Behavior of Pile Extension Connections to Slab Bridges under Cyclic Loading

Mohamed Ayoub, Graduate Assistant

David H. Sanders, PhD, Project PI

UNR Report No. CCEER 10-06

Report for the
California Department of Transportation
Sacramento, CA

Caltrans Contract 59A0501

November 2010

Center for Earthquake Engineering Research
Department of Civil and Environmental Engineering
University of Nevada
Reno, Nevada 89557-0258

Abstract

The California Transportation Department (Caltrans) has a large number of highway bridges; and many of them are slab bridges. Although slab bridges are a common type of bridge, the current version of the Bridge Design Specification and the Seismic Design Criteria provide limited design guidance for pile extension connection details for slab bridges. Unlike the column to box-girder bridge connections which have been discussed and tested extensively, slab-bridge connections have not been tested. The objectives were to develop standard details that can be used to update the existed details for the slab bridge joints and to establish design procedure for the joint regions with and without drop caps. To accomplish these objectives eight large-scale pile-slab bridge connection specimens (16-in. diameter piles) were tested under cyclic loading at the University of Nevada, Reno (UNR). The first two specimens were based on the existing Caltrans specification. The primary difference was that one specimen had a flat-slab detail while the second specimen had a drop-cap detail. The remaining six specimens were based on 24-in. diameter piles. Since there are no standard details for 24-in. diameter piles, box-girder design methodology was used. Both the drop cap T-joint and Knee-joint with the 24-in. diameter piles had plastic hinging in the pile. The flat-slab T-joint and Knee-joint both did not perform well, where failure occurred in the slab. From the experimental visual observations and the reinforcement strains recorded for 24-in. pile specimens, strut-and-tie models (STM's) were used to develop the last two specimens. The modified specimens performed well and provided the basis for revised design methodology and standard details for the connection of larger diameter piles in slab bridges.

Overall the results have shown that the specifications for the box-girder design are good for slab-bridge joints with some modifications. Guidelines for the modification of the slab-bridge joints are discussed in detail.

Acknowledgments

The research presented in this document was funded by the California Department of Transportation (Caltrans) Agreement No. 59A0501. Thanks are given to Dr. Saad El-Azazy and Dr. Ahmed Ibrahim, the Caltrans contract monitors, for their support and advice.

We would like to thank the staff of the UNR Large Scale Structures Laboratory, Patrick Laplace, Paul Lucas, Chad Lyttle, Robby Nelson and Todd Lyttle, for their help and support during the portion of this research.

This report was prepared by the first author as a part of this authors' doctoral dissertation and supervised by the second author. Opinions expressed in this report are those of the authors and do not necessarily reflect the views of the funding organization.

Table of Contents

Table of Contents ..... **iii**
List of Tables ..... **ix**
List of Figures ..... **xi**

Chapter 1 Introduction and Literature Review **1**
1.1 General Perspective 1
1.2 Literature Review 1
1.2.1 Bridge Column Connection Research 1
1.2.2 Column-Slab Building Research 4
1.2.3 Pile to Pile-Cap Research 4
1.2.4 Existing Code Provisions 4
1.3 Caltrans Slab Bridges 5
1.4 Problem Statement 5
1.5 Research Objectives 5
1.6 Scope of work 6
1.7 Document Layout 6

Chapter 2 Preliminary Analysis and Specimen Selection **6**
2.1 Introduction 6
2.2 Model Selection 6
2.2.1 Pile Length Selection 6
2.2.2 Slab Dimensions Selection 7
2.3 Reinforcement Design 7
2.3.1 Pile Reinforcement 7
2.3.2 Slab Reinforcement 8
2.4 Joint Design 8
2.5 Moment Capacity 9
2.6 Punching Shear 10
2.7 Preliminary Analysis 10
2.7.1 Moment-Curvature Analysis 12
2.7.2 Material Models 12
2.7.2.1 Unconfined Concrete 12
2.7.2.2 Confined Concrete 13
2.7.2.3 Nonlinear Reinforcing Steel Model 14
2.8 Pushover Analysis 14

Chapter 3 Experimental Program **14**
3.1 Introduction 14
3.2 Pile-Slab Bridge Model Construction 14
3.3 Measured Material Properties 14
3.3.1 Measured Concrete Properties 14
3.3.2 Testing of Steel Samples 14
3.4 Experimental Test Set-Up 15

3.4.1 Experimental Test Setup for T-Joints 15
3.4.2 Experimental Test Set-Up for Knee-Joints 16
3.5 Loading Program 17
3.6 Instrumentation 17
3.6.1 Strain Gauges 17
3.6.2 Displacement Transducer Devices 18
3.6.3 Load Measurements 18
3.6.4 Axial Load 20
3.6.5 Global Displacements 20

Chapter 4 Experimental Test Results 20
4.1 Introduction 20
4.2 DCRCC1 Results 20
4.2.1 Observed Response of the Specimen, DCRCC1 20
4.2.2 Force-Displacement Relationships 20
4.2.3 Strain Gauge Data 21
4.2.4 Curvature Measurements 22
4.3 FSRCC1 Results 22
4.3.1 Observed Response of the Specimen, FSRCC1 22
4.3.2 Force-Displacement Relationships 23
4.3.3 Strain Gauge Data 23
4.3.4 Curvature Measurements 23
4.4 DCRCC24 Results 24
4.4.1 Observed Response of the Specimen, DCRCC24 24
4.4.2 Force-Displacement Relationships 24
4.4.3 Strain Gauge Data 25
4.4.4 Curvature Measurements 25
4.5 FSRCC24 Results 25
4.5.1 Observed Response of the Specimen, FSRCC24 25
4.5.2 Force-Displacement Relationships 26
4.5.3 Strain Gauge Data 27
4.5.4 Curvature Measurements 27
4.6 DCKJ24 Results 27
4.6.1 Observed Response of the Specimen, DCKJ24 27
4.6.2 Force-Displacement Relationships 28
4.6.3 Strain Gauge Data 29
4.6.4 Curvature Measurements 29
4.7 FSKJ24 Results 30
4.7.1 Observed Response of the Specimen, FSKJ24 30
4.7.2 Force-Displacement Relationships 30
4.7.3 Strain Gauge Data 31
4.7.4 Curvature Measurements 31

Chapter 5 Strut-and-Tie Models 33
5.1 Introduction 33

5.2 Strut-and-Tie Model for T-joint (Specimen FSRCC24) 33
5.2.1 Boundary Forces 33
5.2.2 Measured Joint Reinforcement Force-Transfer Contributions 34
5.2.2.1 Joint Stirrups 34
5.2.2.2 Pile Reinforcement 34
5.2.2.3 Slab Reinforcement 34
5.2.3 Strut-and-Tie Model Development for FSRCC24 35
5.3 Strut-and-Tie Model Verification 36
5.3.1 Ties Verification 36
5.3.2 Strut Verification 38
5.3.3 The Design Shortages of Specimen FSRCC24 38
5.4 Design of Specimen FSRCC24-M 39
5.4.1 Additional Reinforcement in Slab Top 39
5.4.2 Additional Reinforcement in Slab Bottom 39
5.4.3 Area of the Vertical Joint Stirrup Reinforcement 39
5.4.4 Area of the additional stirrups on the pile face 40
5.5 Strut-and-Tie Model for Knee-joint 40
5.5.1 Boundary Forces 40
5.5.2 Strut-and-Tie Model Development for DCKJ24 41
5.5.3 Measured Joint Reinforcement Force-Transfer Contributions 42
5.5.3.1 Joint Stirrups 42
5.5.3.2 Pile Reinforcement 42
5.5.3.3 Slab Reinforcement 42
5.5.4 Strut-and-Tie Model Verification 43
5.5.4.1 Closing Moment Case 43
5.5.4.2 Opening Moment Case: 44
5.5.4.3 Strut Verification 45
5.6 Strut-and-Tie Model for FSKJ24 46
5.6.1 Boundary Forces 46
5.6.2 Measured Joint Reinforcement Force-Transfer Contributions 46
5.6.2.1 Joint Stirrups 46
5.6.2.2 Pile Reinforcement 46
5.6.2.3 Slab Reinforcement 46
5.6.2.4 Joint Cracks Development 47
5.6.3 Strut-and-Tie Model Verification 48
5.6.3.1 Closing Moment Case 48
5.6.3.2 Opening Moment Case 49
5.6.3.3 Strut Verification 50
5.7 Design of Specimen FSKJ24-M 50
5.7.1 Design Modification 51
5.7.1.1 Width of the slab 51
5.7.1.2 Better load distribution method. 51
5.7.1.3 Slab Thickness 51
5.7.1.4 Specimen Reinforcement 51
5.8 Summary and Conclusions 53

Chapter 6 Modified Specimens 55
6.1 Introduction 55
6.2 FSRCC24-M Results 55
6.2.1 Observed Response of the Specimen, FSRCC24-M 55
6.2.2 Force-Displacement Relationships 56
6.2.3 Strain Gauges Data 56
6.2.4 Curvature Measurements 57
6.3 FSKJ24-M Results 57
6.3.1 Observed Response of the Specimen, FSKJ24-M 57
6.3.2 Force-Displacement Relationships 57
6.3.3 Strain Gauge Data 58
6.3.4 Curvature Measurements 59
6.4 Strut-and-Tie Model 59
6.4.1 Specimen FSRCC24-M 59
6.4.1.1.1 Measured Joint Reinforcement Force-Transfer Contributions 59
6.4.1.1.2 Joint Stirrups 59
6.4.1.1.3 Pile Reinforcement 59
6.4.1.1.4 Slab Reinforcement 60
6.4.1.2 Strut-and-Tie Model Verification for FSRCC24-M 60
6.4.1.2.1 Tie Model Verification 60
6.4.1.2.2 Strut Verification 62
6.4.2 Specimen FSKJ24-M 62
6.4.2.1 Measured Joint Reinforcement Force-Transfer Contributions 62
6.4.2.1.1 Joint Stirrups 62
6.4.2.1.2 Pile Reinforcement 62
6.4.2.1.3 Slab Reinforcement 63
6.4.2.2 Strut-and-Tie Model Verification for FSKJ24-M 63
6.4.2.2.1 Closing Moment Case 63
6.4.2.2.2 Opening Moment Case 67
6.4.2.3 Strut Verification 69
6.5 Performance Evaluation of the Modified Specimens 69
6.5.1 Force Transfer Evaluation 69
6.5.2 Specimen FSRCC24 and FSRCC24-M Comparison 69
6.5.3 Specimen FSKJ24 and FSKJ24-M Comparison 70
6.6 Simplified Strut-and-Tie Model 70
6.6.1 T-Joint 70
6.6.2 Knee-Joint 70

Chapter 7 Post-Test Analysis 72
7.1 Introduction 72
7.2 Finite Element Modeling 72
7.2.1 Concrete Modeling 72
7.2.1.1 Stress-Strain Relations for Concrete 72
7.2.1.2 Biaxial Stress Failure Criterion of Concrete 73
7.2.1.2.1 Compressive Failure 73

7.2.1.2.2 Tensile Failure 73
7.2.2 Numerical model 74
7.2.3 Reinforcement Modeling 74
7.2.4 Boundary Conditions and Loading Program 74
7.3 Impact of Variables on the Analytical Results 75
7.4 Analytical Results 76
7.4.1 Load-Displacement Relationship 76
7.4.2 Cracks Pattern 77
7.5 Updated Moment Curvature Results 78

Chapter 8 Design Recommendations 79
8.1 Introduction 79
8.2 Superstructure Design of the Slab Bridges 79
8.2.1 Superstructure Seismic Forces 79
8.2.2 Joint Dimensions 79
8.2.2.1 Connection Type 79
8.2.2.2 Drop Cap Width 80
8.2.2.3 Effective Width for Flat Slabs 80
8.2.3 Principal Joint Stresses 80
8.2.4 Punching Shear 81
8.3 T-Joint Reinforcement Recommendations 81
8.3.1 Vertical Joint Stirrups 81
8.3.2 Horizontal Joint Stirrups 82
8.3.3 Splice-Transfer Reinforcement 82
8.3.4 Slab Longitudinal Reinforcement in the Transverse Direction of the Bridge 83
8.3.5 Horizontal Side Reinforcement 83
8.4 Knee-Joint Reinforcement Recommendations 83
8.4.1 Vertical Joint Stirrups for Knee-Joints 83
8.4.2 Horizontal Joint Stirrups 83
8.4.3 Splice-Transfer Reinforcement for the Knee-Joints 84
8.4.4 Slab Longitudinal Reinforcement in the Transverse Direction of the Bridge 84
8.4.5 Horizontal Side Reinforcement: 84
8.4.6 Horizontal Cap End Ties 85
8.5 Pile Transverse Reinforcement 85
8.6 Pile Longitudinal Reinforcement 85
8.7 Reinforcement Recommendations for 16-in. Pile Diameter Joints 86

Chapter 9 Summary and Conclusions 87
9.1 Summary 87
9.2 Conclusions 88
9.2.1 Experimental Testing and Observation Conclusions 88
9.2.2 Analytical Modeling Conclusions 88

References **90**

Appendix A **353**
Appendix B **385**
Appendix C **410**
Appendix D **442**
Appendix E **472**
Appendix F **503**
Appendix G **539**
Appendix H **586**

List of Tables

Table 2-1: Variables Matrix for the Prototype Bridges 93
Table 2-2: Variables Matrix for Tested Specimens 93
Table 2-3: Specimen Dimensions 94
Table 2-4: Scaling Factors 94
Table 2-5: Steel Properties for Preliminary Analysis 95
Table 2-6: Concrete Properties for Preliminary Analysis 95
Table 2-7: Pushover Analysis Calculations 96

Table 3-1: Concrete Strength 97
Table 3-2: Measured Reinforcement Properties 98

Table 4-1: Maximum and Minimum Measured Force and Displacement of DCRCC1 ... 99
Table 4-2: Maximum and Minimum Measured Strain (micro strain) in the Reinforcement of DCRCC1 100
Table 4-3:Maximum and Minimum Displacements (inches) of DCRCC1 105
Table 4-4:Maximum and Minimum Measured Force and Displacement of FSRCC1 ... 107
Table 4-5: Maximum and Minimum Measured Strain (micro strain) in the Reinforcement of FSRCC1 108
Table 4-6: Maximum and Minimum Measured Displacements (inches) of FSRCC1.... 112
Table 4-7: Maximum and Minimum Measured Force and Displacement of DCRCC24 113
Table 4-8: Maximum and Minimum Measured Strain (micro strain) in the Reinforcement of DCRCC24 114
Table 4-9: Maximum and Minimum Measured Displacements (inches) of DCRCC24 118
Table 4-10: Maximum and Minimum Measured Force and Displacement of FSRCC24 120
Table 4-11: Maximum and Minimum Measured Strain (micro strain) in the Reinforcement of FSRCC24 121
Table 4-12: Maximum and Minimum Measured Displacements (inches) of FSRCC24 126
Table 4-13: Maximum and Minimum Measured Force and Displacement of DCKJ24. 128
Table 4-14: Maximum and Minimum Measured Strain (micro strain) in the Reinforcement of DCKJ24 129
Table 4-15: Maximum and Minimum Measured Displacements (inches) of DCKJ24 .. 134
Table 4-16: Maximum and Minimum Measured Force and Displacement of FSKJ24.. 135
Table 4-17: Maximum and Minimum Measured Strain (micro strain) in the Reinforcement of FSKJ24 136
Table 4-18: Maximum and Minimum Measured Displacements (inches) of FSKJ24 ... 141

Table 5-1: Strut-and-Tie Model Coordinates for FSRCC24 142
Table 5-2: Strut-and-Tie Model Forces for FSRCC24 142
Table 5-3: Factored Strut-and-Tie Model Forces for FSRCC24 143
Table 5-4: Strut-and-Tie Model Coordinates for DCKJ24, Closing Moment Case and Opening Moment Case 143

Table 5-5: Strut-and-Tie Model Forces for DCKJ24 in the Closing Moment Case and Opening Moment Case 144
Table 5-6: Strut-and-Tie Model Coordinates for FSKJ24, Closing Moment Case and Opening Moment Case 144
Table 5-7: Strut-and-Tie Model Forces for FSKJ24 in the Closing Moment Case and Opening Moment Case 145
Table 5-8: Strut-and-Tie Model Coordinates for Modified FSKJ24 in the Closing Moment Case and Opening Moment Case 146
Table 5-9: Strut-and-Tie Model Factored Forces for Modified FSKJ24 in the Closing Moment Case and Opening Moment Case 147

Table 6-1: Maximum and Minimum Measured Force and Displacement of FSRCC24-M 148
Table 6-2: Maximum and Minimum Measured Strain (micro strain) in the Reinforcement of FSRCC24-M 149
Table 6-3: Maximum and Minimum Measured Displacements of FSRCC24-M..... 156
Table 6-4: Maximum and Minimum Measured Force and Displacement of FSKJ24-M158
Table 6-5: Maximum and Minimum Measured Strain (micro strain) in the Reinforcement of FSKJ24-M 159
Table 6-6: Maximum and Minimum Measured Displacements of FSKJ24-M 166
Table 6-7: Strut-and-Tie Model Coordinates for FSRCC24-M..... 167
Table 6-8: Strut-and-Tie Model Forces for FSRCC24-M 167
Table 6-9: Strut-and-Tie Model Coordinates for Modified FSKJ24-M in the Closing Moment Case and Opening Moment Case 168
Table 6-10: Strut-and-Tie Model Forces for Modified FSKJ24-M in the Closing Moment Case and Opening Moment Case 169
Table 6-11: Tension Demands in Reinforcement Concrete T-Joint Using the Modified Strut-and-Tie Model..... 170
Table 6-12: Tension Demands in Reinforcement Concrete Knee-Joint Using the Modified Strut-and-Tie Model..... 171

Table 7-1: Experimental and Analytical Measured Force-Displacement..... 172
Table 7-2: Confined Concrete Parameters..... 172
Table 7-3: Updated Pushover Analysis Calculations..... 173
Table 7-4: Measured Force-Displacement in Positive Direction..... 173

Table 8-1: Caltrans Reinforcement Requirements for T-Joints[5]..... 174
Table 8-2: Caltrans Reinforcement Requirements for Knee-Joints[5]..... 175
Table 8-3: Test Ductility and drift Summary..... 176

List of Figures

Figure 1-1: Modified External Joint Transfer Strut-and-Tie Model[1] 177
Figure 1-2: Model Forces in D-Region of Short Specimen Beam[2] 177
Figure 1-3: Stut-and-Tie Model for Flared Column Bent[3] 178
Figure 1-4: UGNP 2-D Strut-and-Tie Model[4] 178
Figure 1-5: Four Different Joint Failure Modes[6] 179

Figure 2-1: Inelastic Deformations of Bridge Piles (Test Model) 180
Figure 2-2: Moment Diagram in the Transverse Direction of the Bridge 180
Figure 2-3: Piles Reinforcment and Dimensions 181
Figure 2-4: Support Types 181
Figure 2-5: Dimensions and Reinforcement Details for Specimen DCRCC1 182
Figure 2-6: Dimensions and Reinforcement Details for Specimen FSRCC1 183
Figure 2-7: Dimensions and Reinforcement Details for Specimen DCRCC24 184
Figure 2-8: Dimensions and Reinforcement Details for Specimen FSRCC24 185
Figure 2-9: Dimensions and Reinforcement Details for Specimen DCKJ24 186
Figure 2-10: Dimensions and Reinforcement Details for Specimen FSKJ24 187
Figure 2-11: Dimensions and Reinforcement Details for Specimen FSRCC24-M 188
Figure 2-12: Dimensions and Reinforcement Details for Specimen FSKJ24(M) 189
Figure 2-13: Moment Curvature Curve 190
Figure 2-14: Confined and Unconfined Concrete Model[19] 190
Figure 2-15: Steel Stress Strain Model 191
Figure 2-16: DCRCC1 Pile M-ϕ 191
Figure 2-17: FSRCC1 Pile M-ϕ 192
Figure 2-18: DCRCC24 Pile M-ϕ 192
Figure 2-19: FSRCC24 and FSRCC24-M Pile M-ϕ 193
Figure 2-20: DCKJ24 Pile M-ϕ 194
Figure 2-21: FSKJ24 and FSKJ24-M Pile M-ϕ 194

Figure 3-1: Slab Reinforcement Prior to Cast 195
Figure 3-2: FSRCC24 Casting 196
Figure 3-3: FSRCC24 and DCRCC24 Sonotube Placement 196
Figure 3-4: Experimental Test Set-Up Schematic for Specimen FSRCC1 197
Figure 3-5: Hinge Locations 197
Figure 3-6: Experimental Test Set-Up for Specimen DCRCC1 198
Figure 3-7: Experimental Test Set-Up for Specimen FSRCC24-M 198
Figure 3-8: Experimental Test Set-Up for Specimen DCKJ24 199
Figure 3-9: Experimental Test Set-Up Schematic for Specimen DCKJ24 200
Figure 3-10: Variable Axial Load Mechanism 201
Figure 3-11: SAP2000 Lumped Plasticity Model 201
Figure 3-12: DCKJ24 Axial Loading Protocol 202
Figure 3-13: FSKJ24 and FSKJ24-M Axial Loading Protocol 202
Figure 3-14: Experimental Test Set-Up Schematic for Specimen FSKJ24-M 203
Figure 3-15: DCRCC1 and FSRCC1 Horizontal Loading Protocol 204

Figure 3-16: DCRCC24, FSRCC24 and FSRCC24-M Horizontal Loading Protocol.... 204
Figure 3-17: DCKJ24 Horizontal Loading Protocol..... 205
Figure 3-18: FSKJ24 nd FSKJ24-M Horizontal Loading Protocol 205
Figure 3-19: DCRCC1 Strain Gauge Locations 206
Figure 3-20: FSRCC1 Strain Gauge Locations 207
Figure 3-21: DCRCC24 Strain Gauge Locations 208
Figure 3-22: FSRCC24 Strain Gauge Locations 209
Figure 3-23: FSRCC24 Pile Strain Gauge Locations 210
Figure 3-24: DCKJ24 Strain Gauge Locations..... 211
Figure 3-25: FSKJ24 Strain Gauge Locations..... 212
Figure 3-26: FSRCC24-M Pile Strain Gauge Locations 213
Figure 3-27: FSRCC24-M Pile Strain Gauge Locations 214
Figure 3-28: FSKJ24-M Slab Strain Gauge Locations..... 215
Figure 3-29: FSKJ24-M Pile Strain Gauge Locations..... 216
Figure 3-30: DCRCC1 Displacement Transducer Device Locations 217
Figure 3-31: FSRCC1 Displacement Transducer Device Locations 217
Figure 3-32: DCRCC24 Displacement Transducer Device Locations 218
Figure 3-33: FSRCC24 and FSRCC24-M Displacement Transducer Device Locations 218
Figure 3-34: DCKJ24 Displacement Transducer Device Locations..... 219
Figure 3-35: FSKJ24 Displacement Transducer Device Locations..... 219
Figure 3-36: FSKJ24-M Displacement Transducer Device Locations..... 220
Figure 3-37: Curvature Calculation Parameters 220
Figure 3-38: Head Rotation Correction in the Test Setup 221

Figure 4-1: DCRCC1 Cracking (1 Δy) 222
Figure 4-2: DCRCC1 Cracking (2 Δy) 222
Figure 4-3: DCRCC1 Cracking (3 Δy) 222
Figure 4-4: DCRCC1 Cracking (5 Δy) 223
Figure 4-5: DCRCC1 Cracking (5 Δy) 223
Figure 4-6: Plastic Hinge Deformation at the End of DCRCC1 Testing..... 223
Figure 4-7: Force-Displacement Hysteretic Response for DCRCC1 224
Figure 4-8: Measured Curvature Envelope along the Plastic Hinge of DCRCC1..... 224
Figure 4-9: FSRCC1 Cracking (1 Δy) 225
Figure 4-10: FSRCC1 Cracking (2 Δy) 225
Figure 4-11: FSRCC1 Cracking (3 Δy) 225
Figure 4-12: FSRCC1 Cracking (4 Δy) 226
Figure 4-13: FSRCC1 Cracking (5 Δy) 226
Figure 4-14: FSRCC1 Slab Cracking (5 Δy) 226
Figure 4-15: Plastic Hinge Deformation at the End of DCRCC1 Testing..... 227
Figure 4-16: Force-Displacement Hysteretic Response for FSRCC1 227
Figure 4-17: Measured Curvature Envelope along the Plastic Hinge of FSRCC1..... 228
Figure 4-18: DCRCC24 Cracks (0.25 fy)..... 228
Figure 4-19: DCRCC24 Cracks (0.75 fy)..... 229
Figure 4-20: DCRCC24 Cracks (1 Δy)..... 229
Figure 4-21: DCRCC24 Cracks (2 Δy)..... 230

Figure 4-22: DCRCC24 Cracks (3 Δy) 230
Figure 4-23: Force-Displacement Hysteretic Response for DCRCC24 231
Figure 4-24: Measured Curvature Envelope along the Plastic Hinge of DCRCC24..... 231
Figure 4-25: FSRCC24 Cracks (0.25fy) 232
Figure 4-26: FSRCC24 Cracks (0.75fy) 232
Figure 4-27: FSRCC24 Slab Cracks (1 Δy) 232
Figure 4-28: FSRCC24 Cracks (2 Δy) 233
Figure 4-29: FSRCC24 Cracks (2.5 Δy) 233
Figure 4-30: FSRCC24 Slab Cracks (3.5 Δy) 234
Figure 4-31: FSRCC24 Cracks (4 Δy) 234
Figure 4-32: The End of FSRCC24 Testing 235
Figure 4-33: Force-Displacement Hysteretic Response for FSRCC24 236
Figure 4-34: Measured Curvature Envelope along the Plastic Hinge of FSRCC24..... 236
Figure 4-35: DCKJ24 Cracks (1 Δy) 237
Figure 4-36: DCKJ24 Cracks (1.5 Δy) 237
Figure 4-37: DCKJ24 Cracks (2 Δy) 238
Figure 4-38: DCKJ24 Cracks (3 Δy) 238
Figure 4-39: DCKJ24 Cracks (4 Δy) 239
Figure 4-40: DCKJ24 Cracks (5 Δy) 239
Figure 4-41: DCKJ24 Cracks (6 Δy) 240
Figure 4-42: DCKJ24 at the End of The Test 240
Figure 4-43: Force-Displacement Hysteretic Response for DCKJ24..... 241
Figure 4-44: Measured Curvature Envelope along the Plastic Hinge of DCKJ24 241
Figure 4-45: FSKJ24 Cracks (0.25fy)..... 242
Figure 4-46: FSKJ24 Cracks (0.5fy)..... 242
Figure 4-47: FSKJ24 Cracks (0.75fy)..... 243
Figure 4-48: FSKJ24 Cracks (1Δy) 243
Figure 4-49: FSKJ24 Cracks (1.5Δy) 244
Figure 4-50: FSKJ24 Cracks (2 Δy) 244
Figure 4-51: FSKJ24 Cracks (2.5Δy) 245
Figure 4-52: FSKJ24 Cracks (3Δy) 245
Figure 4-53: FSKJ24 at the End of The Test 246
Figure 4-54: Force-Displacement Hysteretic Response for FSKJ24..... 247
Figure 4-55: Measured Curvature Envelope along the Plastic Hinge of FSKJ24 247

Figure 5-1: Tension and Compression Centroids of Pile..... 248
Figure 5-2: Tension and Compression Centroids of the Flat-Slab in Positive and Negative Moment 248
Figure 5-3:Boundary Forces –Full Specimen 249
Figure 5-4: Strut-and-Tie Model for Specimen FRCC24..... 249
Figure 5-5: Joint Stirrup Strain for FSRCC24 South Cycle 2 250
Figure 5-6: Joint Stirrup Strain for FSRCC24 North Cycle 2 250
Figure 5-7: Joint Stirrup Strain for FSRCC24 South Cycle 2 251
Figure 5-8: Joint Stirrup Strain for FSRCC24 North Cycle 2 251
Figure 5-9: Joint Stirrup Strain for FSRCC24 South Cycle 2 252

Figure 5-10: Joint Stirrup Strain for FSRCC24 North Cycle 2 252
Figure 5-11: Longitudinal Pile Strain for FSRCC24 South Cycle 2 253
Figure 5-12: Longitudinal Pile Strain for FSRCC24 North Cycle 2 253
Figure 5-13: Spiral Reinforcement Strain for FSRCC24 South Cycle 2 254
Figure 5-14: Spiral Reinforcement Strain for FSRCC24 North Cycle 2 254
Figure 5-15: Slab Top Reinforcement for FSRCC24 South Cycle 2..... 255
Figure 5-16: Slab Top Reinforcement for FSRCC24 North Cycle 2..... 255
Figure 5-17: Slab Bottom Reinforcement Strainfor FSRCC24 South Cycle 2 256
Figure 5-18: Slab Bottom Reinforcement Strainfor FSRCC24 North Cycle 2 256
Figure 5-19: Tension and Compression Centroids of Slab..... 257
Figure 5-20: Tension and Compression Centroids of the Drop-Cap Slab in Positive and Negative Moment..... 257
Figure 5-21: Boundary Forces for DCKJ24 in Openning Position..... 258
Figure 5-22: Boundary Forces for DCKJ24 in Clossing Position 258
Figure 5-23: Strut-and-Tie Model for Specimen DCKJ24 (Closing Moment)..... 259
Figure 5-24: Strut-and-Tie Model for Specimen DCKJ24 (Opening Moment) 259
Figure 5-25: Horizontal Cap End Ties Strain for DCKJ24 South Cycle 2..... 260
Figure 5-26: Horizontal Cap End Ties Strain for DCKJ24 North Cycle 2..... 260
Figure 5-27: Joint Stirrup Strain for DCKJ24 South Cycle 2..... 261
Figure 5-28: Joint Stirrup Strain for DCKJ24 North Cycle 2..... 261
Figure 5-29: Joint Stirrup Strain for DCKJ24 South Cycle 2..... 262
Figure 5-30: Joint Stirrup Strain for DCKJ24 North Cycle 2..... 262
Figure 5-31: Joint Stirrup Strain for DCKJ24 South Cycle 2..... 263
Figure 5-32: Joint Stirrup Strain for DCKJ24 North Cycle 2..... 263
Figure 5-33: Longitudinal Pile Strain for DCKJ24 South Cycle 2..... 264
Figure 5-34: Longitudinal Pile Strain for DCKJ24 North Cycle 2..... 264
Figure 5-35: Spiral Reinforcement Strain for DCKJ24 South Cycle 2 265
Figure 5-36: Spiral Reinforcement Strain for DCKJ24 North Cycle 2 265
Figure 5-37: Slab Bottom Reinforcement Strainfor DCKJ24 South Cycle 2..... 266
Figure 5-38: Slab Bottom Reinforcement Strainfor DCKJ24 North Cycle 2..... 266
Figure 5-39: Slab Bottom Reinforcement Strain for DCKJ24 South Cycle 2..... 267
Figure 5-40: Slab Bottom Reinforcement Strain for DCKJ24 North Cycle 2..... 267
Figure 5-41: Slab Top Reinforcement Strain for DCKJ24 South Cycle 2 268
Figure 5-42: Slab Top Reinforcement Strain for DCKJ24 North Cycle 2 268
Figure 5-43: Slab Top Reinforcement Strain for DCKJ24 South Cycle 2 269
Figure 5-44: Slab Top Reinforcement Strain for DCKJ24 North Cycle 2 269
Figure 5-45: Spiral Reinforcement Tie Representation in Knee-Joint 270
Figure 5-46: Horizontal Cap End Ties Strain for FSKJ24 South Cycle 2..... 270
Figure 5-47: Horizontal Cap End Ties Strain for FSKJ24 North Cycle 2..... 271
Figure 5-48: Joint Stirrup Strain for FSKJ24 South Cycle 2..... 271
Figure 5-49: Joint Stirrup Strain for FSKJ24 North Cycle 2..... 272
Figure 5-50: Joint Stirrup Strain for FSKJ24 South Cycle 2..... 272
Figure 5-51: Joint Stirrup Strain for FSKJ24 North Cycle 2..... 273
Figure 5-52: Joint Stirrup Strain for FSKJ24 South Cycle 2..... 273
Figure 5-53: Joint Stirrup Strain for FSKJ24 North Cycle 2..... 274

Figure 5-54: Longitudinal Pile Strain for FSKJ24 South Cycle 2 274
Figure 5-55: Longitudinal Pile Strain for FSKJ24 North Cycle 2 275
Figure 5-56: Spiral Reinforcement Strain for FSKJ24 South Cycle 2..... 275
Figure 5-57: Spiral Reinforcement Strain for FSKJ24 North Cycle 2..... 276
Figure 5-58: Slab Bottom Reinforcement Strain for FSKJ24 South Cycle 2 276
Figure 5-59: Slab Bottom Reinforcement Strain for FSKJ24 North Cycle 2 277
Figure 5-60: Slab Bottom Reinforcement Strain for FSKJ24 South Cycle 2 277
Figure 5-61: Slab Bottom Reinforcement Strain for FSKJ24 North Cycle 2 278
Figure 5-62: Slab Top Reinforcement Strain for FSKJ24 South Cycle 2..... 278
Figure 5-63: Slab Top Reinforcement Strain for FSKJ24 North Cycle 2..... 279
Figure 5-64: Slab Top Reinforcement Strain for FSKJ24 South Cycle 2..... 279
Figure 5-65: Slab Top Reinforcement Strain for FSKJ24 North Cycle 2..... 280
Figure 5-66: Bottle Shaped Strut Configuration..... 280
Figure 5-67: Strut-and-Tie Model FSKJ24 (Closing Moment) 281
Figure 5-68: Strut-and-Tie Model FSKJ24 (Opening Moment)..... 281
Figure 5-69: Modified Strut-and-Tie Model for FSKJ24 (Closing Moment)..... 282
Figure 5-70: Modified Strut-and-Tie Model for FSKJ24 (Opening Moment) 282

Figure 6-1: FSRCC24-M Cracks (0.75fy) 283
Figure 6-2: FSRCC24-M Cracks (1Δy)..... 283
Figure 6-3: FSRCC24-M Cracks (2Δy)..... 284
Figure 6-4: FSRCC24-M Cracks (2.5Δy)..... 284
Figure 6-5: FSRCC24-M Cracks (3Δy)..... 285
Figure 6-6: FSRCC24-M Cracks (3.5Δy)..... 285
Figure 6-7: FSRCC24-M Cracks (4Δy)..... 286
Figure 6-8: FSRCC24-M Cracks (5Δy)..... 286
Figure 6-9: FSRCC24-M Cracks (6Δy)..... 287
Figure 6-10: Force-Displacement Hysteretic Response for FSRCC24-M 287
Figure 6-11: Measured Curvature Envelope along the Plastic Hinge of FSRCC24-M.. 288
Figure 6-12: FSKJ24-M Cracks (0.75fy)..... 288
Figure 6-13: FSKJ24-M Cracks (1Δy) 289
Figure 6-14: FSKJ24-M Cracks (1.5Δy) 289
Figure 6-15:FSKJ24-M Cracks (2Δy) 290
Figure 6-16:FSKJ24-M Cracks (2.5Δy) 290
Figure 6-17: FSKJ24-M Cracks (3Δy) 290
Figure 6-18: FSKJ24-M Cracks (4Δy) 290
Figure 6-19: FSKJ24-M Cracks (6Δy) 291
Figure 6-20: Force-Displacement Hysteretic Response for FSKJ24-M..... 292
Figure 6-21: Measured Curvature Envelope along the Plastic Hinge of FSKJ24-M 292
Figure 6-22: Joint Stirrup Strain for FSRCC24-M South Cycle 2 293
Figure 6-23: Joint Stirrup Strain for FSRCC24-M North Cycle 2 293
Figure 6-24: Joint Stirrup Strain for FSRCC24-M South Cycle 2 294
Figure 6-25: Joint Stirrup Strain for FSRCC24-M North Cycle 2 294
Figure 6-26: Joint Stirrup Strain for FSRCC24-M South Cycle 2 295
Figure 6-27: Joint Stirrup Strain for FSRCC24-M North Cycle 2 295

Figure 6-28: Joint Stirrup Strain for FSRCC24-M South Cycle 2 296
Figure 6-29: Joint Stirrup Strain for FSRCC24-M North Cycle 2 296
Figure 6-30: Joint Stirrup Strain for FSRCC24-M South Cycle 2 297
Figure 6-31: Joint Stirrup Strain for FSRCC24-M North Cycle 2 297
Figure 6-32: Joint Stirrup Strain for FSRCC24-M South Cycle 2 298
Figure 6-33: Joint Stirrup Strain for FSRCC24-M North Cycle 2 298
Figure 6-34: J-bars Joint Reinforcement Strain for FSRCC24-M South Cycle 2 299
Figure 6-35: J-bars Joint Reinforcement Strain for FSRCC24-M North Cycle 2 299
Figure 6-36: J-bars Joint Reinforcement Strain for FSRCC24-M South Cycle 2 300
Figure 6-37: J-bars Joint Reinforcement Strain for FSRCC24-M North Cycle 2 300
Figure 6-38: Longitudinal Pile Strain for FSRCC24-M South Cycle 2..... 301
Figure 6-39: Longitudinal Pile Strain for FSRCC24-M North Cycle 2..... 301
Figure 6-40: Spiral Reinforcement Strain for FSRCC24-M South Cycle 2 302
Figure 6-41: Spiral Reinforcement Strain for FSRCC24-M North Cycle 2 302
Figure 6-42: Slab Bottom Reinforcement Strain for FSRCC24-M South Cycle 2..... 303
Figure 6-43: Slab Bottom Reinforcement Strain for FSRCC24-M North Cycle 2..... 303
Figure 6-44: Slab Bottom Reinforcement for FSRCC24-M South Cycle 2 304
Figure 6-45: Slab Bottom Reinforcement Strain for FSRCC24-M North Cycle 2..... 304
Figure 6-46: Slab Top Reinforcement Strain for FSRCC24-M South Cycle 2 305
Figure 6-47: Slab Top Reinforcement Strain for FSRCC24-M North Cycle 2 305
Figure 6-48: Slab Top Reinforcement Strain for FSRCC24-M South Cycle 2 306
Figure 6-49: Slab Top Reinforcement Strain for FSRCC24-M North Cycle 2 306
Figure 6-50: Boundary Forces –Full Specimen 307
Figure 6-51: Joint Stirrup Strain for FSKJ24-M South Cycle 2 307
Figure 6-52: Joint Stirrup Strain for FSKJ24-M North Cycle 2 308
Figure 6-53: Joint Stirrup Strain for FSKJ24-M South Cycle 2 308
Figure 6-54: Joint Stirrup Strain for FSKJ24-M North Cycle 2 309
Figure 6-55: Joint Stirrup Strain for FSKJ24-M South Cycle 2 309
Figure 6-56: Joint Stirrup Strain for FSKJ24-M North Cycle 2 310
Figure 6-57: Horizontal Cap End Ties Strain for FSKJ24-M South Cycle 2 310
Figure 6-58: Horizontal Cap End Ties Strain for FSKJ24-M North Cycle 2 311
Figure 6-59: J-bars Joint Reinforcement Strain for FSKJ24-M South Cycle 2..... 311
Figure 6-60: J-bars Joint Reinforcement Strain for FSKJ24-M North Cycle 2..... 312
Figure 6-61: Longitudinal Pile Strain for FSKJ24-M South Cycle 2 312
Figure 6-62: Longitudinal Pile Strain for FSKJ24-M North Cycle 2 313
Figure 6-63: Spiral Reinforcement Strain for FSKJ24-M South Cycle 2..... 313
Figure 6-64: Spiral Reinforcement Strain for FSKJ24-M North Cycle 2..... 314
Figure 6-65: Slab Top Reinforcement for FSKJ24-M South Cycle 2 314
Figure 6-66: Slab Top Reinforcement Strain for FSKJ24-M North Cycle 2..... 315
Figure 6-67: Slab Top Reinforcement for FSKJ24-M South Cycle 2 315
Figure 6-68: Slab Top Reinforcement Strain for FSKJ24-M North Cycle 2..... 316
Figure 6-69: Slab Top Reinforcement Strain for FSKJ24-M South Cycle 2..... 316
Figure 6-70: Slab Top Reinforcement Strain for FSKJ24-M North Cycle 2..... 317
Figure 6-71: Slab Bottom Reinforcement Strain for FSKJ24-M South Cycle 2 317
Figure 6-72: Slab Bottom Reinforcement Strain for FSKJ24-M North Cycle 2 318

Figure 6-73: Slab Bottom Reinforcement Strain for FSKJ24-M South Cycle 2 318
Figure 6-74: Slab Bottom Reinforcement Strain for FSKJ24-M North Cycle 2 319
Figure 6-75: Slab Bottom Reinforcement Strain for FSKJ24-M South Cycle 2 319
Figure 6-76: Slab Bottom Reinforcement Strain for FSKJ24-M North Cycle 2 320
Figure 6-77: Modified Strut-and-Tie Model For FSKJ24 (Closing Moment)..... 321
Figure 6-78: Bottle Shaped Strut Configuration for Strut C_{CG} in Closing Case..... 321
Figure 6-79: Final Modified Strut-and-Tie Model For FSKJ24 (Closing Moment) 321
Figure 6-80: Modified Strut-and-Tie Model For FSKJ24 (Opening Moment) 322
Figure 6-81: Bottle Shaped Strut Configuration for Strut C_{CG} in Opening Case 322
Figure 6-82: Final Modified Strut-and-Tie Model For FSKJ24 (Opening Moment)..... 322
Figure 6-83: Force-Dispacement for Specimens FSRCC24 and FSRCC24-M..... 323
Figure 6-84: Force-Dispacement for Specimens FSKJ24 and FSKJ24-M..... 323
Figure 6-85: Force Transfer Mechanis Inside and Outside Pile Core Reigon..... 324

Figure 7-1: Uniaxial stress-strain law for concrete[28] 325
Figure 7-2: Biaxial failure function for concrete[28] 325
Figure 7-3: Finite Element Types 326
Figure 7-4: Finite Element Modeling for T-joint Specimens 327
Figure 7-5: Finite Element Modeling for Knee-joint Specimens 327
Figure 7-6: Analytical Results versus Experimental Results for DCRCC1 328
Figure 7-7: Analytical Results versus Experimental Results for FSRCC1..... 328
Figure 7-8: Analytical Results versus Experimental Results for DCRCC24 329
Figure 7-9: Analytical Results versus Experimental Results for FSRCC24..... 329
Figure 7-10: Analytical Results versus Experimental Results for DCKJ24..... 330
Figure 7-11: Analytical Results versus Experimental Results for FSKJ24..... 330
Figure 7-12: Analytical Results versus Experimental Results for FSRCC24-M..... 331
Figure 7-13: Analytical Results versus Experimental Results for FSKJ24-M 331
Figure 7-14: Actual and Predicted Cracks Pattern for Specimen DCRCC1..... 332
Figure 7-15: Actual and Predicted Cracks Pattern for Specimen FSRCC1..... 332
Figure 7-16: Actual and Predicted Cracks Pattern for Specimen DCRCC24..... 333
Figure 7-17: Actual and Predicted Cracks Pattern for Specimen FSRCC24..... 333
Figure 7-18: Actual and Predicted Cracks Pattern for Specimen DCKJ24 334
Figure 7-19: Actual and Predicted Cracks Pattern for Specimen FSKJ24 334
Figure 7-20: Actual and Predicted Cracks Pattern for Specimen FSRCC24-M..... 335
Figure 7-21: Actual and Predicted Cracks Pattern for Specimen FSKJ24-M 335
Figure 7-22: DCRCC1 Pile M-ϕ Post Analysis 336
Figure 7-23: FSRCC1 Pile M-ϕ Post Analysis 336
Figure 7-24: DCRCC24 Pile M-ϕ Post Analysis 337
Figure 7-25: FSRCC24 Pile M-ϕ Post Analysis 337
Figure 7-26: DCKJ24 Pile M-ϕ Post Analysis (Max. Load Case)..... 338
Figure 7-27: DCKJ24 Pile M-ϕ Post Analysis (Min. Load Case) 338
Figure 7-28: FSKJ24 Pile M-ϕ Post Analysis (Max. Load Case)..... 339
Figure 7-29: FSKJ24 Pile M-ϕ Post Analysis (Min. Load Case)..... 339
Figure 7-30: FSRCC24-M Pile M-ϕ Post Analysis 340
Figure 7-31: FSKJ24-M Pile M-ϕ Post Analysis (Max. Load Case)..... 340

Figure 7-32: FSKJ24-M Pile M-ϕ Post Analysis (Min. Load Case) 341
Figure 7-33: DCRCC1 Slab Positive M-ϕ Post Analysis 341
Figure 7-34: DCRCC1 Slab Negative M-ϕ Post Analysis 342
Figure 7-35: FSRCC1 Slab Positive M-ϕ Post Analysis 342
Figure 7-36: FSRCC1 Slab Negative M-ϕ Post Analysis 343
Figure 7-37: DCRCC24 Slab Positive M-ϕ Post Analysis 343
Figure 7-38: DCRCC24 Slab Negative M-ϕ Post Analysis 344
Figure 7-39: FSRCC24 Slab Positive M-ϕ Post Analysis 344
Figure 7-40: FSRCC24 Slab Negative M-ϕ Post Analysis 345
Figure 7-41: DCKJ24 Slab Positive M-ϕ Post Analysis 345
Figure 7-42: DCKJ24 Slab Negative M-ϕ Post Analysis 346
Figure 7-43: FSKJ24 Slab Positive M-ϕ Post Analysis 346
Figure 7-44: FSKJ24 Slab Negative M-ϕ Post Analysis 347
Figure 7-45: FSRCC24-M Slab Positive M-ϕ Post Analysis 347
Figure 7-46: FSRCC24-M Slab Negative M-ϕ Post Analysis 348
Figure 7-47: FSKJ24-M Slab Positive M-ϕ Post Analysis 348
Figure 7-48: FSKJ24-M Slab Negative M-ϕ Post Analysis 349

Figure 8-1: Plan View of Joint Reinforcement Locations for the T-Joint 350
Figure 8-2: Recommended Joint Reinforcement Details 350
Figure 8-3: Plan View of Joint Reinforcement Locations for the Knee-Joint 351
Figure 8-4: FSRCC24 Failure Mode 352

Figure A - 1: Measured Strain in Gauge No.1 for DCRCC1 354
Figure A - 2: Measured Strain in Gauge No.2 for DCRCC1 354
Figure A - 3: Measured Strain in Gauge No.3 for DCRCC1 355
Figure A - 4: Measured Strain in Gauge No.4 for DCRCC1 355
Figure A - 5: Measured Strain in Gauge No.5 for DCRCC1 356
Figure A - 6: Measured Strain in Gauge No.6 for DCRCC1 356
Figure A - 7: Measured Strain in Gauge No.8 for DCRCC1 357
Figure A - 8: Measured Strain in Gauge No.9 for DCRCC1 357
Figure A - 9: Measured Strain in Gauge No.10 for DCRCC1 358
Figure A - 10: Measured Strain in Gauge No.11 for DCRCC1 358
Figure A - 11: Measured Strain in Gauge No.12 for DCRCC1 359
Figure A - 12: Measured Strain in Gauge No.13 for DCRCC1 359
Figure A - 13: Measured Strain in Gauge No.14 for DCRCC1 360
Figure A - 14: Measured Strain in Gauge No.15 for DCRCC1 360
Figure A - 15: Measured Strain in Gauge No.16 for DCRCC1 361
Figure A - 16: Measured Strain in Gauge No.18 for DCRCC1 361
Figure A - 17: Measured Strain in Gauge No.19 for DCRCC1 362
Figure A - 18: Measured Strain in Gauge No.20 for DCRCC1 362
Figure A - 19: Measured Strain in Gauge No.21 for DCRCC1 363
Figure A - 20: Measured Strain in Gauge No.22 for DCRCC1 363
Figure A - 21: Measured Strain in Gauge No.23 for DCRCC1 364
Figure A - 22: Measured Strain in Gauge No.24 for DCRCC1 364

Figure A - 23: Measured Strain in Gauge No.25 for DCRCC1 365
Figure A - 24: Measured Strain in Gauge No.26 for DCRCC1 365
Figure A - 25: Measured Strain in Gauge No.27 for DCRCC1 366
Figure A - 26: Measured Strain in Gauge No.29 for DCRCC1 366
Figure A - 27: Measured Strain in Gauge No.30 for DCRCC1 367
Figure A - 28: Measured Strain in Gauge No.32 for DCRCC1 367
Figure A - 29: Measured Strain in Gauge No.33 for DCRCC1 368

Figure A - 30: Measured Strain in Gauge No.34 for DCRCC1 368
Figure A - 31: Measured Strain in Gauge No.35 for DCRCC1 369
Figure A - 32: Measured Strain in Gauge No.36 for DCRCC1 369
Figure A - 33: Measured Strain in Gauge No.38 for DCRCC1 370
Figure A - 34: Measured Strain in Gauge No.39 for DCRCC1 370
Figure A - 35: Measured Strain in Gauge No.40 for DCRCC1 371
Figure A - 36: Measured Strain in Gauge No.41 for DCRCC1 371
Figure A - 37: Measured Strain in Gauge No.42 for DCRCC1 372
Figure A - 38: Measured Strain in Gauge No.43 for DCRCC1 372
Figure A - 39: Measured Strain in Gauge No.44 for DCRCC1 373
Figure A - 40: Measured Strain in Gauge No.45 for DCRCC1 373
Figure A - 41: Measured Strain in Gauge No.46 for DCRCC1 374
Figure A - 42: Measured Strain in Gauge No.47 for DCRCC1 374
Figure A - 43: Measured Strain in Gauge No.48 for DCRCC1 375
Figure A - 44: Measured Strain in Gauge No.49 for DCRCC1 375
Figure A - 45: Measured Strain in Gauge No.50 for DCRCC1 376
Figure A - 46: Measured Strain in Gauge No.51 for DCRCC1 376
Figure A - 47: Measured Strain in Gauge No.52 for DCRCC1 377
Figure A - 48: Measured Strain in Gauge No.53 for DCRCC1 377
Figure A - 49: Measured Strain in Gauge No.54 for DCRCC1 378
Figure A - 50: Measured Strain in Gauge No.55 for DCRCC1 378
Figure A - 51: Measured Strain in Gauge No.57 for DCRCC1 379
Figure A - 52: Measured Strain in Gauge No.58 for DCRCC1 379
Figure A - 53: Measured Strain in Gauge No.59 for DCRCC1 380
Figure A - 54: Measured Strain in Gauge No.60 for DCRCC1 380
Figure A - 55: Measured Strain in Gauge No.61 for DCRCC1 381
Figure A - 56: Measured Strain in Gauge No.62 for DCRCC1 381
Figure A - 57: Measured Strain in Gauge No.63 for DCRCC1 382
Figure A - 58: Measured Strain in Gauge No.64 for DCRCC1 382
Figure A - 59: Measured Strain in Gauge No.65 for DCRCC1 383
Figure A - 60: Measured Strain in Gauge No.66 for DCRCC1 383
Figure A - 61: Measured Strain in Gauge No.67 for DCRCC1 384
Figure A - 62: Measured Strain in Gauge No.68 for DCRCC1 384

Figure B - 1: Measured Strain in Gauge No.1 for FSRCC1 386
Figure B - 2: Measured Strain in Gauge No.3 for FSRCC1 386
Figure B - 3: Measured Strain in Gauge No.4 for FSRCC1 387
Figure B - 4: Measured Strain in Gauge No.5 for FSRCC1 387
Figure B - 5: Measured Strain in Gauge No.6 for FSRCC1 388
Figure B - 6: Measured Strain in Gauge No.7 for FSRCC1 388
Figure B - 7: Measured Strain in Gauge No.9 for FSRCC1 389
Figure B - 8: Measured Strain in Gauge No.10 for FSRCC1 389
Figure B - 9: Measured Strain in Gauge No.11 for FSRCC1 390
Figure B - 10: Measured Strain in Gauge No.12 for FSRCC1 390
Figure B - 11: Measured Strain in Gauge No.13 for FSRCC1 391

Figure B - 12: Measured Strain in Gauge No.15 for FSRCC1 391
Figure B - 13: Measured Strain in Gauge No.16 for FSRCC1 392
Figure B - 14: Measured Strain in Gauge No.17 for FSRCC1 392
Figure B - 15: Measured Strain in Gauge No.18 for FSRCC1 393
Figure B - 16: Measured Strain in Gauge No.19 for FSRCC1 393
Figure B - 17: Measured Strain in Gauge No.21 for FSRCC1 394
Figure B - 18: Measured Strain in Gauge No.23 for FSRCC1 394
Figure B - 19: Measured Strain in Gauge No.24 for FSRCC1 395
Figure B - 20: Measured Strain in Gauge No.25 for FSRCC1 395
Figure B - 21: Measured Strain in Gauge No.26 for FSRCC1 396
Figure B - 22: Measured Strain in Gauge No.27 for FSRCC1 396
Figure B - 23: Measured Strain in Gauge No.28 for FSRCC1 397
Figure B - 24: Measured Strain in Gauge No.29 for FSRCC1 397
Figure B - 25: Measured Strain in Gauge No.31 for FSRCC1 398
Figure B - 26: Measured Strain in Gauge No.32 for FSRCC1 398
Figure B - 27: Measured Strain in Gauge No.33 for FSRCC1 399
Figure B - 28: Measured Strain in Gauge No.35 for FSRCC1 399
Figure B - 29: Measured Strain in Gauge No.36 for FSRCC1 400
Figure B - 30: Measured Strain in Gauge No.39 for FSRCC1 400
Figure B - 31: Measured Strain in Gauge No.40 for FSRCC1 401
Figure B - 32: Measured Strain in Gauge No.41 for FSRCC1 401
Figure B - 33: Measured Strain in Gauge No.44 for FSRCC1 402
Figure B - 34: Measured Strain in Gauge No.45 for FSRCC1 402
Figure B - 35: Measured Strain in Gauge No.46 for FSRCC1 403
Figure B - 36: Measured Strain in Gauge No.48 for FSRCC1 403
Figure B - 37: Measured Strain in Gauge No.49 for FSRCC1 404
Figure B - 38: Measured Strain in Gauge No.50 for FSRCC1 404
Figure B - 39: Measured Strain in Gauge No.52 for FSRCC1 405
Figure B - 40: Measured Strain in Gauge No.53 for FSRCC1 405
Figure B - 41: Measured Strain in Gauge No.54 for FSRCC1 406
Figure B - 42: Measured Strain in Gauge No.55 for FSRCC1 406
Figure B - 43: Measured Strain in Gauge No.56 for FSRCC1 407
Figure B - 44: Measured Strain in Gauge No.57 for FSRCC1 407
Figure B - 45: Measured Strain in Gauge No.58 for FSRCC1 408
Figure B - 46: Measured Strain in Gauge No.59 for FSRCC1 408
Figure B - 47: Measured Strain in Gauge No.61 for FSRCC1 409
Figure B - 48: Measured Strain in Gauge No.62 for FSRCC1 409

Figure C - 1: Measured Strain in Gauge No.1 for DCRCC24.....411
Figure C - 2: Measured Strain in Gauge No.2 for DCRCC24.....411
Figure C - 3: Measured Strain in Gauge No.3 for DCRCC24.....412
Figure C - 4: Measured Strain in Gauge No.4 for DCRCC24.....412
Figure C - 5: Measured Strain in Gauge No.5 for DCRCC24.....413
Figure C - 6: Measured Strain in Gauge No.6 for DCRCC24.....413
Figure C - 7: Measured Strain in Gauge No.7 for DCRCC24.....414

Figure C - 8: Measured Strain in Gauge No.9 for DCRCC24 414
Figure C - 9: Measured Strain in Gauge No.10 for DCRCC24 415
Figure C - 10: Measured Strain in Gauge No.11 for DCRCC24 415
Figure C - 11: Measured Strain in Gauge No.12 for DCRCC24 416
Figure C - 12: Measured Strain in Gauge No.13 for DCRCC24 416
Figure C - 13: Measured Strain in Gauge No.14 for DCRCC24 417
Figure C - 14: Measured Strain in Gauge No.15 for DCRCC24 417
Figure C - 15: Measured Strain in Gauge No.16 for DCRCC24 418
Figure C - 16: Measured Strain in Gauge No.17 for DCRCC24 418
Figure C - 17: Measured Strain in Gauge No.18 for DCRCC24 419
Figure C - 18: Measured Strain in Gauge No.20 for DCRCC24 419
Figure C - 19: Measured Strain in Gauge No.21 for DCRCC24 420
Figure C - 20: Measured Strain in Gauge No.22 for DCRCC24 420
Figure C - 21: Measured Strain in Gauge No.23 for DCRCC24 421
Figure C - 22: Measured Strain in Gauge No.24 for DCRCC24 421
Figure C - 23: Measured Strain in Gauge No.25 for DCRCC24 422
Figure C - 24: Measured Strain in Gauge No.26 for DCRCC24 422
Figure C - 25: Measured Strain in Gauge No.27 for DCRCC24 423
Figure C - 26: Measured Strain in Gauge No.28 for DCRCC24 423
Figure C - 27: Measured Strain in Gauge No.30 for DCRCC24 424
Figure C - 28: Measured Strain in Gauge No.31 for DCRCC24 424
Figure C - 29: Measured Strain in Gauge No.32 for DCRCC24 425
Figure C - 30: Measured Strain in Gauge No.33 for DCRCC24 425
Figure C - 31: Measured Strain in Gauge No.34 for DCRCC24 426
Figure C - 32: Measured Strain in Gauge No.35 for DCRCC24 426
Figure C - 33: Measured Strain in Gauge No.36 for DCRCC24 427
Figure C - 34: Measured Strain in Gauge No.37 for DCRCC24 427
Figure C - 35: Measured Strain in Gauge No.38 for DCRCC24 428
Figure C - 36: Measured Strain in Gauge No.39 for DCRCC24 428
Figure C - 37: Measured Strain in Gauge No.40 for DCRCC24 429
Figure C - 38: Measured Strain in Gauge No.41 for DCRCC24 429
Figure C - 39: Measured Strain in Gauge No.42 for DCRCC24 430
Figure C - 40: Measured Strain in Gauge No.43 for DCRCC24 430
Figure C - 41: Measured Strain in Gauge No.45 for DCRCC24 431
Figure C - 42: Measured Strain in Gauge No.46 for DCRCC24 431
Figure C - 43: Measured Strain in Gauge No.47 for DCRCC24 432
Figure C - 44: Measured Strain in Gauge No.49 for DCRCC24 432
Figure C - 45: Measured Strain in Gauge No.50 for DCRCC24 433
Figure C - 46: Measured Strain in Gauge No.52 for DCRCC24 433
Figure C - 47: Measured Strain in Gauge No.53 for DCRCC24 434
Figure C - 48: Measured Strain in Gauge No.54 for DCRCC24 434
Figure C - 49: Measured Strain in Gauge No.55 for DCRCC24 435
Figure C - 50: Measured Strain in Gauge No.56 for DCRCC24 435
Figure C - 51: Measured Strain in Gauge No.58 for DCRCC24 436
Figure C - 52: Measured Strain in Gauge No.59 for DCRCC24 436

Figure C - 53: Measured Strain in Gauge No.61 for DCRCC24 437
Figure C - 54: Measured Strain in Gauge No.62 for DCRCC24 437
Figure C - 55: Measured Strain in Gauge No.63 for DCRCC24 438
Figure C - 56: Measured Strain in Gauge No.64 for DCRCC24 438
Figure C - 57: Measured Strain in Gauge No.65 for DCRCC24 439
Figure C - 58: Measured Strain in Gauge No.66 for DCRCC24 439
Figure C - 59: Measured Strain in Gauge No.67 for DCRCC24 440
Figure C - 60: Measured Strain in Gauge No.68 for DCRCC24 440
Figure C - 61: Measured Strain in Gauge No.70 for DCRCC24 441

Figure D - 1: Measured Strain in Gauge No.1 for FSRCC24 443
Figure D - 2: Measured Strain in Gauge No.2 for FSRCC24 443
Figure D - 3: Measured Strain in Gauge No.3 for FSRCC24 444
Figure D - 4: Measured Strain in Gauge No.4 for FSRCC24 444
Figure D - 5: Measured Strain in Gauge No.5 for FSRCC24 445
Figure D - 6: Measured Strain in Gauge No.6 for FSRCC24 445
Figure D - 7: Measured Strain in Gauge No.7 for FSRCC24 446
Figure D - 8: Measured Strain in Gauge No.9 for FSRCC24 446
Figure D - 9: Measured Strain in Gauge No.10 for FSRCC24 447
Figure D - 10: Measured Strain in Gauge No.11 for FSRCC24 447
Figure D - 11: Measured Strain in Gauge No.12 for FSRCC24 448
Figure D - 12: Measured Strain in Gauge No.13 for FSRCC24 448
Figure D - 13: Measured Strain in Gauge No.15 for FSRCC24 449
Figure D - 14: Measured Strain in Gauge No.16 for FSRCC24 449
Figure D - 15: Measured Strain in Gauge No.17 for FSRCC24 450
Figure D - 16: Measured Strain in Gauge No.18 for FSRCC24 450
Figure D - 17: Measured Strain in Gauge No.19 for FSRCC24 451
Figure D - 18: Measured Strain in Gauge No.20 for FSRCC24 451
Figure D - 19: Measured Strain in Gauge No.21 for FSRCC24 452
Figure D - 20: Measured Strain in Gauge No.22 for FSRCC24 452
Figure D - 21: Measured Strain in Gauge No.23 for FSRCC24 453
Figure D - 22: Measured Strain in Gauge No.26 for FSRCC24 454
Figure D - 23: Measured Strain in Gauge No.27 for FSRCC24 454
Figure D - 24: Measured Strain in Gauge No.28 for FSRCC24 455
Figure D - 25: Measured Strain in Gauge No.29 for FSRCC24 455
Figure D - 26: Measured Strain in Gauge No.31 for FSRCC24 456
Figure D - 27: Measured Strain in Gauge No.32 for FSRCC24 456
Figure D - 28: Measured Strain in Gauge No.33 for FSRCC24 457
Figure D - 29: Measured Strain in Gauge No.35 for FSRCC24 457
Figure D - 30: Measured Strain in Gauge No.37 for FSRCC24 458
Figure D - 31: Measured Strain in Gauge No.38 for FSRCC24 458
Figure D - 32: Measured Strain in Gauge No.40 for FSRCC24 459
Figure D - 33: Measured Strain in Gauge No.41 for FSRCC24 459
Figure D - 34: Measured Strain in Gauge No.42 for FSRCC24 460
Figure D - 35: Measured Strain in Gauge No.43 for FSRCC24 460

Figure D - 36: Measured Strain in Gauge No.44 for FSRCC24 461
Figure D - 37: Measured Strain in Gauge No.45 for FSRCC24 461
Figure D - 38: Measured Strain in Gauge No.47 for FSRCC24 462
Figure D - 39: Measured Strain in Gauge No.48 for FSRCC24 462
Figure D - 40: Measured Strain in Gauge No.49 for FSRCC24 463
Figure D - 41: Measured Strain in Gauge No.50 for FSRCC24 463
Figure D - 42: Measured Strain in Gauge No.51 for FSRCC24 464
Figure D - 43: Measured Strain in Gauge No.52 for FSRCC24 464
Figure D - 44: Measured Strain in Gauge No.53 for FSRCC24 465
Figure D - 45: Measured Strain in Gauge No.54 for FSRCC24 465
Figure D - 46: Measured Strain in Gauge No.56 for FSRCC24 466
Figure D - 47: Measured Strain in Gauge No.58 for FSRCC24 466
Figure D - 48: Measured Strain in Gauge No.59 for FSRCC24 467
Figure D - 49: Measured Strain in Gauge No.60 for FSRCC24 467
Figure D - 50: Measured Strain in Gauge No.61 for FSRCC24 468
Figure D - 51: Measured Strain in Gauge No.63 for FSRCC24 468
Figure D - 52: Measured Strain in Gauge No.64 for FSRCC24 469
Figure D - 53: Measured Strain in Gauge No.65 for FSRCC24 469
Figure D - 54: Measured Strain in Gauge No.66 for FSRCC24 470
Figure D - 55: Measured Strain in Gauge No.67 for FSRCC24 470
Figure D - 56: Measured Strain in Gauge No.68 for FSRCC24 471
Figure D - 57: Measured Strain in Gauge No.69 for FSRCC24 471

Figure E - 1: Measured Strain in Gauge No.1 for DCKJ24 473
Figure E - 2: Measured Strain in Gauge No.3 for DCKJ24 473
Figure E - 3: Measured Strain in Gauge No.5 for DCKJ24 474
Figure E - 4: Measured Strain in Gauge No.7 for DCKJ24 474
Figure E - 5: Measured Strain in Gauge No.8 for DCKJ24 475
Figure E - 6: Measured Strain in Gauge No.9 for DCKJ24 475
Figure E - 7: Measured Strain in Gauge No.10 for DCKJ24 476
Figure E - 8: Measured Strain in Gauge No.11 for DCKJ24 476
Figure E - 9: Measured Strain in Gauge No.12 for DCKJ24 477
Figure E - 10: Measured Strain in Gauge No.13 for DCKJ24 477
Figure E - 11: Measured Strain in Gauge No.14 for DCKJ24 478
Figure E - 12: Measured Strain in Gauge No.16 for DCKJ24 478
Figure E - 13: Measured Strain in Gauge No.18 for DCKJ24 479
Figure E - 14: Measured Strain in Gauge No.19 for DCKJ24 479
Figure E - 15: Measured Strain in Gauge No.20 for DCKJ24 480
Figure E - 16: Measured Strain in Gauge No.21 for DCKJ24 480
Figure E - 17: Measured Strain in Gauge No.22 for DCKJ24 481
Figure E - 18: Measured Strain in Gauge No.23 for DCKJ24 481
Figure E - 19: Measured Strain in Gauge No.24 for DCKJ24 482
Figure E - 20: Measured Strain in Gauge No.25 for DCKJ24 482
Figure E - 21: Measured Strain in Gauge No.26 for DCKJ24 483
Figure E - 22: Measured Strain in Gauge No.27 for DCKJ24 483

Figure E - 23: Measured Strain in Gauge No.28 for DCKJ24.....484
Figure E - 24: Measured Strain in Gauge No.29 for DCKJ24.....484
Figure E - 25: Measured Strain in Gauge No.30 for DCKJ24.....485
Figure E - 26: Measured Strain in Gauge No.31 for DCKJ24.....485
Figure E - 27: Measured Strain in Gauge No.32 for DCKJ24.....486
Figure E - 28: Measured Strain in Gauge No.33 for DCKJ24.....486
Figure E - 29: Measured Strain in Gauge No.34 for DCKJ24.....487
Figure E - 30: Measured Strain in Gauge No.36 for DCKJ24.....487
Figure E - 31: Measured Strain in Gauge No.37 for DCKJ24.....488
Figure E - 32: Measured Strain in Gauge No.38 for DCKJ24.....488
Figure E - 33: Measured Strain in Gauge No.39 for DCKJ24.....489
Figure E - 34: Measured Strain in Gauge No.40 for DCKJ24.....489
Figure E - 35: Measured Strain in Gauge No.41 for DCKJ24.....490
Figure E - 36: Measured Strain in Gauge No.42 for DCKJ24.....490
Figure E - 37: Measured Strain in Gauge No.43 for DCKJ24.....491
Figure E - 38: Measured Strain in Gauge No.44 for DCKJ24.....491
Figure E - 39: Measured Strain in Gauge No.45 for DCKJ24.....492
Figure E - 40: Measured Strain in Gauge No.46 for DCKJ24.....492
Figure E - 41: Measured Strain in Gauge No.47 for DCKJ24.....493
Figure E - 42: Measured Strain in Gauge No.48 for DCKJ24.....493
Figure E - 43: Measured Strain in Gauge No.50 for DCKJ24.....494
Figure E - 44: Measured Strain in Gauge No.53 for DCKJ24.....494
Figure E - 45: Measured Strain in Gauge No.55 for DCKJ24.....495
Figure E - 46: Measured Strain in Gauge No.56 for DCKJ24.....495
Figure E - 47: Measured Strain in Gauge No.57 for DCKJ24.....496
Figure E - 48: Measured Strain in Gauge No.60 for DCKJ24.....496
Figure E - 49: Measured Strain in Gauge No.61 for DCKJ24.....497
Figure E - 50: Measured Strain in Gauge No.62 for DCKJ24.....497
Figure E - 51: Measured Strain in Gauge No.63 for DCKJ24.....498
Figure E - 52: Measured Strain in Gauge No.65 for DCKJ24.....498
Figure E - 53: Measured Strain in Gauge No.66 for DCKJ24.....499
Figure E - 54: Measured Strain in Gauge No.67 for DCKJ24.....499
Figure E - 55: Measured Strain in Gauge No.68 for DCKJ24.....500
Figure E - 56: Measured Strain in Gauge No.69 for DCKJ24.....500
Figure E - 57: Measured Strain in Gauge No.71 for DCKJ24.....501
Figure E - 58: Measured Strain in Gauge No.72 for DCKJ24.....501
Figure E - 59: Measured Strain in Gauge No.75 for DCKJ24.....502

Figure F - 1: Measured Strain in Gauge No.1 for FSKJ24.....504
Figure F - 2: Measured Strain in Gauge No.2 for FSKJ24.....504
Figure F - 3: Measured Strain in Gauge No.3 for FSKJ24.....505
Figure F - 4: Measured Strain in Gauge No.4 for FSKJ24.....505
Figure F - 5: Measured Strain in Gauge No.5 for FSKJ24.....506
Figure F - 6: Measured Strain in Gauge No.6 for FSKJ24.....506
Figure F - 7: Measured Strain in Gauge No.7 for FSKJ24.....507

Figure F - 8: Measured Strain in Gauge No.8 for FSKJ24 507
Figure F - 9: Measured Strain in Gauge No.9 for FSKJ24 508
Figure F - 10: Measured Strain in Gauge No.10 for FSKJ24 508
Figure F - 11: Measured Strain in Gauge No.11 for FSKJ24 509
Figure F - 12: Measured Strain in Gauge No.12 for FSKJ24 509
Figure F - 13: Measured Strain in Gauge No.13 for FSKJ24 510
Figure F - 14: Measured Strain in Gauge No.14 for FSKJ24 510
Figure F - 15: Measured Strain in Gauge No.15 for FSKJ24 511
Figure F - 16: Measured Strain in Gauge No.16 for FSKJ24 511
Figure F - 17: Measured Strain in Gauge No.17 for FSKJ24 512
Figure F - 18: Measured Strain in Gauge No.18 for FSKJ24 512
Figure F - 19: Measured Strain in Gauge No.19 for FSKJ24 513
Figure F - 20: Measured Strain in Gauge No.20 for FSKJ24 513
Figure F - 21: Measured Strain in Gauge No.21 for FSKJ24 514
Figure F - 22: Measured Strain in Gauge No.22 for FSKJ24 514
Figure F - 23: Measured Strain in Gauge No.23 for FSKJ24 515
Figure F - 24: Measured Strain in Gauge No.24 for FSKJ24 515
Figure F - 25: Measured Strain in Gauge No.25 for FSKJ24 516
Figure F - 26: Measured Strain in Gauge No.26 for FSKJ24 516
Figure F - 27: Measured Strain in Gauge No.27 for FSKJ24 517
Figure F - 28: Measured Strain in Gauge No.28 for FSKJ24 517
Figure F - 29: Measured Strain in Gauge No.29 for FSKJ24 518
Figure F - 30: Measured Strain in Gauge No.30 for FSKJ24 518
Figure F - 31: Measured Strain in Gauge No.31 for FSKJ24 519
Figure F - 32: Measured Strain in Gauge No.32 for FSKJ24 519
Figure F - 33: Measured Strain in Gauge No.33 for FSKJ24 520
Figure F - 34: Measured Strain in Gauge No.34 for FSKJ24 520
Figure F - 35: Measured Strain in Gauge No.35 for FSKJ24 521
Figure F - 36: Measured Strain in Gauge No.36 for FSKJ24 521
Figure F - 37: Measured Strain in Gauge No.37 for FSKJ24 522
Figure F - 38: Measured Strain in Gauge No.38 for FSKJ24 522
Figure F - 39: Measured Strain in Gauge No.39 for FSKJ24 523
Figure F - 40: Measured Strain in Gauge No.40 for FSKJ24 523
Figure F - 41: Measured Strain in Gauge No.41 for FSKJ24 524
Figure F - 42: Measured Strain in Gauge No.42 for FSKJ24 524
Figure F - 43: Measured Strain in Gauge No.44 for FSKJ24 525
Figure F - 44: Measured Strain in Gauge No.45 for FSKJ24 525
Figure F - 45: Measured Strain in Gauge No.46 for FSKJ24 526
Figure F - 46: Measured Strain in Gauge No.47 for FSKJ24 526
Figure F - 47: Measured Strain in Gauge No.50 for FSKJ24 527
Figure F - 48: Measured Strain in Gauge No.51 for FSKJ24 527
Figure F - 49: Measured Strain in Gauge No.52 for FSKJ24 528
Figure F - 50: Measured Strain in Gauge No.53 for FSKJ24 528
Figure F - 51: Measured Strain in Gauge No.54 for FSKJ24 529
Figure F - 52: Measured Strain in Gauge No.55 for FSKJ24 529

Figure F - 53: Measured Strain in Gauge No.56 for FSKJ24 530
Figure F - 54: Measured Strain in Gauge No.58 for FSKJ24 530
Figure F - 55: Measured Strain in Gauge No.60 for FSKJ24 531
Figure F - 56: Measured Strain in Gauge No.61 for FSKJ24 531
Figure F - 57: Measured Strain in Gauge No.63 for FSKJ24 532
Figure F - 58: Measured Strain in Gauge No.64 for FSKJ24 532
Figure F - 59: Measured Strain in Gauge No.65 for FSKJ24 533
Figure F - 60: Measured Strain in Gauge No.66 for FSKJ24 533
Figure F - 61: Measured Strain in Gauge No.67 for FSKJ24 534
Figure F - 62: Measured Strain in Gauge No.68 for FSKJ24 534
Figure F - 63: Measured Strain in Gauge No.69 for FSKJ24 535
Figure F - 64: Measured Strain in Gauge No.70 for FSKJ24 535
Figure F - 65: Measured Strain in Gauge No.71 for FSKJ24 536
Figure F - 66: Measured Strain in Gauge No.72 for FSKJ24 536
Figure F - 67: Measured Strain in Gauge No.73 for FSKJ24 537
Figure F - 68: Measured Strain in Gauge No.74 for FSKJ24 537
Figure F - 69: Measured Strain in Gauge No.75 for FSKJ24 538

Figure G - 1: Measured Strain in Gauge No.1 for FSRCC24-M 540
Figure G - 2: Measured Strain in Gauge No.2 for FSRCC24-M 540
Figure G - 3: Measured Strain in Gauge No.3 for FSRCC24-M 541
Figure G - 4: Measured Strain in Gauge No.4 for FSRCC24-M 541
Figure G - 5: Measured Strain in Gauge No.5 for FSRCC24-M 542
Figure G - 6: Measured Strain in Gauge No.6 for FSRCC24-M 542
Figure G - 7: Measured Strain in Gauge No.7 for FSRCC24-M 543
Figure G - 8: Measured Strain in Gauge No.8 for FSRCC24-M 543
Figure G - 9: Measured Strain in Gauge No.9 for FSRCC24-M 544
Figure G - 10: Measured Strain in Gauge No.10 for FSRCC24-M 544
Figure G - 11: Measured Strain in Gauge No.13 for FSRCC24-M 545
Figure G - 12: Measured Strain in Gauge No.14 for FSRCC24-M 545
Figure G - 13: Measured Strain in Gauge No.15 for FSRCC24-M 546
Figure G - 14: Measured Strain in Gauge No.16 for FSRCC24-M 546
Figure G - 15: Measured Strain in Gauge No.17 for FSRCC24-M 547
Figure G - 16: Measured Strain in Gauge No.18 for FSRCC24-M 547
Figure G - 17: Measured Strain in Gauge No.19 for FSRCC24-M 548
Figure G - 18: Measured Strain in Gauge No.20 for FSRCC24-M 548
Figure G - 19: Measured Strain in Gauge No.21 for FSRCC24-M 549
Figure G - 20: Measured Strain in Gauge No.22 for FSRCC24-M 549
Figure G - 21: Measured Strain in Gauge No.23 for FSRCC24-M 550
Figure G - 22: Measured Strain in Gauge No.25 for FSRCC24-M 551
Figure G - 23: Measured Strain in Gauge No.26 for FSRCC24-M 551
Figure G - 24: Measured Strain in Gauge No.27 for FSRCC24-M 552
Figure G - 25: Measured Strain in Gauge No.28 for FSRCC24-M 552
Figure G - 26: Measured Strain in Gauge No.30 for FSRCC24-M 553
Figure G - 27: Measured Strain in Gauge No.31 for FSRCC24-M 553

Figure G - 28: Measured Strain in Gauge No.32 for FSRCC24-M 554
Figure G - 29: Measured Strain in Gauge No.33 for FSRCC24-M 554
Figure G - 30: Measured Strain in Gauge No.34 for FSRCC24-M 555
Figure G - 31: Measured Strain in Gauge No.35 for FSRCC24-M 555
Figure G - 32: Measured Strain in Gauge No.36 for FSRCC24-M 556
Figure G - 33: Measured Strain in Gauge No.37 for FSRCC24-M 556
Figure G - 34: Measured Strain in Gauge No.38 for FSRCC24-M 557
Figure G - 35: Measured Strain in Gauge No.39 for FSRCC24-M 557
Figure G - 36: Measured Strain in Gauge No.40 for FSRCC24-M 558
Figure G - 37: Measured Strain in Gauge No.41 for FSRCC24-M 558
Figure G - 38: Measured Strain in Gauge No.42 for FSRCC24-M 559
Figure G - 39: Measured Strain in Gauge No.43 for FSRCC24-M 559
Figure G - 40: Measured Strain in Gauge No.45 for FSRCC24-M 560
Figure G - 41: Measured Strain in Gauge No.46 for FSRCC24-M 560
Figure G - 42: Measured Strain in Gauge No.47 for FSRCC24-M 561
Figure G - 43: Measured Strain in Gauge No.49 for FSRCC24-M 561
Figure G - 44: Measured Strain in Gauge No.50 for FSRCC24-M 562
Figure G - 45: Measured Strain in Gauge No.51 for FSRCC24-M 562
Figure G - 46: Measured Strain in Gauge No.52 for FSRCC24-M 563
Figure G - 47: Measured Strain in Gauge No.53 for FSRCC24-M 563
Figure G - 48: Measured Strain in Gauge No.54 for FSRCC24-M 564
Figure G - 49: Measured Strain in Gauge No.55 for FSRCC24-M 564
Figure G - 50: Measured Strain in Gauge No.56 for FSRCC24-M 565
Figure G - 51: Measured Strain in Gauge No.58 for FSRCC24-M 565
Figure G - 52: Measured Strain in Gauge No.59 for FSRCC24-M 566
Figure G - 53: Measured Strain in Gauge No.63 for FSRCC24-M 566
Figure G - 54: Measured Strain in Gauge No.64 for FSRCC24-M 567
Figure G - 55: Measured Strain in Gauge No.66 for FSRCC24-M 567
Figure G - 56: Measured Strain in Gauge No.67 for FSRCC24-M 568
Figure G - 57: Measured Strain in Gauge No.68 for FSRCC24-M 568
Figure G - 58: Measured Strain in Gauge No.69 for FSRCC24-M 569
Figure G - 59: Measured Strain in Gauge No.70 for FSRCC24-M 569
Figure G - 60: Measured Strain in Gauge No.71 for FSRCC24-M 570
Figure G - 61: Measured Strain in Gauge No.73 for FSRCC24-M 570
Figure G - 62: Measured Strain in Gauge No.74 for FSRCC24-M 571
Figure G - 63: Measured Strain in Gauge No.75 for FSRCC24-M 571
Figure G - 64: Measured Strain in Gauge No.76 for FSRCC24-M 572
Figure G - 65: Measured Strain in Gauge No.77 for FSRCC24-M 572
Figure G - 66: Measured Strain in Gauge No.81 for FSRCC24-M 573
Figure G - 67: Measured Strain in Gauge No.82 for FSRCC24-M 573
Figure G - 68: Measured Strain in Gauge No.83 for FSRCC24-M 574
Figure G - 69: Measured Strain in Gauge No.84 for FSRCC24-M 574
Figure G - 70: Measured Strain in Gauge No.85 for FSRCC24-M 575
Figure G - 71: Measured Strain in Gauge No.86 for FSRCC24-M 575
Figure G - 72: Measured Strain in Gauge No.87 for FSRCC24-M 576

Figure G - 73: Measured Strain in Gauge No.88 for FSRCC24-M 576
Figure G - 74: Measured Strain in Gauge No.89 for FSRCC24-M 577
Figure G - 75: Measured Strain in Gauge No.90 for FSRCC24-M 577
Figure G - 76: Measured Strain in Gauge No.91 for FSRCC24-M 578
Figure G - 77: Measured Strain in Gauge No.92 for FSRCC24-M 578
Figure G - 78: Measured Strain in Gauge No.93 for FSRCC24-M 579
Figure G - 79: Measured Strain in Gauge No.94 for FSRCC24-M 579
Figure G - 80: Measured Strain in Gauge No.95 for FSRCC24-M 580
Figure G - 81: Measured Strain in Gauge No.96 for FSRCC24-M 580
Figure G - 82: Measured Strain in Gauge No.97 for FSRCC24-M 581
Figure G - 83: Measured Strain in Gauge No.98 for FSRCC24-M 581
Figure G - 84: Measured Strain in Gauge No.100 for FSRCC24-M 582
Figure G - 85: Measured Strain in Gauge No.101 for FSRCC24-M 582
Figure G - 86: Measured Strain in Gauge No.102 for FSRCC24-M 583
Figure G - 87: Measured Strain in Gauge No.103 for FSRCC24-M 583
Figure G - 88: Measured Strain in Gauge No.104 for FSRCC24-M 584
Figure G - 89: Measured Strain in Gauge No.106 for FSRCC24-M 584
Figure G - 90: Measured Strain in Gauge No.108 for FSRCC24-M 585

Figure H - 1: Measured Strain in Gauge No.1 for FSKJ24-M.....587
Figure H - 2: Measured Strain in Gauge No.3 for FSKJ24-M.....587
Figure H - 3: Measured Strain in Gauge No.4 for FSKJ24-M.....588
Figure H - 4: Measured Strain in Gauge No.5 for FSKJ24-M.....588
Figure H - 5: Measured Strain in Gauge No.6 for FSKJ24-M.....589
Figure H - 6: Measured Strain in Gauge No.7 for FSKJ24-M.....589
Figure H - 7: Measured Strain in Gauge No.8 for FSKJ24-M.....590
Figure H - 8: Measured Strain in Gauge No.9 for FSKJ24-M.....590
Figure H - 9: Measured Strain in Gauge No.15 for FSKJ24-M.....591
Figure H - 10: Measured Strain in Gauge No.16 for FSKJ24-M.....591
Figure H - 11: Measured Strain in Gauge No.18 for FSKJ24-M.....592
Figure H - 12: Measured Strain in Gauge No.19 for FSKJ24-M.....592
Figure H - 13: Measured Strain in Gauge No.20 for FSKJ24-M.....593
Figure H - 14: Measured Strain in Gauge No.21 for FSKJ24-M.....593
Figure H - 15: Measured Strain in Gauge No.22 for FSKJ24-M.....594
Figure H - 16: Measured Strain in Gauge No.23 for FSKJ24-M.....594
Figure H - 17: Measured Strain in Gauge No.24 for FSKJ24-M.....595
Figure H - 18: Measured Strain in Gauge No.25 for FSKJ24-M.....595
Figure H - 19: Measured Strain in Gauge No.26 for FSKJ24-M.....596
Figure H - 20: Measured Strain in Gauge No.27 for FSKJ24-M.....596
Figure H - 21: Measured Strain in Gauge No.28 for FSKJ24-M.....597
Figure H - 22: Measured Strain in Gauge No.30 for FSKJ24-M.....597
Figure H - 23: Measured Strain in Gauge No.31 for FSKJ24-M.....598
Figure H - 24: Measured Strain in Gauge No.33 for FSKJ24-M.....598
Figure H - 25: Measured Strain in Gauge No.34 for FSKJ24-M.....599
Figure H - 26: Measured Strain in Gauge No.35 for FSKJ24-M.....599

Figure H - 27: Measured Strain in Gauge No.37 for FSKJ24-M.....600
Figure H - 28: Measured Strain in Gauge No.38 for FSKJ24-M.....600
Figure H - 29: Measured Strain in Gauge No.39 for FSKJ24-M.....601
Figure H - 30: Measured Strain in Gauge No.40 for FSKJ24-M.....601
Figure H - 31: Measured Strain in Gauge No.41 for FSKJ24-M.....602
Figure H - 32: Measured Strain in Gauge No.42 for FSKJ24-M.....602
Figure H - 33: Measured Strain in Gauge No.43 for FSKJ24-M.....603
Figure H - 34: Measured Strain in Gauge No.44 for FSKJ24-M.....603
Figure H - 35: Measured Strain in Gauge No.45 for FSKJ24-M.....604
Figure H - 36: Measured Strain in Gauge No.47 for FSKJ24-M.....604
Figure H - 37: Measured Strain in Gauge No.48 for FSKJ24-M.....605
Figure H - 38: Measured Strain in Gauge No.50 for FSKJ24-M.....605
Figure H - 39: Measured Strain in Gauge No.51 for FSKJ24-M.....606
Figure H - 40: Measured Strain in Gauge No.52 for FSKJ24-M.....606
Figure H - 41: Measured Strain in Gauge No.53 for FSKJ24-M.....607
Figure H - 42: Measured Strain in Gauge No.54 for FSKJ24-M.....607
Figure H - 43: Measured Strain in Gauge No.55 for FSKJ24-M.....608
Figure H - 44: Measured Strain in Gauge No.57 for FSKJ24-M.....608
Figure H - 45: Measured Strain in Gauge No.59 for FSKJ24-M.....609
Figure H - 46: Measured Strain in Gauge No.60 for FSKJ24-M.....609
Figure H - 47: Measured Strain in Gauge No.61 for FSKJ24-M.....610
Figure H - 48: Measured Strain in Gauge No.62 for FSKJ24-M.....610
Figure H - 49: Measured Strain in Gauge No.63 for FSKJ24-M.....611
Figure H - 50: Measured Strain in Gauge No.64 for FSKJ24-M.....611
Figure H - 51: Measured Strain in Gauge No.65 for FSKJ24-M.....612
Figure H - 52: Measured Strain in Gauge No.66 for FSKJ24-M.....612
Figure H - 53: Measured Strain in Gauge No.67 for FSKJ24-M.....613
Figure H - 54: Measured Strain in Gauge No.68 for FSKJ24-M.....613
Figure H - 55: Measured Strain in Gauge No.69 for FSKJ24-M.....614
Figure H - 56: Measured Strain in Gauge No.70 for FSKJ24-M.....614
Figure H - 57: Measured Strain in Gauge No.71 for FSKJ24-M.....615
Figure H - 58: Measured Strain in Gauge No.72 for FSKJ24-M.....615
Figure H - 59: Measured Strain in Gauge No.73 for FSKJ24-M.....616
Figure H - 60: Measured Strain in Gauge No.74 for FSKJ24-M.....616
Figure H - 61: Measured Strain in Gauge No.75 for FSKJ24-M.....617
Figure H - 62: Measured Strain in Gauge No.78 for FSKJ24-M.....617
Figure H - 63: Measured Strain in Gauge No.79 for FSKJ24-M.....618
Figure H - 64: Measured Strain in Gauge No.80 for FSKJ24-M.....618
Figure H - 65: Measured Strain in Gauge No.81 for FSKJ24-M.....619
Figure H - 66: Measured Strain in Gauge No.82 for FSKJ24-M.....619
Figure H - 67: Measured Strain in Gauge No.83 for FSKJ24-M.....620
Figure H - 68: Measured Strain in Gauge No.84 for FSKJ24-M.....620
Figure H - 69: Measured Strain in Gauge No.85 for FSKJ24-M.....621
Figure H - 70: Measured Strain in Gauge No.86 for FSKJ24-M.....621
Figure H - 71: Measured Strain in Gauge No.87 for FSKJ24-M.....622

Figure H - 72: Measured Strain in Gauge No.88 for FSKJ24-M.....622
Figure H - 73: Measured Strain in Gauge No.89 for FSKJ24-M.....623
Figure H - 74: Measured Strain in Gauge No.90 for FSKJ24-M.....623
Figure H - 75: Measured Strain in Gauge No.91 for FSKJ24-M.....624
Figure H - 76: Measured Strain in Gauge No.92 for FSKJ24-M.....624
Figure H - 77: Measured Strain in Gauge No.94 for FSKJ24-M.....625
Figure H - 78: Measured Strain in Gauge No.95 for FSKJ24-M.....625
Figure H - 79: Measured Strain in Gauge No.96 for FSKJ24-M.....626
Figure H - 80: Measured Strain in Gauge No.97 for FSKJ24-M.....626
Figure H - 81: Measured Strain in Gauge No.98 for FSKJ24-M.....627
Figure H - 82: Measured Strain in Gauge No.99 for FSKJ24-M.....627
Figure H - 83: Measured Strain in Gauge No.100 for FSKJ24-M.....628
Figure H - 84: Measured Strain in Gauge No.101 for FSKJ24-M.....628
Figure H - 85: Measured Strain in Gauge No.1 02for FSKJ24-M.....629
Figure H - 86: Measured Strain in Gauge No.104 for FSKJ24-M.....629
Figure H - 87: Measured Strain in Gauge No.105 for FSKJ24-M.....630
Figure H - 88: Measured Strain in Gauge No.106 for FSKJ24-M.....630
Figure H - 89: Measured Strain in Gauge No.107 for FSKJ24-M.....631
Figure H - 90: Measured Strain in Gauge No.108 for FSKJ24-M.....631
Figure H - 91: Measured Strain in Gauge No.109 for FSKJ24-M.....632
Figure H - 92: Measured Strain in Gauge No.110 for FSKJ24-M.....632

Chapter 1
Introduction and Literature Review

1.1 General Perspective

Slab bridges are structures where the pile works as a pile under the soil level and as a column above the soil level. The pile is then directly connected to the superstructure. The California Transportation Department (Caltrans) has a large number of highway bridges, and many of them are slab bridges. Although slab bridges are a common type of bridge, the current version of the Bridge Design Specification (BDS) and the Seismic Design Criteria (SDC) provide limited design guidance for pile extension connection details for slab bridges. Unlike the column to box-girder bridge connections, which have been discussed and tested extensively, slab-bridge connections have not been tested. It is important that large-scale tests be conducted on these connections.

Eight large-scale pile-slab bridge connections were the target of the research. The research focused on loading in the transverse direction of the bridge. The first two specimens used 16-in. diameter piles with details based on the existing Bridge Design Aids (BDA). The primary difference was that one specimen had a flat-slab detail while the second specimen had a drop-cap detail. Twenty-four-in diameter piles were suggested by Caltrans to be used in the next four specimens instead of the 16-in. pile in the first two specimens. The last two specimens were designed based on the recommendation of the previous six specimens. This study focused on T-joint and knee-joint connections. The results of the research provided standardized details as well as rational methodology for designing and analyzing these connections. Experimental testing enabled verification of the procedures.

1.2 Literature Review

Little information is known about the behavior of bridge column connections for slab bridges. The literature review can be divided into four areas: bridge column connection research, column-slab building research, pile-pile cap research, and the existing code provisions. The column/pile connection research, whether for bridges or buildings, helps to provide insight into methodologies for design slab connection regions. These consist of evaluating principal stresses, following the flow of forces with strut-and-tie models. While not complete, the existing code provisions give insight into the state-of-the-art of connection design. The conclusion of the literature review was that while there was research that was close to the subject of the project, none was found that directly related to the pile extension connections in slab bridges.

1.2.1 Bridge Column Connection Research

A mechanism based on research conducted at UCSD[1] on transverse behavior of bridge bent T-joints is shown in Figure 1-1. This model uses what is known as the splice transfer mechanism. The splice transfer mechanism model requires more reinforcement on the negative moment side of the joint (left side) of Figure 1-1 than on the positive moment side of the joint (right side). In these models, single compression struts were used to represent the stress state on either side of the joint. This model works well for bent caps with solid sections where centerline of the columns coincides with the centerline of the cap beam. For these cases, a 2-D strut-and-tie model works well to represent the flow of forces through the joint.

The primary focus in two past Caltrans projects[2,3] conducted at the University of Nevada, Reno, was the connection between the column and bent cap in a standard box-girder bridge. One project had circular columns[2] while the other one had flared columns[3]. In the first project there were three specimens in which the only variable was the specimen's height. Strut-and-tie models (STM) were used as shown in Figure 1-2 to understand the flow of forces in medium specimen. This model is basically for connecting the forces generated at the adjoining column sections.

For flared column bents the variables were column height as well as flare and gap details. Also in this case, the column had moment connections at the top and hinge connections at the base. STMs were developed for modeling the connection in the bent cap as well as the hinge connection between the left and right column and the footing as shown in Figure 1-3. Figure 1-3 shows that the yielding of the flare hoops was caused by a spreading of the forces into the flare. Limiting this reinforcement would limit the spreading of forces into the flare. The STM results were used in calculating the system capacity by evaluating the forces in the ties that represent the base hinge dowels, the flare hoops and the column longitudinal bars at the gap region. The recommendations of the past two projects were a good start to understand the STM mechanism of slab-bridge connections.

In a project sponsored by the Nevada Department of Transportation, four 40% scaled column-girder subsystems were developed and tested at the University of Nevada, Reno[4]. These systems were subjected to reverse cyclic loading in the longitudinal direction of the bridge only. Three specimens were built to investigate the effect of post-tensioning on the connection performance by failing the girder-to-bent cap connection and limiting inelastic behavior in the column. The joints of these specimens were detailed using Caltrans guidelines with additional vertical stirrups in the column core region[5]. The fourth specimen was developed to represent a conventional bridge design in which failure occurs in the column while the girders and joints remain essentially elastic. Figure 1-4 shows the strut-and-tie model (STM) for the conventional bridge design specimen. Joint details for the fourth specimen were developed from a strut-and-tie model in order to take the advantages of post-tensioning, which are not included in the Caltrans design. The actual failure mode in the four specimens was a large horizontal joint crack, delaminating the upper of the deck above the joint, forcing failure in the girder soffit to occur. Based on the experimental results and the strut-and-tie model, the study recommended providing additional vertical reinforcement at the top of the joint to limit crack size. The developed STM was helpful to start the STM for the current study.

A study on the failure modes of the bridge joints[6] showed that the failure may occur in four different modes[6]. The first mode is compression failure, which occurs as a result of concrete crushing of the struts in the joints. The second failure mode is tension failure. This typically develops in reinforced concrete joints when shear reinforcement, responsible for mobilizing the joint compression field, is subjected to large inelastic strain. The third failure mode is anchorage failure, which mainly occurs in the knee-joints. The fourth failure mode is lab splice failures, which occur if the lap length between the reinforcement is not sufficient to transfer the column tension force to the beam reinforcement. Figure 1-5 summarizes the four different modes of failure.

1.2.2 Column-Slab Building Research

There are tremendous amounts of research that have been done in the column-slab area, with or without beams, for building applications. Much of this work has involved slabs with a column above and below the connection. This is not directly related to the project, but there are design criteria for slabs with only a column below. The following are examples of the type of work that exists.

Research on this topic was documented by ACI-ASCE Committee-352 in "Recommendations for Design of Beam-Column Connection in Monotonic Reinforced Concrete in Monolithic Reinforced Concrete Structures"[7] and "Recommendations for Design of Slab-Column Connection in Monotonic Reinforced Concrete in Monolithic Reinforced Concrete Structures"[8]. Both provide insight into the details that work for building applications. The recommendations state that for high seismic zones, columns framing into a slab can have inadequate shear and moment transfer capacity at the connection. Again, while not a direct application, this adds to the data surrounding the subject of the research; therefore, these details can be applied to find applicable details for slab- bridge connections.

1.2.3 Pile to Pile-Cap Research

Work has been done on pile to pile-cap connections and plastic hinge behavior in piles. As with the column-bent cap connection, the pile to pile-cap connection research helps but does not directly apply. Typically the piles are anchored in a large stiff block that represents the pile cap. The following are examples of the type of work that exists.

In New Zealand a prestressed concrete pile connected to a pile cap was subjected to simulate seismic loading[9]. The piles were pretensioned concrete with octagonal cross section and spiral reinforcement. The range of pile to pile-cap connection details that were tested included piles with the end embedded in the cap, either with or without the ends of the longitudinal steel exposed, and the use of longitudinal steel dowel bars. The test results showed that well-detailed prestressed concrete piles and pile to pile-cap connections are capable of undergoing large post-elastic deformations without significant loss in strength when subjected to severe seismic loading.

In an investigation on the capacity of square pile to pile-cap connections[10], a prestressed pile was simply embedded in the cast-in-place pile cap. It showed that the plain embedment can develop the flexural capacity of the pile without distress to the pile cap or connection region, provided that a sufficient embedment length was furnished. Equations for determining the required embedment length were provided.

1.2.4 Existing Code Provisions

The Caltrans design charts are for a well-defined set of slab bridges. The provisions are derived from tests on box girder bridges instead of slab bridges. Because of the lack of information on pile to slab-bridge connections, the equations and recommendations of box-girder bridge design are used to design slab bridges. The Caltrans criteria from MTD 20-6[11] states that the superstructure must have an appropriate strength reserve above the demands generated from probable column plastic hinging. No direct guidelines for the joint shear or detailing information are provided for prestressed and non-prestressed piles.

Caltrans Bridge Design Aid (BDA 4-10)[12] states that fixed or pinned connection at the top of the pile needs to be designed based on Seismic Design Criteria and that it may be necessary to provide a bent to achieve the necessary development. Details provided in

BDA 4-10 show details for spans with bent caps and those without, but these details have not been tested. Details are provided for cast-in-place reinforced concrete piles, precast prestressed concrete piles and cast-in-drilled holes concrete piles for round and octagonal cross sections.

Provisions in the Seismic Design Criteria (SDC)[5] discuss box-girder joint and column design extensively, so these can be extrapolated to piles, but there are differences. Specifically for the joint, the section is much shallower, and drop caps need to be detailed carefully. Other codes such as ACI 318[13] and AASHTO LRFD[14] have some provisions detailing for connections, but they are very limited. The discussions only deal with longitudinal pile bar extension in the cap and how long the plastic hinge region extends into the column, but there are no details about the joint reinforcement.

1.3 Caltrans Slab Bridges

In order to start the project, drawings for several slab bridges were provided by Caltrans to UNR. The drawings showed the reinforcement details and the geometry of each bridge, and large variation in the columns/piles reinforcement. The drawings were useful to decide the average height of the piles and the typical detailing of column/pile-slab joints; this will be discussed in detail in Chapter 2.

1.4 Problem Statement

The current version of the Caltrans Bridge Design Specifications (BDS)[15] and Seismic Design Criteria (SDC)[5] provide little direct design guidance for pile extension connection details for slab bridges. There is also no guidance in the latest AASHTO Bridge Specification[14] and data in the literature is limited. There is extensive discussion on the column to box-girder bridge connections both in specifications and the literature but not for slab bridges. While these connections have the same purpose as a column to cap beam connection in box-girder bridges, the size of the column verses slab thickness are much different than what exists in the column-cap beam connection in a box-girder bridge.

Slab bridges are very common and yet, the critical details have not been tested. Because of the lack of experimental data on slab-bridge connections, box-girder connections guidelines are used to design the slab bridge connections, which could cause overdesign or unsafe design. Therefore, this project was undertaken.

1.5 Research Objectives

This project focuses on the design and detailing of connection regions for pile extensions for slab bridges. The pile to slab connections investigated were T-joints and knee-joints. The pile-slab bridge connections varied so as to have some that require drop caps and other that have just a flat slab. All the connections were with full moment connections. The objectives were as follows:

1- Develop standard details that can be used to update the existing details.
2- Establish design procedure for the joint regions with and without drop caps.
3- Develop simplified methods as well as strut-and-tie models for design.
4- Conduct tests to verify and develop the details and design procedures for bridge joints.
5- Propose changes to Caltrans Seismic Design Criteria (SDC).

1.6 Scope of work

To satisfy the objectives, eight large-scale specimens were designed and tested. The joints were tested in the Large Scale Structures Laboratory (LSSL) at the University of Nevada, Reno (UNR) and were subjected to reverse cyclic loading. Analytical strut-and-tie models and finite element models were developed and compared to the measured results. The combination of the analytical and experimental results of this research leads to recommendations for joint design.

1.7 Document Layout

This document contains eight more chapters as follows:

Chapter 2: Preliminary Analysis and Specimens Construction
Chapter 3: Experimental Program
Chapter 4: Experimental Test Results
Chapter 5: Strut-and-Tie Models
Chapter 6: Modified Specimens
Chapter 7: Post-Test Analysis
Chapter 8: Design Recommendations
Chapter 9: Summary and Conclusions

Chapter 2
Preliminary Analysis and Specimen Selection

2.1 Introduction

Eight large-scale specimens were tested at the UNR large-scale structural lab. The specimens were designed such that the effects of potentially critical parameters of the pile-slab bridge joints could be simulated and studied. The research focused on loading in the transverse direction of the bridge. This chapter illustrates the procedures used to develop the specimens and describes the final design of the first six specimens.

2.2 Model Selection

In order to select the model, a survey was done on the existing bridges in California. Drawings of previous projects and some of the existing slab-bridges in California were provided by Caltrans to UNR. The models in the experimental program were designed using the dimensions of the existing bridges. After data were collected, the following variables were evaluated:

- Column/pile diameter
- Column/pile length
- Slab type (with or without a drop-cap)
- Amount of column/pile longitudinal reinforcement
- Amount of column/pile transverse reinforcement
- Column shape (circular - hexagonal)
- Connection type (full moment - hinge)

Table 2-1 summarizes the prototype values collected from the drawings of the existing bridges of Caltrans. The collected values of Table 2-1 include the longitudinal and transverse reinforcement ratio and whether or not the column has a hinge in the base, slab thickness, pile shape (circular or hexagonal) and slab type (flat-slab or drop-cap). The numbers of variables are large (see Table 2-1). It was decided to focus on the number of variables for this research. The slab thickness, slab type and pile diameter are used as the variables in this research. The test matrix as well as the order of testing was finalized in cooperation with Caltrans engineers. The variables matrix for the tested specimens is given in Table 2-2**.**

2.2.1 Pile Length Selection

The embedded length of the pile into the soil varies according to the soil type. In the plans submitted by Caltrans to UNR, the height of the pile above the ground ranged from 9D to 16D, where “D” stands for pile diameter. Therefore, an average height of the pile above the soil surface equals 12.5D. The point of the maximum moment for the individual pile can be approximated at D to 2D under the surface of the soil. This increases the average total length to 13.5D to 14.5D. The pile inflection point will be approximately halfway between the pile top and maximum moment point in the soil. Piles with shear spans equal to or greater than 6D are considered flexural members, as shown in Figure 2-1. Therefore, the heights of the eight specimens were chosen to be in the range of 6D and 7.75D. For specimens DCRCC1 (Drop-Cap T-Joint with 16-in. diameter pile) and FSRCC1 (Flat-Slab T-Joint with 16-in. diameter pile), the pile height was chosen to be 7.75D. For specimens DCRCC24 (Drop-Cap T-Joint with 24-in.

diameter pile), FSRCC24 (Flat-Slab T-Joint with 24-in. diameter pile), FSRCC24-M (Modified Flat-Slab T-Joint with 16-in. diameter pile), DCKJ24 (Drop-Cap Knee-Joint with 24-in. diameter pile), FSKJ24 (Flat-Slab Knee-Joint with 24-in. diameter pile) and FSKJ24-M (Modified Flat-Slab Knee-Joint with 24-in. diameter pile), the pile height was chosen to be 6D, (see Table 2-2).

2.2.2 Slab Dimensions Selection

When a bridge is subjected to earthquake motion in the transverse direction, a moment diagram is created, as shown in Figure 2-2. The length of the specimen in the transverse bridge direction was determined by the distance between the points of zero moment due to lateral load, which equals the pile spacing distance. When the bridge is under a combination of dead and lateral load, the position of the inflection points will shift slightly. The maximum distance between the piles on the transverse direction of the bridge based on the SDC[5] was determined to be 126 inches. The drop-cap connection was considered as a T-section. The T-connection effective width (B_{eff}) was determined according to Section 8.10.2 of ACI 318-08[13] as shown in Equation 2-1 to Equation 2-3.

B_{eff} = One-quarter of the span length of the beam — Equation 2-1

B_{eff} = Web width + one half the clear distance to the next web on each side — Equation 2-2

B_{eff} = Web width + eight times the slab thickness on each side — Equation 2-3

B_{cap}=Dc+2 (ft) — Equation 2-4

The minimum bent cap width, based on Caltrans Specifications, is shown in Equation 2-4. The width of the drop-cap connection was chosen to the minimum of Equation 2-2 through Equation 2-4.

For the flat slab-pile connection, the equations of the T-beam are not applicable. The width of the flat slab was chosen to be no less than Equation 2-4 or two times the width of the beam, where the stirrup width in the transverse direction was considered as the beam width. The basic dimensions for the eight specimens are listed in Table 2-3**.**

2.3 Reinforcement Design

2.3.1 Pile Reinforcement

For specimens DCRCC1 and FSRCC1 the pile reinforcement was chosen to represent the Cast-in-Drilled Hole Concrete Pile. The pile diameter was 16-in. based on Caltrans BDA[12]. Longitudinal reinforcement was 7#7 with W5@ 1.55-in. for the spirals, as stated in BDA[12]. For specimens DCRCC24, FSRCC24 and FSRCC24-M, the pile diameter was 24-in., and the longitudinal reinforcement was 9#9 with #3@ 2.5-in. for the spirals. The reinforcement ratios for the longitudinal (ρ_L=2%) and the transverse reinforcement (ρ_t=0.61%) were approximately the same for all the specimens. The T-joint specimens were full scale. The height of the full-scale knee-joint was higher than the reaction wall, so it was hard to attach the actuator. A 2/3-scale was used for the knee-joint specimens; the scaling factors are listed in Table 2-4. The knee-joint piles were 16-in. with 9#6 as longitudinal reinforcement and W5@ 1.7-in. as spirals. Figure 2-3 shows the reinforcement details for the piles.

2.3.2 Slab Reinforcement

The reinforcement of the slab is different depending on the support configuration. There are five types of support, as shown in Figure 2-4. The slab reinforcement details for specimens DCRCC1 and FSRCC1 represent the current existing details for slab bridges. Specimen DCRRC1 represents support type V[12], with span length of 24-ft (see Figure 2-5), while specimen FSRRC1 represents support type III[12] with span length of 34-ft (see Figure 2-6).

When the 24-in. pile diameter was used instead of 16-in. pile diameter the demand on the slab increased. Additional shear and longitudinal reinforcement were added to the joint to satisfy Caltrans' requirements for joint design requirements[5]; see Section 2.4. The longitudinal and transverse reinforcement of the slab were redesigned in order to satisfy the moment capacity as shown in Section 2.5. Punching shear was checked as well (see Section 2.6). Specimen DCRCC24 represents support type III[12] with span length of 20-ft (see Figure 2-7), while specimens FSRCC24 and FSRCC24-M represent support type III[12] with span length of 34-ft. For specimen FSRCC24 details, see Figure 2-8. Specimen DCKJ24 represents support type III with span length of 24-ft (see Figure 2-9). Specimens FSKJ24 and FSKJ24-M represent support type III with span length of 26-ft. For specimen FSKJ24 details, see Figure 2-10. The reinforcement details of specimen FSRCC24-M were redesigned based on the analytical results of the STM for specimen FSRCC24 and Caltrans' requirements for joint design, moment capacity and punching shear (see Figure 2-11). The reinforcement details of specimen FSRCC24-M will be discussed in detail in Section 5.4. The reinforcement details of specimen FSKJ24-M were redesigned based on the analytical results of STM for specimen FSKJ24. The new design for FSKJ24-M also fulfilled Caltrans' requirements for joint design, moment capacity and punching shear (see Figure 2-12). The reinforcement details of specimen FSKJ24-M will be discussed in detail in Section 5.7.

2.4 Joint Design

Because of the lack of slab-pile joint research, the design of the slab-pile joints was designed based on Caltrans Seismic Design Criteria for the box-girder joints[5]. From Mohr's circle of stress, the principal stresses in the joint can be calculated using Equation 2-5 through Equation 2-10.

$$p_c, p_t = \frac{(f_h + f_v)}{2} \pm \sqrt{\left(\frac{f_h - f_v}{2}\right)^2 + v^2_{jv}} \qquad \text{Equation 2-5}$$

$$v_{jv} = \frac{T_c}{A_{jv}} \qquad \text{Equation 2-6}$$

$$A_{jv} = l_{ac} \times B_{cap} \qquad \text{Equation 2-7}$$

$$f_v = \frac{P_c}{A_{jh}} \qquad \text{Equation 2-8}$$

$$A_{jh} = (D_c + D_S) \times B_{cap} \qquad \text{Equation 2-9}$$

$$f_h = \frac{P_b}{B_{cap} \times D_s}$$ Equation 2-10

where

p_c, p_t = Principal compression and tension stresses

f_v, f_h = Average vertical and horizontal axial stresses

v_{jv} = Joint shear stress

A_{jh} = Effective horizontal joint area

A_{jv} = Effective vertical joint area

B_{cap} = Bent cap width

D_s = Bent cap depth

l_{ac} = Length of pile reinforcement embedded in the bent cap

P_c = Pile axial force including the effective overturning load

P_b = Effective beam axial force at the center of the joint including the prestressing force

T_c = Column tensile force defined as $M_u(col)/h$, where h is the distance from c.g. of column tensile force to centroid of compressive force on the section and $M_u(col)$ is the column/pile ultimate moment capacity. Alternatively, T_c can be obtained from the moment curvature analysis of the cross section.

If the principal tension stress, p_t, is less than or equal to $3.5 \times \sqrt{f'_c}$ psi, no additional joint reinforcement is required. When the principal tension stress p_t exceeds the limitation of $3.5 \times \sqrt{f'_c}$ psi, additional vertical stirrups, horizontal stirrups and side reinforcement must be designed according to Caltrans Seismic Design Criteria (SDC) [5]. The equations which control the additional steel and minimum volumetric stirrups ratio are listed in the SDC [5]. The horizontal joint compression, f_h, can typically be ignored without significantly effecting the principal stress calculation, unless prestressing force is applied on the joint. All the superstructure-column (pile) moment resisting joints shall be proportioned to satisfy Equation 2-11 and Equation 2-12.

The principal tension $p_t \leq 12\sqrt{f'_c}$ psi Equation 2-11

The principal compression $p_c \leq 0.25 f'_c$ psi Equation 2-12

2.5 Moment Capacity

Based on Caltrans Seismic Criteria[5], the nominal moment capacity of the slab must be at least 1.2 times that of the ultimate moment capacity of the pile (see Equation 2-12).

$(M_n)_{slab} = 1.2(M_u)_{pile}$ Equation 2-13

All the specimens were designed to satisfy Equation 2-13 except specimen DCRCC1 and FSRCC1. DCRCC1 and FSRCC1 were detailed based on standard details of Caltrans[12]. The main difference between the T-joints and the knee-joints is that in the T-joint, the slab is designed assuming that the moment will be distributed on both sides of the T-joint slab evenly. This means that each side of the joint resists $0.6(M_u)_{pile}$. On the other hand, for the knee-joint, the slab was designed to resist $1.2(M_u)_{pile}$ from one side. The moment capacities of specimens FSRCC24-M and FSKJ24-M were designed based on recommendations of the analytical results of the strut-and-tie model (STM) of

specimens FSRCC24 and FSKJ24 respectively; their design procedures will be discussed in detail in Chapter 5.

2.6 Punching Shear

The specimens were checked to make sure they were safe against punching shear. Equation 2-14 through Equation 2-19[8] are directly applicable to square cross sections; therefore, the pile cross sections were transformed into a square section. The following steps should be followed in order to conduct the punching shear check:

For non-seismic loads:

$$V_n = V_c = 4 \times A_{cs}\sqrt{f_c'} \qquad \text{Equation 2-14}$$

$$V_o = \varphi V_n > V_u \qquad \text{Equation 2-15}$$

For seismic loads:

$$V_n = Cv.V_c \qquad \text{Equation 2-16}$$

$$V_o = \varphi V_n > V_u \qquad \text{Equation 2-17}$$

Check Moment Transfer:

$$V_u + \alpha(M_u)/b_o < V_o \qquad \text{Equation 2-18}$$

Check Maximum Permitted Vertical Shear:

$$V_{max} = 0.4V_c > V_u \qquad \text{Equation 2-19}$$

where

V_n =Nominal shear strength in the absence of the moment transfer

V_c =Basic shear strength of concrete

A_{cs} =Cross sectional area of the slab critical section

f_c' = Concrete compressive strength

Cv =0.75 for weight light concrete, and equals 1 for regular concrete

φ = Strength reduction factor

V_o =Design shear strength in the absence of the moment transfer

M_u = Moment transfer to the pile

α = 5 for interior Joints and 3.5 for exterior joint

2.7 Preliminary Analysis

The preliminary analysis was used to predict the behavior of each specimen, to be sure that each specimen could reach failure before exceeding the actuator capacity. The preliminary analysis was used to plan an effective instrumentation scheme. For the preliminary analysis, XTRACT[16] program was used to determine the moment and curvature capacities for pile and slab cross sections. SAP2000[17] was used to calculate the moment, shear and reaction. For the post analysis, a finite element program called Atena[18] was used.

2.7.1 Moment-Curvature Analysis

Moment-curvature analysis is essential in order to calculate the plastic hinge length, the yield moment capacity, yielding displacement, plastic moment capacity and the

ultimate displacement of each specimen. The initial moment (M) - curvature (ϕ) analysis was based on the expected material properties shown in Table 2-5 and Table 2-6. $M-\phi$ analysis derives the curvatures associated with a range of moments for a cross section based on the principles of strain compatibility and equilibrium of forces. The $M-\phi$ curve can be idealized with an elastic perfectly plastic response to estimate the plastic moment capacity of a member's cross section. The elastic portion of the idealized curve should pass through the point, marking the first reinforcing bar yield. The idealized plastic moment capacity is obtained by balancing the areas between the actual and the idealized $M-\phi$ curves beyond the first reinforcing bar yield point (see Figure 2-13).

2.7.2 Material Models

Constitutive material models for the concrete and reinforcement need to be specified in a moment-curvature analysis. There are numerous models available for both concrete and reinforcement in the literature. Tensile capacity of concrete was not included in the preliminary moment-curvature analysis. The materials' models chosen for the preliminary analysis are summarized in the subsequent sections.

2.7.2.1 Unconfined Concrete

For the primary analysis, Mander Model[19] was used for the unconfined concrete. The basic stress-strain behavior is shown in Figure 2-14. The equation for the stress-strain behavior is given as:

$$f_c=\frac{f'_{co}\,xr}{r-1+x^r} \qquad \text{Equation 2-20}$$

where

$$x=\frac{\varepsilon_c}{\varepsilon_{co}}$$

$$r=\frac{E_c}{E_c-E_{sec}}$$

$$E_c=57000\sqrt{f'_{co}}\ \text{(psi)}$$

$$E_{sec}=\frac{f'_{co}}{\varepsilon_{co}}$$

where ε_{co} is the unconfined concrete strain at ultimate strength; ε_c is the longitudinal compressive concrete strain at the unconfined stress-strain curve, where the stress is required to be calculated, and f'_{co} is the unconfined concrete compressive strength. Equation 2-20 applies to $2\varepsilon_{co}$, after which the stress-strain behavior decreases linearly until the spalling strain, ε_{sp} is reached, as shown in Figure 2-14.

2.7.2.2 Confined Concrete

To calculate the failure displacement, a representative constitutive model for concrete is needed. The primary points of the stress-strain relationship for concrete are the peak stress and the failure strain. Other parameters such as shape of the stress-strain

relationship do not generally affect the outcome[20]. The peak stress and failure strain are sensitive to the amount and distribution of the confinement steel. Many models have been developed for the constitutive relationship of confined concrete. Modified Mander stress-strain model[19] was used to model confined concrete. The strength of confined concrete, f'_{cc}, is related to confining pressure, f'_l, provided by the lateral reinforcement, which is given as

$$f'_l = 0.5 k_e \rho_s f_{yh} \qquad \text{Equation 2-21}$$

where

k_e = Confinement effectiveness coefficient, which is equal to 0.95 for circular section

ρ_s = Volumetric ratio of the lateral steel

f_{yh} = Yield stress of lateral steel

For circular section, or square sections, with equally confining steel in both directions, the confined concrete strength is:

$$f'_{cc} = f'_{co}\left(-1.254 + 2.254\sqrt{1 + \frac{7.94 f'_l}{f'_{co}}} - \frac{2 f'_l}{f'_{co}}\right)$$

$$\varepsilon_{cc} = 0.002\left[1 + 5\left(\frac{f'_{cc}}{f'_{co}} - 1\right)\right]$$

f'_{cc} = unconfined concrete compressive strength

$$\rho = \frac{D\pi \times \mathrm{A1}}{\mathrm{A} \times S}$$

where

D = Diameter of confined steel (in)

A1 = Area of confined steel (in^2)

A = Area of column cross section (in^2)

S = Confined steel spacing (in)

To find the ultimate strain of concrete at failure, Mander *et al.*[19] applied a strain energy approach. In this method, the longitudinal compressive concrete strain at failure corresponds to the first fracture in the hoops. Paulay and Priestley[20] adopted a modified version of the Mander *et al.* model to determine the ultimate stress-strain behavior. The modified model prescribes an ultimate strain, ε_{cu}, as follows:

$$\varepsilon_{cu} = 0.004 + \frac{1.4 \times \rho_s \times f_{yh} \times \varepsilon_{sm}}{f`_{cc}} \qquad \text{Equation 2-22}$$

where ε_{sm}= Steel strain at maximum tensile stress.

The used values of ε_{sm} were based on the Seismic Design Criteria[5].

2.7.2.3 Nonlinear Reinforcing Steel Model

Reinforcing steel was modeled with a stress-strain relationship that exhibits an initial linear elastic portion, a yield plateau, and a strain hardening range in which the stress increases with strain. The yield point was defined by the expected yield stress of the steel, f_{ye}. The length of the yield plateau shall be a function of the steel strength and bar size. The strain-hardening curve can be modeled as a parabola or other non-linear

relationship and should terminate at the ultimate tensile strain, ε_{su} (see Figure 2-15). It is Caltrans' practice to reduce the ultimate strain by up to thirty-three percent to decrease the probability of fracture of the reinforcement.

2.8 Pushover Analysis

The ultimate displacement of each specimen can be calculated by adding the plastic displacement of each specimen, Δ_p, to its corresponding yield displacement, Δ_y. The yield displacement, Δ_y, of each pile is calculated using the moment-curvature values shown in Figure 2-16 to Figure 2-21. The values used for the preliminary analysis are listed in Table 2-7, based on Equation 2-23 to Equation 2-27.

$\Delta_m = \Delta_y + \Delta_p$ Equation 2-23

$\Delta y = \frac{L^2}{3} \times \Phi_y$ Equation 2-24

$L_P = 0.08L + 0.15 f_{ye} d_{bL} \geq 0.3 f_{ye} d_{bL}$ Equation 2-25

$\Delta_p = \theta_p \times (H - L_p/2)$ Equation 2-26

$\theta_p = (\Phi_u - \Phi_y) \times L_p \Delta_p$ Equation 2-27

where

Δ_m = maximum lateral displacement

Δ_y= yield displacement (obtained from analysis)

Δ_p= plastic displacement

Φy= yield curvature of column section (from XTRACT analysis)

L= the pile/column length

θp= plastic rotation

Φu=ultimate curvature of column section (from XTRACT analysis)

H = pile clear height

L_p = plastic hinge length (Paulay and Priestley empirical equations)

d_{bL}= diameter of longitudinal reinforcement of the pile

Chapter 3
Experimental Program

3.1 Introduction

The experimental portion of this project consisted of testing eight connection models subjected to reverse cyclic loading in the transverse direction. This chapter discusses the construction process, the measured material properties, test setup, instrumentation and the selected loading protocol for each specimen. The instrument layout was used to capture displacements, forces, and strain actions during the experiments.

3.2 Pile-Slab Bridge Model Construction

All of the specimens were constructed by a local contractor. The specimens were constructed outside the Large Scale Structures Laboratory (LSSL) at UNR. The general procedures for constructing the specimens can be divided into three steps, which are discussed in the following paragraph.

The specimen is tested up-side down. Accordingly, the first step in the construction was to place the reinforcement for the slab, and then the reinforcement for the pile. Figure 3-1 shows the slab and pile reinforcement for specimens FSRCC24-M and FSKJ44-M respectively. Figure 3-2 shows the concrete slab casting for specimen FSRCC24. The second step was to stand the sonotube form for the pile (see Figure 3-3). The last step was to place the reinforcement for the pile head, and then cast the pile and the head.

3.3 Measured Material Properties

Materials were tested to be sure of their proper quality and strength. These tests were conducted on concrete samples taken from each cast. For the reinforcement, a tension test was done on each bar size for each specimen.

3.3.1 Measured Concrete Properties

Two casts were required for each specimen. During each cast, 12 concrete cylinders were made then tested at seven days, 28 days and on the test day. The last three cylinders were extras, in case of loss or damage of the other cylinders. The main purpose of testing the cylinders in this sequence was to track the progression of concrete strength to ensure they would satisfy the minimum strength requirements of the specification shown in Table 2-6. The concrete strengths for the specimens are listed in Table 3-2.

3.3.2 Testing of Steel Samples

The reinforcement for the first six specimens were delivered to UNR in pairs, which means that specimens DCRCC1 and FSRCC1 had the same reinforcement properties, specimens DCRCC24 and FSRCC24 had the same reinforcement properties, and specimens DCKJ24 and FSKJ24 had the same reinforcement properties. Specimen FSRCC24-M and specimen FSKJ24-M each had their own properties. Each specimen had several bars sizes. Table 3-1 summarizes the reinforcement properties for each specimen.

3.4 Experimental Test Set-Up

In the research project, two test set-ups were adopted for the testing programs: one for the T-joints, and the second for the knee-joints. The main purpose of the experimental test set-ups was to simulate the forces and deformations of the pile-slab bridge joint prototype as discussed in Section 2-2.

3.4.1 Experimental Test Setup for T-Joints

Five out of the eight specimens were T-joint connections. Figure 3-4 shows the experimental test set-up schematic for specimen FSRCC1. The first step in the test set-up was to attach two W12x26 beams to the strong floor of the laboratory. For specimen FSRCC24-M, two HSS10x10x5/8 were used instead of W12x26. Each beam was attached to the floor through four $1\frac{3}{8}$-in. Dywidag. In order to enable the slab edges to rotate during the test, a set of hinges was used. The hinges were attached on the top of the beams and to the slab through threaded rods that were embedded during the casting of the slab. After attaching the hinges to the beams, the specimens were placed on the top of the hinges, as shown in Figure 3-5.

The transfer of axial loads to the specimen was accomplished through a steel I-beam that was placed across the top of the pile, as shown in Figure 3-6 and Figure 3-7. The flange width, flange thickness and web thickness of the steel beam were 12 in., 2 in. and 1 in. respectively. The beam length was 5 ft and the overall depth was 2 ft. Four holes were drilled in the bottom flange of the beam to allow the passage of the anchor bolts that were embedded in the pile head. The cross beam was then placed in position and secured to the top of the pile.

Two hydraulic jacks were placed at the top of the steel cross beam, and then two $1\frac{3}{8}$-in. Dywidag bars were extended vertically through the top of the hydraulic jacks to the bottom of the slab through two transverse beams. The transverse beams applied the load to two longitudinal beams attached to the bottom of the specimen through a 1-in. diameter rod at each side of the transverse beams (see Figure 3-7). The rod roller enabled the beams to shift during the test; therefore, their stiffness did not influence the behavior. The axial load was held constant in the Dywidag bars, while subjected to lateral load reversals with increasing drift levels. To minimize axial load fluctuation caused by variation in the prestressing bar length under different drift levels, a pressure accumulator was hooked to the hydraulic system between the pump and the jacks. At the beginning of each test, the desired axial load was applied prior to lateral loading.

The lateral load was applied by means of a MTS hydraulic actuator. The actuator base was first connected to the reaction wall through a steel plate, and then the actuator was extended and connected to the top of the pile. The actuator was attached to the top of the pile through the cross beam web of specimens DCRCC1 and FCRCC1. For specimens DCRCC24, FSRCC24, and FSRCC24-M, the actuator was attached directly to the pile head. For specimens DCRCC1 and FSRCC1, one ±220-kip MTS Actuator with a stroke of ±15 in. was used to provide the lateral force. A ±350-kip MTS Actuator with a stroke of ±20 in. was used to provide the lateral load for specimens DCRCC24, FSRCC24 and FSRCC24-M. The axial load for specimen DCRCC1 was 76.5-kips, and 35-kips for specimen DCRCC24, while the axial load for specimens FSRCC1, FSRCC24 and FSRCC24-M was 70.5-kips. The axial load was calculated based on the span length of the bridge and the number of piles for each bent cap[12]. To move the specimen safety

from outside the laboratory to the test position, a set of U-shaped steel bars was anchored in the slab before casting. The U-shaped bars made moving the specimen easier for the forklift.

3.4.2 Experimental Test Set-Up for Knee-Joints

Three out of the eight tested specimens were knee-joint connections. For the deformation of the knee-joint, the test set-up was not symmetrical and had two mechanisms: 1) an opening mechanism and 2) a closing mechanism.

The first step in the test set-up was to attach a W12x36 beam to the strong floor. The beam was attached to the floor through three $1\frac{3}{8}$-in. Dywidag bars (see Figure 3-8 and Figure 3-9). To fix the end of the specimen in the horizontal direction, a buttress support was used in the back of the specimen. The buttress was attached to the floor using three $1\frac{3}{8}$-in. Dywidag bars.

On the top of the beam, a set of 1-in. steel bars was placed along the center line of the longitudinal direction of the beam to enable the specimen to rotate during the closing mechanism. Then the specimen was placed on the top of the W12x36 beam; the distance between the longitudinal center line of the beam and the center line of the pile was equal to 42 inches. In order to enable the specimen to rotate during the opening moment, rubber pads were placed on the top side of the slab at 42 inches. from the pile center. A W8x40 beam was placed on the top of the rubber pads, then the beam was stressed to the floor through three $1\frac{3}{8}$-in. Dywidag bars.

The flange width, flange thickness and web thickness of the steel beam were 12 in., 2 in. and 1 in., respectively. The beam length was 5 ft and the overall depth was 2 ft. Four holes were drilled in the bottom flange of the beam to allow the passage of the anchor bolts, which were embedded in the pile head. The cross beam was then placed in position and secured to the pile top by means of four nuts (see Figure 3-9 and Figure 3-10).

The axial load for the knee-joints was a function of their displacement. The lumped plasticity model shown in Figure 3-11 was used to find the reaction using SAP2000 program[17]. The plastic hinge properties and the geometry of the model were based on the discussion in Sections 2.7 and 2.8. Figure 3-12 and Figure 3-13 show the function of variable axial load for specimens DCKJ24, FSKJ24 and FSKJ24-M, respectively. The variable axial load was the main difference between the axial load for the T-joint connections and the knee-joint connection. To apply the variable axial load on the pile, two Dywidag bars were used to apply the axial load. The variable axial load was applied through a single hydraulic jack; the working mechanism for the jack is shown in detail in Figure 3-10. The jack was placed at the top of the steel cross beam, then the prestressing bars were extended vertically and anchored at the top of the jacks and the bottom of the slab through transverse beams. For specimens DCKJ24 and FSKJ24, rubber pads were used between the transverse beam and the bottom surface of the slab to enable the specimen to rotate during the test.

For specimen FSKJ24-M, two Dywidag bars were extended vertically and anchored at the top of the jacks and the bottom of the slab through two transverse beams. A 1-in. rod was used on each side of the transverse beams as a roller to transfer the load to two longitudinal beams which were attached to the slab. The 1-in. roller rod was used mainly to enable the transverse beams to move during testing; therefore, their stiffness was

excluded from calculations. For more clarification about the test set-up, see Figure 3-14. The lateral load was applied by means of a ±220-kip MTS Actuator with a stroke of ±15 in. The actuator base was first connected to the reaction wall through a steel plate, then extended and connected to the pile head.

3.5 Loading Program

Each specimen was subjected to two loads, one load in the horizontal direction and the other in the vertical direction. The lateral loading system consisted of cyclic loading at increasing amplitudes until failure of the specimen was reached. The loading program can be divided into two parts: 1) force controlled, and 2) displacement controlled. Initial cycles were run in force control; the specimen was loaded gradually until it reached 75% of the predicted effective yield load. When 75% of the predicted effective yield load amplitude cycle was reached, the displacement was recorded and defined as 75% of the yield displacement, Δy. To obtain the experimental yield displacement, $0.75\Delta y$ was multiplied by 4/3. The subsequent cycles were run in displacement control, starting with the measured Δy and continuing in multiples of Δy until failure was reached. At the displacement-controlled stage, the specimen was considered to be failed when the lateral capacity became 80% of its maximum capacity. Figure 3-15 to Figure 3-18 show the horizontal load protocol for the different specimens. The used yield force and displacement during the test were based on the values shown in Table 2-7.

The vertical loading system was nearly the same for all the specimens. The only difference was that the axial load for the T-joints remained constant, but was variable for the knee-joints, as mentioned in Section 3.4.1 and Section 3.4.2, respectively.

3.6 Instrumentation

The most important point of the instrumentation process was to identify the location and objectives of each instrument. Overall instrumentation objectives can be summarized as follows:

1- Reinforcement strains of the pile-slab bridge connection and pile reinforcement.
2- Curvature, rotation, and deformation measurements in the connections model.
3- Lateral and vertical applied loads.
4- Global displacements of the pile-slab bridge connection.

The instrumentation layout of each specimen was designed to record strains, curvatures, displacements and forces generated at critical sections during testing. Each instrumentation type is individually discussed in the following subsections.

3.6.1 Strain Gauges

Strain measurements were collected using YFLA-2-5L series strain gauges manufactured by Tokyo Sokki Kenkyujo Co., Ltd. Strain gauges were used to record the strains generated in the rebar at the critical sections during testing. The critical section for the pile was the bottom part of the pile, where the plastic hinge was expected. One longitudinal bar was instrumented on each side of the pile. Transverse reinforcement was also instrumented. Strain gauge locations along the length of the slab were variable for each specimen; longitudinal and transverse reinforcement of the slab were instrumented. The orientation of the strain gauges is shown in Figure 3-19 to Figure 3-29.

In order to minimize strain gauge damage during the construction process, the following steps were used to attach the strain gauges:

1- Mark where the strain gauge will be attached.
2- Prepare surface for gauge attachment.
   - Grind a smooth surface on reinforcement using sandpaper.
   - Clean the surface from contaminants using cleaner.
3- Attach gauge using CN-Y adhesive.
4- Protect gauge with electrical tape. After gauge is covered, fold the wire over the top of the taped gauge and tape again.
5- Protect shielded wire with heat shrink tubing (1/8 in.), and group wires together with larger heat shrink tube (0.5 in. or 1 in.) in protected locations to avoid damage from construction process.
6- Number each strain gauge, then route wires to an exit point in the specimen, trying to avoid an exit point in areas of high compression.

3.6.2 Displacement Transducer Devices

Displacement Transducer Devices (DTD) TR-50 (±1-in. stroke), TR-75 (±1.5-in. stroke), and TR-100 (±2-in. stroke) were used to measure relative displacements. Accordingly, average curvatures and average rotations were measured in the critical plastic hinge and pile-slab connection regions. Additionally, a shear panel, consisting of a Displacement Transducer Device, was used to determine average joint strains for each specimen. DTD locations used to measure these quantities are shown in Figure 3-30 through Figure 3-36. The instruments were attached to 5/16 in. threaded rods embedded into the concrete during the casting process. The main purpose of the DTD was to determine curvatures and strains at the critical sections during testing. The average strain at each location was calculated from the measured deflection divided by the gauge length (see Figure 3-37). Once the average strains from both sides of the specimen were calculated at each section level, the average curvature over the gauge length was calculated, as shown in Equation 1.

$$\phi_{avg}=\frac{\phi_1+\phi_2}{2}=\frac{0.5(\varepsilon_1-\varepsilon_2)}{D/2+X} \qquad \text{Equation 1}$$

where

ε_1 = strain in level i at tension position,

ε_2 = strain in level i at compression position,

X = distance from instrument to pile surface at level i, on the left side of the specimen, and

D = diameter of the pile section.

3.6.3 Load Measurements

Two types of actuators were used: 1) 220-kip MTS Actuator with an internal load cell, and 2) 350-kip MTS Actuator, with pressure cell (delta-p). Since 350-kip MTS Actuator does not directly measure the force, it has friction along the shaft which must be included in the amount of force being applied to the column. Vertical load was measured by load cells attached to the vertical hydraulic jacks.

3.6.4 Axial Load

The column axial load was applied through post-tensioning the column (see Figure 3-38). Depending on the horizontal displacement and the corresponding rotational angle of the axial load, the load can be divided into horizontal and vertical components[21]. To calculate the column head displacement and rotation, a set of string pots was attached to the pile head (see Figure 3-38). The actual lateral force to the pile is:

$$F' = [F - P\sin(\theta)] \qquad \text{Equation 3-2}$$

And the vertical load is:

$$P' = P\cos(\theta) \qquad \text{Equation 3-3}$$

Note that $P' \simeq P$, since θ is typically small.

3.6.5 Global Displacements

Global displacements were measured using string pots capable of 40 inches of stroke. String pots were used to measure the horizontal displacement of the pile head in the transverse direction. The placement of the string pots are shown in Figure 3-30 to Figure 3-36.

Chapter 4
Experimental Test Results

4.1 Introduction

In this chapter, four T-joint connections and two knee-joint connections were subjected to reverse cyclic loading. Observations and the damage propagation of each specimen are discussed in detail. In addition, the measurement results obtained from each test are also presented in this chapter. The most representative data are discussed while the less critical data are shown in Appendices A through F.

4.2 DCRCC1 Results

4.2.1 Observed Response of the Specimen, DCRCC1

Before starting the first cycle, pre-cracks were marked. Most of the pre-cracks were formed in the pile, and no significant cracks were seen in the slab; the cracks were due to shrinkage and temperature. Experimental testing of DCRCC1 consisted of 12 load stages done over two days. The loading protocol is shown in Figure 3-15. The first six load stages (force controlled) were completed on the first day, while the remaining six load stages (displacement controlled) were completed on the second day. The concrete crack development was monitored and recorded during the peak positive and negative amplitude of the second cycle for each load stage.

A constant axial load equal to 76.50-kips was applied to the specimen. The axial load was applied by means of two hydraulic jacks. A pressure accumulator was used to minimize axial load fluctuations during the test. Lateral cyclic load was applied through a single 220-kip MTS actuator, with a stroke of ±15 in.; the experimental test setup is discussed in detail in Section 3.4.1 and illustrated in Figure 3-4.

Starting from the first load stage (0.05 f_y), up to and including load stage 6 (0.75 f_y), cracks were hairline and concentrated in the bottom part of the pile. At load stage 7, where the ductility level was equal to 1Δy, minor cracks were observed at the pile base, and no cracks were observed in the slab, as shown in Figure 4-1. During the second excursion of load stage 8 (2Δy), the cracks of the pile base extended and became wider on both sides, as shown in Figure 4-2. As the specimen was pushed to load stage 9 (3Δy), the concrete cover at the base of the pile spalled off on both sides of the pile, as shown in Figure 4-3. At load stage 10 (4Δy), flexural cracks developed along the pile height, and during the first excursion of load stage 11 (5Δy), cracks started to become wider at the bottom where the spirals and longitudinal reinforcement of the pile were exposed, as shown in Figure 4-4. When the specimen was pushed to load stage 12 (6Δy), longitudinal bars on the compression side buckled, and one of the longitudinal bars on the tension side fractured. In addition, the spirals fracture and the pile core was damaged, as shown in Figure 4-5. At this stage it was decided to stop the test, since the resisting shear force capacity of the pile dropped to less than 80% of the maximum shear strength. At the end of the test the slab was very stiff with no significant cracks, and there was failure in the pile (see Figure 4-6).

4.2.2 Force-Displacement Relationships

As mentioned in Section 3.6.4, the shear load applied to the specimen needs to be corrected to account for the angle of the axial load. The corrected force-displacement

hysteretic behavior for specimen DCRCC1 is shown in Figure 4-7. Cycles in the west direction (positive sign) are pushing force values. Cycles in the east direction (negative sign) are pulling force values. The following points summarize the force-displacement hysteretic behavior of specimen DCRCC1:

1- The force-displacement relationship was linear until it reached 75% of the yielding force. At a load equal to 8.60-kips (75% of the yielding load), displacement of the pile head was equal to 1.60 in.
2- After the yielding point, the force-displacement relationship became nonlinear. The ultimate force in the positive direction was equal to 13.43-kips, recorded at load stage 8 (2Δy), while the ultimate force in the negative direction was equal to 12.91-kips at the same load stage.
3- The specimen reached the failure point when the ultimate force dropped to 80% of its value. The displacement was equal to 6.6 inches (2.8 Δy) in the positive direction. The specimen was more ductile in the negative direction, where the displacement was equal to 7 inches (2.9 Δy) at 80% of the ultimate load.
4- The specimen was pushed farther until reaching displacements of 13.90 inches (5.8 Δy) in the positive direction and 14.45 inches (6.1 Δy) in the negative direction. At this point, it was decided to stop the test, since the maximum resisting shear force became less than 35% of the ultimate shear force.

String pots were fixed to the cross beam on the top of the pile. Table 4-1 includes the average displacement of the string pots plus the displacement reading from the actuator and the force reading for each cycle.

4.2.3 Strain Gauge Data

The number and position of strain gauges on the longitudinal and transverse reinforcement of the pile and slab of specimen DCRCC1 are shown in Figure 3-19. Due to the large number of strain gauges, hysteresis plots of displacement vs. strain for each recorded gauge are provided in Appendix A. During the casting, some of the gauges were damaged, and therefore are not included in the plots. Additionally, some of the gauges were working well during the test up to a certain point, but were then damaged. After the gauges were damaged, the data was truncated from the plots. At each loading cycle, the maximum and minimum measured strains for each strain gauge were tabulated, as shown in Table 4-2. Positive values in both Table 4-2 and Appendix A plots are tensile strains while negative values are compressive strains. From Table 4-2, the bad gauges can be easily discovered. The strain gauges have a rating of 15 to 20% strain (150000 – 200000 microstrain); therefore, values in this range or above generally indicate the point at which the gauge was damaged. These tables do not include the gauges which were damaged before testing or gauges which showed large jumps in strain values from one cycle to the next.

A review of the strain gauge data revealed that yielding occurred in the longitudinal bars of the pile at load stage 7 (1 Δy). Some of the spirals towards the end of the test attained high strains but did not yield. Yielding in the longitudinal steel of the slab, SG4 and SG21, occurred at load stage 7 (1 Δy) of the test. The rest of the longitudinal bars did not show any significant strain at any other location. None of the slab stirrups yielded. The plots of the strain gauges are shown in Appendix A, and all of the readings are tabulated in Table 4-2**.** The force and strain yielding limit values of the reinforcement bars are listed in Table 3-1.

4.2.4 Curvature Measurements

The method discussed in Section 3.6.2 was used to calculate curvatures of the pile for each load cycle. The measured curvature envelope along the potential plastic hinge location was obtained from the Displacement Transducers Devices (DTD) reading as shown in Table 4-3. Figure 4-8 shows that the curvature of the pile was calculated based on the listed displacement readings of DTD in Table 4-3, and using Equation 3-1. To find the actual plastic hinge length, these curvatures are plotted against the pile height. The actual plastic hinge length can be determined from the intersection point between the curvature envelope of the pile and the yielding limit envelop. Yielding limit was determined based on the cross sectional analysis using XTRACT program[16] (see Figure 7-21). The extension of the top part of the right envelope intersects with yield limit envelope at 18.5 in. from the pile base (15% of pile length).

4.3 FSRCC1 Results

4.3.1 Observed Response of the Specimen, FSRCC1

The experimental test took place in two days. Experimental testing of FSRCC1 consisted of 13 load stages. The loading protocol is shown in Figure 3-15. The first six load stages (force controlled) were completed on the first day, while the remaining five load stages (displacement controlled) were completed on the second day. Before starting the first cycle, pre-cracks were marked. Most of the pre-cracks formed in the bottom region of the pile, and no significant cracks were seen in the slab. The cracks were due to shrinkage and temperature. Before starting this test, a constant axial load equal to 70.40-kips was applied to the specimen. The axial load was applied using two hydraulic jacks. A pressure accumulator was used to minimize axial load fluctuations during the test. Lateral cyclic load was applied through a single 220-kip MTS actuator with a stroke of ±15 in., as shown in Figure 3-4. The experimental test setup was discussed in detail in Section 3.4.1.

Starting from the first load stage (0.05 f_y), up to and including load stage 6 (0.75 f_y), the cracks were hairline and concentrated in the bottom part of the pile. No cracks observed in the slab. At load stage 7, where the ductility level was equal to 1 Δy, minor cracks were observed at the pile base and no cracks were observed in the slab, as shown in Figure 4-9. During the first excursion of load stage 8 (2 Δy), the cracks of the pile base extended and became wider on both sides. When the specimen was taken to the second cycle of 2 Δy, concrete started to spall on both sides of the pile, as shown in Figure 4-10. As the specimen was pushed to load stage 9 (3 Δy), the concrete cover at the base of the pile spalled off at an increasing rate, as shown in Figure 4-11. At load stage 10 (4 Δy), flexural cracks developed along the pile height, as shown in Figure 4-12. During the first excursion of load stage 11 (5 Δy), cracks started to become wider, and the spirals and longitudinal steel became exposed, as shown in Figure 4-13. During the second excursion of load stage 11 (5 Δy), parts of the slab cover spalled off, as shown in Figure 4-14. When the specimen was pushed to load stage 12 (6 Δy), two of the longitudinal bars fractured. The longitudinal bars on the compression side buckled, and another longitudinal bar on the tension side fractured. The spirals fractured and the pile core was completely damaged, as shown in Figure 4-15. After load stage 13, it was decided to stop the test since the resisting force dropped to less than 80% of the maximum shear load. At the end of the test, the slab had no significant cracks and failure in the pile.

4.3.2 Force-Displacement Relationships

As mentioned in Section 3.6.4, load applied to the specimen needs to be corrected to account for the angle of axial load. The corrected force-displacement hysteretic behavior for specimen FSRCC1 is shown in Figure 4-16. Cycles in the west direction (positive sign) are pushing force values while cycles in the east direction (negative sign) are pulling force values. The following points summarize the force-displacement hysteretic behavior of specimen FSRCC1:

1- The force-displacement relationship was linear until it reached 50% of the yielding force, where the displacement was equal to 0.88 in.
2- The force-displacement relationship was almost linear until it reached 75% of the yielding force, where the force was equal to 8.83-kips at 1.62-in. displacement.
3- After the yielding point, the force-displacement relationship became nonlinear. The ultimate force in the positive direction was equal to 13.16-kips, recorded at load stage 8 ($2\Delta y$), while the ultimate force in the negative direction was equal to 13.58-kips.
4- When the load reached 80% of the ultimate load, it can be said that the specimen reached the failure point. The displacement was equal to 8.20 inches ($3.9\ \Delta y$) in the positive direction. The specimen was more ductile in the negative direction, where the displacement was equal to 8.55 inches ($4.1\ \Delta y$) at 80% of the ultimate load.
5- The specimen was pushed farther until reaching a displacement equal to 14.50 inches ($6.93\ \Delta y$) in the positive direction and 13.72 inches ($6.7\ \Delta y$) in the negative direction. At this point, it was decided to stop the test, since the maximum resisting shear force (7-kips) became less than 53% of the ultimate shear force. Table 4-4 includes the displacement readings from the string pots, actuator force and displacement.

4.3.3 Strain Gauge Data

The numbering and position of strain gauges of the longitudinal and transverse reinforcement of the pile and the slab of specimen FSRCC1 are shown in Figure 3-20. At each load cycle, the maximum measured strains generated in the positive and negative direction for each strain gauge were tabulated, as shown in Table 4-5. Positive values in both Table 4-5 and Appendix B plots are tensile strains, while negative values are compressive strains. From Table 4-5 the bad gauges of unreasonable maximum response could be easily discovered. These tables do not include the gauges which were damaged before testing or the gauges which showed large jumps in strain values from one cycle to the next.

A review of the strain gauge data revealed that yielding occurred in the longitudinal bars of the pile at stage 7 ($1\ \Delta y$). Some of the spirals towards the end of the test attained high strains but did not yield. Yielding in the longitudinal steel of the slab occurred in SG4 and SG21 at load stage 7 ($1\ \Delta y$) of the test, while the rest of the longitudinal bars did not show any significant strain at any other location. None of the slab stirrups yielded. The plots of the strain gauges are shown in Appendix B. The force and strain yielding values of the reinforcement bars are listed in Table 3-1.

4.3.4 Curvature Measurements

The curvature of the pile was calculated based on the listed displacement reading of the Displacement Transducer Devices (DTD) in Table 4-6, and using Equation 3-1. The method discussed in Section 3.6.2 was used to calculate curvatures of the pile for each load cycle. The measured curvature envelope along the potential plastic hinge was

obtained from the DTD reading and presented in Figure 4-17. To find the actual plastic hinge length, these curvatures are plotted against the height of the pile. The actual plastic hinge length can be determined from the intersection point between the curvature envelope of the pile and the yield limit envelope. The yielding limit was determined based on the cross sectional analysis using XTRACT program[16] (see Figure 7-22). The extension of the top part of the right envelope intersects with yield limit envelope at 19.4 in. from the pile base (15.9% of pile length).

4.4 DCRCC24 Results

4.4.1 Observed Response of the Specimen, DCRCC24

Lateral cyclic load was applied through a single 350-kip MTS actuator with a stroke of ±20 in. Loading protocol is shown in Figure 3-16. The experimental test setup was discussed in detail in Section 3.4.1, and illustrated in Figure 3-4. Before starting this test, a constant axial load equal to 76.50-kips was applied to the specimen. Before starting the test, all the shrinkage and the pretest cracks were marked. At load stage 4 ($0.25f_y$), no significant cracks were marked on the specimen as shown in Figure 4-18. During the second excursion of load stage 5 ($0.5\ f_y$), cracks spread all over the lower part of the pile. When the specimen was taken to the second cycle of load stage 6 ($0.75\ f_y$), cracks became wider on both sides of the pile, as shown in Figure 4-19. As the specimen was pushed to a ductility $1\Delta y$, the cracks in the pile base became continuous, as shown in Figure 4-20. When the specimen was pushed to the second extrusion of load stage 8 ($2\ \Delta y$), radial cracks appeared in the pile base. Some hairline cracks appeared on the top surface of the slab, while shear cracks appeared above the hinge area on the column, as shown in Figure 4-21. During the first excursion of load stage 9 ($3\Delta y$), the flexural cracks along the pile base became wider and the concrete cover started to spall off the pile, as shown in Figure 4-22. The reaction force in the slab support hinge area caused extension of shear and flexure cracks, especially in the corners of the slab where parts of concrete spalled off. The hinge support became unable to transfer load from specimen to the strong floor of the laboratory, therefore the test was concluded.

4.4.2 Force-Displacement Relationships

As mentioned in Section 3.6.4, force-displacement hysteretic behavior needs to be corrected to account for the incline of the axial load and the actuator friction effect. The corrected force-displacement hysteretic behavior for specimen DCRCC24 is shown in Figure 4-23. Cycles in the north direction (positive sign) are pushing force, while cycles in the south direction (negative sign) are pulling force. The following points summarize the force-displacement hysteretic behavior of specimen DCRCC24:

1- The force-displacement relationship was linear until it reached 50% of the yielding force. The maximum force at this stage in the positive direction was equal to 14.13-kips, and the displacement was equal to 0.88 in. The maximum force in the negative direction was equal to 15.12-kips, and the displacement was equal 1.49 in.

2- The force-displacement relationship became nonlinear at 75% of the yielding force. The specimen was stiffer in the positive direction than the negative direction. The maximum force at this stage in the positive direction was equal to 22.05-kips, and the displacement was equal to 1.79 in. The maximum force in the negative direction was equal to 22.53-kips, and the displacement was equal to 2.22 in.

3- At ductility level (1Δy), the force-displacement relationship became nonlinear. The force in the positive direction was equal to 33-kips, and the displacement was equal to 2.82 in. The force in the negative direction was equal to 27.43-kips, and the displacement was equal to 2.72 in.
4- In load stage 9 (3Δy) the shear force was equal to 43.72-kips, and the displacement was 8.08 in.; after this stage it was decided to stop the test because of the shear cracks in the slab corners, as mentioned previously in Section 4.4.1.

Table 4-7 includes the displacement reading of the actuator, the force reading for each cycle and the average displacements of the string pots.

4.4.3 Strain Gauge Data

The number and position of strain gauges of the longitudinal and transverse reinforcement of the pile and slab of specimen DCRCC24 are shown in Figure 3-21. A review of the strain gauge data revealed that yielding occurred in the longitudinal pile reinforcement during load stage 7 (1Δy). The spiral showed high strain by the end of the test, but only SG54 reached the yield limit. Strain gauges on the longitudinal reinforcement of the slab did not reach their yield limit. Strain gauges SG6, SG7 and SG26 obtained strain values close to the yield value. All the readings of the strain gauges are listed in Table 4-8. Plots of the strain gauges for specimen DCRCC24 are provided in Appendix C. The force and strain yielding values of the reinforcement bars are listed in Table 3-1.

4.4.4 Curvature Measurements

The curvature of the pile was calculated based on the displacement readings of the DTDs in Table 4-9, and using Equation 3-1. To find the actual plastic hinge length, the measured curvature along the plastic hinge length was plotted, as shown in Figure 4-24. The actual plastic hinge can be determined from the intersection point between the curvature envelope of the pile and the yield limit envelope. The yielding limit was determined based on the cross sectional analysis using XTRACT program[16] (see Figure 7-23). The extension of the top part of the left envelope intersects with the yield limit envelope at 24.5 in. from the pile base (17% of pile length).

4.5 FSRCC24 Results

4.5.1 Observed Response of the Specimen, FSRCC24

Lateral cyclic load was applied through a single 350-kip MTS actuator with a stroke of ±20 in. The experimental test setup was discussed in detail in Section 3.4.1, and illustrated in Figure 3-4. Before starting this test, a constant axial load of 70.50-kips was applied to the specimen. All the shrinkage cracks were marked to differentiate between the shrinkage cracks and cracks which occurred during the test. The shrinkage cracks were minimal. Experimental testing of FSRCC1 consisted of 12 load stages. The loading protocol is shown in Figure 3-16. The experiment took place in two days. The first six load stages, which were force controlled, were on the first day, while the remaining six load stages, which were displacement controlled, were completed on the second day.

The cracks during the first four stages were hairline cracks, mainly in the pile with no cracks observed in the slab. During the second excursion of load stage 4 ($0.5f_y$), small hairline cracks spread over the lower part of the pile (see Figure 4-25), and no cracks

were seen in the slab. When the specimen was taken to the second cycle of load stage 6 ($0.75f_y$), which is the end of the force controlled loading, a few hairline cracks spread in the slab, and more hairline cracks spread in the bottom part of the pile, as shown in Figure 4-26. As the specimen was pushed to 1Δy, wide cracks extended to the bottom of the pile and more hairline cracks spread in the slab, as shown in Figure 4-27. When the specimen was pushed to the second cycle load stage 8 (2 Δy), small parts of the pile concrete cover spalled, and slab cracks extended and became wider; some cracks appeared on the bottom surface of the slab, as shown in Figure 4-28. During the second excursion of load stage 9 (2.5Δy), small parts of the concrete cover of the pile spalled off from both sides of the pile base. A big part of the upper slab surface cover spalled off, and cracks on the bottom side of the slab became wider, as shown in Figure 4-29. Despite the existence of large cracks in the slab at this stage, it was decided to keep pushing the specimen to observe the behavior of the specimen after this stage. As the pile head was pushed farther, load stage 11 (3.5Δy), a crushing sound was heard in the slab. The cracks on the top and bottom surfaces of the slab became wider, more parts of the slab cover spalled off and the transverse reinforcement of the top surface of the slab became exposed. Pile cracks did not change at this stage. The pile-slab connection was substantially damaged at this stage, as shown in Figure 4-30. When the specimen was pushed to the first cycle stage 12, parts from the bottom side of the slab cover started to fall to the floor, as shown in Figure 4-31, and the transverse reinforcement of the bottom side of the slab became exposed. At this stage it was decided to stop testing.

By the end of the test, the pile cracks stopped propagating after load stage 9 (2.5Δy), where the ultimate load was recorded. The cracks spreading in the slab became more dramatic after stage 9 (2.5Δy). None of the longitudinal reinforcement or transverse reinforcement of the pile was exposed at the end of the test, as shown in Figure 4-32.

4.5.2 Force-Displacement Relationships

The corrected force-displacement hysteretic behavior for specimen FSRCC24 is shown in Figure 4-33. Cycles in the north direction (positive sign) are pushing, while cycles in the south direction (negative sign) are pulling. The following points summarize the force-displacement hysteretic behavior of specimen FSRCC24:

1- The force-displacement relationship was linear until it reached 50% of the yielding force. The ultimate force at this stage in the positive direction was equal to 20.30-kips and the displacement was equal to 1.38 in. The maximum force at this stage in the negative direction was equal to 20.10-kips, and the displacement was equal to 1.29 in.

2- The force-displacement relationship became slightly nonlinear at 75% of the yielding force. The maximum force at this stage in the positive direction was equal to 29.33-kips, and the displacement was equal to 2.27 in. The maximum force in the negative direction was equal to 26.50-kips, and the displacement was equal to 2.01 in.

3- At ductility level of 1Δy, the force-displacement relationship became nonlinear. The maximum force in the positive direction was equal to 36.01-kips, and the displacement was equal to 3.10 in. The maximum force in the negative direction was equal to 34.69-kips, and the displacement was equal to 3.10 in.

4- The maximum force at load stage 8 (2Δy) was equal to 42.73-kips, with 6.01 in. displacement in the positive direction. In the negative direction, the maximum force was equal to 42.84-kips and 6.01 in. displacement.

5- The ultimate recorded force during the test was 42.86-kips, during load stage 9 (2.5Δy) in the positive direction.
6- At ductility level (3Δy), force in the positive direction dropped to 60% of the ultimate force. In negative direction, the force dropped to 50% of the ultimate force.
7- The specimen was pushed farther until reaching a displacement of 12.06 in. (4Δy). The recorded force at this stage was equal to 21.35-kips in the positive direction and 17.58-kips in the negative direction.

Table 4-10 includes the force, the displacement of the actuator and the average displacements of the string pots at each cycle. The string pots were used to check the readings of the actuator. Figure 4-33 shows the force-displacement relationship of the actuator.

4.5.3 Strain Gauge Data

The numbers and positions of the strain gauges of the longitudinal and transverse reinforcement of the pile and slab of specimen FSRCC24 are shown in Figures 3-22 and 3-23. As the specimen was pushed to 0.75 f_y, strain gauge readings showed that SG31, SG37, SG41, SG43, SG45, SG49, SG65, SG67 and SG69 in the longitudinal bars of the pile reached the yield limit, and none of the transverse reinforcement of the pile or slab reinforcement reached yield at this stage. All of the readings for the strain gauges during each cycle are listed in Table 4-11 and Appendix D. A review of strain gauge readings at ductility 1Δy showed that SG32 at 20 in. from the pile base in the stirrups yielded. SG56 in the longitudinal reinforcement of the pile also reached the yield limit. Slab strain gauges showed significant high strain but did not reach yield. At ductility level 3Δy, strain gauges SG2, SG12 and SG20 in the longitudinal reinforcement of the slab reached their yield value.

The longitudinal and transverse reinforcement of the pile passed the yield limit at the end of the test. The longitudinal reinforcement of the slab also reached the yield limit, but none of the joint shear reinforcement reached the yield limit.

4.5.4 Curvature Measurements

The curvature of the pile was calculated based on the listed displacement readings in Table 4-12, and using Equation 3-1. To find the actual plastic hinge length, the measured curvature along the plastic hinge length was plotted, as shown in Figure 4-34. The actual plastic hinge can be determined from the intersection point between the curvature envelope of the pile and the yield limit envelope. The yield limit for specimen FSRCC24 pile is shown in Figure 7-24. The extension of the top part of the right envelope intersects with yield limit envelope at 23 in. from the pile base (16% of pile length).

4.6 DCKJ24 Results

4.6.1 Observed Response of the Specimen, DCKJ24

Experimental testing of specimen DCKJ24 took place in one day. Lateral cyclic load was applied through a single 220-kip MTS actuator with a stroke of ±15 in. The experimental test setup was discussed in detail in Section 3.4.1, and illustrated in Figure 3.9. A variable axial load was applied to the specimen during the test (see Figure 3-12). Before starting the test, all of the shrinkage cracks were marked to differentiate between the shrinkage cracks and cracks which occurred during the test. In order to make the

cracks easier to see during the test, a white water base primer was applied to the specimen.

The cracks during the first load stage ($0.15f_y$) were hairline cracks, mainly in the pile, with no cracks observed in the slab. During load stage 1 ($0.5f_y$), small hairline cracks spread all over the pile, and some hairline cracks appeared on the top surface of the slab. When the specimen was taken to the second cycle of load stage 4 ($0.75\Delta y$), more hairline cracks spread in the slab, and hairline cracks spread in the bottom part of the pile.

As the specimen was pushed to ductility ($1\Delta y$), an extended crack at the pile slab interface appeared, and more hairline cracks spread in the slab, as shown in Figure 4-35. More hairline cracks spread in the pile and the slab at load stage 6 ($1.5\Delta y$), as shown in Figure 4-36. At load stage 7 ($2\Delta y$), small parts of the pile cover spalled off, while the cracks in the slab became wider (see Figure 4-37). At load stage 8 ($3\Delta y$), parts of the pile cover spalled off to a height of 8 inches, while hairline cracks kept propagating in the slab, as shown in Figure 4-38. When the specimen was pushed to ductility $4\Delta y$, large horizontal cracks around (1/8–inch wide) were seen in the pile base, as shown in Figure 4-39. During the second excursion of stage 10 ($5\Delta y$), the concrete cover of the pile started to spall off from the inner side of the pile (pile face which is closer to the hinge), to a height of 20 inches. The pile spirals were exposed as well. The cracks on the outside of the pile became wider, and more cracks spread all over the slab, as shown in Figure 4-40. When the specimen was pushed to ductility level $6\Delta y$, two of the spirals ruptured and three of the longitudinal bars in the inner side buckled. Technically, the specimen can be considered failed after this stage, as shown in Figure 4-41.

The general observation for the specimen at the end of the test was that none of the slab longitudinal reinforcement or slab transverse reinforcement was exposed. A crack in the top side of the slab was marked at 10 in. from the pile face; This was the same place where the U-bars ended, as shown in Figure 4-42. Other inclined cracks were marked on both sides of the slab; large parts of the cover of the pile were lost from both sides of the pile, as shown in Figure 4-42.

4.6.2 Force-Displacement Relationships

The corrected force-displacement hysteretic behavior for specimen DCKJ24 is shown in Figure 4-43. Cycles in the north direction (positive sign) are pushing force, while cycles in the south direction (negative sign) are pulling force. The following points summarize the force-displacement hysteretic behavior of specimen DCKJ24:

1- The force-displacement relationship was linear until it reached 50% of the yielding force. It was obvious at this early stage that the specimen was stiffer in the negative direction (opening the joint) rather than positive direction (closing the joint). The maximum force in the positive direction was equal to 12.02-kips, and the displacement was equal to 1.21 in. The maximum force in the negative direction was equal to 7.81-kips, and the displacement was equal to 0.67 in.

2- The force-displacement relationship became slightly nonlinear at 75% of the yielding force. The maximum force in the positive direction was equal to 14.87-kips and the displacement was equal to 1.53 in. The maximum force in the negative direction was equal to 11.41-kips, and the displacement was equal to 1.20 in.

3- At ductility level 1Δy, the maximum force in the positive direction was equal to 18.76-kips, and the displacement was equal to 2.44 in. The maximum force in the negative direction was equal to 11.83-kips, and the displacement was equal to 2.43 in.
4- The ultimate recorded force in the positive direction during the test was recorded at ductility level 1.5Δy, 20.61-kips and 3.66 in. displacement, while in the negative direction, the force was equal to 14.07-kips and 3.65 in. displacement.
5- The force in the positive direction started decreasing after ductility level 1.5Δy, while in the negative direction, the force was still increasing after ductility level 1.5Δy.
6- At ductility level 4Δy, the load dropped to 78% of the ultimate force, in the positive direction, where the recorded force was equal to 18.02-kips with 9.75 in. displacement, while in negative direction, the ultimate force was 17.32-kips, with a displacement equal to 9.74 in. The longitudinal bars in the positive direction buckled, and this caused the force to drop in the positive direction.
7- At ductility level 5Δy, the maximum force in the positive direction was 16.21-kips with 12.18 in. displacement. In the negative direction, the force was equal to 14.80-kips (85% of the ultimate recorded force), with 11.85 in. displacement.
8- When the specimen was pushed to ductility level 6Δy in the positive direction, one of the longitudinal bars fractured and the force dropped to 9.21-kips (44% of the ultimate force).

Table 4-13 includes the force, the displacement of the actuator and the average displacements of the string pots at each cycle. Figure 4-43 shows the force-displacement relationship of the actuator.

4.6.3 Strain Gauge Data

The number and position of strain gauges of the longitudinal and transverse reinforcement of the pile and slab of specimen DCKJ24 are shown in Figure 3-25. As the specimen was pushed to 0.75 f_y, a review of strain gauge readings showed that SG3, SG7, SG9, SG11, SG13, SG19, SG21, SG23, SG25 and SG27 on the longitudinal bars of the pile reached yielding, but none of the transverse reinforcement of the pile did. SG56 and SG69 on the longitudinal reinforcement of the slab reached yield at this stage. All of the readings for the strain gauges during each cycle are listed in Table 4-14, and the strain gauge plots are provided in Appendix E.

A review of strain gauge readings at ductility 1.5Δy showed that SG5 yielded in the longitudinal reinforcement of the pile. SG34 yielded on the horizontal cap end ties. SG55 and SG60 reached the yield limit on the longitudinal reinforcement of the slab. At ductility 5Δy, SG18 and SG20 yielded on the pile spirals. SG29 and SG32 also yielded on the horizontal stirrups. The transverse stirrups of the slab reached yield only at one location: SG38.

The longitudinal reinforcement of the pile reached the yield limit at early stage. Transverse reinforcement of the pile yielded at the end of the test. The longitudinal reinforcement of the slab reached the yield limit. None of the vertical U-bars in joint shear reinforcement reached the yield limit.

4.6.4 Curvature Measurements

The curvature of the pile was calculated based on the displacements of DTDs in Table 4-15, and using Equation 3-1. To find the actual plastic hinge length, the measured curvature along the plastic hinge length was plotted, as shown in Figure 4-44. The actual

plastic hinge can be determined from the intersection point between the curvature envelope of the pile and the yield limit, which is shown in Figure 7-25. The extension of the top part of the right envelope intersects with yield limit envelope at 19.15 in. from the pile base (20% of pile length).

4.7 FSKJ24 Results

4.7.1 Observed Response of the Specimen, FSKJ24

Experimental testing of specimen FSKJ24 took place in one day. Lateral cyclic load was applied through a single 220-kip MTS actuator with a stroke of ±15 in. The experimental test setup was discussed in detail in Section 3.4.1, and illustrated in Figure 3.9. A variable axial load was applied to the specimen during the test (see Figure 3-13). Before starting the test, all of the shrinkage cracks were marked to differentiate between the shrinkage cracks and cracks which occurred during the test. In order see the cracks easier during the test, a white water based primer was applied to the specimen. It was obvious that the shrinkage cracks were minimal.

The cracks during the first two load stages were hairline cracks in the pile and horizontal cracks in the slab, as shown in Figure 4-45. During the second excursion of load stage 3 ($0.5f_y$), small hairline cracks spread all over the pile, and hairline cracks appeared on the top surface of the slab, as shown in Figure 4-46. At the first excursion of $0.75\Delta y$, more cracks spread on the top surface and sides of the slab (see Figure 4-47), and hairline cracks spread on the bottom part of the pile. As the specimen was pushed to $1\Delta y$, a crack started to extend at the pile-slab interface and more hairline cracks spread in the slab, as shown in Figure 4-48. When the specimen was pushed to $1.5\Delta y$, the pile-slab interface crack became wider. Cracks stopped propagating at the pile at this stage and wide diagonal cracks on both sides of the slab appeared, Figure 4-49. When the specimen was pushed to a higher displacement than $2\Delta y$, concrete spalled off the slab's bottom and the sides, and the slab cracks became wider, especially when in the joint closed, as shown in, Figure 4-50.

During the second excursion of load stage 8 ($2.5\Delta y$), no more new cracks were observed in the pile and more parts of the slab cover fell to the floor (Figure 4-51). It was decided to push the specimen farther to observe the behavior of the specimen. As the specimen was pushed to higher ductility level, $3\Delta y$, more cracks were seen on both sides of the slab and on the top, as shown in Figure 4-52. Figure 4-53 shows the specimen at the end of the test, where all the major cracks were in the slab, and the concrete cover of the pile was still in place.

4.7.2 Force-Displacement Relationships

The corrected force-displacement hysteretic behavior for specimen FSKJ24 is shown in Figure 4-54. Cycles in the north direction (positive sign) are pushing force, while cycles in the south direction (negative sign) are pulling force. The following points summarize the force-displacement hysteretic behavior of specimen FSKJ24:

1- The force-displacement relationship was non linear beginning at 50% of the yielding force. The specimen was stiffer in the negative direction (opening the joint) rather than positive direction (closing the joint). The maximum force in the positive direction was equal to 8.76-kips, and the displacement was equal to 1.28 in. The

maximum force in the negative direction was equal to 7.19-kips, and the displacement was equal to 1.36 in.

2- At 75% of the yielding force, the shear force in the positive direction was equal to 13.23-kips, and the displacement was equal to 2.44 in. The maximum force in the negative direction was equal to 10.50-kips, and the displacement was equal to 2.77 in. The specimen was more flexible in the opening position.

3- At 1Δy, the maximum force in the positive direction was equal to 15.71-kips, and the displacement was equal to 3.18 in. The maximum force in the negative direction was equal to 12.03-kips, and the displacement was equal to 3.22 in.

4- The ultimate force of 16.85-kips, in the positive direction, was recorded at a ductility level of 1.5Δy, with 4.86 in. displacement. The ultimate force in the negative direction was equal to 13.54-kips, with 4.20 in. displacement, at load ductility level 2Δy.

5- At ductility level 2.5Δy, the load dropped to 86% of the ultimate force in the positive direction, where the recorded force was equal to 15.96-kips and 8.70 in. displacement. While in the negative direction, the load dropped to 9.50-kips, 70% of the ultimate force in the negative direction, at displacement equal to 7.97 in.

6- It was decided to observe the behavior of the specimen when pushed farther. When the specimen was pushed to ductility level 3.5Δy, the force dropped to 8.50-kips in the positive direction (75.7% of the ultimate force). While in the negative direction, the force dropped to 36.4% of the ultimate force.

Table 4-16 includes the force, the displacement of the actuator and the average displacements of the string pots at each cycle.

4.7.3 Strain Gauge Data

The number and position of strain gauges of the longitudinal and transverse reinforcement of the pile and slab of specimen FSKJ24 are shown in Figure 3-25. A review of the strain gauge data at load stage 4 ($0.75f_y$), revealed that strain gauges SG1, SG9, SG13, SG17, SG25 in the longitudinal reinforcement of pile reached the yield limit, while SG67 in the bottom longitudinal reinforcement of the slab yielded. At load stage 6 (1.5Δy), more strain gauges yielded in the longitudinal bars of the pile: SG3, SG5, SG7, SG11, SG13, SG15, SG19, SG23 and SG27. Strain gauge SG38 reached the yield limit. In the longitudinal reinforcement of the slab, additional strain gauges reached the yield limit: SG54, SG55, SG58, SG60, SG66 and SG68. Strain gauges SG70, SG73 and SG75 in the vertical U-bars reached the yield limit. All measured strain readings for pile and slab reinforcement are shown in Table 4-17. At the end of the test, none of the horizontal cap end ties showed yield, while strain gauges SG44 and SG47 in the horizontal stirrups in the slab yielded. The plots of the strain gauges for specimen FSKJ24 are shown in Appendix F.

4.7.4 Curvature Measurements

The curvature of the pile was calculated based on readings in Table 4-18, and using Equation 3-1. To find the actual plastic hinge length, the measured curvature along the plastic hinge length was plotted, as shown in Figure 4-55. The actual plastic hinge can be determined from the intersection point between the curvature envelope of the pile and the yield limit envelope; the yield limit is shown in Figure 7-26. The extension of the top part

of the right envelope intersects the yield limit envelope at 19.15 in. from the pile base (19.9% of pile length) (see Figure 4-55).

Chapter 5
Strut-and-Tie Models

5.1 Introduction

The strut-and-tie models were developed based on the reinforcement strain for each specimen and the experimental observations made during each experiment. This chapter focuses on the development of STMs for specimens FSRCC24, DCKJ24 and FSKJ24, which each have high strains in the pile and the slab. The strain levels for the slab reinforcements of specimens FSRCC1, DCRCC1 and DCRCC24 were too low, so it was hard to improve the developed STMs for them. After the STM models were developed, the models were verified against the measured data. In the strut-and-tie model, the external forces are transferred to the structural body through a combination of struts and ties. The joints connecting the struts and ties are called nodes; at these nodes, equilibrium is to be maintained for calculating member forces. In this document, dashed lines represent struts while solid lines represent ties.

In order to calculate forces, a free java based program called Fachwerk[22], developed specifically for strut-and-tie models, was used. Fachwerk has many advantages; the program does not depend on the member stiffness, so equilibrium condition is the only condition to determine the member forces. Another advantage of the program is that force magnitudes can be assigned to members if the system is indeterminate.

The experimental results and the STM for specimen FSRCC24 were used to develop specimen FSRCC24-M, while the experimental results and the STM for specimens DCKJ24 and FSKJ24 were used to develop FSKJ24-M; these will be discussed in detail in Chapter 6.

5.2 Strut-and-Tie Model for T-joint (Specimen FSRCC24)

The STM for specimen FSRCC24 was developed using measured joint strains and experimental observations. The following steps illustrate the steps to develop the STM for specimen FSRCC24.

5.2.1 Boundary Forces

The STM was developed for the full specimen, not just the pile-slab connection region. The first step in developing the force transfer model was to determine the magnitude and location of the boundary forces. There were three positions where the boundary forces were calculated at: the pile-slab interface, and the slab at distance equal to half of the slab thickness from both sides of the pile face. These boundary forces were determined at the ultimate lateral load condition. The ultimate lateral load, 43.84-kips, was recorded during load stage 8 ($2\Delta y$), as shown in Figure 4-33. The axial load on the pile was equal to 70.50-kips. Moment, shear, and axial force values were calculated based on the experimental test results, using XTRACT[16] software.

The next step was to represent the moments acting on the joint boundaries in terms of compression and tension force resultants. This was accomplished through the moment curvature analysis techniques discussed in Section 2.7.1. Figure 5-1 and Figure 5-2 show graphically the forces in the pile and the slab. Notice that an x-z coordinate system was defined for the model in order to easily describe the nodal locations and determine the angles. The origin of the coordinate system adopted for this model and all subsequent models presented in this chapter is positioned so the longitudinal x-axis and vertical z-

axis directions are located in the middle of the slab-pile interface. Figure 5-3 summarizes the boundary forces for the system. The proposed STM that was developed is shown in Figure 5-4, while the coordinates of the STM are provided in Table 5-1.

5.2.2 Measured Joint Reinforcement Force-Transfer Contributions

In order to develop the STM, the force-transfer through the reinforcement was known from the peak measured strains during the test. The peak strain values listed in Table 4-12 are provided in this section as plots; in order to understand the various joint reinforcement component contributions to the force-transfer process, see Figure 5-5 to Figure 5-18. These plots are helpful to visualize the major joint reinforcement contributors to the force-transfer process at various load levels, and are instrumental in developing a new, more robust force-transfer model capable of handling several incremental increases in lateral load.

5.2.2.1 Joint Stirrups

Measured strains recorded on the vertical and horizontal joint stirrups for specimen FSRCC24 are shown in Figure 5-5 to Figure 5-10. The loading direction and strain gauge identification are indicated on the figures. It is evident from these plots that none of the vertical stirrups or horizontal stirrups reached the yield limit, although some gauges showed high strain in varying degrees.

5.2.2.2 Pile Reinforcement

Measured strains for specimen FSRCC24 pile longitudinal reinforcement at different load stages are shown in Figure 5-11 for the south cycle and Figure 5-12 for the north cycle. The joint/pile interface is represented as zero in the figures with a negative y-axis distance extending into the joint (slab) and a positive y-axis distance extending into the joint. All the strain gauges along the longitudinal reinforcement yielded at an early stage. Notice that the pile longitudinal reinforcement yielded at 12 inches into the bent cap. This indicates that the bars are still being developed into the joint. Similar plots for the pile transverse spirals extending into the joint are shown in Figure 5-13 and Figure 5-14 for the south and north cycles, respectively. Both plots show substantially large strain at a distance of 12 in. into the joint and at 20 in. height from the pile-slab interface, the spirals yielded.

5.2.2.3 Slab Reinforcement

Measured strains for reinforcement at the top and bottom of the slab are plotted along the slab length for various FSRCC24 load stages in Figure 5-15 to Figure 5-18. For the slab distance on the x-axis of these plots, zero indicates the joint center with negative x-axis values extending north along the slab, and positive x-axis values extending south. The purpose of the plots was to indicate how the slab tension was transferred inside the joint. Figure 5-15 and Figure 5-16 indicate that the slab reinforcement yielded in different locations at load stage 16.

5.2.3 Strut-and-Tie Model Development for FSRCC24

This section shows the procedures taken in order to generate the strut-and-tie model. The following steps focus on node and member locations in the x-axis and z-axis and how to determine each of them.

a) External Forces Coordinates

The first step is to determine boundary forces and force resultants as discussed before. Pile compression resultant, C_p, and pile shear force, V_p, are applied to Node W, while the pile tension resultant T_p is applied to Node F (see Figure 5-3). Nodes X and V represent the hinge supports location, where one half of the shear force was applied on each node. The external force applied at Nodes Y and Z is one-half of the applied axial forces on each pile.

b) Internal Forces Coordinates

1) Locate Nodes A, B, I and J coordinates.

The x-coordinate of Node A was chosen to be at a distance equal to half of the slab thickness from the right outer face of the pile. The z-coordinate was found from the moment curvature analysis using XTRACT[16], as mentioned previously in Section 5.2.1. Node A is meant to represent the compression centroid in the top part of the slab. Node B has the same x-coordinate as Node A and is located at the tension centroid of the bottom reinforcement on right side of the slab. The z-coordinate was calculated from the moment curvature analysis. Once Nodes A and B were determined, Tie T_{AB} was calculated.

The x-coordinate of Node I was chosen to be at a distance equal to half of the slab thickness from the outer left face of the pile. The z-coordinate was calculated from the moment curvature analysis, as mentioned before. Node I was located at the tension force centroid in the top part of the left side of the slab. Node J had the same x-coordinate as Node I and was at the compression centroid of the bottom part of the left side of the slab. Once Nodes J and I were determined, Tie T_{JI} was calculated.

2) Locate Node D

The x coordinate of Node D was located at the T_c resultant (see Figure 5-4). Node D represents the end of the minimum anchorage length of the pile tension bars based on bond stress from the longitudinal bars to the concrete. In order to locate the z-coordinate of Node D, it was assumed that the pile tension bars could be extended with a maximum bond stress of $30\sqrt{f'_c}\,psi$; this value was measured from pile bent cap experiments by other researchers[23]. Assuming this maximum bond stress is uniform; a minimum anchorage length was expressed as:

$$l_a = \frac{A_b f_{s\,avg}}{\pi d_b U}\ (in) \qquad \text{Equation 5-1}$$

where A_b is the reinforcement bar area; $f_{s\,avg}$ is the average stress in the tension reinforcement consisting of pile tension resultant, T_c; d_b is the reinforcement bar diameter; and U is the uniform bond stress taken as $30\sqrt{f'_c}\,psi$; Equation 5-1 was simplified to:

$$l_a = \frac{d_b f_{s\,avg}}{120\sqrt{f_c'}}\ (in) \qquad \text{Equation 5-2}$$

where $f_{s\,avg}$ and $\sqrt{f_c'}$ are given in terms of psi. Once Node D is located, Strut C_{DA} was determined.

3) Locate Node W and H

The x and z-coordinates of Node W were located at the pile compression resultant centroid, C_P, as mentioned in the external forces coordinates section. Strut C_{WH} represents the force resultant at Node W resulting from C_P and V_P. Node H was located by the extension of force action line at point B horizontally until it intersected with the force resultant of Node W. The z-coordinate of Node H is the z-coordinate of Node B. The x-coordinate of Node H was the resultant of Strut C_{HW} intersection with the Tie T_{BH} (see Figure 5-4).

4) Locate Node E and C

Node E had the same x-coordinate as point D. The z-coordinate of point E was the center line of the pile's spirals as shown in Figure 5-19. This point will be discussed in detail later. Node C had the same z-coordinate as Node I and the same x-coordinates as node D (see Figure 5-4).

5) Locate Node G

Node G had the same z-coordinate as point E. The x-coordinate of Node G was dependent upon the desired magnitude of Tie T_{EG} and thus is up to the designer. Once Node G was located, Strut C_{CG}, Tie T_{CD} and Tie T_{CI} were determined from the equilibrium of Node C. From the equilibrium of Node D, Strut C_{DG} and Tie T_{DE} were determined. Strut C_{GH} and Tie T_{GI} were determined from equilibrium equations of Node G. Strut C_{HJ} and Tie T_{HB} were determined from the equilibrium of Node H.

At this stage the struts and ties of the pile-slab joint were known. For convenience, when the STM was extended to the supports, the z-coordinate of Node K was the same z-coordinate as Node J. Nodes O and L had the same x-coordinate as Node I. Nodes Q and U had the same z-coordinate as Node A. Nodes R and T had the same z-coordinate as joint B. The x-coordinate of Node O was determined from the force resultant at support intersection with the horizontal Tie T_{OL}, the same as point U. The coordinates for all of the points are listed in Table 5-1.

5.3 Strut-and-Tie Model Verification

5.3.1 Ties Verification

In this section, the experimentally developed strut-and-tie model is applied to specimen FSRCC24 at the ultimate lateral load determined from the experimental test results. The ultimate lateral load, 43.84-kips, was recorded in stage 9 during the first excursion of 2.5Δy. Solving the STM requires Node G to be located such that an appropriate value for Tie T_{EG} was determined. Tie T_{EG} represents the force in the spiral reinforcement in joint center, as shown in Figure 5-19. Tie T_{EG} is assumed to be resisted by the pile spirals inside the slab; Equation 5-3 illustrates the calculation method of Tie T_{EG}.

$$T_{EG} = 2\left[\frac{\left(L_{above} + L_b\right)}{S} + 1\right] A_{sp} f_{sp} \qquad \text{Equation 5-3}$$

where L_{above} is the distance between Node D and the end of pile spirals, L_b is the distance between Node D and the tension reinforcement of the slab; "S" is the spiral pitch, A_{sp} is the spiral reinforcement area, and f_{sp} is the spiral stress. The "+ 1" term in Equation 5-3 is for the spiral turn that is next to the last space, and the "2" term accounts for 2 spiral

areas are in each pitch. The following steps summarize the verification of the model for each member:

a) The x-coordinates of Node G were determined based on the magnitude of Tie T_{EG}. The amount of tension was determined based on the average maximum readings of the strain gauges SG61, SG64, SG66 and SG68 in the spirals at ductility level 2.5Δy. Tie T_{EG} was calculated using Equation 5-1, where L =13.5 in., s = 2.5 in., A_{sp} = 0.11 in^2, and the resulting average strain for 981 microstrains. Tie T_{EG} was determined to be 40.80-kips. Node X-coordinates of Node G was adjusted until Tie T_{EG} was representative of the above value.
b) Tie T_{IC} (341.4-kips) represented the top reinforcement of the slab inside the pile-slab joint with an area of 4.74 in^2 and a strain of 2520 microstrains. Strain for gauge SG20 in the top reinforcement of the slab inside the pile-slab joint was equal to 2234 microstrains. Both the strains in the experiment and the STM are located in the yielding plateau, so the force from the experiment and the STM agree very well.
c) Tie T_{LI} (136-kips) represented the top reinforcement of the slab outside the pile-slab joint with an area of 4.74 in^2 and a strain of 1004 microstrains. Strain for gauge SG26 in the top reinforcement of the slab outside the pile-slab joint was equal to 1052 microstrains; this agrees very well with the strut-and-tie model.
d) Tie T_{HB} (338-kips) represented the bottom reinforcement of the slab inside the pile-slab joint with an area of 4.74 in^2 and a strain of 2495 microstrains. The average strain for gauges SG12 and SG18 on the bottom reinforcement of the slab inside the pile-slab joint was equal to 1768 microstrains; which was less than the predicted value of the strut-and-tie model.
e) Tie T_{BR} (114.5-kips) represented the bottom reinforcement of the slab outside the pile-slab joint with an area of 4.74 in^2 and a strain of 845 microstrains. The strain for gauge SG6 on the bottom reinforcement of the slab outside the pile-slab joint was equal to 803 microstrains; this agrees well with the strut-and-tie model.
f) Tie T_{DE} (329.4-kips) represented the top part of the pile reinforcement, which was considered half of the longitudinal reinforcements of the pile with an area of 4.5 in^2 and a strain of 2258 microstrains. The average strain for gauges SG63 and SG65 in the top part of the pile reinforcement was equal to 2093 microstrains; this agrees well with the strut-and-tie model.
g) Tie T_{CD} (318-kips) represented the tension force in the vertical stirrups which transfer the force from the pile longitudinal reinforcement to the top mat of slab reinforcement, with an area of 1.24 in^2. The strain for SG13 was equal to 554 microstrains, which means that 22-kips was transferred by the vertical stirrups, leaving 307-kips to be transferred by the concrete; this caused some parts of the bottom side of the slab to spall (see Figure 4-32). The vertical stirrups did not yield because the stirrups were too widely spaced at 61 in. and unable to mobilize the tension force from the pile to the top reinforcement of the joint; this was also true for Tie T_{IJ} and Tie T_{AB}.
h) Tie T_{IJ} (116.4-kips) and Tie T_{LK} represent the vertical stirrups on the compression side of the pile face with an area of 1.24 in^2. The average strains for gauges SG1 and SG7 in vertical stirrups on the compression side was equal to 671 microstrains. The vertical stirrups in this case had a resisting force equal to only 25.8-kips, leaving approximately 73.3-kips to be resisted by the concrete, which was too high.

i) Tie T_{AB} (65.8-kips) represented the vertical stirrups on the tension side of the pile face with an area of 1.24 in^2. The average strain for gauges SG19 and SG25 in the vertical stirrups on the tension side was equal to 450 microstrains. The vertical stirrups in this case had a resisting force equal to only 17.3-kips, leaving approximately 48.5-kips to be resisted by the concrete. This high tension force caused tension failure in the slab surface.

5.3.2 Strut Verification

The effective compressive strength of the concrete f_{ce} shall be taken as[13]:

$$f_{ce} = \phi\, 0.85 \beta_s \cdot f'_c \qquad \text{Equation 5-4}$$

The strength reduction factor ϕ was taken as 1.0 to check the existing design, and 0.75 for the new design. βs is the strut strength factors and is taken as 0.75 for the critical struts, to account for the spreading effect. Based on the concrete strength of the slab, as shown in Table 3-1 and Equation 5-4, the permissible compressive strength of struts is equal to f_{ce} =2.9-kips.

Strut C_{GH} (511-kips) was an important strut; this strut was chosen because it was considered as the main diagonal strut in the model (see Figure 5-4 and Table 5-2). Other researchers have also determined this strut to be the most critical[1,24] and have suggested to calculate the stress at mid-height of the joint. The area for C_{GH} was calculated at Node G. The effective strut width on one side of Node G was taken as half the horizontal distance between Node G and Node E[4] (9.27 in.), meaning this distance also extended to the left of Node G. The thickness of the strut at Node H was 25.91 in., which was determined as the pile diameter at point W (24 in.) plus the width due to force spreading between Node W and Node H (1.91 in). The computed Strut C_{GH} stresses for the specimen was 2.13-ksi, less than the permissible compressive strength (2.9-ksi).

5.3.3 The Design Shortages of Specimen FSRCC24

Based on the experimental test results of specimen FSRCC24, which were discussed in Section 4.5, and the STM of FSRCC24, the following issues need modification for the pile-slab joint based on the experimental and analytical results:

- Yielding of the longitudinal reinforcement occurred in the slab before the ultimate force in the pile. Based on Caltrans guidelines, the slab is to be elastic when the pile reaches the ultimate load. The design concept of the slab was based on $(M_n)_{slab}=1.2(M_u)_{pile}$. Despite this, the longitudinal reinforcement of the slab yielded. This means the slab needed more reinforcement and better detailing.
- There were no vertical stirrups or j-bars into the joint to transfer force from the pile to the top part of the slab. The existence of such stirrups or j-bars would sustain the force of Tie T_{CD} (343.6-kips) which was 68% of the pile load.
- Vertical stirrups were not distributed properly. The vertical stirrups were too widely spaced. For better force transfer, additional stirrups with smaller spacing were needed near the pile.

5.4 Design of Specimen FSRCC24-M

Specimen FSRCC24-M was designed based on the experimental results of specimen FSRCC24 and the STM. The pile capacity in the STM was increased by 1.2(Mu) of its

capacity, then the internal forces were calculated based on this factored force. The coordinates of the nodes and the forces in the STM are shown in Table 5-1 and Table 5-3, respectively. From the section analysis results, using XTRACT[16] program of the 24 in. diameter pile, the pile tension force T_p (507.5-kips) was determined. Equation 5-5 is the same as that developed by Priestley *et al.*[23], except that the constant was changed from 0.50 to 0.53 to be consistent with the XTRACT[16] results.

$$T_p = 0.53 A_{SC} \lambda_a f_{yc} \qquad \text{Equation 5-5}$$

where, A_{sc}, λ_a and f_{yc} are the total pile longitudinal bar area, over strength factor of the pile longitudinal reinforcement from the rebar test (1.57), and yield strength of pile longitudinal bars (67-ksi), respectively.

5.4.1 Additional Reinforcement in Slab Top

The formation of Strut C_{GI} imposes tension demand in the top reinforcement resulting from the clamping mechanism (see Figure 5-4). The additional force from Table 5-3 over the slab moment was equal to T_{IC}-T_{IL}=409.6-163.2=246.4-kips=0.485 T_p. Based on Equation 5-5, the area of the additional longitudinal reinforcement in the top part of the beam, A_{tb}, was calculated as:

$$A_{tb} = (0.485) \times 0.53 \times A_{sc}\, \lambda_a \frac{f_{yc}}{f_{yb}} = 0.257 \times A_{sc}\, \lambda_a \frac{f_{yc}}{f_{yb}}$$

A_{tb}=0.257×9×1.57×1.13=4.1 in^2

where f_{yb}=yield strength of beam longitudinal reinforcement

5.4.2 Additional Reinforcement in Slab Bottom

The formation of Strut C_{EB} imposes tension demand in the bottom reinforcement resulting from the clamping mechanism (see Figure 5-4). The additional force equals T_{HB}-T_{BR}=(405.7-137.4)=268.3kip= 0.53 T_p. Based on Equation 5-5, the area of the additional longitudinal reinforcement in the bottom part of the beam A_{bb} was calculated as:

$$A_{bb} = (0.53) \times 0.53 \times A_{sc}\, \lambda_a \frac{f_{yc}}{f_{yb}} = 0.28 \times A_{sc}\, \lambda_a \frac{f_{yc}}{f_{yb}}$$

A_{bb}=0.28×9×1.57×1.13=4.47in^2

Priestley *et al.*[23] recommended extending the reinforcement to a distance not less than $\frac{D}{2} + l_a$ from both sides of the pile. For more convenience the additional top and bottom reinforcement was the same, five #8. This reinforcement should be placed in both the longitudinal and transverse directions of the bridge, as shown in Figure 2-10.

5.4.3 Area of the Vertical Joint Stirrup Reinforcement

In the current design recommendation there are no j-bars in the joint, and vertical stirrups are far away from the pile to transfer force from the pile to the top part of the slab (Splice Transfer Mechanism). The existence of such stirrups or j-bars would help to carry the force of Tie $(T_{CD})_{1.2Mp}$ = 381.6-kips, which is 75% of the pile unfactored tension force. Based on Equation 2, the area of the joint vertical stirrups A_{js} was calculated as:

$$A_{js} = 0.75 \times 0.53 \times A_{sc}\, \lambda_a \frac{f_{yc}}{f_{yv}} = 0.4 \times A_{sc}\, \lambda_a \frac{f_{yc}}{f_{yv}}$$

$A_{js}=0.4\times9\times1.57\times1.1=6.2$ in^2
where f_{yv} =yield strength of vertical stirrups.

The location of Tie T_{CD} changes depends on the loading directions; therefore, the area of the additional vertical stirrups should be twice A_{js}, 4 sets of (6# 6 j-bars plus #5 stirrups), as shown in Figure 2-11.

5.4.4 Area of the additional stirrups on the pile face

The splice transfer mechanism imposed additional tension demand in the vertical direction in the beam region adjacent to the pile compression face. This demand could be quantified using the STM and the experimental results of specimen FSRCC24. The factored force in Tie T_{IJ}, which represents the vertical stirrups was equal to 139.6-kips. The area of the additional stirrups was equal to (139.6)/60=2.32 in^2. To fulfill the required steel area of the modified specimen, 2#5 two legged stirrups (each side of the pile) were placed in addition to the existing 2#5 vertical stirrups. Priestley *et al.*, 1996[23] and Sritharan, 2005[25], recommended spreading these stirrups at a distance of not more than the beam height to the pile face. The width of those stirrups was equal to minimum bent cap width $B_{cap}=D_c+2$ (ft) =48 in. The reinforcement details for specimen FSRCC24-M are shown in Figure 2-10.

5.5 Strut-and-Tie Model for Knee-joint

The STM for specimen DCKJ24 was developed using measured joint strains and experimental observations. Based on the STM for specimens DCKJ24 and FSKJ24, specimen FSKJ24-M was designed. The behavior of the specimen was different in the opening and closing case. The following steps illustrate the process in order to develop the STM for DCKJ24.

5.5.1 Boundary Forces

The STM was developed for the full specimen, not just the pile-slab connection region. The first step in developing the model was to determine the magnitude and location of the boundary forces. There were two positions where the internal boundary should be known. The first position was the surface of the pile-slab interface; the location was at the slab at a distance equal to (h_b/2) from the pile face, where h_b is the slab thickness. These boundary forces were determined at the ultimate lateral load condition. The second step was to transfer the moments which act on the joint boundaries to compression and tension forces. Moment curvature software XTRACT[16] was used to determine the tension, compression forces and the coordinates for the opening and closing case, as shown in Figure 5-20. The highest shear force in the closing case was equal to 20.61-kips at stage 6, and the highest shear force in the opening case was equal to 17.32-kips at stage 9, as mentioned in Section 4.6.2. The third step was to apply those loads on the specimen. The boundary conditions for the system, the z-coordinates, x-coordinates and the magnitude of the boundary forces are listed in Table 5-4 and Table 5-5, respectively.

5.5.2 Strut-and-Tie Model Development for DCKJ24

The following steps focus on node and member locations in the x-axis and z-axis, and how to determine each of them. Pile compression resultant, C_P, and the pile shear force, V_P, are applied to Node W, while the pile tension resultant, T_P, was applied to Node

D, as shown Figure 5-21 and Figure 5-22. Node D had the same x-coordinate as point F; the z-coordinate was defined in the following steps, and the external forces were applied at Node R, as shown Figure 5-21 and Figure 5-22.

1) Locate Nodes A and B coordinates:

The x-coordinate of Node A was chosen to be at a distance equal to one half the slab thickness of the pile face. The z-coordinate was found from the moment curvature analysis as mentioned in Section 5.5.1. Node A was meant to represent the tension centroid in the top part of the slab (Closing Moment) and the compression centroid in the bottom part of the slab (Opening Moment).

Node B had the same x-coordinate as Node A and was located at the tension centroid of the bottom reinforcement on the right side of the slab. The z-coordinate was calculated from the moment curvature analysis. Node B was meant to represent the compression centroid in the top part of the slab (Closing Moment) and the tension centroid in the bottom part of the slab (Opening Moment).

2) Locate Node D

The x-coordinate of Node D was located at the T_p resultant. The concept of locating the z-coordinate of Node D was the same as discussed in Section 5.2.3. Once Node D was located, Strut C_{DA} was determined.

3) Locate Node F, Node W and Node H

Node F had the same x-coordinate as point D; the z-coordinate of point F was considered as the centroid of the longitudinal bottom rebar of the slab. The x- and z-coordinates of Node W was located at the pile compression resultant centroid, $C_{P,}$ as determined in step 1. Strut C_{WH} represents the force resultant at Node W resulting from C_P and V_P. The z-coordinate of Node H was the z-coordinate of Node F. The x-coordinate of Node H was the resultant of Strut C_{HW} intersection with the Tie T_{BH}, as shown in Figure 5-23 and Figure 5-24.

4) Locate Nodes F, E and H

Node E had the same x-coordinate as point D; z-coordinate of point E was the half way point between Node D and Node H, while Node C had the same the z-coordinate as Node A and the same x-coordinate as node D, as shown in Figure 5-23 and Figure 5-24.

5) Locate Node G

The method of locating Node G was different in the closing moment than the opening moment case.

a) <u>Closing Moment Case:</u>

Node G had the same z-coordinate as Node D. The x-coordinate of Node G was the same as Node H. The magnitude of Tie T_{DG} was set based on the experimental results, as shown in Equation 5-6. Once Node G was located and the value of Tie T_{DG} became known from the equilibrium of Node I, Node C and D, then Strut $C_{CG,}$ Tie T_{DE}, and Strut C_{DH} were known. From the equilibrium of Node H, Strut C_{DH} and Tie T_{HN} were determined. At this stage the struts and ties of the pile-slab joint were known. For convenience, when the STM extended to the supports, z-coordinates of Nodes K and L were the same z-coordinate as Node A. Nodes J and M had the same x-coordinate as Node B.

b) <u>Opening Moment Case:</u>

Node G had the same z-coordinate as Node D. The x-coordinate of Node G was the same as Node H. The magnitude of Tie T_{DG} was designed based on Equation 5-6. Once

Node G was located and the value of Tie T_{DG} became known from the equilibrium of Node I, Nodes C and D, Strut C_{CG}, Strut C_{HD} and Strut C_{DB} were known. From the equilibrium of Node H, Strut C_{HG} and Tie T_{HB} were determined. At this stage the struts and ties of the pile-slab joint were known. For more convenience, when the STM extended to the supports, z-coordinates of Nodes K and L were the same z-coordinate as Node A. Nodes J and M had the same x-coordinate as Node B.

6) Node X and Y

The location of Nodes X and Y were determined based on the discussion shown in Section 5.6.2.4.

5.5.3 Measured Joint Reinforcement Force-Transfer Contributions

The peak measured strain values listed in Table 4-14 are provided in this section as plots in order to understand the various joint reinforcement component contributions to the force-transfer process (see Figure 5-25 to Figure 5-44).

5.5.3.1 Joint Stirrups

Measured strains recorded on the vertical and horizontal joint stirrups are plotted for specimen DCKJ24 in Figure 5-25 to Figure 5-32. It is evident from these plots that none of the vertical stirrups reached the yield limit, while strain gauge SG45 at 20 in. from the pile face yielded. The horizontal cap end ties shown in Figure 5-26 yielded early at load stage 12 N. The horizontal stirrups yielded at load stage 18N, as shown in Figure 5-28.

5.5.3.2 Pile Reinforcement

Measured strains for the pile longitudinal reinforcement for specimen DCKJ24 are shown in Figure 5-33 for the south cycle and Figure 5-34 for the north cycle. The joint/pile interface is represented as zero in the figures with a negative y-axis distance extending into the joint (slab), and a positive y-axis distance extending into the joint. The yield occurred at 8 in. from the pile-slab interface in the pile direction load stage 8N, as shown in Figure 5-34. Notice there is still an appreciable amount of strain in pile longitudinal reinforcement 8 in. into the bent cap. This indicates that the bars are still being developed, suggesting that Equation 5-2 is a good choice to represent the effective anchorage length. Similar plots for the pile transverse spirals extending into the joint generated from Table 4-14 are shown in Figure 5-35 and Figure 5-36 for the south and north cycles, respectively. Both plots show that the stirrups yielded at an early stage along the pile height and inside the joint.

5.5.3.3 Slab Reinforcement

Measured strains for reinforcement at the top and bottom of the slab are plotted along the slab length for various DCKJ24 load stages in Figure 5-37 to Figure 5-43. For the slab distance on the x-axis of these plots, zero indicates the joint center with negative x-axis values extending north along the slab and positive x-axis values extending south. The purpose of the plots was to indicate how the slab tension was transferred inside the joint. From Figure 5-37 to Figure 5-43, the yielding occurred in the bottom reinforcement of the slab at an early stage compared to the top reinforcement.

5.5.4 Strut-and-Tie Model Verification

5.5.4.1 Closing Moment Case

Ties Verification:

In this section, the experimentally developed strut-and-tie model is applied to the specimen at the ultimate lateral load determined at closing moment from the experimental test results. The ultimate lateral load, 20.61-kips, was recorded in stage 6 during the first excursion of (1.5Δy). To solve the STM, the value for Tie $T_{DG,}$ must be determined. Tie T_{DG} represents the force in the pile hoops and the force in the horizontal cap end ties, as shown in Figure 5-45.

$$T_{DG} = 2[N]A_H f_H + 4 \times A_{HC} f_{HC} \qquad \text{Equation 5-6}$$

where N is the number of hoops, A_H is the hoop reinforcement area and f_{sp} is the hoop stress. The "2" term in the equation accounts for two hoops in each pitch. The "4" term accounts for the number, and A_{HC} is the area of horizontal cap end ties; f_{sp} is its stress. The strut-and-tie model was applied to specimen DCKJ24 for the measured ultimate load during stage 6. The following steps summarize the verification of the model for each member:

a) Tie T_{DG} was adjusted to match the experimentally measured force in the pile hoops and the horizontal cap end ties. The average maximum strains of hoops were calculated from Table 4-14 based on the values of tension strain gauges SG8, SG10 and SG12 at load stage 6; the average of these were equal to 387 microstrains, and the average strain in the horizontal cap end ties was based on the values of the compression strain gauges SG33 and SG34 at load stage 6, which had an average value of 1494 microstrains. Tie T_{EG} was determined to be 34.6-kips, where Tie T_{EG} was calculated from Equation 5-6, using N = 7 hoops, $A_H = A_{HC} = 0.11$ in^2.
b) Tie T_{KL} (162.5-kips) represented the top reinforcement of the slab outside the pile-slab joint with an area of 2.64 in^2 and a strain of 2105 microstrains. Strain for gauge SG60 at load stage 6 was equal to 2197 microstrains, which agrees very well with the strut-and-tie model.
c) Tie T_{KA} (162.5-kips) represented the top reinforcement of the slab outside the pile-slab joint, with an area 2.64 in^2 and a strain of 2105 microstrains. Strain for gauge SG55 at load stage 6 equaled 2420 microstrains. Although this strain looks slightly higher than the predicted, this strain was in the range of yield plateau; therefore, the generated force due to this strain equaled 162.36-kips; this agrees very well with the predicted force of the strut-and-tie model.
d) Tie T_{IA} (201.2-kips) represented the top reinforcement of the slab inside the pile-slab joint. This force was the summation of the force in the top longitudinal rebar of the slab and the force in the 7#4 u-bars.
   -The top reinforcement of the slab had an area equal to 2.64 in^2. The average strains on gauges SG53, SG54, SG57 and SG58 at load stage 6 were equal to 1518 microstrains which gave a force equal to 117.4-kips.
   -The 7#4 u-bars had an area equal to 1.40 in^2. The strain for gauge SG71 at load stage 6 was equal to 1520 microstrains, which gave a force equal to 125.17-kips.

-The summation of the previous two forces was equal to 183.78-kips (117.40+66.38), which agrees well with the predicted force of the strut-and-tie model.

- Tie T_{CO} (185.2-kips) represented the top reinforcement of the slab inside the pile-slab joint. This force is the summation of the force in the top longitudinal rebar of the slab and the force in the 7#4 u-bars.
  -The top reinforcement of the slab had an area equal to 2.64 in^2. The strain for gauge SG56 at load stage 6 was equal to 1776 microstrains, which gave a force equal to 137.31-kips.
  -The 7#4 u-bars had an area equal to 1.40-in^2. The strain for gauge SG75 at load stage 6 was equal to 1461 microstrains, which gave a force equal to 62.67-kips.
  -The summation of the previous two forces was equal to 200-kips (137.31+62.67), which agrees well with the predicted force of the strut-and-tie model.
- Tie T_{NH} (129.0-kips) represented the bottom reinforcement of the slab inside the pile-slab joint. This force is a summation of the force in the top longitudinal rebar of the slab and the force in the 7#4 u-bars.
  -The top of the bottom reinforcement of the slab had an area equal to 2.64 in^2. The average strain for gauges SG61, SG62, SG66, and SG67 at load stage 6 was equal to 971 microstrains, which gave a force equal to 75.05-kips.
  -The 7#4 u-bars have an area equal to 1.40 in^2. The average strain for gauge SG72 at load stage 6 was equal to 1442 microstrains, which gave a force equal to 61.85-kips.
  -The summation of the previous two forces is equal to 136.9-kips (75.05+61.85), which agrees very well with the predicted force of the strut-and-tie model.
- Tie T_{AB} (11.30-kips) represented the vertical stirrup on the internal side of the pile face with an area of 2 in^2 and a strain of 189 microstrains. The average strain for gauges SG48 and SG50 at load stage 6 was equal to 167 microstrains, which agrees with the strut-and-tie model.
- Tie T_{ON} (44.7-kips) represented the force in the vertical stirrups (vertical u-bars) on the outside part of the pile face. Unfortunately, there were no strain gauges in the u-bars in the vertical direction.
- Tie T_{CD} (26.7-kips) and Tie T_{XY} (48.6-kips) represented the vertical stirrups in the joint region. The vertical stirrups area was 2.40 in^2 and the average strain for gauges SG37 and SG39 at load stage 6 was equal to 407 microstrains or 30.2-kips. The strain in the stirrups was low, and no cracks occurred; this means that the remaining force was resisted by the concrete ties.

5.5.4.2 Opening Moment Case:

Ties Verification:

In this section, the experimentally developed strut-and-tie model was applied to the specimen at the ultimate lateral load determined for the opening moment from the experimental test results. The ultimate lateral load at opening case was 17.32-kips at stage 9 ($4\Delta y$). The following steps summarize the verification of the model for each member:

- Tie T_{DG} was adjusted to match the experimentally measured force in the pile hoops and the horizontal cap end ties. The average maximum strains of hoops were calculated from Table 4-14 based on the tension strain gauges SG8, SG10 and SG12 at load stage 9; the average equaled 1117 microstrains. The average strain in the

horizontal cap end ties was based on the values of the strain gauges SG33 and SG34 at load stage 9 which was equal to 1810 microstrains. Tie T_{DG} was calculated from Equation 5-6, N=7 hoops, $A_H = A_{HC} = 0.11$ in^2. Tie T_{DG} was determined to be 74.94-kips (23.78+51.16).

- Tie T_{MJ} (153.2-kips) represented the bottom reinforcement of the slab outside the pile-slab joint with an area of 2.64 in^2 and a strain of 1980 microstrains. Strain for gauge SG65 at load stage 9 was 2164 microstrains, which agrees well with the strut-and-tie model.
- Tie T_{BJ} (153.2-kips) represented the bottom reinforcement of the slab outside the pile-slab joint with an area of 2.64 in^2 and a strain of 1980 microstrains. Strain for gauge SG69 at load stage 9 was 1942 microstrains, which agrees very well with the predicted strut-and-tie model.
- Tie T_{BH} (182.4-kips) represented the bottom reinforcement of the slab inside the pile-slab joint. This force is the summation of the force in the top longitudinal rebar of the slab and the force in the 7#4 u-bars.

  -The bottom reinforcement of the slab had an area equal to 2.64 in^2. The average strain for gauges SG61, SG62, SG66 and SG67 at load stage 9 was 1350 microstrains, which gave a force of 104.37-kips.

  -The 7#4 u-bars had an area equal to 1.40 in^2. The average strain for gauge SG72 at load stage 9 was 1089 microstrains, which gave a force of 47.34-kips.

  -The summation of the previous two forces was equal to 151.71-kips (104.37+47.34), which is less than the predicted strut-and-tie model results.
- Tie T_{AB} (18.6-kips) represented the vertical stirrup on the internal side of the pile face with an area of 2 in^2 and a strain of 300 microstrains. The average strain for gauges SG48 and SG50 at load stage 9 was 282 microstrains, which agrees very well with the strut-and-tie model results.
- Tie T_{CD} (36-kips) and Tie T_{XY} (19.3-kips) represented the vertical stirrups in the joint region. The vertical stirrups area was 2.4 in^2, and the average strain for gauges SG37 and SG39 at load stage 9 was 751 microstrains; this was equal to 53.7-kips, which agrees very well with the expected force from the STM.

5.5.4.3 Strut Verification

Based on concrete strength of the slab, Table 3-1 and Equation 5-4, the permissible compressive strength of struts is equal to f_{ce}=2.83-kips.

Strut C_{DH} (248.1-kips) in the opening case is an important strut; this strut was chosen because it is considered the main diagonal strut in the model (see Figure 5-24 and Table 5-4). Other researchers have also determined this strut to be the most critical[1,24] and have suggested to calculate the stress at mid-height of the joint. The area for C_{DH} was calculated at Node D. The effective strut width on one side of Node D was taken as half the horizontal distance between Node D and Node G[4] (7.82 in.), meaning this distance also extended to the left of Node D. The thickness of the strut at Node H equaled (17.93 in.), which equaled the pile diameter at point W (16 in.) plus width due force spreading between Node W and Node H (1.93 in.). The computed Strut C_{DH} stresses for the specimen was 1.77-ksi, less than the permissible compressive strength (2.83-ksi).

5.6 Strut-and-Tie Model for FSKJ24

5.6.1 Boundary Forces

The procedures to find the boundary forces for FSKJ24 were the same as DCKJ24. The highest shear force in the closing case was equal to 16.85-kips at stage 6, and the highest shear force in the opening case was equal to 13.54-kips at stage 7.

5.6.2 Measured Joint Reinforcement Force-Transfer Contributions

The peak measured strain values listed in Table 4-17 are provided in this section as plots, in order to understand the various joint reinforcement component contributions to the force-transfer process (see Figure 5-46 to Figure 5-65).

5.6.2.1 Joint Stirrups

Measured strains recorded on the vertical and horizontal joint stirrups plotted verses the load cycle for specimen FSKJ24 are shown in Figure 5-46 to Figure 5-53. The loading direction and strain gauge identification are indicated on the figures. It is evident from these plots that none of the vertical stirrups yielded, although some of them showed high strain. The horizontal stirrups showed high strain, where strain gauges SG44 and SG46 at 5 in. from the pile face yielded.

5.6.2.2 Pile Reinforcement

Measured strains for the pile longitudinal reinforcement for specimen FSKJ24 are shown in Figure 5-54 for the south cycle and Figure 5-55 for the north cycle. The joint/pile interface was represented as zero in the figures with a negative y-axis distance extending into the joint (slab) and a positive y-axis distance extending into the joint. In general, the maximum strains occurred inside the joint at 8 in. from the pile-slab interface; this indicates that the bars were still being developed into the joint, suggesting that Equation 5-2 is a good choice to represent the effective anchorage length. All the strain gauges along the longitudinal reinforcement of the pile yielded. Similar plots for the pile transverse spirals extending into the joint were generated from Table 4-17, and are shown in Figure 5-56 and Figure 5-57 for the south and north cycles, respectively. None of the strain gauge in the stirrups yielded except the strain gauge at 8 in. inside the slab at load cycle 20N.

5.6.2.3 Slab Reinforcement

Measured strains for reinforcement at the top and bottom of the slab are plotted along the slab length for various FSKJ24 load stages in Figure 5-58 to Figure 5-65. For the slab distance on the x-axis of these plots, zero indicates the joint center, with negative x-axis values extending north along the slab and positive x-axis values extending south. Figure 5-58 to Figure 5-61 show that the bottom longitudinal bars yielded at different locations. Figure 5-62 to Figure 5-65 show also that top longitudinal bars yielded at different locations.

5.6.2.4 Joint Cracks Development

Based on the discussion and the experimental observations, which were provided in Section 4.7.1 for this specimen, the lateral load capacity was governed by the

development of large diagonal joint cracks. As a result of load reversal, the inclined cracks spread across the two sides of the slab. The vertical reinforcement crossing these cracks were insufficient to keep the cracks' width small. These cracks limited the ability of force transfer in the joint. Cracks altered the ability of struts which cross these cracks to anchor the pile tension force. Cover separation from the slab reduced the moment arm between the compression and tension force resultants and caused the magnitudes of these resultants to increase in order to compensate. Since the slab reinforcement was limited in its ability to provide moment resistance, it would be expected that the specimen would experience a drop in lateral load. This drop in lateral load was observed during stage 7 ($2\Delta y$) for the closing moment, while the drop was observed for the opening moment during stage 6 ($1.5\Delta y$), as shown in Section 4.7.2.

a) Closing Moment Case

From the experimental observations for specimen FSKJ24 diagonal cracks due to tension force are shown in Figure 4-53. To predict the tension demand resulting from the above described situation, Strut C_{NE} was considered bottle-shaped as shown in Figure 5-66. In this figure, Tie T_{XY} represents the splitting tension resulting from spreading, and θ represents the spreading angle determined by assuming Strut C_{EX} is horizontal. Determining θ in this manner results in a spread angle smaller than the 2:1 ratio recommend in literature[25]. The final STM for the closing case is shown in Figure 5-67. When comparing the initial joint crack formation for the specimen, the cracking pattern suggests that tension perpendicular to Strut C_{NE} caused the crack to develop. A likely cause of this tension was the result from Strut C_{NE} spreading into the joint. Based on the strut-and-tie model shown in Figure 5-67, this compression force must be used to anchor a significant portion of the pile tension; this required Strut C_{NE} to be redirected by Tie $T_{ON,}$ thus requiring the strut to spread up to Node E.

b) Opening Moment Case

From the experimental observations in the opening case, the diagonal joint crack developed near Node D and traveled nearly parallel to the Strut C_{AD} (see Figure 4-53). When comparing the initial joint crack formation for the specimen, the cracking pattern suggests that tension perpendicular to Strut C_{DA} caused the crack to develop. A likely cause of this tension is a result of Strut C_{DA} spreading into the joint. Based on the strut-and-tie model shown in Figure 5-68, this compression force must be used to anchor a significant portion of the pile tension; this required Strut C_{DA} to be redirected by Tie T_{AB}, thus requiring the strut to spread up to Node D.

5.6.3 Strut-and-Tie Model Verification

5.6.3.1 Closing Moment Case

Ties Verification:

In this section, the experimentally developed strut-and-tie model is applied to the specimen at the ultimate lateral load determined at closing moment from the experimental test results. The ultimate lateral load, 16.85-kips, was recorded in stage 6 during the first excursion of ($1.5\Delta y$). To solve the STM, the value for Tie T_{EG} must be determined. Tie T_{EG} represented the force in the pile hoops and the force in the horizontal cap end ties (Equation 5-6). The strut-and-tie model was applied to specimen FSKJ24 for the measured ultimate load during stage 6. The following steps summarize the verification of the model for each member:

a) Tie T_{DG} was adjusted to match the experimentally measured force in the pile hoops and the horizontal cap end ties. The average maximum strains of hoops were calculated from Table 4-17 based on the maximum strain values in gauges SG2, SG4, SG6, SG10 and SG12 at load stage 6. The average was 477 microstrains. The average maximum strain in the horizontal cap end ties was based on the values of gauges SG33, SG34 and SG35 at load stage 6, which was 924 microstrains. Tie T_{DG} was determined to be 22.0-kips, where Tie T_{DG} was calculated from Equation 5-5, using N = 3 hoops, $A_H = A_{HC} = 0.11$ in^2.

b) Tie T_{KL} (268.5-kips) represented the top reinforcement of the slab outside the pile-slab joint at 20 in. from the joint center with an area of 4.4 in^2 and a strain of 2081 microstrains. Strain for gauge SG60 at load stage 6 was 2111 microstrains, which agrees very well with the strut-and-tie model.

c) Tie T_{KA} (268.5-kips) represented the top reinforcement of the slab outside the pile-slab joint at 34 in. from the joint center, with an area of 4.4 in^2 and a strain of 2081 microstrains. Strain for SG55 at load stage 6 were equal to 3116. The generated force due to this strain was equal to 270.6-kips, which agrees with the strut-and-tie model.

d) Tie T_{IA} (339.3-kips) represented the top reinforcement of the slab inside the pile-slab joint. This force was the summation of the force in the top longitudinal rebar of the slab and the force in the 7#4 u-bars.

   -The top reinforcement of the slab had an area equal to 4.4 in^2. The force generated due to strain readings on gauges SG53, SG54 and SG58 at load stage 6 was 298.6-kips.

   -The 7#4 u-bars had an area equal to 1.40 in^2. The average strain for gauges SG71 and SG74 at load stage 6 was 1734 microstrains, which had a force of 74.37-kips.

   -The summation of the previous two forces was 37.92-kips, which agrees well with the strut-and-tie model.

e) Tie T_{CO} (326.7-kips) represented the top reinforcement of the slab inside the pile-slab joint. This force was the summation of the force in the top longitudinal rebar of the slab and the force in the 7#4 u-bars.

   -The top reinforcement of the slab had an area equal to 4.4 in^2. The average strain for gauges SG52 and SG56 at load stage 6 was equal to 1868 microstrains, which gave a force equal to 240.50-kips.

   -The 7#4 u-bars have an area equal to 1.40 in^2. The average strain for gauges SG70 and SG75 at load stage 6 was 2265 microstrains, which gave a force of 90-kips.

   -The summation of the previous two forces was equal to 330.50-kips, which agrees very well with the strut-and-tie model.

f) Tie T_{YH} (355.8-kips) represented the bottom reinforcement of the slab inside the pile-slab joint. This force was the summation of the force in the top longitudinal rebar of the slab and the force in the 7#4 u-bars.

   -The bottom reinforcement of the slab had an area equal to 4.4 in^2. The average strain for gauge SG61, SG66 and SG67 at load stage 6 was 1972 microstrains, which gave a force of 254.15-kips.

   -The 7#4 u-bars had an area equal to 1.40 in^2. The average strain for gauge SG72 and SG73 at load stage 6 was 1770 microstrains, which gave a force of 76.96-kips.

   -The summation of the previous two forces was equal to 335.11-kips, which agrees very well with the results from the strut-and-tie model.

g) Tie T_{AB} (20.1-kips) represented the vertical stirrup on the internal side of the pile face with an area of 1.86 in^2 and a strain of 349 microstrains. The average strain for SG50 at load stage 6 was 701 microstrains, which was more than the expected strain using the strut-and-tie model.
h) Tie T_{ON} (62.1-kips) and Tie T_{XY} (63-kips) represented the vertical stirrup and the u-bars on the external side of the pile face with an area of 1.24 in^2 for the vertical stirrup and 1.4 in^2 for the u-bars. The average strain was 1388 microstrains. The average strain for gauges SG37 and SG39 at load stage 6 was 856 microstrains, which means that 70.16-kips was transferred by the vertical stirrups leaving 54.94-kips to be transferred by the concrete. Tension demands from splitting Strut $C_{NE,}$ represented by Tie T_{XY} = 63-kips, contributed to the concrete tension demand of Tie T_{CD} to develop the horizontal joint crack shown in Figures 4-53 and Figure 5-67. Providing adequate reinforcement for Tie T_{NO} and T_{XY} would allow force transfer across the crack by keeping the crack width small.

5.6.3.2 Opening Moment Case

Ties Verification:

In this section, the experimentally developed strut-and-tie model is applied to the specimen at the ultimate lateral load determined for the opening moment from the experimental test results. The ultimate lateral load at the opening case was 13.54-kips at load stage 7 (2 Δy).

a) Tie T_{DG} was adjusted to match the experimentally measured force in the pile hoops and the horizontal cap end ties. The average maximum strain for the hoops was calculated from Table 4-17 based on the values of gauges SG2, SG4, SG6, SG10 and SG12 at load stage 7, which was 736 microstrains. The average strain in the horizontal cap end ties was based on the values of gauges SG33, SG34 and SG35 at load stage 7, which was equal to 712 microstrains. Tie T_{DG} was determined to be 23.86-kips. Where Tie T_{DG} was calculated from Equation 4, using N = 3 hoops, A_H = A_{HC} = 0.11 in^2.
b) Tie T_{JM} (209.4-kips) represented the bottom reinforcement of the slab outside the pile-slab joint with an area of 4.4 in^2 and a strain of 1627 microstrains. Strain for gauges SG65 at load stage 7 was 1810 microstrains, which agrees well with the predicted results of the strut-and-tie model.
c) Tie T_{BJ} (209.4-kips) represented the bottom reinforcement of the slab outside the pile-slab joint with an area of 4.4 in^2 and a strain of 1627 microstrains. The strain for gauges SG64 and SG69 at load stage 7 was 1968 microstrains, which is bigger than the predicted strut-and-tie model.
d) Tie T_{HB} (333.8-kips) represented the top reinforcement of the slab inside the pile-slab joint. This force was the summation of the force in the top longitudinal rebar of the slab and the force in the 7#4 u-bars.
   -The top reinforcement of the slab had an area equal to 4.4 in^2. The average strain for gauges SG63, SG67 and SG68 at load stage 7 was 1897 microstrains, which equates to a force of 244.4-kips.
   -The 7#4 u-bars had an area equal to 1.40 in^2. The average strain for gauges SG71 and SG74 at load stage 7 was 1692 microstrains, which gave a force of 72.6-kips.

-The summation of the previous two force is equal to 317-kips which agrees very well with the strut-and-tie model.

e) Tie T_{AB} (50.8-kips) and Tie T_{XY} (52.9-kips) represented the vertical stirrup on the internal side of the pile face with an area of 1.86 in^2 and a strain of 1763 microstrains. The average strain for gauge SG50 at load stage 7 was 872 microstrains. The measure strain equated to 46.22-kips, leaving approximately 57.48-kips to be resisted by concrete ties. Tension demands from splitting Strut $C_{AD,}$ represented by Tie T_{XY}(52.9-kips), contributed to the concrete tension demand of Tie T_{CD} to develop the horizontal joint crack shown in Figures 4-53 and Figure 5-68. In any case, providing adequate reinforcement for Tie T_{CD} and T_{XY} would allow force transfer across the crack by keeping the crack width small.

5.6.3.3 Strut Verification

Based on concrete strength of the slab, Table 3-1 and Equation 5-4, the permissible compressive strength of struts is equal to f_{ce}=2.93-kips.

Strut C_{DH} (348.9-kips) in the opening case was an important strut; this strut was chosen because it was considered the main diagonal strut in the model (see Figure 5-68 and Table 5-7). Other researchers have also determined this strut to be the most critical[1,24] and have suggested to calculate the stress at mid-height of the joint. The area for C_{DH} was calculated at Node D. The effective strut width on one side of Node D was taken as half the horizontal distance between Node D and Node G[4] (9.3 in.), meaning this distance also extended to the left of Node D. The thickness of the strut at Node H equals (17.75-in.), which equals the pile diameter at point W (16 in.) plus width due force spreading between Node W and Node H (1.75 in.). The computed Strut C_{DH} stresses for the specimen is 2.11-ksi, less than the permissible compressive strength (2.93-ksi).

5.7 Design of Specimen FSKJ24-M

The design of the proposed flat slab knee-joint specimen was based on the experimental results of the previous two tests, DCKJ24 and FSKJ24, the STM, and previous research[4,23,26]. The flat slab knee-joint FSKJ24 failed mainly due to damage in the slab. The primary reasons were lack of flexural slab reinforcement and the lack of the vertical reinforcement to transfer the force from the pile longitudinal reinforcement to the longitudinal reinforcement of the slab.

5.7.1 Design Modification

The following issues need modification for the pile-slab joint based on the experimental and analytical results:

a) Width of the slab,
b) Load distribution method,
c) Slab thickness,
d) Lack of j-bars or vertical stirrups reinforcement, and
e) Yielding of slab reinforcement.

5.7.1.1 Width of the slab

In order to develop the struts force outside the joint bigger slab width was used. The width of specimen FSKJ24 (48 in.) was chosen based on Equation 2-4, which equaled the minimum bent cap width. The method for the effective width calculation for the new

specimen FSKJ24-M was the same as the width for the flat slab T-joints, where the slab width was to chosen to be twice the effective width of the beam. The effective beam width was considered to be the same as the width of the stirrups in the transverse direction of the bridge. The prototype width was 104 in. (2(52)) and the scaled width was 70 in.

5.7.1.2 Better load distribution method.

In order to make the dead load distribution closer to the actual distribution, two loading points were used for FSKJ24-M instead of using a single loading point, as in FSJK24 and DCKJ24 (see Figure 3-13).

5.7.1.3 Slab Thickness

The smallest thickness for the slab which can satisfy the punching shear requirements shown in Section 2.6 was 16.5 in. (prototype). The STM stress limits do not take into account confinement, plus the calculation of strut and node areas is extremely complicated. The concrete inside the pile core is highly confined, so it was decide to depend only on the punching shear to choose the slab thickness. The reinforcement was designed based on the STM for the 16.5 in. slab. The coordinates of the nodes and the forces in the modified STM are shown in Table 5-1 and Figure 5-2, respectively.

5.7.1.4 Specimen Reinforcement

The pile capacity in the STM was increased by 1.2 to determine the internal forces.

1- Additional longitudinal reinforcement in slab.

From Figure 5-69 and Table 5-8, it was observed that the formation of Strut C_{DH} (Opening Moment) imposed tension demand in the bottom reinforcement resulting from the clamping mechanism. The force, over the slab moment, was equal to T_{HB} (522-kips). The area of the slab reinforcement was 8.7 in^2 (522-kips/60 ksi). The area of the required longitudinal reinforcement was 7.1 in^2 (8.7-in^2 – 8 Vertical U bars # 4), therefore 12#7 was the total reinforcement in the bottom side of the slab; this means that 7#7 additional reinforcement was used. The maximum force in the top reinforcement of the slab was in Tie T_{CI} (336.9-kips). In order to make the section symmetric, the same reinforcement was used in the top. Based on the recommendations of the previous researches[23], the same amount of additional reinforcement, 7#7, was placed in the transverse direction.

2- Area of the vertical joint stirrup reinforcement

The stirrups on the pile face showed low strain compared to what the STM predicted; this was because the stirrups were far away from the pile. The opening moment was the most critical case where the splice transfer mechanism for Struts C_{YA} and C_{DB} imposed additional tension demand on Tie T_{AB} adjacent to the pile tension face(see Figure 5-69). This demand could be quantified using the STM. Based on the STM results in the opening case, Tie T_{DC} (9-kips) and Tie T_{XY} (73.1-kips) represented the j-bars on the internal side of the pile face. The total force on the pile face was equal to 80.1-kips (9+73.1). The area of the required vertical joint stirrup reinforcement was calculated as 1.34 in^2 (80.1-kips/60 ksi); therefore 12#3 j-bars were placed on each side of the joint. The j-bars were spread at 18 in. from the pile center.

For the vertical force on the pile face, T_{AB} (72.8-kips), the opening moment case also was the governing case. From Section 5.5.4.2, the current vertical reinforcement in Tie

T_{AB} position was able to resist 18.6-kips force. The additional reinforcement needed was 9 in^2 ((72.8-18.6)/60), therefore 2#4 two branch stirrups were used on each side of the joint.

3- Shear Reinforcement Details

Based on Caltrans recommendations for designing the knee-joint, there were two cases for the joint detailing:

i. 'S' < $D_c/2$

ii. 'S' < L_d or 'S' < D_c

where

S=Distance between the pile face and the cantilever edge of the specimen

D_c=Column/Pile Diameter

L_d= Straight bar develop length for the main bent cap reinforcement

Therefore, the first case was used for design, where S= Dc/2=8 in.

(a) Bent cap top and bottom reinforcement within the bent cap width shall be in the form of continuous u-bars[5]. This reinforcement shall be a minimum of 33% of the total area of pile reinforcement anchored in the joint A_{st}, (9#6).

$$A_s^{u-bar}\ \min\ = 0.33 \times A_{st} \qquad \text{Equation 5-7}$$

Based on Equation 5-7, 8#4 was used as vertical u-bars.

(b) Vertical Stirrups[5]:

$$A_s^{jv} = 0.2 \times A_{st} \qquad \text{Equation 5-8}$$

Vertical stirrups should be placed transversely within a distance 0.5 D_c from the interior face of the pile[1,8]. Based on Equation 5-8, 4#3 as vertical stirrups @8" distance from the internal face of the pile were placed.

(c) Horizontal Stirrups[5]:

BDC[5] states that the horizontal stirrups or ties shall be placed transversely around the vertical stirrups or ties in two or more intermediate layers spaced vertically at not more than 18 in.

$$A_s^{jh} = 0.1 \times A_{st} \qquad \text{Equation 5-9}$$

Based on Equation 5-9, 2#4 horizontal stirrups were placed transversely around the vertical stirrups.

(d) Horizontal Side Reinforcement[5]:

BDC[5] states that the total longitudinal side face reinforcement A_s^{sf} in the bent cap shall be at least equal to the greater of the areas specified in Equation 5-10.

$$A_s^{sf} \geq \begin{cases} 0.1 \times A_{cap}^{top} \\ \text{or} \\ 0.1 \times A_{cap}^{bot} \end{cases} \qquad \text{Equation 5-10}$$

A_{cap} = Area of bent cap top or bottom flexural steel

Therefore, 2#6 stirrups were placed near the side faces of the bent cap with a maximum spacing of 12 in.

(e) Horizontal Cap End Ties[5]:

BDC[5] states that the Horizontal ties placed at the end of the bent cap shall be equal to the area specified in Equation 5-11.

$$A_s^{jhc} = 0.33 \times A_s^{u-bar} \min \qquad \text{Equation 5-11}$$

Therefore, 4#3(0.44 in^2) was placed around the intersection of the bent cap horizontal side reinforcement and the continuous bent cap U-bar reinforcement, spaced at not more than 12 in. vertically and horizontally.

(f) Transverse Reinforcement[5]

Transverse reinforcement in the joint region shall consist of #4@2- in hoops with a minimum reinforcement ratio specified by Equation 5-12.

$$\rho_s = 0.6 \times \frac{\rho_l \cdot D_c}{l_{ac}} \qquad \text{Equation 5-12}$$

5.8 Summary and Conclusions

This chapter presented the development of strut-and-tie models to explain the force transfer that occurs in the joint connecting the slab bridge superstructure to the substructure. Strain measurements on joint reinforcement of three specimens were used to develop the strut-and-tie models capable of handling numerous loading situations. Based on the work of this chapter, three primary issues become apparent with the current design method of Caltrans.

First, although the slab moment capacity was designed based on Caltrans Seismic Design Criteria[5], where the slab moment capacity was 1.2 times the moment capacity of the pile, as discussed previously in Section 2.5, the slab failed in specimens FSRCC24 and FSKJ24. This means that Equation 2-12 is not sufficient enough to keep the slab elastic while the pile reaches the failure mode. Additional flexure reinforcement in the slab is needed. Caltrans Seismic Criteria[5] did not specify the effective width of the slab section where the moment capacity should be calculated or where the additional flexural reinforcement should be added.

The second issue with current joints design methods was large cracking in the slab. The cracking occurred due to high tension demands resulting from the pile tension being transferred to the longitudinal reinforcement of the slab in the T-joint, as mentioned in Section 5.3.3. The flat slab knee-joint cracking in the slab was due to the potential splitting of the slab compression strut on the positive moment side of the joint, as mentioned in Section 5.6.2.4. Therefore, it is necessary to provide additional vertical reinforcement to account for this tension. Providing vertical reinforcement at the joint top will limit crack widths. Currently, Caltrans Seismic Criteria[5] of Caltrans only requires vertical reinforcement in the pile core region for skew bridges. Priestley, M.J.N[23] recommended providing an amount of vertical reinforcement in the pile core region for transferring 50% of the column tension. Based on the experimental results in the current research, the ratio of the transferred force from the pile to the slab longitudinal reinforcement is more than 50%. This will be discussed in detail in Chapter 6.

Third, the distance between the two legs of the vertical stirrups were too wide, so the force transfer through the vertical stirrups was not sufficient. Additional less wide vertical stirrups on the pile face region is recommended, where the stirrups width should not be more than the minimum bent cap width mentioned in Equation 2-4. The experimentally developed strut-and-tie models for the T-joints presented in this chapter indicate that the transferred force in the vertical stirrups on the negative moment side is higher than the force transferred on the positive moment side. This same observation was made by other researchers[6,23] investigating force transfer in the transverse direction. The

force in the negative side is the controlling force for the vertical stirrups on the pile face. From the STM for the knee-joint, the opening moment case is the governor for the vertical stirrups design.

Chapter 6
Modified Specimens

6.1 Introduction

In this chapter, observations of the experimental test of the modified specimens FSRCC24-M and FSKJ24-M, including the behavior and the damage propagation of each specimen, are discussed in detail. In addition, the measured results from each test are presented. Comparison between the performance of the original design and modified specimens are discussed in detail. The most represented data are discussed in this chapter while the less critical data are shown in Appendixes G and H.

6.2 FSRCC24-M Results

Failure occurred in specimen FSRCC24 in the slab; therefore, specimen FSRCC24-M was modified in order to keep the slab with minimum cracks while reaching failure in the pile.

6.2.1 Observed Response of the Specimen, FSRCC24-M

The experimental test occurred over two days. The first six load stages, which were force controlled, were completed on the first day. The remaining eight load stages, which were displacement, were control completed on the second day. The loading protocol is shown in Figure 3-16. Before starting the test, all the shrinkage cracks were marked to differentiate between the shrinkage cracks and cracks which occurred during the test. In order to make the cracks easier to see during the test, a water based primer mix was applied to the specimen.

The cracks during the first five stages were hairline cracks mainly in the pile, and no cracks were observed in the slab. When the specimen was taken to the first cycle of load stage 6 (0.75fy), a few hairline cracks spread in the slab around the pile and more hairline cracks spread in the bottom part of the pile, as shown in Figure 6-1. As the specimen was pushed to higher ductility (1Δy), more cracks spread at the pile base, and cracks spread in the slab around the pile, as shown in Figure 6-2. When the specimen was pushed to the second cycle of load stage 8 (2Δy), the cracks in the pile extended. A wide crack between the pile and the slab interface appeared, and hairline cracks spread in the slab (see Figure 6-3). During the second excursion of load stage 9 (2.5Δy), small parts of the concrete cover of the pile spalled off from one side, and more hairline cracks spread in the slab (see Figure 6-4). More concrete cover of the pile spalled off, and the hairline cracks in the slab extended more when the slab was pushed to ductility 3Δy, and then to 3.5Δy (see Figure 6-5 and Figure 6-6, respectively). As the specimen was pushed further to load stage 12 (4Δy), the spiral of the pile was exposed and concrete cover on the top surface of the slab spalled off, as shown in Figure 6-7. As the specimen was pushed to load stage 13(5Δy), more concrete cover spalled off the pile, and the slab reinforcement close to the pile became exposed, as shown in Figure 6-8. When the specimen was at the final load stage, load stage 14(6Δy), more concrete cover spalled off, and some cracks spread on the bottom side of the slab, as shown in Figure 6-9.

6.2.2 Force-Displacement Relationships

The corrected force-displacement hysteretic behavior for specimen FSRCC24-M is shown in Figure 6-10. Cycles in the north direction (positive sign) are pushing force,

while cycles in the south direction (negative sign) are pulling force. The following points summarize the force-displacement hysteretic behavior of specimen FSRCC24-M:

1- The force-displacement relationship was linear until it reached 50% of the yield force. The specimen was stiffer in the negative direction (pulling) rather than the positive direction (pushing). The force in the positive direction was equal to 13.28-kips, and the displacement was equal to 0.88 in. The force in the negative direction was equal to 19.37-kips, and the displacement was equal to 0.98 in.
2- At 0.75% of the yielding force, the shear force in the positive direction was equal to 19.93-kips, and the displacement was equal to 1.29 in. The force in the negative direction was equal to 28.97-kips, and the displacement was equal to 1.96 in.
3- At ductility level 1Δy, the force in the positive direction was equal to 31.85-kips, and the displacement was equal to 2.77 in. The force in the negative direction was equal to 40.05-kips, and the displacement was equal to 2.82 in.
4- The ultimate force in the positive direction 42.96-kips was at a ductility level 3.5Δy at 9.71 in. displacement. The ultimate force in the negative direction 44.68-kips was at a ductility level 3Δy, 8.24 in. displacement.
5- The force in the positive direction started decreasing after 3.5Δy, while in the negative direction, it started decreasing after ductility level 3Δy.
6- At the second cycle of load stage 13 (5Δy), the load dropped to 81.5% of the ultimate force in the positive direction, where the force at the second cycle of load stage 13 was equal to 34.10-kips at 13.07 in. displacement. In the negative direction, the load was dropped to 33.95-kips, 74.4% of the ultimate force at 13.07 in. Since the ultimate force dropped to less than 80% of the ultimate force, the specimen at this stage was considered failed.

The specimen was pushed farther to a ductility level of 6Δy. Table 6-1 includes the force, the displacement of the actuator and the average displacements of the string pots at each cycle. The string pots were used to check the readings of the actuator.

6.2.3 Strain Gauges Data

A review of the strain gauge data at load stage 4 (0.75fy) revealed that strain gauges SG77, SG81, SG83, SG85, SG86, SG89, SG91, SG95 and SG103 in the longitudinal reinforcement of pile reached the yield limit, while none of the slab reinforcement reached the yield limit. The ultimate load in the negative direction was at load stage 9 (2.5Δy). Many strain gauges passed the yielded limit in the longitudinal bars of the pile (SG73, SG76, SG80, SG81, SG93, SG96, SG101 and SG107), and none of the strain gauges in the slab reached the yield limit. The ultimate positive load was at load stage 11 (3.5Δy); strain gauge SG49 in the longitudinal bottom reinforcement of the slab yielded. At load stage 13 (5Δy), where the specimen considered to be collapsed, strain gauges SG28, SG39 and SG41 in the top reinforcement of the slab yielded, and strain gauges SG33, SG36, SG46 and SG49 in the bottom longitudinal reinforcement of the slab yielded. At load stage14 (6Δy), strain gauges SG21and SG47 in the horizontal stirrups yielded, and SG41 in the vertical stirrups yielded. All measured strain readings for the pile and slab reinforcement are shown in Table 6-2, and the plots of the strain gauges for specimen FSRCC24-M are shown in Appendix G.

6.2.4 Curvature Measurements

The curvature of the pile was calculated based on the listed readings of the DTDs in Table 6-3 and using Equation 3-1. To find the actual plastic hinge length, the measured curvature along the plastic hinge length was plotted, as shown in Figure 6-11. The actual plastic hinge can be determined from the intersection point between the curvature envelope of the pile and the yield limit. The extension of the top part of the left envelope intersects with yield limit envelope at 23 in. from the pile base (24% of pile length). The yield limit for the pile is shown in Figure 7-44.

6.3 FSKJ24-M Results

6.3.1 Observed Response of the Specimen, FSKJ24-M

The experimental test occurred over two days. The first four load stages, which were force control, were completed on the first day. The loading protocol is shown in Figure 3-18. The remaining eight load stages, which are displacement control were completed on the second day. Before starting the test, all of the shrinkage cracks were marked to differentiate between the shrinkage cracks and cracks which occurred during the test. In order to make the cracks easier to see during the test, a water based primer mix was applied to the specimen.

The cracks during the first three stages were hairline cracks in the slab and the pile base. When the specimen was taken to load stage 4 (0.75Δy), more hairline cracks spread in the slab, and radial hairline cracks spread in the bottom part of the pile (see Figure 6-12). As the specimen was pushed to a higher ductility, 1Δy, the crack at the slab surface extended to the sides of the slab and more hairline cracks spread in the pile base, as shown in Figure 6-13. At load stage 6 (1.5Δy), more hairline cracks spread in the pile base and the slab (see Figure 6-14). At load stages 7 (2Δy) and load stage 8 (2.5Δy), small parts of the pile cover spalled off, while no more new cracks in the slab were seen at these stages (see Figure 6-15 and Figure 6-16, respectively). At load stage 9 (3Δy), parts of the pile cover spalled off, a large crack at the pile-slab interface appeared and no more new cracks were observed at this stage, as shown in Figure 6-17. When the specimen was pushed to ductility 4Δy, four horizontal cracks, around 1/8 in. were seen in the pile base, and the pile cover spalled off to 7 in. height (see Figure 6-18). During the first excursion of load stage 12 (6Δy), the concrete cover of the pile spalled off from the pile to 14 in. height, the longitudinal bars buckled, and two stirrups fractured. During the second excursion of load stage 12 (6Δy), one of the longitudinal bars fractured and parts of the slab cover spalled (see Figure 6-19).

The general observation for the specimen at the end of the test was that none of the slab longitudinal reinforcement or the slab transverse reinforcement was exposed. Fracture occurred in the pile, and minimum cracks were seen in the slab.

6.3.2 Force-Displacement Relationships

The corrected force-displacement hysteretic behavior for specimen FSKJ24-M is shown in Figure 6-20. Cycles in the north direction (positive sign) are pushing force, while cycles in the south direction (negative sign) are pulling force. The following points summarize the force-displacement hysteretic behavior of specimen FSKJ24-M:

1- The force-displacement relationship was almost linear until it reached 0.50% of the yield force. The force in the positive direction was equal to 9.37-kips, and the

displacement was equal to 0.53 in. The force in the negative direction was equal to 9.47-kips, and the displacement was equal to 0.98 in.

2- The force-displacement relationship became nonlinear at 0.75% of the yield force, where the force in the positive direction was equal to 14.13-kips and the displacement was equal to 1.16 in. The force in the negative direction was equal to 13.97-kips, and the displacement was equal to 1.97 in. At this stage the specimen was stiffer in the positive direction (closing the joint) than in the negative direction (opening the joint); therefore, it was decided to use a different ductility level for each loading direction. The displacements at ductility (1Δy) in the positive direction were 1.54 in. and 2.64 in. in the negative direction.

3- At load stage 11 (1Δy), the force in the positive direction was equal to 17.01-kips, and the displacement was equal to 1.54 in. The force in the negative direction was equal to 16.85-kips, and the displacement was equal to 2.62 in.

4- The ultimate force during the test was at load stage 9 (3Δy) for the positive direction and load stage 10 (4Δy) for the negative direction. In the positive direction, the force was equal to 22.21-kips at 4.62 in. displacement, while in the negative direction the force was equal to 22.71-kips and 10.46 in. displacement.

5- The force decreased with increasing displacement after ductility level 4Δy. The load dropped at the second extrusion of load stage 12 (4Δy) in the positive direction to 17.42-kips (78.4% of the ultimate load) and 9.73 in. displacement. The force in the negative direction was equal to 12.68-kips (55.8% of the ultimate load) at 15.62 in. displacement. After this stage the force dropped to less than 80% of the ultimate load. The longitudinal bars in the positive direction buckled, and one on them was fractured.

Table 6-4 includes the force, the displacement of the actuator and the average displacements of the strain pots at each cycle. The string pots were used to check the readings of the actuator. Figure 6-20 shows the force-displacement relationship of the actuator.

6.3.3 Strain Gauge Data

As the specimen was pushed to 0.75 fy, a review of strain gauge readings showed that SG4, SG8, SG16, SG20, SG22, SG24, SG21 and SG28 in the longitudinal bars of the pile reached the yield limit, and none of the transverse pile reinforcement did. None of the longitudinal reinforcement of the slab reached the yield limit at this stage. All of the readings for the strain gauges during each cycle are listed in Table 6-5 and Appendix G.

A review of strain gauge readings at 4Δy showed that strain gauges SG6 and SG26 in the longitudinal reinforcement of the pile yielded. Strain gauge SG15 in the spirals at 4 in. from the pile and strain gauge SG45 in the additional vertical stirrups at the center of the pile yielded. Strain gauges SG87, SG90, SG91, SG92 and SG95 in the j-bars, and strain gauges SG109 and SG110 in the longitudinal reinforcement of the slab reached the yield limit.

At ductility 6Δy, strain gauge SG18 in the longitudinal reinforcement of the pile yielded. Strain gauge SG38 in the U-stirrups yielded. Strain gauges SG62 and SG107 in the longitudinal reinforcement of the slab and strain gauges SG89 and SG94 in the j-bars reached the yield limit.

6.3.4 Curvature Measurements

The curvature of the pile was calculated based on the listed readings of the DTDs in Table 6-6 and using Equation 3-1. To find the actual plastic hinge length, the measured curvature along the plastic hinge length was plotted, as shown in Figure 6-21. The actual plastic hinge can be determined from the intersection point between the curvature envelope of the pile and the yield limit. The extension of the top part of the left envelope intersects with yield limit envelope at 18.50 in. from the pile base (19.3% of pile length). The yield limit for the pile and slab are shown in Figures 7-45 and 7-46.

6.4 Strut-and-Tie Model

The STM for the modified specimens was developed based on the strain in the reinforcement of the modified specimens and the experimental observations made during each of the experiments. The processes and the equations used to develop the STM for specimen FSRCC24-M are the same as specimen FSRCC24; the processes and the equations used to develop the STM for specimen FSKJ24-M are the same as specimen FSKJ24.

6.4.1 Specimen FSRCC24-M

6.4.1.1 Measured Joint Reinforcement Force-Transfer Contributions

The peak measured strain values for specimen FSRCC24-M are listed in Table 6-2 and are provided in this section in plots, in order to understand the various joint reinforcement component contributions to the force-transfer process. These plots are helpful to visualize the major joint reinforcement contributors to the force-transfer process at various load levels, and are instrumental in developing a force-transfer model capable of handling several incremental increases in lateral load.

6.4.1.1.1 Joint Stirrups

Measured strain in the vertical and horizontal joint stirrups plotted for specimen FSRCC24-M are shown in Figure 6-22 to Figure 6-33. A similar plot for j-bars (Dowel) reinforcement placed in the pile core region is shown in Figure 6-34 to Figure 6-37. The load direction and strain gauge identification are indicated on the figures. It is evident from these plots that none of the vertical stirrups reached the yield limit, while strain gauge SG47 on the horizontal stirrups yielded; the rest of strain gauges on the horizontal stirrups showed high strain. The j-bars strain shown in Figure 6-34 to Figure 6-37 also indicate active force-transfer participation for the j-bars; this indicates that pile tension was being transferred to the deck reinforcement and should also be included in the force transfer model.

6.4.1.1.2 Pile Reinforcement

Measured strain for the pile longitudinal reinforcement for specimen FSRCC24-M are shown in Figure 6-38 for the south cycle and Figure 6-39 for the north cycle. The load direction and strain gauge identification are indicated on the figures. The joint/pile interface is represented as zero in the figures with a negative y-axis distance extending into the joint (slab) and a positive y-axis distance extending into the joint. In general, maximum strain occurred in the pile at 5 in. from the pile-slab interface. There was still

an appreciable amount of strain in pile longitudinal reinforcement 12 in. into the bent cap. This indicates that the bars were still being developed further into the joint, suggesting that Equation 5-2 is a good choice to represent the effective anchorage length. Similar plots for the pile transverse spirals extending into the joint are shown in Figure 6-40 and Figure 6-41 for the south and north cycles, respectively. Both plots show large strain at a distance of 12 in. into the joint at load cycle 26. The measured strain values in the pile are below the yield strain.

6.4.1.1.3 Slab Reinforcement

Measured strain for reinforcement at the top and bottom of the slab is plotted along the slab length for various FSRCC24-M load stages in Figure 6-42 to Figure 6-49. For the slab distance on the x-axis of these plots, zero indicates the joint center with negative x-axis values extending north along the slab and positive x-axis values extending south. The purpose of the plots was to indicate how the slab tension was transferred inside the joint. Figure 6-42 to Figure 6-49 indicate that slab reinforcement started to reach the yield limit at load stage 20 ($3\Delta y$).

6.4.1.2 Strut-and-Tie Model Verification for FSRCC24-M

6.4.1.2.1 Tie Model Verification

The procedures to find the boundary conditions for specimen FSRCC24-M are the same for the boundary conditions for specimen FSRCC24, as shown in Section 5.2.1. The final boundary condition for specimen FSRCC24-M is shown in Figure 6-50. The following steps summarize the verification of the model for each member:

1) The location of Node G was adjusted to match the experimentally measured force in the pile spirals. The x-coordinates of Node G can be determined based on the magnitude of Tie T_{EG}, as shown in Figures 5-4 and 5-19. Strains were calculated from Table 6-2, based on the values of strain gauges SG98, SG100, SG102, SG104, SG106 and SG108 at load stage 10. The Tie T_{EG} can be calculated from Equation 5-3, using La = 2 in., L = 11.2 in., s = 1.5 in., A_{sp} = 0.11 in^2, the measured strain of 608 microstrains, and E = 29,000 ksi. Tie T_{EG} was determined to be 40.23 kips. Node G was adjusted in the model development until Tie T_{EG} was representative of the above value.
2) Tie T_{IC} (367.2 kips) represented the top reinforcement of the slab inside the pile-slab joint with an area of 8.69 in^2 and a strain of 1351 microstrains. The average strain of strain gauges SG33, SG36, SG46 and SG49 at load stage 10 was 1410 microstrains, which agrees very well with the strut-and-tie model.
3) Tie T_{LI} (146.2 kips) represented the top reinforcement of the slab outside the pile-slab joint with an area of 8.69 in^2 and a strain of 537 microstrains. The average strain of strain gauges SG20 and SG23 at load stage 10 was 526 microstrains, which agrees very well with the strut-and-tie model.
4) Tie T_{HB} (345.7 kips) represented the bottom reinforcement of the slab inside the pile-slab joint with an area of 8.69 in^2 and a strain of 1269 microstrains. The average strain in strain gauges SG26, SG28, SG39 and SG41 at load stage 10 was 1152 microstrains, which agrees very well with the strut-and-tie model.

5) Tie T_{BR} (126.2 kips) represented the bottom reinforcement of the slab outside the pile-slab joint with an area of 8.69 in^2 and a strain of 463 microstrains. The average strain of strain gauges SG52 and SG55 at load stage 10 was 403 microstrains, which agrees with the strut-and-tie model.
6) Tie T_{DE} (334.4 kips) represented the top part of the pile reinforcement, which can be considered as half the longitudinal reinforcements of the pile with an area of 4.5 in^2 and a strain of 2214 microstrains. The average strain in strain gauges SG101 and SG103 at load stage 10 was 18328 microstrains, which is larger than the predicted strain but still in the yielding plateau; this means that the force is the same.
7) Tie T_{CD} (322.2 kips) represented the tension force in the top part of the slab. The force is transferred from the pile bars to the top mat of the slab reinforcement through the j-bars and the 61 in. wide vertical stirrups.

a) The area of j-bars reinforcement included in the calculation of Tie T_{CD} was equal to 7.92 in^2 (18 × 0.44 in^2). The j-bars were instrumented with a larger number of strain gauges to know exactly whether the additional j-bars were effective. The average strain for strain gauges SG9, SG14, SG15, SG25, SG38, SG42, SG43, SG51 and SG56 at load stage 10 was 846 microstrains, which equaled a force of 219.6- kips.
b) The area of the 61 in. wide vertical stirrups was equal to 2.64-in^2 (3 stirrups with two branches for each stirrup) (3 × 2 × 0.44 in^2). The measured strain in strain gauges SG24, SG31 and SG37 at load stage 10 was 916 microstrains. This was equal to a resisting force equal to 79.2- kips.

The summation of the predicted forces equaled 298.8-kips (219.6+79.2), which agrees very well with the predicted value from the STM.

8) Tie T_{IJ} (117.8 kips) represented the vertical stirrups and the j-bars on the compression side of the pile face. The forces were carried by the following steel:

a) First were the 61 in. wide vertical stirrups with an area of 1.76 in^2 (2 stirrups with two branches for each stirrup) (2 × 2 × 0.44 in^2). The average strain in strain gauges SG8 and SG17 at load stage 10 was 199 microstrains, which equaled a force of 11.5 -kips.
b) Second are the 48 in. vertical stirrups with an area of 1.24 in^2 (2 stirrups with two branches for each stirrup) (2 × 2 × 0.31 in^2); the average strain in strain gauges SG16 and SG18 at load stage 10 was 843 microstrains, which equaled a force of 31.5- kips.
c) Third were the j-bars on the compression side of the joint; six j-bars (1.76 in^2) were included. The average strain in gauges SG15 and SG19 at load stage 10 was 916 microstrains, which equaled a force of 79.2-kips.

The summation of the predicted forces was 122.2-kips (11.5+31.5+79.2), which agrees very well with the predicted value from the STM.

9) Tie T_{AB} (70 kips) represented the shear force on the tension side of the pile face. The forces were carried by the vertical stirrups and the j-bars as follows:

a) First were the 61 in. wide vertical stirrups with an area of 1.76 in^2 (2 stirrups with two branches for each stirrup) (2 × 2 × 0.44 in^2). The average strain in strain gauges SG50 and SG59 at load stage 10 was 272 microstrains, which equaled a force of 15.7-kips.
b) Second were the 48 in. vertical stirrups with an area of 1.24 in^2 (2 stirrups with two branches for each stirrup) (2 × 2 × 0.31 in^2). The strain in strain gauge SG58 at load stage 10 was 324 microstrains, which equaled a force of 12.6- kips.

The summation of the predicted forces was equal to 28.3-kips (15.7+12.6), which is less than the predicted force values from the STM. This means that the proposed STM is more conservative.

6.4.1.2.2 Strut Verification

Based on concrete strength of the slab shown in Table3-1 and Equation 5-4, the permissible compressive strength of struts is equal to $f_{ce} = 2.72 - ksi$.

Strut C_{GH} (525.5-kips) was an important strut; it was chosen because it was considered the main diagonal strut in the model (see Figure 5-4 and Table 6-8). Other researchers have also determined this strut to be the most critical[1,24] and have suggested to calculate the stress at mid-height of the joint. The area for C_{GH} was calculated at Node G. The effective strut width on one side of Node G was taken as half the horizontal distance between Node G and Node E4 (9.24 in.), meaning this distance also extended to the left of Node G. The thickness of the strut at Node H equaled 25.98 in., which equaled the pile diameter at point W (24 in.) plus width due force spreading between Node W and Node H (1.98 in). The computed Strut C_{GH} stresses for the specimen is 2.19-ksi, which was less than the permissible compressive strength (2.72-ksi).

6.4.2 Specimen FSKJ24-M

6.4.2.1 Measured Joint Reinforcement Force-Transfer Contributions

The peak measured strain values listed in Table 6-5 are provided in this section as plots, in order to understand the various joint reinforcement component contributions to the force-transfer process.

6.4.2.1.1 Joint Stirrups

Measured strains in the vertical and horizontal joint stirrups are shown in Figure 6-51 to Figure 6-58. A similar plot for the j-bars (Dowel) reinforcement placed in the pile core region is shown in Figure 6-59 and Figure 6-60. The loading direction and strain gauge identification are indicated on the figures. It is evident from these plots that none of the vertical stirrups reached the yield limit, while strain gauge SG45 at 6 in. from the pile face in the horizontal stirrups yielded at load stage 5. The j-bars strain shown in Figure 6-59 and Figure 6-60 also indicate that strain gauges SG87, SG89, SG90, SG91, SG92, SG94 and SG95 yielded. The high strain was due to active force-transfer participation for the j-bars; this indicates that pile tension was being transferred to the deck reinforcement and should also be included in the force transfer model.

6.4.2.1.2 Pile Reinforcement

Measured strain for the pile longitudinal reinforcement for specimen FSKJ24-M is shown in Figure 6-61 for the south cycle and Figure 6-62 for the north cycle. The joint/pile interface is represented as zero in the figures, with a negative y-axis distance extending into the joint (slab) and a positive y-axis distance extending into the joint. In general, maximum strain occurred in the pile at the pile-slab interface. Notice there was still an appreciable amount of strain in pile longitudinal reinforcement 8 in. into the bent cap. This indicates that the bars were still being developed into the joint, suggesting that Equation 5-2 is a good choice to represent the effective anchorage length. Similar plots

for the pile transverse spirals extending into the joint generated from Table 6-5 are shown in Figure 6-63 and Figure 6-64 for the south and north cycles, respectively. Both plots show a large strain at the pile-slab interface at load cycle 24. The measured strain values in the pile are over the yield strain until 8 in. from the pile-slab interface.

6.4.2.1.3 Slab Reinforcement

Measured strains for reinforcement at the top and bottom of the slab are plotted along the slab length for various FSKJ24-M load stages in Figure 6-66 to Figure 6-76. For the slab distance on the x-axis of these plots, zero indicates the joint center with negative x-axis values extending north along the slab and positive x-axis values extending south. The purpose of the plots was to indicate how the slab tension was transferred inside the joint. For the longitudinal reinforcement of the slab yield, Figure 6-66 and Figure 6-68 show the bars which reached the yield limit.

6.4.2.2 Strut-and-Tie Model Verification for FSKJ24-M

The boundary conditions of specimen FSKJ24-M in the closing and opening case are the same as FSKJ24 (Section 5.3.2.1, Section 6.4.2.2.1 and Section 6.4.2.2.2 show in detail the verification of the STM in the closing and opening case, respectively).

6.4.2.2.1 Closing Moment Case

In this section, the experimentally developed strut-and-tie model shown in Figure 6-77 is applied to the specimen at the ultimate lateral load, determined at the closing moment from the experimental test results. The ultimate lateral load (22.21-kips) was at load stage 9 (3Δy), for the closing case. To solve the STM for the closing moment case, the value for Tie T_{EG} should be determined. The location of Tie T_{EG} is shown in Figure 5-45. The following steps summarize the verification of the model for each member:

1) Tie T_{DG} was adjusted to match the experimentally measured force in the pile hoops and the horizontal cap end ties. The strain of hoops was calculated from Table 6-5 based on the reading of strain gauges SG3, SG6 and SG7 at load stage 9 (3Δy). The average value was 835 microstrains, and the strain in the horizontal cap end ties was based on the values of the strain gauges SG50 and SG51 at load stage 9 (3Δy), which was 1437 microstrains. Using Equation 5-3, Tie T_{DG} force was determined to be 61-kips, where, N = 4 hoops, $A_H = A_{HC} = 0.11$ in^2.
2) Tie T_{KL} (284.8-kips) represented the top reinforcement of the slab outside the pile-slab joint; this force was the summation of the force in the 12#7 bars and the force in 6#3 bars in the experiment.

a) The 12#7 bars had an area equal to 7.2 in^2. The measured strain in strain gauge SG79 at load stage 9 (3Δy) was 1033 microstrains, which equaled a force of 244-kips.
b) The 6#3 bars had an area equal to 0.66 in^2. Strain gauge SG110 at load stage 9 (3Δy) reached the yield limit, where the force equaled a force of 40.3-kips.
   The summation of the previous two forces was equal to 284.3-kips (244+40.33), which agrees very well with the predicted force of the strut-and-tie model.

3) Tie T_{KA} (284.8-kips) represented the top reinforcement of the slab outside the pile-slab joint. This force was the summation of the force in the 12#7 bars and the force in 6#3 bars.

a) The 12#7 bars had an area equal to 7.2 in^2. The measured strain in strain gauge SG78 at load stage 9 (3Δy) was 1046 microstrains, which equaled a force of 246.9-kips.
b) The 6#3 bars had an area equal to 0.66 in^2. The strain gauge SG109 at load stage 9 (3Δy) reached the yield limit, which equaled a force of 46.93-kips.
The summation of the previous two forces was 286.93-kips (246.9+40.33), which agrees very well with the predicted force of the strut-and-tie model.

4) Tie T_{IA} (327.3-kips) represented the top reinforcement of the slab outside the pile-slab joint; this force was the summation of the forces in the 12#7 bars, the force in 6#3 bars and the force in 8#4 vertical u-bars.

a) The 12#7 bars had an area equal to 7.2 in^2. The average strain in strain gauges SG63 and SG64 at load stage 9 (3Δy) was 1100 microstrains, which equals a force of 259.7-kips.
b) The 6#3 bars had an area equal to 0.66 in^2. The average strain in strain gauges SG107 and SG108 at load stage 9 (3Δy) was 1772 microstrains, which equaled a force of 32.87-kips.
c) The 8#4 vertical u-bars had an area equal to 1.6 in^2. The average strain in strain gauges SG37 and SG42 at load stage 9 (3Δy) was 826 microstrains, which equaled a force of 42.2-kips.
The summation of the previous forces was equal to 334.77-kips (259.70+32.87+42.2), which agrees very well with the predicted force of the strut-and-tie model.

5) Tie T_{IC} (357.7-kips) represented the top reinforcement of the slab inside the pile-slab joint; this force was the summation of the forces in the 12#7 bars, the force in 6#3 bars and the force in 8#4 vertical u-bars.

a) The 12#7 bars had an area equal to 7.2 in^2. The average strain in strain gauges SG75 and SG62 at load stage 9 (3Δy) was 1309 microstrains, which equaled a force of 309.30-kips.
b) The 6#3 bars had an area equal to 0.66 in^2. The average strain in strain gauges SG106 at load stage 9 (3Δy) was 959 microstrains, which equaled a force of 21.43-kips.
c) The 8#4 vertical u-bars had an area equal to 1.6 in^2. The strain in strain gauge SG41 at load stage 9 (3Δy) was 814 microstrains, which equaled a force of 35.6-kips.
The summation of the previous force was equal to 366.33-kips (309.30+21.43+35.6), which agrees very well with the predicted force of the strut-and-tie model.

6) Tie T_{CP} (223.8-kips) represented the top reinforcement of the slab inside the pile-slab joint; this force was the summation of the force in the 12#7 bars, the force in 6#3 bars and the force in 8#4 vertical u-bars.

a) The 12#7 bars had an area equal to 7.2 in^2. The average strain in strain gauges SG61 and SG74 at load stage 9 (3Δy) was 653 microstrains, which equaled a force of 154.3-kips.
b) The 6#3 bars had an area equal to 0.66 in^2. The average strain in strain gauge SG105 at load stage 9 (3Δy) was 718 microstrains, which equaled a force of 13.84-kips.
c) The 8#4 vertical u-bars had an area equal to 1.6 in^2. The average strain in strain gauge SG41 at load stage 9 (3Δy) was 814 microstrains, which equaled a force of 41.6-kips.
The summation of the previous forces was equal to 209.74-kips (154.3+13.84+41.6), which agrees very well with the predicted force of the strut-and-tie model.

7) Tie T_{PO} (171-kips) represented the top reinforcement of the slab inside the pile-slab joint; this force was the summation of the force in the 12#7 bars, the force in 6#3 bars and the force in 8#4 vertical u-bars.

a) The 12#7 bars had an area equal to 7.2 in^2. The average strain in strain gauges SG60 and SG73 at load stage 9 (3Δy) was 196 microstrains, which equaled a force of 46.1-kips.

b) The 6#3 bars had an area equal to 0.66 in^2. The measured strain in strain gauge SG104 at load stage 9 (3Δy) was 97 microstrains, which equaled a force of 1.9-kips.

c) The 8#4 vertical u-bars had an area equal to 1.6 in^2. The measured strain in strain gauge SG41 at load stage 9 (3Δy) was 814 microstrains, which equaled a force of 41.6-kips.

The summation of the previous forces was equal to 89.6-kips (46.1+1.9+41.6), which was less than the predicted forces from the STM, which means that the STM was more conservative.

8) Tie T_{NY} (103.8-kips) represented the bottom reinforcement of the slab outside the pile-slab joint; this force was the summation of the force in the 12#7 bars, the force in 6#3 bars and the force in 8#4 vertical u-bars.

a) The 12#7 bars had an area equal to 7.2 in^2. The average strain in strain gauges SG66 and SG80 at load stage 9 (3Δy) was 225 microstrains, which equaled a force of 53.2-kips.

b) The 6#3 bars had an area equal to 0.66 in^2. The average strain in strain gauge SG97 at load stage 9 (3Δy) was 94 microstrains, which equaled a force of 3.1-kips.

c) The 8#4 vertical u-bars had an area equal to 1.6 in^2. The average strain in strain gauges SG33 and SG38 at load stage 9 (3Δy) was 1067 microstrains, which equaled a force of 54.4-kips.

The summation of the previous forces was equal to 110.7-kips (53.2+3.1+54.4), which agrees well with the predicted force of the strut-and-tie model.

9) Tie T_{YH} (215.1-kips) represented the bottom reinforcement of the slab inside the pile-slab joint; this force was the summation of the force in the 12#7 bars, the force in 6#3 bars and the force in 8#4 vertical u-bars.

a) The 12#7 bars had an area equal to 7.2 in^2. The average strain in strain gauges SG67, SG68, SG81, and SG82 at load stage 9 (3Δy) was 774 microstrains, which equaled a force of 182.8-kips.

b) The 6#3 bars had an area equal to 0.66 in^2. The average strain in strain gauges SG98 and SG99 at load stage 9 (3Δy) was 435 microstrains, which equaled a force of 14.4-kips.

c) The 8#4 vertical u-bars had an area equal to 1.6 in^2. The average strain in strain gauges SG33 and SG38 at load stage 9 (3Δy) was 1067 microstrains, which equaled a force of 54.4-kips.

The summation of the previous forces was equal to 251.8-kips (183+14.4+54.4), which agrees well with the predicted force of the strut-and-tie model.

10) Tie T_{CD} (47.8-kips) represented the forces in the 20#3. The 20#3 bars had an area equal to 2.2 in^2. The average strain in strain gauges SG87, SG88, SG89, SG90, SG91, SG92, SG94, SG95, and SG99 at load stage 9 (3Δy) was 1661 microstrains, which equals a force of 106.3-kips. The strut-and-tie shown in Figure 6-77 model did not predict the force in Tie T_{CD} (j-bars and vertical stirrups) in an accurate way. The force

in the j-bars and the vertical stirrups was lower than the force from the strut-and-tie model. To predict the tension demand in the j-bars and the vertical stirrups, strut C_{CG} inside the joint was considered bottle-shaped, as shown in Figure 6-78. Tie $T_{X'Y'}$ represented the splitting tension resulting from spreading, and θ represented the spreading angle determined by assuming strut C_{CG} was horizontal. Determining θ in this manner resulted in a spread angle smaller than the 2:1 ratio recommend in literature[25.]

By adding the force in Tie $T_{X'Y'}$ =52.6-kips to the force of Tie T_{CD} =47.8-kips, the summation, 100.4-kips, agrees very well with the force (106.3-kips) from the experimental results. Based on the previous discussion, the final STM for the closing case be as shown in Figure 6-79.

11) Tie T_{XY} (39.8-kips) represented the forces in the vertical stirrups as follows:

a) The area of the 4#5 main vertical stirrups equaled 2.48 in^2. The average strain in strain gauges SG57 and SG59 at load stage 9 (3Δy) was 210 microstrains, which equaled a force of 16.4-kips.

b) The area of the 2#4 main vertical stirrups was 0.8 in^2. The average strain in strain gauges SG44 and SG47 at load stage 9 (3Δy) was 367 microstrains, which equaled a force of 9.4-kips.

The summation of the previous forces was equal to 25.8-kips (16.4+9.4), which was less than the predicted force of the strut-and-tie model.

12) Tie T_{AB} (13-kips) represented the vertical stirrup and the j-bars on the internal side of the pile face; this force was the summation of the following forces:

a) The area of the main vertical stirrups (3#5) was 1.86 in^2. The average strain in strain gauges SG52, SG53, SG54 and SG55 at load stage 9 (3Δy) was 188 microstrains, which equaled a force of 11-kips.

b) The area of the additional vertical stirrups 2#4 was 0.8 in^2. The average strain in strain gauge SG30 at load stage 9 (3Δy) was 242 microstrains, which equaled a force of 6.2-kips.

c) The area of the additional vertical stirrups, 2#4, was 0.8 in^2. The average strain in strain gauges SG45 and SG48 at load stage 9 (3Δy) was 1354 microstrains, which equaled a force of 34.5-kips.

d) The area of the j-bars on the compression side was 0.44-in^2(four j-bars). The strain of strain gauge SG86 at load stage 9 was 221 microstrains, which equaled a force of 2.3-kips.

The summation of the previous forces was equal to 54-kips (11+6.2+34.5+2.3), which was less than the predicted force of the strut-and-tie model. The force of Tie T_{AB} in the opening case governed, as shown in Section 6.4.2.2.2; therefore, it is the one used for design, rather than the value in the closing case.

13) Tie T_{ON} (39.9-kips) represented the force in vertical u-bars in the outside part of the pile face. The area of the 8#4 u-bars was 1.6 in^2 and the average strain in strain gauges SG35 and SG40 at load stage 9 (3Δy) was 105 microstrains, which equaled 5.36-kips. The force in the u-bars (5.36-kips) was so lower than the predicted force (39.9-kips) because the longitudinal bars were hooked, therefore it took a shear from the vertical force.

6.4.2.2.2 Opening Moment Case

In this section, the experimentally developed strut-and-tie model was applied to the specimen at the ultimate lateral load for the opening. The ultimate lateral load (22.71-kips) was at load stage 10 (4Δy) for the closing case. To solve the STM for the opening moment case, shown in Figure 6-80, the value for Tie T_{EG} should be determined, where the location of Tie T_{EG} is shown in Figure 5-45. The following steps summarize the verification of the model for each member:

1) Tie T_{DG} was adjusted to match the experimentally measured force in the pile hoops and the horizontal cap end ties. The strain of hoops was calculated from Table 6-4, where the average strain in strain gauges SG3, SG6 and SG7 at load stage 10 (4Δy) was 847 microstrains. The strain in the horizontal cap end ties was based on the values of strain gauges SG50 and SG51 at load stage 10 (4Δy), which was 1574 microstrains. Tie T_{DG} was determined to be 63.4-kips, where Tie T_{EG} can be calculated from Equation 5-5, using N = 4 hoops, $A_H = A_{HC} = 0.11$ in^2.
2) Tie T_{MJ} (301.1-kips) represented the bottom reinforcement of the slab. This force was the summation of the forces in the 12#7 bars and the force in 6#3 bars.

a) The 12#7 bars had an area equal to 7.2 in^2. The measured strain in strain gauge SG72 at load stage 10 (4Δy) was 1186 microstrains, which equaled a force of 280.2-kips.
b) The 6#3 bars had an area equal to 0.66 in^2. The strain in strain gauge SG102 at load stage 10 (4Δy) was 1373 microstrains, which equaled a force of 26.4-kips.
   The summation of the previous forces was equal to 306.6-kips (280.2+26.4), which agrees very well with the predicted force of the strut-and-tie model.

3) Tie T_{BJ} (301.1-kips) represented the bottom reinforcement of the slab outside this force and was the summation of the forces in the 12#7 bars and the force in 6#3 bars.

a) The 12#7 bars had an area of 7.2 in^2. The average strain in strain gauges SG71 and SG85 at load stage 10 (4Δy) was 1125 microstrains, which equaled a force of 265.8-kips.
b) The 6#3 bars had an area equal to 0.66-in^2. The strain gauge SG103 was damaged during testing so the reading of the closest strain gauge SG102 was used. The measured strain in gauge SG102 at load stage 10 (4Δy) was 1373 microstrains , which equaled a force of 26.4-kips.
   -The summation of the previous forces was equal to 292.2-kips (265.8+26.4), which agrees very well with the predicted force of the strut-and-tie model.

4) Tie T_{BH} (440.4-kips) represented the bottom reinforcement of the slab inside the pile-slab joint; this force was the summation of the forces in the 12#7 bars, the force in 6#3 bars and the force in 8#4 vertical u-bars.

a) The 12#7 bars had an area equal to 7.2 in^2. The average strain in strain gauges SG68, SG69, SG70, SG82, SG83 and SG84 at load stage 10 (4Δy) was 1322 microstrains, which equaled a force of 312-kips.
b) The 6#3 bars had an area equal to 0.66 in^2. The average strain in strain gauges SG99, SG100 and SG101 at load stage 10 (4Δy) was 1145 microstrains, which equaled a force of 37.6-kips.
c) The 8#4 vertical u-bars had an area equal to 1.6 in^2. The average strain in strain gauges SG34 and SG39 at load stage 10 (4Δy) was 879 microstrains, which equaled a force of 44.8-kips.

-The summation of the previous forces was equal to 394.4-kips (312+37.6+44.8), which agrees well with the predicted force of strut-and-tie model.

5) Tie T_{AB} (60.7-kips) represented the vertical stirrup and the j-bars on the internal side of the pile face; this force was the summation of the following forces:

a) The area of the main vertical stirrups 3#5 was 1.86 in^2. The average strain in strain gauges SG52, SG53, SG54 and SG55 at load stage 10 (4Δy) was 185 microstrains, which equaled a force of 10.8-kips.

b) The area of the additional vertical stirrups 2#4 was 0.8 in^2. The average strain in strain gauge SG30 at load stage 10 (4Δy) was 261 microstrains, which equaled a force of 6.7-kips.

c) The area of the additional vertical stirrups 4#3 was 0.88 in^2. The average strain in strain gauges SG45 and SG48 at load stage 10 (4Δy) was 1402 microstrains, which equaled a force of 41.8-kips.

d) The area of the j-bars on the compression side of the joint (six j-bars (0.66-in^2)) was included. The strain of strain gauge SG86 at load stage 10 was 290 microstrains; the resisting force was 2.4-kips.

-The summation of the previous forces was equal to 61.7-kips (10.8+6.7+41.8+2.4), which agrees very well with the predicted force of the strut-and-tie model.

6) Tie T_{CD} (23.4-kips) and T_{XY} (64.6-kips) represented the forces in the vertical stirrups and the j-bars. These forces were the summation of the forces in the 20#3 j-bars bars in the tension side, the force in the 4#5 main vertical stirrups bars and the force in the 2#4 additional vertical stirrups.

a) The 20#3 bars had an area equal to 1.98 in^2. The average strain in strain gauges SG87, SG88, SG89, SG90, SG91, SG92, SG94, SG95 and SG99 at load stage 10 (4Δy) was 1756 microstrains, which equaled a force of 101-kips

b) The area of the 4#5 main vertical stirrups was 2.48 in^2. The average strain in strain gauges SG59 and SG57 at load stage 10 (4Δy) was 258 microstrains, which equaled a force of 20.4-kips.

c) The area of the 2#4 main vertical stirrups was 0.8 in^2. The average strain in strain gauges SG44 and SG47 at load stage 10 (4Δy) was 4076 microstrains, which equaled a force of 10.4-kips.

The summation of the previous force was equal to 131.8-kips (101+20.4+10.4), which is less than the predicted force of the strut-and-tie model.

The strut-and-tie model did not predict the force in the j-bars and the vertical stirrups in an accurate way. The experimental force was lower than the force from the strut-and-tie model. To predict the tension demand resulting in the vertical stirrups and j-bars, strut C_{CG} inside the joint is considered bottle-shaped as shown in Figure 6-81. In this figure, Tie $T_{X'Y'}$ represents the splitting tension resulting from spreading and θ represents the spreading angle determined by assuming strut C_{CG} is horizontal. Determining θ in this manner results in a spread angle smaller than the 2:1 ratio recommend in literature[25].

The force in Tie $T_{X'Y'}$ was 26.3-kips. By adding this force to the forces of Tie T_{CD} (23.4-kips) and T_{XY} (64.6-kips), the summation was 114.3-kips, compared to 131.8-kips from the measured strain. Based on the previous discussion, the final STM for the opening case is shown in Figure 6-82.

6.4.2.3 Strut Verification

Based on concrete strength of the slab, Table 3-1 and Equation 5-4, the permissible compressive strength of struts is equal to $f_{ce} = 4.93 - ksi$.

Strut C_{DH} (479.7-kips) in the opening case was an important strut; this strut was chosen because it was considered the main diagonal strut in the model (see Figure 6-80 and Table 6-10). Other researchers have also determined this strut to be the most critical[1,24] and have suggested to calculate the stress at mid-height of the joint. The area for C_{DH} was calculated at Node D. The effective strut width on one side of Node D was taken as half the horizontal distance between Node D and Node G[4] (7.91 in.), meaning this distance also extended to the left of Node D. The thickness of the strut at Node H equaled 17.93 in., which equaled the pile diameter at point W (16 in.) plus width due force spreading between Node W and Node H (1.93 in.). The computed Strut C_{DH} stresses for the specimen was 3.38-ksi, less than the permissible compressive strength (4.93-ksi).

6.5 Performance Evaluation of the Modified Specimens

The performance evaluation of the modified specimens included the force transfer method and comparison between the original and modified design.

6.5.1 Force Transfer Evaluation

The experimental results and the approved strut-and-tie models showed good performance for the modified specimens and the proposed reinforcement detailing. The good performance of the joint means that the force was effectively transferred through the joint. The force transferred in the joint through the splice mechanism, which transfer pile tension to the slab reinforcement through the j-bars and vertical stirrups. The T-joint splice transfer tie was represented by Tie T_{CD} for T-joints. The knee-joints' splice transfer tie was represented by Ties T_{CD} and T_{XY} in the closing case, and Ties T_{CD}, T_{XY} and $T_{X'Y'}$ in the opening case. The splice transfer mechanism was separated into an inside joint splice transfer mechanism and outside splice transfer mechanism. The inside joint splice transfer mechanism assumed that force transfer from the longitudinal bars to the j-bars reinforcement was through a set of strut and ties through the concrete, as shown in Figure 6-85; this mechanism transferred the majority of the pile tension to the top mat slab reinforcement. The outside splice transfer mechanism, assumed that the remaining pile tension in the strut-and-tie model was transferred to the deck reinforcement by the vertical joint stirrups outside the pile core region, with the mechanism shown in Figure 6-85.

6.5.2 Specimen FSRCC24 and FSRCC24-M Comparison

As mentioned previously in Section 4.5.1, specimen FSRCC24 failed in the slab region, and this was undesired mode of failure. The modified specimen FSRCC24-M was modified in order to overcome the performance issues of specimen FSRCC24. Additional vertical stirrup, j-bars and longitudinal reinforcement were added to FSRCC24-M. Figure 6-83 shows the force-displacement curve for specimen FSRCC24, which was designed based on using the SDC, and the modified specimen FSRCC24-M, which was used based on the recommendations of the STM and the experimental results. The initial stiffness for both specimens was almost the same. The value of the ultimate force was almost the same, but the ductility for FSRCC24-M was larger than FSRCC24. The hysteresis loop

for specimen FSRCC24-M was larger than FSRCC24; this means that the modified specimen has better ability for energy dissipation.

6.5.3 Specimen FSKJ24 and FSKJ24-M Comparison

As mentioned previously in Section 4.7.1, specimen FSKJ24 failed in the slab region; this was undesired failure mode. The modified specimen FSKJ24-M was modified in order to overcome this problem in design. Additional vertical stirrup, j-bars and longitudinal reinforcement were added to FSKJ24-M. Figure 6-84 shows the force-displacement curve for both specimens. The initial stiffness for the modified specimen FSKJ24-M was stiffer than FSKJ24. The value of the ultimate force FSKJ24-M and the ductility for FSKJ24-M were larger than FSKJ24, and the hysteresis loop for specimen FSKJ24-M was larger than FSKJ24. This means that the modified specimen has better ability for energy dissipation.

6.6 Simplified Strut-and-Tie Model

In order to make the design process simple, tables and equations were developed. The strut-and-tie models were applied to twenty three T-joints and twenty three knee-joints with 24 in. piles, for different V, II, III support configurations. The different support configuration is shown in Figure 2-4. The results from the approved STM are shown in Table 6-11 and Table 6-12 for the T-joint and knee-joint, respectively. The following section shows in detail the previous discussion.

6.6.1 T-Joint

Tension demand values shown in Table 6-11 were calculated based on the approved STM for specimen FSRCC24-M, shown in Figure 5-4. The listed values represented four different force demands on the joint as follows:

1- Additional tension demand on the top reinforcement of the slab (T_{bt}), where T_{bt} equaled $T_{IC} - T_{LI}$;

2- Additional tension demand on the bottom reinforcement of the slab (T_{bb}), where T_{bb} equaled T_{HB} -T_{BR};

3- Tension demand on the stirrups outside the joint (T_{es}), which was the larger value of T_{AB} and T_{IJ}; and

4- Tension demand on j-bars inside the joint (T_{JV}), which was represented in the STM by Tie T_{CD}.

6.6.2 Knee-Joint

Tension demand values shown in Table 6-12 were calculated based on the approved STM for the knee-joint shown in Figure 6-79 and Figure 6-82. The listed values were the maximum values in the opening and closing case. The listed values represent four different force demands on the joint as follows:

1- Additional demand on the top reinforcement of the slab (T_{bt}), where T_{bt} equaled $T_{AK} - T_{AI}$.;

2- Additional demand on the bottom reinforcement of the slab (T_{bb}), where T_{bt} equaled T_{HB} -T_{BJ};

3- Tension demand on the stirrups outside the joint (T_{es}), which was the bigger value of T_{AB} in the opening and T_{AB} in the closing case; and

4- Tension demand on j-bars inside the joint (T_{JV}), which was represented by the maximum of Ties (T_{CD} and $T_{X'Y'}$) in the closing case and Ties (T_{CD}, $T_{X'Y'}$ and T_{XY}) in opening case.

From the force values shown in Table 6-11 and Table 6-12, the force demand in the joint for the 30-ft span was too large. Therefore, it is recommended to use a drop-cap joint for the 30-ft span instead of the flat slab-joint. The additional reinforcement needed in the top and bottom of the slab and vertically in the joint were determined using the STM. The forces shown in Table 6-11 and Table 6-12 were transferred into equations; this will be discussed in detail in Chapter 8.

Chapter 7
Post-Test Analysis

7.1 Introduction

The focus of this chapter is on the analytical modeling of the specimens. The results from the analytical model show the push-over curve, crack pattern, type of failure and the locations where failure occurred. This helps to identify the critical elements and joints in each specimen, which in turn helps to determine the cause of failure and how to control it.

To perform this analysis on the eight specimens, a 3-D finite element model was developed for each specimen, using the Atena program[18]. The Atena program, which is used for nonlinear finite element analysis of structures, offers tools specially designed for computer simulation of concrete and reinforced concrete structural behavior.

The Atena program system consists of a solution core and several user interfaces. The solution core offers a wide range of 2D and 3D continuum models, libraries of finite elements, material models and solution methods. Atena 3D program is designed for 3D nonlinear analysis of solids with special tools for reinforced concrete structures. The program has three main functions:

1- Pre-processing including input of geometrical objects (concrete, reinforcement, interfaces, etc.), loading and boundary conditions, meshing and solution parameters;
2- Analysis that makes it possible for real time monitoring of results during calculations; and
3- Post-processing with access to a wide range of graphical and numerical results.

The program allows the comparisons of cracking patterns. The results from the Atena program were used to compare against the measured experimental results for each specimen in order to see the validity of modeling assumptions and the correlation between the analytical and experimental results. By using the program, it was also possible to examine the ultimate behavior of specimen DCRCC24 since the experiment had to be terminated early due to support failure. Also in this chapter, force and displacement results from moment curvature analysis are updated, and the results are compared to the force-displacement results from the experimental test.

7.2 Finite Element Modeling

The finite element modeling included the material modeling of concrete and steel, the modeling of the support condition, the element meshing and the element type.

7.2.1 Concrete Modeling

For concrete modeling, Atena provides stress-strain relationship based on the Kupfer's[28,29] model. This is the only model specifically provided by Atena. In the concrete material model, called SBETA, the effects of concrete stress-strain curve is combined with specified failure envelope and a crack model. The program allows the user to include or neglect the tension capacity of concrete.

7.2.1.1 Stress-Strain Relations for Concrete

The nonlinear behavior of concrete in the biaxial stress state is described by means of an effective stress, σ_c^{ef}, and the equivalent uniaxial strain, ε^{eq}. The effective stress is in

most cases, a principal stress. The equivalent uniaxial strain is introduced in order to eliminate the Poisson's effect in the plane stress state.

$$\varepsilon^{eq} = \frac{\sigma_{ci}}{E_{ci}} \qquad \text{Equation 7-1}$$

The equivalent uniaxial strain can be considered as the strain that would be produced by the stress, σ_{ci} in a uniaxial test with modulus, E_{ci}, associated with the direction, i. With this assumption, the nonlinearity is caused only by the governing stress, σ_{ci}. The numbers of the points in Figure 7-1 (material state numbers) are used to indicate the state of concrete damage. The peak values of stress in compression, f'^{ef}_{c}, and tension, f'^{ef}_{t}, are calculated according to the biaxial stress state. Thus, the equivalent uniaxial stress-strain law reflects the biaxial stress state. Detailed description of the stress-strain law is given in the following subsections.

7.2.1.2 Biaxial Stress Failure Criterion of Concrete

7.2.1.2.1 Compressive Failure

A biaxial stress failure criterion according to Kupfer[28,29] is used as shown in Figure 7-2. Equation 7-2 is the compression-compression stress state failure function:

$$f_c'^{ef} = \frac{1+3.65a}{(1+a)^2} f_c', \; a = \frac{\sigma_{c1}}{\sigma_{c2}} \qquad \text{Equation 7-2}$$

where σ_{c1} and σ_{c2} are the principal stresses in concrete, and f_c' is the uniaxial cylinder strength. In the biaxial stress state, the strength of concrete is predicted under the assumption of a proportional stress path. In the tension-compression state, the failure function continues linearly from the point $\sigma_{c1}= 0$ to the point $\sigma_{c2}= f_c'$, into the tension-compression region with a linearly decreasing strength, see Equation 7-3.

$$f_c'^{ef} = f_c' r_{ec}, r_{ec} = \left(1 + 5.3278\frac{\sigma_{c1}}{f_c'}\right), 1.0 \geq r_{ec} \geq 0.9 \qquad \text{Equation 7-3}$$

where r_{ec} is the reduction factor of the compressive strength in the principal direction 2 due to the tensile stress in the principal direction 1.

7.2.1.2.2 Tensile Failure

In the tension-tension state, the tensile strength is constant and equal to the uniaxial tensile strength f'_t. In the tension-compression state, the tensile strength is reduced by the relation shown in Equation 7-4.

$$f_t'^{ef} = f_t' r_{et}, r_{et} = \left(1\text{-}0.8\frac{\sigma_{c2}}{f_c'}\right) \qquad \text{Equation 7-4}$$

where r_{et} is the reduction factor of the tensile strength in the direction 1 due to the compressive stress in the direction 2.

7.2.2 Numerical model

Numerical model is generated based on geometrical model and represents a numerical approximation of the structural analysis problem. The mesh generator in Atena makes possible to generate automatically meshes for solid and reinforcing objects or the mesh size can be adjusted by user. As a consequence of independent macroelements the finite element meshes are made for each macroelement independently. Thus, when two macroelements are connected as neighboring objects, there are two surfaces belonging to

each object on the shared boundary. There are two sets of nodes on the shared boundary that, which may, but need not to coincide. The connection between the nodes of neighboring objects can be perfect, or there may be a contact element to model other types of interaction between the nodes. A perfect connection means that the elements work as one material. For the current study the contact between the macroelements was chosen to be a perfect connection.

For concrete meshing, Atena has three types of elements: tetrahedron and brick and wedge element, each type of elements has different number of nodes and sides as shown Figure 7-3. Brick elements are best when modeling uniform members. Any irregularity, such as an opening, line or joint or areas where refinement is required, such as a corner, is difficult to model with a brick element. Tetrahedron and mixed meshes are more flexible. Thus brick-tetra element mesh was used for the analysis. After several iterations the mesh dimension was chosen to be 6 in. for the full-scale specimens and 4 in. for the 2/3-scale specimens.

7.2.3 Reinforcement Modeling

A multi-linear stress-strain diagram was used to model the reinforcement. The multi-linear stress-strain diagram allows modeling all four stages of steel behavior: elastic state, yield plateau, hardening and fracture. The input values for the stress and strain are listed in Table 3-2. All of the reinforcement bars were assumed to be perfectly bonded, except for the longitudinal bars of the pile where a slip law by CEB-FIB[28] model code 1990 was adopted. CEB-FIB model code 1990 was based on the concrete compressive strength, reinforcement diameter and reinforcement type. For bond slip modeling Atena has two cases for the concrete condition: 1) confined concrete and 2) unconfined; the pile-slab connection was chosen to be confined.

Reinforcement can be modeled in two ways. The first way is a discrete bar, which is defined as a geometrical multi-linear object. It is embedded in solid objects. Its geometry is defined independently of the macroelement. Thus one reinforcing bar can be embedded in any number of macroelements; Second way is a smeared reinforcement, defined as a composite material, which has no effect on geometrical model. The distribution of the steel in the elements is irregular, thus, the discrete bar was used in this study.

7.2.4 Boundary Conditions and Loading Program

For the T-joint specimens, the detailing of the finite element model was the same for specimens DCRCC1, FSRCC1, DCRCC24, FSRCC24 and FSRCC24-M. The pile head was assumed to be elastic and perfectly attached to the top of the pile. The supports, hinges and beams, attached to the bottom of the slab, were assumed to be elastic and perfectly attached to the slab. For the boundary, the slab was considered to be fixed in the X and Z directions, and free in the Y direction. The final configuration for the T-joint specimens is shown in Figure 7-4.

For the knee-joint specimens, the detailing of the finite element model was the same for specimens DCKJ24, FSKJ24 and FSKJ-M. The support, which represents the inflection point in the slab, was fixed in Z direction and free in X and Y directions as shown in Figure 7-5. At the end of the specimen, the supports were fixed in X, Y and Z directions. The pile head was assumed to be elastic and perfectly attached to the top of the pile; the beams on the top of the specimens were modeled as elastic members and perfectly connected to the pile.

The loading program was divided into two parts: 1) vertical load and 2) horizontal load. The vertical constant axial load was applied to the center of the pile top. For the horizontal load, the specimen was pushed laterally at the center of the pile head under a constant increment of displacement until the specimen failed. From the pushover curve, the peak forces and displacements can be determined for each specimen.

7.3 Impact of Variables on the Analytical Results

Many trials were done in order to reach the final results. Some factors improve Atena results; these factors can be summarized as following:

1. Mesh Size

The mesh size was an important factor which affects the results. If the mesh size is too large, Atena will not start running. In order to find the mesh size which gives the closest result to the actual push-over results for the full scale specimens, 8 in., 7 in. and 6-in. were used as mesh sizes. It was observed that the smaller mesh size, the closer initial stiffness to the actual stiffness is. The smaller mesh size than 6-in did not improve the results and increased the number of points in the model which increase the run time, thus 6 in. was used as mesh size for the full-scale specimens.

For the 2/3-scale specimens 6 in., 5 in. and 4 in. were used as trails for mesh. The mesh size less than 4 in. didn't improve the push-over results and the bigger mesh sizes were less accurate, thus 4 in. was used as a mesh size for the 2/3-scale specimens.

2. Boundary Conditions

The boundary conditions for the head of the pile were important. The specimen was pushed laterally at the center of the pile head. When the pile head was not prevented from moving laterally, the program was unstable. Therefore, the head was fixed in the perpendicular direction of loading and free in the loading direction and in the vertical direction. The rest of the boundary conditions were mentioned in Section 7.2.4.

3. Bond Slip Effect

Bond slip was included in the modeling of the longitudinal reinforcement of the pile. When the bond slip was included in the modeling the push-over results were closer to the actual results. The push-over curve for the model without including the bond slip has higher the initial stiffness than the model with bond slip.

4. Materials Selection

The predicted crack pattern and the push-over results are close to the measured results when the actual properties were used. The pile head material was modeled as an elastic plastic material to prevent failure due to the applied lateral point load..

7.4 Analytical Results

7.4.1 Load-Displacement Relationship

The following section compares the load-displacement envelop of each specimen from the experiments to the finite element (Atena) results. As a general trend, the Atena pushover results for the T-joints were stiffer than the experimental results for the following reasons:

1) The actual response was cyclic rather than just simply pushing.
2) The Atena program does not model the full flexibility of the supports, where the deformation of the I-beams used as supports was neglected in the model.

For the same two reasons mentioned previously the expected yield force was higher than the measured yield force values. Table 7-1 shows the maximum yield and ultimate in the positive and negative values for the experimental and Atena results.

a) Specimen DCRCC1

The post-analysis pushover curve for specimen DCRCC1 is shown in Figure 7-6. The Atena yield force was 2% more than the actual force in the positive direction and 8% more in the negative direction. The predicted ultimate force was almost the same in both positive and negative direction. The predicted pushover curve from Atena has a stiffer response.

b) Specimen FSRCC1

The post-analysis pushover curve for specimen FSRCC1 is shown in Figure 7-7. The predicted pushover curve from Atena had a stiffer response. The predicted yield load in the positive direction was 33% more than the actual load, while in the positive direction it was 30% more. The ultimate predicted load in the positive and negative direction was almost identical. The predicted curve after the ultimate point tracked the measured behavior well.

c) Specimen DCRCC24

The supports of Specimen DCRCC24 failed prematurely, thus the test was stopped before reaching to a complete failure for the joint. In order to investigate the behavior of specimen after the ultimate point, the Atena program was used to predict the pushover curve for specimen DCRCC24 as shown in Figure 7-8. The predicted pushover curve from finite element results was stiffer than the actual responses. The predicted yield load in the positive was 14% more than the actual yield load, while in the negative loading direction it was 40% more than the actual yield load. The predicted ultimate loads in the positive and negative loading direction were almost identical. The predicted load dropped at ductility level of 5.8 Δy in the positive direction and at 5 Δy in the negative direction. This proves that the performance of the specimen and the corresponding details would have performed fine if the supports had not fail prematurely.

d) Specimen FSRCC24

The post-analysis pushover curve for specimen FSRCC24 is shown in Figure 7-9. The predicted yield load in the positive direction was 16% more than the actual yield load, while in the negative loading direction it was 21% more than the actual yield load. The predicted ultimate loads in the positive and negative loading direction were almost identical. The predicted curve in the negative direction shows the drop in the force, while in the positive direction the predicted curve could not track the drop in the measured curve.

e) Specimen DCKJ24

The post-analysis pushover curve for specimen DCKJ24 is shown in Figure 7-10. The predicted initial stiffness in the positive and negative direction of loading was very close to the measured stiffness. The ultimate and yield predicted loads were almost the same as the measured load, in the negative and positive direction.

f) Specimen FSKJ24

The post-analysis pushover curve for specimen FSKJ24 is shown in Figure 7-11. The predicted initial stiffness in the positive and negative direction of loading was close to the measured stiffness. The predicted yield load was 12% more that the measured yield load

in the positive direction, while in the negative direction it was 20% more. The predicted ultimate loads were almost the same as the measured load.

g) Specimen FSRCC24-M

The post-analysis pushover curve for specimen FSRCC24-M is shown in Figure 7-12. The pushover curve in the negative direction was able to track the measured pushover curve very well. In the positive direction the predicted curve was stiffer than the measured curve. The predicted yield load was 25% more than the actual yield load. The predicted and measured ultimate loads were almost the same in both directions.

h) Specimen FSKJ24-M

The post-analysis pushover curve for specimen FSKJ24-M is shown in Figure 7-13. The predicted initial stiffness in the positive and negative directions of loading was nearly identical. The predicted load at yield was almost the same as the measured load in the positive direction, while the ultimate predicted load was 8% less. In the negative direction the predicted yield load was almost the same as the measured yield load, while the predicted ultimate load at ultimate was 5% less than the measured.

7.4.2 Cracks Pattern

One major advantage of Atena was the ability to predict the crack pattern at each loading stage. Figure 7-14 through Figure 7-21 show the predicted crack patterns for each specimen. For the finite element results, the darker the color the higher amount of cracks.

a) DCRCC1 and FSRCC1

The actual and predicted crack patterns for specimens DCRCC1 and FSRCC1 are shown in Figure 7-14 and Figure 7-15 respectively. From there figures, the cracks concentrated at the pile base region, which was the same as the actual failure mode and cracking.

b) DCRCC24

The actual and predicted crack patterns for DCRCC24 using Atena software are shown in Figure 7-16. Most of the predicted cracks were concentrated at the pile hinge region with some cracks in the drop cap near the supports. For the actual failure mode, cracks spread at the pile base and parts of slab concrete cover spalled off. The hinge support became unable to transfer the load from specimen to the strong floor of the laboratory; therefore the test was concluded. The crack pattern shows that if the experimental test had continued, plastic hinging would have occurred in the pile, with some damage in the drop cap portion of the slab.

c) FSRCC24

The actual and predicted crack patterns for FSRCC24 using Atena software are shown in Figure 7-17. The failure in specimen FSRCC24 occurred mainly due to the slab failure; the predicted crack patterns showed the spreading of cracks in the top and bottom surface of the slab. The predicted cracks in the pile base were more than the actual cracks.

d) DCKJ24

The actual and predicted cracks in pull and push patterns for FSKJ24 using Atena software are shown in Figure 7-18. From the test photos, a good correlation can be seen between the actual and predicted failure mode and the cracking pattern in the pull direction. The pattern was slightly off the actual behavior in the push direction, as shown from Figure 7-18. Atena showed more cracks in the pile base, but the actual behavior showed more cracks in the slab.

e) FSKJ24

The actual and predicted cracks in pull and push patterns for FSKJ24 using Atena software is shown in Figure 7-19. From the test photos, a good correlation can be seen between the actual and predicted failure mode and the cracking pattern in the pull direction. The pattern is slightly off the actual behavior in the push direction, as shown from Figure 7-19. Atena showed more cracks in the pile base, but the actual behavior showed more cracks in the slab.

f) FSRCC24-M

The actual and predicted crack patterns for specimen FSRCC24-M is shown in Figure 7-20. The cracks concentrated at the pile base region, which was the same as the actual failure mode and cracking.

g) FSKJ24-M

The actual and predicted cracks in pull and push patterns for FSKJ24-M using Atena software are shown in Figure 7-21. From the test photos, a good correlation can be seen between the actual and predicted failure mode and cracking pattern in the pushing and in pulling direction.

7.5 Updated Moment Curvature Results

The moment curvature plots discussed in Section 2.7.1 are updated in this section to reflect the measured material properties for each specimen. The confined and unconfined concrete material models presented in Table 2-6 are updated in Table 7-2. Strain parameters for the unconfined concrete are the same as those provided in Table 2-6. The reinforcement properties used are from Table 3-2. Figure 7-22 through Figure 7-32 show the moment curvature plots for the piles, while Figure 7-33 through Figure 7-48 show the moment curvature for the slab.

Based on the updated moment curvature results, Table 2-7 for the pushover preliminary analysis are updated as shown in Table 7-3. Table 7-3 shows the actual and predicted yield load, ultimate load and displacement using Paulay and Priestley[20] empirical equations shown in Section 2.8. Table 7-3 shows that the predicted yield and ultimate loads are close to the measured force, while the calculated displacements are less than the actual displacement. The reason of the difference in the expected and actual value was because the predicted values are based on the first confined fiber reaching the failure, while actual values are based on the crushing penetration to the core. The actual lengths of the plastic hinge in the piles are determined from the experimental results and are shown in Chapters 4 and 6. The plastic hinge length in both the experimental and using Paulay and Priestley[20] empirical equations are very close, see Table 7-3.

All the specimens were designed to satisfy Equation 2-12, except for specimens DCRCC1 and FSRCC1. DCRCC1 and FSRCC1 were detailed based on standard details of Caltrans[12] as mentioned in Section 2.5. The ratio between $(M_n)_{slab}$ and $(M_u)_{pile}$ is listed in Table 7-4, where these values were based on the moment curvature calculation shown in Figure 7-22 through Figure 7-48. Although the ratio $(M_n)_{slab}/(M_u)_{pile}$ for all specimen was greater than or equal to 1.2, the failure in specimens FSRCC1 and FSKJ24 occurred in the slab. Based on the previous discussion, it can be said that Equation 2-12 was not sufficient to avoid the failure to occur in the pile, and additional reinforcement was needed. The additional reinforcement requirement will be discussed in detail in Chapter 8.

Chapter 8
Design Recommendations

8.1 Introduction

Chapter 8 consolidates the previously presented experimental and analytical research into a set of design guidelines that can be used for the design of T-joints and knee-joints of slab bridges. These design guidelines focus on the joint reinforcement details for the proposed 24 in. pile diameters. While the provisions focus on 24 in. diameter pile joints, the rules could be used for other diameter piles. The recommendations enable the force and moment to be effectively transferred between the pile and slab of the superstructure. The tension force demand inside the 24-in. diameter pile slab-bridge joints for different configurations are summarized in Tables 6-12 and 6-13. The current specifications for slab-bridge joints cover 16-in. diameter piles. Guidelines for larger piles are limited; thus, box-girder specifications were used to design slab-bridge joints. The box-girder specifications were not sufficient for larger diameter piles. The guidelines for the currently used 16 in. pile are discussed in Section 8.7. Recommendations for the effective width of the slab are discussed in this chapter.

8.2 Superstructure Design of the Slab Bridges

The experimentally validated strut-and-tie models presented in Chapters 5 and 6 were applied to 46 different joint configurations for 24-in. diameter piles. Based on the results from the strut-and-tie models, the following section provides recommendations for designing of T-joints and knee-joints for pile-slab bridges.

8.2.1 Superstructure Seismic Forces

In general, the superstructure of slab bridges should be designed to remain essentially elastic during a seismic event in order to concentrate the majority of inelastic behavior to the pile above the ground where the repairs can be made easily. In order to satisfy the above statement, Caltrans[5] requires the superstructure seismic capacity for moment-resisting joints to be 1.2 times greater than the pile ultimate moment capacity for T-joints and knee-joints, as shown in Equation 2-12. It was found in this study that the 1.2 ratio was not sufficient to keep the slab elastic, and additional reinforcement was needed; this will be discussed in detail in Sections 8.3.4 and 8.4.4 for T-joints and knee-joints, respectively.

8.2.2 Joint Dimensions

From the STM and experimental results, guidelines have been established for the basic joint dimensions that should be used in the analysis and design. These guidelines include when a drop cap is needed, drop cap width and effective width in a flat slab.

8.2.2.1 Connection Type

From the STM results, it was recommended that for slab depths less than 17 inches a drop cap be used. The strut-and-tie model results showed a large increase in the required additional reinforcement for slab depths less than 17-in. with 24-in. diameter piles (see Tables 6-11 and 6-12). This means that slabs with span lengths less than 32 ft should use drop-cap joints, and for span lengths equal to or more than 32 ft, a flat slab can be used.

8.2.2.2 Drop Cap Width

The drop cap width should be wide enough to provide sufficient room for the stirrups outside the pile core region on either side of the joint. The recommended drop-cap width by BDA[27] is 36 in. for the 16-in. pile diameter, which is also the effective width of the drop-cap where the main longitudinal reinforcement is concentrated. The width for drop-cap specimens with 24-in. pile diameter was 36 in. The main reinforcement was also concentrated within this width. The performance of the drop-cap specimens was good with the failure occurring in the piles as mentioned before in Sections 4.2.1 and 4.6.1. The knee-joint specimen (DCKJ24) was 2/3 scale. Because of this, the 24-in. diameter pile was 16 inches in diameter in the experiment. The width of the drop cap was 24 inches. This is equivalent to a 16-in. diameter pile with a 24 in. wide drop cap. The specimen performed very well. Therefore, it is sufficient to take the drop cap width as pile diameter plus 1 ft.

8.2.2.3 Effective Width for Flat Slabs

Based on ACI recommendations for beam-column connections[7], the effective width for the flat slab specimen was chosen to be two times the width of the stirrups in the transverse direction for specimens FSRCC24, FSRCC24-M and FSKJ24-M. The experimental results, in Sections 4.5.1 and 4.5.3 for specimen FSRCC24, showed even with slab failure, the legs of the transverse stirrups had strains less than half of yield, because the stirrups legs were located at distance of 18.5 in. from the pile face; this stirrup spacing would require an effective width of 61 in. The failure in the slab occurred within a width less than 4 ft, as shown in Figure 8-4. The longitudinal reinforcement should be concentrated in the strip where the failure occurred.

The minimum bent-cap width based on Caltrans recommendations[5] was equal to the pile diameter plus 2 ft. In the modification for specimen FSRCC24, additional transverse stirrups with smaller width, equal to the minimum bent-cap width, were used, and the main longitudinal reinforcement was concentrated inside this width. The performance of the modified specimen, FSRCC24-M, with the small width transverse stirrups, was very good; the failure occurred in the pile, and the strain of additional transverse stirrups was higher compared to the strain for the transverse stirrups of specimen FSRCC24.

The STM (see Sections 5.3, 5.6, 6.4.1.2 and 6.4.22) showed that the compression struts outside the joint were spreading in a distance equal to half of the slab thickness ($h_b/2$), which generated tension forces in Ties T_{AB} and T_{IJ}, see Figure 5-4. This means that the stirrups legs should be located at distance equals ($h_b/2$) from the pile face in order to carry the tension force T_{AB} and T_{IJ}. Therefore, it is recommended that the effective width should be equal to the pile diameter plus the slab thickness. This is requirement is slightly different than what is current specified by Caltrans (Dc + 2 ft). The change was made due the STM results. Within this effective width, the transverse reinforcement and moment reinforcement should be placed.

8.2.3 Principal Joint Stresses

The equations for the principal stresses are included in Section 2.4. These equations are used by Caltrans for joint detailing. It is recommended to use the Caltrans[5] maximum principal stress limits of $3.5\sqrt{f_c'}$(psi) for tension and $0.25f'_c$ for compression. If the compression stress is more than $0.25f'_c$, the slab thickness should be increased.

If principal tensile stresses are below $3.5\sqrt{f_c'}$(psi) then it is recommended to provide minimum joint reinforcement to control the cracks. The minimum joint reinforcement should be provided by extending the pile transverse reinforcement into the joint. The requirements for the longitudinal reinforcement of the slab should be satisfied according to Sections 8.3.4 and 8.4.4, for T-joints and knee-joints, respectively. Equation 8-1[5] is used to determine the minimum reinforcement ratio in the joint for the T-joints and knee-joints.

$$\rho_{s\,min} = 3.5\sqrt{f_c'}/f_y \text{(psi)} \qquad \text{Equation 8-1}$$

where, f_c' = the concrete strength, f_y = the yield strength of the longitudinal reinforcement of the pile.

If the tensile principal stress exceeds $3.5\sqrt{f_c'}$(psi), then a detailed joint design procedure should be performed using the recommendations of the experimentally developed strut-and-tie models in Chapters 5 and 6, which is summarized in Section 8.3 for T-joints and Section 8.4 for knee-joints.

8.2.4 Punching Shear

Slab-bridge joints must be safe against punching shear[8]. Equation 2-13 through Equation 2-18 can be used to check the punching shear. The equations are directly applicable to square cross sections; therefore, circular pile cross sections should be transformed into square sections. From the current study it can be said that the flat slab joints are more critical for punching shear than the drop-cap joints.

8.3 T-Joint Reinforcement Recommendations

Equation 8-2 is an equation developed by Priestley *et al.*[23], and gives good agreement with the results of the cross-section analysis, as mentioned previously in Section 5.4.

$$T_C = 0.5A_{st}\lambda_a f_{yc} \qquad \text{Equation 8-2}$$

where, A_{st}, λ_a and f_{yc} are the total pile longitudinal bar area, overstrength factor of the pile longitudinal reinforcement from the rebar test, and yield strength of pile longitudinal bars, respectively. For simplicity, λ_a was assumed to be[5] 1.4 and all of the joint reinforcement was assumed to have the same yield strength. Equation 8-2 can then be written as shown in Equation 8-3.

$$T_C = 0.7A_{st}f_{yc} \qquad \text{Equation 8-3}$$

8.3.1 Vertical Joint Stirrups

Vertical joint stirrup reinforcement is based on the larger of Tie T_{IJ} or T_{AB} in the strut-and-tie model shown in Figure 5-4 for the T-joint. The vertical stirrups should be placed in both sides of the pile in zones 3 and 4 within a distance equal to half the column/pile diameter (Dc/2), based on Caltrans recommendations, as shown in Figure 8-1. Other researchers[23, 26] recommend that the stirrups should be distributed within a distance equal to the beam/slab height (h_b/2) from the pile face. So it is recommended to place the stirrups from the pile face within a distance equal to half the beam height (h_b/2) or half the column diameter (Dc/2), whichever is smaller.

Based on Caltrans specifications, shown in Table 8-1, the vertical stirrups on both sides of the joint should be 20% of the total area of the pile longitudinal reinforcement. This amount of reinforcement was determined not to be sufficient for the 24 in. pile diameter joints, and additional vertical stirrup were needed. Equation 8-4 and Equation 8-5 were derived from the strut-and-tie results mentioned in Section 6-6, and using Equation 8-3. The vertical stirrups' reinforcement should be equal on both sides of the joint. Equation 8-4 is used for the drop-cap joints, while Equation 8-5 used for flat-slab joint.

$A_s^{jv} = 0.2 \times A_{st}$ (Drop Cap-joint T-joint) Equation 8-4

$A_s^{jv} = 0.3 \times A_{st}$ (Flat Slab-joint T-joint) Equation 8-5

where

A_s^{jv} = area of the vertical stirrups,

A_{st} = area of the longitudinal reinforcement of the pile/column extended inside the joint.

8.3.2 **Horizontal Joint Stirrups**

The horizontal stirrups specified by Caltrans[5] were not changed (see **Table 8-1).** Horizontal stirrups or ties shall be placed transversely around the vertical stirrups or ties in two or more intermediate layers spaced vertically at not more than 18 in. This horizontal reinforcement, $A_s^{jh} = 0.1 \times A_{st}$, shall be placed around the vertical joint stirrups specified in Section 8.3.1.

8.3.3 Splice-Transfer Reinforcement

The Seismic Design Criteria[5] has no recommendations to provide j-bars in the pile slab joint core for straight bridges. Almer, K.[4], recommended additional vertical steel in the joint area based on his study on the box-girder bridges loaded in the longitudinal direction. The location of Tie T_{CD} from the centroid of the joint changes, depending on the loading direction (see Figure 5-4). The vertical stirrup and j-bars, A_s^{j+s}, inside the pile core, are responsible for transferring part of the pile tension to the top mat of the slab reinforcement. A_s^{j+s} should be able to resist twice the tension demand, T_{JV}, of Tie T_{CD}. The tension demand, T_{JV}, is equal to 0.75 times the tension force in the longitudinal reinforcement of the pile (see Table 6-11).

Based on the experimental results, it is recommended to place A_s^{j+s} in zones 1, 2 and 5, as shown in Figure 8-1. The reinforcement in zone 5 should be j-bars, while outside the pile core in zones 1 and 2 should be stirrups, as shown in Figure 8-2. It is also recommended to stagger the length of the j-bars if the development length and joint configuration permits it. It was recommended by other researchers [4] that the j-bars' length should be at least 2/3 of the joint depth and longer if more development length is needed.

Based on the strut-and-tie model results for the T-joints, shown in Section 6-6 and using Equation 8-3, the area of j-bars and stirrups needed to resist Tie T_{CD} is given by Equation 8-6, where A_s^{j+s} is the area of the j-bars and the vertical stirrups. It is recommended to concentrate the majority of A_s^{j+s} inside the pile core zone 5 as j-bars and the rest as vertical stirrups in zones 1 and 2 (see Figure 8-1).

$A_s^{j+s} = 1.05\ A_{st}$ Equation 8-6

8.3.4 Slab Longitudinal Reinforcement in the Transverse Direction of the Bridge

The longitudinal reinforcement in the slab must satisfy $(Mn)_{slab}/(Mu)pile=1.2$; also, additional reinforcement in the joint region must be added based on the STM results.

The SDC[5] does not require additional longitudinal reinforcement in T-joints. In order to find the additional reinforcement for the bottom reinforcement of the slab, a simplified STM, shown in Section 6-6 and Equation 8-3, were used to derive Equation 8-7 and Equation 8-8. Both of these equations are applicable for the 24 in. pile diameter.

$A_{bt} = A_{bb} = 0.25\ A_{st}$ (Drop-Cap Joint) Equation 8-7

$A_{bt} = A_{bb} = 0.35\ A_{st}$ (Flat-Slab Joint) Equation 8-8

where, A_{bt} and A_{bb} are the additional longitudinal reinforcement in the top and bottom of the slab, respectively. The additional longitudinal reinforcement should be extended at least a distance (L_d + the longer of Dc/2 or $h_b/2$) beyond pile face on both sides. It is also recommended to stagger the length of the additional longitudinal reinforcement.

8.3.5 Horizontal Side Reinforcement

The horizontal side reinforcement from Caltrans recommendations[5] was not changed. The total longitudinal side face reinforcement in the bent cap shall be at least equal to the greater of the areas specified in Table 8-1 and shall be placed near the side faces of the joint, with a maximum spacing of 12 in.

8.4 Knee-Joint Reinforcement Recommendations

8.4.1 Vertical Joint Stirrups for Knee-Joints

Vertical joint stirrup reinforcement calculations for the knee-joint are based on the larger tension value of Tie T_{AB} in the strut-and-tie model for the opening and closing cases (see Figures 6-79 and 6-82). The vertical stirrups should be placed in zones 3 and 4 (see Figure 8-3), within a distance equal to half the column/pile diameter (Dc/2) from the pile face, based on Caltrans recommendations. Other researchers[23, 26] recommend that the stirrups should be placed within a distance equal to half the beam/slab height ($h_b/2$), so it is recommended to place the stirrups from the pile face within a distance equal to half the beam height ($h_b/2$) or half the column diameter (Dc/2), whichever is smaller.

Based on Caltrans specification[5] for the knee-joint shown in Table 8-2, the vertical stirrups on the interior side of the pile should be 20% of the total area of the pile longitudinal reinforcement (see Equation 8-9 and Equation 8-10). Based on the experimental study and STM, this ratio was sufficient, but the width for the vertical stirrups should not be more than the pile diameter (24 in.) plus the smaller slab thickness or pile diameter.

$A_s^{jv} = 0.2 \times A_{st}$ (Drop-Cap Knee-Joint) Equation 8-9

$A_s^{jv} = 0.2 \times A_{st}$ (Flat-Slab Knee-Joint) Equation 8-10

8.4.2 Horizontal Joint Stirrups

The horizontal joint stirrups specified by Caltrans[5] were not changed. Horizontal stirrups or ties shall be placed transversely around the vertical stirrups or ties in two or more intermediate layers spaced vertically at not more than 18 in. This horizontal

reinforcement, $A_s^{jh} = 0.1 \times A_{st}$, shall be placed around the vertical joint stirrups specified in Section 8.4.1.

8.4.3 Splice-Transfer Reinforcement for the Knee-Joints

The splice-transfer and splitting reinforcement requirement are based on the tension developed at the top of the joint described by Ties T_{CD} and (T_{XY} and $T_{X'Y'}$), respectively (see Figures 6-79 and 6-82). The location of Tie T_{CD} from the centroid changes with the changing of the loading direction. The vertical stirrups and j-bar reinforcement, A_s^{j+s}, inside the pile core are responsible for transferring a portion of the pile tension to the top mat of the slab reinforcement. A_s^{j+s} should be able to resist twice the tension demand, T_{JV}, of Ties T_{CD}, T_{XY} and $T_{X'Y'}$. The tension demand, T_{JV}, is equal to 0.6 times the tension force in the longitudinal reinforcement of the pile (see Table 6-12). Based on the experimental results, it is recommended to place A_s^{j+s} in zones 1, 2 and 5, as shown in Figure 8-3. The reinforcement in zone 5 should be j-bars, while outside the pile core in zones 1 and 2 should be stirrups, as shown in Figure 8-2.

Based on the strut-and-tie model results for the knee-joints, the area of j-bars and stirrups needed to resist Tie T_{CD} force is given by Equation 8-11, where A_s^{j+s} is the area of the j-bars and the vertical stirrups.

$$A_s^{j+s} = 0.85\, A_{st} \qquad \text{Equation 8-11}$$

It is recommended to concentrate the majority of A_s^{j+s} inside the pile core zone 5 as j-bars and the rest as vertical stirrups in zones 1 2 (see Figure 8-3).

8.4.4 Slab Longitudinal Reinforcement in the Transverse Direction of the Bridge

The longitudinal reinforcement in the slab must satisfy $(Mn)_{slab}/(Mu)pile=1.2$; also, additional reinforcement in the joint region must be added based on the STM results. The SDC[5] of Caltrans also required additional flexural reinforcement at the top and bottom in the transverse direction within the bentcap width for the knee-joint. This provision was met with continuous u-bars. Caltrans recommended that the u-bars reinforcement should be a minimum of 33% of the pile reinforcement. According to the STM, this ratio was not sufficient to fulfill the flexural requirements for the knee-joint. In order to find the additional reinforcement for the top and bottom reinforcement of the slab, the results of Section 6-6 was used to derive Equation 8-12. Equation 8-12 is applicable for the top and bottom reinforcement for the 24-in. pile diameter.

$$T_{bt}=T_{bb} = 0.5\, T_c \text{ (Drop-Cap Joint and Flat Slab Joint)} \qquad \text{Equation 8-12}$$

Splices in u-bars should not be located within a distance (L_d + the larger of Dc/2 or $h_b/2$) beyond the interior pile face. Based on Equation 8-12, the area of the u-bars, A_s^{u-bar}, can be rewritten as a ratio of the longitudinal reinforcement of the pile, A_{st}; by substituting Equation 8-3 into Equation 8-12 (see Equation 8-13).

$$A_s^{u-bar} \min = 0.35 \times A_{st} \qquad \text{Equation 8-13}$$

8.4.5 Horizontal Side Reinforcement:

The horizontal side reinforcement specified by Caltrans[5] was not changed. Based on Caltrans recommendations[5], the total longitudinal side face reinforcement in the bent cap

shall be at least equal to the greater of the areas specified Table 8-2 and shall be placed near the side faces of the joint, with a maximum spacing of 12 in.

8.4.6 Horizontal Cap End Ties

Based on Caltrans recommendations[5], the horizontal cap end ties are only used when the bent cap short stub length, S, is less than Dc/2 (see case 1 in Figure 8-3). The area of the horizontal ties, A_s^{jhc}, placed at the end of the bent cap shall be equal to the area specified in Equation 8-14. This reinforcement shall be placed around the intersection of the bent cap horizontal side reinforcement and the continuous bent cap u-bar reinforcement, spaced at not more than 12 in. vertically and horizontally. This horizontal reinforcement shall extend through the pile cage to the interior face of the pile.

$$A_s^{jhc} = 0.33 \times A_s^{u-bar} \text{ min} \qquad \text{Equation 8-14}$$

8.5 Pile Transverse Reinforcement

The pile transverse reinforcement specified by Caltrans[5] was not changed. The force in the transverse reinforcement of the pile inside the joint region based on the proposed strut-and-tie design models did not exceed 8% and 25% of the tension force of the pile for the T-joints and knee-joints, respectively. This means the area of the transverse stirrups should be at least 18% of the longitudinal reinforcement of the pile (see Equation 8-15).

$$A_s = 0.18\ A_{st} \qquad \text{Equation 8-15}$$

where A_s= area of the pile transverse stirrups.

When the principal stress exceed the limits of $3.5\sqrt{f_c'}$(psi) for tension, the SDC[5] recommends Equation 8-16 with the minimum of Equation 8-1 to find the transverse stirrups for the T-joint and knee-joint bent-cap with short stub length, S equals Dc/2 < S <Dc or L_d. For the knee-joint bent-cap with short stub length, S less than Dc/2, Equation 8-17 should be used with the minimum of Equation 8-1.

$$\rho_{s\,min} = 0.4\frac{A_{st}}{l_{ac}^{\ 2}} \qquad \text{Equation 8-16}$$

$$\rho_{s\,min} = 0.6\frac{\rho_l D_c}{l_{ac}} \qquad \text{Equation 8-17}$$

where

ρ_l = ratio of the longitudinal reinforcement of the pile,

D_c = pile diameter, and

l = length of the pile/column embedded into the bent cap.

The SDC[5] recommended that the ductility of the flexural members should be larger than 3, based on the ductility calculated at 80% of the ultimate load. As shown in Table 8-3, the ductility at 80% of the ultimate load is higher than 3, for specimens DCKJ24, FSRCC24-M and FSKJ24-M. The failure occurred in the pile at a sufficient ductility level, so there was no need for additional confinement for the pile.

8.6 Pile Longitudinal Reinforcement

It is recommended to extend the main reinforcement of the pile as deep as possible in the joint in order to provide a more efficient load transfer path. The farther the pile main

longitudinal reinforcement extended into the joint, the higher Node D in the strut-and-tie model could be located. The higher Node D was in the strut-and-tie, the lower the vertical tie demand to direct the joint compression strut (C_{AD}) and (C_{AD} and C_{AG}) for the T-joint and knee-joint, respectively, as shown in Figures 5-4, 6-79 and 6-82. Another benefit of locating Node D as far into the joint as possible was that lower horizontal tie demands were needed in order to direct the main compression strut to Nodes H and B for the T-Joint and knee-joint as well.

8.7 Reinforcement Recommendations for 16-in. Pile Diameter Joints

From the 16-in. pile experimental results, plastic hinging occurred in the pile, and no cracks were seen in the slab. From Table 8-3, the ductility of pile for specimen DCRCC1 was 2.8, which was less than the SDC[5] recommendation for ductility value (3); therefore, it is recommended to increase the confinement of the pile by increasing the confinement ratio of the pile.

Based on Caltrans Seismic Design Criteria[5], the nominal moment capacity of the slab must be at least 1.2 times the pile capacity (see Equation 2-12). For the specimens with 16 in. pile diameter, the ratio between $(Mn)_{slab}$ and $(Mu)_{pile}$ for specimens DCRCC1 and FSRCC1 was 4.83 and 2.86, respectively, which was higher than the 1.2 ratio, as shown in Table 7-4. The current flexural reinforcement specifications[27] for the 16-in. pile joints are sufficient to keep the slab elastic while the pile reached failure.

If principal tensile stresses are below $3.5\sqrt{f_c'}$(psi) then it is recommended to provide minimum joint reinforcement to control the cracks. The minimum joint reinforcement shown in Equation 8-1[5] should be provided by extending the pile transverse reinforcement into the joint. If the flexural reinforcement mentioned in BDA[27] for the slab-bridge joint for the 16-in. pile is changed, the ratio $(Mn)_{slab}/(Mu)_{pile}$ should be 1.2 or larger, and the additional flexural reinforcement shown in Sections 8.3.4 and 8.4.4 should be added, depending on the joint type. If principal tensile stresses are larger than $3.5\sqrt{f_c'}$(psi) in tension for the 16-in. pile, it is recommended to use Sections 8.3 to 8.6 for the joint design.

Chapter 9
Summary and Conclusions

9.1 Summary

This study was done to investigate the behavior of slab bridge joints for Caltrans. Although slab bridges are a common type of bridge, the current version of the Bridge Design Specification (BDS)[30] and the Seismic Design Criteria (SDC)[5] provide limited design guidance for pile extension connection details for slab bridges; therefore, the box-girder bridge connections guidelines must be used to design the slab-bridge joints, which were not predesigned.

The primary objective of this project was to understand the behavior of pile-slab connections. This was done by an experimental testing program that included existing slab bridge details for the 16 in. diameter pile and the proposed slab-bridge joints for 24 in. diameter piles. Through testing and evaluation, the adequacy details for slab-bridge joints could be determined, and design guideline recommendations for Caltrans could be made.

In order to satisfy the research objectives, a survey of Caltrans slab bridges was done to find the typical joint details and the critical variables. Little information was known about the behavior of bridge pile/column connections for slab bridges, so the column/pile connection research, whether for bridges or buildings, was used to provide insight into methodologies for design of slab connection regions.

Ultimately, models of five full-scale slab bridge T-joints and three 2/3-scale slab bridge knee-joints were constructed, instrumented, and experimentally tested at the Large Scale Structures Laboratory at the University of Nevada, Reno (UNR). The first two specimens, DCRCC1 and FSRCC1, represented existing slab-bridge joints for 16-in. diameter piles. The difference between the first two specimens was that specimen DCRCC1 was a drop-cap T-joint, while FSRCC1 was flat-slab T-joint.

Caltrans suggested 24-in. diameter piles to be used in the next six specimens since they were used in situations where liquefaction could occur. Since there were no standard details, the reinforcement and the dimensions of the 24-in. diameter pile specimens were based on the box-girder bridge design procedures. The third and fourth specimens, DCRCC24 and FSRCC24, were T-joints with the 24-in. diameter piles. Specimen DCRCC24 was a drop-cap joint, while FSRCC24 was a flat-slab joint. The fifth and sixth specimens, DCKJ24 and FSKJ24, were knee-joints with 24-in. diameter piles. DCKJ24 was a drop-cap joint, while FSKJ24 was a flat-slab joint. The seventh and eighth specimens, FSRCC24-M and FSKJ24-M, were flat-slab joints with a 24-in. diameter pile. FSRCC24-M was a T-joint, while FSKJ24-M was a knee joint. The slabs were designed to stay essentially elastic. Each specimen was designed to fulfill the Caltrans Seismic Design Criteria[5] requirements, where the nominal moment capacity of the slab should be 1.2 times the pile ultimate capacity.

Each specimen was subjected to reverse cyclic loading at increasing amplitudes using actuators attached to the pile. Axial load was applied on the pile top of each specimen. The axial load for the T-joints was held constant. For the knee joint, the axial load was variable. Data was collected during the loading of each specimen using strain gauges, displacement transducers, load cells, and photos of damage and crack patterns

after each loading stage. Post-analysis analytical modeling was conducted to predict force-displacement response and compared against the experimental data. The finite element program, Atena[18], was used to develop an analytical model for each specimen in order to examine the causes of failure in the joints. For the force transfer between the pile and the slab, strut-and-tie models were developed based on experimental data collected for each specimen. The last two specimens were designed based on the experimental results and the developed strut-and-tie models.

Based on both the experimental and analytical results from the research, design recommendations were proposed for slab bridge T and knee-joints. The design recommendations were provided in equation format to make them easier to use.

9.2 Conclusions

The main conclusions resulting from the experimental testing and analytical modeling of the slab-bridge joints, subjected to reverse cyclic loading in the transverse direction of the bridge, are summarized in the following subsections.

9.2.1 Experimental Testing and Observation Conclusions

The conclusions based on experimental testing and observations are presented below.

1- The failure mode for the 16-in. diameter pile slab bridge T-joints occurred in the pile with a few hairline cracks seen in the slab; this behavior was true for the flat slab (FSRCC1) and drop cap (DCRCC1) using the existing Caltrans design procedures. The ductility at 80% of the ultimate load for specimen DCRCC1 was 2.8 and 3.9 for specimen FSRCC1; Caltrans recommends that the ductility[5] at 80% should be at least 3. Further confinement of the pile would help the system to reach the desired ductility level.

2- The failure mode for the 24-in. diameter pile T-joints based on the existing design procedure using a drop cap (DCRCC24) was mainly in the pile with some cracks in the slab support hinge location. When the 24-in diameter pile used a flat slab, the failure occurred in the slab (FSRCC24), which was not desired as a failure mode.

3- The failure for the 24in. diameter pile knee-joint with a drop cap (DCKJ24) was mainly in the pile with some small cracks in the slab. When the 24-in. diameter pile knee-joint used a flat slab (FSKJ24), the joint failed in the slab, which was not desired failure mode.

4- When the flat slab 24-in. diameter pile specimens, T-joint (FSRCC24-M) and knee-joint (FSKJ24-M), were redesigned, none of the slab longitudinal reinforcement or the slab transverse reinforcement were exposed at the end of the test. Failure occurred in the pile, and minimum cracks were seen in the slab.

   The results showed that the existing design procedures for slab-bridge joints with a 24-in. diameter pile was not sufficient when a flat slab joint was used, but was sufficient for a drop cap. The proposed details for flat slabs in a T-joint or knee-joint configuration did well.

9.2.2 Analytical Modeling Conclusions

The following conclusions are based on the analytical work, which included the strut-and-tie model and the results from Atena program. Strut-and-tie models were developed based on the reinforcement strain and the observations needed during each

experiment. The strain levels for the slab reinforcement of specimens DCRCC1 (16-in. diameter pile drop cap T-joint), FSRCC1 (16-in. diameter pile flat slab T-joint) and DCRCC24 (24-in. diameter pile drop cap T-joint) were low; therefore, it was hard to verify the STM for them. After the STM models were developed for the remaining specimens, the models were verified against the measured data. The recommended reinforcement details were tested in specimens FSRCC24-M (modified 24-in. diameter pile flat slab T-joint) and FSKJ24-M (modified 24-in. diameter pile flat slab knee-joint). The additional reinforcement showed high strain, which meant that the additional reinforcement worked actively in the force transfer inside the joint. The box-girder design procedures are generally applicable to slab-bridge joints, but modifications are needed. Guidelines for the modification of the slab-bridge joints were discussed in detail in Chapter 8. The STM showed that there were some shortages in the design of slab-pile connections:

1- Although the nominal moment capacity of the slab in specimens FSRCC24 (24-in. diameter pile flat slab T-joint) and FSKJ24 (16-in. diameter pile flat slab knee-joint) were 1.2 times of the pile ultimate capacity, as recommended by Caltrans[5], both specimens FSRCC24 and FSKJ24, failed in the slab and the longitudinal reinforcement yielded. Additional flexural longitudinal reinforcement was needed in order to keep the slab elastic while the pile reached failure.
2- In order to be effective, the flexural longitudinal reinforcement must be distributed within the effective width. The effective width of the flat slab is recommended to be equal to the diameter of the pile plus the slab thickness. For the drop-cap joints, the effective width is recommended to be equal to the pile diameter plus 1 ft.
3- Slab failure occurred also due to the lack of j-bars in the pile core. The j-bars inside the pile core were needed for transferring a portion of tension force in the longitudinal pile reinforcement to the top mat slab reinforcement.
4- Vertical stirrups were insufficient and not distributed properly in the transverse direction of the bridge. For better force transfer, additional stirrups with smaller spacing were needed near the external pile face. Additional vertical stirrups were recommended to be distributed within a distance from the pile face not more than the smaller of half the pile diameter or half the slab thickness in the transverse direction of the bridge.
5- It was recommended that the flat-slab depth should not be less than 17 in. This means that the joints for spans less than 32 ft should use drop-cap joints, and for spans equal to or more than 32 ft, the joints should use flat-slab joints. The strut-and-tie model results showed that a large amount of additional reinforcement was needed for flat slabs with a slab thickness of less than 17 in. with 24-in. pile diameters.

The force-displacement response given by the post-analysis using Atena[18] program agreed very well with the measured response for the knee-joints and T-joints. In the T-joints, the program was able to model the force, but the predicted stiffness was higher than the measured stiffness. This could have been due to the cyclic loading or the test setup flexibility. The predicted crack pattern using the Atena program agreed very well with the measured crack patterns.

References:

1-Sritharan, S., “Strut-and-Tie Analysis of Bridge Tee Joints Subjected to Seismic Actions,” *Journal of Structural Engineering*, Vol. 131, No. 9, September 2005, pp. 1321-1333.

2-Moustafa, K., Sanders, D., and Saiidi, M., "Impact of Aspect Ratio on Two-Column Bent Seismic Performance," Center for Civil Engineering Earthquake Research, Department of Civil Engineering, University of Nevada, Reno, Nevada, Report No. CCEER-04-3, February 2004.

3-Nada, H., Sanders, D., and Saiidi, M., “Seismic Performance of RC Bridge Frames with Architectural-Flared Columns,” Civil Engineering Department, University of Nevada, Reno, Report No. CCEER 03-3, January 2003.

4-Almer, K, and D. Sanders, “Longitudinal Seismic Performance of Precast Bridge Girders Integrally Connected to a Cast-in-Place Bentcap”, University of Nevada, Reno, Dissertation Report, December 2008.

5-Caltrans, Seismic Design Criteria, Version 1.3, California Department of Transportation, Sacramento, CA, June 2006.

6-Sritharan Sri, M.J.Ingham “application of strut-Tie Concepts to Prestressed Concrete Bridge Joints in Seismic Regions” PCI Journal July-August 2003.

7-ACI-ASCE Committee 352, “*Recommendations for Design of Beam-Column Connection in Monotonic Reinforced Concrete in Monolithic Reinforced Concrete Structures*”; Committee ACI 352R-02, American Concrete Institute, Farmington Hill, MI, 2002.

8-ACI-ASCE Committee 352, “*Recommendations for Design of Slab-Column Connection in Monotonic Reinforced Concrete in Monolithic Reinforced Concrete Structures*”; Committee ACI 352.1R-89(Reproved 1997), American Concrete Institute, Farmington Hill, MI, 2002.

9-Joen, P.H. and Park, R.,*”Simulated Seismic Load Testes on Prestressed Concrete Piles and Pile-Pile Cap Connections,”* PCI Journal, v35, n6, Nov-Dec, 1990, p 42-61.

10-Harries, K. and F. Petrou,” Behavior of Precast, Prestressed Concrete Pile to Cast-in-Place Pile Cap Connections,” PCI Journal, v46, n4, July-August, 2001, p 82-92.

11-Land, R., “Seismic Strength of Concrete Bridge Superstructures,” Memo to Designers 20-6, California Department of Transportation, Sacramento, CA, August 2001.

12-Caltrans, Bridge Design Aids, California Department of Transportation, Sacramento, CA, July 1990.

13-ACI Committee 318, "Building Code Requirements for Structural Concrete (ACI 318R-2008)," American Concrete Institute, Farmington Hills, Michigan, 2008, 464 pp.

14-AASHTO, LRFD Bridge Design Specifications, 4th Edition, American Association of State Highway Transportation Officials, Washington, D.C., 2007.

15-Caltrans, Bridge Design Specifications, California Department of Transportation, Sacramento, CA, September 2004.

16-XTRACT, V2.6.0, 2002, Imbsen Software Systems, Sacramento, CA.

17-SAP2000 Advanced 12.0.1, Computers and Structures, Inc (CSI), 2007, Berkeley,CA.
18-Atena version 4.1.4.0, Cervenka Consulting, Czech Republic.

19-Mander, J.B., Priestley, M.J.N., and Park, R., "Theoretical Stress-Strain Model for Confined Concrete," Journal of Structural Engineering, Vol. 114, No.8, August 1988, pp. 1804-1826.

20-Paulay,T., and Priestley, M.J.N, "*Seismic Design of Reinforced Concrete and Masonry Buildings*", John Wiley and Sons, Inc, 1992, New York, NY.

21-Esmaeily, A and Xiao, Y. "Seismic Behavior of Bridge Columns Subjected to Various Loading Patterns" Research Report PEER, DEC. 2002, CA.

22-Fachwerk, Version 0.3.1, http://fachwerk.berlios.de/index_en.html, 2007.

23-Priestley, M.J.N, Seible, F., Calvi, G.M., *Seismic Design and Retrofit of Bridge*, John Wiley and Sons, Inc., 1996, 686 pp.

24-Holombo, J., Priestly, M.J.N., and Sieble, F, "Continuity of Precast Prestressed Spliced-Girder Bridges Under Seismic Loads," *PCI Journal*, Vol. 45, No. 2, March-April 2000, pp.40-63.

25-Schlaich, J., and Schafer, K. "Design and detailing of structural concrete using strut and-tie models," *The Structural Engineer*, Vol. 69, No. 6, March 1991.

26-Sritharan, S., "Improved Seismic Design Procedure for Concrete Bridge Joints", *Journal of Structural Engineering*, Vol. 131, No.9, September 2005.

27-Caltrans, Bridge Design Aids, California Department of Transportation, Sacramento, CA, April 2009.

28-Vladimír Červenka, Libor Jendele,and Jan Červenka *ATENA Program Documentation Theory,* Prague, May 12, 2009.

29-Park, R., and Paulay, T., *Reinforced Concrete Structures*, John Wiley & Sons, 1975, New York, NY.

Table 2-1: Variables Matrix for the Prototype Bridges

Bridge Name	Bird Ditch Widening	Pruitt Creek Bridges	Mark West Creek Bridge	Mormon Slough Bridge	Puritan Mine Road UC
Length/ Diameter	13	11	16	9	5
Column Longitudinal Reinforcement Ratio	2.12%	1.325%	1.325%	1.66%	2.50%
Column Transverse Reinforcement Ratio	1.51%	0.968%	0.968%	0.7%	0.53%
Hinge At Base	with	without	without	without	without
Slab Thickness (in)	16	14.75	16	15.25	20.50
Pile Shape	Circular	Hexagonal	Hexagonal	Hexagonal	Circular
Slab Type	Flat-Slab	Flat-Slab	Drop-Cap	Drop-Cap	Drop-Cap

Table 2-2: Variables Matrix for Tested Specimens

Specimen Number	Pile Diameter	Joint Shape	Joint Configuration	Scale
DCRCC1	16-in	T-Joint	Drop-Cap	Full
FSRCC1	16-in	T-Joint	Flat Slab	Full
DCRCC24	24-in	T-Joint	Drop-Cap	Full
FSRCC24	24-in	T-Joint	Flat-Slab	Full
DCKJ24	24-in	Knee-Joint	Drop-Cap	2/3 Scale
FSKJ24	24-in	Knee-Joint	Flat-Slab	2/3 Scale
FSRCC24-M	24-in	T-Joint	Flat-Slab	Full
FSKJ24-M	24-in	Knee-Joint	Flat-Slab	2/3 Scale

Table 2-3: Specimen Dimensions

Specimen	Pile length (in)	Slab Thickness (in)	Specimen Width (in)
DCRCC1	124	13.50	96
FSRCC1	124	17.50	122
DCRCC24	144	12.00	80
FSRCC24	144	17.50	122
DCKJ24	96	8.00	32
FSKJ24	96	9.67	36
FSRCC24-M	144	17.5	122
FSKJ24-M	96	13.33	36

Table 2-4: Scaling Factors

	2/3 Scale		Full Scale	
Quantity	**Model Factor**	**Required**	**Model Factor**	**Required**
Geometric Length, L	$\lambda L=1$	0.67	$\lambda L=1$	1.00
Elastic Modulus, E	$\lambda E=1$	1.00	$\lambda E=1$	1.00
Forces, f	$\lambda f=\lambda E*\lambda L^2$	0.44	$\lambda f=1$	1.00
Stress, s	$\lambda \sigma=\lambda E$	1.00	$\lambda \sigma=1$	1.00
Strain, ε	$\lambda \varepsilon=1$	1.00	$\lambda \varepsilon=1$	1.00
Area, A	$\lambda A=\lambda L^2$	0.44	$\lambda A=1$	1.00
Volume, V	$\lambda V=\lambda L^2$	0.30	$\lambda V=1$	1.00
Second Moment of Area, I	$\lambda I=\lambda L^4$	0.20	$\lambda I=1$	1.00
Moment,	$\lambda M=\lambda f*\lambda L$	0.30	$\lambda M=1$	1.00

Table 2-5: Steel Properties for Preliminary Analysis

Material Properties		Specimen
Grade 60 #8 and less	f_{sy}(ksi)	68
	f_{su}(ksi)	95
	E_s(ksi)	29000
	ε_{sh}	0.0125
	ε_{su}	0.12
	ε_{sm}	0.09
Grade 60 #9	f_{sy}(ksi)	68
	f_{su}(ksi)	95
	E_s(ksi)	29000
	ε_{sh}	0.015
	ε_{su}	0.12
	ε_{sm}	0.09

Table 2-6: Concrete Properties for Preliminary Analysis

Material Properties		Specimen		
		DCRCC1 and FSRCC1	DCRCC24, FSRCC24 and FSRCC24-M	DCKJ24, FSKJ24 and FSKJ24-M
Unconfined Concrete	f'_{co}(ksi)	4		
	ε_o	0.002		
	ε_{sp}	0.006		
Pile Confined Concrete	$f`_{cc}$ (ksi)	5.13	5.21	5.13
	ε_{cc}	0.0034	0.0035	0.0034
	ε_{cu}	0.0135	0.0172	0.0151

Table 2-7: Pushover Analysis Calculations

	Δy (in)	Δp (in)	Δu (in)	Lp (in)	Fy (ksi)	Fu (ksi)
DCRCC1	1.58	6.37	7.95	17.89	13.92	13.20
FSRCC1	1.34	6.62	7.95	17.89	13.48	13.10
DCRCC24	1.60	10.48	12.07	23.00	33.86	37.33
FSRCC24 FSRCC24-M	1.58	10.04	11.61	23.00	35.26	38.12
DCKJ24	1.10	5.25	6.34	15.33	16.57	17.05
FSKJ24 FSKJ24-M	1.10	5.07	6.17	15.33	16.89	17.18

Δy: yield displacement,

Δp: plastic displacement,

Δu: ultimate displacement

Fy: yield force,

Fu: ultimate Force,

Lp: plastic hinge length

Table 3-1: Concrete Strength

Specimen Name		Testing Results		
		At 7 Days	At 28 Days	At the Testing Day
DCRCC1	Slab	5.34 ksi	5.59 ksi	6.24 ksi
	Pile	4.59 ksi	4.9 ksi	5.18 ksi
FSRCC1	Slab	5.34 ksi	5.59 ksi	6.34 ksi
	Pile	4.59 ksi	4.9 ksi	5.18 ksi
DCRCC24	Slab	3.33 ksi	4.44 ksi	4.52 ksi
	Pile	2.91 ksi	3.92 ksi	4.2 ksi
FSRCC24	Slab	3.33 ksi	4.44 ksi	4.55 ksi
	Pile	2.91 ksi	3.92 ksi	4.22 ksi
DCKJ24	Slab	2.48 ksi	4.39 ksi	4.45 ksi
	Pile	3.14 ksi	6.59 ksi	7.1 ksi
FSKJ24	Slab	2.48 ksi	4.39 ksi	4.59 ksi
	Pile	3.14 ksi	6.59 ksi	7.15 ksi
FSRCC24-M	Slab	2.84 ksi	3.86 ksi	4.27 ksi
	Pile	4.17 ksi	5.66 ksi	6.09 ksi
FSKJ24-M	Slab	3.90 ksi	5.51 ksi	7.74 ksi
	Pile	3.94 ksi	6.32 ksi	7.69 ksi

Table 3-2: Measured Reinforcement Properties

Specimen Name			W 5	#3	#4	#5	#6	#7	#8	#9
DCRCC1, FSRCC1	fy	(ksi)	57.2	68.2	65.2	66.12	65.2	62.95	65.21	66.5
	ε_{ye}		0.0028	0.002	0.0022	0.0021	0.0027	0.0023	0.0028	0.0025
	ε_{sh}		0.0028	0.015	0.009	0.016	0.0145	0.015	0.016	0.0126
	fu	(ksi)	72	105.1	95.25	97.52	97.58	93	103.69	104.2
	ε_{su}		0.125	0.125	0.15	0.14	0.13	0.125	0.122	0.132
DCRCC24, FSRCC24	fy	(ksi)		60.12	63.25	64.86	62.55	65.74	60	67.98
	ε_{ye}			0.0021	0.003	0.0025	0.0022	0.0022	0.002	0.0021
	ε_{sh}			0.009	0.009	0.016	0.015	0.015	0.016	0.013
	fu	(ksi)		97.75	101.77	92.14	98.23	103.15	101.21	106.1
	ε_{su}			0.17	0.14	0.18	0.18	0.16	0.15	0..16
DCKJ24, FSKJ24	fy	(ksi)	57.2	60.71	65.2	67.06	61.5	61.5		
	ε_{ye}		0.0028	0.0022	0.0021	0.0023	0.0021	0.002		
	ε_{sh}		0.0028	0.01	0.007	0.007	0.012	0.008		
	fu	(ksi)	72	98.18	98.18	101.31	97.1	93		
	ε_{su}		0.125	0.154	0.15	0.155	0.17	0.18		
FSRCC24-M	fy	(ksi)		66.72	63.31	65.81	68.82	67.67	65.73	68
	ε_{ye}			0.0021	0.0018	0.002	0.0021	0.0021	0.0021	0.002
	ε_{sh}			0.011	0.025	0.0022	0.09	0.055	0.04	0.03
	fu	(ksi)		100.91	102.27	104.42	94.28	105.97	104.92	114.97
	ε_{su}			0.16	0.19	0.15	0.15	0.14	0.16	0.14
FSKJ24-M	fy	(ksi)	57.2	61.11	67	65.97	68.8	68.9		
	ε_{ye}		0.0028	0.0021	0.0021	0.0022	0.002	0.002		
	ε_{sh}		0.0028	0.0063	0.005	0.006	0.005	0.017		
	fu	(ksi)	72	107.21	111.15	109.81	107.71	111.12		
	ε_{su}		0.125	0.13	0.14	0.13	0.16	0.15		

Table 4-1: Maximum and Minimum Measured Force and Displacement of DCRCC1

Stage	Ductility	Average String Pot Displacement at Max. and Min. Force (in)		Actuator Displacement at Max. and Min. Force (in)		Actuator Force (kips)	
Number	Level	Max.	Min.	Max.	Min.	Max.	Min.
Stage (1)	$0.05f_y$	0.16	-0.05	-0.03	-0.12	0.57	-0.57
Stage (2)	$0.10\ f_y$	0.13	-0.02	0.02	-0.18	1.15	-1.15
Stage (3)	$0.15\ f_y$	0.23	-0.07	0.07	-0.25	1.72	-1.72
Stage (4)	$0.25\ f_y$	0.36	-0.22	0.23	-0.41	2.87	-2.87
Stage (5)	$0.5\ f_y$	0.96	-0.92	0.88	-0.94	5.73	-5.73
Stage (6)	$0.75\ f_y$	1.74	-1.63	1.60	-1.72	8.61	-8.62
Stage (7)	$1\ \Delta y$	2.38	-2.39	2.28	-2.37	10.63	-10.52
Stage (8)	$2\ \Delta y$	4.73	-4.77	4.62	-4.72	13.43	-12.91
Stage (9)	$3\ \Delta y$	7.14	-7.12	7.11	-7.20	12.63	-12.42
Stage (10)	$4\ \Delta y$	9.52	-9.33	9.30	-9.55	9.02	-9.62
Stage (11)	$5\ \Delta y$	11.89	-11.77	11.76	-11.86	7.31	-7.35
Stage (12)	$6\ \Delta y$	14.50	-13.95	13.90	-14.45	5.02	-2.93

Table 4-2: Maximum and Minimum Measured Strain (micro strain) in the Reinforcement of DCRCC1

		Stage (1)	Stage (2)	Stage (3)	Stage (4)	Stage (5)	Stage (6)	Stage (7)	Stage (8)	Stage (9)	Stage (10)	Stage (11)	Stage (12)
Gauge		$0.05f_y$	$0.10f_y$	$0.15f_y$	$0.25f_y$	$0.5f_y$	$0.75f_y$	1 Δy	2 Δy	3 Δy	4 Δy	5 Δy	6 Δy
SG1	Max.	30	30	30	30	23	23	45	53	53	90	60	70
	Min.	-23	-15	-23	-23	-38	-38	-30	-30	-21	-65	-21	-11
SG2	Max.	15	15	15	15	8	0	15	23	38	30	38	38
	Min.	-38	-30	-38	-38	-45	-53	-45	-30	-30	-30	-45	-30
SG3	Max.	53	53	53	53	45	45	83	98	76	120	76	120
	Min.	7	7	7	7	-15	-8	15	38	45	0	0	53
SG4	Max.	-8	68	151	369	956	1702	2387	15240	22731	30427	30427	46163
	Min.	-151	-181	-211	-294	-489	-482	-678	-663	22	0	-678	2101
SG5	Max.	23	23	30	30	23	15	30	30	45	45	45	45
	Min.	-30	-22	-30	-30	-30	-37	-22	-22	-38	-7	-38	-15
SG6	Max.	8	8	8	15	0	0	23	30	8630	38	8630	38
	Min.	-38	-38	-38	-38	-53	-60	-45	-38	-1589	-30	-1589	-23
SG8	Max.	68	60	60	60	23	23	68	83	90	105	105	113
	Min.	8	8	15	8	-23	-30	0	15	-38	0	-38	38
SG9	Max.	67	67	67	67	22	22	75	90	22581	120	22581	128
	Min.	15	15	15	15	-31	-23	15	30	45	0	0	67
SG10	Max.	38	38	38	38	38	38	45	83	105	68	105	60
	Min.	-8	-8	-8	-15	-30	-38	-68	-60	-68	-75	-75	-98
SG11	Max.	38	45	38	53	30	22	53	68	23299	83	23299	83
	Min.	-8	-8	-8	-8	-30	-30	-15	0	-4204	0	-4204	22
SG12	Max.	45	45	52	52	45	45	15	22	37	45	45	45
	Min.	-15	0	0	-8	-8	-23	-53	-38	-45	-23	-53	-15
SG13	Max.	23	23	23	16	31	-0	-7	-45	-72	-45	-72	-60
	Min.	-76	-83	-76	-83	-113	-121	-121	-113	-166	-46	-166	-46
SG14	Max.	8	8	8	23	30	15	76	106	113	128	128	136
	Min.	-45	-45	-45	-45	-90	-105	-83	-45	-30	-22	-83	-15
SG15	Max.	60	60	60	60	22	30	67	90	12231	113	12231	120
	Min.	15	7	15	15	-30	-15	0	30	45	0	0	60

Cont. Table 4-2: Maximum and Minimum Measured Strain (micro strain) in the Reinforcement of DCRCC1

		Stage (1)	Stage (2)	Stage (3)	Stage (4)	Stage (5)	Stage (6)	Stage (7)	Stage (8)	Stage (9)	Stage (10)	Stage (11)	Stage (12)
Gauge		$0.05f_y$	$0.10f_y$	$0.15f_y$	$0.25f_y$	$0.5f_y$	$0.75f_y$	1 Δy	2 Δy	3 Δy	4 Δy	5 Δy	6 Δy
SG16	Max.	1340	1348	1340	1348	1333	1333	1371	1378	1408	1408	1408	1423
	Min.	1295	1295	1288	1288	1273	0	1273	1273	15	0	0	1310
SG18	Max.	45	45	45	53	38	45	53	60	68	75	75	75
	Min.	0	-8	-8	-8	-8	-15	-8	0	-45	0	-45	7
SG19	Max.	60	68	68	83	75	98	158	324	610	1107	1107	30976
	Min.	8	0	-7	-7	-38	-38	-7	-15	-83	0	-83	625
SG20	Max.	15	23	23	23	8	8	46	68	98	98	98	128
	Min.	-22	-30	-30	-37	-52	-60	-45	-45	-92	-92	-45	-15
SG21	Max.	-8	30	75	173	625	1325	1958	5686	15597	25771	25771	25771
	Min.	-113	-144	-181	-264	-565	-580	-889	-2147	-1989	-6560	-6560	-6560
SG22	Max.	60	68	68	83	60	90	150	188	203	211	211	218
	Min.	15	15	15	15	-8	-15	23	23	-16	0	-46	53
SG23	Max.	76	76	83	83	38	38	91	106	22870	136	22870	143
	Min.	23	30	30	30	-22	-22	23	30	45	0	0	68
SG24	Max.	15	15	15	15	15	8	15	23	3613	23	3613	15
	Min.	-30	-38	-30	-38	-45	-45	-45	-38	-1792	-38	-1792	-45
SG25	Max.	8	8	8	15	0	0	23	23	113	30	113	30
	Min.	-37	-37	-45	-45	-68	-83	-75	-68	-52	-60	-75	-45
SG26	Max.	8	8	8	8	8	0	23	38	121	53	121	61
	Min.	-37	-37	-37	-37	-52	-60	-45	-30	-30	-30	-45	-30
SG27	Max.	45	52	45	52	15	22	60	75	9916	98	9916	105
	Min.	0	0	-8	-8	-45	-38	-8	22	-1709	0	-1709	45
SG29	Max.	45	45	45	45	0	15	68	76	20611	91	20611	226
	Min.	-7	-7	-7	-15	-52	-52	-15	-7	-5204	-7	-5204	-45
SG30	Max.	38	45	45	45	7	15	45	53	21106	68	21106	120
	Min.	-8	-8	-8	-8	-45	-45	-15	0	7	0	-15	-23
SG32	Max.	-150	-105	-68	38	625	648	2011	6672	8946	13141	13141	16861
	Min.	-271	-316	-361	-467	-783	-1077	-1288	-1830	-1318	-1423	-1830	-474

Cont. Table 4-2: Maximum and Minimum Measured Strain (micro strain) in the Reinforcement of DCRCC1

		Stage (1)	Stage (2)	Stage (3)	Stage (4)	Stage (5)	Stage (6)	Stage (7)	Stage (8)	Stage (9)	Stage (10)	Stage (11)	Stage (12)
Gauge		$0.05f_y$	$0.10f_y$	$0.15f_y$	$0.25f_y$	$0.5f_y$	$0.75f_y$	1 Δy	2 Δy	3 Δy	4 Δy	5 Δy	6 Δy
SG33	Max.	7	7	7	7	22	15	15	15	8	7	8	7
	Min.	-38	-46	-46	-46	-30	-38	-38	-38	-46	-46	-46	-53
SG34	Max.	-53	15	75	218	753	1453	2063	10725	12592	16885	16885	2.00E+05
	Min.	-189	-226	-271	-377	-678	-678	-1010	-979	22	0	-1010	2666
SG35	Max.	776	784	784	784	761	761	806	814	821	829	829	836
	Min.	731	731	731	731	716	0	738	746	-68	0	-68	761
SG36	Max.	-188	-120	-60	113	783	813	2334	8944	17399	29581	29581	2.00E+05
	Min.	-339	-407	-459	-572	-949	-1250	-1438	-2356	-3433	-806	-3433	-3.00E+05
SG38	Max.	-15	38	75	188	805	1566	2221	2868	9991	14644	14644	2.00E+05
	Min.	-136	-166	-203	-301	-602	-602	-964	-1739	-1604	-3825	-3825	-4420
SG39	Max.	15	15	15	22	7	0	30	97	1062	158	1062	180
	Min.	-38	-31	-38	-38	-53	-61	-53	-38	-60	-8	-60	22
SG40	Max.	-113	-67	-22	106	625	655	2048	8494	17432	29781	29781	2.00E+05
	Min.	-241	-293	-339	-444	-805	-1076	-1257	-1844	-2695	-2522	-2695	25338
SG41	Max.	15	15	22	22	15	22	45	75	98	2605	2605	75
	Min.	-30	-30	-30	-38	-60	-60	-60	-38	-128	-4683	-4683	-38
SG42	Max.	0	68	128	286	851	1619	2282	14058	20654	28237	28237	2.00E+05
	Min.	-143	-188	-233	-346	-685	-685	-994	-971	241	-3253	-3253	-2.00E+05
SG43	Max.	30	37	30	37	0	0	83	90	67	67	90	143
	Min.	-23	-15	-15	-15	-53	-53	-30	-8	-173	-249	-249	-331
SG44	Max.	-166	-106	-38	113	866	888	2522	11936	19240	26568	26568	2.00E+05
	Min.	-294	-347	-399	-505	-881	-1198	-1401	-2147	-5746	-10581	-10581	-37993
SG45	Max.	60	60	60	60	30	527	467	489	1175	519	1175	519
	Min.	15	15	15	8	-37	-15	407	429	241	0	0	459
SG46	Max.	-45	-45	-45	-37	-52	68	211	241	369	414	414	701
	Min.	-98	-98	-98	-98	-120	-128	-105	-90	-15	0	-105	121
SG47	Max.	52	52	52	60	45	52	67	308	504	624	624	2.00E+05
	Min.	0	-8	-15	-15	-61	-53	-23	0	210	0	-23	353

Cont. Table 4-2: Maximum and Minimum Measured Strain (micro strain) in the Reinforcement of DCRCC1

		Stage (1)	Stage (2)	Stage (3)	Stage (4)	Stage (5)	Stage (6)	Stage (7)	Stage (8)	Stage (9)	Stage (10)	Stage (11)	Stage (12)
Gauge		$0.05f_y$	$0.10f_y$	$0.15f_y$	$0.25f_y$	$0.5f_y$	$0.75f_y$	1 Δy	2 Δy	3 Δy	4 Δy	5 Δy	6 Δy
SG48	Max.	-144	-106	-68	37	632	655	2018	12662	23902	32685	32685	2.00E+05
	Min.	-257	-302	-339	-430	-693	-965	-1183	-1635	-3224	-5379	-5379	-1.00E+05
SG49	Max.	0	8	8	8	-7	0	31	68	2.00E+05	98	2.00E+05	98
	Min.	-45	-45	-52	-52	-97	-97	-90	-60	-43281	-15	-4328	-7
SG50	Max.	-7	46	91	204	814	1981	2726	17830	28048	41654	41654	2.00E+05
	Min.	-128	-158	-203	-316	-602	-594	-1137	-1099	-1460	-4322	-4322	-5752
SG51	Max.	53	60	68	75	60	75	128	271	979	1687	1687	61683
	Min.	0	0	0	-8	-38	-45	-15	15	-37	0	-37	346
SG52	Max.	-173	-121	-75	113	723	738	2154	13645	23028	29919	29919	40582
	Min.	-279	-316	-347	-377	-535	-640	-723	-919	7	0	-919	18020
SG53	Max.	52	52	60	60	30	30	75	90	1258	105	1258	105
	Min.	7	15	7	7	-31	-38	-8	15	22	0	-8	45
SG54	Max.	37	45	52	52	75	67	256	391	1182	1152	1182	2.00E+05
	Min.	-15	-8	-23	-30	-68	-61	0	60	0	0	0	-3.00E+05
SG55	Max.	90	90	90	90	52	60	97	278	15137	1211	15137	1392
	Min.	30	37	30	22	-38	-30	7	30	-2154	0	-2154	767
SG57	Max.	52	60	60	60	45	60	105	165	602	843	843	1521
	Min.	0	7	0	-8	-31	-31	0	15	-339	0	-339	248
SG58	Max.	-30	7	60	158	467	1061	1641	2326	4502	8605	8605	14627
	Min.	-121	-136	-158	-226	-347	-339	-482	-1453	-2168	-2146	-2168	-1702
SG59	Max.	53	53	61	68	76	106	181	241	422	550	550	1009
	Min.	8	8	0	-7	-30	0	45	68	-38	0	-38	241
SG60	Max.	0	0	7	7	83	83	534	1001	1219	1302	1302	1362
	Min.	-60	-68	-83	-136	-264	-347	-414	-708	-911	-979	-979	-1077
SG61	Max.	15	15	23	38	68	196	444	941	1069	1167	1167	1295
	Min.	-38	-45	-45	-60	-173	-196	-279	-625	-821	-889	-889	-979
SG62	Max.	60	68	75	98	203	346	437	678	1393	1792	1792	2883
	Min.	0	8	0	-7	-45	-15	121	151	37	0	0	926

Cont. Table 4-2: Maximum and Minimum Measured Strain (micro strain) in the Reinforcement of DCRCC1

		Stage (1)	Stage (2)	Stage (3)	Stage (4)	Stage (5)	Stage (6)	Stage (7)	Stage (8)	Stage (9)	Stage (10)	Stage (11)	Stage (12)
Gauge		$0.05f_y$	$0.10f_y$	$0.15f_y$	$0.25f_y$	$0.5f_y$	$0.75f_y$	1 Δy	2 Δy	3 Δy	4 Δy	5 Δy	6 Δy
SG63	Max.	75	75	75	75	52	52	226	670	28500	1377	28500	1701
	Min.	22	22	22	22	-38	-23	37	83	-15	0	-15	655
SG64	Max.	0	0	0	7	7	0	113	248	941	376	941	406
	Min.	-45	-45	-53	-68	-106	-136	-173	-279	-354	-384	-384	-422
SG65	Max.	7	7	15	15	53	38	68	150	2.00E+05	1347	2.00E+05	1393
	Min.	-45	-53	-53	-60	-53	-60	-38	-15	135	0	-38	233
SG66	Max.	30	38	38	45	23	45	106	211	1386	287	1386	317
	Min.	-15	-15	-15	-15	-52	-52	-90	-226	-301	-331	-331	-354
SG67	Max.	45	37	37	45	0	7	45	60	90	83	90	90
	Min.	-8	-8	-8	-8	-53	-45	-30	7	7	0	-30	30
SG68	Max.	8	8	8	8	8	8	15	15	38	23	38	83
	Min.	-37	-37	-37	-45	-53	-53	-37	-30	-30	-37	-37	-113

Table 4-3:Maximum and Minimum Displacements (inches) of DCRCC1

		Stage (1)	Stage (2)	Stage (3)	Stage (4)	Stage (5)	Stage (6)	Stage (7)	Stage (8)	Stage (9)	Stage (10)	Stage (11)	Stage (12)
Gauge		$0.05f_y$	$0.10f_y$	$0.15f_y$	$0.25f_y$	$0.5f_y$	$0.75f_y$	1 Δy	2 Δy	3 Δy	4 Δy	5 Δy	6 Δy
DTD 1	Max.	-0.004	-0.003	-0.002	0.001	0.01	0.011	0.037	0.1	1.291	0.029	1.291	0.767
	Min.	-0.006	-0.006	-0.008	-0.01	-0.016	-0.024	-0.031	-0.067	-0.205	-0.182	-0.205	-0.287
DTD 2	Max.	0.024	0.002	0.003	0.006	0.016	0.037	0.053	0.153	0.235	0.125	0.235	0.957
	Max.	-0.003	-0.003	-0.004	-0.006	-0.012	-0.012	-0.025	-0.058	-0.373	-0.684	-0.684	-0.32
DTD 3	Min.	0	0	0.001	0.002	0.012	0.014	0.031	0.111	0.758	0.679	0.768	0.644
	Max.	-0.002	-0.002	-0.002	-0.003	-0.006	-0.009	-0.012	-0.034	0.012	-0.006	-0.034	-0.768
DTD 4	Min.	0	-0.008	-0.008	-0.008	-0.008	0	-0.01	0.018	0.24	0.628	0.628	0.314
	Max.	-0.042	-0.009	-0.009	-0.01	-0.013	-0.013	-0.02	-0.036	-0.157	-0.471	-0.471	-0.795
DTD 5	Max.	-0.002	-0.002	0	0.002	0.014	0.015	0.032	0.091	1.291	0.489	1.291	1.291
	Min.	-0.004	-0.004	-0.006	-0.008	-0.015	-0.024	-0.03	-0.055	-0.148	-0.026	-0.148	0
DTD 6	Max.	-0.001	0.001	0.001	0.003	0.014	0.025	0.035	0.09	0.243	0.721	0.721	0.904
	Max.	-0.003	-0.004	-0.005	-0.006	-0.014	-0.015	-0.029	-0.054	-0.049	-0.01	-0.054	-0.34
DTD 7	Min.	0.001	0.001	0.001	0.001	-0.007	0	0.012	0.035	0.078	0	0.078	-0.007
	Max.	-0.001	-0.001	-0.001	-0.033	-0.016	-0.022	-0.026	-0.044	-0.1	-0.101	-0.101	-0.107
DTD 8	Min.	0	0.001	0.002	0.004	0.012	0.022	0.031	0.069	0.131	0.082	0.131	0.043
	Max.	-0.002	-0.002	-0.003	-0.004	-0.011	-0.012	-0.028	-0.046	-0.054	-0.055	-0.055	-0.058
DTD 9	Max.	0	0	0	0	0	0	0.168	0.065	0.065	0.065	0.168	0.065
	Min.	-0.001	-0.001	-0.001	-0.001	-0.001	-0.001	-0.046	0.064	0	0	-0.046	0.064
DTD 10	Max.	0.001	0.002	0.001	0.001	0.002	0.001	0.001	-0.002	0.002	0	0.002	-0.014
	Max.	-0.002	-0.001	-0.001	-0.001	-0.001	-0.001	-0.005	-0.005	-0.005	-0.017	-0.017	-0.017
DTD 11	Max.	0.001	0.001	0.001	0.001	0.001	0.001	0.002	0.002	0.002	0.002	0.002	0.002
	Min.	0	-0.001	0	0	-0.001	-0.001	-0.001	-0.001	-0.005	0	-0.005	0
DTD 12	Max.	0	0	0	0	0	0	0	0	0	0	0	-0.001
	Min.	-0.001	0	0	-0.001	0	0	-0.001	-0.001	-0.002	-0.002	-0.002	-0.002
DTD 13	Max.	0.002	0.002	0.002	0.002	0.002	0.002	0.002	0.002	0.002	0.002	0.002	0.002
	Min.	0	0	0	0	0	0	0	0	-0.002	0	-0.002	0
DTD 14	Max.	-0.003	-0.003	-0.003	-0.003	-0.002	0	-0.003	-0.003	-0.003	0	0	-0.003
	Min.	-0.004	-0.004	-0.004	-0.004	-0.003	-0.004	-0.004	-0.004	-0.023	-0.004	-0.023	-0.004

Cont. Table 4-3:Maximum and Minimum Displacements (inches) of DCRCC1

		Stage (1)	Stage (2)	Stage (3)	Stage (4)	Stage (5)	Stage (6)	Stage (7)	Stage (8)	Stage (9)	Stage (10)	Stage (11)	Stage (12)
Gauge		$0.05f_y$	$0.10f_y$	$0.15f_y$	$0.25f_y$	$0.5f_y$	$0.75f_y$	1 Δy	2 Δy	3 Δy	4 Δy	5 Δy	6 Δy
DTD 15	Max.	-0.021	-0.021	-0.021	-0.021	-0.021	0	-0.021	-0.021	0.0837	0	0.0837	-0.021
	Min.	-0.023	-0.023	-0.023	-0.023	-0.023	-0.023	-0.023	-0.023	-0.104	-0.023	-0.104	-0.023
DTD 16	Max.	-0.004	-0.004	-0.004	-0.004	-0.004	0	-0.004	-0.004	-0.002	0	0	-0.005
	Max.	-0.005	-0.005	-0.005	-0.005	-0.005	-0.005	-0.005	-0.005	-0.006	-0.006	-0.006	-0.006
DTD 17	Min.	-0.002	-0.001	-0.001	-0.001	-0.001	0	-0.001	-0.001	-0.001	0	0	-0.002
	Max.	-0.002	-0.003	-0.002	-0.002	-0.002	-0.002	-0.002	-0.002	-0.006	-0.003	-0.006	-0.003
DTD 18	Min.	-0.001	-0.001	-0.001	-0.001	-0.001	0	-0.001	-0.002	-0.002	0	0	-0.001
	Max.	-0.001	-0.001	-0.001	-0.001	-0.001	-0.002	-0.002	-0.002	-0.004	-0.002	-0.004	-0.002

Table 4-4:Maximum and Minimum Measured Force and Displacement of FSRCC1

Stage	Ductility	Average String Pot Displacement at Max. and Min. Force (in)		Actuator Displacement at Max. and Min. Force (in)		Actuator Force (kips)	
Number	Level	Max.	Min.	Max.	Min.	Max.	Min.
Stage (1)	$0.05f_y$	0.03	-0.05	0.05	-0.03	0.58	-0.59
Stage (2)	$0.10f_y$	0.07	-0.09	0.09	-0.07	1.17	-1.17
Stage (3)	$0.15f_y$	0.11	-0.15	0.15	-0.12	1.77	-1.78
Stage (4)	$0.25f_y$	0.27	-0.27	0.27	-0.27	2.94	-3
Stage (5)	$0.5f_y$	0.77	-0.88	0.89	-0.88	5.89	-5.9
Stage (6)	$0.75f_y$	1.53	-1.62	1.62	-1.53	8.83	-8.84
Stage (7)	1 Δy	2.09	-2.37	2.39	-2.08	11.204	-10.65
Stage (8)	2 Δy	4.18	-4.17	4.18	-4.17	13.16	-13.58
Stage (9)	3 Δy	6.17	-5.96	5.95	-6.07	12.65	-13.3
Stage (10)	4 Δy	8.36	-8.30	8.26	-8.36	10.44	-11.3
Stage (11)	5 Δy	10.46	-10.44	10.44	-10.46	8.94	-9.56
Stage (12)	6 Δy	12.56	-12.54	12.55	-12.56	7.86	-4.91
Stage (13)	7 Δy	13.71	-14.50	14.50	-13.72	5.79	-3.27

Table 4-5: Maximum and Minimum Measured Strain (micro strain) in the Reinforcement of FSRCC1

		Stage (1)	Stage (2)	Stage (3)	Stage (4)	Stage (5)	Stage (6)	Stage (7)	Stage (8)	Stage (9)	Stage (10)	Stage (11)	Stage (12)	Stage (13)
Gauge		$0.05f_y$	$0.10f_y$	$0.15f_y$	$0.25f_y$	$0.5f_y$	$0.75f_y$	1 Δy	2 Δy	3 Δy	4 Δy	5 Δy	6 Δy	7 Δy
SG1	Max.	53	53	53	53	61	53	38	30	38	38	46	46	91
	Min.	-7	0	8	0	0	0	-22	-22	-22	-30	-15	-7	-60
SG3	Max.	8	8	8		30	23	8	15	15	23	30	45	30
	Min.	-37	-45	-37	-37	-45	-37	-60	-68	-60	-60	-60	-68	-60
SG4	Max.	53	60	60	68	68	60	45	53	45	53	68	68	128
	Min.	7	7	15	7	-8	0	-23	-23	-30	-23	-23	-15	-38
SG5	Max.	75	90	83	90	90	83	75	83	90	98	105	105	105
	Min.	30	30	38	23	23	30	7	15	15	23	23	30	30
SG6	Max.	83	91	83	91	106	113	98	189	241	256	279	279	272
	Min.	38	38	46	38	23	31	8	23	76	98	106	128	136
SG7	Max.	68	68	75	75	75	68	53	53	45	53	53	60	60
	Min.	23	23	23	30	23	23	0	0	0	0	8	15	0
SG9	Max.	8	15	15	15	38	23	23	45	45	53	53	53	106
	Min.	-30	-38	-30	-38	-45	-45	-68	-83	-83	-83	-83	-83	-128
SG10	Max.	53	53	60	60	68	60	45	53	53	60	68	76	128
	Min.	0	8	8	8	0	0	-30	-22	-22	-22	-15	-15	-60
SG11	Max.	60	60	52	60	68	68	68	83	98	105	113	113	113
	Min.	7	0	7	0	0	7	0	0	7	15	15	22	15
SG12	Max.	45	45	45	45	90	113	105	158	173	195	218	233	233
	Min.	0	-8	-8	-8	-15	0	-30	-46	-38	-23	0	37	45
SG13	Max.	-23	-23	-23	-23	-8	-8	-15	-23	-23	-30	-23	-30	-30
	Min.	-68	-68	-68	-68	-75	-60	-68	-75	-83	-90	-90	-90	-90
SG15	Max.	7	7	7	7	30	15	-8	-8	-8	15	30	30	15
	Min.	-38	-38	-38	-38	-46	-46	-91	-113	-106	-106	-98	-106	-106
SG16	Max.	8	8	8	8	23	8	0	8	16	16	16	16	16
	Min.	-45	-37	-37	-45	-45	-45	-60	-60	-60	-60	-52	-52	-60
SG17	Max.	68	68	68	68	83	75	90	135	166	196	233	241	248
	Min.	15	23	23	23	15	30	38	60	83	105	120	158	166

Cont. Table 4-5: Maximum and Minimum Measured Strain (micro strain) in the Reinforcement of FSRCC1

		Stage (1)	Stage (2)	Stage (3)	Stage (4)	Stage (5)	Stage (6)	Stage (7)	Stage (8)	Stage (9)	Stage (10)	Stage (11)	Stage (12)	Stage (13)
Gauge		$0.05f_y$	$0.10f_y$	$0.15f_y$	$0.25f_y$	$0.5f_y$	$0.75f_y$	1 Δy	2 Δy	3 Δy	4 Δy	5 Δy	6 Δy	7 Δy
SG18	Max.	90	98	98	105	105	105	105	136	128	143	143	166	158
	Min.	38	45	45	53	30	30	-7	-7	-15	0	0	23	38
SG19	Max.	22	22	22	22	37	30	22	15	7	15	7	30	120
	Min.	-30	-30	-23	-30	-30	-15	-30	-38	-45	-45	-45	-45	-106
SG21	Max.	23	23	23	23	53	45	45	45	23	15	68	68	331
	Min.	-22	-22	-22	-30	-30	-22	-45	-53	-68	-75	-68	-98	-437
SG23	Max.	113	113	113	121	121	121	106	113	121	128	143	158	151
	Min.	60	60	68	68	45	60	38	38	45	53	53	68	60
SG24	Max.	61	61	61	68	76	68	53	46	38	38	38	46	46
	Min.	8	16	16	16	8	16	-15	-15	-15	-15	-7	0	-7
SG25	Max.	61	68	61	68	68	61	46	46	46	46	46	53	46
	Min.	8	15	15	15	0	8	-7	-7	-7	-7	-7	-7	-7
SG26	Max.	0	0	0	0	8	15	23	0	-7	-7	-7	-7	8
	Min.	-38	-45	-45	-60	-60	-53	-53	-68	-60	-68	-60	-68	-75
SG27	Max.	30	30	30	30	45	38	30	45	53	60	68	68	90
	Min.	-15	-23	-23	-15	-23	-23	-38	-45	-45	-38	-38	-38	-83
SG28	Max.	30	38	38	38	38	38	30	30	38	45	45	45	38
	Min.	-15	-15	-15	-15	-15	-15	-38	-38	-38	-30	-30	-30	-45
SG29	Max.	75	83	83	83	91	83	75	91	98	106	113	128	128
	Max.	23	30	38	30	23	23	8	15	15	30	30	53	53
SG31	Min.	90	98	98	105	166	218	203	196	241	173	203	369	301
	Max.	45	45	45	53	53	60	15	30	53	60	30	60	83
SG32	Min.	-91	-61	-30	37	708	1393	1785	9693	9460	9783	11380	12404	12028
	Max.	-181	-196	-219	-287	-467	-610	-746	1740	1190	851	30	75	-30

Cont. Table 4-5: Maximum and Minimum Measured Strain (micro strain) in the Reinforcement of FSRCC1

		Stage (1)	Stage (2)	Stage (3)	Stage (4)	Stage (5)	Stage (6)	Stage (7)	Stage (8)	Stage (9)	Stage (10)	Stage (11)	Stage (12)	Stage (13)
Gauge		$0.05f_y$	$0.10f_y$	$0.15f_y$	$0.25f_y$	$0.5f_y$	$0.75f_y$	1 Δy	2 Δy	3 Δy	4 Δy	5 Δy	6 Δy	7 Δy
SG33	Max.	53	46	53	61	106	143	121	189	279	445	670	776	753
	Min.	0	0	0	-15	-22	23	-22	0	68	91	68	15	23
SG35	Max.	38	46	46	61	143	174	181	287	580	806	889	897	1055
	Min.	-15	-22	-22	-30	-37	-15	-30	0	159	302	347	520	520
SG36	Max.	0	8	8	23	106	113	106	144	98	113	174	144	-60
	Min.	-45	-45	-37	-45	-67	-82	-128	-203	-436	-723	-775	-1001	-813
SG39	Max.	83	90	90	90	105	105	98	188	504	678	949	1378	2296
	Max.	38	38	38	45	38	45	15	75	233	256	188	233	459
SG40	Min.	-83	-46	-16	60	692	1422	1867	11254	13475	16682	20364	22103	23142
	Max.	-174	-196	-219	-287	-467	-573	-663	2386	1257	308	-193608	-229971	-10759
SG41	Min.	22	30	22	22	97	75	45	165	308	474	941	1099	1401
	Max.	-31	-31	-38	-38	-46	-46	-204	-113	7	15	-159	-106	-339
SG44	Min.	-53	-23	7	67	775	1483	1912	15146	21063	28787	35140	45604	66630
	Max.	-136	-151	-174	-234	-399	-490	-573	4870	4253	4117	3229	4419	-57845
SG45	Max.	-128	-98	-60	68	587	1310	1649	5390	13068	19429	25624	239306	239306
	Min.	-233	-271	-301	-384	-700	-956	-1091	-1648	-1362	836	249	10546	-254016
SG46	Max.	98	106	106	113	136	159	159	234	226	98	497	8629	243016
	Min.	53	53	53	61	46	61	46	83	-52	-263	-331	362	6672
SG48	Max.	-53	-31	7	67	609	1249	1663	2943	17941	23415	29265	34091	40716
	Min.	-128	-143	-166	-219	-347	-452	-558	-1341	3147	22	-1032	-234	-317
SG49	Max.	30	30	30	37	45	45	22	22	15	15	15	22	15
	Max.	-23	-15	-15	-23	-23	-15	-38	-53	-53	-53	-45	-45	-45
SG50	Min.	-151	-121	-91	15	511	1640	2212	15745	19471	36684	42622	51963	28232
	Max.	-249	-286	-324	-407	-761	-1099	-1340	1031	-1694	-6804	-130337	-255241	-255241
SG52	Min.	-45	-30	0	76	618	1251	1627	9929	12460	17341	22184	21913	10885
	Max.	-120	-128	-143	-188	-331	-361	-399	2464	1695	-1649	-2960	-1868	-2945
SG53	Min.	-165	-143	-113	60	708	1446	1913	14712	18710	28769	37653	31246	10654
	Max.	-248	-271	-301	-346	-557	-708	-813	2997	196	45	-421	-85793	-241622

Cont. Table 4-5: Maximum and Minimum Measured Strain (micro strain) in the Reinforcement of FSRCC1

		Stage (1)	Stage (2)	Stage (3)	Stage (4)	Stage (5)	Stage (6)	Stage (7)	Stage (8)	Stage (9)	Stage (10)	Stage (11)	Stage (12)	Stage (13)
Gauge		$0.05f_y$	$0.10f_y$	$0.15f_y$	$0.25f_y$	$0.5f_y$	$0.75f_y$	1 Δy	2 Δy	3 Δy	4 Δy	5 Δy	6 Δy	7 Δy
SG54	Max.	-45	-7	15	83	760	1490	1912	2619	5426	12334	18513	23126	24285
	Min.	-128	-143	-165	-218	-383	-542	-685	-1482	-2348	-895	-301	2032	2717
SG55	Max.	60	68	68	76	76	68	45	38	45	38	53	53	45
	Min.	15	23	23	23	15	15	-7	-15	-7	-15	-7	0	-7
SG56	Max.	-68	-61	-46	0	316	835	1234	2130	3342	9613	10871	9892	7355
	Min.	-136	-143	-151	-189	-271	-279	-324	-1077	-1235	-151	-889	-3080	-3095
SG57	Max.	31	31	38	46	181	272	279	385	595	799	791	784	24164
	Max.	-15	-22	-22	-22	23	68	38	31	151	385	189	-82542	-2518
SG58	Min.	-68	-53	-45	22	361	1099	1634	2304	11965	17033	24352	21046	6272
	Max.	-143	-166	-181	-226	-414	-565	-686	-1416	-911	-678	-512	564	3561
SG59	Min.	30	30	30	38	61	61	45	83	121	143	174	174	174
	Max.	-15	-15	-22	-15	-15	-7	-37	-75	-67	-45	-30	-7	8
SG61	Min.	38	45	60	68	166	263	407	700	768	806	888	843	45
	Max.	-15	-15	-15	-30	-136	-203	-271	-474	-663	-851	-1039	-1122	-1092
SG62	Max.	165	165	165	173	180	180	203	278	316	361	391	399	391
	Min.	112	120	120	120	67	112	97	127	150	173	195	225	233

Table 4-6: Maximum and Minimum Measured Displacements (inches) of FSRCC1

		Stage (1)	Stage (2)	Stage (3)	Stage (4)	Stage (5)	Stage (6)	Stage (7)	Stage (8)	Stage (9)	Stage (10)	Stage (11)	Stage (12)	Stage (13)
Gauge		$0.05f_y$	$0.10f_y$	$0.15f_y$	$0.25f_y$	$0.5f_y$	$0.75f_y$	1 Δy	2 Δy	3 Δy	4 Δy	5 Δy	6 Δy	7 Δy
DTD 1	Max.	-0.024	-0.023	-0.022	-0.016	0.006	0.035	0.064	0.179	0.275	0.622	1.125	0.8	0.955
	Min.	-0.027	-0.028	-0.028	-0.031	-0.043	-0.059	-0.062	-0.112	-0.138	-0.009	0.228	0.392	0.021
DTD 2	Max.	-0.002	-0.002	-0.002	0.001	0.01	0.031	0.048	0.154	0.338	0.566	0.945	0.75	1.066
	Min.	-0.003	-0.004	-0.005	-0.006	-0.014	-0.023	-0.028	-0.06	-0.026	0.117	0.222	0.216	0.261
DTD 3	Max.	0.001	0.001	0.001	0.002	0.012	0.024	0.032	0.1	0.244	0.232	0.181	0.003	0.325
	Min.	0	-0.001	-0.001	-0.001	-0.005	-0.01	-0.014	-0.033	-0.125	-0.531	-0.728	-0.728	-0.728
DTD 4	Max.	0	0	0	0	0	0	-0.002	-0.003	0.026	-0.058	-0.091	0	0
	Max.	-0.002	-0.002	-0.002	-0.002	-0.004	-0.007	-0.009	-0.017	-0.084	-0.471	-0.694	0	0
DTD 5	Min.	0	0.001	0.001	0.003	0.013	0.023	0.03	0.082	0.132	0.209	0.34	0.412	0.433
	Max.	-0.001	-0.002	-0.002	-0.004	-0.009	-0.017	-0.022	-0.045	-0.066	-0.074	0.018	0.015	-0.123
DTD 6	Min.	-0.003	-0.003	-0.002	0.001	0.012	0.022	0.028	0.079	0.146	0.242	0.448	0.351	0
	Max.	-0.004	-0.005	-0.006	-0.007	-0.016	-0.025	-0.029	-0.058	-0.176	-0.08	-0.035	-0.305	-0.28
DTD 7	Min.	-0.001	0	0	0.001	0.01	0.021	0.027	0.057	0.061	0.06	0.081	0.111	0.094
	Max.	-0.002	-0.003	-0.004	-0.005	-0.01	-0.017	-0.021	-0.037	-0.042	-0.04	-0.044	-0.042	-0.04
DTD 8	Max.	-0.002	-0.001	-0.001	0.003	0.022	0.055	0.081	0.171	0.223	0.217	0.191	0.182	0.12
	Min.	-0.004	-0.005	-0.005	-0.007	-0.013	-0.021	-0.024	-0.041	-0.041	-0.064	-0.083	-0.044	0
DTD 9	Max.	0	0	0	0	0.001	0.001	0.001	0.001	0.001	0.001	0.001	0.001	0.001
	Min.	-0.001	0	-0.001	-0.001	-0.001	0	0.001	0.001	0.001	0.001	0	0	0
DTD 10	Max.	0.001	0.001	0.002	0.001	0.002	0.001	0.001	0.001	0.001	0.002	0.001	0.002	0.002
	Min.	0	0	0	0	-0.001	-0.001	-0.001	-0.001	-0.001	-0.001	-0.001	-0.001	-0.001
DTD 11	Max.	0.001	0.001	0.001	0.001	0.001	0.001	0.001	0.001	0.001	0.001	0.001	0.001	0.001
	Max.	-0.001	-0.001	-0.001	-0.001	-0.001	-0.002	-0.001	-0.001	-0.001	-0.001	-0.001	-0.001	-0.002
DTD 12	Min.	0.006	0.006	0.006	0.006	0.007	0.006	0.007	0.007	0.007	0.007	0.007	0.007	0.007
	Max.	0.006	0.006	0.006	0.006	0.005	0.005	0.006	0.006	0.006	0.006	0.006	0.006	0.006
DTD 13	Min.	-0.001	-0.001	-0.001	-0.001	-0.001	-0.002	-0.001	-0.001	-0.001	-0.001	-0.001	0	0
	Max.	-0.002	-0.002	-0.002	-0.002	-0.005	-0.003	-0.002	-0.002	-0.002	-0.002	-0.002	-0.002	-0.001
DTD 14	Min.	-0.002	-0.002	-0.002	-0.002	-0.002	-0.004	-0.003	-0.003	-0.003	-0.003	-0.003	-0.002	-0.002
	Max.	-0.002	-0.002	-0.002	-0.002	-0.022	-0.004	-0.004	-0.004	-0.004	-0.004	-0.004	-0.004	-0.004
DTD 15	Min.	-0.001	-0.001	-0.001	-0.001	-0.001	-0.001	-0.001	-0.001	-0.002	-0.002	-0.002	-0.002	-0.002
	Max.	-0.002	-0.002	-0.002	-0.002	-0.002	-0.002	-0.002	-0.002	-0.002	-0.002	-0.003	-0.003	-0.003

Table 4-7: Maximum and Minimum Measured Force and Displacement of DCRCC24

Stage Number	Ductility Level	Average String Pot Displacement at Max. and Min. Force (in)		Actuator Displacement at Max. and Min. Force (in)		Actuator Force (kips)	
		Max.	Min.	Max.	Min.	Max.	Min.
Stage (1)	$0.05f_y$	0.12	-0.14	0.14	-0.12	1.66	-1.69
Stage (2)	$0.10f_y$	0.16	-0.18	0.18	-0.17	6.42	-6.18
Stage (3)	$0.15f_y$	0.27	-0.28	0.27	-0.28	7.15	-6.20
Stage (4)	$0.25f_y$	0.45	-0.46	0.46	-0.45	9.50	-8.95
Stage (5)	$0.5f_y$	1.48	-0.89	0.88	-1.49	14.13	-15.12
Stage (6)	$0.75f_y$	2.21	-1.79	1.79	-2.22	22.05	-22.53
Stage (7)	$1\ \Delta y$	2.71	-2.72	2.82	-2.72	33.00	-27.43
Stage (8)	$2\ \Delta y$	5.36	-5.47	5.45	-5.37	42.06	-42.18
Stage (9)	$3\ \Delta y$	5.36	-8.18	8.08	-5.37	43.75	-42.04

Table 4-8: Maximum and Minimum Measured Strain (micro strain) in the Reinforcement of DCRCC24

		Stage (1)	Stage (2)	Stage (3)	Stage (4)	Stage (5)	Stage (6)	Stage (7)	Stage (8)	Stage (9)
Gauge		$0.05f_y$	$0.10f_y$	$0.15f_y$	$0.25f_y$	$0.5f_y$	$0.75f_y$	1 Δy	2 Δy	3 Δy
SG1	Max.	62	69	69	83	90	111	145	505	457
	Min.	7	28	35	28	35	-7	7	0	35
SG2	Max.	62	55	42	138	145	194	221	1882	2200
	Min.	-14	-7	0	-21	0	-83	-104	-180	-48
SG3	Max.	48	55	55	76	83	104	69	173	298
	Min.	-7	14	14	14	28	7	14	7	21
SG4	Max.	35	35	48	55	62	76	42	55	48
	Min.	-14	0	7	0	7	-14	-14	-14	-14
SG5	Max.	62	62	69	83	97	111	83	623	464
	Min.	7	28	28	28	48	7	0	14	7
SG6	Max.	55	55	55	83	90	111	55	1016	1390
	Min.	-7	0	0	-7	-7	-83	-111	-159	83
SG7	Max.	69	69	62	131	138	159	277	1342	1680
	Min.	7	14	21	21	28	-7	0	-14	104
SG9	Max.	104	104	104	125	132	152	138	900	1190
	Min.	42	69	69	69	83	35	42	42	242
SG10	Max.	125	132	132	194	201	228	256	512	588
	Min.	35	62	97	76	83	-42	-35	0	228
SG11	Max.	62	55	55	90	90	104	125	616	388
	Min.	-7	21	21	21	42	7	14	21	62
SG12	Max.	55	55	48	90	90	118	76	602	1660
	Min.	0	7	14	7	7	-35	-35	-35	194
SG13	Max.	62	62	62	90	104	249	436	637	782
	Min.	-14	-7	14	-14	7	-7	48	-42	-42
SG14	Max.	28	21	28	35	42	69	90	235	450
	Min.	-21	-14	-14	-14	-7	-7	-69	-201	-339
SG15	Max.	28	28	21	35	28	35	28	28	28
	Min.	-21	-14	-14	-21	-21	-21	-21	-28	-21
SG16	Max.	76	69	76	97	97	118	69	166	201
	Min.	14	28	35	14	21	-35	-42	-42	55
SG17	Max.	69	69	69	90	97	111	69	152	159
	Min.	7	21	28	28	42	7	0	-7	-28

Cont. Table 4-8: Maximum and Minimum Measured Strain (micro strain) in the Reinforcement of DCRCC24

		Stage (1)	Stage (2)	Stage (3)	Stage (4)	Stage (5)	Stage (6)	Stage (7)	Stage (8)	Stage (9)
Gauge		$0.05f_y$	$0.10f_y$	$0.15f_y$	$0.25f_y$	$0.5f_y$	$0.75f_y$	1 Δy	2 Δy	3 Δy
SG18	Max.	111	125	118	152	166	221	62	740	962
	Min.	21	76	76	83	90	-69	-55	0	221
SG20	Max.	62	76	69	159	166	214	539	1175	1313
	Min.	-7	7	14	7	14	0	0	-28	97
SG21	Max.	76	69	83	104	104	125	360	561	526
	Min.	14	35	35	35	48	14	28	83	159
SG22	Max.	28	28	14	55	69	221	242	470	270
	Min.	-35	-35	-35	-48	-42	-55	-42	-21	-14
SG23	Max.	48	48	48	83	90	104	325	727	838
	Min.	-7	14	7	7	14	-7	0	62	55
SG24	Max.	55	55	55	83	83	104	145	429	533
	Min.	-7	7	14	14	21	-42	-21	28	145
SG25	Max.	118	111	111	125	125	138	249	651	824
	Min.	62	69	76	69	69	55	28	-69	-35
SG26	Max.	76	83	83	138	145	201	574	1155	1418
	Min.	7	28	35	28	35	0	14	-7	28
SG27	Max.	69	69	69	90	97	111	69	304	408
	Min.	7	28	28	35	48	7	14	-962	83
SG28	Max.	62	69	69	97	104	118	76	118	152
	Min.	0	28	35	35	42	-7	7	7	7
SG30	Max.	55	48	55	76	76	97	104	263	318
	Min.	-14	14	14	14	21	-28	-21	-41	-28
SG31	Max.	187	194	35	865	879	1571	1841	2270	2249
	Min.	-166	-201	-194	-616	-609	-886	-1170	-1958	-2173
SG32	Max.	83	97	90	159	166	208	215	291	325
	Min.	14	35	42	42	62	28	14	28	48
SG33	Max.	235	305	305	1461	1447	2070	2845	7581	14601
	Min.	-187	-180	-7	-526	-519	-955	-1094	-1350	318
SG34	Max.	69	83	83	228	228	277	325	339	568
	Min.	14	28	42	28	48	28	28	35	97
SG35	Max.	221	221	35	1384	1384	2449	3045	13458	15423
	Min.	-215	-256	-249	-803	-789	-1190	-1564	-2505	-1038

Cont. Table 4-8: Maximum and Minimum Measured Strain (micro strain) in the Reinforcement of DCRCC24

		Stage (1)	Stage (2)	Stage (3)	Stage (4)	Stage (5)	Stage (6)	Stage (7)	Stage (8)	Stage (9)
Gauge		$0.05f_y$	$0.10f_y$	$0.15f_y$	$0.25f_y$	$0.5f_y$	$0.75f_y$	1 Δy	2 Δy	3 Δy
SG36	Max.	97	104	97	159	159	187	201	304	374
	Min.	21	35	48	42	76	55	42	48	55
SG37	Max.	221	270	263	1336	1329	1889	2581	2817	2872
	Min.	-125	-118	35	-388	-381	-858	-1031	-2187	-2360
SG38	Max.	76	76	55	138	152	201	214	298	270
	Min.	-7	-7	0	0	55	42	35	48	35
SG39	Max.	221	221	55	990	997	1862	2215	2900	2962
	Min.	-166	-201	-201	-713	-692	-1017	-1370	-2498	-2844
SG40	Max.	7	14	7	62	62	111	76	131	159
	Min.	-55	-55	-42	-55	-28	-21	-62	-104	-166
SG41	Max.	249	298	291	1591	1584	2173	2816	14150	17160
	Min.	-118	-118	42	-471	-464	-941	-1162	-477	-1142
SG42	Max.	90	90	90	173	166	187	208	298	443
	Min.	28	42	48	48	83	48	62	48	90
SG43	Max.	277	277	69	1156	1149	2021	2353	2990	14833
	Min.	-194	-228	-228	-754	-734	-1038	-1398	-2609	-5662
SG45	Max.	208	256	242	1370	1357	1883	2464	11731	14161
	Min.	-138	-138	0	-443	-436	-893	-1073	-955	-408
SG46	Max.	83	90	76	173	173	228	263	394	374
	Min.	14	21	28	28	76	55	55	35	42
SG47	Max.	221	228	62	1183	1211	2263	2547	19462	14949
	Min.	-166	-201	-194	-706	-678	-1045	-1440	-2637	-4436
SG49	Max.	228	284	277	1578	1578	2152	2844	13814	23849
	Min.	-145	-138	28	-436	-429	-927	-1135	-2187	1128
SG50	Max.	69	76	55	118	125	145	152	263	726
	Min.	0	0	7	0	35	0	0	0	42
SG51	Max.	76	76	62	166	180	263	277	1702	2097
	Min.	0	0	14	-35	-35	-111	-263	-3529	-55313
SG52	Max.	125	131	131	166	166	187	138	166	201
	Min.	55	76	90	83	111	83	76	21	7
SG53	Max.	201	249	249	1176	1176	1681	2325	2712	18392
	Min.	-111	-104	35	-325	-318	-782	-976	-2367	187

Cont. Table 4-8: Maximum and Minimum Measured Strain (micro strain) in the Reinforcement of DCRCC24

		Stage (1)	Stage (2)	Stage (3)	Stage (4)	Stage (5)	Stage (6)	Stage (7)	Stage (8)	Stage (9)
Gauge		$0.05f_y$	$0.10f_y$	$0.15f_y$	$0.25f_y$	$0.5f_y$	$0.75f_y$	1 Δy	2 Δy	3 Δy
SG54	Max.	2188	2188	2160	2222	2222	2243	2243	2291	2305
	Min.	2098	2091	2098	2098	2132	2042	2070	2070	2049
SG55	Max.	62	69	69	104	104	125	125	187	374
	Min.	-7	14	28	14	35	0	42	48	48
SG56	Max.	70	67	55	112	209	276	380	468	728
	Min.	16	15	45	110	180	265	26	300	500
SG58	Max.	187	242	235	1108	1018	1212	1184	1634	644
	Min.	-173	-166	-35	-422	-408	-665	-852	-893	-263
SG59	Max.	125	131	111	194	201	228	159	394	733
	Min.	-62	-69	-76	-69	-190	-155	-142	-148	-297
SG61	Max.	48	55	55	97	111	173	311	429	574
	Min.	0	14	21	14	28	14	35	55	62
SG62	Max.	187	187	7	865	865	1612	1930	7823	2262
	Min.	-145	-166	-166	-374	-367	-463	-457	-457	1238
SG63	Max.	118	118	35	644	671	1626	2076	2581	2636
	Min.	-104	-111	-104	-346	-346	-498	-650	-1619	-1709
SG64	Max.	311	305	311	360	374	401	374	588	803
	Min.	256	263	270	263	284	256	249	-48	-173
SG65	Max.	242	263	263	928	935	1503	2534	2957	16765
	Min.	35	42	118	-104	-104	-332	-443	-1738	215
SG66	Max.	76	76	62	138	152	187	228	346	305
	Min.	7	14	14	14	83	62	69	83	97
SG67	Max.	76	76	76	104	111	131	83	152	401
	Min.	14	28	35	35	55	14	21	-7	48
SG68	Max.	76	76	76	111	111	152	138	388	422
	Min.	14	35	28	21	28	7	28	69	138
SG70	Max.	131	138	152	221	228	256	284	464	477
	Min.	28	76	111	90	104	21	-14	-35	83

Table 4-9: Maximum and Minimum Measured Displacements (inches) of DCRCC24

		Stage (1)	Stage (2)	Stage (3)	Stage (4)	Stage (5)	Stage (6)	Stage (7)	Stage (8)	Stage (9)
Gauge		$0.05f_y$	$0.10f_y$	$0.15f_y$	$0.25f_y$	$0.5f_y$	$0.75f_y$	1 Δy	2 Δy	3 Δy
DTD 1	Max.	0.003	0.003	-0.001	0.015	0.015	0.040	0.046	0.129	0.129
	Min.	-0.004	-0.005	-0.005	-0.013	-0.013	-0.017	-0.027	-0.070	-0.140
DTD 2	Max.	0.003	0.004	0.004	0.023	0.023	0.039	0.059	0.167	0.270
	Min.	-0.003	-0.003	0.000	-0.009	-0.009	-0.019	-0.024	-0.057	-0.073
DTD 3	Max.	0.001	0.000	0.000	0.001	0.000	0.000	-0.002	0.004	0.004
	Min.	0.000	0.000	0.000	-0.003	-0.003	-0.014	-0.016	-0.029	-0.061
DTD 4	Max.	0.001	0.001	0.001	0.001	0.000	0.000	0.000	-0.001	0.040
	Min.	0.000	0.000	0.000	-0.004	-0.004	-0.009	-0.011	-0.024	-0.022
DTD 5	Max.	0.003	0.003	0.000	0.015	0.015	0.035	0.034	0.097	0.099
	Min.	-0.003	-0.003	-0.003	-0.010	-0.010	-0.013	-0.018	-0.035	-0.060
DTD 6	Max.	0.002	0.002	0.002	0.013	0.013	0.020	0.028	0.100	0.164
	Min.	-0.003	-0.003	-0.001	-0.006	-0.006	-0.010	-0.012	-0.024	-0.025
DTD 7	Max.	0.001	0.001	-0.001	0.009	0.010	0.020	0.025	0.064	0.063
	Min.	-0.003	-0.003	-0.003	-0.009	-0.009	-0.011	-0.015	-0.028	-0.032
DTD 8	Max.	0.001	0.001	0.001	0.014	0.014	0.020	0.026	0.062	0.116
	Min.	-0.001	-0.001	0.000	-0.005	-0.005	-0.010	-0.012	-0.019	-0.017
DTD 9	Max.	0.001	0.001	0.001	0.001	0.000	0.004	0.001	0.006	-0.001
	Min.	0.000	-0.001	0.000	-0.004	-0.003	-0.007	-0.011	-0.020	-0.024
DTD 10	Max.	0.002	0.003	0.003	0.014	0.014	0.021	0.029	0.062	0.086
	Min.	-0.002	-0.002	0.000	-0.006	-0.006	-0.009	-0.011	-0.016	-0.014
DTD 11	Max.	-0.005	-0.005	-0.005	-0.005	-0.005	-0.005	0.001	0.021	0.027
	Min.	-0.007	-0.007	-0.007	-0.007	-0.007	-0.007	-0.007	-0.001	0.006
DTD 12	Max.	-0.005	-0.006	-0.006	-0.006	-0.007	-0.007	-0.009	0.005	0.010
	Min.	-0.006	-0.007	-0.007	-0.008	-0.008	-0.010	-0.012	-0.015	-0.008
DTD 13	Max.	-0.013	-0.013	-0.013	-0.013	-0.013	-0.013	-0.009	0.007	0.009
	Min.	-0.015	-0.015	-0.015	-0.015	-0.015	-0.015	-0.015	-0.011	0.003
DTD 14	Max.	-0.020	-0.043	-0.049	-0.051	-0.061	-0.007	-0.058	-0.062	-0.060
	Min.	-0.043	-0.048	-0.051	-0.063	-0.067	-0.073	-0.067	-0.066	-0.065
DTD 15	Max.	0.000	0.000	0.000	0.000	0.000	0.004	0.003	0.007	0.001
	Min.	-0.001	-0.001	-0.001	-0.001	-0.001	-0.001	0.001	-0.009	-0.013
DTD 16	Max.	-0.001	-0.001	-0.001	-0.001	-0.001	-0.001	-0.002	-0.001	0.000
	Min.	-0.003	-0.003	-0.002	-0.003	-0.003	-0.004	-0.004	-0.004	-0.004

Cont. Table 4-9: Maximum and Minimum Measured Displacements (inches) of DCRCC24

		Stage (1)	Stage (2)	Stage (3)	Stage (4)	Stage (5)	Stage (6)	Stage (7)	Stage (8)	Stage (9)
Gauge		$0.05f_y$	$0.10f_y$	$0.15f_y$	$0.25f_y$	$0.5f_y$	$0.75f_y$	1 Δy	2 Δy	3 Δy
DTD 17	Max.	-0.054	-0.054	-0.054	-0.052	-0.052	-0.050	-0.049	-0.045	-0.044
	Min.	-0.055	-0.055	-0.055	-0.055	-0.052	-0.053	-0.051	-0.053	-0.054
DTD 18	Max.	-0.001	-0.001	-0.001	-0.001	-0.001	-0.001	-0.002	-0.001	0.000
	Min.	-0.003	-0.003	-0.003	-0.003	-0.003	-0.004	-0.004	-0.004	-0.004
DTD 19	Max.	-0.038	-0.038	-0.039	-0.038	-0.038	-0.038	-0.053	-0.039	-0.032
	Min.	-0.040	-0.040	-0.040	-0.040	-0.040	-0.056	-0.056	-0.054	-0.041
DTD 20	Max.	-0.004	-0.004	-0.004	-0.003	-0.003	-0.002	-0.011	-0.001	0.003
	Min.	-0.004	-0.004	-0.004	-0.004	-0.004	-0.020	-0.013	-0.012	-0.012
DTD 21	Max.	0.002	0.002	0.002	0.009	0.009	0.016	0.032	0.081	0.115
	Min.	0.000	0.000	0.000	-0.004	-0.004	-0.007	-0.007	-0.016	-0.021
DTD 22	Max.	0.001	0.001	0.011	0.011	0.011	0.011	0.017	0.099	0.117
	Min.	-0.001	0.000	0.000	-0.003	-0.013	-0.007	-0.007	-0.018	-0.021

Table 4-10: Maximum and Minimum Measured Force and Displacement of FSRCC24

Stage	Ductility	Average String Pot Displacement at Max. and Min. Force (in)		Actuator Displacement at Max. and Min. Force (in)		Actuator Force (kips)	
Number	Level	Max.	Min.	Max.	Min.	Max.	Min.
Stage (1)	$0.05f_y$	0.05	-0.02	0.02	-0.04	3.77	-3.58
Stage (2)	$0.10f_y$	0.23	-0.21	0.18	-0.24	4.31	-4.39
Stage (3)	$0.15f_y$	0.25	-0.21	0.23	-0.25	6.25	-6.12
Stage (4)	$0.25f_y$	0.56	-0.56	0.55	-0.56	9.33	-10.23
Stage (5)	$0.5f_y$	1.26	-1.37	1.38	-1.29	20.30	-20.10
Stage (6)	$0.75f_y$	2.11	-2.25	2.27	-2.01	29.33	-26.50
Stage (7)	1 Δy	2.86	-2.97	3.01	-2.80	36.01	-34.69
Stage (8)	2 Δy	5.77	-6.01	6.01	-5.81	42.73	-42.84
Stage (9)	2.5 Δy	7.43	-7.45	7.45	-7.38	42.86	-35.39
Stage (10)	3 Δy	8.87	-8.91	8.91	-8.86	25.60	-21.68
Stage (11)	3.5 Δy	10.57	-10.55	10.51	-10.49	22.93	-17.78
Stage (12)	4 Δy	12.07	-12.03	12.06	-12.02	21.35	-17.58

Table 4-11: Maximum and Minimum Measured Strain (micro strain) in the Reinforcement of FSRCC24

		Stage (1)	Stage (2)	Stage (3)	Stage (4)	Stage (5)	Stage (6)	Stage (7)	Stage (8)	Stage (9)	Stage (10)	Stage (11)	Stage (12)
Gauge		$0.05f_y$	$0.10f_y$	$0.15f_y$	$0.25f_y$	$0.5f_y$	$0.75f_y$	1 Δy	2 Δy	2.5 Δy	3 Δy	3.5 Δy	4 Δy
SG 1	Max.	-21	-21	-21	-14	0	69	318	809	885	664	547	374
	Min.	-62	-62	-62	-62	-55	-42	-35	125	228	297	291	228
SG 2	Max.	-28	-35	-21	-21	21	187	470	976	1259	22287	22287	22287
	Min.	-69	-76	-83	-83	-104	-104	-7	263	713	1280	22287	22287
SG 3	Max.	-7	-14	7	14	55	187	332	768	1405	62	-14	-48
	Min.	-62	-55	-42	-48	-55	-48	-14	48	-187	-657	-796	-125
SG 4	Max.	-14	-21	-7	-7	7	42	173	560	609	512	512	387
	Min.	-62	-55	-55	-55	-48	-35	-21	97	291	270	249	325
SG 5	Max.	-7	-7	0	7	28	62	145	256	374	339	367	242
	Min.	-48	0	-42	-42	-35	-28	-14	55	215	132	132	228
SG 6	Max.	28	21	35	42	48	48	76	845	803	692	1128	318
	Min.	-21	-21	-14	-28	-42	-55	-42	-62	215	132	132	228
SG 7	Max.	-28	-28	-14	-14	-21	7	180	374	457	388	360	256
	Min.	-69	-35	-69	-69	-76	-69	-48	42	118	145	145	132
SG 9	Max.	-14	-14	-7	-7	35	173	318	616	734	747	734	256
	Min.	-55	-48	-55	-62	-62	-62	-76	-42	208	208	201	201
SG 10	Max.	-21	-21	-14	-7	35	429	561	678	692	630	616	471
	Min.	-55	-55	-48	-55	-48	-14	256	256	284	298	305	312
SG 11	Max.	-21	-21	-14	0	42	187	325	505	775	976	969	699
	Min.	-62	-55	-55	-48	-48	-242	-249	-104	325	374	422	381
SG 12	Max.	-28	-35	-14	0	35	367	685	1038	2187	222573	-230931	-230931
	Min.	-76	-76	-76	-83	-90	-62	28	-159	-90	-230931	-230931	-230931
SG 13	Max.	-7	-7	-7	0	0	42	221	574	554	422	360	242
	Min.	-48	-48	-48	-48	-55	-55	-21	42	145	221	187	131
SG 14	Max.	19893	19907	20170	20322	20938	21789	22377	23996	2390	29781	-7494	-13991
	Min.	19630	19679	19644	19824	19873	19762	10919	-512	-4055	-14690	-15008	-14489
SG 15	Max.	367	574	865	844	921	844	588	768	395	-806	-865	-865
	Min.	111	395	104	-48	-48	-62	69	138	-28	893	893	-865

Cont. Table 4-11: Maximum and Minimum Measured Strain (micro strain) in the Reinforcement of FSRCC24

		Stage (1)	Stage (2)	Stage (3)	Stage (4)	Stage (5)	Stage (6)	Stage (7)	Stage (8)	Stage (9)	Stage (10)	Stage (11)	Stage (12)
Gauge		$0.05f_y$	$0.10f_y$	$0.15f_y$	$0.25f_y$	$0.5f_y$	$0.75f_y$	1 Δy	2 Δy	2.5 Δy	3 Δy	3.5 Δy	4 Δy
SG 16	Max.	-21	-14	-14	-7	35	214	408	768	630	533	519	367
	Min.	-62	-55	-55	-55	-48	-21	55	83	180	298	291	270
SG 17	Max.	7	0	7	14	35	69	104	422	353	464	321	327
	Min.	-42	-35	-35	-42	-35	-14	-42	-208	-325	-1107	-1111	-1121
SG 18	Max.	-48	-55	-35	-28	14	665	921	1440	11796	1350	3621	1184
	Min.	-97	-97	-97	-111	-97	-62	69	145	35	-339	692	796
SG 19	Max.	-7	-7	-7	0	-7	48	152	284	297	263	242	214
	Min.	-48	-48	-48	-48	-69	-62	-21	42	90	152	97	118
SG 20	Max.	62	55	76	131	346	740	982	1522	2235	2318	22203	-23140
	Min.	7	7	-7	-14	-69	-97	76	180	464	865	-23140	-23140
SG 21	Max.	-97	-90	-83	-83	-55	-35	69	436	671	443	715	457
	Min.	-131	-131	-131	-145	-166	-152	-111	-62	48	-228	-221	-131
SG 22	Max.	-14	-14	-7	0	104	651	789	927	810	824	768	512
	Min.	-55	-48	-48	-48	-42	21	242	284	374	450	450	401
SG 23	Max.	7	0	14	21	76	429	613	645	630	230	-30	739
	Min.	-42	-42	-42	-48	-48	-104	-145	-2	-23	83	48	637
SG 24	Max.	-35	-28	-14	0	48	235	32182	34667	17361	42160	32570	20731
	Min.	-76	-69	-76	-76	-76	-35	48	249	-21	-1017	-754	17638
SG 25	Max.	-14	-14	0	0	14	104	145	533	602	685	609	325
	Min.	-55	-48	-48	-55	-42	-42	21	76	187	284	277	215
SG 26	Max.	7	0	7	21	14	48	152	955	1052	913	982	858
	Min.	-35	-35	-35	-42	-55	-28	-14	83	408	533	623	623
SG 27	Max.	-28	-21	-14	0	55	228	429	796	1189	870	796	312
	Min.	-62	-62	-69	-76	-104	-111	-48	21	145	125	152	242
SG 28	Max.	-7	-14	0	7	7	42	83	180	180	194	194	166
	Min.	-48	-48	-48	-48	-48	-35	-21	7	69	111	125	125
SG 29	Max.	14	21	21	28	21	21	21	21	21	21	422	7
	Min.	-28	-21	-28	-21	-28	-21	-42	-35	-22381	-42	-22381	-28

Cont. Table 4-11: Maximum and Minimum Measured Strain (micro strain) in the Reinforcement of FSRCC24

		Stage (1)	Stage (2)	Stage (3)	Stage (4)	Stage (5)	Stage (6)	Stage (7)	Stage (8)	Stage (9)	Stage (10)	Stage (11)	Stage (12)
Gauge		$0.05f_y$	$0.10f_y$	$0.15f_y$	$0.25f_y$	$0.5f_y$	$0.75f_y$	1 Δy	2 Δy	2.5 Δy	3 Δy	3.5 Δy	4 Δy
SG 30	Max.	-7	-14	0	0	7	21	48	235	588	4271	24485	-23137
	Min.	-55	-48	-48	-55	-69	-76	-76	-13022	-23137	-23137	-23137	-23137
SG 31	Max.	-42	-62	7	318	1335	2255	2830	2844	2179	1003	844	28
	Min.	-194	-297	-387	-547	-1232	-1764	-2041	-2740	-2269	-1432	-1273	-401
SG 32	Max.	-42	-55	-21	125	734	1675	2513	214358	-239377	-239377	-239377	-239377
	Min.	-111	-152	-166	-235	-478	-519	-533	-239377	-239377	-239377	-239377	-239377
SG 33	Max.	19	0	20	60	40	137	433	2722	2998	2602	2799	2445
	Min.	-96	-100	-100	-120	-157	-80	-40	-237	-1163	-1519	-1776	-1776
SG 35	Max.	14	7	21	21	21	14	14	7	21	28	35	-7
	Min.	-28	-35	-28	-28	-28	-35	-42	-62	-55	-55	-55	-48
SG 37	Max.	-42	76	159	436	1806	3010	3833	13721	9825	4809	4442	3204
	Min.	-208	-180	-242	-457	-948	-1405	-1778	-1944	-131	1218	1467	3003
SG 38	Max.	-7	-7	7	21	76	138	180	249	201	145	145	90
	Min.	-48	-55	-48	-62	-42	-35	-14	-28	21	42	48	55
SG 39	Max.	879	1156	1896	2367	1703	1190	1689	4139	2028	1384	879	1204
	Min.	-782	-429	-298	-21	-1260	-1827	-1883	-6721	-3800	-2381	-1578	-609
SG 40	Max.	-14	-14	7	21	76	159	194	457	367	242	242	201
	Min.	-55	-55	-62	-62	-48	-28	0	28	125	138	152	166
SG 41	Max.	-62	69	152	498	1702	2616	2789	12615	9010	4636	4249	3121
	Min.	-215	-194	-242	-477	-920	-1377	-1765	-1771	62	1252	1495	3003
SG 42	Max.	-14	-14	0	0	48	111	138	187	138	131	138	111
	Min.	-55	-62	-55	-69	-62	-35	-28	-28	-14	28	35	76
SG 43	Max.	-35	-55	0	270	1204	2041	2601	3479	2518	1280	1121	201
	Min.	-152	-221	-277	-401	-858	-1294	-1563	-3998	-1937	-567	-450	118
SG 44	Max.	-7	14	35	62	90	166	201	485	436	291	291	187
	Min.	-55	-55	-62	-83	-62	-28	-7	62	132	28	111	118
SG 45	Max.	-35	42	111	256	1322	2457	2810	13034	9490	5074	4721	3641
	Min.	-152	-138	-180	-374	-754	-1184	-1537	-1599	775	2056	2284	3509

Cont. Table 4-11: Maximum and Minimum Measured Strain (micro strain) in the Reinforcement of FSRCC24

		Stage (1)	Stage (2)	Stage (3)	Stage (4)	Stage (5)	Stage (6)	Stage (7)	Stage (8)	Stage (9)	Stage (10)	Stage (11)	Stage (12)
Gauge		$0.05f_y$	$0.10f_y$	$0.15f_y$	$0.25f_y$	$0.5f_y$	$0.75f_y$	1 Δy	2 Δy	2.5 Δy	3 Δy	3.5 Δy	4 Δy
SG 47	Max.	-55	-83	-7	318	1314	2221	2636	12189	7402	6254	6136	3936
	Min.	-194	-270	-325	-457	-927	-1390	-1716	-27754	1384	2933	3127	3805
SG 48	Max.	7	7	21	35	55	90	125	388	457	381	353	242
	Min.	-42	-48	-42	-48	-35	-28	-21	21	152	166	166	180
SG 49	Max.	-48	35	104	214	1314	2365	2904	6209	5705	2877	2455	1452
	Min.	-173	-159	-207	-408	-768	-1238	-1563	-2711	-304	194	401	1376
SG 50	Max.	-14	-21	-7	-7	0	14	55	145	90	111	118	76
	Min.	-55	-62	-69	-76	-76	-62	-48	-42	-21	7	14	35
SG 51	Max.	-48	-14	14	83	686	1413	1773	5311	4217	222730	-231093	-231093
	Min.	-118	-111	-125	-166	-125	-97	-42	69	1586	-231093	-231093	-231093
SG 52	Max.	-14	-14	-14	-7	-7	0	0	35	21	222996	-230734	-230734
	Min.	-62	-62	-62	-90	-90	-111	-125	-104	-69	-230734	-230734	-230734
SG 53	Max.	21	21	21	21	21	21	21	28	28	21	21	21
	Min.	-21	-21	-28	-28	-21	-28	-21	-28	-21	-28	-21	-28
SG 54	Max.	-7	-7	0	0	7	7	0	28	14	35	48	28
	Min.	-55	-55	-55	-83	-111	-138	-145	-138	-132	-55	-48	-7
SG 56	Max.	-7	-28	21	228	1156	1904	2444	2728	2395	223352	-230370	-230370
	Min.	-111	-173	-222	-305	-630	-879	-997	-2035	-1828	-230370	-230370	-230370
SG 58	Max.	-55	-62	-48	-42	7	48	0	69	76	212690	-240870	-240870
	Min.	-97	-97	-97	-97	-97	-97	-111	-208	-256	-240870	-240870	-240870
SG 59	Max.	-69	-76	-55	90	706	1280	1785	2948	2394	1903	1772	-111
	Min.	-118	-125	-131	-131	-138	-138	-138	-325	-498	-491	-484	-228
SG 60	Max.	-48	-48	-42	-42	35	263	332	574	270	298	304	42
	Min.	-90	-90	-90	-97	-90	-83	-83	-69	-90	-55	-55	-7
SG 61	Max.	-35	-42	-28	-14	35	28	76	301	301	408	410	401
	Min.	-90	-90	-97	-104	-111	-83	-48	-118	-110	-102	-111	-92
SG 63	Max.	-21	-14	-7	0	69	291	367	1197	222498	-231106	-231106	-231106
	Min.	-62	-55	-55	-55	-62	-35	28	83	-231106	-231106	-231106	-231106

Cont. Table 4-11: Maximum and Minimum Measured Strain (micro strain) in the Reinforcement of FSRCC24

		Stage (1)	Stage (2)	Stage (3)	Stage (4)	Stage (5)	Stage (6)	Stage (7)	Stage (8)	Stage (9)	Stage (10)	Stage (11)	Stage (12)
Gauge		$0.05f_y$	$0.10f_y$	$0.15f_y$	$0.25f_y$	$0.5f_y$	$0.75f_y$	1 Δy	2 Δy	2.5 Δy	3 Δy	3.5 Δy	4 Δy
SG 64	Max.	-7	-7	0	7	48	194	235	623	1011	1053	1553	1753
	Min.	-48	-48	-48	-42	-48	-21	76	-180	-304	-301	-330	-200
SG 65	Max.	-62	-7	48	159	1280	2519	2990	17233	15143	68109	64655	4713
	Min.	-152	-138	-166	-291	-526	-657	-962	-194	5032	-23182	-23182	4623
SG 66	Max.	-48	-48	-42	-42	-14	83	201	1924	2300	220993	-232605	-232605
	Min.	-90	-83	-83	-90	-83	-83	-90	-62	76	-232605	-232605	-232605
SG 67	Max.	-48	21	97	256	1640	2733	7818	11610	4947	2892	2774	1003
	Min.	-159	-138	-194	-346	-692	-1114	-104	-60449	-8233	-4809	-3383	851
SG 68	Max.	519	567	540	616	616	540	422	478	314	55923	325	166
	Min.	436	478	415	381	388	-62	14	-62	-125	-232590	-263	118
SG 69	Max.	-55	-76	-21	159	1191	2166	3246	22243	-23118	-23118	-23118	-23118
	Min.	-152	-208	-242	-339	-637	-872	-1038	-23118	-23118	-23118	-23118	-23118
SG 70	Max.	-14	-14	0	7	35	62	131	42867	44022	59982	50272	42618
	Min.	62	55	55	55	55	90	138	394	291	533	233940	-37766

Table 4-12: Maximum and Minimum Measured Displacements (inches) of FSRCC24

		Stage (1)	Stage (2)	Stage (3)	Stage (4)	Stage (5)	Stage (6)	Stage (7)	Stage (8)	Stage (9)	Stage (10)	Stage (11)	Stage (12)
Gauge		$0.05f_y$	$0.10f_y$	$0.15f_y$	$0.25f_y$	$0.5f_y$	$0.75f_y$	1 Δy	2 Δy	2.5 Δy	3 Δy	3.5 Δy	4 Δy
DTD1	Max.	0.003	0.000	0.002	0.003	0.032	0.072	0.102	0.284	0.323	0.346	0.251	0.044
	Min.	-0.002	-0.004	-0.004	-0.007	-0.019	-0.040	-0.067	-0.242	-0.439	-0.794	-1.027	-1.027
DTD2	Max.	0.002	0.000	0.001	0.006	0.028	0.060	0.109	0.246	0.324	0.189	0.029	0.889
	Min.	-0.257	-0.003	-0.004	-0.007	-0.018	-0.038	-0.056	-0.257	-0.570	-0.984	-0.984	-0.984
DTD3	Max.	0.002	0.002	0.002	0.002	0.002	0.001	-0.001	-0.004	-0.003	-0.005	-0.005	-0.006
	Min.	-0.019	0.000	0.000	-0.001	-0.004	-0.008	-0.011	-0.019	-0.009	-0.008	-0.079	-0.111
DTD4	Max.	0.001	-0.001	-0.001	-0.001	-0.001	-0.001	-0.004	0.046	0.060	0.045	0.024	0.022
	Min.	-0.001	-0.001	-0.001	-0.002	-0.007	-0.013	-0.018	-0.033	-0.001	-0.071	-0.187	-0.227
DTD5	Max.	0.001	0.001	0.002	0.007	0.021	0.039	0.049	0.142	0.096	0.047	0.038	0.033
	Min.	-0.002	-0.001	-0.002	-0.004	-0.010	-0.018	-0.024	-0.038	-0.029	-0.024	-0.019	-0.146
DTD6	Max.	0.001	0.000	0.001	0.002	0.013	0.037	0.055	0.163	0.271	0.322	0.371	-0.502
	Min.	-0.001	-0.001	-0.002	-0.005	-0.013	-0.022	-0.037	-0.130	-0.300	-0.425	-0.606	-0.752
DTD7	Max.	0.002	0.002	0.003	0.004	0.017	0.022	0.027	0.078	0.060	0.033	0.029	0.025
	Min.	-0.001	0.000	0.000	-0.003	-0.009	-0.014	-0.019	-0.026	-0.018	-0.012	-0.008	-0.008
DTD8	Max.	0.001	0.003	0.004	0.009	0.024	0.038	0.050	0.082	0.054	0.038	0.031	0.028
	Min.	-0.001	0.001	0.000	-0.002	-0.007	-0.013	-0.015	-0.025	-0.017	-0.009	-0.008	-0.007
DTD9	Max.	0.001	0.001	0.007	0.007	0.021	0.044	0.053	0.066	0.043	0.031	0.029	0.025
	Min.	-0.001	-0.002	-0.002	-0.001	-0.009	-0.013	-0.016	-0.020	-0.014	-0.008	-0.002	-0.002
DTD10	Max.	0.001	0.001	0.001	0.001	0.001	0.001	0.001	-0.001	-0.004	-0.005	-0.006	-0.006
	Min.	-0.001	-0.001	-0.001	-0.005	-0.013	-0.022	-0.026	-0.036	-0.028	-0.032	-0.014	-0.012
DTD11	Max.	0.008	-0.001	-0.001	-0.001	-0.001	-0.001	-0.001	0.018	0.003	-0.001	0.015	0.015
	Min.	-0.003	-0.003	-0.003	-0.003	-0.003	-0.003	-0.003	-0.002	0.000	-0.004	-0.003	0.013
DTD12	Max.	0.001	0.011	0.011	0.011	0.011	0.009	0.009	0.009	0.040	0.039	0.050	0.050
	Min.	-0.002	0.011	0.009	0.009	0.008	0.008	0.005	-0.002	0.035	0.038	0.037	0.049
DTD13	Max.	0.001	0.024	0.024	0.024	0.024	0.024	0.024	0.041	0.039	0.039	0.062	0.062
	Min.	0.002	0.022	0.022	0.022	0.022	0.023	0.022	0.023	0.025	0.037	0.037	0.060
DTD14	Max.	-0.001	-0.054	-0.054	-0.054	-0.054	-0.054	-0.046	-0.027	-0.023	-0.022	-0.019	-0.019
	Min.	-0.001	-0.056	-0.056	-0.056	-0.056	-0.056	-0.056	-0.048	-0.028	-0.025	-0.024	-0.021

Cont. Table **4-12: Maximum and Minimum Measured Displacements (inches) of FSRCC24**

		Stage (1)	Stage (2)	Stage (3)	Stage (4)	Stage (5)	Stage (6)	Stage (7)	Stage (8)	Stage (9)	Stage (10)	Stage (11)	Stage (12)
Gauge		$0.05f_y$	$0.10f_y$	$0.15f_y$	$0.25f_y$	$0.5f_y$	$0.75f_y$	1 Δy	2 Δy	2.5 Δy	3 Δy	3.5 Δy	4 Δy
DTD15	Max.	0.090	0.085	0.085	0.085	0.085	0.085	0.085	0.090	0.081	0.086	0.085	0.085
	Min.	0.055	0.085	0.085	0.085	0.085	0.085	0.084	0.055	0.076	0.084	0.073	0.084
DTD16	Max.	0.132	0.001	0.002	0.006	0.019	0.030	0.039	0.132	0.103	0.083	0.073	0.061
	Min.	-0.044	-0.001	-0.002	-0.005	-0.010	-0.018	-0.022	-0.044	-0.030	-0.006	-0.003	-0.001
DTD17	Max.	0.204	-0.001	0.000	0.001	0.014	0.037	0.067	0.204	0.136	0.102	-0.310	-0.809
	Min.	-0.111	-0.005	-0.005	-0.007	-0.015	-0.032	-0.043	-0.111	-0.324	-0.698	-0.810	-0.938

Table 4-13: Maximum and Minimum Measured Force and Displacement of DCKJ24

Stage	Ductility	Axial Force (Kips)		Average String Pot Displacement at Max. and Min. Force (in)		Actuator Displacement at Max. and Min. Force (in)		Actuator Force (kips)	
Number	Level	Max.	Min.	Max.	Min.	Max.	Min.	Max.	Min.
Stage (1)	$0.15f_y$	33.78	33.82	0.19	-0.21	0.17	-0.22	4.70	-4.00
Stage (2)	$0.25f_y$	33.44	26.00	0.28	-0.27	0.26	-0.23	4.55	-4.54
Stage (3)	$0.5f_y$	52.2	21.00	0.70	-1.22	1.21	-0.67	12.02	-7.81
Stage (4)	$0.75f_y$	57.44	9.58	1.20	-1.54	1.53	-1.19	14.87	-11.41
Stage (5)	1 Δy	60.04	5.04	2.41	-2.56	2.44	-2.43	18.76	-11.83
Stage (6)	1.5Δy	60.74	4.62	3.61	-3.63	3.66	-3.65	20.61	-14.07
Stage (7)	2 Δy	58.62	4.52	4.81	-5.01	4.98	-4.87	20.57	-15.17
Stage (8)	3 Δy	56.62	2.52	7.71	-7.44	7.35	-7.17	19.51	-16.74
Stage (9)	4 Δy	55.14	5.63	9.84	-9.74	9.75	-9.82	18.02	-17.32
Stage (10)	5 Δy	56.76	9.82	11.88	-12.18	12.18	-11.85	16.21	-17.27
Stage (12)	6 Δy	57.58	9.82	11.29	-14.61	14.61	-11.85	14.07	-17.27

Table 4-14: Maximum and Minimum Measured Strain (micro strain) in the Reinforcement of DCKJ24

		Stage (1)	Stage (2)	Stage (3)	Stage (4)	Stage (5)	Stage (6)	Stage (7)	Stage (8)	Stage (9)	Stage (10)	Stage (11)
Gauge		$0.15f_y$	$0.25f_y$	$0.5f_y$	$0.75f_y$	1 Δy	1.5 Δy	2 Δy	3 Δy	4 Δy	5 Δy	6 Δy
SG 1	Max.	321	269	361	1686	1194	1935	2191	3010	4480	6539	9379
	Min.	-243	144	85	-944	-413	-1115	-1423	-1482	-997	-1292	-512
SG 3	Max.	118	118	924	2438	2923	140087	210128	210128	210128	162064	210128
	Min.	-85	-46	-177	-636	59	-219415	-219415	-219415	-219415	-219415	-219415
SG 5	Max.	170	177	734	1488	2314	6582	10660	19459	28946	39941	48287
	Min.	-197	-184	-446	-715	-1134	-1108	-426	229	708	1875	4839
SG 7	Max.	256	275	1488	2649	5882	10281	2826	1397	1410	1318	1003
	Min.	-275	-256	-531	-846	-1049	13	-157	-885	-1016	-3803	-656
SG 8	Max.	98	105	170	931	347	623	531	524	518	655	1390
	Min.	-118	7	7	-518	-426	-413	-518	-551	-459	7	-413
SG 9	Max.	249	242	1042	1992	2556	9725	16620	30828	44583	58542	69821
	Min.	-242	-223	-623	-996	-1416	-1966	-1134	452	3585	9018	12727
SG 10	Max.	59	79	92	131	111	144	138	446	721	761	721
	Min.	-20	-13	-20	-7	13	-52	-79	39	-177	-603	-761
SG 11	Max.	190	197	1612	2910	5073	13411	18616	1298	33672	38706	210061
	Min.	-275	-249	-662	-1023	-1475	-2255	-3795	282	-15849	-17678	-219507
SG 12	Max.	105	85	157	236	295	393	518	29057	2111	2865	2845
	Min.	-39	-13	-13	20	33	39	111	-11504	400	1278	-1495
SG 13	Max.	190	190	1173	2406	8082	12487	18184	31602	44575	57737	75961
	Min.	-275	-282	-721	-1127	-1114	-924	-518	184	2314	6175	5198
SG 14	Max.	52	66	59	131	157	164	131	105	210	374	4678
	Min.	-33	-13	-20	7	33	0	-72	-216	-394	-643	-656
SG 16	Max.	66	72	105	164	203	275	354	721	1384	2308	8328
	Min.	-46	-26	-20	-7	13	20	39	184	236	525	1161

Cont. Table 4-14: Maximum and Minimum Measured Strain (micro strain) in the Reinforcement of DCKJ24

		Stage (1)	Stage (2)	Stage (3)	Stage (4)	Stage (5)	Stage (6)	Stage (7)	Stage (8)	Stage (9)	Stage (10)	Stage (11)
Gauge		$0.15f_y$	$0.25f_y$	$0.5f_y$	$0.75f_y$	1 Δy	1.5 Δy	2 Δy	3 Δy	4 Δy	5 Δy	6 Δy
SG 17	Max.	216	210	1212	63635	68773	72103	81101	88251	96246	103344	109314
	Min.	-269	-295	-655	-1016	-1252	-1593	-1507	308	3178	8552	14025
SG 18	Max.	0	13	39	92	105	105	688	642	944	1835	2202
	Min.	-98	-85	-98	-85	-59	-39	-26	111	131	190	813
SG 19	Max.	453	479	1766	3237	5397	13276	15705	22271	29801	38219	41501
	Min.	-315	-302	-788	-1182	-1595	-2423	-1589	-2475	-3808	-4524	-14786
SG 20	Max.	105	105	170	197	243	315	308	479	1311	2308	2452
	Min.	-33	33	13	72	85	105	66	-203	-229	118	361
SG 21	Max.	203	203	1318	2360	3029	11303	13795	21761	28521	35405	42493
	Min.	-269	-262	-656	-1023	-1220	-1193	-66	20	905	2065	308
SG 22	Max.	85	79	131	315	387	426	446	997	1088	1285	-219445
	Min.	-20	-7	-7	52	66	98	177	236	341	-219445	-219445
SG 23	Max.	210	223	1436	2341	2505	2590	2970	16557	38596	31521	210867
	Min.	-289	-249	-721	-1056	-1515	-1947	-2151	-218861	-218861	-218861	-218861
SG 24	Max.	288	288	1337	2261	3120	10047	11266	885	20337	2536	27107
	Min.	-328	-341	-819	-1095	-1186	-1167	184	111	-131	485	1134
SG 25	Max.	79	66	138	203	282	361	387	1514	1574	1934	1718
	Min.	-46	-33	-13	0	26	46	79	478	538	747	-219506
SG 26	Max.	72	59	92	190	256	223	229	282	833	1639	1737
	Min.	-20	-7	-13	-13	46	33	66	-7	72	544	721
SG 27	Max.	334	387	1797	3291	3580	13087	15421	22588	28351	33111	209782
	Min.	-472	-466	-1003	-1442	-1862	-2374	-1593	-643	131	-15192	-219912
SG 28	Max.	118	118	301	426	452	478	557	812	1114	1232	1409
	Min.	-46	-39	-20	144	170	190	216	347	269	236	380
SG 29	Max.	85	72	407	1188	1326	1431	1490	1720	2061	2218	2087
	Min.	-26	0	-13	39	144	79	98	92	131	276	210
SG 30	Max.	72	72	92	144	203	747	1095	1455	1757	1993	1927
	Min.	-20	0	0	-13	33	72	308	400	531	662	623

Cont. Table 4-14: Maximum and Minimum Measured Strain (micro strain) in the Reinforcement of DCKJ24

		Stage (1)	Stage (2)	Stage (3)	Stage (4)	Stage (5)	Stage (6)	Stage (7)	Stage (8)	Stage (9)	Stage (10)	Stage (11)
Gauge		$0.15f_y$	$0.25f_y$	$0.5f_y$	$0.75f_y$	1 Δy	1.5 Δy	2 Δy	3 Δy	4 Δy	5 Δy	6 Δy
SG 31	Max.	98	85	157	190	190	275	361	564	1055	1265	1351
	Min.	-26	20	20	-20	20	20	79	105	229	406	315
SG 32	Max.	52	52	282	800	977	1199	1252	1357	1573	4122	4830
	Min.	-46	-20	-26	52	131	210	229	223	249	223	2373
SG 33	Max.	52	66	85	518	610	793	997	1298	1521	2065	2334
	Min.	-33	-7	0	-157	-98	-125	138	256	315	531	682
SG 34	Max.	223	98	151	1311	1580	2196	2236	5081	2236	13137	16063
	Min.	-7	0	-7	-7	46	144	138	-229	-236	-380	-479
SG 36	Max.	46	39	85	138	577	1022	1291	1383	1697	1776	1671
	Min.	-52	-46	-52	-79	-20	-7	26	356	242	315	374
SG 37	Max.	39	39	46	72	72	151	151	1514	131	190	230
	Min.	-52	-20	-46	-66	-111	-79	-20	105	-52	-39	-20
SG 38	Max.	1023	714	649	551	649	983	1259	157	2320	2537	2648
	Min.	354	551	347	59	79	66	164	146	478	603	662
SG 39	Max.	39	26	52	46	348	662	859	1816	1371	1639	1712
	Min.	-52	-39	-52	-52	-46	-7	98	282	164	236	249
SG 40	Max.	72	59	79	125	125	157	171	1102	617	721	735
	Min.	-20	-20	-20	7	33	33	13	111	85	184	243
SG 41	Max.	39	46	118	210	184	223	302	308	1232	1449	1344
	Min.	-52	-20	-39	-20	-20	-20	-13	39	125	302	341
SG 42	Max.	72	66	72	144	151	184	203	590	459	734	800
	Min.	-20	-7	-13	13	26	33	46	39	125	197	203
SG 43	Max.	39	46	52	98	118	125	249	243	905	1062	1082
	Min.	-52	-39	-46	-26	-13	0	0	72	79	144	203
SG 44	Max.	52	52	66	98	118	125	151	597	832	1147	1186
	Min.	-33	-33	-26	7	7	7	26	33	177	387	367

Cont. Table 4-14: Maximum and Minimum Measured Strain (micro strain) in the Reinforcement of DCKJ24

		Stage (1)	Stage (2)	Stage (3)	Stage (4)	Stage (5)	Stage (6)	Stage (7)	Stage (8)	Stage (9)	Stage (10)	Stage (11)
Gauge		$0.15f_y$	$0.25f_y$	$0.5f_y$	$0.75f_y$	1 Δy	1.5 Δy	2 Δy	3 Δy	4 Δy	5 Δy	6 Δy
SG 46	Max.	66	46	66	92	111	125	138	164	551	977	1016
	Min.	-39	-7	-20	7	7	20	13	-7	13	131	125
SG 47	Max.	52	59	59	92	105	131	151	387	767	1029	1055
	Min.	-33	-33	-33	-13	7	20	13	59	111	170	170
SG 48	Max.	52	39	118	125	118	131	138	216	321	406	374
	Min.	-59	-26	-46	-26	-20	-7	0	33	52	118	144
SG 49	Max.	66	72	85	302	151	210	289	472	393	485	518
	Min.	-59	-13	-20	-92	-98	-164	-138	-61	-39	171	66
SG 50	Max.	72	59	105	197	197	203	210	203	243	249	236
	Min.	-33	-7	-13	-13	0	-7	-7	13	-7	59	46
SG 53	Max.	98	105	407	1141	1285	1574	1672	1941	1993	1049	1023
	Min.	-111	-118	-269	-361	-511	-577	-498	-656	-754	-433	-308
SG 54	Max.	793	767	780	1173	846	918	1167	1029	918	780	787
	Min.	406	551	551	-728	-577	-583	-485	-544	-498	478	256
SG 55	Max.	230	269	1135	1883	2066	2420	2532	2663	3122	7635	7045
	Min.	-157	-105	-321	-479	-584	-649	-636	-610	-1036	-885	2184
SG 56	Max.	354	321	636	2156	1239	1776	2052	1848	1658	1750	1783
	Min.	-151	223	210	-1022	-852	-924	-937	-891	-1016	413	-990
SG 57	Max.	118	118	649	1226	1370	1613	1731	1816	2197	5921	5698
	Min.	-59	-59	-164	-256	-262	-302	-262	-308	-446	-479	2262
SG 58	Max.	131	131	597	1489	1640	1968	2105	2433	2939	4113	4021
	Min.	-125	-112	-282	-439	-603	-754	-695	-800	-1299	-1345	-1436
SG 60	Max.	328	374	1154	1732	1876	2197	2984	6275	10592	11681	10632
	Min.	-138	-85	-269	-407	-492	-538	-551	-433	2374	2807	3548
SG 61	Max.	85	79	111	183	439	708	891	865	1298	1593	1651
	Min.	-39	-33	-98	-151	-131	-131	-98	20	-13	164	203
SG 62	Max.	72	85	184	584	840	984	1030	1081	1456	1515	1410
	Min.	-52	-46	-118	-144	-118	-72	-33	-98	33	282	269

Cont. Table 4-14: Maximum and Minimum Measured Strain (micro strain) in the Reinforcement of DCKJ24

		Stage (1)	Stage (2)	Stage (3)	Stage (4)	Stage (5)	Stage (6)	Stage (7)	Stage (8)	Stage (9)	Stage (10)	Stage (11)
Gauge		$0.15f_y$	$0.25f_y$	$0.5f_y$	$0.75f_y$	1 Δy	1.5 Δy	2 Δy	3 Δy	4 Δy	5 Δy	6 Δy
SG 63	Max.	98	92	308	964	1403	1717	1894	1921	1934	2078	2078
	Min.	-59	-59	-157	-125	-46	-33	-20	20	262	387	505
SG 65	Max.	138	125	393	1121	1606	1914	1993	2019	2164	2223	2118
	Min.	-33	-13	-52	-46	-20	-46	-46	-7	243	413	498
SG 66	Max.	79	66	105	184	879	1043	1089	1108	1181	1312	1358
	Min.	-52	-52	-118	-125	-118	-105	-79	-52	-13	7	52
SG 67	Max.	98	92	236	715	945	1148	1286	1292	1463	1660	1686
	Min.	-72	-46	-151	-157	-118	-98	-52	-46	13	184	394
SG68	Max.	118	98	282	761	1187	1502	1613	1646	1653	1744	1587
	Min.	-66	-46	-125	-85	-33	7	39	85	125	157	125
SG 69	Max.	93	82	293	918	1346	1615	1814	1908	1942	1979	1969
	Min.	-50	-55	-147	-125	-30	-30	-10	-70	-45	-10	5
SG 71	Max.	256	236	597	1404	1364	1520	1817	1456	1010	754	656
	Min.	-190	39	-33	-899	-794	-761	-721	-617	-735	-125	-525
SG 72	Max.	256	249	662	1102	1187	1442	1521	1449	1089	610	413
	Min.	33	52	-26	-236	-315	-315	-230	-197	-190	-13	-85
SG 75	Max.	98	98	524	1029	1154	1461	1573	1750	1567	1062	642
	Min.	-33	-7	-46	-33	7	72	79	111	52	-20	-26

Table 4-15: Maximum and Minimum Measured Displacements (inches) of DCKJ24

		Stage (1)	Stage (2)	Stage (3)	Stage (4)	Stage (5)	Stage (6)	Stage (7)	Stage (8)	Stage (9)	Stage (10)	Stage (11)
Gauge		$0.15f_y$	$0.25f_y$	$0.5f_y$	$0.75f_y$	1 Δy	1.5 Δy	2 Δy	3 Δy	4 Δy	5 Δy	6 Δy
DTD 1	Max.	0.0048	0.0047	0.0156	0.0263	0.0523	0.1050	0.1628	-0.0519	0.4111	0.5352	0.6229
	Min.	-0.0029	-0.0030	-0.0128	-0.0264	-0.0287	-0.0519	-0.0758	-0.0758	-0.1689	-0.3173	-0.3254
DTD 2	Max.	0.0047	0.0050	0.0231	0.0535	0.0619	0.1287	0.1289	-0.0645	0.3358	0.3924	0.4025
	Min.	-0.0051	-0.0050	-0.0121	-0.0210	-0.0383	-0.0645	-0.2419	-0.2419	-0.4105	-0.6056	-0.6763
DTD 3	Max.	0.0024	0.0021	0.0129	0.0268	0.0529	0.1032	0.1880	-0.0277	0.4439	0.5888	0.8343
	Min.	-0.0031	-0.0032	-0.0084	-0.0149	-0.0158	-0.0277	-0.0377	-0.0377	-0.0597	-0.0526	-0.0150
DTD 4	Max.	0.0012	-0.0002	0.0120	0.0219	0.0247	0.0666	0.2267	-0.0432	0.2432	0.3155	0.3612
	Min.	-0.0028	-0.0028	-0.0083	-0.0152	-0.0247	-0.0432	-0.0555	-0.0555	-0.2219	-0.2972	-0.6477
DTD 5	Max.	0.0016	0.0015	0.0140	0.0244	0.0368	0.0694	0.1015	-0.0189	0.3133	0.2786	0.2866
	Min.	-0.0031	-0.0032	-0.0098	-0.0138	-0.0139	-0.0189	-0.0253	-0.0253	-0.0512	-0.0580	-0.1838
DTD 6	Max.	0.0048	0.0062	0.0218	0.0372	0.0426	0.0774	0.1114	-0.0339	0.4369	0.5958	0.5968
	Min.	-0.0011	-0.0003	-0.0077	-0.0151	-0.0230	-0.0339	-0.0449	-0.0449	0.0371	0.1784	0.0286
DTD 7	Max.	0.0024	0.0023	0.0119	0.0188	0.0276	0.0411	0.0510	-0.0173	0.1298	0.1983	0.2227
	Min.	-0.0026	-0.0026	-0.0076	-0.0129	-0.0141	-0.0173	-0.0202	-0.0202	-0.0310	-0.0287	-0.0208
DTD 8	Max.	0.0025	0.0028	0.0153	0.0249	0.0270	0.0411	0.0610	-0.0259	0.1196	0.1555	0.1262
	Min.	-0.0036	-0.0036	-0.0093	-0.0134	-0.0194	-0.0259	-0.0303	-0.0303	-0.0491	-0.0442	-0.0097
DTD 9	Max.	0.0004	0.0001	0.0057	0.0146	0.0169	0.0545	0.0866	0.0236	0.2346	0.3095	0.3500
	Min.	-0.0008	-0.0007	-0.0007	-0.0004	-0.0001	0.0013	0.0236	0.0013	0.1052	0.1652	0.1944
DTD 10	Max.	0.0004	0.0005	0.0127	0.0246	0.0274	0.0705	0.1175	0.0117	0.3018	0.3856	0.4013
	Min.	-0.0011	-0.0010	-0.0011	-0.0003	0.0001	0.0010	0.0117	0.0010	0.0606	0.0882	0.0341
DTD 11	Max.	0.0014	-0.0005	-0.0004	0.0120	0.0146	0.0193	0.0272	-0.0005	0.0708	0.1041	0.1523
	Min.	-0.0009	-0.0008	-0.0105	-0.0148	-0.0046	-0.0029	-0.0005	-0.0029	-0.0014	0.0080	0.0426
DTD 12	Max.	-0.0015	-0.0015	0.0247	0.0519	0.0489	0.0607	0.0776	0.0262	0.1268	0.1687	0.1803
	Min.	-0.0024	-0.0023	-0.0024	0.0130	0.0214	0.0220	0.0262	0.0220	0.0490	0.0699	0.0962
DTD 13	Max.	0.0005	0.0004	0.0011	0.0073	0.0117	0.0168	0.0204	0.0000	0.0423	0.0404	0.0364
	Min.	0.0000	0.0001	-0.0011	-0.0014	-0.0004	-0.0007	0.0000	-0.0007	0.0052	0.0070	0.0123
DTD 14	Max.	0.0009	0.0009	0.0174	0.0389	0.0389	0.0412	0.0526	0.0369	0.0737	0.1134	0.1360
	Min.	-0.0011	-0.0009	-0.0009	0.0160	0.0370	0.0369	0.0351	0.0351	0.0614	0.0720	0.1088
DTD 15	Max.	0.0015	0.0018	0.0018	0.0024	0.0013	-0.0004	-0.0026	-0.0044	-0.0155	-0.0253	-0.0428
	Min.	0.0010	0.0013	0.0010	0.0005	-0.0020	-0.0044	-0.0103	-0.0103	-0.0334	-0.0680	-0.0945

Table 4-16: Maximum and Minimum Measured Force and Displacement of FSKJ24

Stage	Ductility	Axial Force (Kips)		String Pot Displacement at Max. and Min. Force (in)		Actuator Displacement at Max. and Min. Force (in)		Actuator Force (kips)	
Number	Level	Max.	Min.	Max.	Min.	Max.	Min.	Max.	Min.
Stage (1)	$0.15f_y$	34.62	28.40	0.37	-0.18	0.19	-0.50	2.73	-3.91
Stage (2)	$0.25f_y$	41.82	15.68	0.86	-0.39	0.38	-0.90	4.47	-5.92
Stage (3)	$0.5f_y$	57.34	8.60	1.31	-1.38	1.28	-1.36	8.76	-7.19
Stage (4)	$0.75f_y$	64.00	1.98	2.66	-2.47	2.44	-2.77	12.73	-10.00
Stage (5)	1 Δy	64.98	1.78	3.19	-3.24	3.18	-3.22	14.61	-10.5
Stage (6)	1.5 Δy	64.94	2.02	4.16	-4.84	4.86	-4.21	16.85	-11.8
Stage (7)	2 Δy	60.42	2.22	6.34	-6.35	6.38	-6.27	15.79	-13.54
Stage (8)	2.5 Δy	58.94	2.42	8.34	-7.94	7.97	-8.37	13.56	-11.2
Stage (9)	3 Δy	58.54	3.62	10.16	-9.98	9.95	-10.06	10.37	-8.84
Stage (10)	3.5 Δy	58.74	4.24	11.16	-11.12	11.08	-11.15	8.50	-6.30

Table 4-17: Maximum and Minimum Measured Strain (micro strain) in the Reinforcement of FSKJ24

		Stage (1)	Stage (2)	Stage (3)	Stage (4)	Stage (5)	Stage (6)	Stage (7)	Stage (8)	Stage (9)	Stage (11)
Gauge		$0.15f_y$	$0.25f_y$	$0.5f_y$	$0.75f_y$	1 Δy	1.5 Δy	2 Δy	2.5 Δy	3 Δy	3.5 Δy
SG 1	Max.	407	879	1855	4701	5855	9284	11808	15532	16575	16627
	Min.	-216	-203	-203	-288	269	-426	-2826	-8248	-15893	-18234
SG 2	Max.	98	282	393	524	544	820	1475	1875	2577	2931
	Min.	-33	0	72	98	92	105	20	-223	-256	-288
SG 3	Max.	79	85	485	1704	3074	7937	14530	21425	25200	28189
	Min.	-197	-275	-334	-321	-26	524	3093	6711	-219362	-219362
SG 4	Max.	52	98	170	426	623	964	1573	2557	2563	2511
	Min.	-26	0	26	125	164	157	170	282	334	302
SG 5	Max.	236	472	1056	1790	2066	2223	1994	1712	1495	1266
	Min.	-151	-184	-315	-426	-439	-479	-498	-348	-177	-66
SG 6	Max.	144	190	138	190	243	262	282	302	256	243
	Min.	-125	-112	-151	-157	-177	-190	39	-230	-256	-439
SG 7	Max.	85	72	531	1560	2012	2700	2700	2720	2183	2196
	Min.	-288	-426	-649	-767	-459	-426	-583	-603	-544	-623
SG 8	Max.	39	92	118	433	511	571	564	538	708	761
	Min.	-39	-39	-26	7	125	184	289	164	354	485
SG 9	Max.	177	341	1692	2715	3056	4945	4348	3548	2984	2466
	Min.	-144	-184	-525	-944	-1108	-1384	-1102	-800	-315	-197
SG 10	Max.	46	92	151	177	210	223	223	229	216	229
	Min.	-20	7	26	92	111	138	144	144	144	157
SG 11	Max.	66	59	721	1816	2340	3290	3389	3271	2550	2405
	Min.	-282	-439	-701	-970	-937	-741	-328	-282	-380	-459
SG 12	Max.	52	72	79	98	131	118	125	151	184	190
	Min.	-33	-20	-7	20	20	39	59	59	85	131
SG 13	Max.	170	872	1698	2661	3507	6214	5316	4254	3586	2970
	Min.	-184	-223	-590	-1029	-1173	-1475	-977	-564	-177	-13
SG 14	Max.	52	125	177	229	275	321	315	295	275	282
	Min.	-7	7	39	111	125	164	144	170	177	177

Cont. Table 4-17: Maximum and Minimum Measured Strain (micro strain) in the Reinforcement of FSKJ24

		Stage (1)	Stage (2)	Stage (3)	Stage (4)	Stage (5)	Stage (6)	Stage (7)	Stage (8)	Stage (9)	Stage (11)
Gauge		$0.15f_y$	$0.25f_y$	$0.5f_y$	$0.75f_y$	1 Δy	1.5 Δy	2 Δy	2.5 Δy	3 Δy	3.5 Δy
SG 15	Max.	59	39	406	1212	1652	2320	2399	2294	1802	1711
	Min.	-229	-380	-603	-800	-878	-885	-603	-288	-315	-367
SG 16	Max.	59	85	118	151	190	197	210	210	210	203
	Min.	-7	13	33	72	85	111	131	131	138	151
SG 17	Max.	157	570	1285	2117	2432	2635	2451	2182	1901	1586
	Min.	-151	-184	-459	-839	-996	-1271	-1258	-1121	-904	-813
SG 18	Max.	59	105	177	236	295	341	341	328	308	321
	Min.	-26	-13	7	59	79	111	125	138	138	144
SG 19	Max.	46	13	347	1278	1684	2294	2333	2137	1658	1573
	Min.	-223	-328	-498	-708	-800	-885	-714	-524	-393	-315
SG 20	Max.	39	59	98	236	295	354	380	380	354	380
	Min.	-20	-20	0	26	79	118	131	138	157	164
SG 21	Max.	131	400	1462	2367	2708	2983	2741	2387	2059	1679
	Min.	-164	-197	-479	-879	-1036	-1338	-1292	-1154	-938	-852
SG 22	Max.	39	92	243	308	354	387	380	367	328	334
	Min.	-33	-13	-20	125	138	138	151	151	151	151
SG 23	Max.	59	0	269	1030	1476	2191	2250	2053	1620	1502
	Min.	-275	-420	-649	-826	-859	-938	-787	-623	-472	-348
SG 24	Max.	46	72	105	144	184	197	203	184	177	184
	Min.	-20	0	20	52	59	92	105	105	105	105
SG 25	Max.	138	433	1317	2130	2451	2648	2399	2071	1776	1435
	Min.	-184	-216	-511	-918	-1068	-1344	-1304	-1180	-983	-905
SG 26	Max.	72	92	216	308	380	400	426	426	426	426
	Min.	0	20	33	79	131	144	157	164	177	184
SG 27	Max.	52	0	282	1233	1692	2393	2393	2144	1646	1547
	Min.	-249	-348	-570	-800	-879	-977	-833	-695	-557	-393
SG 28	Max.	46	65	98	157	177	190	177	170	164	170
	Min.	-20	0	7	72	79	85	92	92	98	111

Cont. Table 4-17: Maximum and Minimum Measured Strain (micro strain) in the Reinforcement of FSKJ24

		Stage (1)	Stage (2)	Stage (3)	Stage (4)	Stage (5)	Stage (6)	Stage (7)	Stage (8)	Stage (9)	Stage (11)
Gauge		$0.15f_y$	$0.25f_y$	$0.5f_y$	$0.75f_y$	1 Δy	1.5 Δy	2 Δy	2.5 Δy	3 Δy	3.5 Δy
SG 29	Max.	269	505	760	1318	1547	1534	996	760	524	269
	Min.	-26	7	46	66	170	-13	-138	-787	-1114	-1134
SG 30	Max.	184	374	676	892	997	1515	1181	-52	-348	-708
	Min.	7	105	125	210	190	262	-131	-1358	-1528	-1541
SG 31	Max.	275	531	872	1180	1291	1645	1639	1272	1278	1285
	Min.	-46	13	33	98	105	20	-321	-642	-813	-603
SG 32	Max.	203	380	649	1167	1344	1580	1593	1868	1868	1809
	Min.	13	85	105	190	210	295	380	780	970	931
SG 33	Max.	66	72	72	72	72	85	79	85	79	98
	Min.	13	7	13	13	20	20	20	20	20	26
SG 34	Max.	98	295	702	1364	1469	1587	1272	997	872	931
	Min.	-39	-33	-26	26	138	72	66	20	157	125
SG 35	Max.	157	459	727	1035	1166	1101	786	314	151	52
	Min.	7	39	98	92	138	111	7	-203	-485	-701
SG 36	Max.	13	-66	52	39	282	662	1527	2006	2236	2498
	Min.	-138	-138	-151	-118	-72	-26	151	328	328	321
SG 37	Max.	52	85	105	223	374	479	748	859	938	997
	Min.	-13	7	33	66	197	334	394	492	531	551
SG 38	Max.	33	-20	72	236	300	472	516	613	613	613
	Min.	-105	-85	-79	-151	-203	-119	-195	-219	-115	-219
SG 39	Max.	39	72	118	334	741	1233	1593	1515	1502	1541
	Min.	-33	-7	20	79	223	413	597	774	623	315
SG 40	Max.	92	151	708	945	1174	1463	1561	1496	1712	1758
	Min.	7	46	66	112	125	66	105	-59	13	361
SG 41	Max.	33	111	308	813	832	1167	1062	1193	1114	1003
	Min.	-39	-13	20	85	203	269	66	216	118	79
SG 42	Max.	98	151	485	892	1088	1233	1410	1495	1548	1646
	Min.	20	52	85	328	374	387	479	485	557	570

Cont. Table 4-17: Maximum and Minimum Measured Strain (micro strain) in the Reinforcement of FSKJ24

		Stage (1)	Stage (2)	Stage (3)	Stage (4)	Stage (5)	Stage (6)	Stage (7)	Stage (8)	Stage (9)	Stage (11)
Gauge		$0.15f_y$	$0.25f_y$	$0.5f_y$	$0.75f_y$	1 Δy	1.5 Δy	2 Δy	2.5 Δy	3 Δy	3.5 Δy
SG 44	Max.	105	190	583	990	1180	1790	2157	3966	4425	4385
	Min.	13	59	79	72	79	170	275	557	1180	1652
SG 45	Max.	46	98	249	931	1246	1659	1580	1443	1207	702
	Min.	-66	-33	-39	20	223	-98	-393	-531	-531	164
SG 46	Max.	66	111	302	846	1062	1160	1134	1940	1934	2196
	Min.	-7	13	52	236	426	511	603	715	898	846
SG 47	Max.	20	98	511	1101	1278	1495	1278	1016	951	760
	Min.	-72	-66	-66	-52	39	-79	203	111	85	52
SG 50	Max.	105	223	374	439	498	701	872	878	583	210
	Min.	-13	59	131	269	321	328	301	295	170	52
SG 51	Max.	59	157	354	709	768	918	925	964	905	859
	Min.	-46	-20	-20	33	125	184	308	387	407	440
SG 52	Max.	118	256	715	1279	1574	1862	2164	2151	1908	1095
	Min.	-33	-52	-52	-92	33	-20	0	66	-184	-11441
SG 53	Max.	20	85	144	190	275	1684	12558	21754	16203	426
	Min.	-105	-98	-66	-33	0	7	105	269	-249	-138
SG 54	Max.	315	492	1127	1744	2124	2517	2746	4575	1593	3015
	Min.	-39	151	157	138	269	302	-1481	-15423	-15423	-596
SG 55	Max.	85	216	1096	1935	2526	3116	3326	2788	2362	2165
	Min.	-138	-171	-138	-138	-20	269	590	643	531	394
SG 56	Max.	92	321	806	1357	1619	1875	1980	2314	2354	2288
	Min.	-208	7	66	170	236	229	157	39	111	-190
SG 58	Max.	367	695	1167	1560	2241	2799	2740	2563	2418	2903
	Min.	-66	-39	-275	-465	-426	-603	-1029	-760	-308	1016
SG 60	Max.	505	806	1206	1678	1927	2111	1894	1652	1403	1167
	Min.	-20	111	-170	-426	-505	-649	-636	-551	-406	-321
SG 61	Max.	85	216	773	1193	1429	1770	2655	3218	3153	-21895
	Min.	-52	-79	-52	0	131	216	210	-21895	-21895	-21895

Cont. Table 4-17: Maximum and Minimum Measured Strain (micro strain) in the Reinforcement of FSKJ24

		Stage (1)	Stage (2)	Stage (3)	Stage (4)	Stage (5)	Stage (6)	Stage (7)	Stage (8)	Stage (9)	Stage (11)
Gauge		$0.15f_y$	$0.25f_y$	$0.5f_y$	$0.75f_y$	1 Δy	1.5 Δy	2 Δy	2.5 Δy	3 Δy	3.5 Δy
SG 63	Max.	59	170	767	1318	1534	1849	2026	1514	1718	1705
	Min.	-118	-144	-118	-33	236	203	190	-26	-275	-354
SG 64	Max.	59	216	997	1659	1961	2407	2807	6293	6293	-21929
	Min.	-85	-59	-13	79	492	571	597	-21929	-21929	-21929
SG 65	Max.	52	138	564	1102	1410	1810	1830	1758	1469	-21851
	Min.	-52	-39	-13	0	7	33	138	374	-21851	-21851
SG 66	Max.	85	302	721	1475	1757	2046	2079	2020	1849	1685
	Min.	-26	0	46	52	164	282	295	249	236	118
SG 67	Max.	282	636	1187	2800	3502	4892	7115	7837	6748	6689
	Min.	-98	-98	-321	-505	-780	-3561	-8427	-11253	-10584	-8440
SG 68	Max.	511	806	839	924	1311	2031	1566	1363	1238	1553
	Min.	92	7	-216	-413	-400	-203	-498	-131	177	406
SG 69	Max.	420	734	1187	1593	1763	1836	1639	1626	1416	1206
	Min.	-46	39	-243	-452	-511	-662	-1029	-1114	-819	-708
SG 70	Max.	164	427	703	1221	1576	2193	2685	3565	3421	3329
	Min.	-13	26	92	72	158	184	309	834	1267	1464
SG 71	Max.	289	551	879	1122	1371	1797	1764	1502	1397	1358
	Min.	-59	-33	-164	-315	-335	-302	-544	-879	-951	-1089
SG 72	Max.	236	518	806	1324	1501	1364	1495	1620	1862	2190
	Min.	-66	-59	-197	-315	-151	-275	-407	-26	498	1161
SG 73	Max.	111	400	918	1738	2118	2177	1777	1659	1738	1679
	Min.	-46	-20	26	138	243	223	249	334	367	374
SG 74	Max.	216	446	721	1199	1520	1671	1619	1494	1330	1212
	Min.	-59	-13	-79	-131	-72	-7	-72	-269	-387	-498
SG 75	Max.	216	419	701	1494	1848	2340	2556	2766	3054	2995
	Min.	20	46	66	72	131	203	341	629	845	1166

Table 4-18: Maximum and Minimum Measured Displacements (inches) of FSKJ24

		Stage (1)	Stage (2)	Stage (3)	Stage (4)	Stage (5)	Stage (6)	Stage (7)	Stage (8)	Stage (9)	Stage (11)
Gauge		$0.15f_y$	$0.25f_y$	$0.5f_y$	$0.75f_y$	1 Δy	1.5 Δy	2 Δy	2.5 Δy	3 Δy	3.5 Δy
DTD 1	Max.	0.001	0.002	0.008	0.030	0.053	0.117	0.155	0.209	0.227	0.281
	Min.	-0.005	-0.009	-0.020	-0.065	-0.097	-0.217	-0.347	-0.539	-0.626	-0.629
DTD 2	Max.	0.006	0.015	0.039	0.115	0.149	0.251	0.368	0.517	0.517	0.496
	Min.	-0.006	-0.008	-0.021	-0.042	-0.065	-0.164	-0.332	-0.544	-0.757	-0.848
DTD3	Max.	0.001	0.001	0.006	0.015	0.018	0.025	0.024	0.021	0.015	0.012
	Min.	-0.002	-0.004	-0.009	-0.013	-0.015	-0.018	-0.018	-0.015	-0.014	-0.012
DTD 4	Max.	0.001	0.001	0.009	0.019	0.022	0.026	0.023	0.021	0.017	0.014
	Min.	-0.001	-0.001	-0.003	-0.008	-0.009	-0.013	-0.013	-0.012	-0.009	-0.009
DTD 5	Max.	0.001	0.000	0.003	0.014	0.018	0.026	0.025	0.023	0.017	0.015
	Min.	-0.002	-0.006	-0.009	-0.013	-0.014	-0.016	-0.014	-0.013	-0.011	-0.009
DTD 6	Max.	0.002	0.009	0.016	0.022	0.025	0.029	0.025	0.022	0.019	0.015
	Min.	-0.002	-0.003	-0.006	-0.013	-0.015	-0.020	-0.020	-0.017	-0.014	-0.013
DTD 7	Max.	0.001	0.000	0.002	0.009	0.012	0.017	0.016	0.014	0.010	0.009
	Min.	-0.002	-0.005	-0.009	-0.013	-0.015	-0.015	-0.015	-0.014	-0.011	-0.010
DTD 8	Max.	-0.001	0.000	0.007	0.016	0.019	0.021	0.019	0.017	0.014	0.012
	Min.	-0.003	-0.004	-0.004	-0.008	-0.010	-0.014	-0.014	-0.011	-0.009	-0.008
DTD 9	Max.	-0.001	-0.003	-0.001	0.003	0.002	0.010	0.008	-0.030	-0.090	-0.218
	Min.	-0.005	-0.008	-0.012	-0.022	-0.031	-0.060	-0.097	-0.215	-0.378	-0.478
DTD 10	Max.	0.000	0.000	0.003	0.013	0.021	0.047	0.051	0.024	-0.051	-0.153
	Min.	-0.004	-0.005	-0.009	-0.012	-0.018	-0.034	-0.083	-0.198	-0.317	-0.387
DTD 11	Max.	-0.002	0.000	0.000	0.002	0.005	0.003	-0.012	0.212	1.245	1.245
	Min.	-0.004	-0.003	-0.001	-0.008	-0.020	-0.074	-0.107	-0.064	0.051	1.243
DTD 12	Max.	0.000	0.004	0.011	0.029	0.036	0.047	0.059	0.077	0.124	0.200
	Min.	-0.003	0.000	0.001	0.002	0.008	0.012	0.016	0.030	0.044	0.080
DTD 13	Max.	0.001	0.001	0.005	0.009	0.015	0.022	0.034	0.066	0.134	0.149
	Min.	-0.001	-0.002	-0.003	-0.003	-0.001	0.001	0.012	0.001	0.001	0.060
DTD 14	Max.	-0.004	0.000	0.003	0.026	0.032	0.046	0.085	0.224	0.316	0.317
	Min.	-0.006	-0.005	-0.001	0.002	0.010	0.012	0.010	0.022	0.034	0.134
DTD 15	Max.	0.002	0.004	0.004	0.004	0.004	0.009	0.074	0.111	0.113	0.114
	Min.	0.001	0.001	0.003	-0.002	-0.002	-0.001	0.006	0.065	0.072	0.073

Table 5-1: Strut-and-Tie Model Coordinates for FSRCC24

Node	Coordinates		Node	Coordinates	
	x (in)	Z (in)		x (in)	Z (in)
A	20.75	16.04	O	-47.23	15.58
B	20.75	1.91	Q	30	16.04
C	4.31	15.58	R	30	1.91
D	4.31	10.92	T	48.45	1.91
E	4.31	6.75	U	48.45	16.04
F	4.31	0	V	48	17.5
G	-5.17	6.75	W	-6.94	0
H	-7.08	1.91	X	-48	17.5
I	-20.75	15.58	Y	-30	17.5
J	-20.75	1.11	Z	30	17.5
K	-30	1.11	L	-30	15.58

Table 5-2: Strut-and-Tie Model Forces for FSRCC24

Strut (kips)		Tie (kips)	
C_{OK}	114.7	T_{OL}	67.6
C_{KJ}	89.4	T_{LK}	71.9
C_{LJ}	127.1	T_{IJ}	116.4
C_{JH}	158.1	T_{LI}	136.0
C_{HW}	579.8	T_{IC}	341.4
C_{HE}	287.1	T_{CD}	318.0
C_{IG}	236.0	T_{DE}	329.4
C_{GD}	101.1	T_{EG}	40.8
C_{HG}	511.0	T_{HB}	325.8
C_{GC}	466.5	T_{AB}	65.8
C_{DA}	97.1	T_{QR}	36.5
C_{EB}	233.0	T_{BR}	114.5
C_{AR}	43.5	T_{RT}	90.8
C_{AQ}	68.8	T_{QU}	21.9
C_{QT}	115.7	T_{UT}	71.7

Table 5-3: Factored Strut-and-Tie Model Forces for FSRCC24

Strut (kips)		Tie (kips)	
1.2 $(Mu)_P$			
C_{OK}	137.64	T_{OL}	81.12
C_{KJ}	107.28	T_{LK}	86.28
C_{LJ}	152.52	T_{IJ}	139.68
C_{JH}	189.72	T_{LI}	163.2
C_{HW}	695.76	T_{IC}	409.68
C_{HE}	344.52	T_{CD}	381.6
C_{IG}	283.2	T_{DE}	395.28
C_{GD}	121.32	T_{EG}	48.96
C_{HG}	613.2	T_{HB}	390.96
C_{GC}	559.8	T_{AB}	78.96
C_{DA}	116.52	T_{QR}	43.8
C_{EB}	279.6	T_{BR}	137.4
C_{AR}	52.2	T_{RT}	108.96
C_{AQ}	82.56	T_{QU}	26.28
C_{QT}	138.84	T_{UT}	86.04

Table 5-4: Strut-and-Tie Model Coordinates for DCKJ24, Closing Moment Case and Opening Moment Case

Closing Moment		
Node	Coordinates	
	x (in)	Z (in)
A	16	14.03
B	16	1.40
C	-2.78	14.03
D	-2.78	11.25
E	-2.78	6.16
F	-2.78	0
G	5.31	11.25
H	5.31	1.75
I	0	14.03
J	29	1.40
K	29	1.75
L	42	14.03
M	42	1.40
N	-15	1.75
O	-15	14.03
W	5.16	0
X	-9.8	6.16
Y	-8	1.75

Opening Moment		
Node	Coordinates	
	x (in)	Z (in)
A	16	14.6
B	16	1.93
C	2.49	14.6
D	2.49	11.05
F	2.49	0
G	-5.33	11.05
H	-5.33	1.925
I	0	14.6
J	29	1.925
K	29	14.6
L	42	14.6
M	42	1.925
W	5.18	0
X	8.59	14.6
Y	9.89	11.05

Table 5-5: Strut-and-Tie Model Forces for DCKJ24 in the Closing Moment Case and Opening Moment Case

Closing Moment			
Strut (kips)		Tie (kips)	
C_{OD}	190.5	T_{OC}	185.2
C_{DI}	83.5	T_{CI}	258.4
C_{DH}	241	T_{IA}	201.2
C_{EH}	145.6	T_{AK}	162.5
C_{EX}	72.3	T_{KL}	162.5
C_{AG}	40.3	$T_{LM}= T_{KJ}$	0
C_{HW}	272.5	T_{AB}	11.3
$C_{HB}= C_{BJ}$	183.6	T_{ON}	44.7
C_{KB}	0	T_{CD}	26.7
C_{JM}	183.6	T_{DE}	99.2
$C_{GL}= C_{LJ}$	0	T_{EF}	211.4
C_{CG}	78.0	$T_{NH}=T_{YH}$	129
C_{HG}	38	T_{DG}	34.6
C_{XN}	72.3	T_{NY}	54.9
C_{EY}	72.3	T_{XY}	47.4

Opening Moment			
Strut (kips)		Tie (kips)	
C_{DH}	248.1	T_{DG}	74.9
C_{HW}	227.7	T_{CD}	36
C_{GH}	41.6	T_{DF}	221.4
C_{GC}	76.8	T_{HB}	182.4
C_{GI}	9.1	T_{AB}	18.6
C_{IC}	7.2	T_{BJ}	153.2
C_{DB}	34.7	T_{JM}	153.2
C_{DX}	33.4	T_{KJ}	0
C_{DY}	33.4	T_{XY}	19.3
C_{YA}	33.4		
C_{XA}	108.3		
C_{CX}	74.9		
C_{AK}	135.7		
C_{AJ}	0		
C_{KM}	0		
C_{KL}	135.7		

Table 5-6: Strut-and-Tie Model Coordinates for FSKJ24, Closing Moment Case and Opening Moment Case

Closing Moment		
Node	Coordinates	
	x (in)	Z (in)
A	12.84	8.17
B	12.84	1.22
C	-2.69	8.17
D	-2.69	6
E	-2.69	3.75
F	-2.69	0
G	5.13	6
H	5.13	1.5
I	0	8.17
J	27.42	1.22
K	27.42	8.17
L	42	8.17
M	42	1.22
N	-15	1.5
O	-15	8.17
W	5.09	0
X	-9.05	3.75
Y	-8.64	1.5

Opening Moment		
Node	Coordinates	
	x (in)	Z (in)
A	12.84	8.54
B	12.84	1.75
C	3.16	8.54
D	3.16	5.71
F	3.16	0
G	-6.14	5.71
H	-6.14	1.75
I	0	8.54
J	27.42	1.75
K	27.42	8.54
L	42	8.54
M	42	1.75
W	-5.99	0
X	7.65	8.54
Y	8.38	5.71

Table 5-7: Strut-and-Tie Model Forces for FSKJ24 in the Closing Moment Case and Opening Moment Case

Closing Moment			
Strut (kips)		Tie (kips)	
C_{OD}	331.7	T_{CO}	326.7
C_{DI}	103.3	T_{CI}	419.6
C_{DH}	321.1	T_{IA}	339.3
C_{EH}	347	T_{XY}	58.5
C_{GA}	73.6	T_{AK}	268.5
C_{NX}	182.5	T_{KL}	268.5
C_{XE}	182.5	$T_{LM}= T_{KJ}$	0
C_{YE}	182.5	T_{AB}	20.1
C_{HW}	252.6	T_{ON}	57.7
C_{HB}	287.7	T_{CD}	25.6
C_{BJ}	286.7	T_{DE}	39.1
C_{KB}	0	T_{EF}	187
C_{JM}	286.7	T_{NY}	173.1
C_{JL}	0	T_{YH}	355.8
C_{CG}	96.4	T_{XY}	58.5
C_{HG}	45.8	T_{DG}	22.2

Opening Moment			
Strut (kips)		Tie (kips)	
C_{DH}	348.9	T_{GD}	23.86
C_{HW}	140.7	T_{CD}	5.8
C_{GH}	7.8	T_{DF}	139.1
C_{GC}	20.2	T_{HB}	333.8
C_{GI}	4.9	T_{AB}	50.8
C_{IC}	4.5	$T_{KJ}= T_{LM}$	0
C_{DB}	134.1	T_{JM}	209.4
C_{DX}	93.8	T_{BJ}	209.4
C_{DY}	93.8	T_{XY}	50.8
C_{YA}	93.8		
C_{XA}	117.6		
C_{AK}	195.9		
C_{KL}	195.9		
C_{CX}	23.9		
$C_{KB}= C_{LJ}$	0		

Table 5-8: Strut-and-Tie Model Coordinates for Modified FSKJ24 in the Closing Moment Case and Opening Moment Case

Closing Moment		
Node	Coordinates	
	x (in)	Z (in)
A	16.25	9.06
B	16.25	1.22
C	-2.21	9.06
D	-2.21	6.23
E	-2.21	3.91
F	-2.21	0
G	5.25	6.23
H	5.25	1.58
I	8	9.06
J	29.13	1.22
K	29.13	9.06
L	42	9.06
M	42	1.22
N	-15	1.58
O	-15	9.06
P	-8	9.06
W	5.10	0
X	-8.74	3.91
Y	-8.37	1.58

Opening Moment		
Node	Coordinates	
	x (in)	Z (in)
A	16.25	9.66
B	16.25	1.75
C	2.27	9.66
D	2.27	6.52
F	2.27	0
G	-5.24	6.52
H	-5.24	1.75
I	-8	9.66
J	29.13	1.75
K	29.13	9.66
L	42	9.66
M	42	1.75
W	-5.14	0
X	8	9.66
Y	9.12	6.52

Table 5-9: Strut-and-Tie Model Factored Forces for Modified FSKJ24 in the Closing Moment Case and Opening Moment Case

Closing Moment			
Strut (kips)		Tie (kips)	
C_{OD}	228.9	T_{CP}	300.8
C_{DP}	86	T_{CI}	404.7
C_{DH}	380.6	T_{IA}	367.9
C_{EH}	285.1	T_{XY}	50.1
C_{GI}	52.7	T_{AK}	323
C_{AG}	47.1	T_{KL}	323
C_{NX}	141.1	T_{LM}	0
C_{XE}	141.1	T_{KJ}	0
C_{YE}	141.1	T_{AB}	14
C_{HW}	365	T_{ON}	49.5
C_{HB}	349.8	T_{CD}	39.5
C_{BJ}	349.3	T_{DE}	153.6
C_{KB}	0	T_{EF}	288
C_{JM}	349.3	T_{NY}	133.2
C_{JL}	0	T_{YH}	272.1
C_{CG}	111.1	T_{DG}	22.17
C_{HG}	91.3	T_{OP}	223.5

Opening Moment			
Strut (kips)		Tie (kips)	
C_{DH}	579	T_{GD}	22.17
C_{GH}	9.1	T_{CD}	9
C_{GC}	24	T_{DF}	313.6
C_{HI}	2.7	T_{HB}	522
C_{DX}	152.2	T_{AB}	72.8
C_{DY}	152.2	T_{KJ}= T_{LM}	0
C_{YA}	152.2	T_{JM}	331.9
C_{XA}	176.6	T_{BJ}	331.9
C_{CX}	21.5	T_{XY}	73.1
C_{DB}	198.4	T_{CI}	0.9
C_{AK}	305.5		
C_{AJ}	0		
C_{KM}	0		
C_{KL}	305.5		
C_{HW}	320		

Table 6-1: Maximum and Minimum Measured Force and Displacement of FSRCC24-M

Stage	Ductility	String Pot Displacement at Max. and Min. Force (in)		Actuator Displacement at Max. and Min. Force (in)		Actuator Force (kips)	
Number	Level	Max.	Min.	Max.	Min.	Max.	Min.
Stage (2)	0.10fy	0.14	-0.11	0.08	-0.12	3.12	-3.1
Stage (3)	0.15fy	0.13	-0.14	0.12	-0.13	4.02	-3.19
Stage (4)	0.25fy	0.25	-0.25	0.22	-0.26	6.64	-9.56
Stage (5)	0.5fy	0.99	-0.88	0.88	-0.98	13.28	-19.37
Stage (6)	0.75fy	1.97	-1.28	1.29	-1.96	19.93	-28.97
Stage (7)	1 Δy	2.84	-2.83	2.77	-2.82	31.85	-40.05
Stage (8)	2 Δy	5.58	-5.44	5.56	-5.43	41.55	-44.12
Stage (9)	2.5 Δy	6.92	-6.91	6.79	-6.93	41.85	-44.55
Stage (10)	3 Δy	8.34	-8.24	8.32	-8.24	41.92	-44.68
Stage (11)	3.5 Δy	9.73	-9.76	9.71	-9.76	42.96	-42.89
Stage (12)	4 Δy	11.01	-10.65	10.55	-10.96	42	-41.81
Stage (13)	5 Δy	13.83	-13.02	12.81	-13.82	42.81	-41.18
Stage (14)	6 Δy	16.64	-16.59	16.67	-16.58	27.52	-25.16

Table 6-2: Maximum and Minimum Measured Strain (micro strain) in the Reinforcement of FSRCC24-M

		Stage (2)	Stage (3)	Stage (4)	Stage (5)	Stage (6)	Stage (7)	Stage (8)	Stage (9)	Stage (10)	Stage (11)	Stage (12)	Stage (13)	Stage (14)
Gauge		0.10fy	0.15fy	0.25fy	0.5fy	0.75fy	1Δy	2Δy	2.5Δy	3Δy	3.5Δy	4Δy	5Δy	6Δy
SG1	Max.	-21	0	0	14	35	48	104	138	166	193	269	366	373
	Min.	-55	-62	-55	-55	-48	-48	-55	-35	-21	-7	28	90	145
SG2	Max.	-26	20	33	39	52	72	105	170	203	209	216	314	340
	Min.	-59	-72	-59	-78	-85	-85	-72	-20	-33	-33	-26	-26	0
SG3	Max.	-62	-28	-21	110	283	407	863	987	1167	1208	904	1200	1484
	Min.	-97	-124	-131	-179	-179	-173	-290	-55	-7	-145	-179	-231	48
SG4	Max.	-20	13	26	26	33	39	118	157	170	170	242	340	517
	Min.	-52	-65	-59	-85	-78	-98	-65	-20	-7	0	20	0	-7
SG5	Max.	-41	-21	-7	-14	-14	-14	83	55	62	62	104	186	186
	Min.	-76	-76	-76	-90	-69	-69	-62	0	-28	-21	0	21	55
SG6	Max.	-7	20	20	26	20	26	72	131	209	360	425	582	517
	Min.	-52	-72	-52	-59	-59	-46	-33	7	65	137	222	275	170
SG7	Max.	-7	20	33	46	111	144	248	262	275	320	412	510	523
	Min.	-46	-59	-39	-59	-13	-7	20	26	26	59	131	229	262
SG8	Max.	-13	7	7	7	7	26	144	242	288	333	359	392	379
	Min.	-52	-59	-59	-65	-65	-46	-26	7	46	65	91	111	163
SG9	Max.	-28	0	7	0	69	186	386	593	697	759	1001	1049	-2305
	Min.	-55	-69	-48	-62	-35	-14	-14	0	-55	-48	-35	-2305	-2305
SG10	Max.	-39	0	26	59	118	157	281	334	373	406	425	523	589
	Min.	-92	-124	-111	-177	-190	-170	-39	-20	-13	-13	-7	-13	-46
SG12	Max.	-69	-41	-28	55	173	283	442	49124	38928	752	939	1325	1470
	Min.	-104	-152	-159	-235	-338	-407	-690	-1132	-808	-739	-469	-159	76
SG13	Max.	-59	0	33	92	144	177	301	386	425	550	759	1407	1740
	Min.	-92	-124	-131	-177	-124	-65	-72	-20	0	13	13	39	412
SG14	Max.	-41	-21	-14	-21	41	159	331	580	849	1132	1415	1746	1594
	Min.	-69	-76	-83	-90	-76	-48	-48	-55	-69	-83	-124	-138	-139

Cont.Table 6-2: Maximum and Minimum Measured Strain (micro strain) in the Reinforcement of FSRCC24-M

		Stage (2)	Stage (3)	Stage (4)	Stage (5)	Stage (6)	Stage (7)	Stage (8)	Stage (9)	Stage (10)	Stage (11)	Stage (12)	Stage (13)	Stage (14)
Gauge		0.10fy	0.15fy	0.25fy	0.5fy	0.75fy	1Δy	2Δy	2.5Δy	3Δy	3.5Δy	4Δy	5Δy	6Δy
SG15	Max.	-20	98	124	52	163	242	268	340	543	621	628	510	-105
	Min.	-65	-111	-268	-216	-163	-288	-268	-262	-183	-196	-399	-857	-1230
SG16	Max.	0	20	20	33	33	46	72	445	746	870	968	1047	975
	Min.	-33	-39	-33	-46	-39	-39	-33	-7	7	-7	7	26	85
SG17	Max.	-28	-14	-7	-7	0	7	76	104	110	138	179	380	400
	Min.	-62	-76	-76	-83	-69	-76	-62	-48	-28	-35	-21	-41	48
SG18	Max.	-16	8	24	16	24	251	730	863	941	1036	1169	1286	1036
	Min.	-55	-86	-62	-86	-62	-47	-8	-47	-71	-62	-40	-55	-62
SG19	Max.	0	33	78	78	399	582	1027	1210	1288	1497	1576	1589	-2191
	Min.	-52	-150	-347	-288	-170	-262	-65	98	163	111	92	-2191	-2191
SG20	Max.	-13	39	46	92	144	183	490	628	641	569	163	-248	-1105
	Min.	-46	-65	-52	-78	-78	-105	-72	-20	-52	-301	-817	-1745	-2249
SG21	Max.	124	338	41	117	442	462	1415	1015	1491	987	1215	1415	1684
	Min.	97	-28	-35	-48	-41	7	-166	-311	-290	-683	-732	-856	-2133
SG22	Max.	-21	-14	0	41	131	304	580	724	807	876	718	980	987
	Min.	-62	-62	-69	-69	-48	-41	-55	-76	-152	-1663	-747	-230	-230
SG23	Max.	13	65	72	111	229	320	445	458	412	444	401	411	300
	Min.	-33	-46	-52	-65	-92	-124	-209	-248	-347	-200	-210	-351	-274
SG24	Max.	-28	-21	-7	-14	-14	28	1201	1346	1429	1277	1346	1539	1615
	Min.	-69	-69	-76	-90	-83	-76	-35	856	663	670	697	732	808
SG25	Max.	-13	20	26	46	144	216	471	661	922	1138	1288	1491	6141
	Min.	-65	-92	-98	-144	-183	-190	-131	0	46	105	118	-33	-2193
SG26	Max.	-72	-26	-7	131	320	399	595	719	863	987	1196	1967	2837
	Min.	-105	-131	-137	-150	-137	-118	-92	-124	-314	-569	-876	-1935	-2797
SG27	Max.	-46	-26	-26	-46	7	7	72	379	732	870	1099	1393	1903
	Min.	-78	-105	-111	-118	-124	-124	-124	-111	-20	65	98	72	-59
SG28	Max.	-46	-13	20	111	451	589	948	1138	1236	1328	1504	2380	3865
	Min.	-78	-118	-118	-163	-105	-98	-190	-334	-706	-1583	-2387	-4892	-7965

Cont.Table 6-2: Maximum and Minimum Measured Strain (micro strain) in the Reinforcement of FSRCC24-M

		Stage (2)	Stage (3)	Stage (4)	Stage (5)	Stage (6)	Stage (7)	Stage (8)	Stage (9)	Stage (10)	Stage (11)	Stage (12)	Stage (13)	Stage (14)
Gauge		0.10fy	0.15fy	0.25fy	0.5fy	0.75fy	1Δy	2Δy	2.5Δy	3Δy	3.5Δy	4Δy	5Δy	6Δy
SG30	Max.	-7	20	33	59	183	261	477	529	575	568	464	464	26
	Min.	-46	-59	-46	-72	-65	-52	-65	-59	-26	-46	-131	-542	-1358
SG31	Max.	7	33	33	39	46	196	621	752	902	1059	1301	1713	1164
	Min.	-26	-33	-39	-39	-33	-13	39	105	163	255	268	229	190
SG32	Max.	-72	-40	65	91	366	294	1327	1327	1098	1235	1549	1856	1039
	Min.	-112	-125	-112	-105	-92	-46	-53	78	97	12	-66	-177	-197
SG33	Max.	39	98	131	209	464	582	1085	1353	1517	1713	2007	3158	4426
	Min.	0	-33	-20	-59	-13	13	78	222	288	386	445	798	1582
SG34	Max.	-41	-28	-21	0	14	48	117	152	304	407	476	518	932
	Min.	-76	-83	-83	-110	-173	-200	-221	-131	-117	7	21	0	-421
SG35	Max.	-26	-7	7	13	33	39	131	33	111	111	-39	-307	-948
	Min.	-59	-85	-59	-92	-137	-268	-229	-229	-242	-451	-928	-1746	-21875
SG36	Max.	85	203	229	392	654	791	1170	1405	1608	1791	1980	2608	2850
	Min.	59	26	26	-33	20	59	222	386	464	542	686	948	745
SG37	Max.	0	20	26	33	52	78	216	333	418	543	713	811	628
	Min.	-46	-59	-46	-46	-46	-39	-46	-7	59	85	111	105	85
SG38	Max.	-7	46	65	346	732	902	1235	1405	1516	1686	1744	1477	653
	Min.	-39	-72	-65	-98	-170	-170	-196	-163	-78	-65	-137	-399	-673
SG39	Max.	-72	-33	-7	105	419	582	739	830	902	1046	1269	2073	2576
	Min.	-124	-150	-150	-209	-203	-177	-163	-118	-118	-262	-615	-3359	-8189
SG40	Max.	-39	7	13	7	46	105	359	503	640	765	876	1255	1470
	Min.	-72	-111	-111	-137	-131	-124	-65	-7	-20	-20	-78	-320	-843
SG41	Max.	-59	-7	0	177	451	667	1014	1282	1609	1975	2432	3171	5597
	Min.	-118	-131	-124	-131	-144	-144	-203	-170	-177	-294	-693	-2308	-3969
SG42	Max.	-26	-13	0	46	137	183	595	634	700	732	726	686	673
	Min.	-65	-78	-65	-78	-72	-65	-46	59	131	183	170	144	-59
SG43	Max.	7	157	216	170	471	588	1000	1072	1471	1608	1685	2097	2097
	Min.	-33	-59	-52	-111	-111	-26	-20	-52	281	307	-2186	-2186	-2186

Cont.Table 6-2: Maximum and Minimum Measured Strain (micro strain) in the Reinforcement of FSRCC24-M

		Stage (2)	Stage (3)	Stage (4)	Stage (5)	Stage (6)	Stage (7)	Stage (8)	Stage (9)	Stage (10)	Stage (11)	Stage (12)	Stage (13)	Stage (14)
Gauge		0.10fy	0.15fy	0.25fy	0.5fy	0.75fy	1Δy	2Δy	2.5Δy	3Δy	3.5Δy	4Δy	5Δy	6Δy
SG45	Max.	-20	33	59	203	294	431	909	1170	1255	1275	1170	1072	7023
	Min.	-59	-150	-203	-294	-360	-320	-301	-353	-346	-281	-170	-78	-2181
SG46	Max.	59	118	123	216	334	500	815	972	1168	1370	1546	2105	2336
	Min.	20	0	-5	-59	-39	10	-25	98	216	334	437	565	996
SG47	Max.	-26	7	13	46	98	183	307	320	399	601	837	994	2680
	Min.	-65	-65	-65	-72	-52	-72	-59	20	92	150	209	235	366
SG49	Max.	29	64	83	172	314	520	967	1172	1349	1580	1830	2228	3444
	Min.	0	-35	-44	-83	-44	10	59	240	280	305	358	486	761
SG50	Max.	-13	7	20	13	13	33	46	85	170	259	316	496	409
	Min.	-65	-65	-52	-65	-52	-59	-152	-152	-139	-227	-227	-227	-320
SG51	Max.	-26	13	39	111	386	471	601	556	314	346	510	2568	20934
	Min.	-78	-98	-137	-124	-131	-235	-281	-373	-530	-543	-497	-503	-2190
SG52	Max.	-82	-15	-15	42	27	54	232	397	5031	8596	10195	1453	1582
	Min.	-178	-232	-259	-341	-479	-479	-560	-355	-274	-109	-82	0	261
SG53	Max.	-59	7	0	131	431	634	1267	1385	1574	1646	1633	1644	1654
	Min.	-118	-150	-150	-150	-163	-157	-131	124	235	307	372	-745	-1163
SG54	Max.	-52	0	7	92	216	262	432	517	595	634	687	1007	1210
	Min.	-85	-111	-124	-150	-216	-255	-307	-301	-229	-124	-59	20	59
SG55	Max.	-39	0	0	26	72	124	307	379	406	393	386	759	1341
	Min.	-79	-118	-118	-124	-105	-65	-26	-33	-65	-72	-52	-20	353
SG56	Max.	-26	7	20	78	314	464	621	555	601	699	797	11819	2711
	Min.	-65	-91	-137	-137	-111	-118	-111	-59	-33	-26	-13	-21767	-21767
SG58	Max.	-35	-14	7	7	14	62	145	228	324	497	828	1359	1387
	Min.	-62	-62	-62	-76	-76	-48	-28	-7	7	62	186	338	690
SG59	Max.	-20	13	7	13	20	13	190	294	373	484	601	660	562
	Min.	-78	-78	-59	-65	-72	-65	-46	0	20	65	118	157	268
SG63	Max.	-39	-7	0	26	98	170	288	327	373	379	353	327	281
	Min.	-72	-85	-85	-85	-59	-59	-7	0	-52	-52	-52	-150	-98

Cont.Table 6-2: Maximum and Minimum Measured Strain (micro strain) in the Reinforcement of FSRCC24-M

		Stage (2)	Stage (3)	Stage (4)	Stage (5)	Stage (6)	Stage (7)	Stage (8)	Stage (9)	Stage (10)	Stage (11)	Stage (12)	Stage (13)	Stage (14)
Gauge		0.10fy	0.15fy	0.25fy	0.5fy	0.75fy	1Δy	2Δy	2.5Δy	3Δy	3.5Δy	4Δy	5Δy	6Δy
SG64	Max.	0	33	52	65	124	124	124	190	203	268	379	608	935
	Min.	-39	-46	-33	-39	-26	-26	-33	-65	-52	-46	-33	39	-20
SG66	Max.	-13	7	20	7	0	0	0	26	72	105	137	216	242
	Min.	-46	-72	-59	-72	-65	-78	-65	-65	-39	-26	0	33	65
SG67	Max.	-13	13	20	20	20	20	72	72	78	111	353	412	39
	Min.	-46	-65	-65	-72	-85	-78	-92	-72	-92	-46	0	-268	-451
SG68	Max.	-39	0	20	72	170	235	412	484	562	621	713	1040	1184
	Min.	-72	-98	-92	-131	-163	-190	-229	-242	-203	-157	-111	-26	72
SG69	Max.	-26	0	0	7	13	20	124	176	209	242	307	412	641
	Min.	-59	-85	-72	-78	-78	-72	-65	-39	-59	-33	-26	-20	72
SG70	Max.	-33	7	7	26	26	20	72	124	157	183	216	229	209
	Min.	-59	-72	-59	-65	-52	-59	-52	-33	-7	0	26	46	65
SG71	Max.	-26	0	13	7	20	13	26	46	59	98	163	346	301
	Min.	-65	-78	-72	-85	-78	-78	-72	-59	-46	-13	33	118	150
SG73	Max.	-69	145	269	1340	2307	2507	8494	11463	13715	15842	17382	18404	12506
	Min.	-104	-331	-311	-635	-939	-1264	-1540	-1457	-1305	-877	-622	-228	1015
SG74	Max.	-21	7	21	55	76	83	152	255	352	400	393	386	172
	Min.	-62	-69	-69	-69	-28	-21	-14	14	21	-14	-117	-172	-172
SG75	Max.	21	62	83	138	200	242	428	601	518	566	656	704	552
	Min.	-21	-55	-35	-41	-55	0	-14	-35	-55	-41	35	76	124
SG76	Max.	-69	456	442	1229	1975	5019	10232	12696	14270	15451	16031	16425	9175
	Min.	-104	-394	-463	-904	-1284	-1402	-2044	-1533	-1519	-1505	-1070	-987	145
SG77	Max.	-83	145	276	1242	2098	2291	2705	10228	12954	15970	19566	22679	14811
	Min.	-110	-373	-345	-676	-1035	-1408	-2215	-2761	-2209	-2209	-1677	-732	1746
SG80	Max.	-48	255	276	1042	1995	2250	10132	13175	16247	18055	18648	20056	11581
	Min.	-83	-262	-338	-780	-1194	-1491	-2146	-38325	-72703	-75036	-11619	-317	2050
SG81	Max.	-55	269	490	1456	2209	2291	10201	12417	14688	17186	19947	22508	14467
	Min.	-90	-317	-317	-656	-966	-1332	-1732	-1684	-2147	-1988	-1311	-676	2064
SG82	Max.	-21	28	55	97	173	207	407	628	952	1187	1442	1705	1304
	Min.	-55	-69	-69	-83	-35	-14	-7	131	200	173	186	228	200

Cont.Table 6-2: Maximum and Minimum Measured Strain (micro strain) in the Reinforcement of FSRCC24-M

		Stage (2)	Stage (3)	Stage (4)	Stage (5)	Stage (6)	Stage (7)	Stage (8)	Stage (9)	Stage (10)	Stage (11)	Stage (12)	Stage (13)	Stage (14)
Gauge		0.10fy	0.15fy	0.25fy	0.5fy	0.75fy	1Δy	2Δy	2.5Δy	3Δy	3.5Δy	4Δy	5Δy	6Δy
SG83	Max.	-48	387	407	1402	2168	7347	13264	16682	18878	20652	21598	23000	13319
	Min.	-90	-311	-387	-856	-1291	-1450	-2389	-1775	-1485	-1809	-3238	-3294	1498
SG84	Max.	0	48	69	110	324	380	884	739	863	953	1070	1187	794
	Min.	-35	-55	-28	-28	0	14	21	21	28	28	21	35	117
SG85	Max.	-65	177	275	1144	2420	2734	16081	20031	23837	28225	32823	38924	26420
	Min.	-98	-386	-353	-706	-1105	-1570	-1746	-687	-3773	-2799	-909	1995	11719
SG86	Max.	-138	752	711	1829	3154	16259	25886	33532	42020	50667	218516	-23375	-23375
	Min.	-173	-607	-711	-1353	-2036	-2298	-5355	428	5107	6908	-23375	-23375	-23375
SG87	Max.	-13	13	26	33	72	150	438	628	824	981	1053	1040	981
	Min.	-46	-59	-59	-72	-46	-26	46	118	170	209	236	137	157
SG88	Max.	13	7	26	26	33	46	111	183	504	543	660	791	802
	Min.	-52	-65	-46	52	72	72	52	33	13	7	-26	39	105
SG89	Max.	-52	242	262	1040	2002	2623	15740	19017	23917	28176	31793	36981	23642
	Min.	-98	-327	-406	-864	-1321	-1688	-2702	-1223	-52	-667	-2205	-20	12632
SG90	Max.	-13	7	26	26	33	46	111	183	504	543	660	791	902
	Min.	-52	-65	-46	-52	-72	-72	-52	-33	-13	-7	26	39	105
SG91	Max.	-52	497	739	1838	3088	5646	19397	23394	27633	76195	92066	209312	209312
	Min.	-85	-340	-353	-752	-975	-543	1197	3134	1596	347	10042	-21941	-21941
SG92	Max.	-35	-21	7	21	97	152	345	380	559	801	918	856	1029
	Min.	-76	-97	-110	-124	-97	-76	-90	-83	-83	-55	-28	-145	-276
SG93	Max.	-59	20	39	300	784	1104	2201	3846	5081	6380	7360	9175	11605
	Min.	-98	-118	-111	-118	-91	-104	-98	333	1770	2978	4166	5081	7118
SG94	Max.	-46	20	79	124	196	170	216	59	196	314	1335	1505	1401
	Min.	-79	-98	-72	-72	-65	-65	-85	-124	-589	-563	-190	-13	13
SG95	Max.	-65	327	530	1903	3988	8408	24172	30149	15123	-1321	6100	21038	-21810
	Min.	-98	-405	-392	-804	-1020	275	2557	4982	-16673	-28795	-11775	-21810	-21810
SG96	Max.	-26	65	157	817	1621	2046	9335	13257	16552	19696	21403	24037	25024
	Min.	-72	-98	-78	-98	-111	-92	-46	5465	8943	11760	13911	14885	14558

Cont.Table 6-2: Maximum and Minimum Measured Strain (micro strain) in the Reinforcement of FSRCC24-M

		Stage (2)	Stage (3)	Stage (4)	Stage (5)	Stage (6)	Stage (7)	Stage (8)	Stage (9)	Stage (10)	Stage (11)	Stage (12)	Stage (13)	Stage (14)
Gauge		0.10fy	0.15fy	0.25fy	0.5fy	0.75fy	1Δy	2Δy	2.5Δy	3Δy	3.5Δy	4Δy	5Δy	6Δy
SG97	Max.	-33	-7	-7	33	164	314	707	1132	1348	1571	2022	1420	1080
	Min.	-65	-79	-92	-72	-46	-52	-144	-151	-170	-177	-79	-14805	-10138
SG98	Max.	-52	-26	-13	52	92	183	510	595	631	660	67326	64122	70183
	Min.	-85	-105	-98	-111	-111	-92	-78	-203	-275	-333	-366	-451	-21839
SG100	Max.	-35	-14	14	104	359	415	511	456	466	415	553	691	608
	Min.	-69	-69	-69	-76	-55	-62	-145	-214	-283	-373	-484	-601	-97
SG101	Max.	-59	98	190	975	1557	1728	5451	10575	14305	18054	21699	27896	57428
	Min.	-92	-216	-222	-399	-857	-1073	-1603	-7	2146	3861	5431	10123	-21862
SG102	Max.	-46	-13	-13	7	46	98	326	424	587	372	385	180	810
	Min.	-78	-98	-85	-85	-59	-46	-13	26	20	-113	-185	-317	-324
SG103	Max.	-85	176	189	954	2678	4696	11626	16740	22350	28137	33152	39187	33499
	Min.	-118	-255	-307	-503	-640	-91	261	3448	5872	9444	13382	15440	15760
SG104	Max.	-20	7	7	26	52	65	157	235	304	320	333	301	124
	Min.	-59	-78	-65	-65	-85	-111	-118	-144	-183	-301	-412	-392	-863
SG106	Max.	-21	0	14	35	69	110	304	414	617	876	1084	1104	904
	Min.	-55	-55	-48	-62	-41	-62	-69	-138	-290	-518	-704	-725	-1263
SG107	Max.	-59	104	131	751	1848	2736	3945	5042	6564	9535	5995	-21865	-21865
	Min.	-91	-183	-202	-372	-503	-366	-725	-594	-274	-21865	-21865	-21865	-21865
SG108	Max.	52	72	52	72	177	262	445	765	1050	1190	1256	2302	3211
	Min.	20	-20	-20	-59	-105	-72	-72	59	248	340	255	13	896

Table 6-3: Maximum and Minimum Measured Displacements of FSRCC24-M

		Stage (2)	Stage (3)	Stage (4)	Stage (5)	Stage (6)	Stage (7)	Stage (8)	Stage (9)	Stage (10)	Stage (11)	Stage (12)	Stage (13)	Stage (14)
Gauge		0.10fy	0.15fy	0.25fy	0.5fy	0.75fy	1Δy	2Δy	2.5Δy	3Δy	3.5Δy	4Δy	5Δy	6Δy
DTD1	Max.	-0.002	0.008	0.007	0.030	0.063	0.097	0.290	0.380	0.458	0.532	0.428	0.467	-0.845
	Min.	-0.002	-0.008	-0.010	-0.022	-0.043	-0.054	-0.134	-0.181	-0.253	-0.402	-0.794	-0.964	-0.964
DTD2	Max.	-0.002	0.005	0.009	0.033	0.063	0.068	0.249	0.330	0.398	0.296	0.053	0.347	-0.899
	Min.	-0.002	-0.007	-0.007	-0.017	-0.033	-0.051	-0.121	-0.180	-0.581	-0.910	-0.910	-0.910	-0.916
DTD3	Max.	0.000	0.000	0.000	-0.001	-0.002	-0.003	-0.004	0.008	0.013	0.015	0.021	0.030	0.027
	Min.	-0.001	-0.002	-0.002	-0.007	-0.011	-0.013	-0.026	-0.030	-0.024	-0.024	-0.020	-0.019	-0.010
DTD4	Max.	0.001	0.002	0.001	0.000	0.000	-0.001	0.064	0.086	0.259	0.937	0.695	0.694	0.611
	Min.	0.001	-0.002	-0.001	-0.004	-0.008	-0.012	-0.028	-0.027	-0.019	0.228	0.449	0.328	0.473
DTD5	Max.	0.000	0.006	0.006	0.020	0.033	0.048	0.157	0.218	0.260	0.302	0.363	0.416	0.256
	Min.	-0.001	-0.003	-0.003	-0.009	-0.015	-0.017	-0.035	-0.041	-0.047	-0.051	-0.046	0.032	0.095
DTD6	Max.	-0.009	-0.004	-0.002	0.013	0.034	0.042	0.099	0.130	0.167	0.199	0.130	0.141	0.068
	Min.	-0.010	-0.011	-0.013	-0.017	-0.020	-0.025	-0.042	-0.047	-0.047	-0.253	-0.062	-0.048	-0.045
DTD7	Max.	0.000	0.005	0.005	0.013	0.025	0.037	0.105	0.122	0.105	0.106	0.112	0.103	0.069
	Min.	-0.001	-0.003	-0.004	-0.009	-0.014	-0.016	-0.027	-0.029	-0.034	-0.035	-0.028	-0.025	-0.012
DTD8	Max.	0.000	0.002	0.003	0.003	-0.001	-0.002	-0.004	-0.009	-0.010	0.049	0.092	0.126	0.102
	Min.	-0.001	-0.002	-0.002	-0.007	-0.011	-0.016	-0.029	-0.034	-0.034	-0.023	-0.016	-0.014	-0.003
DTD9	Max.	0.001	0.001	0.001	0.000	-0.001	-0.002	-0.003	0.008	0.032	0.011	0.172	0.194	0.149
	Min.	0.000	-0.002	-0.002	-0.005	-0.009	-0.011	-0.025	-0.030	-0.036	-0.047	-0.023	0.077	0.108
DTD10	Max.	0.000	0.002	0.003	0.021	0.035	0.041	0.101	0.152	0.193	0.221	0.206	0.194	0.123
	Min.	-0.001	-0.004	-0.004	-0.008	-0.013	-0.017	-0.027	-0.030	-0.028	-0.024	-0.023	-0.022	-0.011
DTD11	Max.	-0.003	-0.002	-0.002	-0.002	-0.002	-0.002	-0.002	-0.001	0.000	0.001	0.002	0.005	0.004
	Min.	-0.004	-0.005	-0.005	-0.005	-0.005	-0.005	-0.005	-0.005	-0.004	-0.003	-0.002	-0.001	0.001
DTD12	Max.	0.004	0.004	0.003	0.003	0.003	0.003	0.003	0.001	0.001	0.000	0.000	0.000	0.000
	Min.	0.003	0.002	0.002	0.002	0.001	0.001	0.000	0.000	-0.001	-0.001	-0.002	-0.002	-0.001
DTD13	Max.	0.002	0.002	0.002	0.002	0.002	0.003	0.002	0.003	0.003	0.003	0.004	0.006	0.007
	Min.	-0.002	-0.002	-0.002	-0.002	-0.002	-0.002	-0.002	-0.002	-0.002	-0.001	-0.001	0.000	0.003
DTD14	Max.	0.001	0.001	0.001	0.001	0.002	0.001	0.008	0.012	0.015	0.019	0.023	0.031	0.031
	Min.	-0.001	-0.002	-0.002	-0.002	-0.002	-0.002	-0.001	0.005	0.007	0.009	0.013	0.016	0.018

Cont.Table 6-3: Maximum and Minimum Measured Displacements of FSRCC24-M

		Stage (2)	Stage (3)	Stage (4)	Stage (5)	Stage (6)	Stage (7)	Stage (8)	Stage (9)	Stage (10)	Stage (11)	Stage (12)	Stage (13)	Stage (14)
Gauge		0.10fy	0.15fy	0.25fy	0.5fy	0.75fy	1Δy	2Δy	2.5Δy	3Δy	3.5Δy	4Δy	5Δy	6Δy
DTD15	Max.	0.001	0.001	0.001	0.001	0.001	0.000	0.000	0.000	0.000	0.000	0.000	0.000	0.000
	Min.	0.000	0.000	0.000	0.000	0.000	0.000	-0.002	-0.003	-0.003	-0.003	-0.003	-0.004	-0.002
DTD16	Max.	-0.001	0.001	0.001	0.006	0.012	0.019	0.076	0.102	0.116	0.130	0.138	0.114	0.007
	Min.	-0.002	-0.002	-0.002	-0.002	-0.002	-0.002	-0.001	0.032	0.046	0.051	0.051	0.002	-0.166
DTD17	Max.	-0.002	0.001	0.001	0.005	0.011	0.016	0.071	0.084	0.100	0.131	0.146	0.100	-0.055
	Min.	-0.002	-0.003	-0.003	-0.003	-0.003	-0.003	-0.003	0.030	0.042	0.056	0.045	-0.060	-0.292

Table 6-4: Maximum and Minimum Measured Force and Displacement of FSKJ24-M

Stage	Ductility	Axial Force (Kips)		String Pot Displacement at Max. and Min. Force (in)		Actuator Displacement at Max. and Min. Force (in)		Actuator Force (kips)	
Number	Level	Max.	Min.	Max.	Min.	Max.	Min.	Max.	Min.
Stage (1)	0.15fy	41.82	25.04	0.11	-0.04	0.04	-0.11	3.01	-2.72
Stage (2)	0.25fy	46.02	14.82	0.25	-0.11	0.11	-0.26	4.57	-4.86
Stage (3)	0.5fy	58	11.82	0.98	-0.54	0.53	-0.98	9.37	-9.47
Stage (4)	0.75fy	60.38	3.98	1.98	-1.18	1.16	-1.97	14.13	-13.97
Stage (5)	1 Δy	63.94	4.1	2.64	-1.56	1.54	-2.62	17.01	-16.85
Stage (6)	1.5 Δy	64.82	4.2	3.95	-2.31	2.31	-4.33	19.56	-21.85
Stage (7)	2 Δy	64.94	4.3	5.24	-3.11	3.11	-5.23	20.81	-21.35
Stage (8)	2.5 Δy	63.22	4.32	6.53	-3.88	3.89	-6.53	21.58	-22.3
Stage (9)	3 Δy	60.54	4.63	7.88	-4.66	4.62	-7.86	22.21	-22.61
Stage (10)	4 Δy	58.24	8.84	10.46	-6.19	6.21	-10.46	21.83	-22.71
Stage (11)	5 Δy	59.04	11.24	13.06	-7.76	7.77	-13.07	21.41	-22.54
Stage (12)	6 Δy	41.82	25.04	15.64	-9.72	9.73	-15.62	20.32	-22.42

Table 6-5: Maximum and Minimum Measured Strain (micro strain) in the Reinforcement of FSKJ24-M

		Stage (1)	Stage (2)	Stage (3)	Stage (4)	Stage (5)	Stage (6)	Stage (7)	Stage (8)	Stage (9)	Stage (10)	Stage (11)	Stage (12)
Gauge		0.15fy	0.25fy	0. 5fy	0.75fy	1 Δy	1.5 Δy	2 Δy	2.5 Δy	3 Δy	4 Δy	5 Δy	6 Δy
SG1	Max.	117	55	76	152	324	324	386	428	421	386	338	297
	Min.	0	0	-14	-283	-276	-124	55	41	-7	-55	-97	-193
SG3	Max.	41	48	55	62	35	41	55	83	110	159	214	311
	Min.	0	-7	-7	-48	-55	-62	-55	-69	-97	-145	-283	-324
SG4	Max.	110	318	1719	4211	5543	9988	13778	21344	30124	47706	66254	84312
	Min.	-131	-228	-435	-283	-90	-1305	-1546	-1560	-932	856	7013	19818
SG5	Max.	26	26	52	150	248	490	588	660	673	667	562	399
	Min.	-52	-33	-59	-26	26	33	52	33	0	-26	-39	-98
SG6	Max.	28	166	994	1995	2671	5626	9250	13481	18182	26251	36598	50210
	Min.	-193	-283	-559	-884	-1063	-1450	-621	511	1691	2989	4079	4839
SG7	Max.	235	62	83	228	759	794	214	228	297	283	304	318
	Min.	-21	-14	-14	-1319	-732	-594	-7	0	-14	-35	-131	-338
SG8	Max.	152	269	594	897	1132	159	-2941	-5295	-8788	-12791	228331	228331
	Min.	-200	-511	-1684	-3168	-6758	-20129	-25327	-36220	-48231	-72040	-13153	-224067
SG9	Max.	85	92	124	137	150	203	314	373	549	700	732	490
	Min.	-20	-39	-78	-98	-137	-170	-196	-216	-209	-144	-190	-883
SG15	Max.	21	28	28	152	3520	3699	3782	3824	3886	3872	3803	23063
	Min.	-55	-62	-97	-138	-3768	-3920	-3906	-3955	-4107	-4693	-5445	-22167
SG16	Max.	124	214	621	917	1179	772	97	-524	-1938	23060	23060	23060
	Min.	-117	-290	-1145	-2786	-5910	-17551	-20641	-29468	-39185	-221352	-221352	-221352
SG18	Max.	26	150	1026	1883	2399	4511	7419	10479	13433	17107	5739	3883
	Min.	-144	-216	-471	-732	-922	-1340	-961	-824	-765	-621	-588	150
SG19	Max.	21	28	28	14	14	7	-14	-14	35	110	366	22983
	Min.	-35	-48	-62	-90	-97	-117	-131	-186	-352	-1132	-1594	-1525
SG20	Max.	172	304	828	1318	1497	23096	23096	23096	23096	23096	23096	23096
	Min.	-145	-352	-1939	-3781	-7057	-22114	-82840	23096	23096	23096	23096	23096
SG21	Max.	78	111	183	142667	307	431	562	798	1000	1327	1556	1451
	Min.	26	33	20	218336	-124	-150	-177	-183	-137	-7	7	320

Cont. Table 6-5: Maximum and Minimum Measured Strain (micro strain) in the Reinforcement of FSKJ24-M

		Stage (1)	Stage (2)	Stage (3)	Stage (4)	Stage (5)	Stage (6)	Stage (7)	Stage (8)	Stage (9)	Stage (10)	Stage (11)	Stage (12)
Gauge		0.15fy	0.25fy	0. 5fy	0.75fy	1 Δy	1.5 Δy	2 Δy	2.5 Δy	3 Δy	4 Δy	5 Δy	6 Δy
SG22	Max.	65	137	1099	2015	2571	4271	6345	9111	11950	17516	23279	26935
	Min.	-164	-255	-569	-844	-994	-1347	-1105	-1033	-857	-536	-222	-124
SG23	Max.	59	59	78	92	111	209	229	294	275	412	928	1320
	Min.	-33	-26	-33	-26	-13	-13	-26	-33	-105	-203	-248	-255
SG24	Max.	131	290	1394	2747	4734	12498	77682	77978	78158	80483	78489	78123
	Min.	-138	-255	-697	-1077	-1318	-1291	-780	-2409	-462	-490	-143799	-1111
SG25	Max.	39	59	92	144	177	222	235	268	301	288	366	373
	Min.	-39	-26	-46	-20	7	33	39	78	105	-170	-438	-700
SG26	Max.	26	78	569	1333	1836	3026	8580	9737	15448	13063	74791	76562
	Min.	-131	-216	-399	-647	-810	-1274	-1059	-1019	-856	-595	-22996	-7
SG27	Max.	41	48	124	110	104	124	304	552	745	973	849	222095
	Min.	-7	-14	-21	14	0	-62	-14	14	-41	-48	-152	-545
SG28	Max.	90	186	1491	2698	4161	10854	12731	17210	20915	27933	33819	37808
	Min.	-104	-193	-580	-966	-1042	-1049	-552	-317	200	828	1642	-230662
SG30	Max.	46	39	39	111	124	170	196	222	242	261	294	333
	Min.	-46	-39	-52	-39	-72	-52	20	39	39	33	46	20
SG31	Max.	21	28	62	152	262	400	462	531	607	710	800	807
	Min.	-28	-41	-62	-41	-7	28	62	69	76	62	69	28
SG33	Max.	65	91	464	876	1026	1209	1176	1189	1176	1196	1176	1104
	Min.	-26	-52	-105	-131	-163	-144	-85	-65	-72	-91	-118	-170
SG34	Max.	39	46	65	222	353	588	667	732	785	791	778	745
	Min.	-39	-33	-39	-33	0	20	59	78	98	105	137	111
SG35	Max.	52	65	59	59	59	72	85	92	85	78	72	52
	Min.	-33	-26	-26	-39	-26	-13	-7	-7	-26	-59	-59	-124
SG37	Max.	39	65	118	333	484	699	791	863	915	974	1020	993
	Min.	-33	-59	-105	-196	-203	-222	-203	-196	-196	-190	-196	-242
SG38	Max.	87	104	249	510	638	866	853	887	957	1148	1301	1226
	Min.	-46	-12	-79	-104	-294	-141	-128	-153	-170	-215	-261	-257

Cont. Table 6-5: Maximum and Minimum Measured Strain (micro strain) in the Reinforcement of FSKJ24-M

		Stage (1)	Stage (2)	Stage (3)	Stage (4)	Stage (5)	Stage (6)	Stage (7)	Stage (8)	Stage (9)	Stage (10)	Stage (11)	Stage (12)
Gauge		0.15fy	0.25fy	0. 5fy	0.75fy	1 Δy	1.5 Δy	2 Δy	2.5 Δy	3 Δy	4 Δy	5 Δy	6 Δy
SG39	Max.	41	62	166	428	573	883	745	787	863	966	1111	1090
	Min.	-35	-48	-55	-35	48	90	76	35	-41	-159	-200	-352
SG40	Max.	28	28	28	55	62	76	97	117	124	152	186	276
	Min.	-21	-21	-34	-14	0	7	21	28	14	-7	21	62
SG41	Max.	48	55	69	221	331	483	614	731	814	966	1042	1132
	Min.	0	-7	-41	-55	-21	7	48	28	14	-14	-21	-28
SG42	Max.	48	69	186	469	614	711	759	780	738	711	607	504
	Min.	-34	-55	-117	-145	-200	-283	-304	-338	-352	-366	-386	-400
SG43	Max.	35	28	62	173	242	331	387	428	435	442	400	352
	Min.	-14	-14	-14	7	55	104	145	159	145	110	83	41
SG44	Max.	13	20	20	33	39	379	490	562	582	628	726	778
	Min.	-39	-33	-52	-39	-52	-26	92	111	131	137	190	157
SG45	Max.	28	28	55	290	1836	1988	2174	2305	2408	2567	2747	2933
	Min.	-21	-21	-28	-14	1636	1656	1718	1753	1774	1801	1856	1877
SG47	Max.	28	28	55	62	76	97	117	124	152	186	276	228
	Min.	14	14	21	28	7	48	62	90	110	124	221	0
SG48	Max.	28	28	28	41	152	317	407	511	607	704	801	821
	Min.	-14	-14	-35	-28	-28	14	104	138	173	193	228	228
SG50	Max.	28	28	145	532	794	994	1091	1222	1332	1519	1712	1774
	Min.	-21	-21	-55	-83	62	90	97	90	69	0	-21	-152
SG51	Max.	59	78	137	628	856	1353	1393	1491	1543	1628	1661	1595
	Min.	-46	-20	-20	7	65	92	137	144	150	137	150	-10859
SG52	Max.	35	83	152	166	179	173	193	200	193	186	193	173
	Min.	-7	-7	-7	14	14	21	28	35	35	35	41	14
SG53	Max.	200	62	117	207	593	655	221	214	221	193	283	221
	Min.	-14	-7	-7	-1076	-559	-490	55	48	48	41	-48	-186
SG54	Max.	21	28	62	69	97	124	152	166	166	179	200	200
	Min.	41	62	166	42	57	88	74	78	86	96	111	109

Cont. Table 6-5: Maximum and Minimum Measured Strain (micro strain) in the Reinforcement of FSKJ24-M

		Stage (1)	Stage (2)	Stage (3)	Stage (4)	Stage (5)	Stage (6)	Stage (7)	Stage (8)	Stage (9)	Stage (10)	Stage (11)	Stage (12)
Gauge		0.15fy	0.25fy	0. 5fy	0.75fy	1 Δy	1.5 Δy	2 Δy	2.5 Δy	3 Δy	4 Δy	5 Δy	6 Δy
SG55	Max.	28	28	28	48	55	110	145	159	173	180	193	200
	Min.	-14	-14	-28	-14	-35	-28	21	35	41	35	35	0
SG57	Max.	39	46	59	78	105	177	203	262	301	366	464	490
	Min.	-46	-39	-59	-39	-39	0	39	52	52	46	98	98
SG59	Max.	52	52	59	65	46	72	98	105	118	150	209	235
	Min.	-33	-26	-46	-33	-33	-13	0	13	20	39	52	39
SG60	Max.	46	52	59	1354	961	785	177	209	288	412	490	844
	Min.	-458	-65	-137	-1844	-817	-1092	-65	-78	-59	7	-340	-124
SG61	Max.	48	55	124	400	511	684	801	911	994	1125	1201	1194
	Min.	-14	-35	-35	21	62	0	-35	-104	-180	-276	-318	-469
SG62	Max.	69	62	283	676	917	1469	1572	1745	1841	1986	2214	2489
	Min.	-21	-21	-28	-14	-34	14	21	7	34	41	152	117
SG63	Max.	41	55	207	525	697	966	1021	1153	1270	1463	1553	1539
	Min.	-35	-62	-145	-228	-283	-311	-269	-283	-269	-297	-276	-324
SG64	Max.	59	105	386	647	752	942	922	942	929	896	831	759
	Min.	-39	-65	-111	-131	-150	-164	-137	-118	-105	-98	-46	-26
SG65	Max.	37	83	294	451	517	662	662	700	712	716	707	683
	Min.	-13	-8	-46	-62	-107	-140	-128	-128	-128	-133	-124	-137
SG66	Max.	18	18	18	255	121	158	207	261	359	395	413	498
	Min.	-73	-31	-42	-103	-207	-97	-25	12	55	97	152	219
SG67	Max.	34	41	117	290	338	448	497	559	559	648	759	814
	Min.	-7	-7	0	14	41	62	90	117	145	159	193	152
SG68	Max.	133	66	265	552	718	982	1010	1087	1154	1237	1292	1298
	Min.	-6	-6	-22	-474	-337	-210	88	99	105	116	83	38
SG69	Max.	166	117	414	904	1125	1491	1498	1601	1657	1719	1781	1802
	Min.	-14	-35	-124	-449	-235	-393	-193	-207	-228	-255	-262	-290
SG70	Max.	531	262	607	938	1111	1373	1325	1352	1325	1297	1235	1145
	Min.	0	97	14	-566	-290	-435	-48	-21	7	41	-83	-214

Cont. Table 6-5: Maximum and Minimum Measured Strain (micro strain) in the Reinforcement of FSKJ24-M

		Stage (1)	Stage (2)	Stage (3)	Stage (4)	Stage (5)	Stage (6)	Stage (7)	Stage (8)	Stage (9)	Stage (10)	Stage (11)	Stage (12)
Gauge		0.15fy	0.25fy	0. 5fy	0.75fy	1 Δy	1.5 Δy	2 Δy	2.5 Δy	3 Δy	4 Δy	5 Δy	6 Δy
SG71	Max.	104	221	552	849	1007	1270	1263	1311	1318	1325	1297	1228
	Min.	-7	7	-41	-83	-110	-166	-138	-152	-152	-159	-145	-159
SG72	Max.	90	248	531	772	897	1124	1131	1186	1186	1186	1165	1124
	Min.	-28	0	-76	-138	-179	-200	-214	-228	-228	-255	-241	-269
SG73	Max.	21	21	21	28	21	62	83	97	103	103	117	103
	Min.	-21	-28	-34	-21	-28	-28	-7	0	0	-7	-14	-21
SG74	Max.	41	35	41	55	62	145	207	262	311	366	414	435
	Min.	-14	-21	-28	-110	-48	-41	14	35	48	55	48	48
SG75	Max.	46	52	118	301	418	582	653	712	778	849	915	915
	Min.	-13	-33	-78	-78	-105	-105	-85	-72	-52	-46	-39	-33
SG78	Max.	161	69	150	397	575	794	920	1012	1046	1082	1058	983
	Min.	-29	-75	-172	-391	-454	-293	-253	-265	-265	-270	-288	-322
SG79	Max.	44	52	182	347	521	747	895	1000	1033	1087	1052	966
	Min.	-44	-78	-130	-182	-217	-253	-261	-278	-374	-305	-313	-525
SG80	Max.	290	55	62	165	648	841	159	152	91	103	207	-7
	Min.	-28	-21	-28	-1165	-689	-469	48	34	-28	-55	-193	-262
SG81	Max.	35	35	48	90	159	235	262	297	324	345	366	331
	Min.	-7	-7	-14	-14	7	28	69	90	83	69	69	21
SG82	Max.	81	90	134	341	493	727	844	950	1058	1219	1453	1659
	Min.	0	-9	-53	-53	-27	-36	-9	9	36	90	296	341
SG83	Max.	62	90	189	511	699	915	1031	1113	1148	1269	1193	1113
	Min.	-27	-53	-117	-170	-216	-269	-269	-278	-296	-313	-322	-341
SG84	Max.	53	72	207	610	789	969	1086	1157	1166	1193	1131	1023
	Min.	-53	-90	-207	-260	-322	-404	-386	-377	-386	-386	-359	-386
SG85	Max.	44	51	121	319	491	648	776	854	889	924	915	863
	Min.	-35	-78	-181	-241	-276	-336	-328	-336	-354	-371	-371	-389
SG86	Max.	28	21	21	48	35	69	110	207	221	290	504	704
	Min.	-28	-35	-41	-35	-62	-55	-28	0	21	-28	-21	-110

Cont. Table 6-5: Maximum and Minimum Measured Strain (micro strain) in the Reinforcement of FSKJ24-M

		Stage (1)	Stage (2)	Stage (3)	Stage (4)	Stage (5)	Stage (6)	Stage (7)	Stage (8)	Stage (9)	Stage (10)	Stage (11)	Stage (12)
Gauge		0.15fy	0.25fy	0. 5fy	0.75fy	1 Δy	1.5 Δy	2 Δy	2.5 Δy	3 Δy	4 Δy	5 Δy	6 Δy
SG87	Max.	20	26	26	203	628	1353	1589	1837	2007	2190	2379	2549
	Min.	-46	-46	-59	-33	20	46	46	33	13	20	39	-7
SG88	Max.	150	39	33	615	360	530	517	595	680	883	1138	1282
	Min.	-33	-52	-78	-477	-438	-92	111	111	124	131	177	131
SG89	Max.	-26	-33	-39	144	307	647	863	1111	1373	1732	2203	2353
	Min.	26	26	46	-26	26	59	85	92	98	105	144	78
SG90	Max.	-20	-33	-52	224	436	851	1051	1279	1467	1652	1856	2264
	Min.	72	65	98	-39	28	-16	-16	-8	8	55	94	208
SG91	Max.	-7	-65	-444	1457	2248	2791	3797	9542	12365	7448	7267	21154
	Min.	118	170	353	-490	-549	-582	-503	59	4228	6673	-6068	-21674
SG92	Max.	-353	-46	-65	1307	869	1418	1732	1961	2059	2262	2386	2536
	Min.	59	131	288	-909	-869	-425	-150	-124	-137	-209	-248	-294
SG94	Max.	-931	-193	-290	973	2290	2849	2511	2656	2821	10112	12377	2281
	Min.	62	-28	-28	-3139	-1497	-862	359	283	172	255	-22817	-2281
SG95	Max.	-20	-20	-59	301	935	7076	2432	1899	2848	3935	4766	4763
	Min.	72	92	78	-85	-25015	-2174	373	-4020	-1725	-18053	-21740	-2174
SG96	Max.	-28	-62	-352	594	783	956	1000	1068	1063	1039	991	894
	Min.	48	76	131	-68	10	48	68	82	43	-130	-242	-13501
SG97	Max.	12	79	92	103	109	103	92	85	94	97	121	128
	Min.	-25	-31	31	-36	36	36	31	25	31	31	18	12
SG98	Max.	14	90	104	117	124	117	104	97	104	110	138	145
	Min.	68	75	55	41	41	41	35	8	35	35	21	14
SG99	Max.	41	48	76	110	145	469	600	704	766	849	980	994
	Min.	-14	-35	-62	-97	-124	-159	-131	-117	-110	-104	-76	-76
SG100	Max.	41	48	90	517	862	1104	1228	1297	1352	1414	1497	1525
	Min.	-28	-41	-83	-117	-117	-145	-138	-138	-138	-145	-131	-131
SG101	Max.	41	55	186	621	773	932	1042	1111	1139	1173	1180	1139
	Min.	-41	-76	-159	-166	-179	-207	-193	-193	-200	-214	-228	-228

Cont. Table 6-5: Maximum and Minimum Measured Strain (micro strain) in the Reinforcement of FSKJ24-M

		Stage (1)	Stage (2)	Stage (3)	Stage (4)	Stage (5)	Stage (6)	Stage (7)	Stage (8)	Stage (9)	Stage (10)	Stage (11)	Stage (12)
Gauge		0.15fy	0.25fy	0. 5fy	0.75fy	1 Δy	1.5 Δy	2 Δy	2.5 Δy	3 Δy	4 Δy	5 Δy	6 Δy
SG102	Max.	35	41	200	414	669	952	1132	1256	1297	1373	1353	1291
	Min.	-62	-131	-235	-276	-311	-359	-352	-359	-373	-386	-400	-414
SG104	Max.	28	28	34	41	34	69	83	90	97	97	97	90
	Min.	-14	-14	-21	-55	-55	-48	-7	14	21	14	21	-21
SG105	Max.	14	14	35	166	373	607	697	739	718	718	711	690
	Min.	-28	-41	-48	-55	7	124	221	214	235	242	255	221
SG106	Max.	28	35	90	311	504	780	870	939	959	994	1049	1042
	Min.	-21	-41	-97	-152	-152	-138	-104	-76	-69	-76	-62	-97
SG107	Max.	35	41	83	745	932	1132	1318	1574	1815	1946	2029	2077
	Min.	-28	-35	-69	-62	0	28	35	41	28	7	7	-35
SG108	Max.	41	62	366	932	1098	1381	1436	1533	1668	1726	1822	1871
	Min.	-28	-41	-90	-69	-69	-55	-62	-55	-69	-83	-69	-110
SG109	Max.	55	69	1111	1594	1974	2608	2657	2864	2926	3022	3064	3133
	Min.	-21	-35	-97	-48	-69	-83	-69	-62	-69	-69	-41	-62
SG110	Max.	76	490	1028	1643	1974	2547	2581	2774	2850	2947	2968	2954
	Min.	-21	7	28	-69	-131	-159	-131	-124	-97	-83	-28	-41

Table 6-6: Maximum and Minimum Measured Displacements of FSKJ24-M

		Stage (1)	Stage (2)	Stage (3)	Stage (4)	Stage (5)	Stage (6)	Stage (7)	Stage (8)	Stage (9)	Stage (10)	Stage (11)	Stage (12)
Gauge		0.15fy	0.25fy	0. 5fy	0.75fy	1 Δy	1.5 Δy	2 Δy	2.5 Δy	3 Δy	4 Δy	5 Δy	6 Δy
DTD 1	Max.	0.001	0.003	0.012	0.027	0.040	0.073	0.111	0.156	0.209	0.295	0.383	0.599
	Min.	-0.004	-0.006	-0.014	-0.028	-0.039	-0.079	-0.096	-0.150	-0.226	-0.383	-0.525	-0.663
DTD 2	Max.	0.003	0.008	0.027	0.053	0.075	0.168	0.198	0.267	0.341	0.348	0.463	0.008
	Min.	-0.002	-0.004	-0.011	-0.022	-0.030	-0.044	-0.062	-0.078	-0.096	-0.339	-0.457	0.002
DTD 3	Max.	0.000	0.000	0.010	0.021	0.027	0.054	0.077	0.096	0.114	0.174	0.231	0.215
	Min.	-0.001	-0.002	-0.005	-0.008	-0.011	-0.025	-0.029	-0.038	-0.032	-0.086	-0.269	-0.019
DTD 4	Max.	0.001	0.002	0.015	0.037	0.040	0.060	0.063	0.108	0.163	0.397	0.525	0.745
	Min.	-0.001	-0.001	-0.005	-0.009	-0.013	-0.019	-0.028	-0.037	-0.048	-0.059	0.029	-0.354
DTD 5	Max.	0.001	0.002	0.011	0.023	0.030	0.037	0.067	0.101	0.139	0.228	0.316	0.417
	Min.	-0.002	-0.003	-0.008	-0.012	-0.017	-0.037	-0.040	-0.046	-0.048	-0.042	-0.014	0.030
DTD 6	Max.	0.001	0.002	0.002	0.007	0.027	0.119	0.154	0.209	0.246	0.340	0.442	0.745
	Min.	-0.001	-0.002	-0.008	-0.012	-0.015	-0.019	-0.023	-0.029	-0.033	-0.038	0.017	-0.354
DTD 7	Max.	0.001	0.002	0.010	0.017	0.019	0.025	0.038	0.051	0.065	0.086	0.121	0.003
	Min.	-0.002	-0.003	-0.006	-0.012	-0.015	-0.026	-0.027	-0.031	-0.033	-0.035	-0.020	0.000
DTD 8	Max.	0.000	0.000	0.008	0.022	0.029	0.063	0.074	0.107	0.143	0.196	0.226	-0.004
	Min.	0.000	-0.001	-0.005	-0.008	-0.010	-0.013	-0.014	-0.017	-0.018	-0.020	-0.021	-0.012
DTD 9	Max.	0.000	0.000	0.004	0.011	0.016	0.051	0.067	0.102	0.144	0.228	0.277	0.337
	Min.	-0.002	-0.002	-0.002	-0.001	0.000	0.000	0.021	0.035	0.058	0.083	0.126	0.132
DTD 10	Max.	0.000	0.000	0.004	0.012	0.017	0.033	0.058	0.078	0.099	0.146	0.228	0.294
	Min.	-0.001	-0.002	-0.002	-0.001	0.000	0.000	0.013	0.027	0.041	0.063	0.102	0.157
DTD 11	Max.	0.001	0.003	0.002	1.883	-0.003	-0.003	-0.007	-0.007	-0.005	-0.006	-0.006	0.002
	Min.	0.000	0.000	0.001	-0.456	-0.004	-0.008	-0.008	-0.007	-0.007	-0.007	-0.007	-0.029
DTD 12	Max.	0.000	0.000	0.000	0.000	-0.002	0.001	0.001	0.003	0.004	0.005	0.006	0.417
	Min.	0.000	-0.002	-0.001	-0.005	-0.005	-0.007	-0.007	-0.007	-0.006	-0.005	-0.004	0.030
DTD 13	Max.	0.000	0.000	0.000	0.000	-0.001	0.000	-0.001	0.004	0.002	0.003	0.004	0.000
	Min.	0.000	0.000	-0.001	-0.003	-0.002	-0.002	-0.003	-0.002	0.000	0.000	0.000	-0.002
DTD 14	Max.	0.001	0.001	0.001	0.002	0.002	0.002	0.002	0.002	0.002	0.002	0.002	0.003
	Min.	0.000	0.000	0.002	0.002	0.002	0.002	0.002	0.002	0.002	0.002	0.002	0.002
DTD 15	Max.	0.001	0.001	0.001	0.001	0.001	0.001	0.000	0.002	0.002	0.002	0.002	0.002
	Min.	0.000	0.000	0.000	-0.011	0.000	0.000	-0.001	0.000	0.000	0.000	0.000	0.000

Table 6-7: Strut-and-Tie Model Coordinates for FSRCC24-M

Node	Coordinates		Node	Coordinates	
	x (in)	Z (in)		x (in)	Z (in)
A	20.75	15.71	O	-47.23	15.53
B	20.75	1.98	Q	30.00	15.71
C	4.34	15.53	R	30.00	1.98
D	4.34	11.03	T	48.45	1.98
E	4.34	7.21	U	48.45	15.71
F	4.34	1.98	V	48.00	17.50
G	-4.90	7.21	W	-6.42	0
H	-6.57	1.98	X	-48.00	17.50
I	-20.75	15.53	Y	-30.00	17.50
J	-20.75	1.41	Z	30.00	17.50
K	-30.00	1.41	L	-30.00	15.53

Table 6-8: Strut-and-Tie Model Forces for FSRCC24-M

Strut (kips)		Tie (kips)	
C_{OK}	121.1	T_{OL}	73.7
C_{KJ}	96.0	T_{LK}	75.3
C_{LJ}	132.2	T_{IJ}	117.8
C_{JH}	168.7	T_{LI}	146.2
C_{HW}	591.9	T_{IC}	367.2
C_{HE}	284.3	T_{CD}	322.2
C_{IG}	250.5	T_{DE}	334.4
C_{GD}	112.0	T_{EG}	40.23
C_{GH}	525.5	T_{HB}	334.1
C_{GC}	488.5	T_{AB}	70.0
C_{DA}	108.1	T_{QR}	40.3
C_{EB}	230.3	T_{BR}	125.9
C_{AR}	48.6	T_{RT}	99.1
C_{AQ}	76.7	T_{QU}	22.3
C_{QT}	124.6	T_{UT}	75.6

Table 6-9: Strut-and-Tie Model Coordinates for Modified FSKJ24-M in the Closing Moment Case and Opening Moment Case

Closing Moment		
Node	Coordinates	
	x (in)	Z (in)
A	16.25	8.96
B	16.25	1.3
C	-2.86	8.96
D	-2.86	6.19
E	-2.86	3.94
F	-2.86	0
G	5.05	6.19
H	5.05	1.69
I	8	8.96
J	29.13	1.3
K	29.13	8.96
L	42	8.96
M	42	1.3
N	-15	1.69
P	-8	8.96
O	-15	8.96
W	4.95	0
X	-9.14	3.94
Y	-9.14	1.69

Opening Moment		
Node	Coordinates	
	x (in)	Z (in)
A	16.25	9.87
B	16.25	1.93
C	3.4	9.87
D	3.4	6.7
F	3.4	0
G	-5.18	6.7
H	-5.18	1.93
I	-8	9.87
J	29.13	1.93
K	29.13	9.87
L	42	9.87
M	42	1.93
W	-5.08	0
X	8	9.87
Y	9.12	6.7

Table 6-10: Strut-and-Tie Model Forces for Modified FSKJ24-M in the Closing Moment Case and Opening Moment Case

Closing Moment			
Strut (kips)		Tie (kips)	
C_{OD}	175.6	T_{CP}	223.8
C_{DP}	60.3	T_{CI}	357.7
C_{DH}	327.7	T_{IA}	327.3
C_{EH}	223.7	T_{XY}	40.6
C_{GI}	42	T_{AK}	284.8
C_{AG}	44.4	T_{KL}	284.8
C_{NX}	111.3	T_{LM}	0
C_{XE}	111.3	T_{KJ}	0
C_{YE}	111.3	T_{AB}	13
C_{HW}	301.2	T_{ON}	39.9
C_{HB}	307.3	T_{CD}	47.9
C_{BJ}	306.9	T_{DE}	141
C_{KB}	0	T_{EF}	242.1
C_{JM}	306.9	T_{NY}	103.8
C_{JL}	0	T_{YH}	215.1
C_{CG}	142.2	T_{DG}	61
C_{HG}	90		

Opening Moment			
Strut (kips)		Tie (kips)	
C_{DH}	479.7	T_{GD}	63.4
C_{GH}	23.4	T_{CD}	23.4
C_{GC}	67.6	T_{DF}	251.9
C_{HI}	4.7	T_{HB}	440.4
C_{DX}	115.4	T_{AB}	60.7
C_{DY}	121.7	$T_{KJ}= T_{LM}$	0
C_{YA}	115.4	T_{JM}	301.1
C_{XA}	178.2	T_{BJ}	301.1
C_{CX}	61.8	T_{XY}	64.6
C_{DB}	151.9	T_{CI}	1.6
C_{AK}	278.7		
C_{AJ}	0		
C_{KM}	0		
C_{KL}	279		
C_{HW}	207.9		

Table 6-11: Tension Demands in Reinforcement Concrete T-Joint Using the Modified Strut-and-Tie Model

		Drop-Cap Joint				Flat-Slab Joint			
Joint Configuration	Span (ft)	16	20	24	28	30	34	40	44
	Tension Demand								
V	Top Reinforcement of the Slab (T_{bt})	0.27	0.25	0.32	0.32	0.39	0.38	0.38	0.36
	Bottom Reinforcement of The Slab (T_{bb})	0.29	0.23	0.27	0.31	0.41	0.34	0.35	0.38
	Stirrups Out of the Joint (T_{es})	0.23	0.21	0.26	0.28	0.28	0.33	0.39	0.43
	Vertical j-bars and Stirrups Inside the Joint (T_{JV})	1.43	1.5	1.44	1.4	1.45	1.46	1.26	1.09
II	Top Reinforcement of the Slab	0.34	0.25	0.3	0.33	0.46	0.45	0.47	0.43
	Bottom Reinforcement of the Slab	0.29	0.24	0.29	0.3	0.66	0.54	0.4	0.36
	Stirrups Out of the Joint	0.23	0.2	0.25	0.28	0.28	0.33	0.38	0.38
	Vertical j-bars and Stirrups Inside the Joint (T_{JV})	1.44	1.46	1.48	1.42	1.47	1.38	1.29	1.32
III	Top Reinforcement of the Slab		0.25	0.30	0.33	0.43	0.44	0.43	0.40
	Bottom Reinforcement of the Slab		0.24	0.24	0.24	0.64	0.43	0.41	0.43
	Stirrups Out of the Joint		0.20	0.24	0.26	0.25	0.29	0.35	0.35
	Vertical j-bars and Stirrups Inside Joint (T_{JV})		1.47	1.50	1.52	1.50	1.54	1.44	1.29

Table 6-12: Tension Demands in Reinforcement Concrete Knee-Joint Using the Modified Strut-and-Tie Model

		Drop-Cap Joint				Flat-Slab Joint			
Joint Configuration	Span (ft)	16	20	24	28	30	34	40	44
	Tension Demand								
V	Top Reinforcement of the Slab	0.41	0.21	0.15	0.15	0.33	0.19	0.18	0.23
	Bottom Reinforcement of the Slab	0.25	0.24	0.23	0.21	0.49	0.29	0.29	0.2
	Stirrups Out of the Joint	0.16	0.16	0.16	0.15	0.23	0.18	0.16	0.15
	Vertical j-bars and Stirrups Inside the Joint (T_{JV})	0.89	0.9	0.88	0.81	1.17	1.02	0.94	0.94
II	Top Reinforcement of the Slab	0.25	0.25	0.23	0.24	0.68	0.5	0.3	0.21
	Bottom Reinforcement of the Slab	0.21	0.25	0.16	0.16	0.68	0.5	0.29	0.25
	Stirrups Out of the Joint	0.16	0.16	0.15	0.16	0.28	0.22	0.17	0.16
	Vertical j-bars Inside the Joint(T_{JV})	0.9	0.91	0.83	0.9	1.12	1.01	0.86	0.88
III	Top Reinforcement of the Slab		0.25	0.23	0.24	0.67	0.5	0.3	0.21
	Bottom Reinforcement of the Slab		0.25	0.16	0.16	0.67	0.5	0.29	0.25
	Stirrups Out of the Joint		0.16	0.15	0.16	0.28	0.22	0.17	0.16
	Vertical j-bars and Stirrups Inside the Joint(T_{JV})		0.91	0.83	0.90	1.12	1.01	0.86	0.88

Table 7-1: Experimental and Analytical Measured Force-Displacement

	Positive Direction					Negative Direction				
	Experimental Test			Atena Results		Experimental Test			Atena Results	
	Δy (in)	Fy (ksi)	Fu (ksi)	Fy (ksi)	Fu (ksi)	Δy (in)	Fy (ksi)	Fu (ksi)	Fy (ksi)	Fu (ksi)
DCRCC1	2.28	10.63	13.43	12.91	13.31	2.37	10.52	12.91	13.20	14.02
FSRCC1	2.19	10.20	13.58	13.61	13.90	2.08	10.65	13.58	13.37	13.77
DCRCC24	2.82	33.00	43.75	38.26	41.63	2.72	27.43	42.18	37.9	40.40
FSRCC24	3.01	36.01	42.84	42.13	43.65	2.80	34.69	42.84	42.31	44.71
DCKJ24	2.44	18.76	20.61	18.62	18.86	2.43	11.83	17.32	11.86	17.02
FSKJ24	3.18	14.61	16.77	16.30	17.25	3.22	10.51	13.54	12.63	13.96
FSRCC24-M	2.77	31.85	42.96	39.78	42.45	2.82	40.05	44.68	41.97	42.85
FSKJ24-M	1.54	17.01	22.21	17.11	20.55	1.54	16.85	22.71	16.21	21.57

Δy: The yield displacement,

Fy: The yield force,

Fu: The ultimate Force

Table 7-2: Confined Concrete Parameters

Material Properties		Specimen							
		DCRCC1	FSRCC1	DCRCC24	FSRCC24	DCKJ24	FSKJ24	FSRCC24-M	FSKJ24-M
Pile Confined Concrete	$f`_c$ (ksi)	5.18	5.18	4.20	4.22	7.10	7.15	6.09	7.69
	$f`_{cc}$ (ksi)	7.05	7.05	5.72	5.73	9.32	9.34	5.51	9.99
	ε_{cc}	0.0037	0.0037	0.0039	0.0039	0.035	0.035	0.004	0.0035
	ε_{cu}	0.017	0.017	0.020	0.020	0.016	0.016	0.0175	0.015
Slab Confined Concrete	$f`_c$ (ksi)	6.24	6.34	4.52	4.55	4.45	4.39	4.27	7.74
	$f`_{cc}$ (ksi)	7.057	11.14	5.18	10.81	5.31	17.31	10.81	10.12
	ε_{cc}	0.0023	0.0069	0.0024	0.011	0.0026	0.003	0.0110	0.0036
	ε_{cu}	0.0128	0.013	0.0115	0.013	0.0145	0.011	0.0111	0.0162

Table 7-3: Updated Pushover Analysis Calculations

	Using Paulay and Priestley						Experimental Test				
	Δy (in)	Δp (in)	Δu (in)	Fy (ksi)	Fu (ksi)	Lp (in)	Δy (in)	Δu (in)	Fy (ksi)	Fu (ksi)	Lp (in)
DCRCC1	1.62	9.98	11.60	12.30	12.62	18.18	2.28	4.62	10.63	13.43	18.50
FSRCC1	1.64	7.65	9.28	12.18	11.84	18.18	2.19	4.17	10.20	13.58	19.40
DCRCC24	1.60	10.66	12.25	33.86	37.33	23.01	2.82	8.08	33.00	43.75	24.50
FSRCC24	1.58	10.04	11.63	35.26	38.12	23.03	3.01	7.45	36.01	42.84	23.00
DCKJ24	0.95	8.06	9.02	16.94	20.73	16.14	2.44	9.02	18.76	20.61	19.15
FSKJ24	0.95	7.89	8.84	17.10	20.01	16.14	3.18	8.84	14.61	16.77	19.15
FSRCC24-M	1.61	9.71	11.33	36.49	43.40	23.03	2.77	11.33	31.85	42.96	23.00
FSKJ24-M	1.04	8.11	9.15	18.29	22.23	18.08	1.54	9.15	17.01	22.21	18.50

Δp: The plastic displacement,

Δu: The ultimate displacement,

Lp: The plastic hinge length

Table 7-4: Measured Force-Displacement in Positive Direction

	Mn (slab) kip-in	Mu (pile) kip-in	Mn(Slab)/ Mu(Pile)	Failure Place
DCRCC1	7562	1565	4.83	Pile
FSRCC1	4202	1468	2.86	Pile
DCRCC24	11320	5376	2.11	Pile
FSRCC24	7247	5489	1.32	Slab
DCKJ24	2782	1990	1.40	Pile
FSKJ24	2295	1921	1.20	Slab
FSRCC24-M	11320	6249	1.81	Pile
FSKJ24-M	5141	2134	2.40	Pile

Table 8-1: Caltrans Reinforcement Requirements[5] and Research Recommendations for T-Joints

	Caltrans	**Recommended**
Flexural Reinforcement	Not less than: $(Mn)_{slab}/(Mu)pile=1.2$	$(Mn)_{slab}/(Mu)pile=1.2$ + $A_{bt} = A_{bb} = 0.25\ A_{st}$ (Drop-Cap Joint) $A_{bt} = A_{bb} = 0.35\ A_{st}$ (Flat-Slab Joint)
J-bars and Vertical Stirrups inside the Joint	----------	$A_s^{j+s} = 1.05\ A_{st}$
Vertical Stirrups Outside the Joint	$A_s^{jv} = 0.2 \times A_{st}$	$A_s^{jv} = 0.2 \times A_{st}$ (Drop Cap-joint T-joint) $A_s^{jv} = 0.3 \times A_{st}$ (Flat Slab-joint T-joint)
Horizontal Stirrups	$A_s^{jh} = 0.1 \times A_{st}$	$A_s^{jh} = 0.1 \times A_{st}$
Horizontal Side Reinforcement	$A_s^{sf} \geq \begin{cases} 0.1 \times A_{cap}^{top} \\ \text{or} \\ 0.1 \times A_{cap}^{bot} \end{cases}$	$A_s^{sf} \geq \begin{cases} 0.1 \times A_{cap}^{top} \\ \text{or} \\ 0.1 \times A_{cap}^{bot} \end{cases}$
Transverse Reinforcement	$\rho_{s\,min}=3.5\sqrt{f_c'}/f_y$(psi) $\rho_s = 0.4 \times \frac{A_{st}}{l_{ac}^2}$	Not less than $A_s = 0.18\ A_{st}$

Table 8-2: Caltrans Reinforcement Requirements[5] and Research Recommendations for Knee-Joints

	Caltrans	Recommended	
Flexural reinforcement	A_s^{u-bar} min $= 0.33 \times A_{st}$ Not less than: $(Mn)_{slab}/(Mu)pile=1.2$	$(Mn)_{slab}/(Mu)pile=1.2$ + A_s^{u-bar} min $= 0.35 \times A_{st}$	
J-bars and Vertical Stirrups inside the Joint	----------	$A_s^{j+s} = 0.85\ A_{st}$	
Vertical Stirrups Outside the Joint	$A_s^{jv} = 0.2 \times A_{st}$	$A_s^{jv} = 0.2 \times A_{st}$	
Horizontal Stirrups	$A_s^{jh} = 0.1 \times A_{st}$	$A_s^{jh} = 0.1 \times A_{st}$	
Horizontal Side Reinforcement	$A_s^{sf} \geq \begin{cases} 0.1 \times A_{cap}^{top} \\ \text{or} \\ 0.1 \times A_{cap}^{bot} \end{cases}$	$A_s^{sf} \geq \begin{cases} 0.1 \times A_{cap}^{top} \\ \text{or} \\ 0.1 \times A_{cap}^{bot} \end{cases}$	
Horizontal Cap End Ties	$A_s^{jhc} = 0.33 \times A_s^{u-bar}$ min	$A_s^{jhc} = 0.33 \times A_s^{u-bar}$ min	
Transverse Reinforcement	$\rho_s = 0.6 \times \frac{\rho_l D_c}{l_{ac}}$	Not less than $A_s = 0.18\ A_{st}$	S < Dc/2*
	$\rho_s = 0.4 \times \frac{A_{st}}{l_{ac}^2}$		Dc/2 < S <Dc or Ld*
* For clarification see Figure 8-3			

Table 8-3: Test Ductility and Drift Summary

DCRCC1	FSRCC1	DCRCC24	FSRCC24	DCKJ24	FSKJ24	FSRCC24-M	FSKJ24-M
Ductility at Peak Load							
2	2	3	2.5	1.5	1.5	3.5	3
Ductility at 80% of Peak Load							
2.8	3.9	3	2.5	3.9	2.5	5	6
Drift at Peak Load							
3.7%	3.4%	5.6%	5.1%	3.8%	5.1%	10%	4.8%
Drift at 80% Peak Load							
5.3%	6.6%	5.6%	5.1%	10.1%	9%	13.6%	10.1%

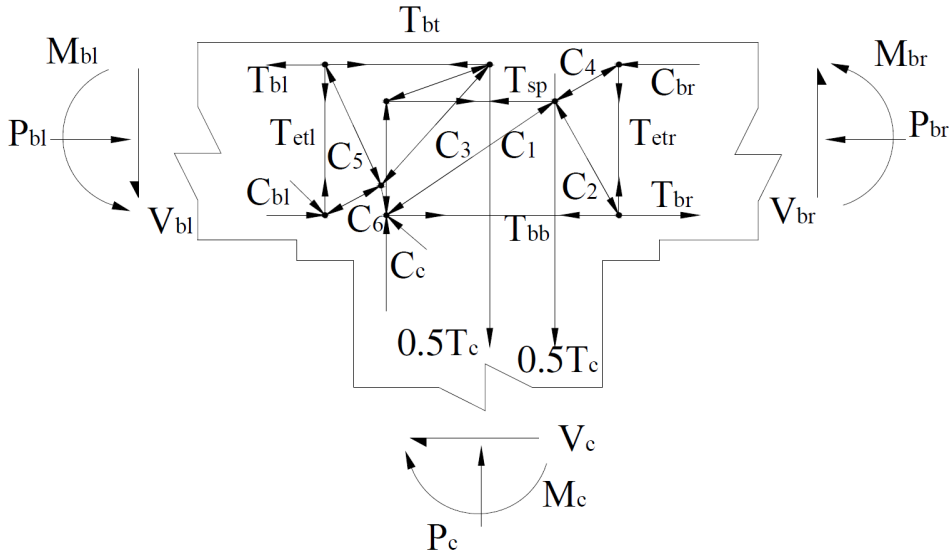

Figure 1-1: Modified External Joint Transfer Strut-and-Tie Model[1]

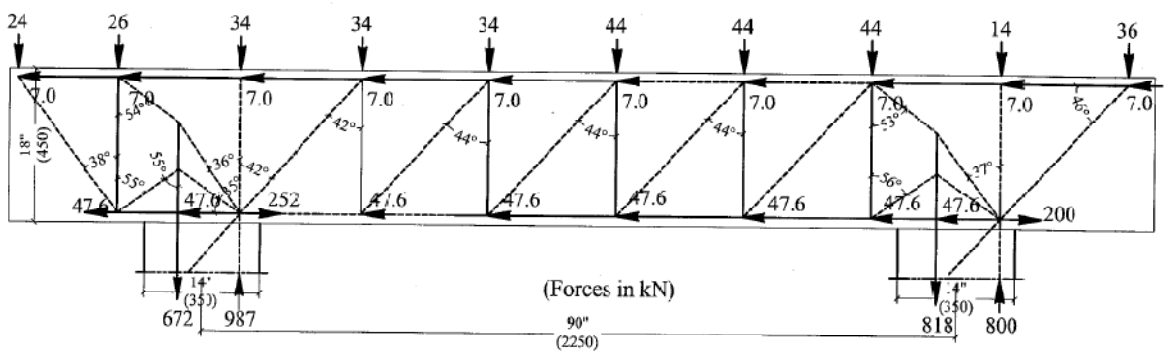

Figure 1-2: Model Forces in D-Region of Short Specimen Beam[2]

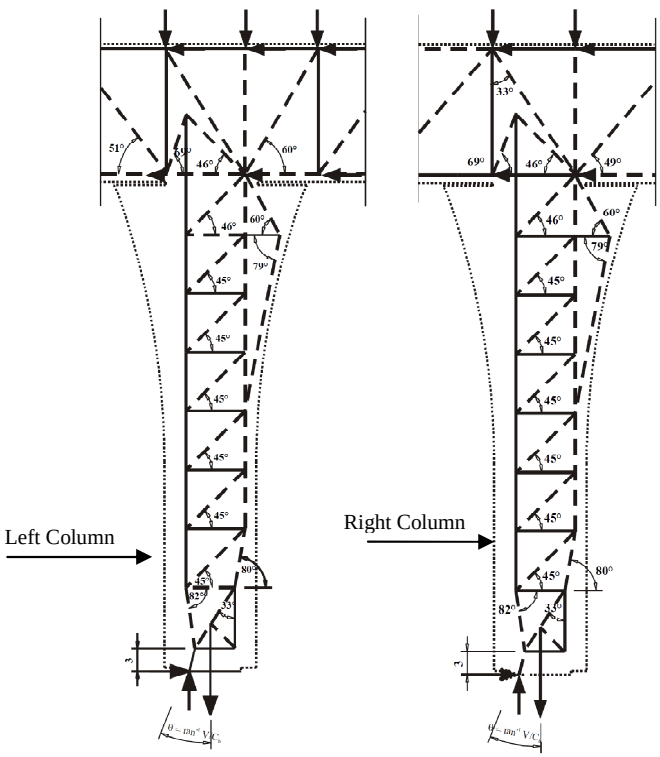

Figure 1-3: Stut-and-Tie Model for Flared Column Bent[3]

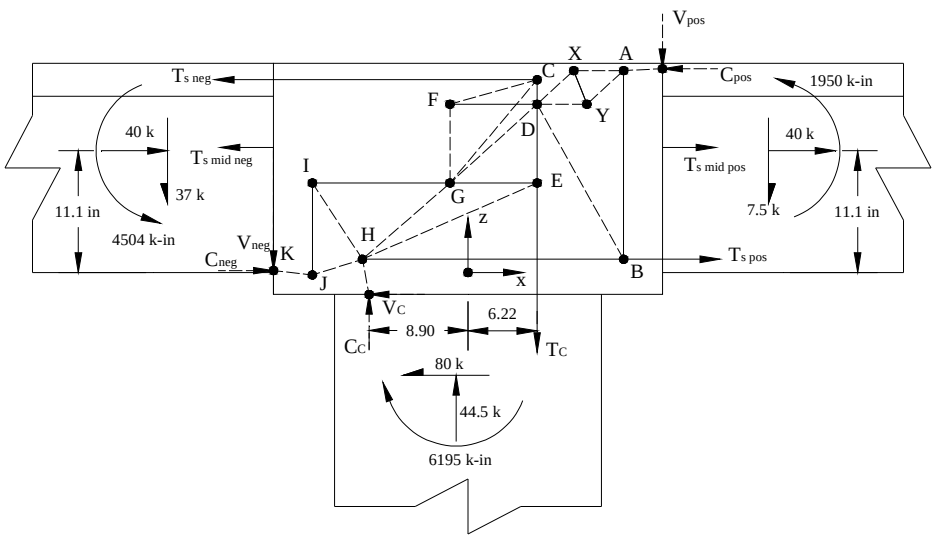

Figure 1-4: UGNP 2-D Strut-and-Tie Model[4]

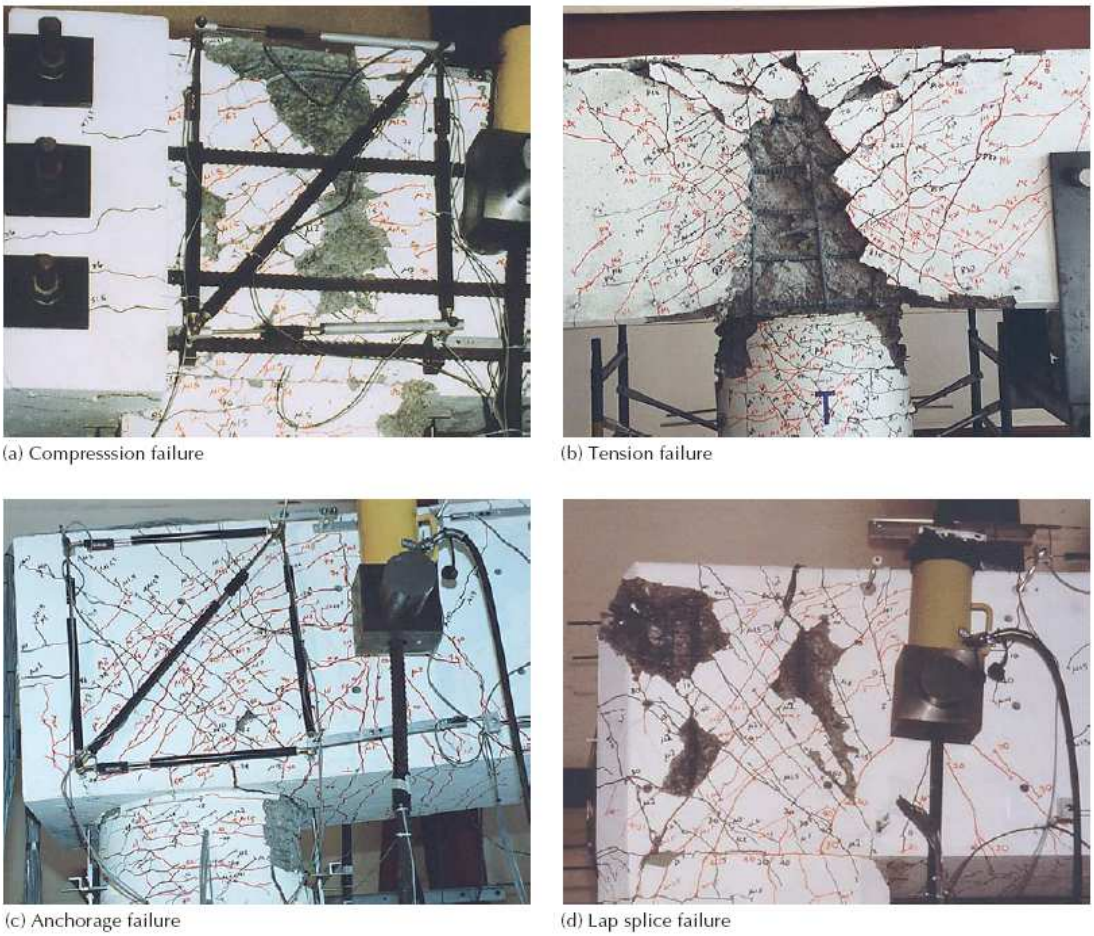

Figure 1-5: Four Different Joint Failure Modes[6]

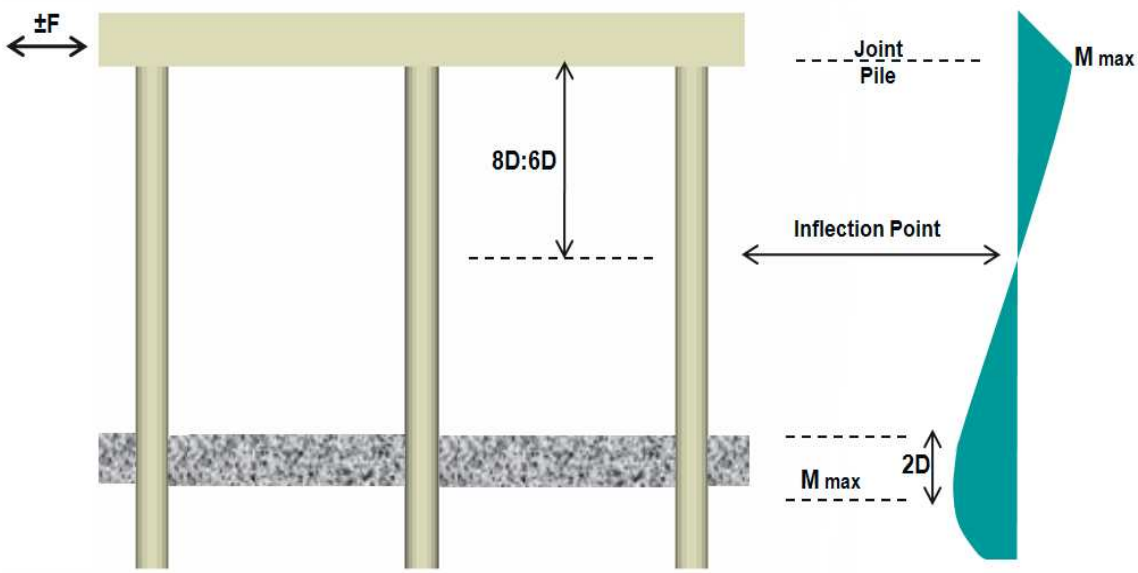

Figure 2-1: Inelastic Deformations of Bridge Piles (Test Model)

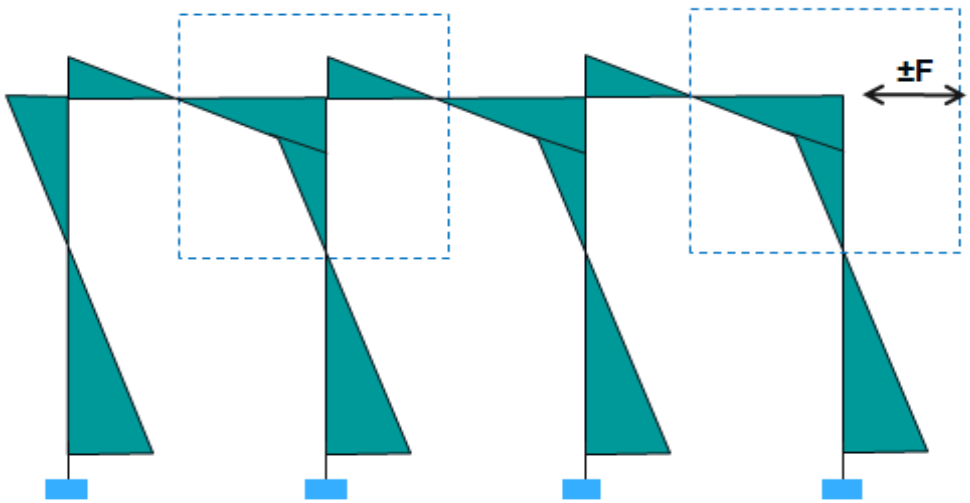

Figure 2-2: Moment Diagram in the Transverse Direction of the Bridge

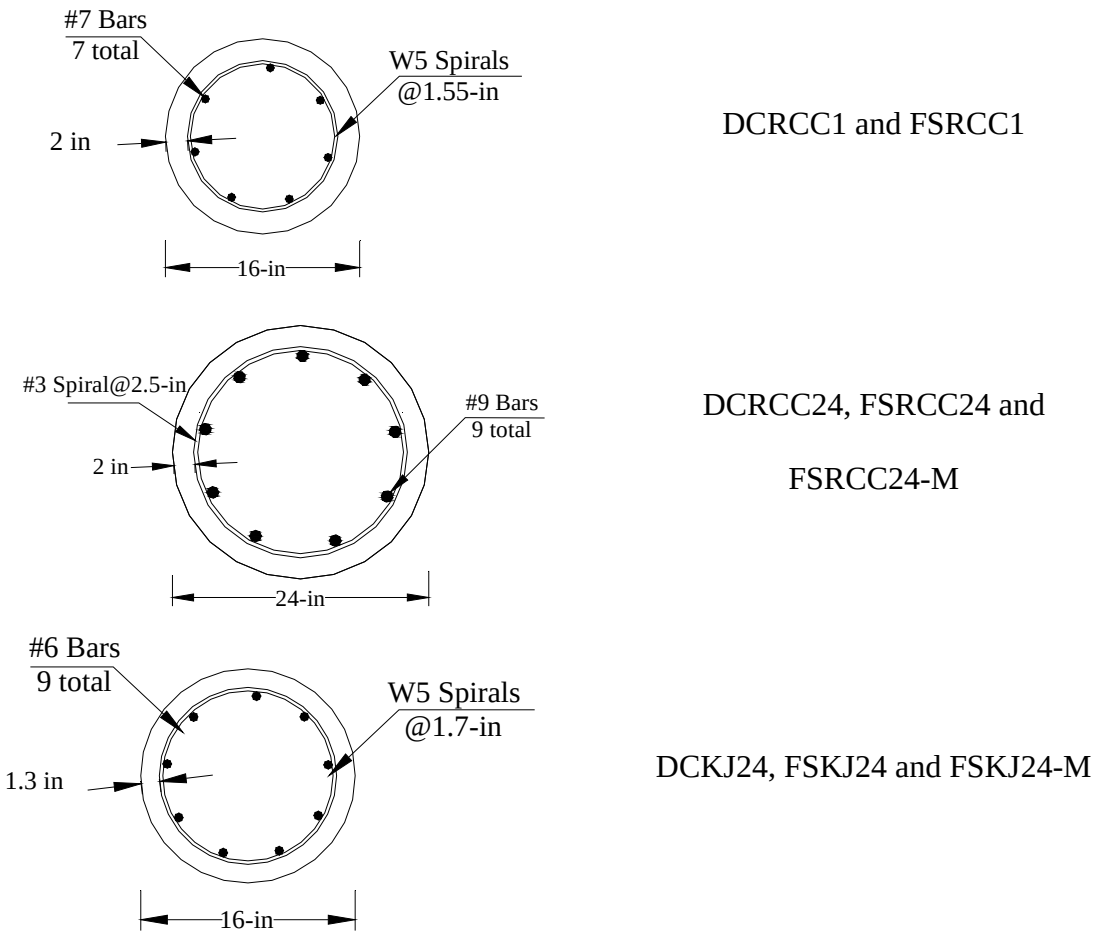

Figure 2-3: Piles Reinforcment and Dimensions

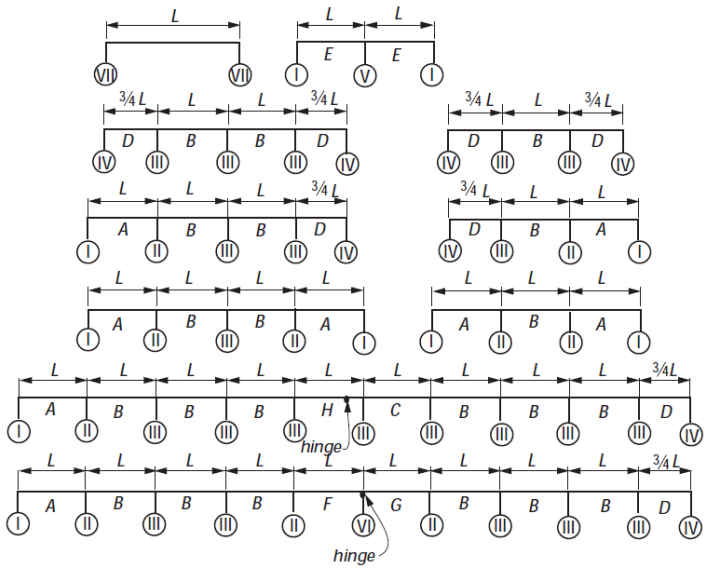

Figure 2-4: Support Types

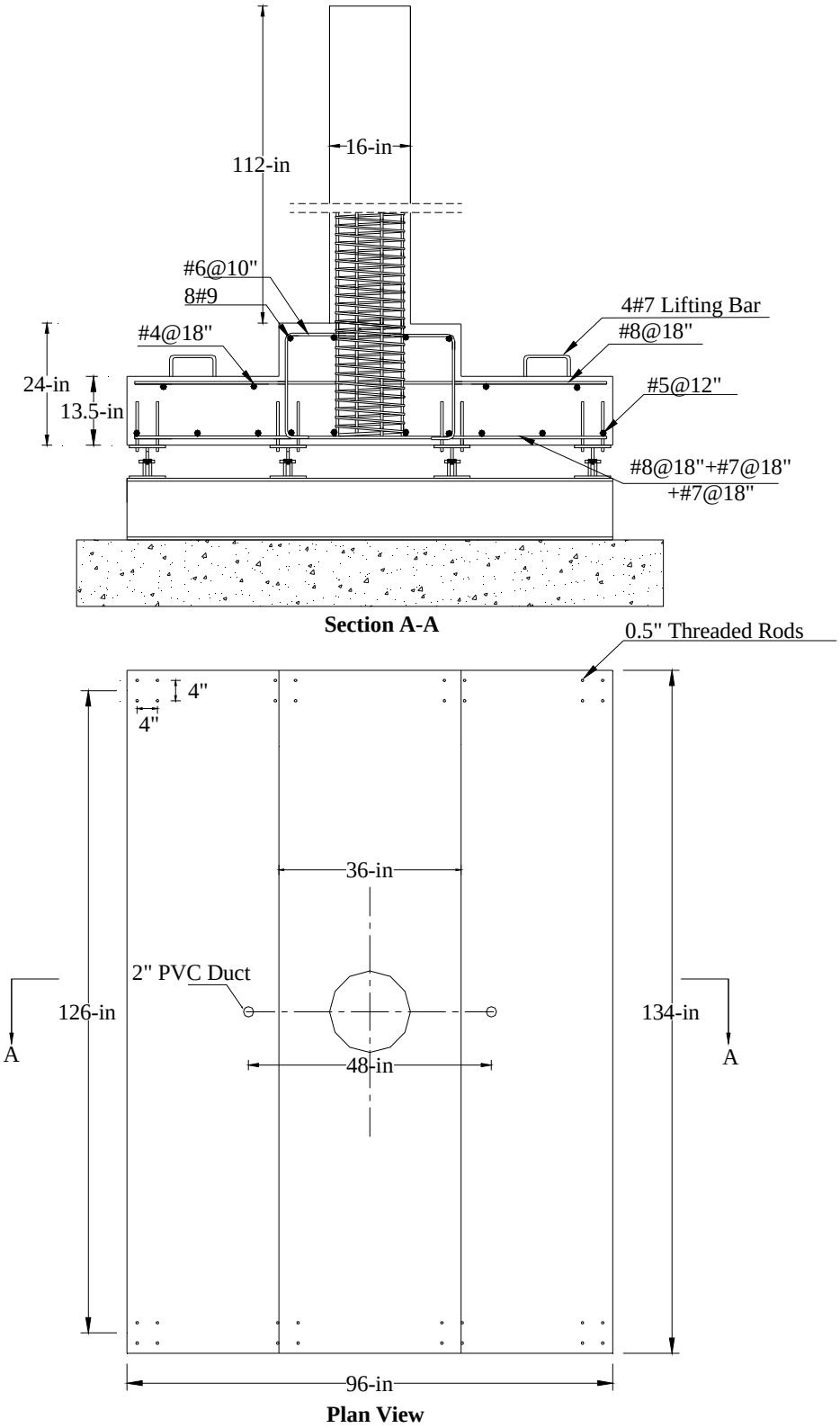

Figure 2-5: Dimensions and Reinforcement Details for Specimen DCRCC1

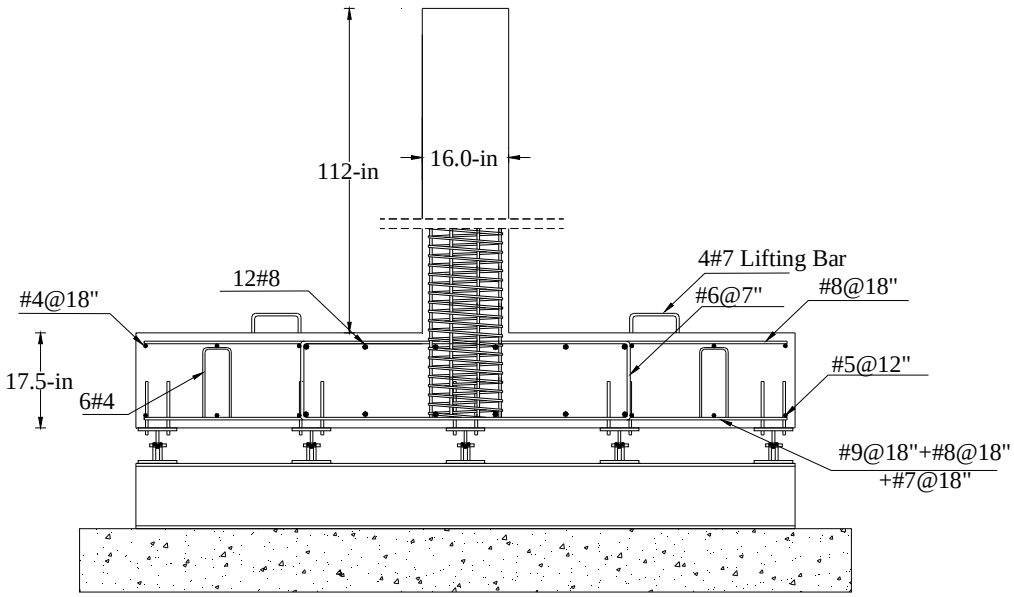

Section A-A

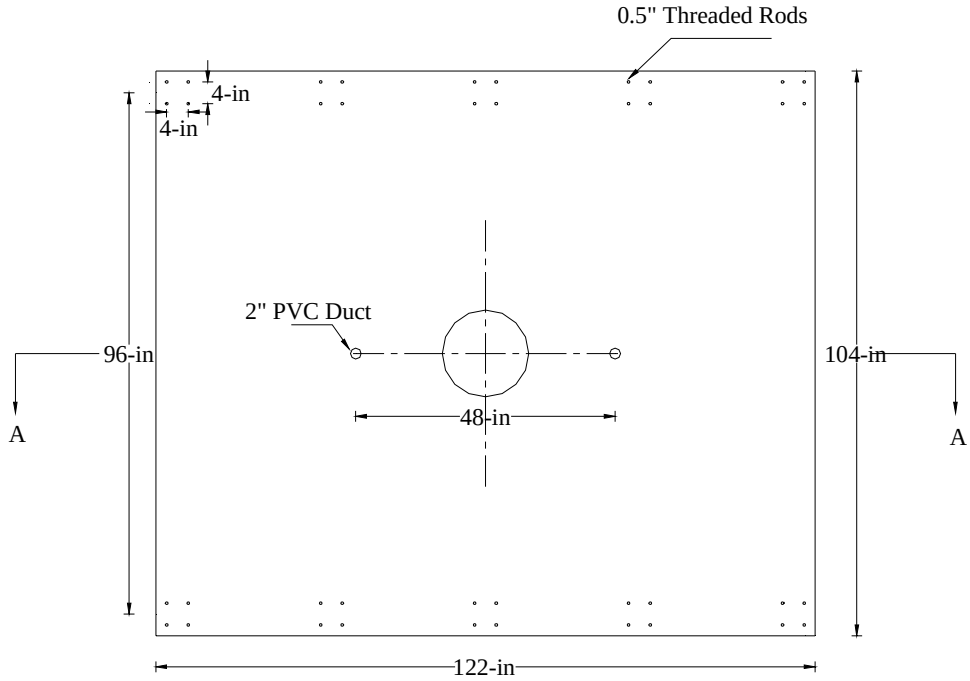

Plan View

Figure 2-6: Dimensions and Reinforcement Details for Specimen FSRCC1

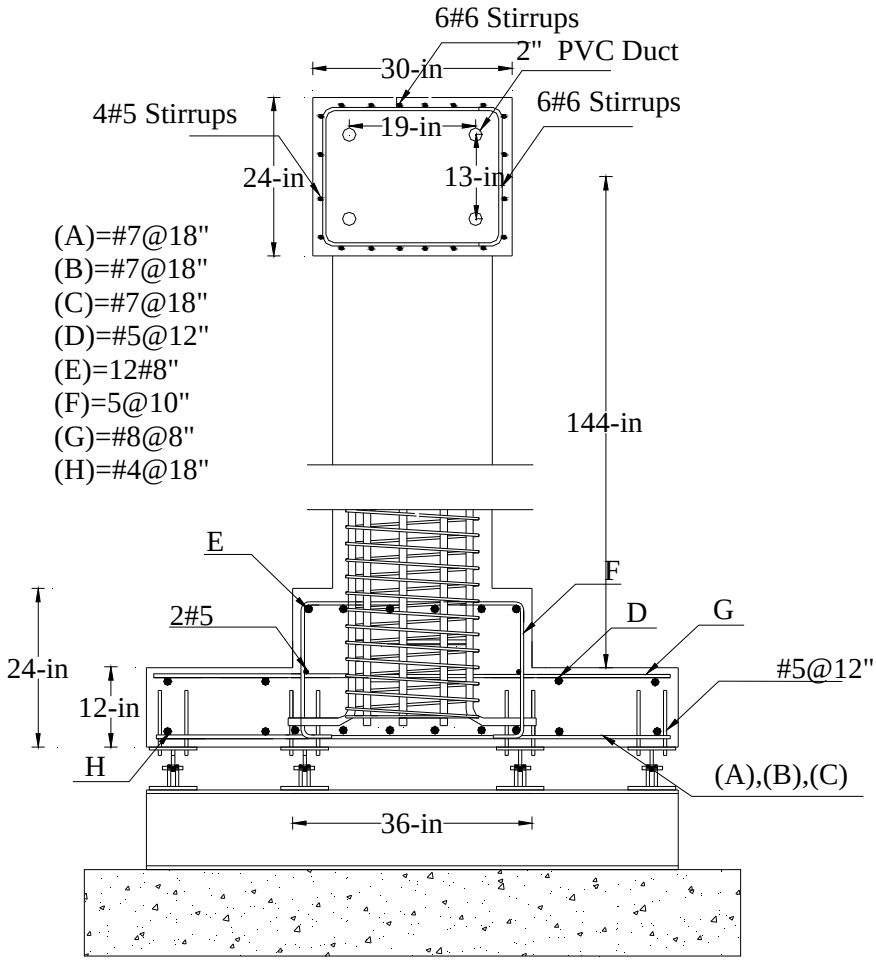

Section A-A

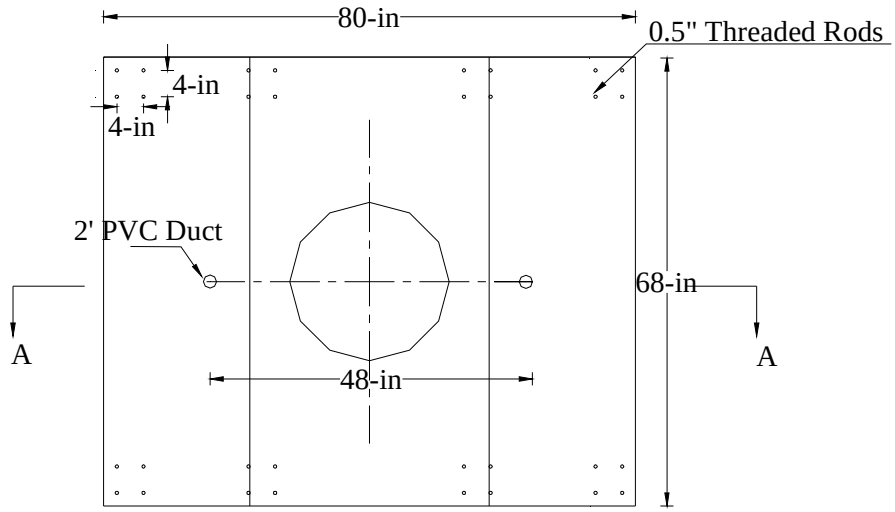

Plan View

Figure 2-7: Dimensions and Reinforcement Details for Specimen DCRCC24

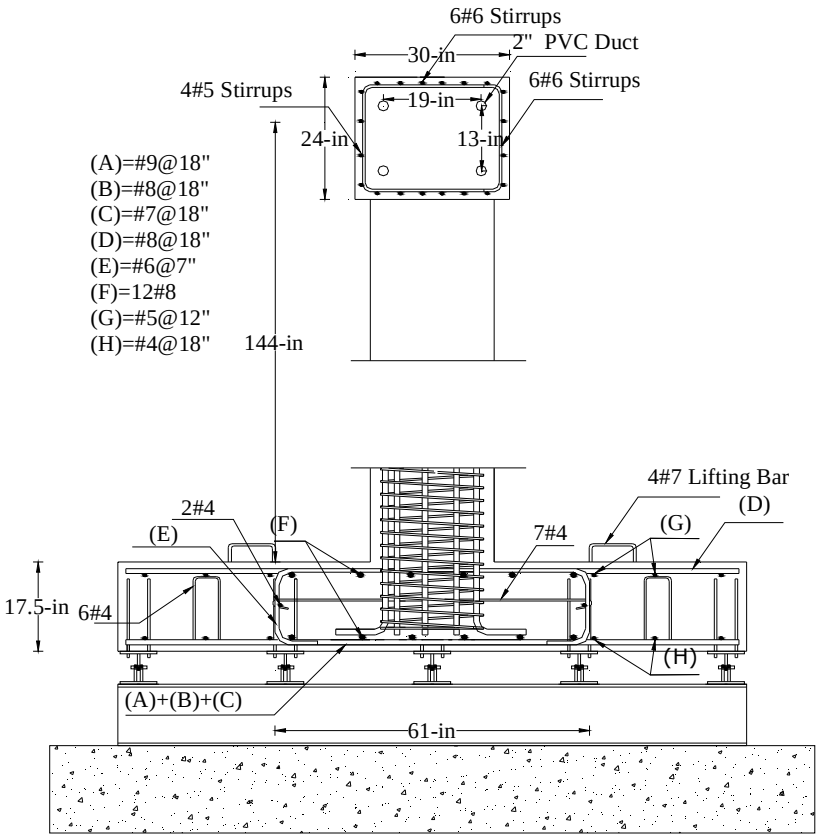

Section A-A

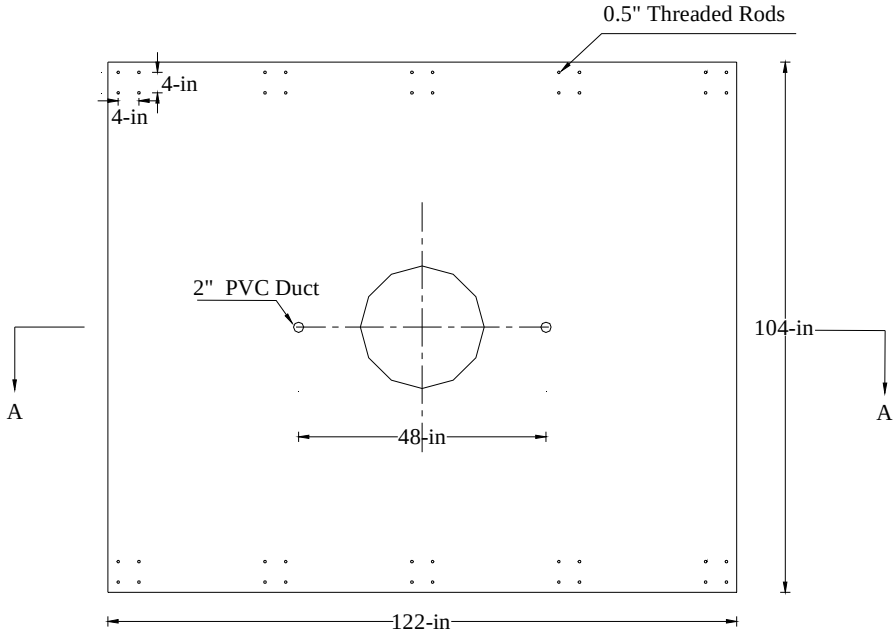

Figure 2-8: Dimensions and Reinforcement Details for Specimen FSRCC24

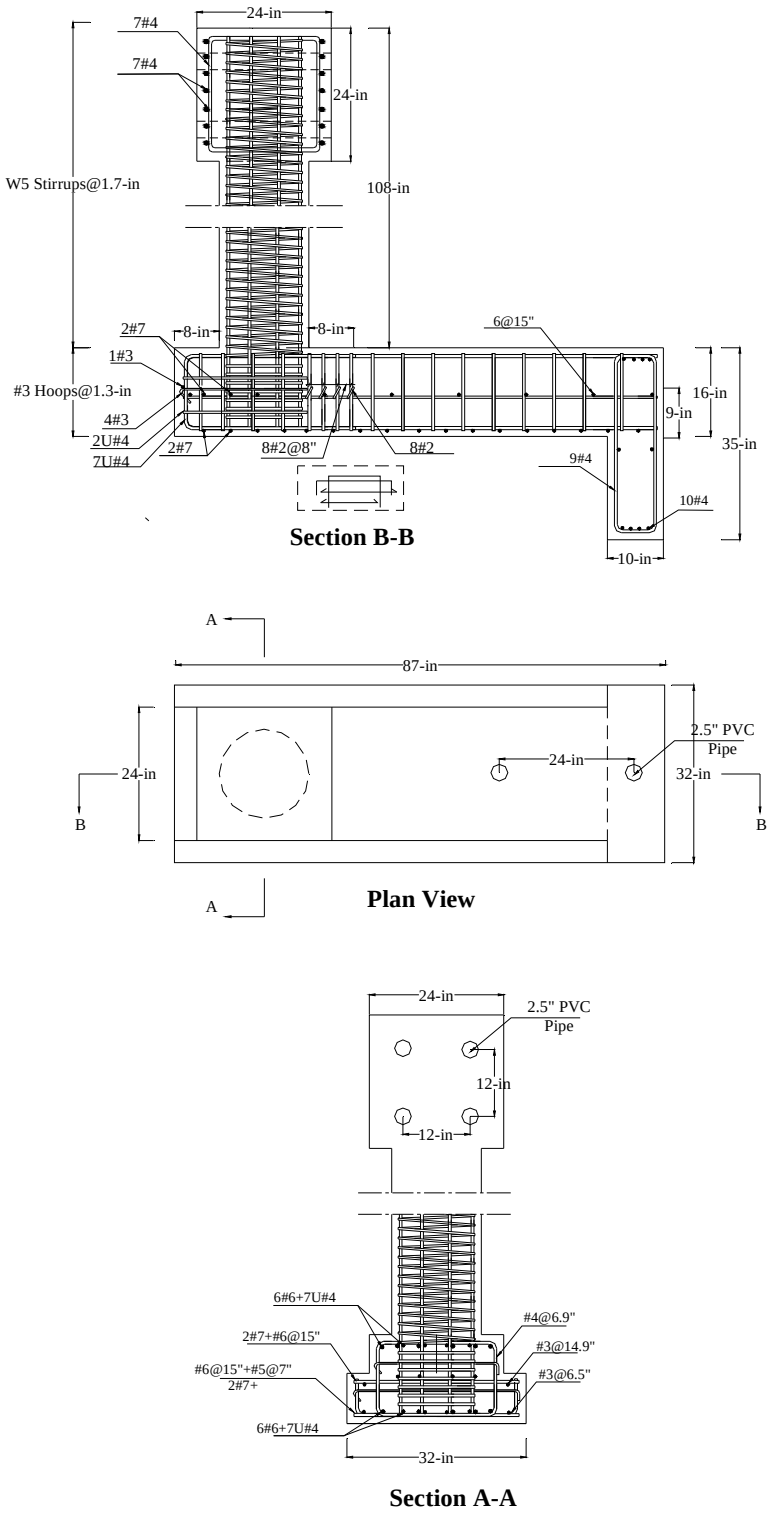

Figure 2-9: Dimensions and Reinforcement Details for Specimen DCKJ24

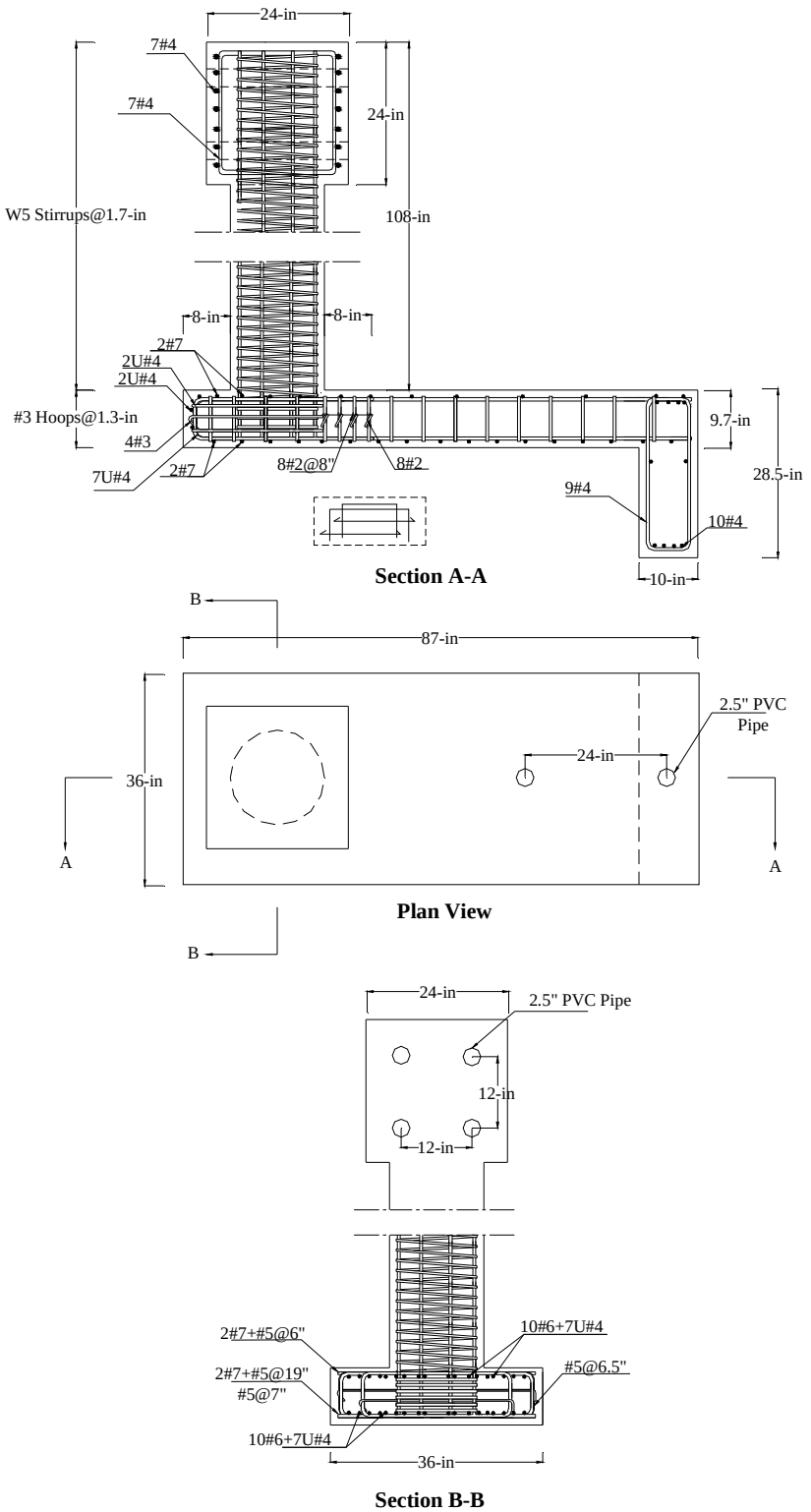

Figure 2-10: Dimensions and Reinforcement Details for Specimen FSKJ24

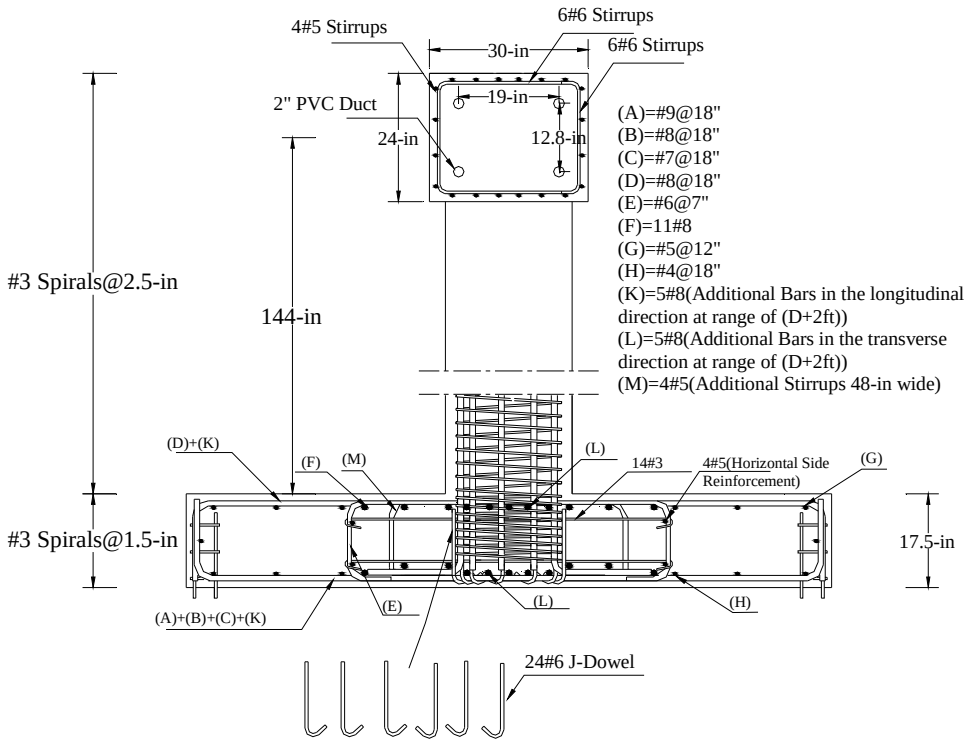

Section A-A

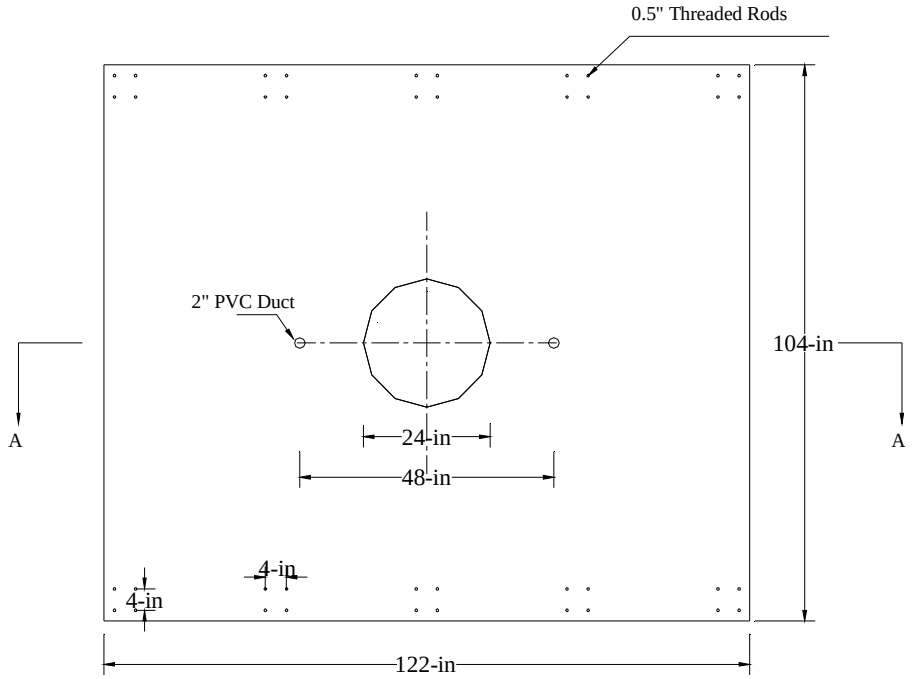

Plan View

Figure 2-11: Dimensions and Reinforcement Details for Specimen FSRCC24-M

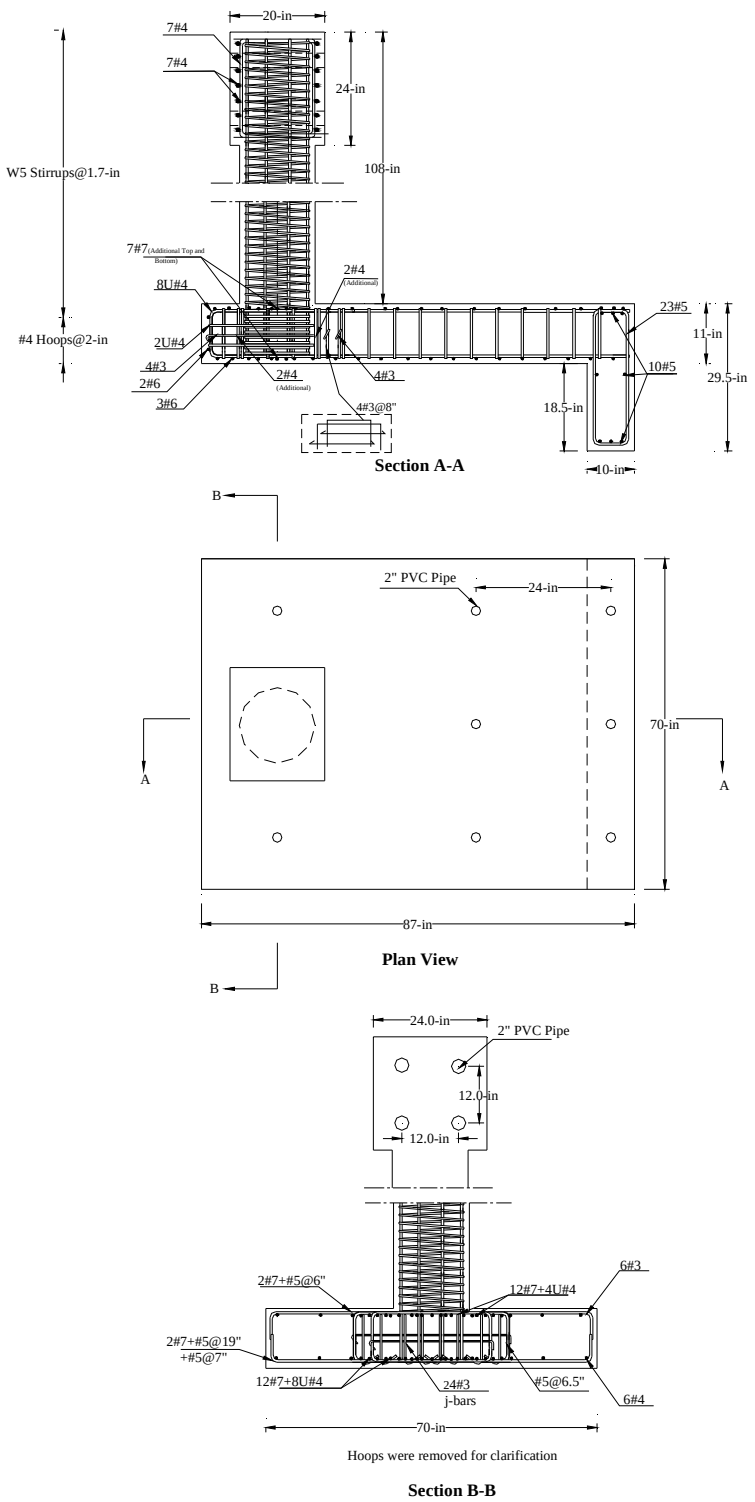

Figure 2-12: Dimensions and Reinforcement Details for Specimen FSKJ24(M)

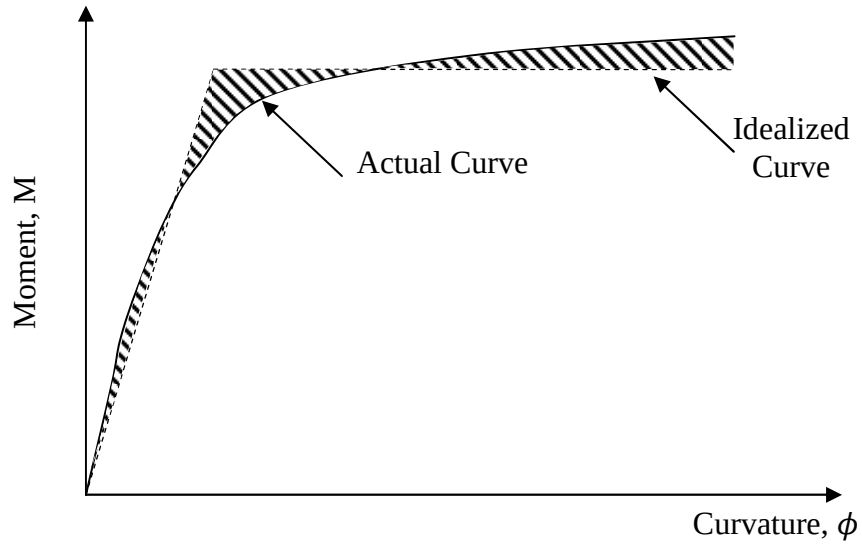

Figure 2-13: Moment Curvature Curve

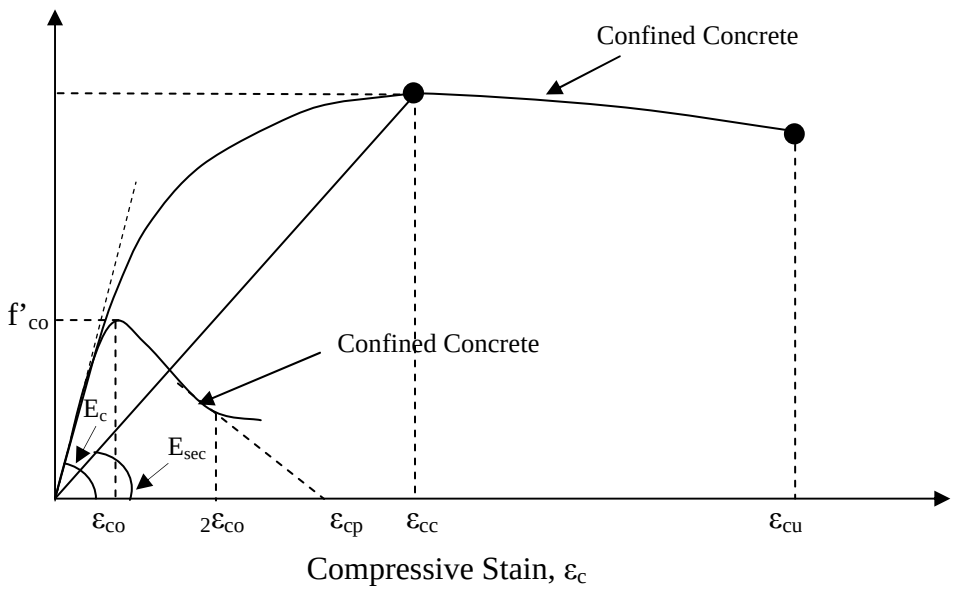

Figure 2-14: Confined and Unconfined Concrete Model[19]

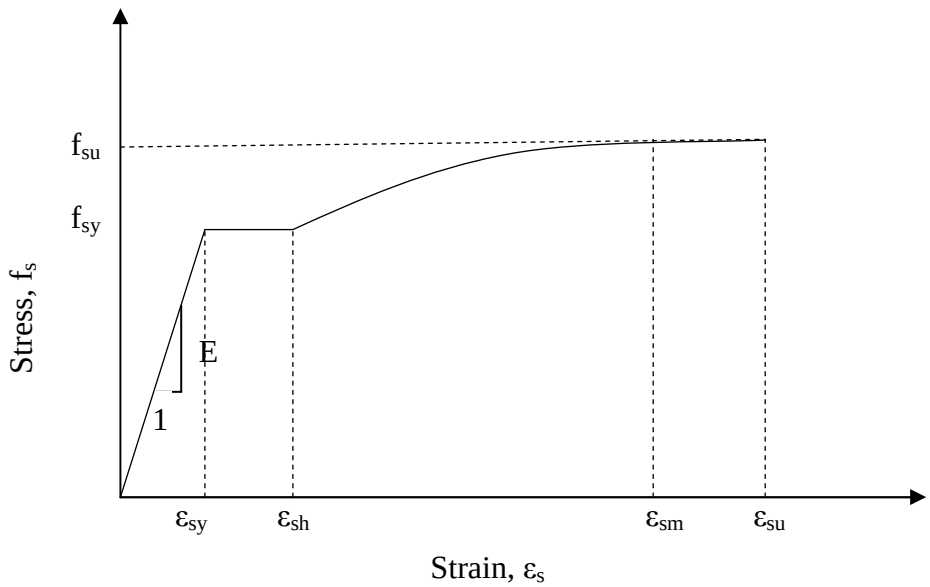

Figure 2-15: Steel Stress Strain Model

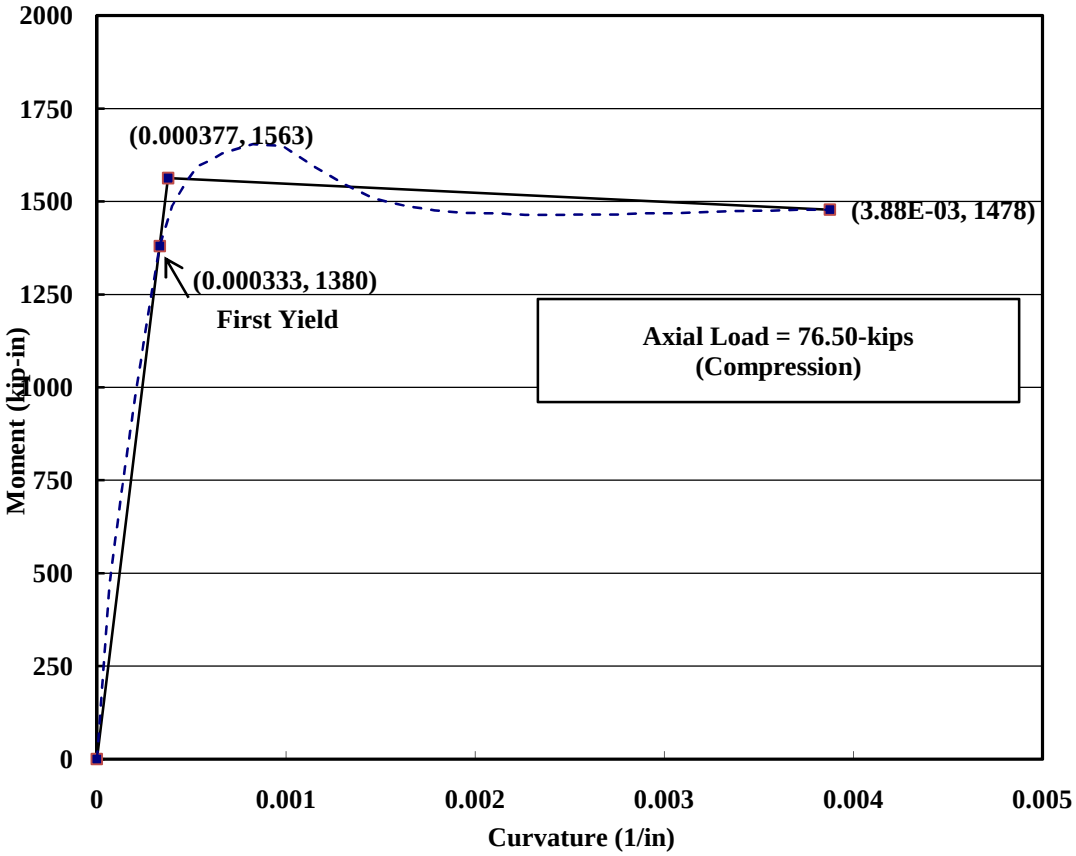

Figure 2-16: DCRCC1 Pile M-ϕ

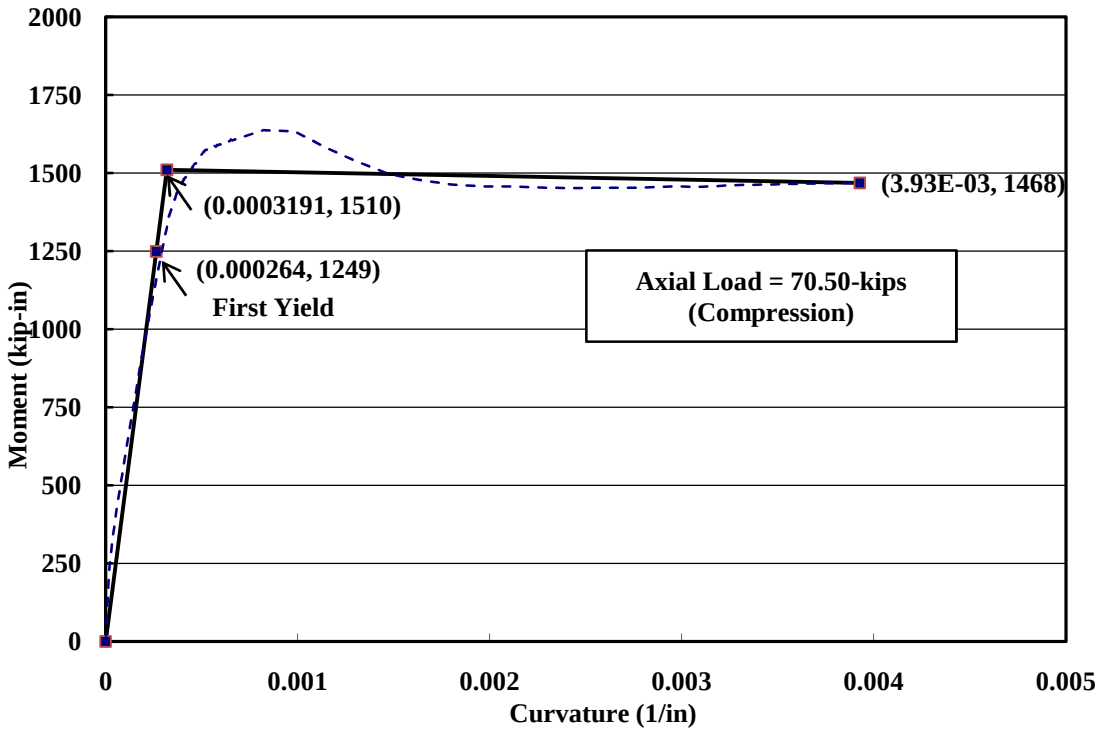

Figure 2-17: FSRCC1 Pile M-ϕ

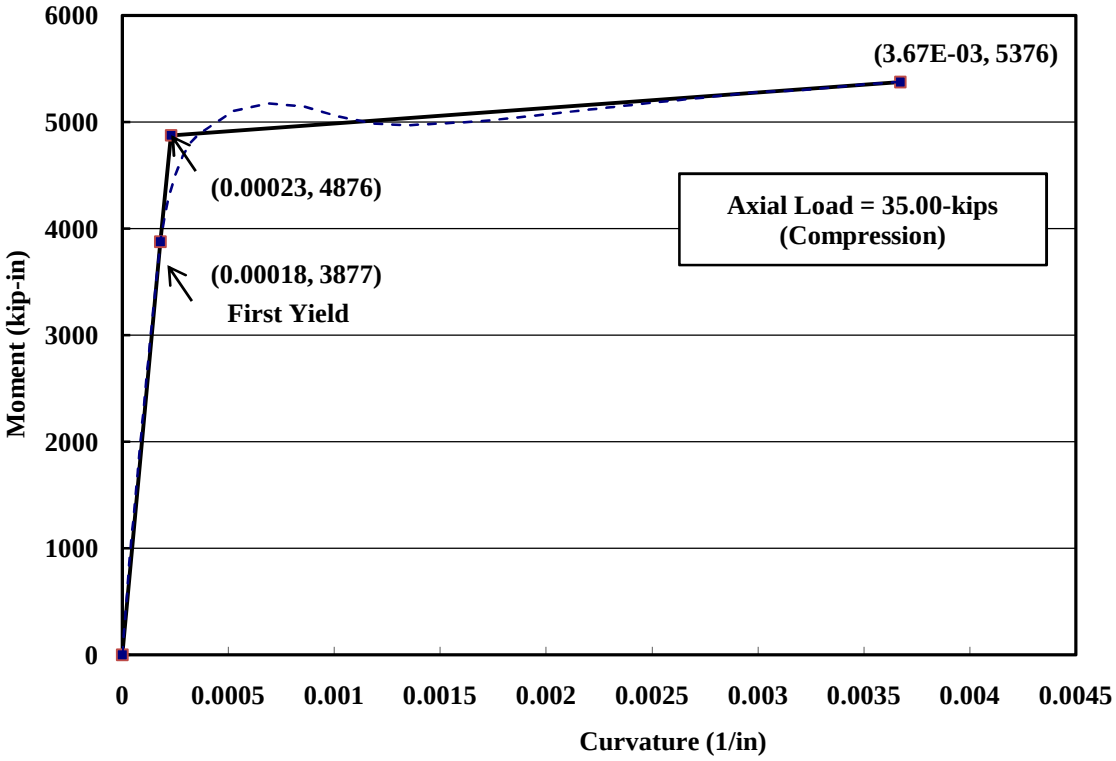

Figure 2-18: DCRCC24 Pile M-ϕ

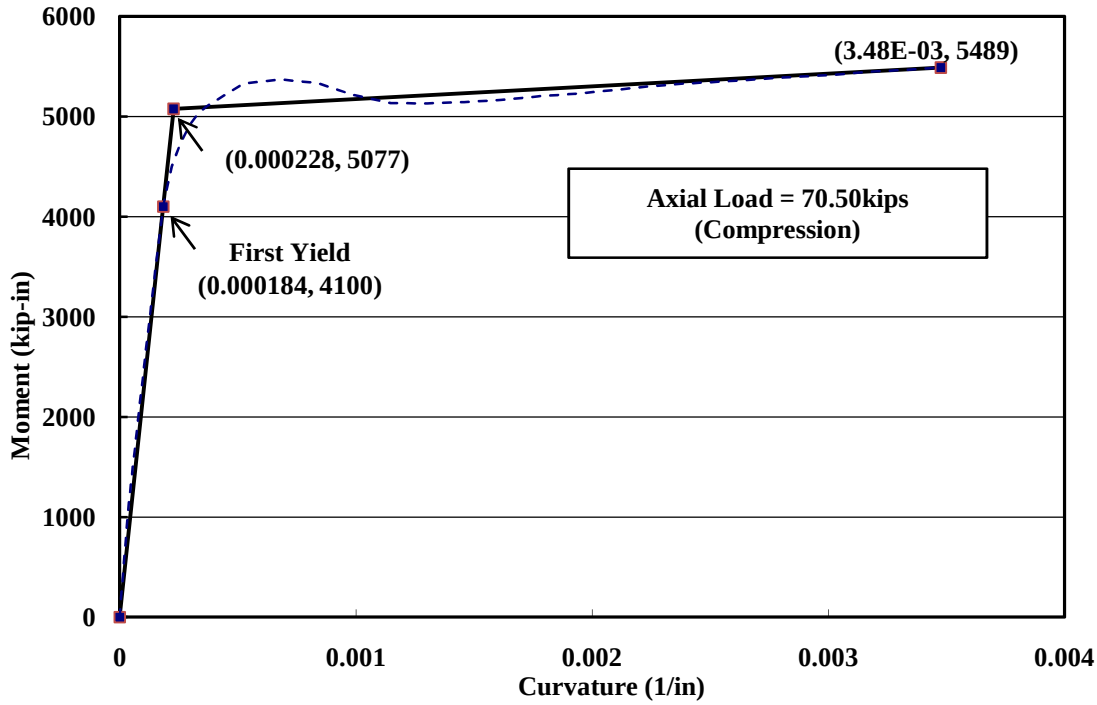

Figure 2-19: FSRCC24 and FSRCC24-M Pile M-ϕ

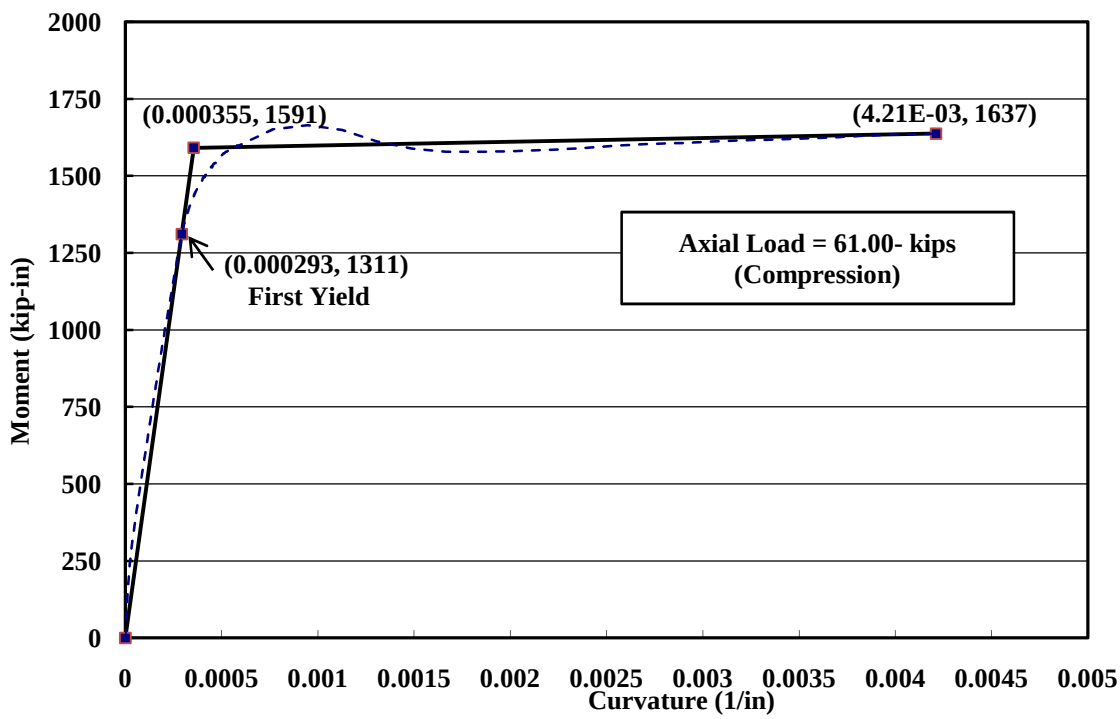

Figure 2-20: DCKJ24 Pile M-ϕ

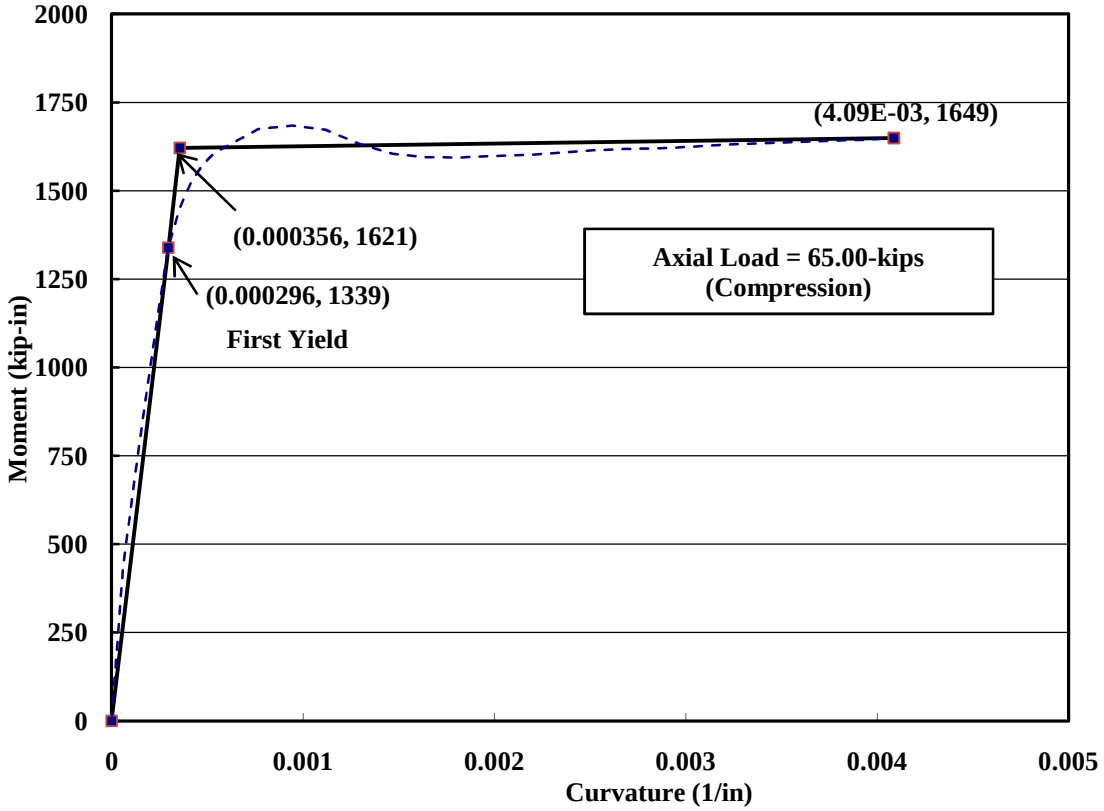

Figure 2-21: FSKJ24 and FSKJ24-M Pile M-ϕ

a) Reinforcment of Specimen FSRCC24-M

b) Reinforcement of Specimen FSKJ24-M

Figure 3-1: Slab Reinforcement Prior to Cast

Figure 3-2: FSRCC24 Casting

Figure 3-3: FSRCC24 and DCRCC24 Sonotube Placement

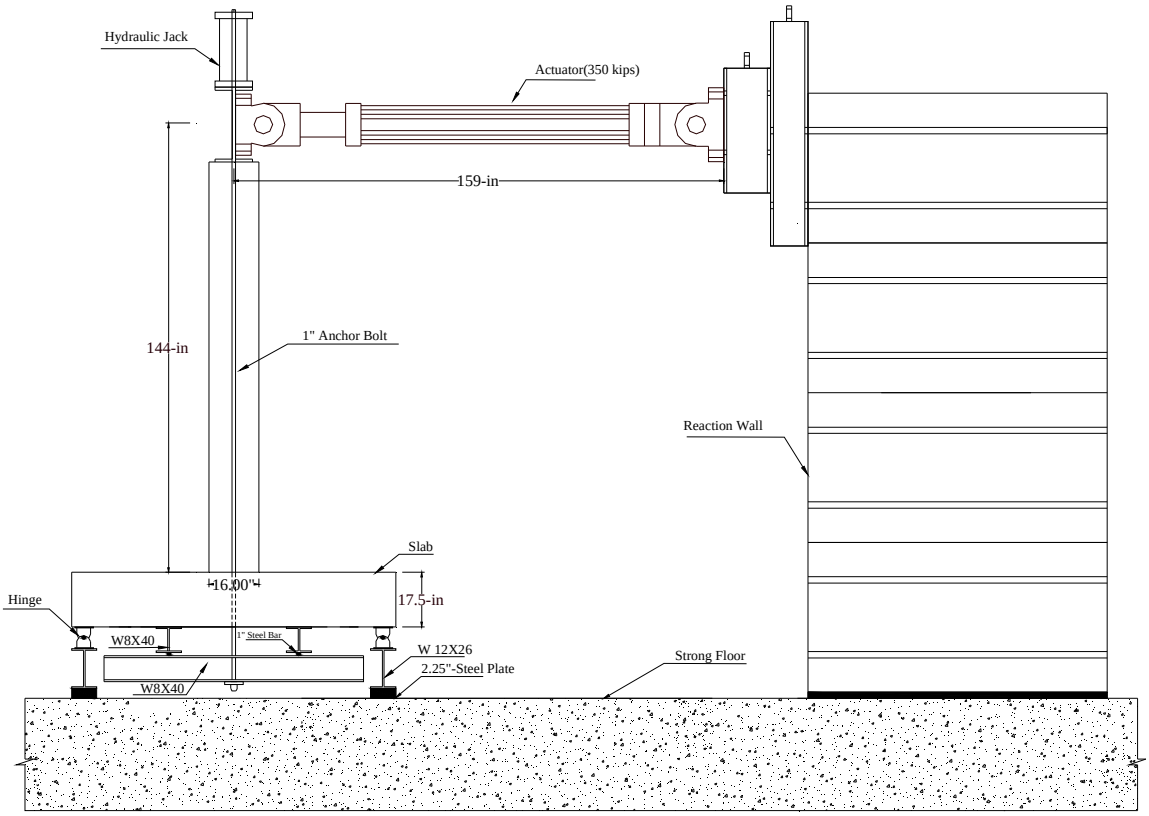

Figure 3-4: Experimental Test Set-Up Schematic for Specimen FSRCC1

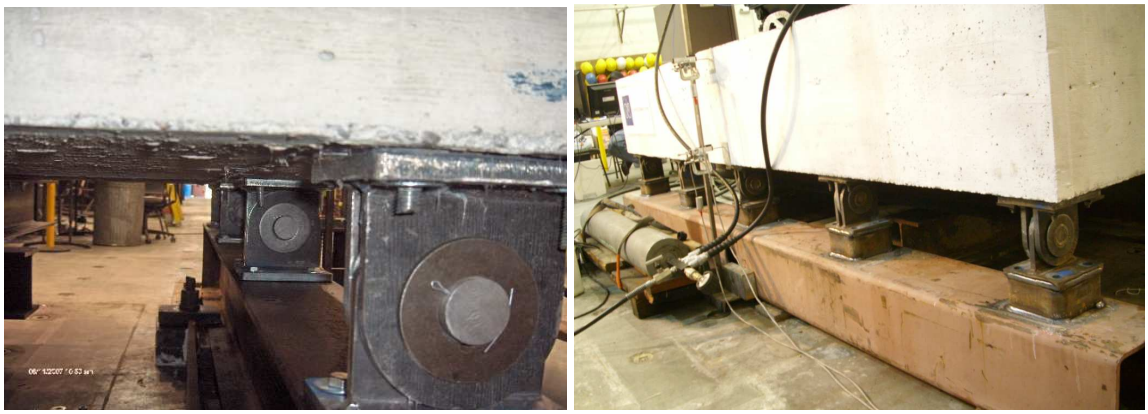

Figure 3-5: Hinge Locations

Figure 3-6: Experimental Test Set-Up for Specimen DCRCC1

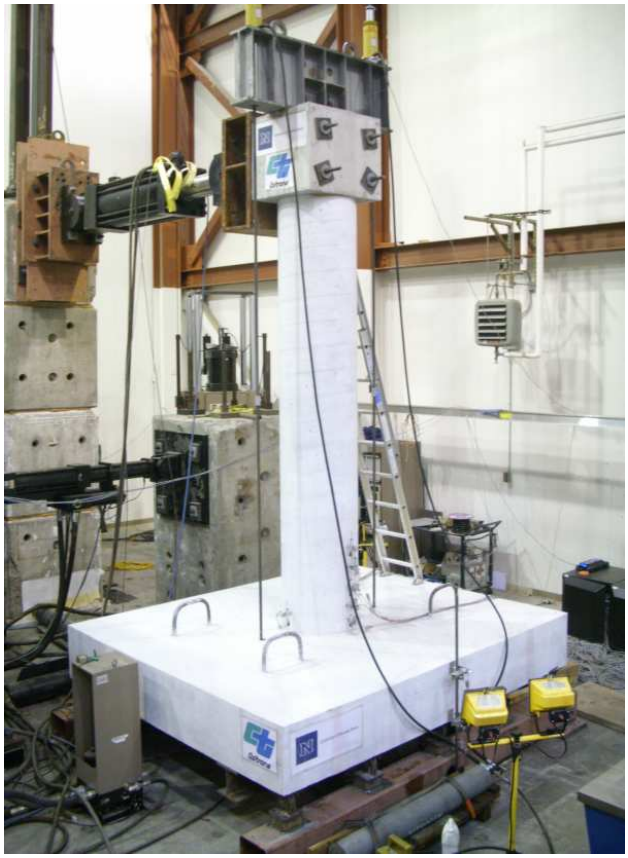

Figure 3-7: Experimental Test Set-Up for Specimen FSRCC24-M

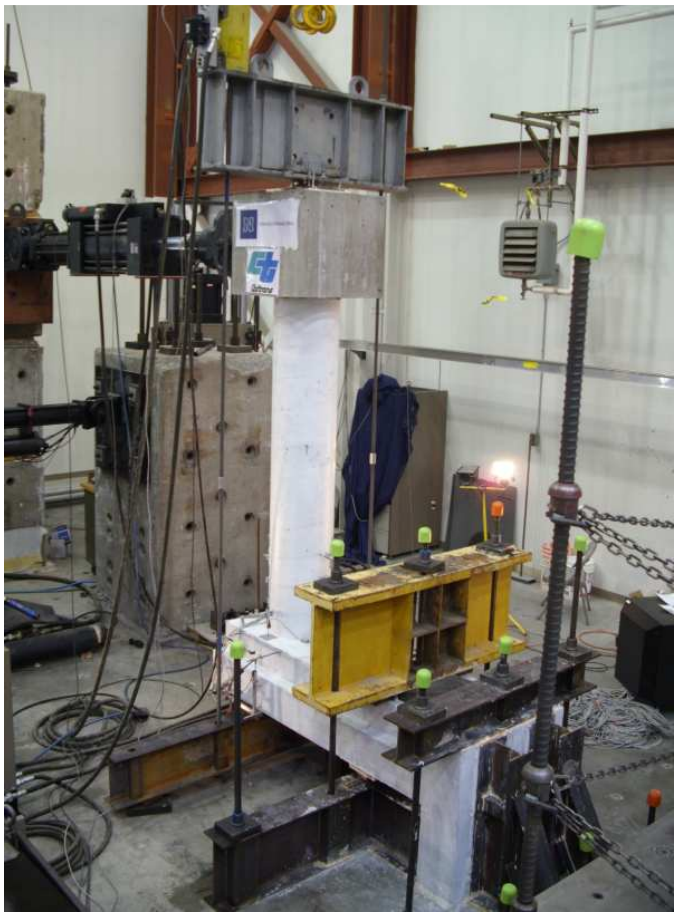

Figure 3-8: Experimental Test Set-Up for Specimen DCKJ24

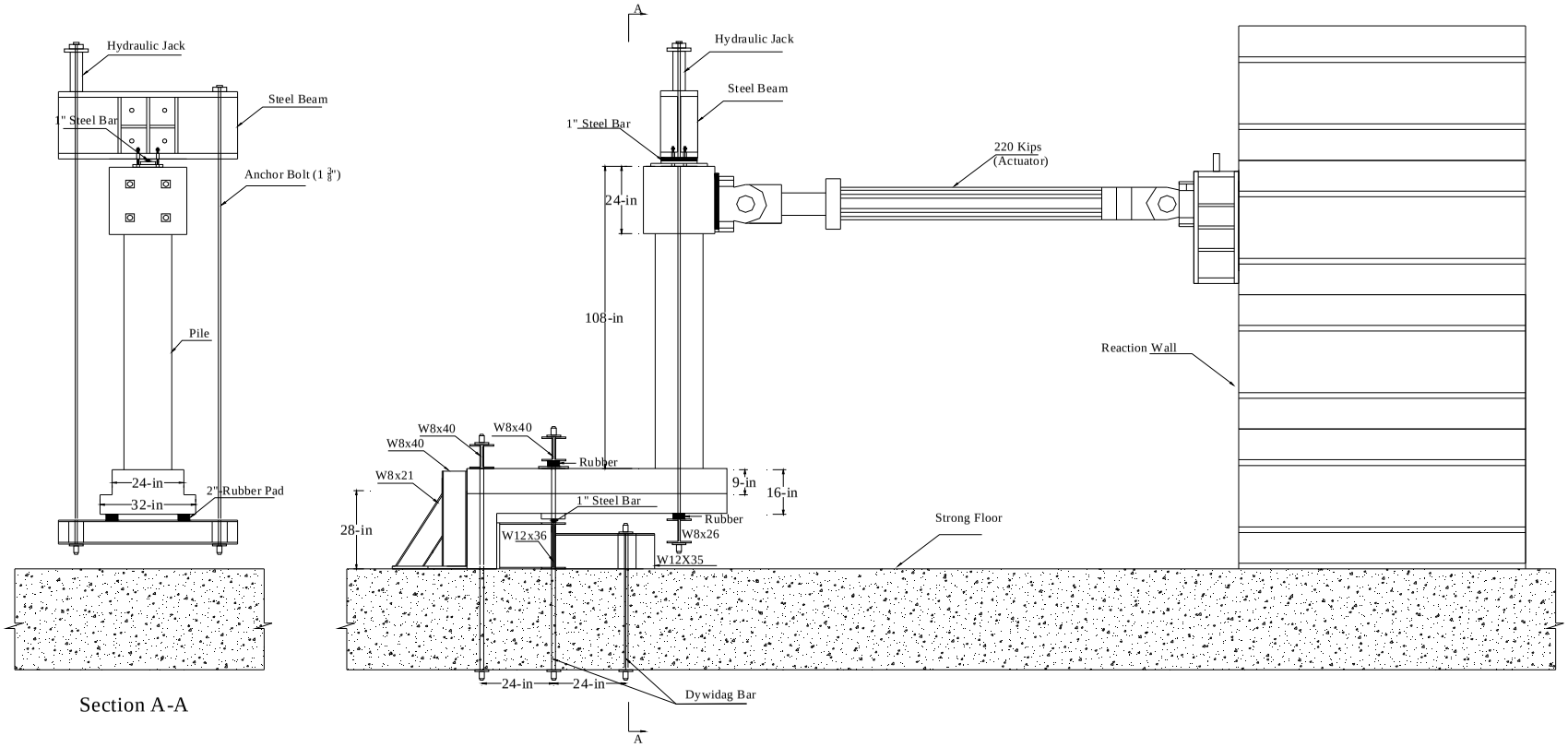

Figure 3-9: Experimental Test Set-Up Schematic for Specimen DCKJ24

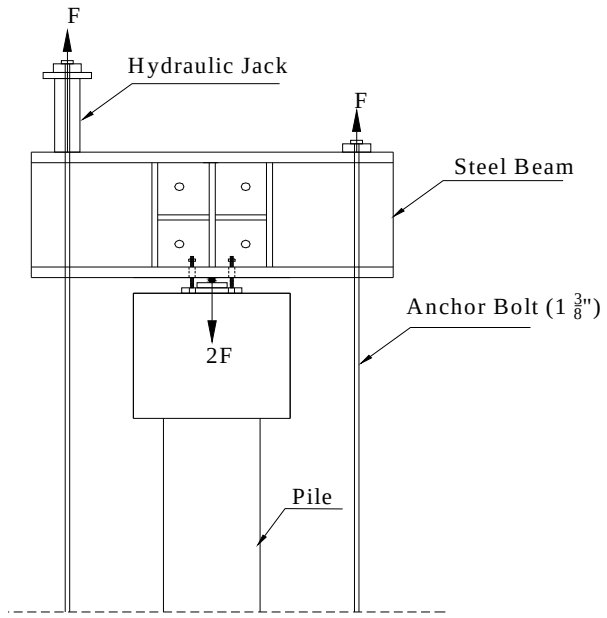

Figure 3-10: Variable Axial Load Mechanism

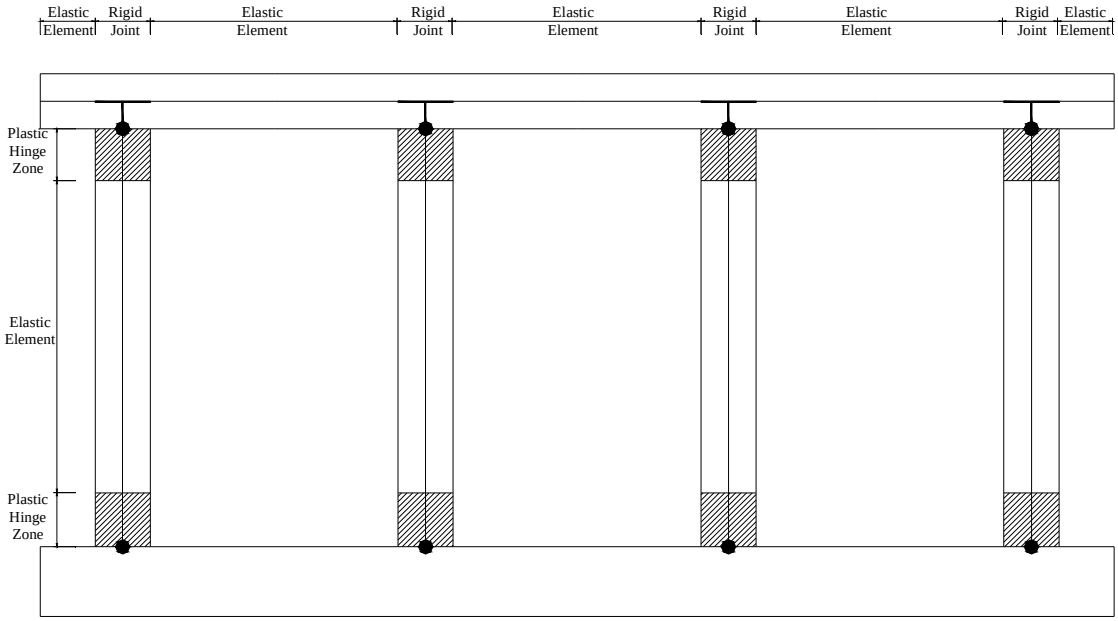

Figure 3-11: SAP2000 Lumped Plasticity Model

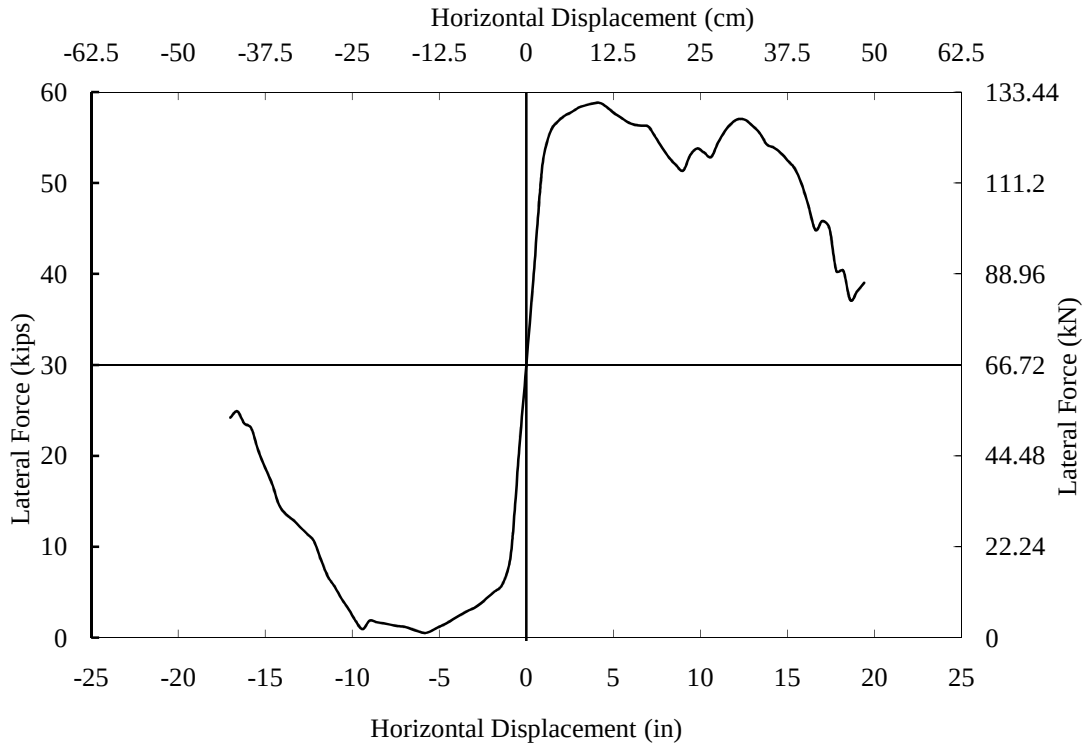

Figure 3-12: DCKJ24 Axial Loading Protocol

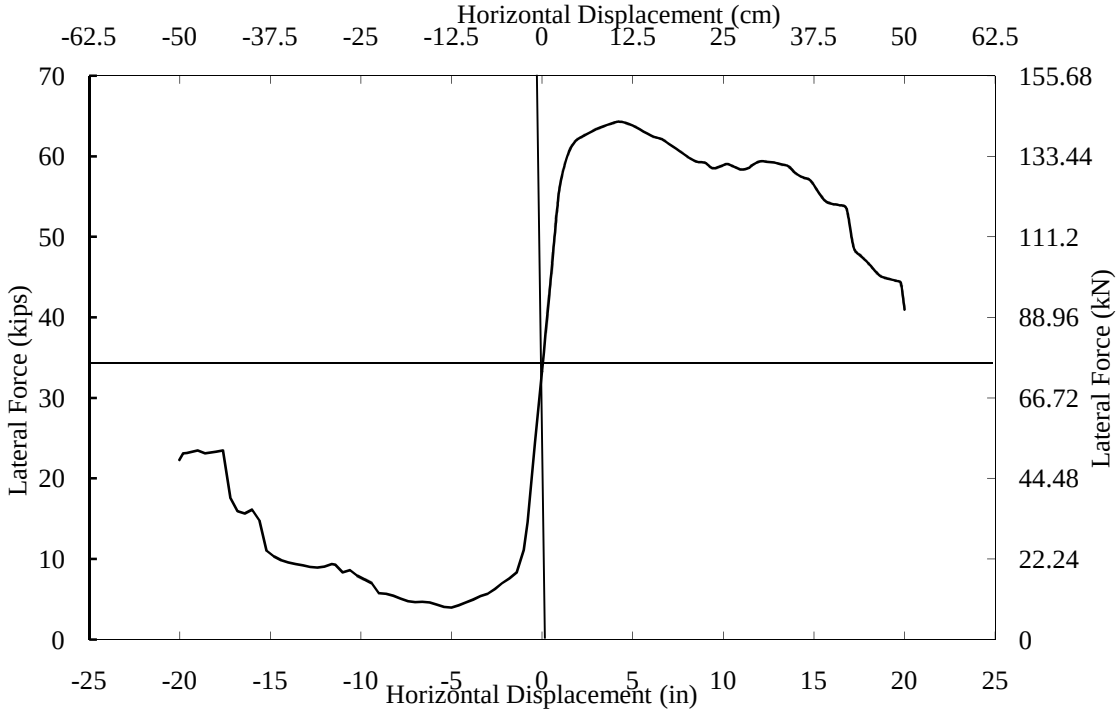

Figure 3-13: FSKJ24 and FSKJ24-M Axial Loading Protocol

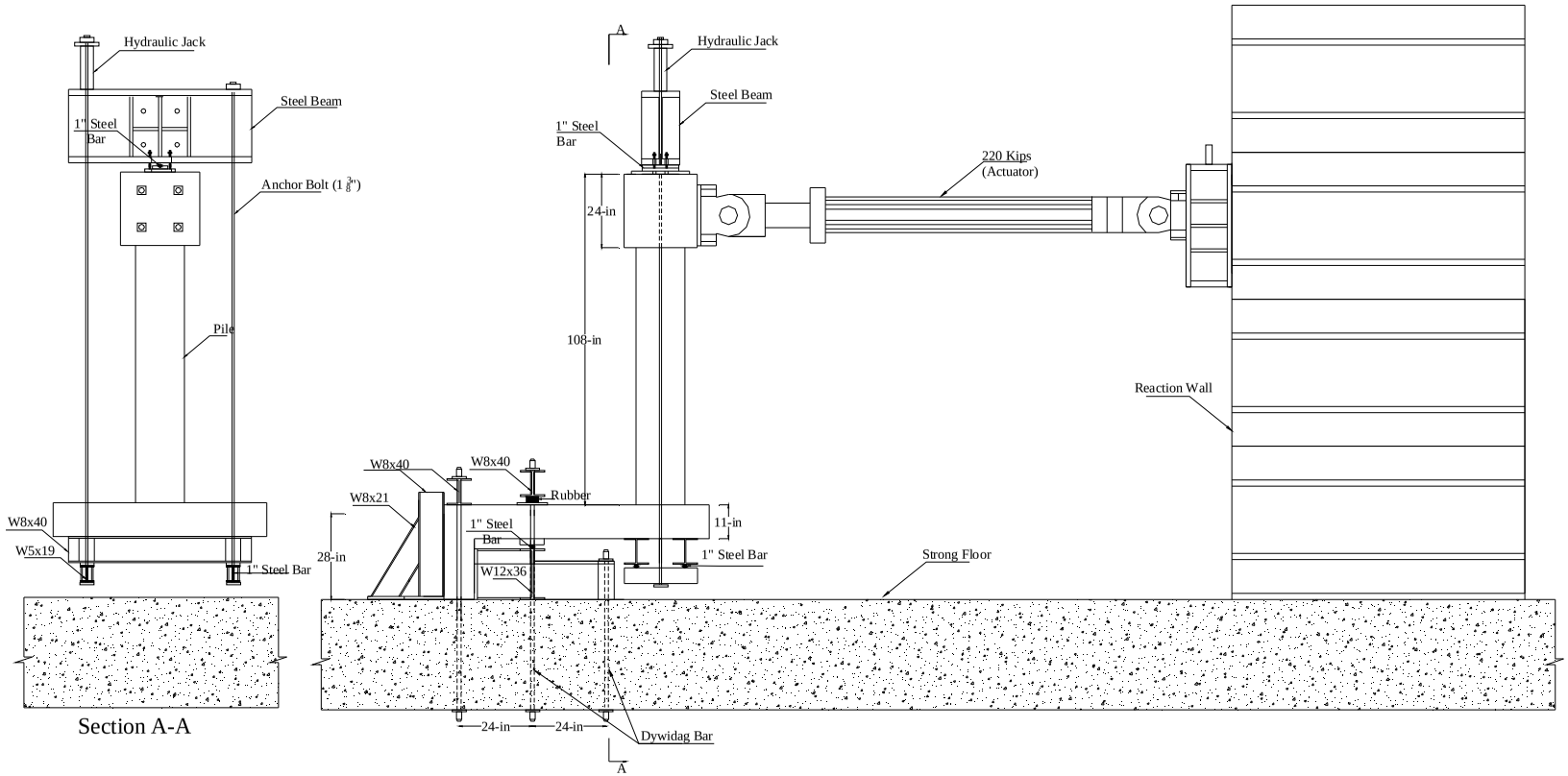

Figure 3-14: Experimental Test Set-Up Schematic for Specimen FSKJ24-M

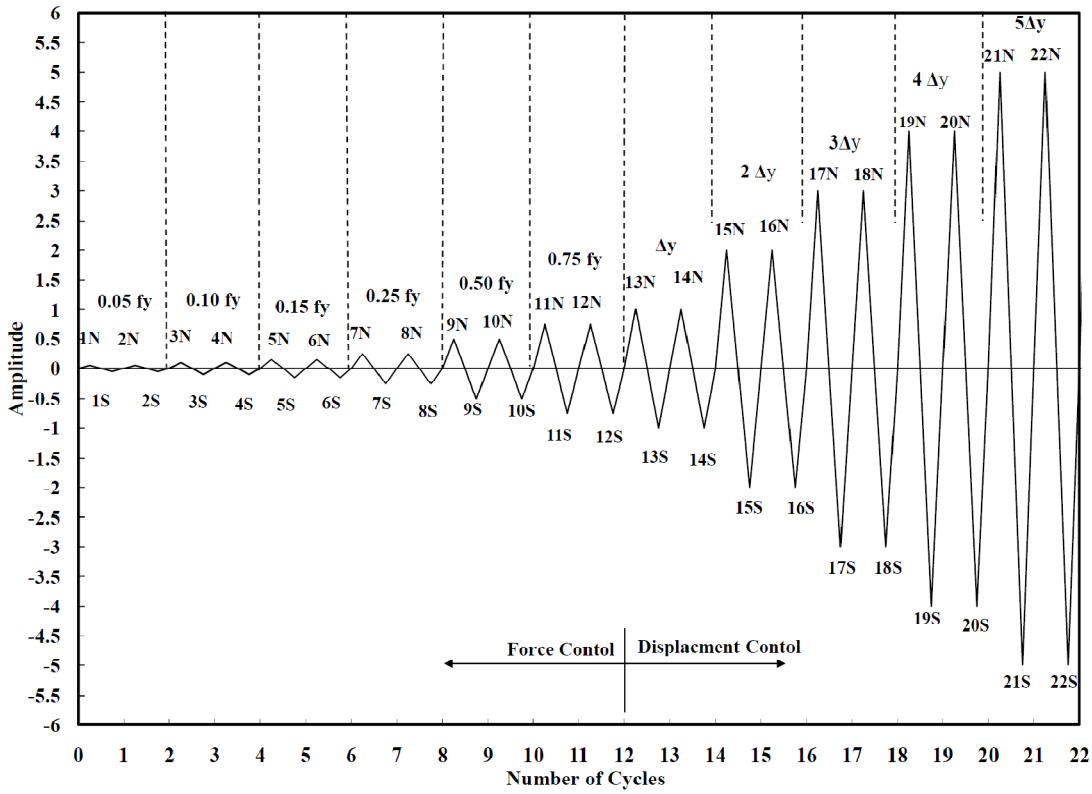

Figure 3-15: DCRCC1 and FSRCC1 Horizontal Loading Protocol

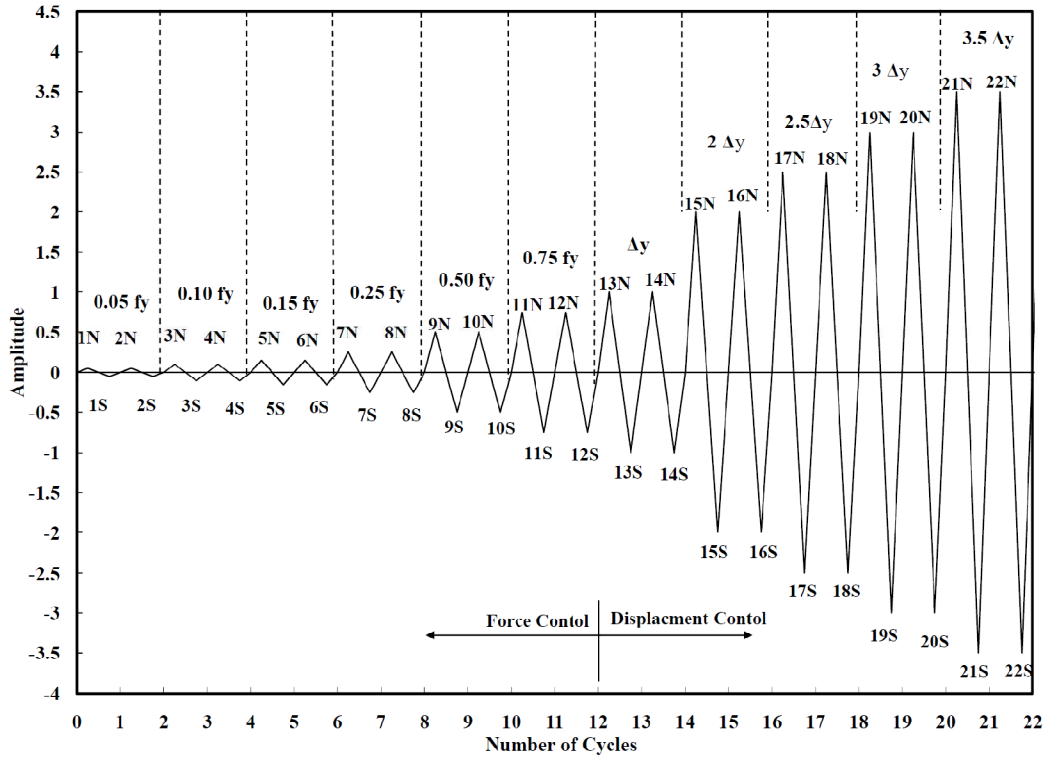

Figure 3-16: DCRCC24, FSRCC24 and FSRCC24-M Horizontal Loading Protocol

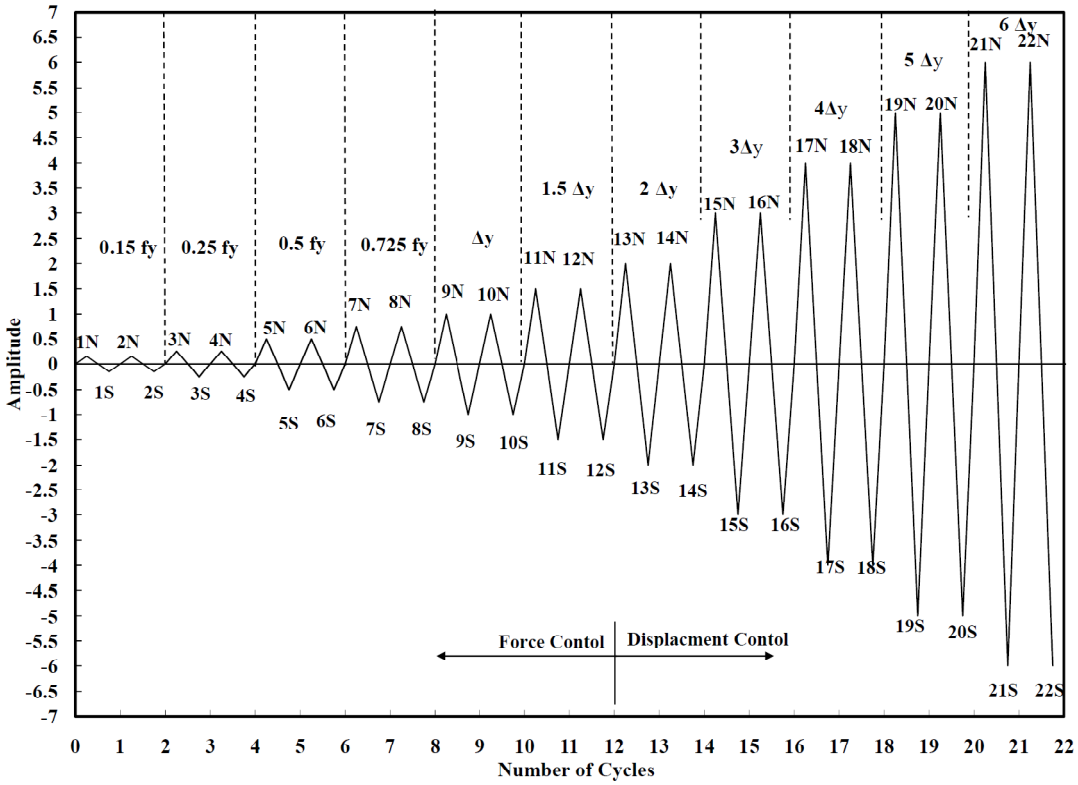

Figure 3-17: DCKJ24 Horizontal Loading Protocol

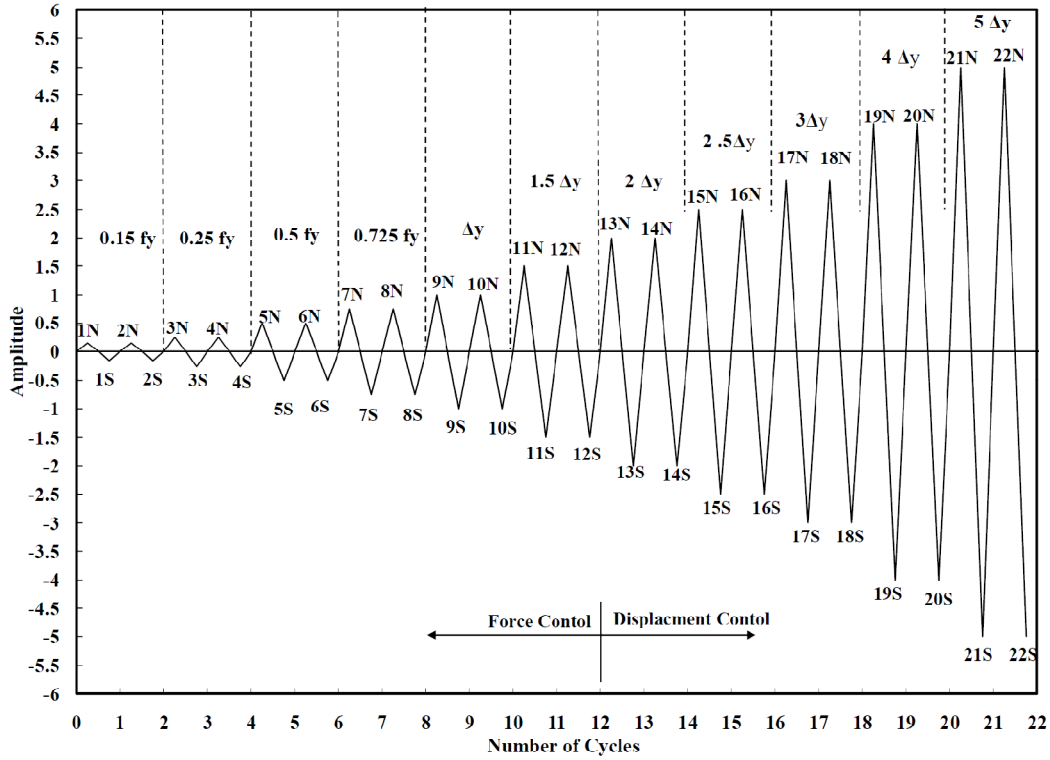

Figure 3-18: FSKJ24 nd FSKJ24-M Horizontal Loading Protocol

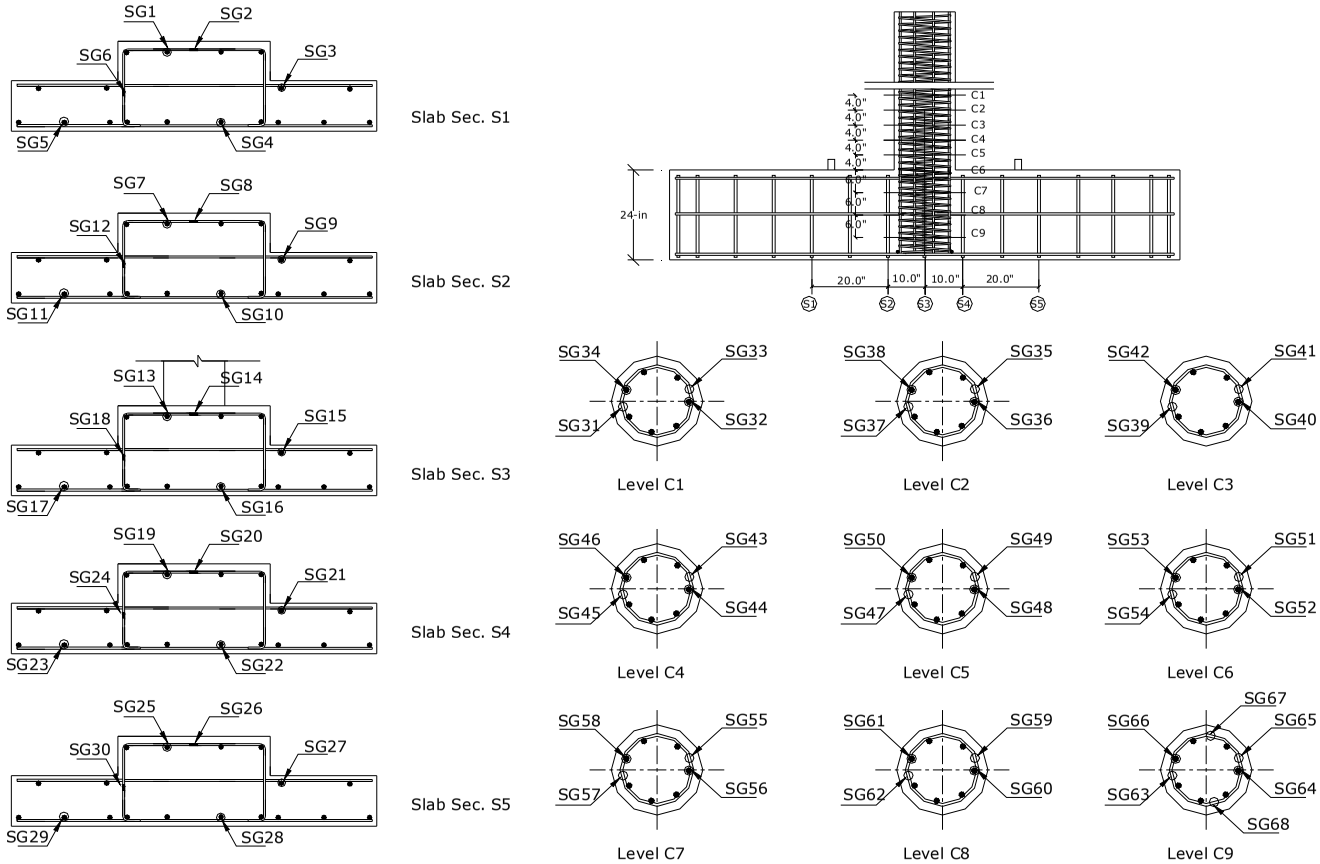

Figure 3-19: DCRCC1 Strain Gauge Locations

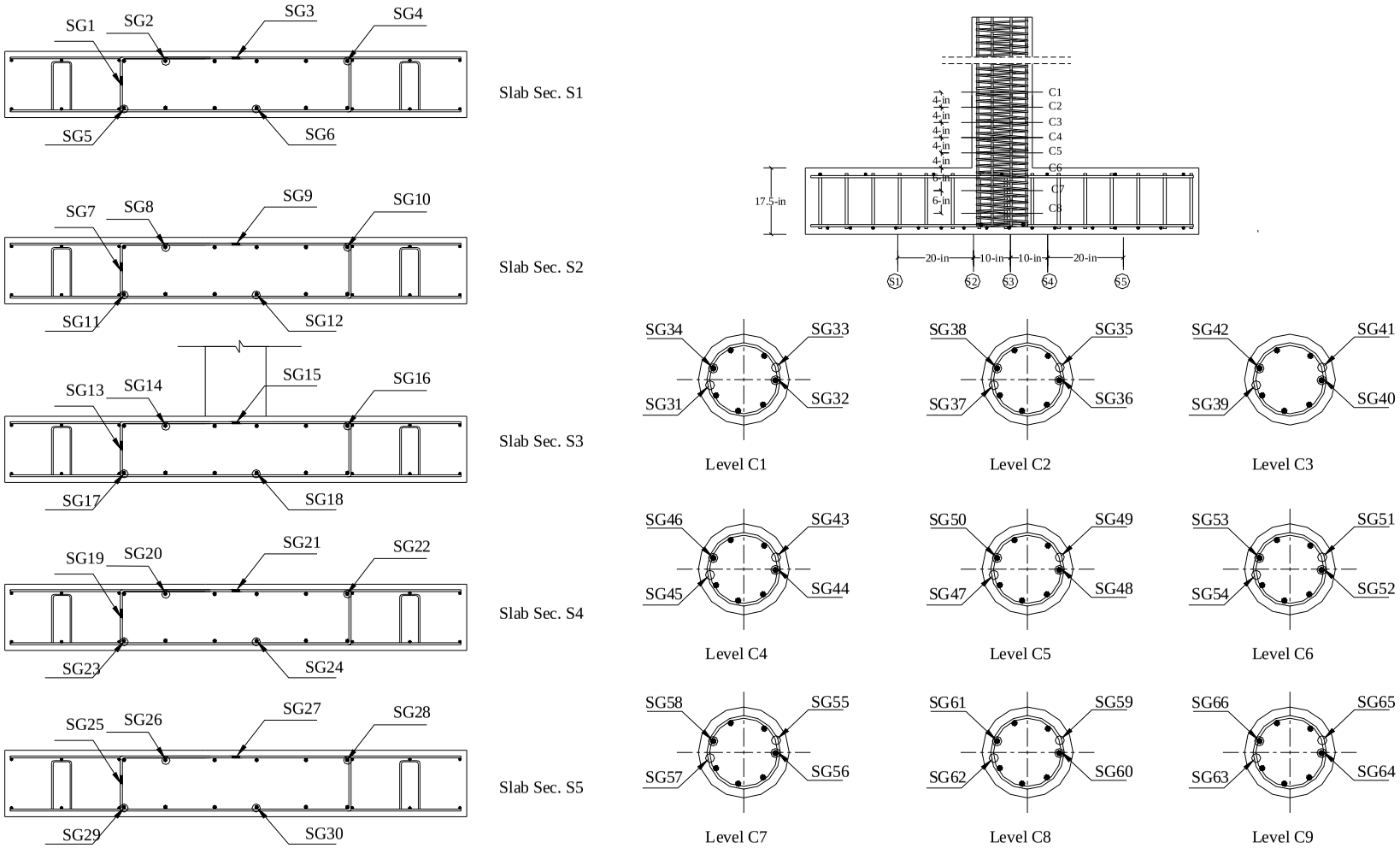

Figure 3-20: FSRCC1 Strain Gauge Locations

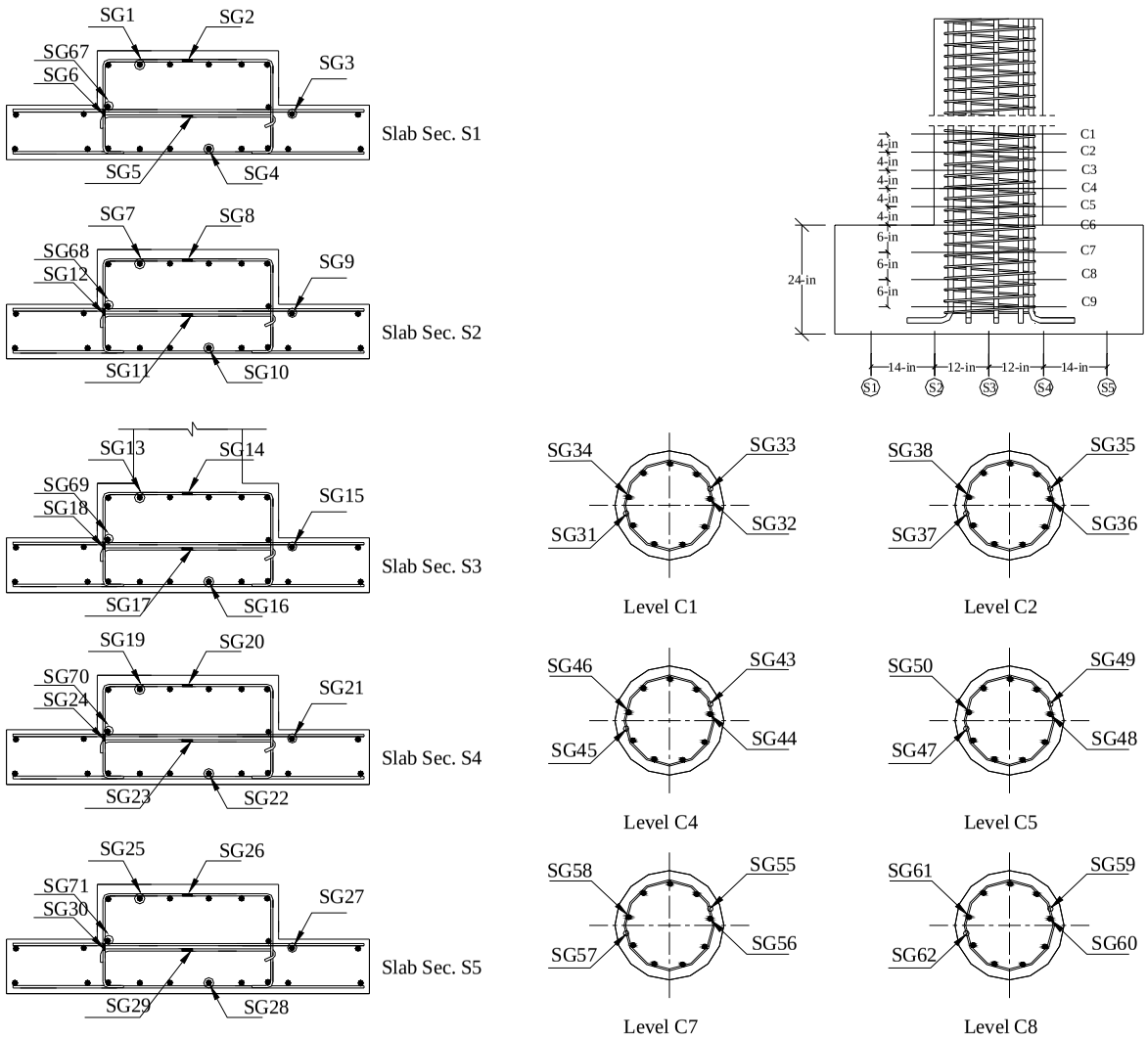

Figure 3-21: DCRCC24 Strain Gauge Locations

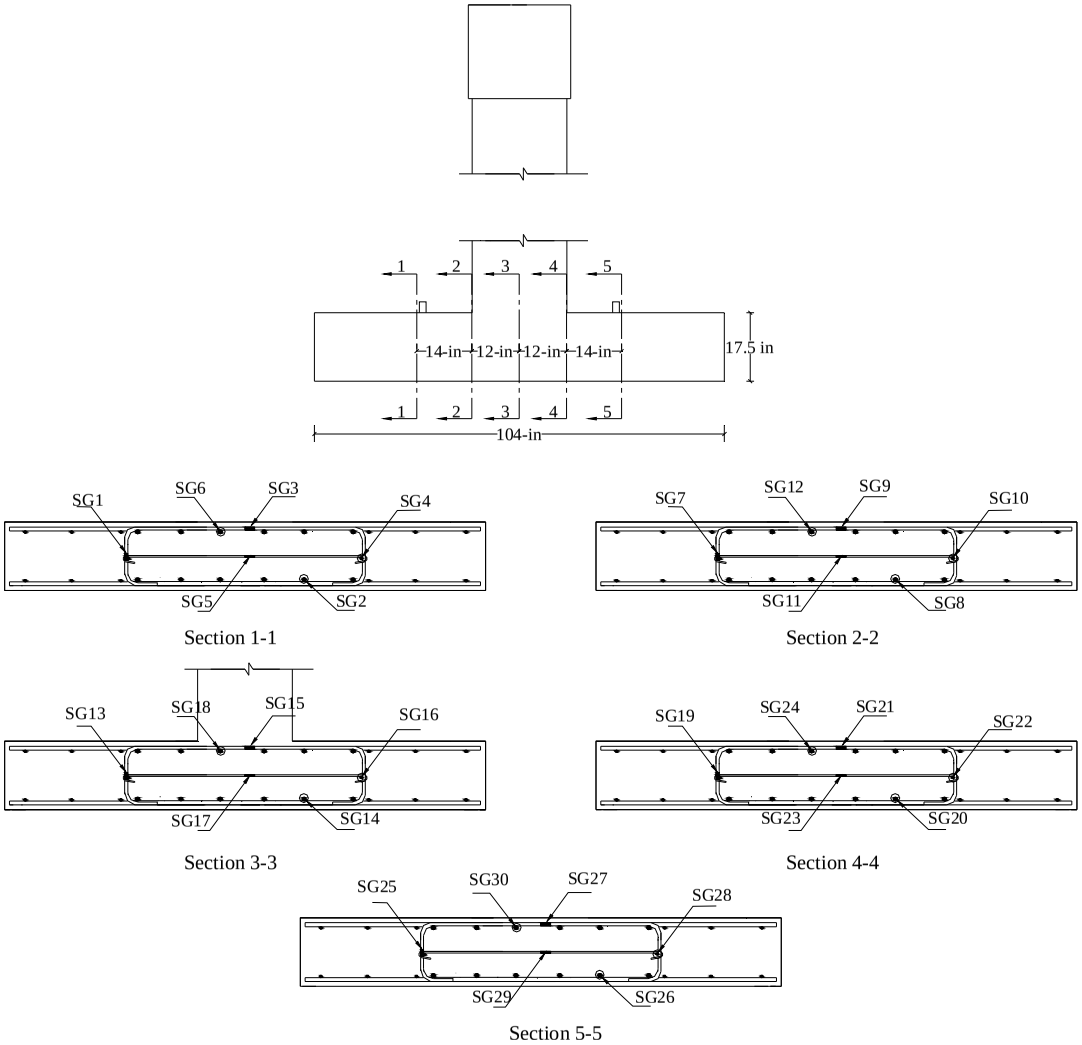

Figure 3-22: FSRCC24 Strain Gauge Locations

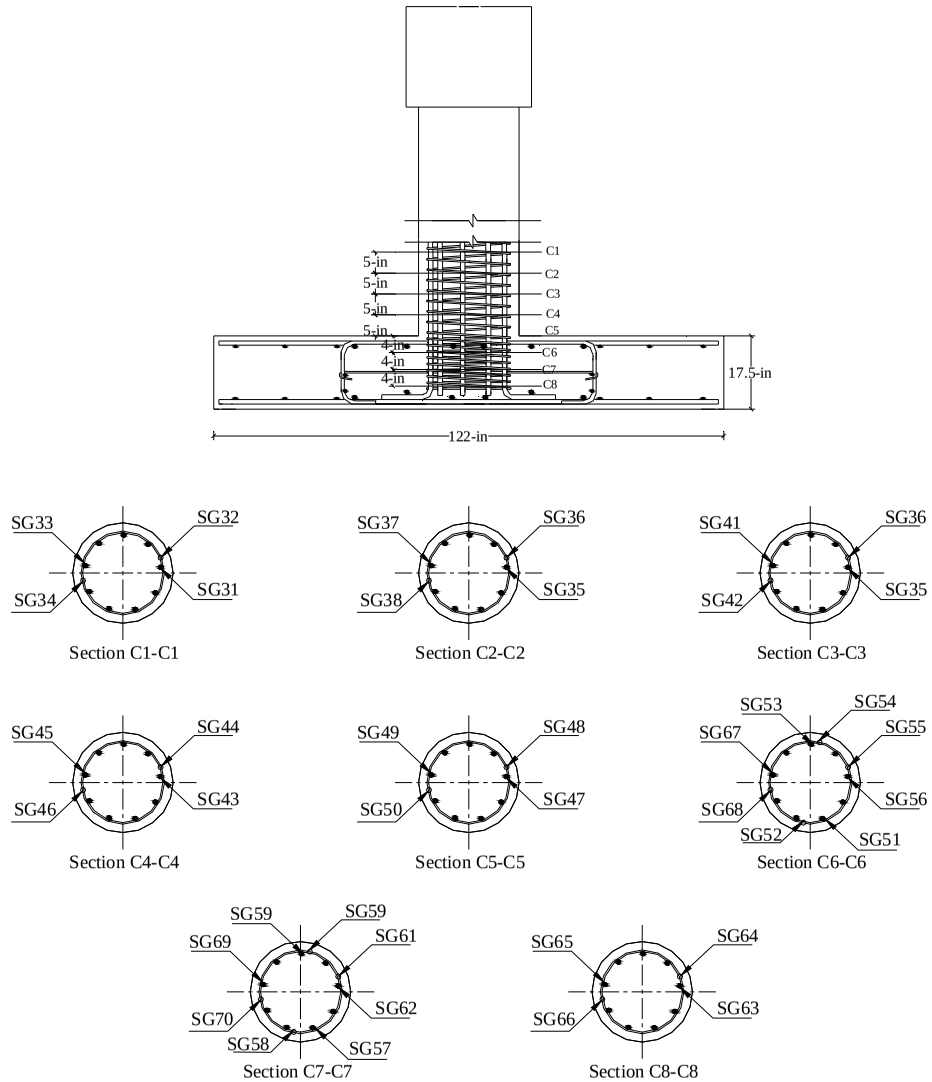

Figure 3-23: FSRCC24 Pile Strain Gauge Locations

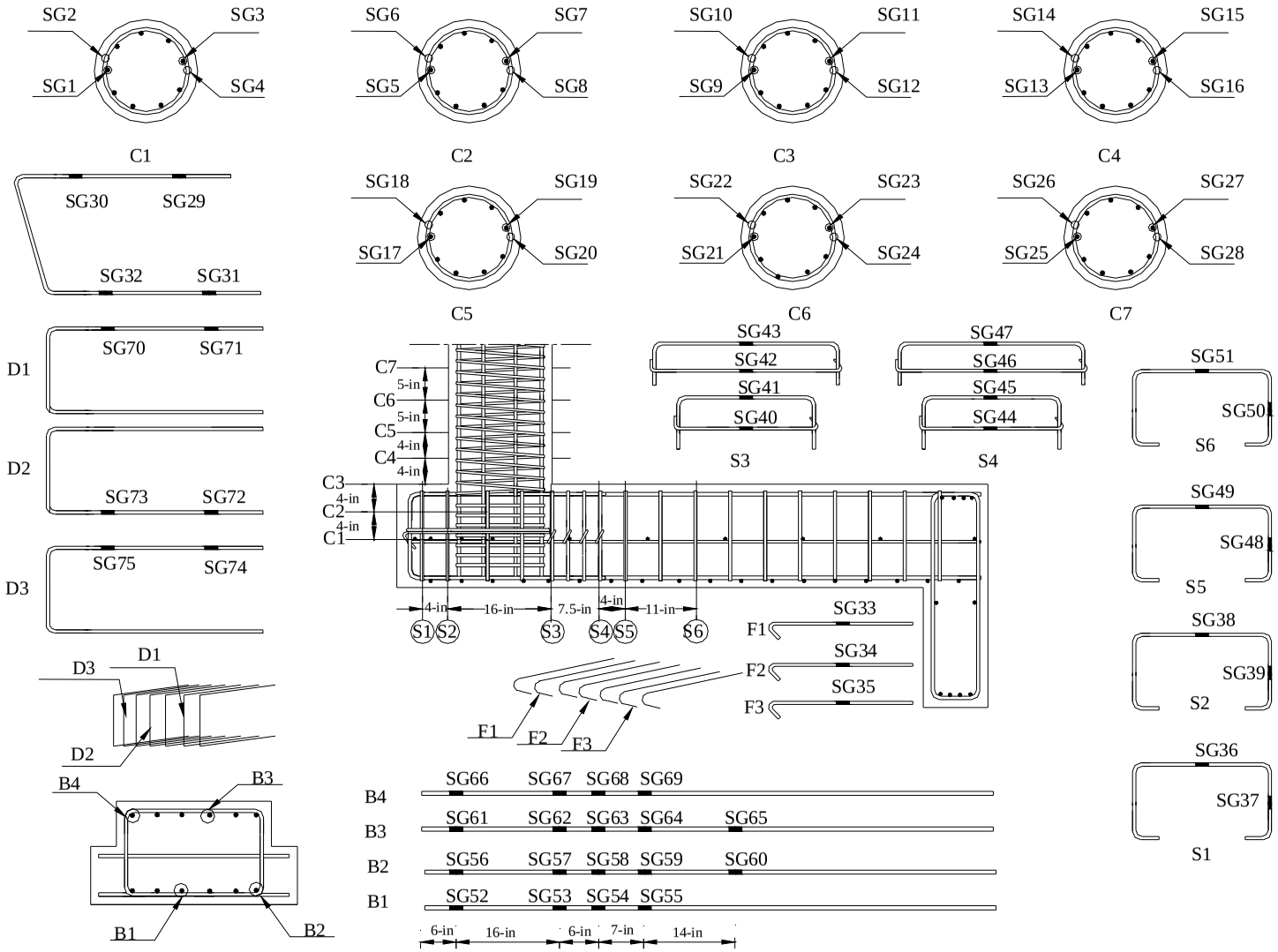

Figure 3-24: DCKJ24 Strain Gauge Locations

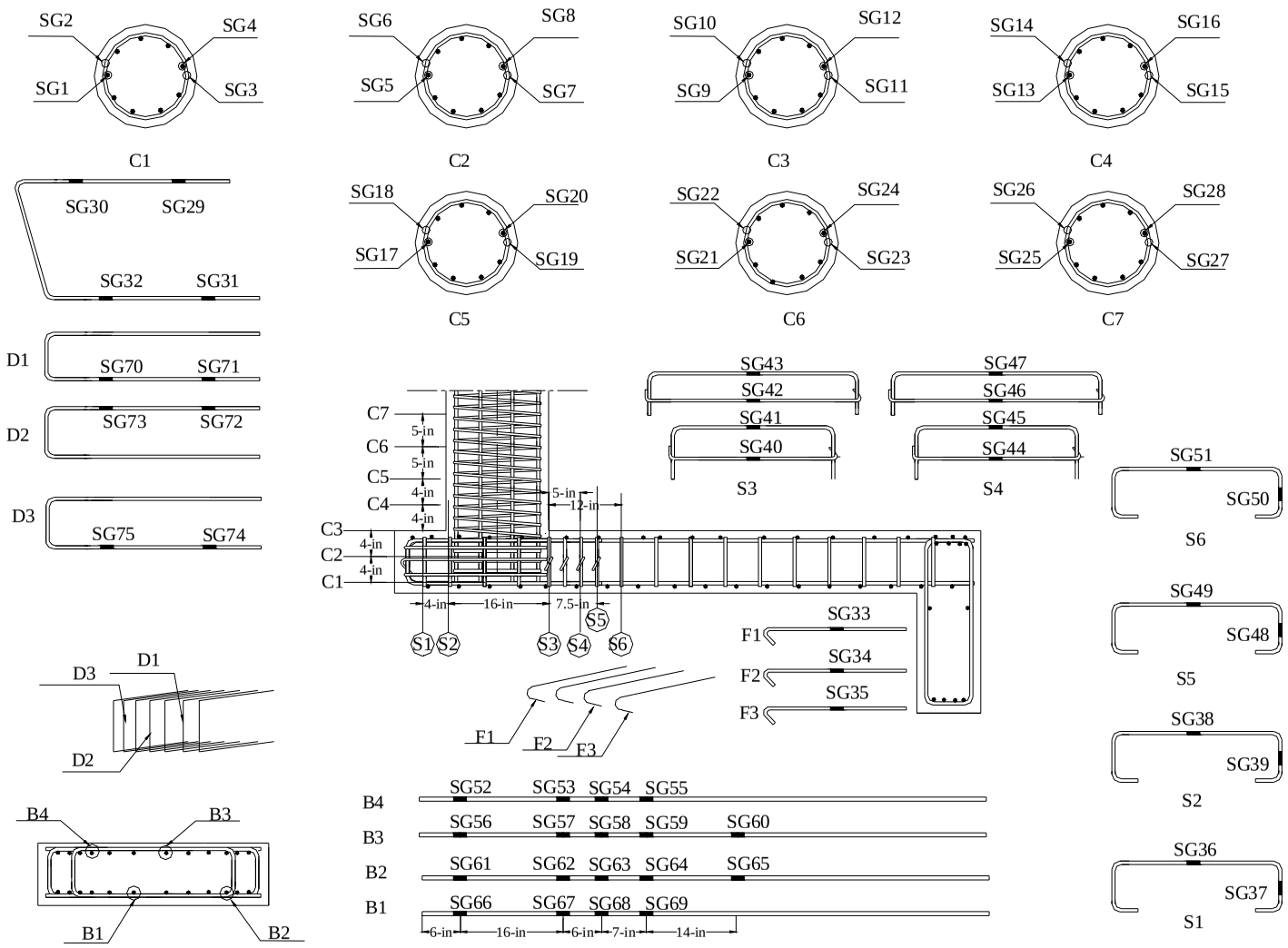

Figure 3-25: FSKJ24 Strain Gauge Locations

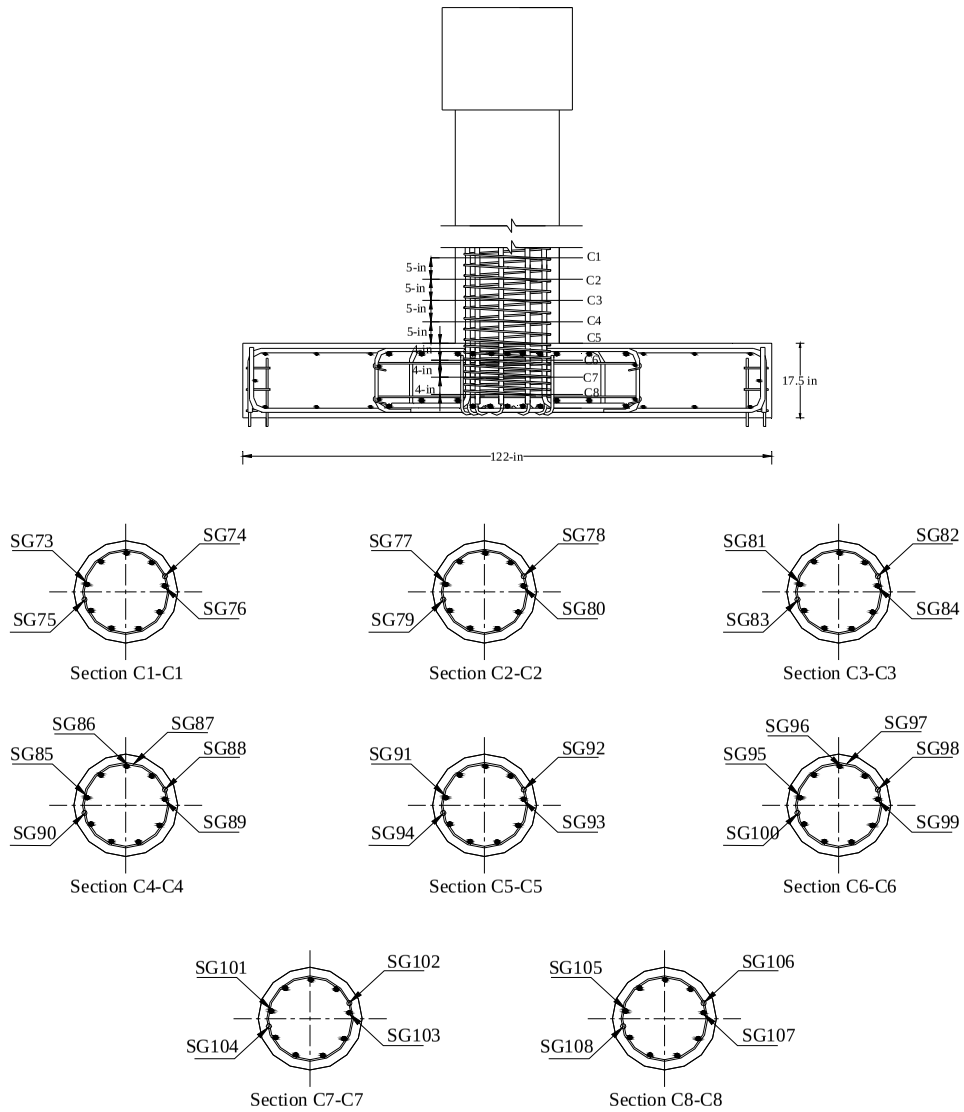

Figure 3-26: FSRCC24-M Pile Strain Gauge Locations

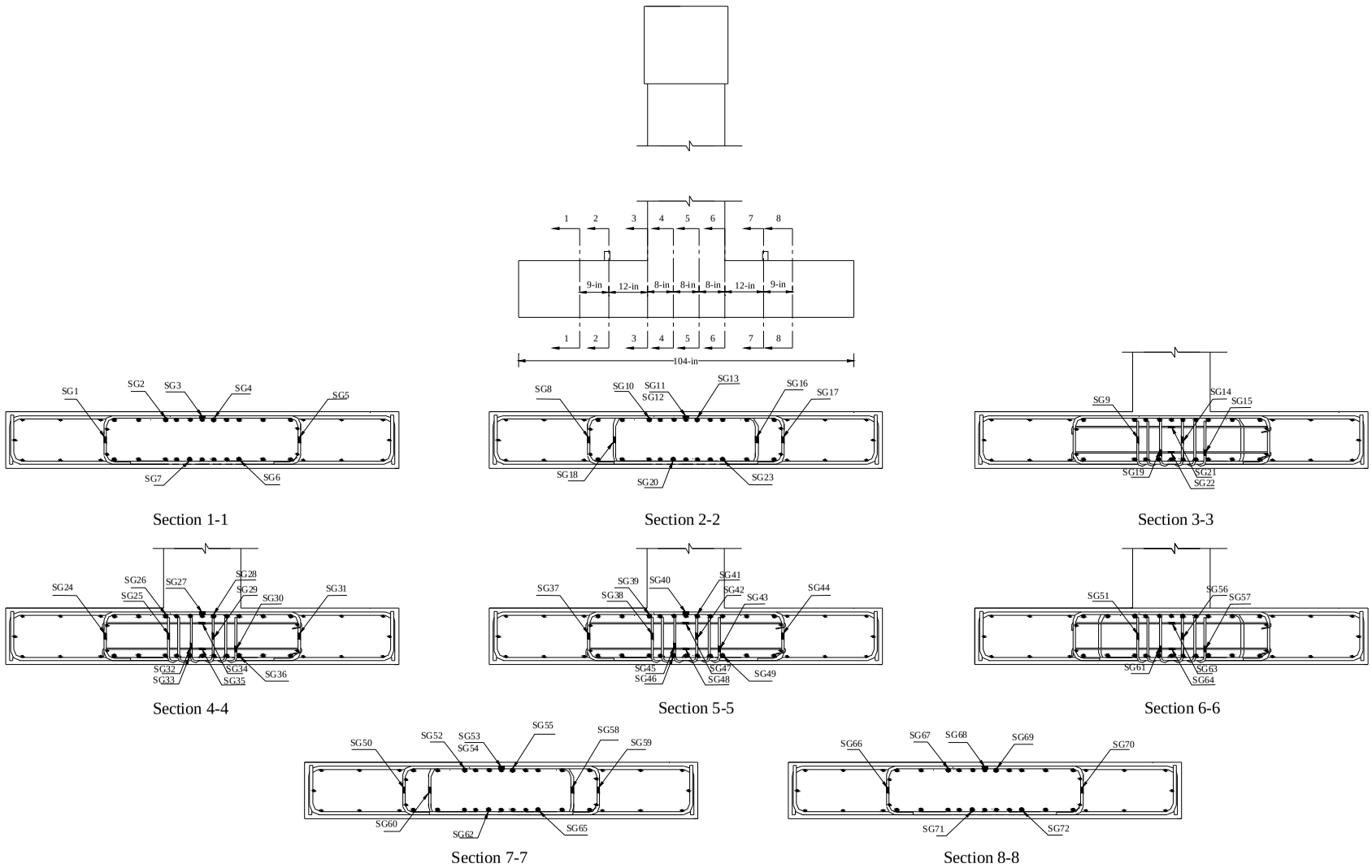

Figure 3-27: FSRCC24-M Pile Strain Gauge Locations

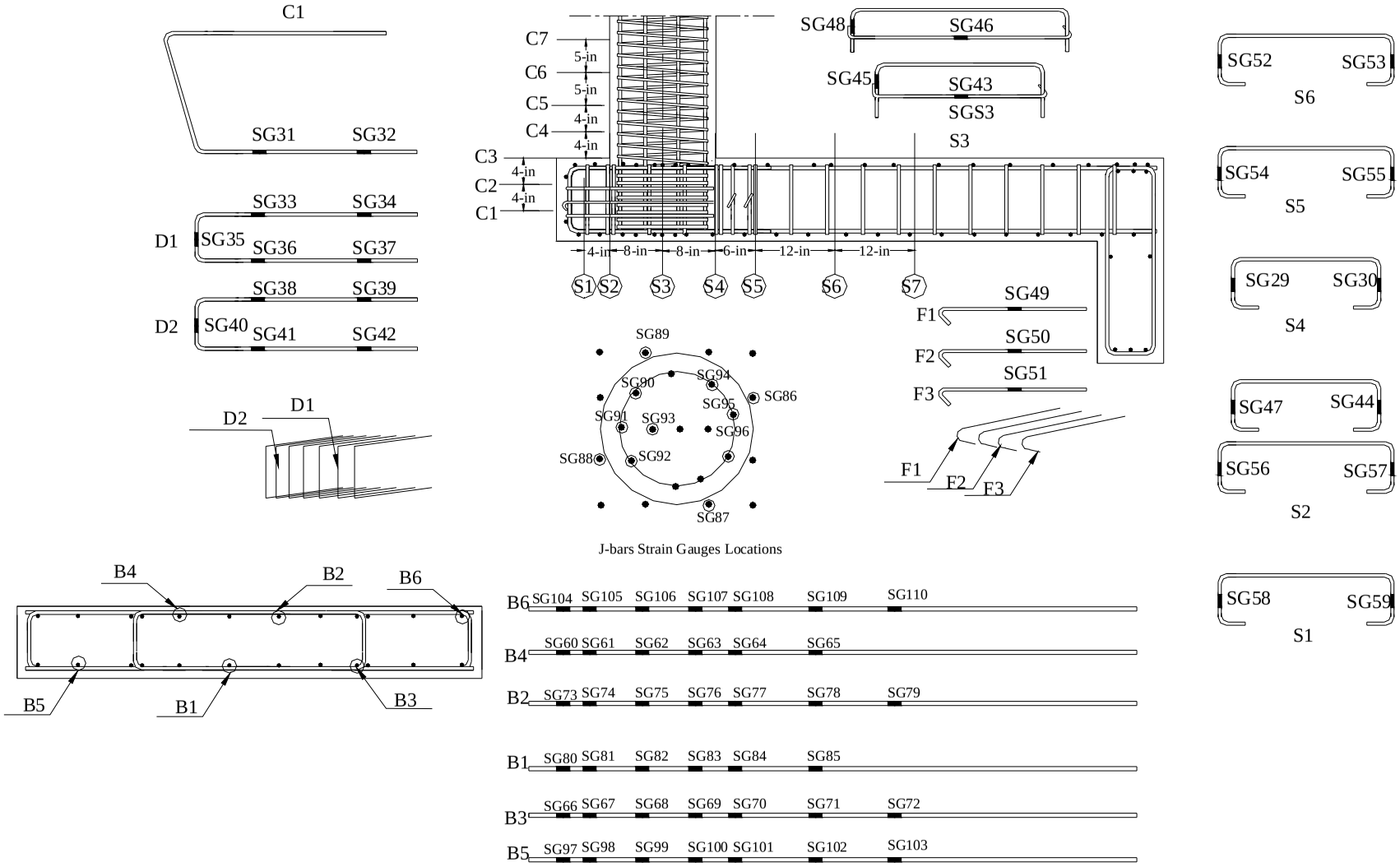

Figure 3-28: FSKJ24-M Slab Strain Gauge Locations

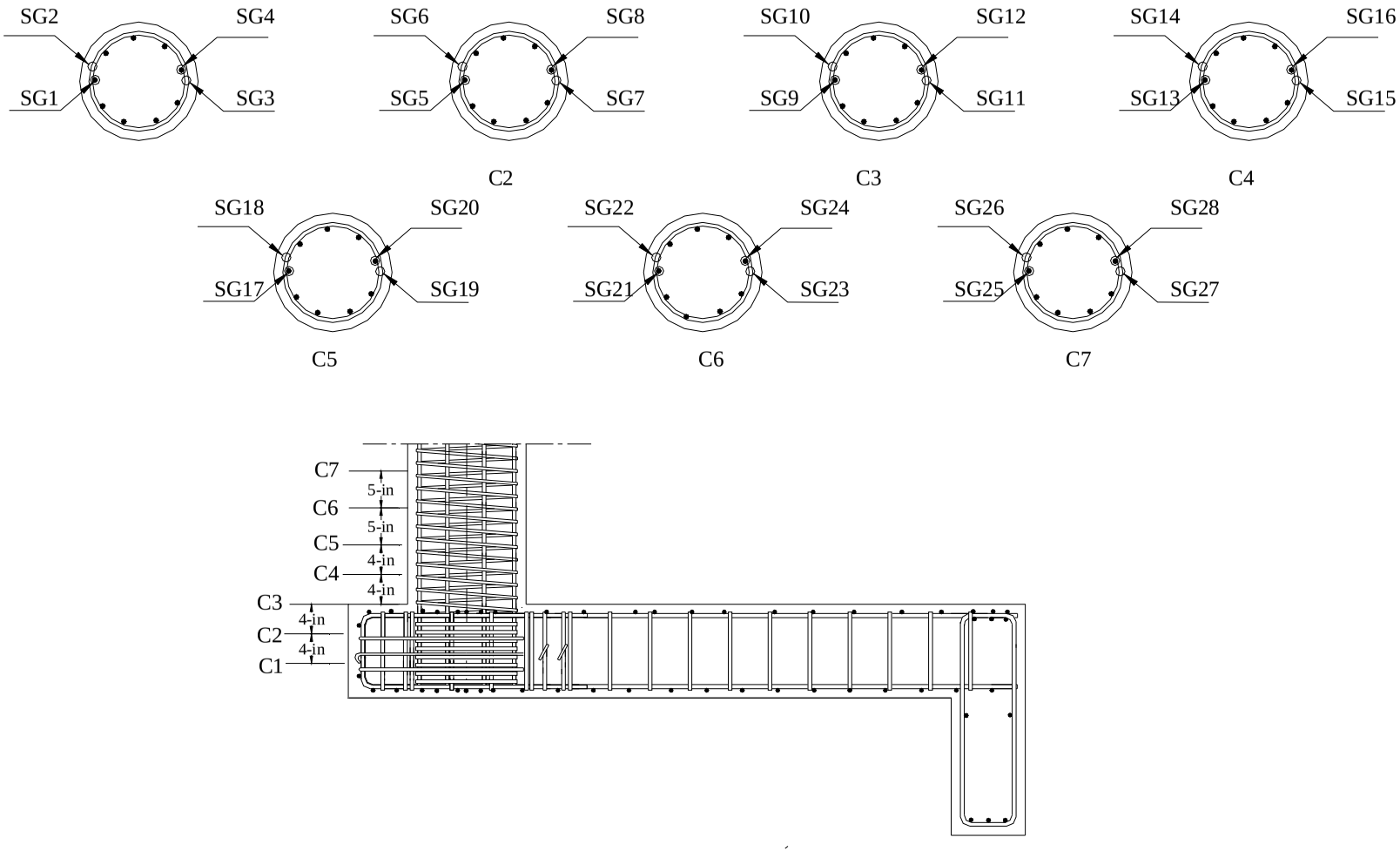

Figure 3-29: FSKJ24-M Pile Strain Gauge Locations

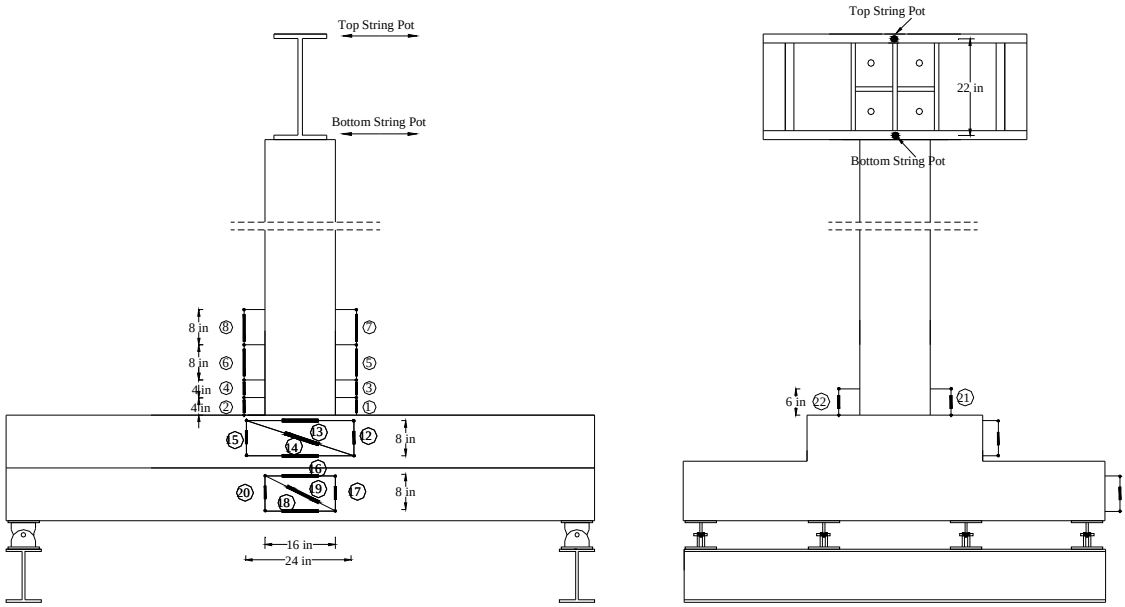

Figure 3-30: DCRCC1 Displacement Transducer Device Locations

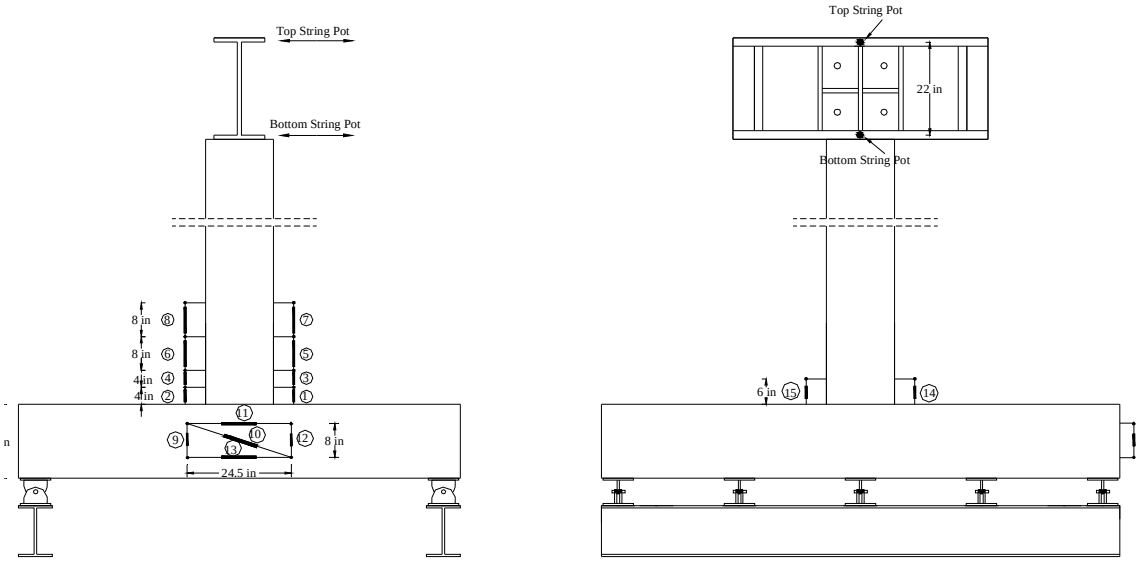

Figure 3-31: FSRCC1 Displacement Transducer Device Locations

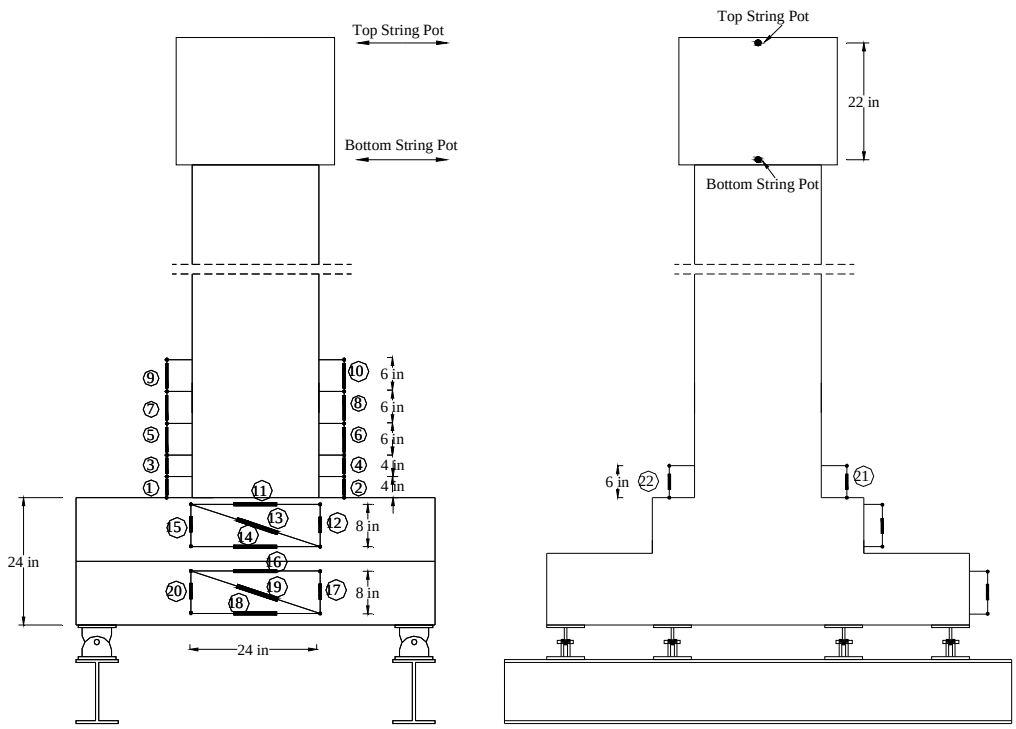

Figure 3-32: DCRCC24 Displacement Transducer Device Locations

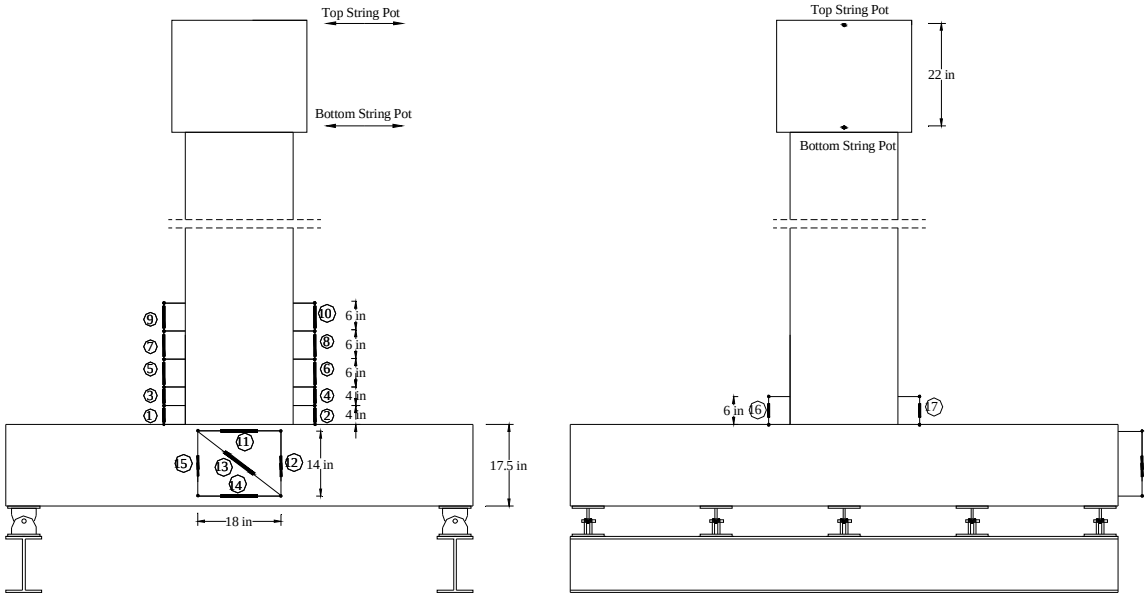

Figure 3-33: FSRCC24 and FSRCC24-M Displacement Transducer Device Locations

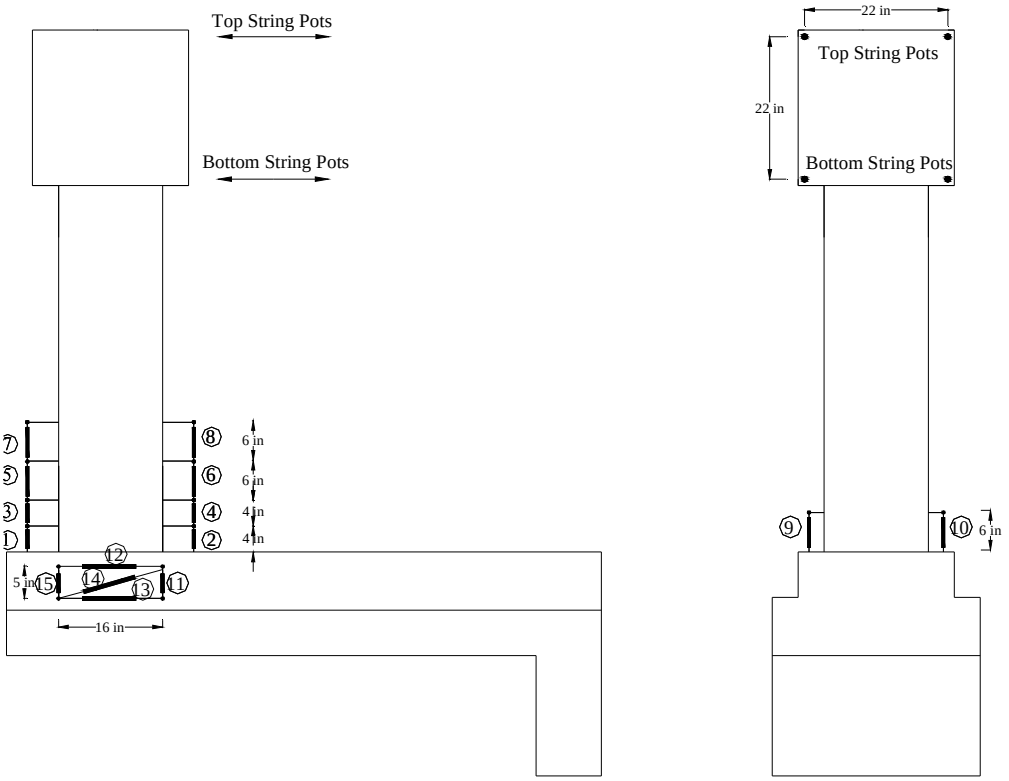

Figure 3-34: DCKJ24 Displacement Transducer Device Locations

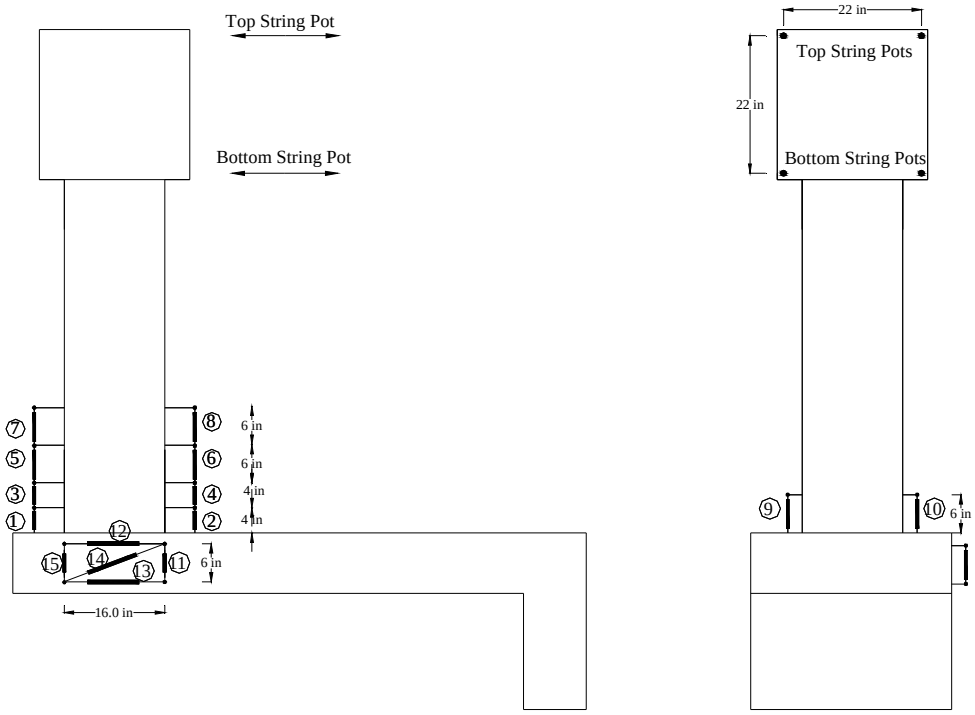

Figure 3-35: FSKJ24 Displacement Transducer Device Locations

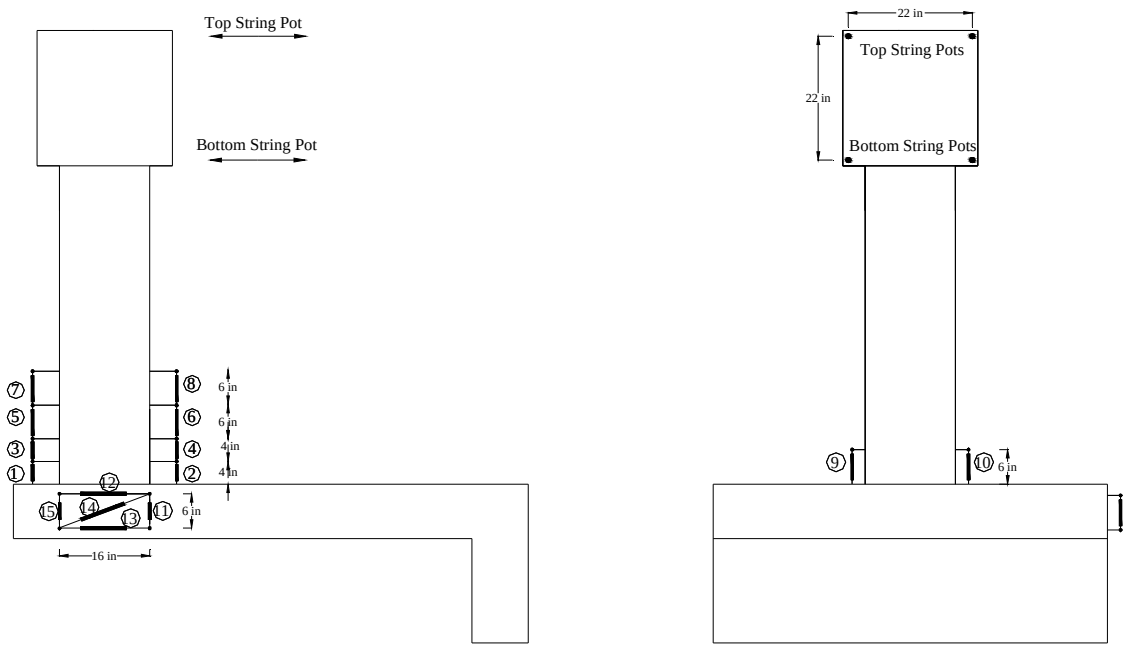

Figure 3-36: FSKJ24-M Displacement Transducer Device Locations

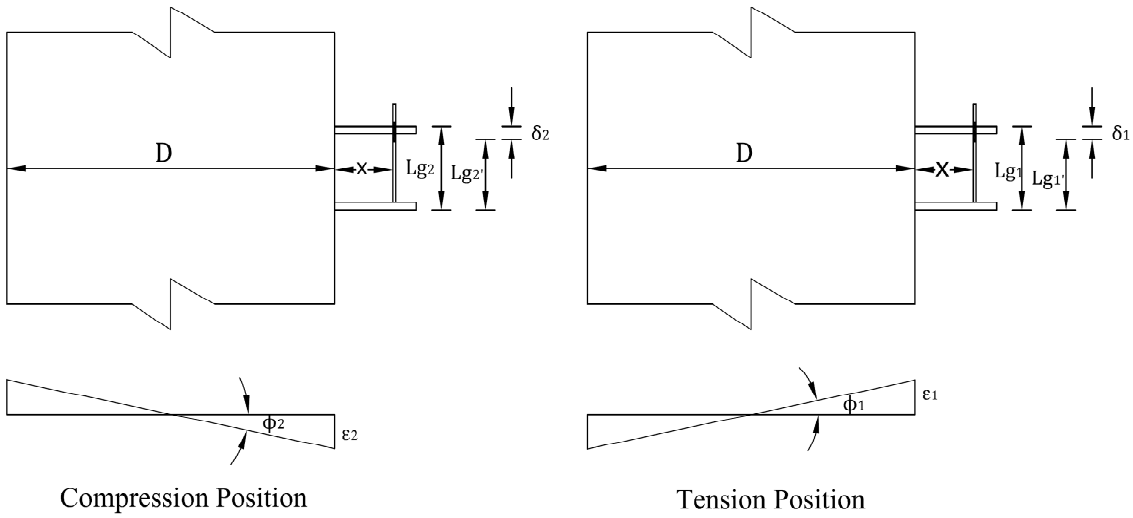

Figure 3-37: Curvature Calculation Parameters

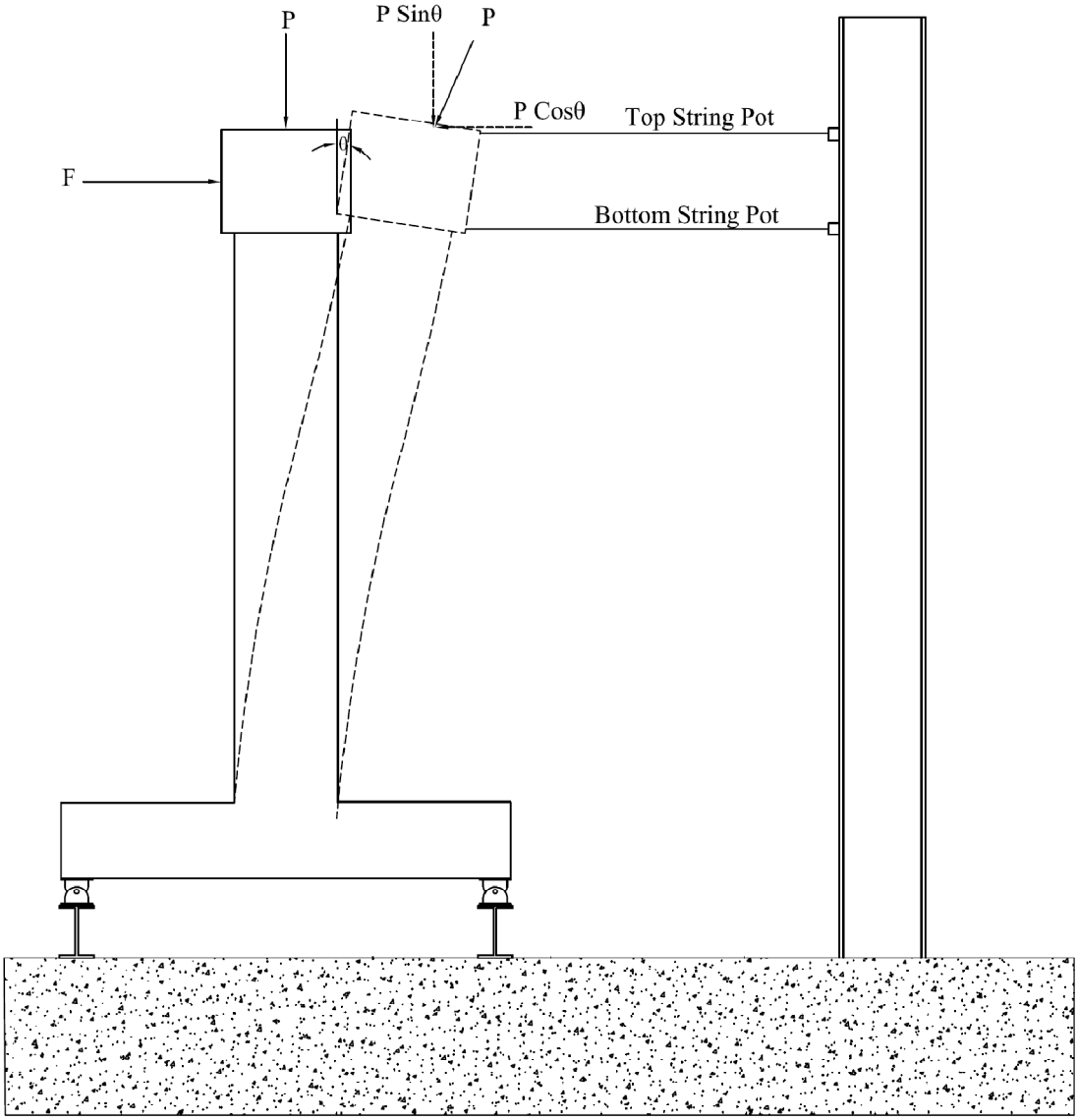

Figure 3-38: Head Rotation Correction in the Test Setup

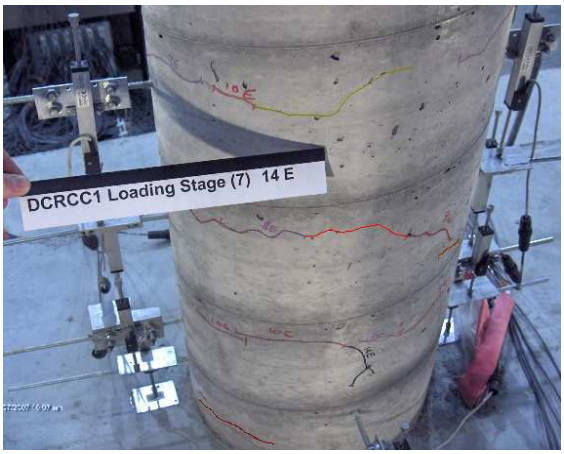

Figure 4-1: DCRCC1 Cracking (1 Δy)

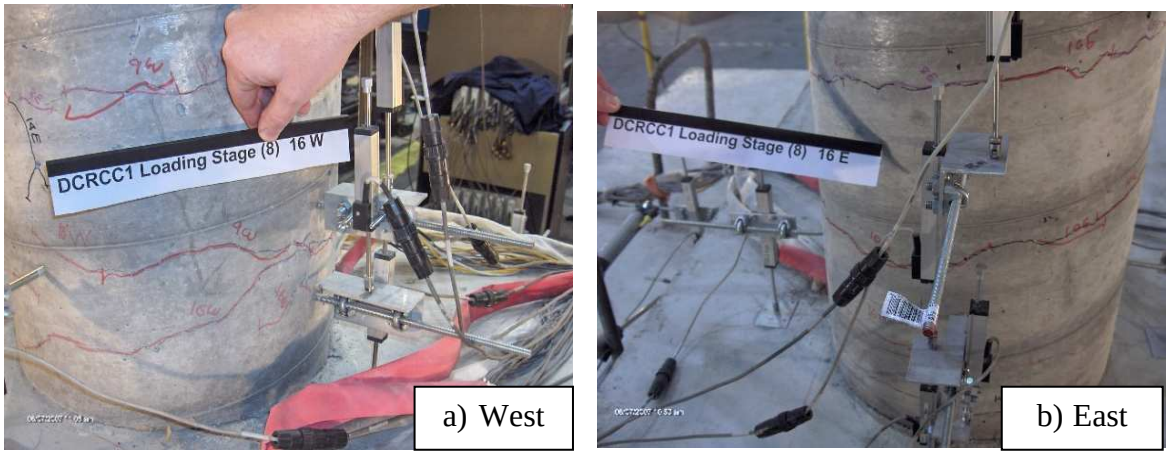

Figure 4-2: DCRCC1 Cracking (2 Δy)

Figure 4-3: DCRCC1 Cracking (3 Δy)

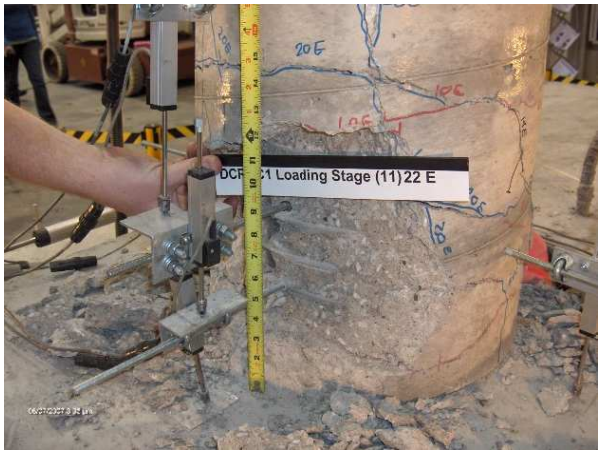

Figure 4-4: DCRCC1 Cracking (5 Δy)

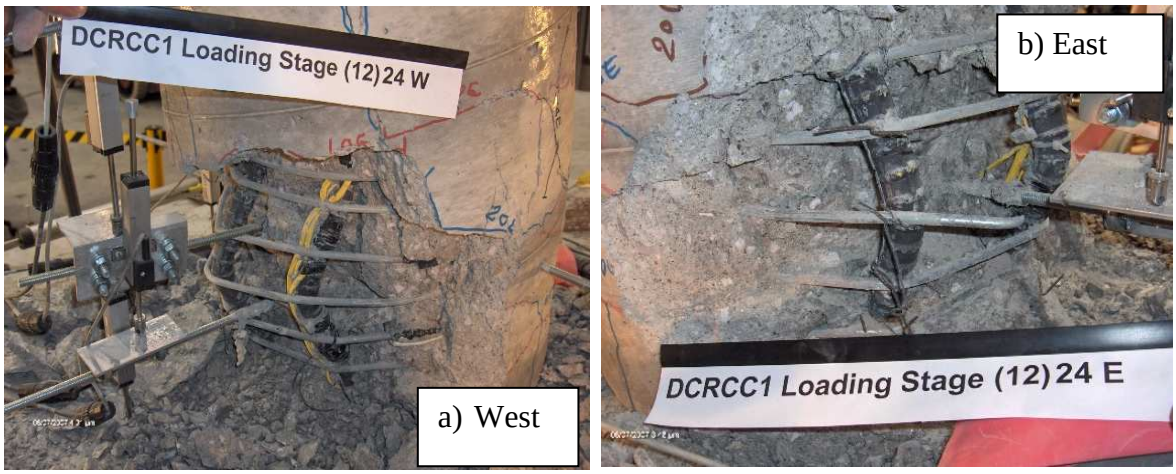

Figure 4-5: DCRCC1 Cracking (5 Δy)

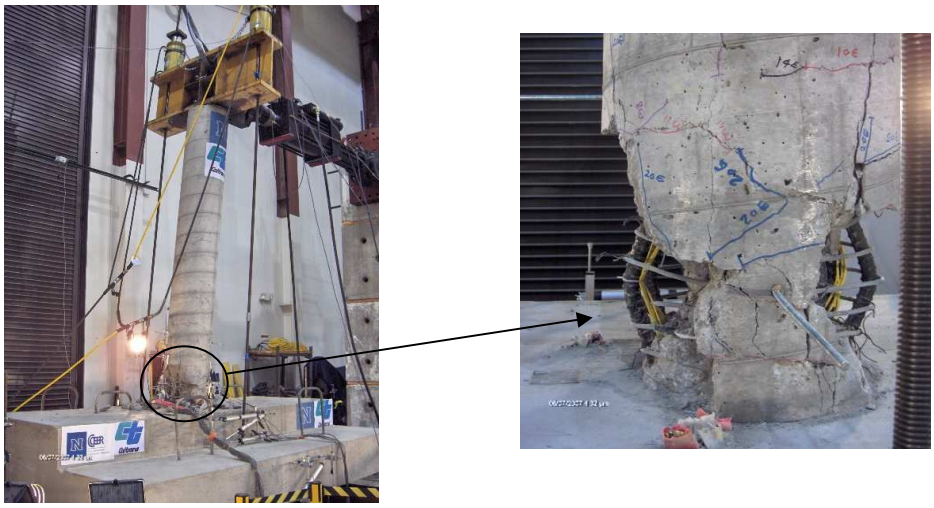

Figure 4-6: Plastic Hinge Deformation at the End of DCRCC1 Testing

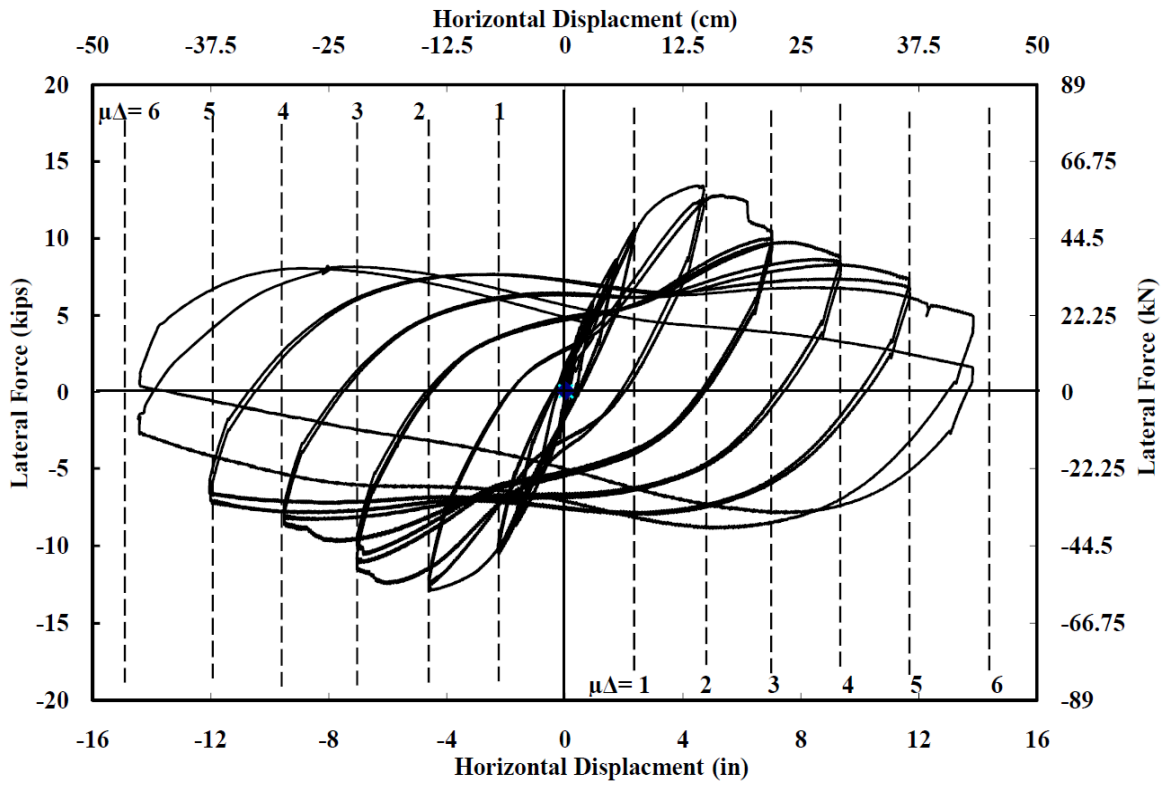

Figure 4-7: Force-Displacement Hysteretic Response for DCRCC1

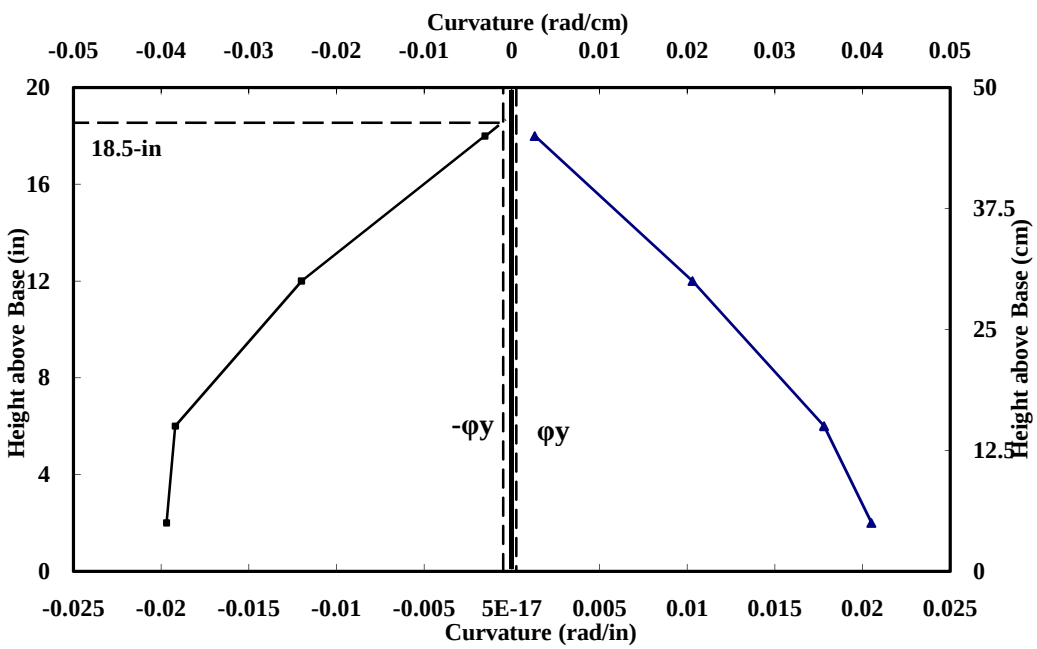

Figure 4-8: Measured Curvature Envelope along the Plastic Hinge of DCRCC1

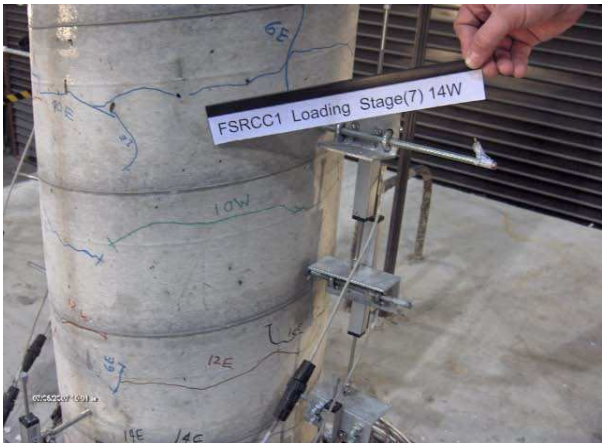

Figure 4-9: FSRCC1 Cracking (1 Δy)

Figure 4-10: FSRCC1 Cracking (2 Δy)

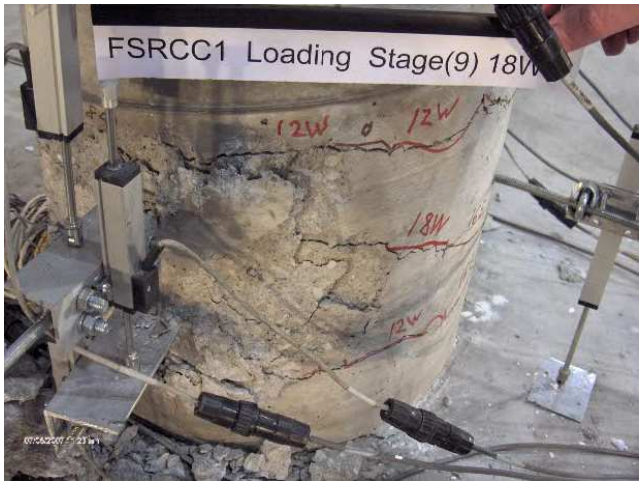

Figure 4-11: FSRCC1 Cracking (3 Δy)

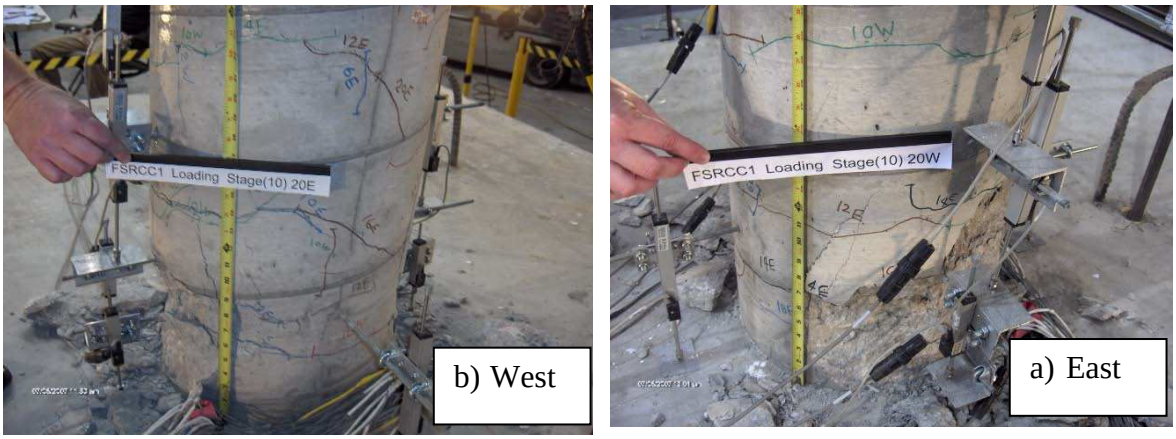

Figure 4-12: FSRCC1 Cracking (4 Δy)

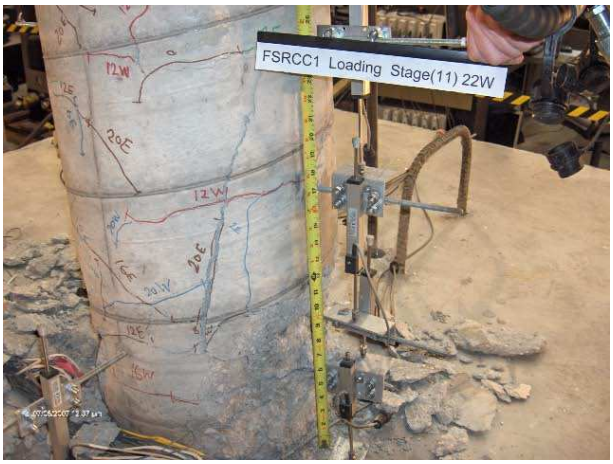

Figure 4-13: FSRCC1 Cracking (5 Δy)

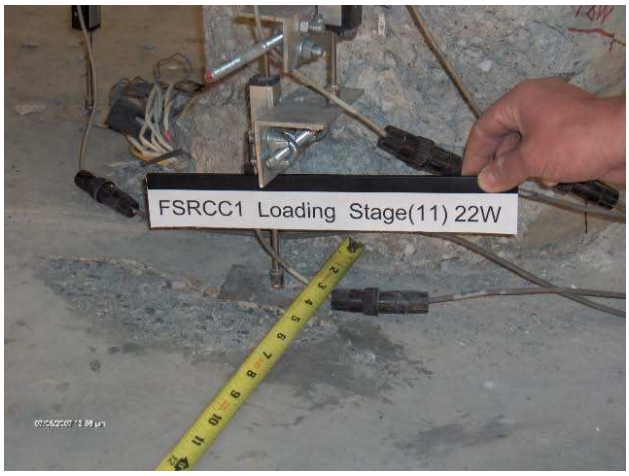

Figure 4-14: FSRCC1 Slab Cracking (5 Δy)

Figure 4-15: Plastic Hinge Deformation at the End of DCRCC1 Testing

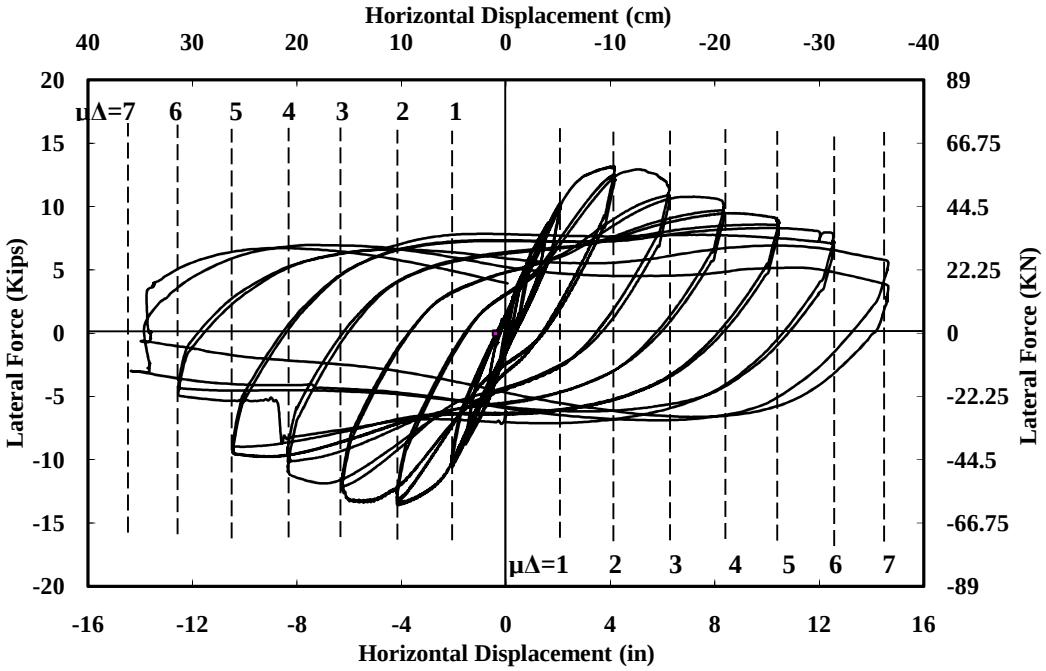

Figure 4-16: Force-Displacement Hysteretic Response for FSRCC1

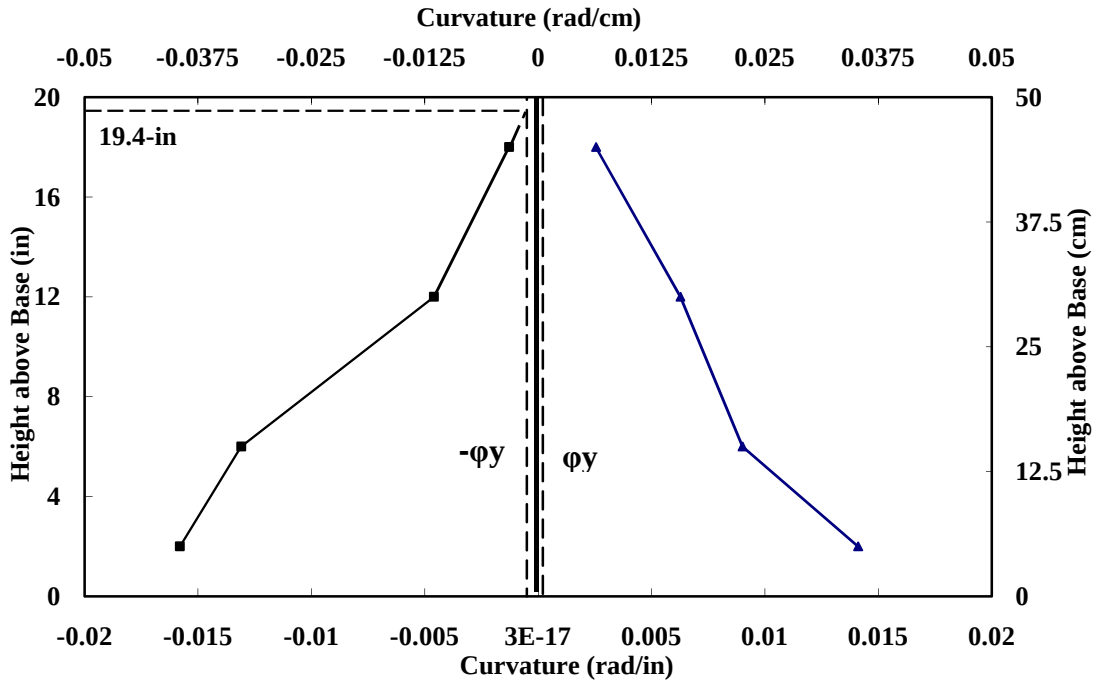

Figure 4-17: Measured Curvature Envelope along the Plastic Hinge of FSRCC1

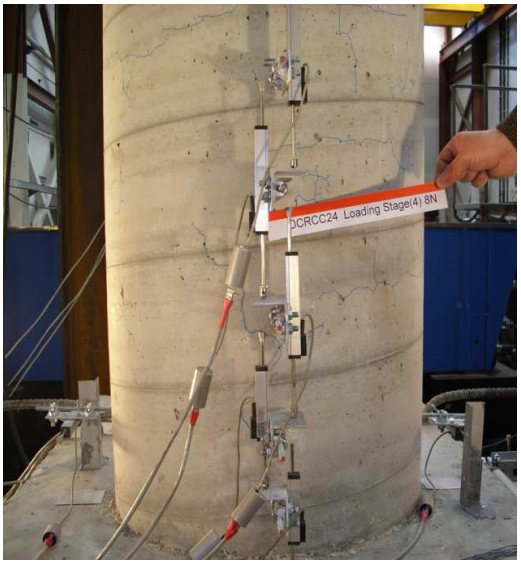

Figure 4-18: DCRCC24 Cracks (0.25 fy)

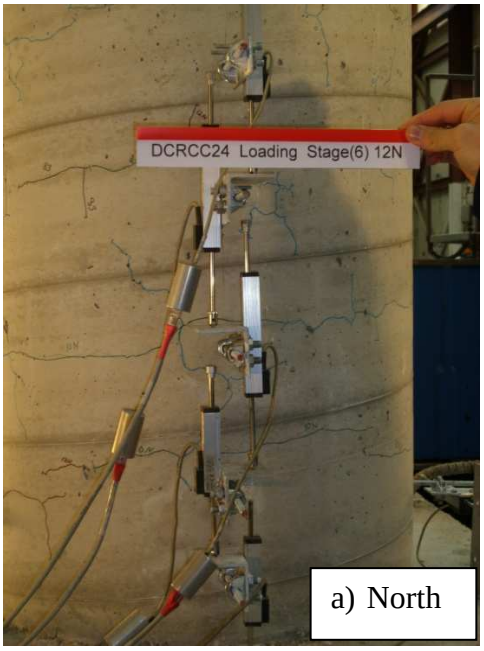

Figure 4-19: DCRCC24 Cracks (0.75 fy)

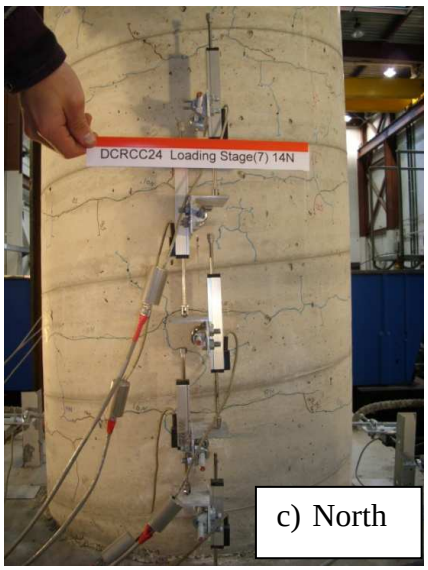

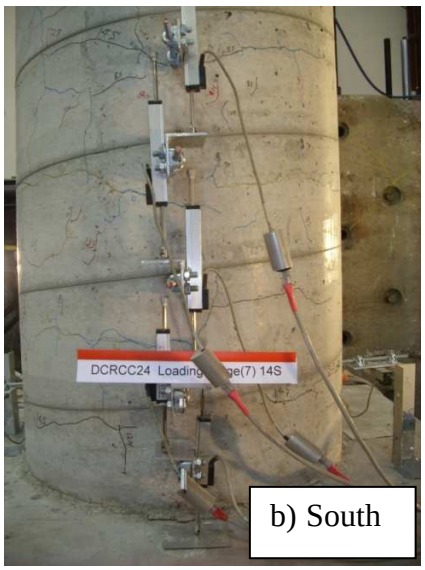

Figure 4-20: DCRCC24 Cracks (1 Δy)

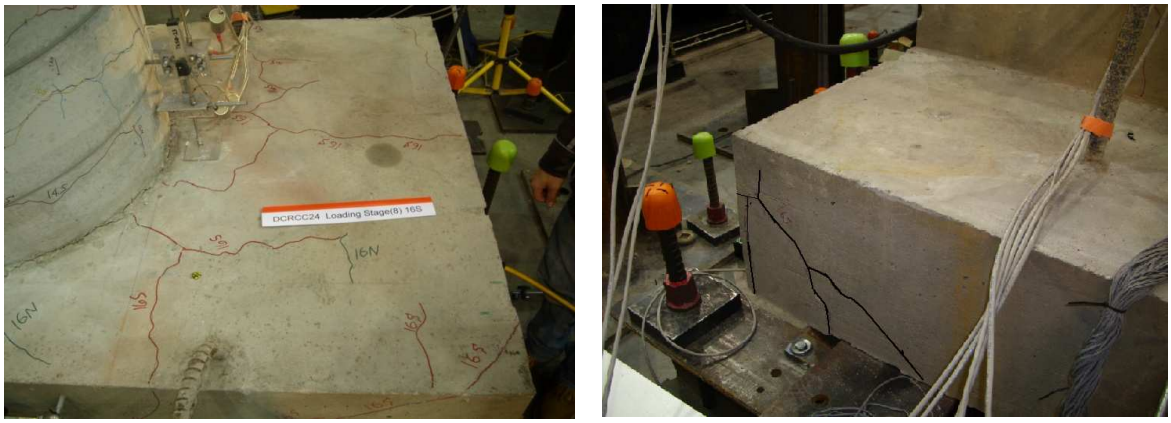

Figure 4-21: DCRCC24 Cracks (2 Δy)

Figure 4-22: DCRCC24 Cracks (3 Δy)

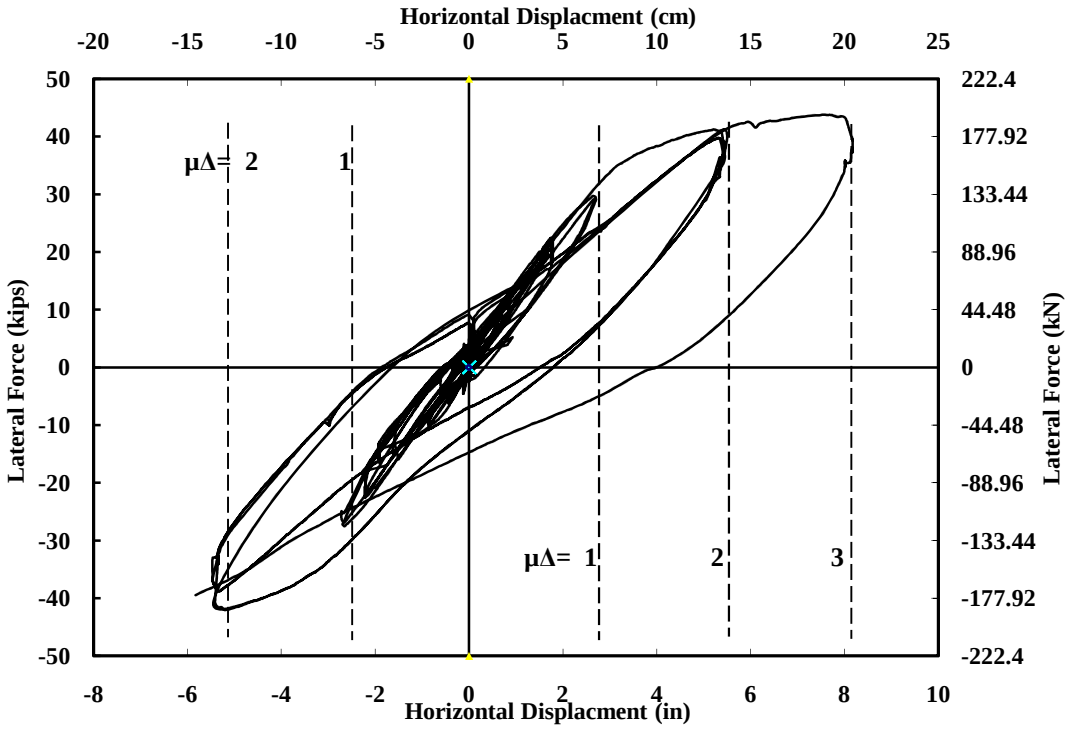

Figure 4-23: Force-Displacement Hysteretic Response for DCRCC24

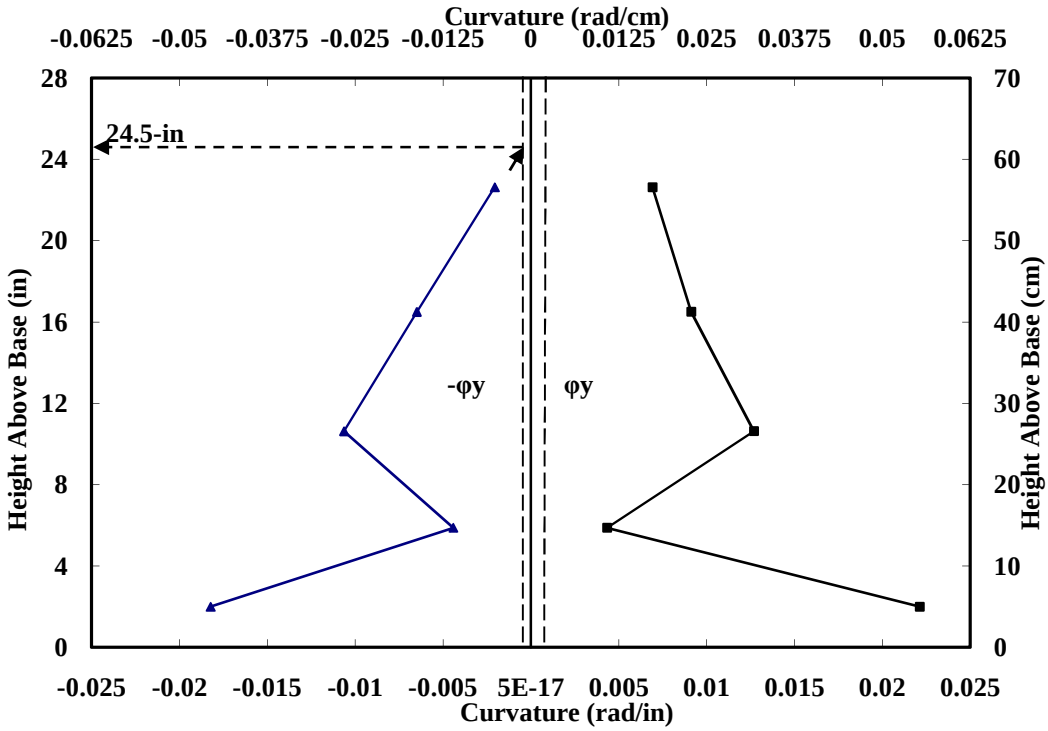

Figure 4-24: Measured Curvature Envelope along the Plastic Hinge of DCRCC24

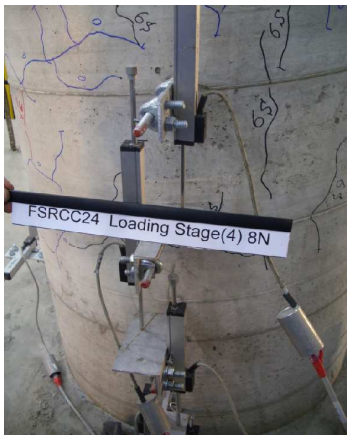

Figure 4-25: FSRCC24 Cracks (0.25fy)

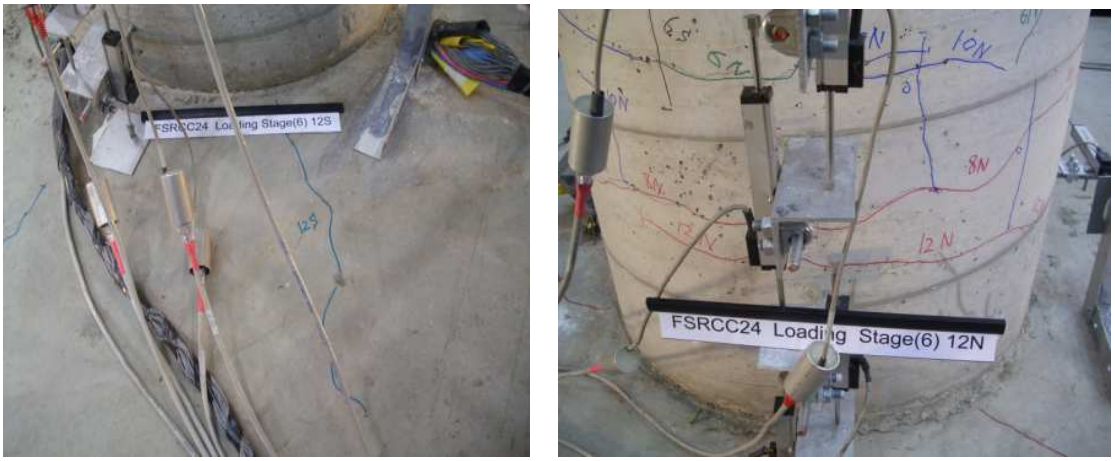

Figure 4-26: FSRCC24 Cracks (0.75fy)

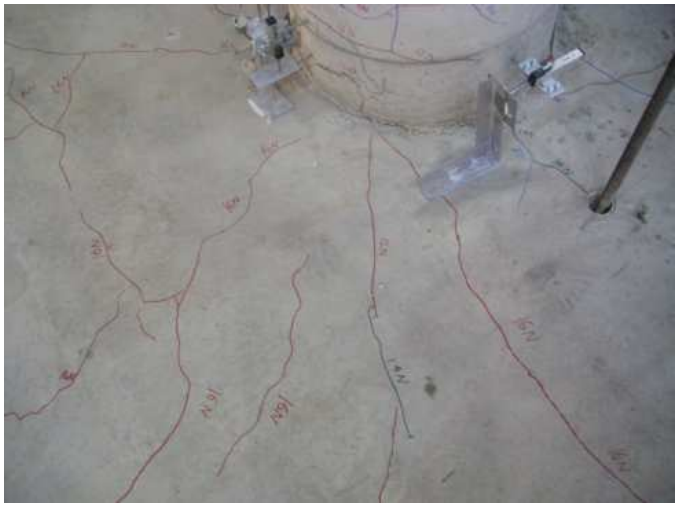

Figure 4-27: FSRCC24 Slab Cracks (1 Δy)

Figure 4-28: FSRCC24 Cracks (2 Δy)

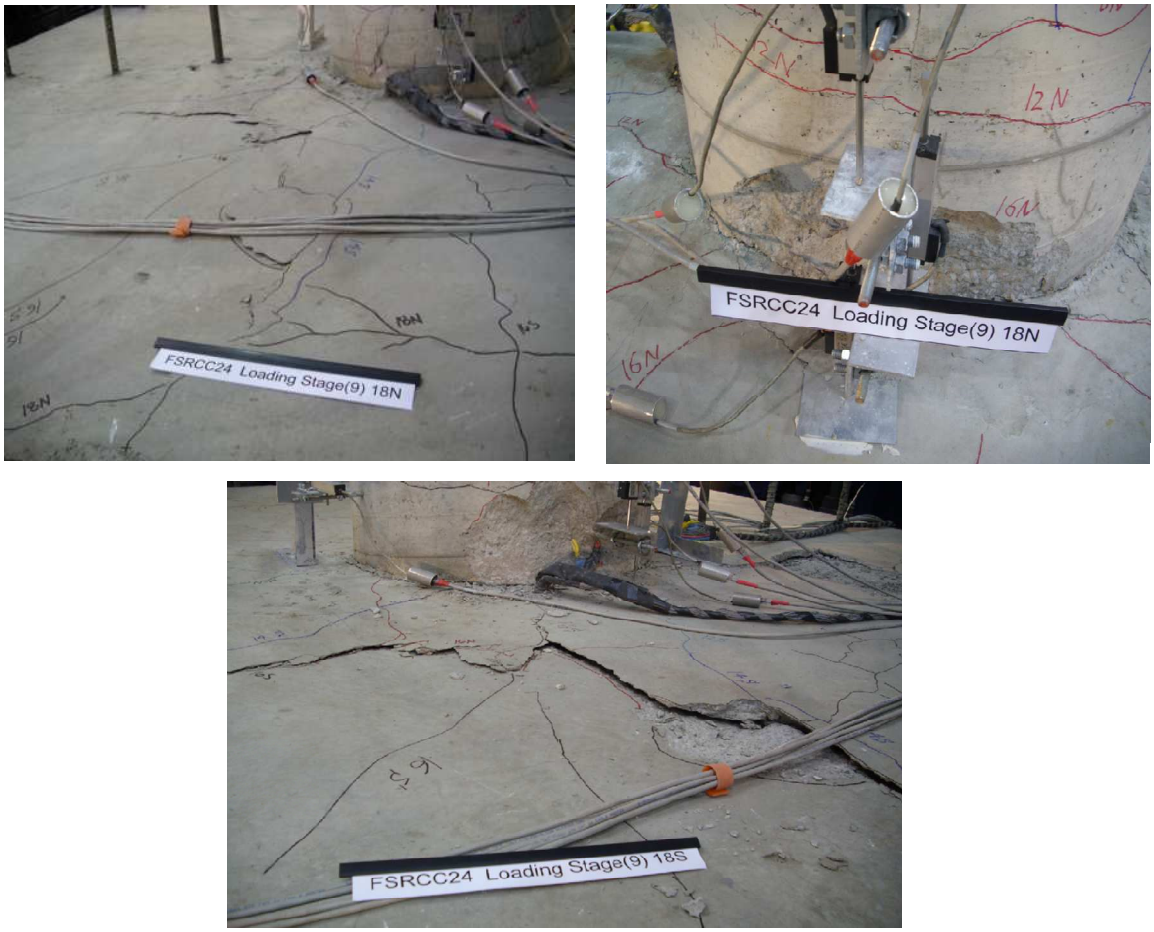

Figure 4-29: FSRCC24 Cracks (2.5 Δy)

Figure 4-30: FSRCC24 Slab Cracks (3.5 Δy)

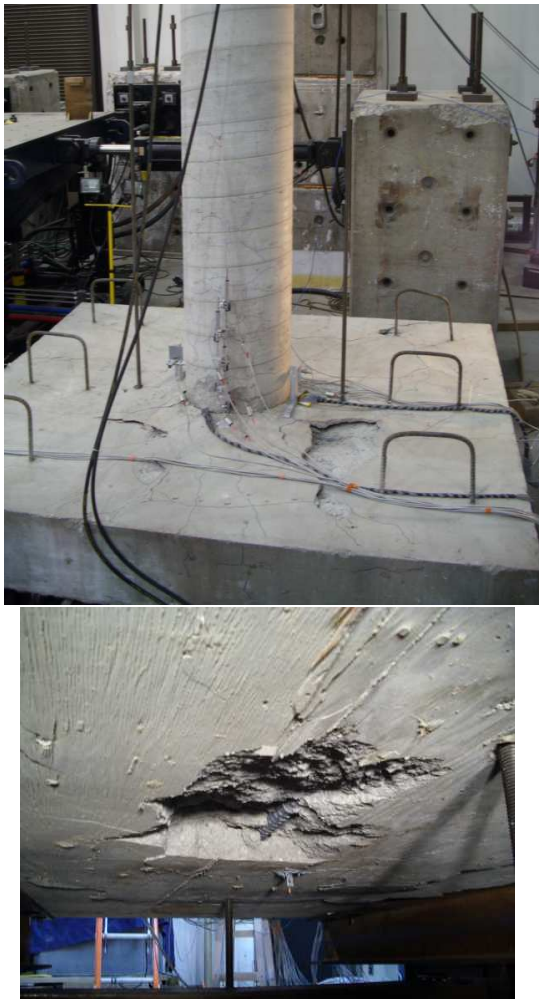

Figure 4-31: FSRCC24 Cracks (4 Δy)

Figure 4-32: The End of FSRCC24 Testing

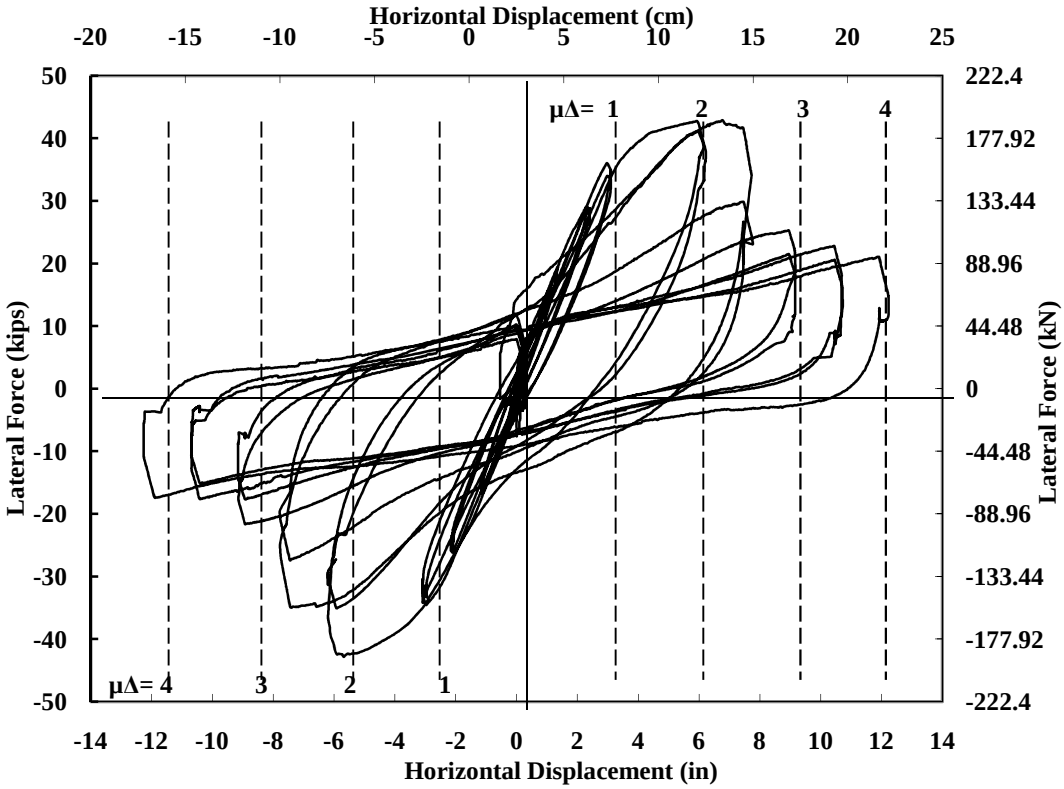

Figure 4-33: Force-Displacement Hysteretic Response for FSRCC24

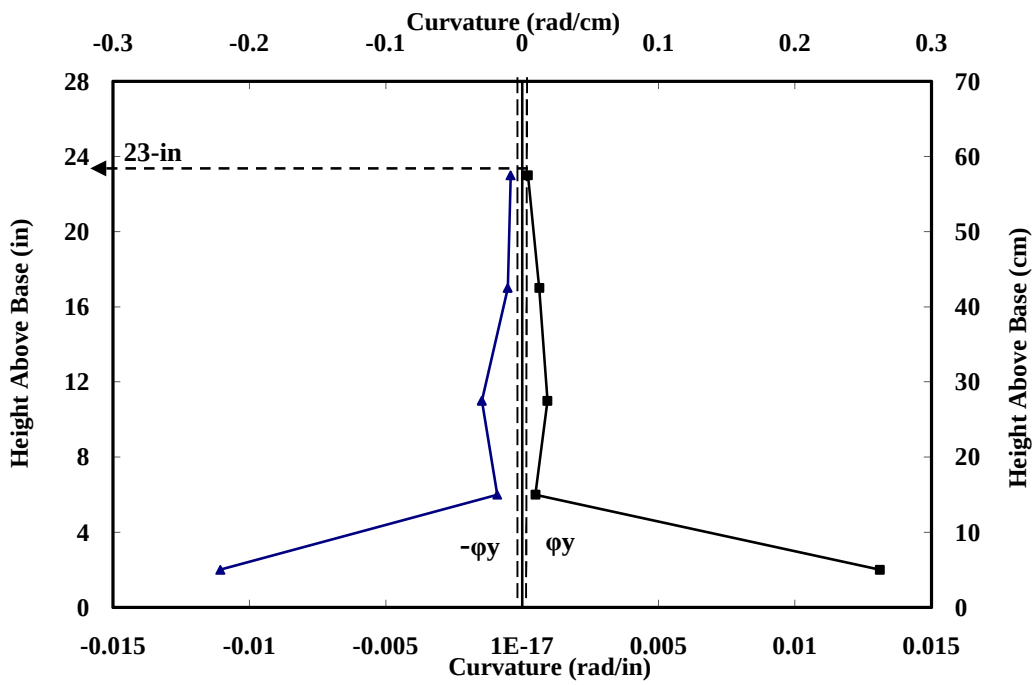

Figure 4-34: Measured Curvature Envelope along the Plastic Hinge of FSRCC24

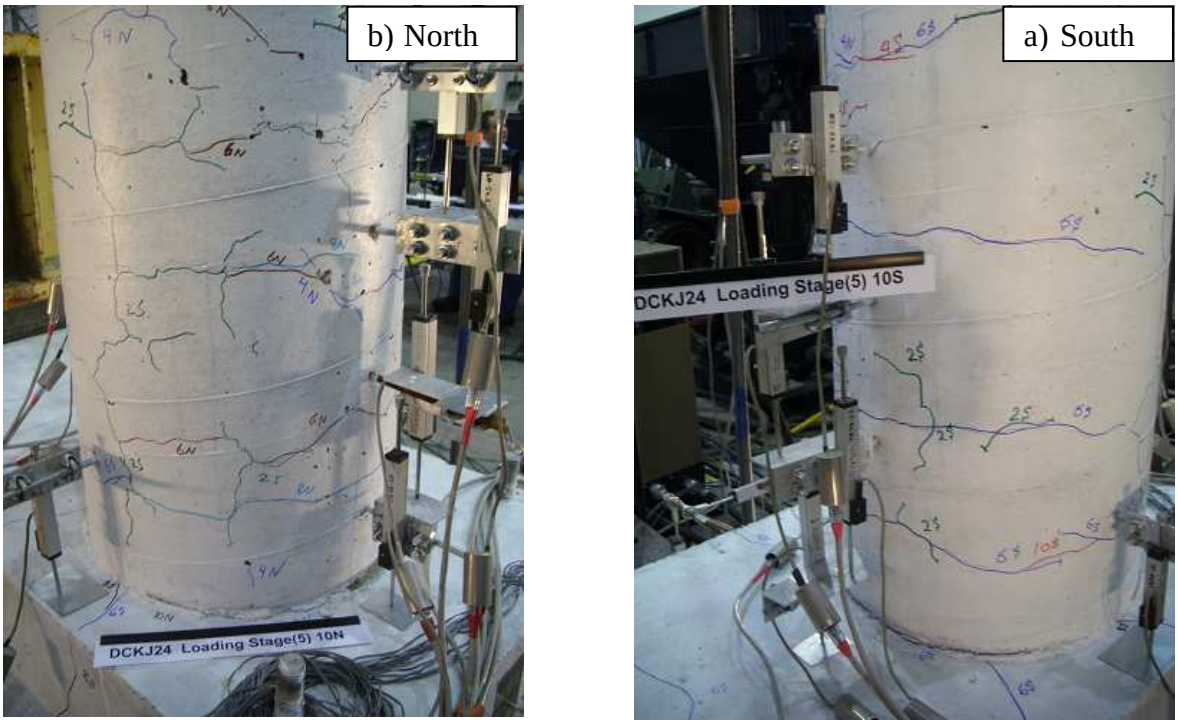

Figure 4-35: DCKJ24 Cracks (1 Δy)

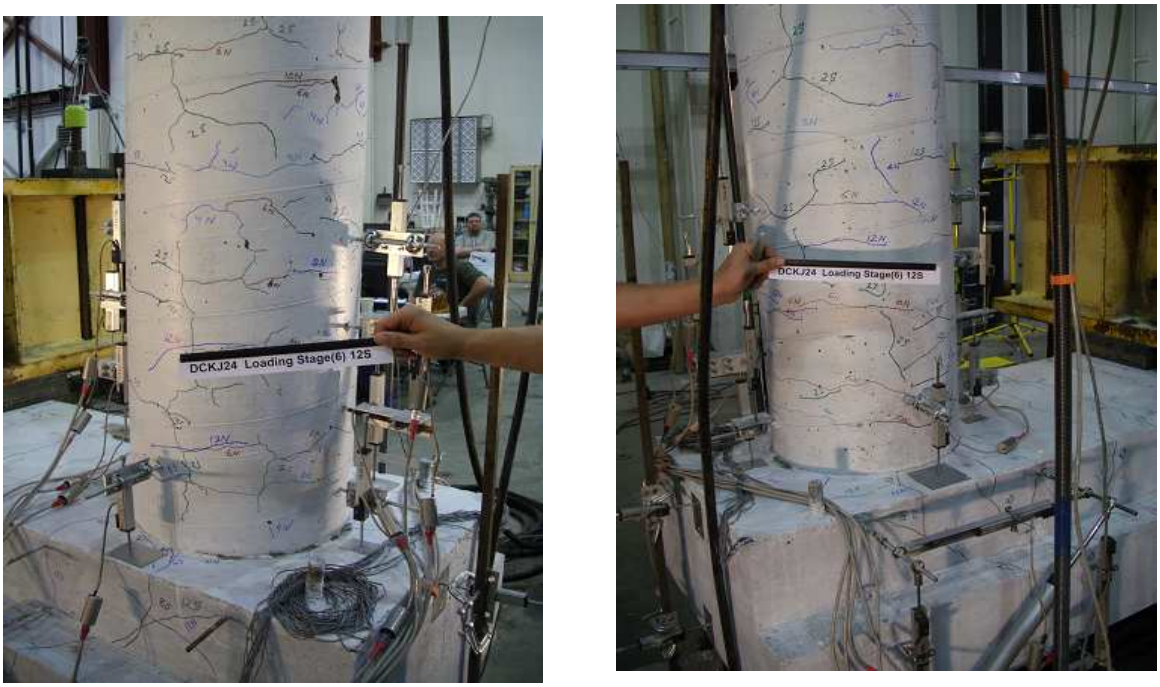

Figure 4-36: DCKJ24 Cracks (1.5 Δy)

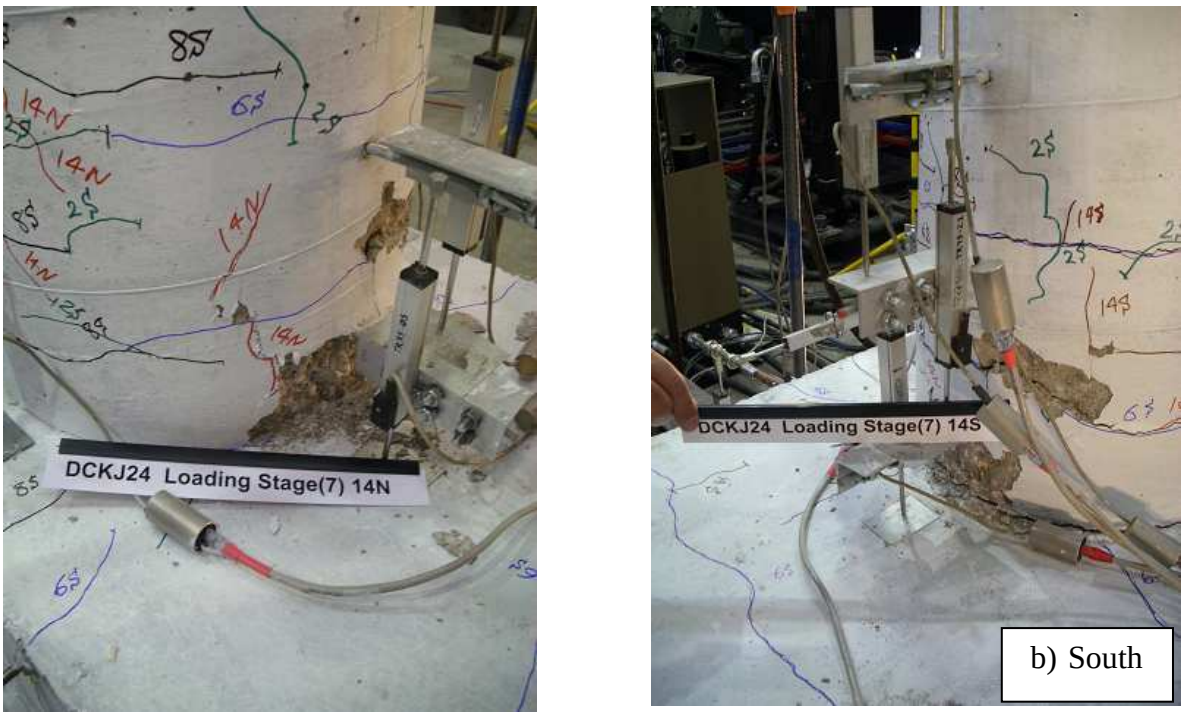

Figure 4-37: DCKJ24 Cracks (2 Δy)

Figure 4-38: DCKJ24 Cracks (3 Δy)

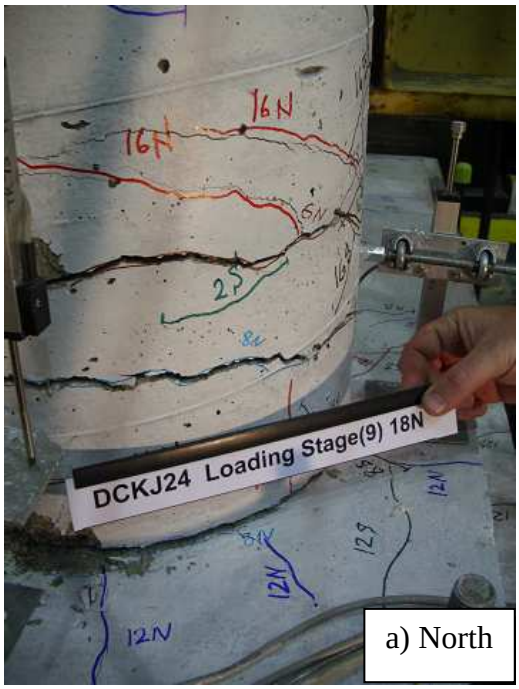

a) North

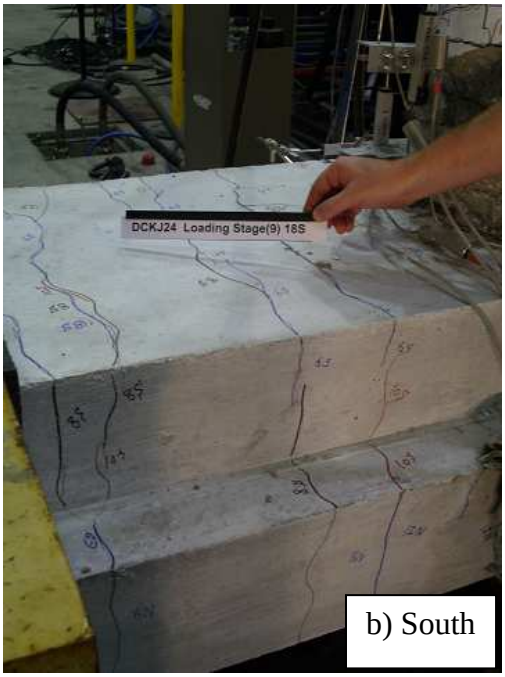

b) South

Figure 4-39: DCKJ24 Cracks (4 Δy)

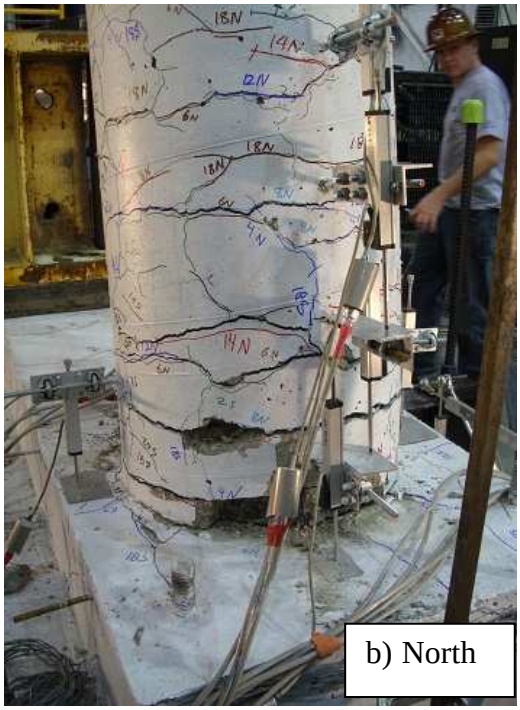

b) North

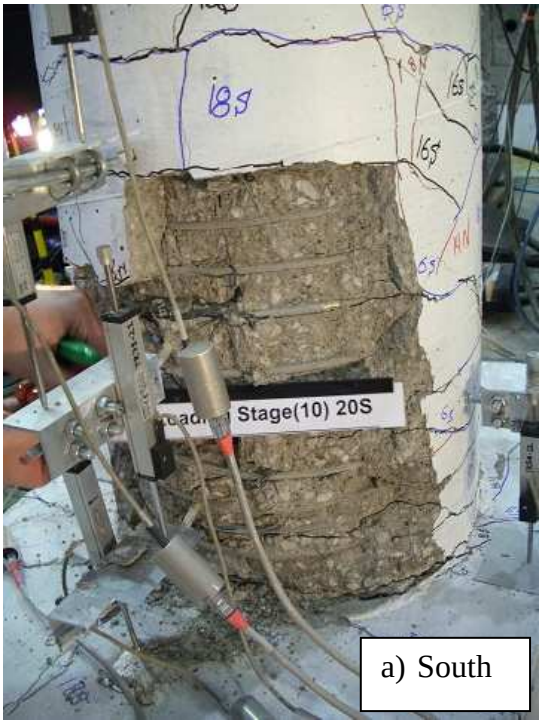

a) South

Figure 4-40: DCKJ24 Cracks (5 Δy)

Figure 4-41: DCKJ24 Cracks (6 Δy)

Figure 4-42: DCKJ24 at the End of The Test

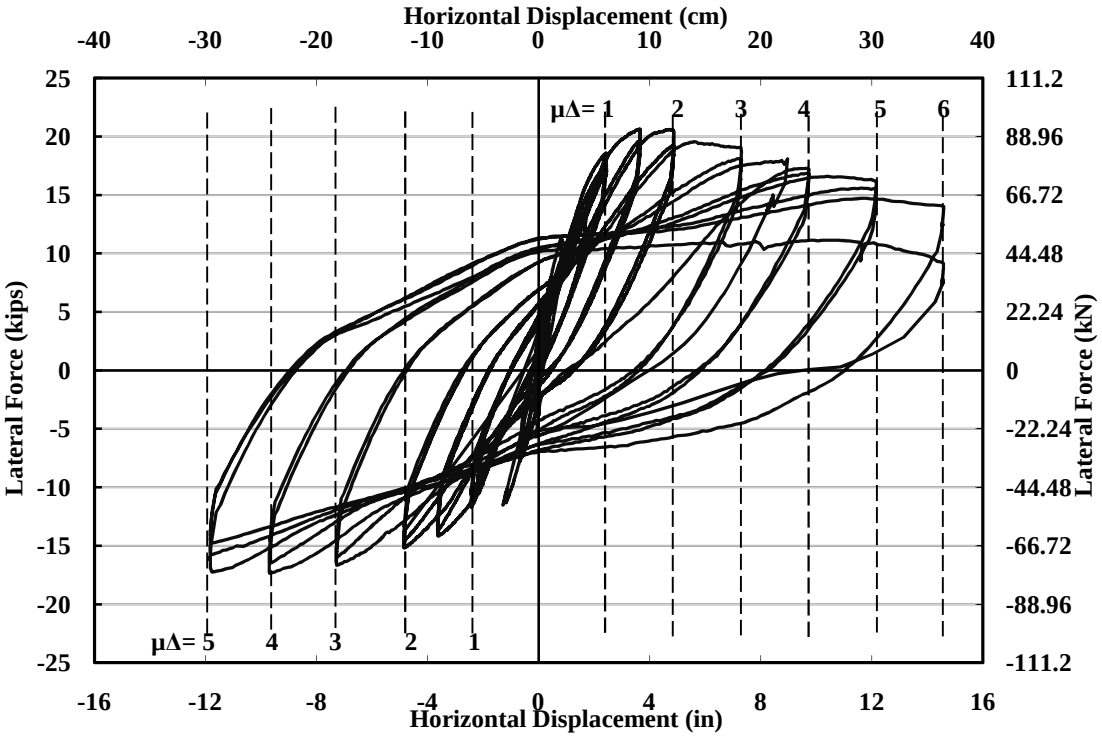

Figure 4-43: Force-Displacement Hysteretic Response for DCKJ24

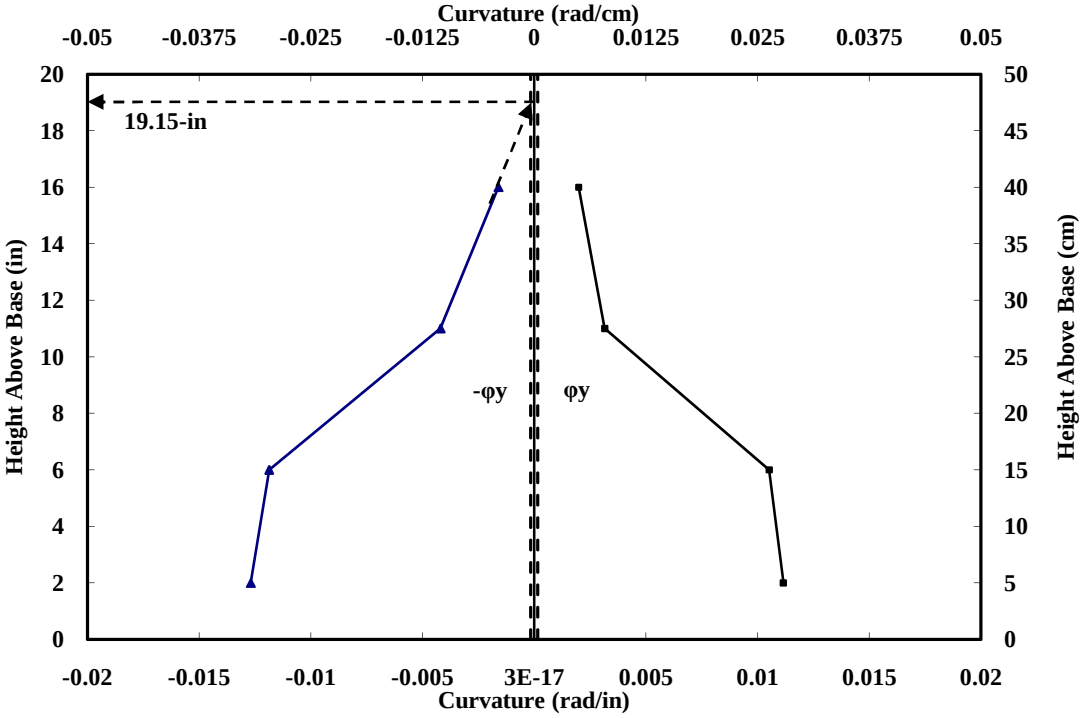

Figure 4-44: Measured Curvature Envelope along the Plastic Hinge of DCKJ24

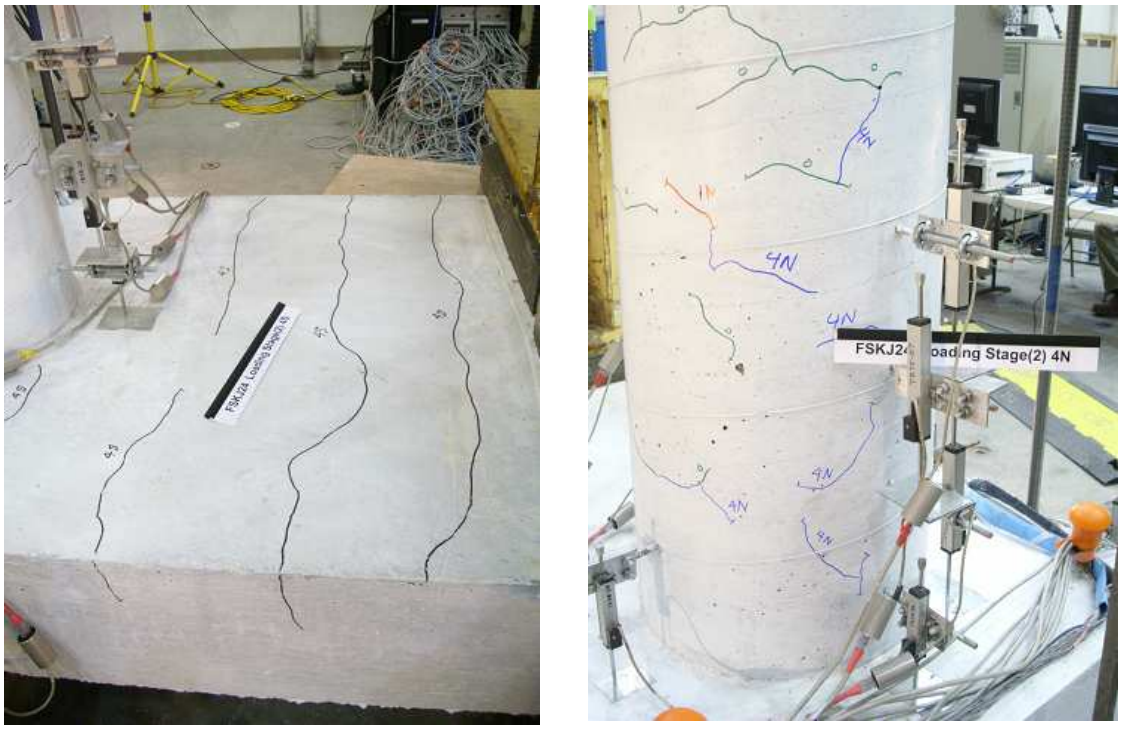

Figure 4-45: FSKJ24 Cracks (0.25fy)

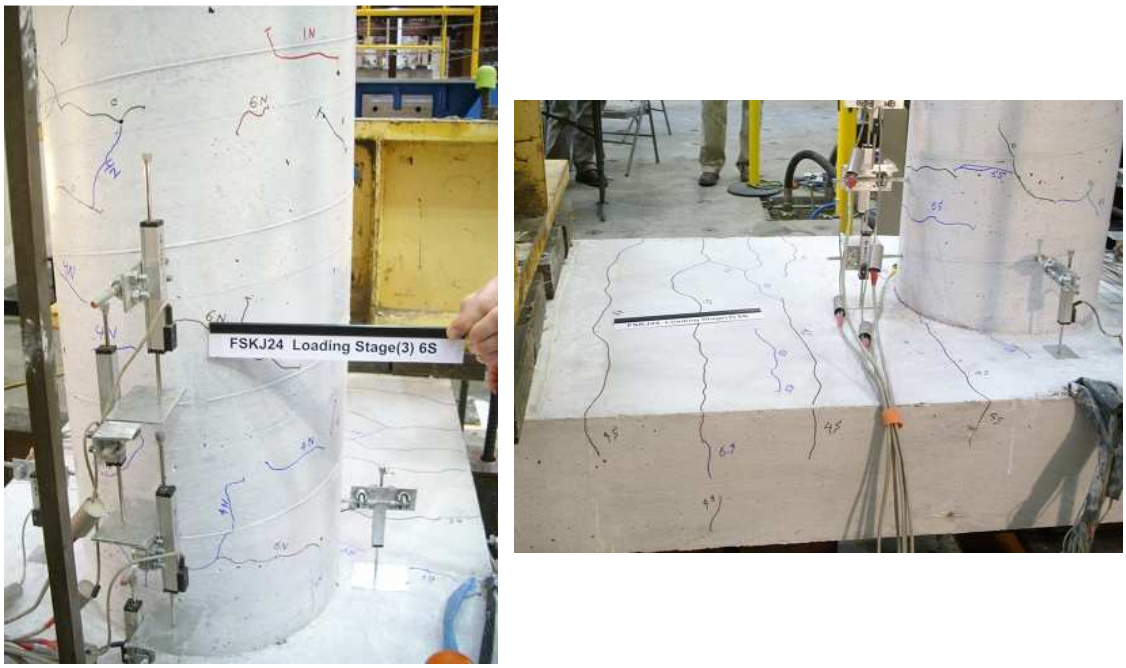

Figure 4-46: FSKJ24 Cracks (0.5fy)

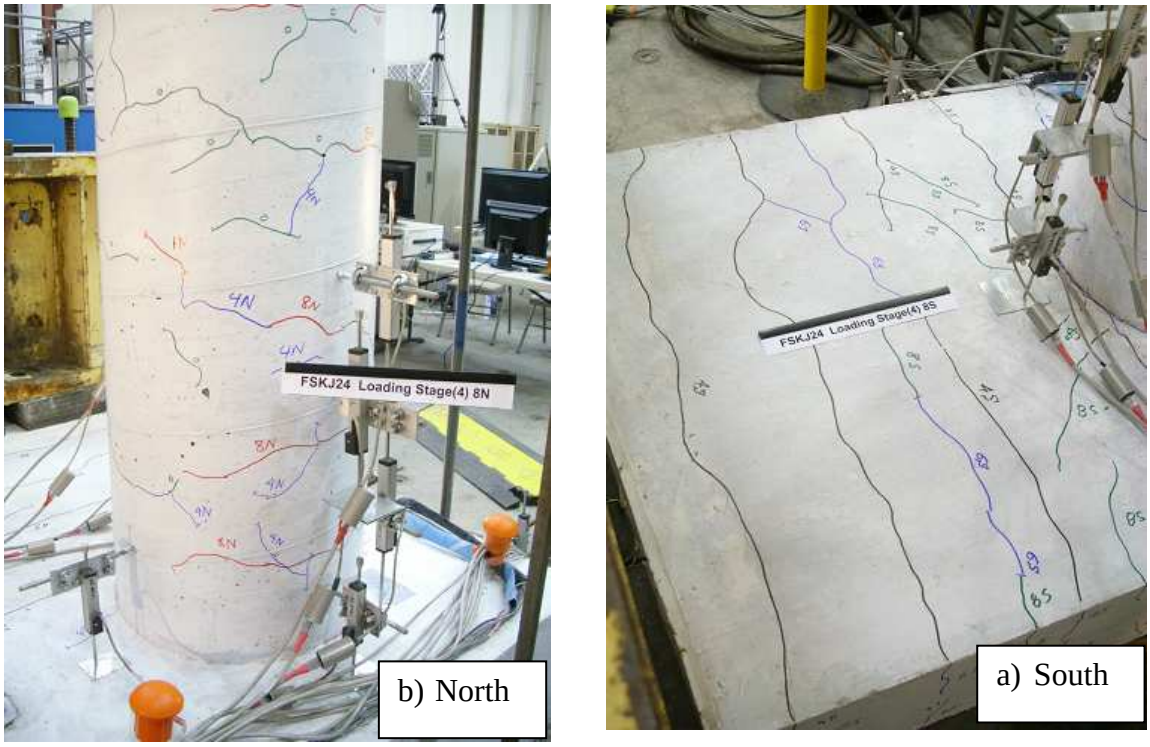

Figure 4-47: FSKJ24 Cracks (0.75fy)

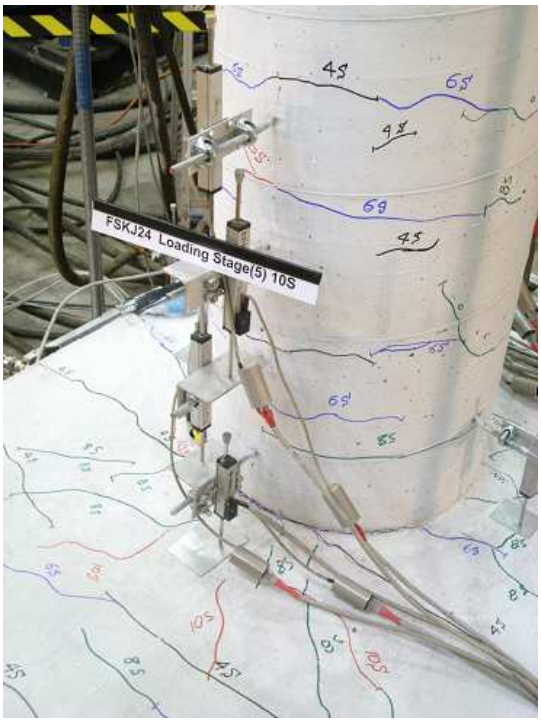

Figure 4-48: FSKJ24 Cracks (1Δy)

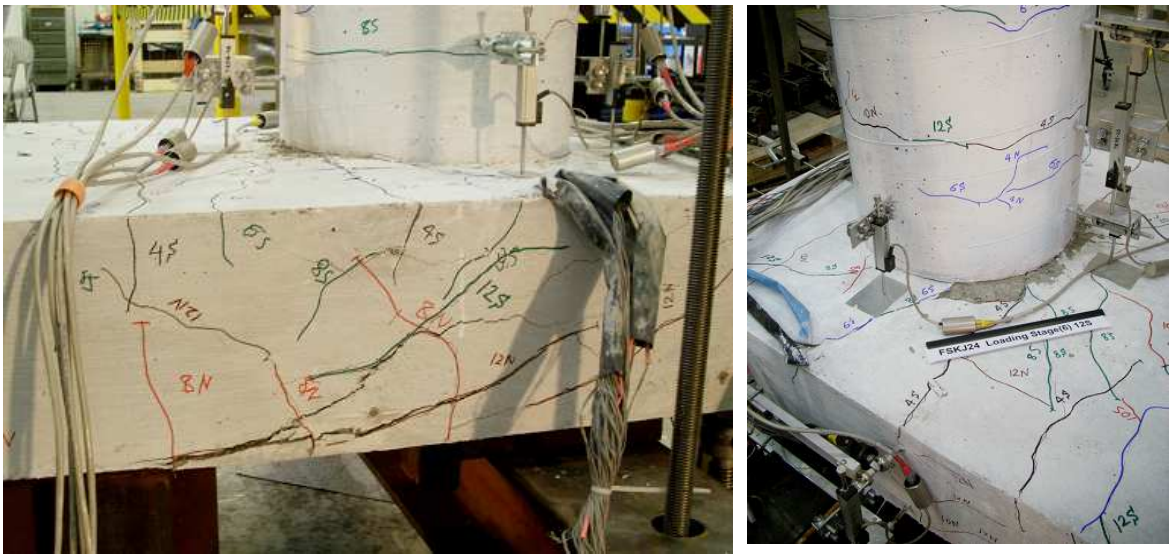

Figure 4-49: FSKJ24 Cracks (1.5Δy)

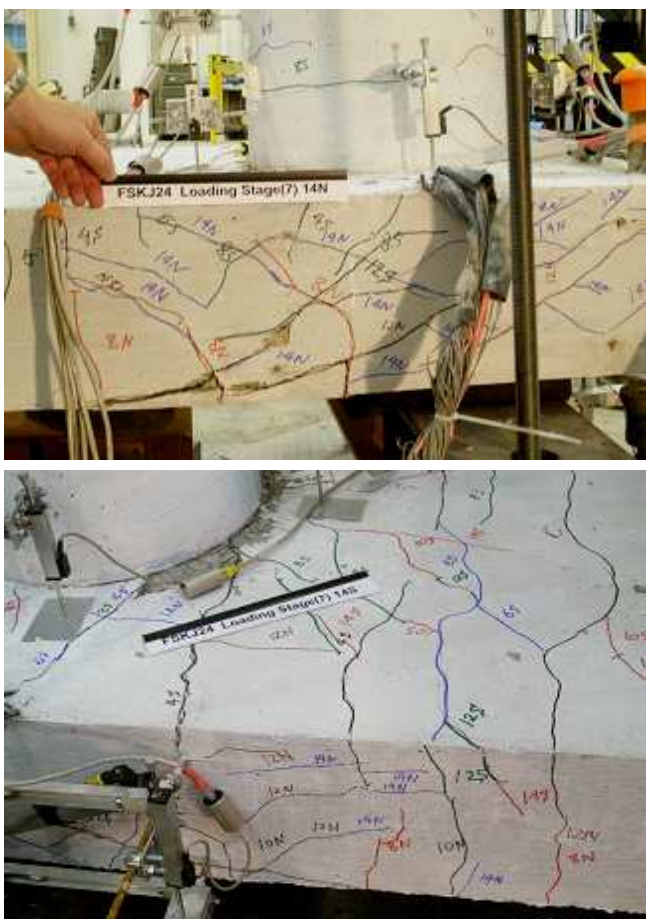

a) North

b) South

Figure 4-50: FSKJ24 Cracks (2 Δy)

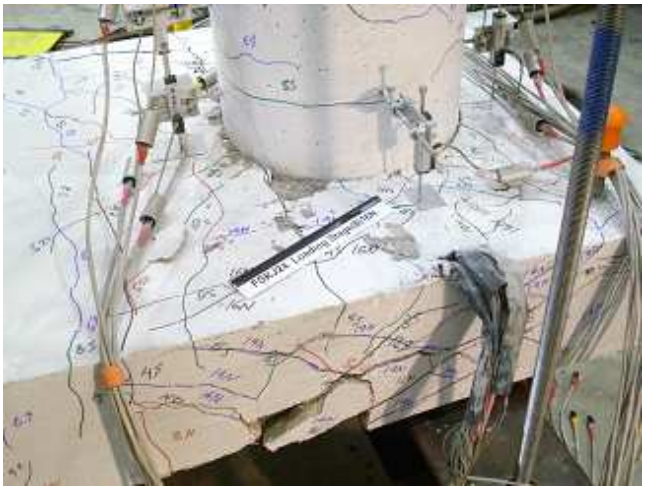

Figure 4-51: FSKJ24 Cracks (2.5Δy)

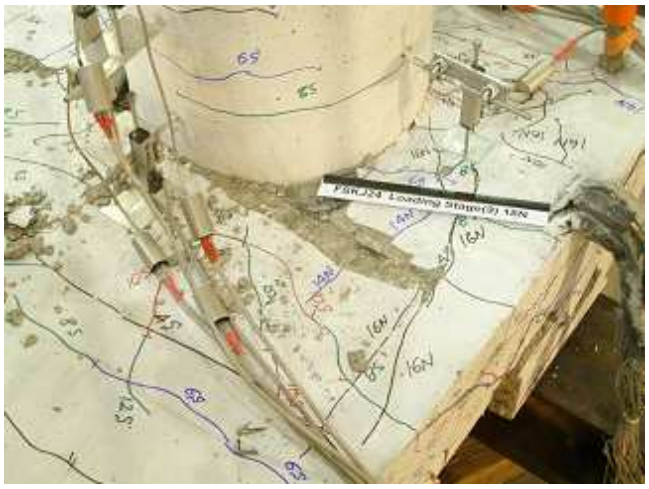

b) North

a) South

Figure 4-52: FSKJ24 Cracks (3Δy)

Figure 4-53: FSKJ24 at the End of The Test

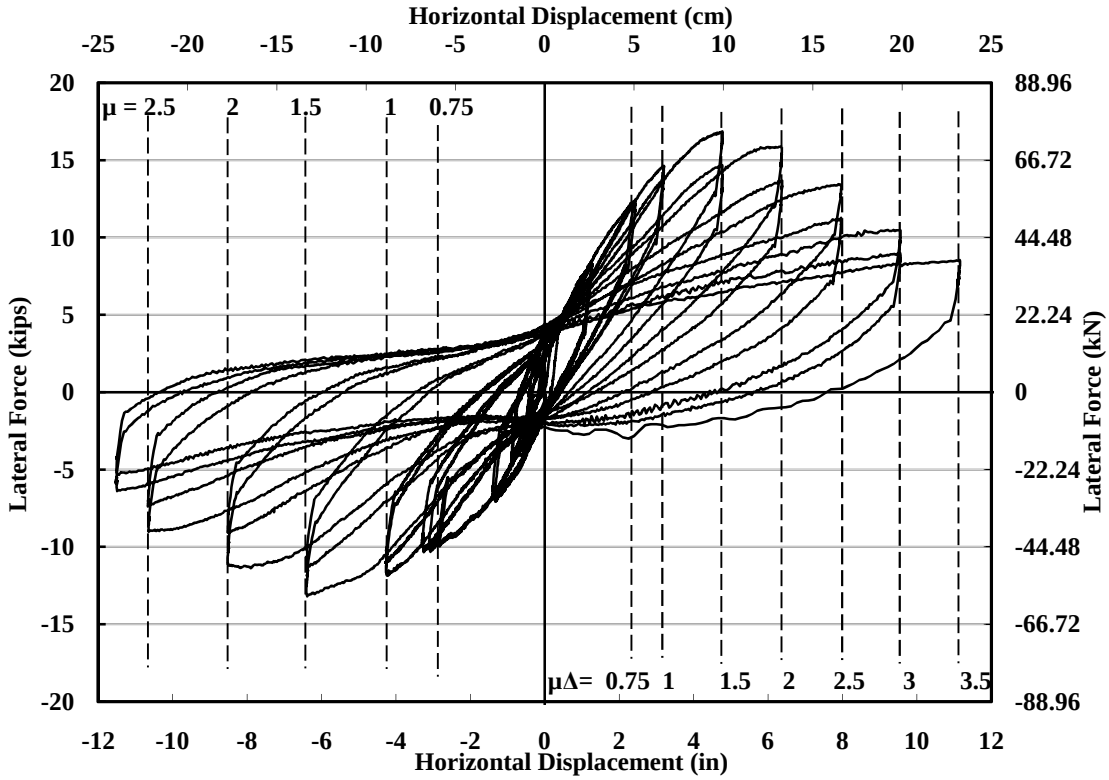

Figure 4-54: Force-Displacement Hysteretic Response for FSKJ24

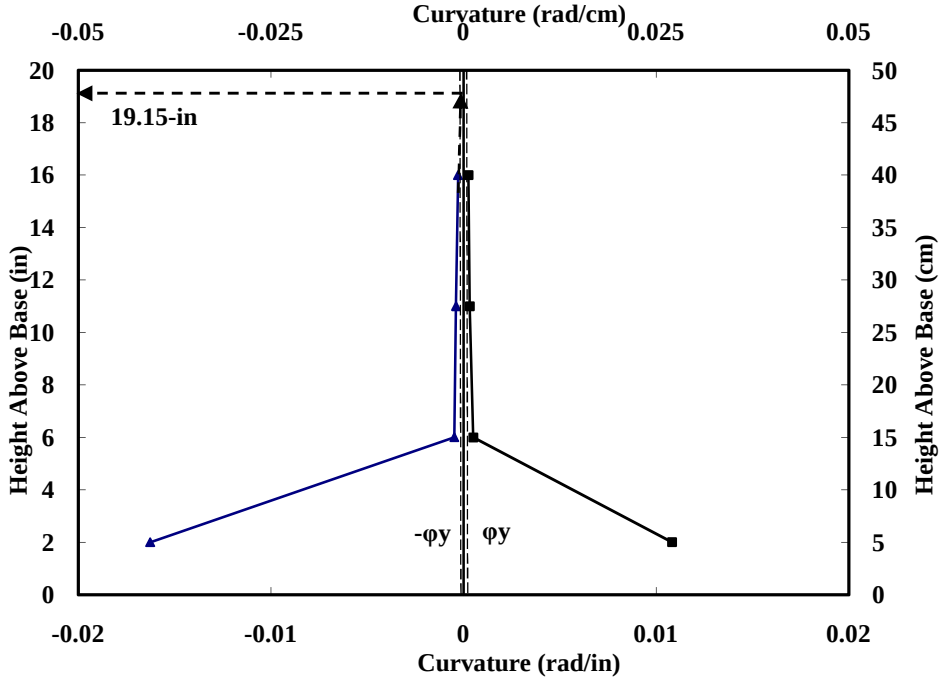

Figure 4-55: Measured Curvature Envelope along the Plastic Hinge of FSKJ24

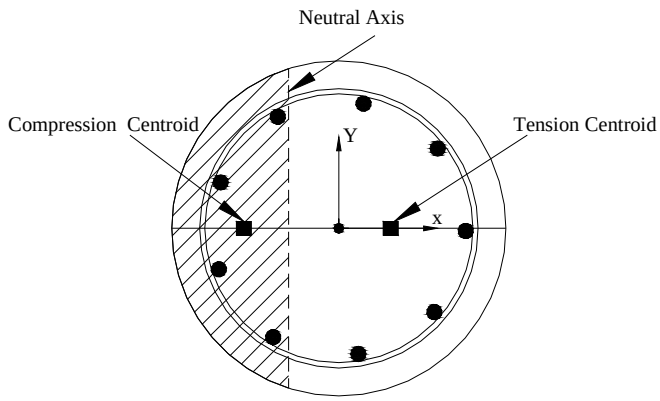

Figure 5-1: Tension and Compression Centroids of Pile

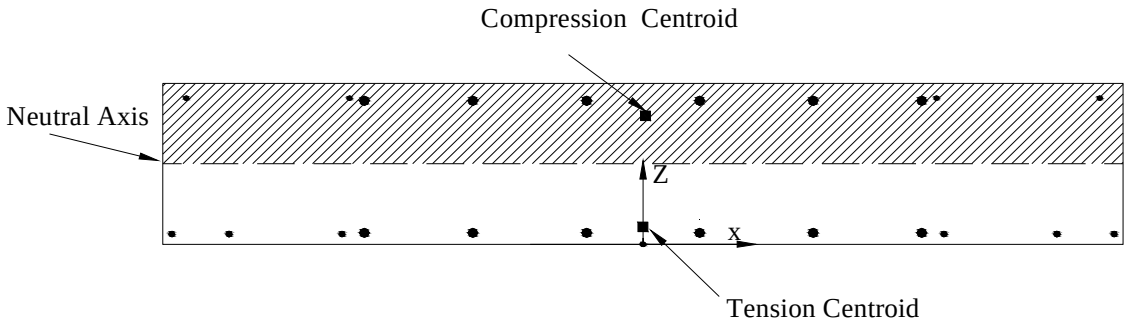

Positive Moment for Flat Slab

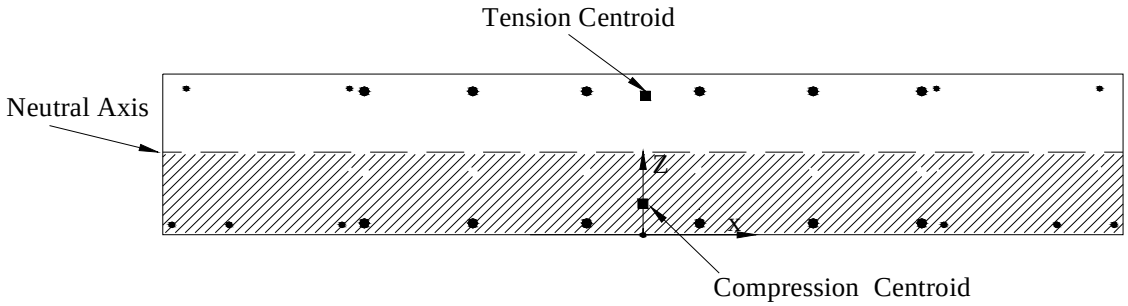

Negative Moment for Flat Slab

Figure 5-2: Tension and Compression Centroids of the Flat-Slab in Positive and Negative Moment

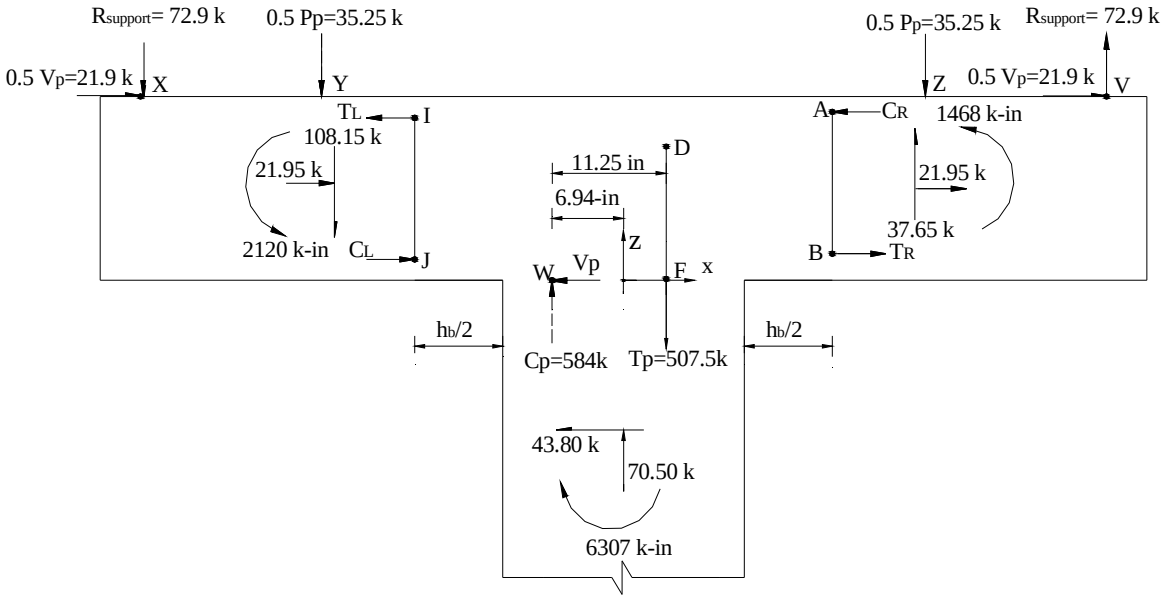

Figure 5-3:Boundary Forces –Full Specimen

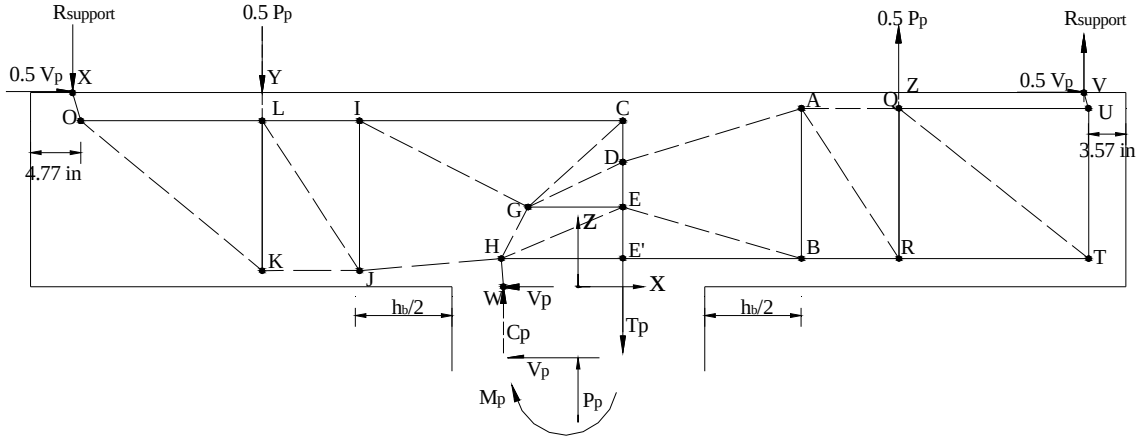

Figure 5-4: Strut-and-Tie Model for Specimen FRCC24

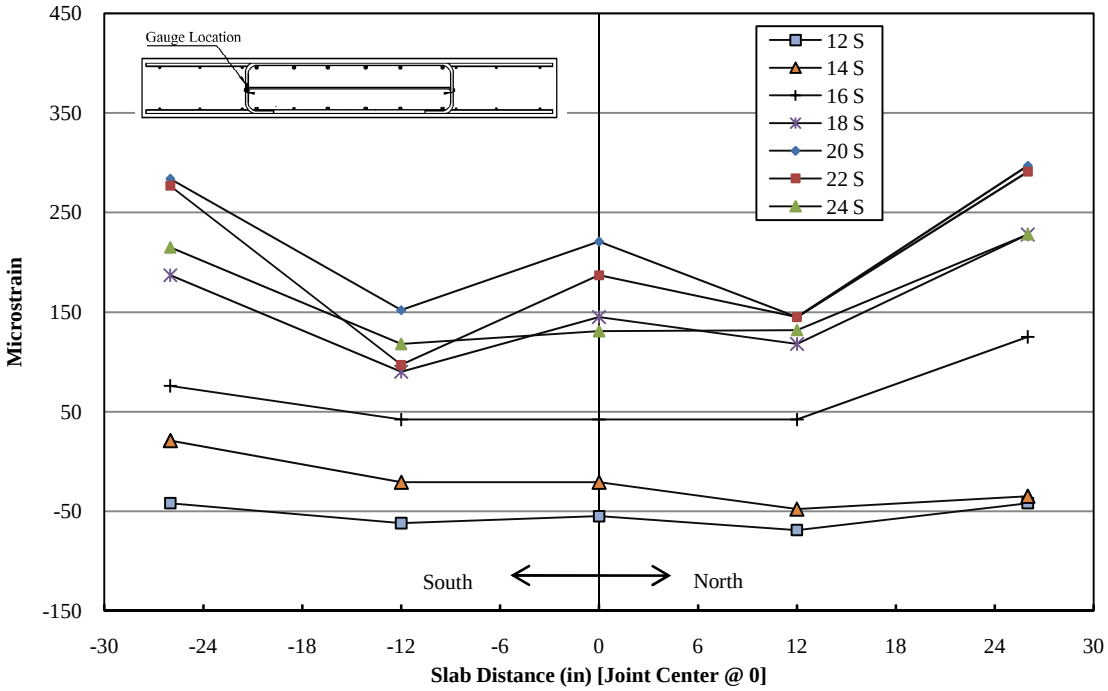

Figure 5-5: Joint Stirrup Strain for FSRCC24 South Cycle 2

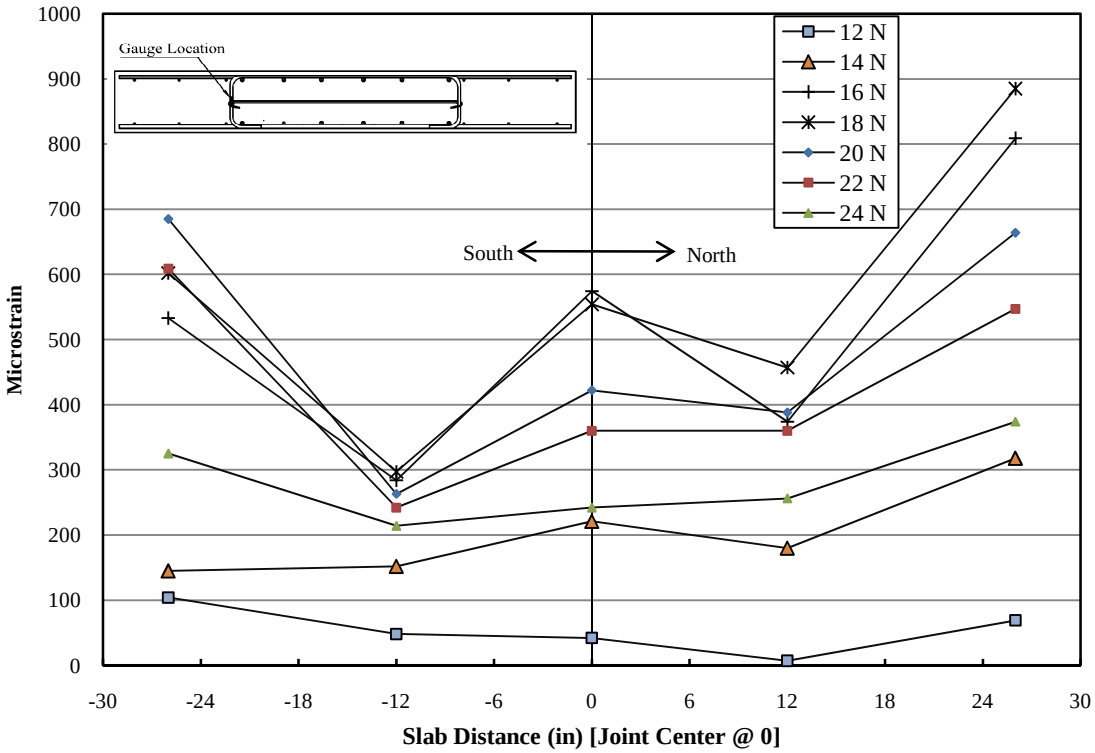

Figure 5-6: Joint Stirrup Strain for FSRCC24 North Cycle 2

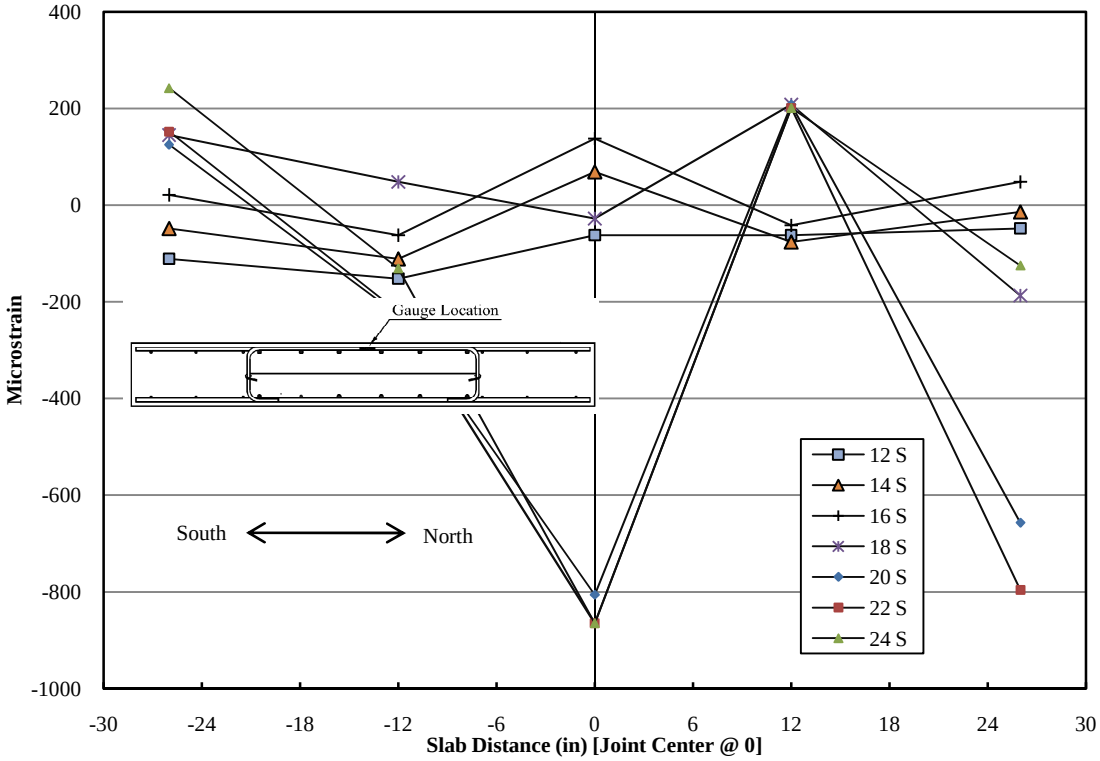

Figure 5-7: Joint Stirrup Strain for FSRCC24 South Cycle 2

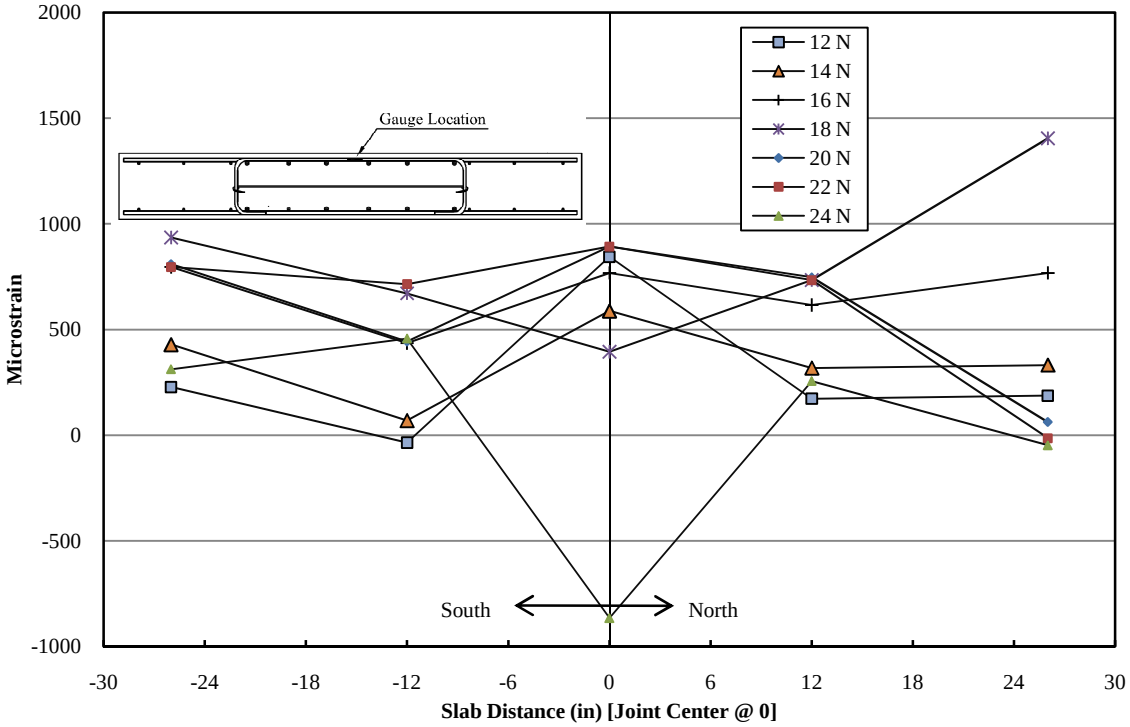

Figure 5-8: Joint Stirrup Strain for FSRCC24 North Cycle 2

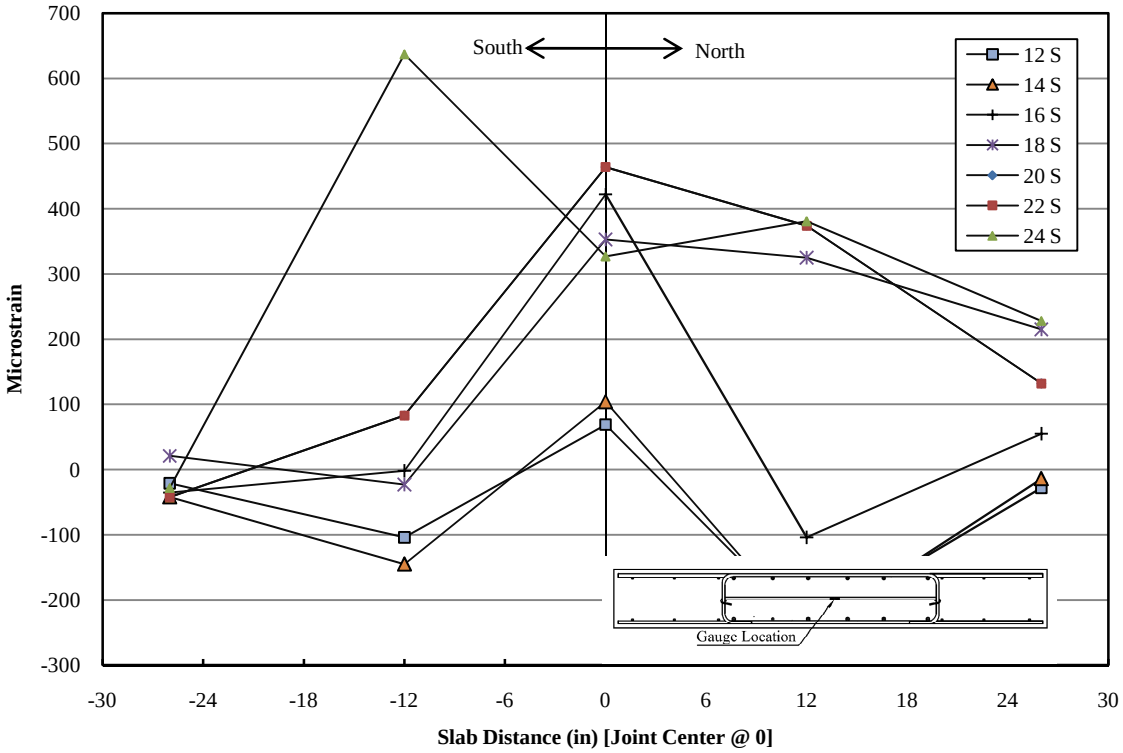

Figure 5-9: Joint Stirrup Strain for FSRCC24 South Cycle 2

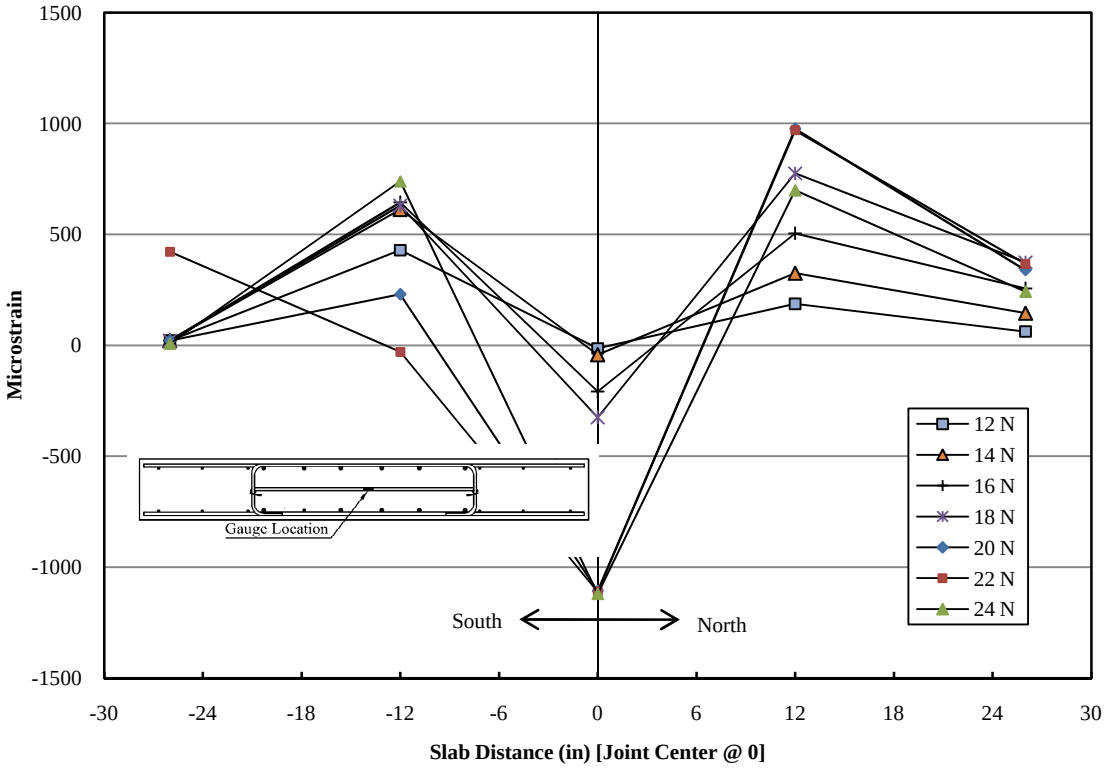

Figure 5-10: Joint Stirrup Strain for FSRCC24 North Cycle 2

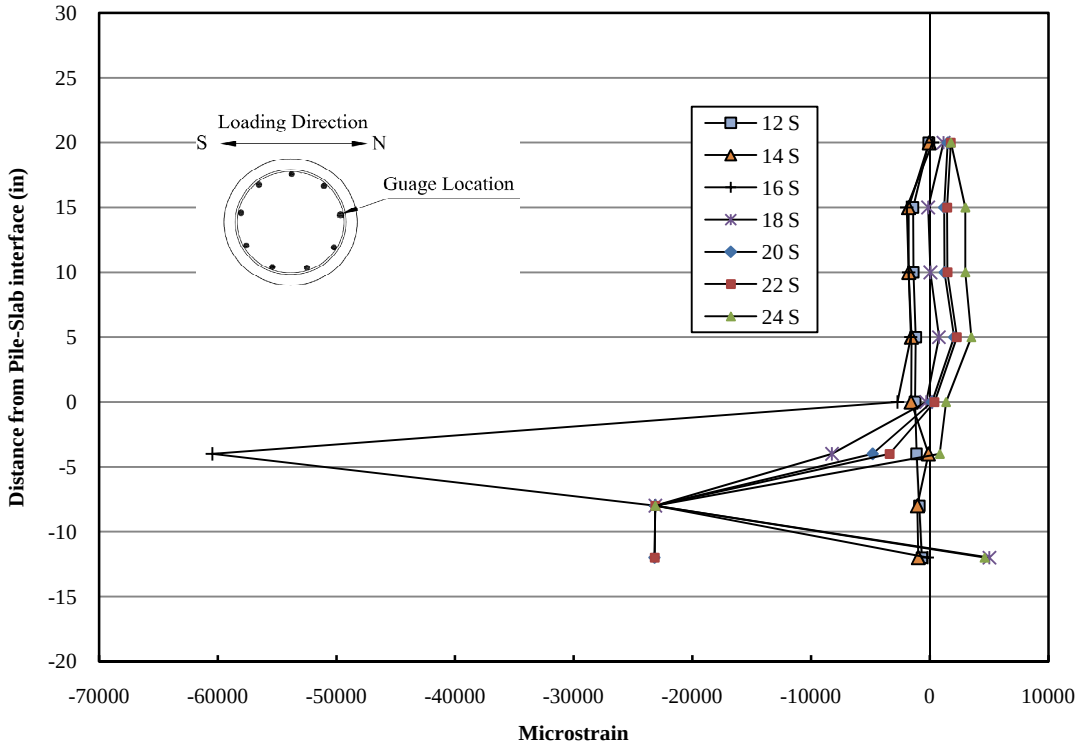

Figure 5-11: Longitudinal Pile Strain for FSRCC24 South Cycle 2

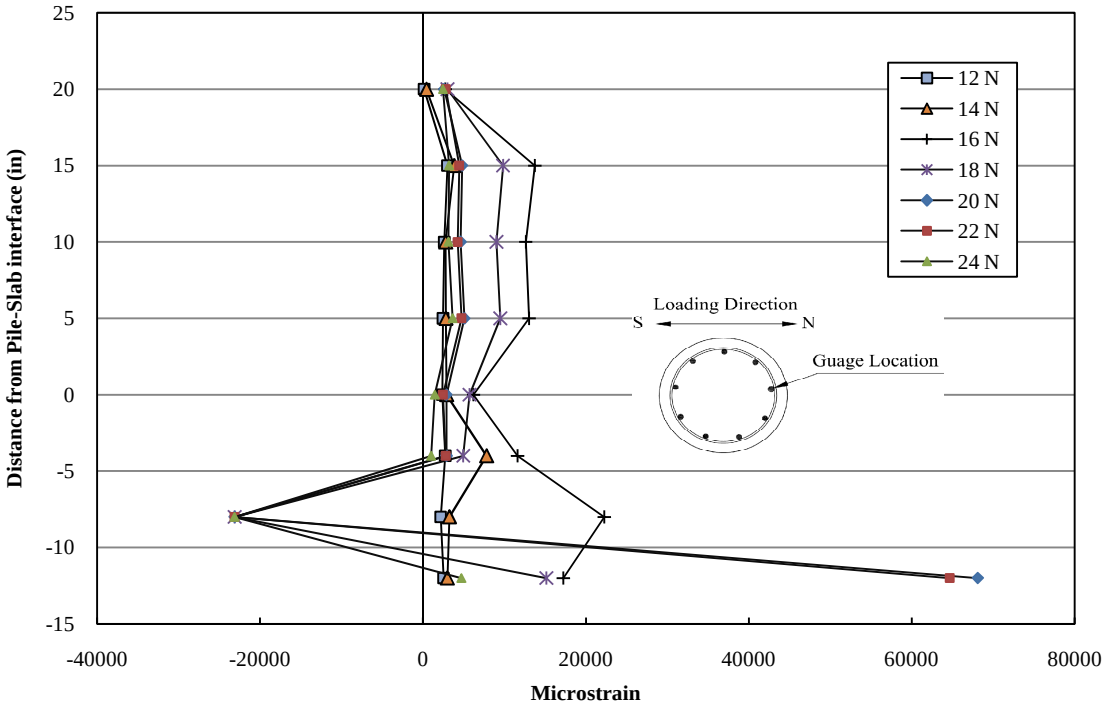

Figure 5-12: Longitudinal Pile Strain for FSRCC24 North Cycle 2

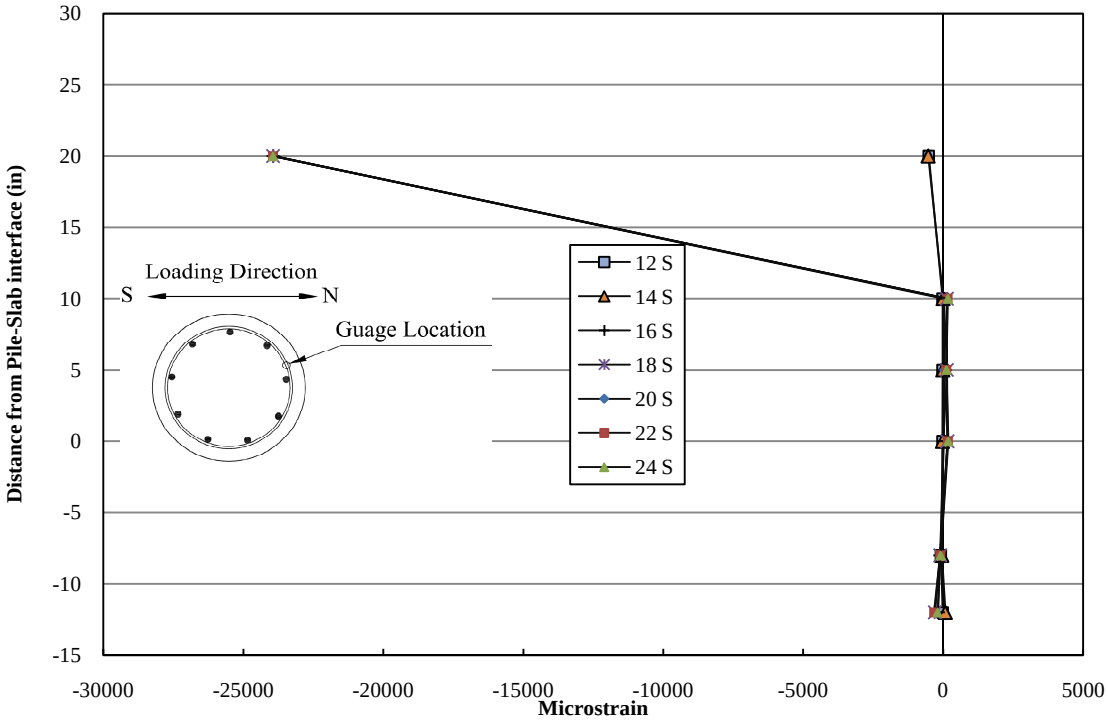

Figure 5-13: Spiral Reinforcement Strain for FSRCC24 South Cycle 2

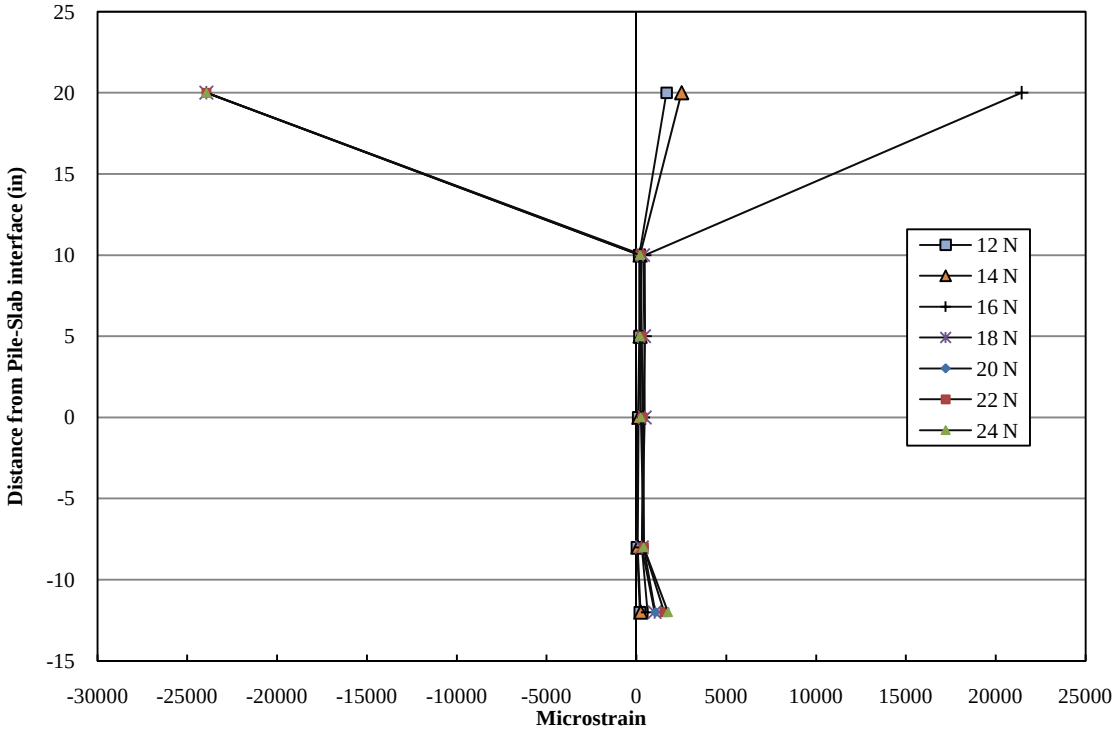

Figure 5-14: Spiral Reinforcement Strain for FSRCC24 North Cycle 2

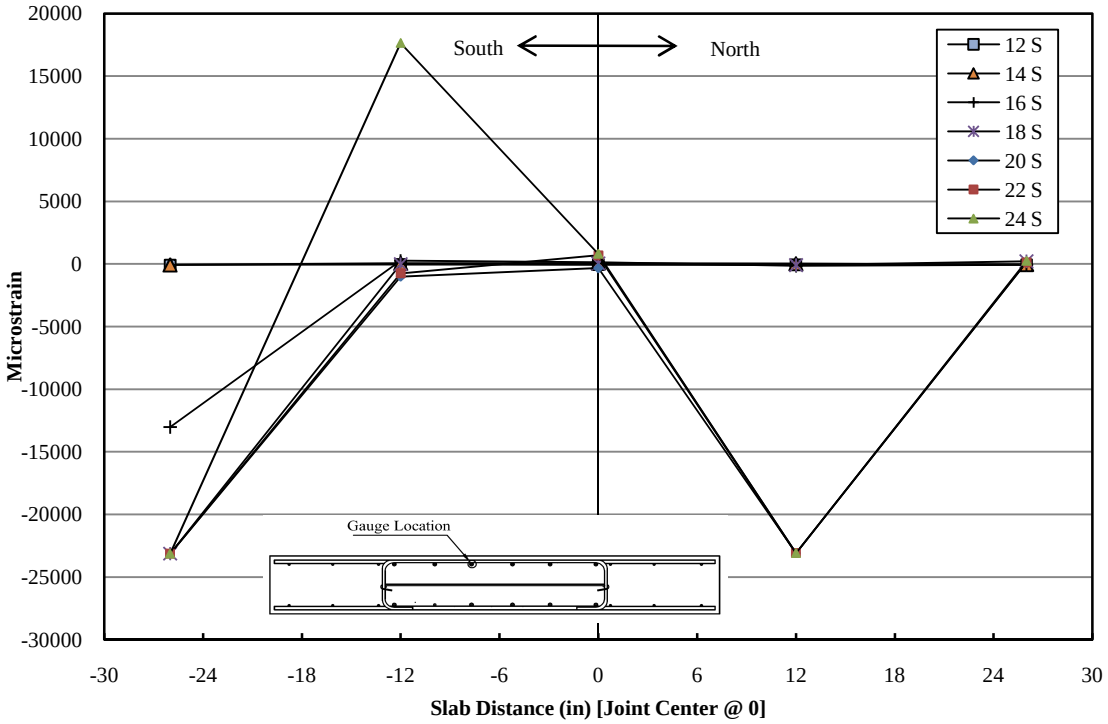

Figure 5-15: Slab Top Reinforcement for FSRCC24 South Cycle 2

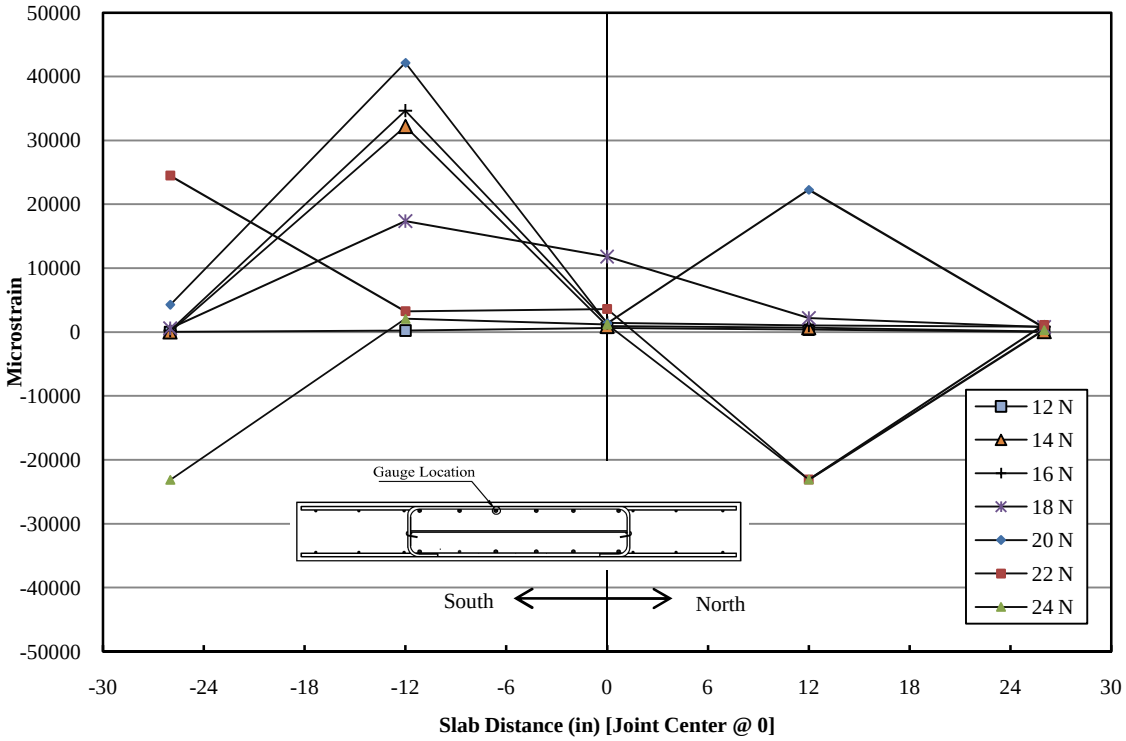

Figure 5-16: Slab Top Reinforcement for FSRCC24 North Cycle 2

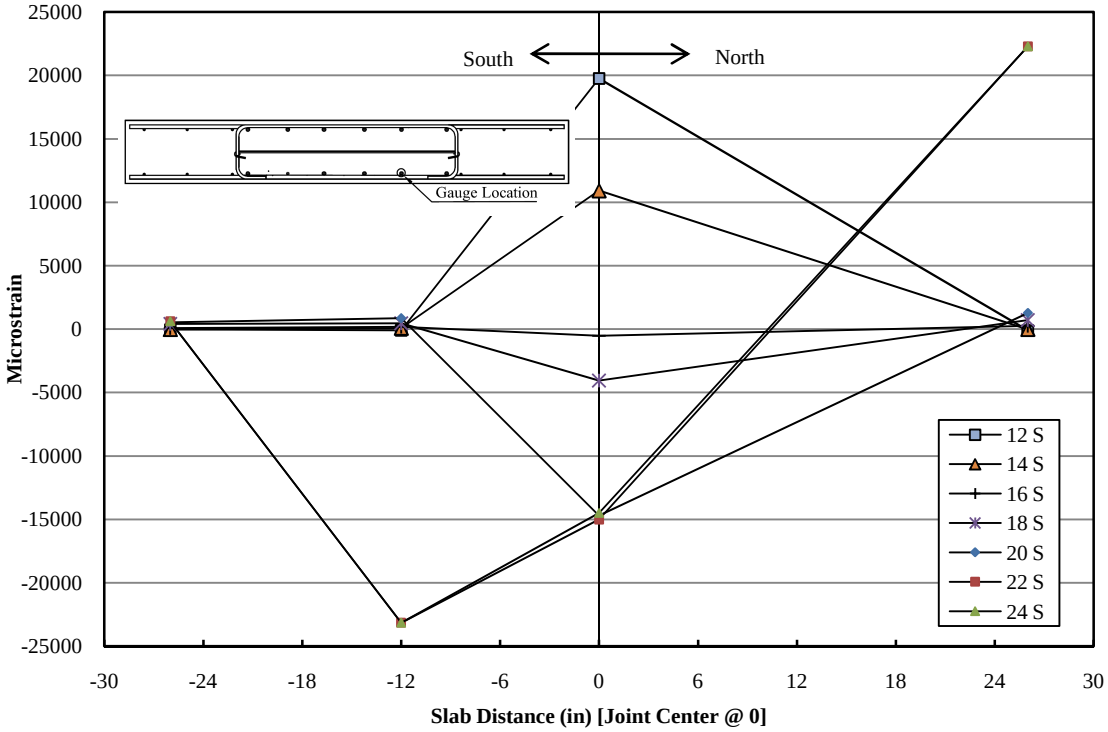

Figure 5-17: Slab Bottom Reinforcement Strainfor FSRCC24 South Cycle 2

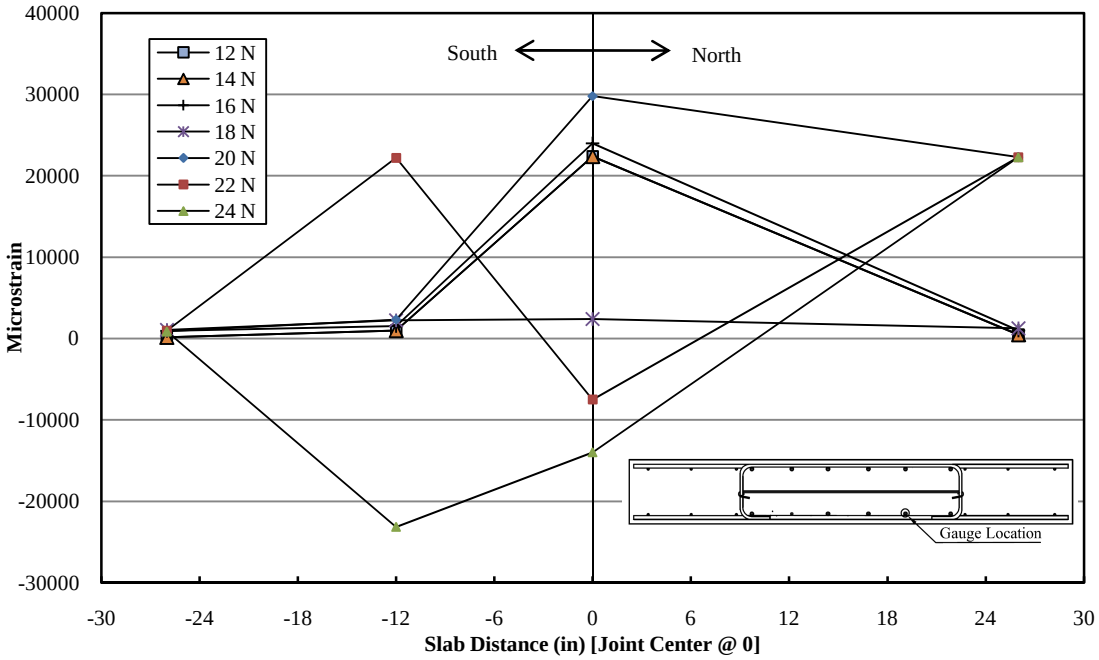

Figure 5-18: Slab Bottom Reinforcement Strainfor FSRCC24 North Cycle 2

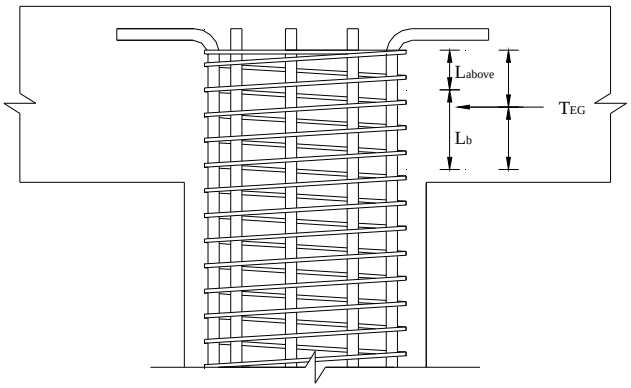

Figure 5-19: Tension and Compression Centroids of Slab

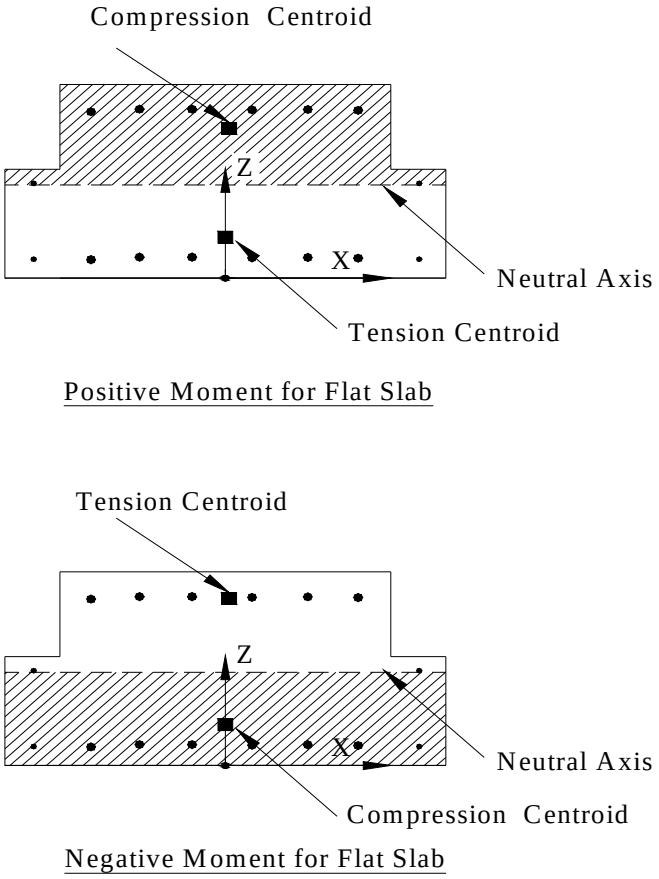

Figure 5-20: Tension and Compression Centroids of the Drop-Cap Slab in Positive and Negative Moment

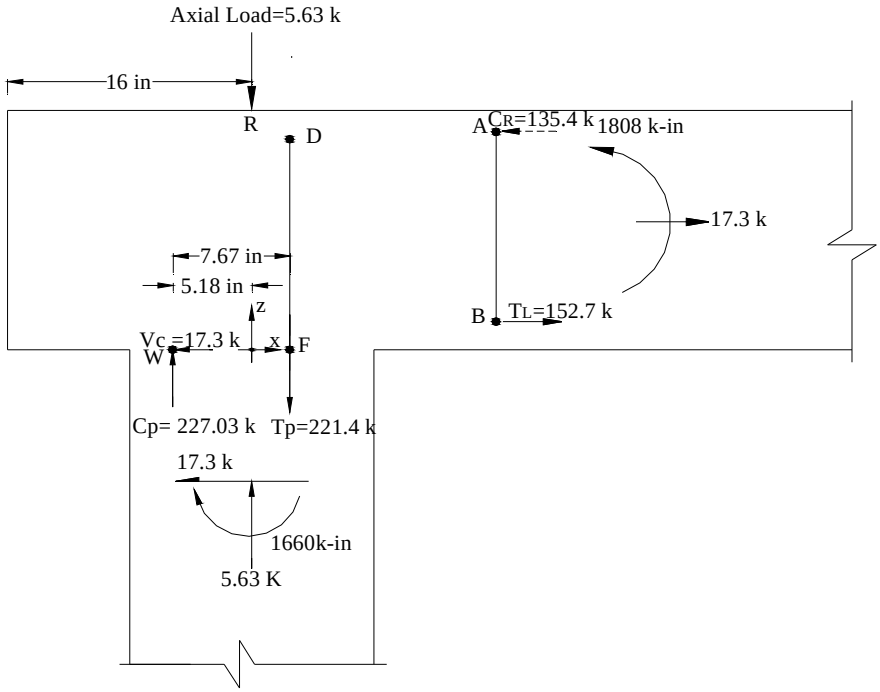

Figure 5-21: Boundary Forces for DCKJ24 in Openning Position

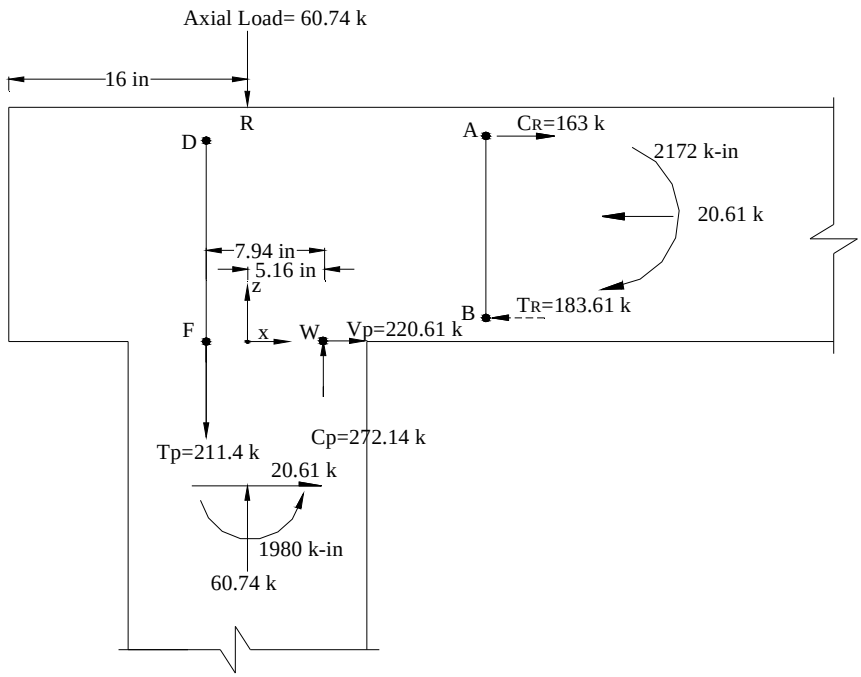

Figure 5-22: Boundary Forces for DCKJ24 in Clossing Position

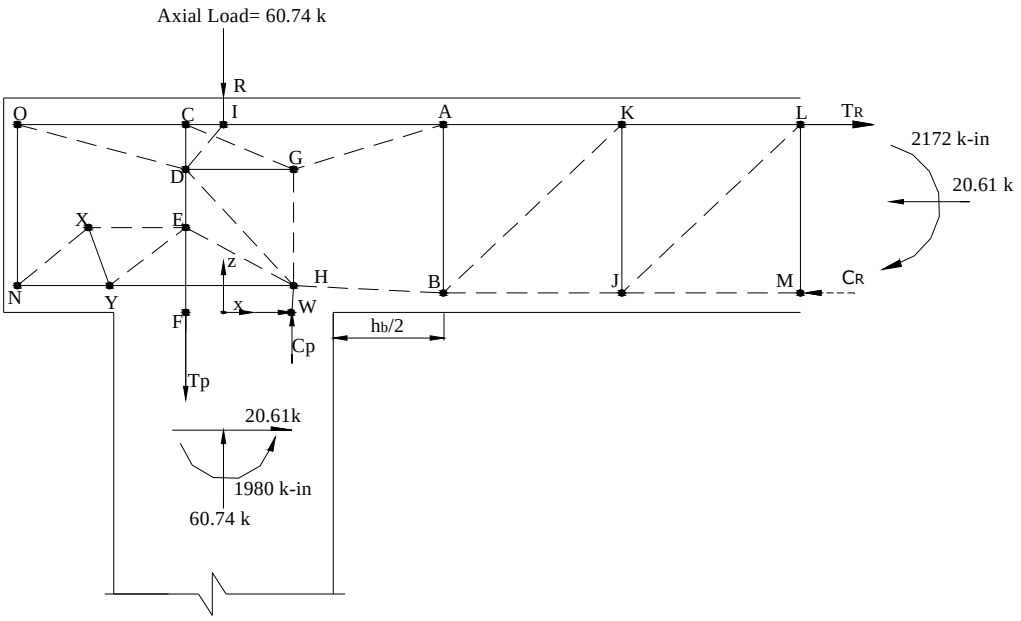

Figure 5-23: Strut-and-Tie Model for Specimen DCKJ24 (Closing Moment)

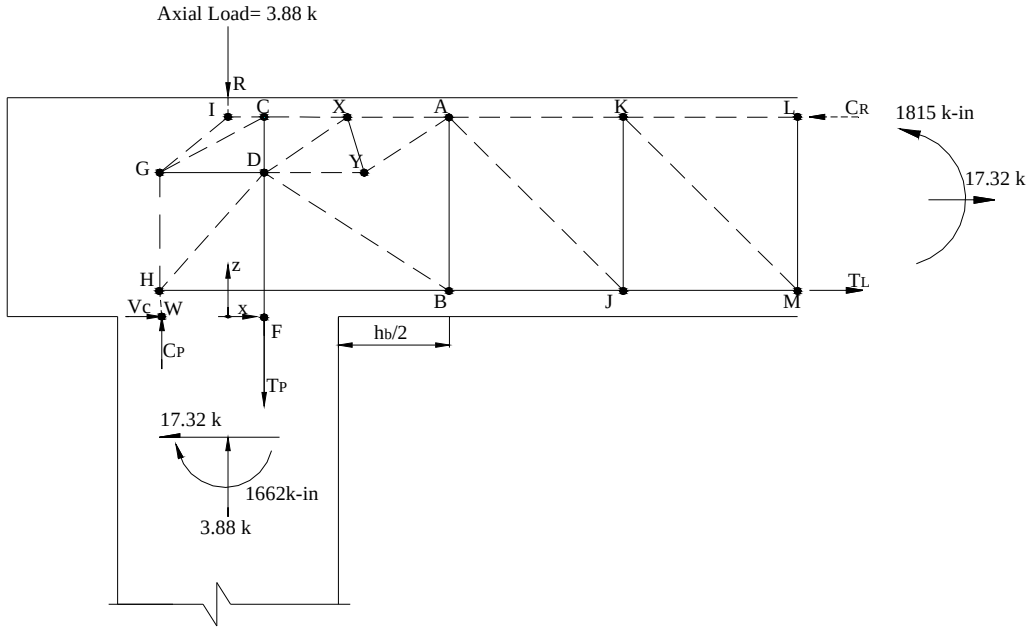

Figure 5-24: Strut-and-Tie Model for Specimen DCKJ24 (Opening Moment)

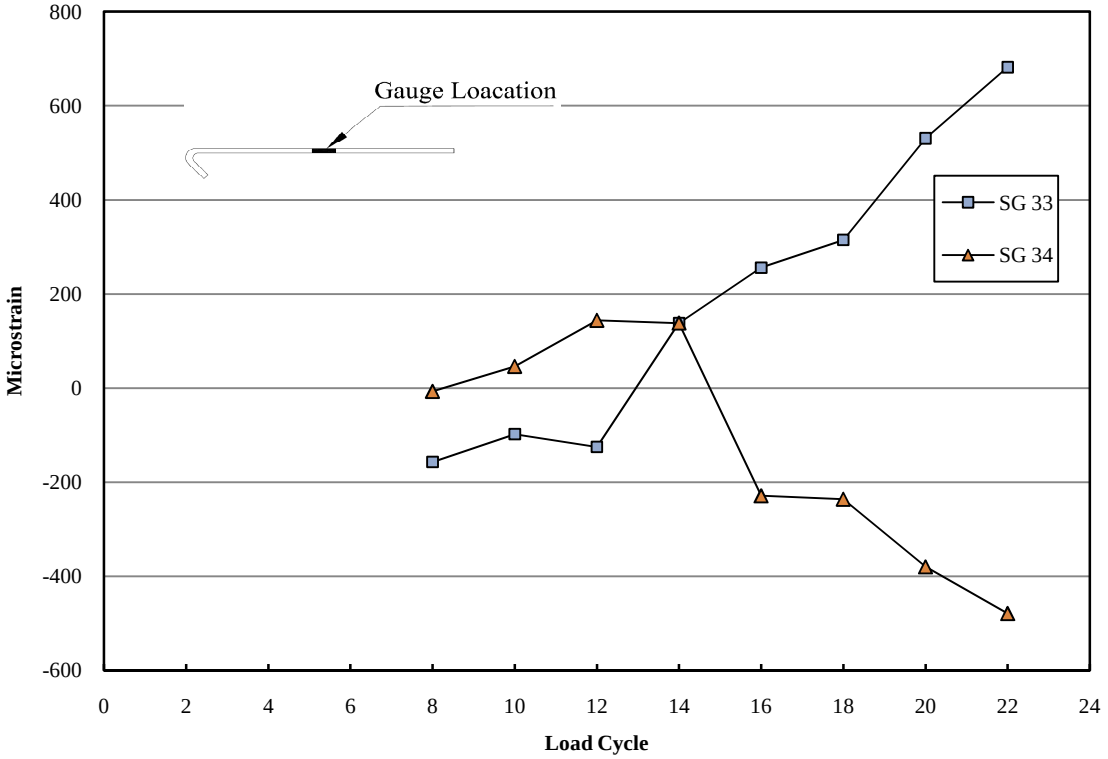

Figure 5-25: Horizontal Cap End Ties Strain for DCKJ24 South Cycle 2

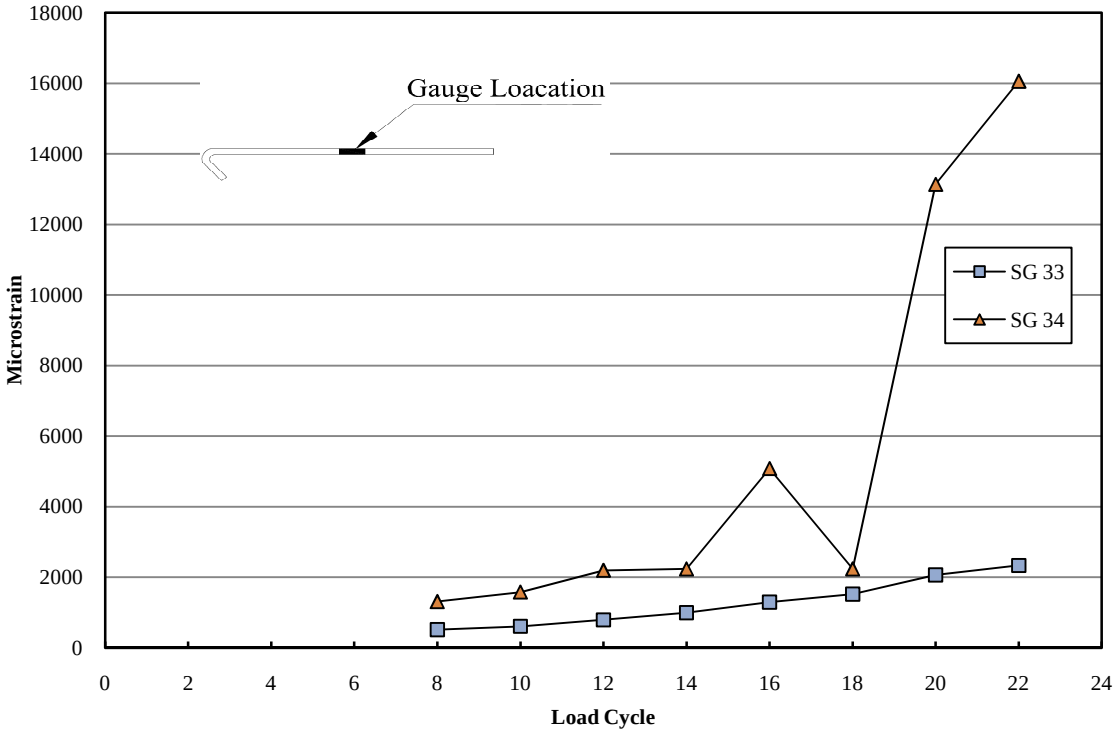

Figure 5-26: Horizontal Cap End Ties Strain for DCKJ24 North Cycle 2

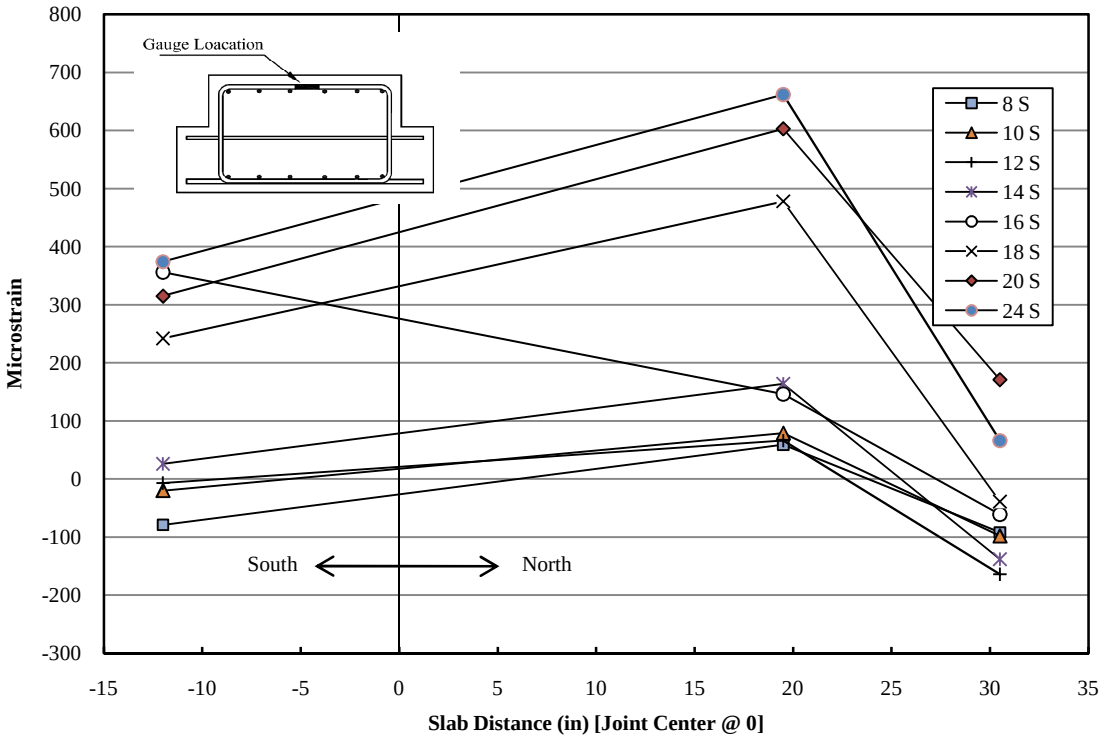

Figure 5-27: Joint Stirrup Strain for DCKJ24 South Cycle 2

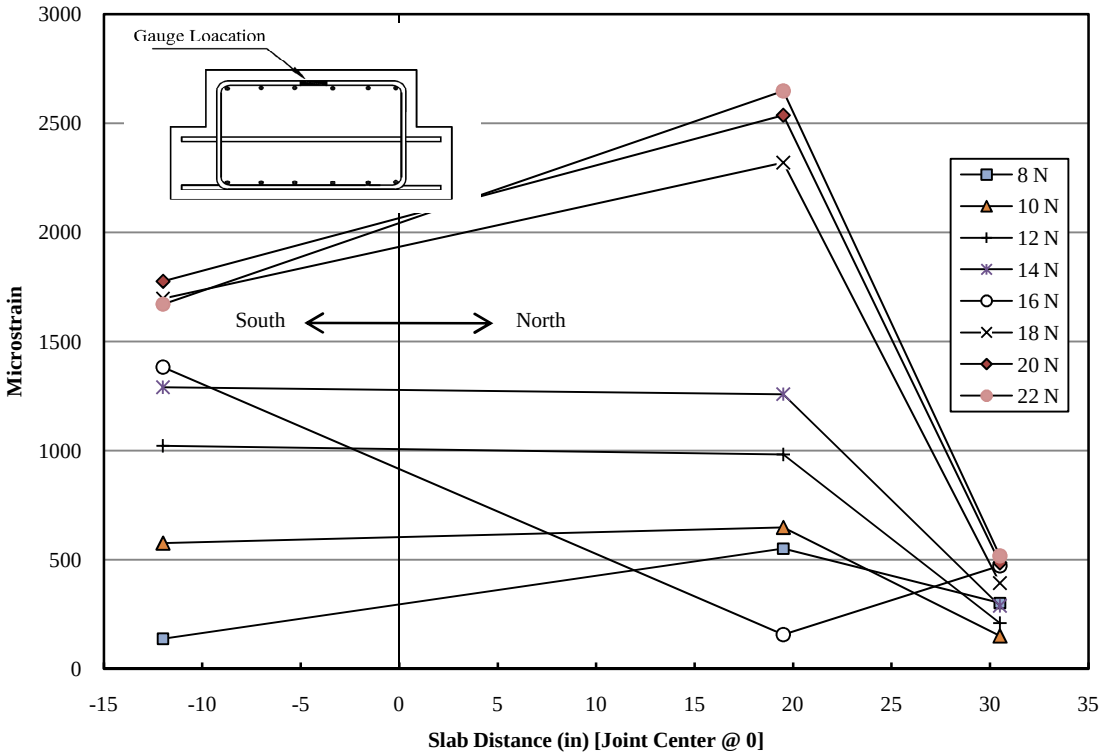

Figure 5-28: Joint Stirrup Strain for DCKJ24 North Cycle 2

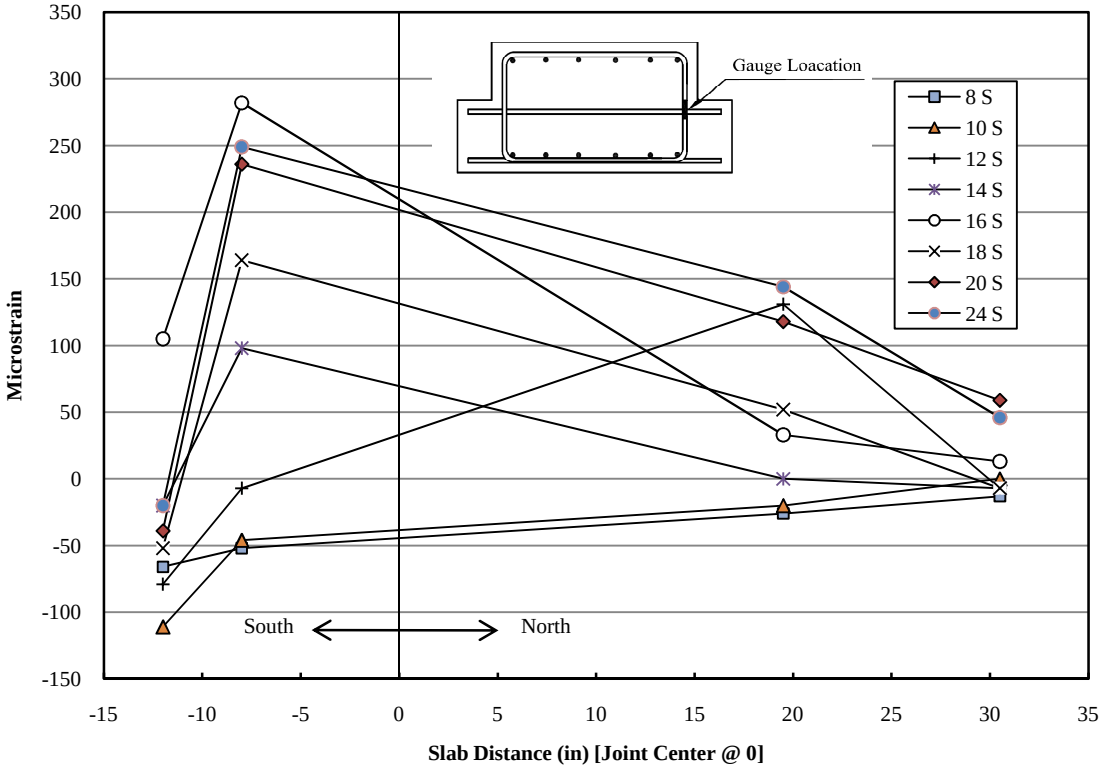

Figure 5-29: Joint Stirrup Strain for DCKJ24 South Cycle 2

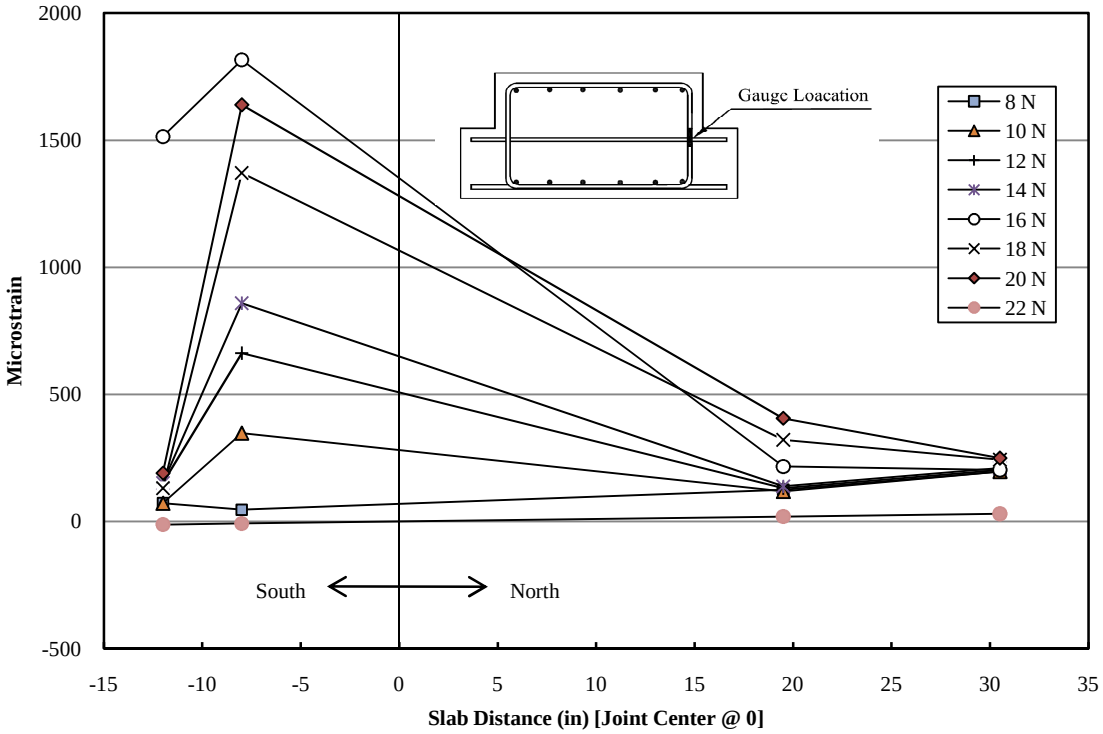

Figure 5-30: Joint Stirrup Strain for DCKJ24 North Cycle 2

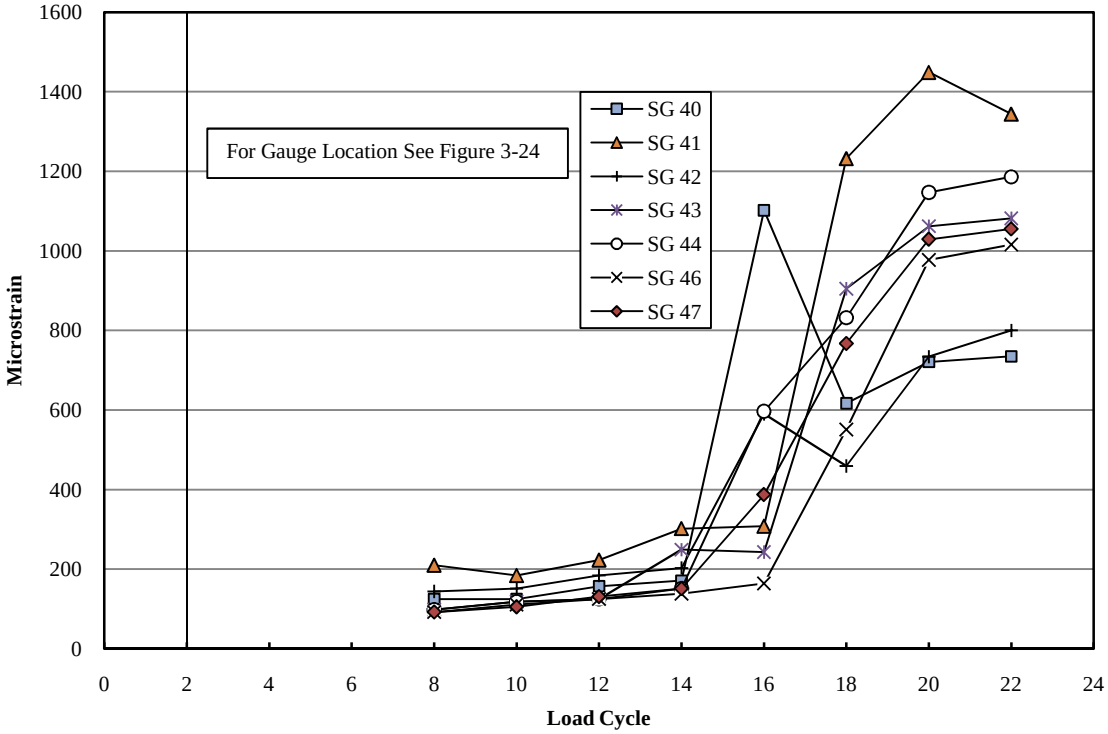

Figure 5-31: Joint Stirrup Strain for DCKJ24 South Cycle 2

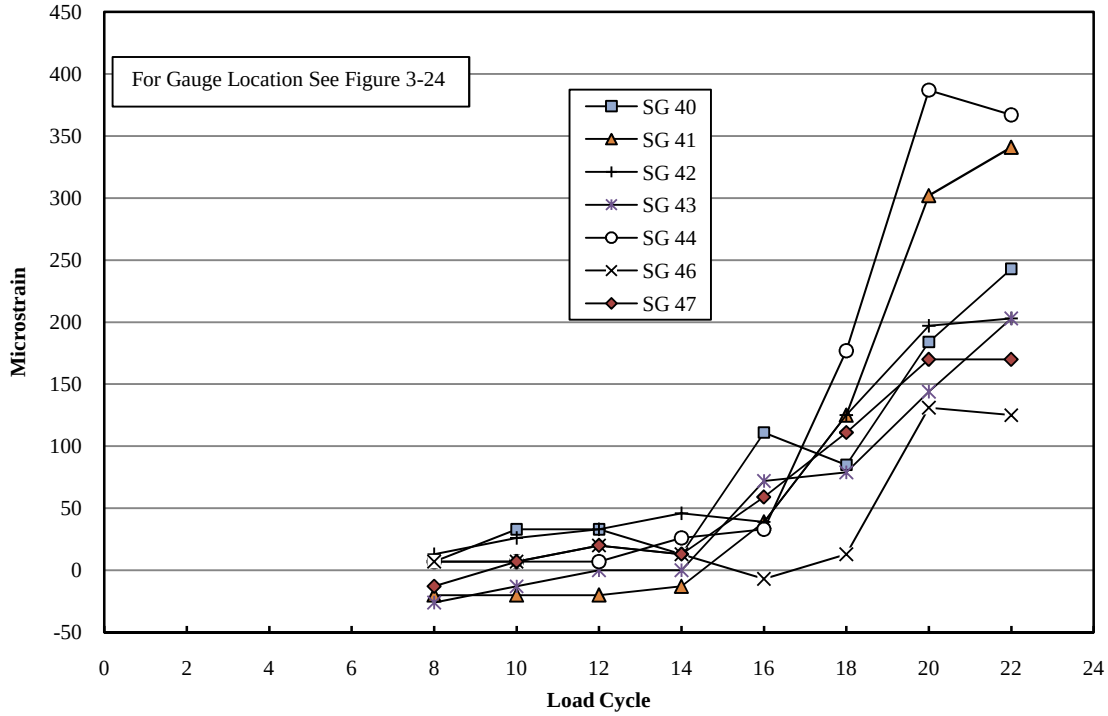

Figure 5-32: Joint Stirrup Strain for DCKJ24 North Cycle 2

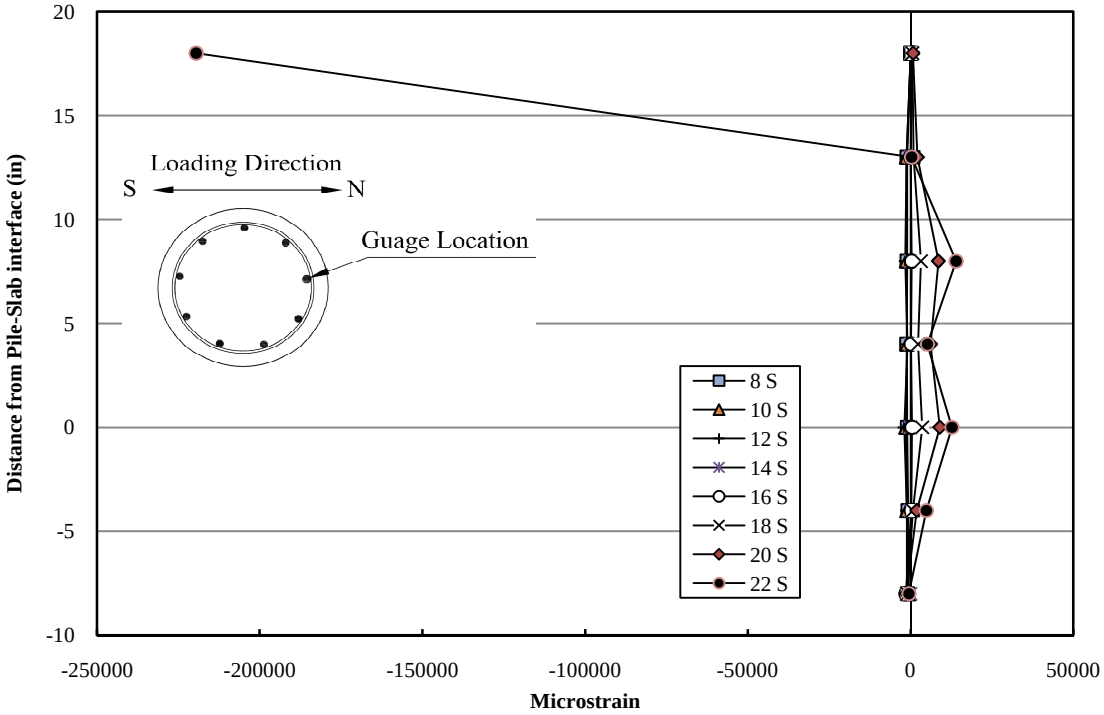

Figure 5-33: Longitudinal Pile Strain for DCKJ24 South Cycle 2

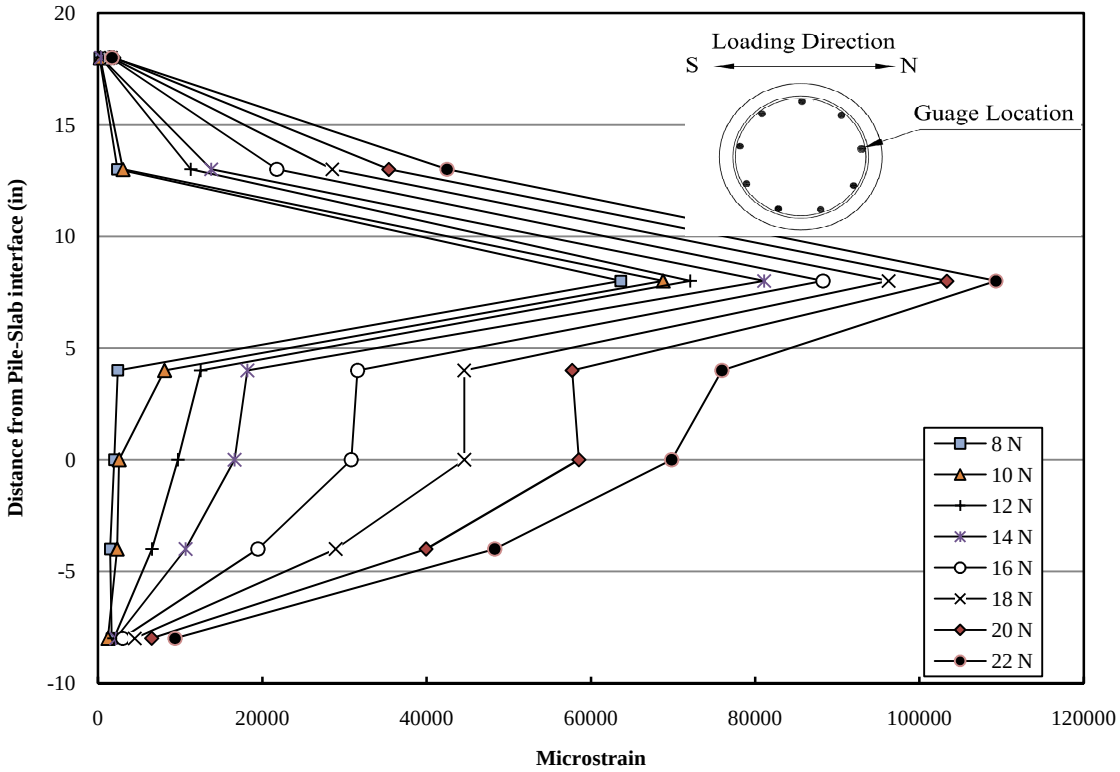

Figure 5-34: Longitudinal Pile Strain for DCKJ24 North Cycle 2

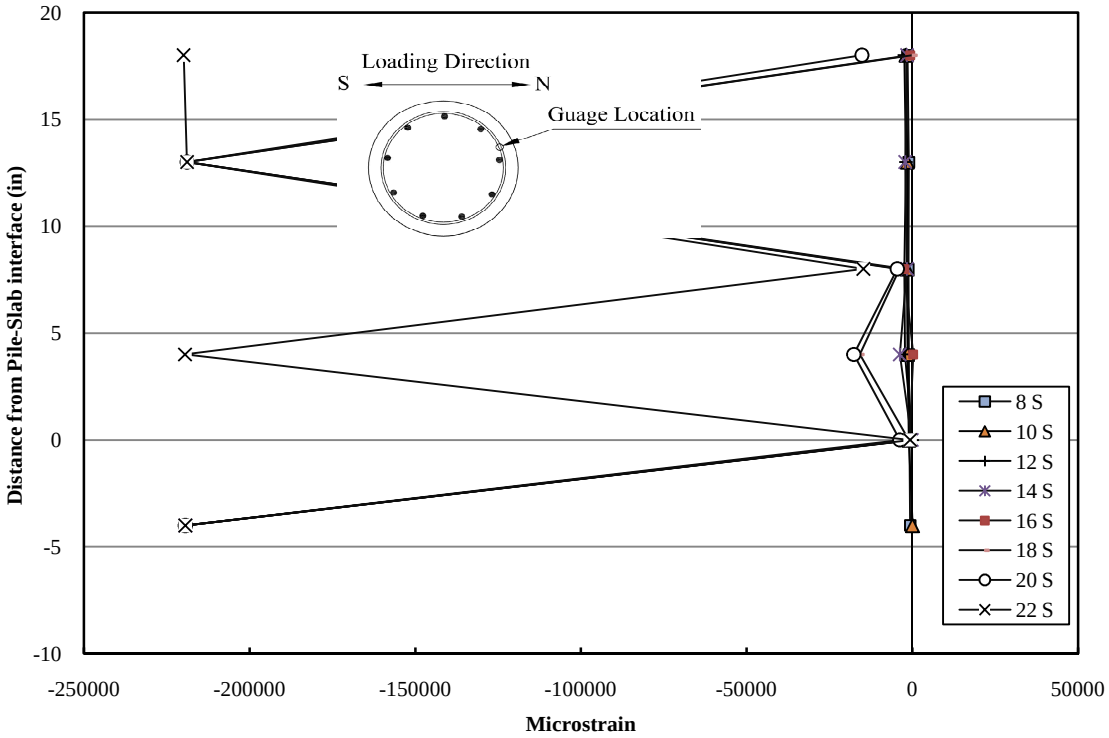

Figure 5-35: Spiral Reinforcement Strain for DCKJ24 South Cycle 2

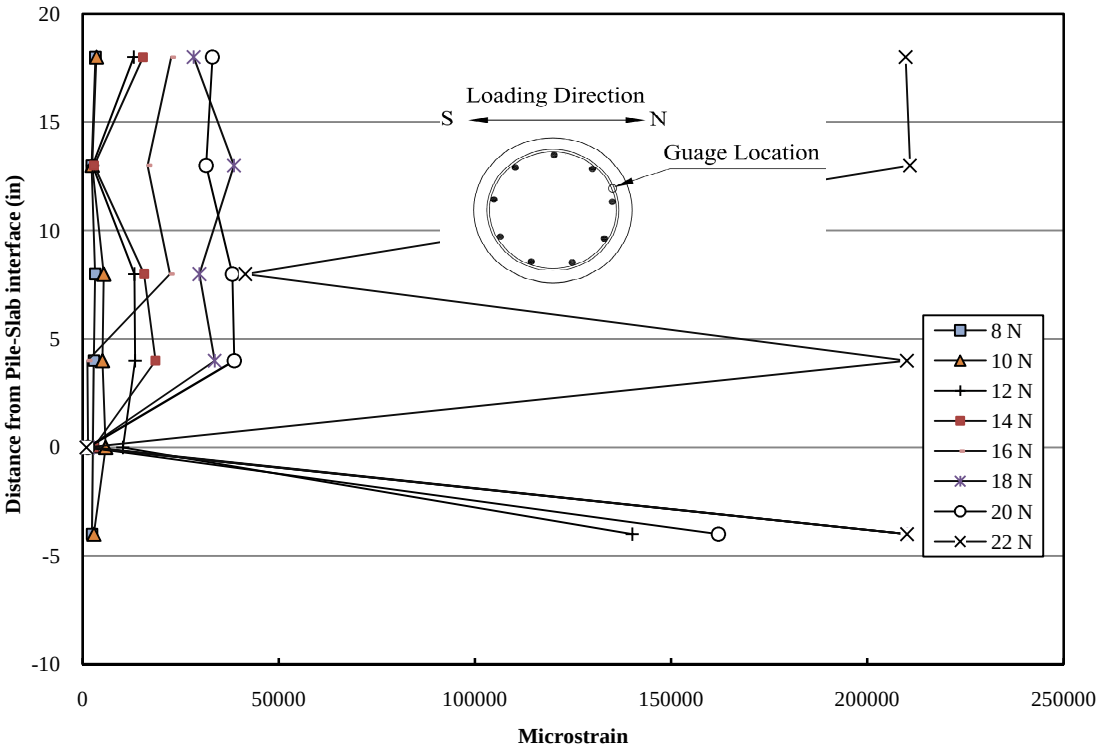

Figure 5-36: Spiral Reinforcement Strain for DCKJ24 North Cycle 2

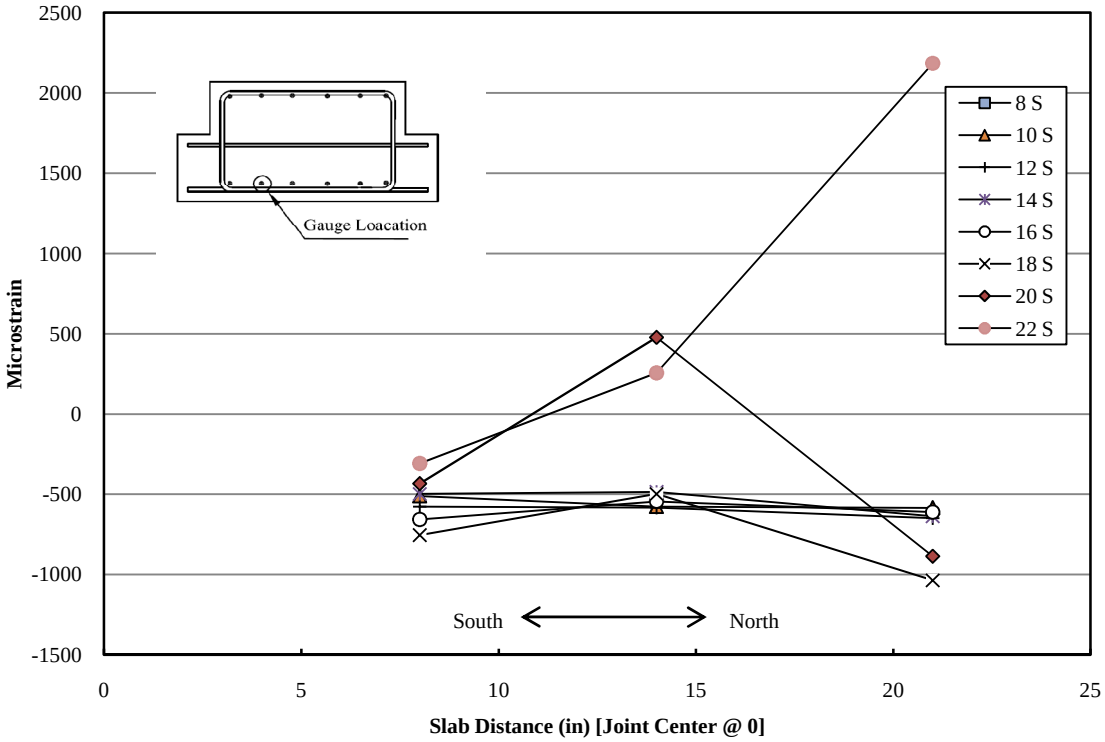

Figure 5-37: Slab Bottom Reinforcement Strainfor DCKJ24 South Cycle 2

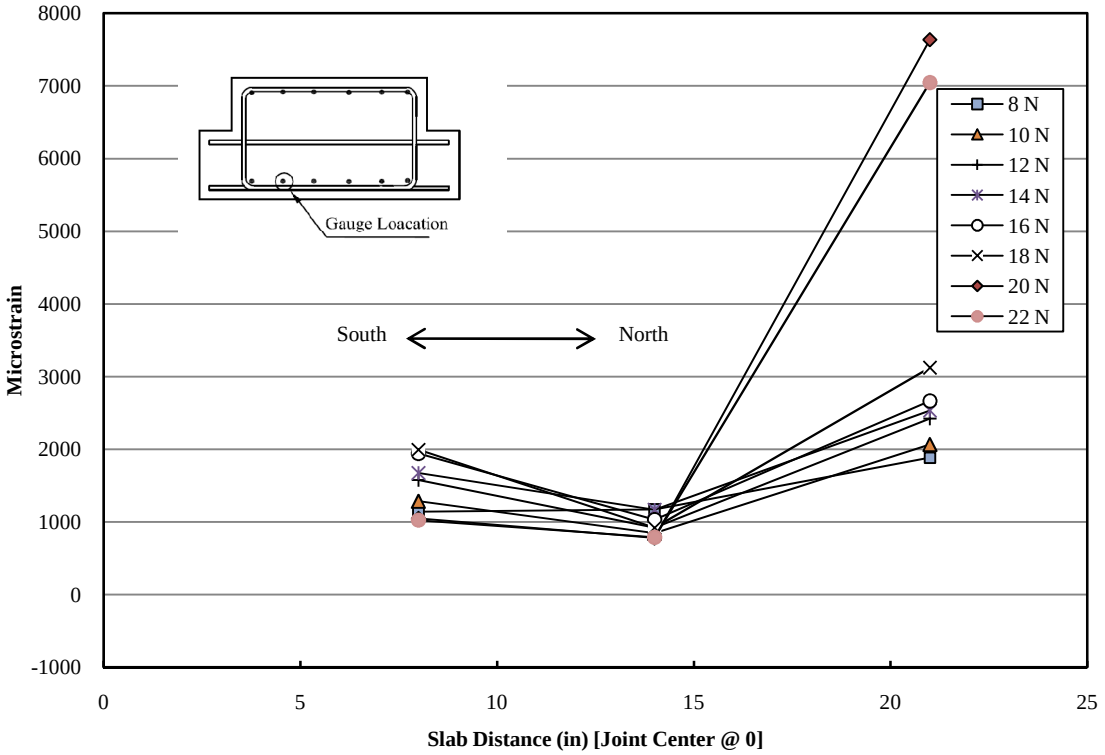

Figure 5-38: Slab Bottom Reinforcement Strainfor DCKJ24 North Cycle 2

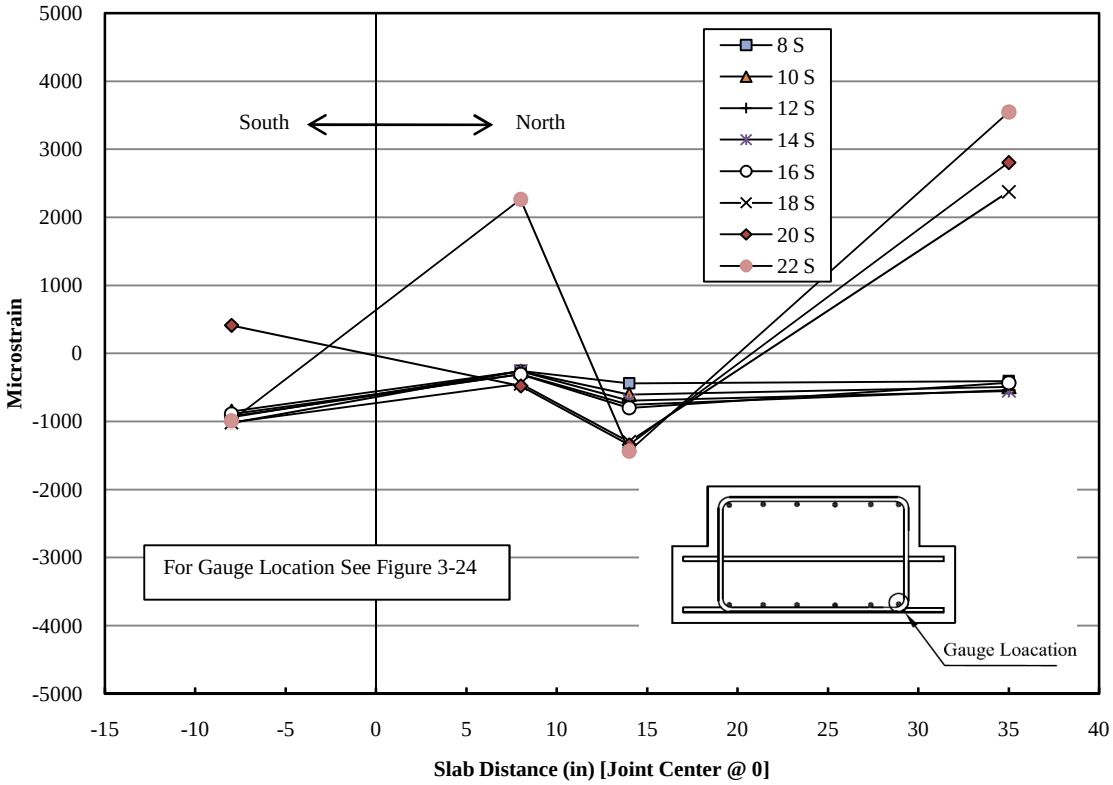

Figure 5-39: Slab Bottom Reinforcement Strain for DCKJ24 South Cycle 2

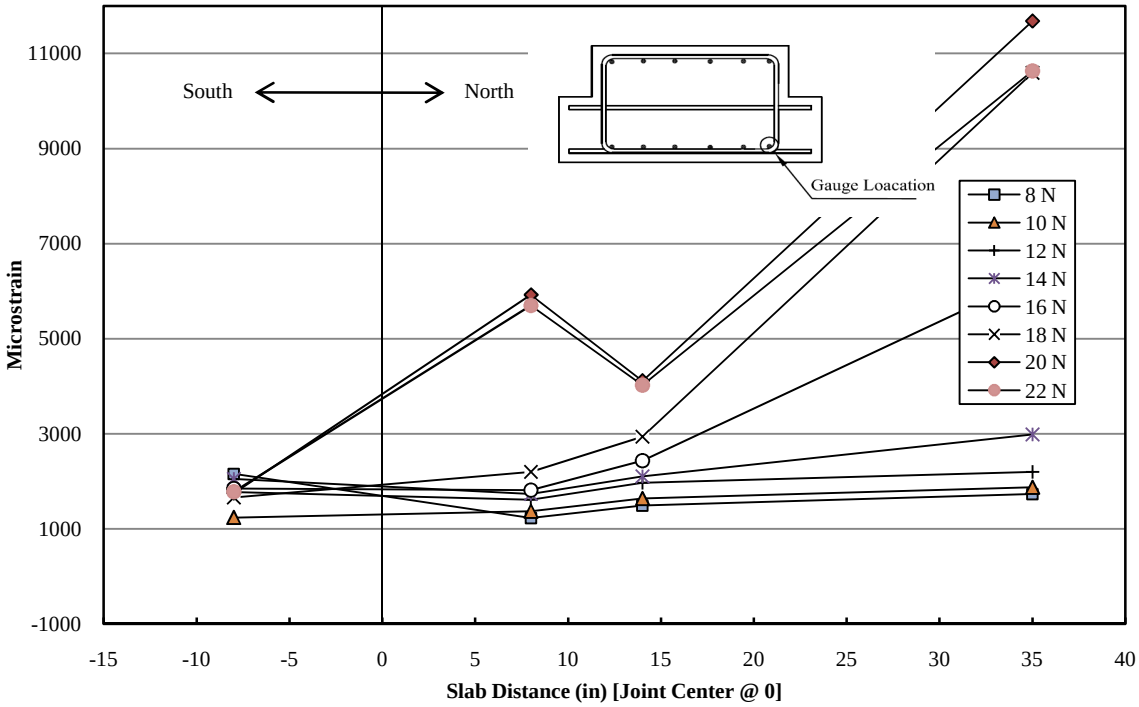

Figure 5-40: Slab Bottom Reinforcement Strain for DCKJ24 North Cycle 2

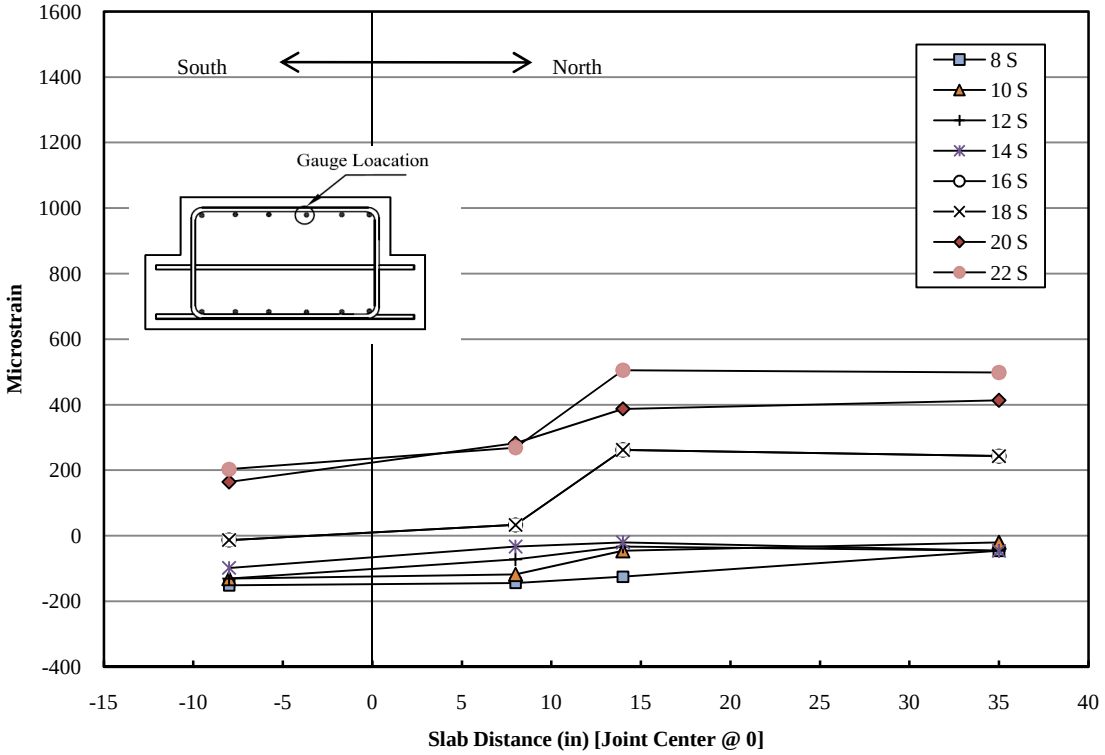

Figure 5-41: Slab Top Reinforcement Strain for DCKJ24 South Cycle 2

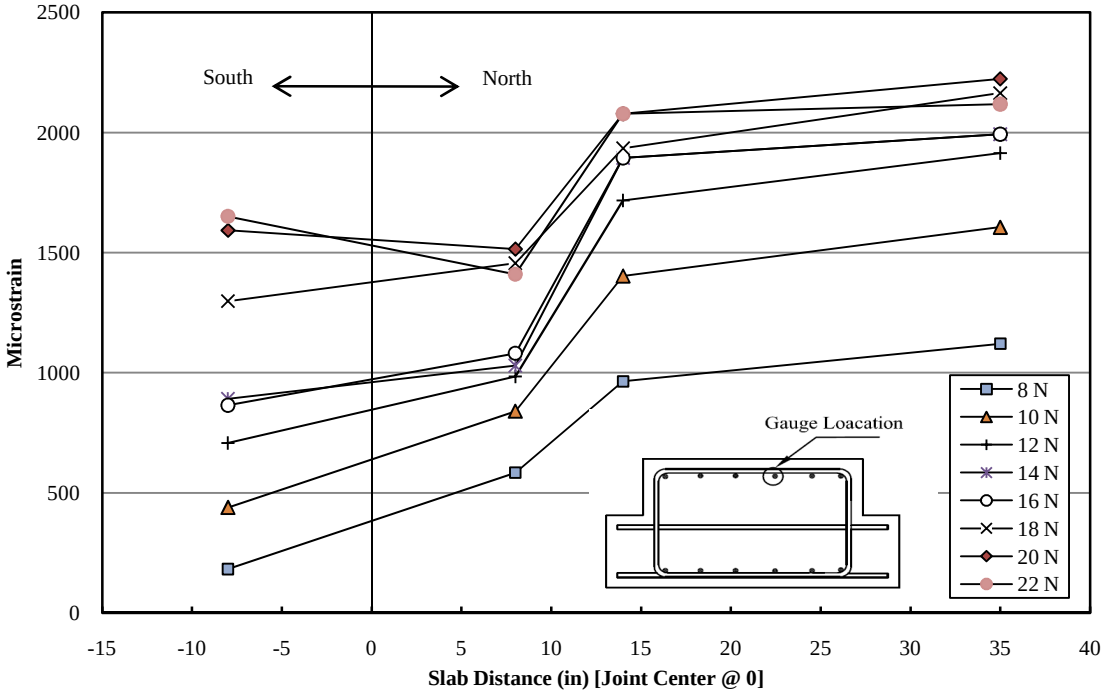

Figure 5-42: Slab Top Reinforcement Strain for DCKJ24 North Cycle 2

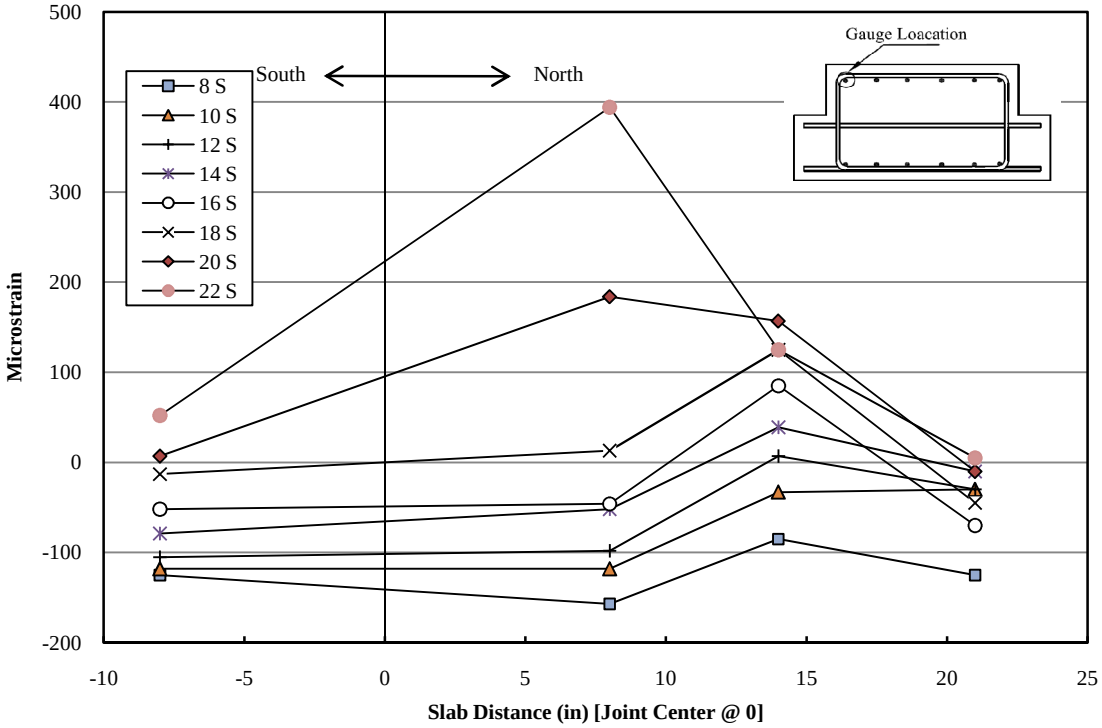

Figure 5-43: Slab Top Reinforcement Strain for DCKJ24 South Cycle 2

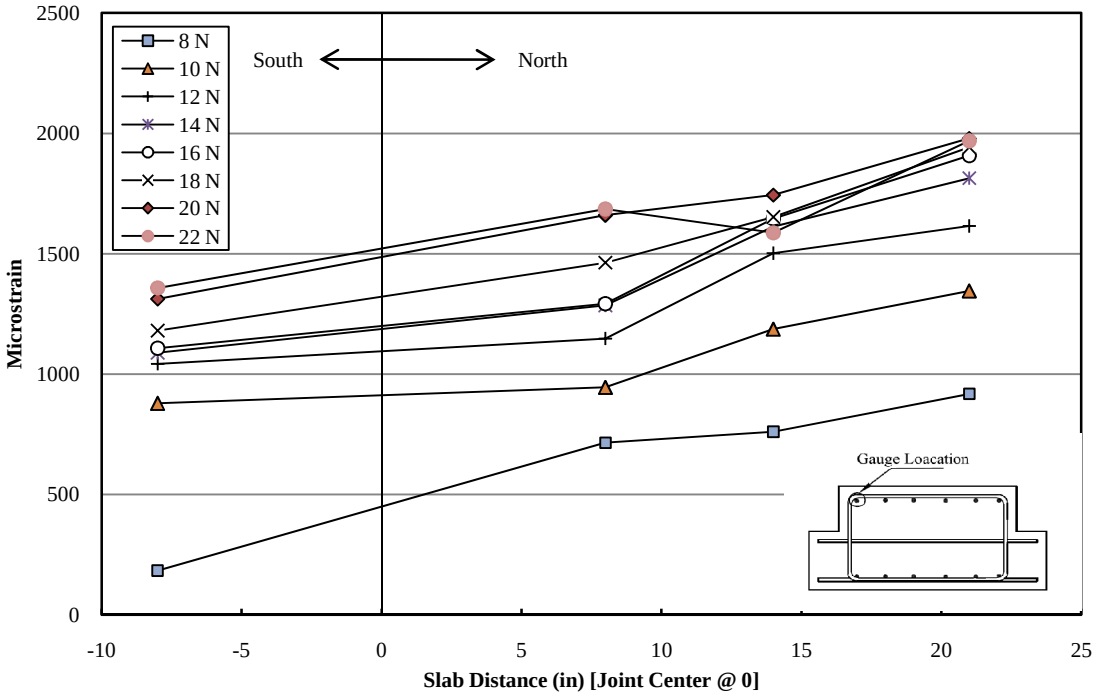

Figure 5-44: Slab Top Reinforcement Strain for DCKJ24 North Cycle 2

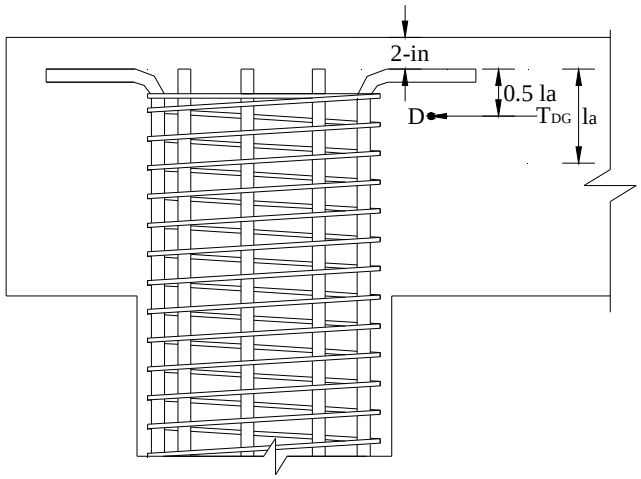

Figure 5-45: Spiral Reinforcement Tie Representation in Knee-Joint

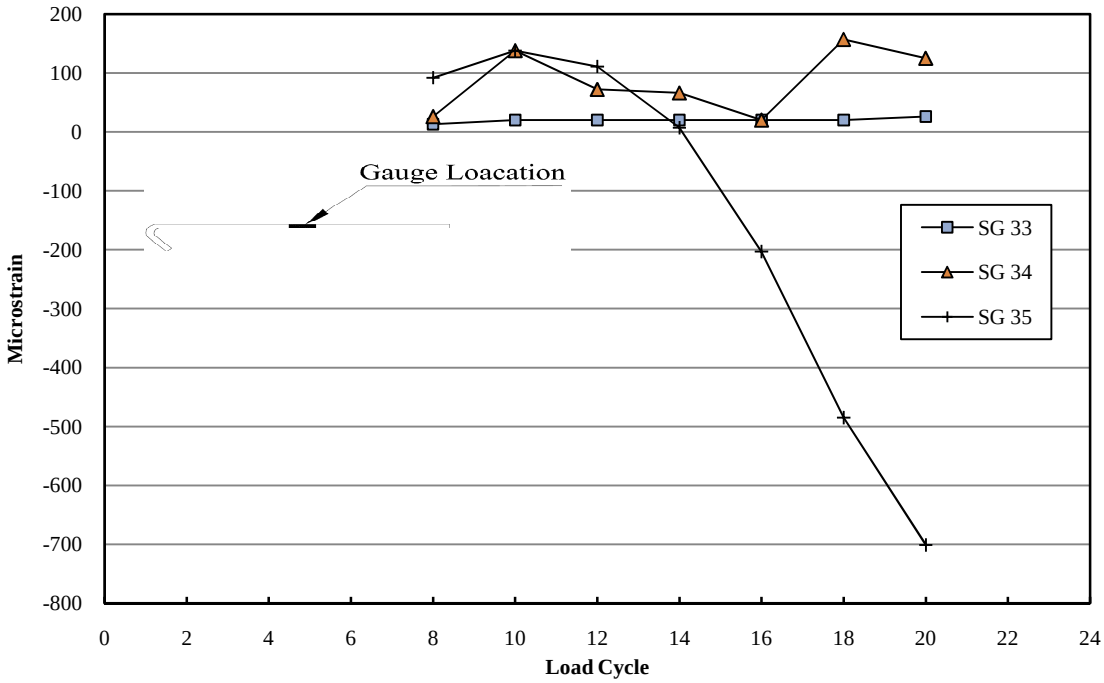

Figure 5-46: Horizontal Cap End Ties Strain for FSKJ24 South Cycle 2

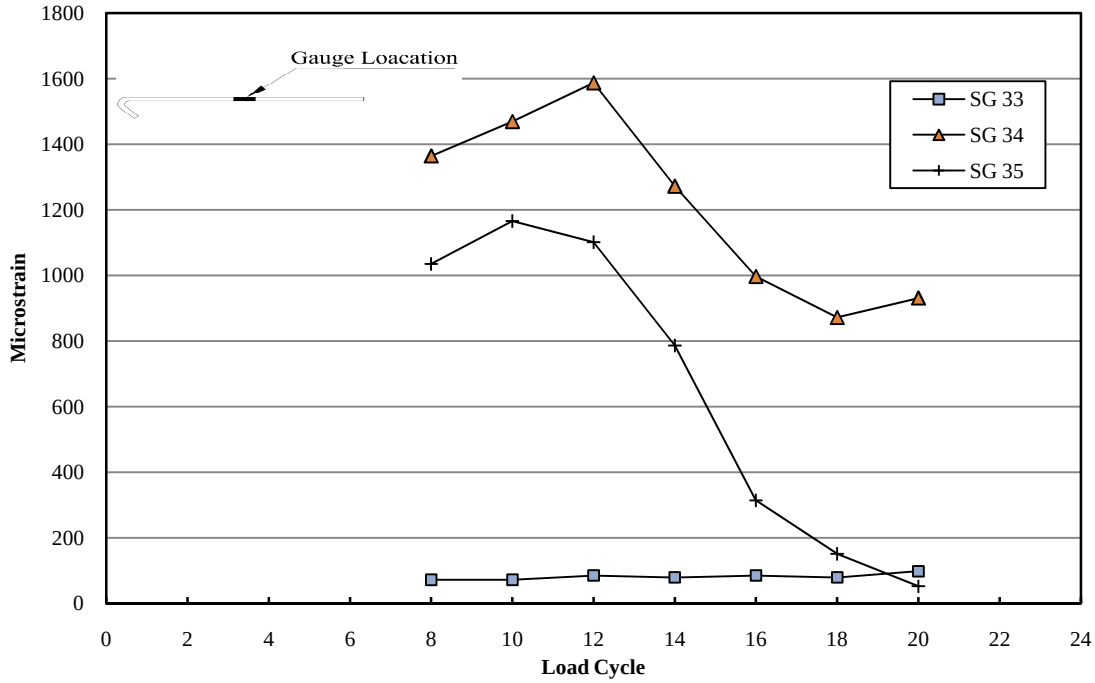

Figure 5-47: Horizontal Cap End Ties Strain for FSKJ24 North Cycle 2

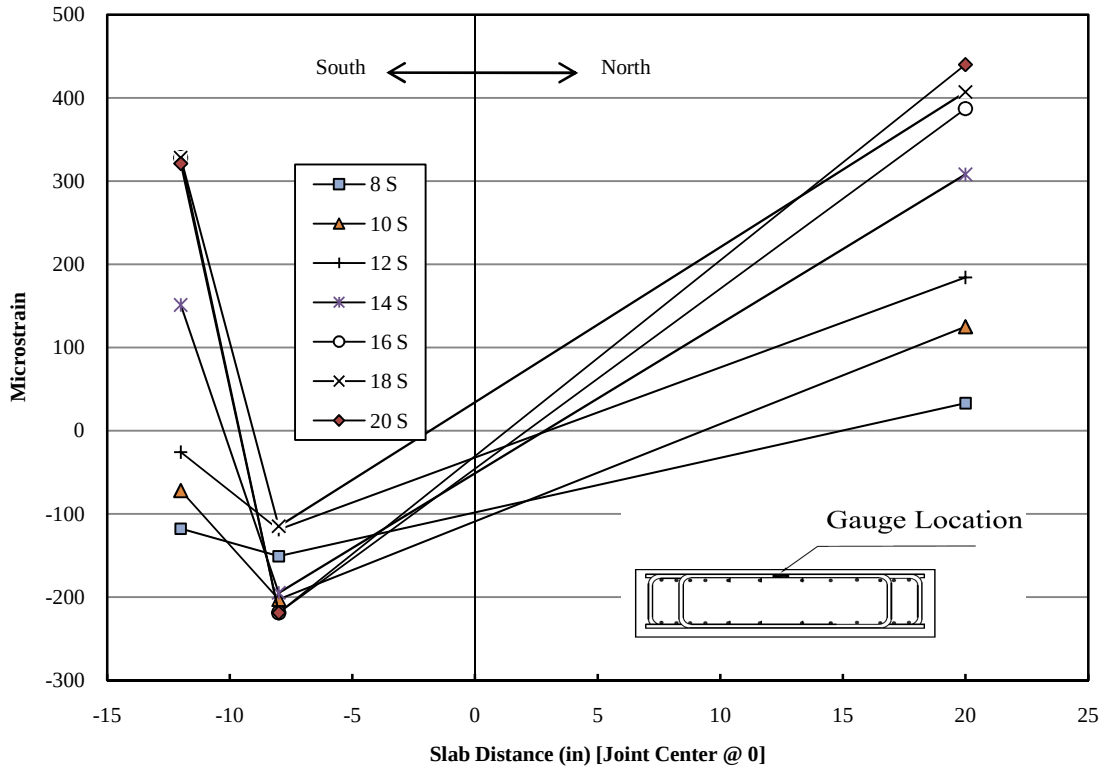

Figure 5-48: Joint Stirrup Strain for FSKJ24 South Cycle 2

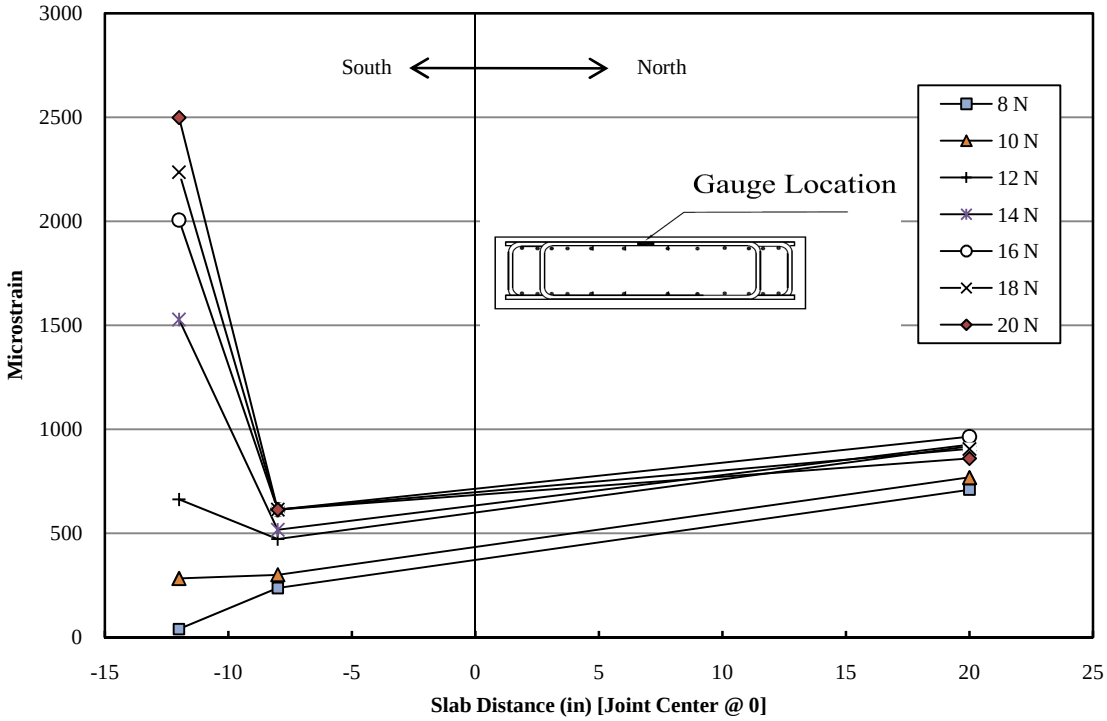

Figure 5-49: Joint Stirrup Strain for FSKJ24 North Cycle 2

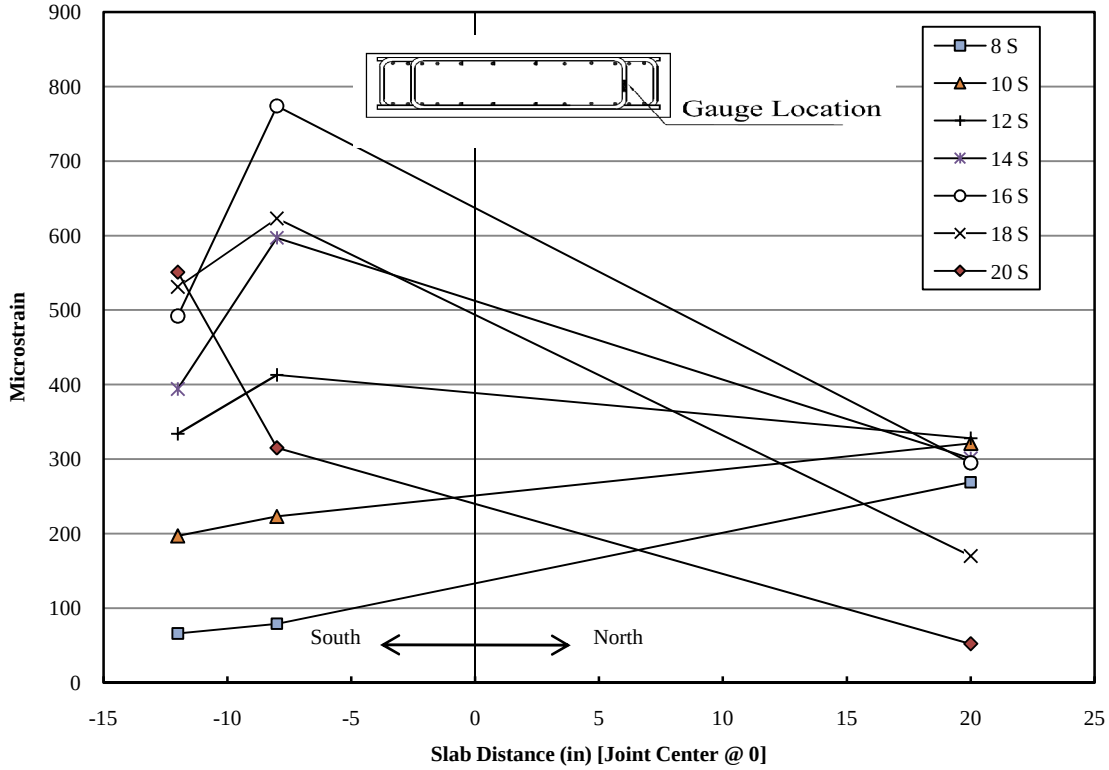

Figure 5-50: Joint Stirrup Strain for FSKJ24 South Cycle 2

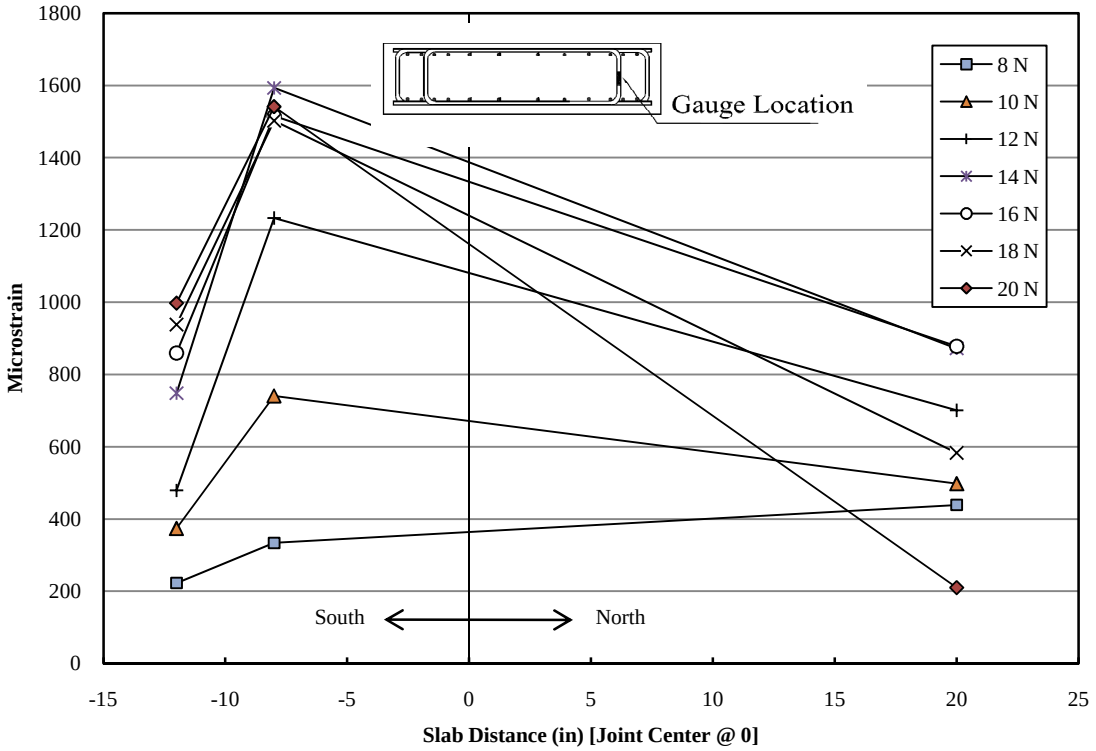

Figure 5-51: Joint Stirrup Strain for FSKJ24 North Cycle 2

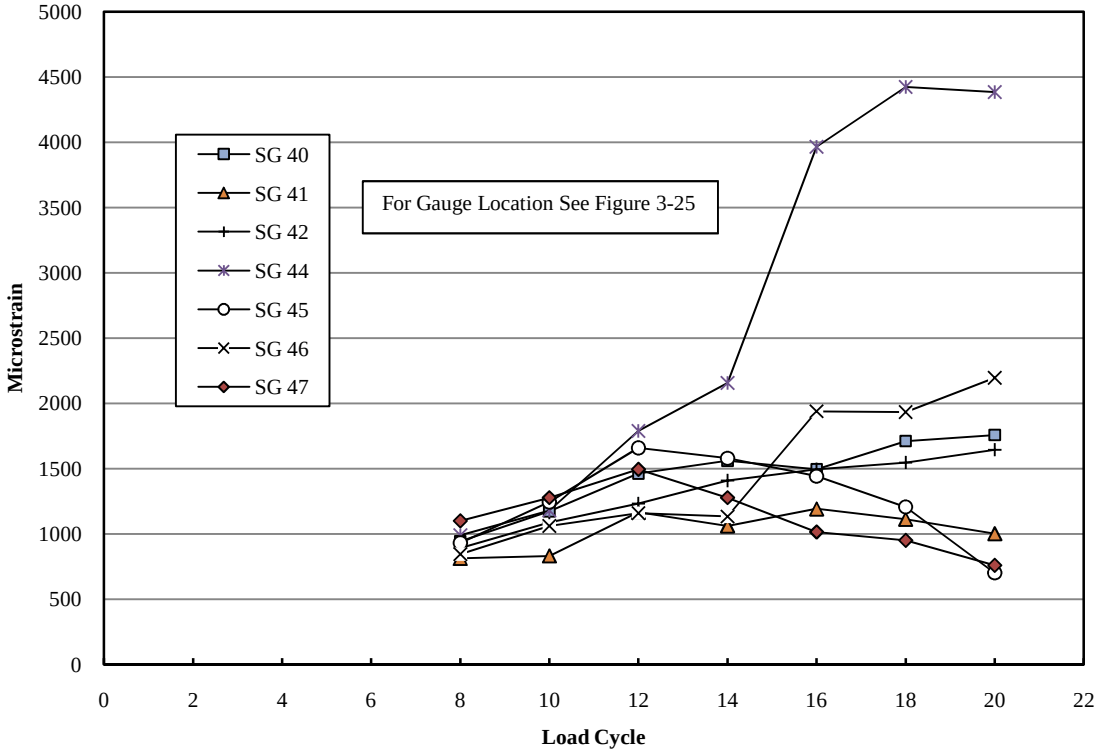

Figure 5-52: Joint Stirrup Strain for FSKJ24 South Cycle 2

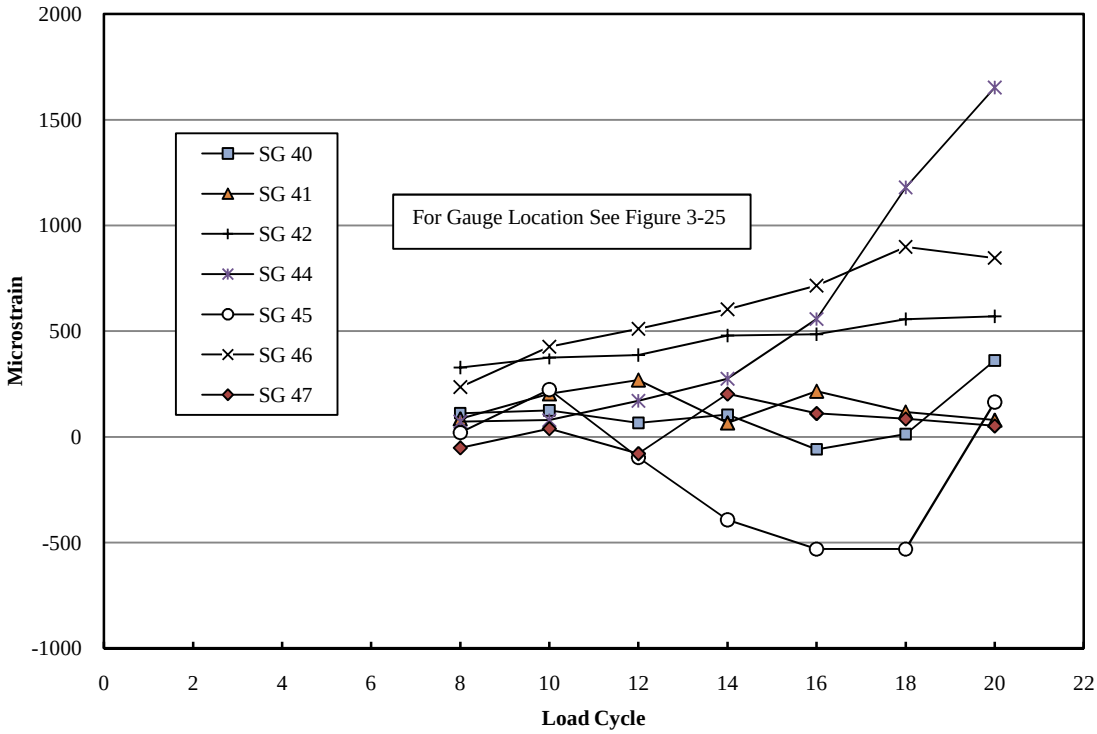

Figure 5-53: Joint Stirrup Strain for FSKJ24 North Cycle 2

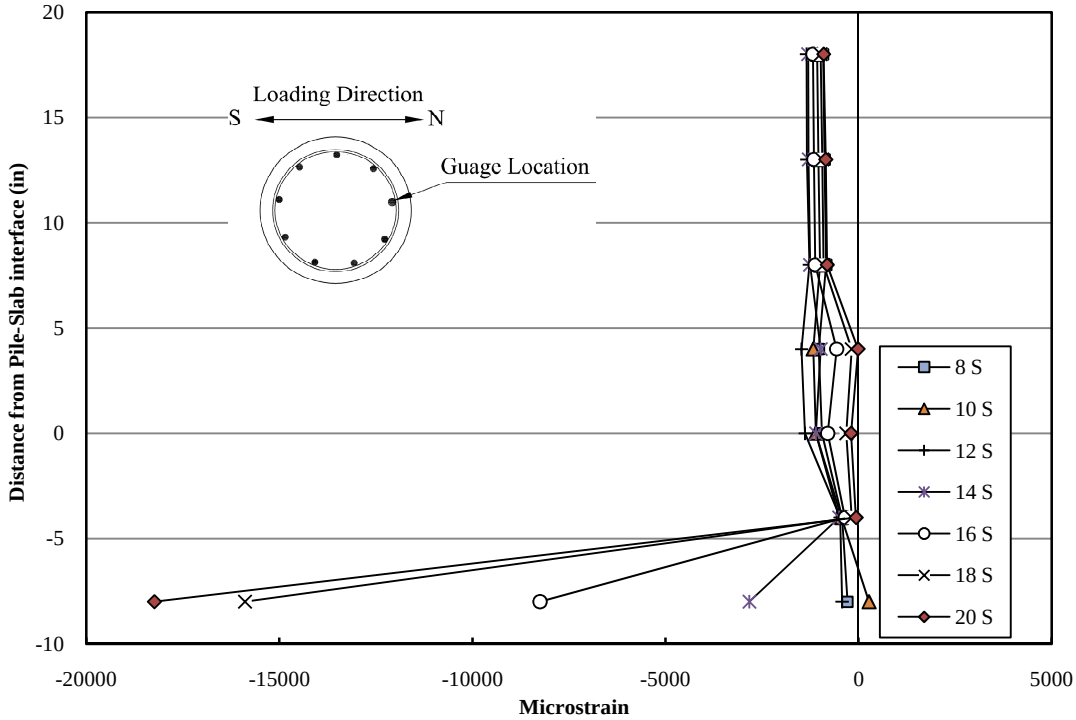

Figure 5-54: Longitudinal Pile Strain for FSKJ24 South Cycle 2

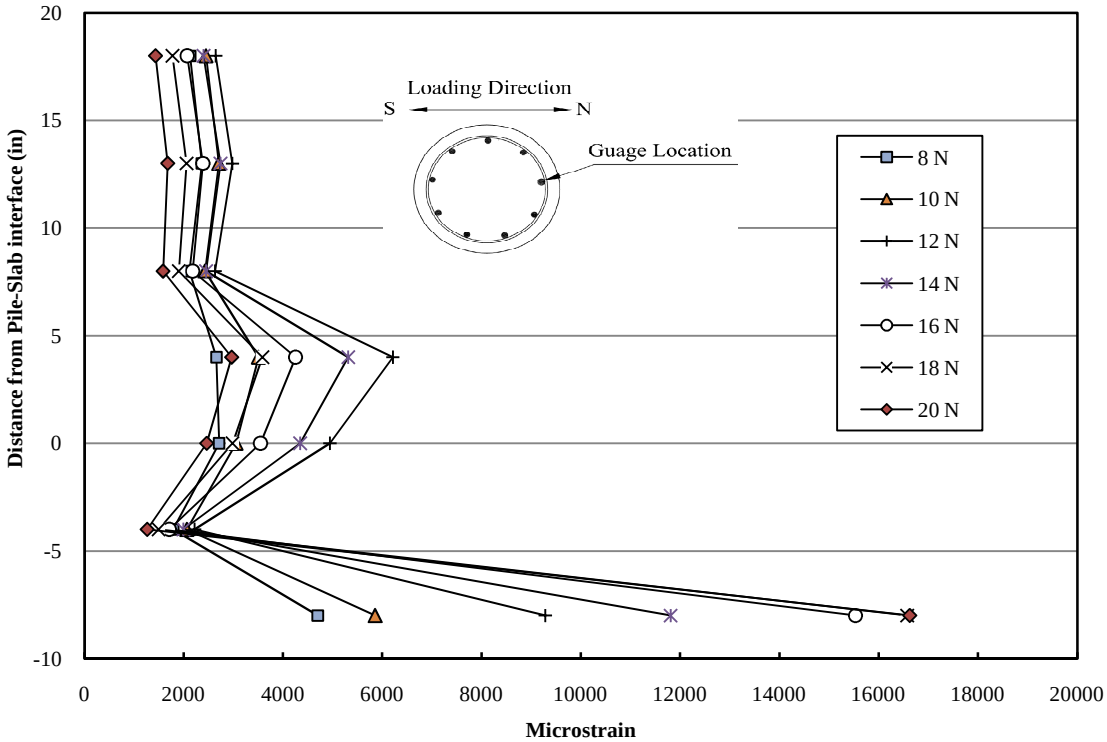

Figure 5-55: Longitudinal Pile Strain for FSKJ24 North Cycle 2

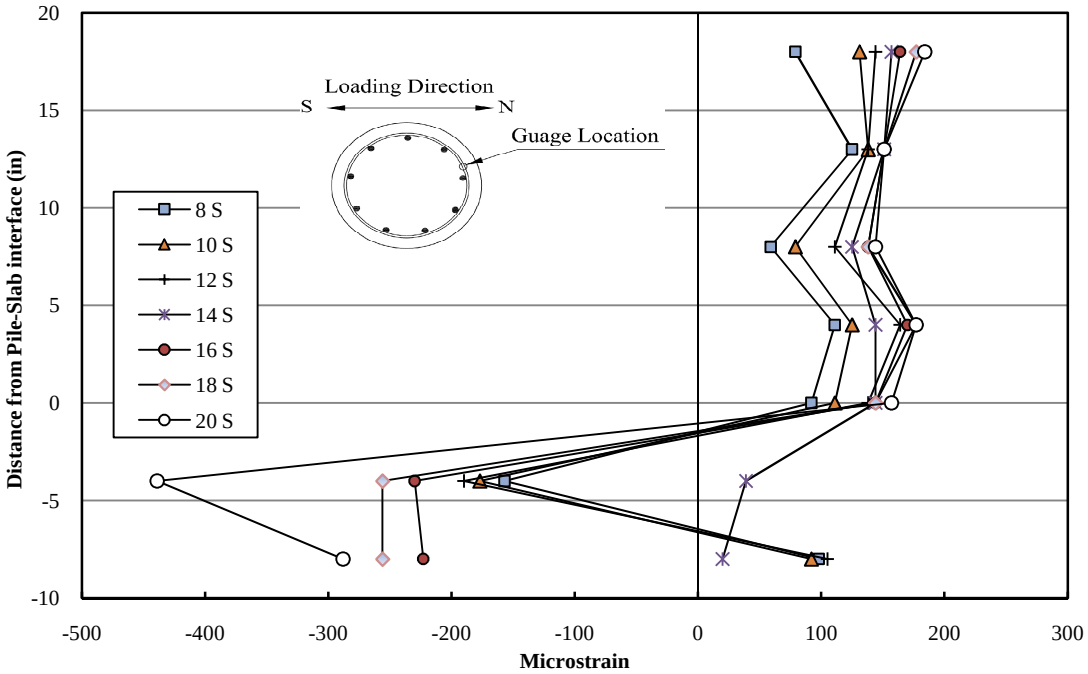

Figure 5-56: Spiral Reinforcement Strain for FSKJ24 South Cycle 2

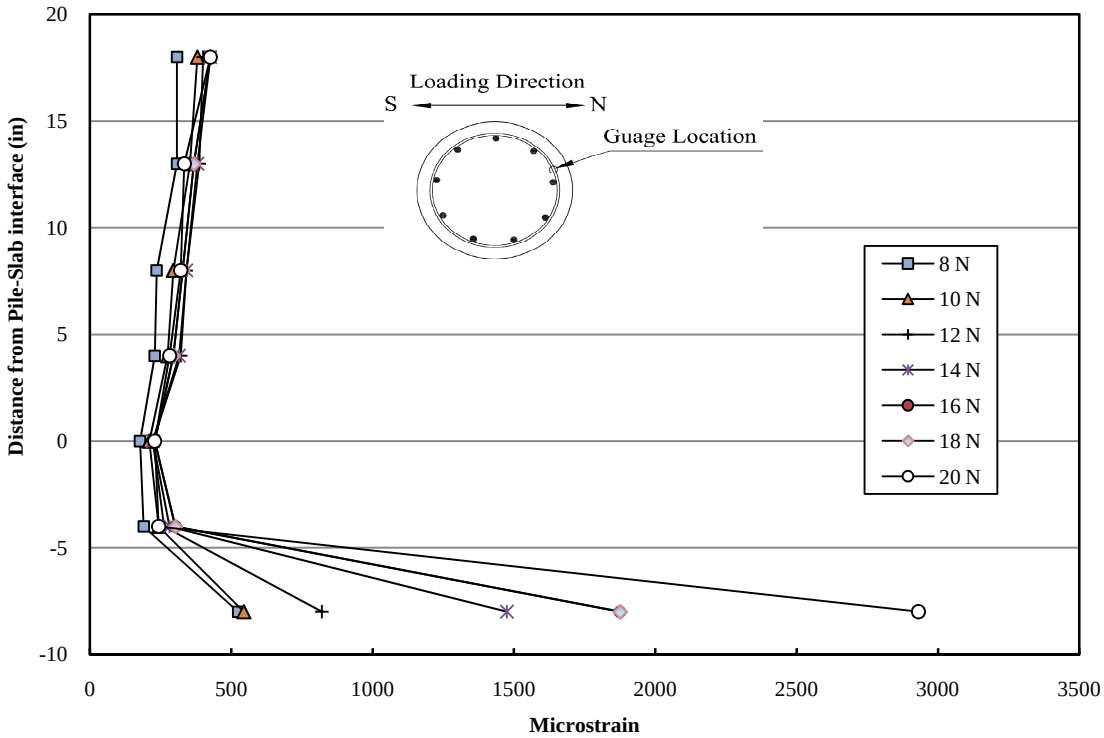

Figure 5-57: Spiral Reinforcement Strain for FSKJ24 North Cycle 2

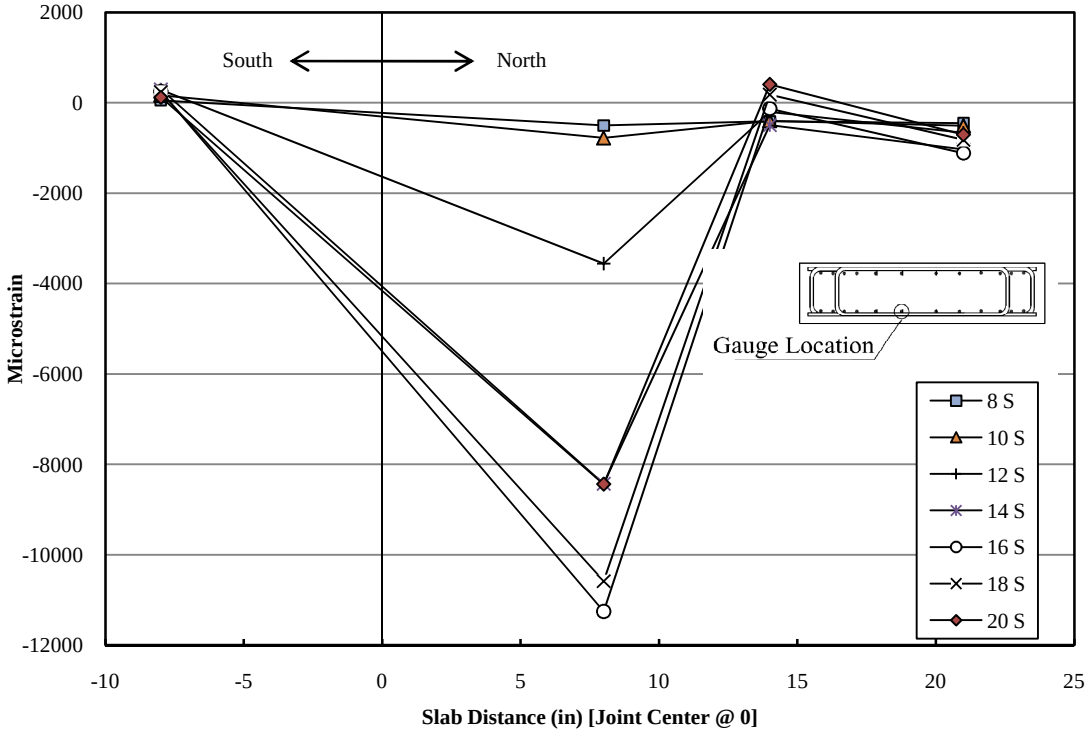

Figure 5-58: Slab Bottom Reinforcement Strain for FSKJ24 South Cycle 2

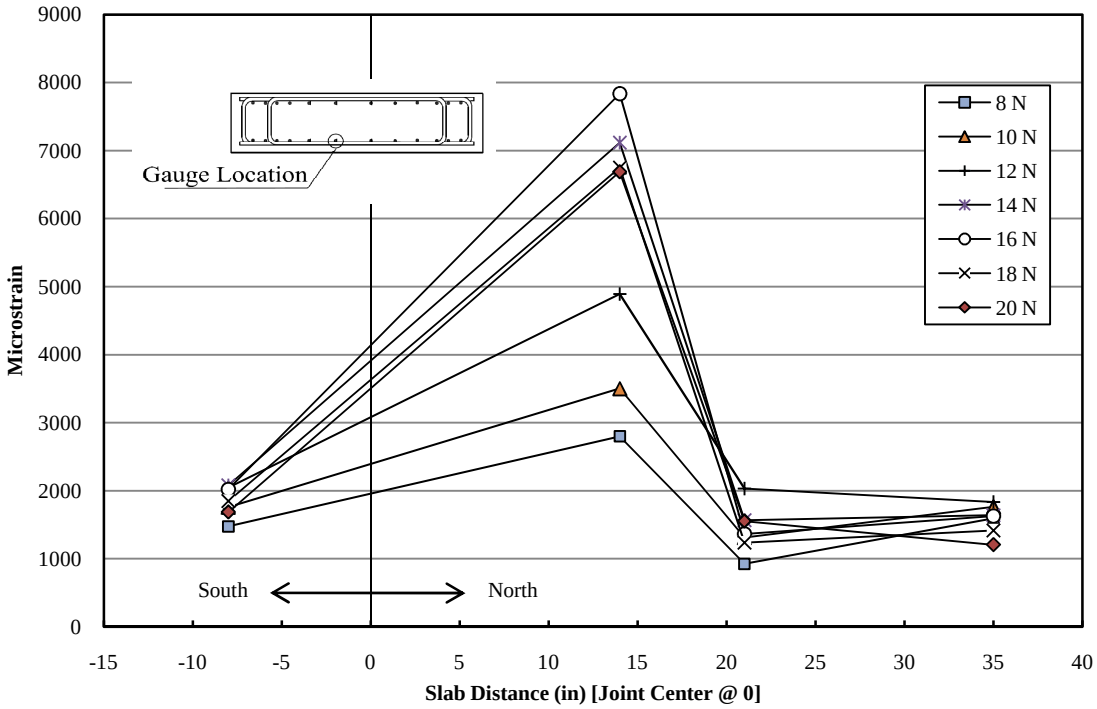

Figure 5-59: Slab Bottom Reinforcement Strain for FSKJ24 North Cycle 2

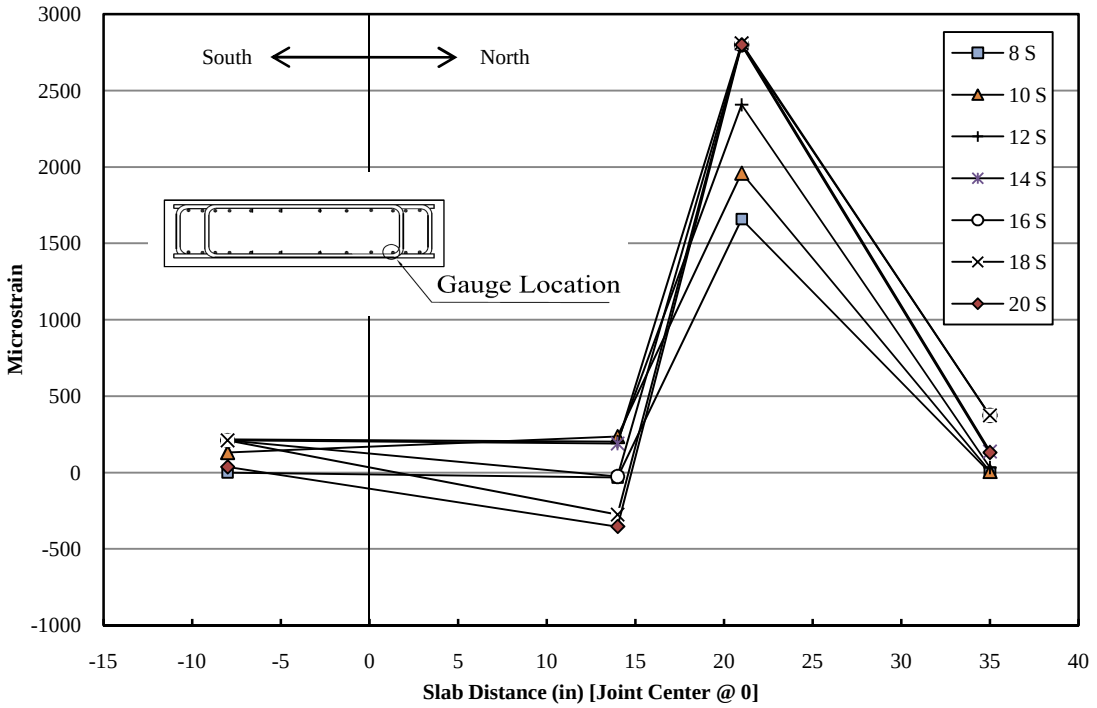

Figure 5-60: Slab Bottom Reinforcement Strain for FSKJ24 South Cycle 2

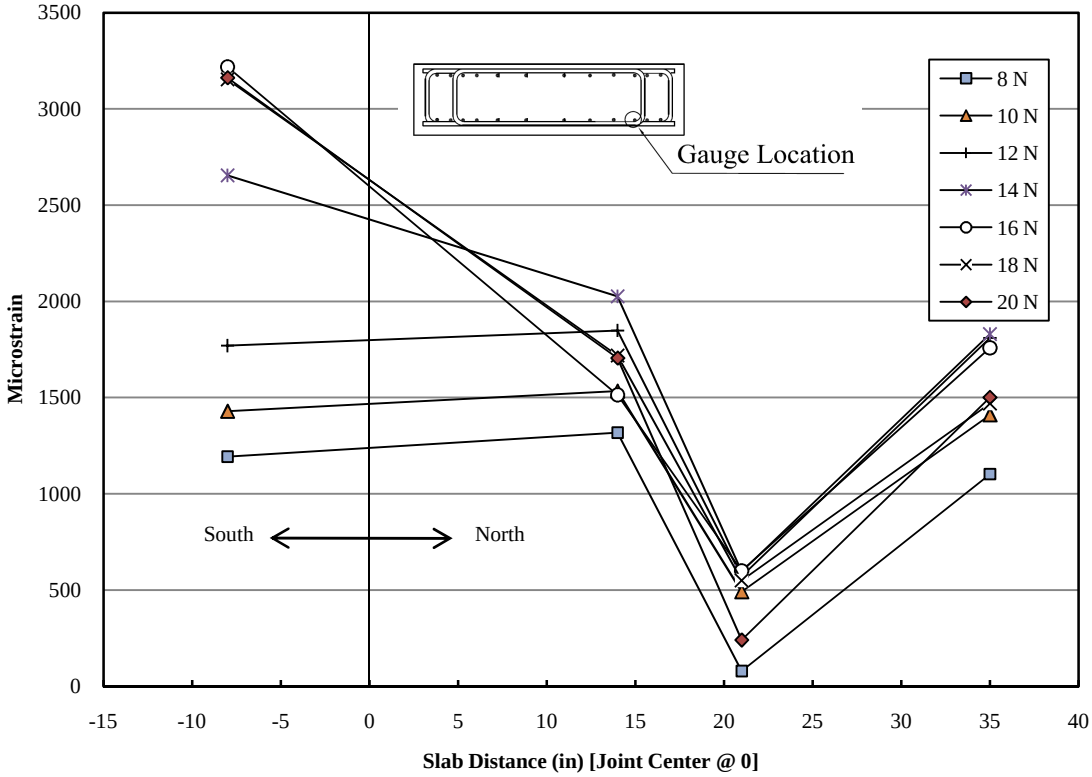

Figure 5-61: Slab Bottom Reinforcement Strain for FSKJ24 North Cycle 2

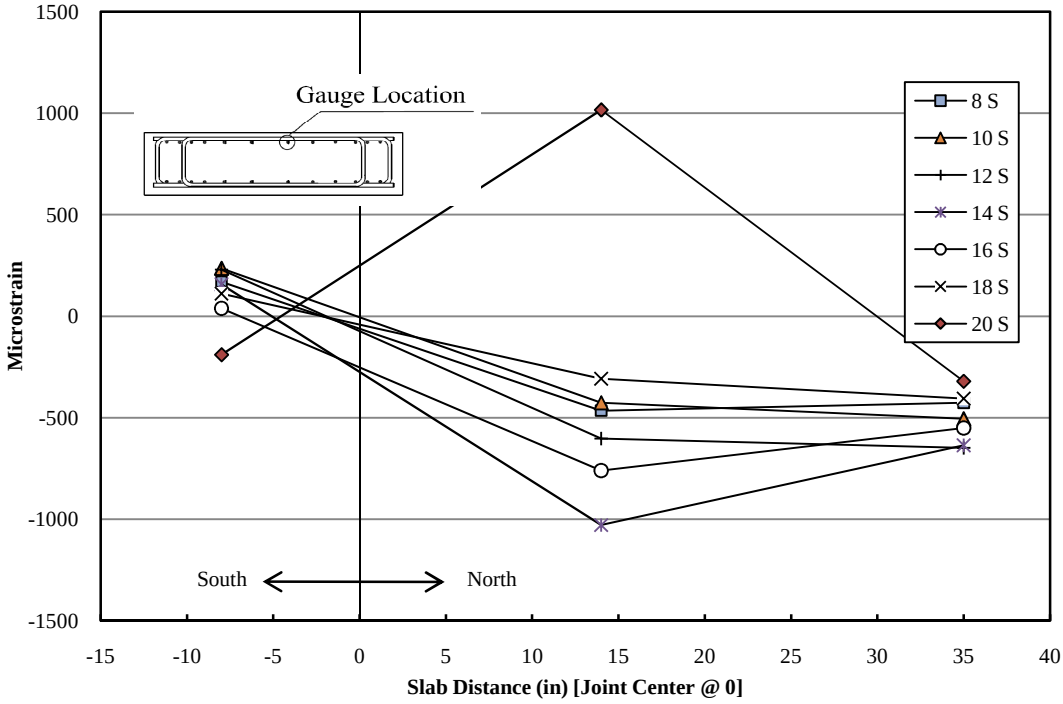

Figure 5-62: Slab Top Reinforcement Strain for FSKJ24 South Cycle 2

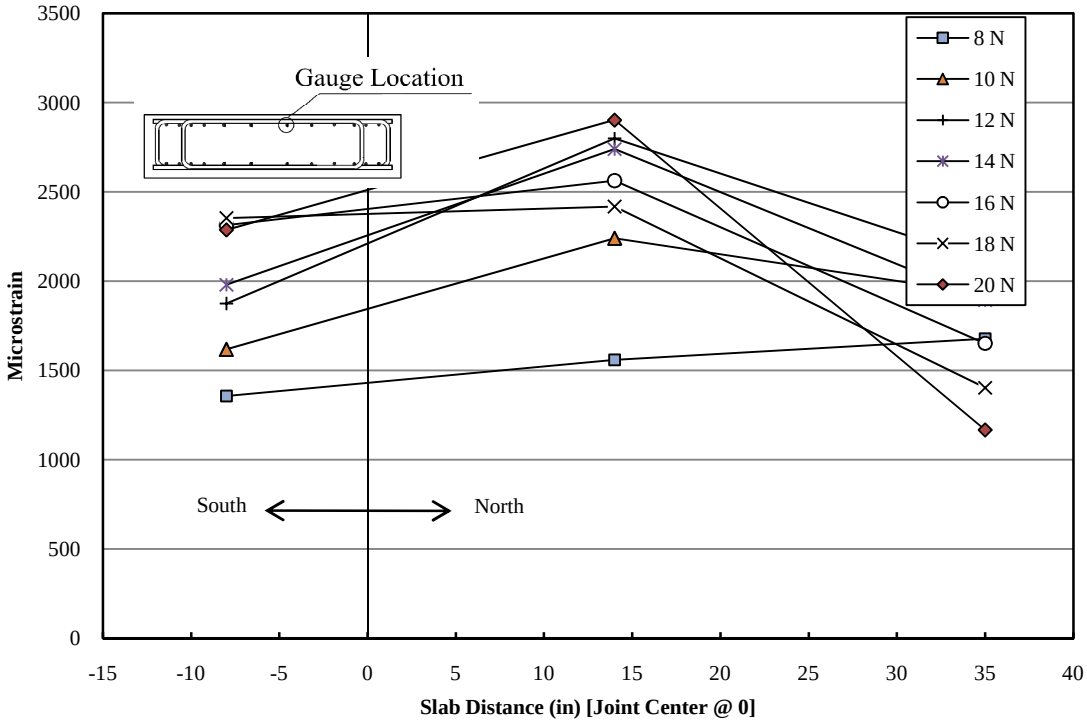

Figure 5-63: Slab Top Reinforcement Strain for FSKJ24 North Cycle 2

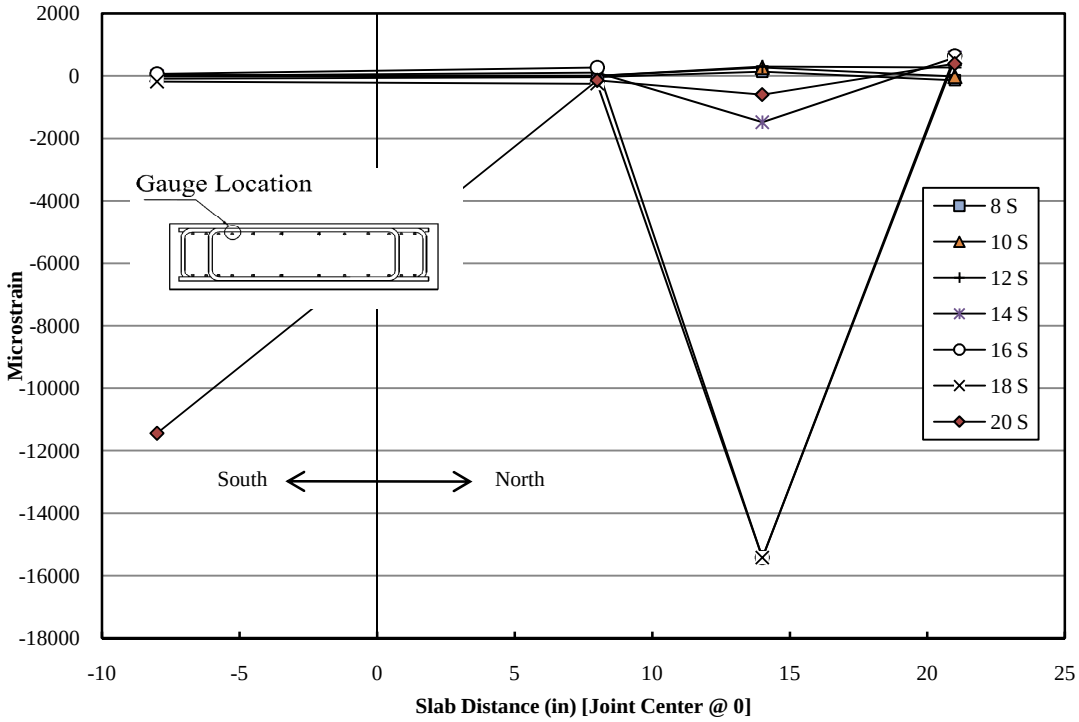

Figure 5-64: Slab Top Reinforcement Strain for FSKJ24 South Cycle 2

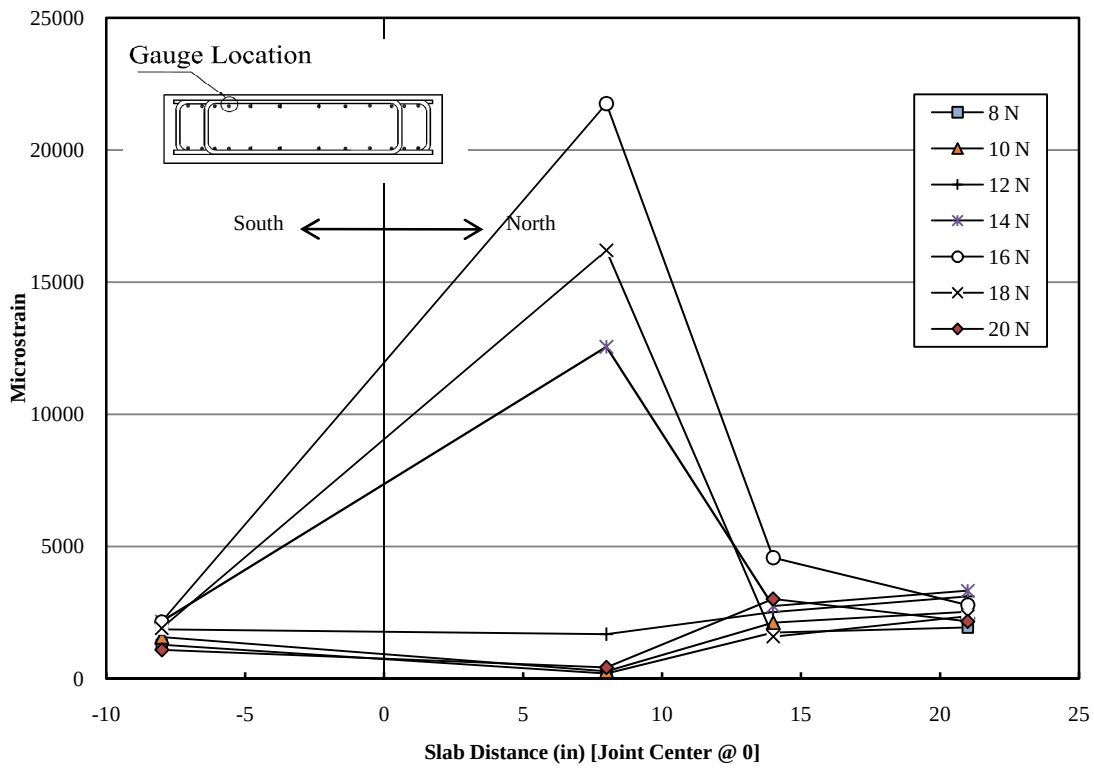

Figure 5-65: Slab Top Reinforcement Strain for FSKJ24 North Cycle 2

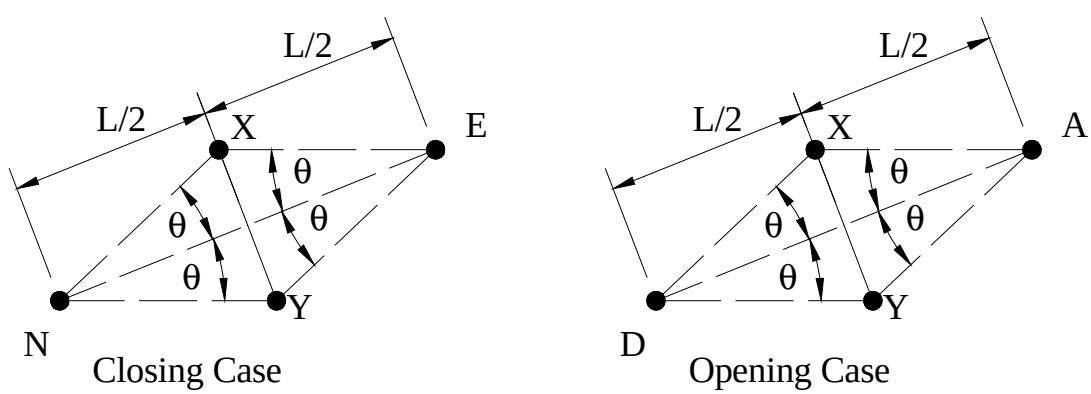

Figure 5-66: Bottle Shaped Strut Configuration

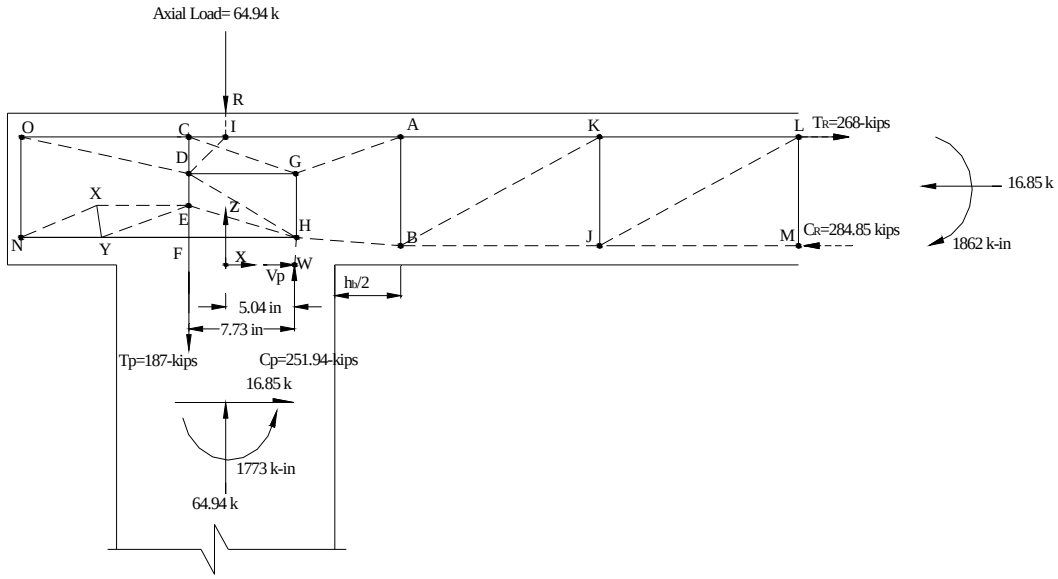

Figure 5-67: Strut-and-Tie Model FSKJ24 (Closing Moment)

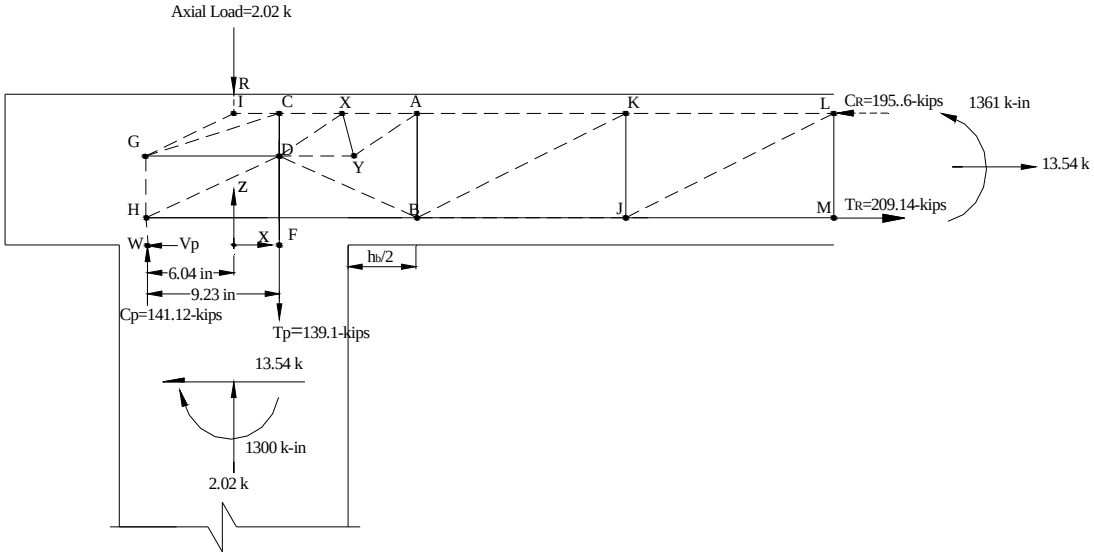

Figure 5-68: Strut-and-Tie Model FSKJ24 (Opening Moment)

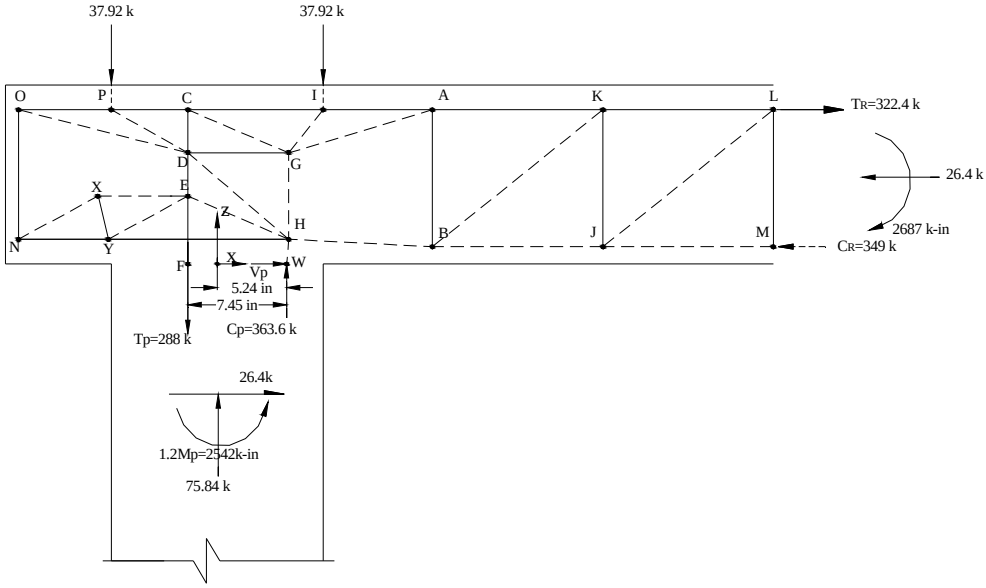

Figure 5-69: Modified Strut-and-Tie Model for FSKJ24 (Closing Moment)

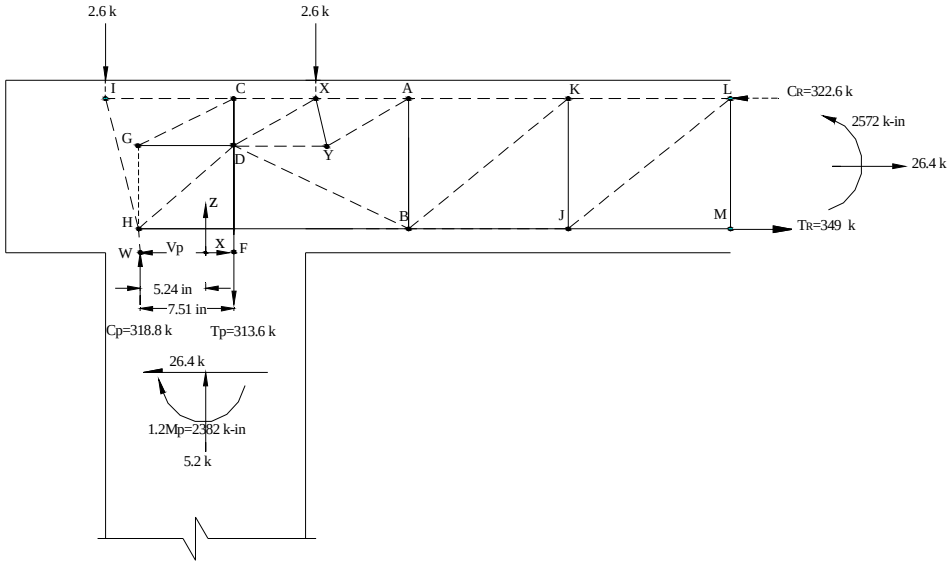

Figure 5-70: Modified Strut-and-Tie Model for FSKJ24 (Opening Moment)

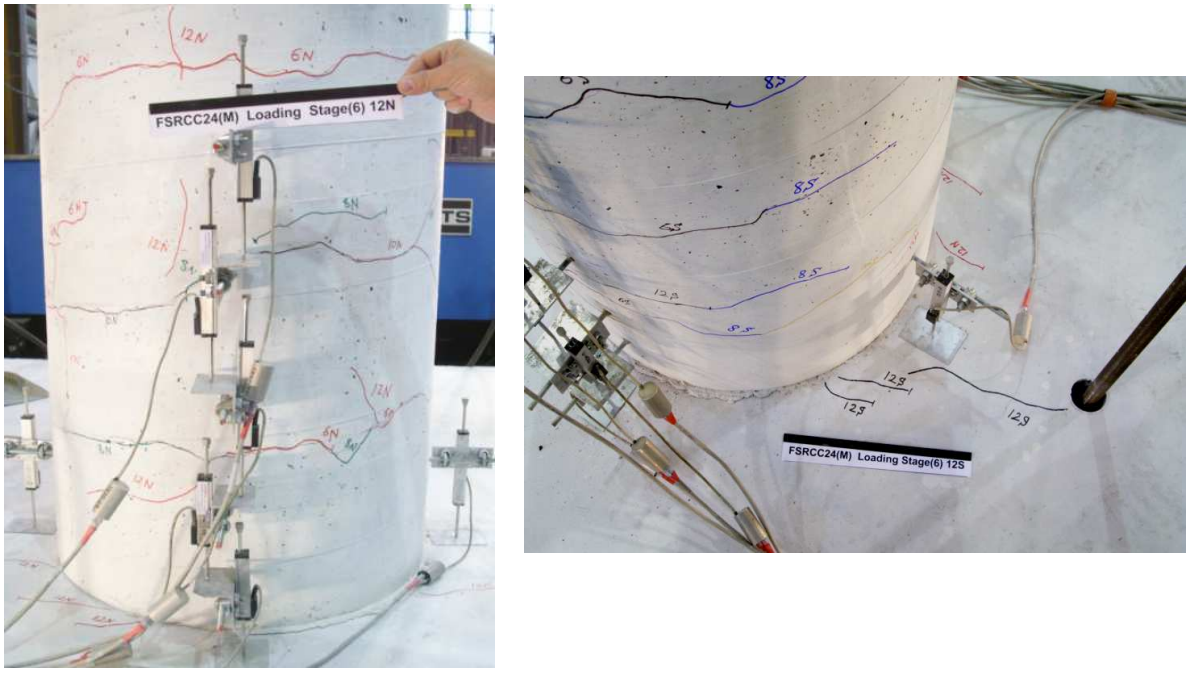

Figure 6-1: FSRCC24-M Cracks (0.75fy)

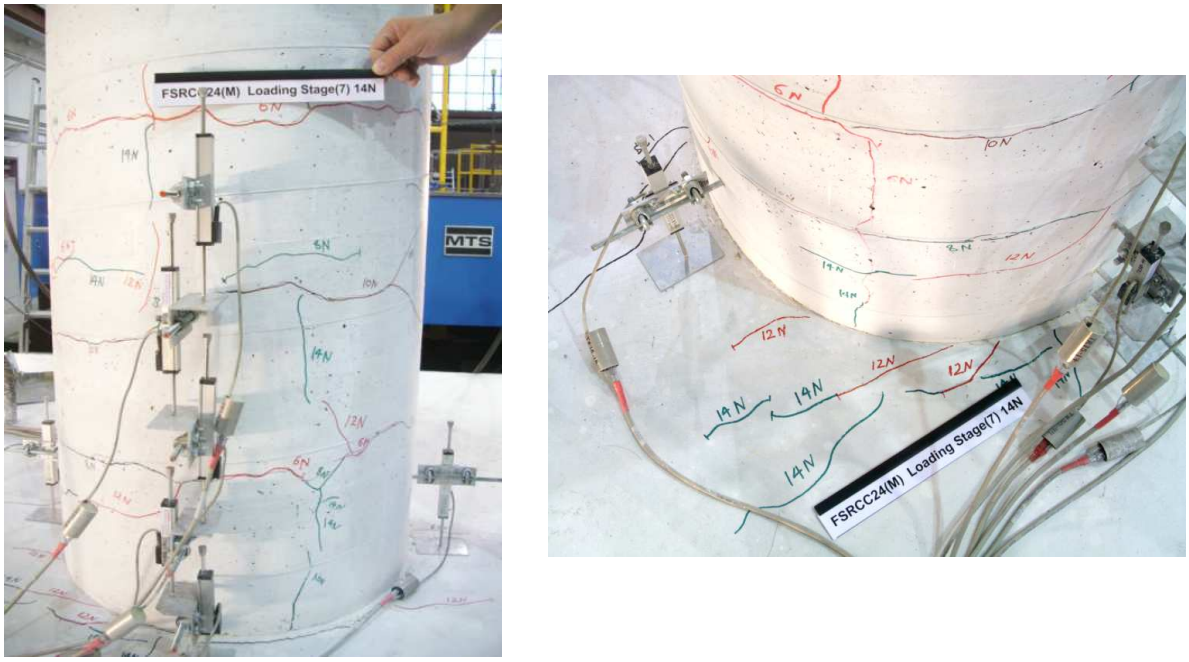

Figure 6-2: FSRCC24-M Cracks (1Δy)

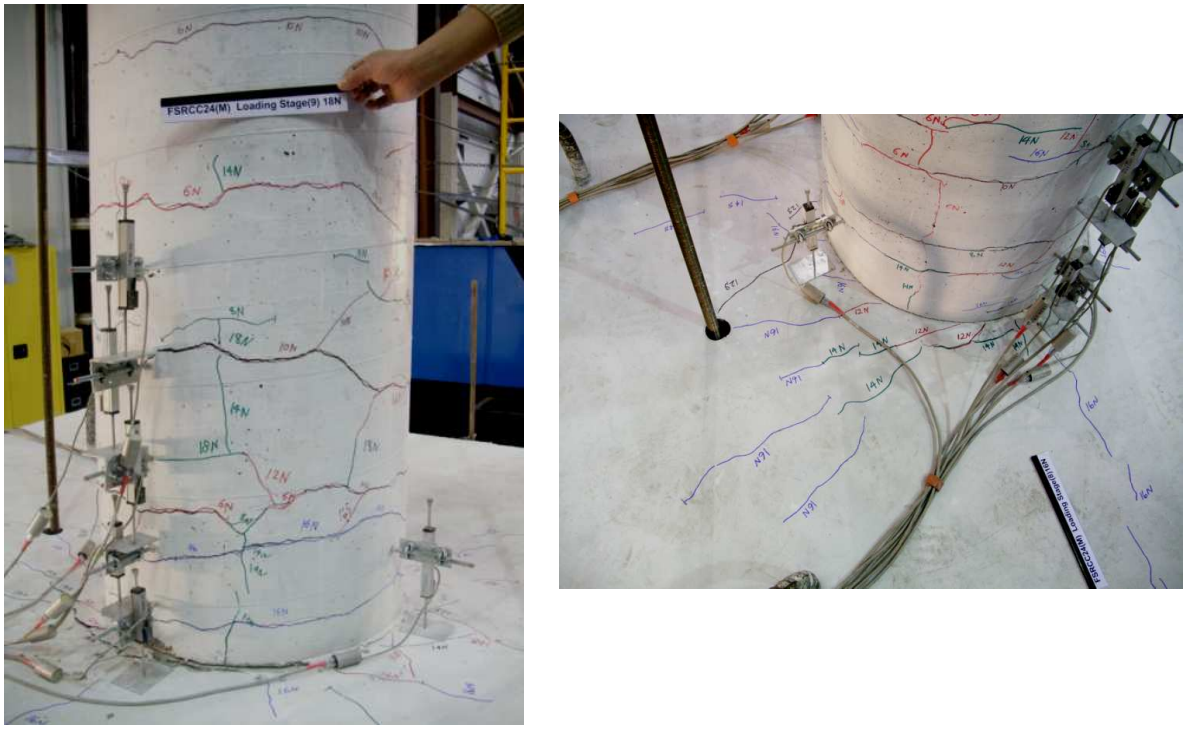

Figure 6-3: FSRCC24-M Cracks (2Δy)

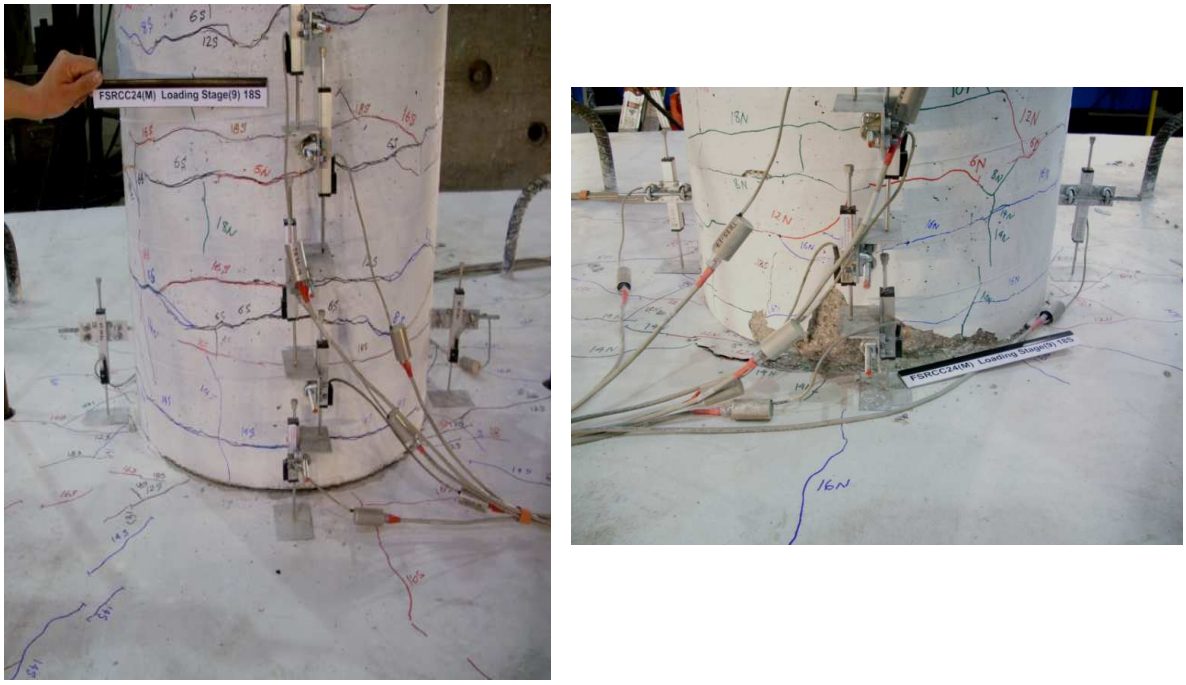

Figure 6-4: FSRCC24-M Cracks (2.5Δy)

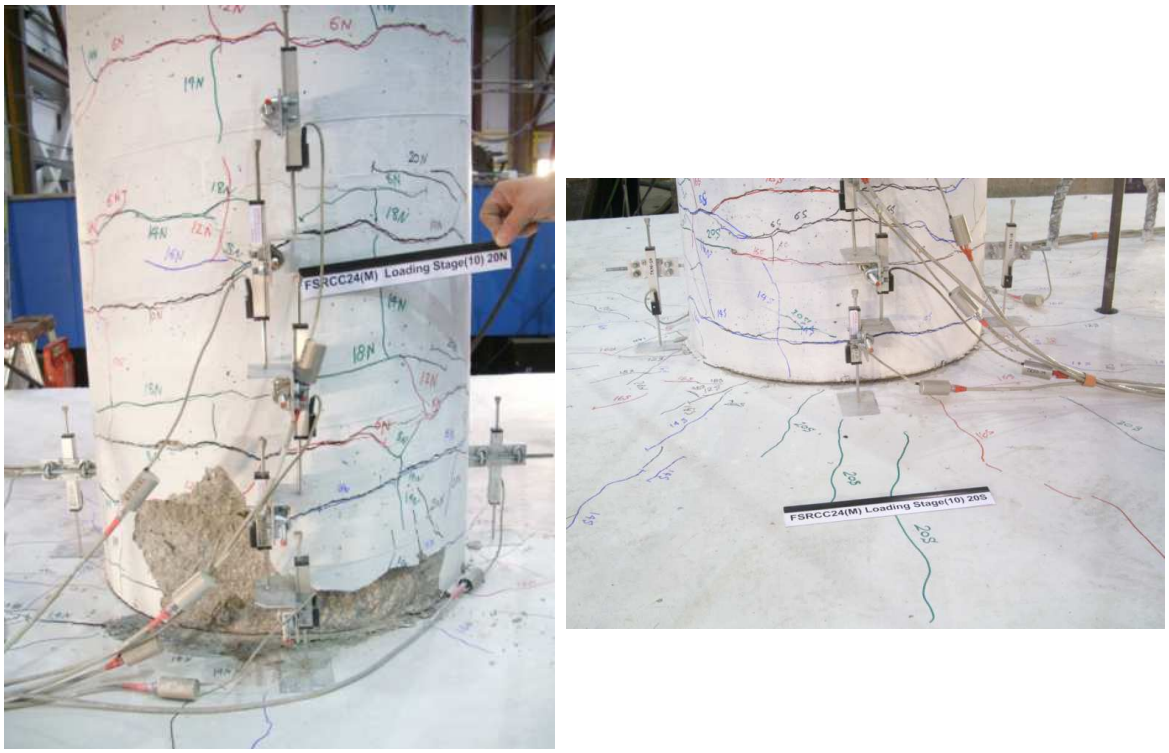

Figure 6-5: FSRCC24-M Cracks (3Δy)

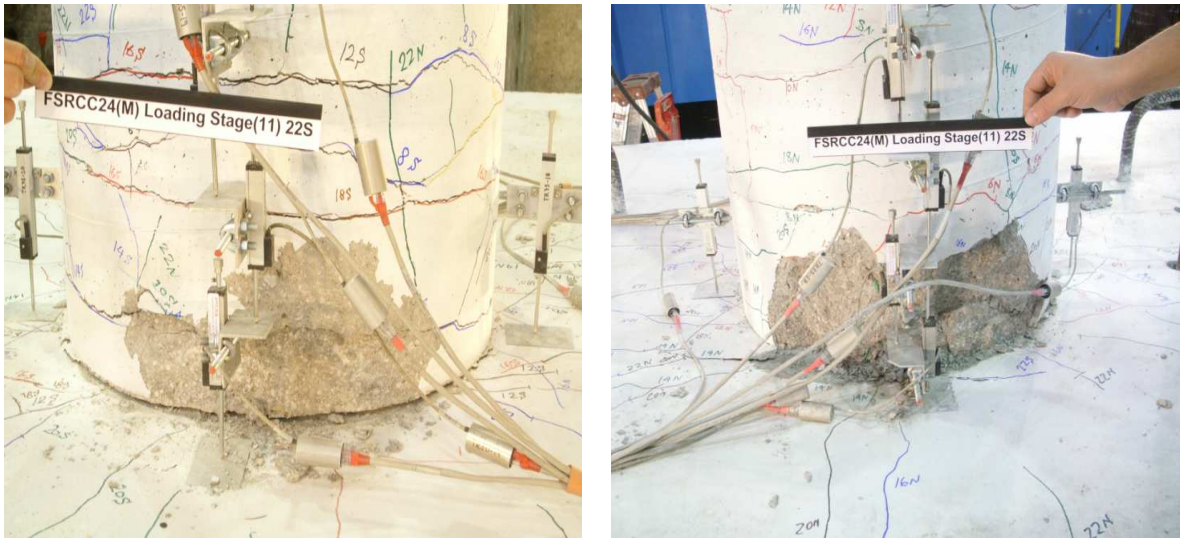

Figure 6-6: FSRCC24-M Cracks (3.5Δy)

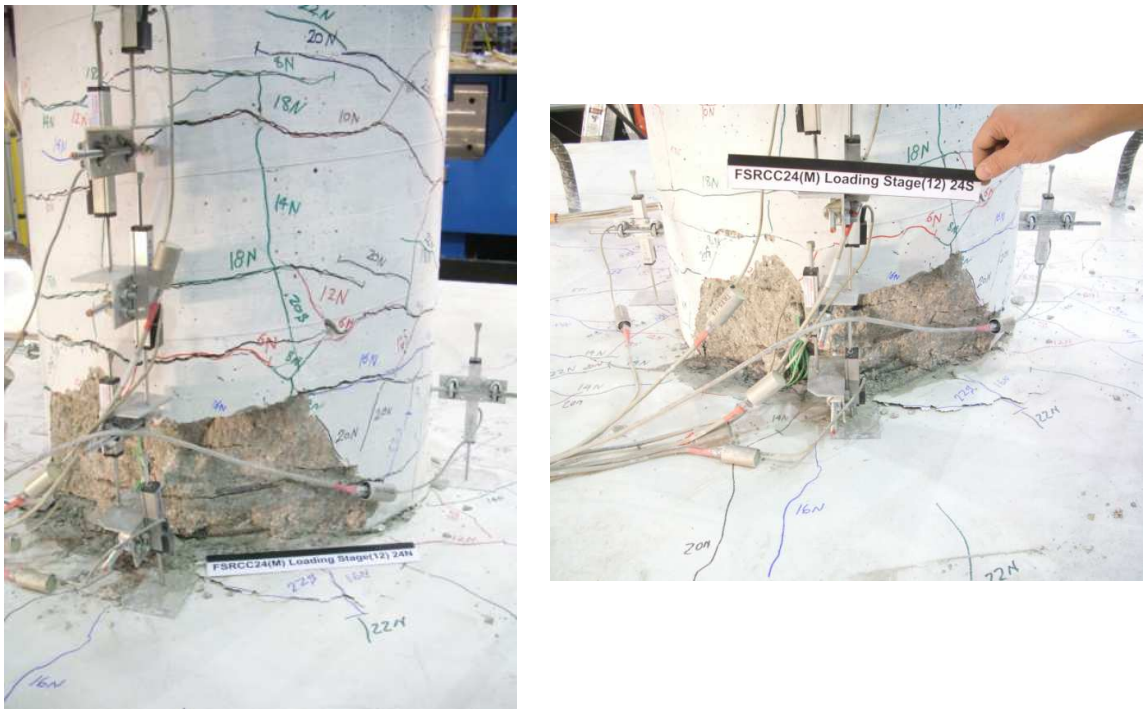

Figure 6-7: FSRCC24-M Cracks (4Δy)

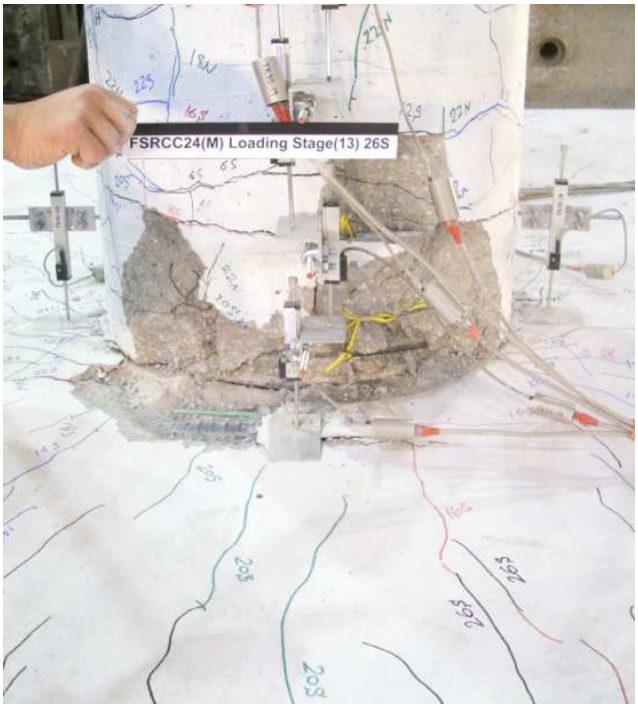

Figure 6-8: FSRCC24-M Cracks (5Δy)

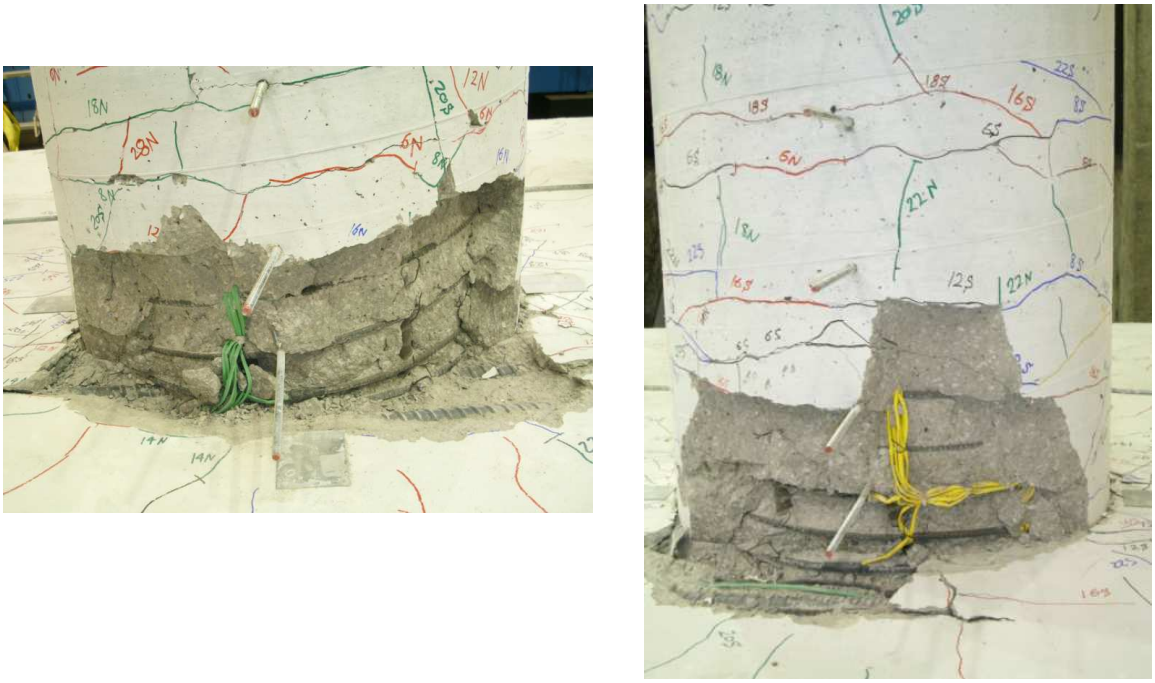

Figure 6-9: FSRCC24-M Cracks (6Δy)

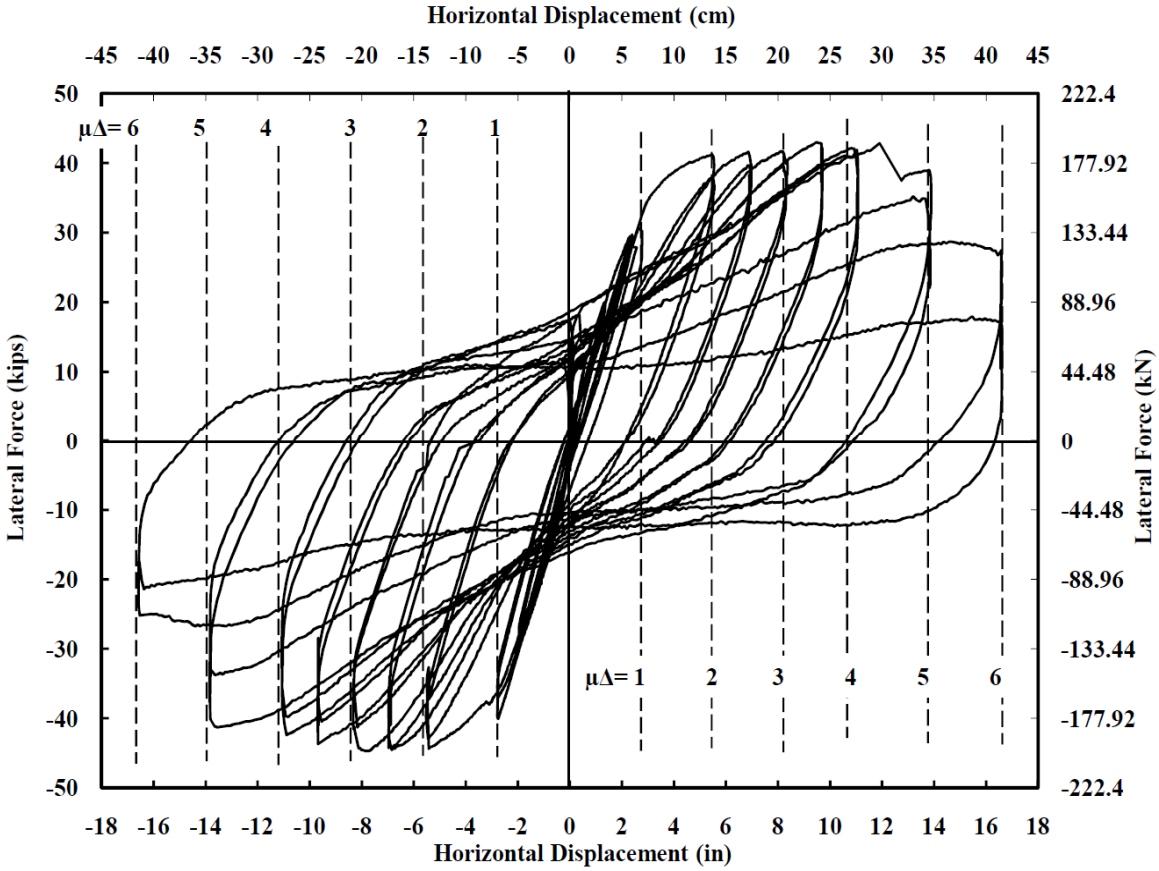

Figure 6-10: Force-Displacement Hysteretic Response for FSRCC24-M

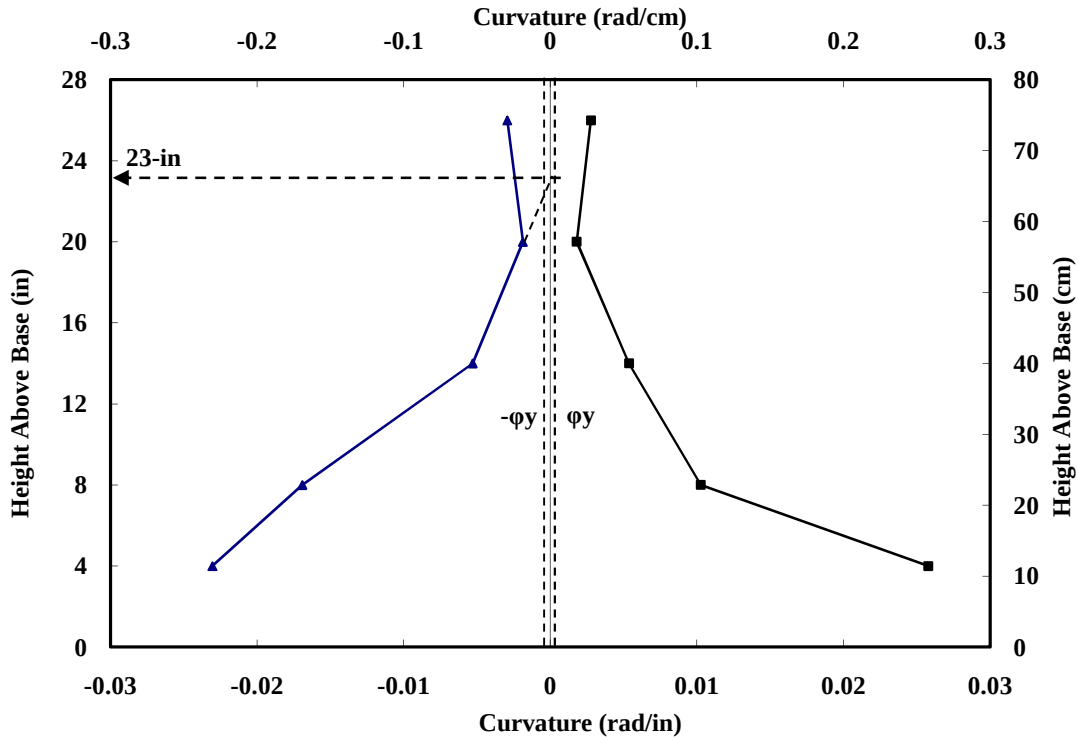

Figure 6-11: Measured Curvature Envelope along the Plastic Hinge of FSRCC24-M

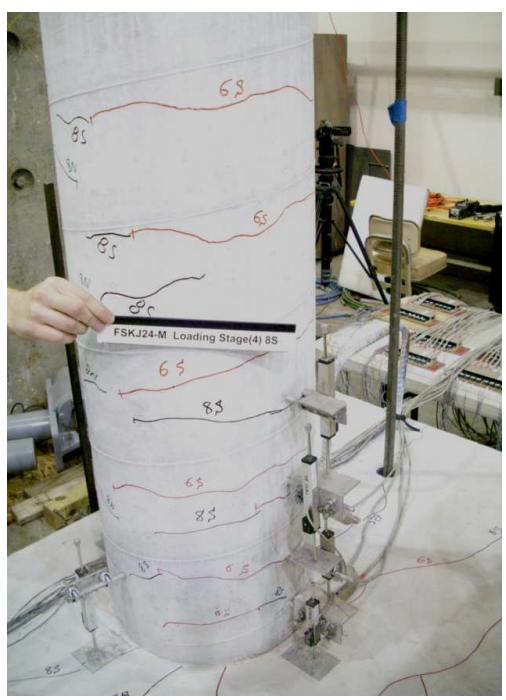

Figure 6-12: FSKJ24-M Cracks (0.75fy)

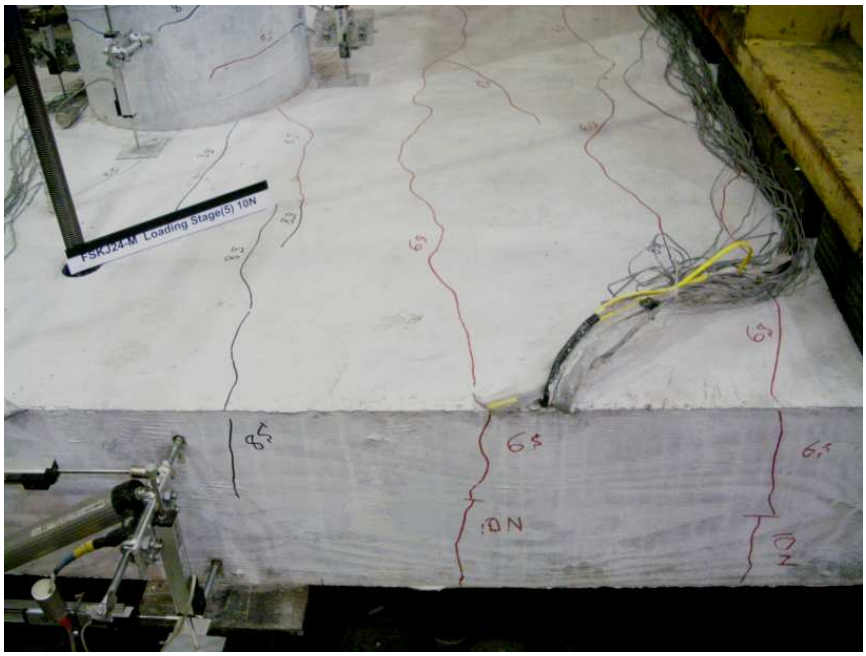

Figure 6-13: FSKJ24-M Cracks (1Δy)

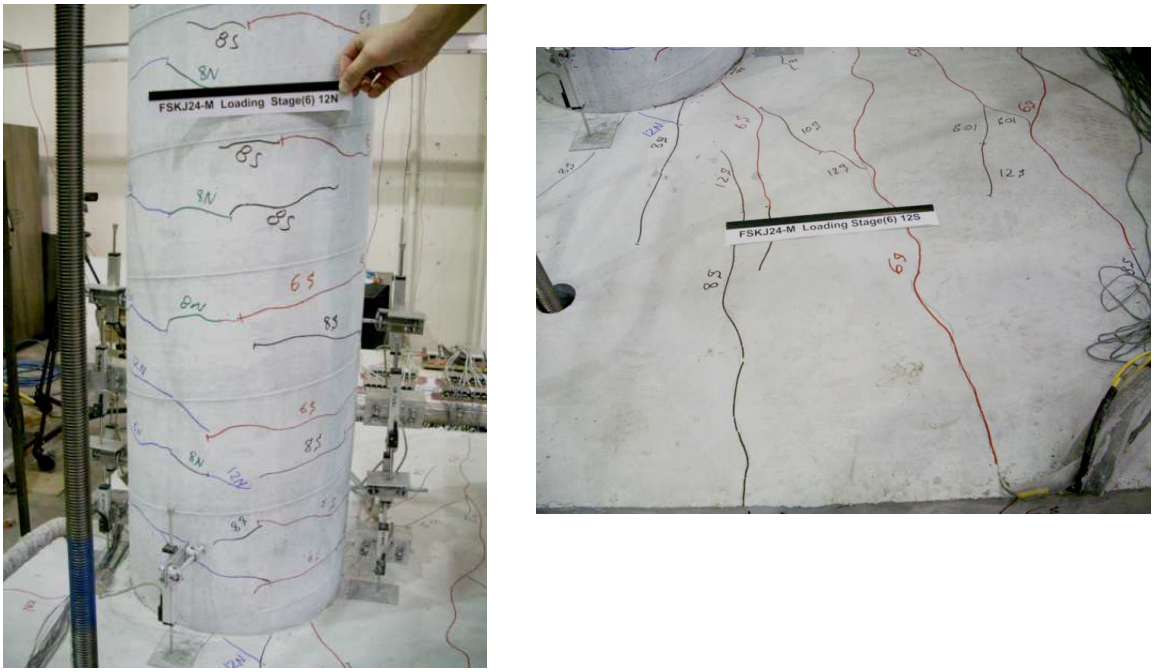

Figure 6-14: FSKJ24-M Cracks (1.5Δy)

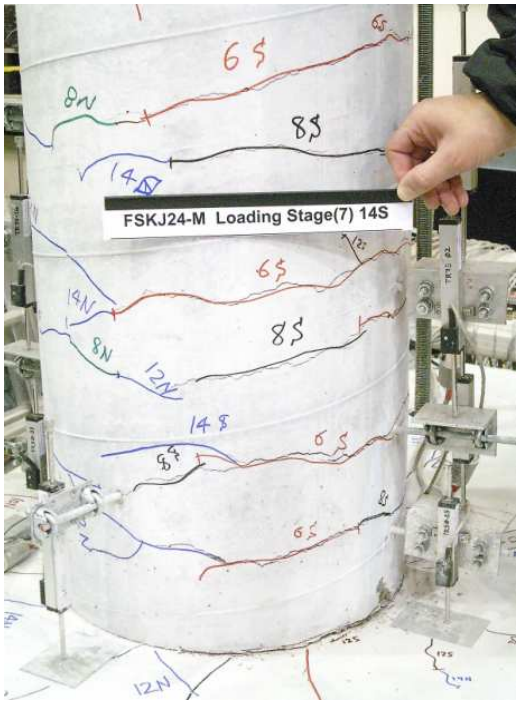

Figure 6-15:FSKJ24-M Cracks (2Δy)

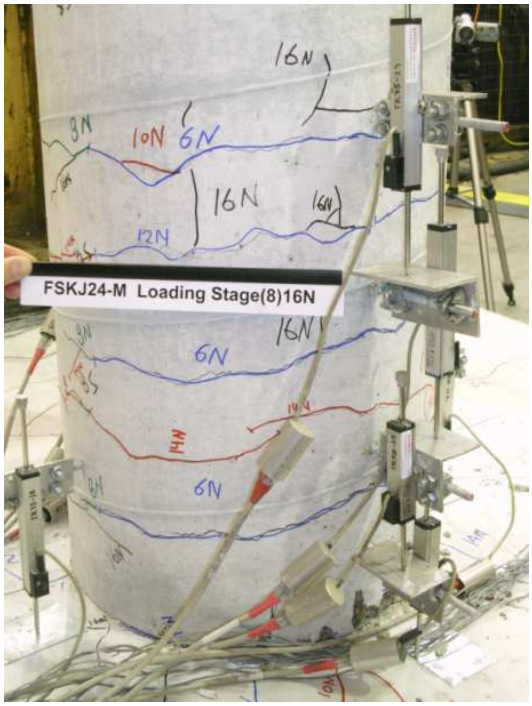

Figure 6-16:FSKJ24-M Cracks (2.5Δy)

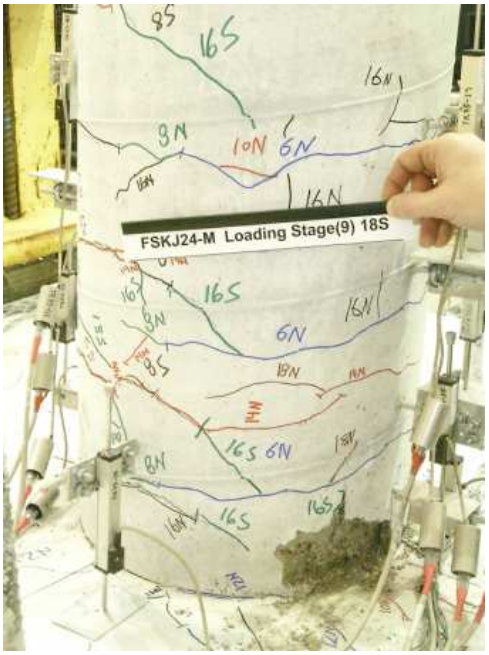

Figure 6-17: FSKJ24-M Cracks (3Δy)

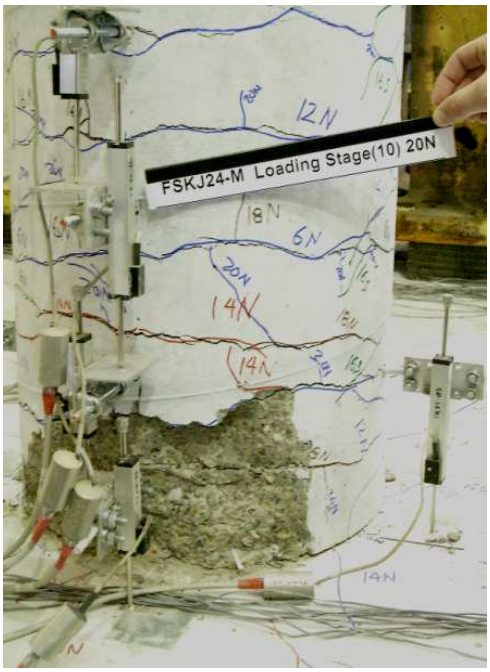

Figure 6-18: FSKJ24-M Cracks (4Δy)

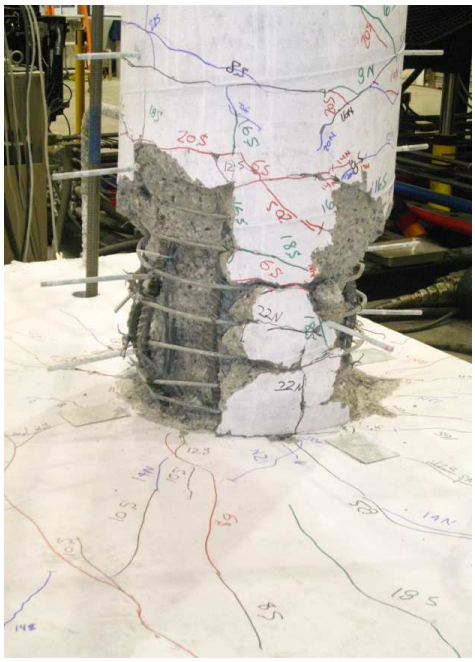

Figure 6-19: FSKJ24-M Cracks (6Δy)

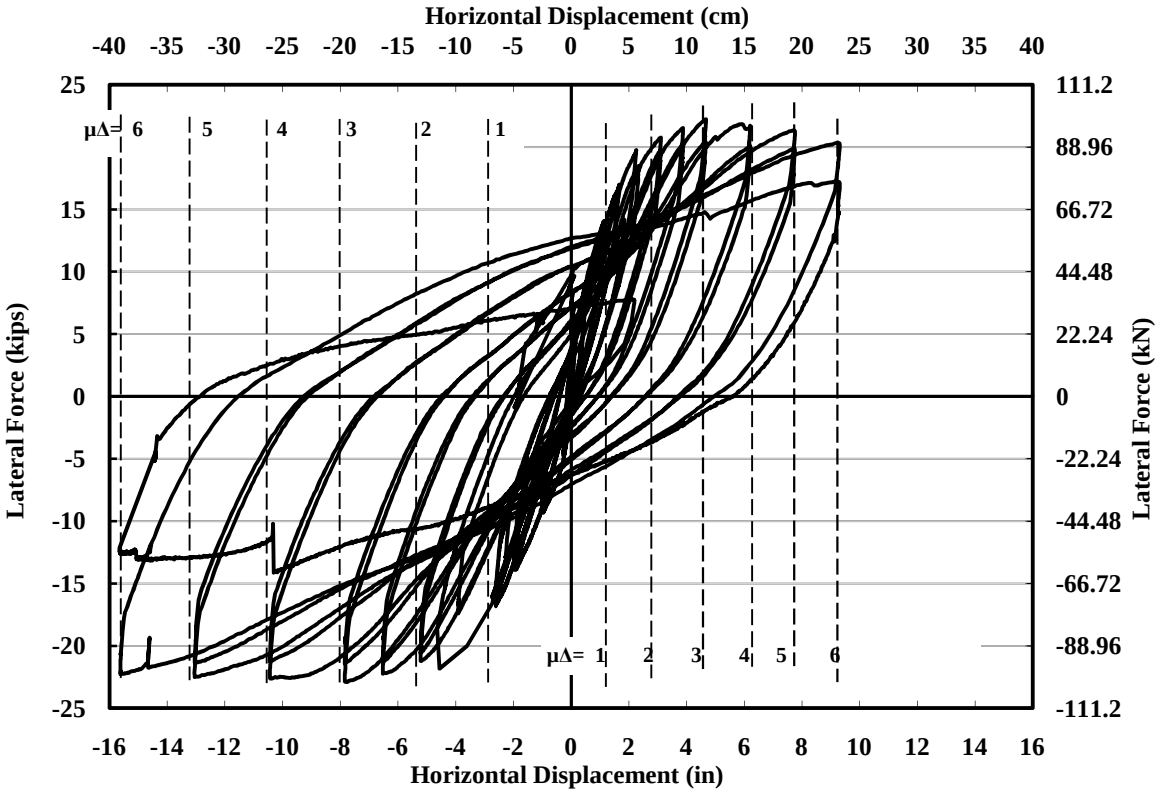

Figure 6-20: Force-Displacement Hysteretic Response for FSKJ24-M

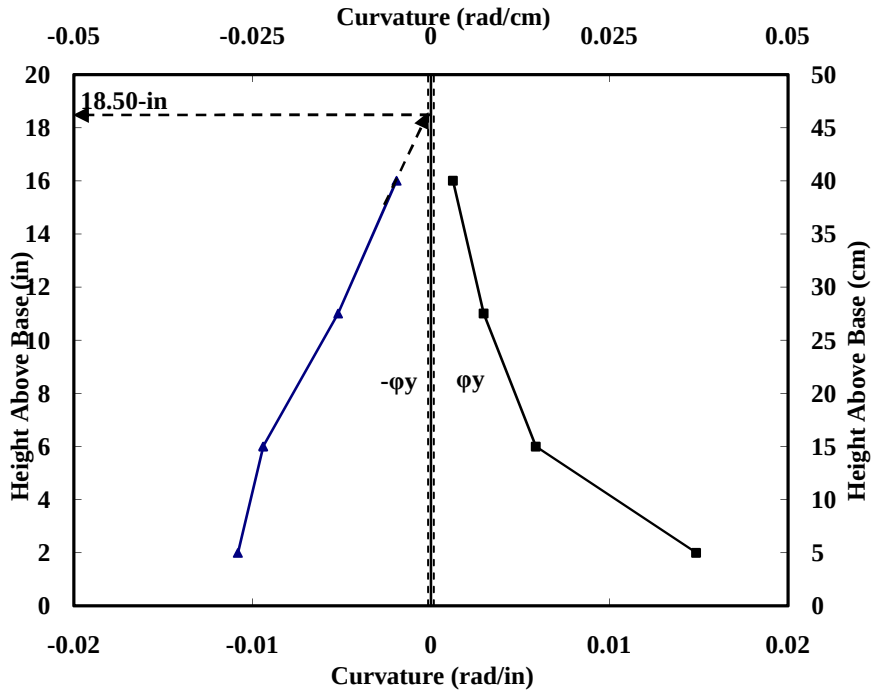

Figure 6-21: Measured Curvature Envelope along the Plastic Hinge of FSKJ24-M

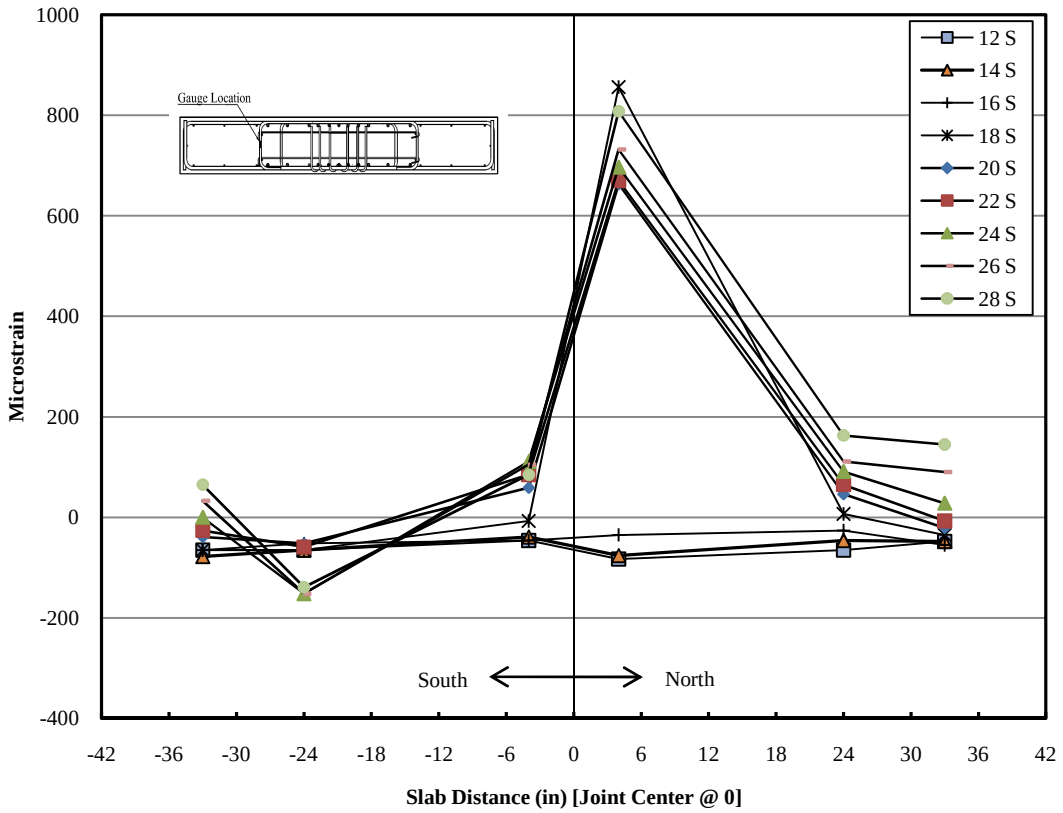

Figure 6-22: Joint Stirrup Strain for FSRCC24-M South Cycle 2

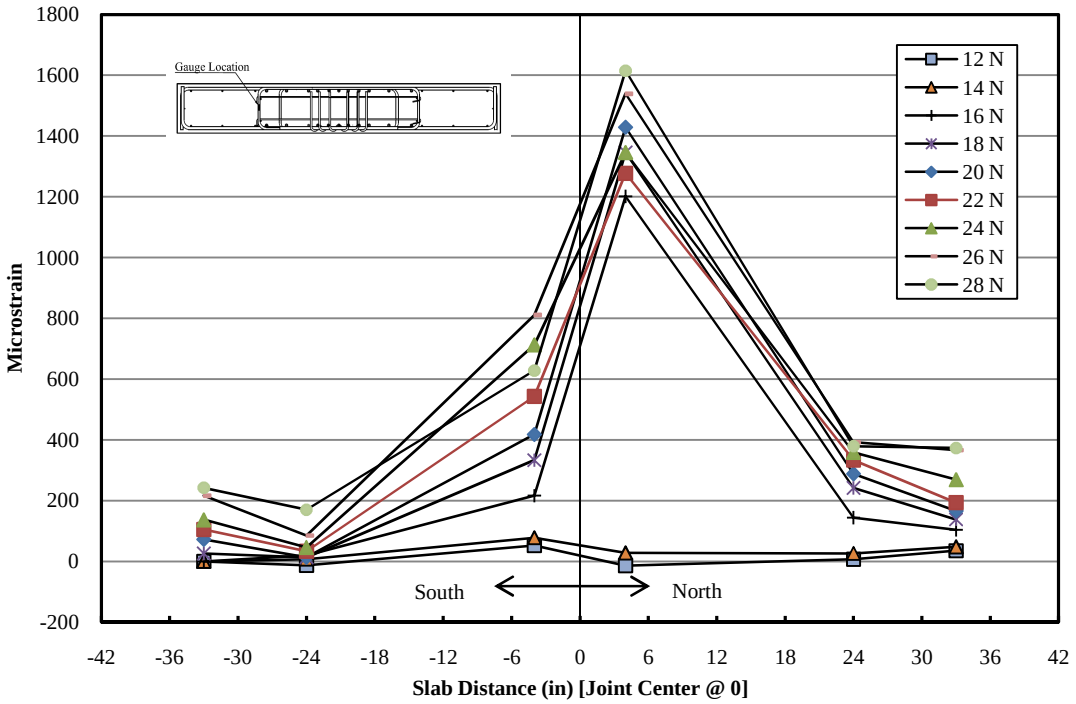

Figure 6-23: Joint Stirrup Strain for FSRCC24-M North Cycle 2

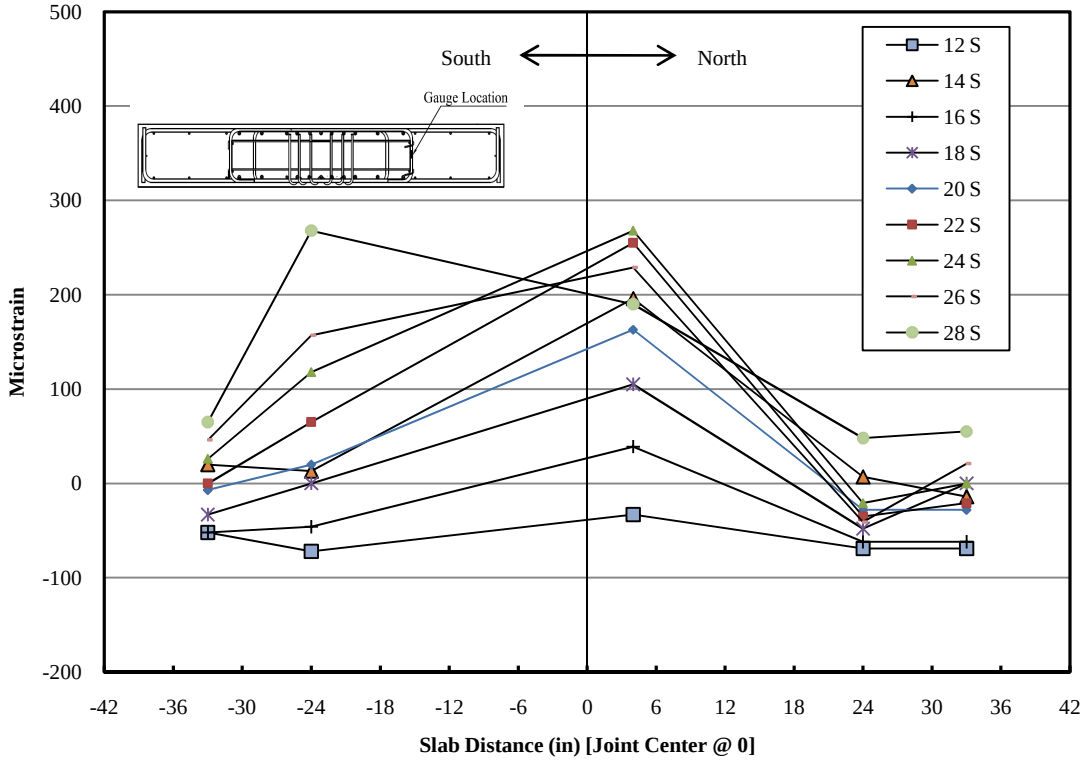

Figure 6-24: Joint Stirrup Strain for FSRCC24-M South Cycle 2

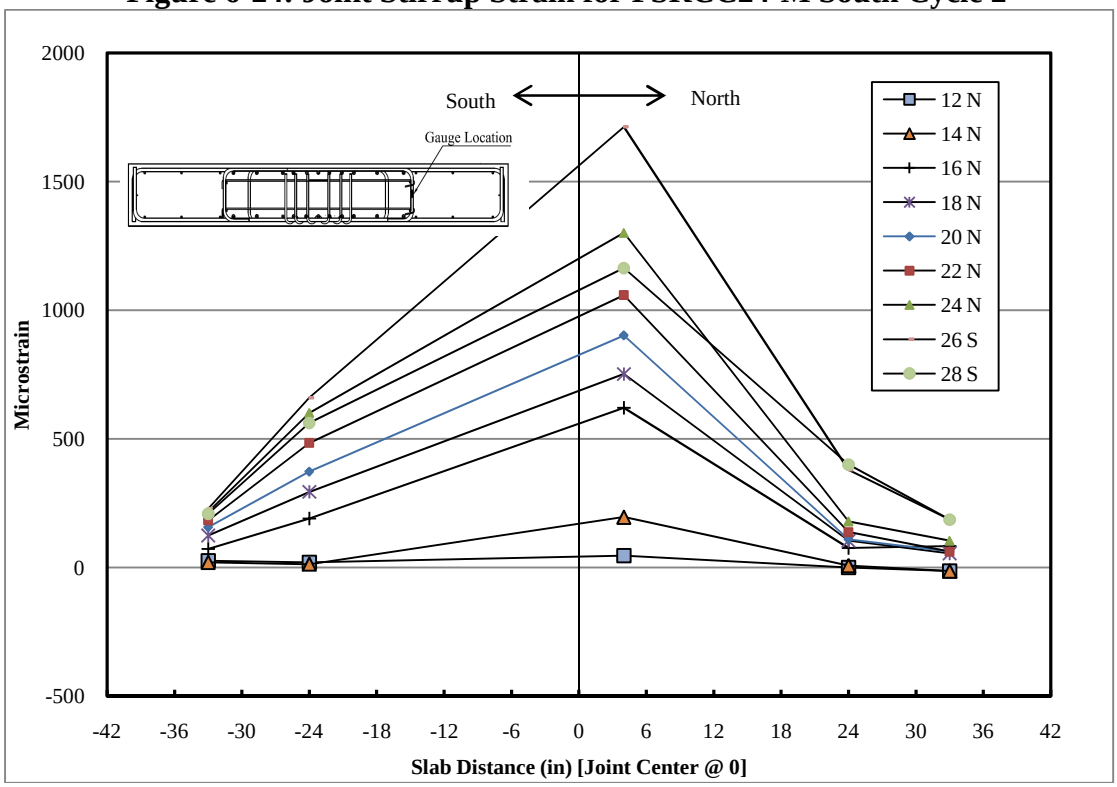

Figure 6-25: Joint Stirrup Strain for FSRCC24-M North Cycle 2

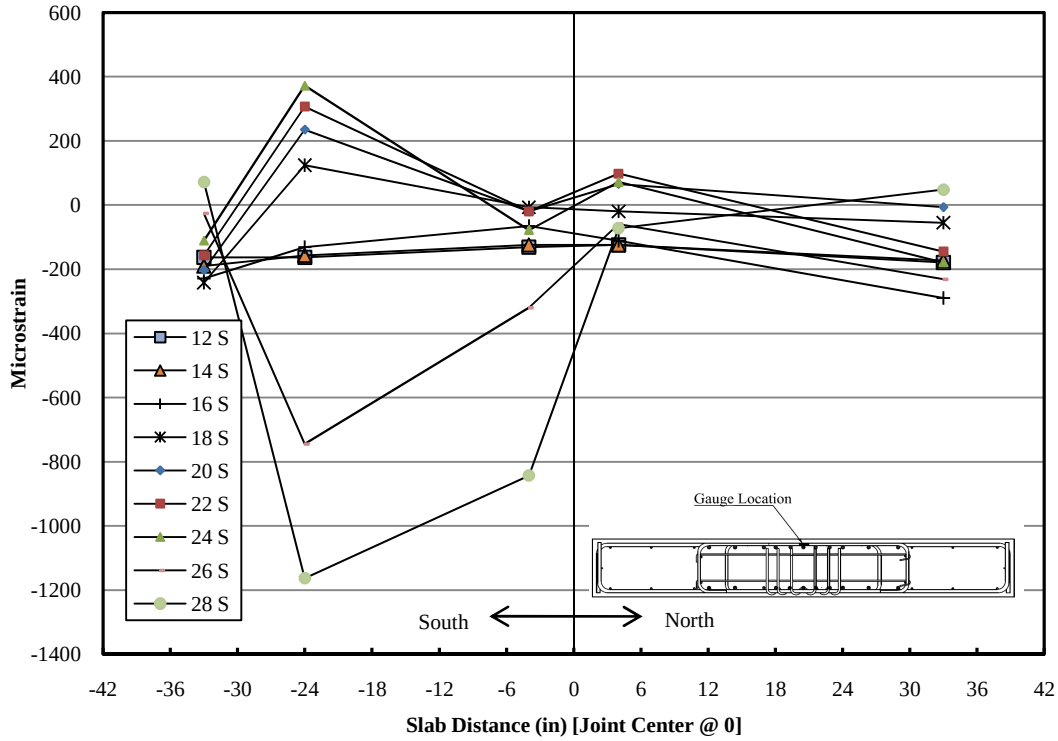

Figure 6-26: Joint Stirrup Strain for FSRCC24-M South Cycle 2

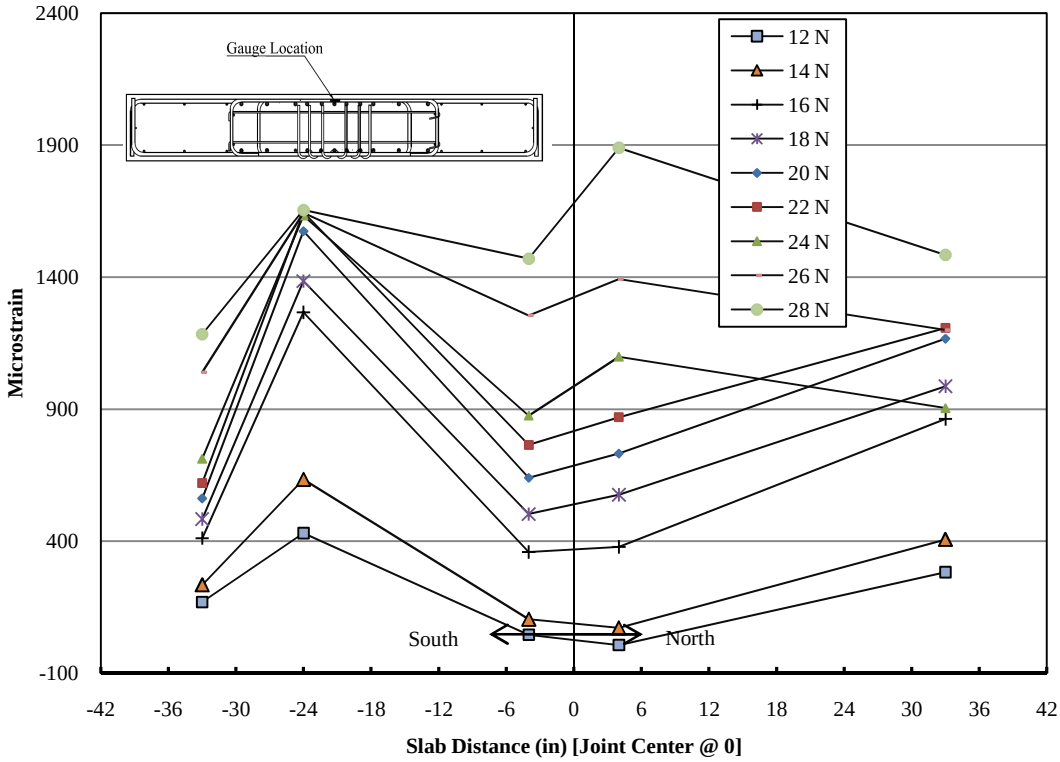

Figure 6-27: Joint Stirrup Strain for FSRCC24-M North Cycle 2

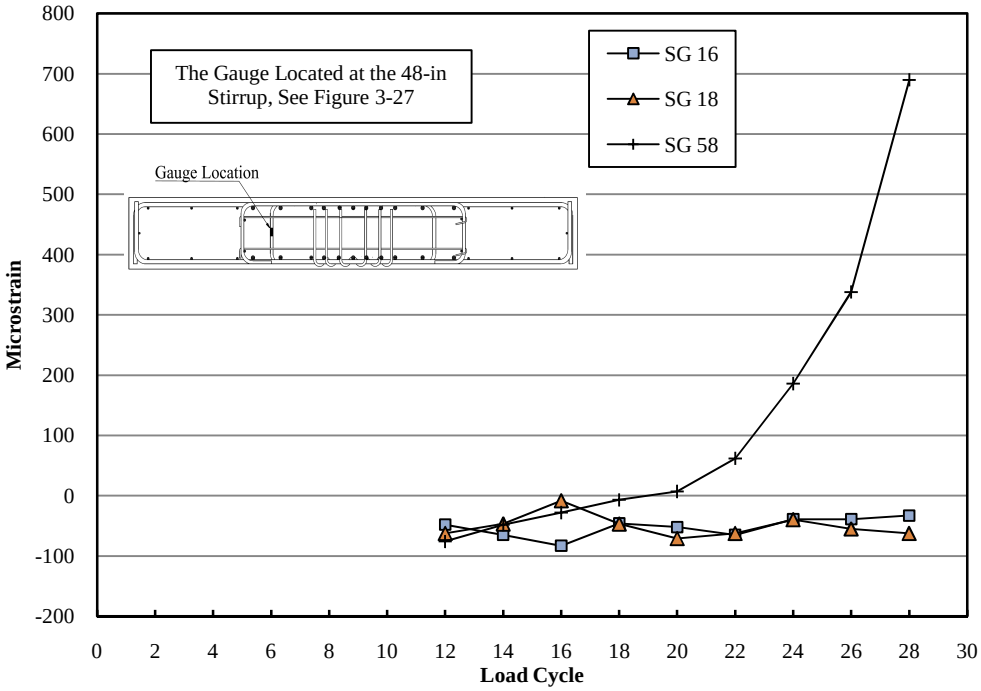

Figure 6-28: Joint Stirrup Strain for FSRCC24-M South Cycle 2

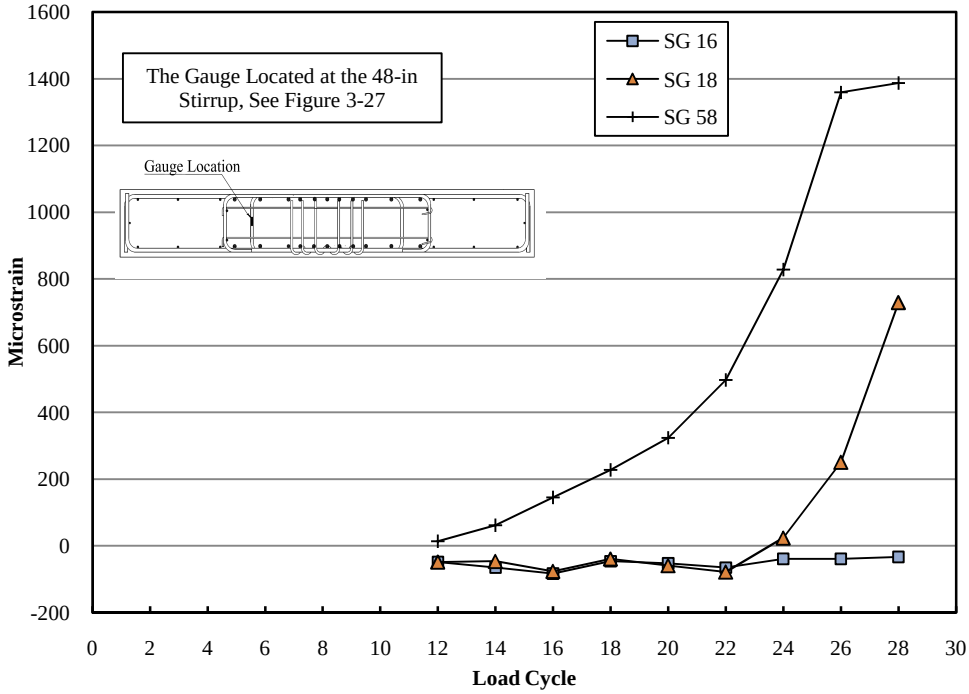

Figure 6-29: Joint Stirrup Strain for FSRCC24-M North Cycle 2

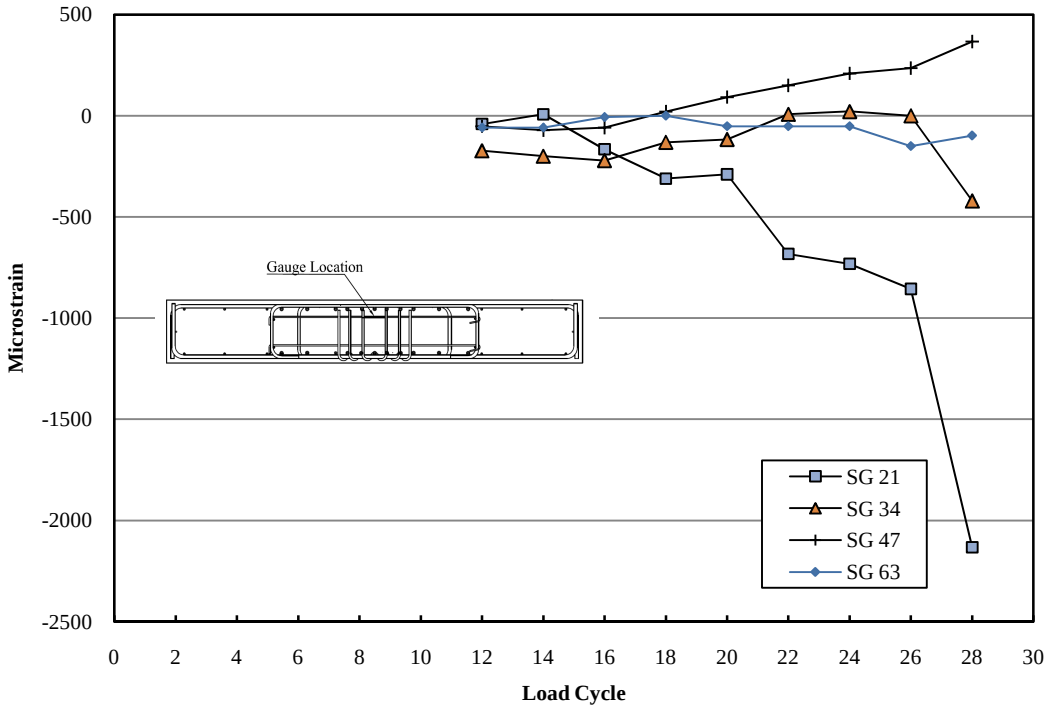

Figure 6-30: Joint Stirrup Strain for FSRCC24-M South Cycle 2

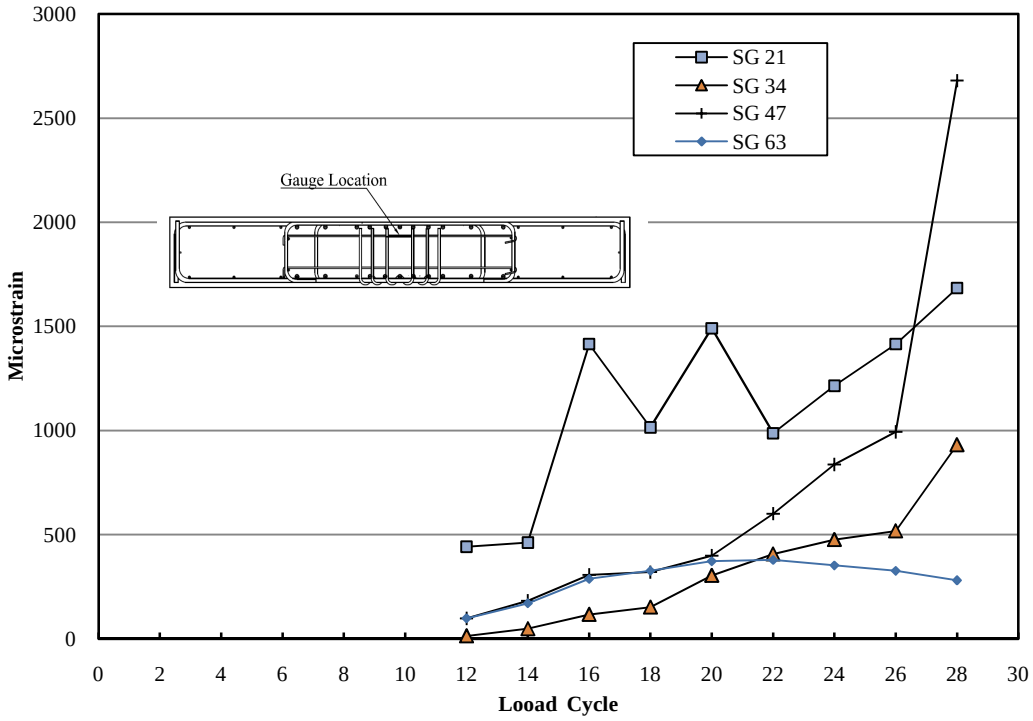

Figure 6-31: Joint Stirrup Strain for FSRCC24-M North Cycle 2

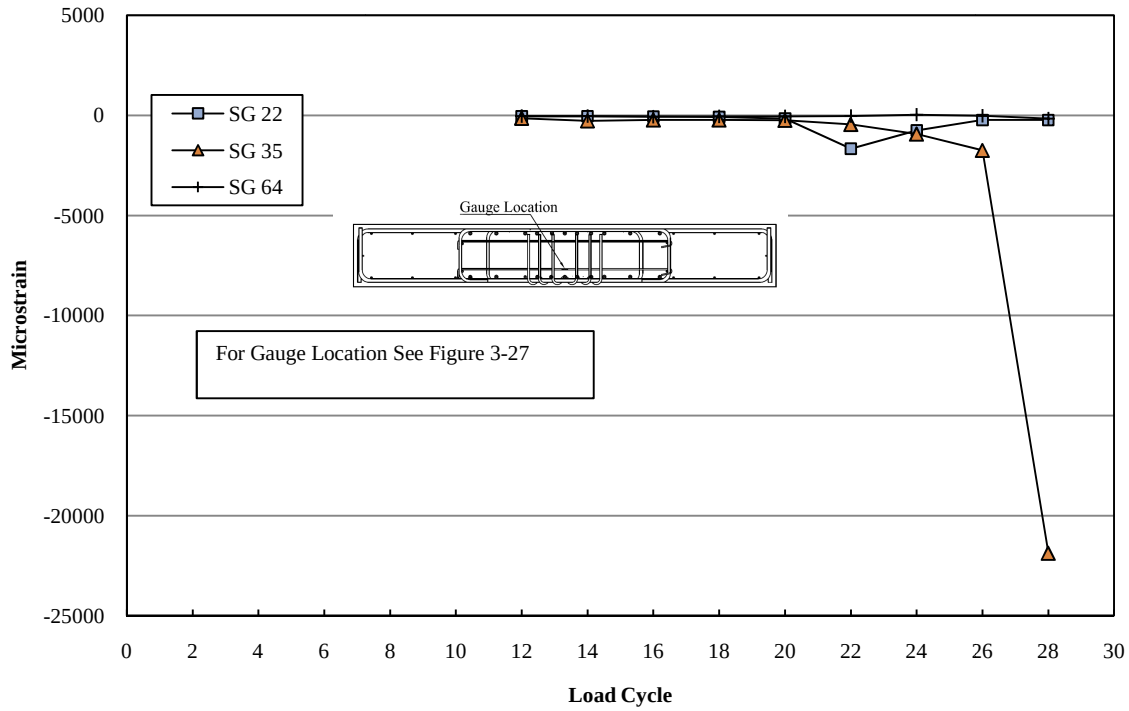

Figure 6-32: Joint Stirrup Strain for FSRCC24-M South Cycle 2

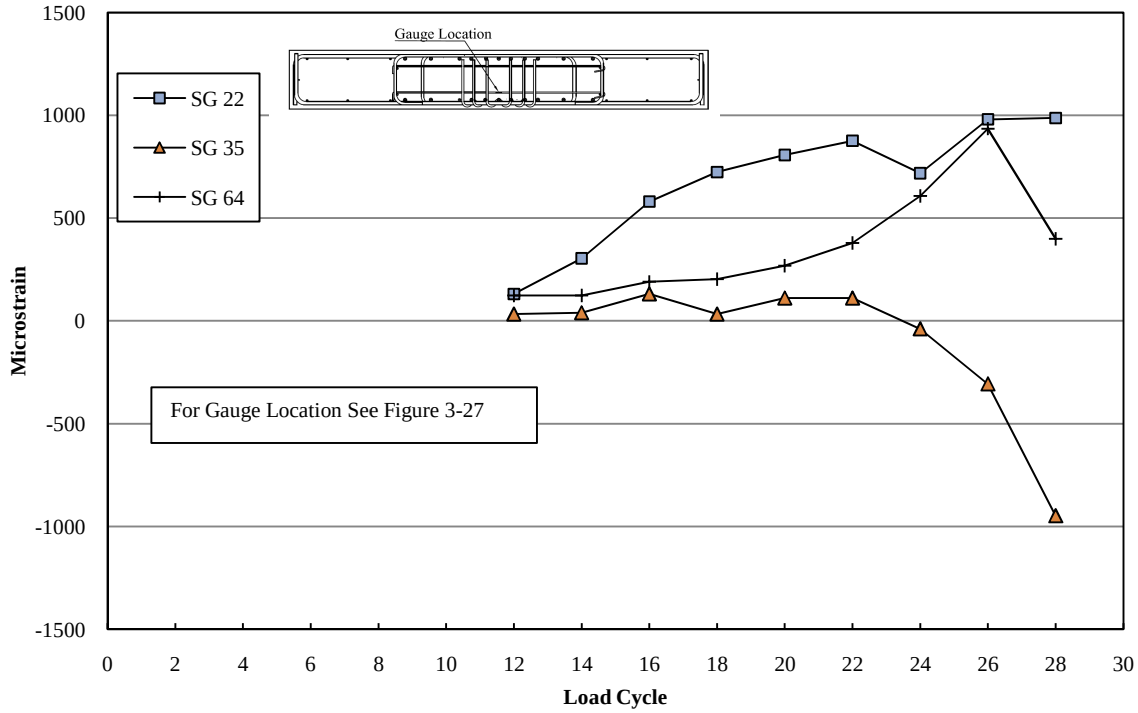

Figure 6-33: Joint Stirrup Strain for FSRCC24-M North Cycle 2

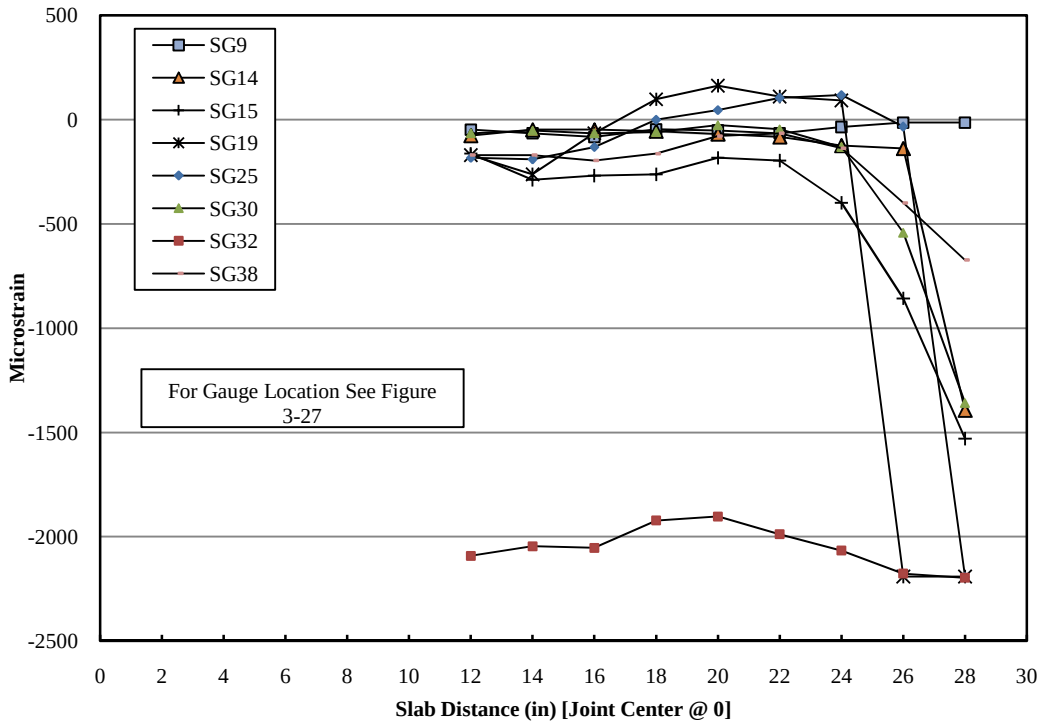

Figure 6-34: J-bars Joint Reinforcement Strain for FSRCC24-M South Cycle 2

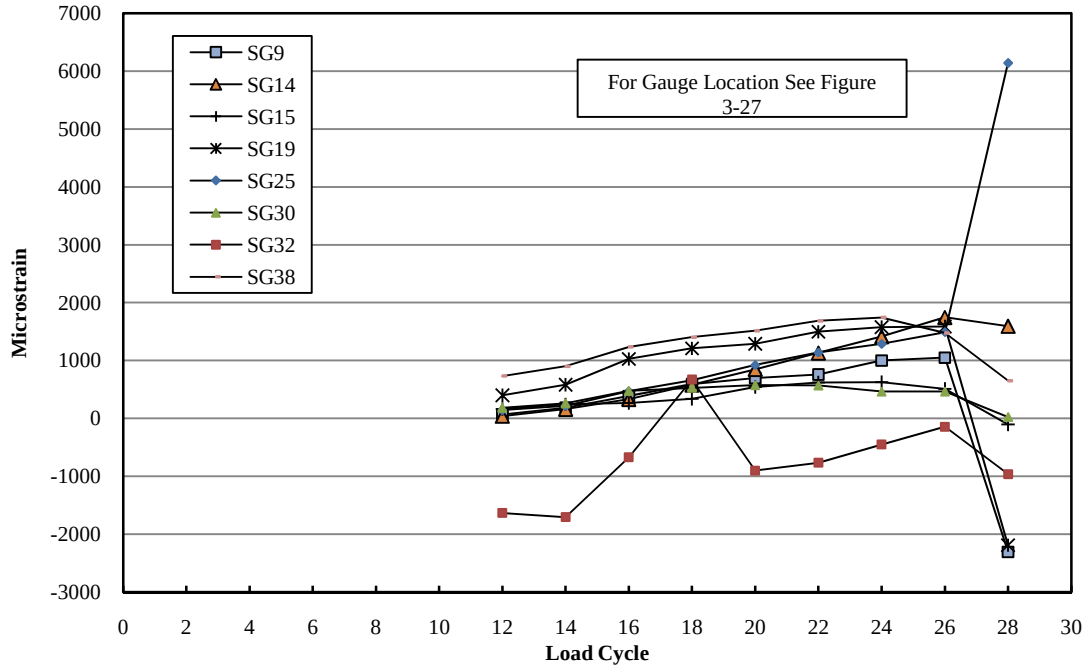

Figure 6-35: J-bars Joint Reinforcement Strain for FSRCC24-M North Cycle 2

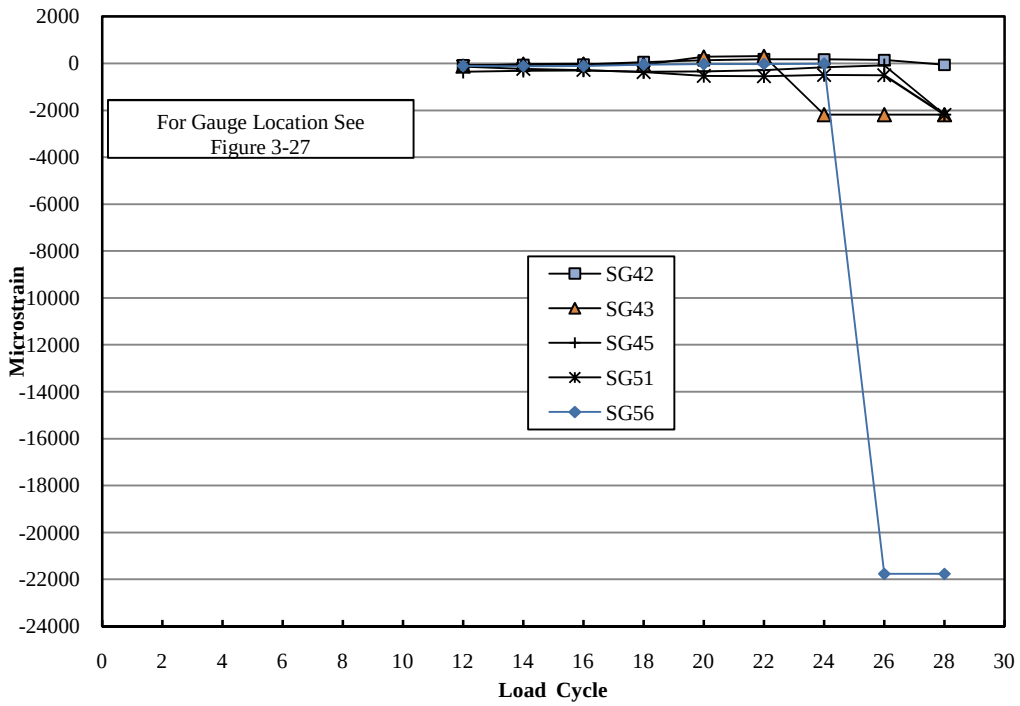

Figure 6-36: J-bars Joint Reinforcement Strain for FSRCC24-M South Cycle 2

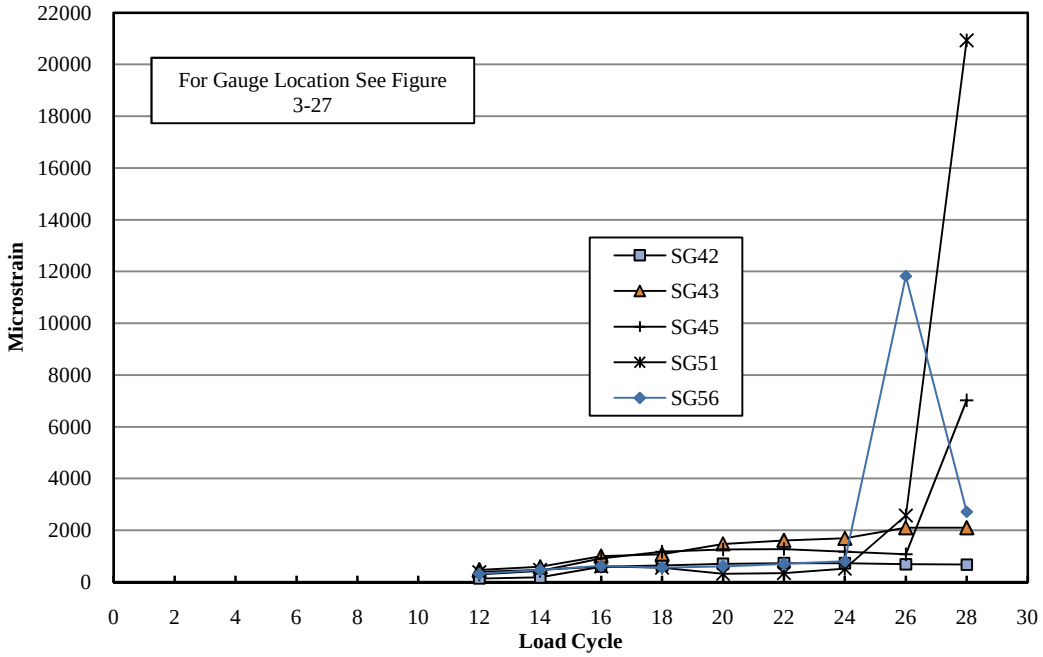

Figure 6-37: J-bars Joint Reinforcement Strain for FSRCC24-M North Cycle 2

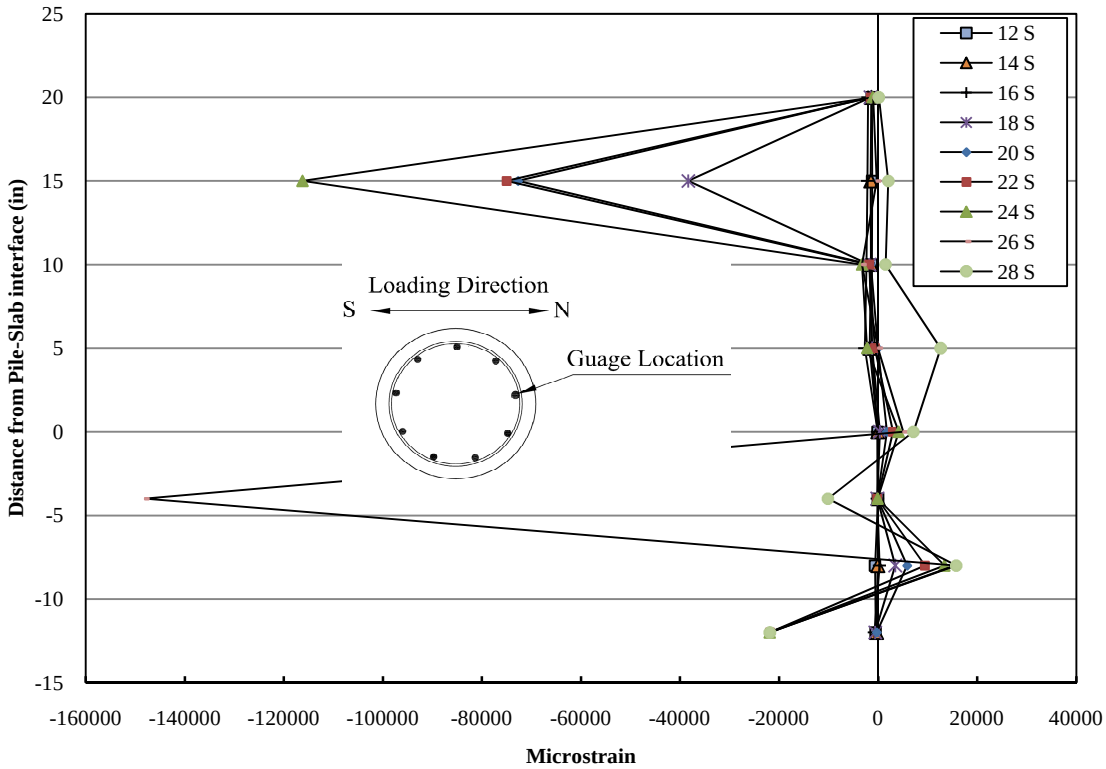

Figure 6-38: Longitudinal Pile Strain for FSRCC24-M South Cycle 2

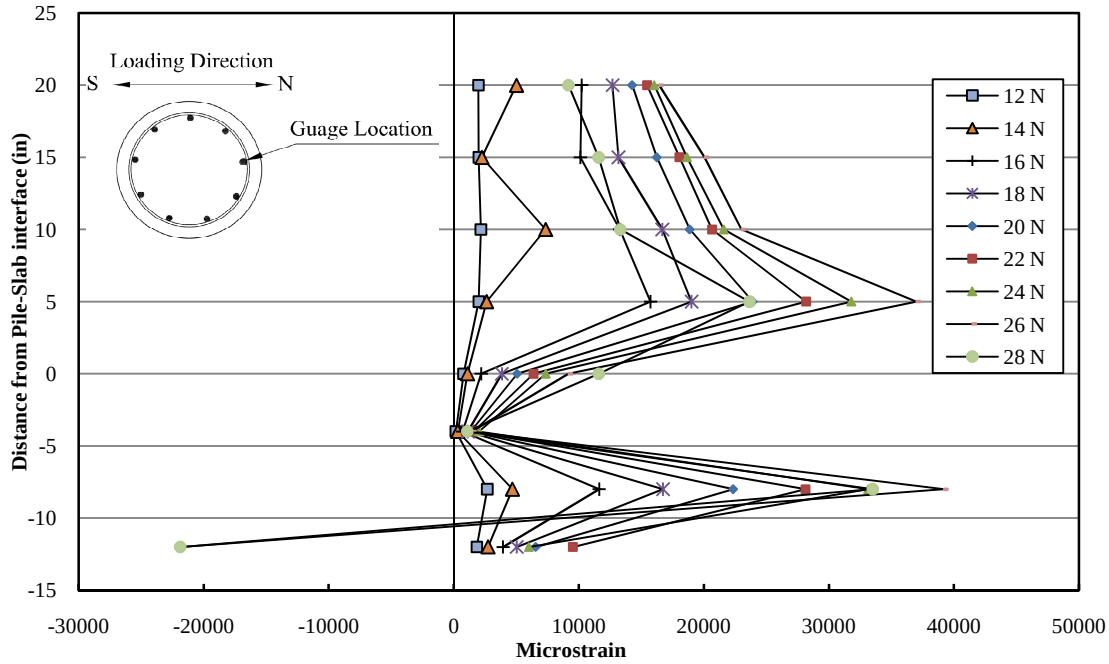

Figure 6-39: Longitudinal Pile Strain for FSRCC24-M North Cycle 2

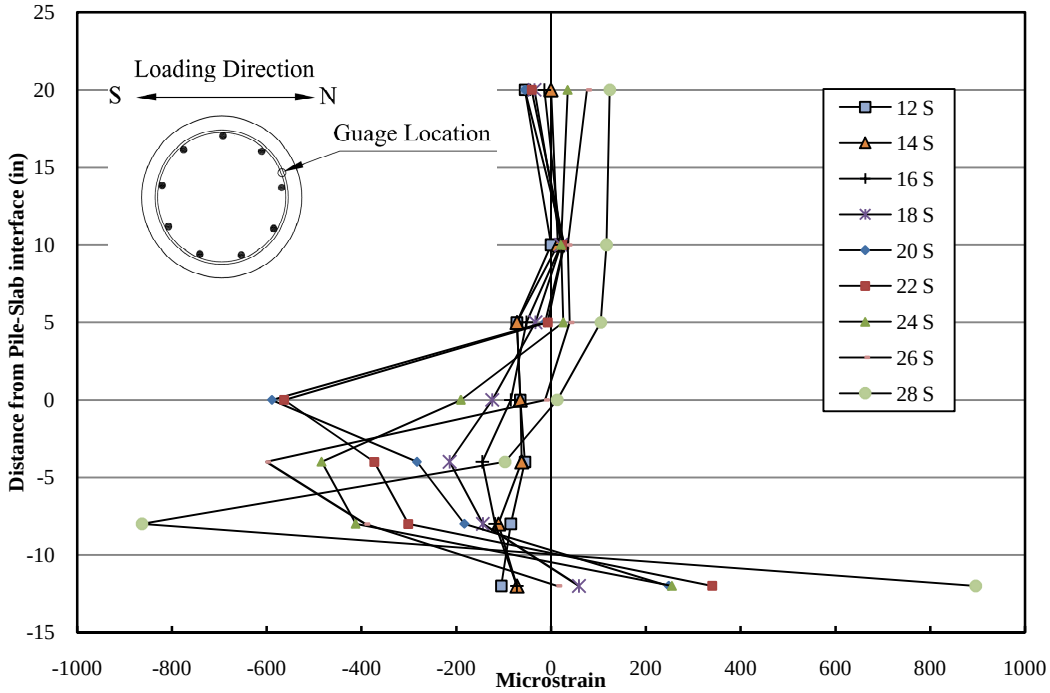

Figure 6-40: Spiral Reinforcement Strain for FSRCC24-M South Cycle 2

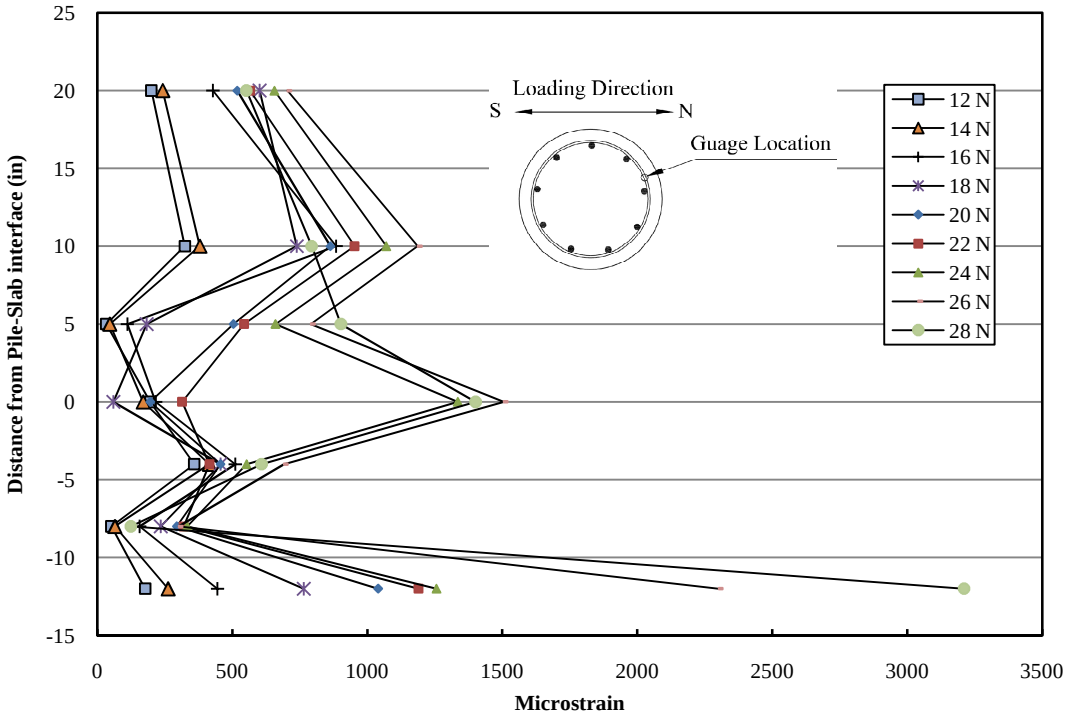

Figure 6-41: Spiral Reinforcement Strain for FSRCC24-M North Cycle 2

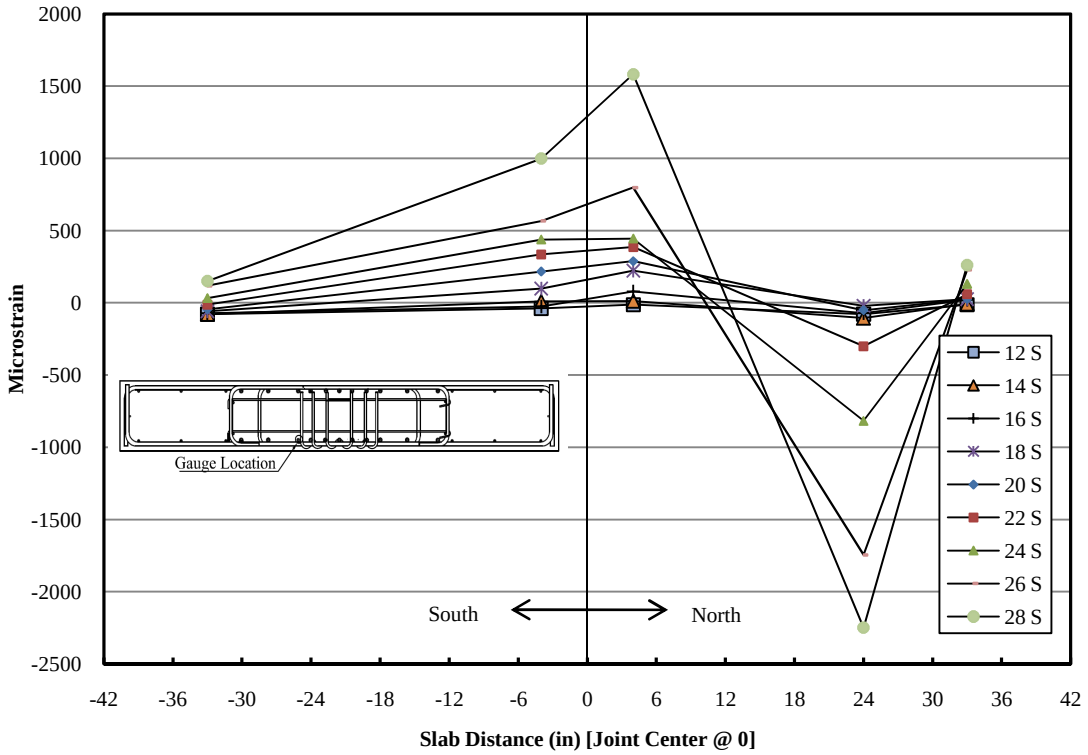

Figure 6-42: Slab Bottom Reinforcement Strain for FSRCC24-M South Cycle 2

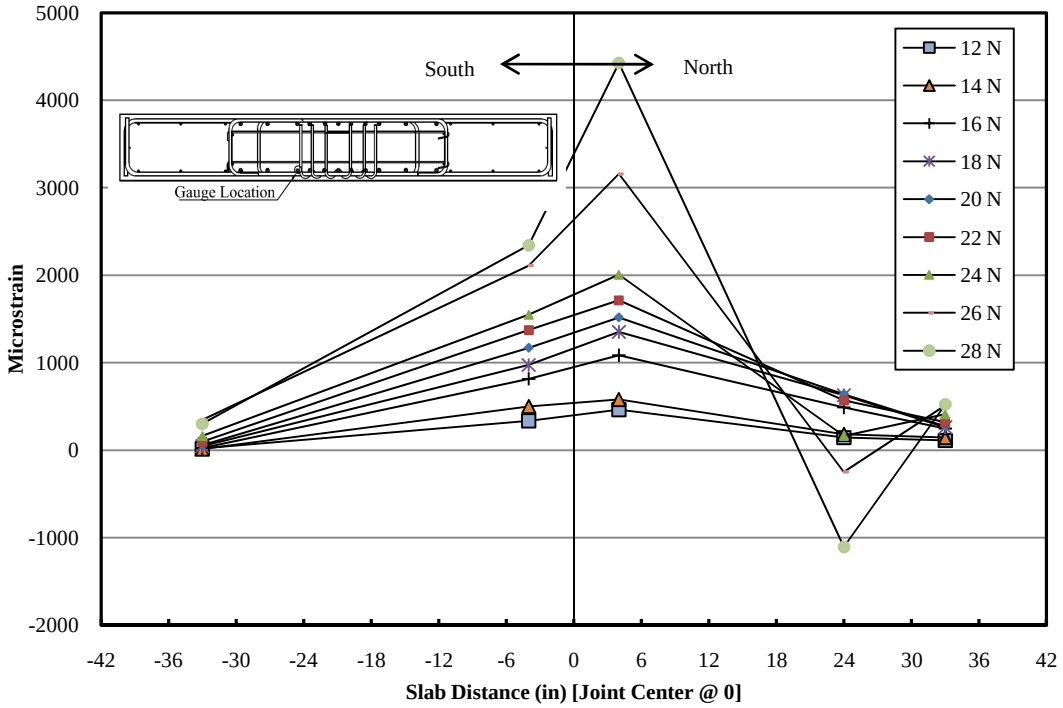

Figure 6-43: Slab Bottom Reinforcement Strain for FSRCC24-M North Cycle 2

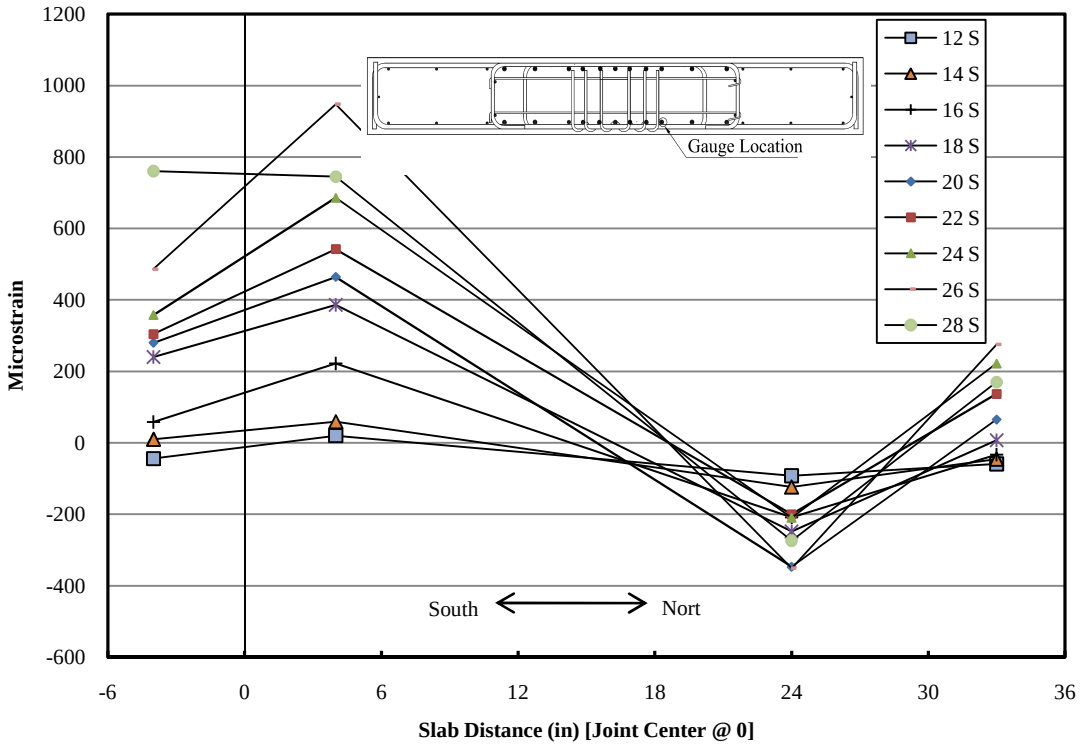

Figure 6-44: Slab Bottom Reinforcement for FSRCC24-M South Cycle 2

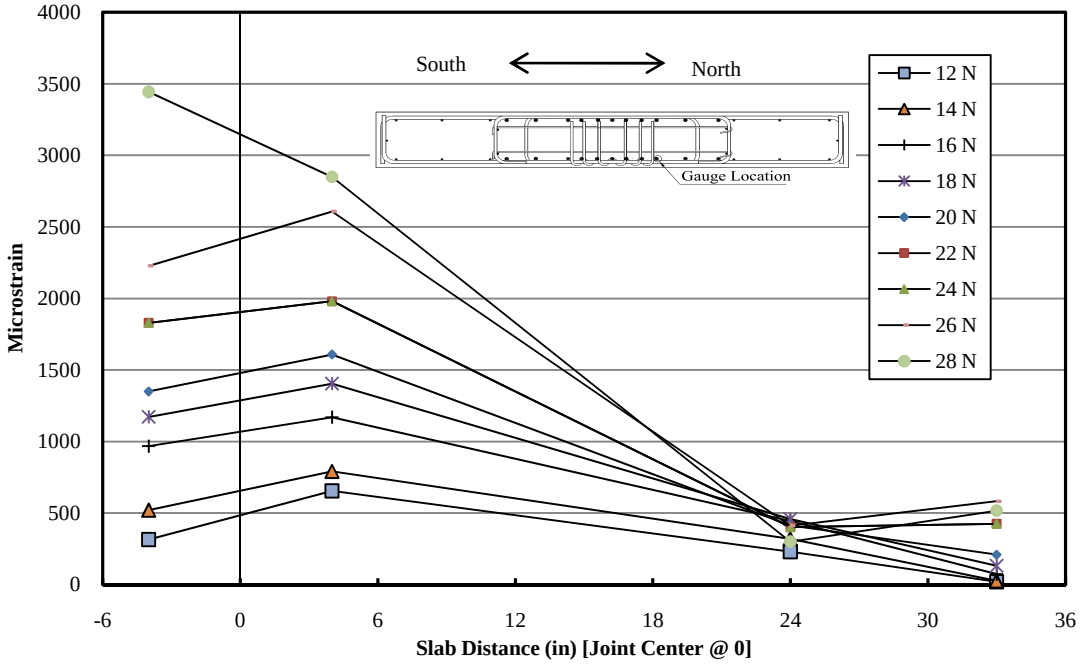

Figure 6-45: Slab Bottom Reinforcement Strain for FSRCC24-M North Cycle 2

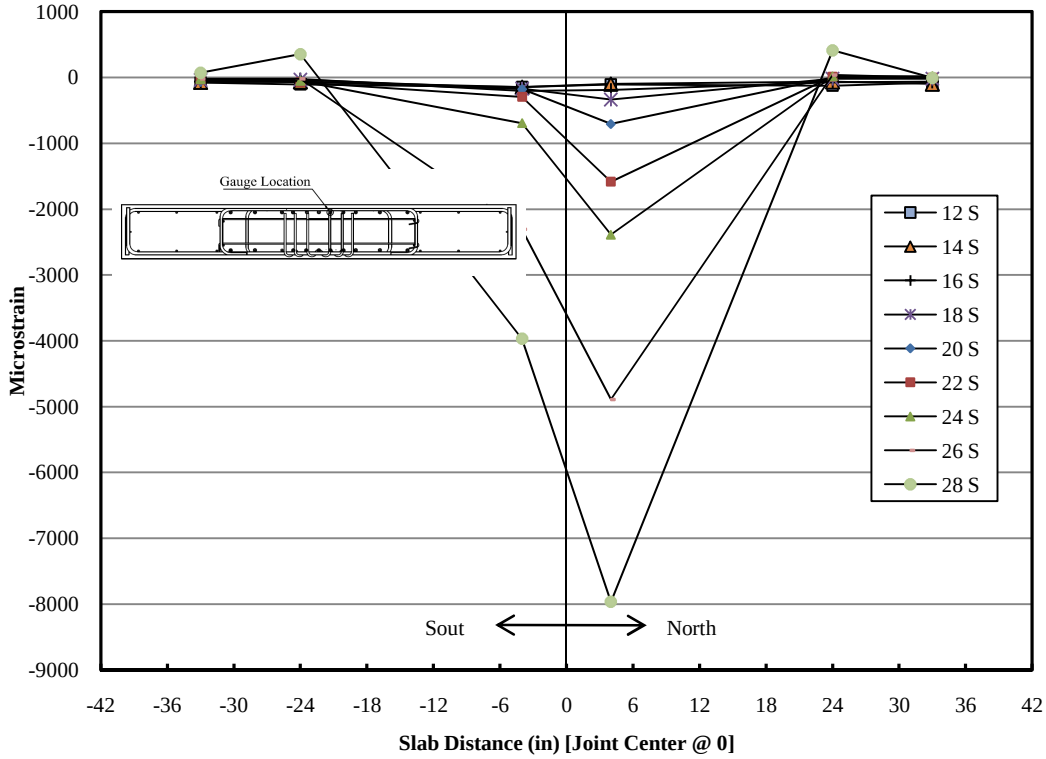

Figure 6-46: Slab Top Reinforcement Strain for FSRCC24-M South Cycle 2

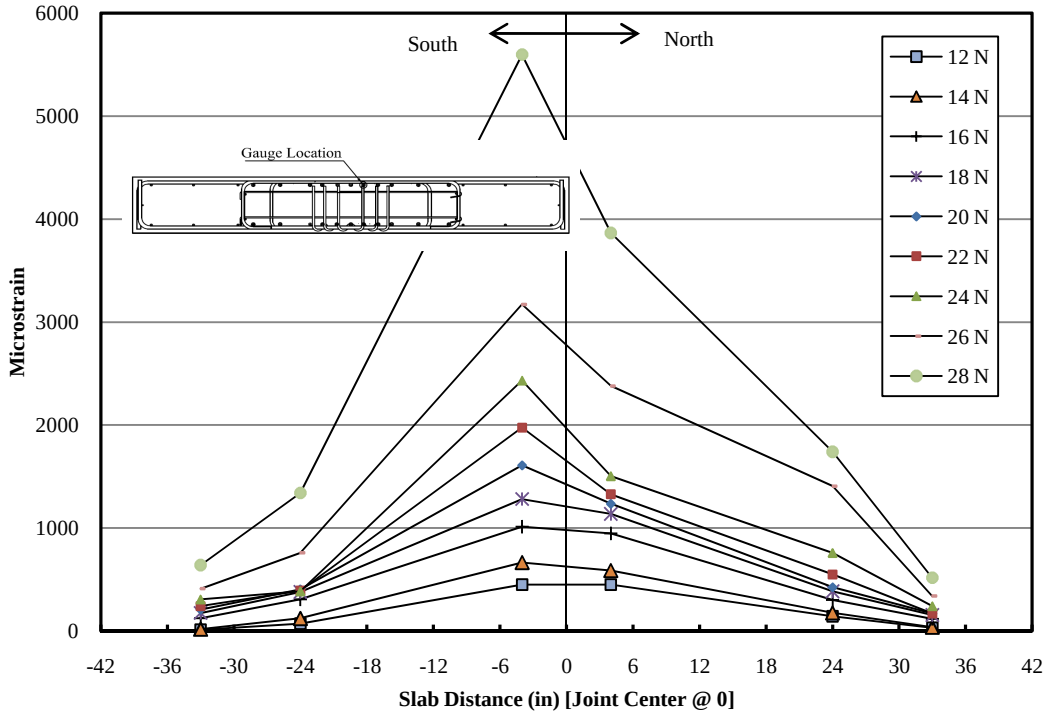

Figure 6-47: Slab Top Reinforcement Strain for FSRCC24-M North Cycle 2

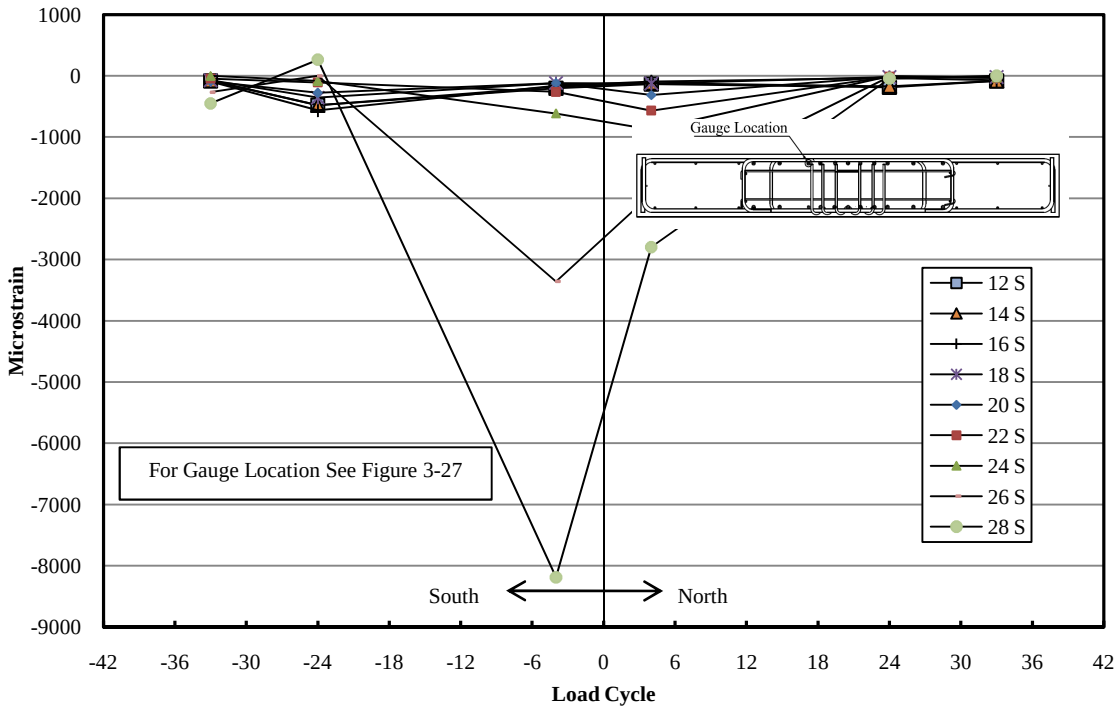

Figure 6-48: Slab Top Reinforcement Strain for FSRCC24-M South Cycle 2

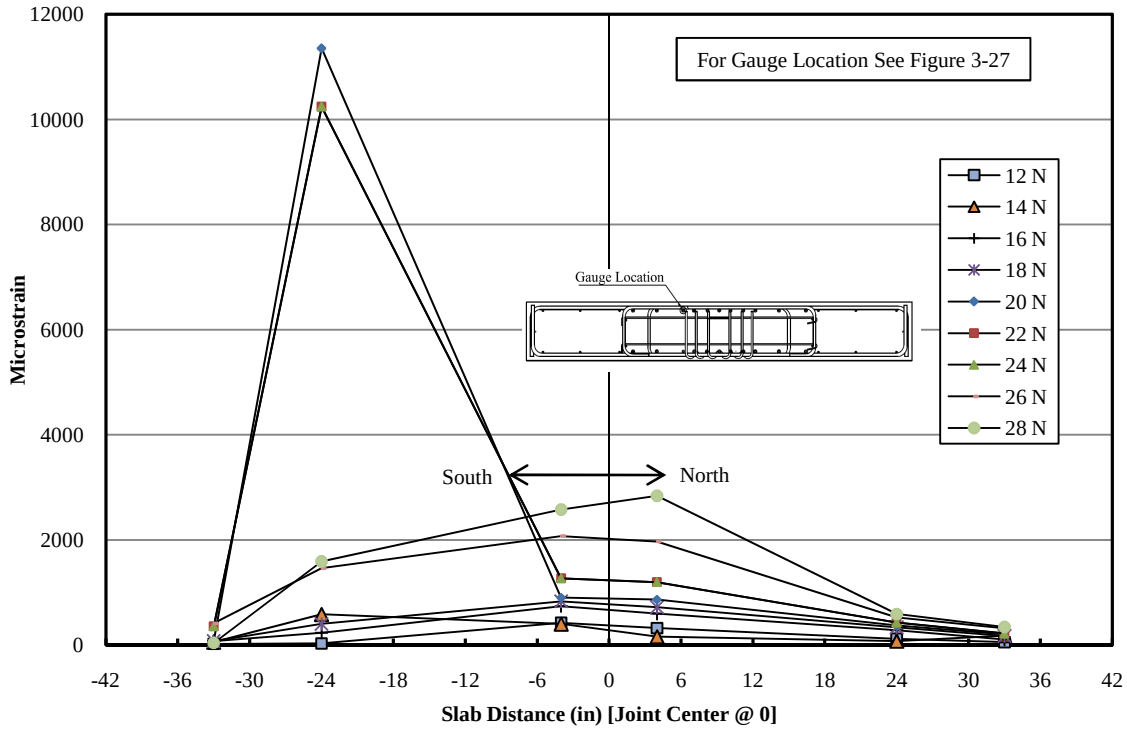

Figure 6-49: Slab Top Reinforcement Strain for FSRCC24-M North Cycle 2

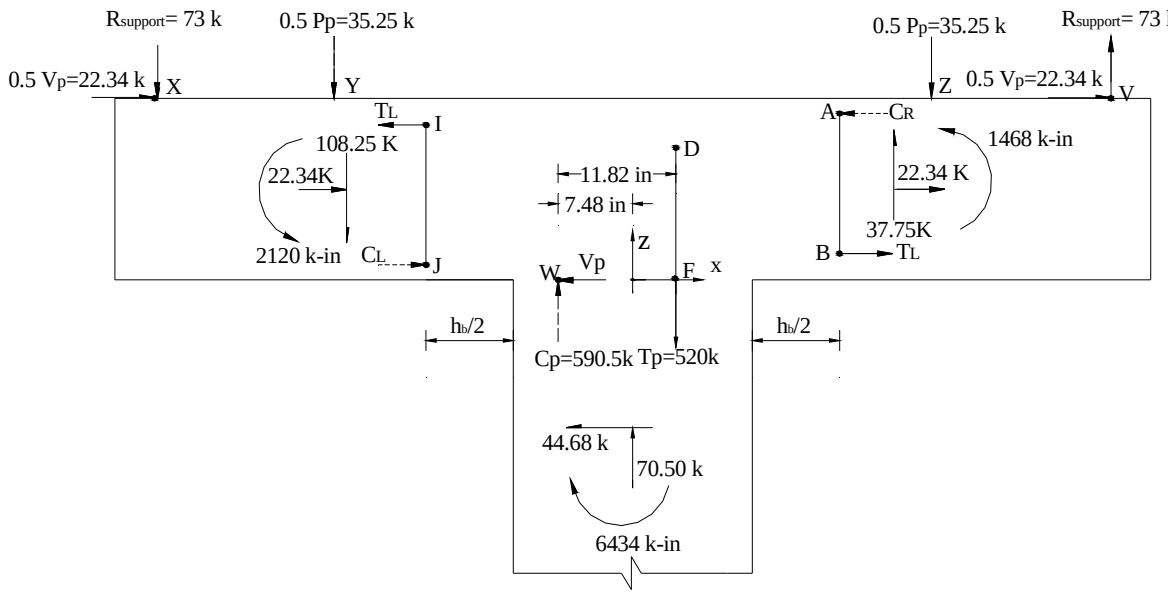

Figure 6-50: Boundary Forces –Full Specimen

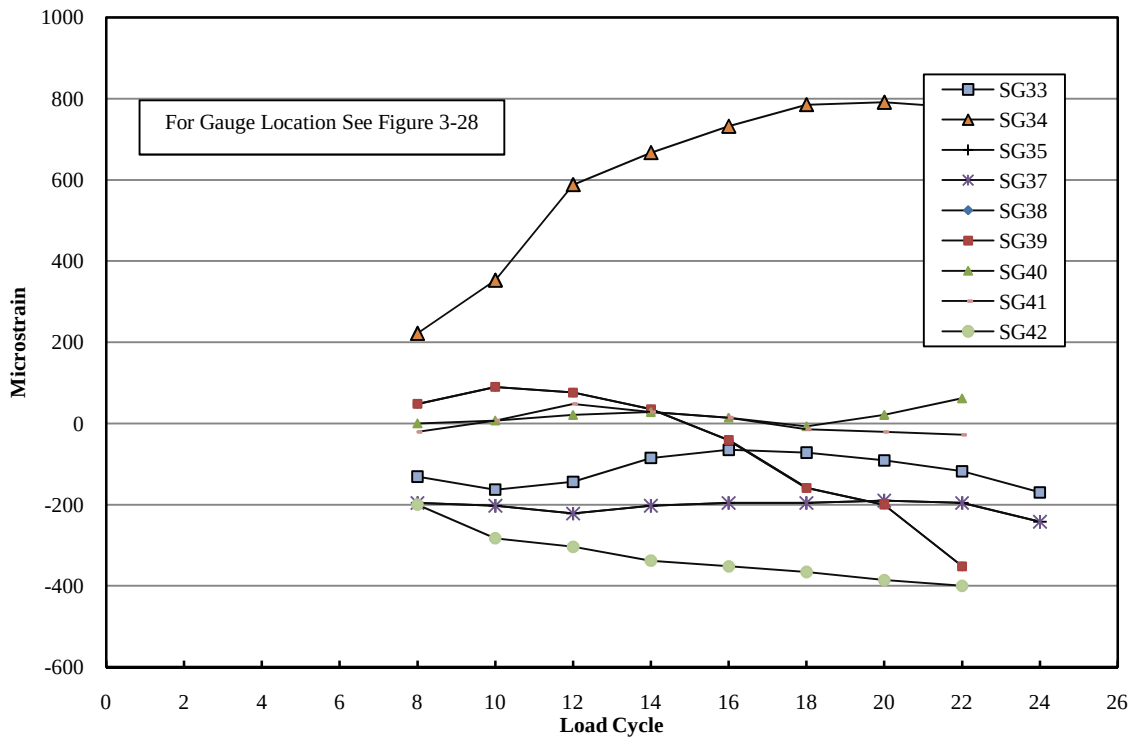

Figure 6-51: Joint Stirrup Strain for FSKJ24-M South Cycle 2

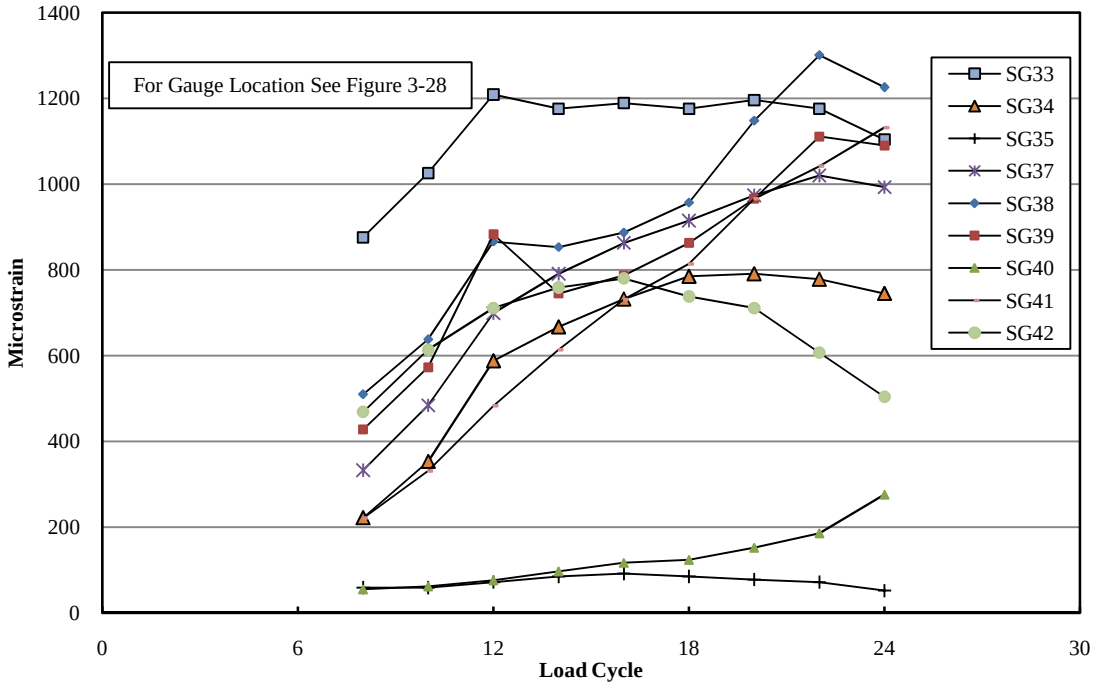

Figure 6-52: Joint Stirrup Strain for FSKJ24-M North Cycle 2

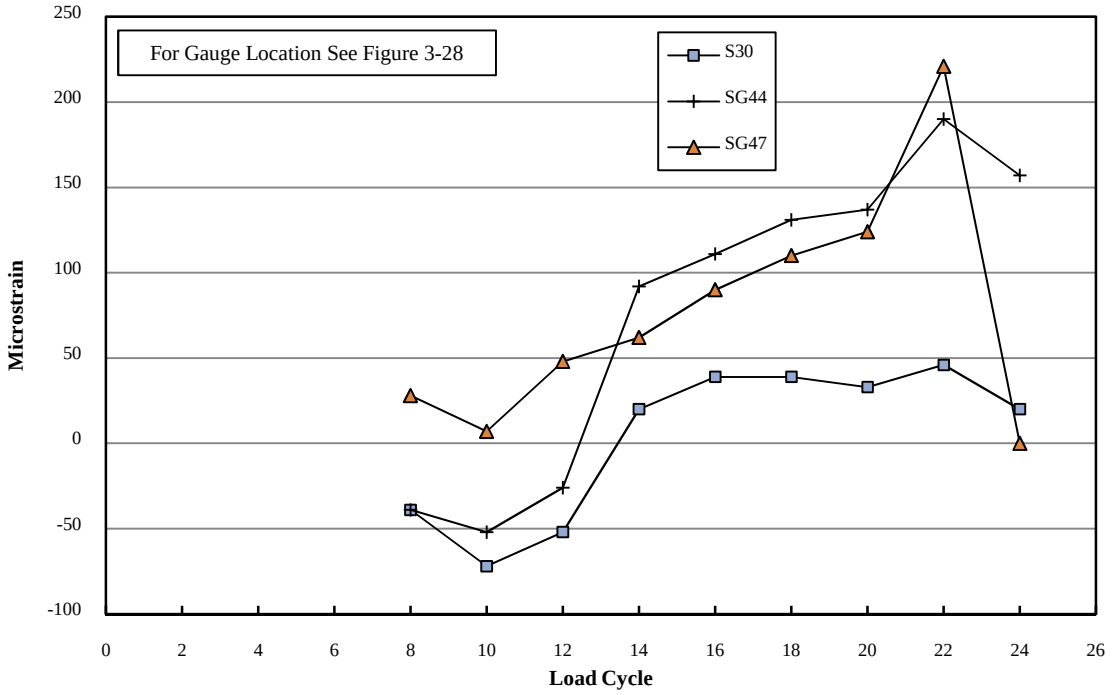

Figure 6-53: Joint Stirrup Strain for FSKJ24-M South Cycle 2

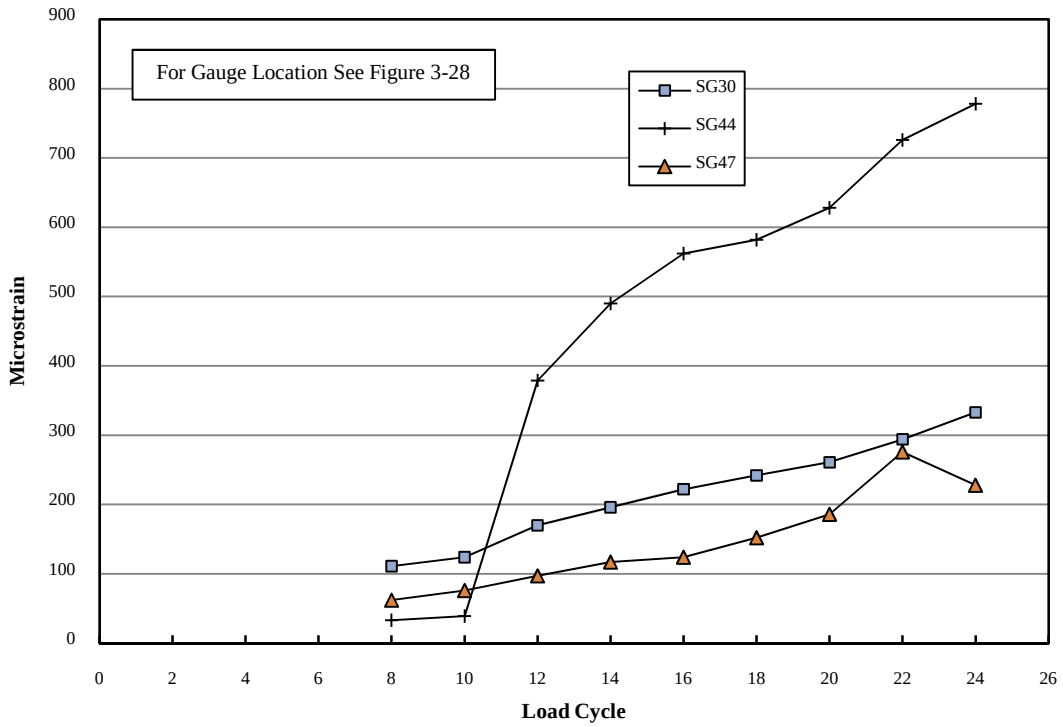

Figure 6-54: Joint Stirrup Strain for FSKJ24-M North Cycle 2

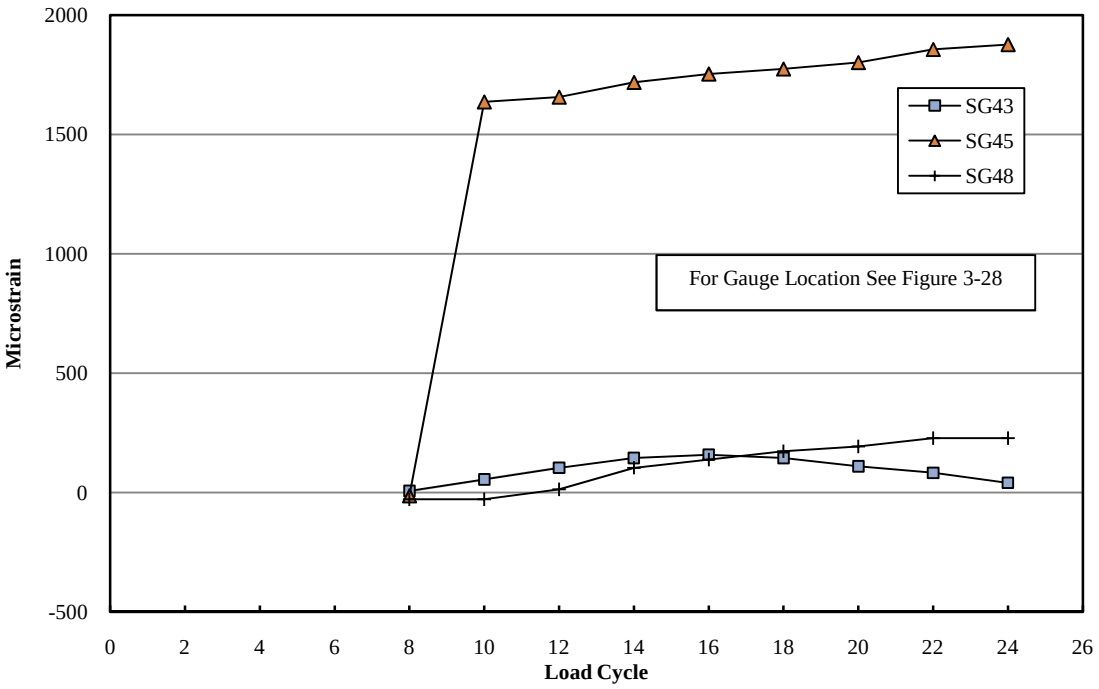

Figure 6-55: Joint Stirrup Strain for FSKJ24-M South Cycle 2

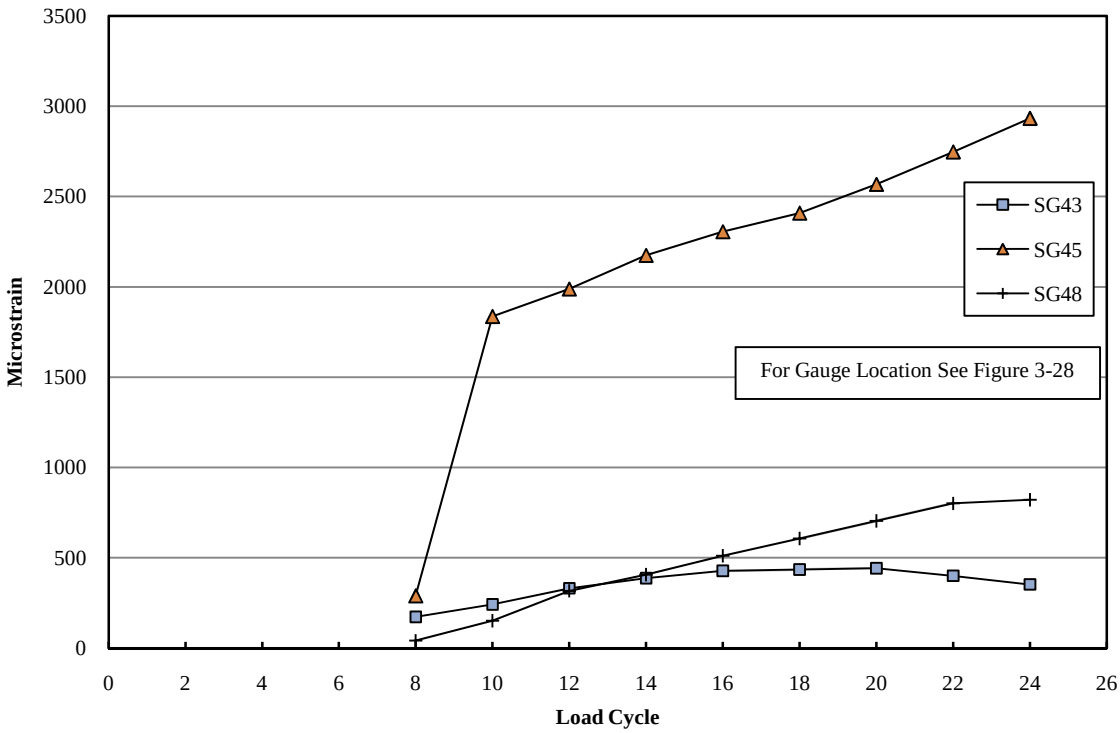

Figure 6-56: Joint Stirrup Strain for FSKJ24-M North Cycle 2

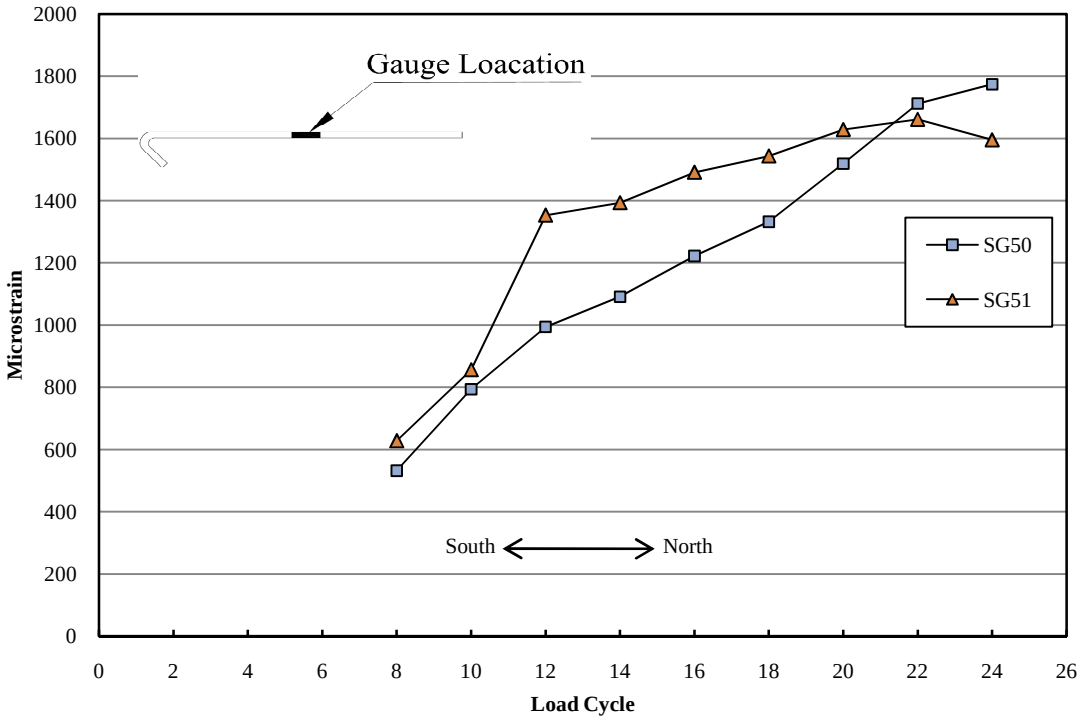

Figure 6-57: Horizontal Cap End Ties Strain for FSKJ24-M South Cycle 2

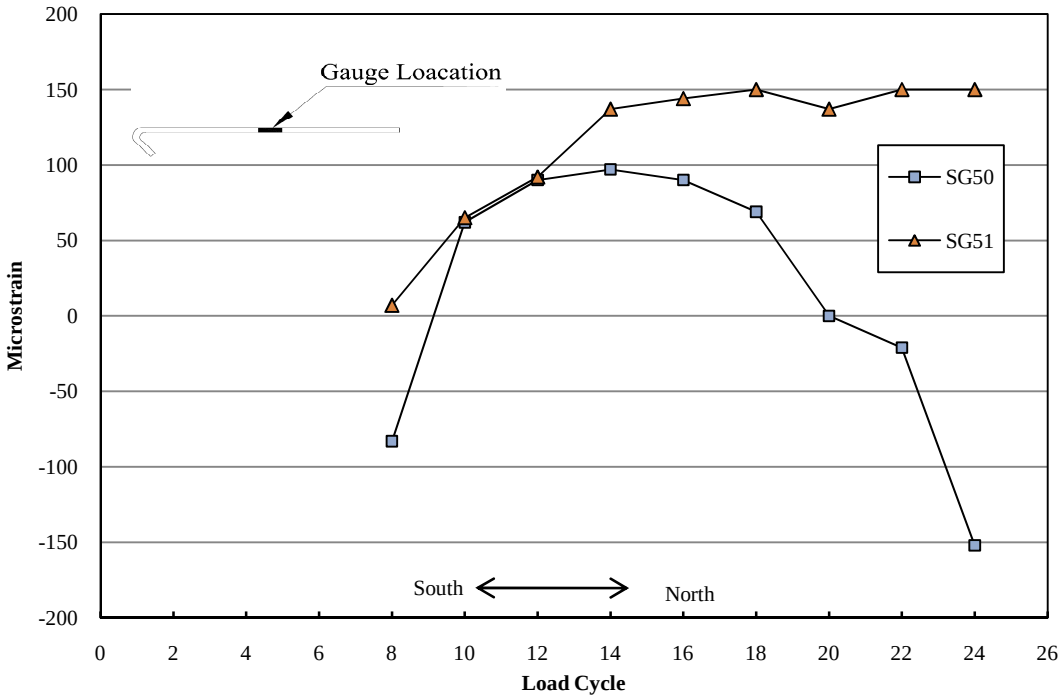

Figure 6-58: Horizontal Cap End Ties Strain for FSKJ24-M North Cycle 2

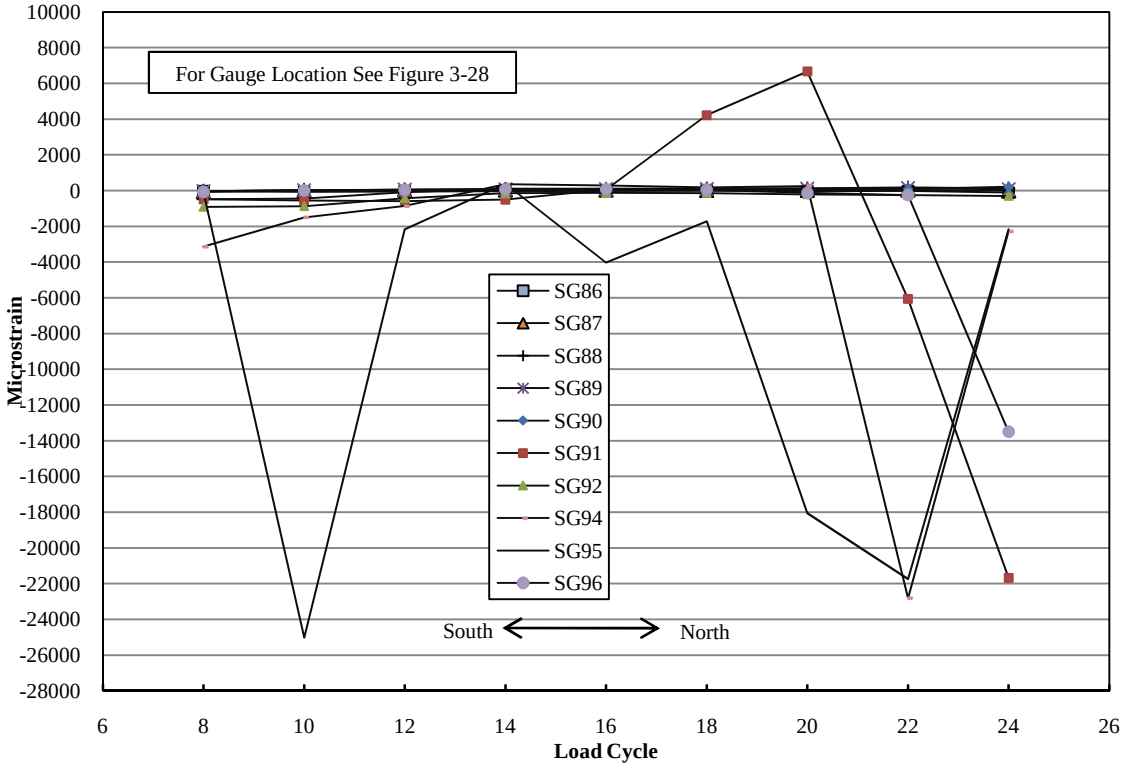

Figure 6-59: J-bars Joint Reinforcement Strain for FSKJ24-M South Cycle 2

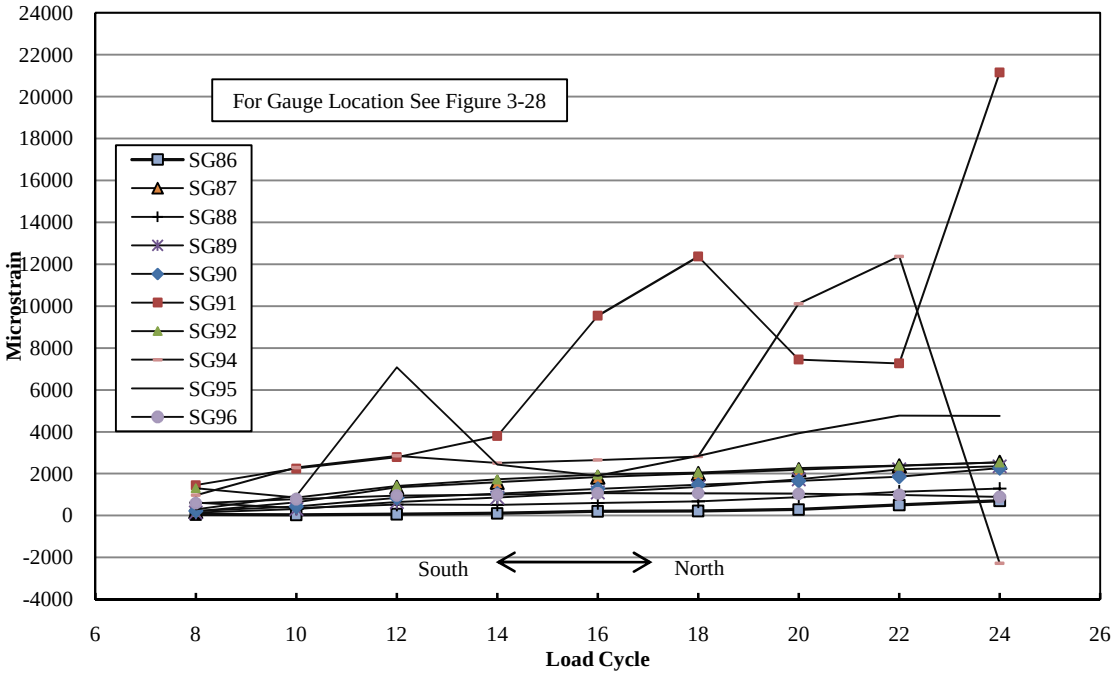

Figure 6-60: J-bars Joint Reinforcement Strain for FSKJ24-M North Cycle 2

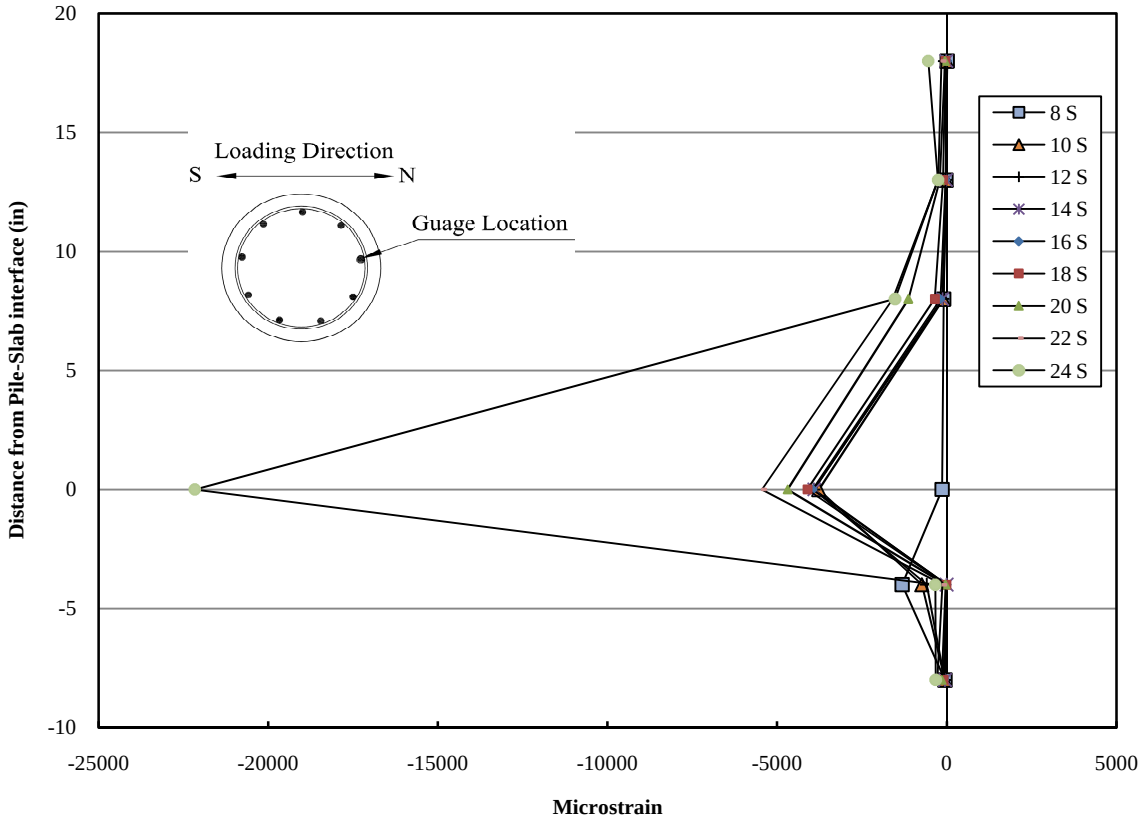

Figure 6-61: Longitudinal Pile Strain for FSKJ24-M South Cycle 2

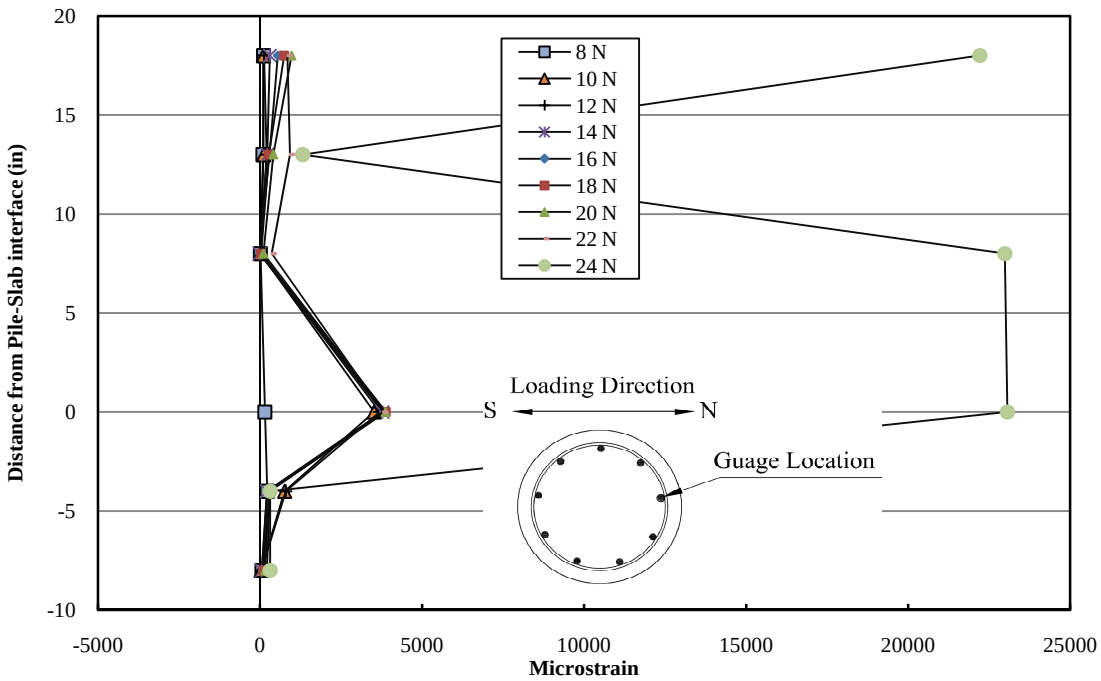

Figure 6-62: Longitudinal Pile Strain for FSKJ24-M North Cycle 2

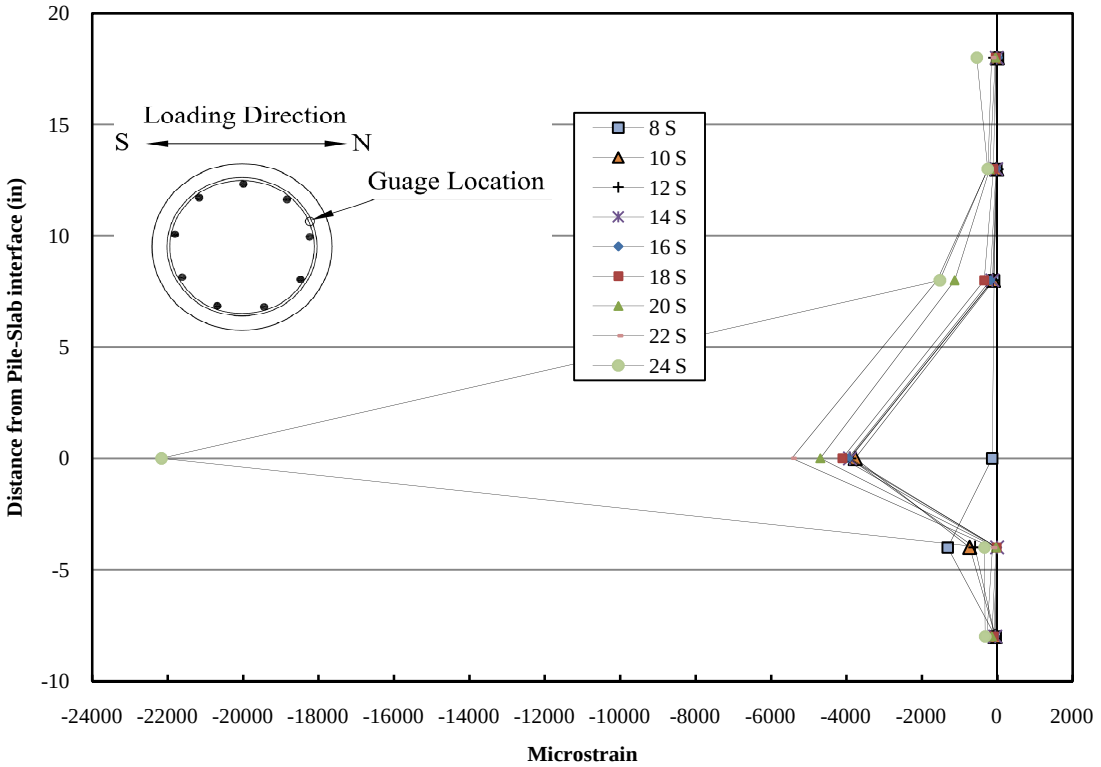

Figure 6-63: Spiral Reinforcement Strain for FSKJ24-M South Cycle 2

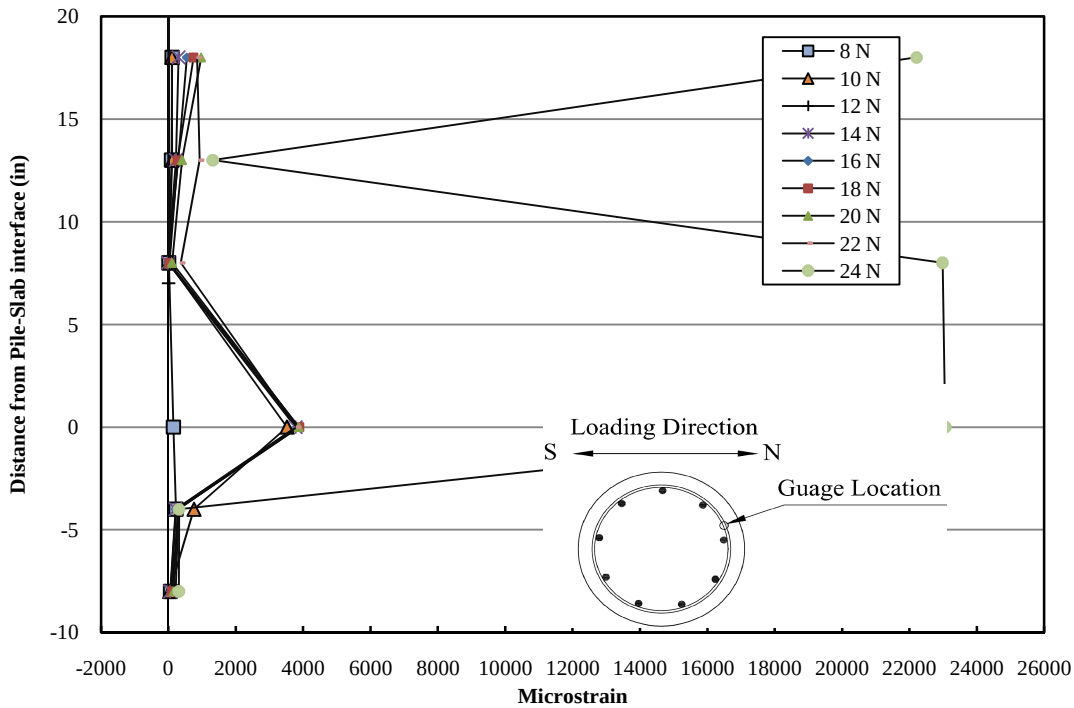

Figure 6-64: Spiral Reinforcement Strain for FSKJ24-M North Cycle 2

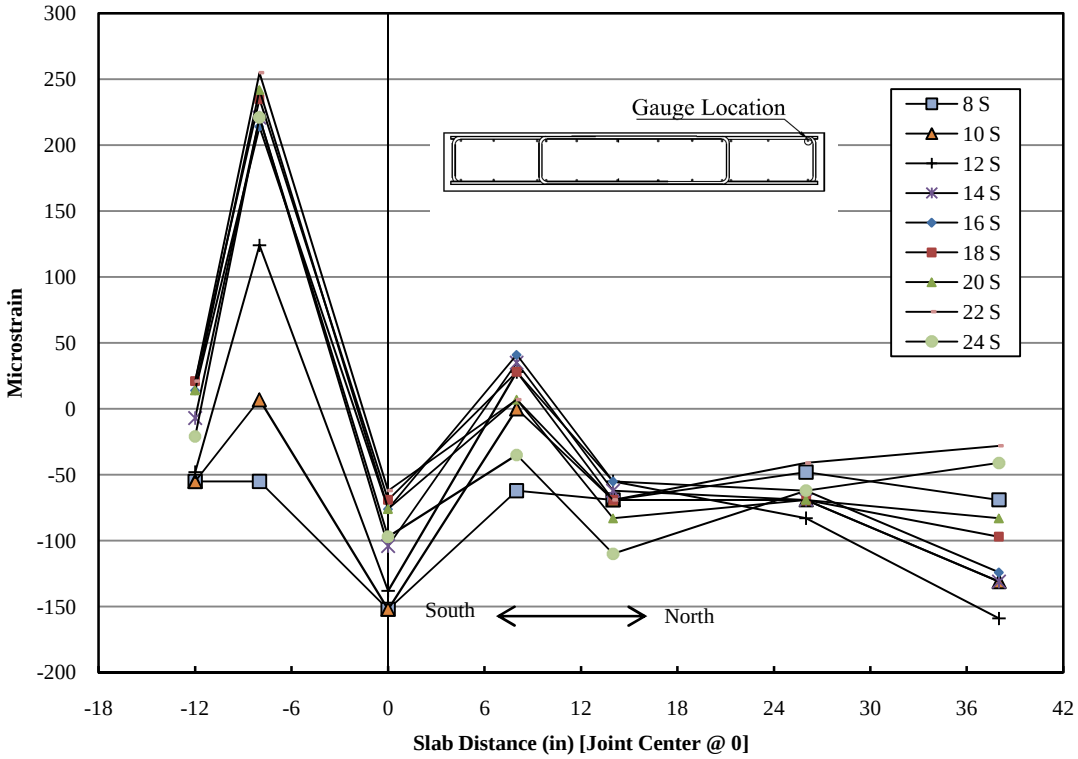

Figure 6-65: Slab Top Reinforcement for FSKJ24-M South Cycle 2

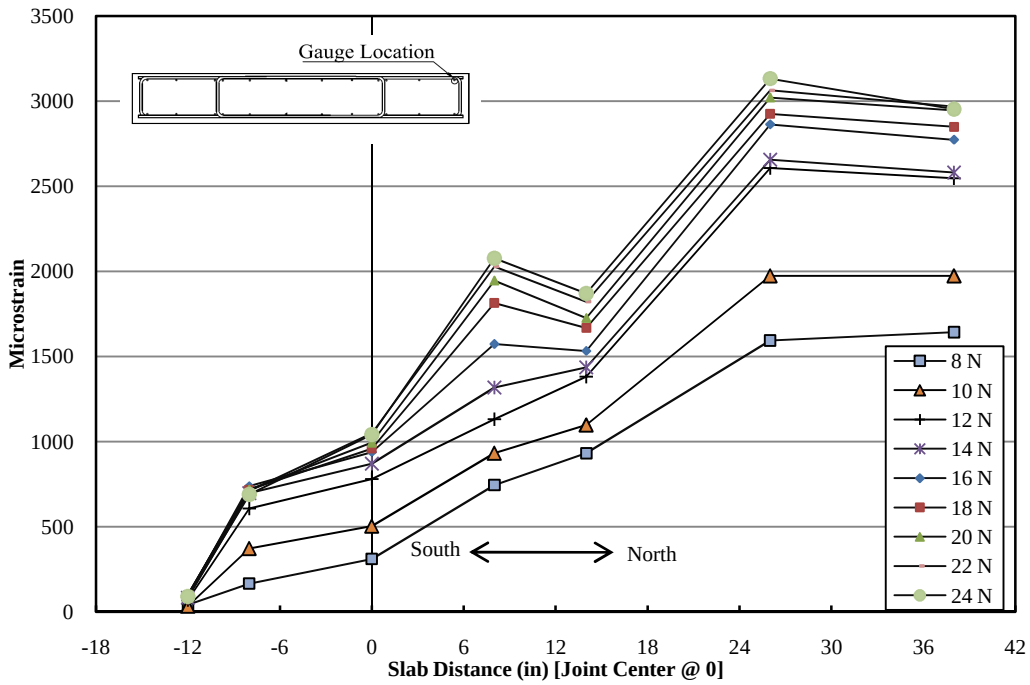

Figure 6-66: Slab Top Reinforcement Strain for FSKJ24-M North Cycle 2

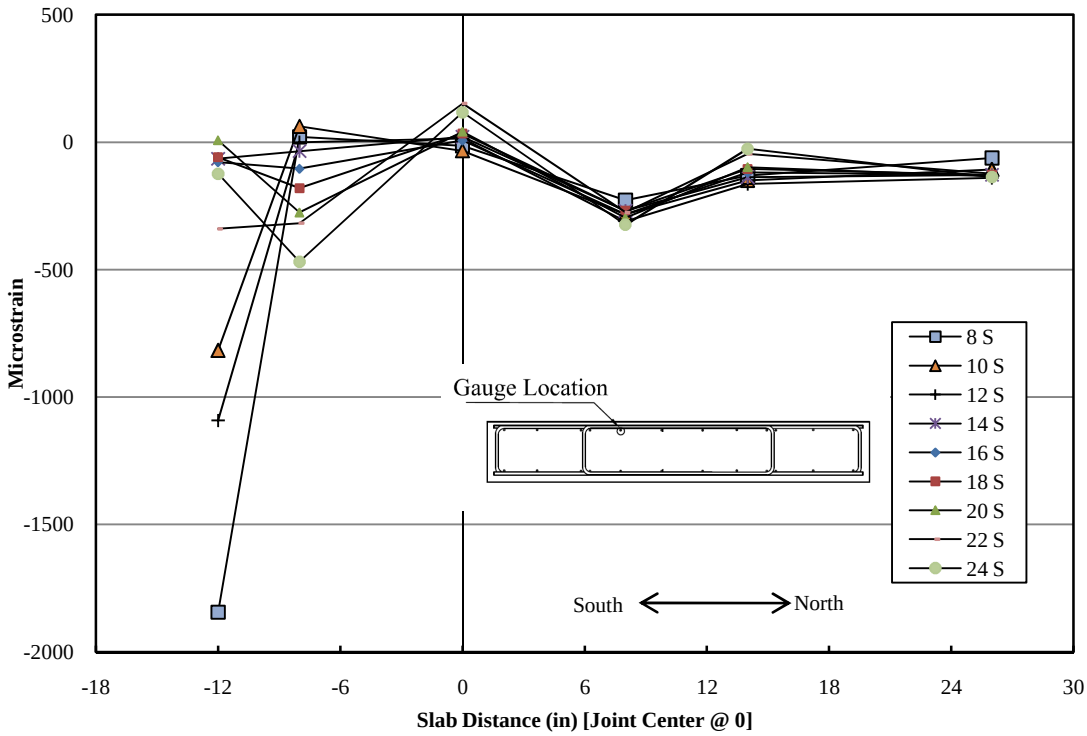

Figure 6-67: Slab Top Reinforcement for FSKJ24-M South Cycle 2

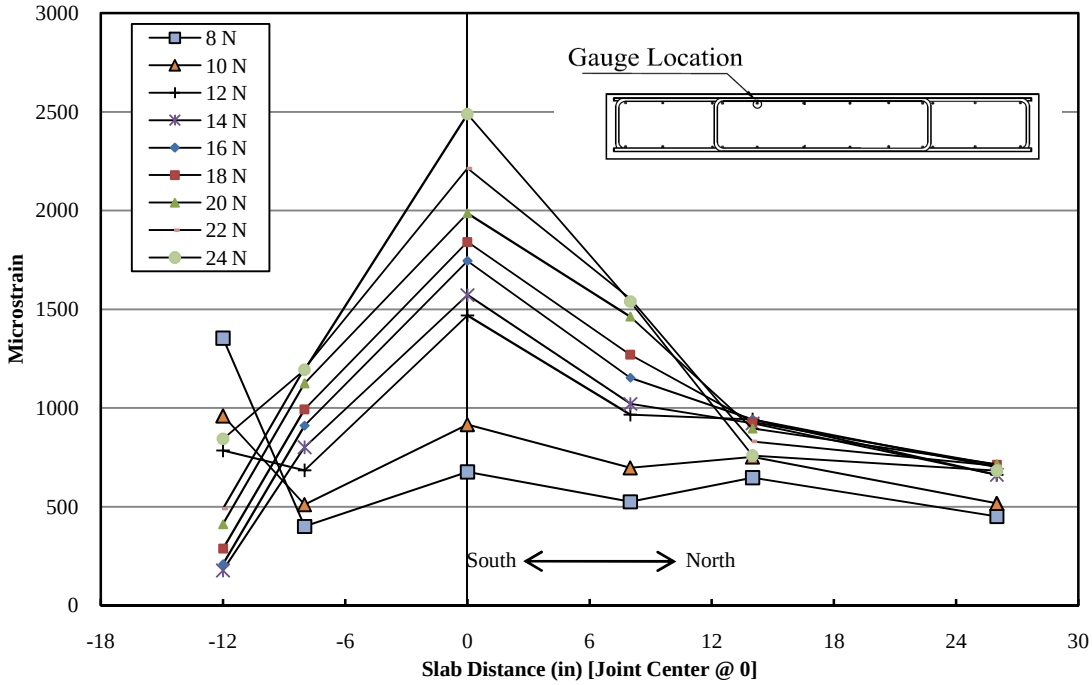

Figure 6-68: Slab Top Reinforcement Strain for FSKJ24-M North Cycle 2

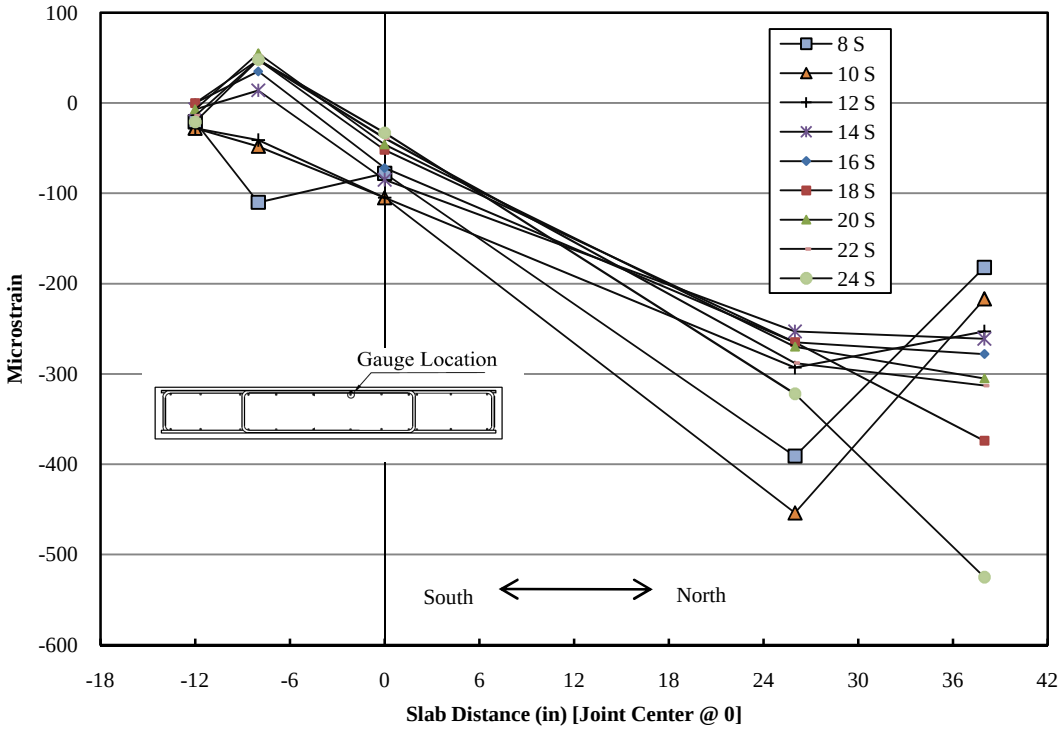

Figure 6-69: Slab Top Reinforcement Strain for FSKJ24-M South Cycle 2

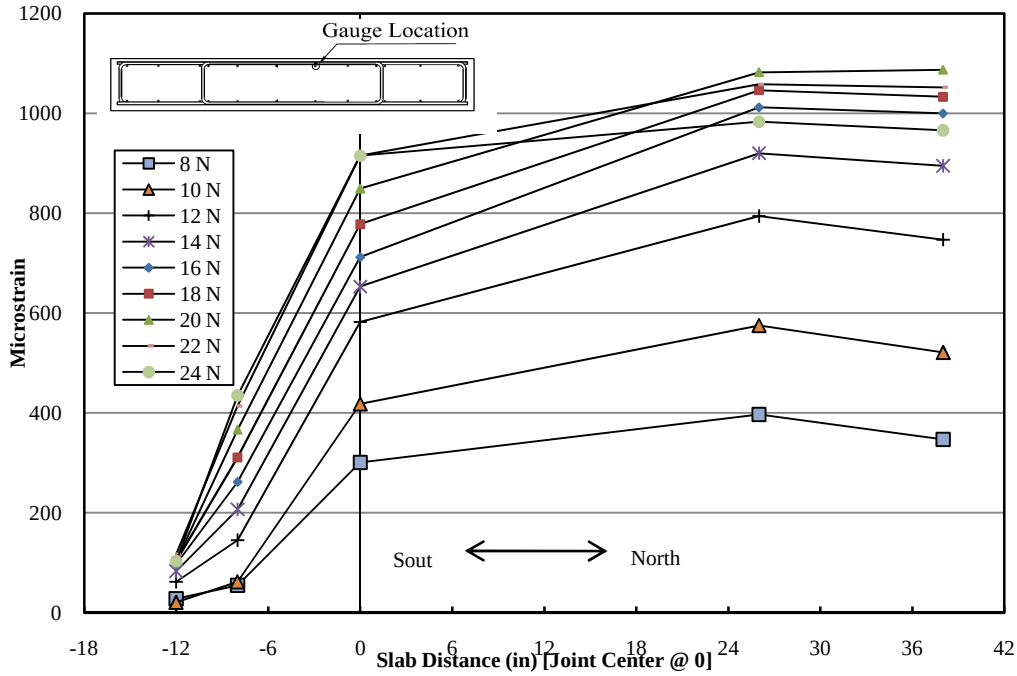

Figure 6-70: Slab Top Reinforcement Strain for FSKJ24-M North Cycle 2

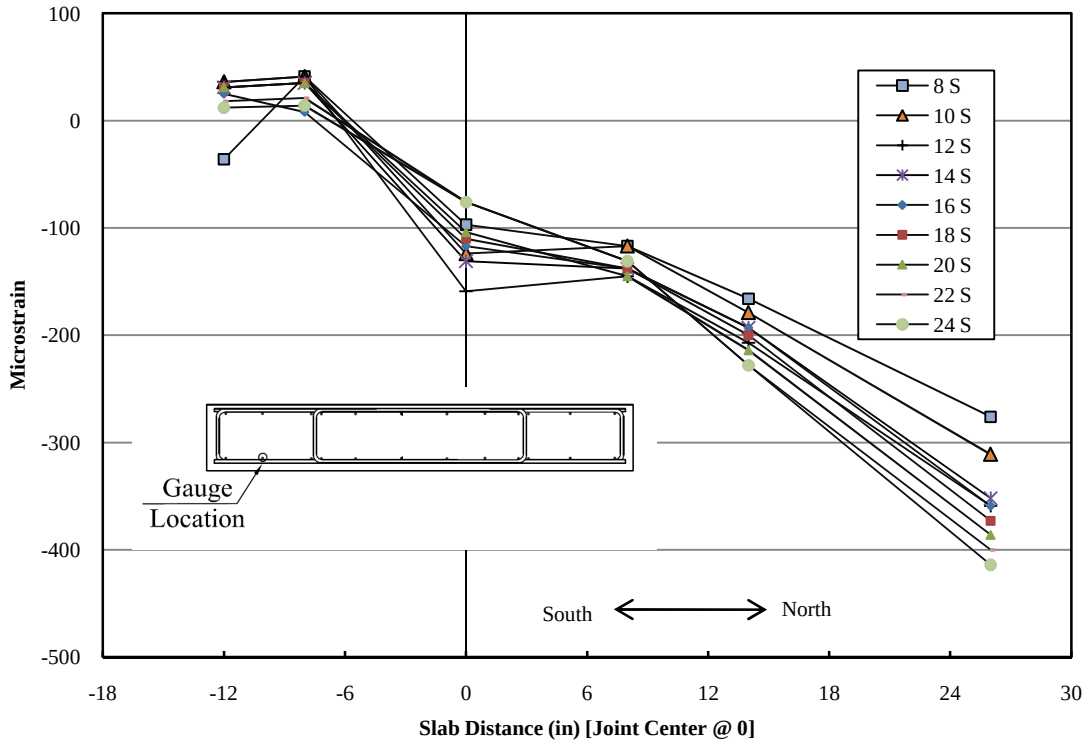

Figure 6-71: Slab Bottom Reinforcement Strain for FSKJ24-M South Cycle 2

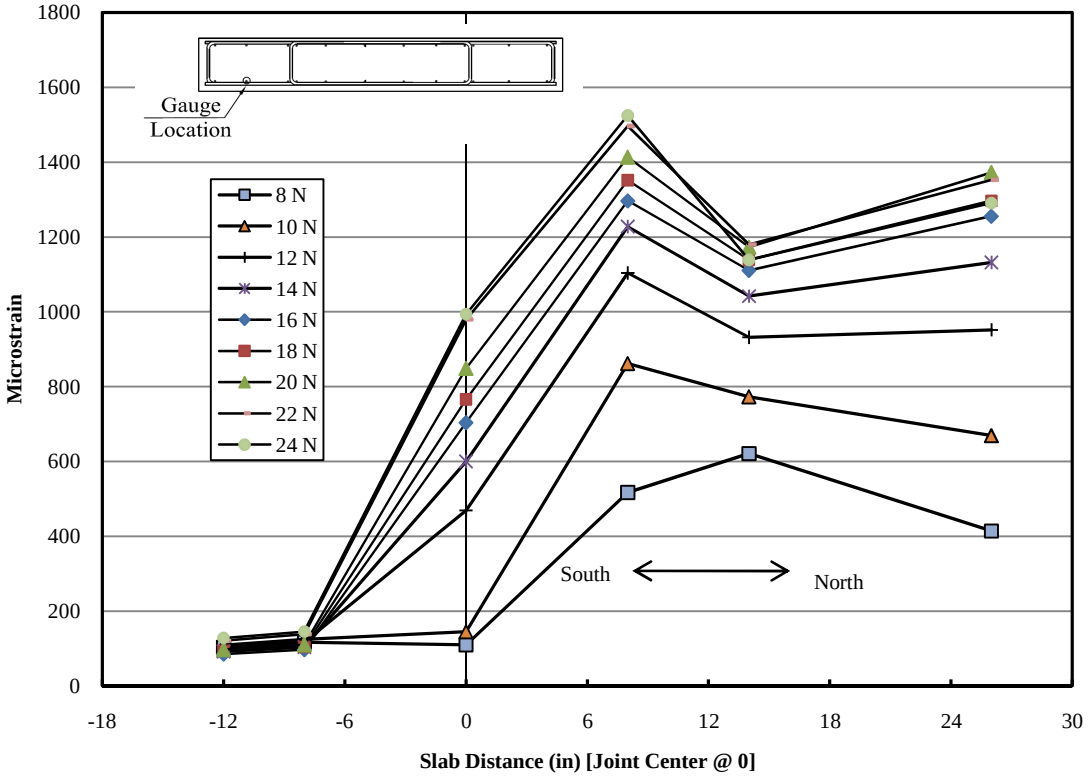

Figure 6-72: Slab Bottom Reinforcement Strain for FSKJ24-M North Cycle 2

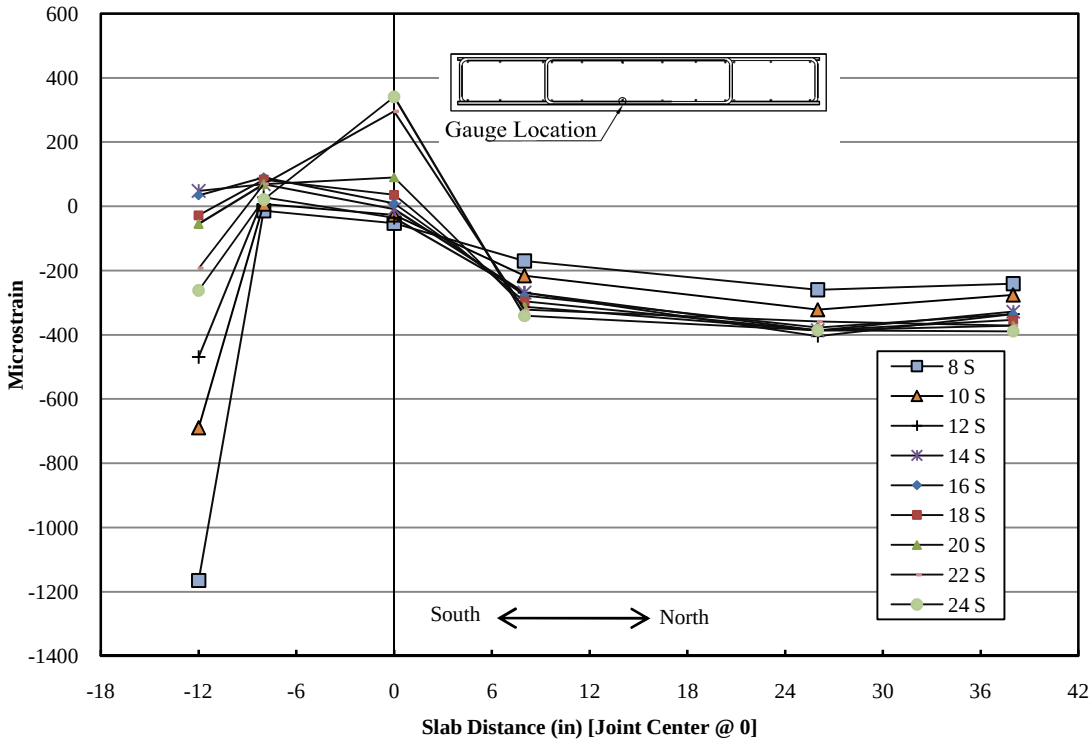

Figure 6-73: Slab Bottom Reinforcement Strain for FSKJ24-M South Cycle 2

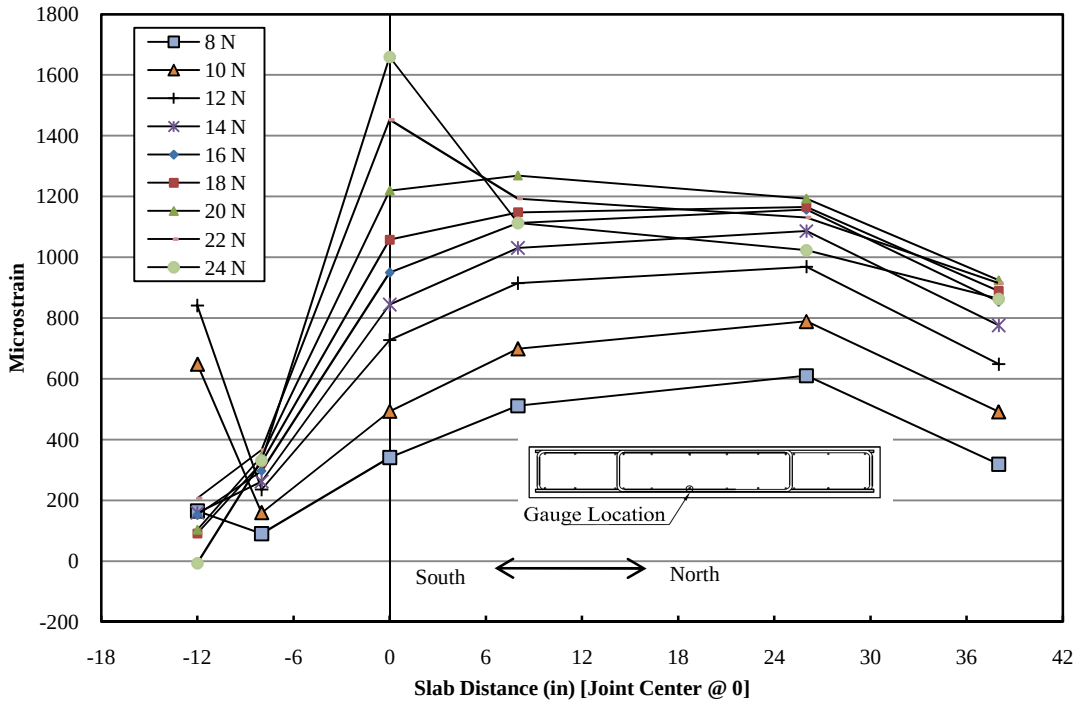

Figure 6-74: Slab Bottom Reinforcement Strain for FSKJ24-M North Cycle 2

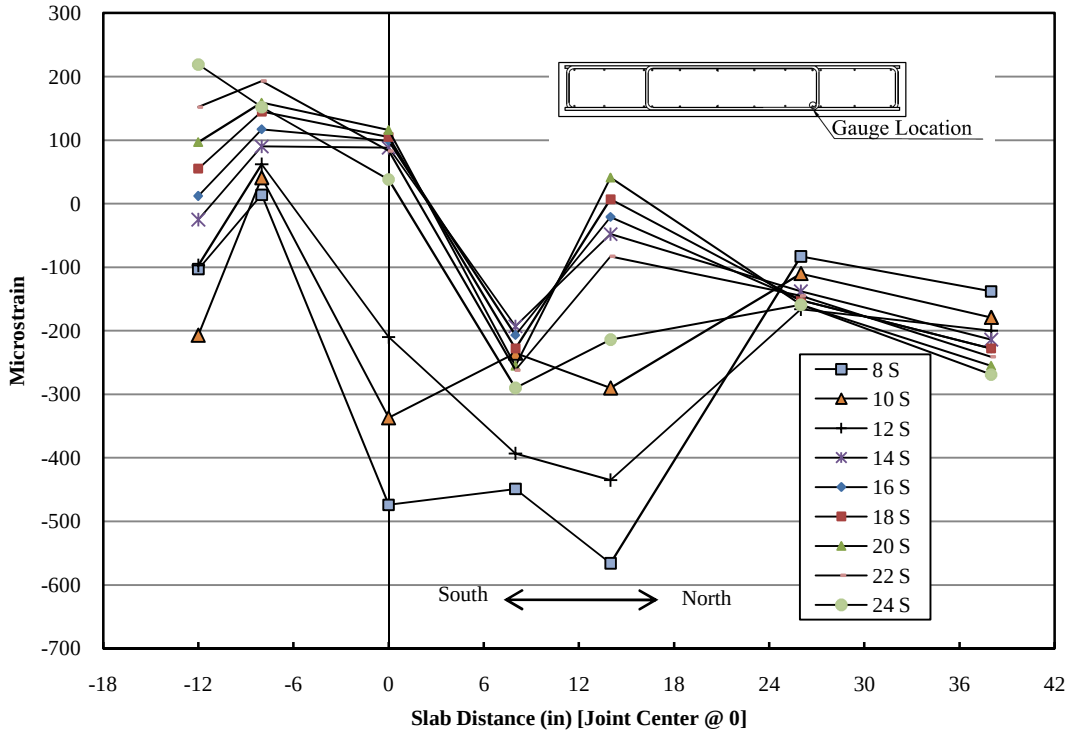

Figure 6-75: Slab Bottom Reinforcement Strain for FSKJ24-M South Cycle 2

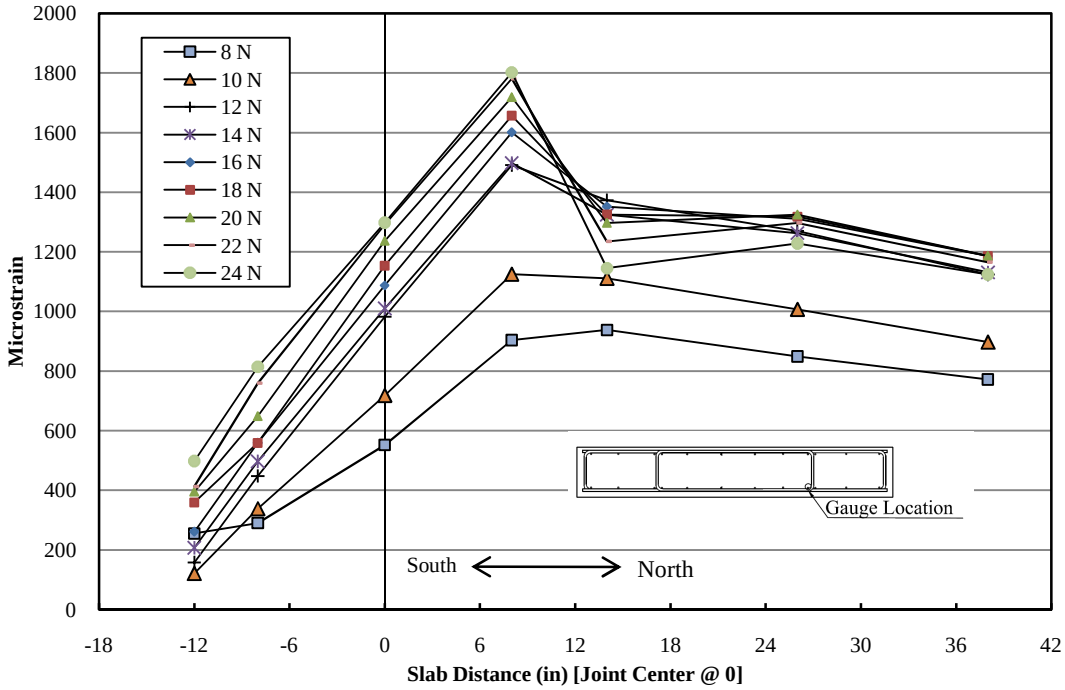

Figure 6-76: Slab Bottom Reinforcement Strain for FSKJ24-M North Cycle 2

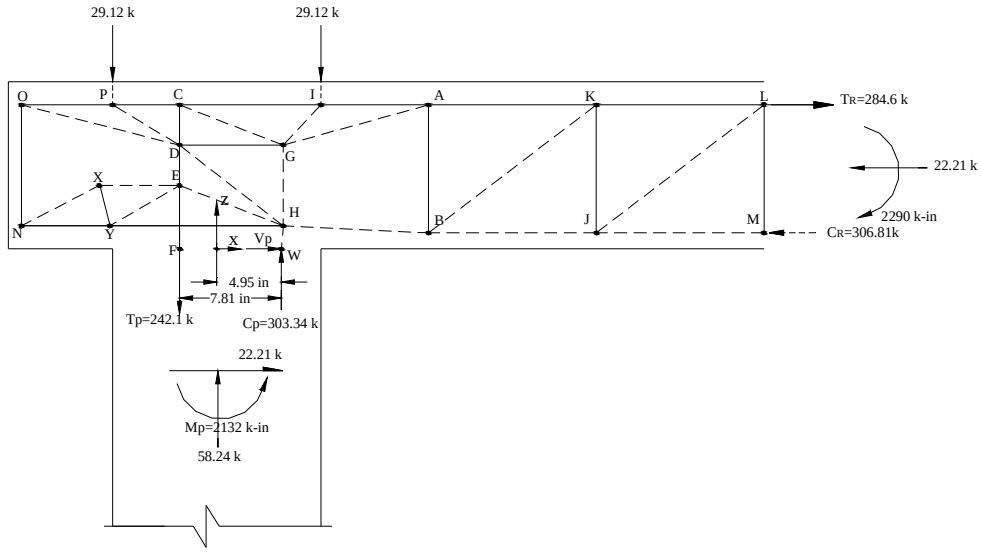

Figure 6-77: Modified Strut-and-Tie Model For FSKJ24 (Closing Moment)

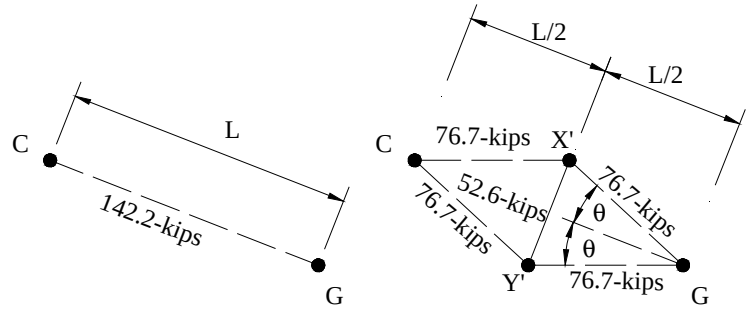

Closing Case

Figure 6-78: Bottle Shaped Strut Configuration for Strut C_{CG} in Closing Case

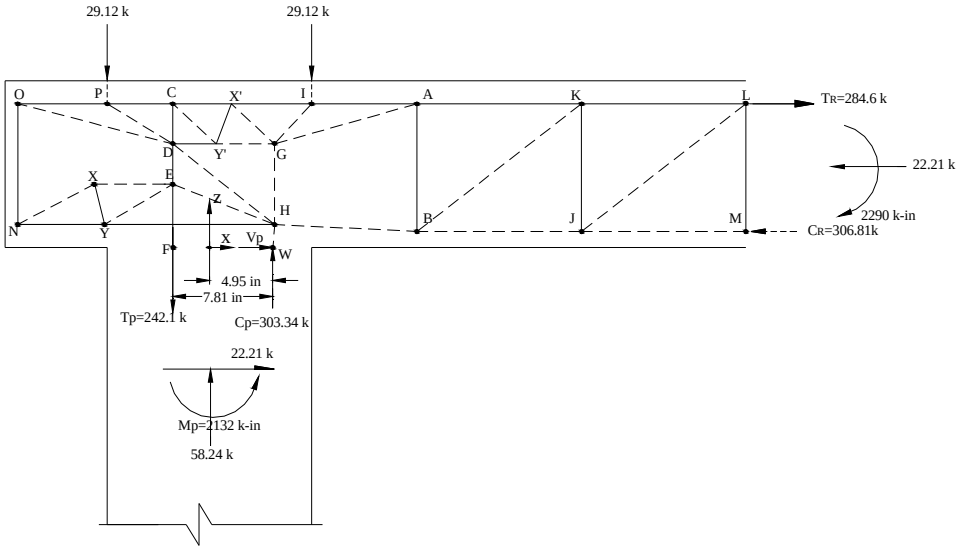

Figure 6-79: Final Modified Strut-and-Tie Model For FSKJ24 (Closing Moment)

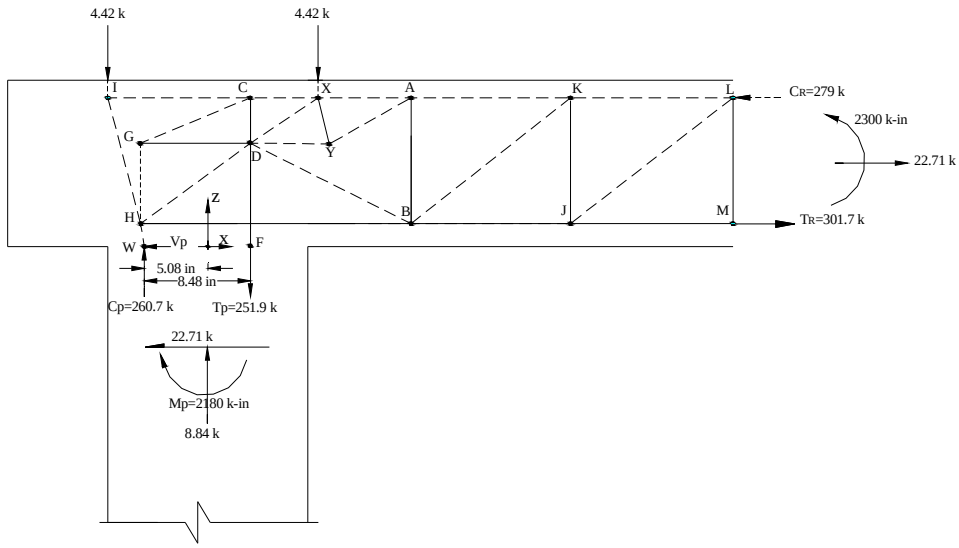

Figure 6-80: Modified Strut-and-Tie Model For FSKJ24 (Opening Moment)

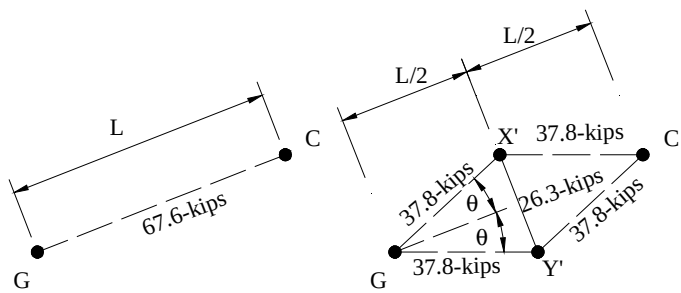

Opening Case

Figure 6-81: Bottle Shaped Strut Configuration for Strut C_{CG} in Opening Case

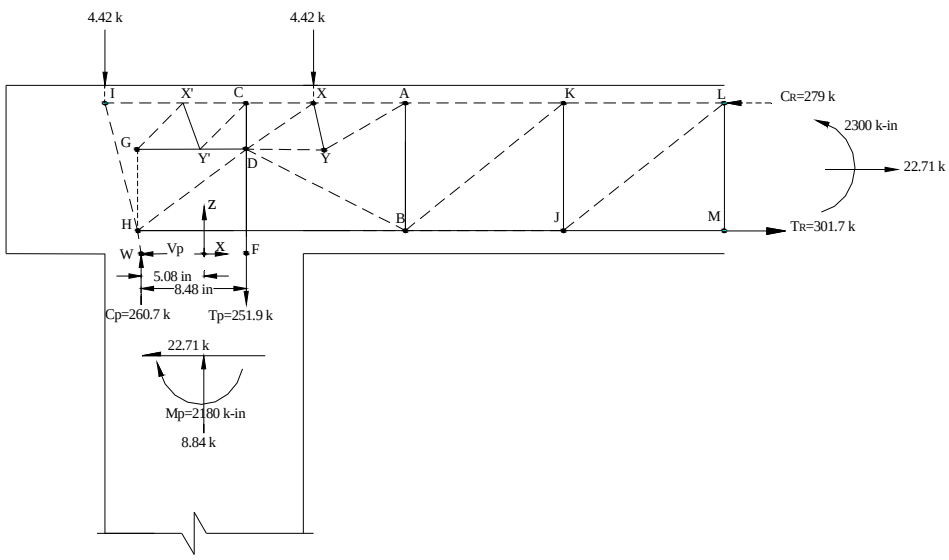

Figure 6-82: Final Modified Strut-and-Tie Model For FSKJ24 (Opening Moment)

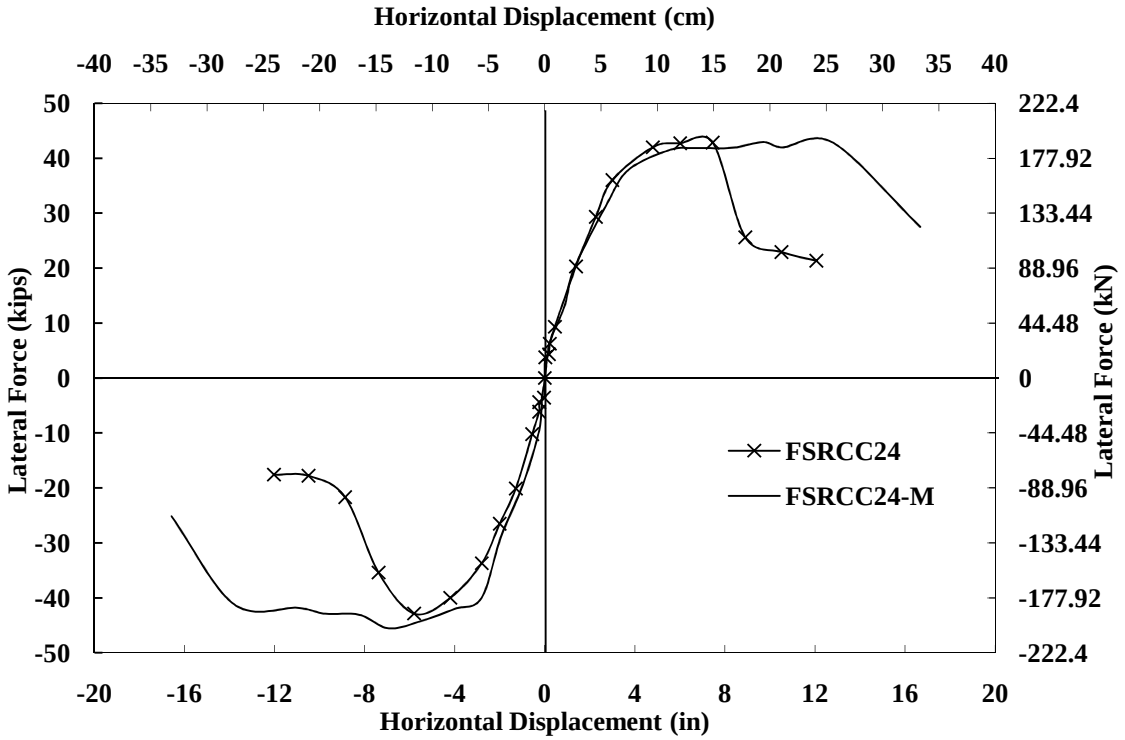

Figure 6-83: Force-Dispacement for Specimens FSRCC24 and FSRCC24-M

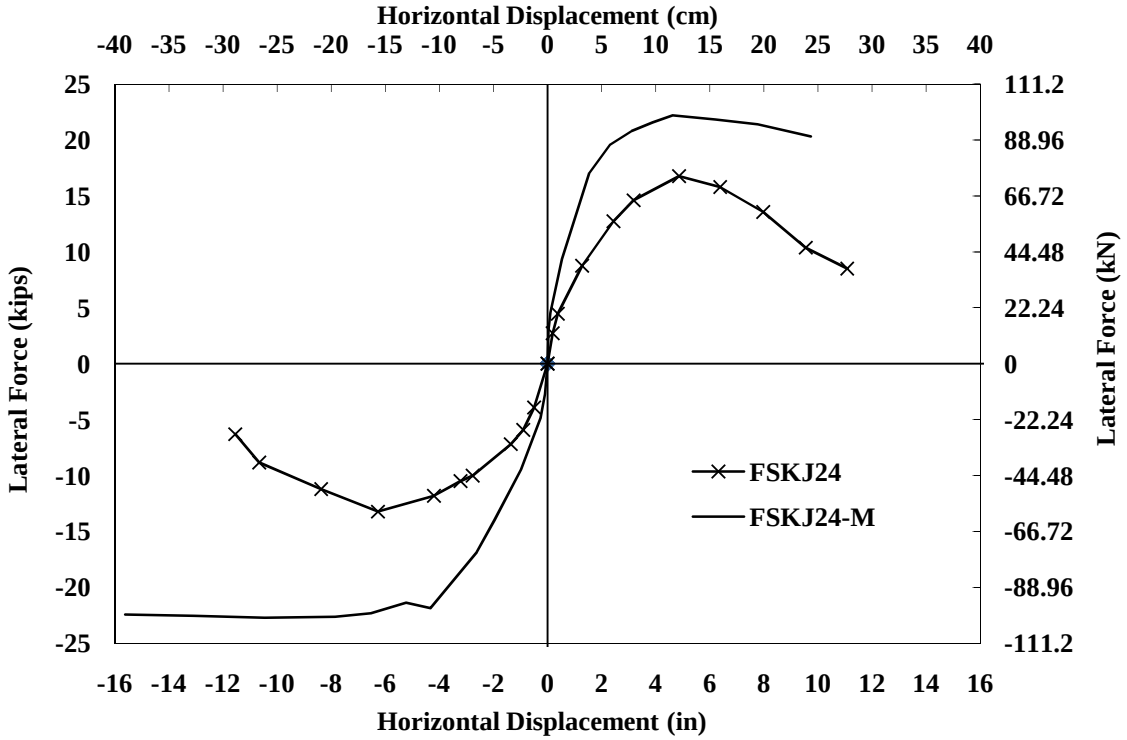

Figure 6-84: Force-Dispacement for Specimens FSKJ24 and FSKJ24-M

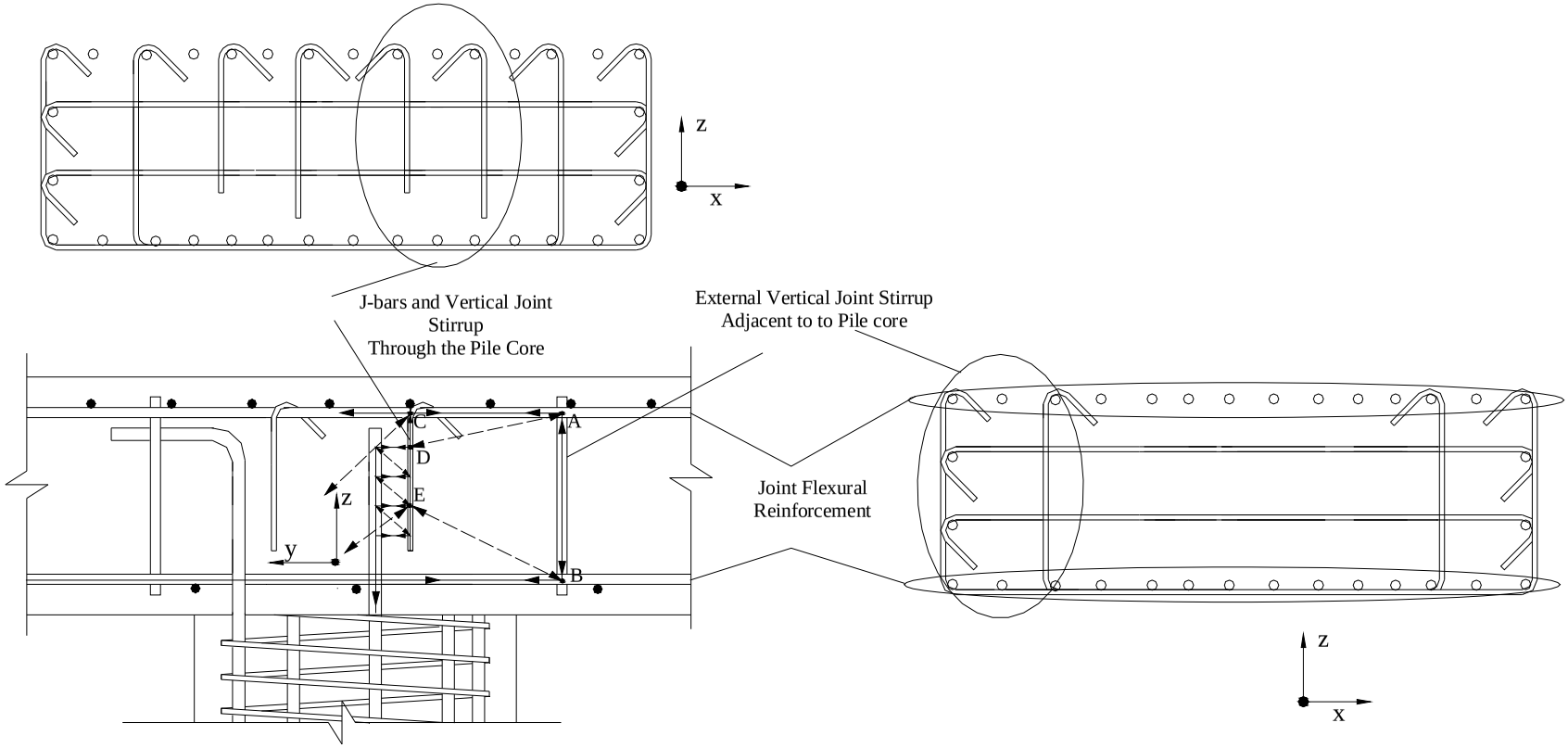

Figure 6-85: Force Transfer Mechanis Inside and Outside Pile Core Reigon

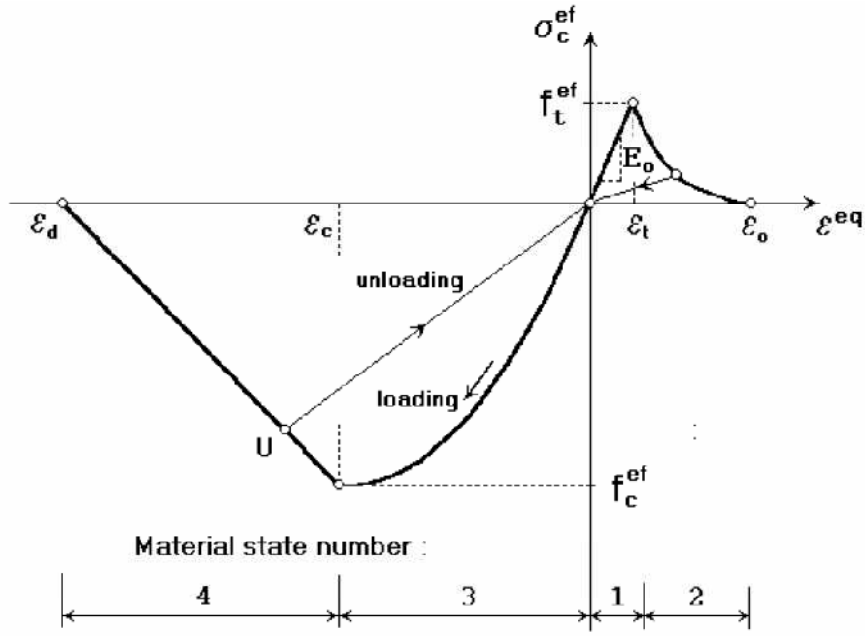

Figure 7-1: Uniaxial stress-strain law for concrete[28]

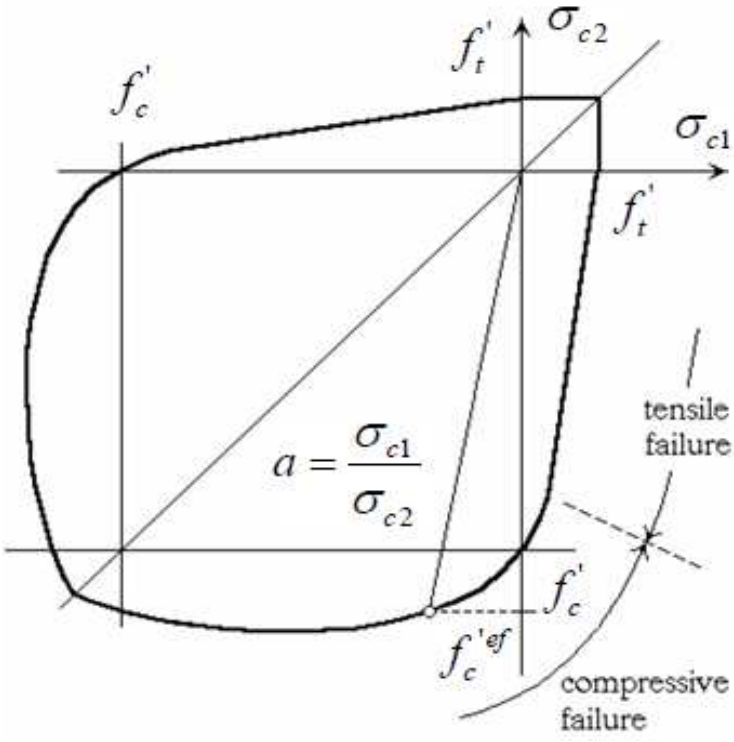

Figure 7-2: Biaxial failure function for concrete[28]

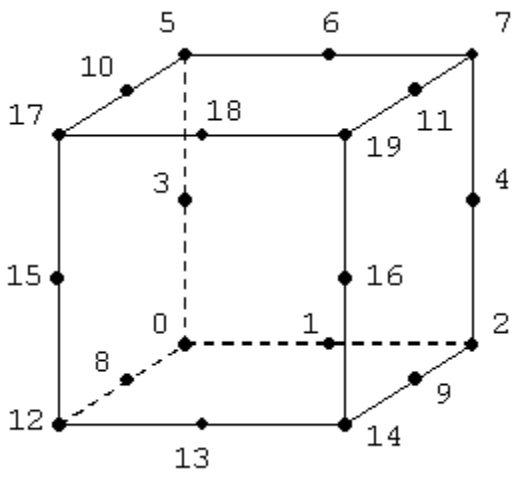

Brick Element

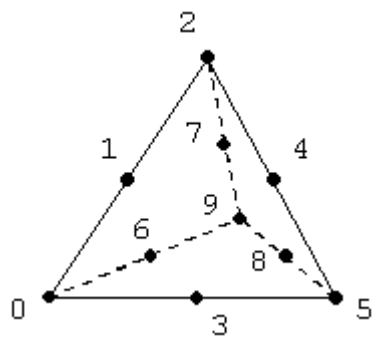

Tetrahedron Element

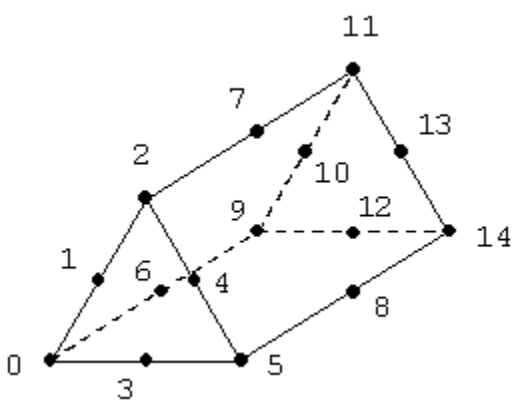

Wedge Element

Figure 7-3: Finite Element Types

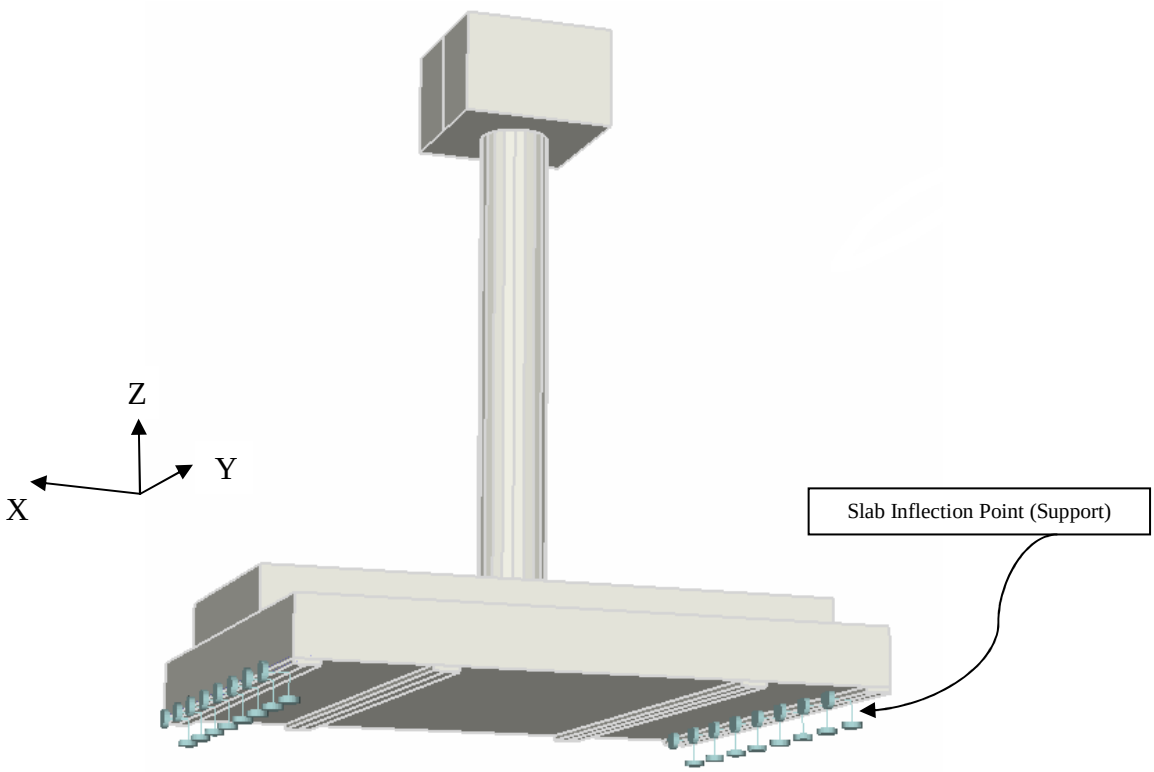

Figure 7-4: Finite Element Modeling for T-joint Specimens

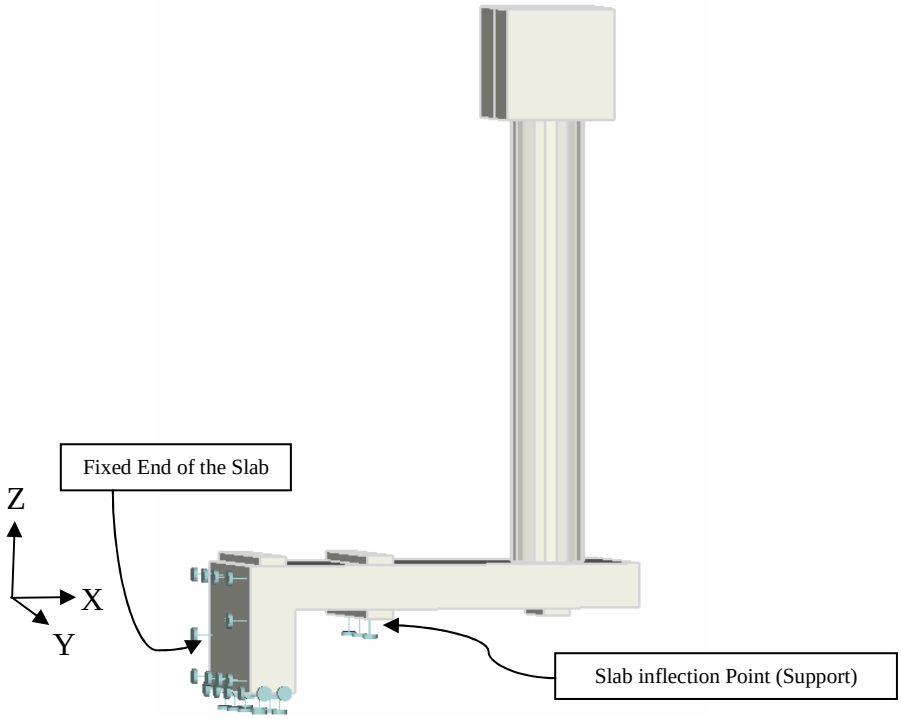

Figure 7-5: Finite Element Modeling for Knee-joint Specimens

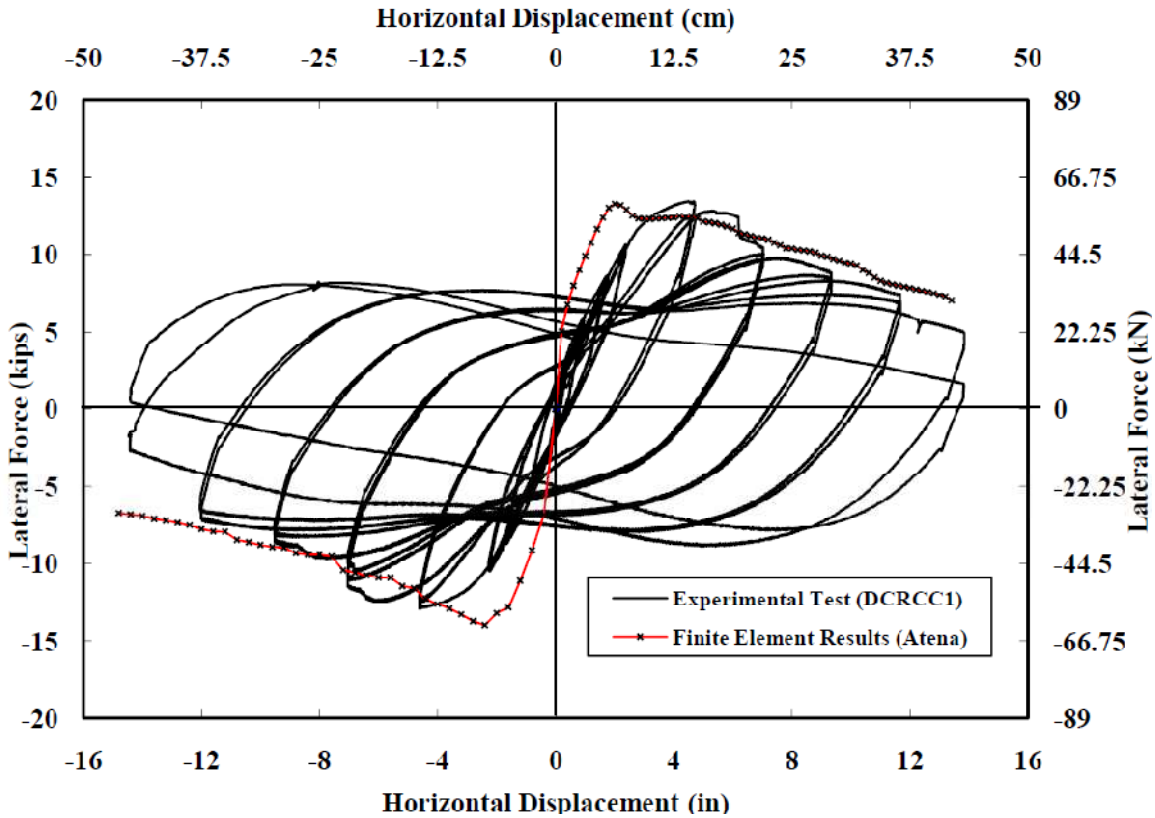

Figure 7-6: Analytical Results versus Experimental Results for DCRCC1

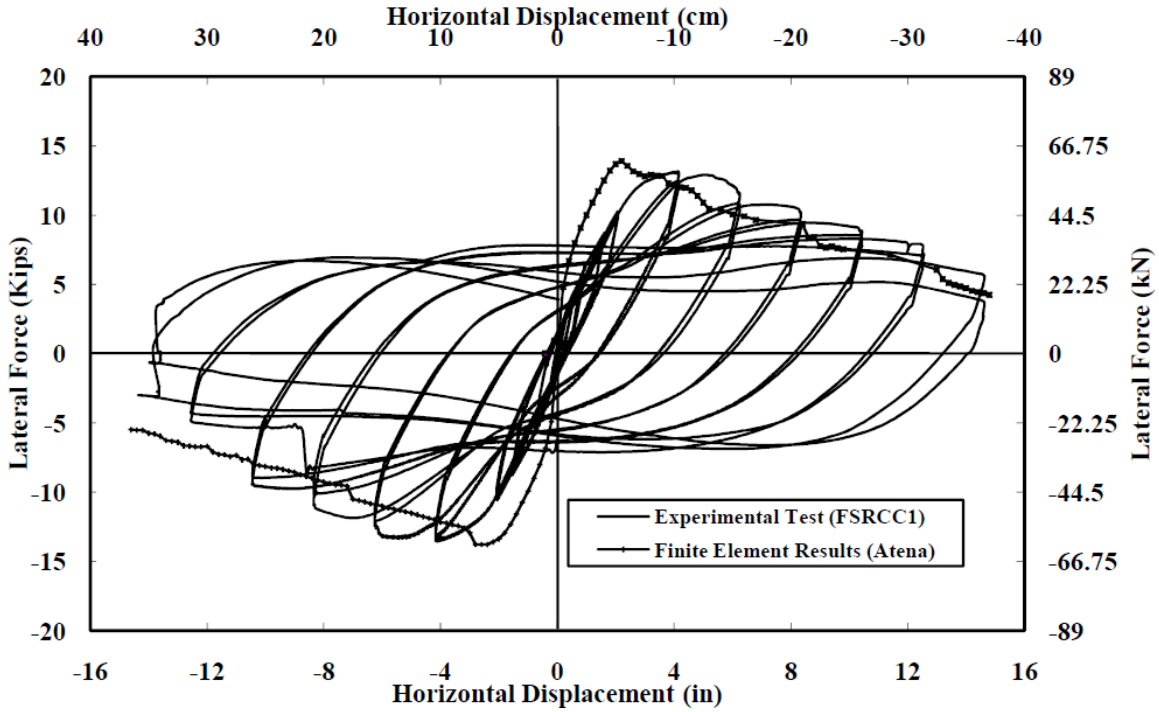

Figure 7-7: Analytical Results versus Experimental Results for FSRCC1

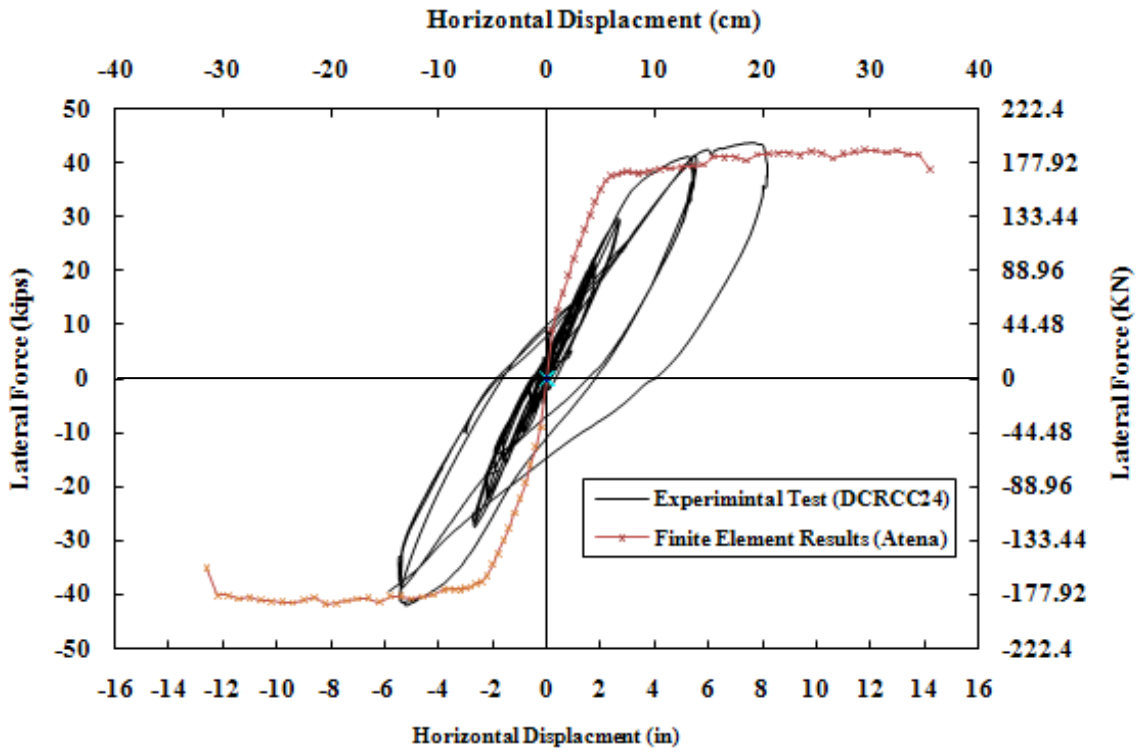

Figure 7-8: Analytical Results versus Experimental Results for DCRCC24

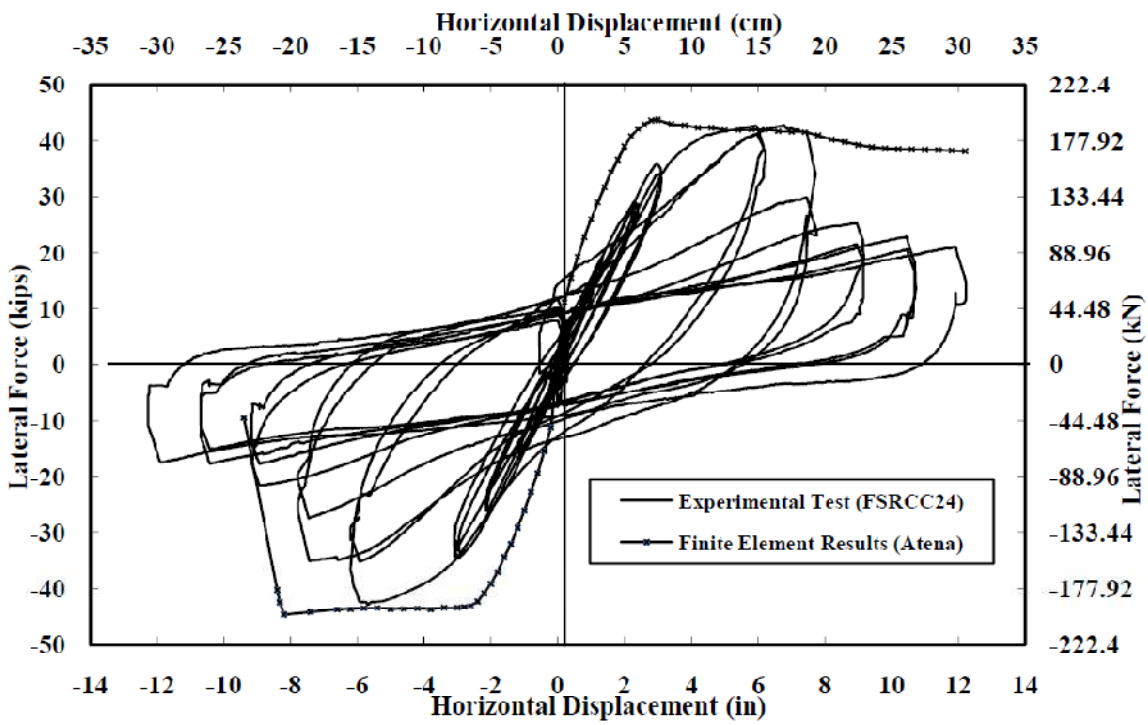

Figure 7-9: Analytical Results versus Experimental Results for FSRCC24

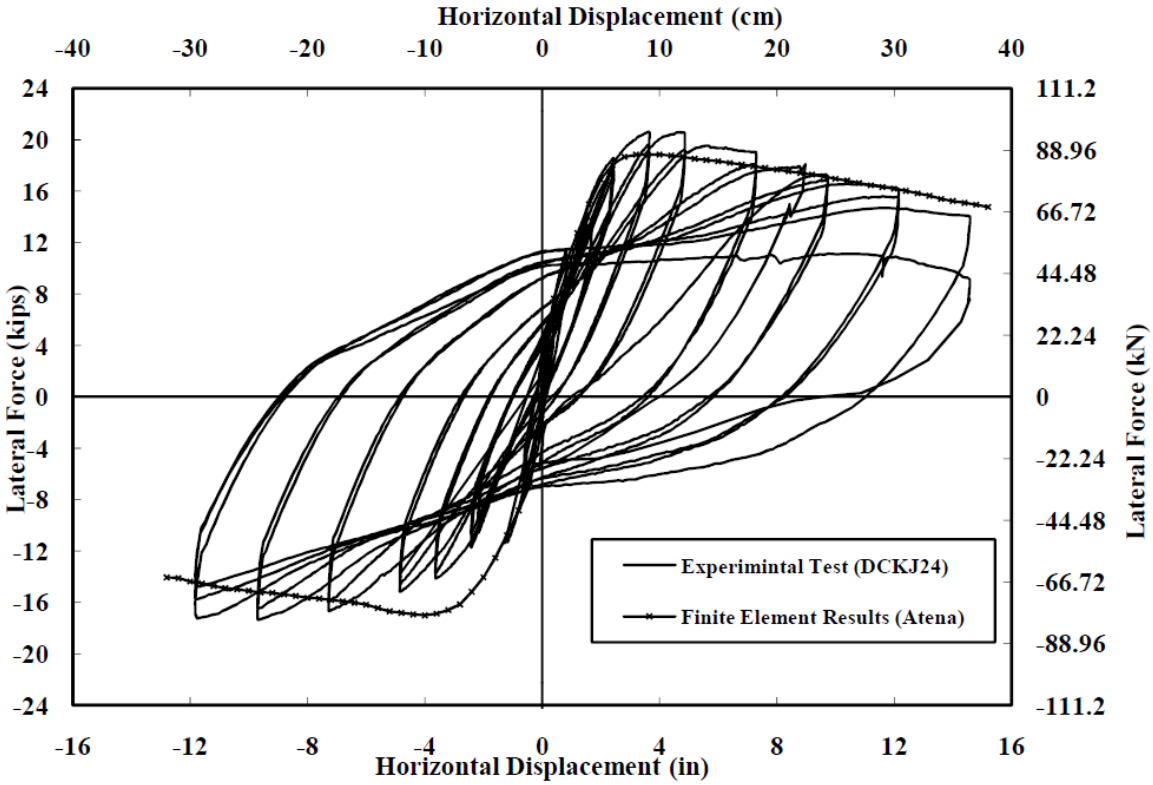

Figure 7-10: Analytical Results versus Experimental Results for DCKJ24

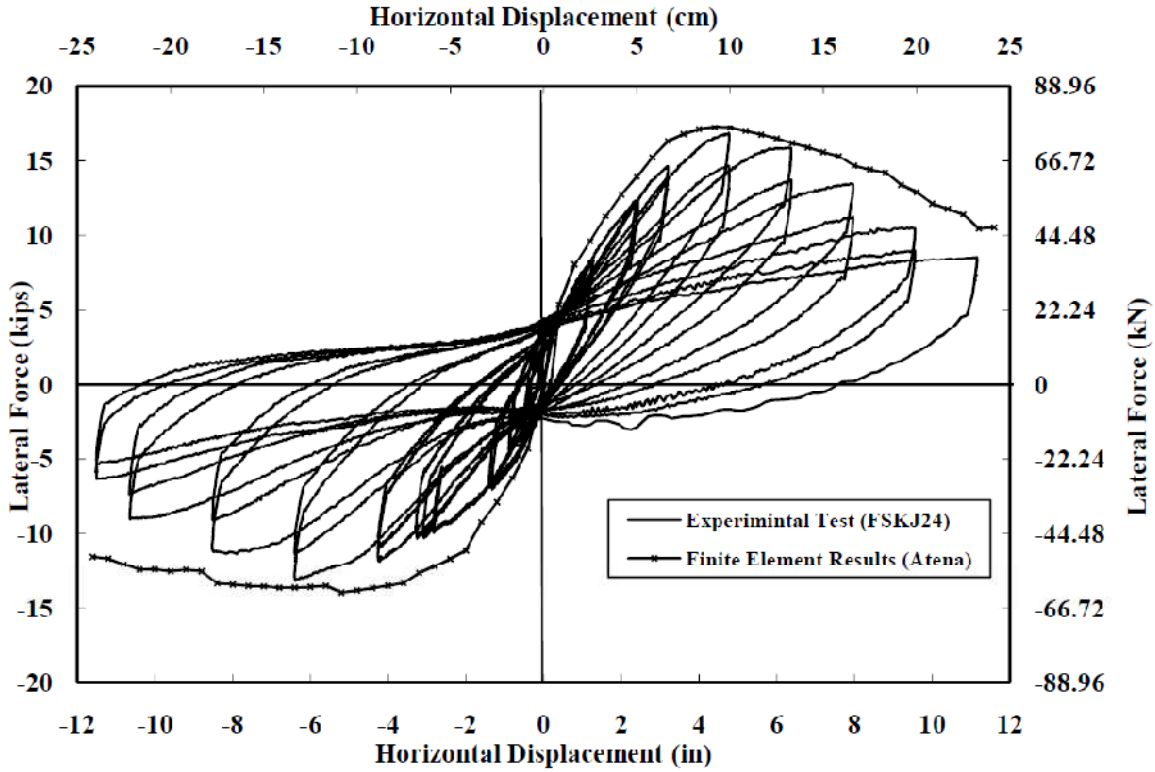

Figure 7-11: Analytical Results versus Experimental Results for FSKJ24

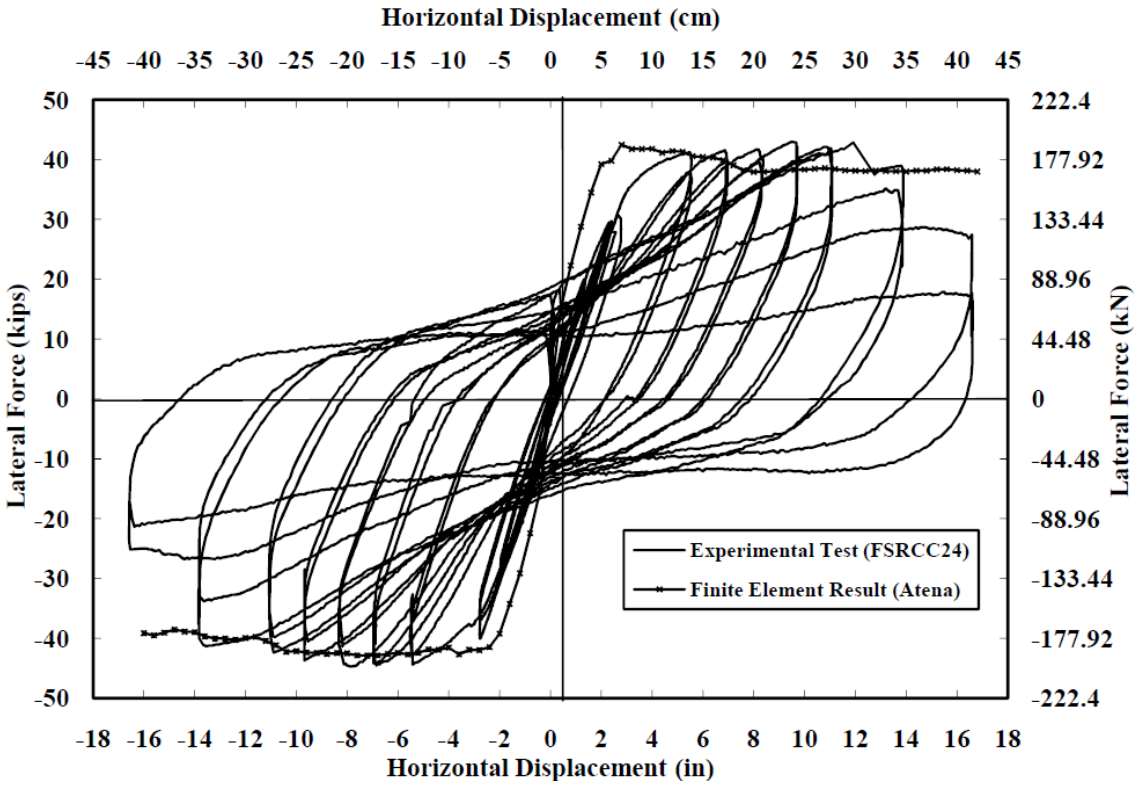

Figure 7-12: Analytical Results versus Experimental Results for FSRCC24-M

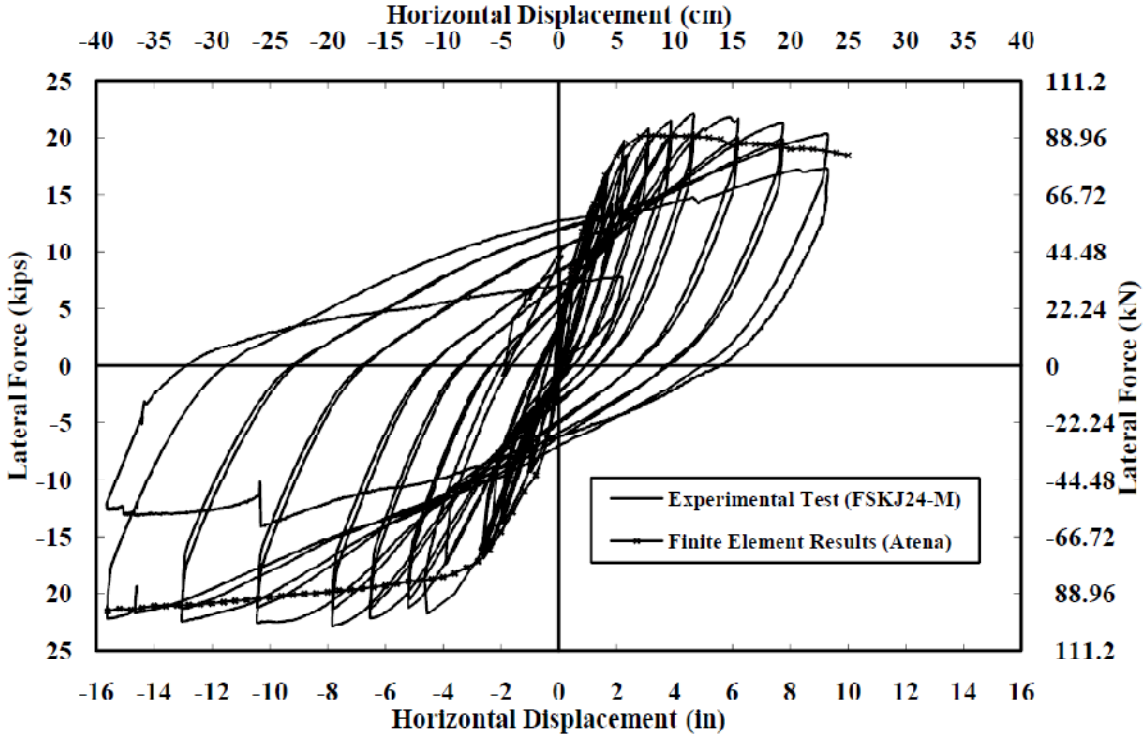

Figure 7-13: Analytical Results versus Experimental Results for FSKJ24-M

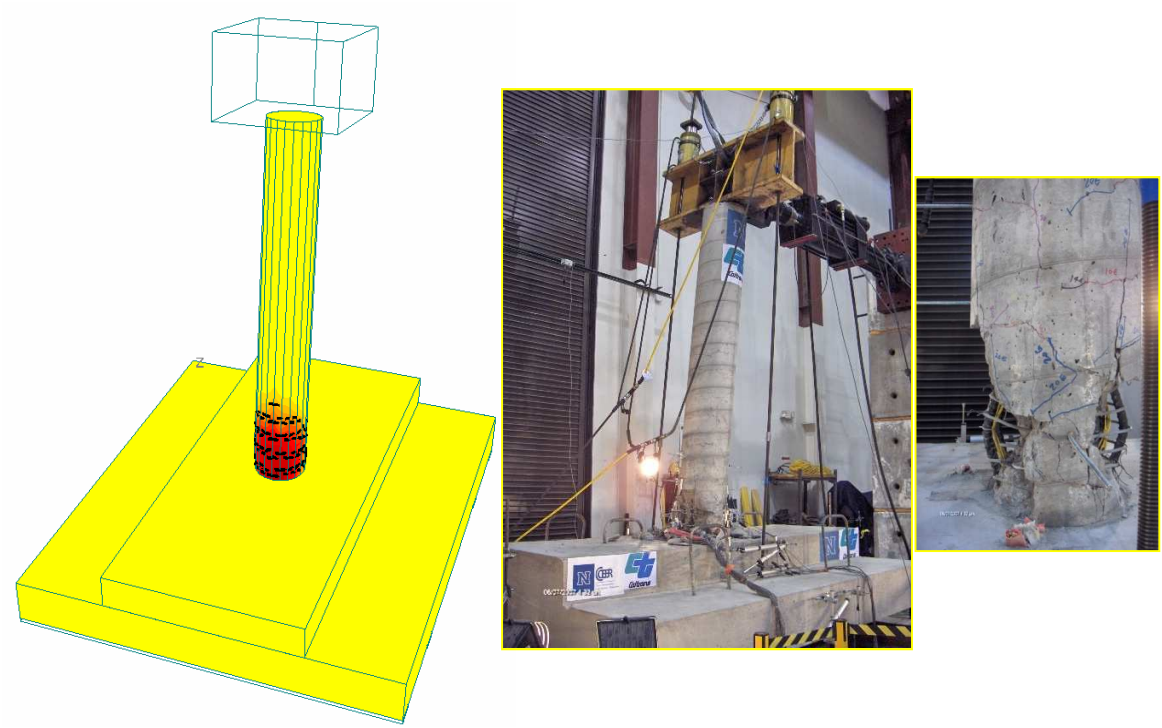

Figure 7-14: Actual and Predicted Cracks Pattern for Specimen DCRCC1

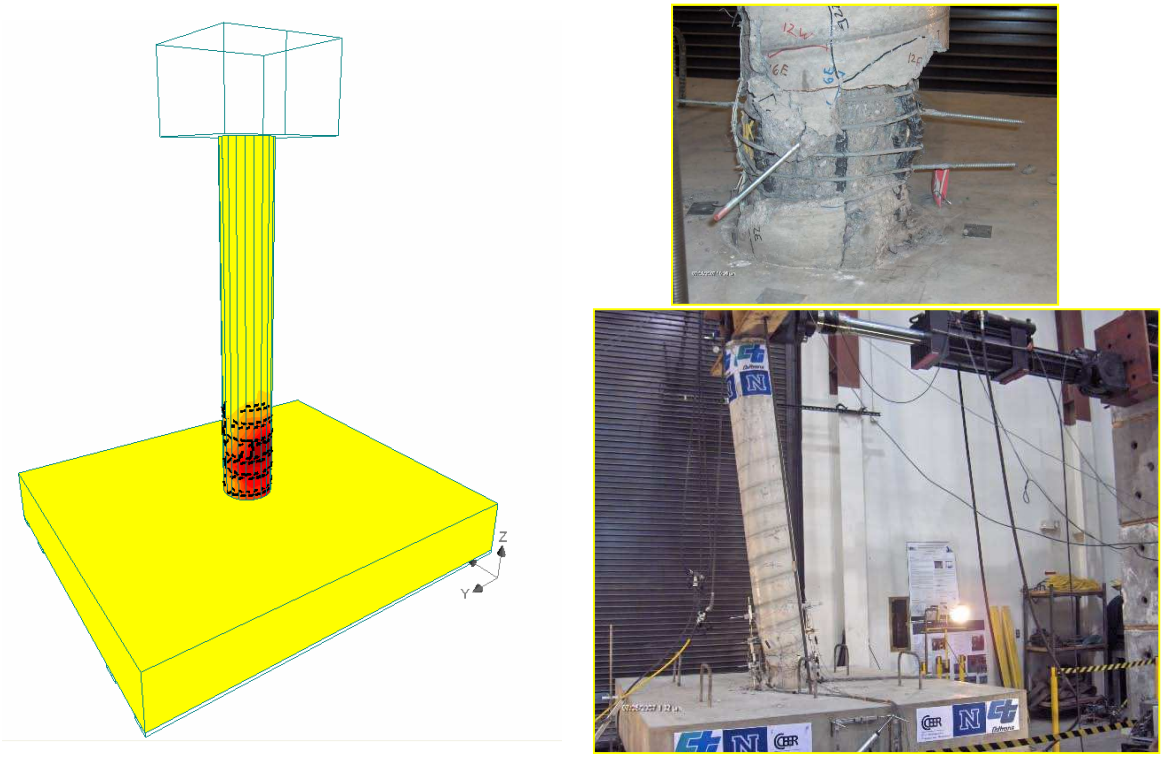

Figure 7-15: Actual and Predicted Cracks Pattern for Specimen FSRCC1

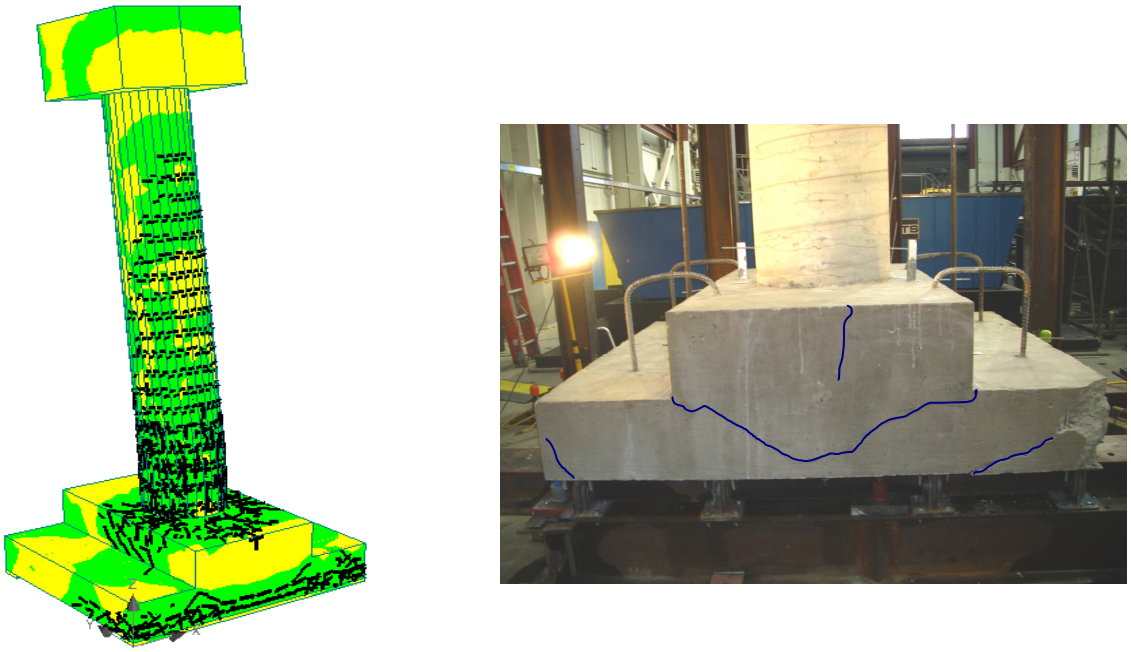

Figure 7-16: Actual and Predicted Cracks Pattern for Specimen DCRCC24

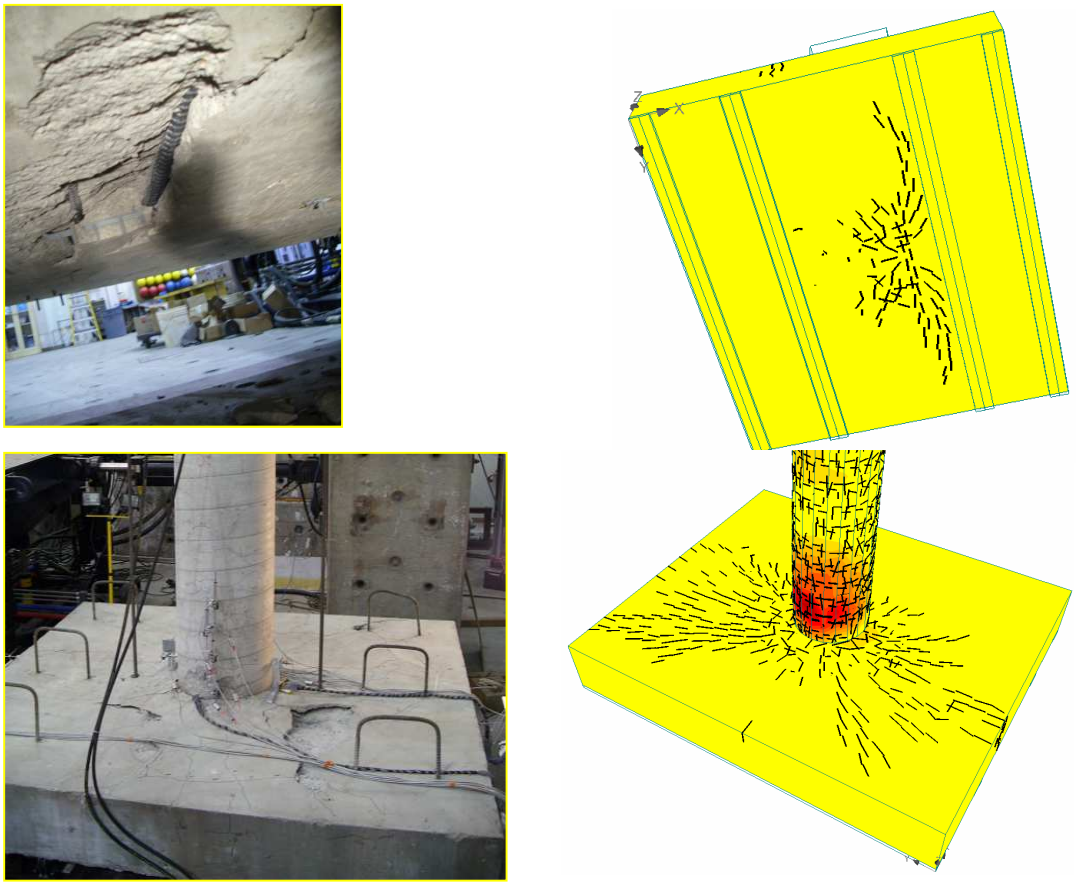

Figure 7-17: Actual and Predicted Cracks Pattern for Specimen FSRCC24

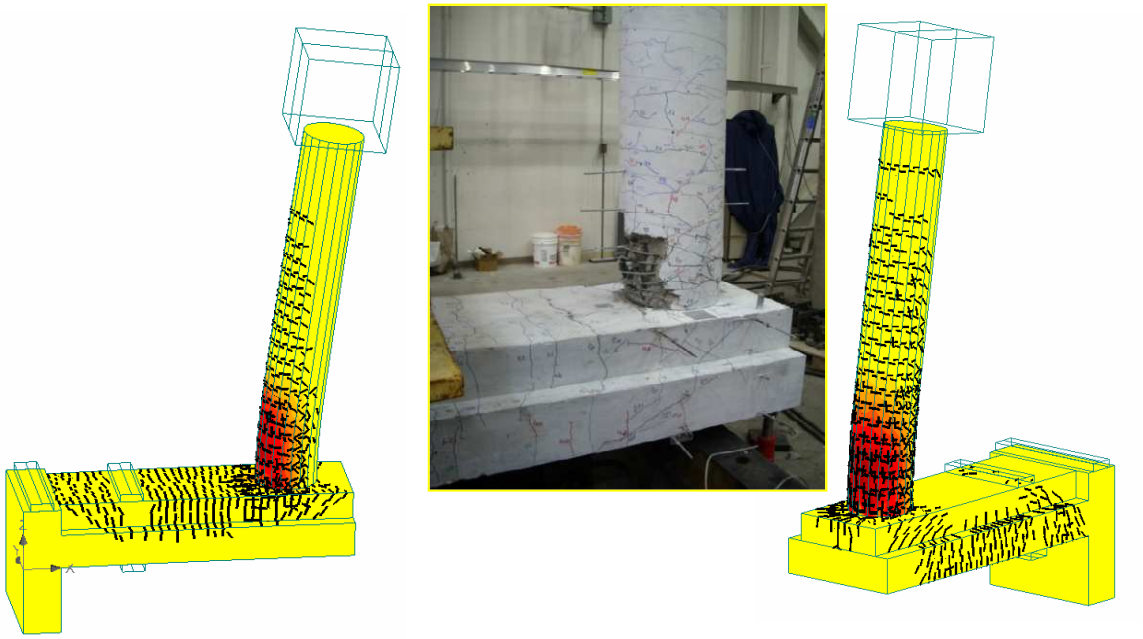

Figure 7-18: Actual and Predicted Cracks Pattern for Specimen DCKJ24

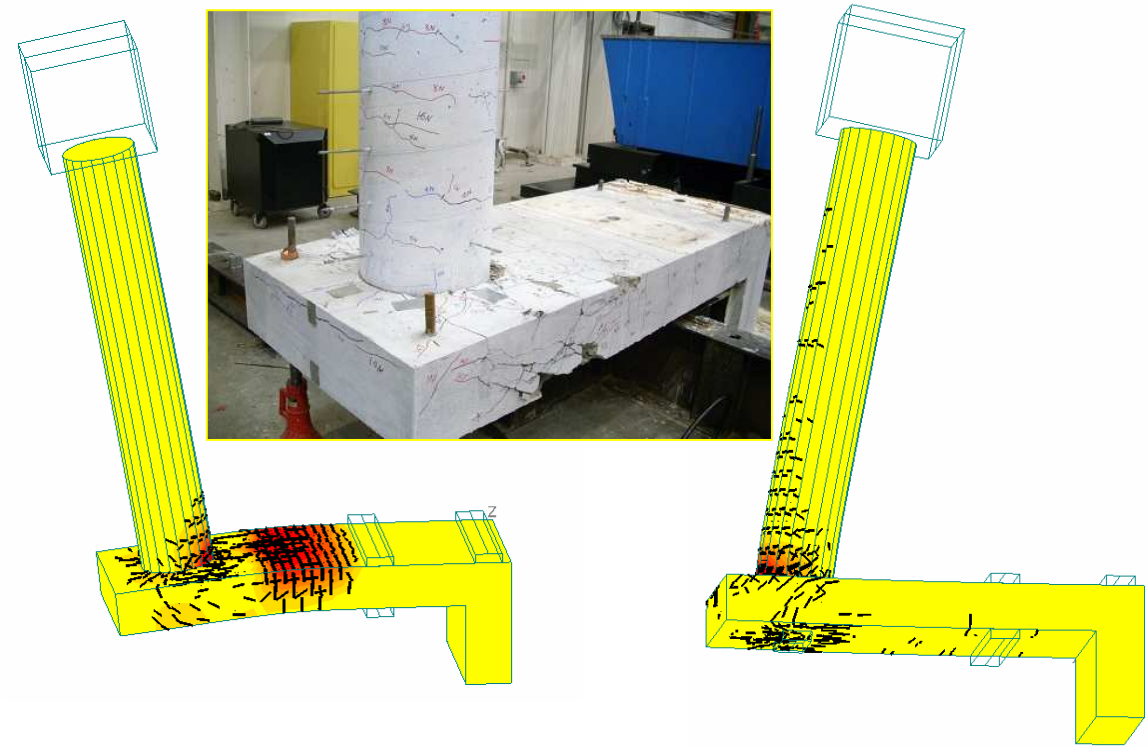

Figure 7-19: Actual and Predicted Cracks Pattern for Specimen FSKJ24

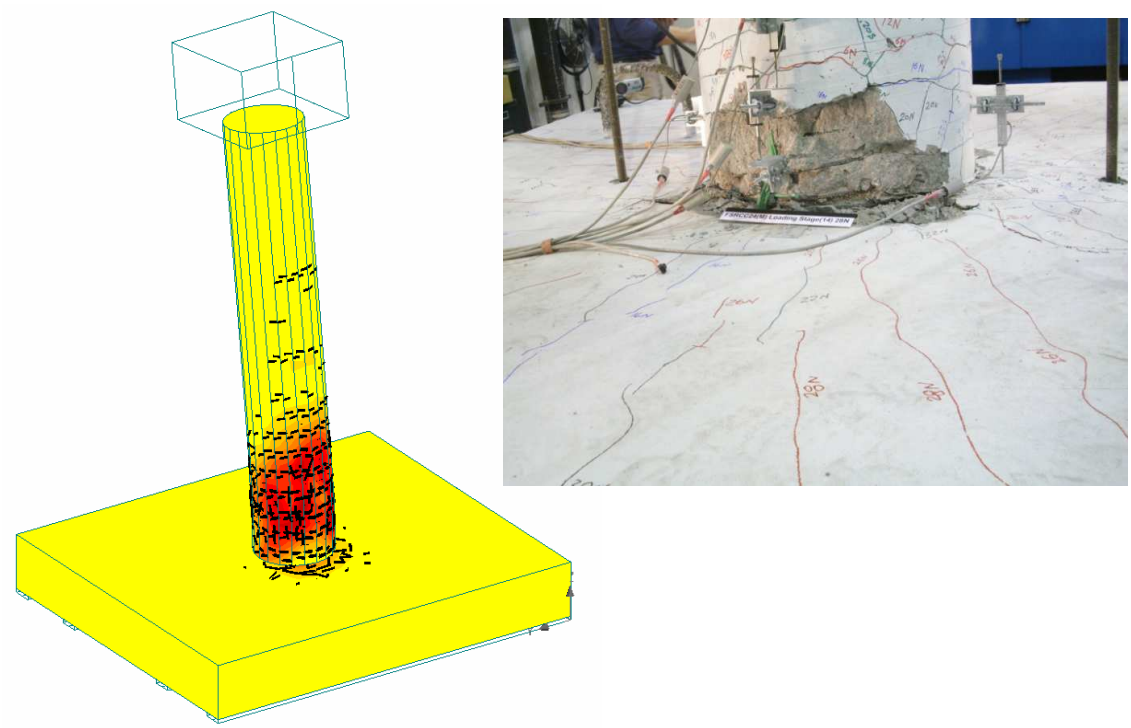

Figure 7-20: Actual and Predicted Cracks Pattern for Specimen FSRCC24-M

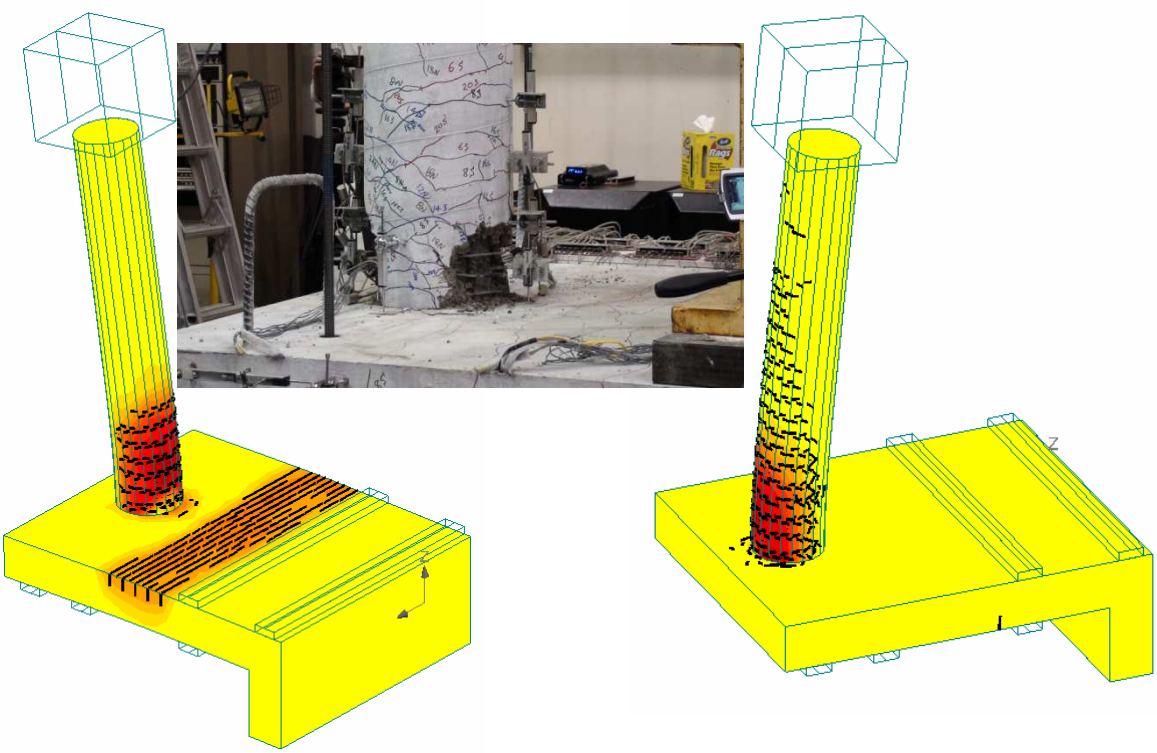

Figure 7-21: Actual and Predicted Cracks Pattern for Specimen FSKJ24-M

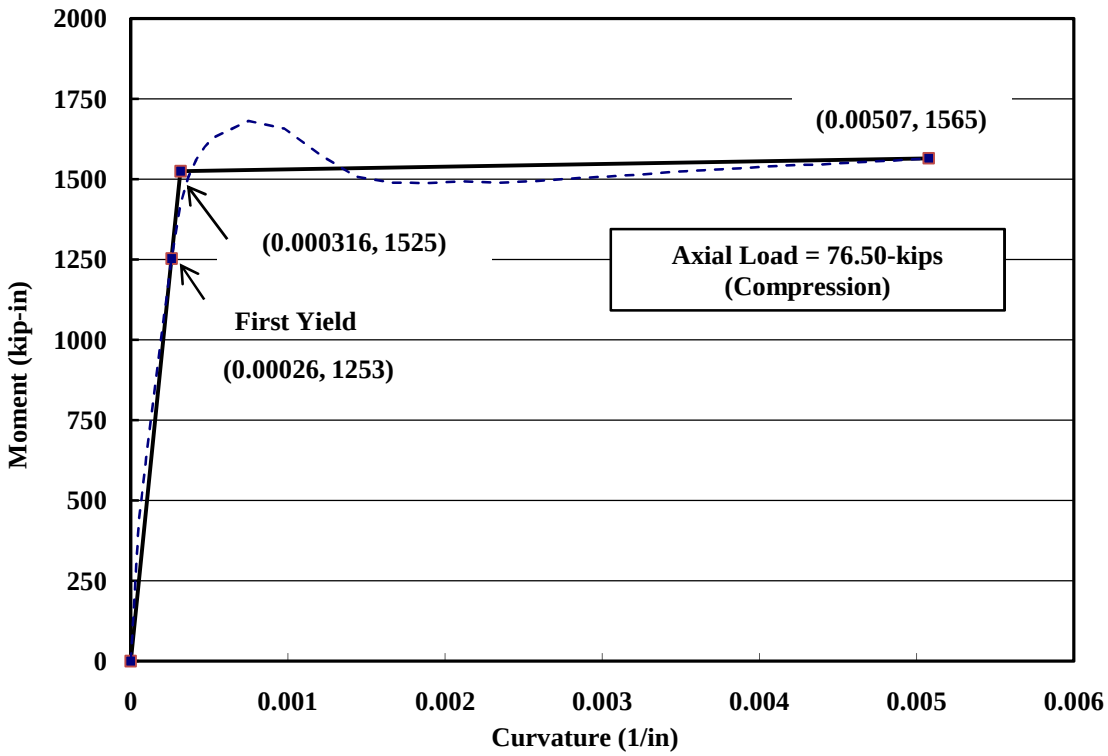

Figure 7-22: DCRCC1 Pile M-ϕ Post Analysis

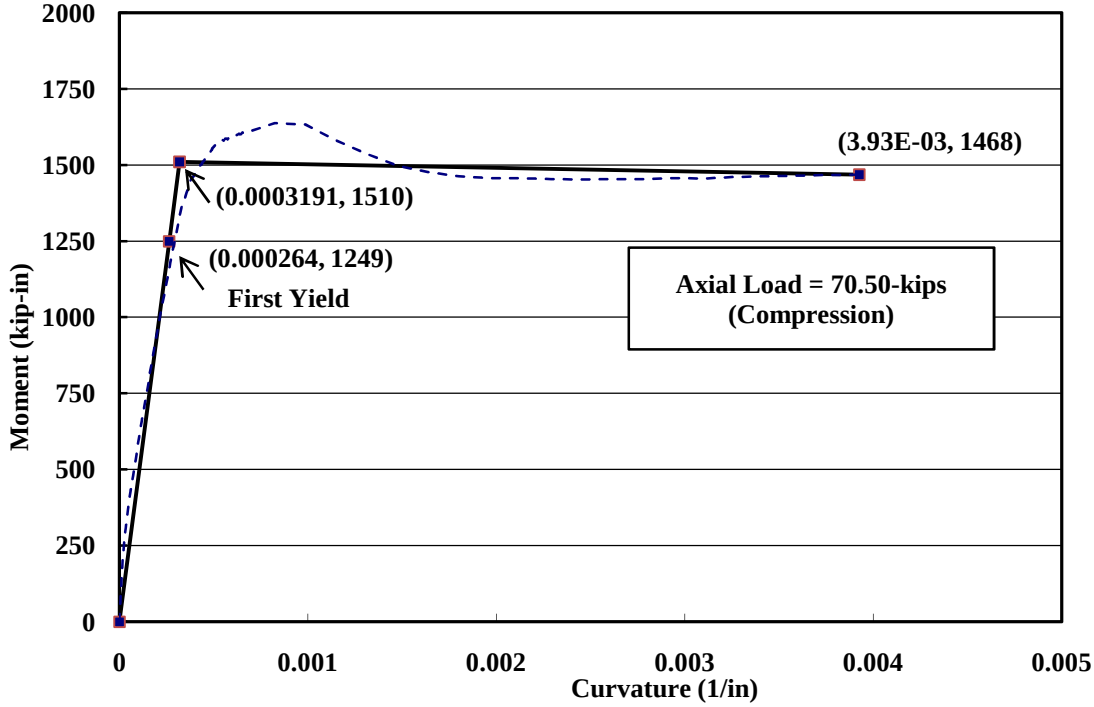

Figure 7-23: FSRCC1 Pile M-ϕ Post Analysis

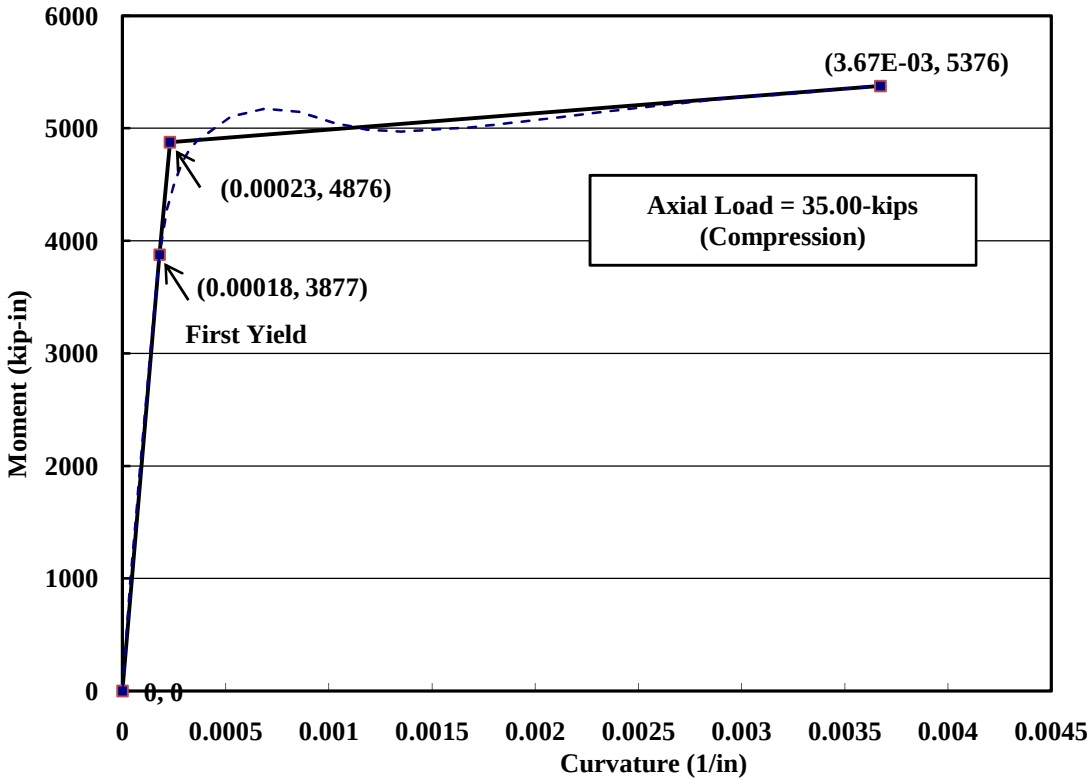

Figure 7-24: DCRCC24 Pile M-ϕ Post Analysis

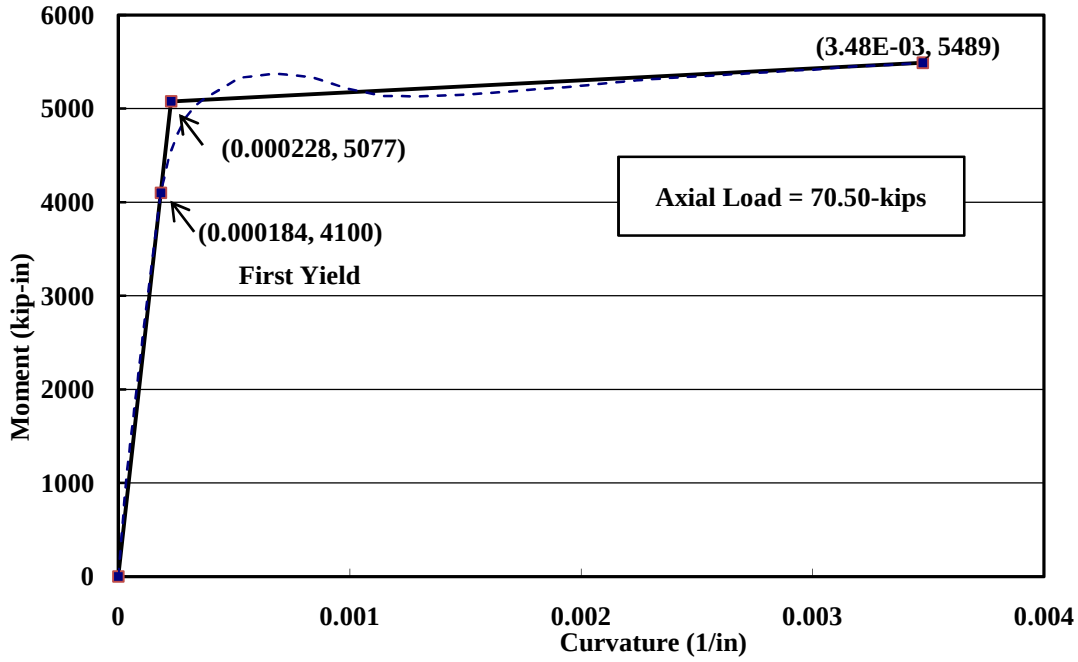

Figure 7-25: FSRCC24 Pile M-ϕ Post Analysis

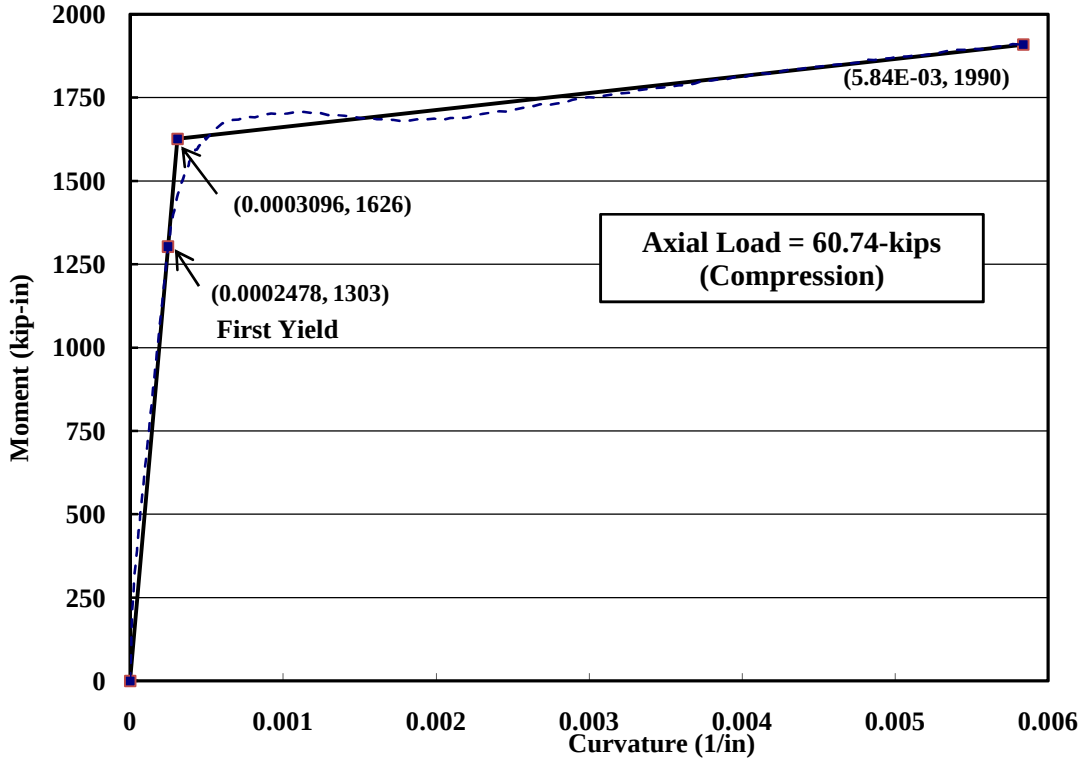

Figure 7-26: DCKJ24 Pile M-ϕ Post Analysis (Max. Load Case)

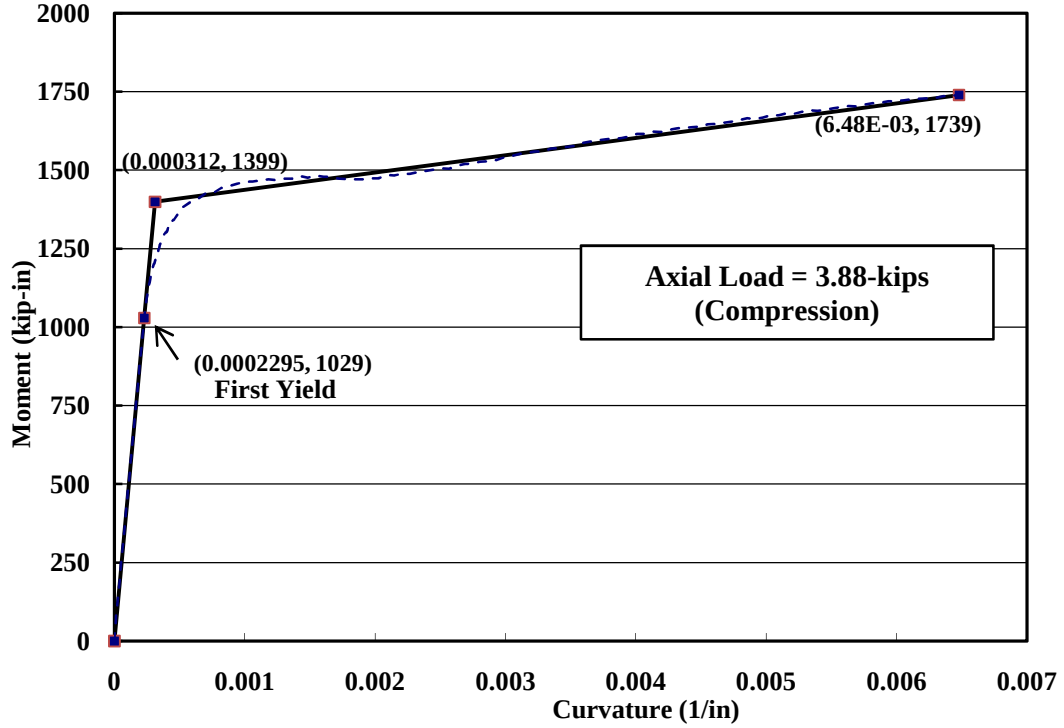

Figure 7-27: DCKJ24 Pile M-ϕ Post Analysis (Min. Load Case)

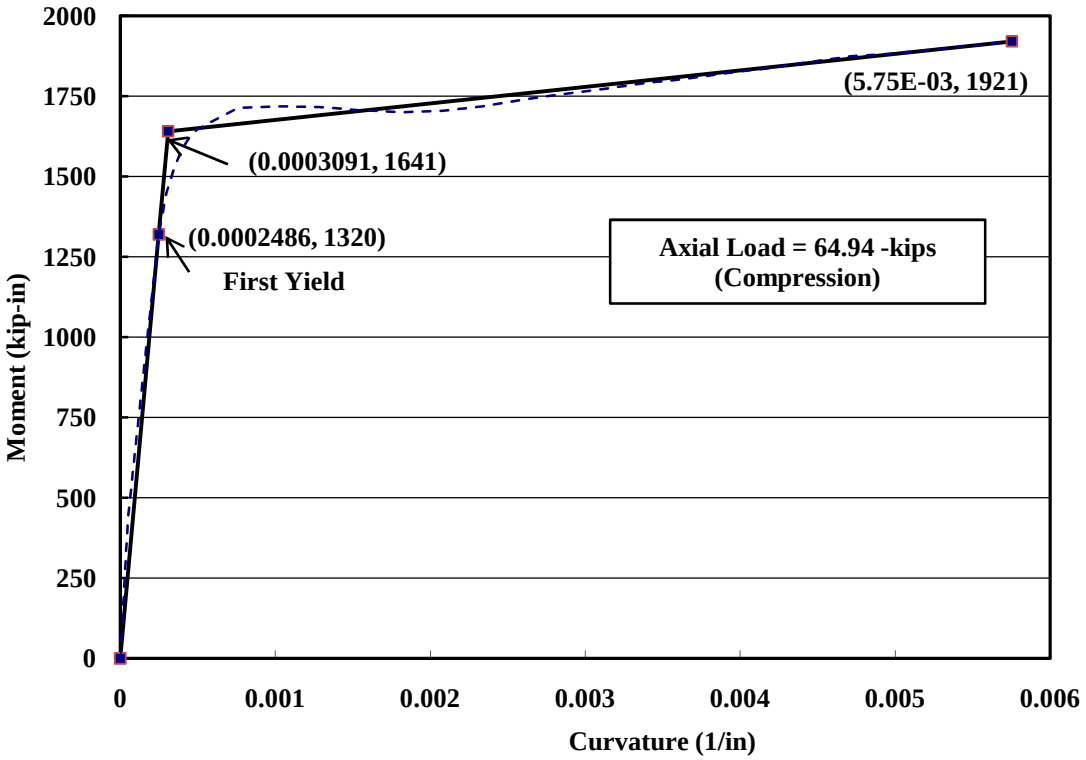

Figure 7-28: FSKJ24 Pile M-ϕ Post Analysis (Max. Load Case)

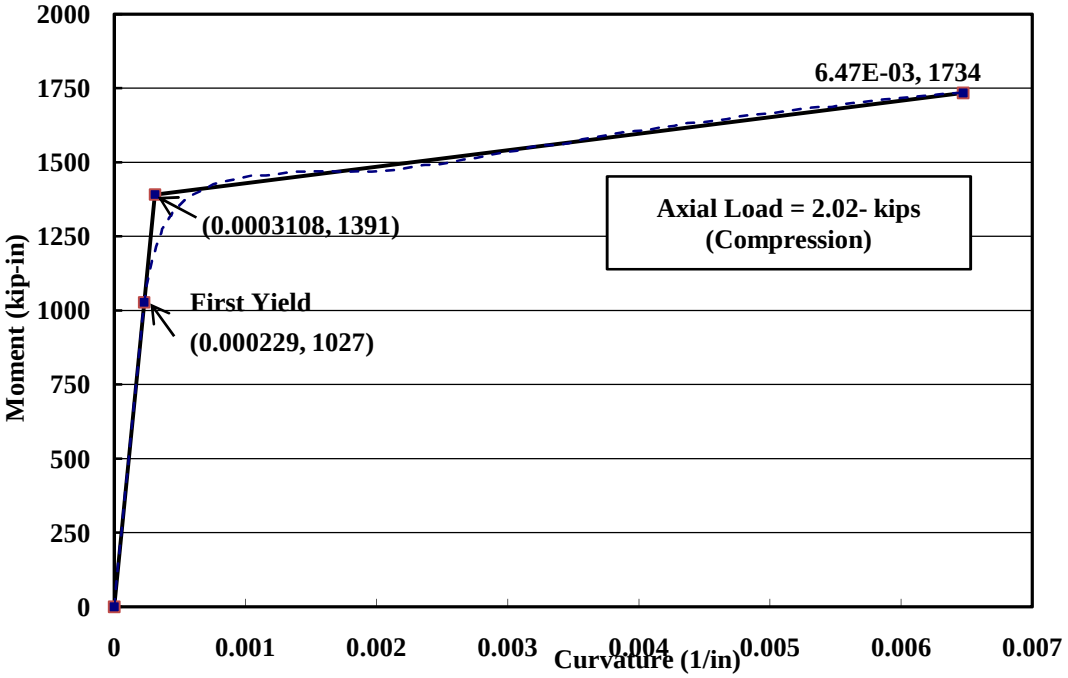

Figure 7-29: FSKJ24 Pile M-ϕ Post Analysis (Min. Load Case)

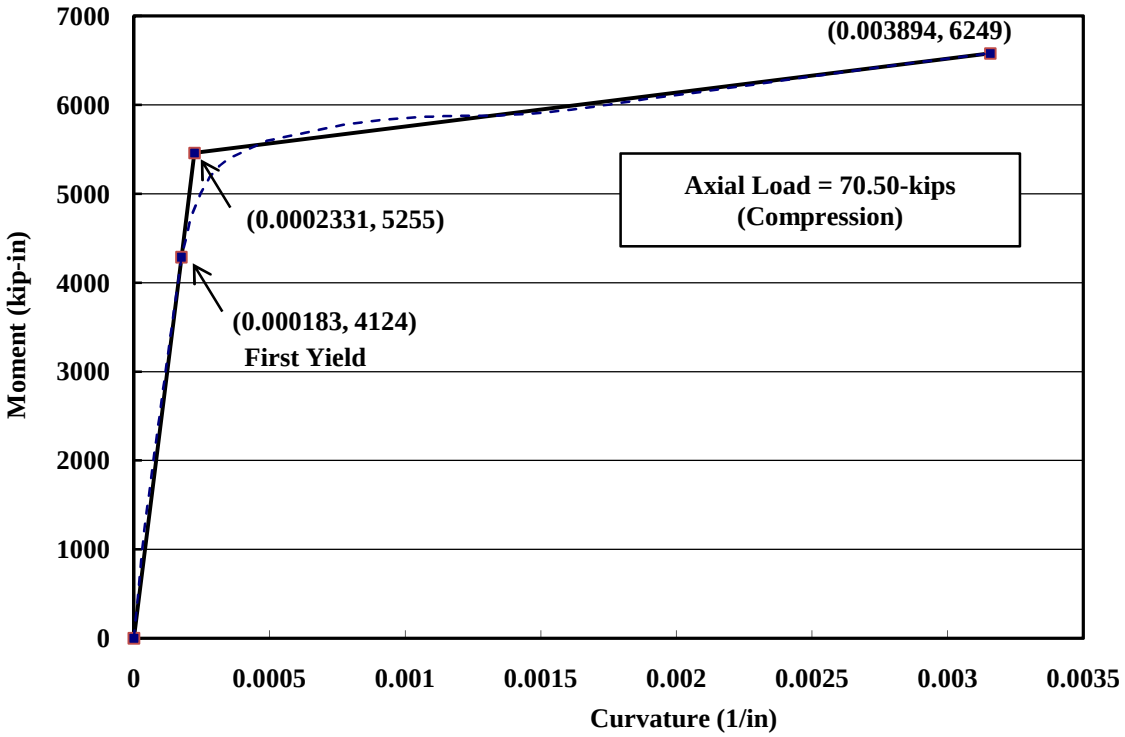

Figure 7-30: FSRCC24-M Pile M-ϕ Post Analysis

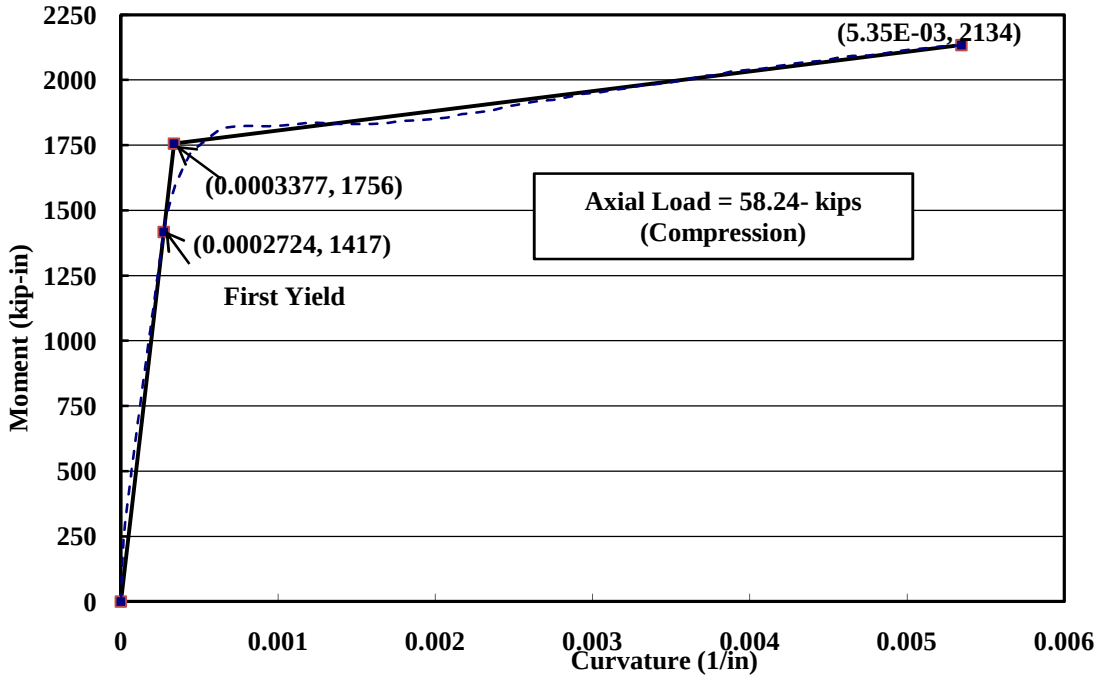

Figure 7-31: FSKJ24-M Pile M-ϕ Post Analysis (Max. Load Case)

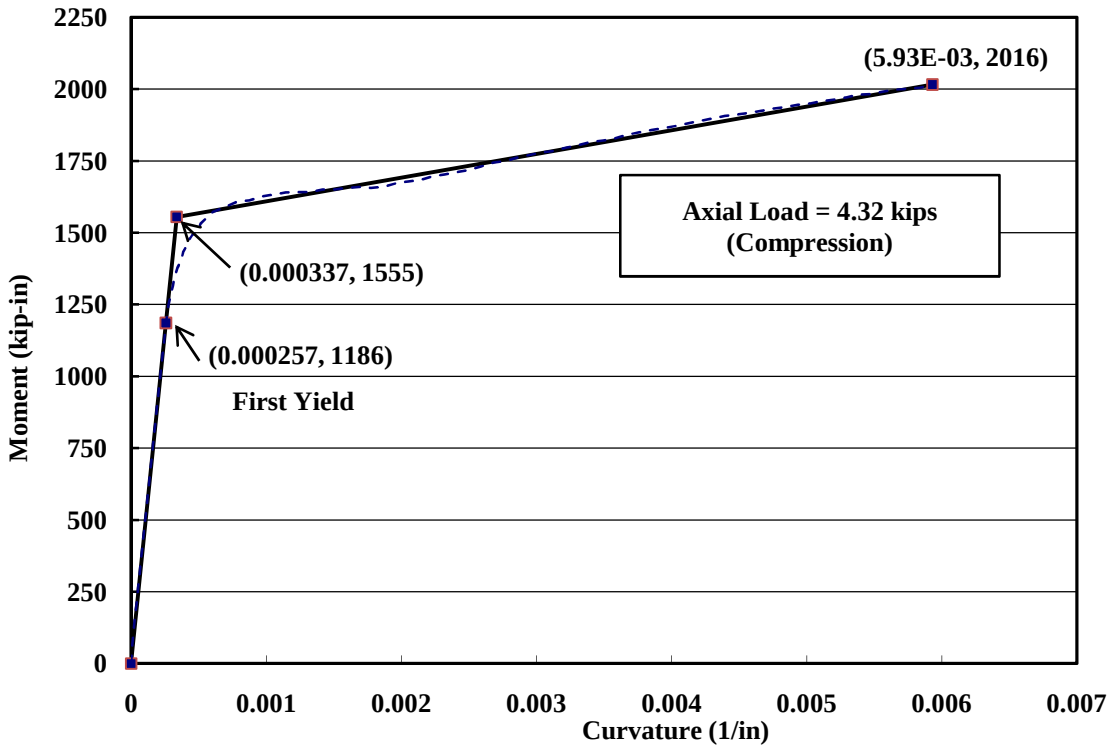

Figure 7-32: FSKJ24-M Pile M-ϕ Post Analysis (Min. Load Case)

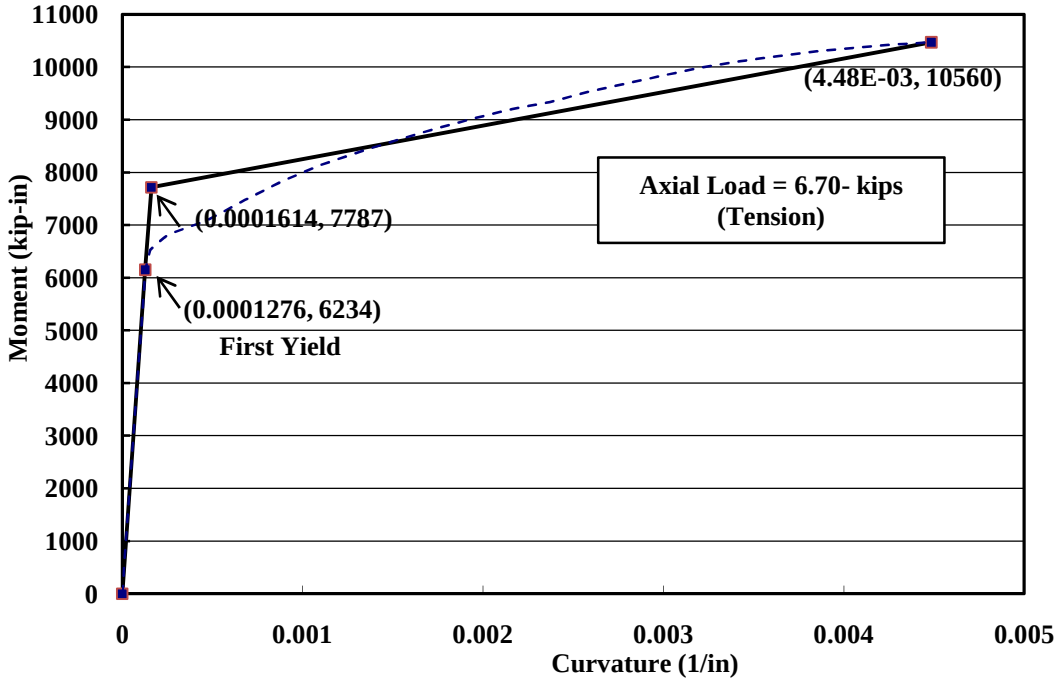

Figure 7-33: DCRCC1 Slab Positive M-ϕ Post Analysis

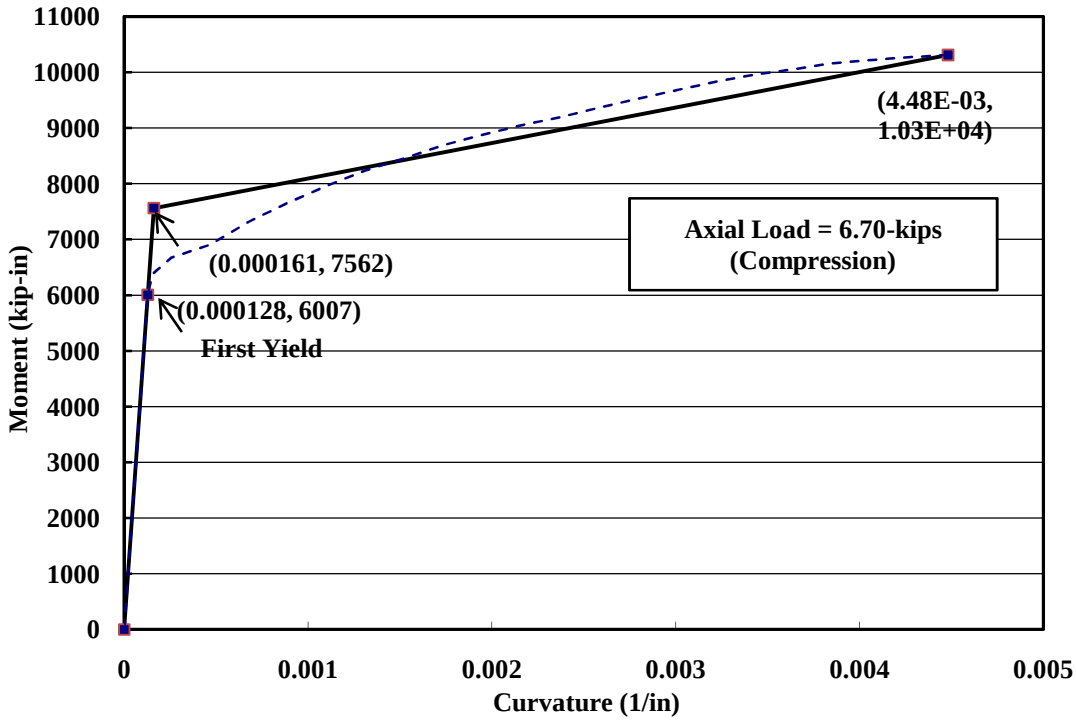

Figure 7-34: DCRCC1 Slab Negative M-ϕ Post Analysis

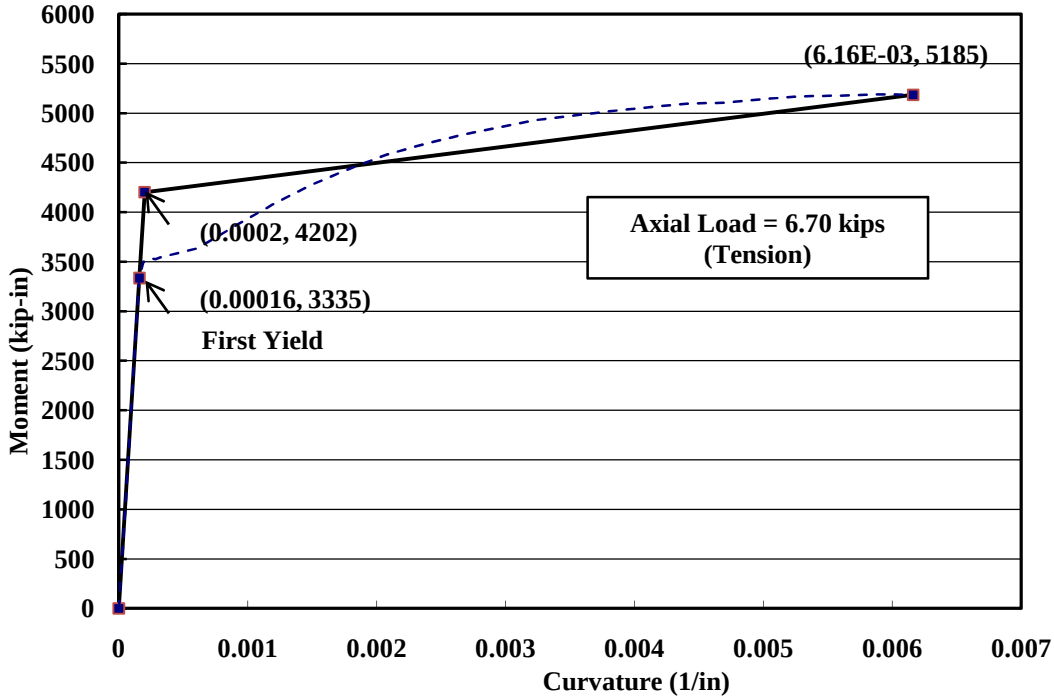

Figure 7-35: FSRCC1 Slab Positive M-ϕ Post Analysis

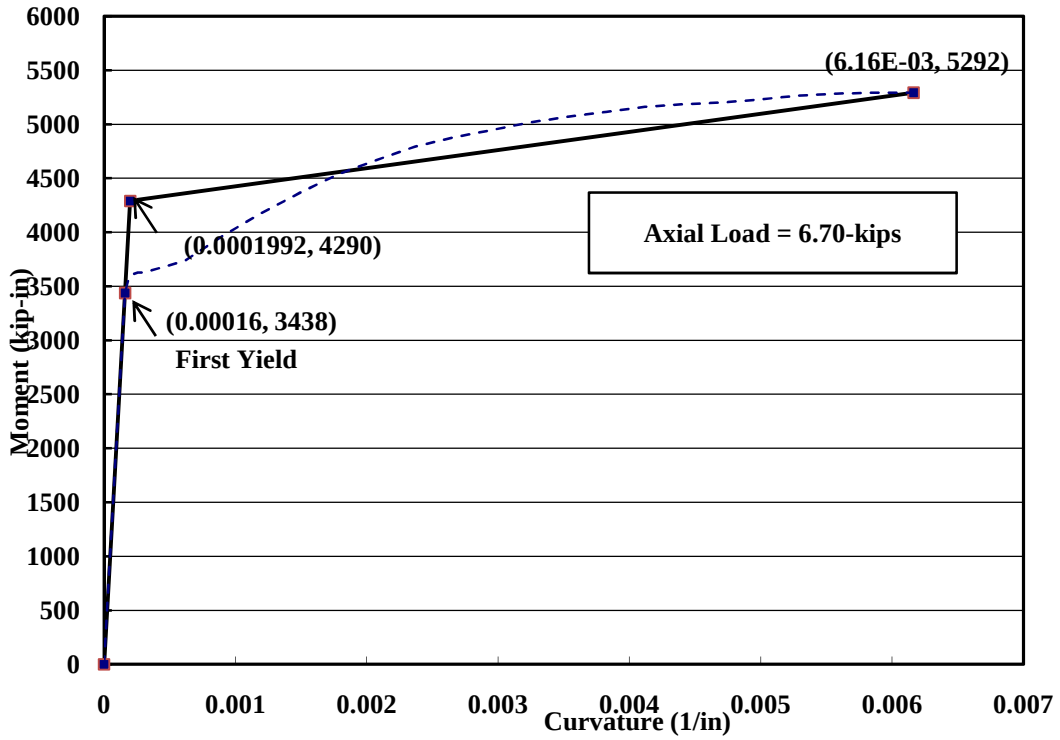

Figure 7-36: FSRCC1 Slab Negative M-ϕ Post Analysis

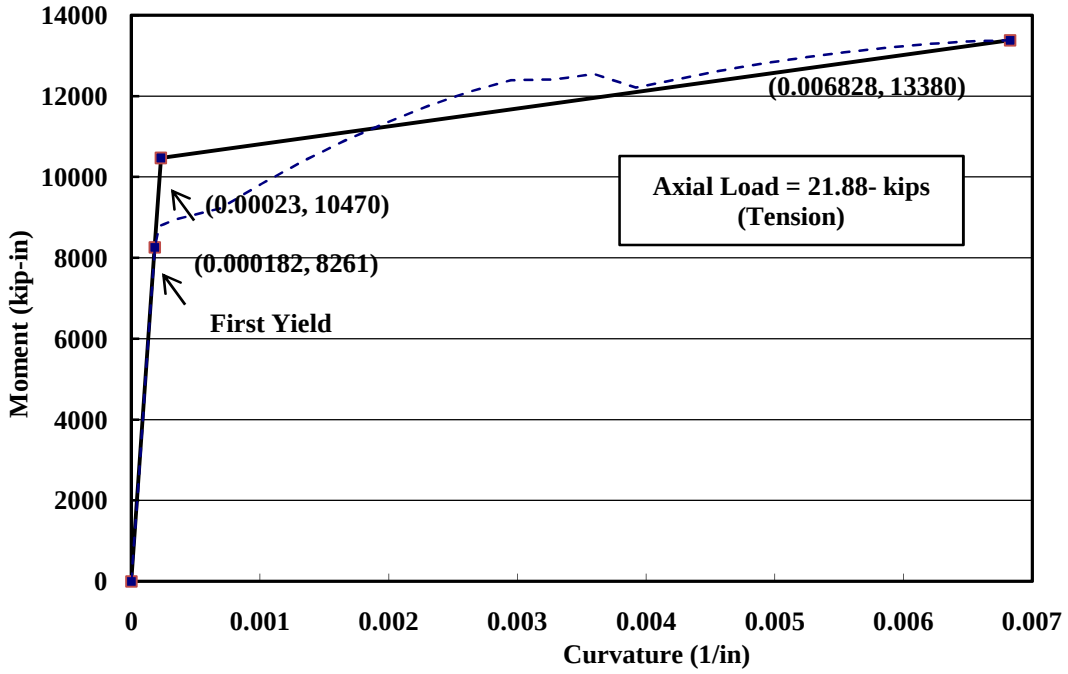

Figure 7-37: DCRCC24 Slab Positive M-ϕ Post Analysis

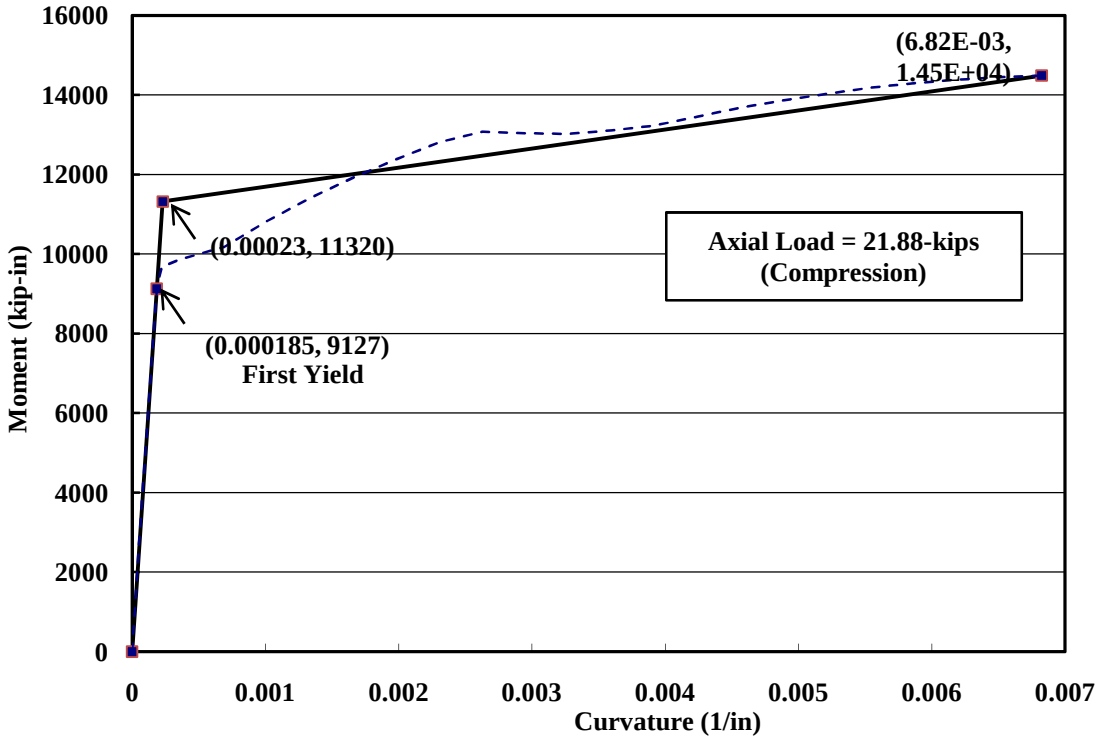

Figure 7-38: DCRCC24 Slab Negative M-ϕ Post Analysis

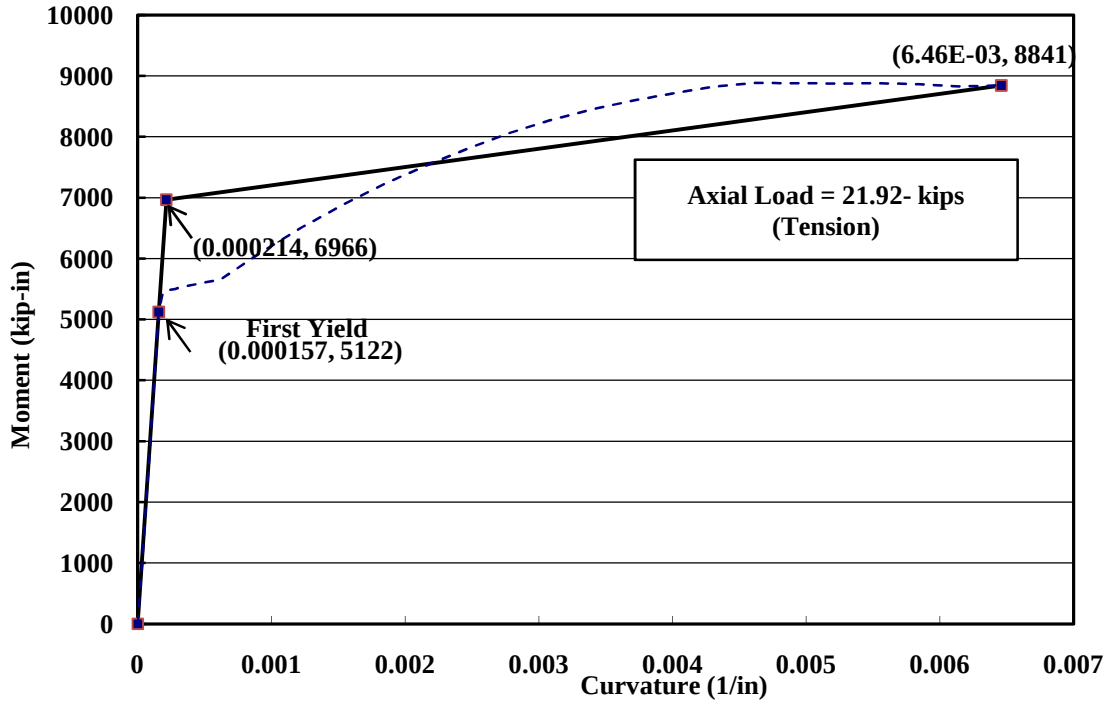

Figure 7-39: FSRCC24 Slab Positive M-ϕ Post Analysis

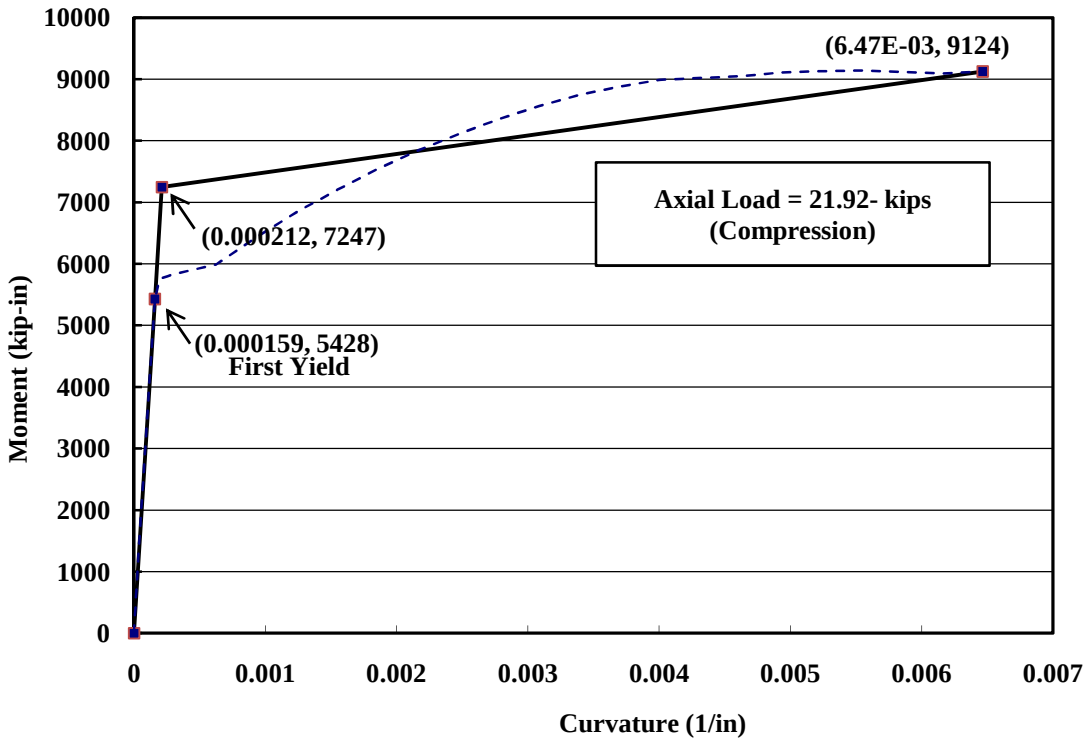

Figure 7-40: FSRCC24 Slab Negative M-ϕ Post Analysis

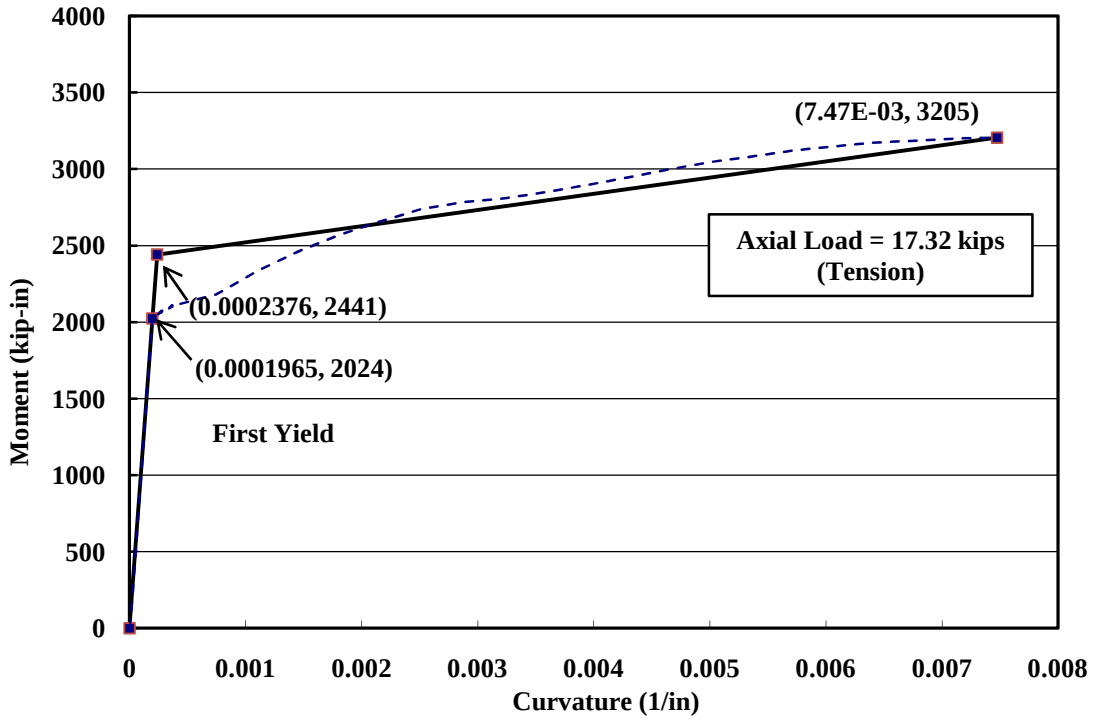

Figure 7-41: DCKJ24 Slab Positive M-ϕ Post Analysis

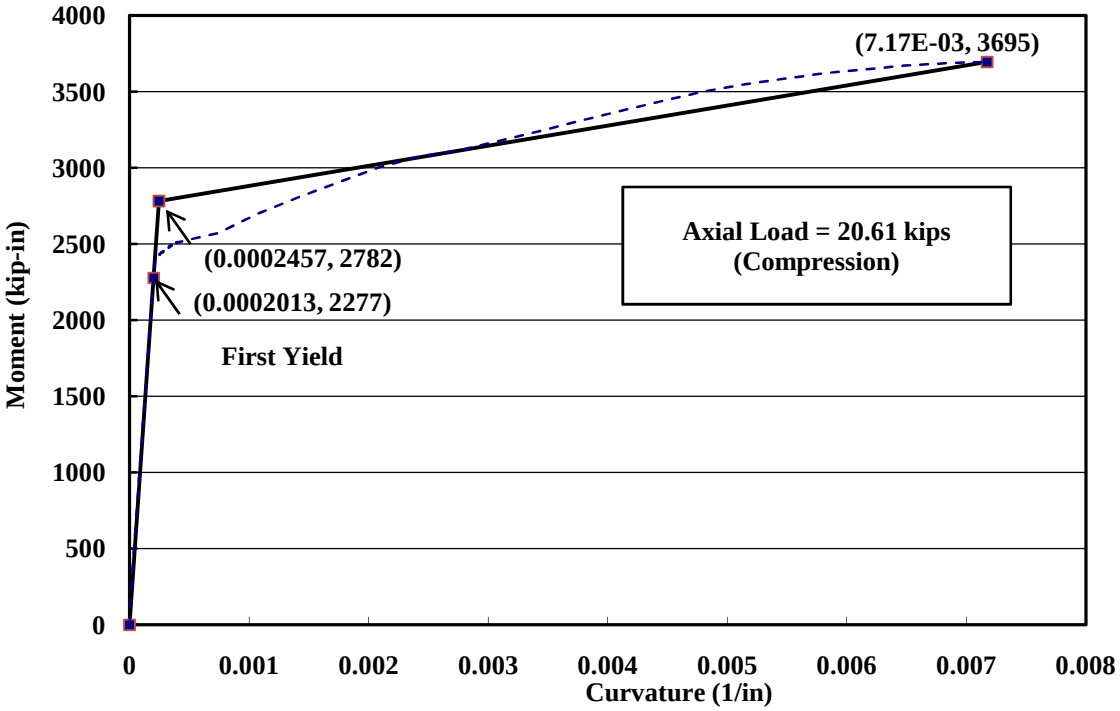

Figure 7-42: DCKJ24 Slab Negative M-ϕ Post Analysis

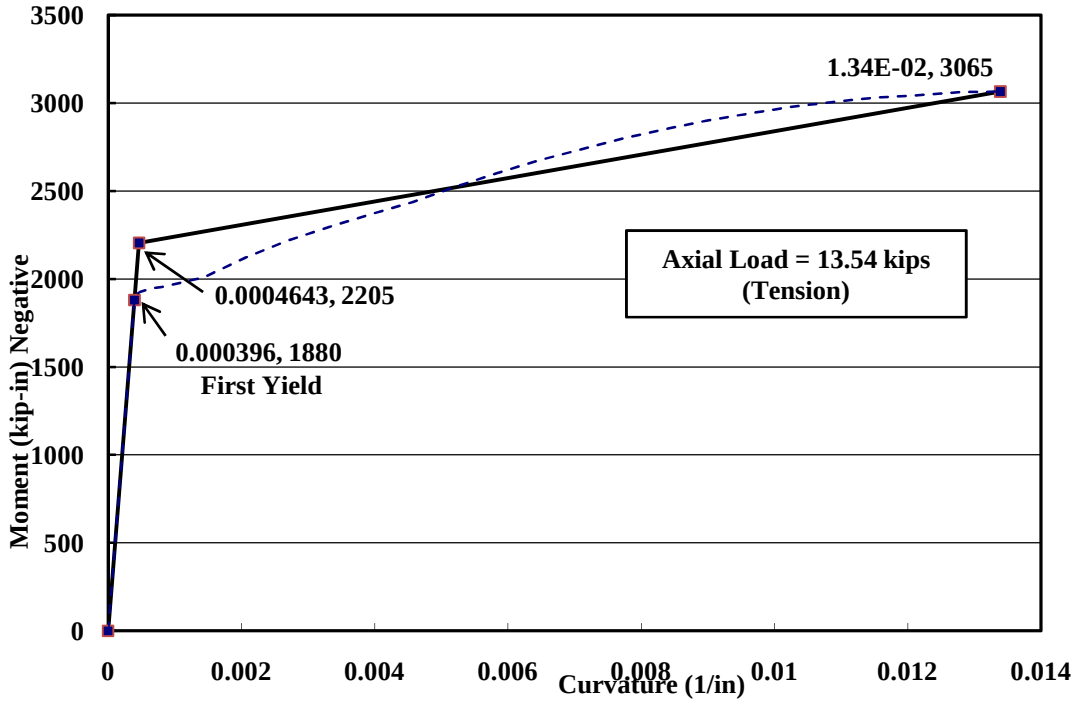

Figure 7-43: FSKJ24 Slab Positive M-ϕ Post Analysis

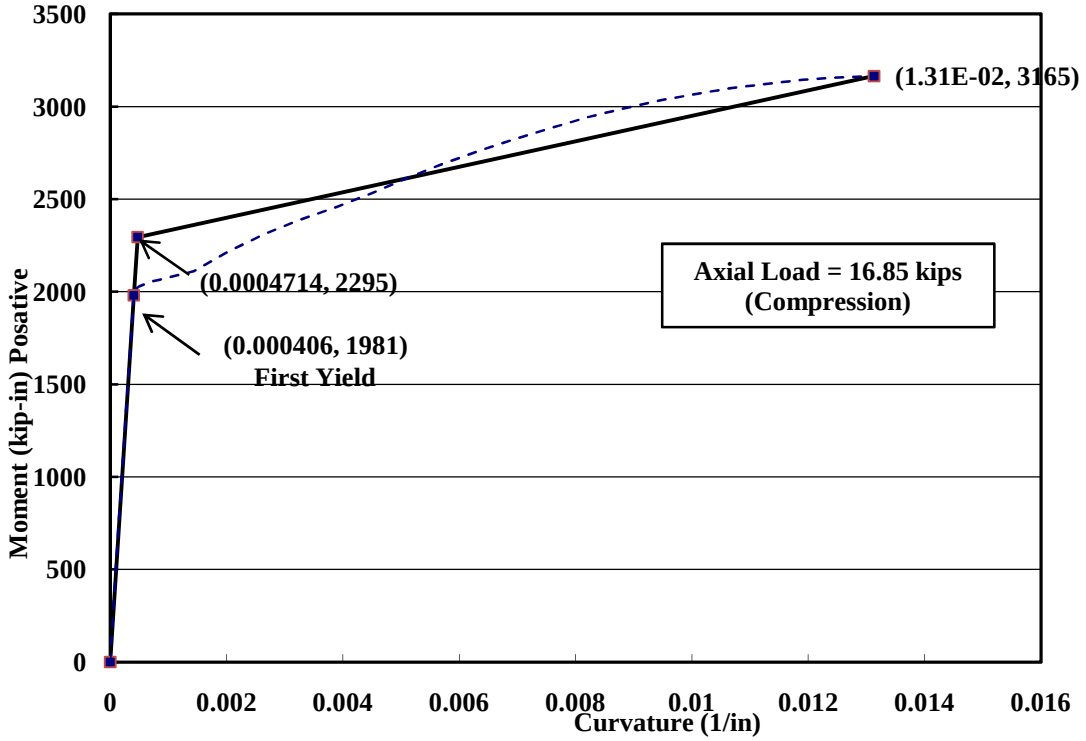

Figure 7-44: FSKJ24 Slab Negative M-ϕ Post Analysis

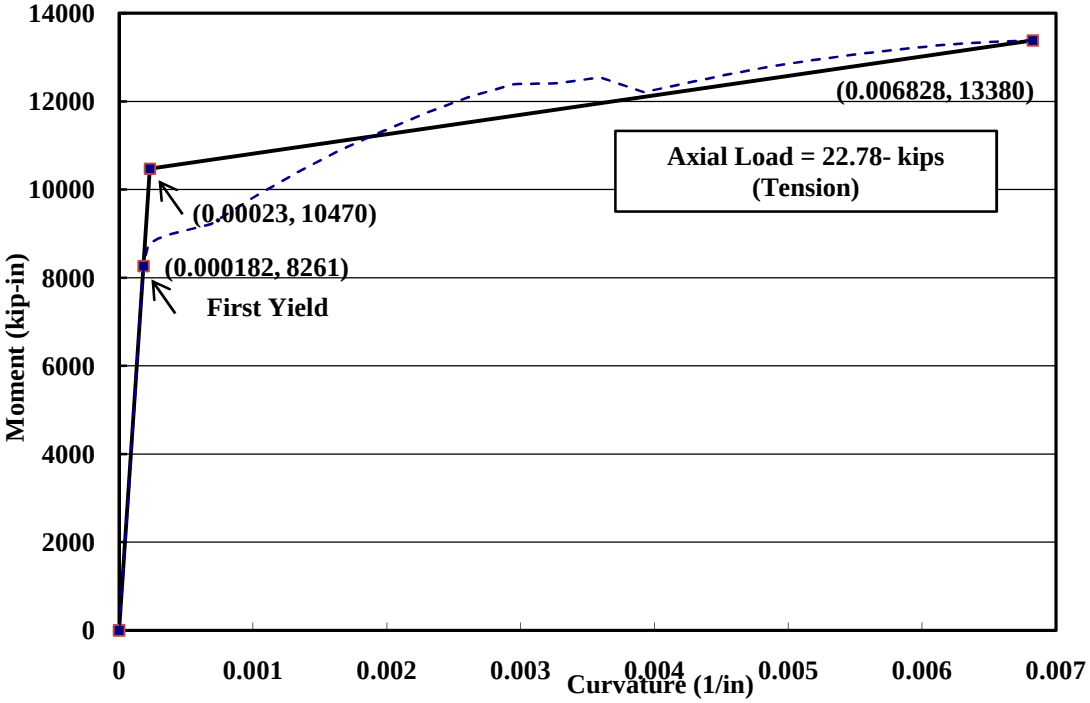

Figure 7-45: FSRCC24-M Slab Positive M-ϕ Post Analysis

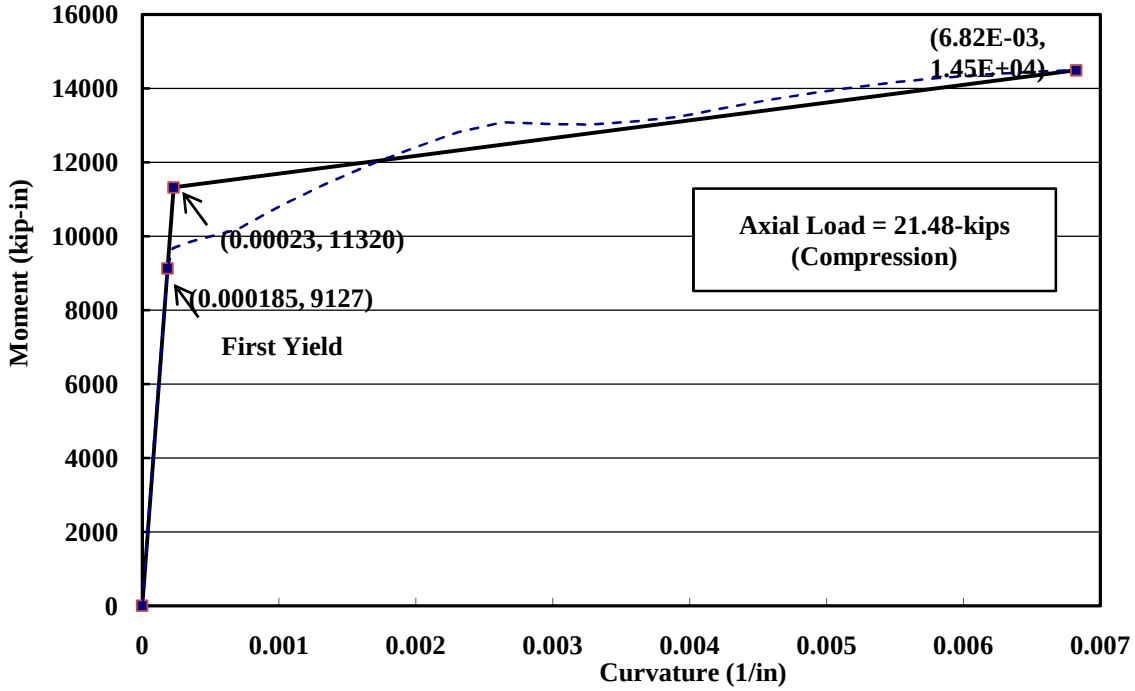

Figure 7-46: FSRCC24-M Slab Negative M-ϕ Post Analysis

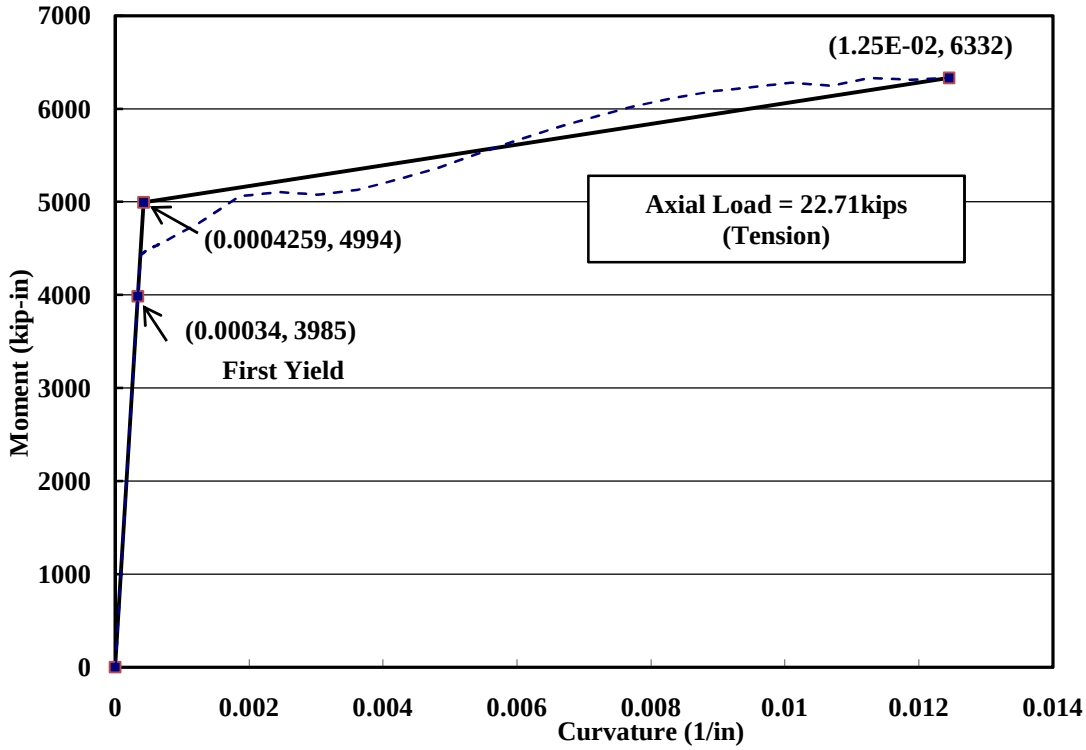

Figure 7-47: FSKJ24-M Slab Positive M-ϕ Post Analysis

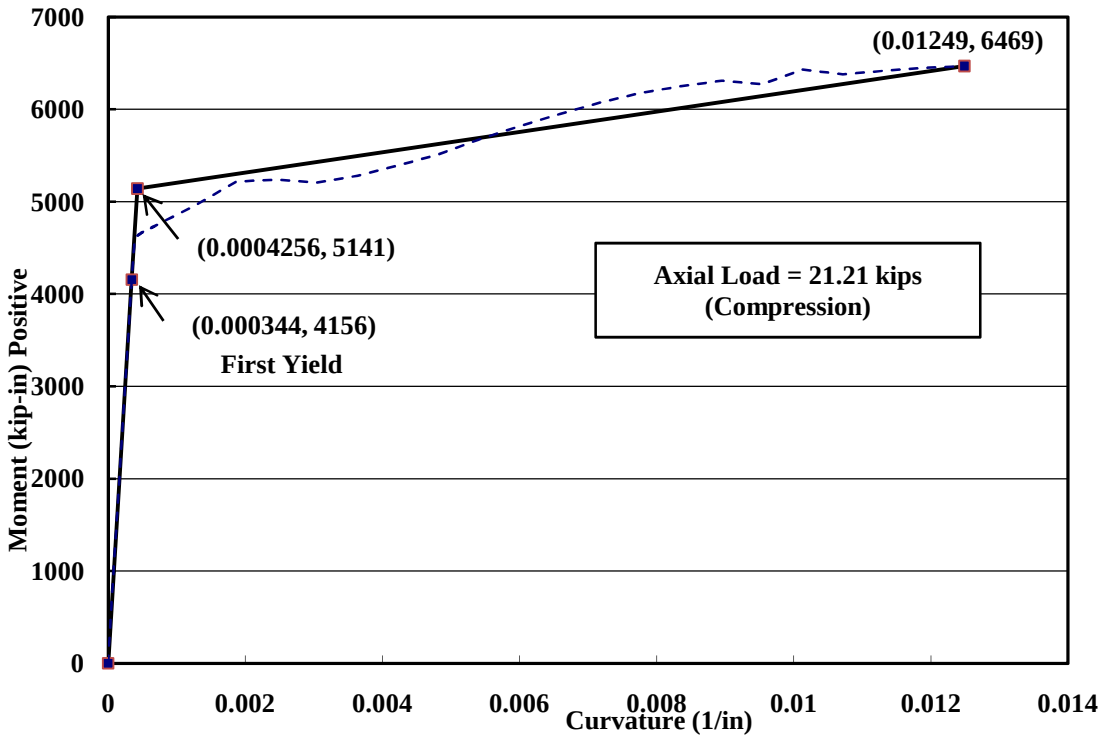

Figure 7-48: FSKJ24-M Slab Negative M-ϕ Post Analysis

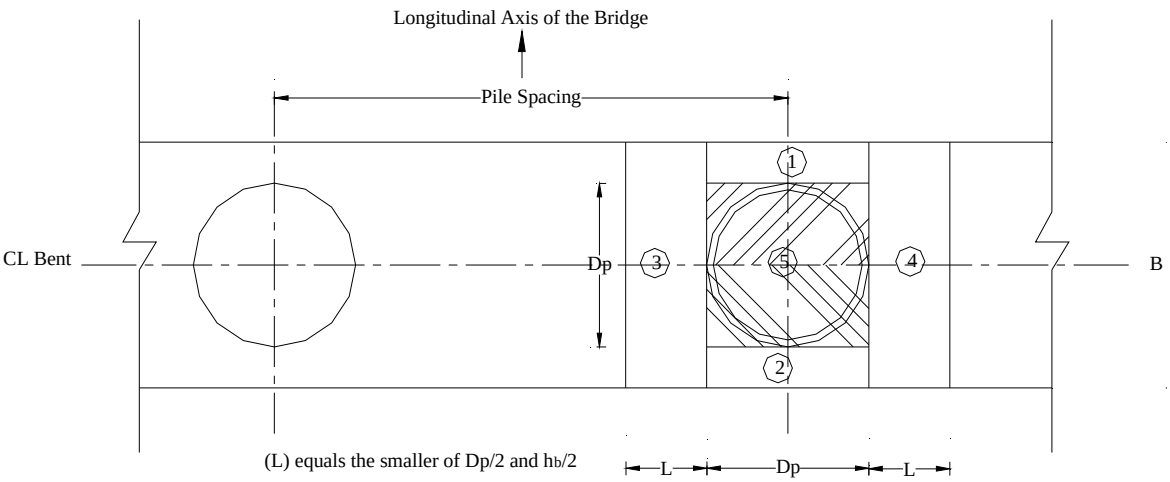

Figure 8-1: Plan View of Joint Reinforcement Locations for the T-Joint

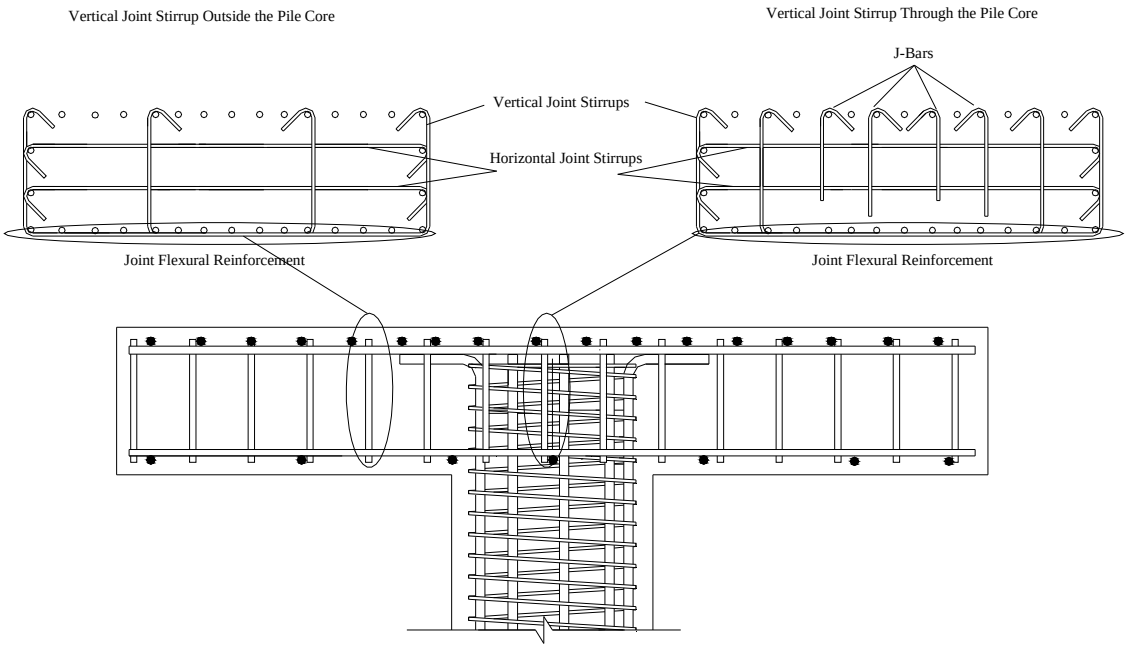

Figure 8-2: Recommended Joint Reinforcement Details

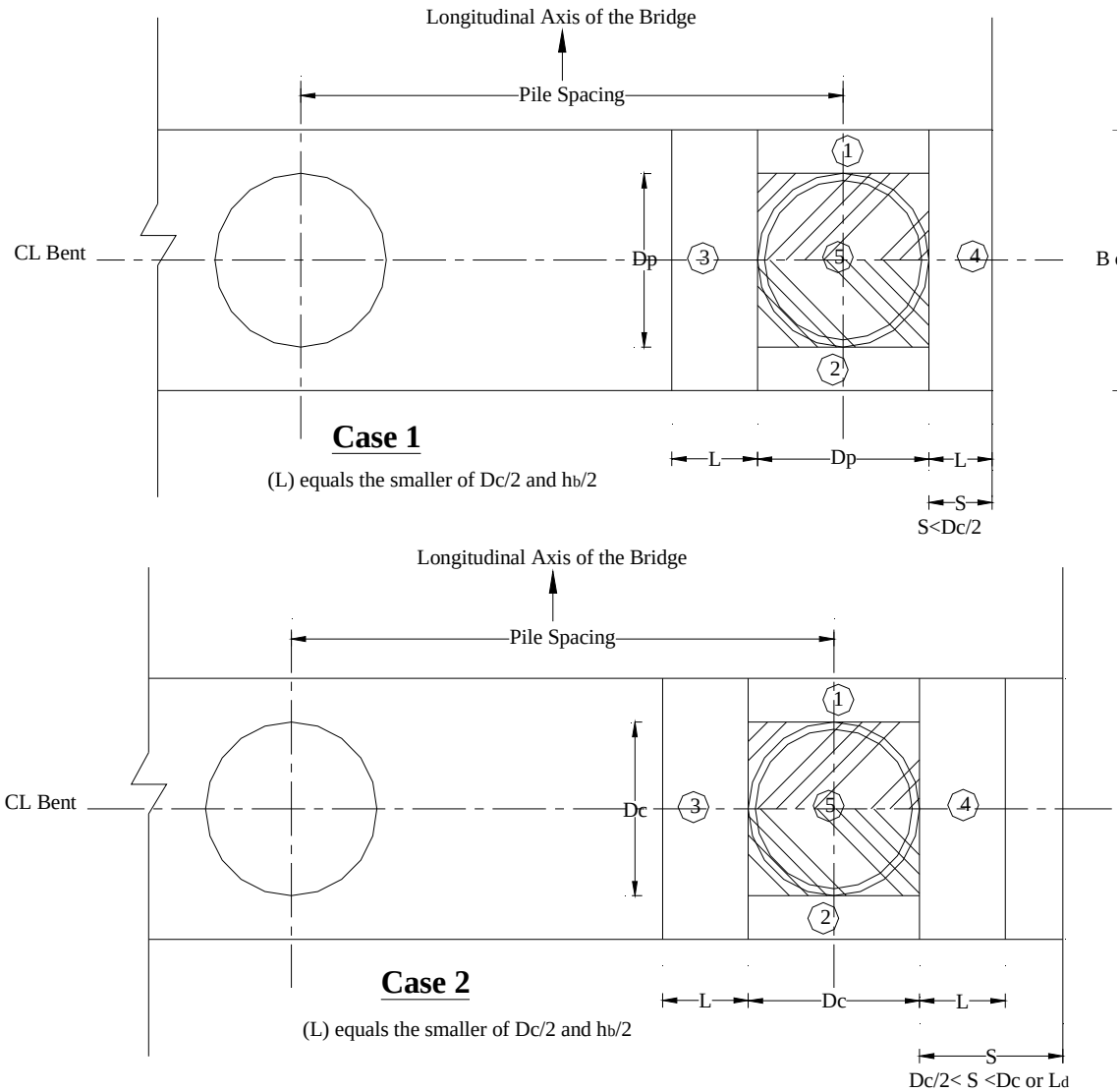

Figure 8-3: Plan View of Joint Reinforcement Locations for the Knee-Joint

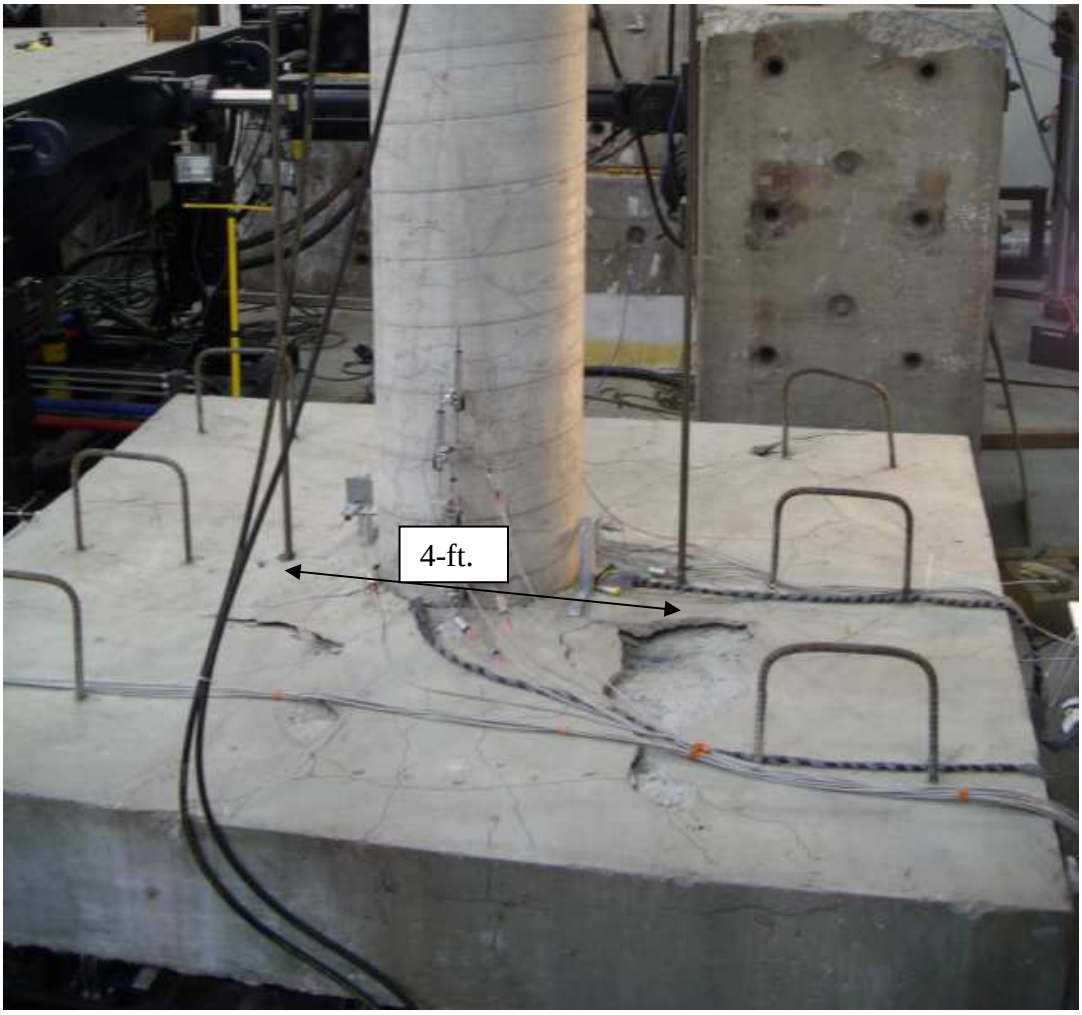

Figure 8-4: FSRCC24 Failure Mode

Appendix A

Specimen DCRCC1

(Drop-Cap T-Joint with 16-in.diameter pile)

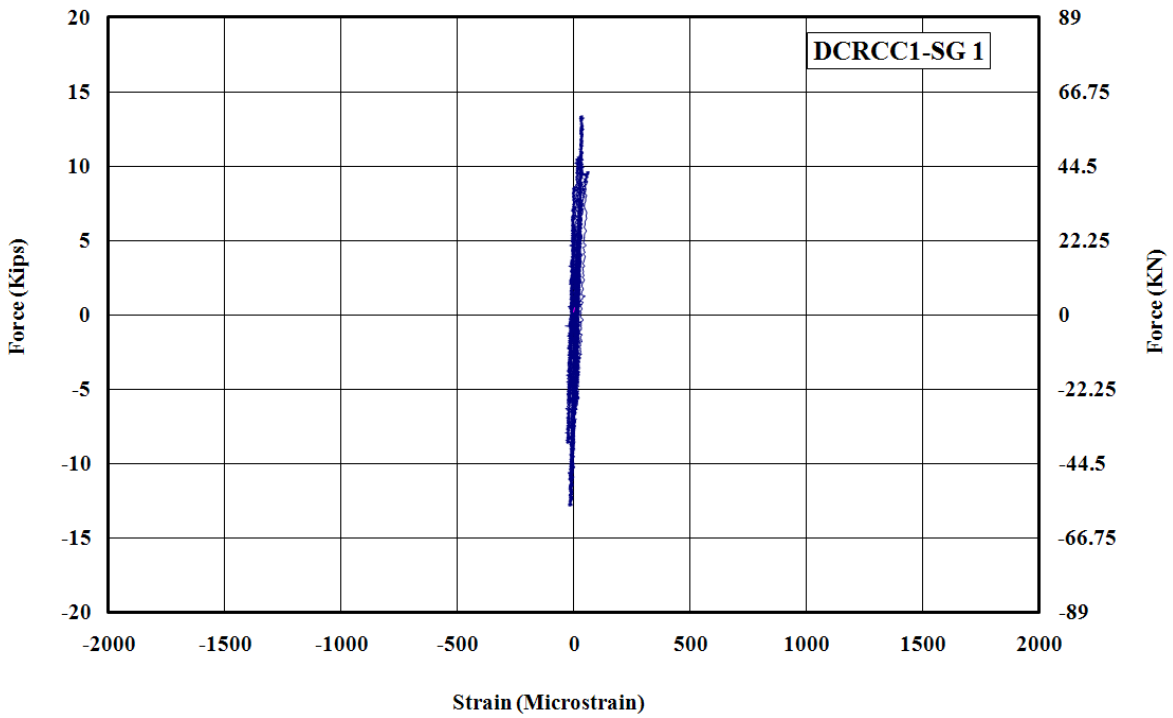

Figure A - 1: Measured Strain in Gauge No.1 for DCRCC1

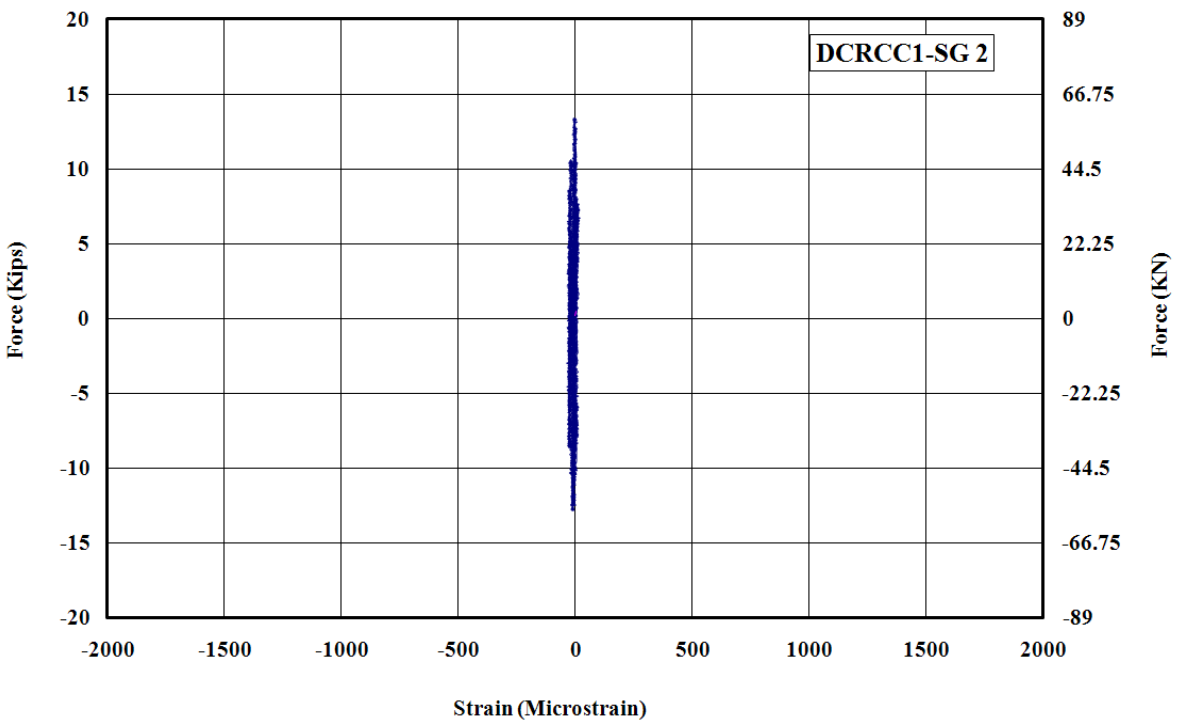

Figure A - 2: Measured Strain in Gauge No.2 for DCRCC1

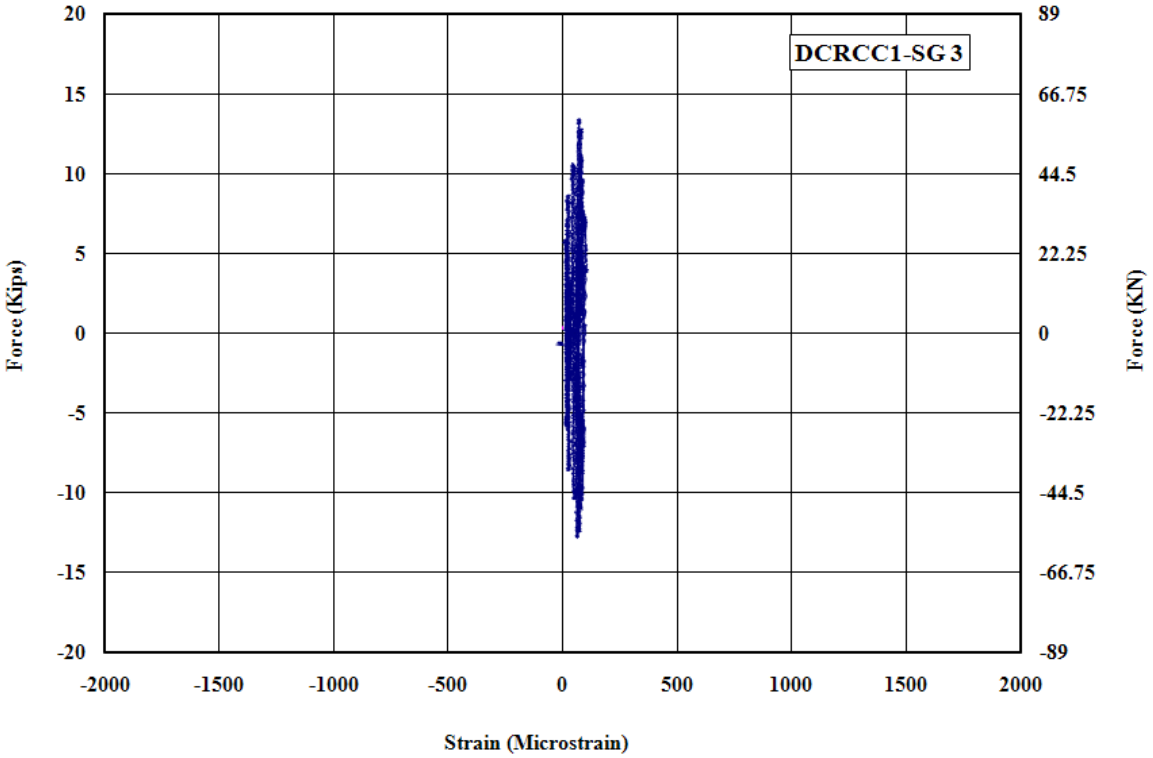

Figure A - 3: Measured Strain in Gauge No.3 for DCRCC1

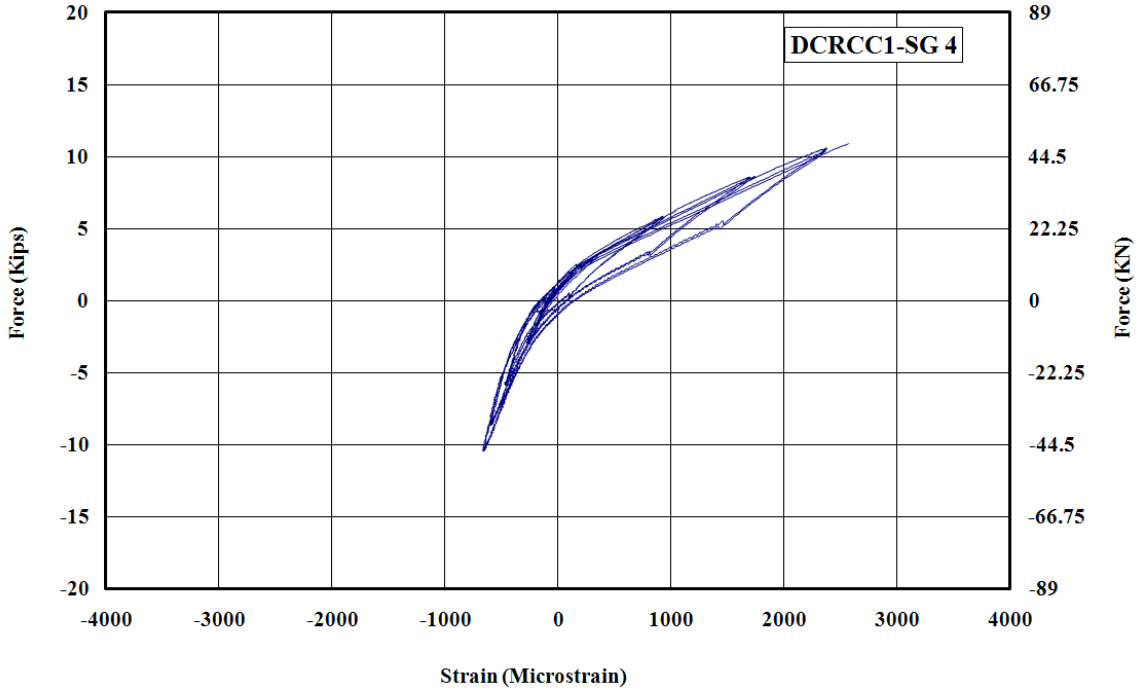

Figure A - 4: Measured Strain in Gauge No.4 for DCRCC1

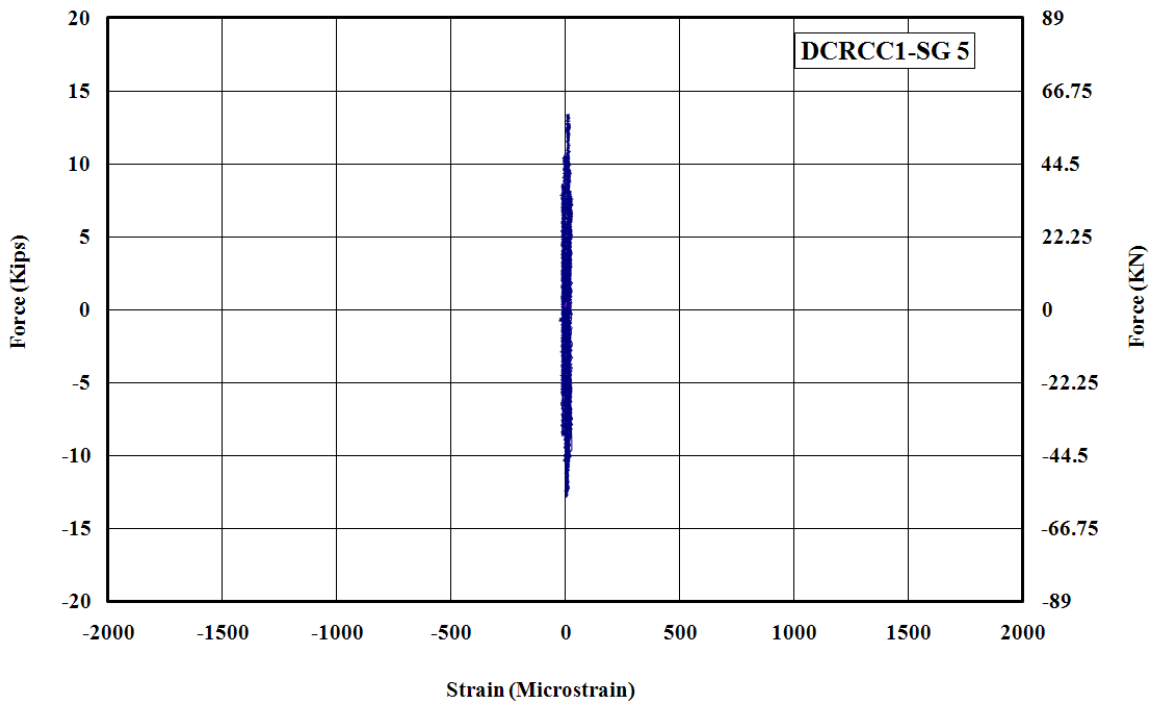

Figure A - 5: Measured Strain in Gauge No.5 for DCRCC1

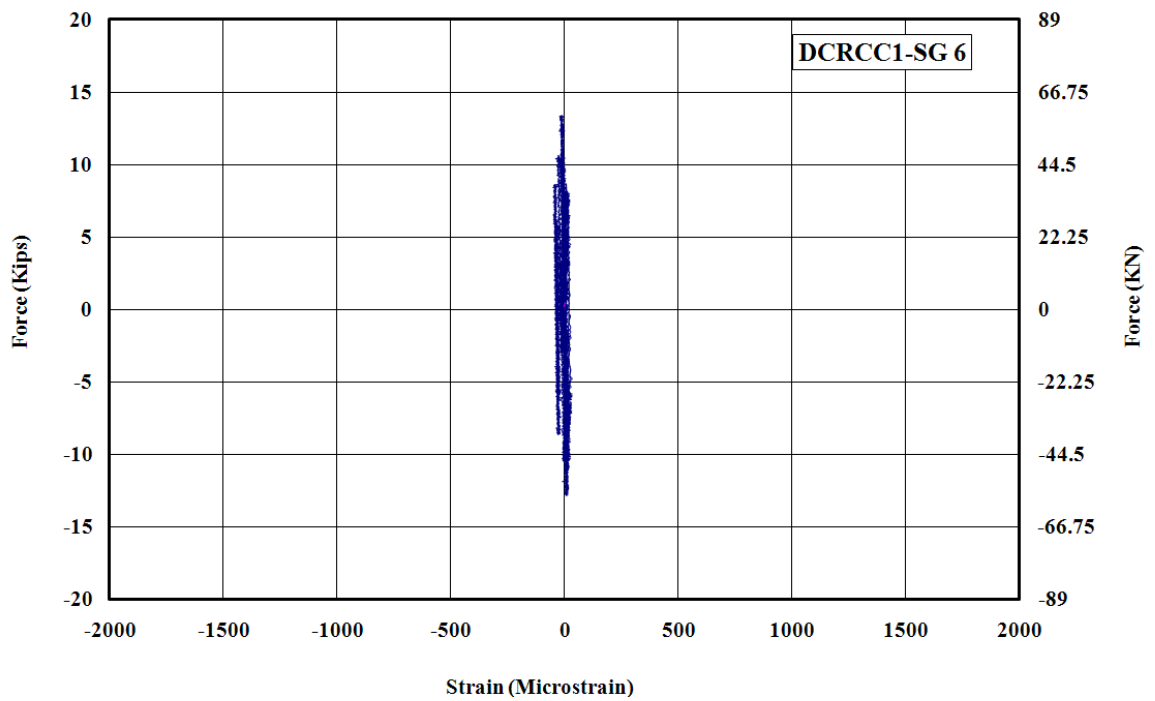

Figure A - 6: Measured Strain in Gauge No.6 for DCRCC1

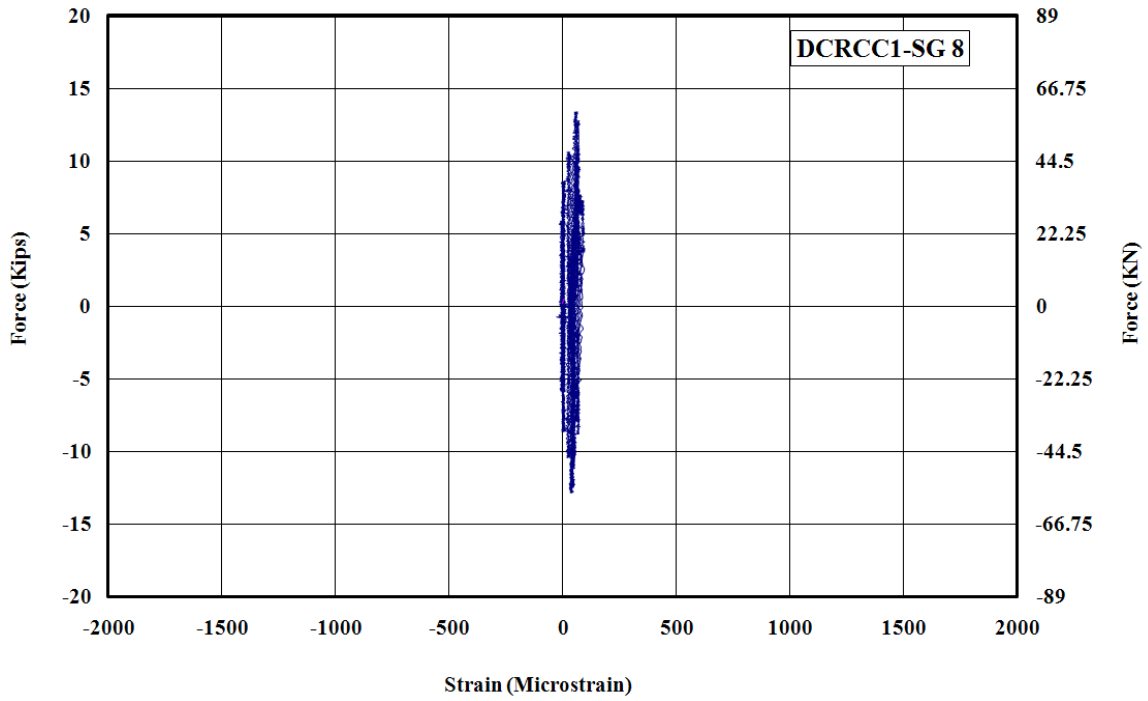

Figure A - 7: Measured Strain in Gauge No.8 for DCRCC1

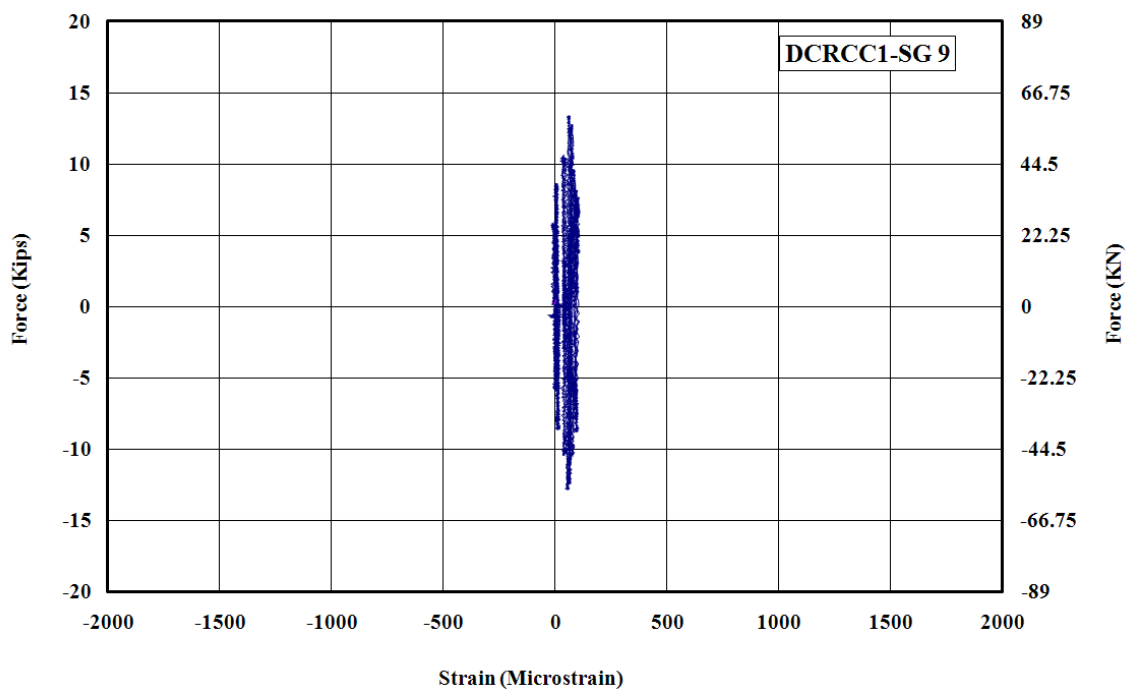

Figure A - 8: Measured Strain in Gauge No.9 for DCRCC1

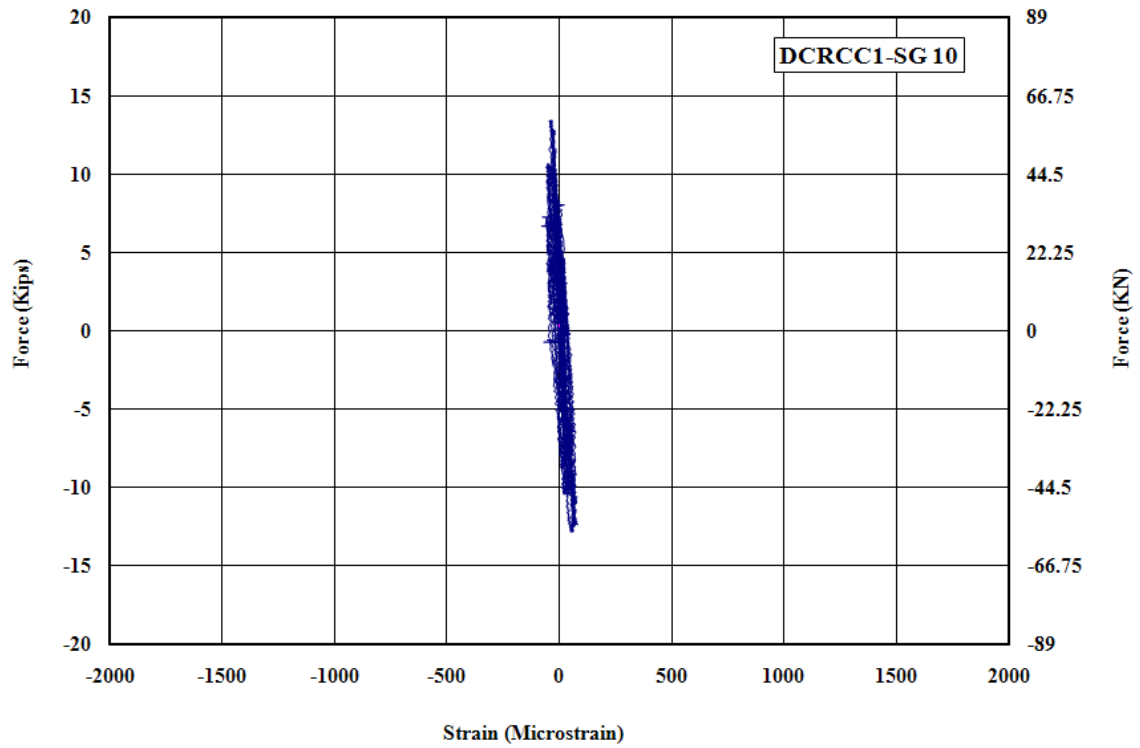

Figure A - 9: Measured Strain in Gauge No.10 for DCRCC1

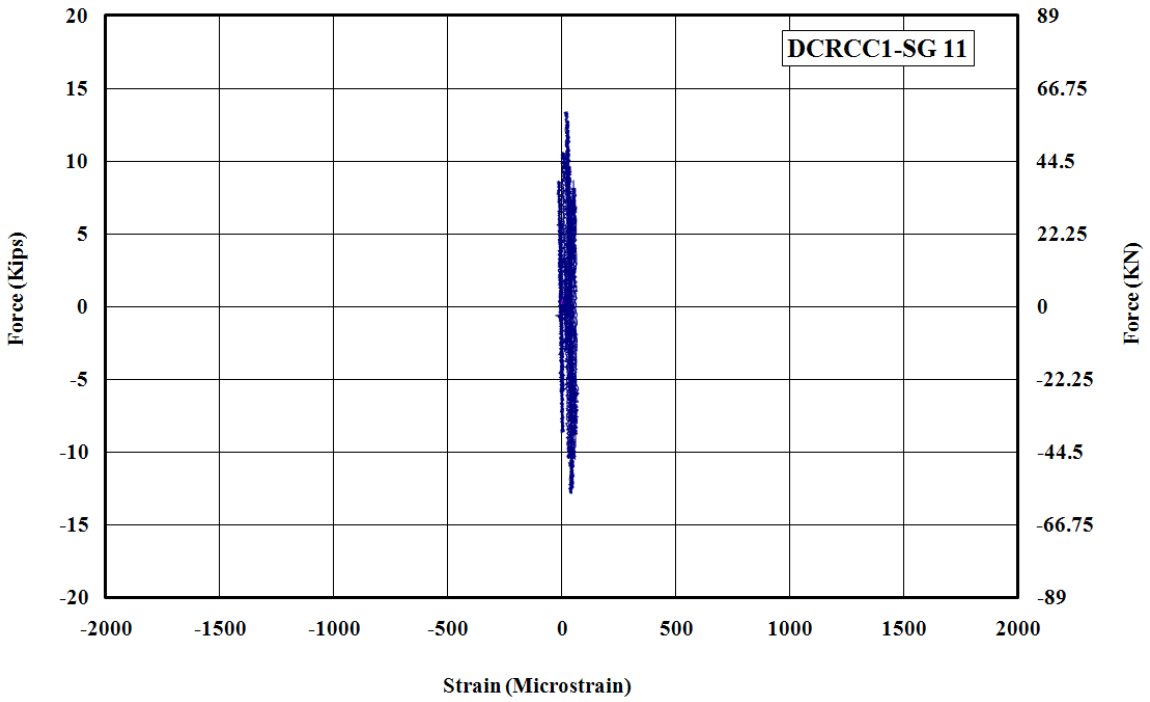

Figure A - 10: Measured Strain in Gauge No.11 for DCRCC1

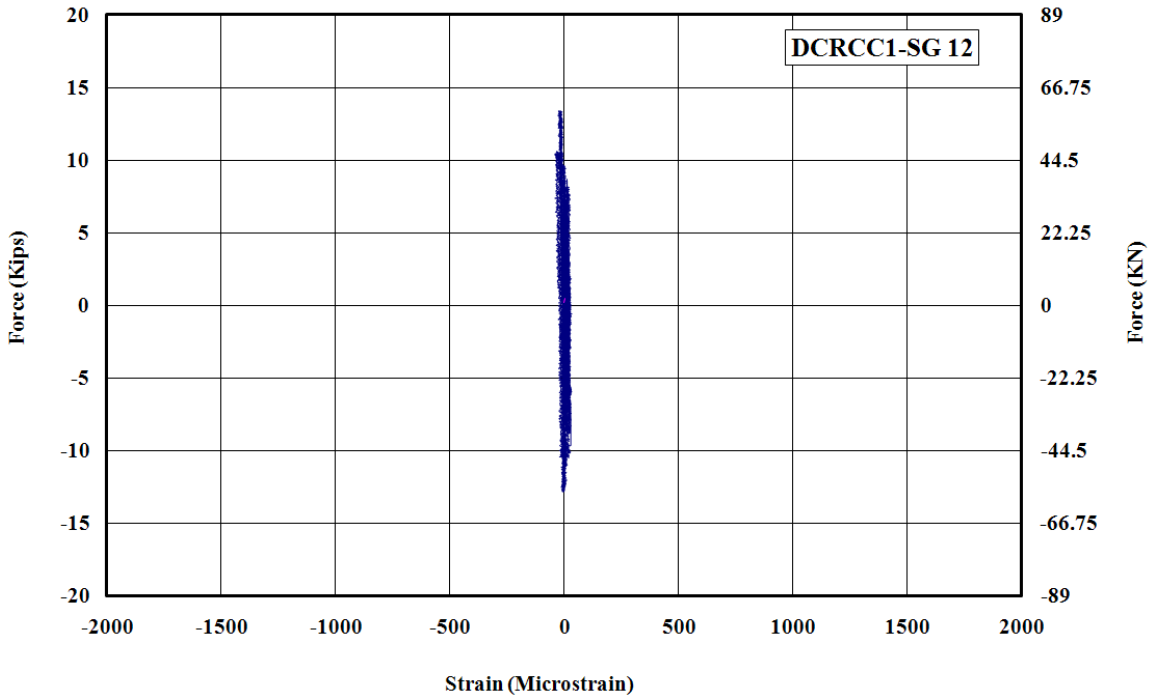

Figure A - 11: Measured Strain in Gauge No.12 for DCRCC1

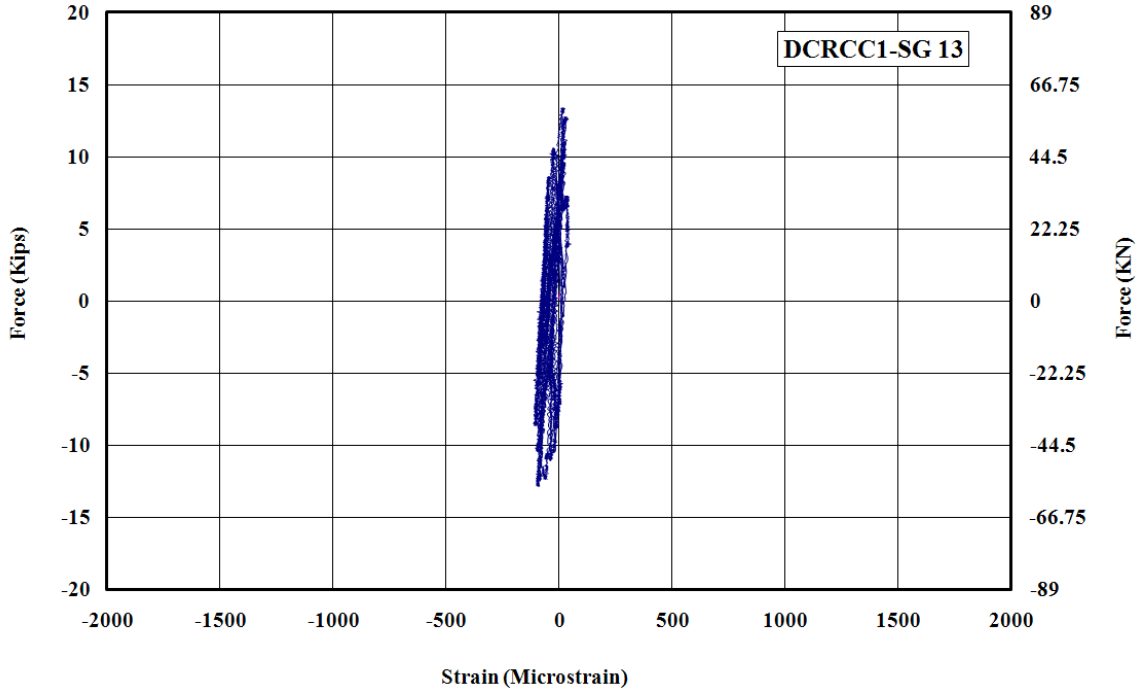

Figure A - 12: Measured Strain in Gauge No.13 for DCRCC1

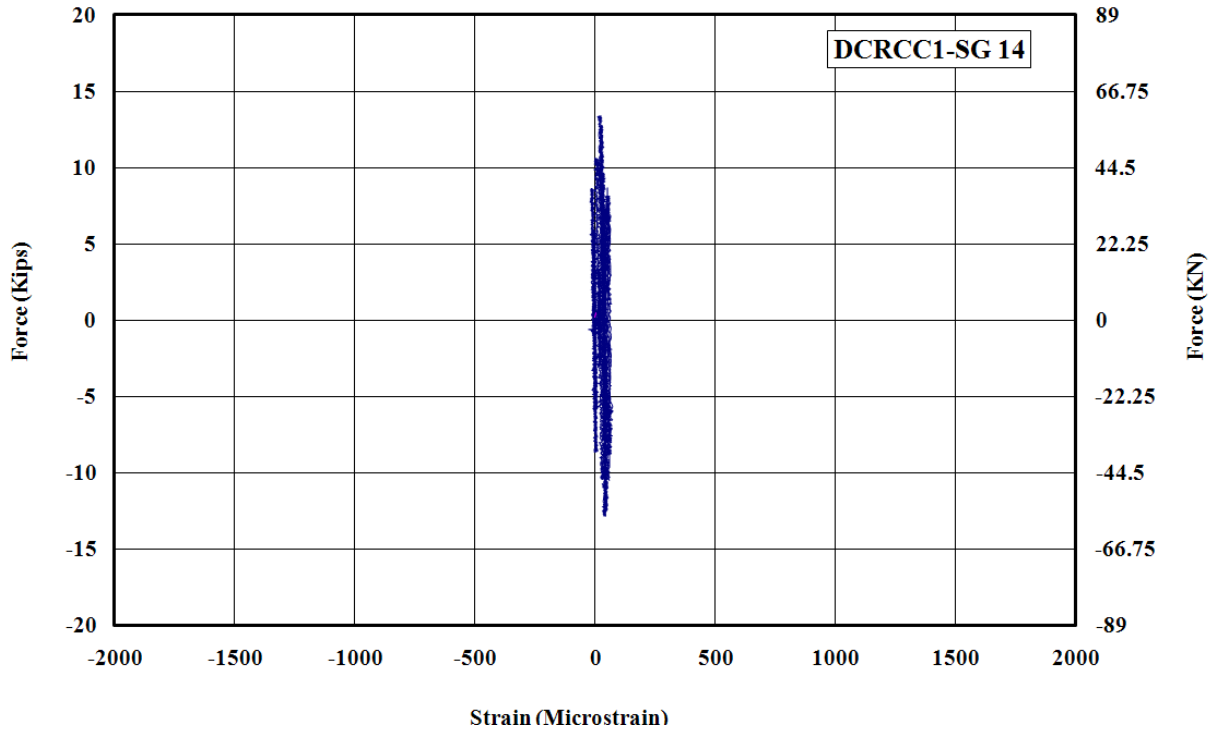

Figure A - 13: Measured Strain in Gauge No.14 for DCRCC1

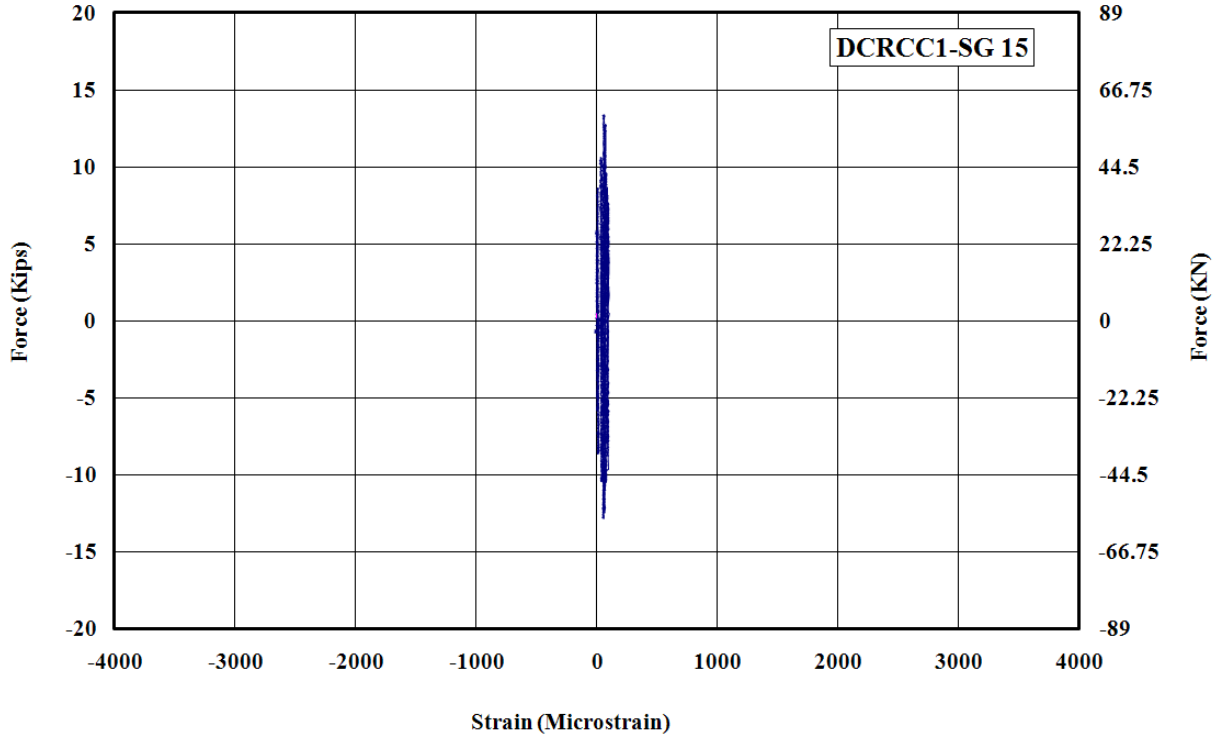

Figure A - 14: Measured Strain in Gauge No.15 for DCRCC1

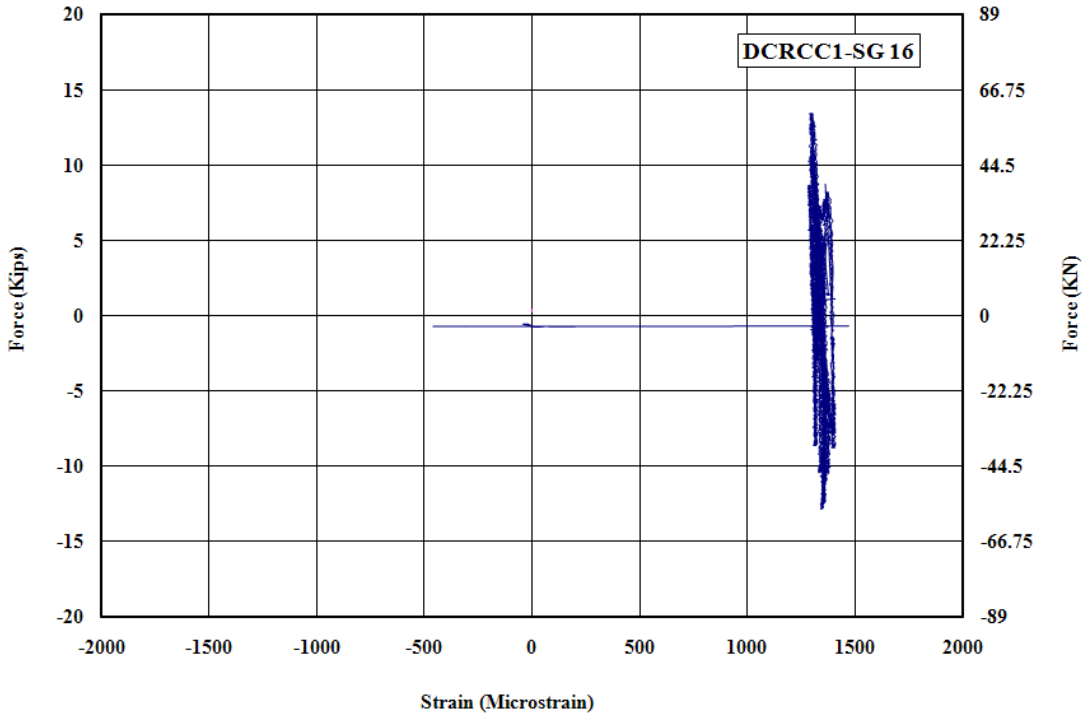

Figure A - 15: Measured Strain in Gauge No.16 for DCRCC1

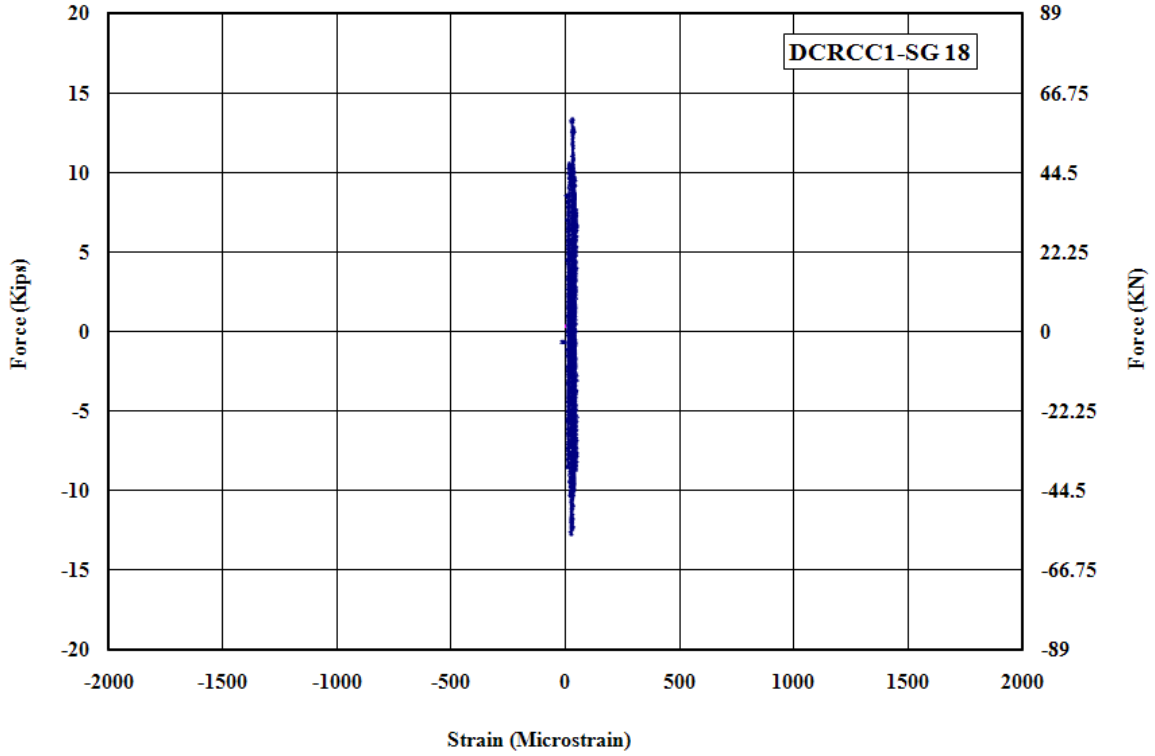

Figure A - 16: Measured Strain in Gauge No.18 for DCRCC1

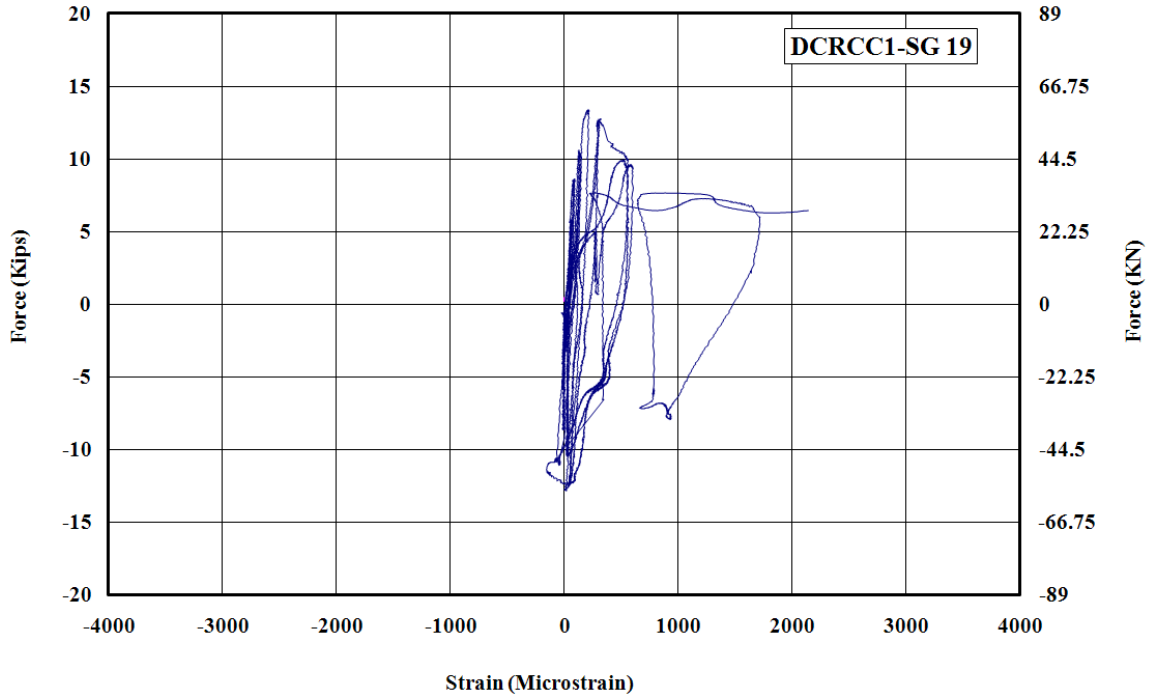

Figure A - 17: Measured Strain in Gauge No.19 for DCRCC1

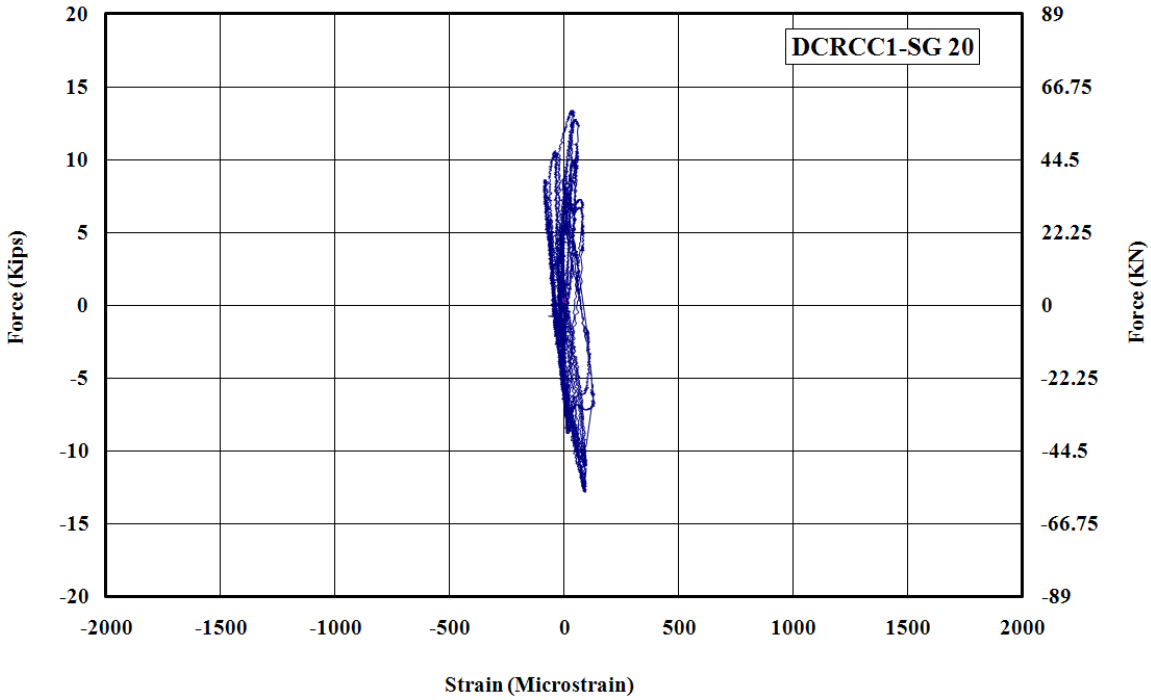

Figure A - 18: Measured Strain in Gauge No.20 for DCRCC1

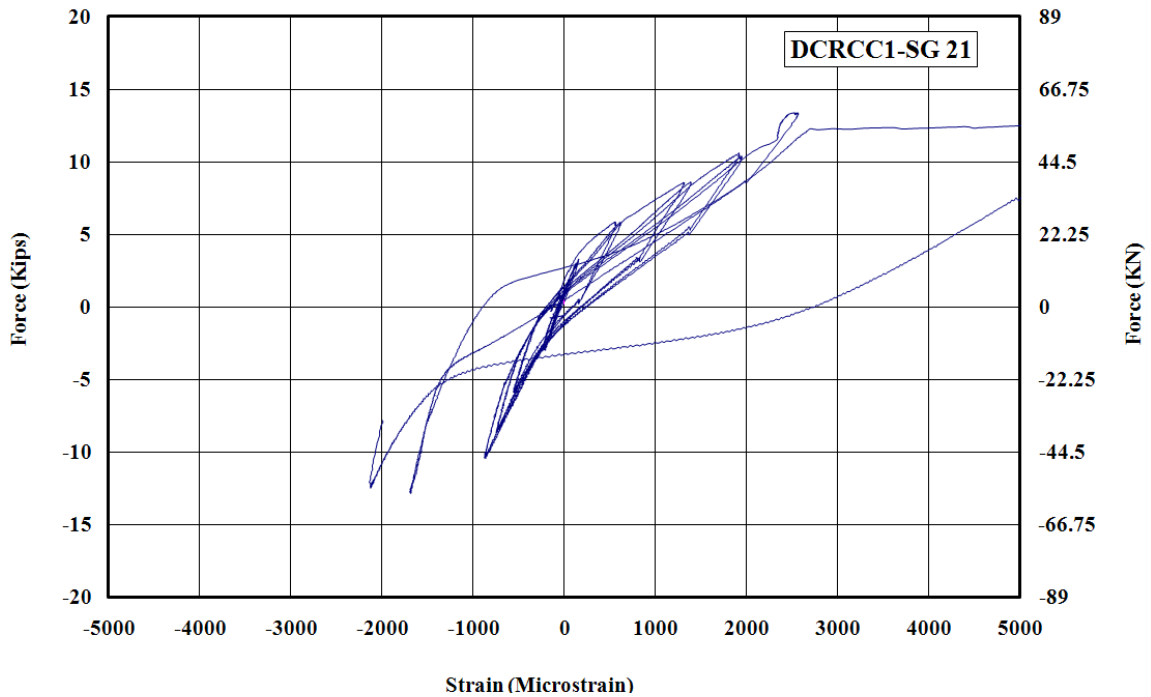

Figure A - 19: Measured Strain in Gauge No.21 for DCRCC1

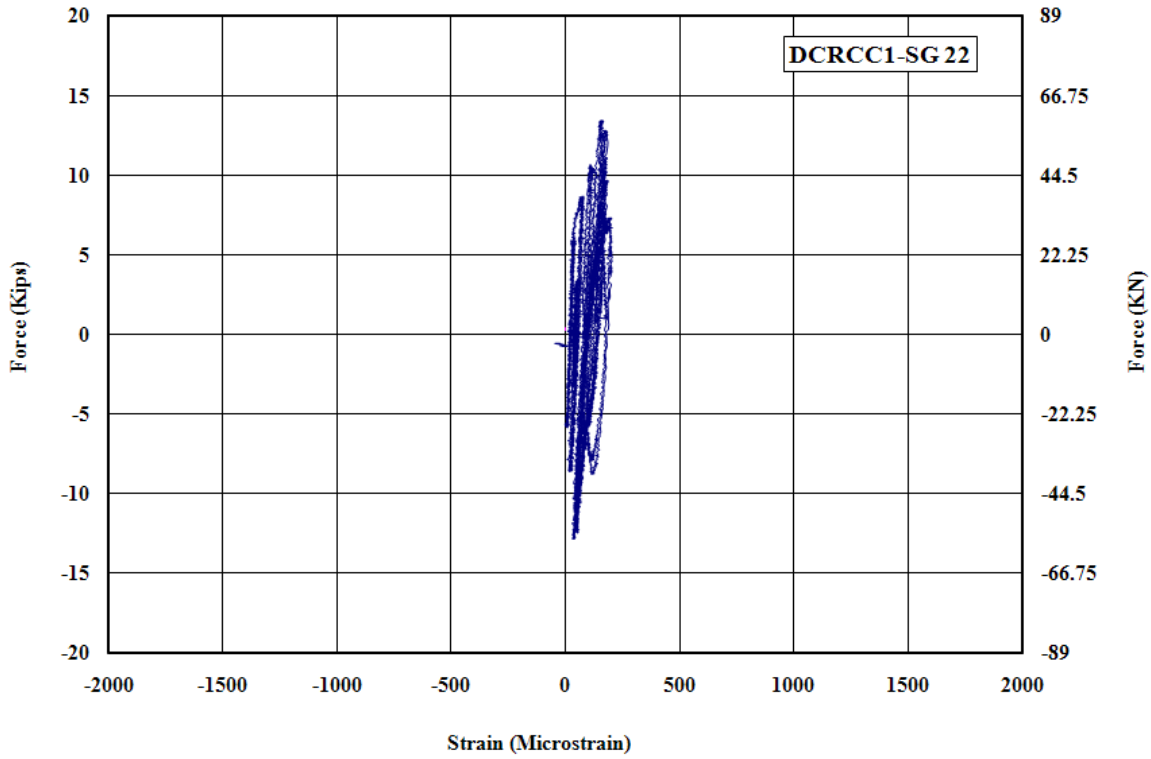

Figure A - 20: Measured Strain in Gauge No.22 for DCRCC1

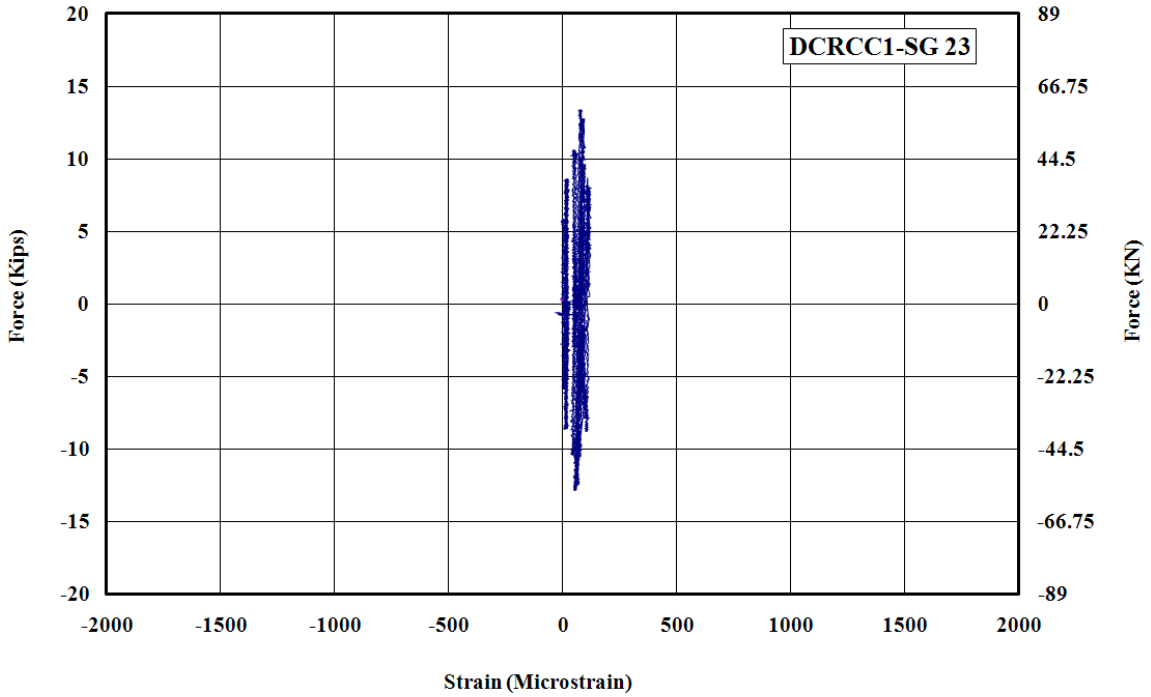

Figure A - 21: Measured Strain in Gauge No.23 for DCRCC1

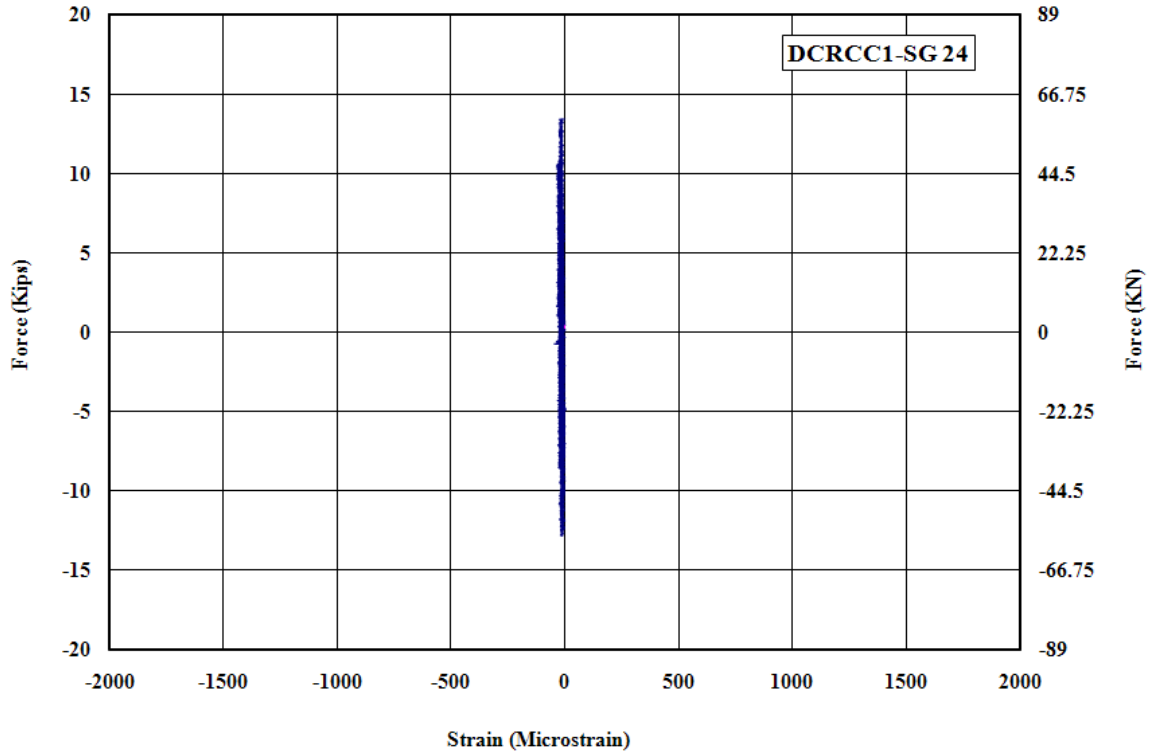

Figure A - 22: Measured Strain in Gauge No.24 for DCRCC1

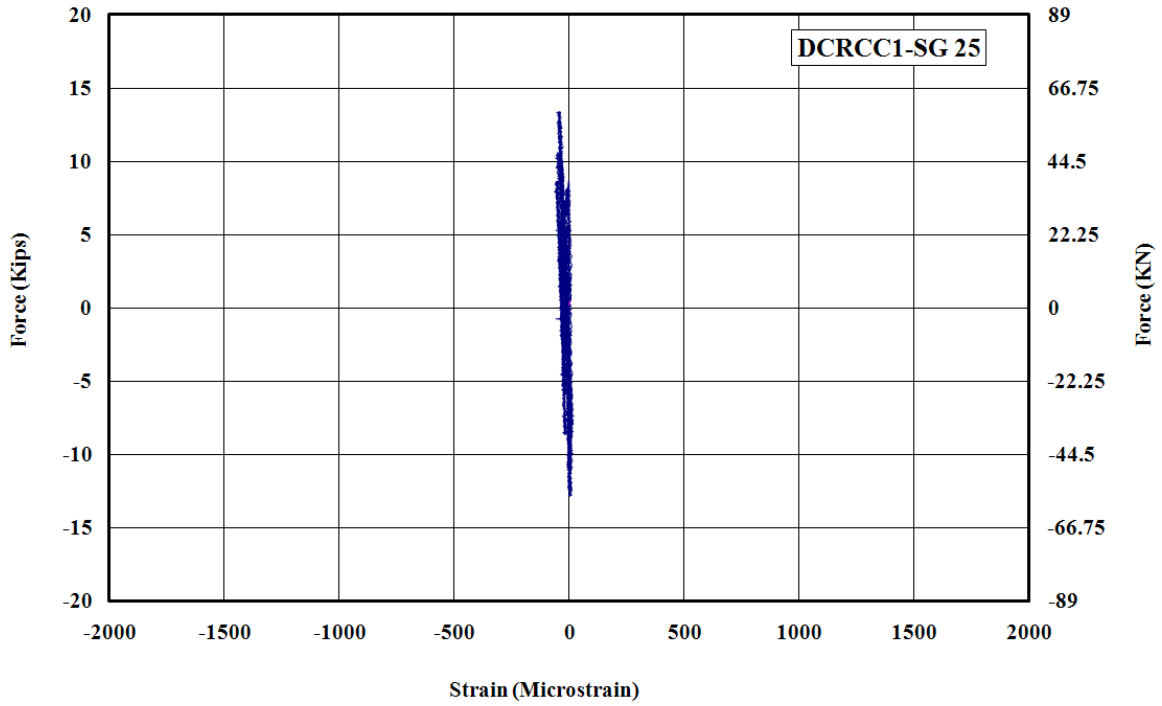

Figure A - 23: Measured Strain in Gauge No.25 for DCRCC1

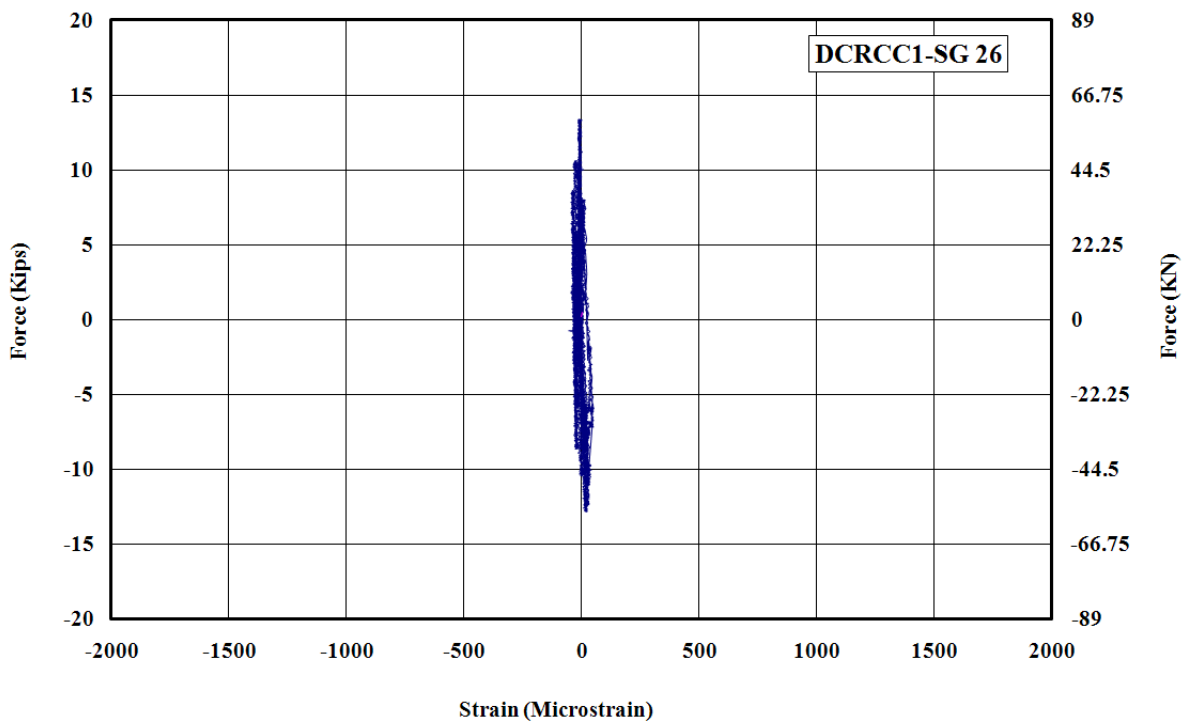

Figure A - 24: Measured Strain in Gauge No.26 for DCRCC1

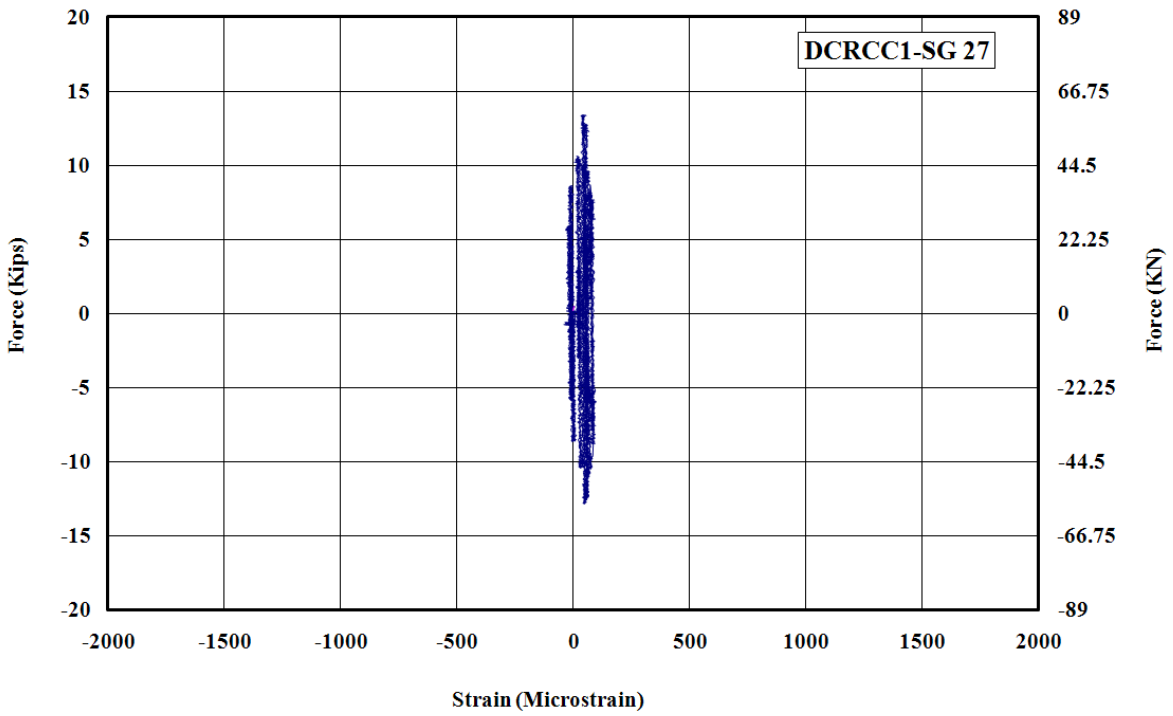

Figure A - 25: Measured Strain in Gauge No.27 for DCRCC1

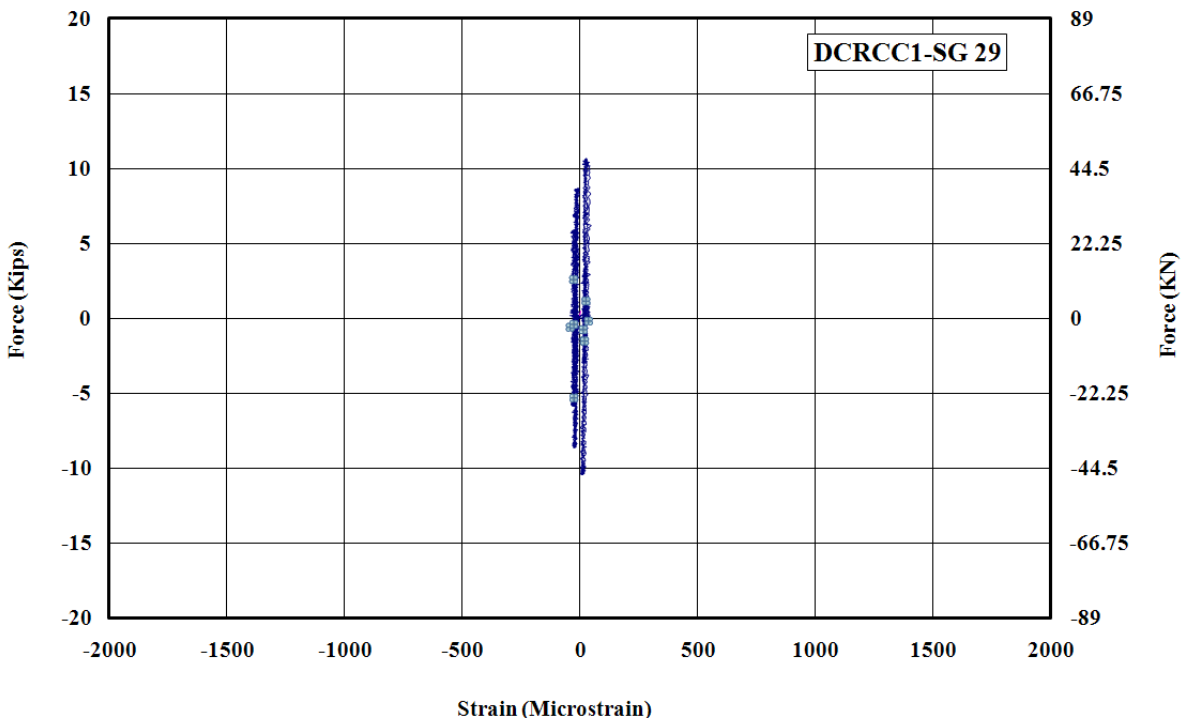

Figure A - 26: Measured Strain in Gauge No.29 for DCRCC1

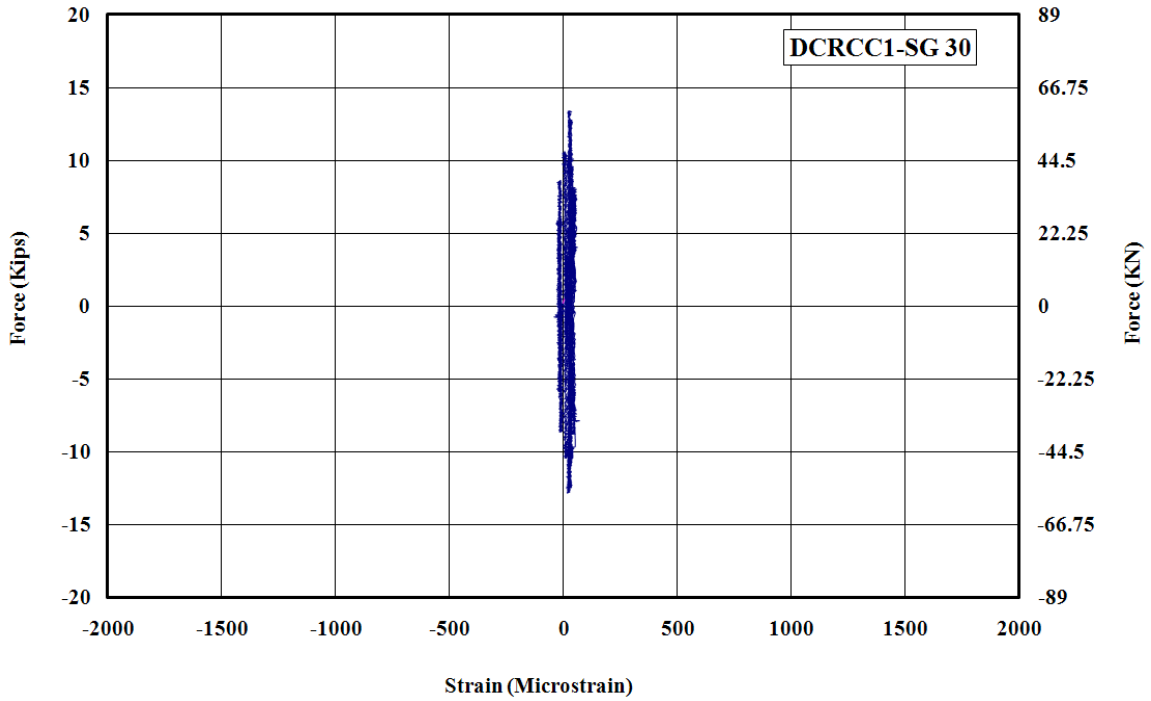

Figure A - 27: Measured Strain in Gauge No.30 for DCRCC1

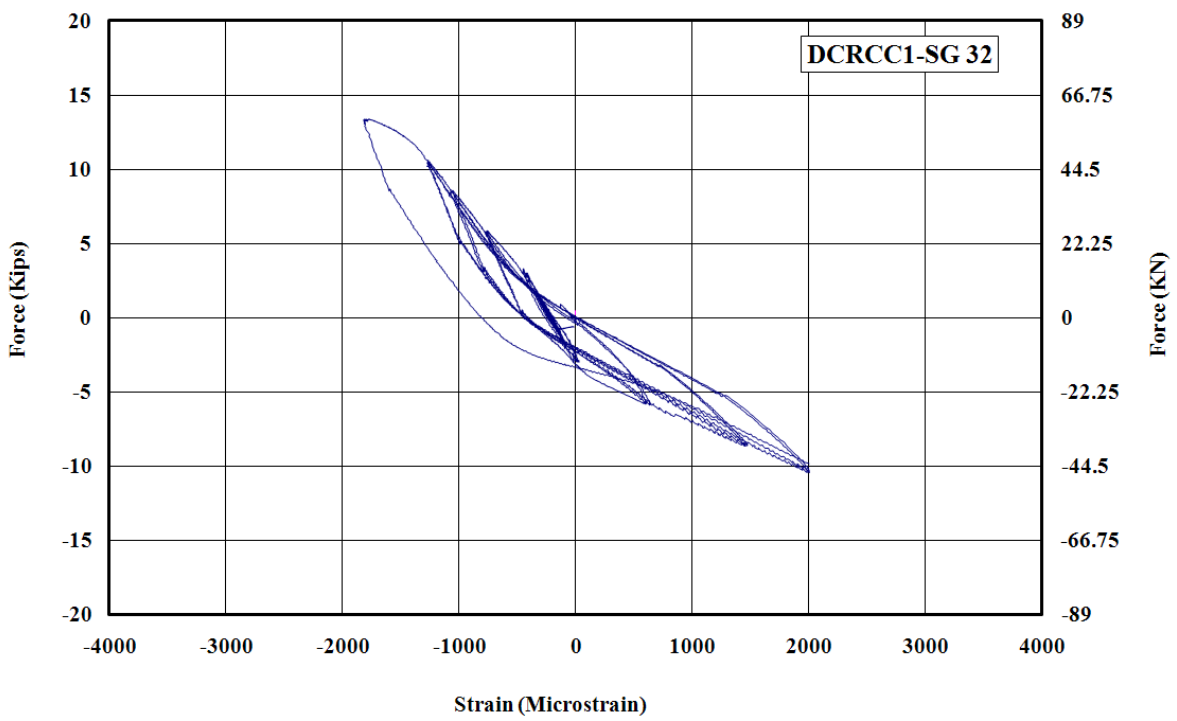

Figure A - 28: Measured Strain in Gauge No.32 for DCRCC1

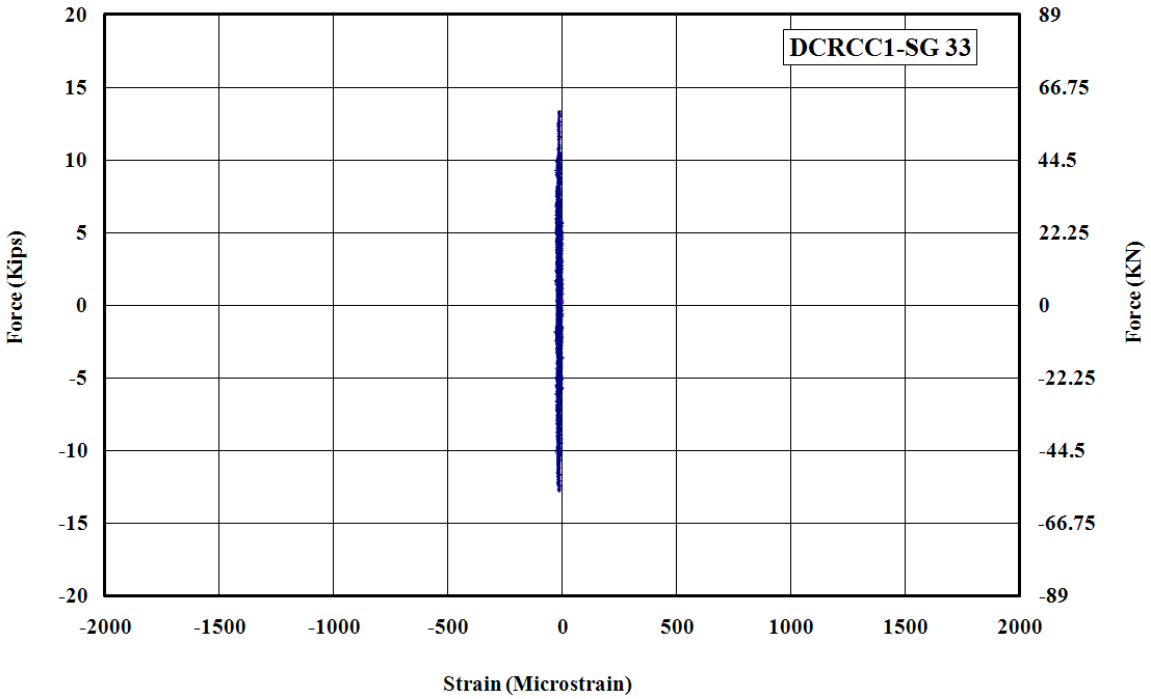

Figure A - 29: Measured Strain in Gauge No.33 for DCRCC1

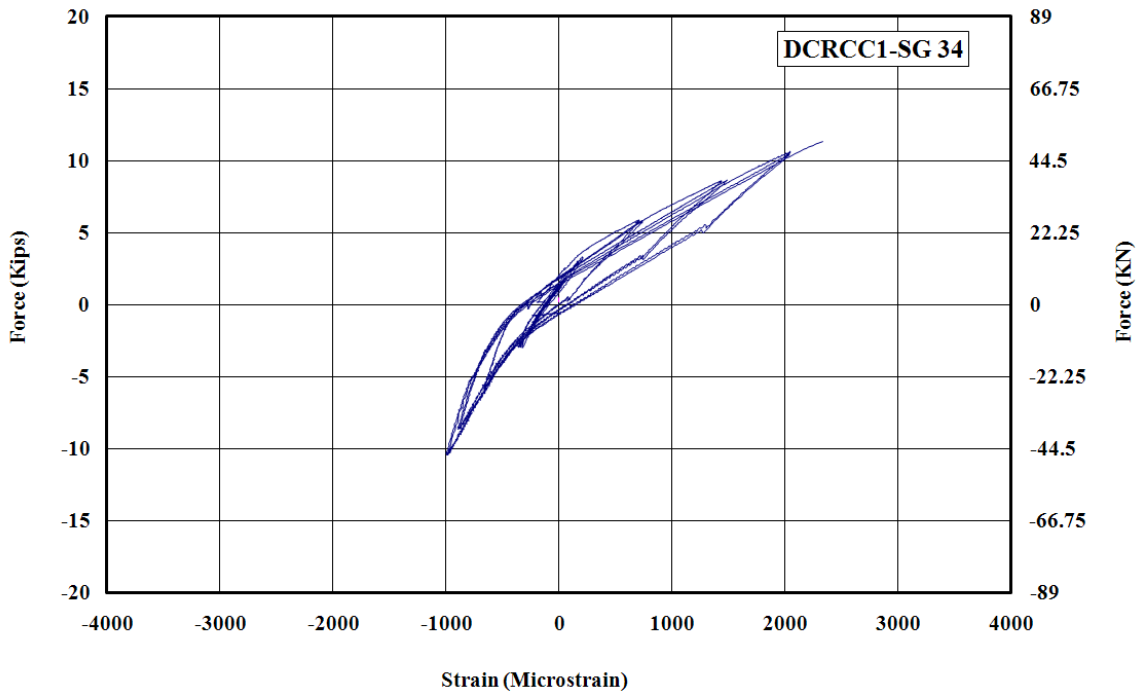

Figure A - 30: Measured Strain in Gauge No.34 for DCRCC1

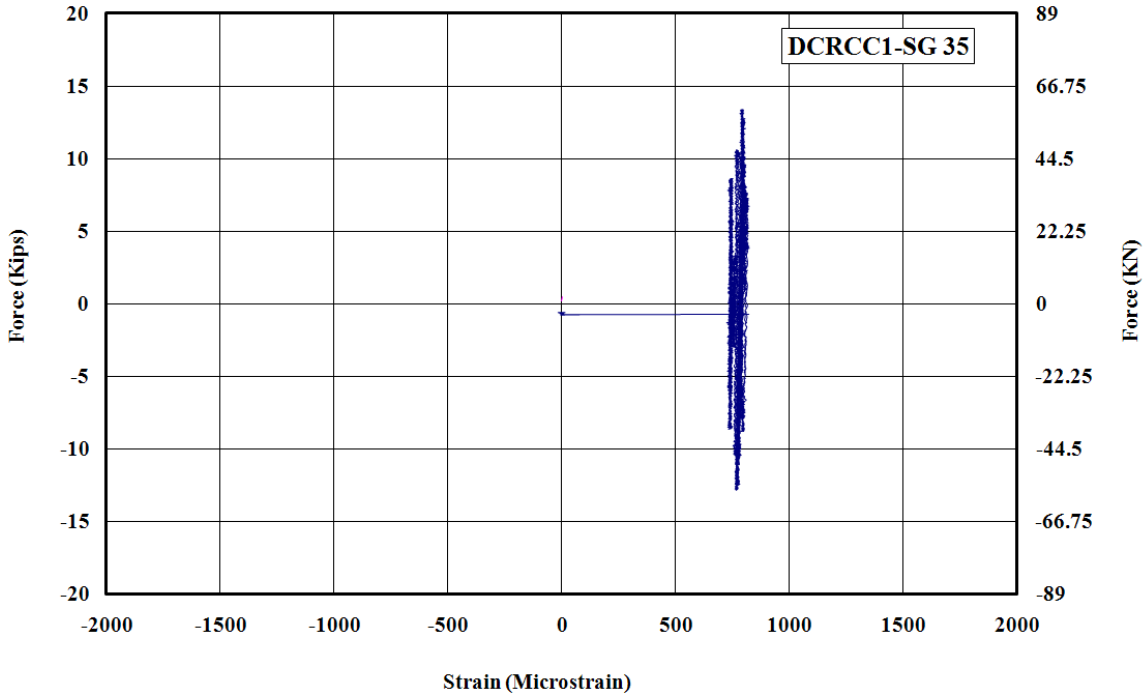

Figure A - 31: Measured Strain in Gauge No.35 for DCRCC1

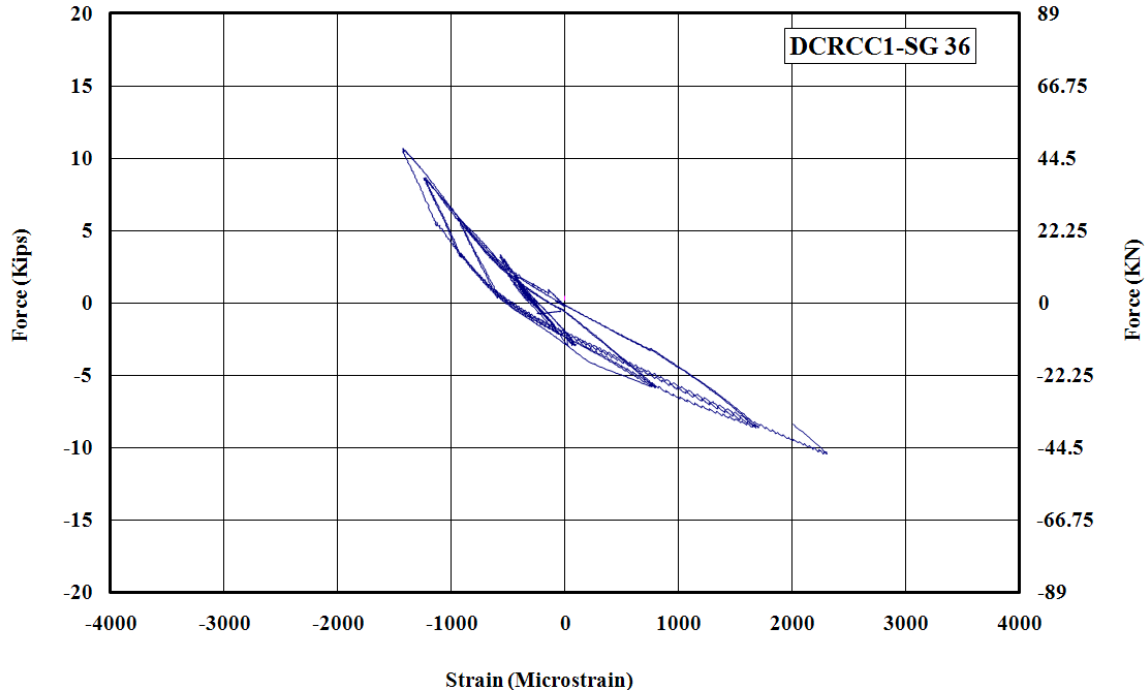

Figure A - 32: Measured Strain in Gauge No.36 for DCRCC1

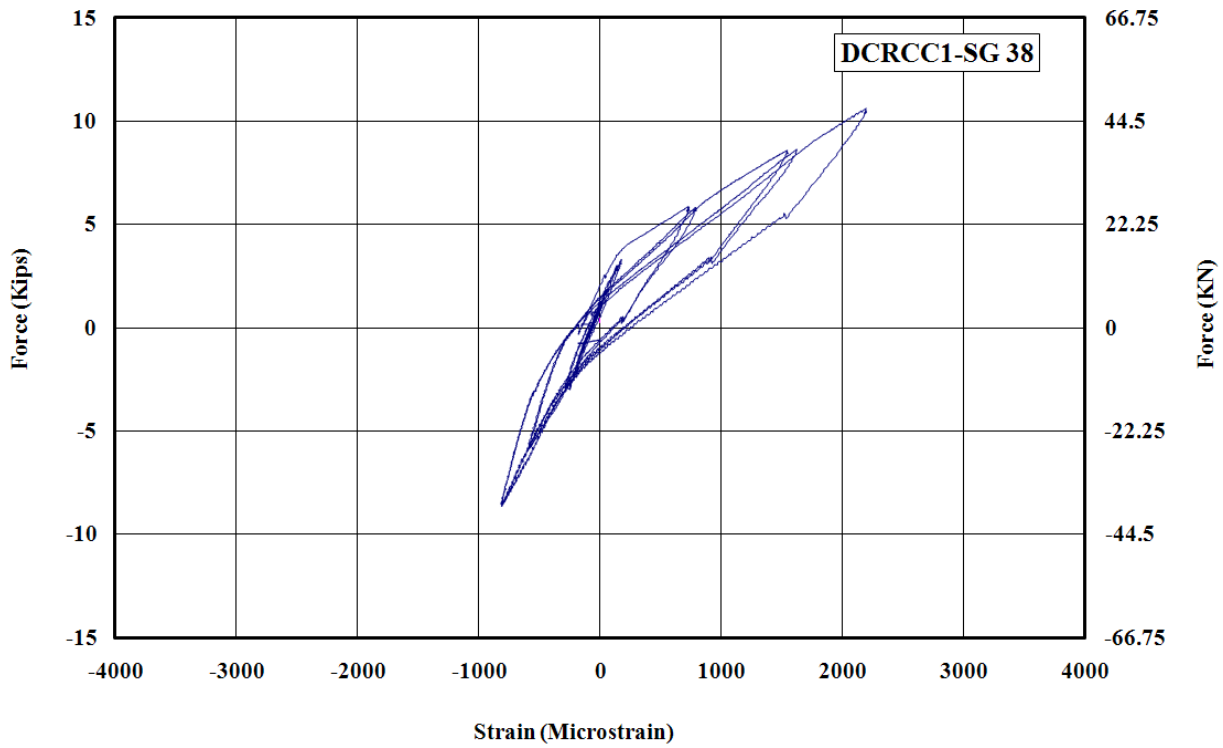

Figure A - 33: Measured Strain in Gauge No.38 for DCRCC1

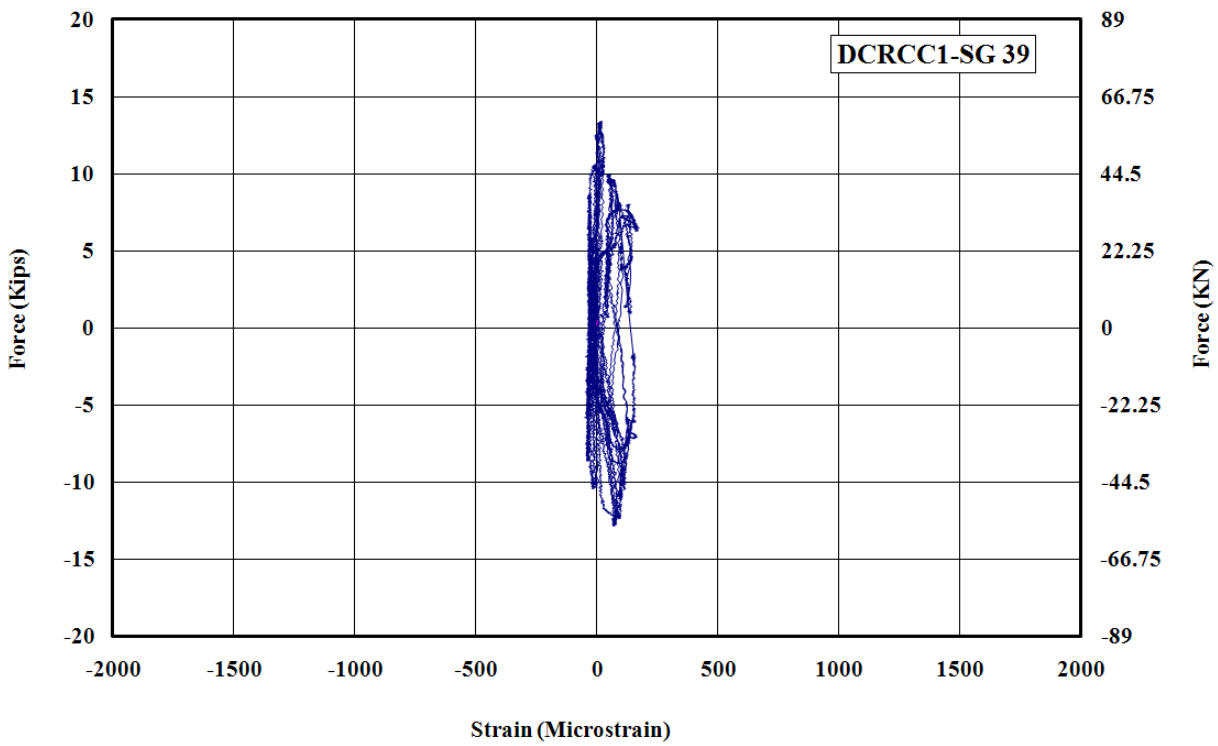

Figure A - 34: Measured Strain in Gauge No.39 for DCRCC1

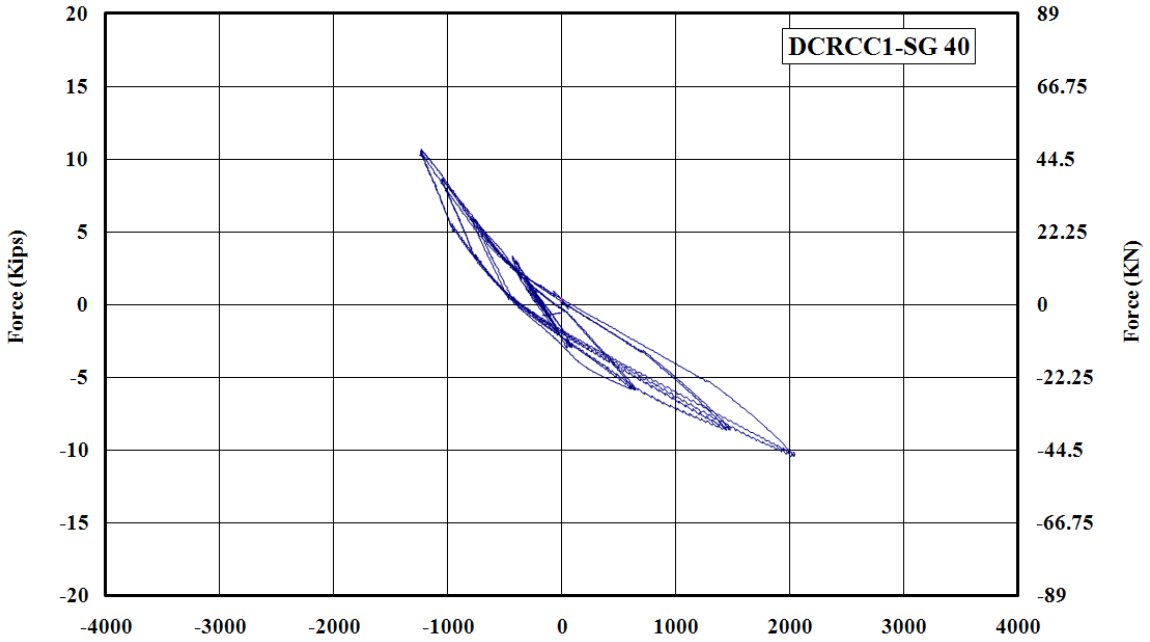

Figure A - 35: Measured Strain in Gauge No.40 for DCRCC1

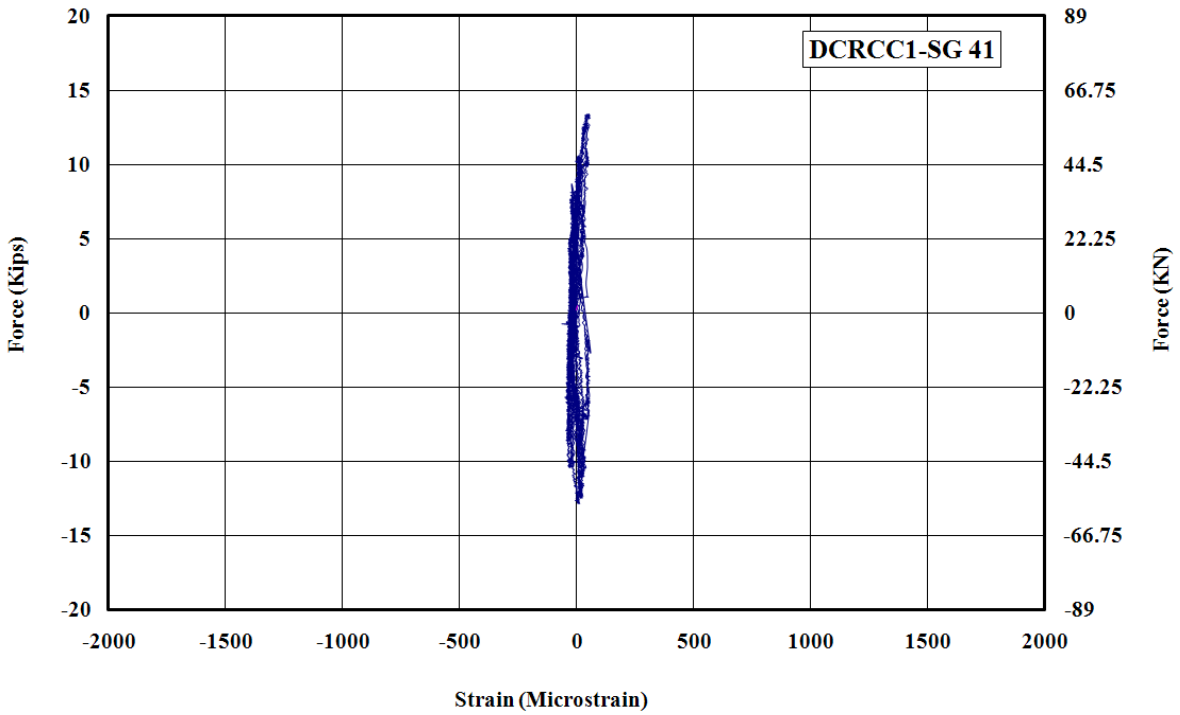

Figure A - 36: Measured Strain in Gauge No.41 for DCRCC1

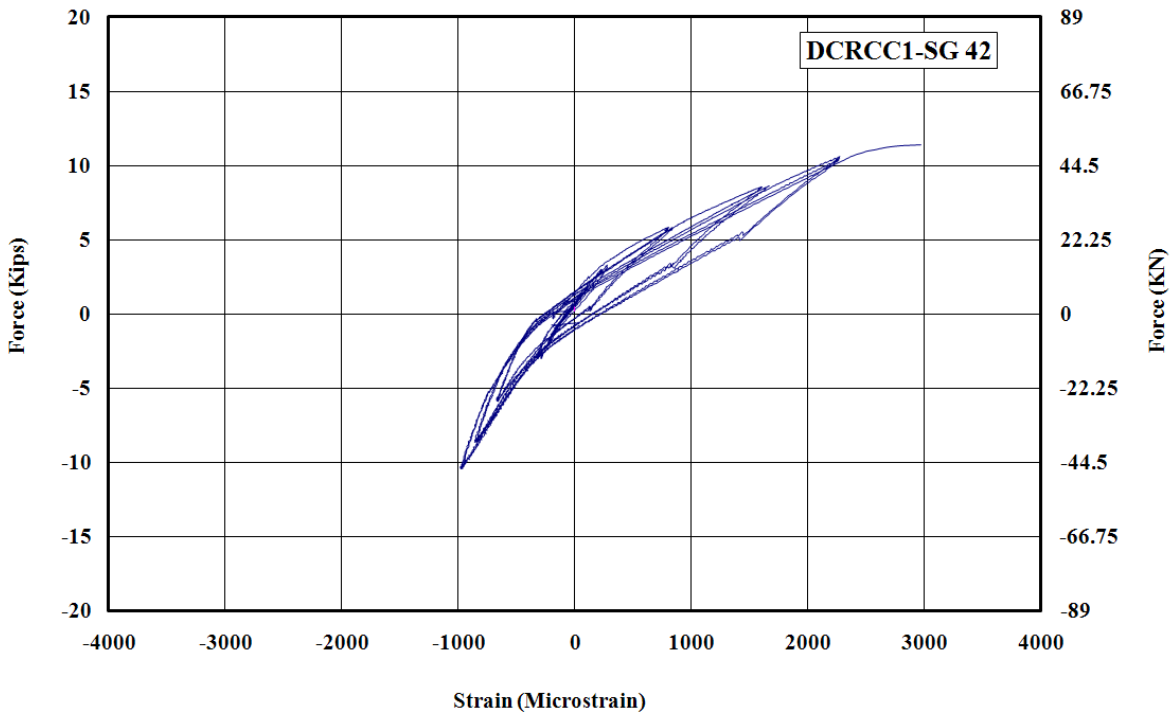

Figure A - 37: Measured Strain in Gauge No.42 for DCRCC1

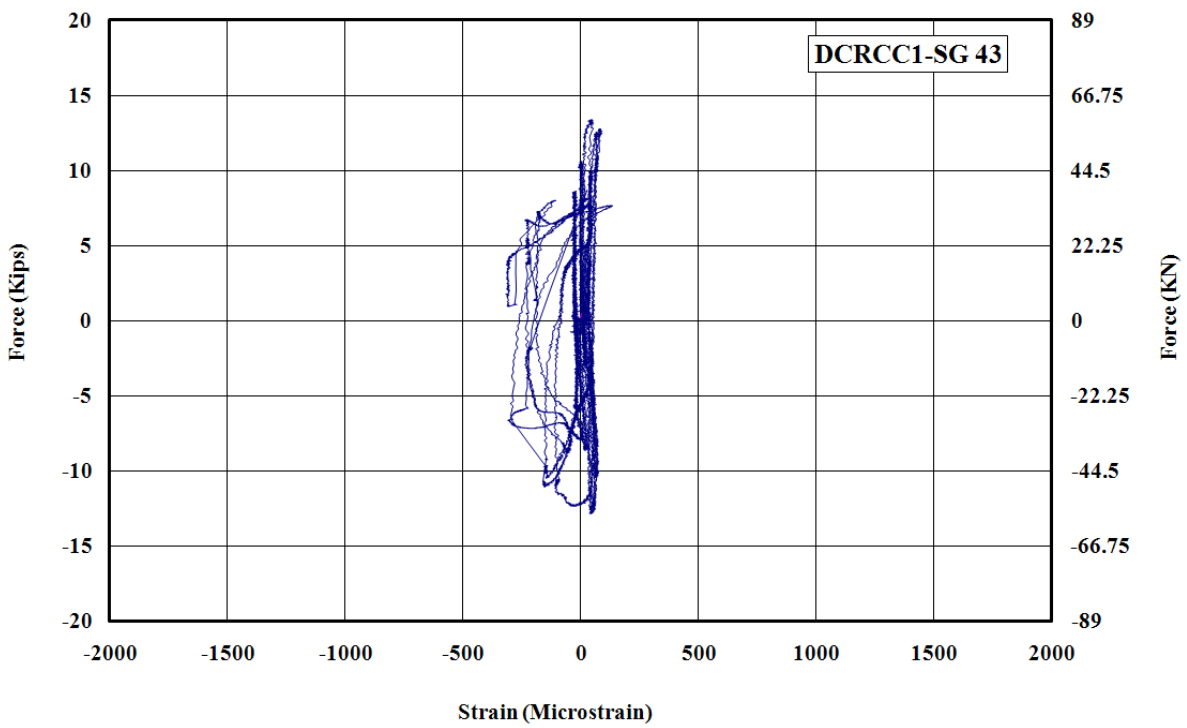

Figure A - 38: Measured Strain in Gauge No.43 for DCRCC1

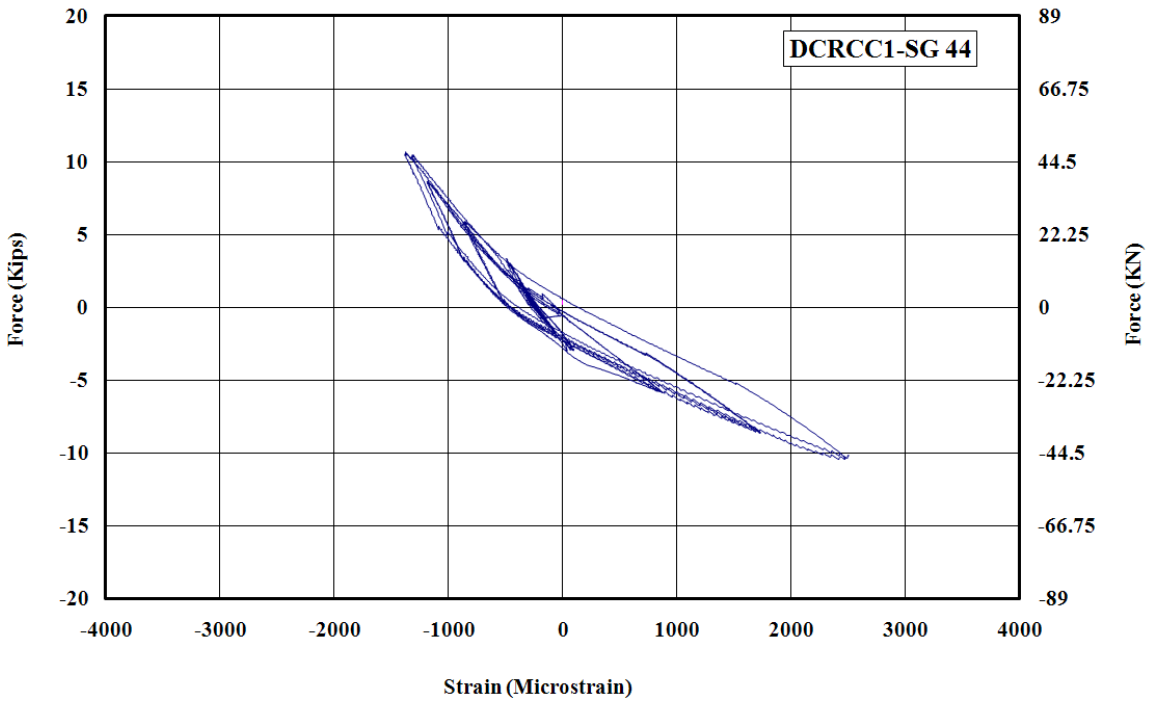

Figure A - 39: Measured Strain in Gauge No.44 for DCRCC1

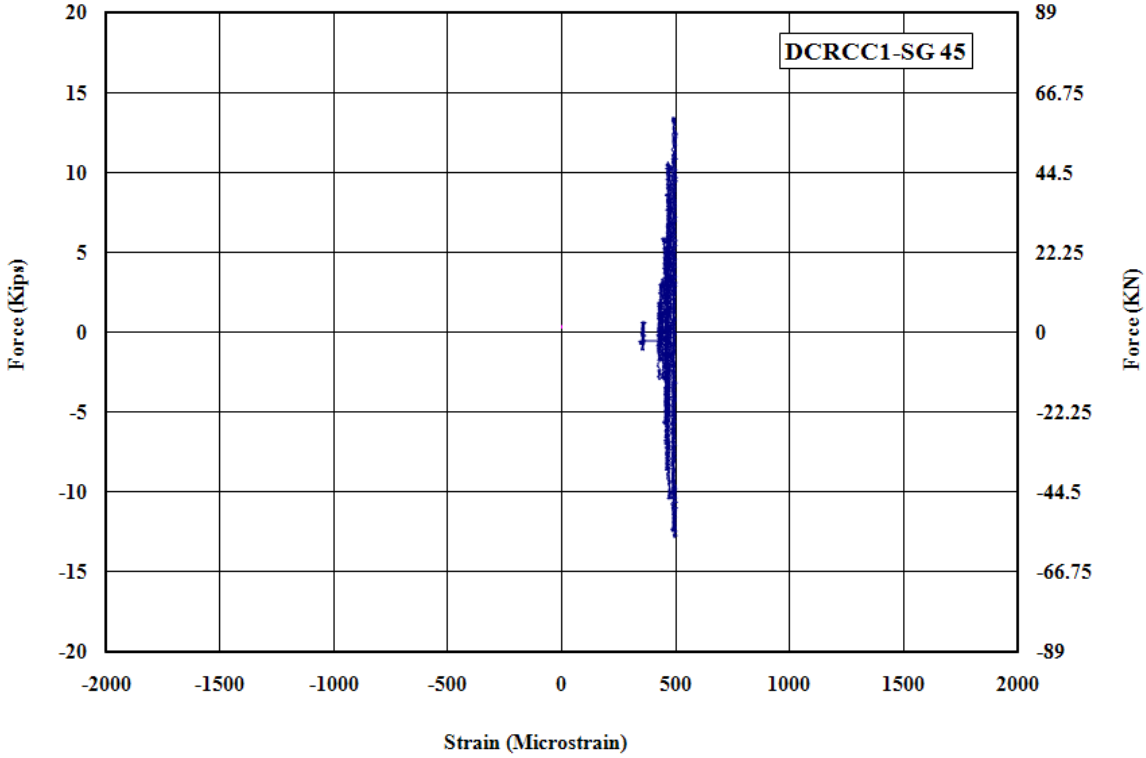

Figure A - 40: Measured Strain in Gauge No.45 for DCRCC1

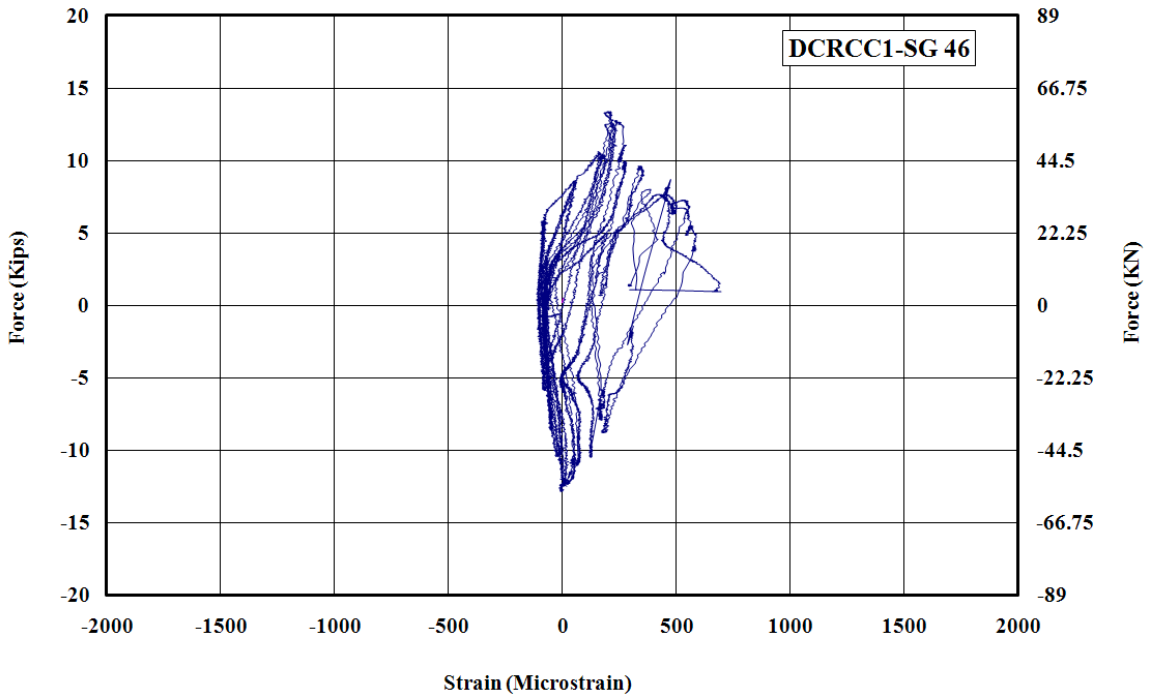

Figure A - 41: Measured Strain in Gauge No.46 for DCRCC1

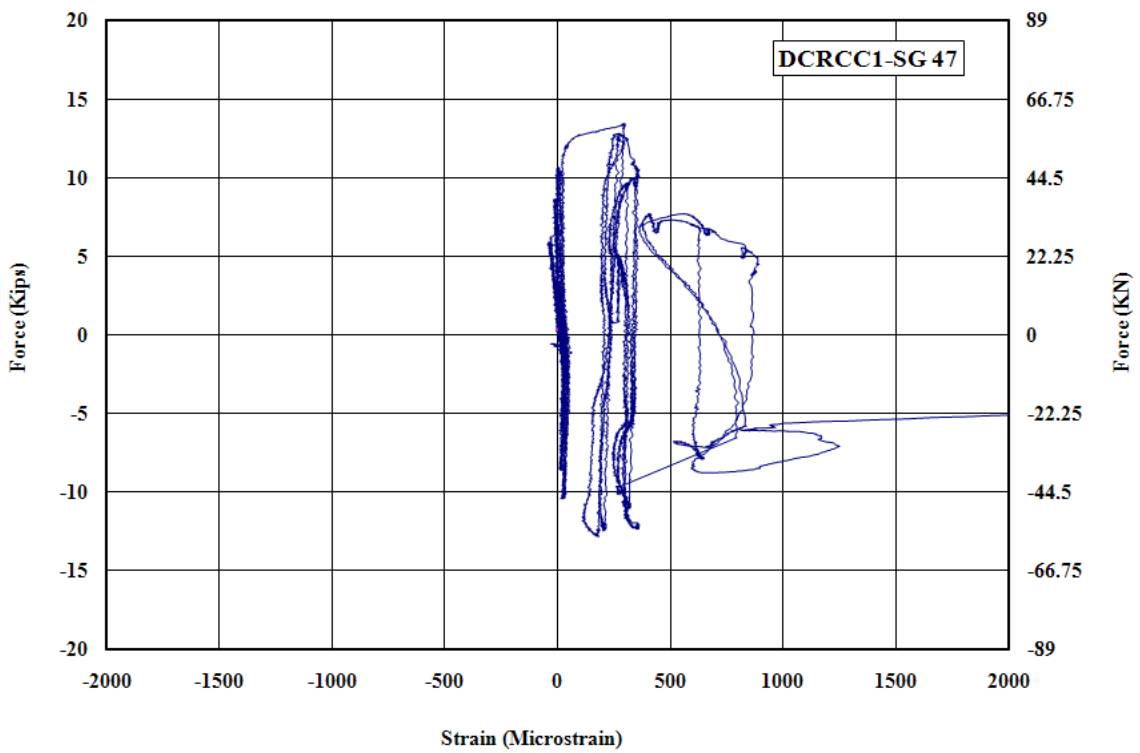

Figure A - 42: Measured Strain in Gauge No.47 for DCRCC1

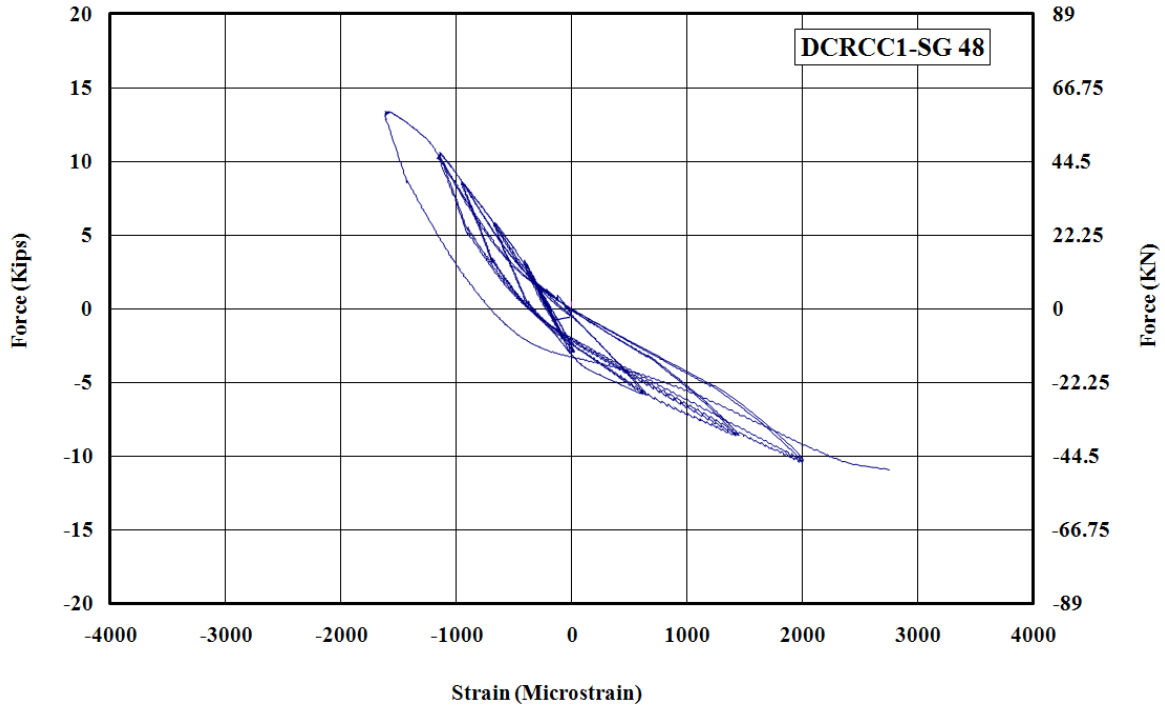

Figure A - 43: Measured Strain in Gauge No.48 for DCRCC1

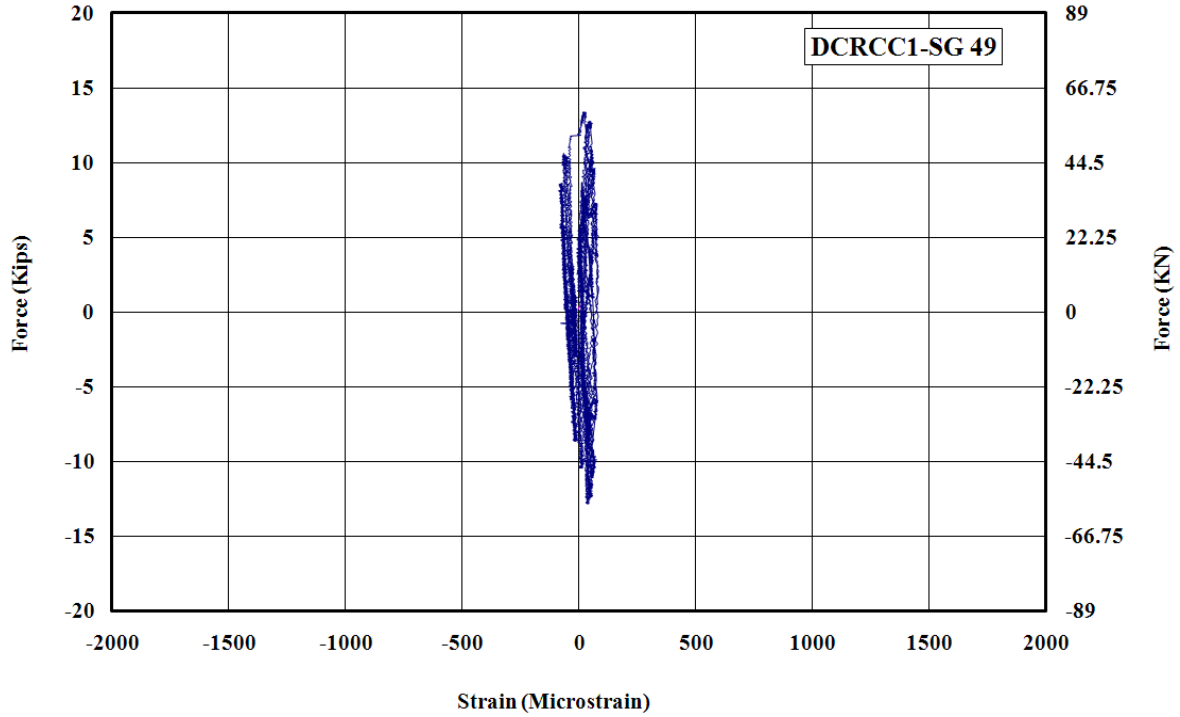

Figure A - 44: Measured Strain in Gauge No.49 for DCRCC1

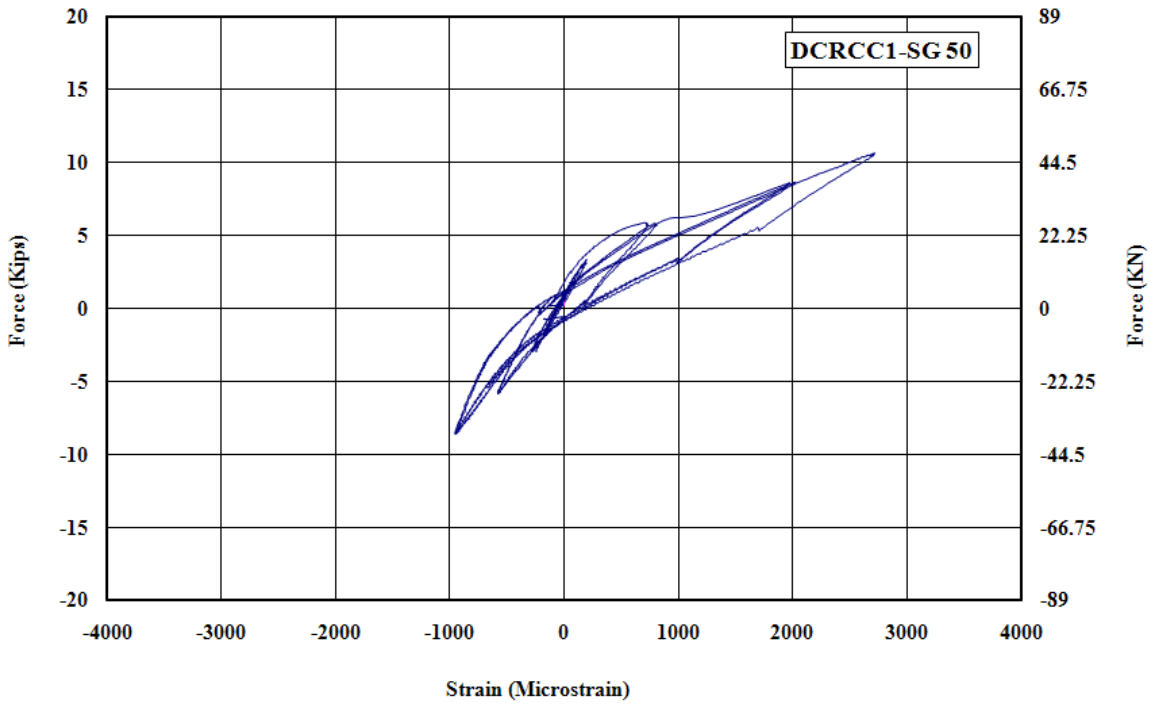

Figure A - 45: Measured Strain in Gauge No.50 for DCRCC1

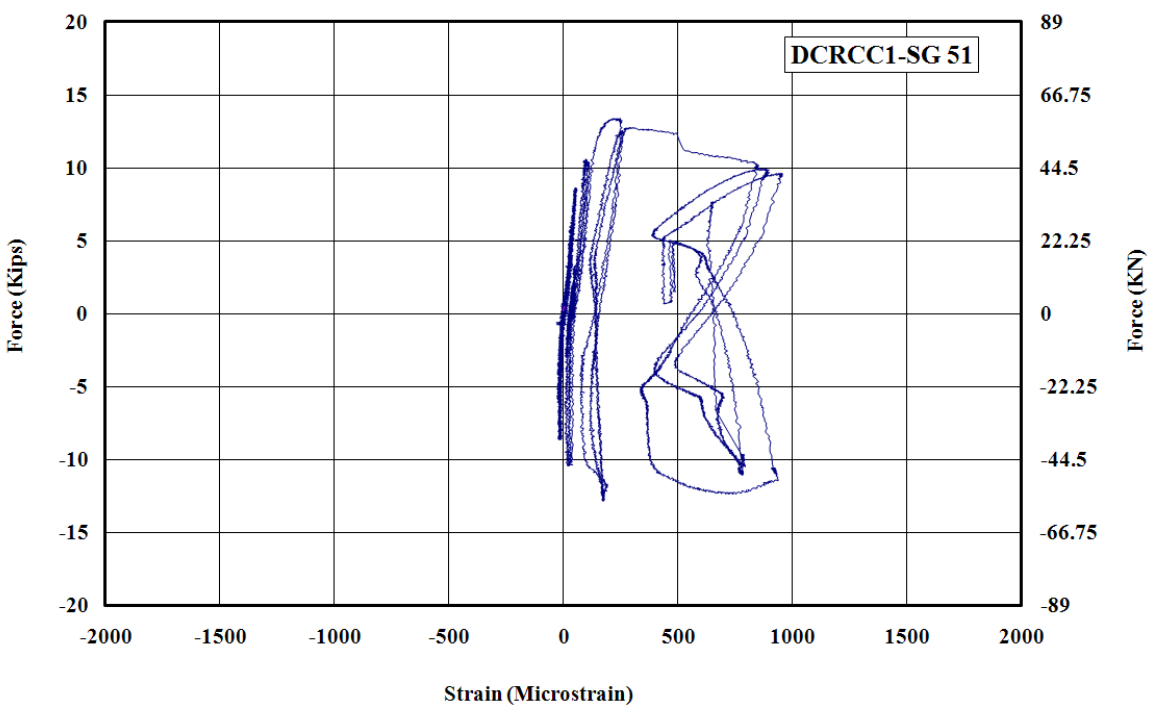

Figure A - 46: Measured Strain in Gauge No.51 for DCRCC1

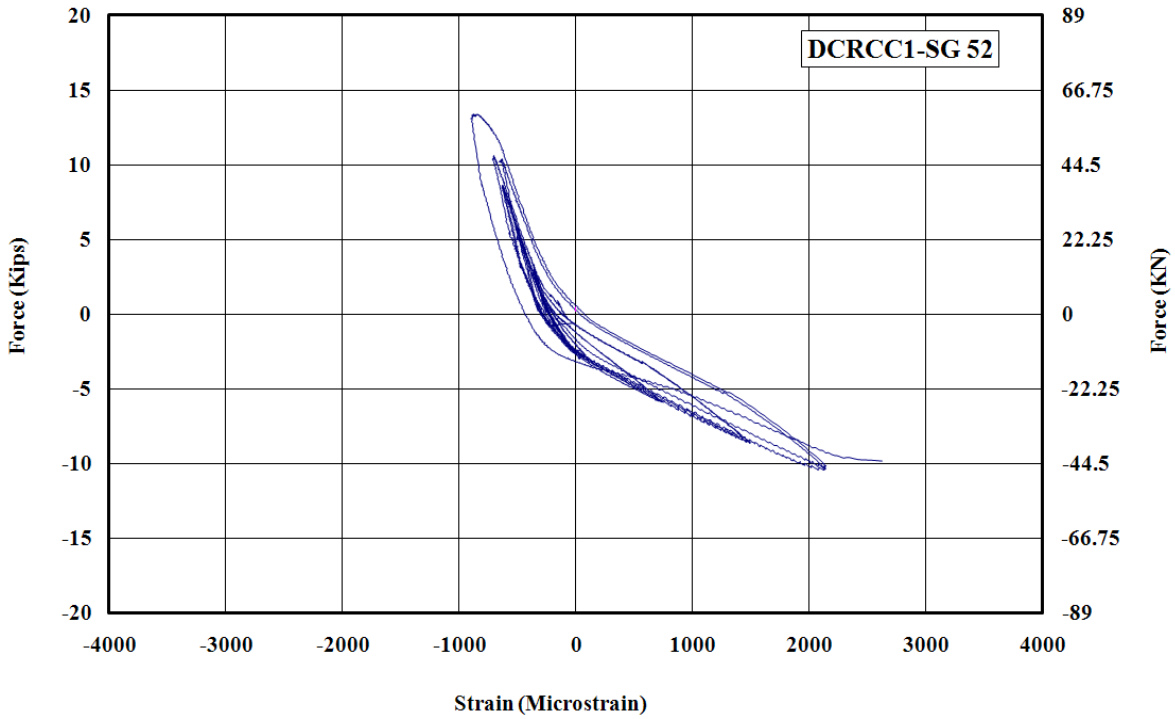

Figure A - 47: Measured Strain in Gauge No.52 for DCRCC1

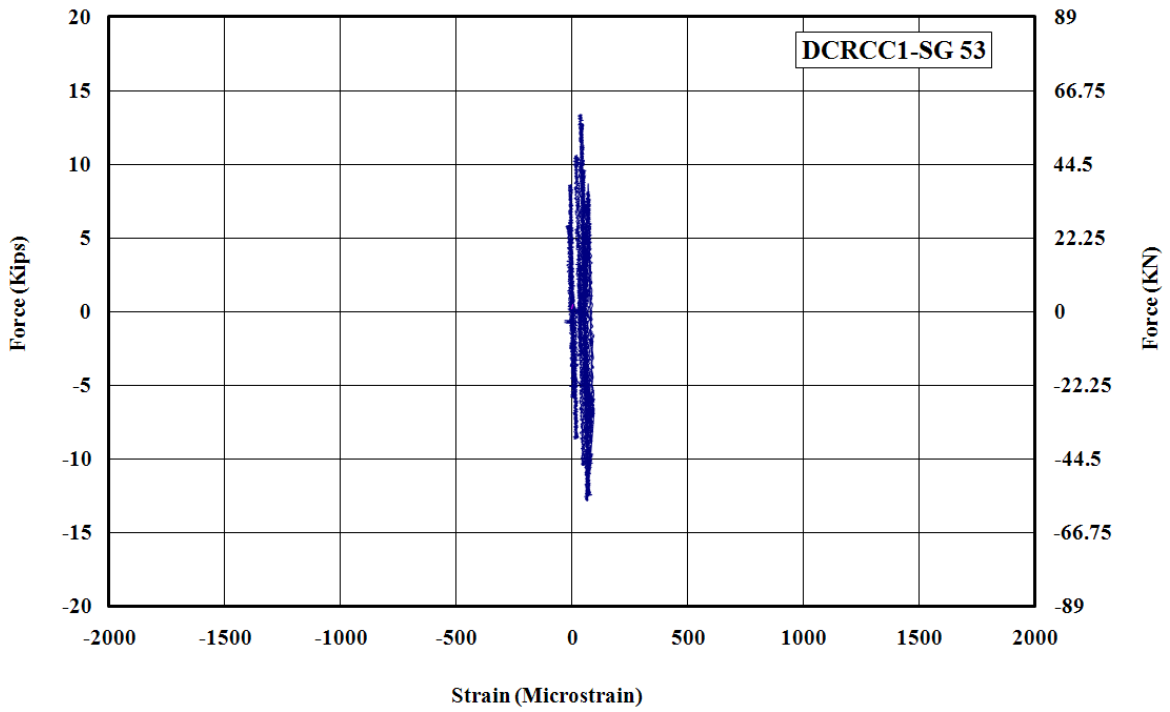

Figure A - 48: Measured Strain in Gauge No.53 for DCRCC1

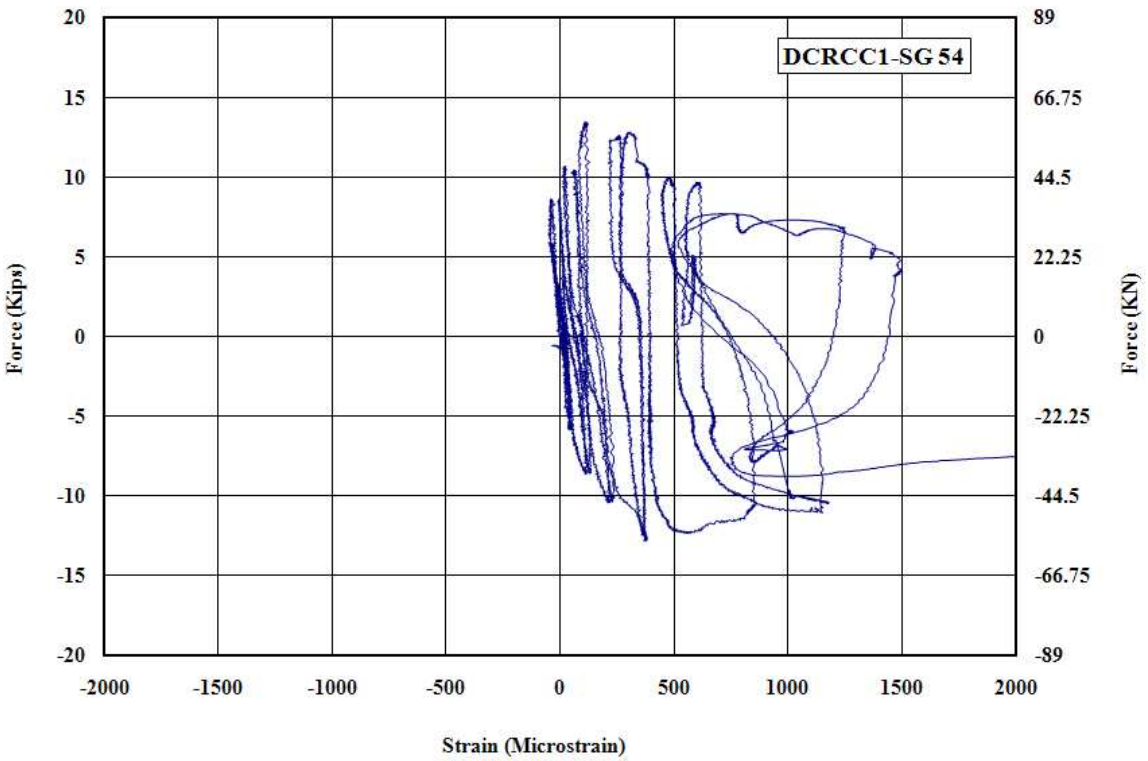

Figure A - 49: Measured Strain in Gauge No.54 for DCRCC1

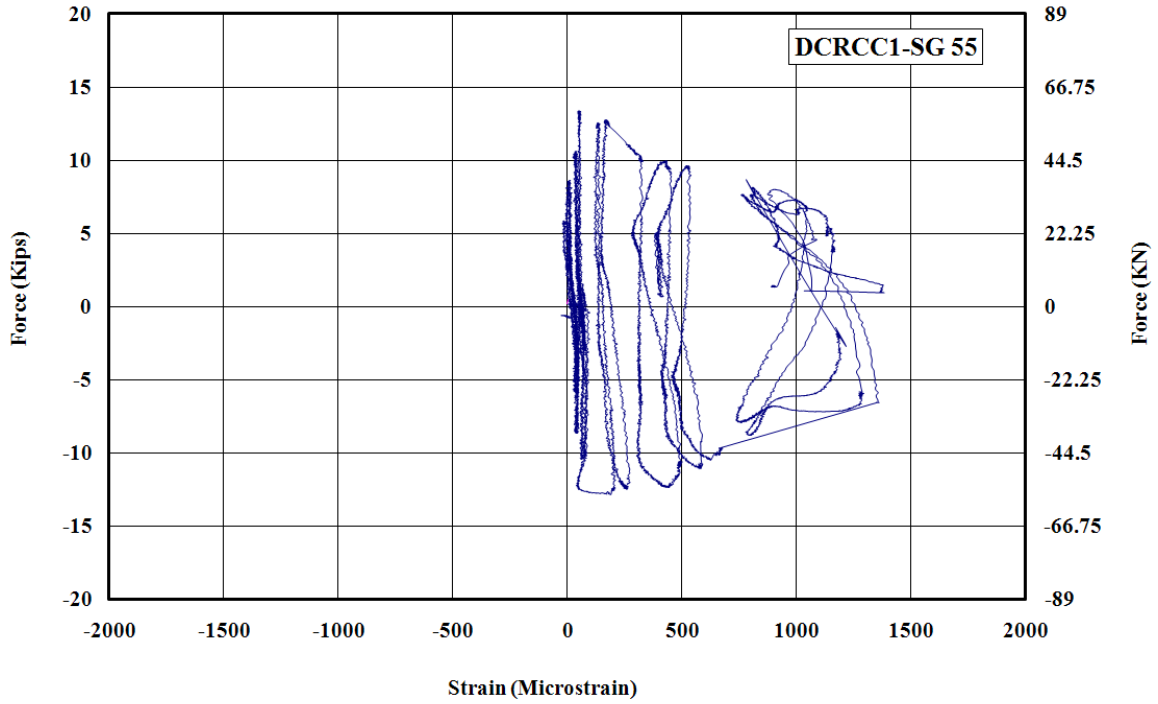

Figure A - 50: Measured Strain in Gauge No.55 for DCRCC1

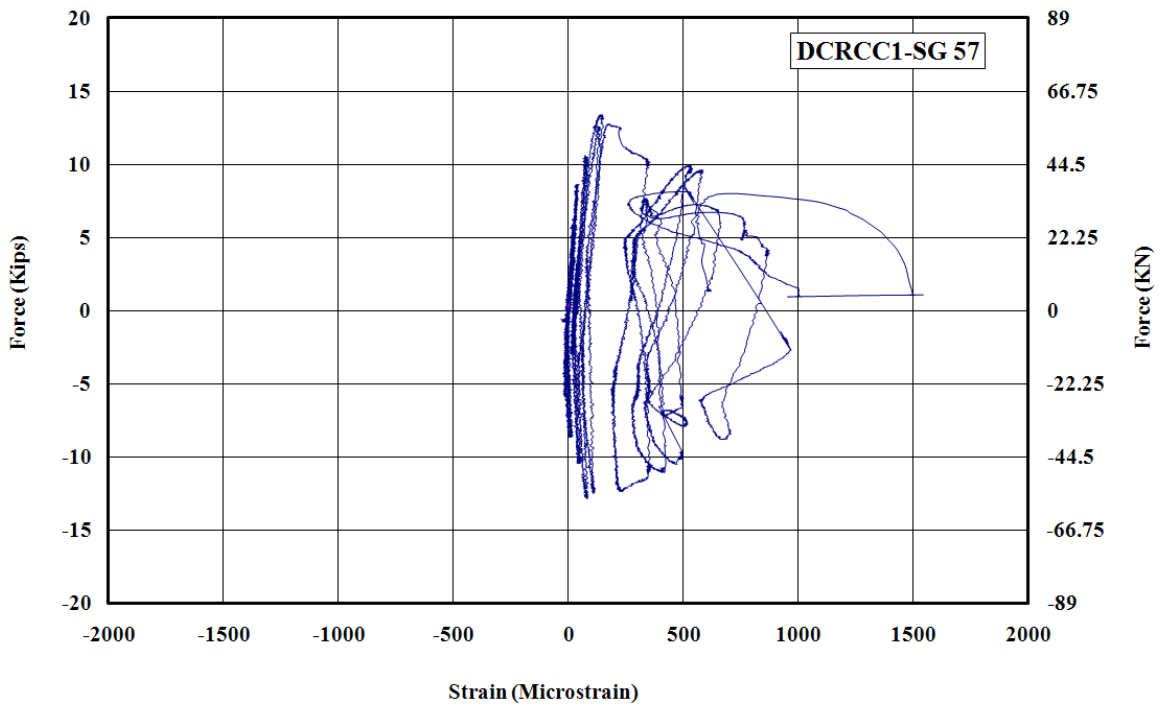

Figure A - 51: Measured Strain in Gauge No.57 for DCRCC1

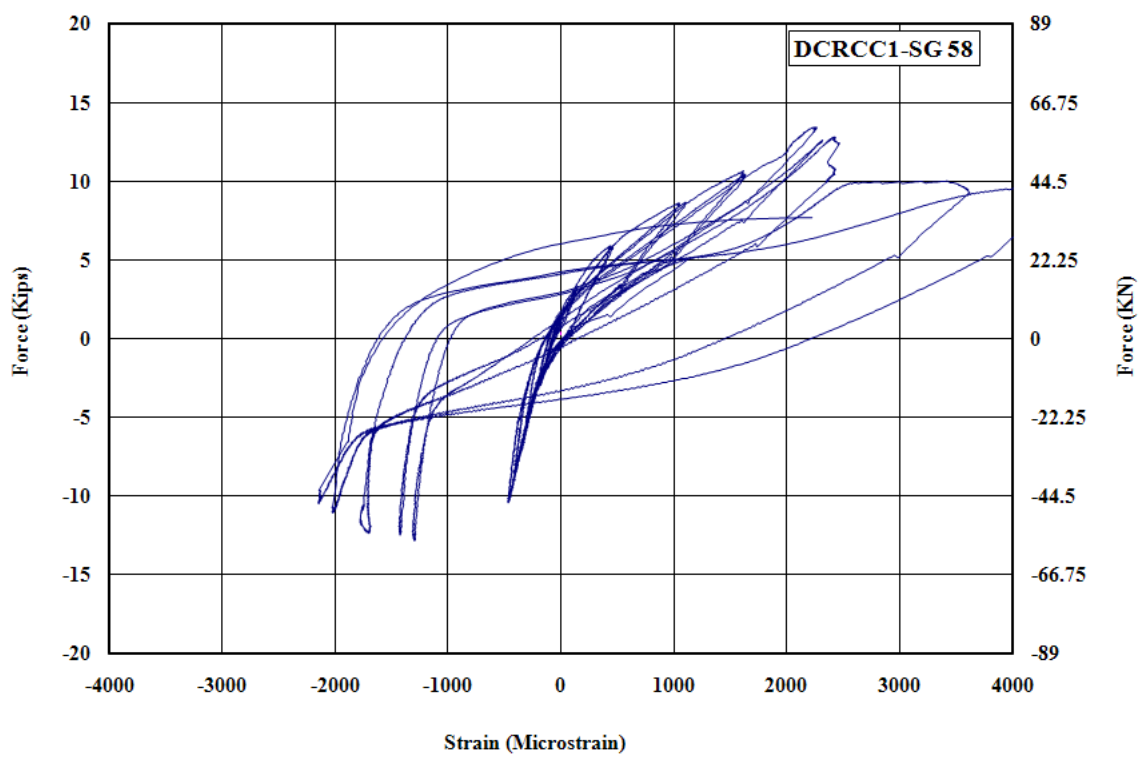

Figure A - 52: Measured Strain in Gauge No.58 for DCRCC1

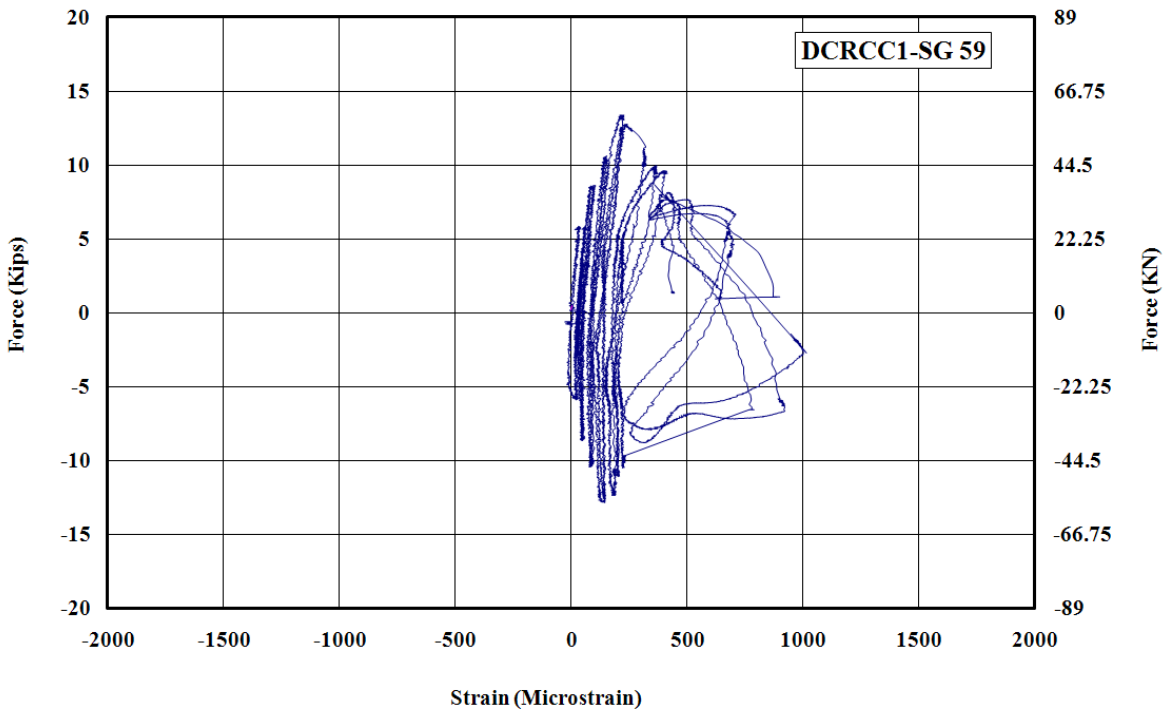

Figure A - 53: Measured Strain in Gauge No.59 for DCRCC1

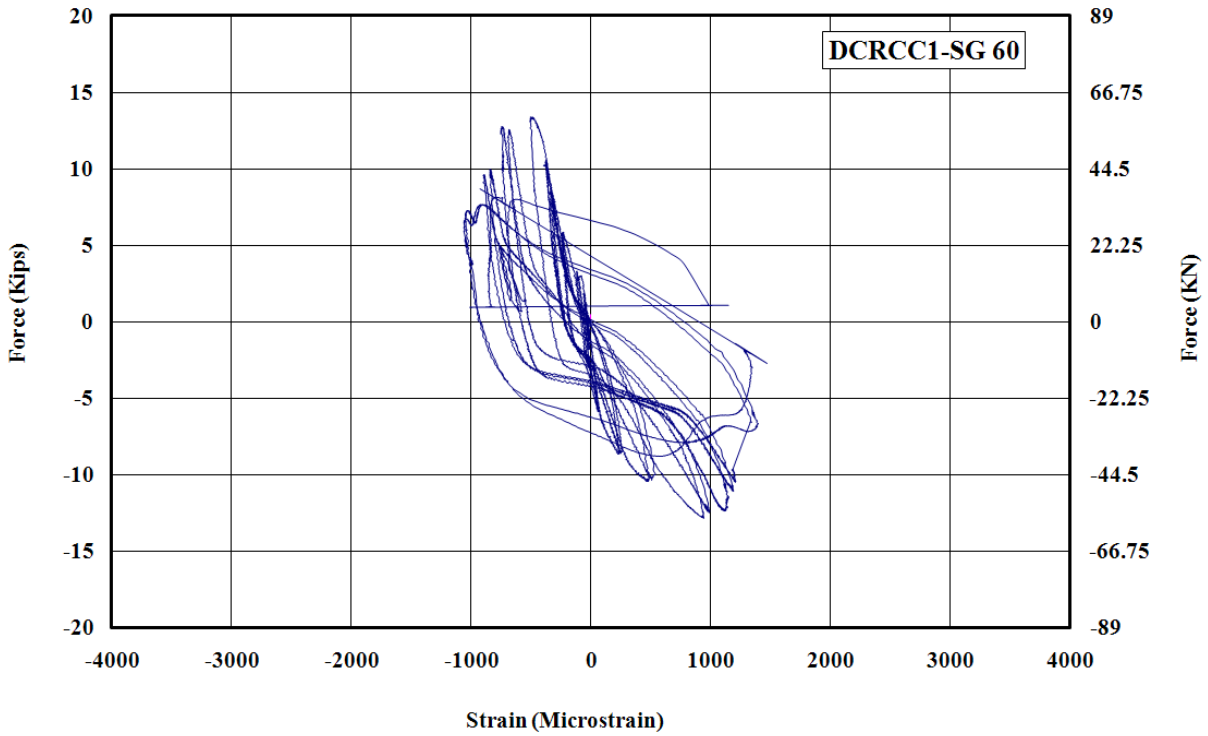

Figure A - 54: Measured Strain in Gauge No.60 for DCRCC1

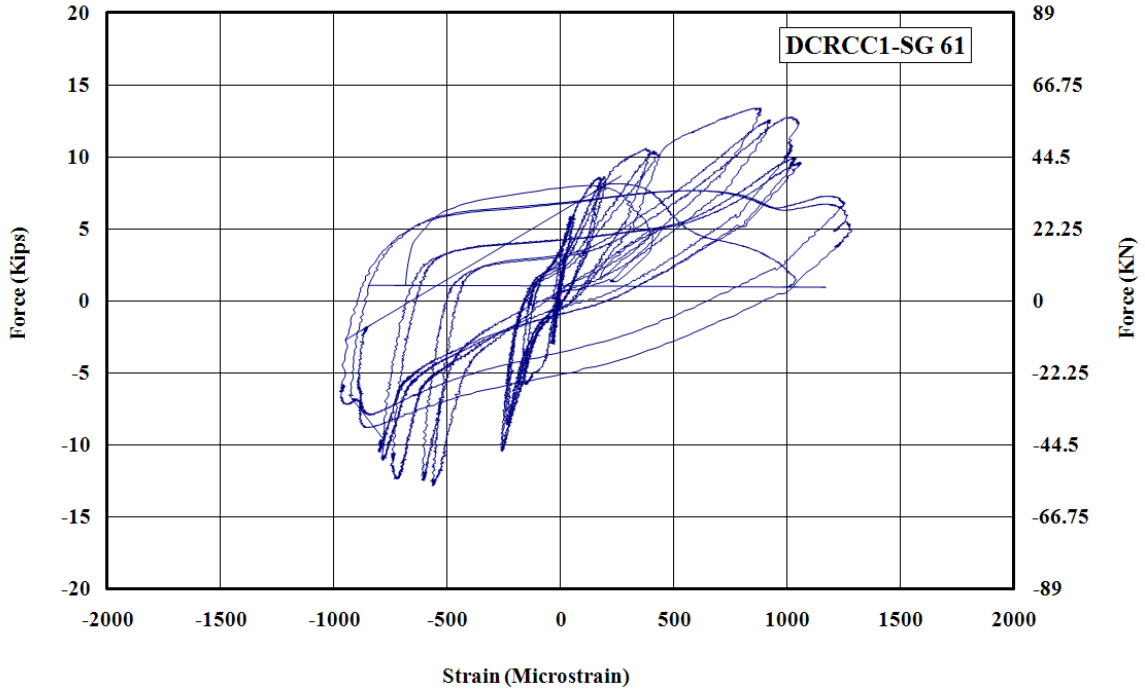

Figure A - 55: Measured Strain in Gauge No.61 for DCRCC1

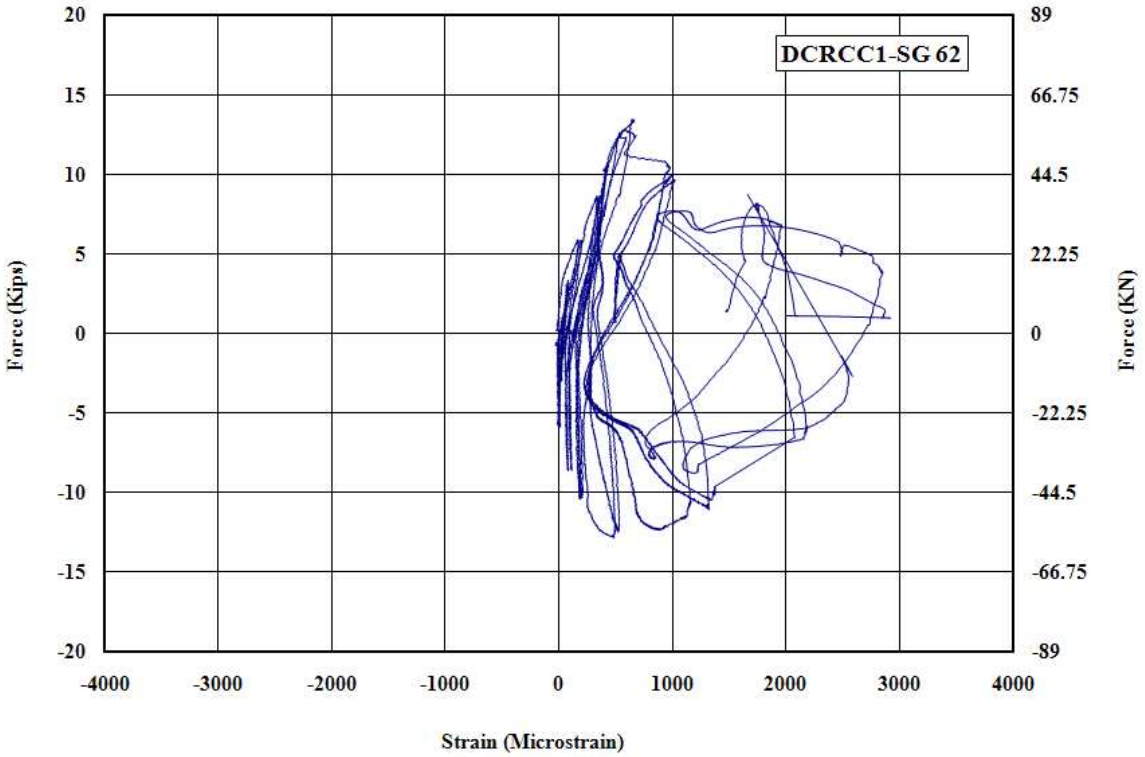

Figure A - 56: Measured Strain in Gauge No.62 for DCRCC1

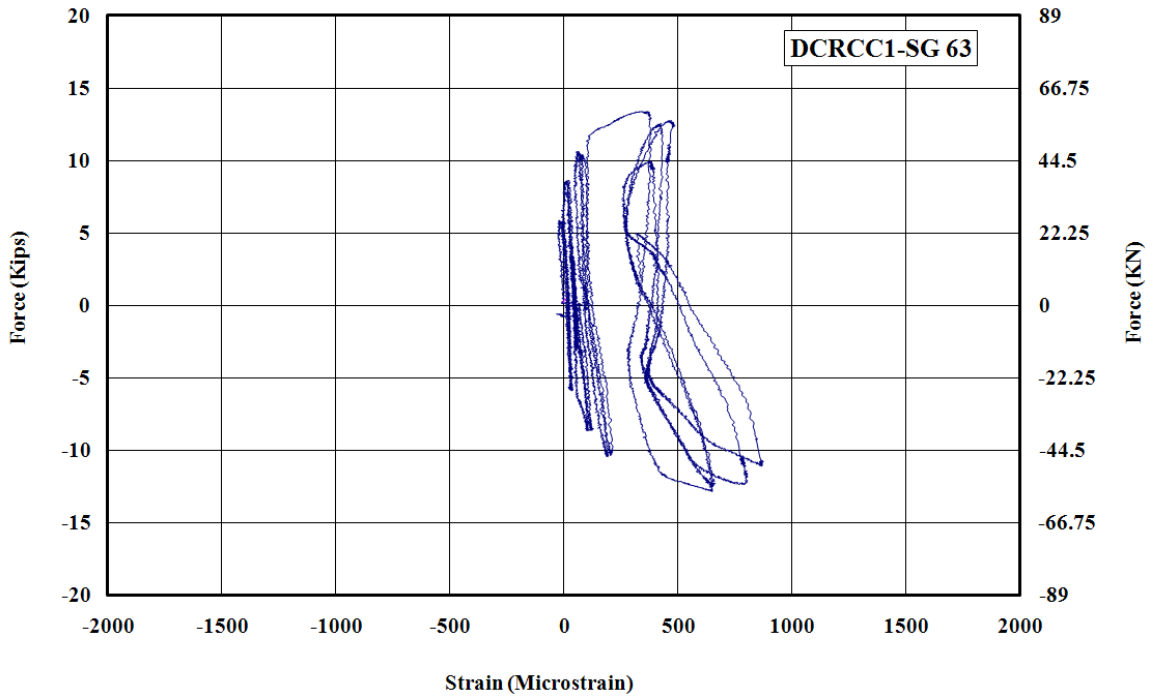

Figure A - 57: Measured Strain in Gauge No.63 for DCRCC1

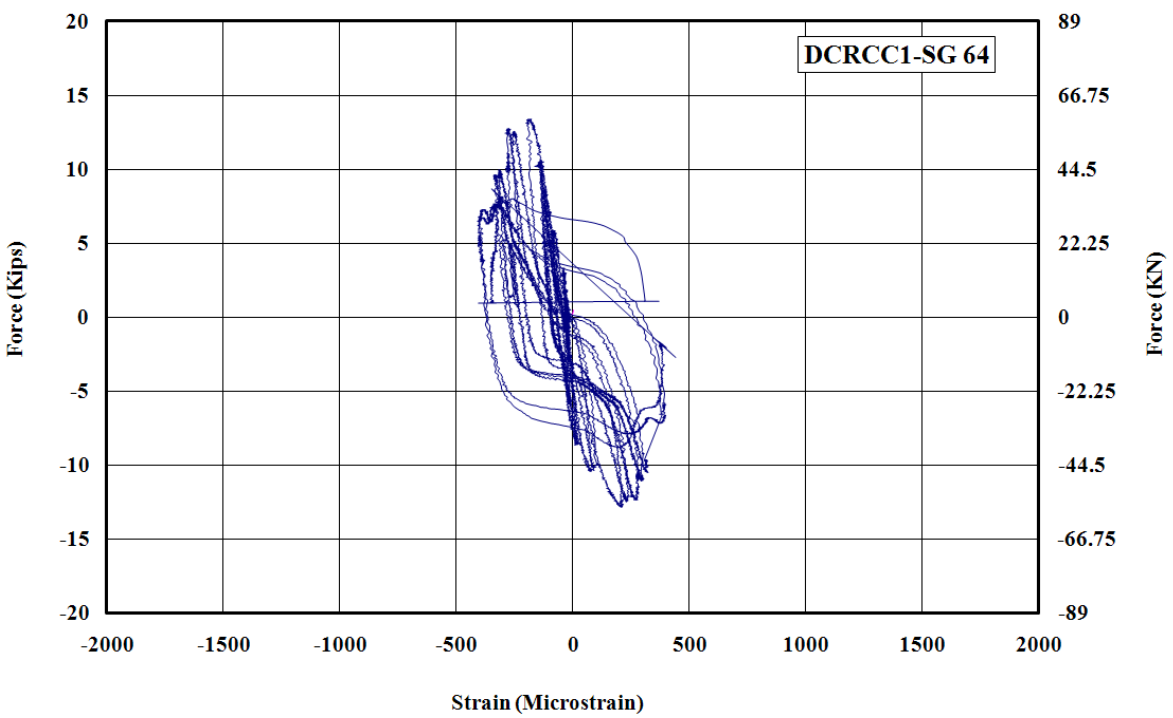

Figure A - 58: Measured Strain in Gauge No.64 for DCRCC1

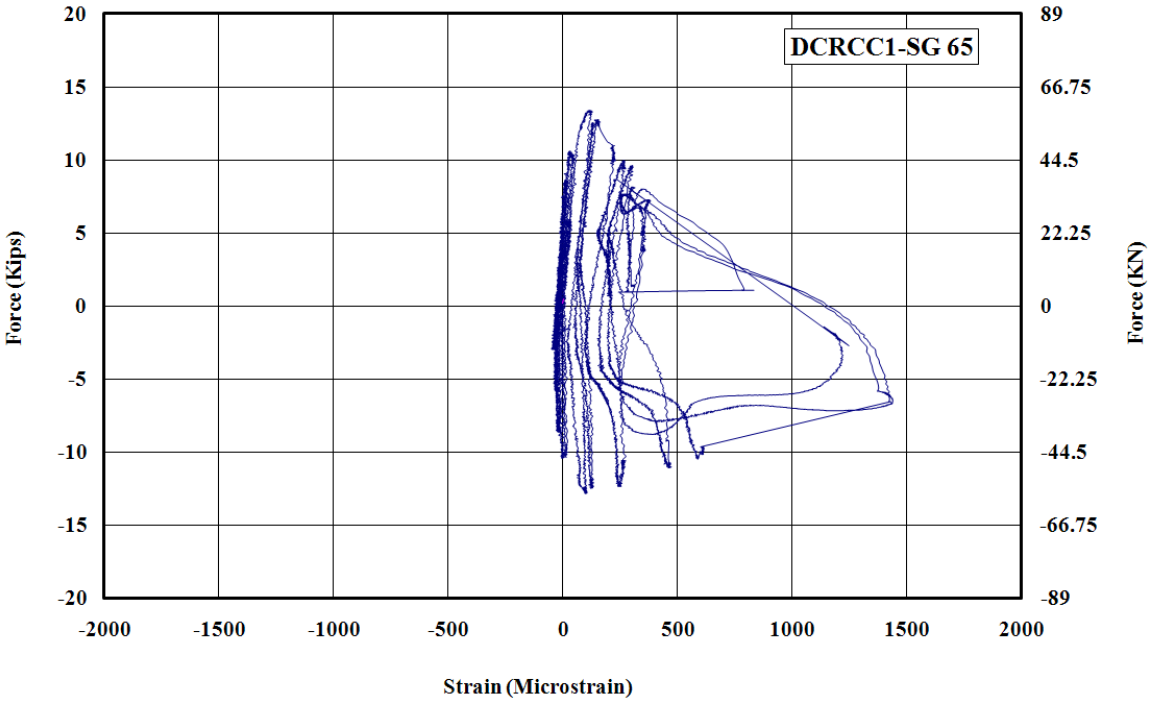

Figure A - 59: Measured Strain in Gauge No.65 for DCRCC1

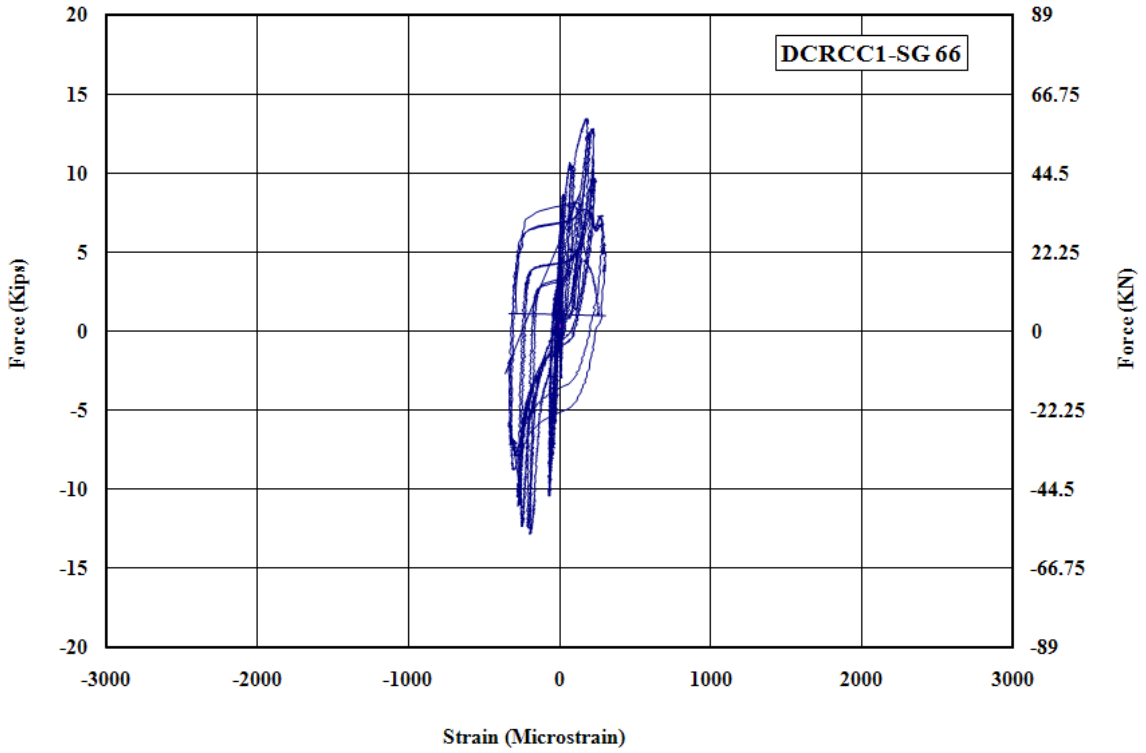

Figure A - 60: Measured Strain in Gauge No.66 for DCRCC1

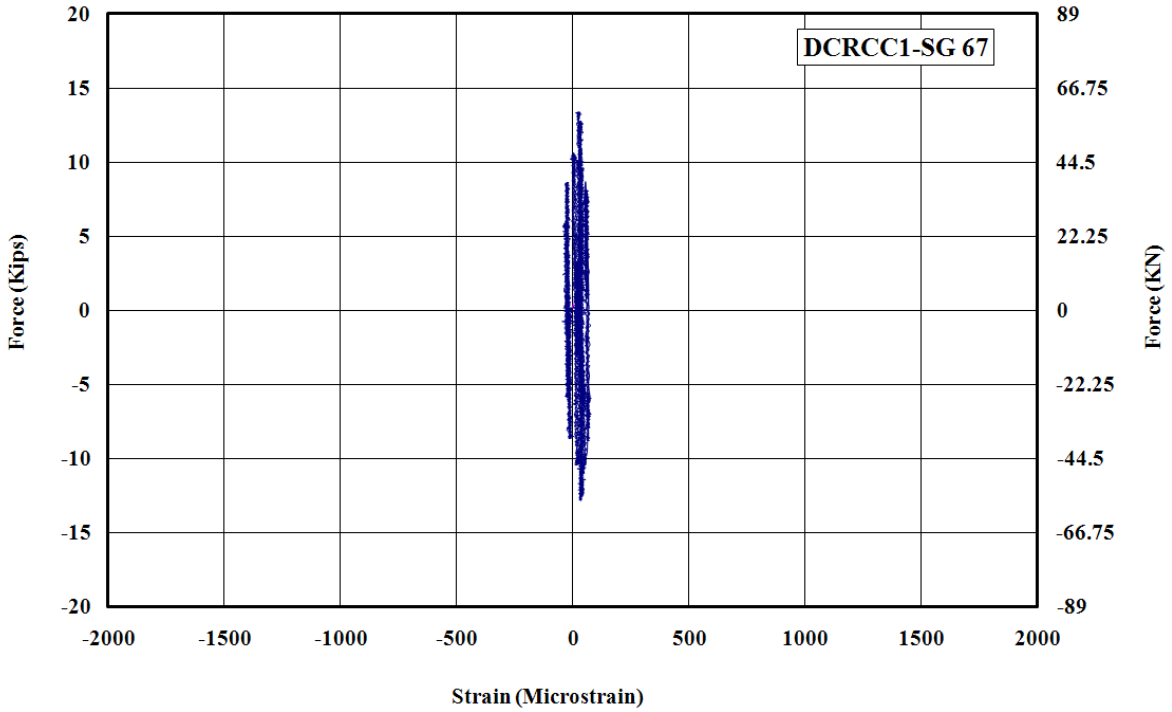

Figure A - 61: Measured Strain in Gauge No.67 for DCRCC1

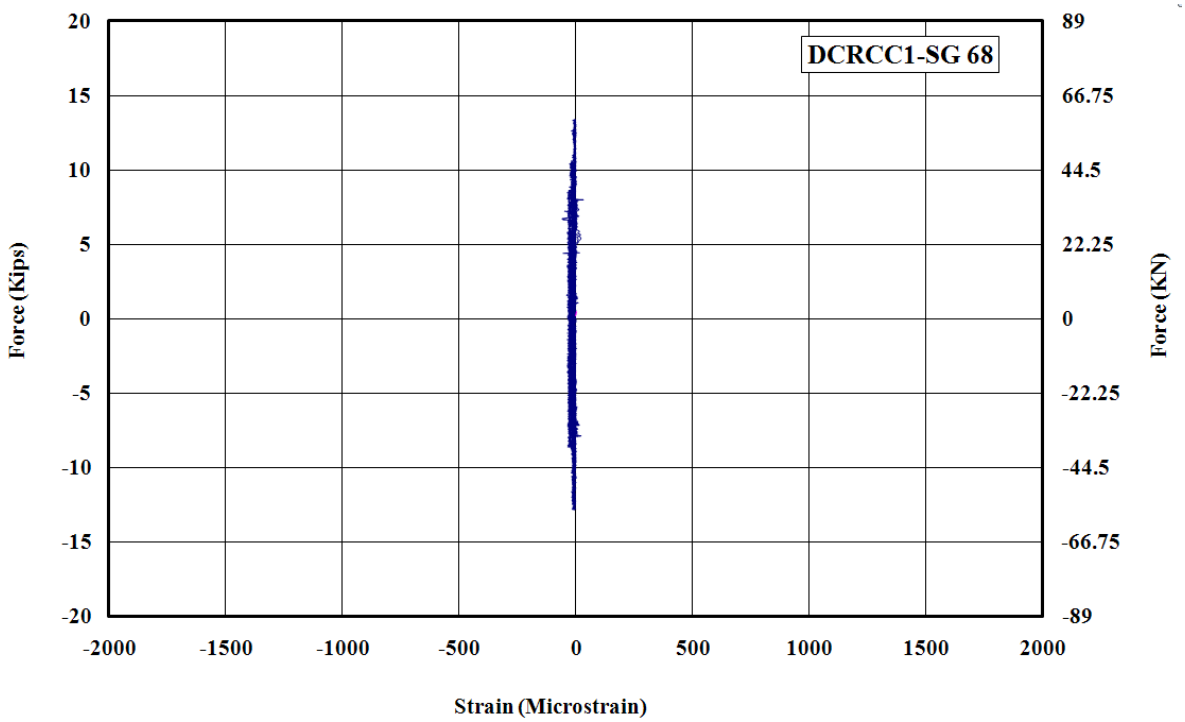

Figure A - 62: Measured Strain in Gauge No.68 for DCRCC1

Appendix B

Specimen FSRCC1

(Flat-Slab T-Joint with 16-in.diameter pile)

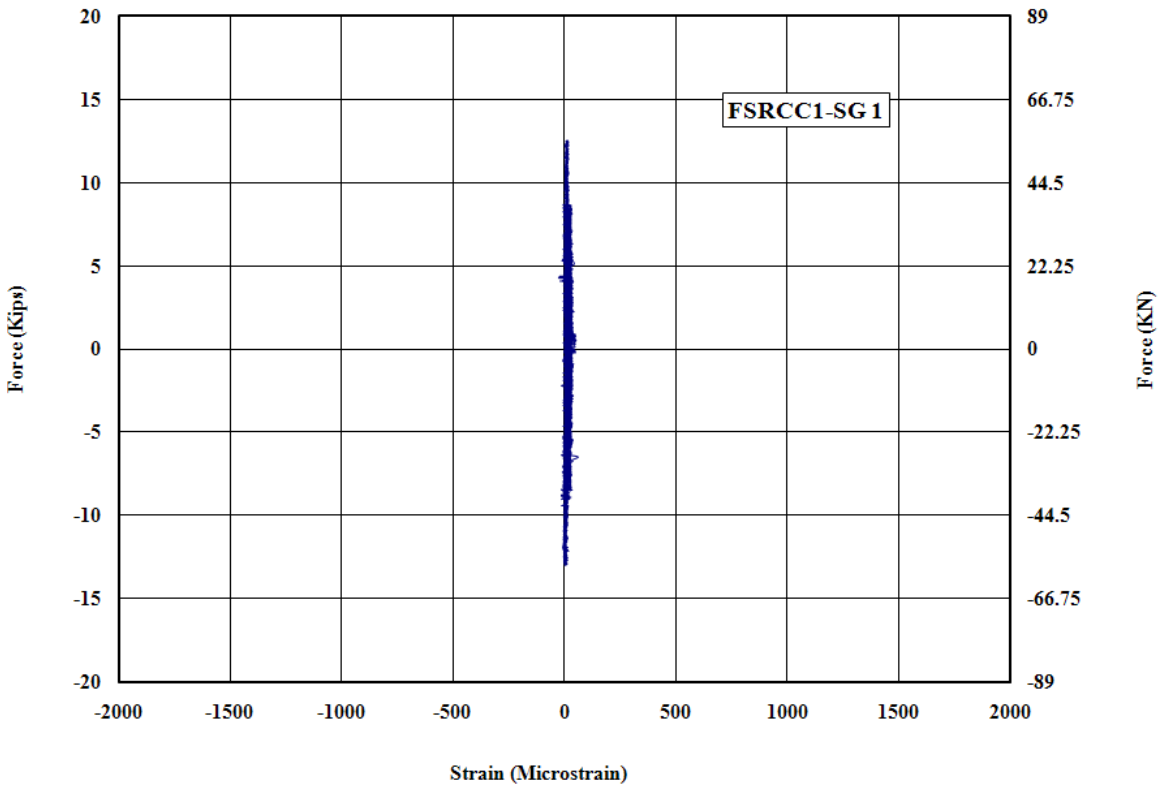

Figure B - 1: Measured Strain in Gauge No.1 for FSRCC1

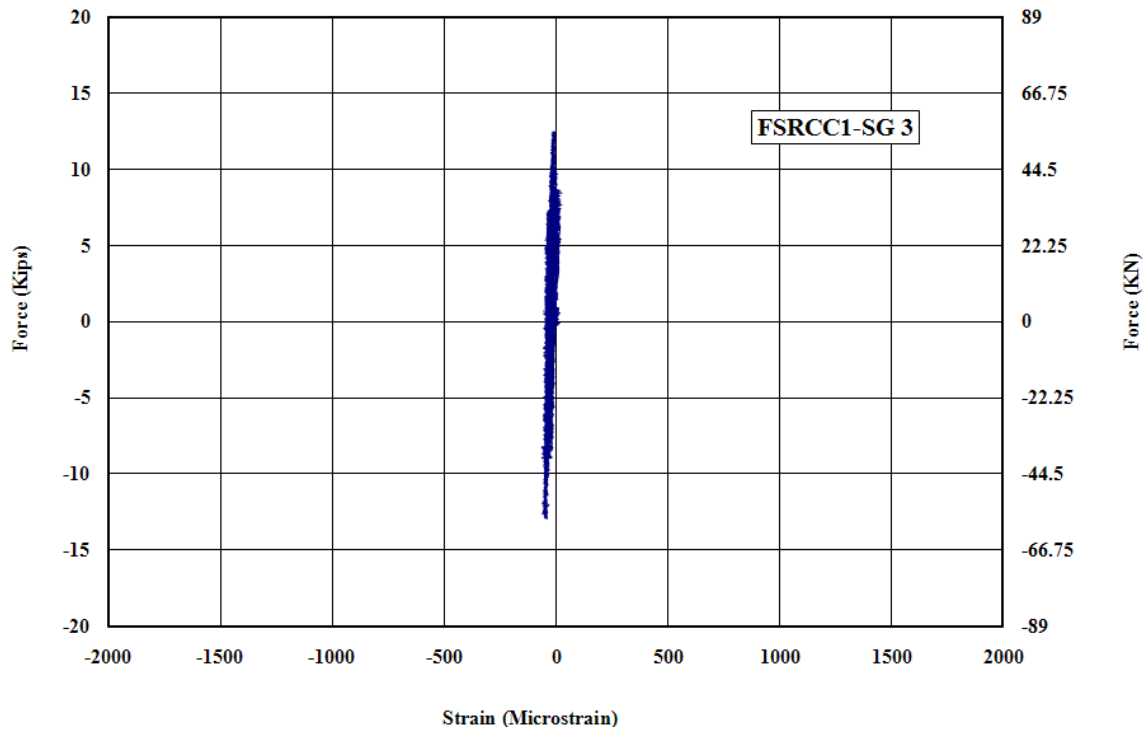

Figure B - 2: Measured Strain in Gauge No.3 for FSRCC1

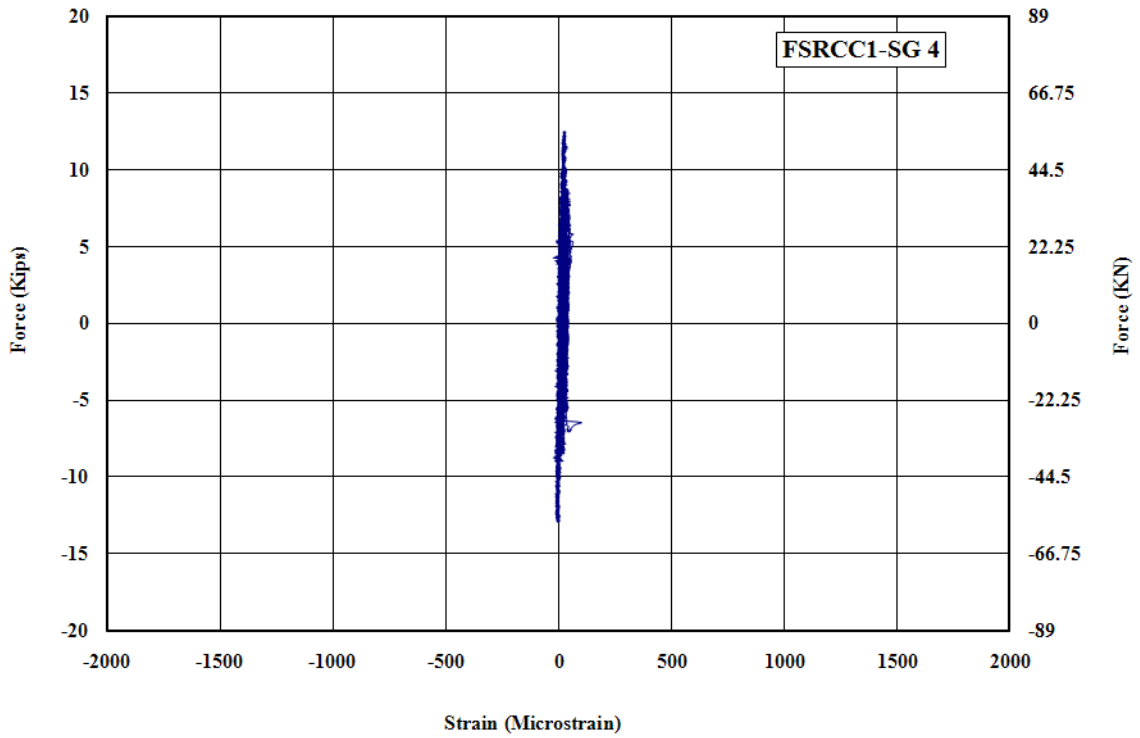

Figure B - 3: Measured Strain in Gauge No.4 for FSRCC1

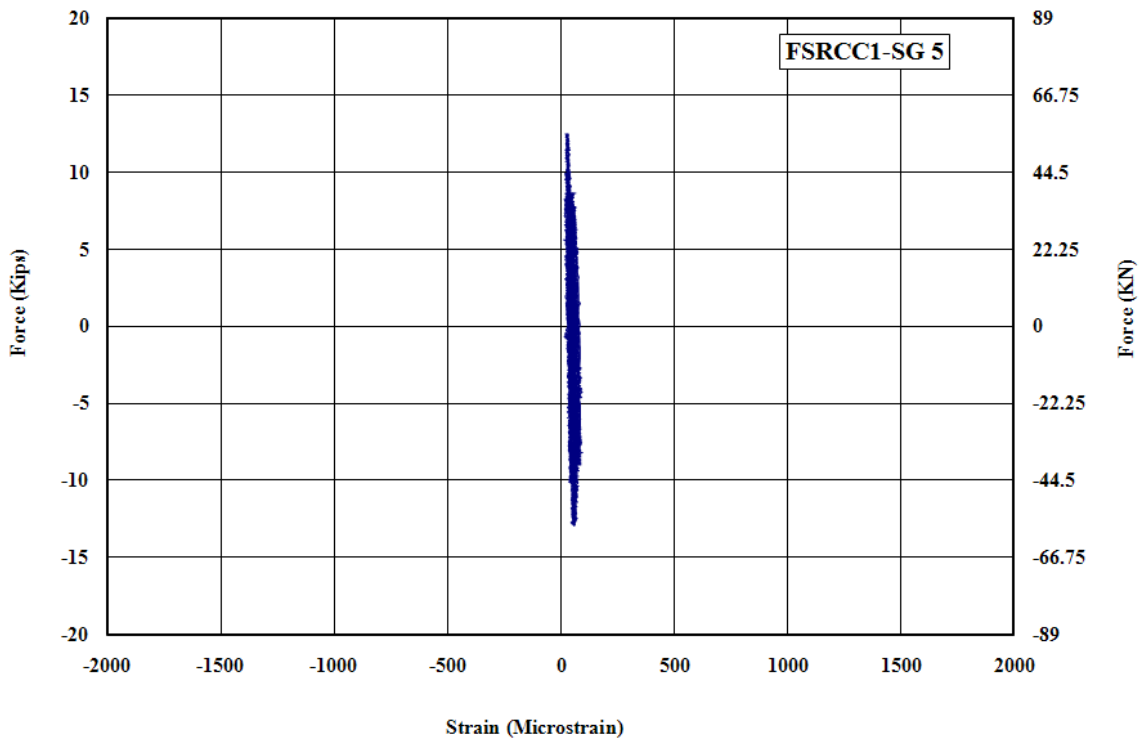

Figure B - 4: Measured Strain in Gauge No.5 for FSRCC1

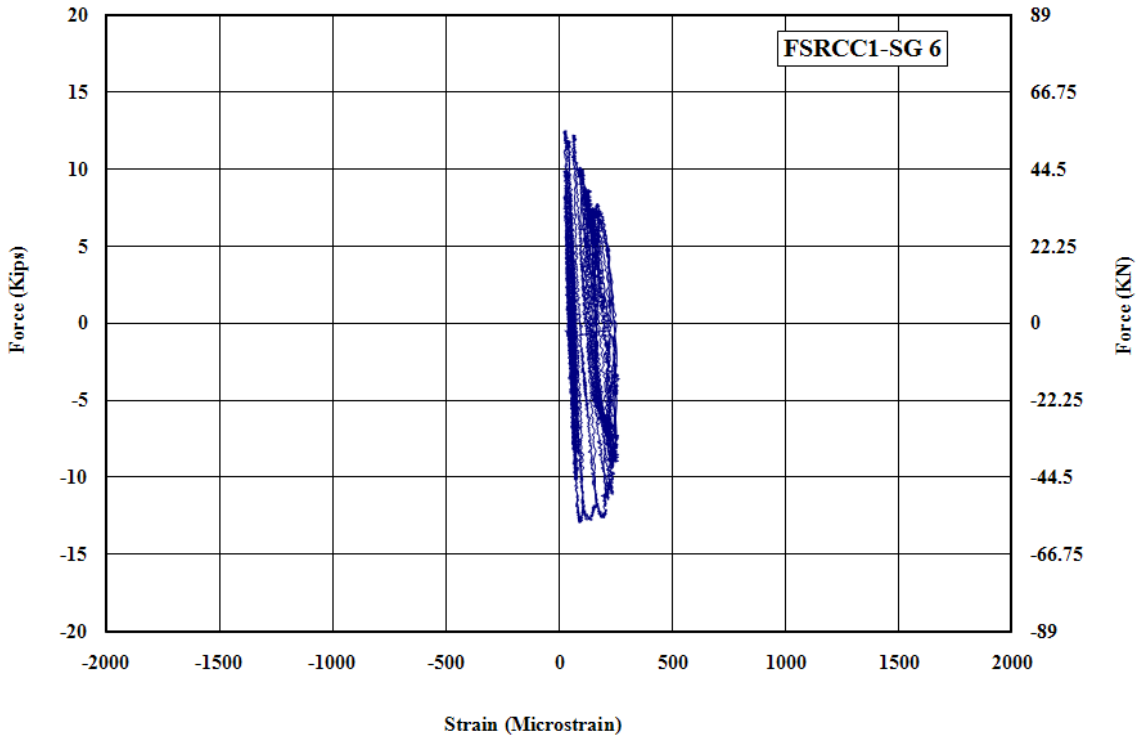

Figure B - 5: Measured Strain in Gauge No.6 for FSRCC1

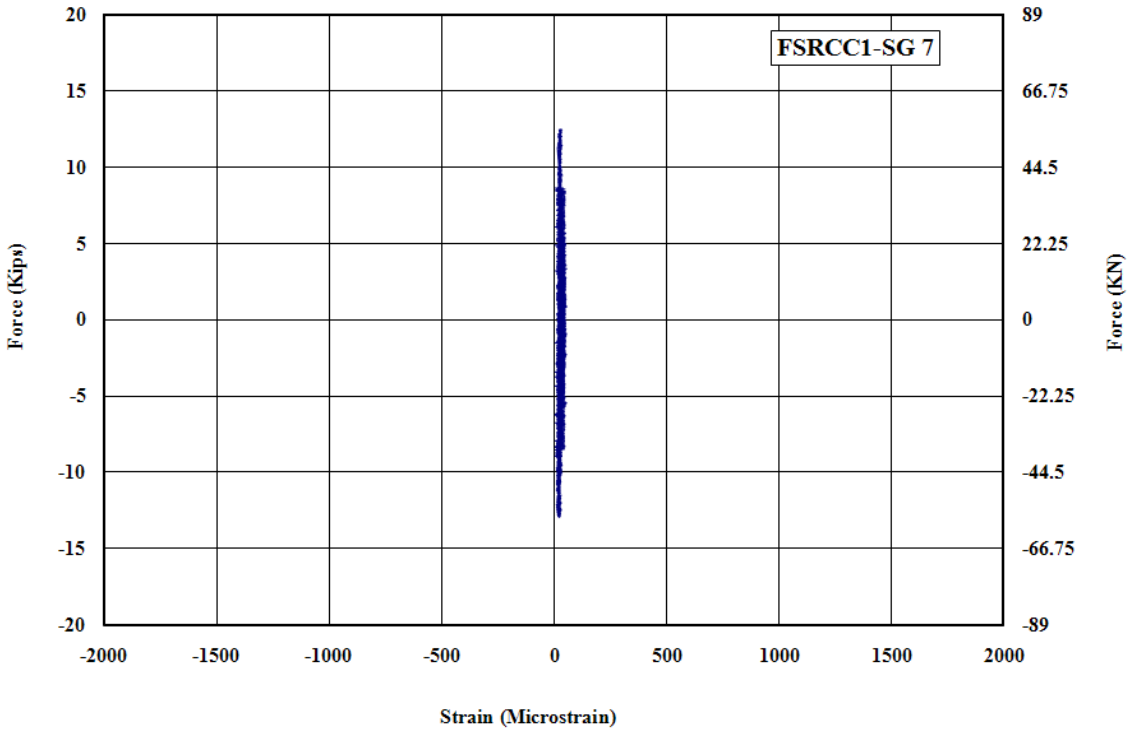

Figure B - 6: Measured Strain in Gauge No.7 for FSRCC1

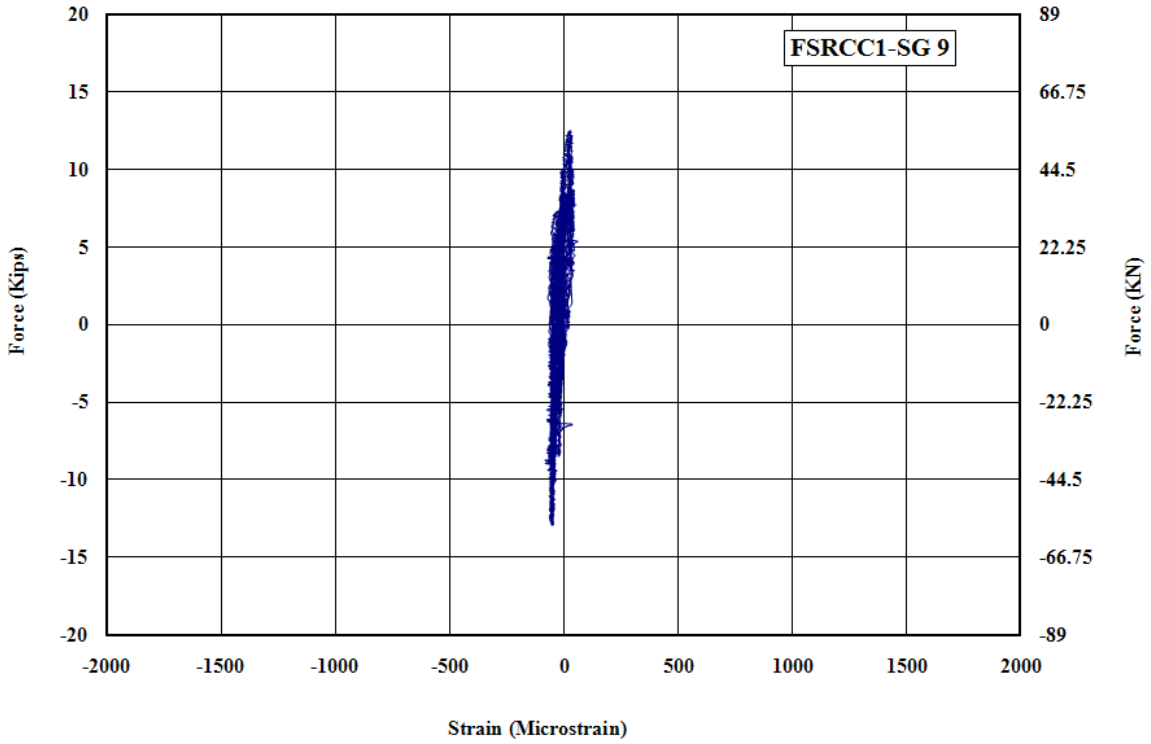

Figure B - 7: Measured Strain in Gauge No.9 for FSRCC1

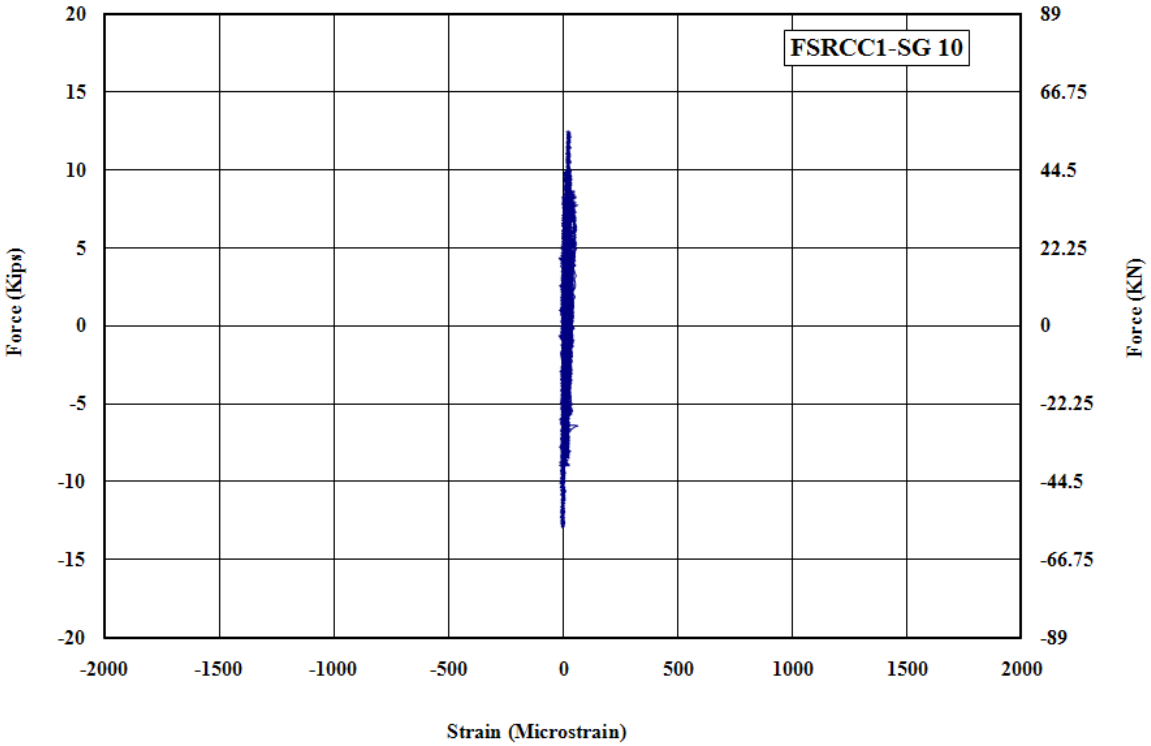

Figure B - 8: Measured Strain in Gauge No.10 for FSRCC1

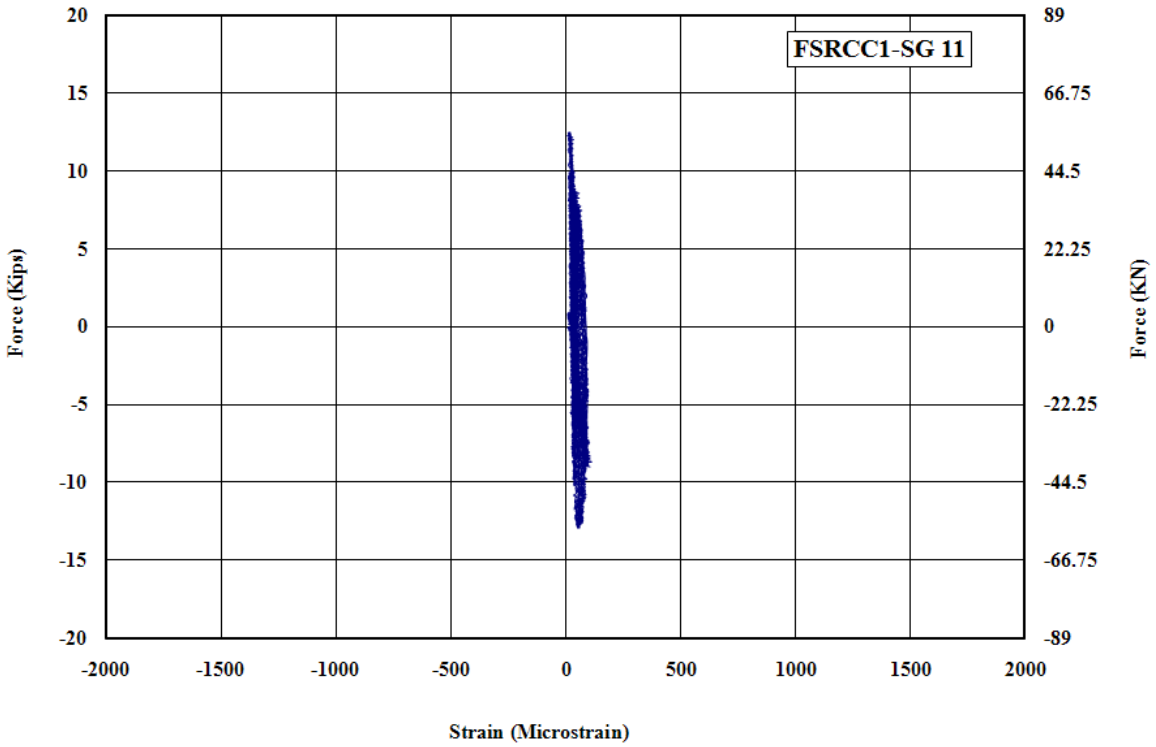

Figure B - 9: Measured Strain in Gauge No.11 for FSRCC1

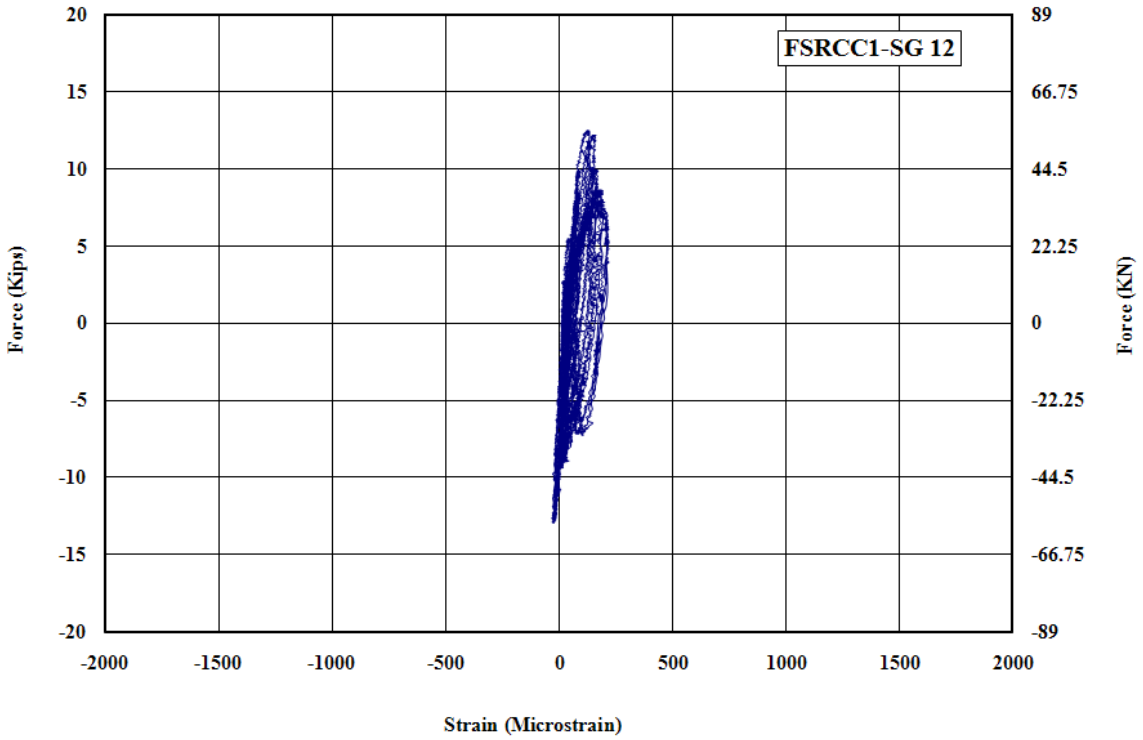

Figure B - 10: Measured Strain in Gauge No.12 for FSRCC1

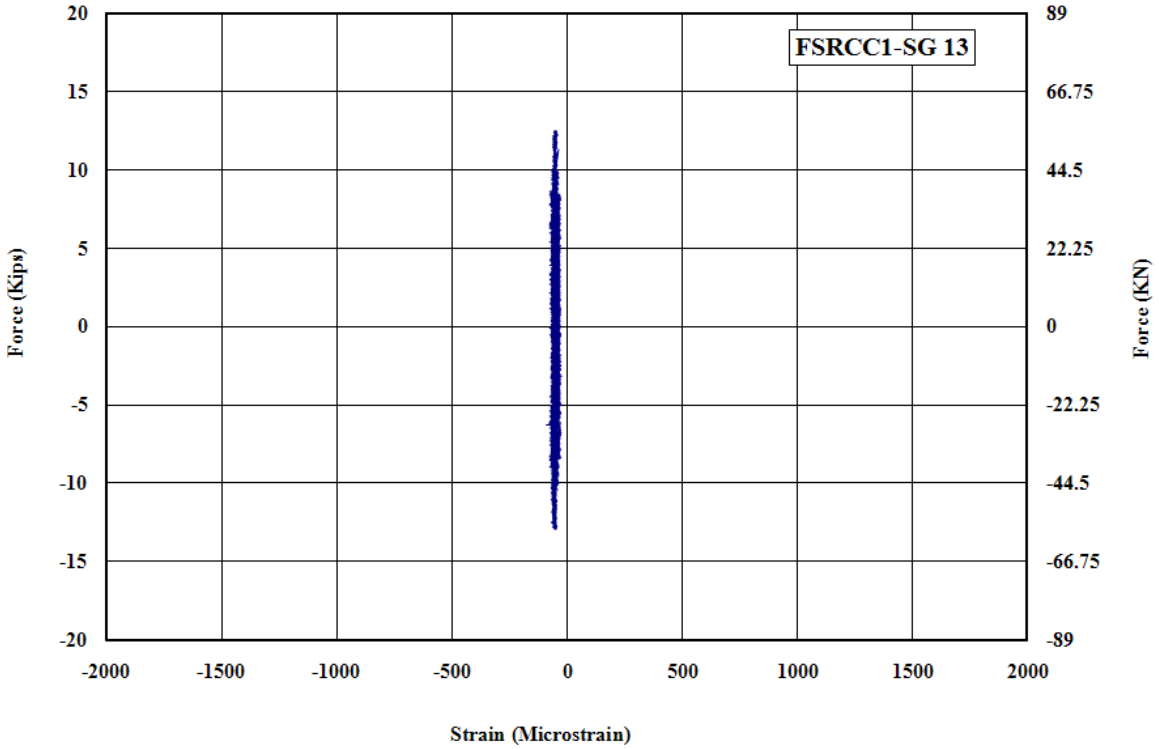

Figure B - 11: Measured Strain in Gauge No.13 for FSRCC1

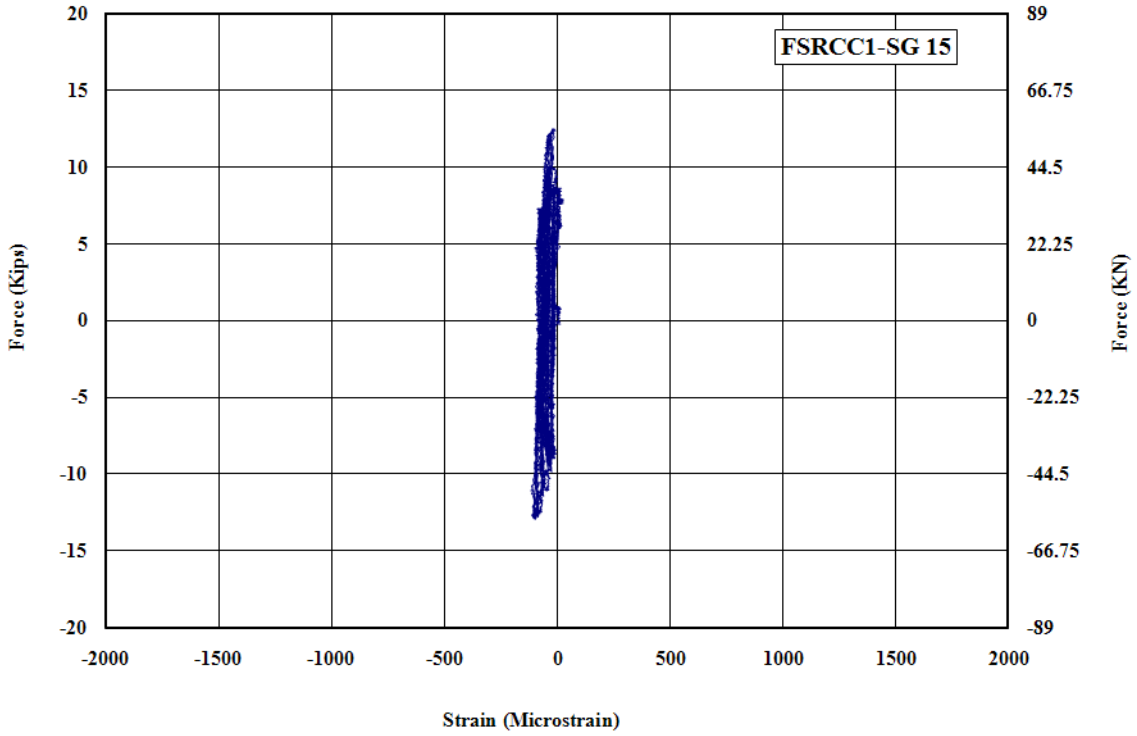

Figure B - 12: Measured Strain in Gauge No.15 for FSRCC1

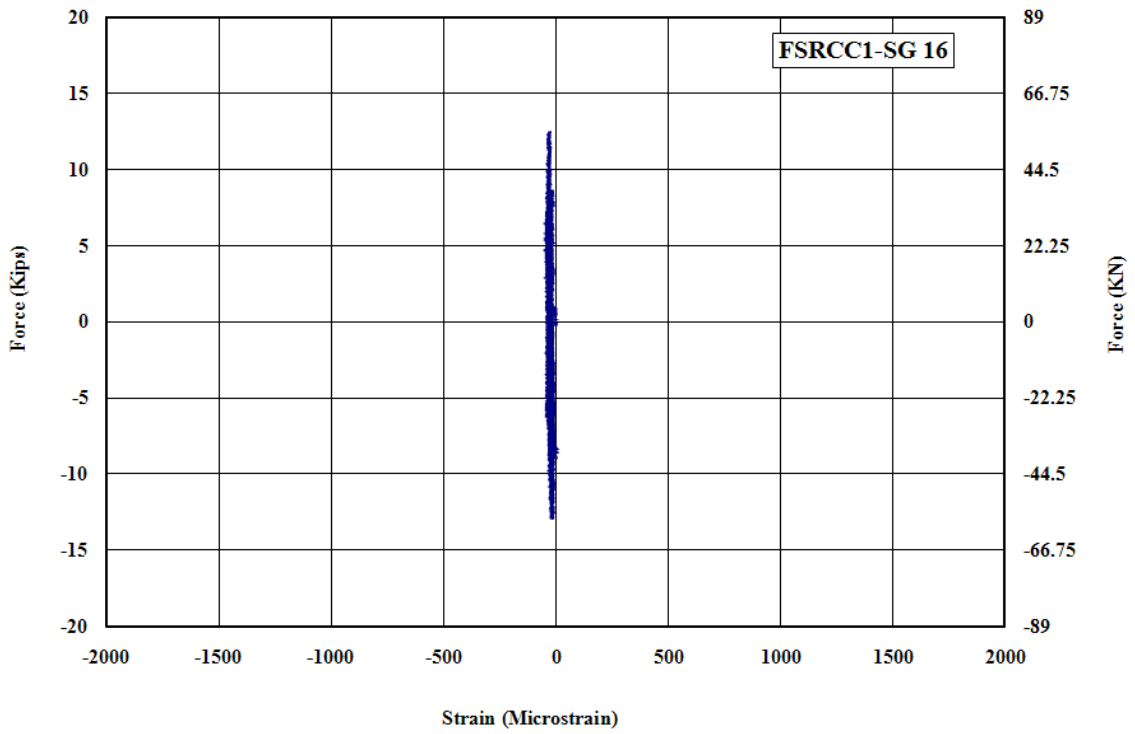

Figure B - 13: Measured Strain in Gauge No.16 for FSRCC1

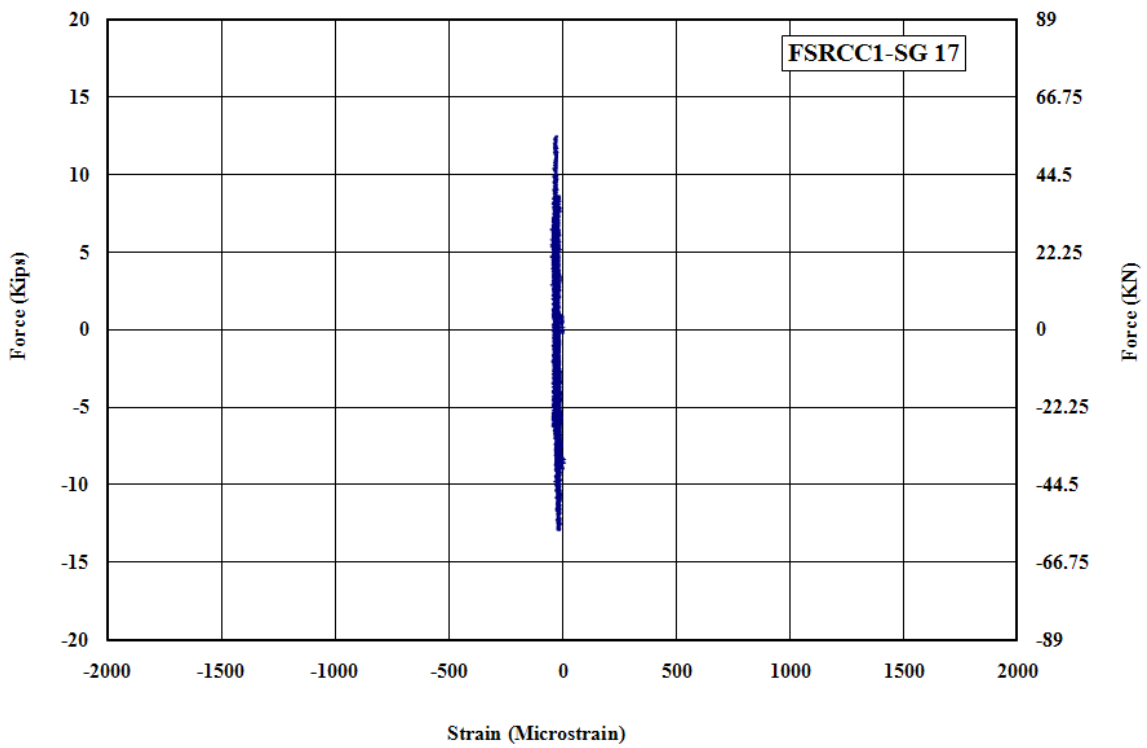

Figure B - 14: Measured Strain in Gauge No.17 for FSRCC1

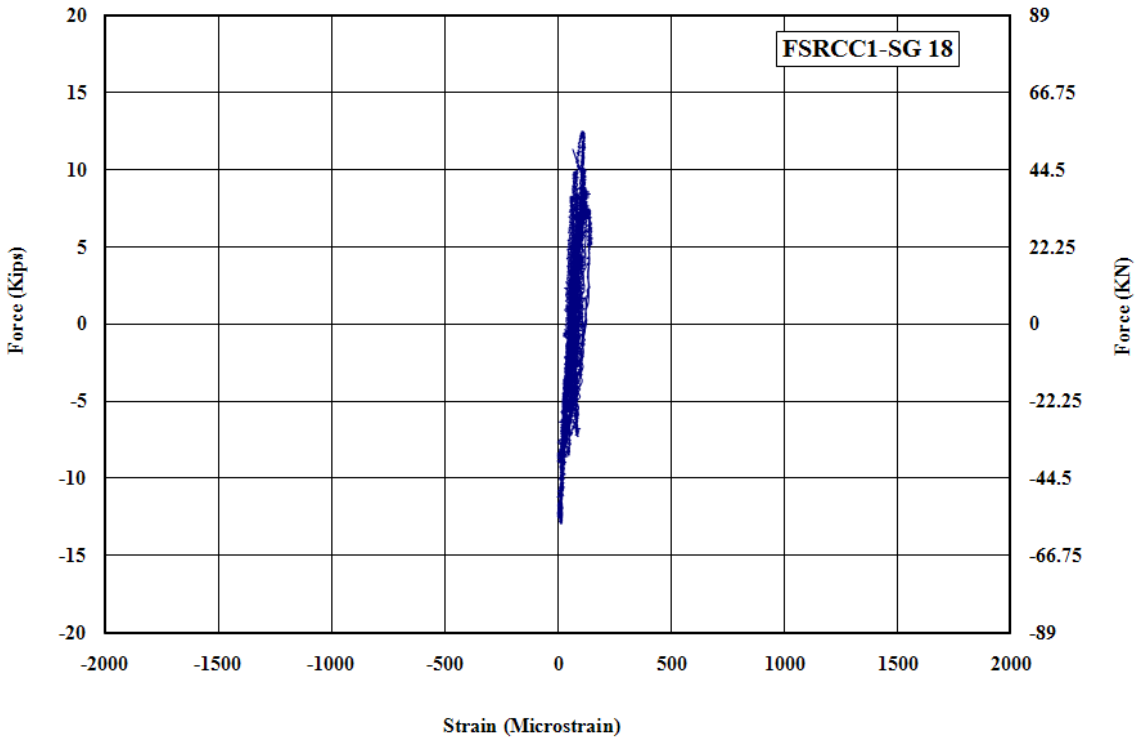

Figure B - 15: Measured Strain in Gauge No.18 for FSRCC1

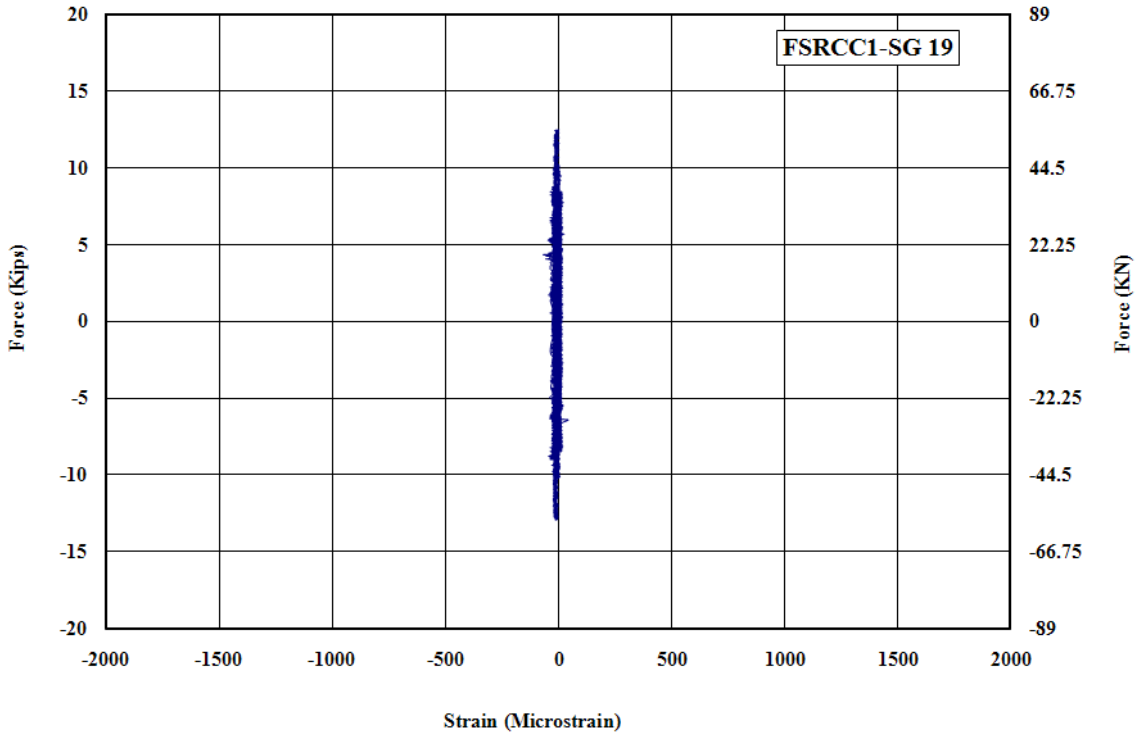

Figure B - 16: Measured Strain in Gauge No.19 for FSRCC1

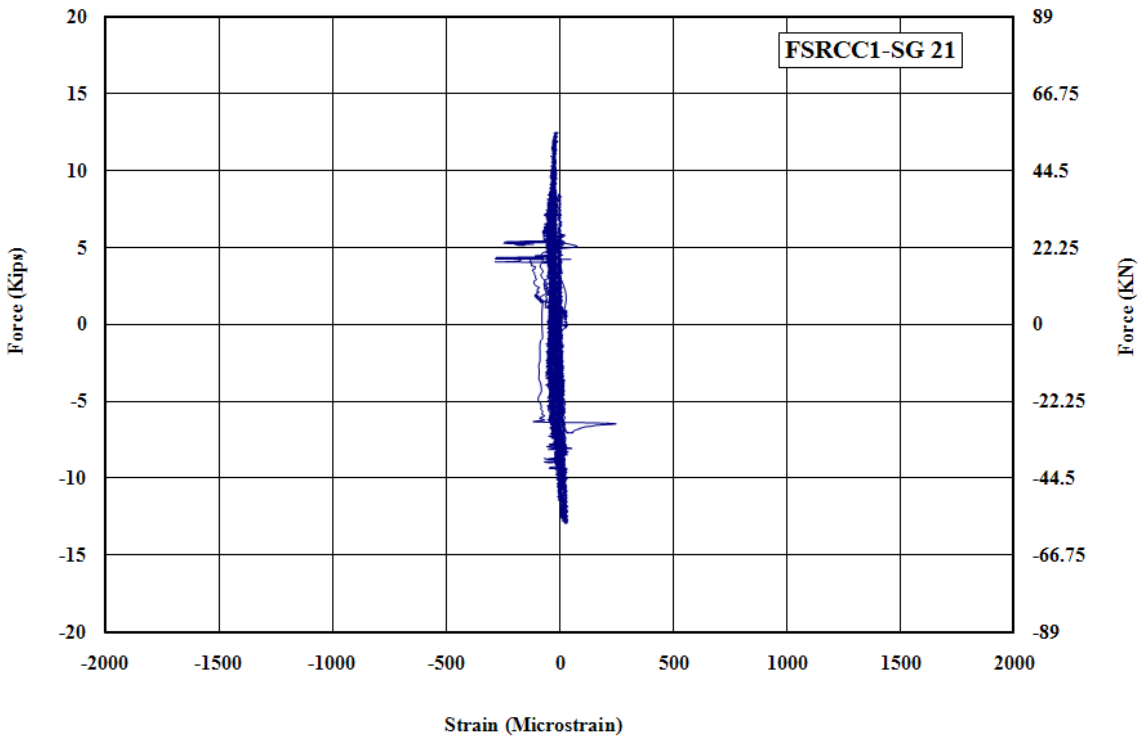

Figure B - 17: Measured Strain in Gauge No.21 for FSRCC1

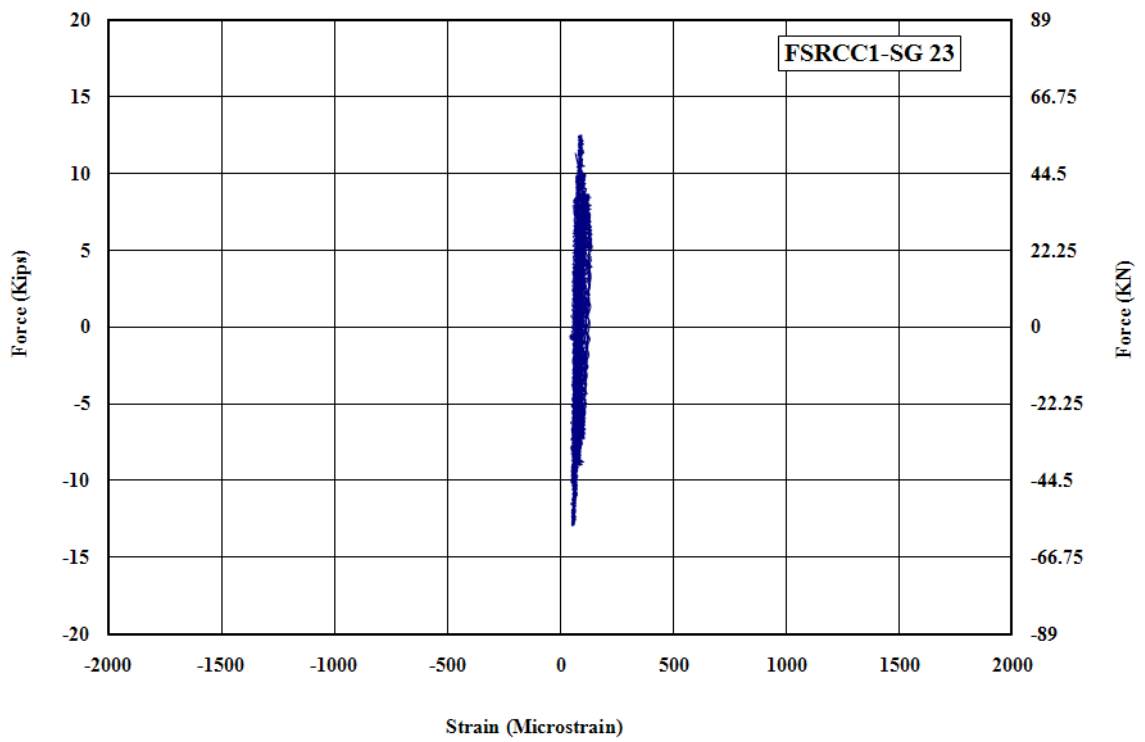

Figure B - 18: Measured Strain in Gauge No.23 for FSRCC1

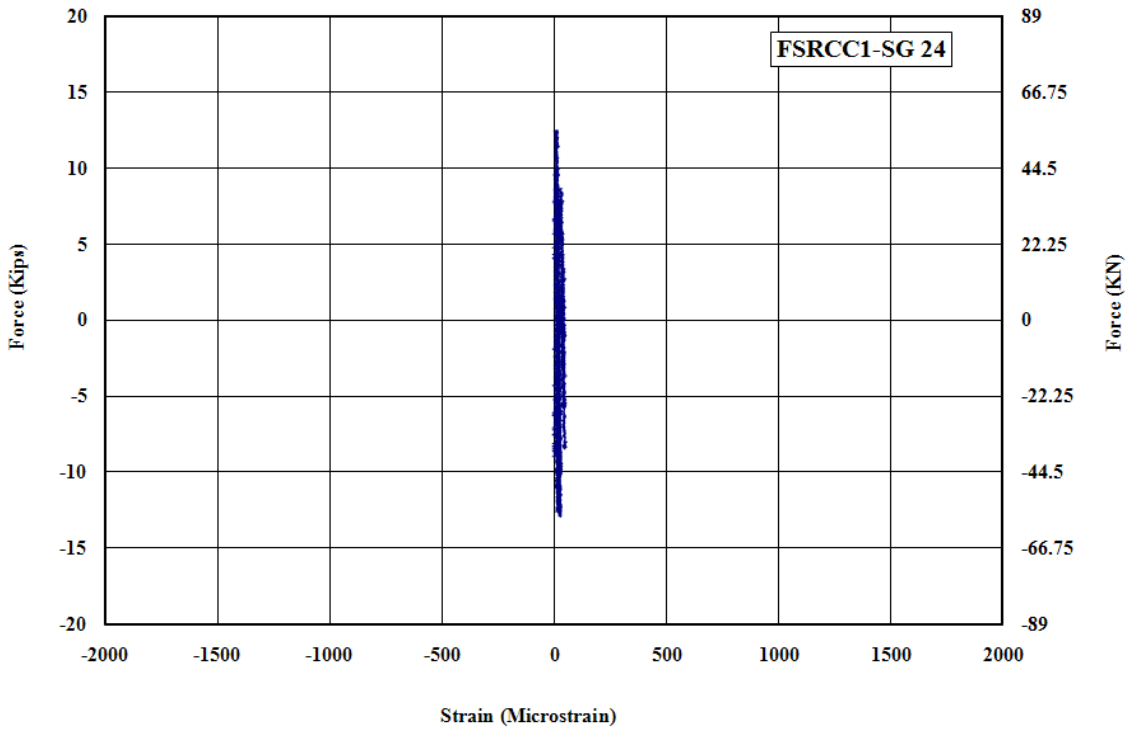

Figure B - 19: Measured Strain in Gauge No.24 for FSRCC1

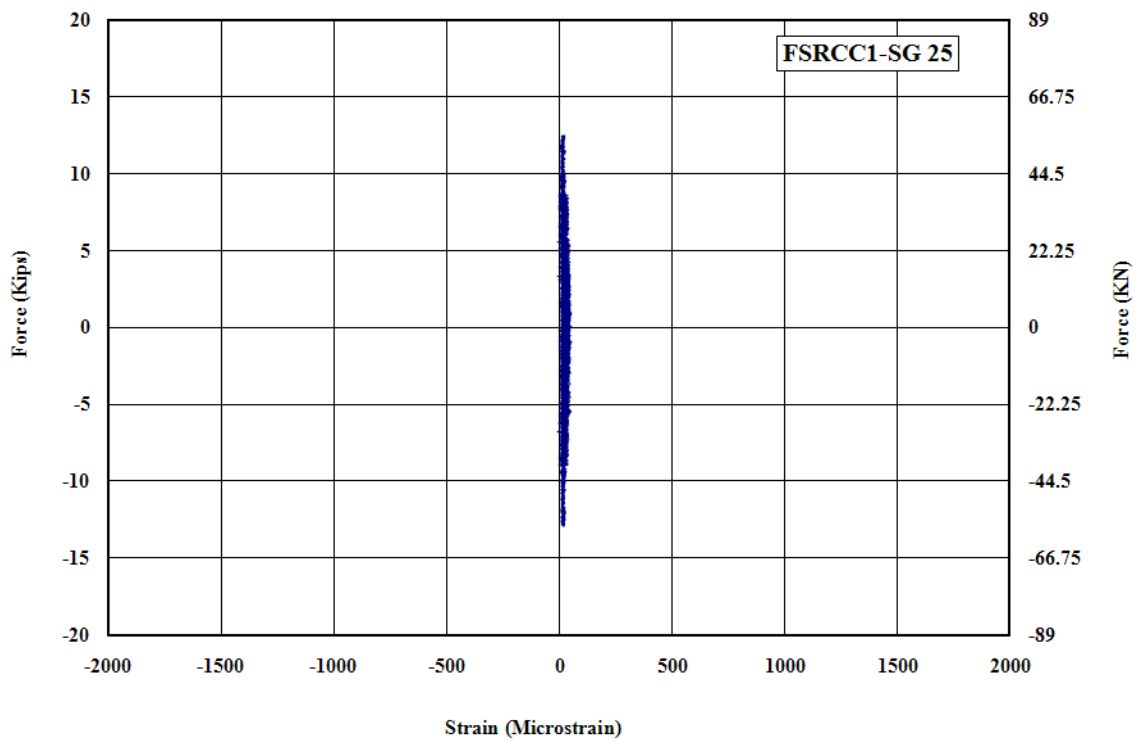

Figure B - 20: Measured Strain in Gauge No.25 for FSRCC1

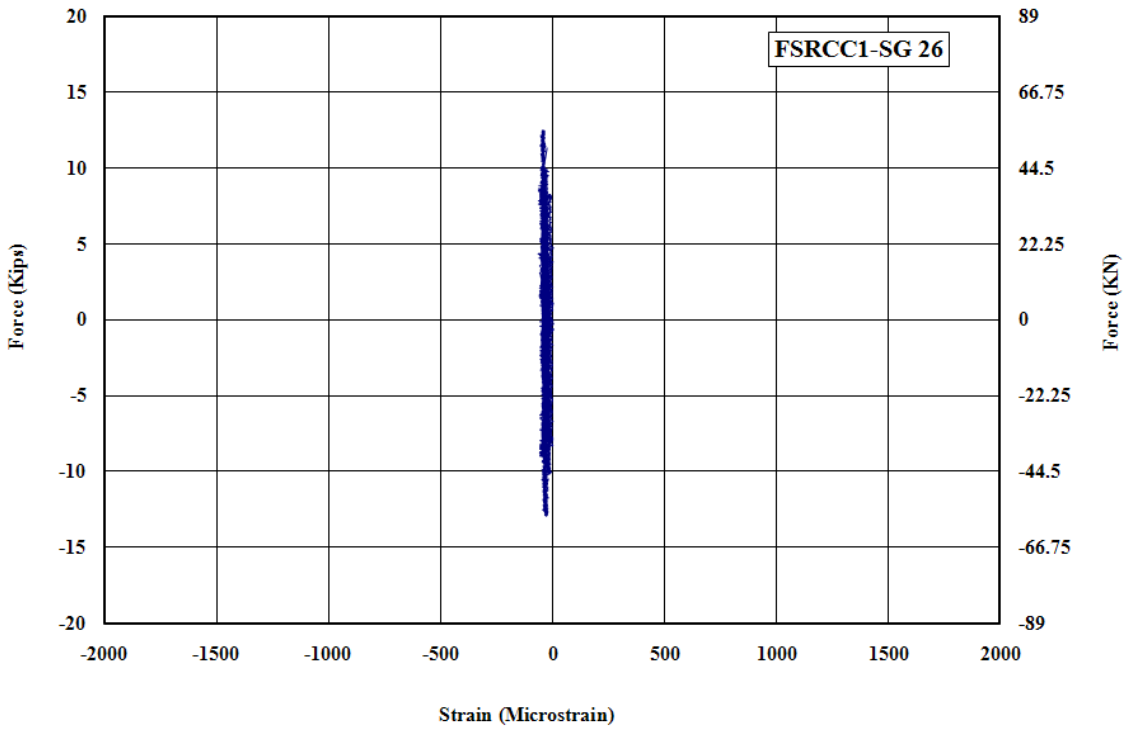

Figure B - 21: Measured Strain in Gauge No.26 for FSRCC1

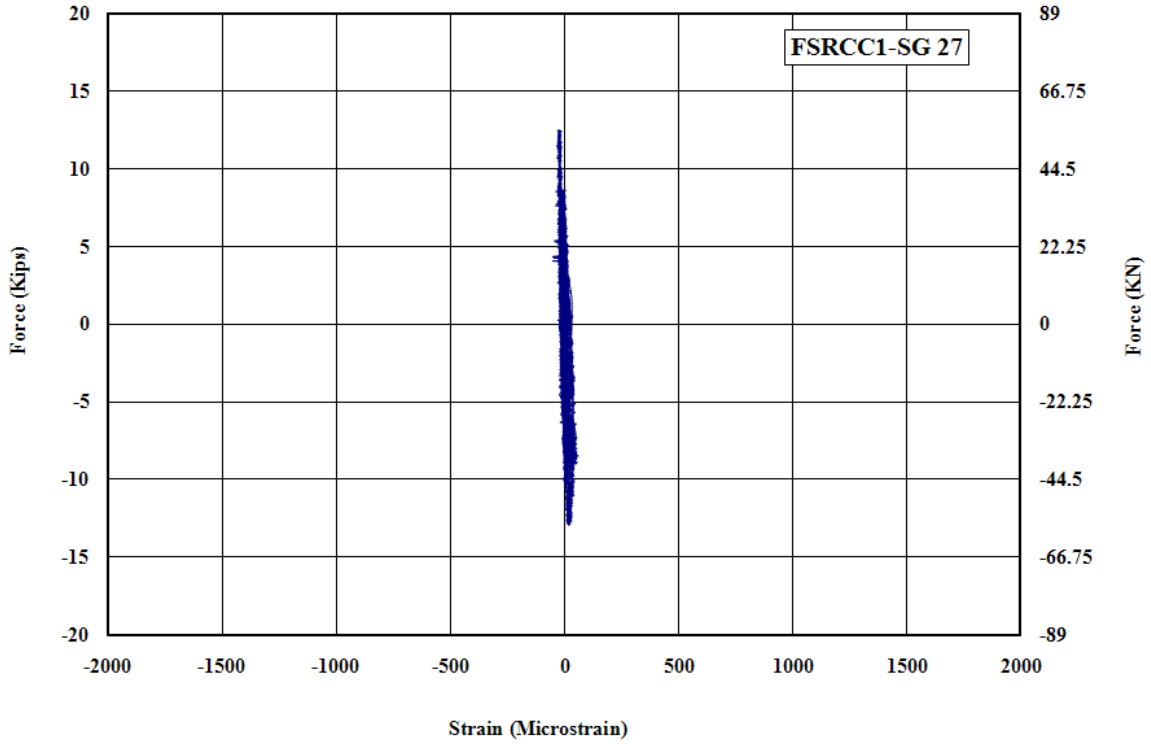

Figure B - 22: Measured Strain in Gauge No.27 for FSRCC1

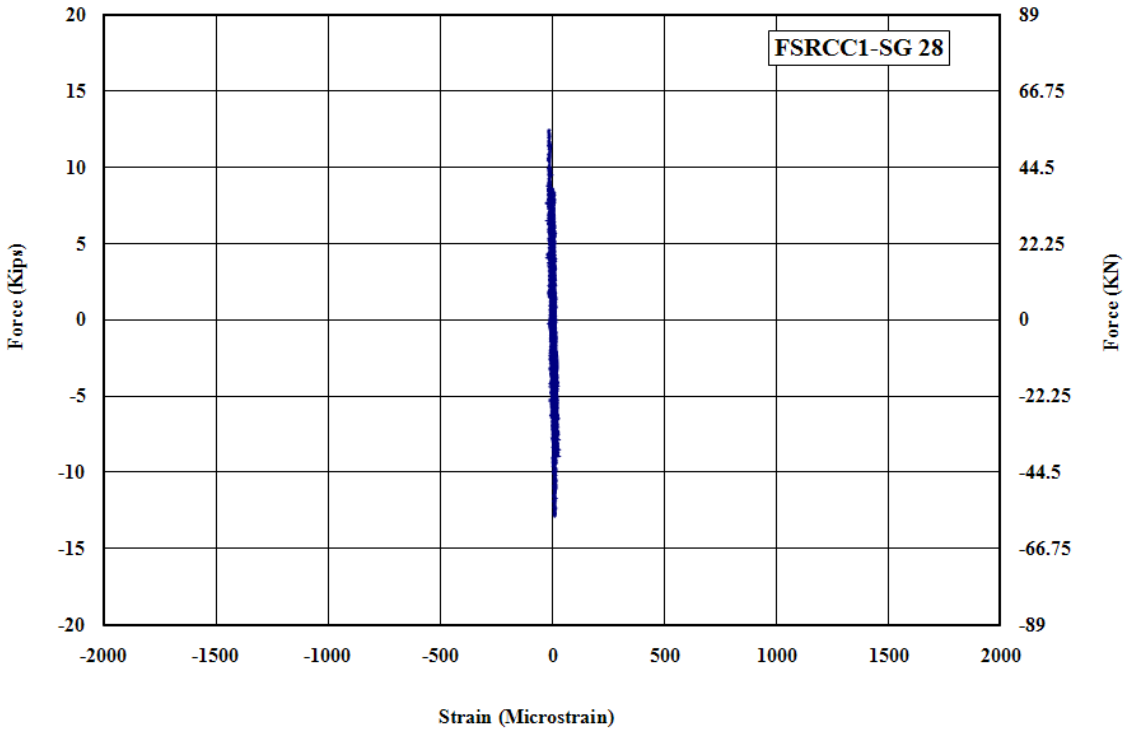

Figure B - 23: Measured Strain in Gauge No.28 for FSRCC1

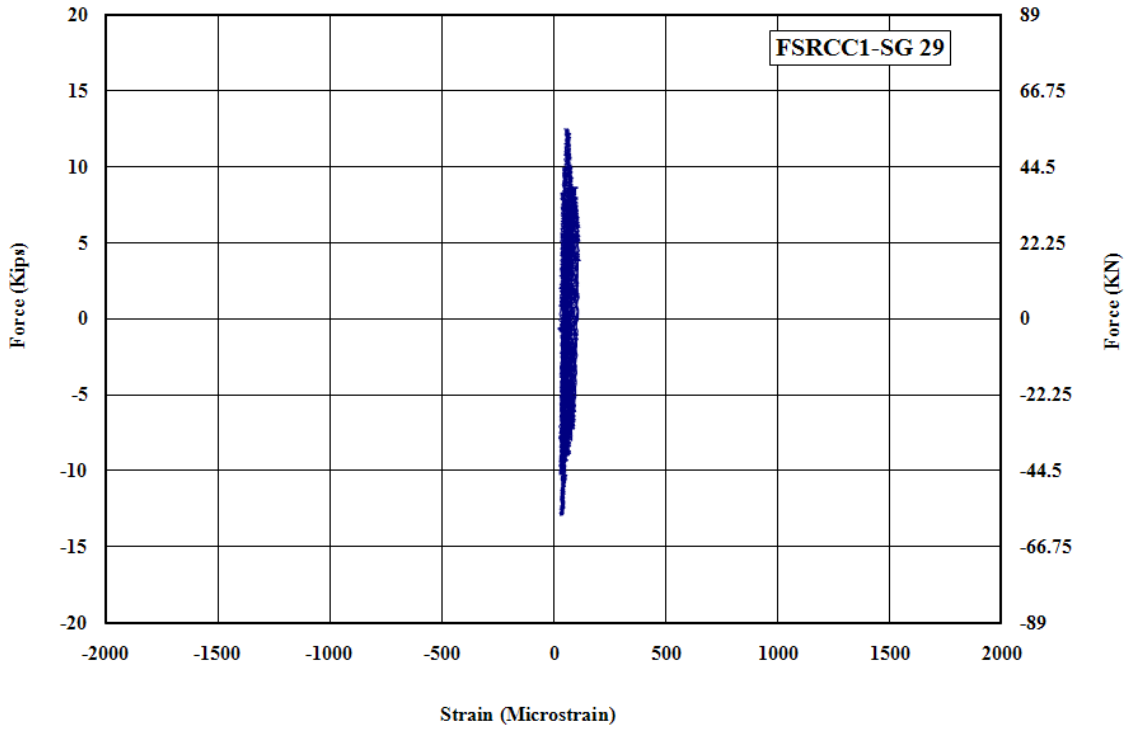

Figure B - 24: Measured Strain in Gauge No.29 for FSRCC1

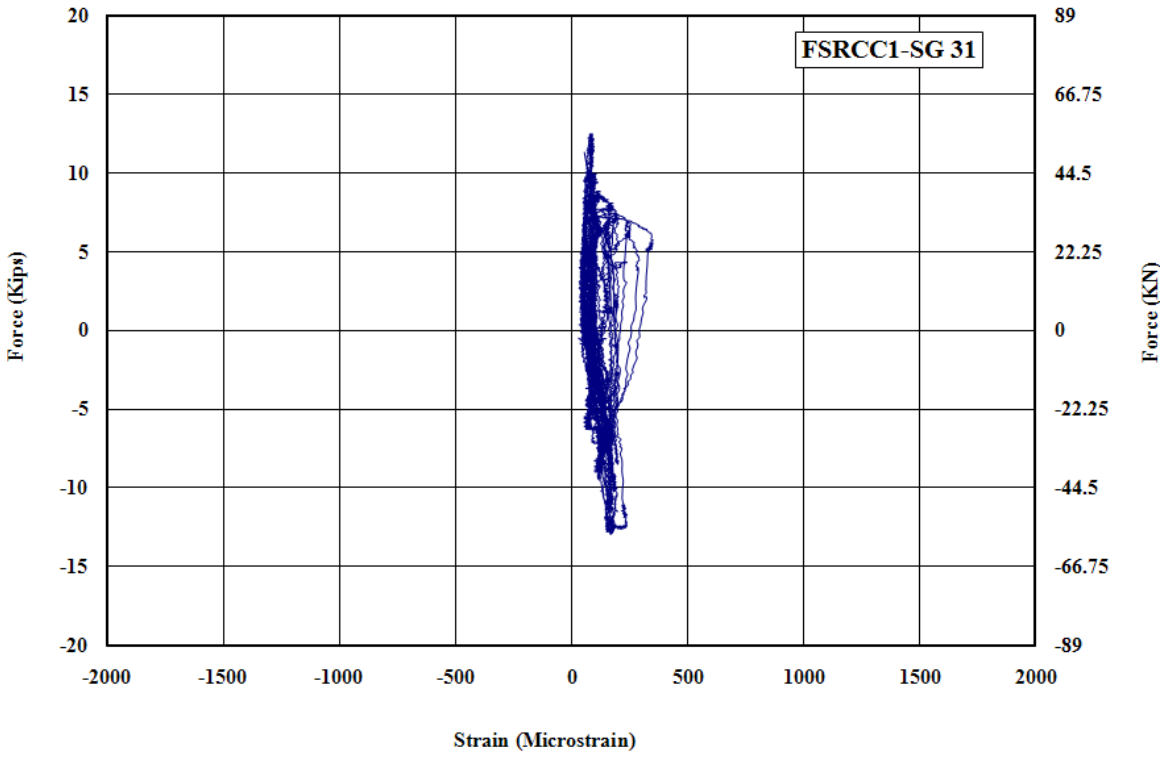

Figure B - 25: Measured Strain in Gauge No.31 for FSRCC1

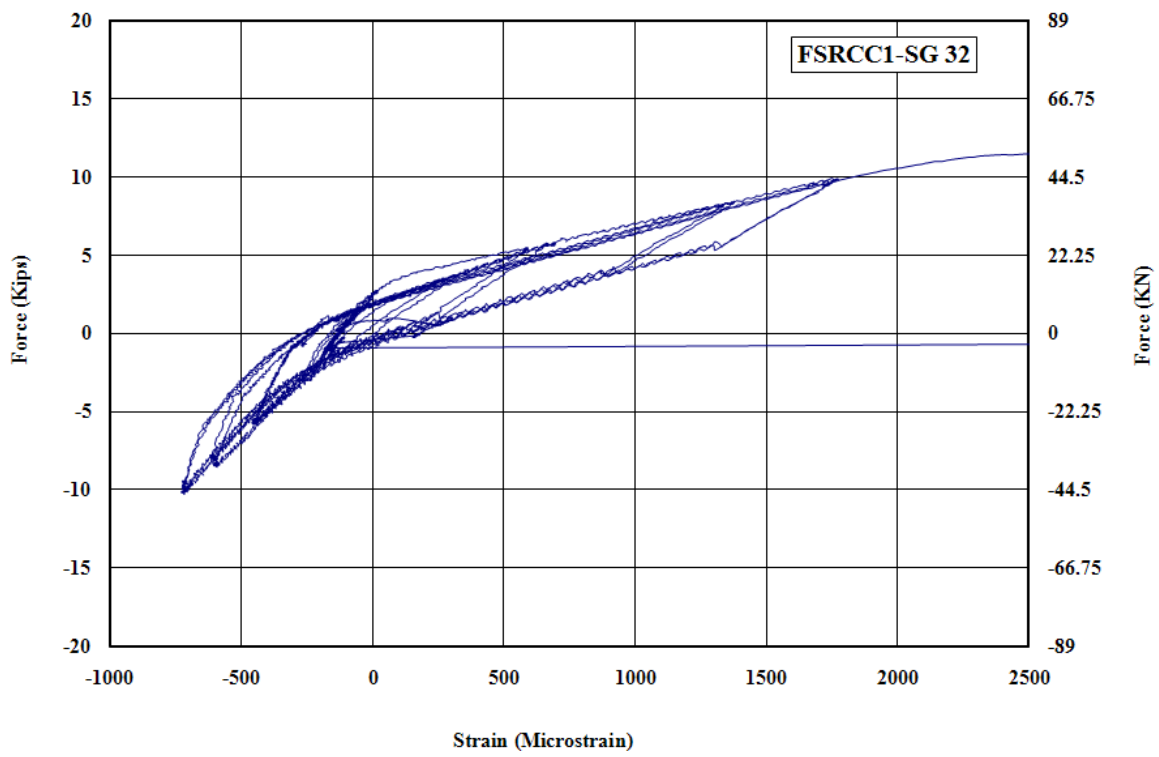

Figure B - 26: Measured Strain in Gauge No.32 for FSRCC1

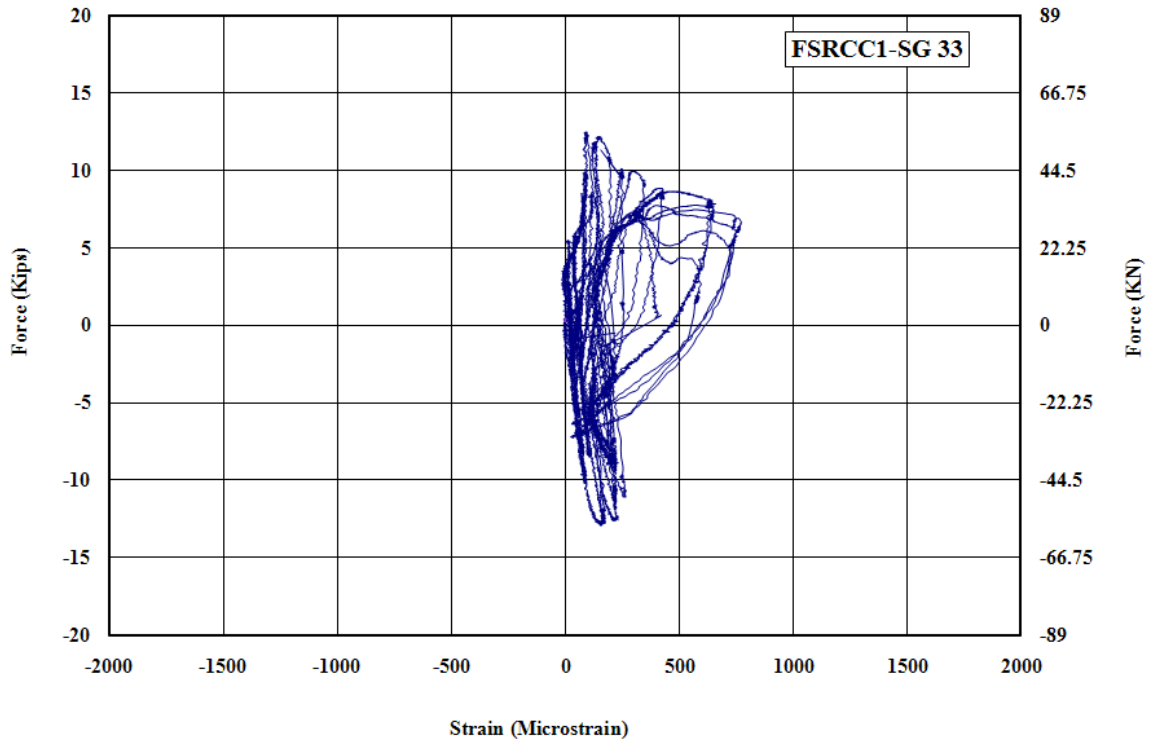

Figure B - 27: Measured Strain in Gauge No.33 for FSRCC1

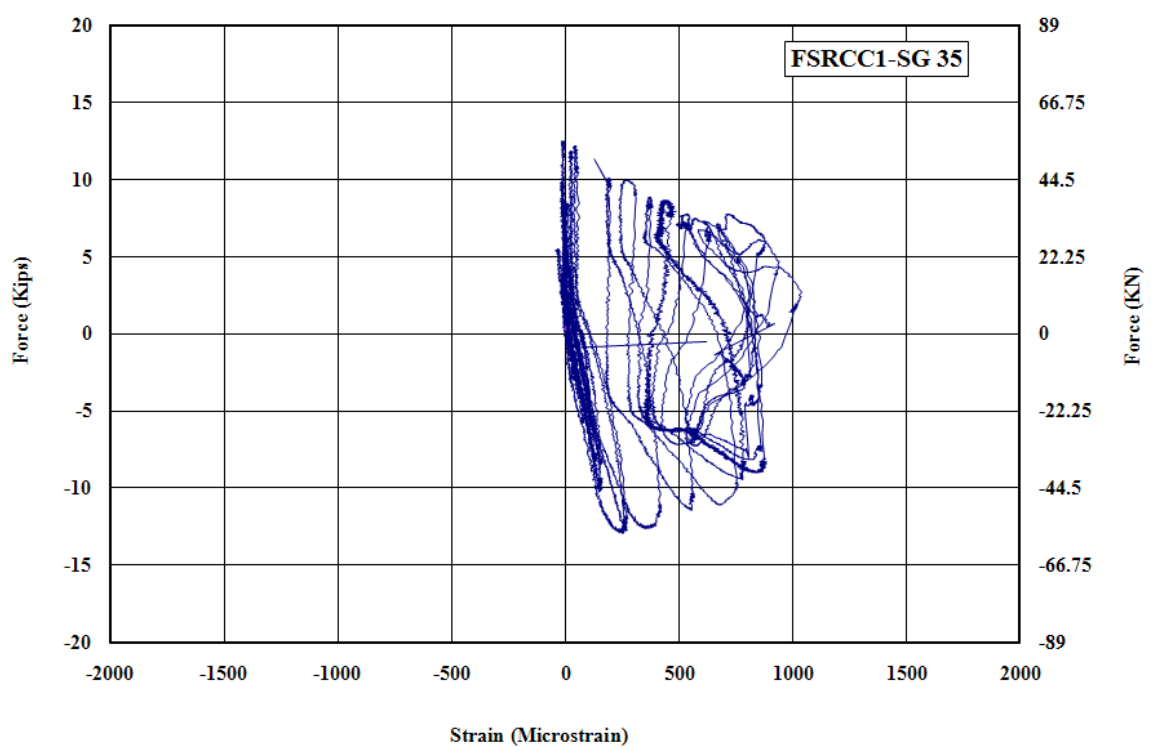

Figure B - 28: Measured Strain in Gauge No.35 for FSRCC1

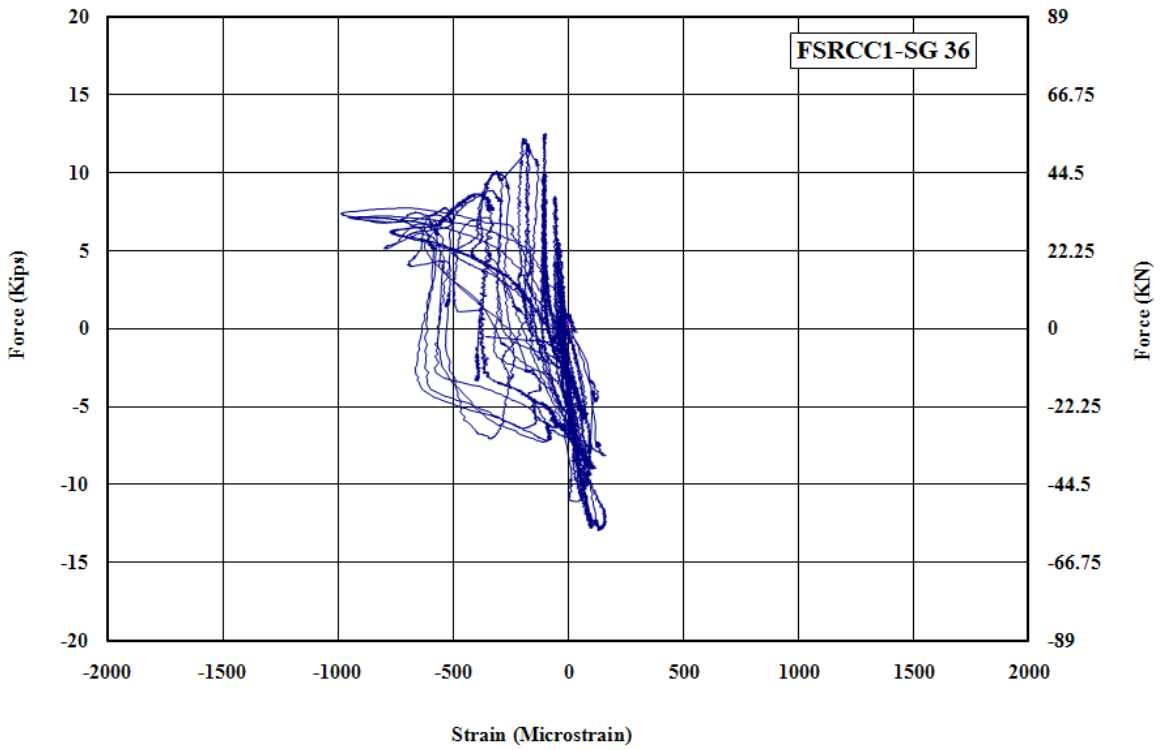

Figure B - 29: Measured Strain in Gauge No.36 for FSRCC1

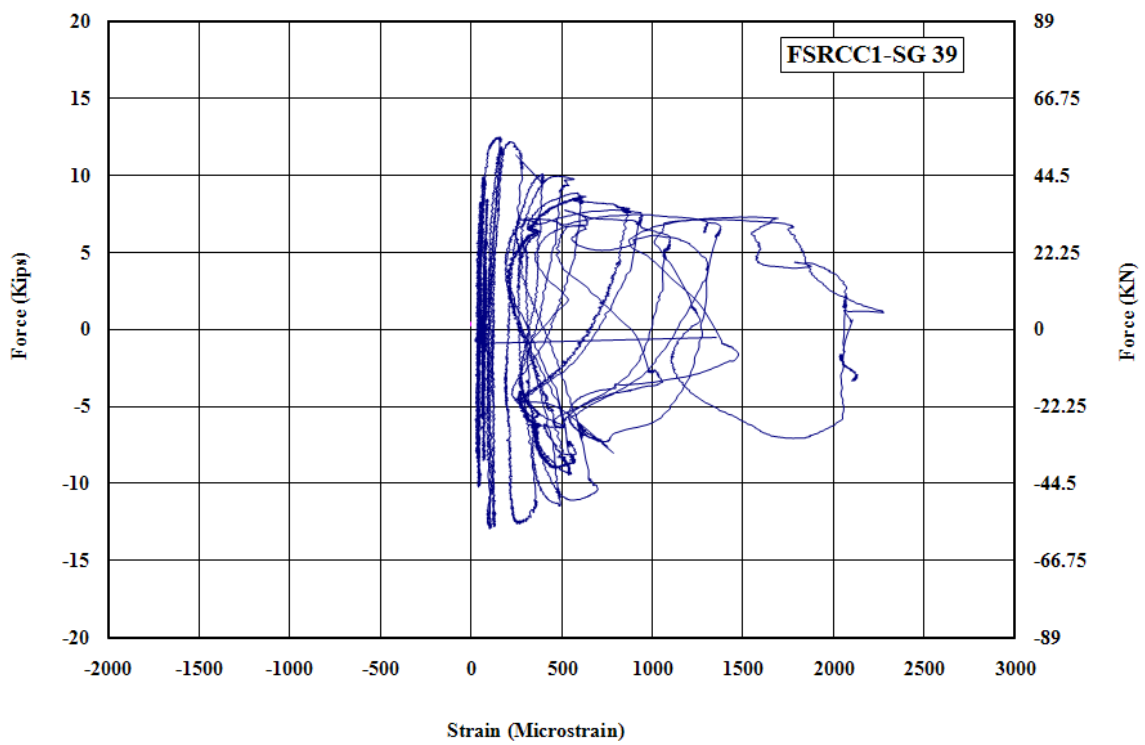

Figure B - 30: Measured Strain in Gauge No.39 for FSRCC1

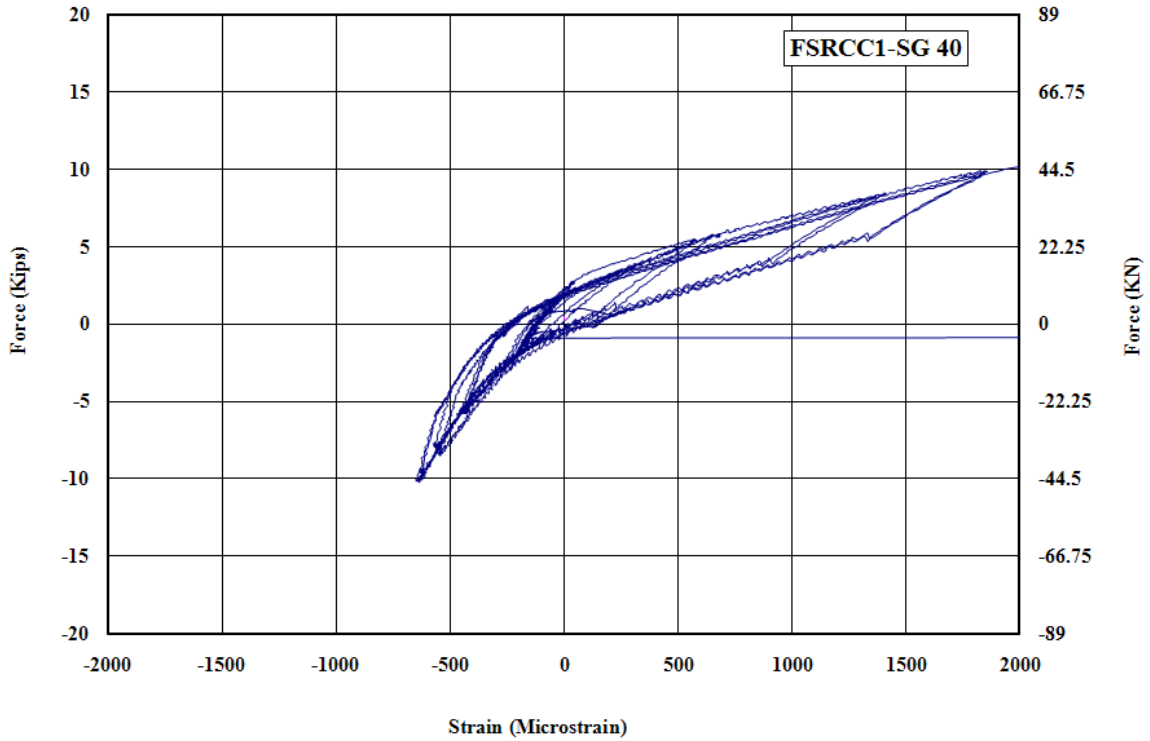

Figure B - 31: Measured Strain in Gauge No.40 for FSRCC1

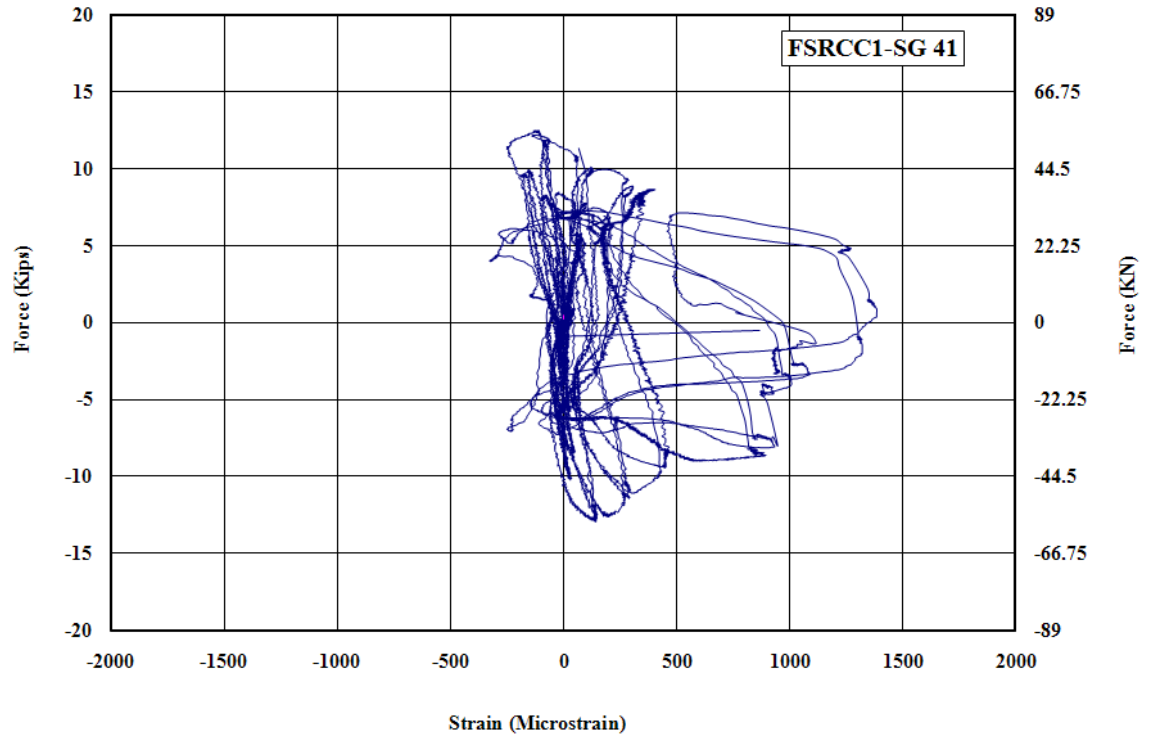

Figure B - 32: Measured Strain in Gauge No.41 for FSRCC1

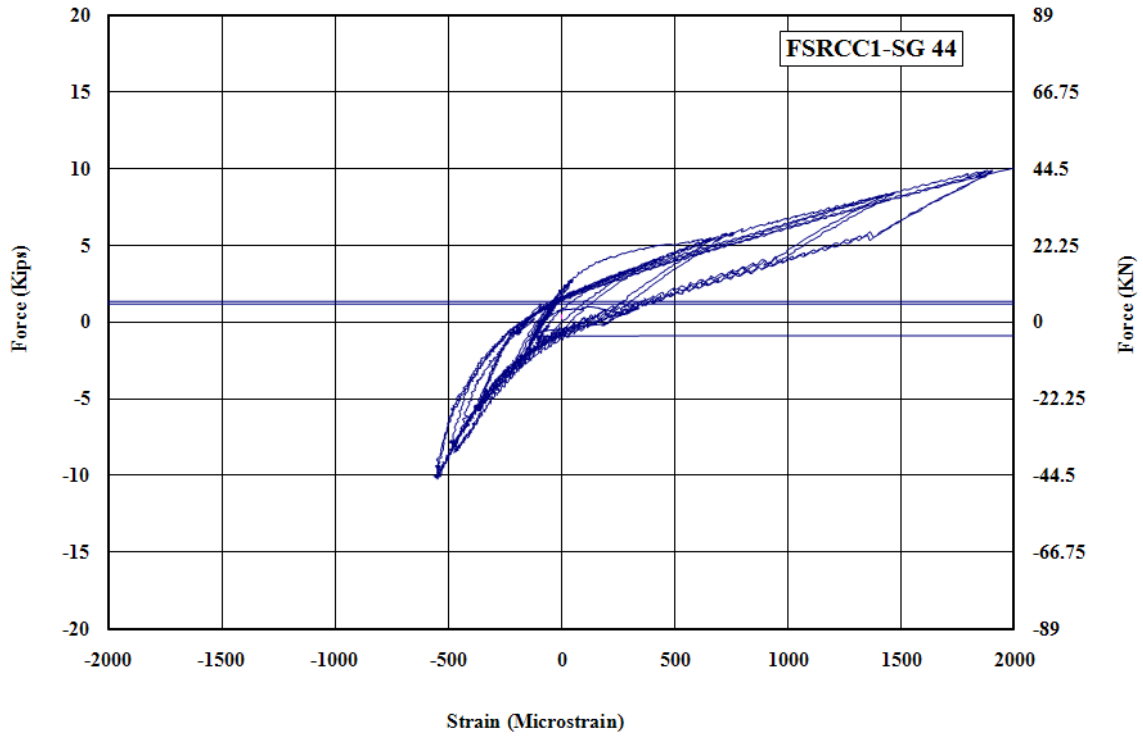

Figure B - 33: Measured Strain in Gauge No.44 for FSRCC1

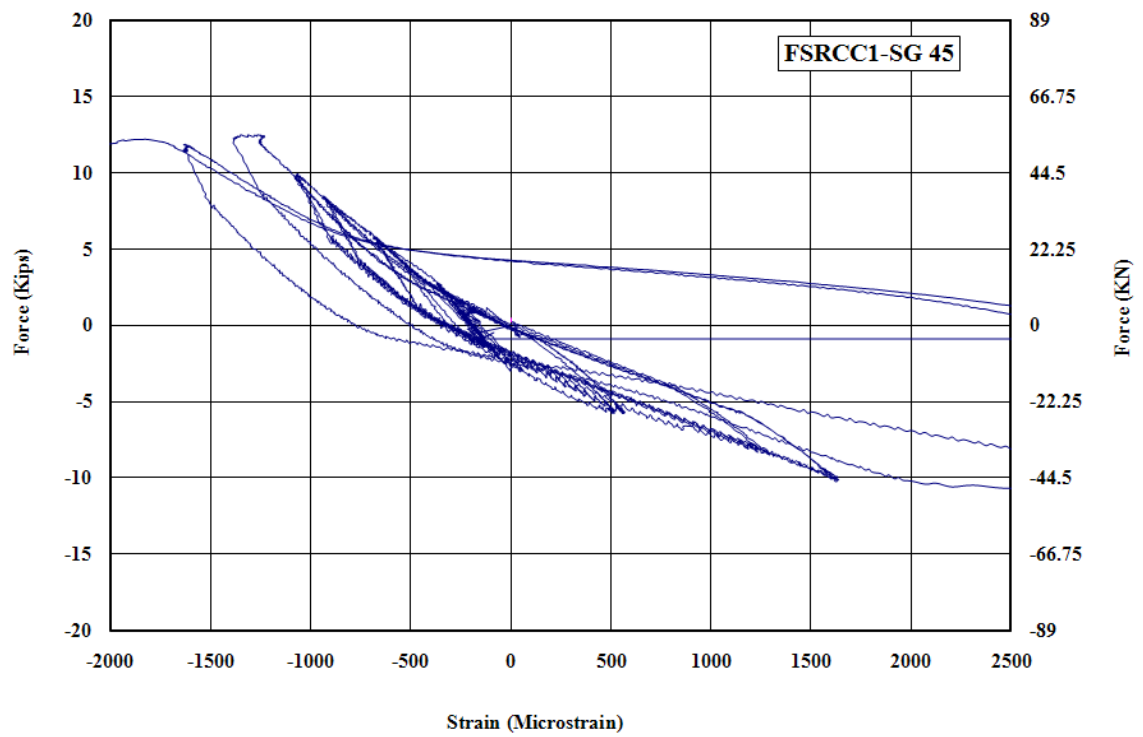

Figure B - 34: Measured Strain in Gauge No.45 for FSRCC1

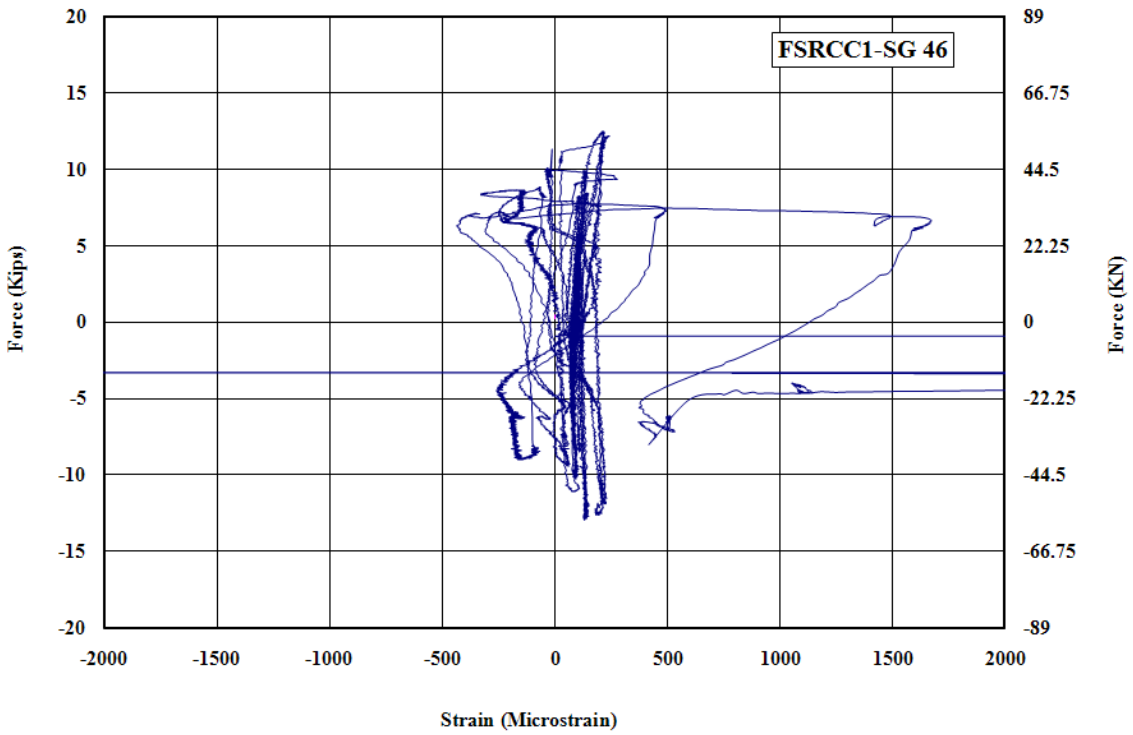

Figure B - 35: Measured Strain in Gauge No.46 for FSRCC1

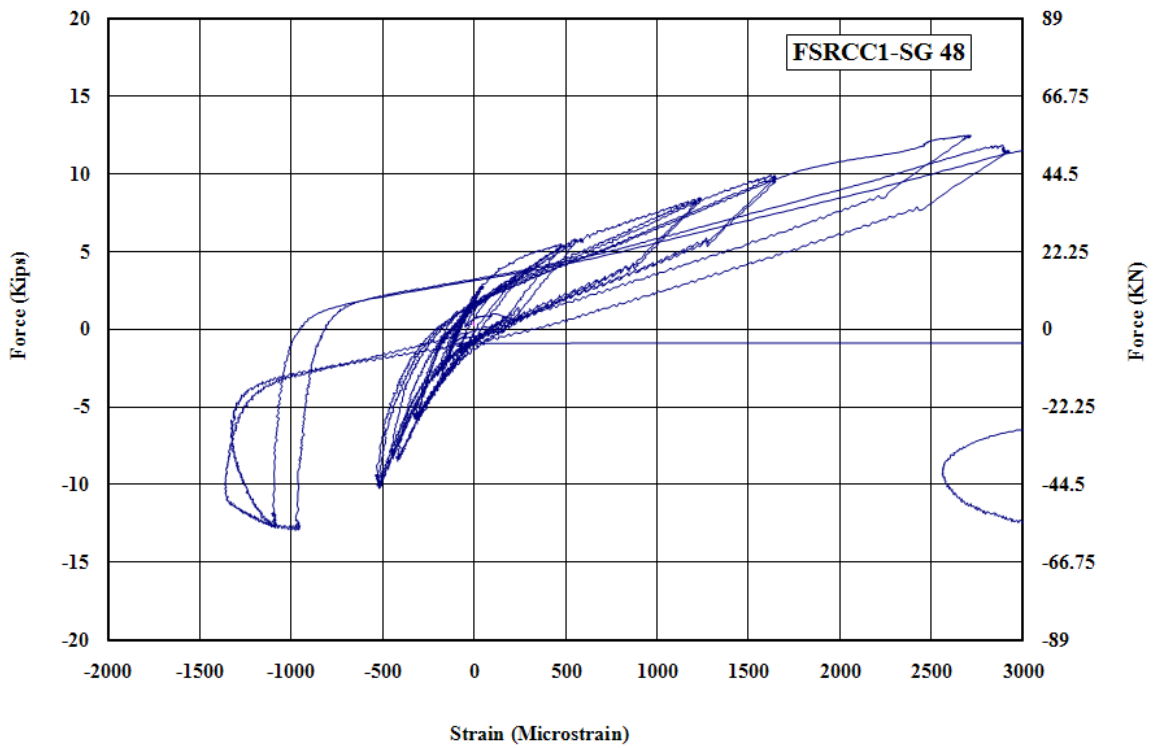

Figure B - 36: Measured Strain in Gauge No.48 for FSRCC1

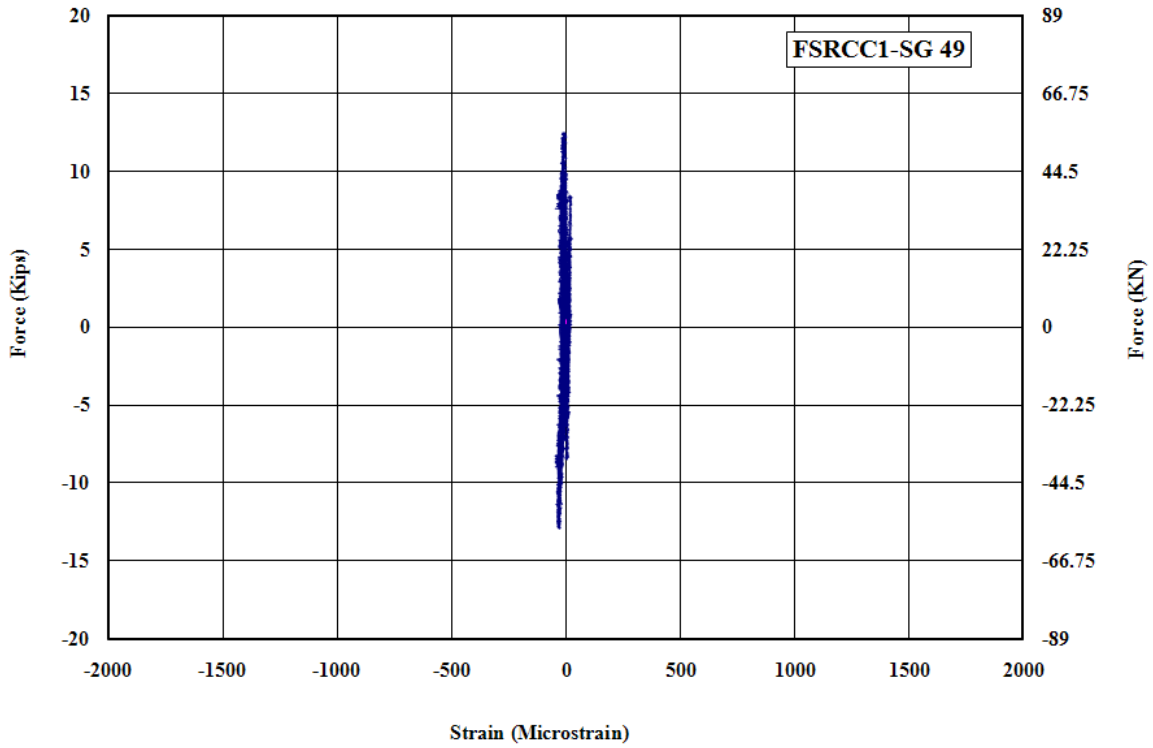

Figure B - 37: Measured Strain in Gauge No.49 for FSRCC1

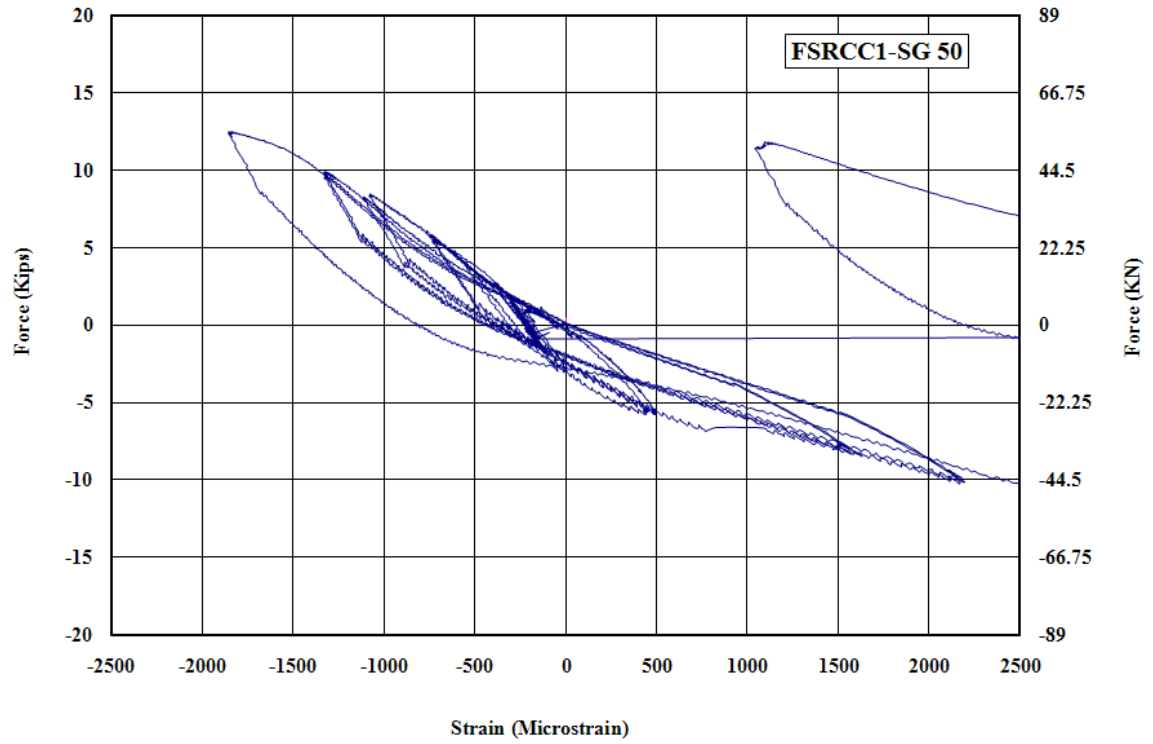

Figure B - 38: Measured Strain in Gauge No.50 for FSRCC1

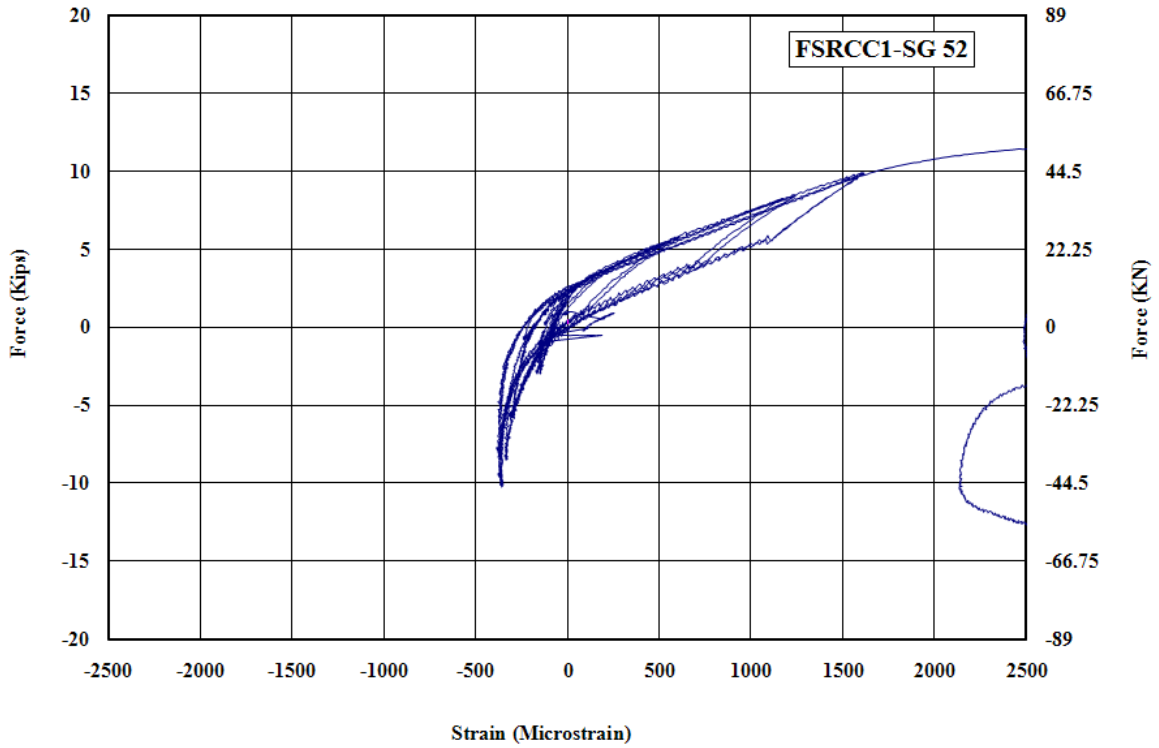

Figure B - 39: Measured Strain in Gauge No.52 for FSRCC1

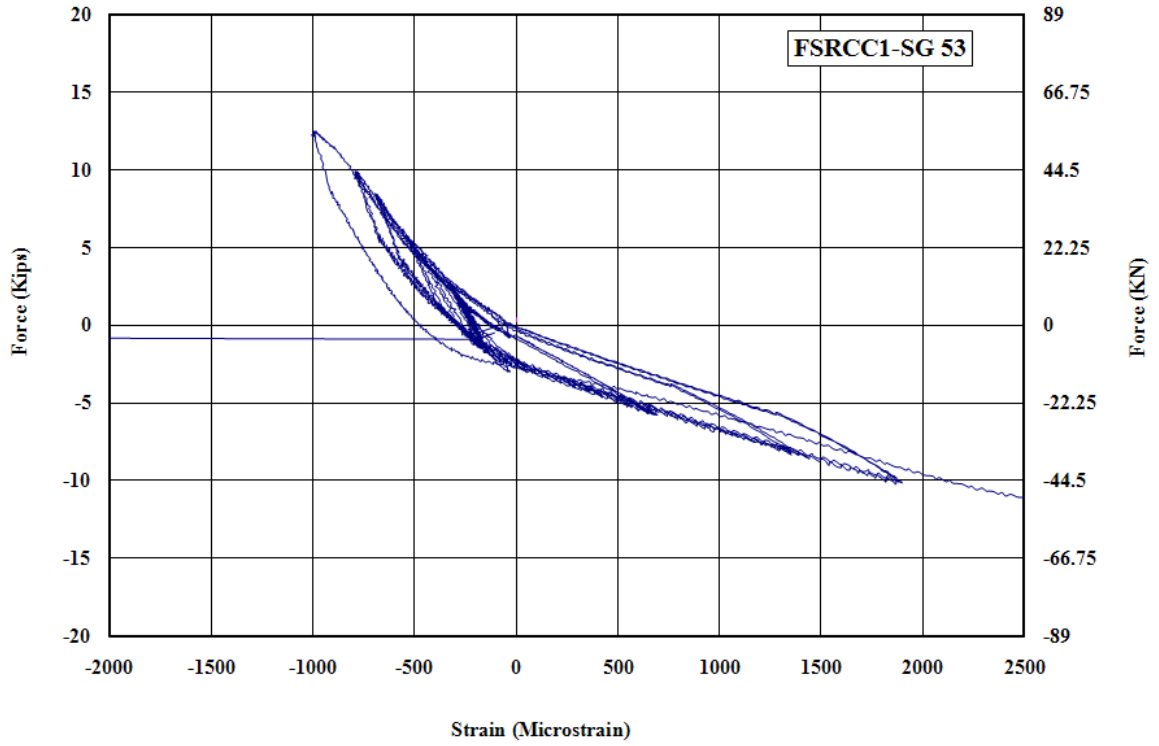

Figure B - 40: Measured Strain in Gauge No.53 for FSRCC1

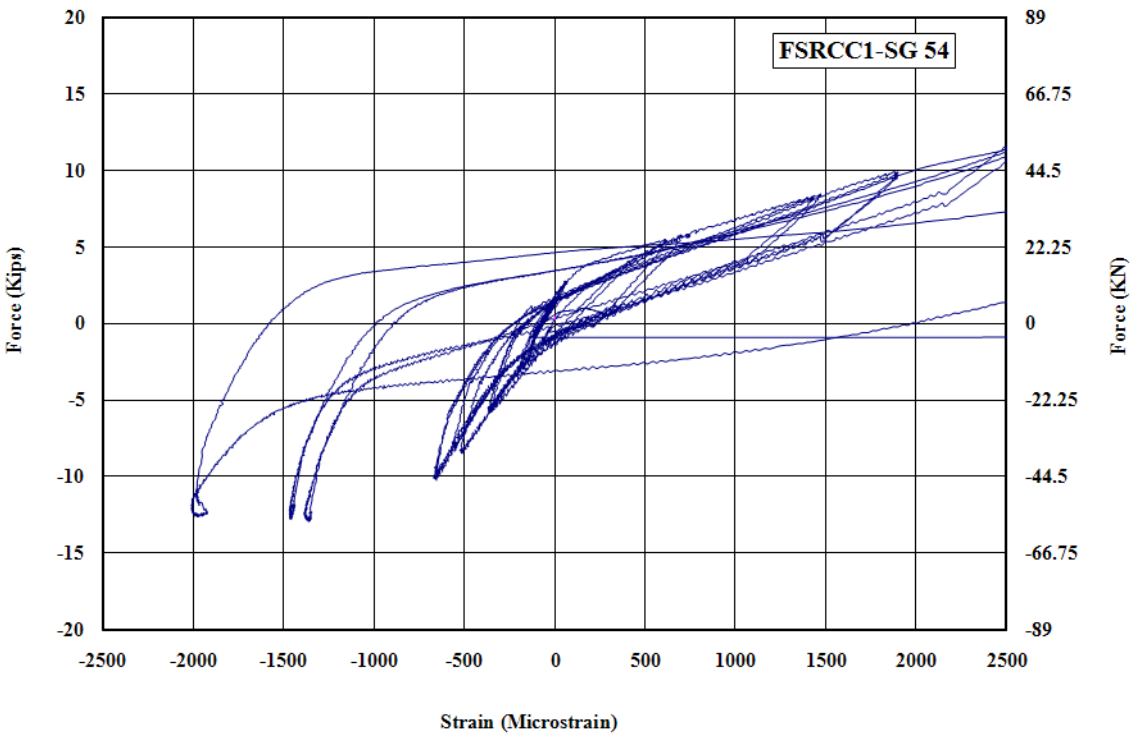

Figure B - 41: Measured Strain in Gauge No.54 for FSRCC1

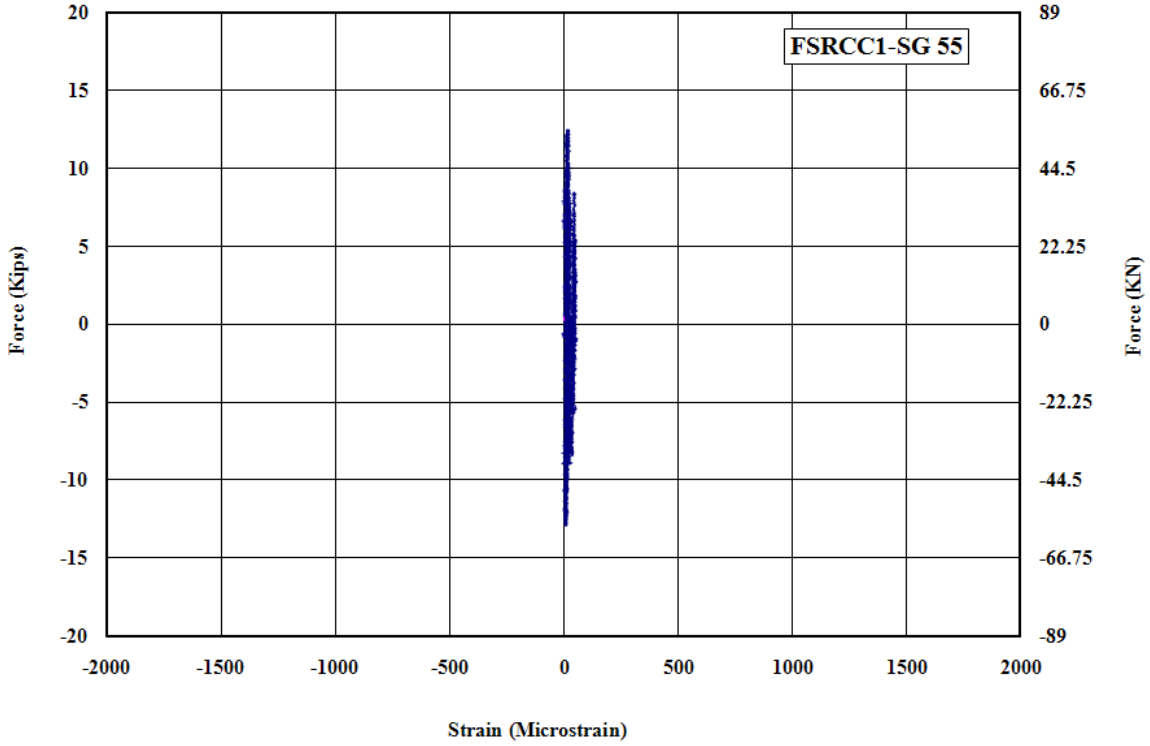

Figure B - 42: Measured Strain in Gauge No.55 for FSRCC1

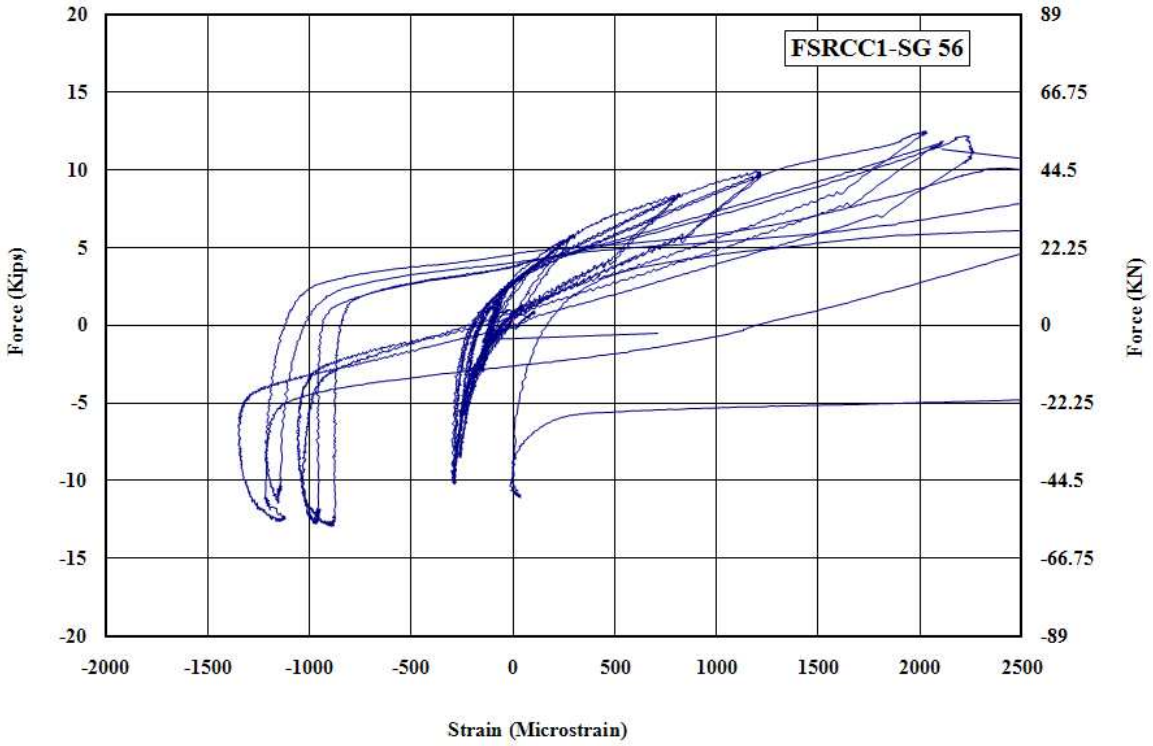

Figure B - 43: Measured Strain in Gauge No.56 for FSRCC1

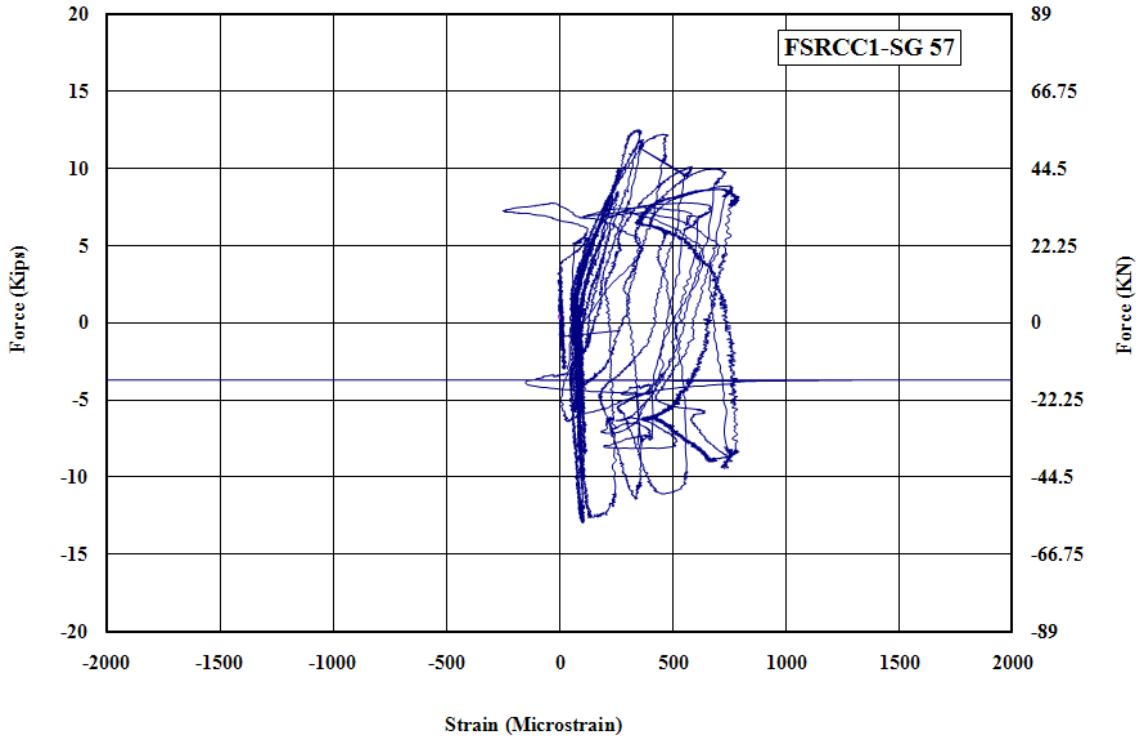

Figure B - 44: Measured Strain in Gauge No.57 for FSRCC1

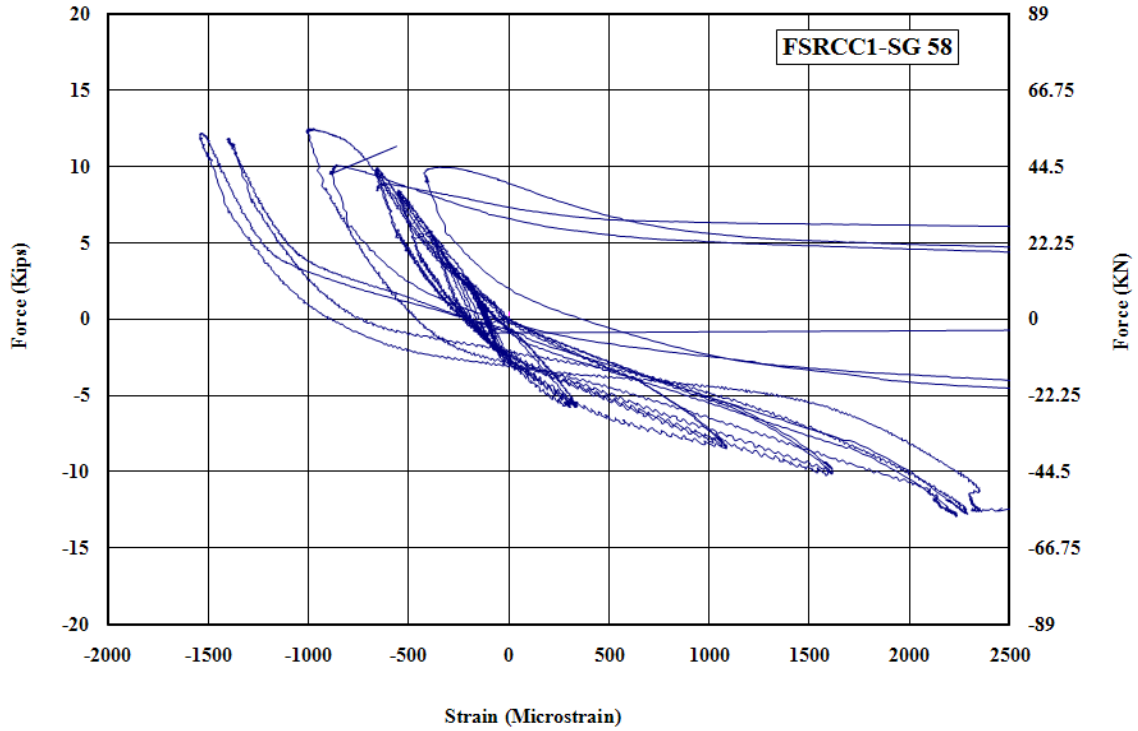

Figure B - 45: Measured Strain in Gauge No.58 for FSRCC1

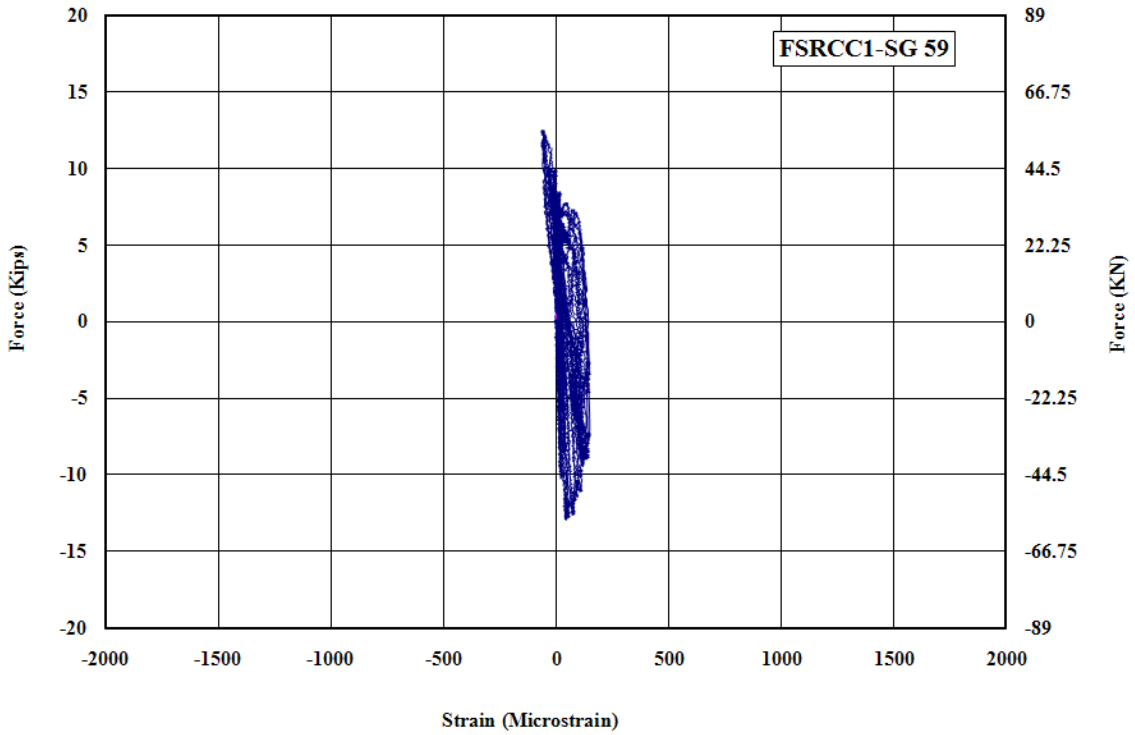

Figure B - 46: Measured Strain in Gauge No.59 for FSRCC1

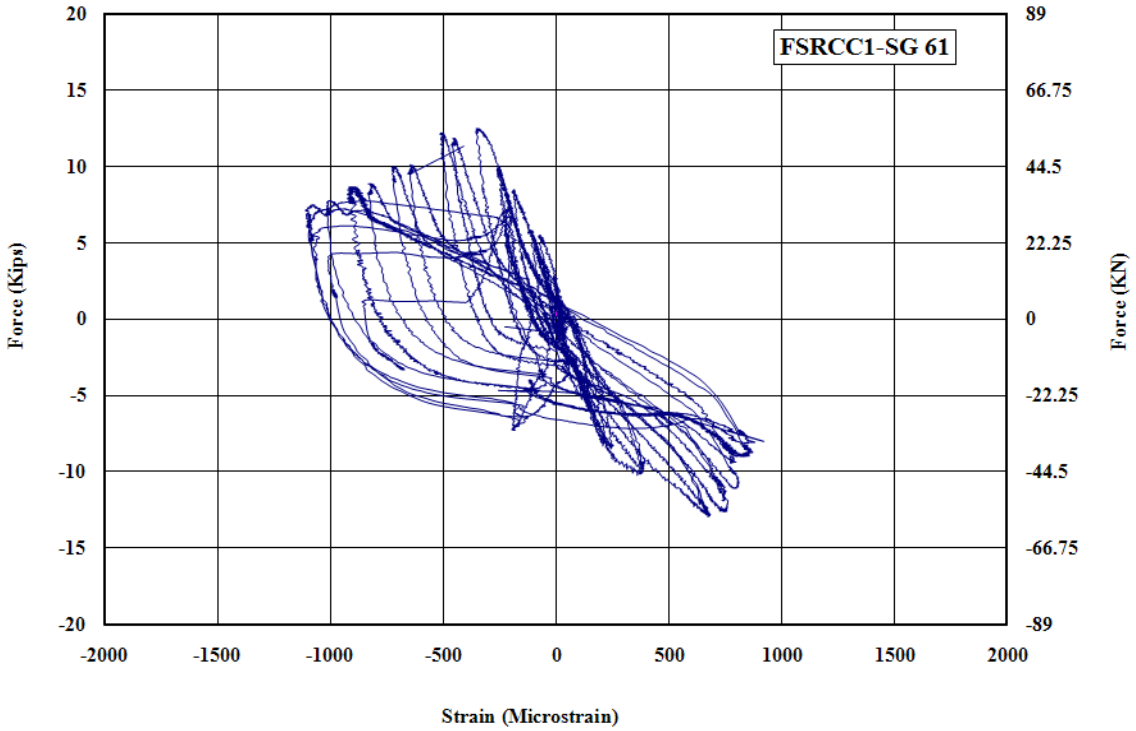

Figure B - 47: Measured Strain in Gauge No.61 for FSRCC1

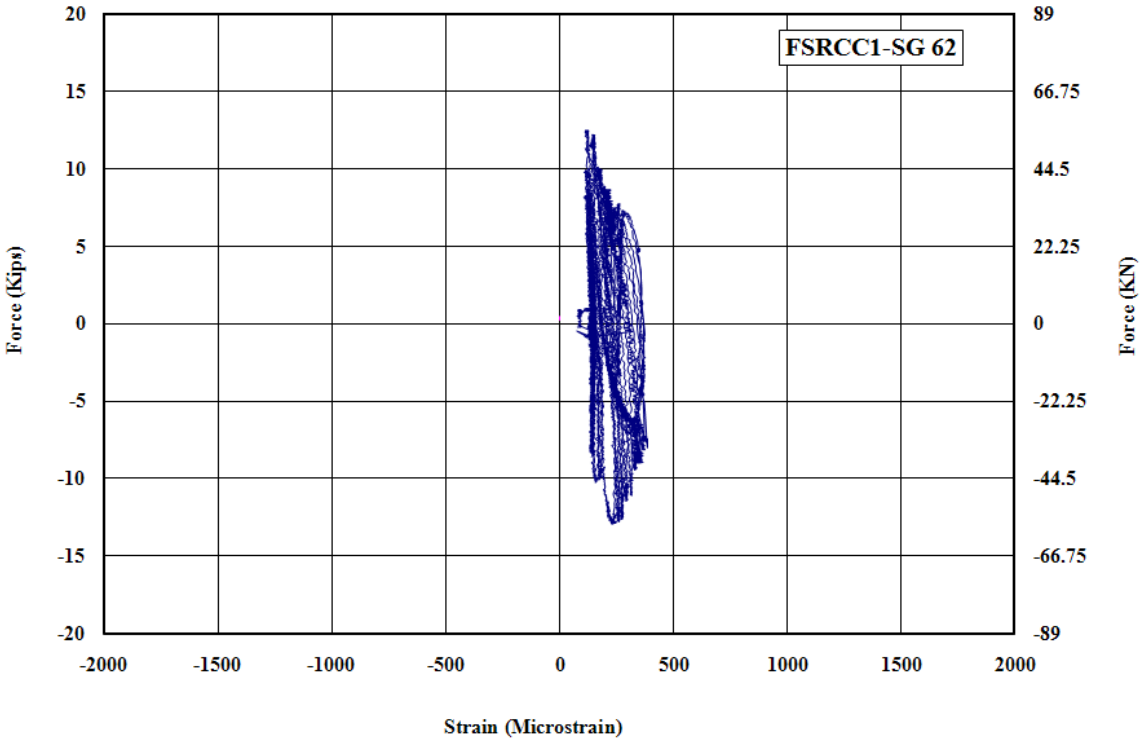

Figure B - 48: Measured Strain in Gauge No.62 for FSRCC1

Appendix C

Specimens DCRCC24

(Drop-Cap T-Joint with 24-in.diameter pile)

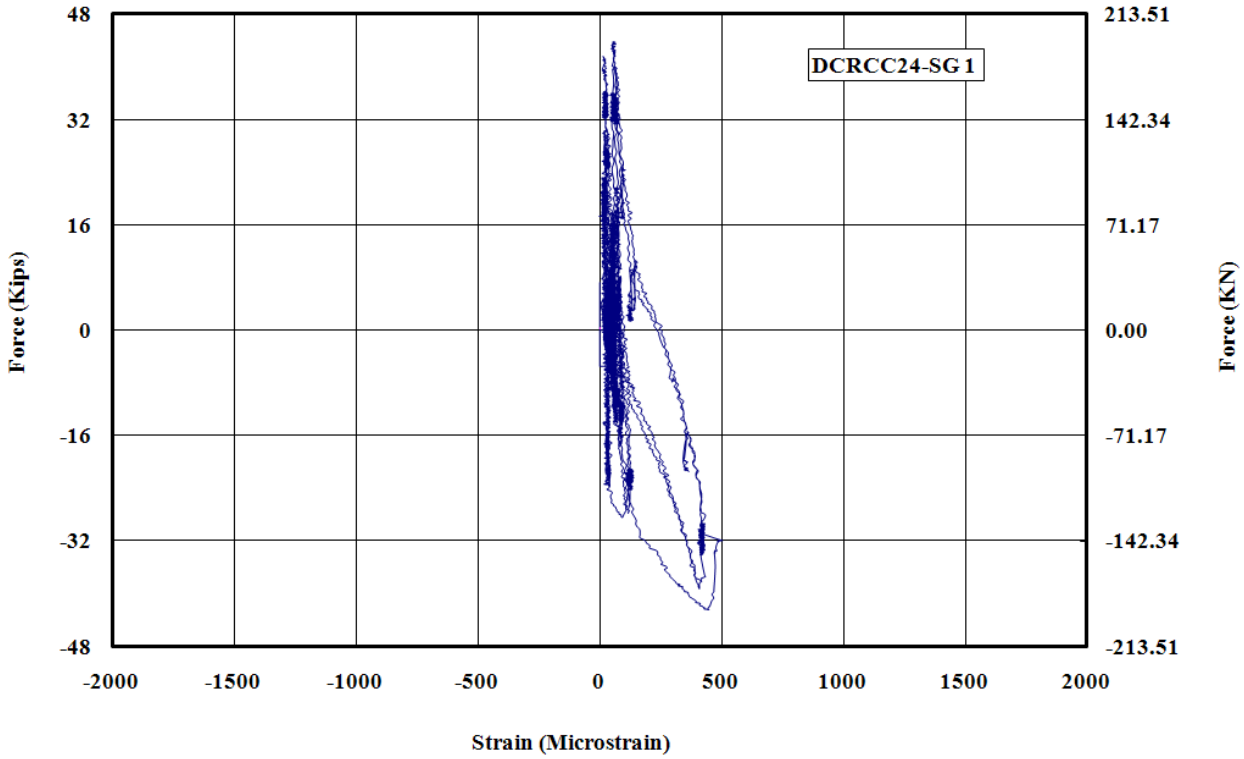

Figure C - 1: Measured Strain in Gauge No.1 for DCRCC24

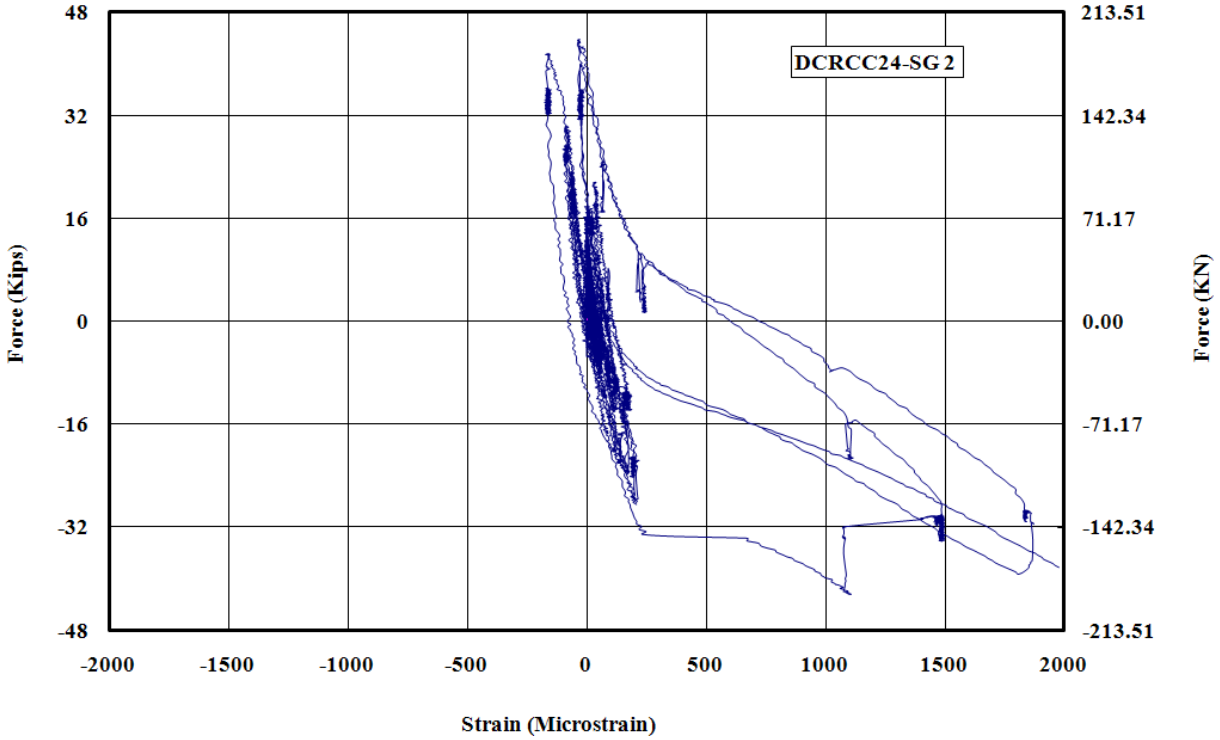

Figure C - 2: Measured Strain in Gauge No.2 for DCRCC24

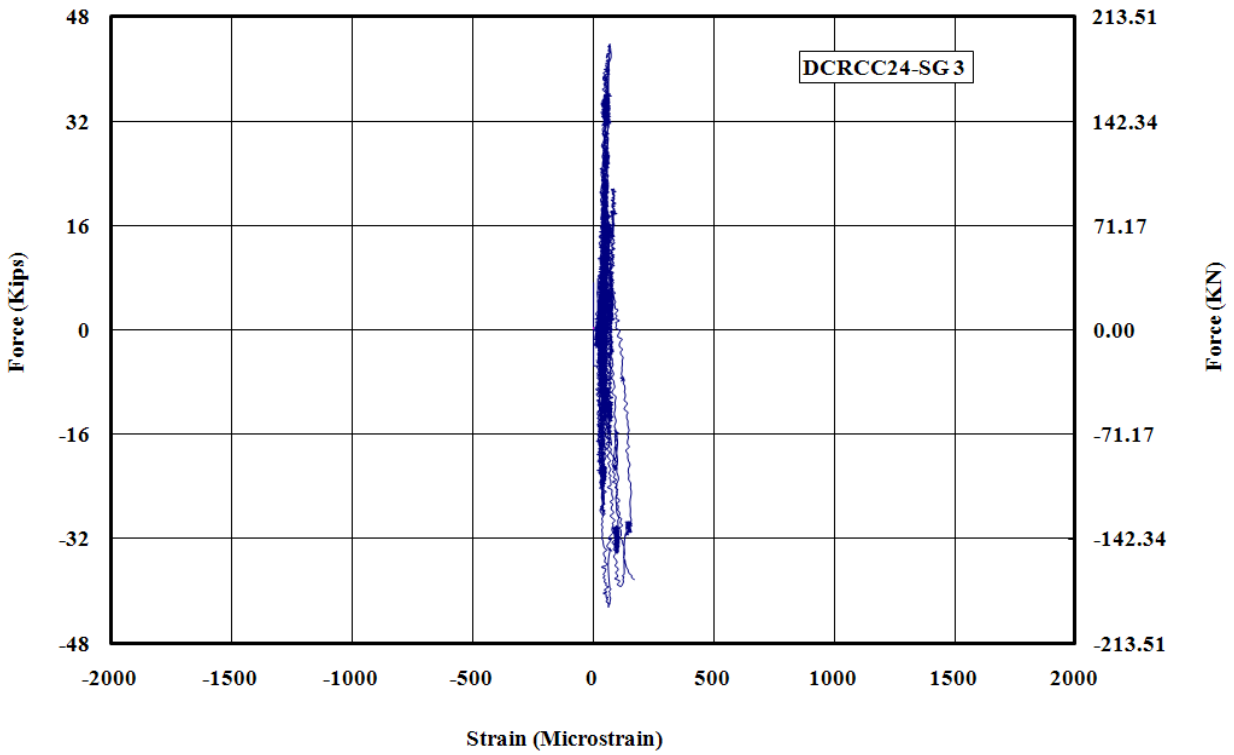

Figure C - 3: Measured Strain in Gauge No.3 for DCRCC24

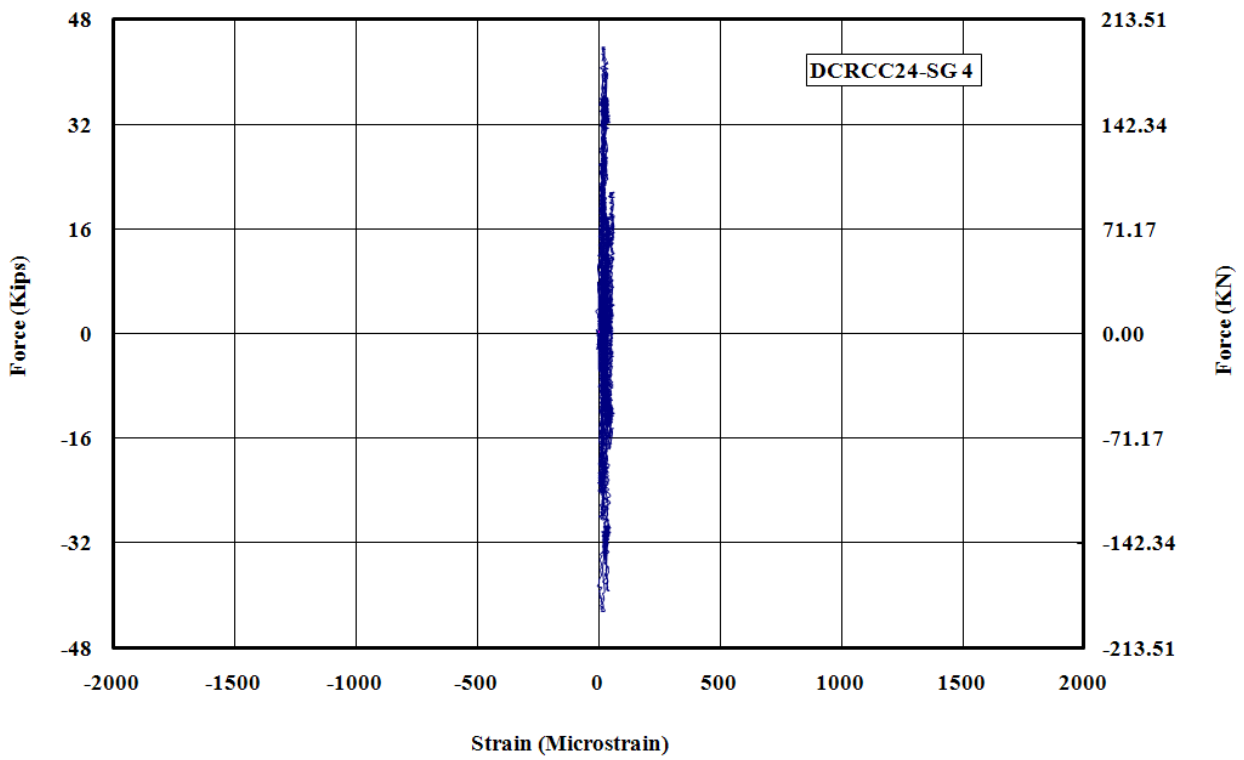

Figure C - 4: Measured Strain in Gauge No.4 for DCRCC24

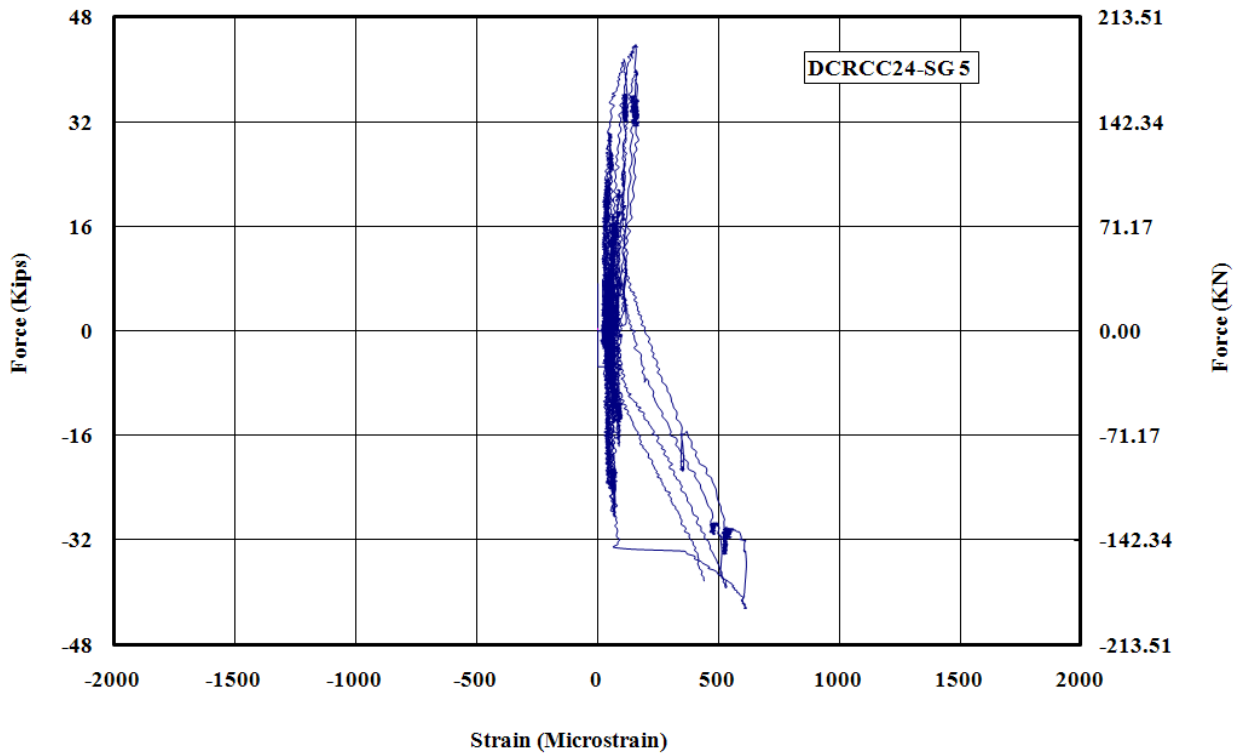

Figure C - 5: Measured Strain in Gauge No.5 for DCRCC24

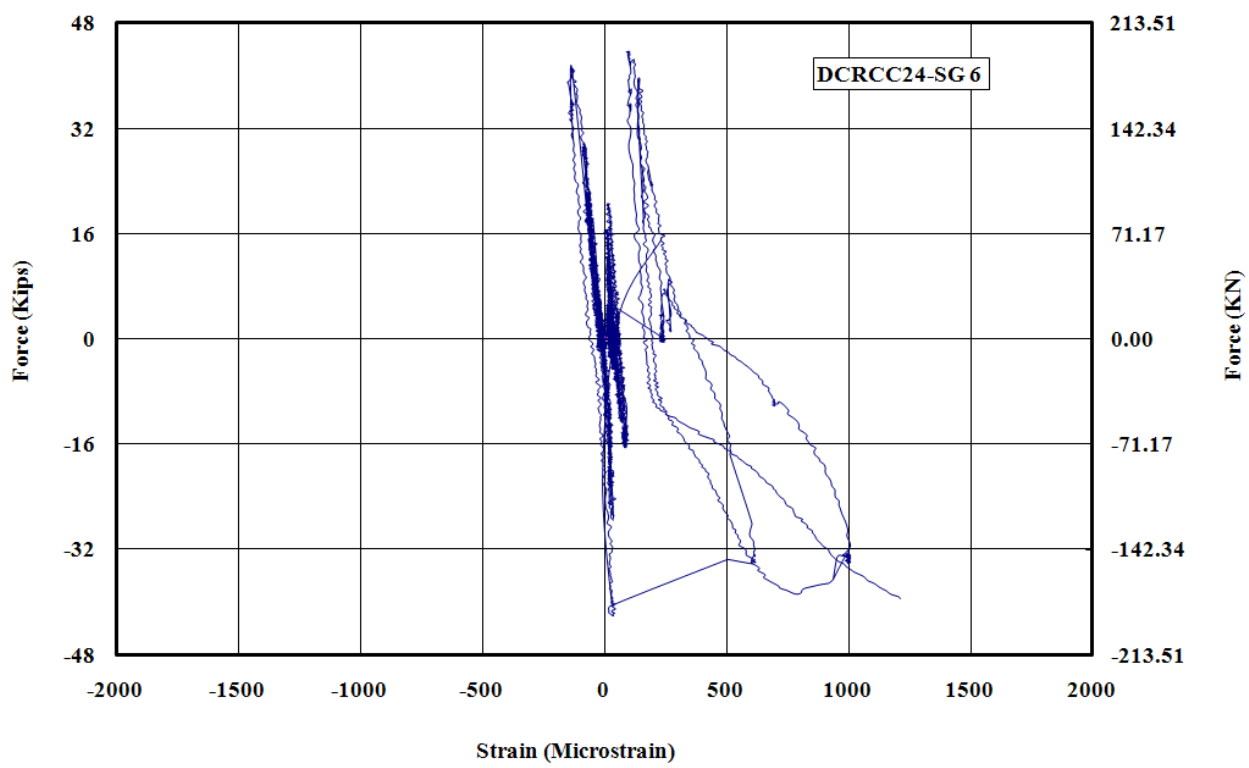

Figure C - 6: Measured Strain in Gauge No.6 for DCRCC24

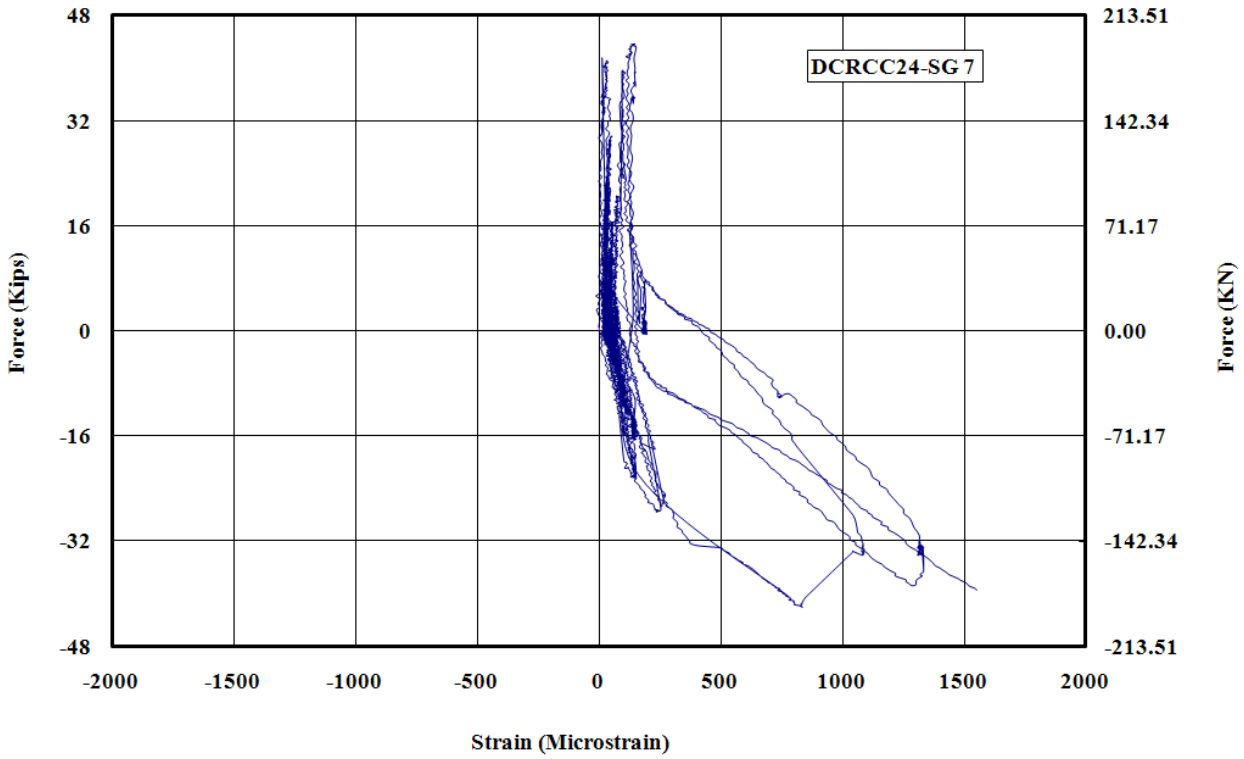

Figure C - 7: Measured Strain in Gauge No.7 for DCRCC24

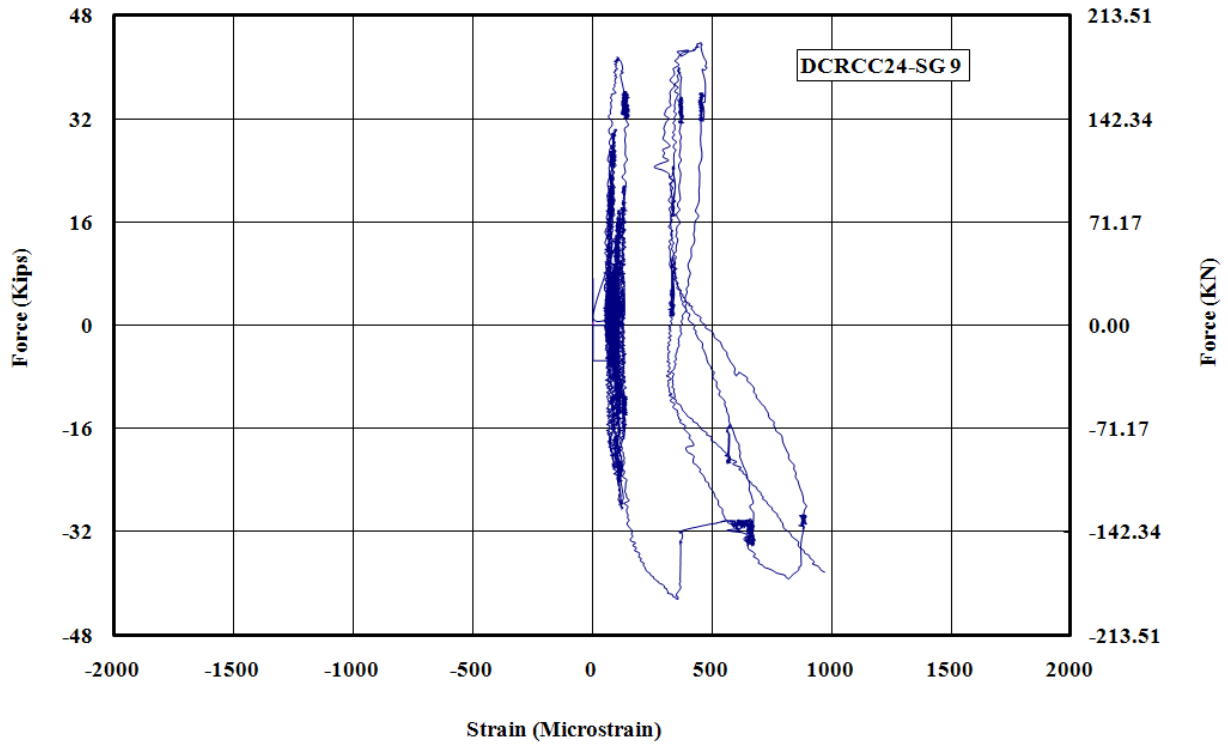

Figure C - 8: Measured Strain in Gauge No.9 for DCRCC24

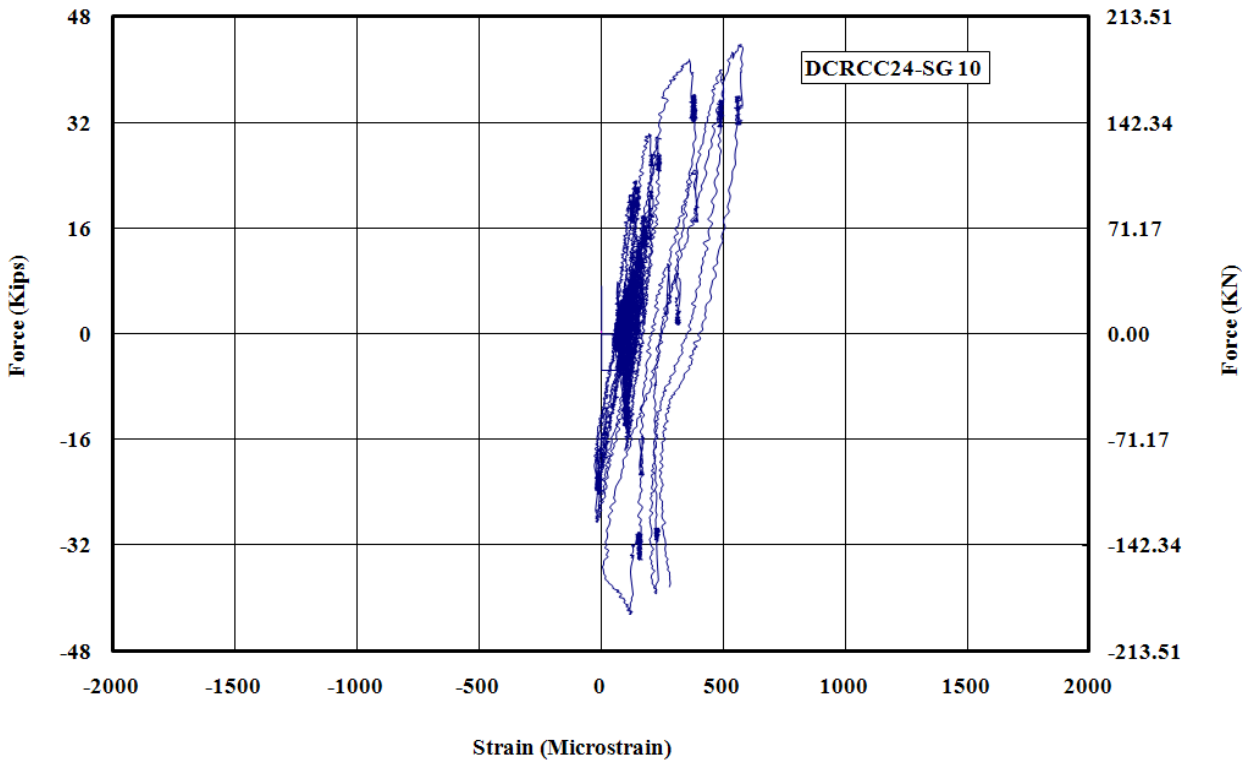

Figure C - 9: Measured Strain in Gauge No.10 for DCRCC24

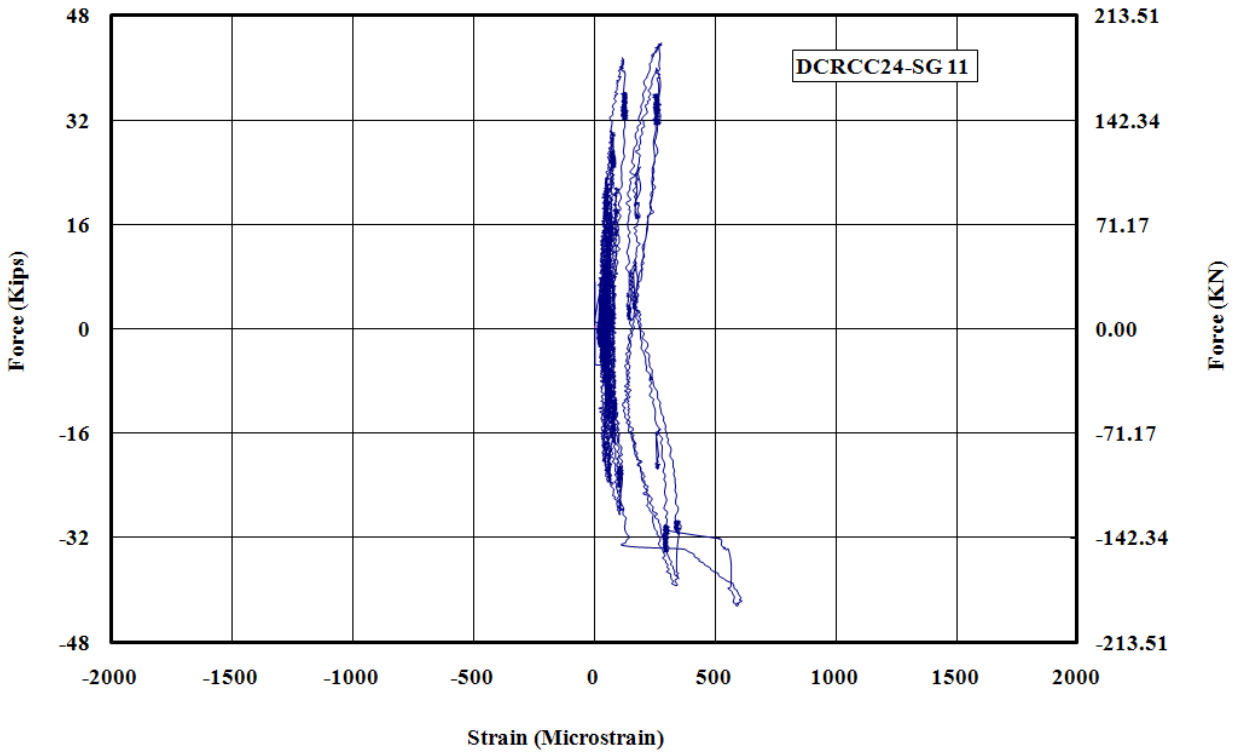

Figure C - 10: Measured Strain in Gauge No.11 for DCRCC24

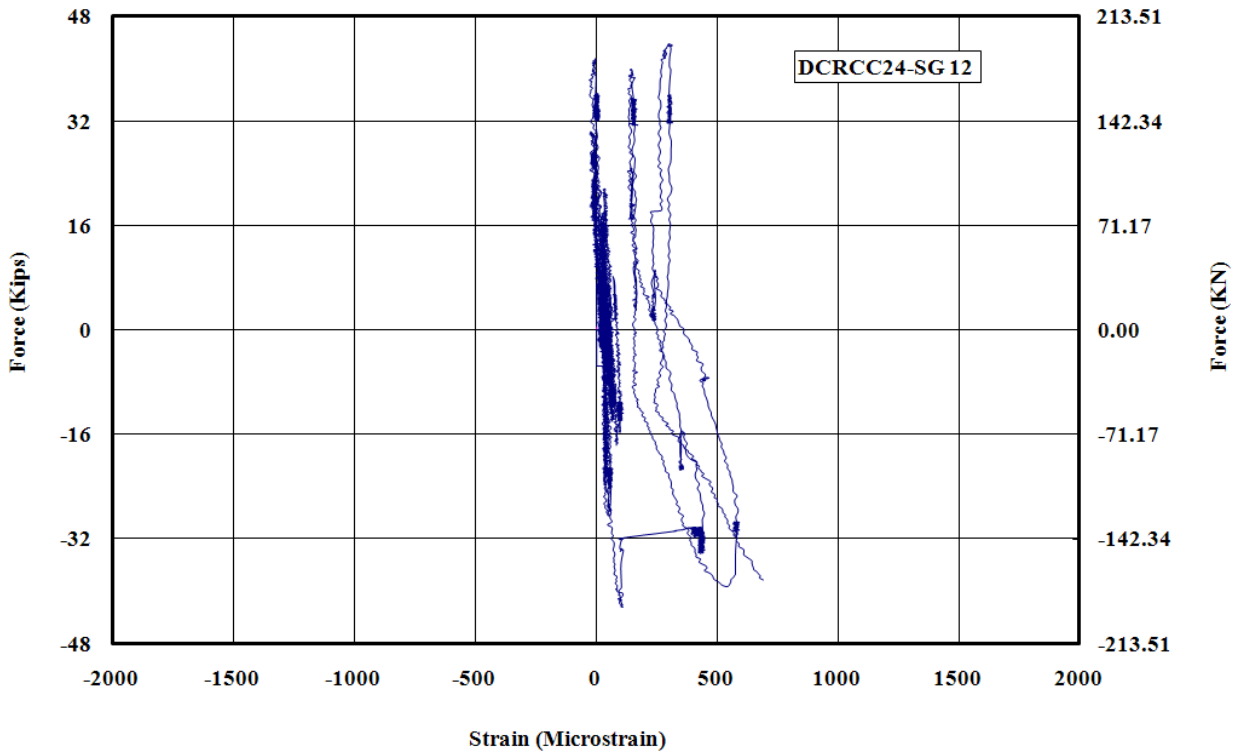

Figure C - 11: Measured Strain in Gauge No.12 for DCRCC24

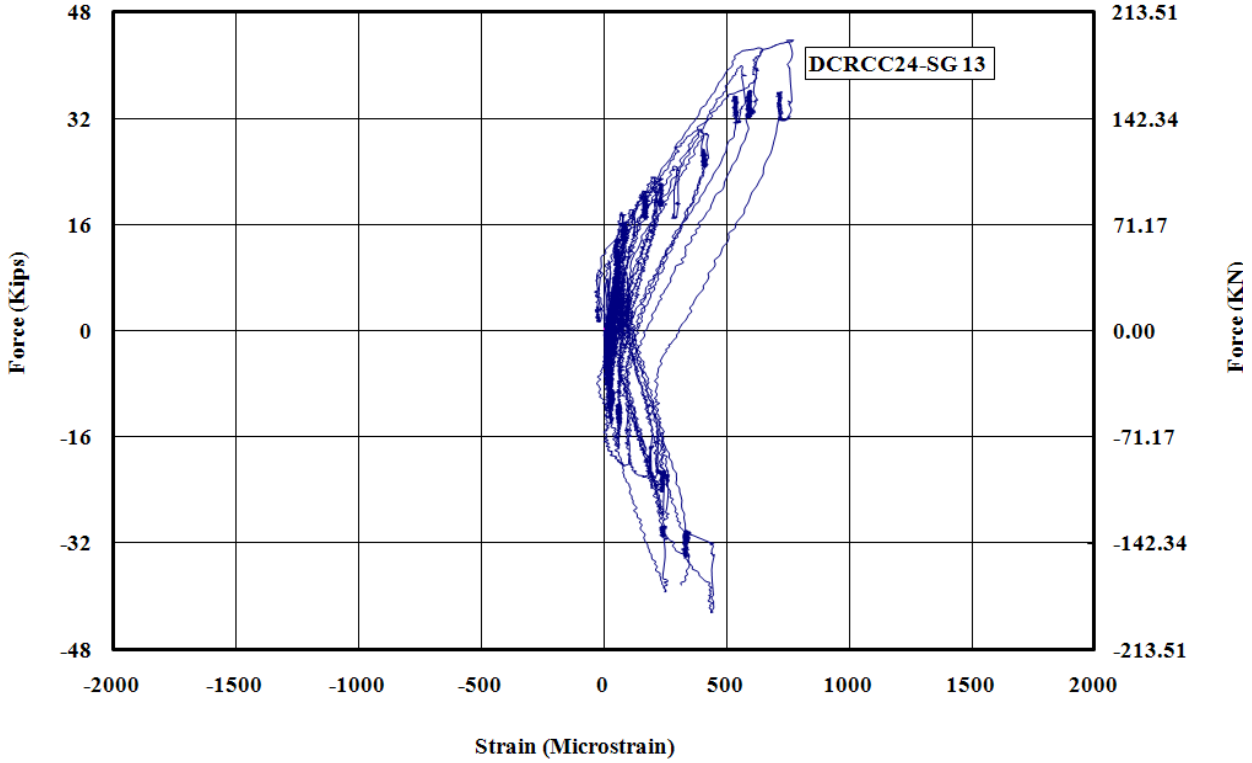

Figure C - 12: Measured Strain in Gauge No.13 for DCRCC24

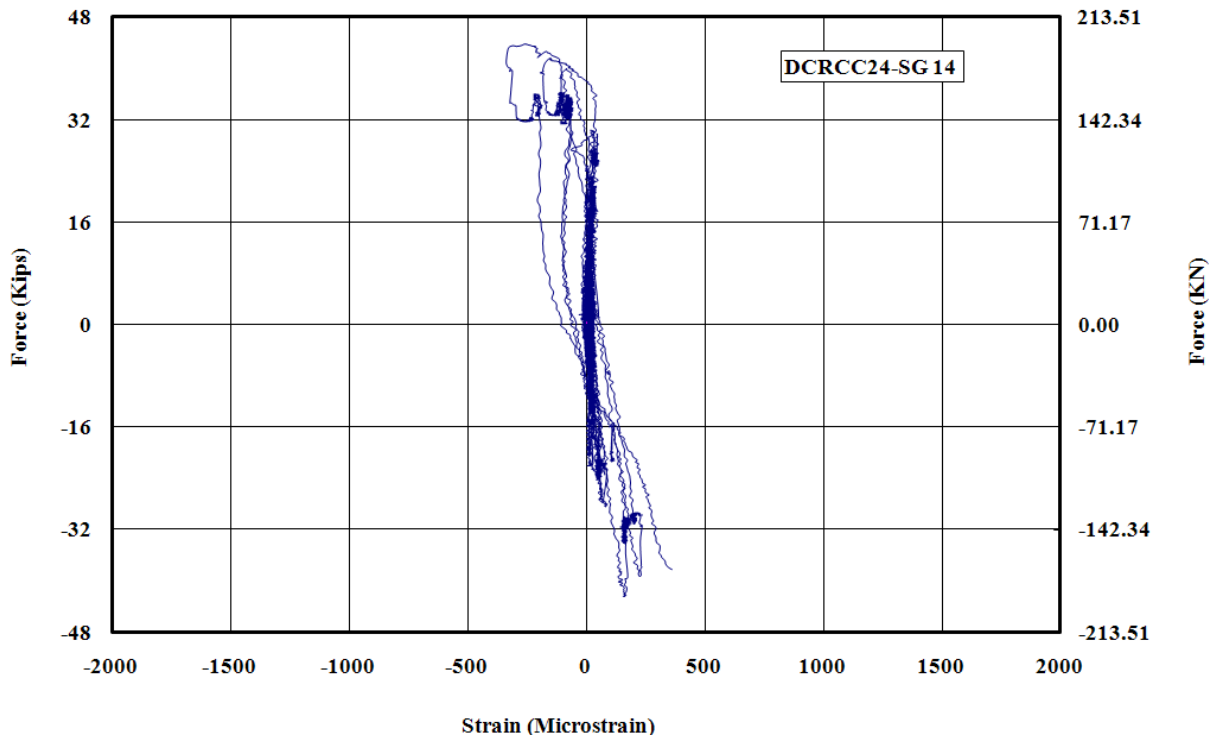

Figure C - 13: Measured Strain in Gauge No.14 for DCRCC24

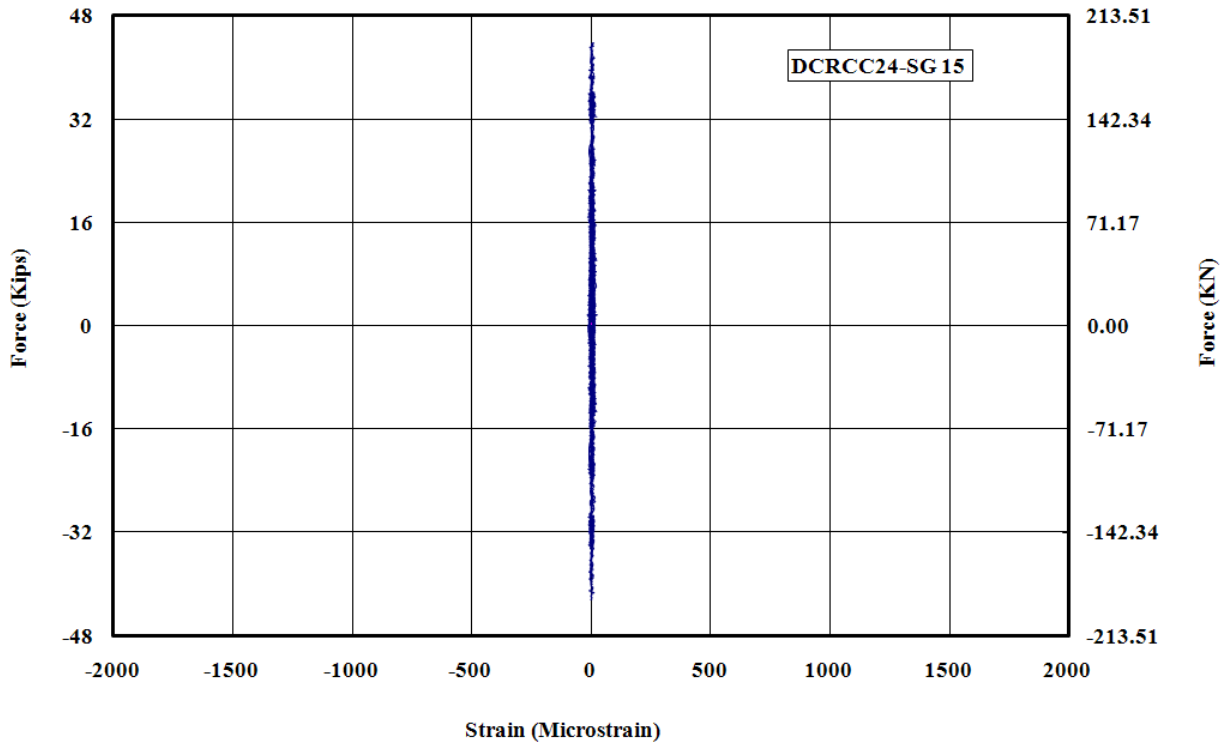

Figure C - 14: Measured Strain in Gauge No.15 for DCRCC24

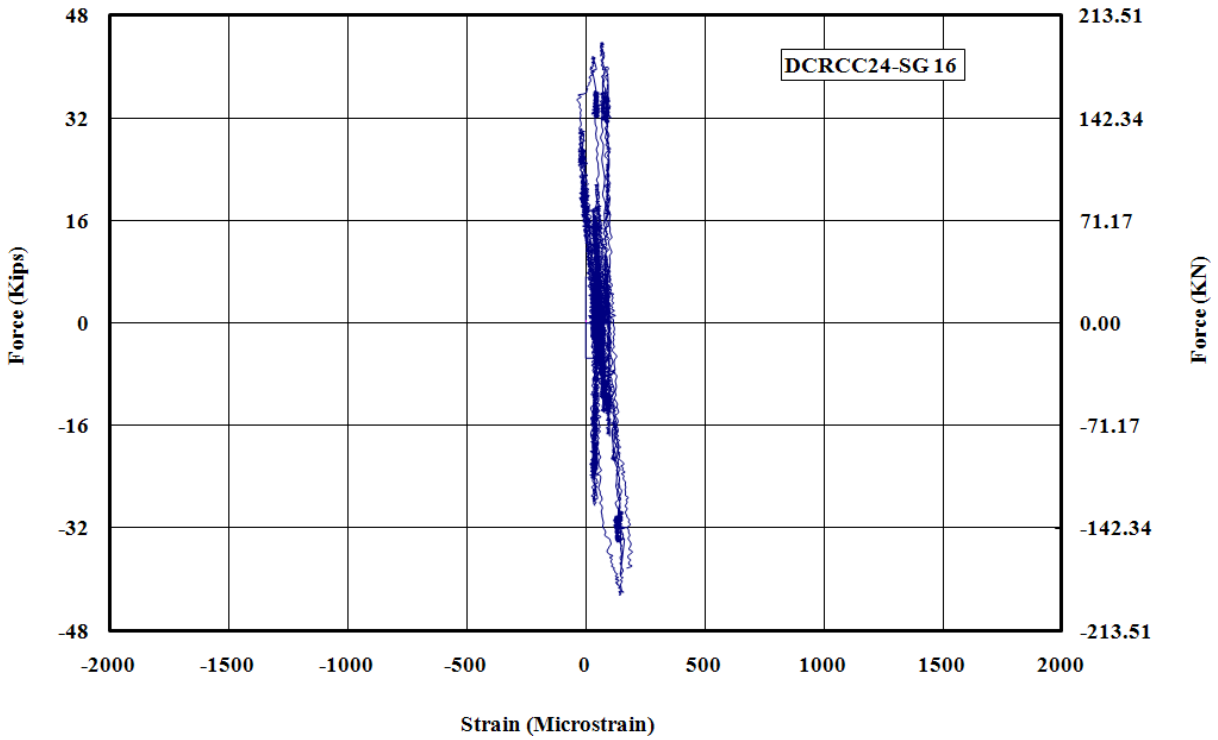

Figure C - 15: Measured Strain in Gauge No.16 for DCRCC24

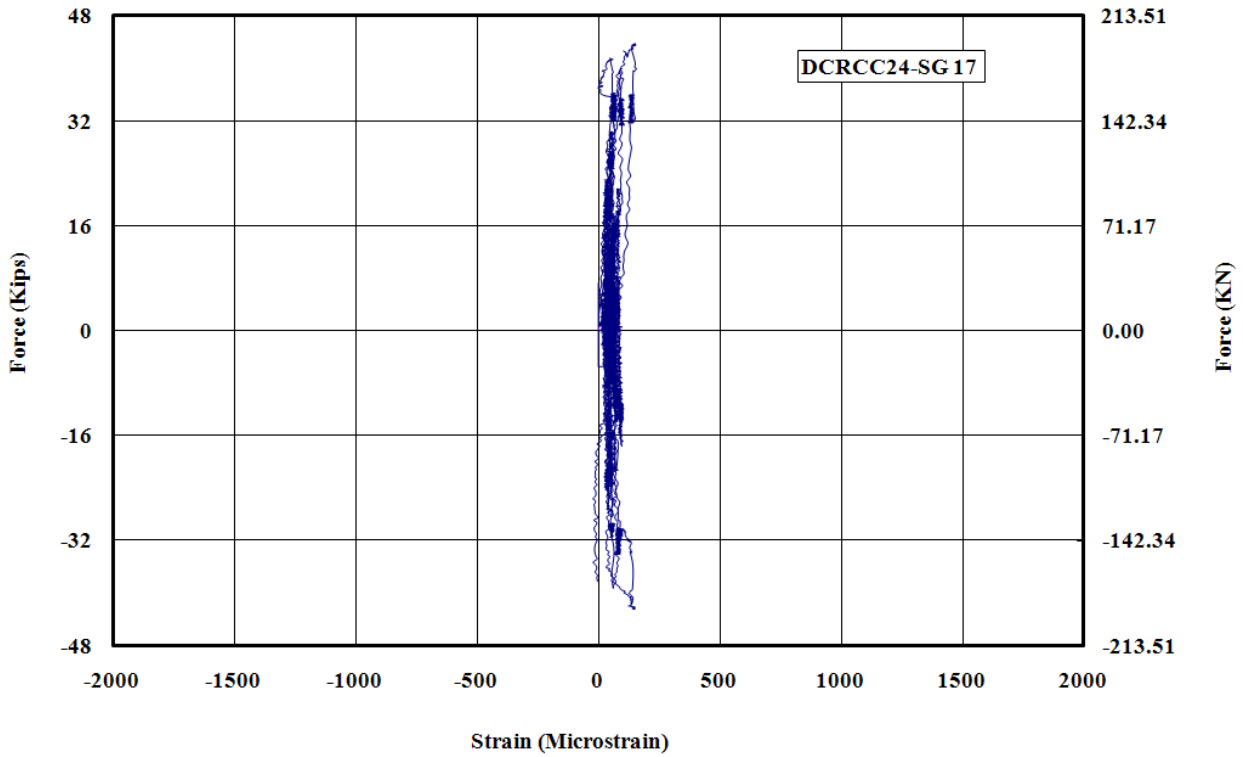

Figure C - 16: Measured Strain in Gauge No.17 for DCRCC24

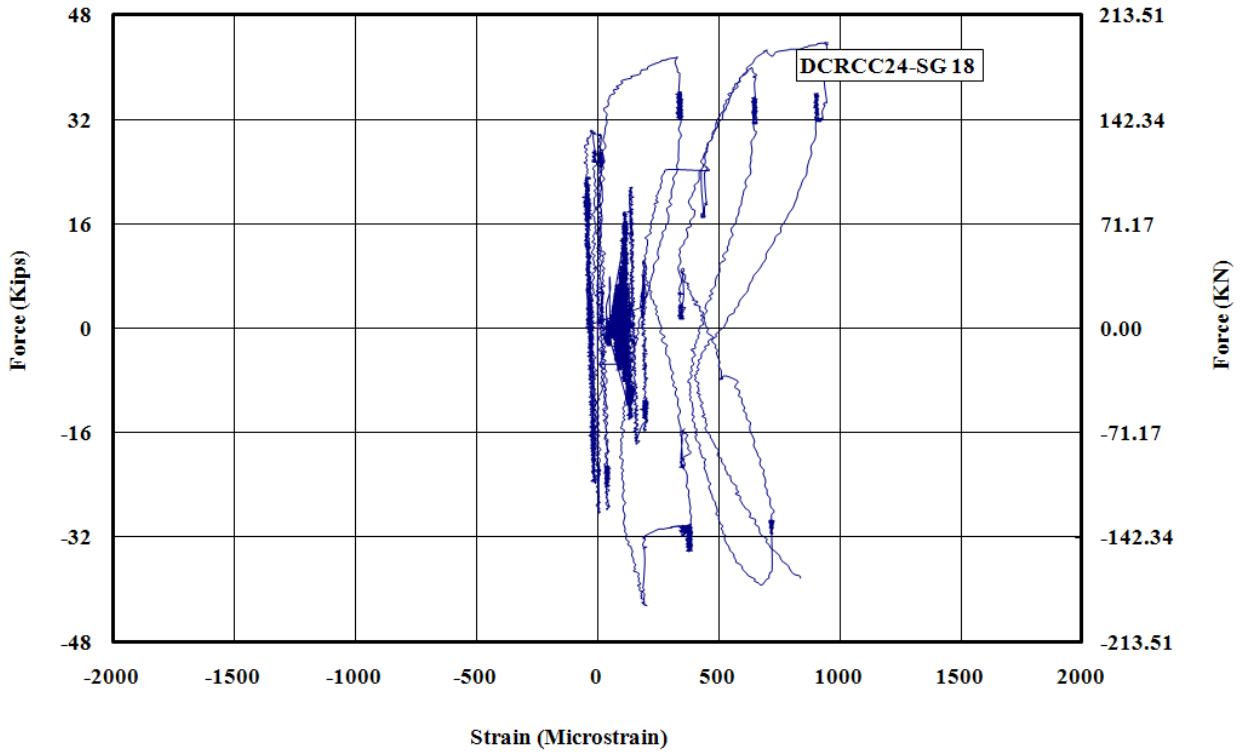

Figure C - 17: Measured Strain in Gauge No.18 for DCRCC24

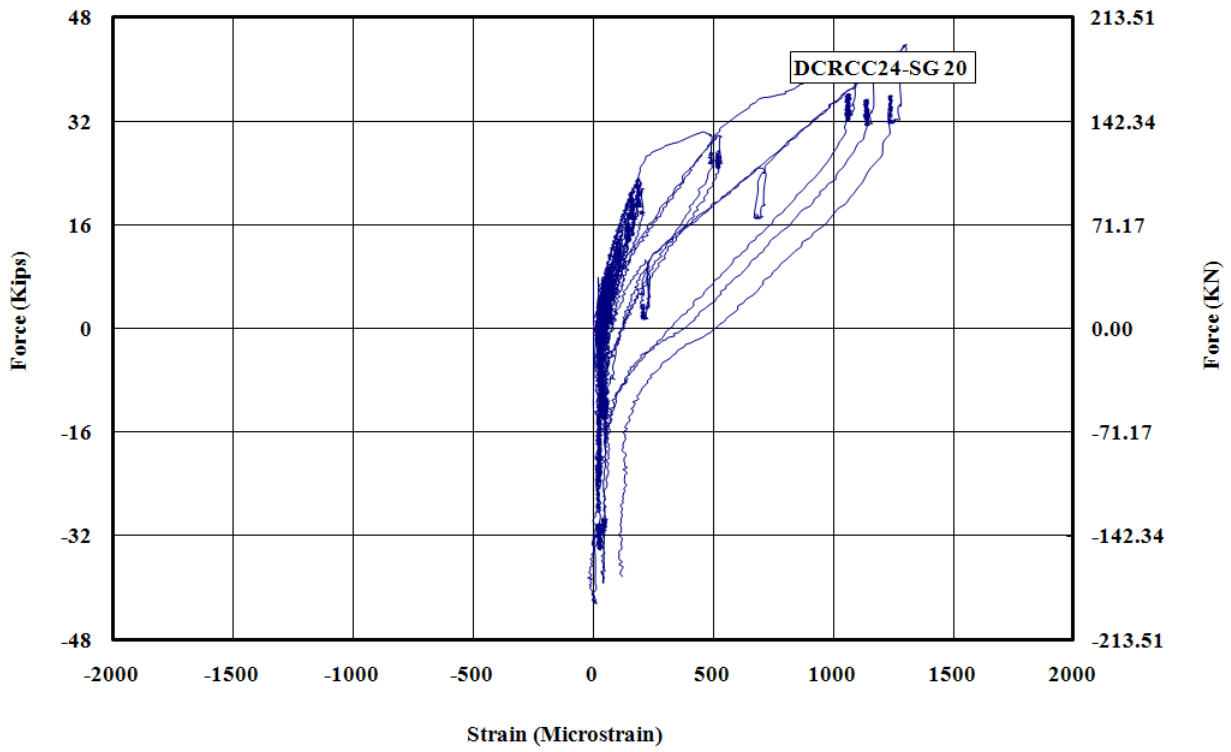

Figure C - 18: Measured Strain in Gauge No.20 for DCRCC24

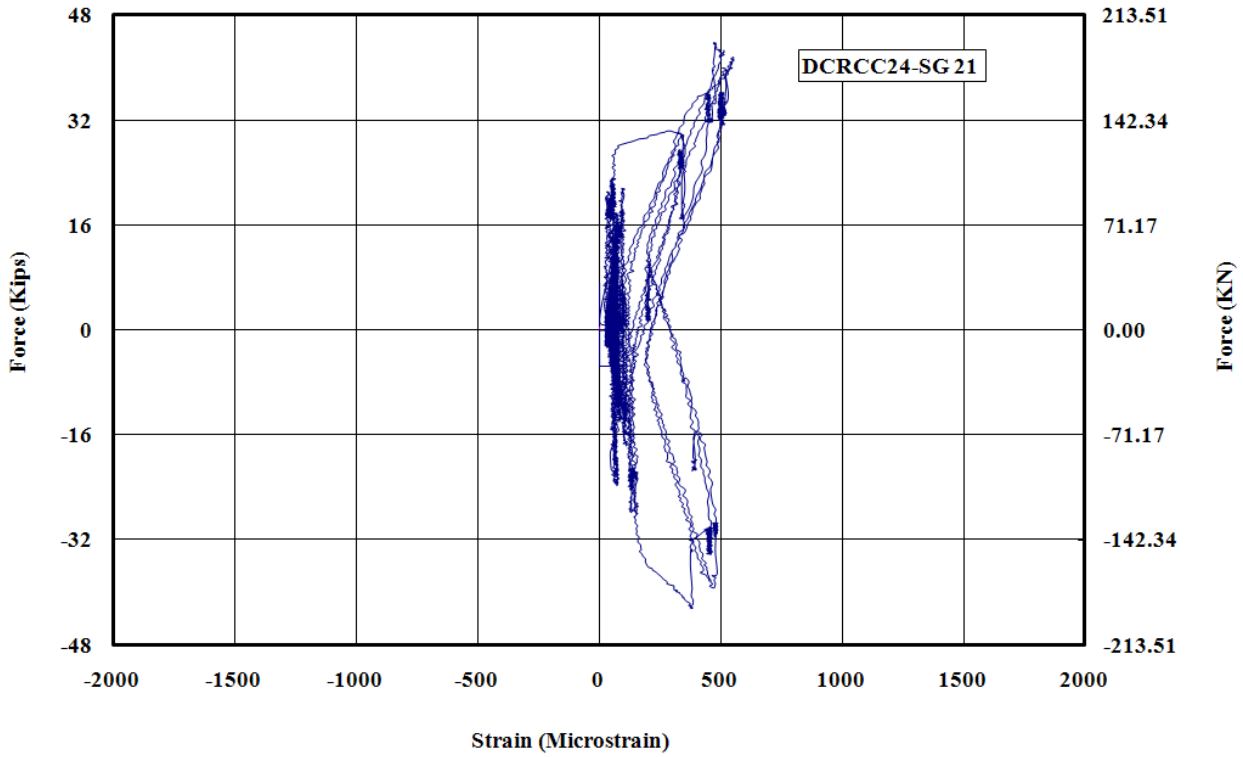

Figure C - 19: Measured Strain in Gauge No.21 for DCRCC24

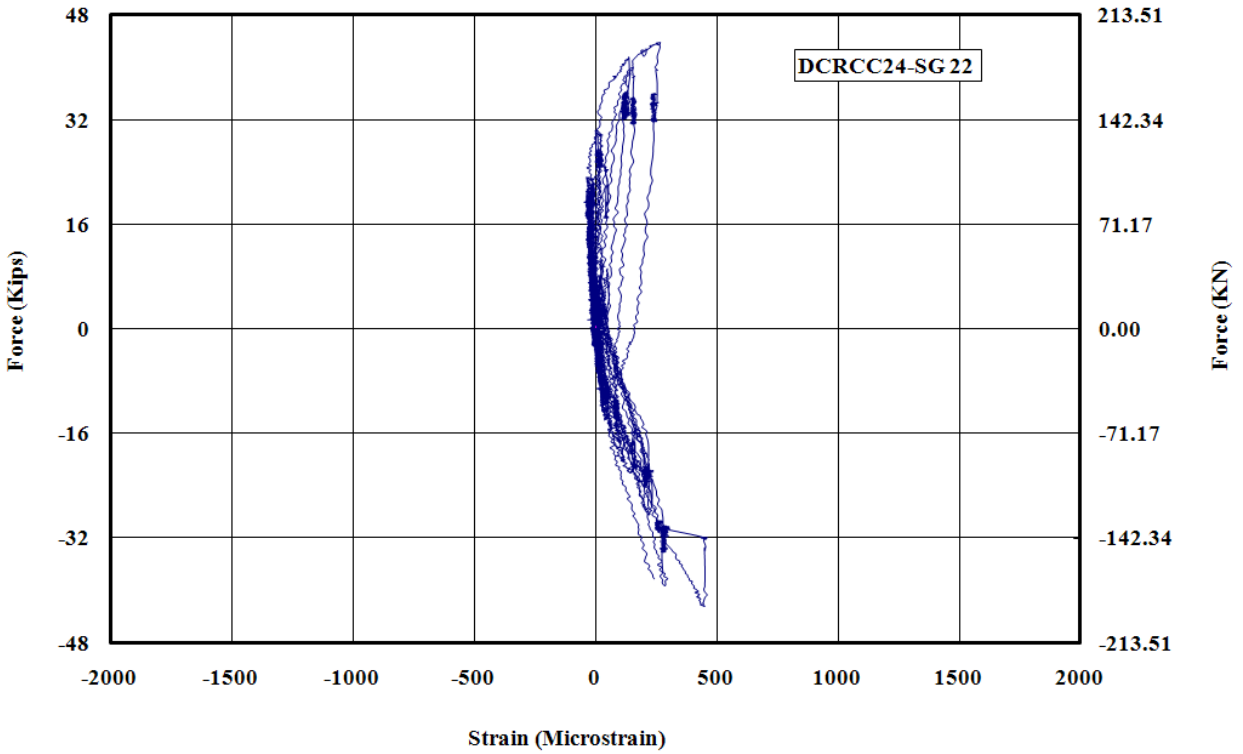

Figure C - 20: Measured Strain in Gauge No.22 for DCRCC24

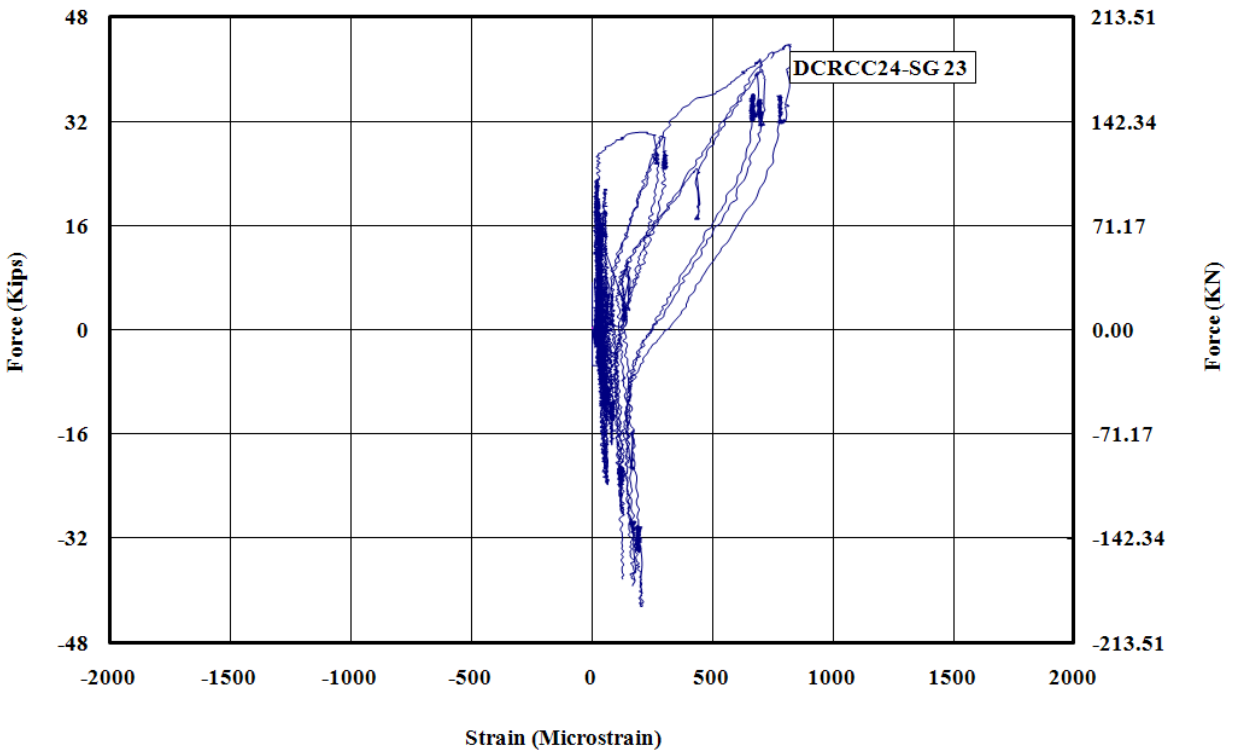

Figure C - 21: Measured Strain in Gauge No.23 for DCRCC24

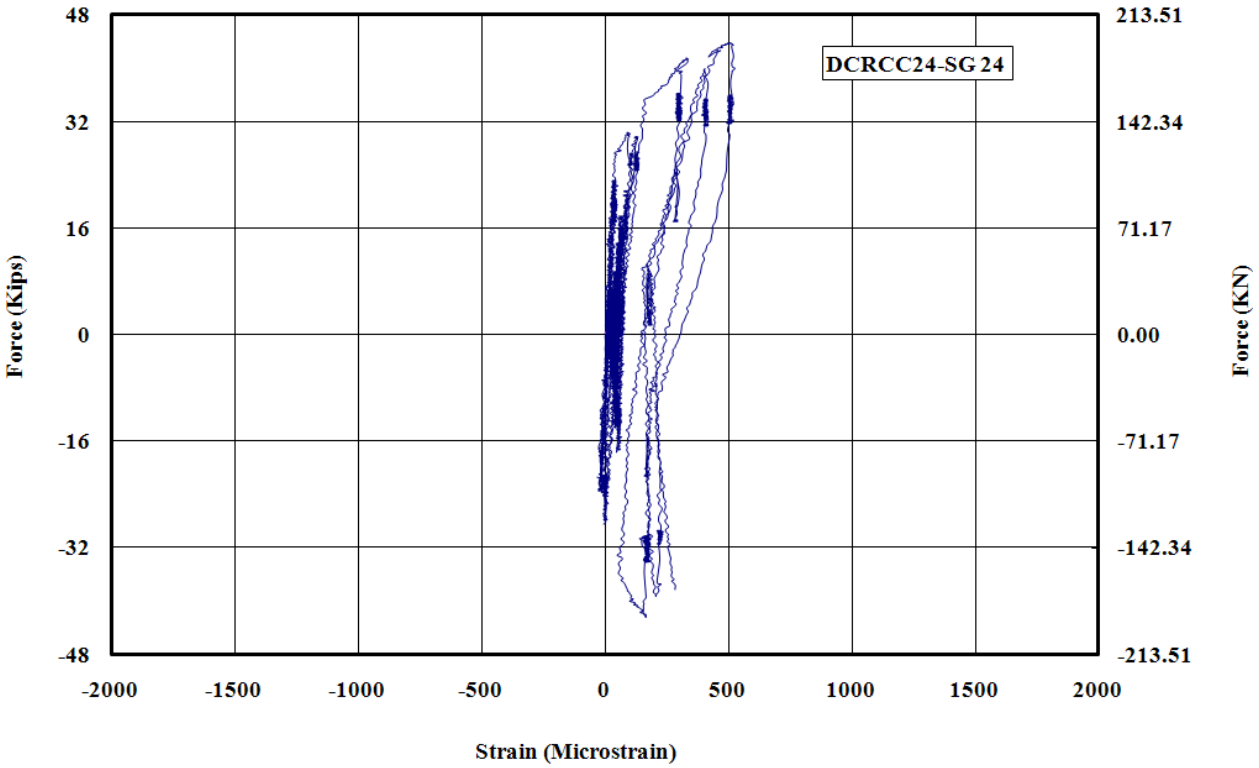

Figure C - 22: Measured Strain in Gauge No.24 for DCRCC24

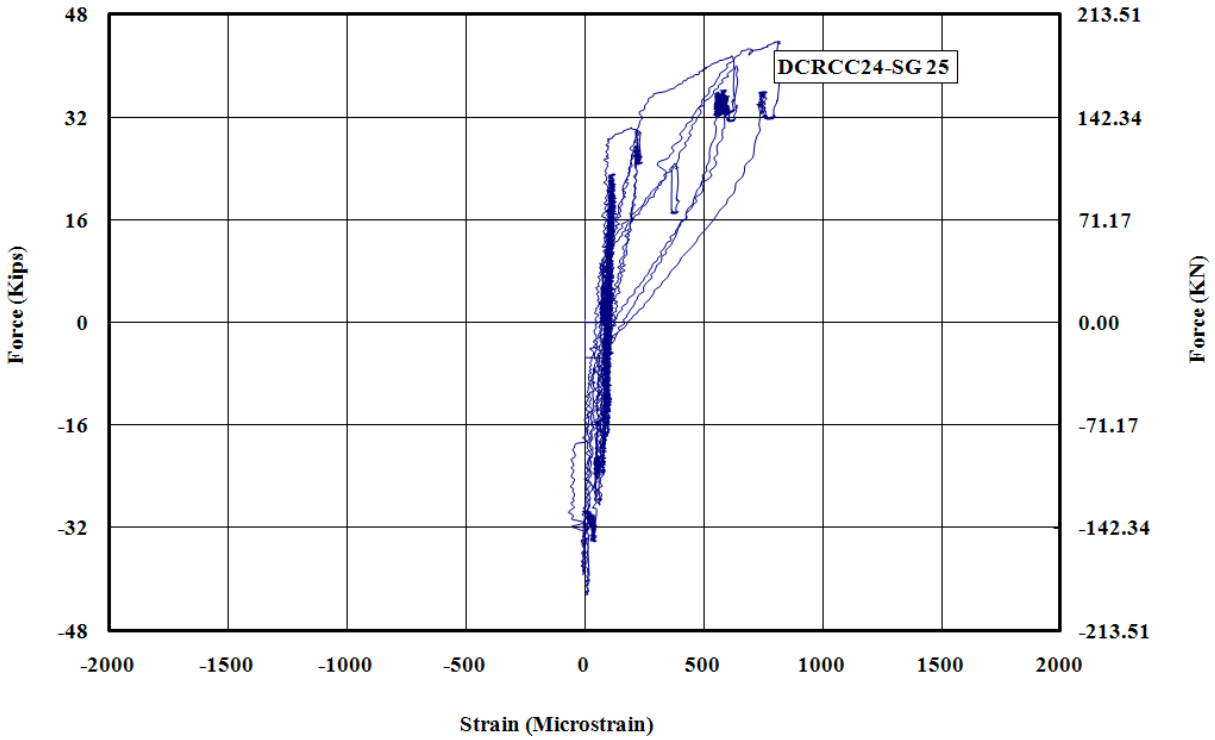

Figure C - 23: Measured Strain in Gauge No.25 for DCRCC24

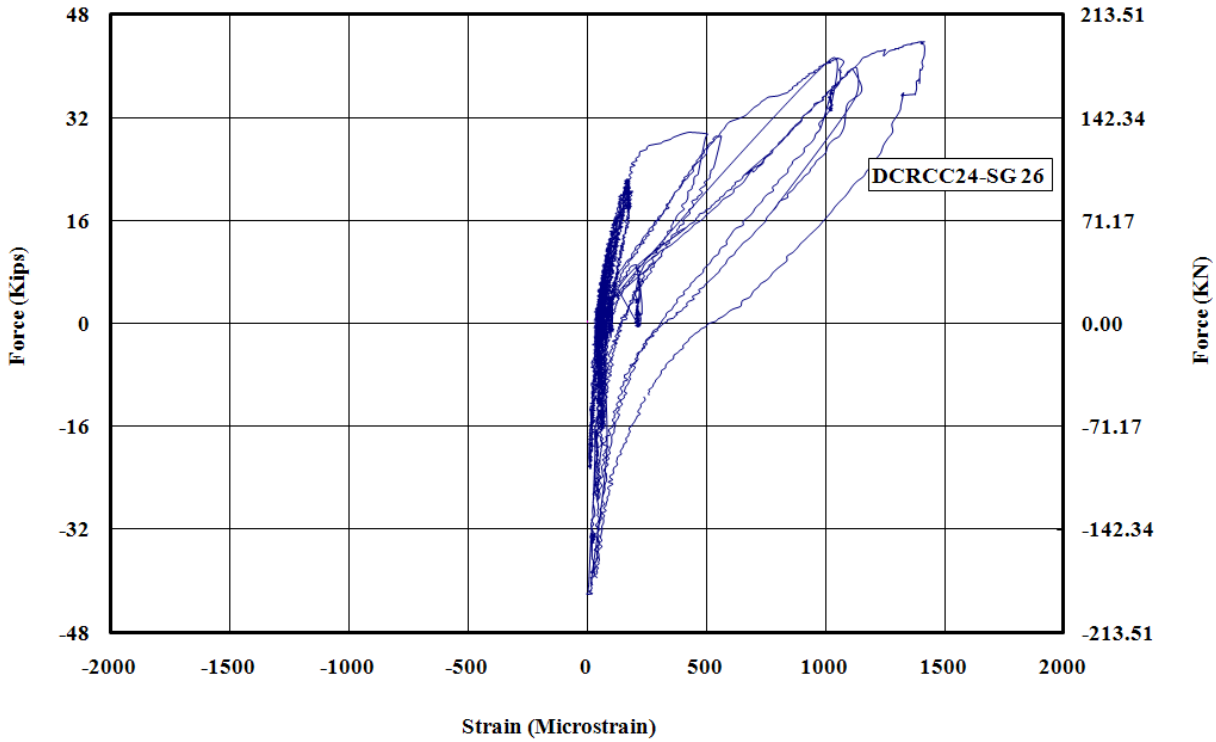

Figure C - 24: Measured Strain in Gauge No.26 for DCRCC24

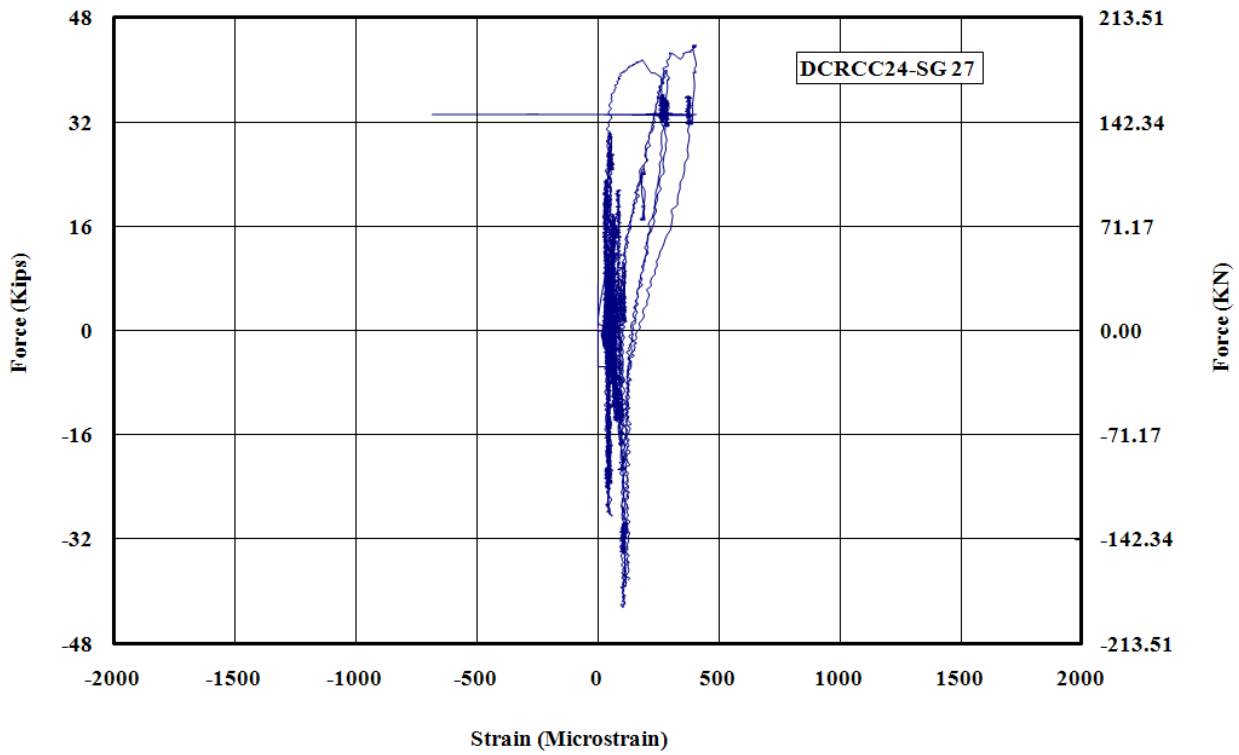

Figure C - 25: Measured Strain in Gauge No.27 for DCRCC24

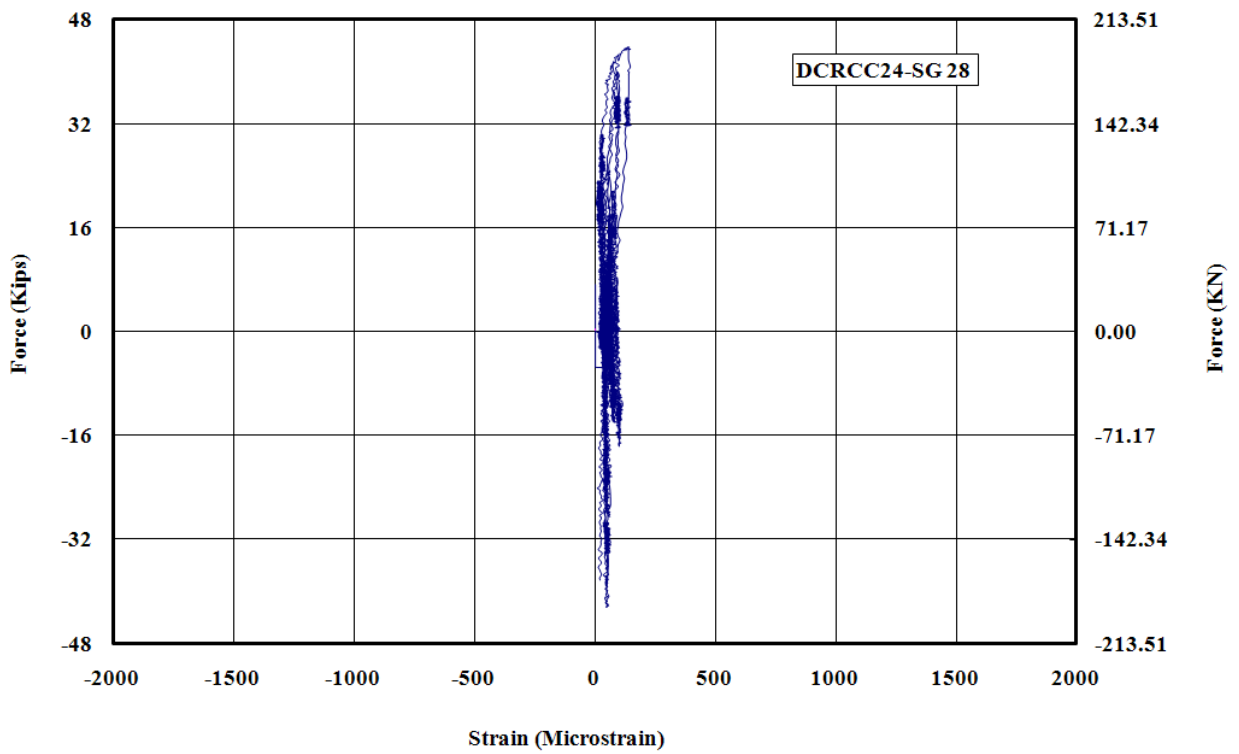

Figure C - 26: Measured Strain in Gauge No.28 for DCRCC24

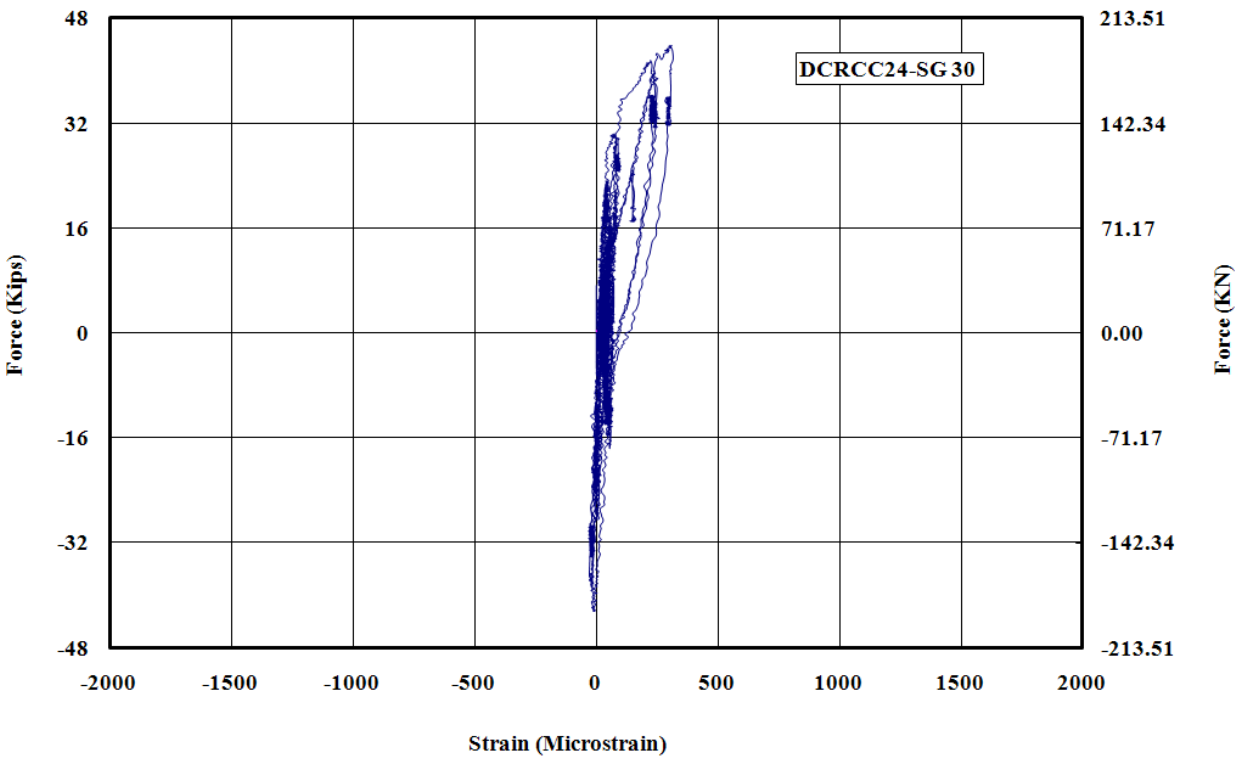

Figure C - 27: Measured Strain in Gauge No.30 for DCRCC24

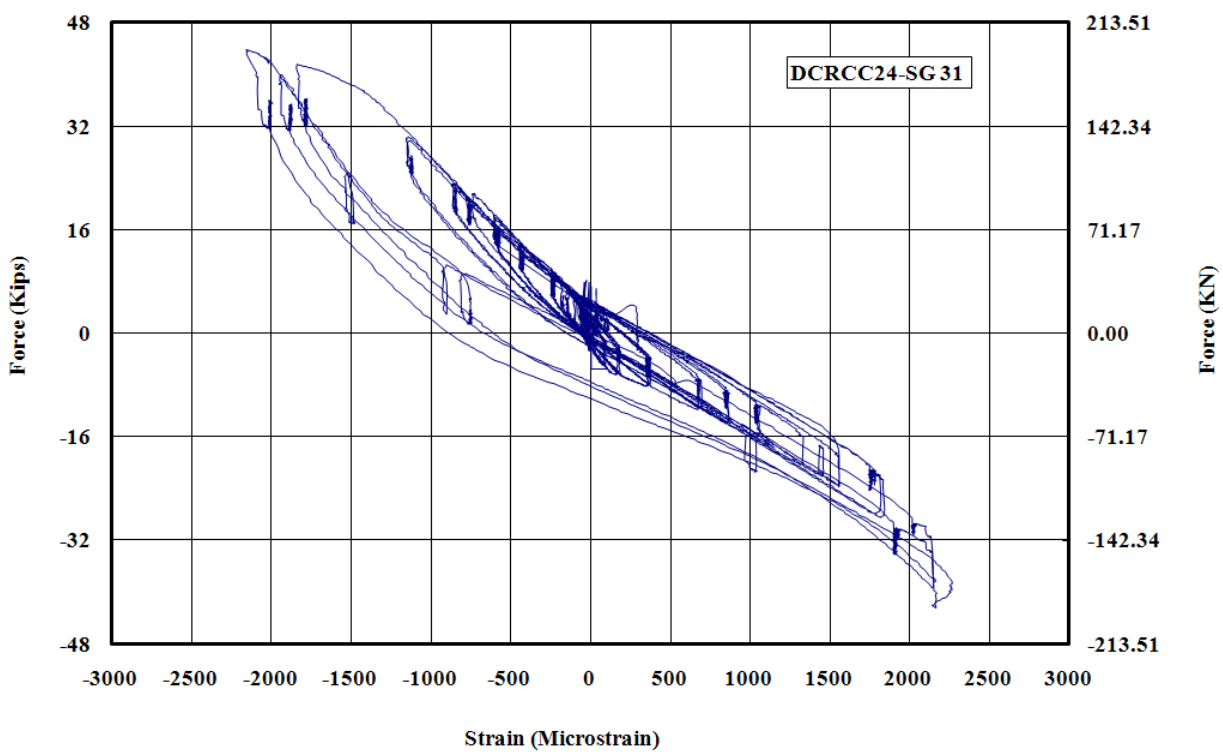

Figure C - 28: Measured Strain in Gauge No.31 for DCRCC24

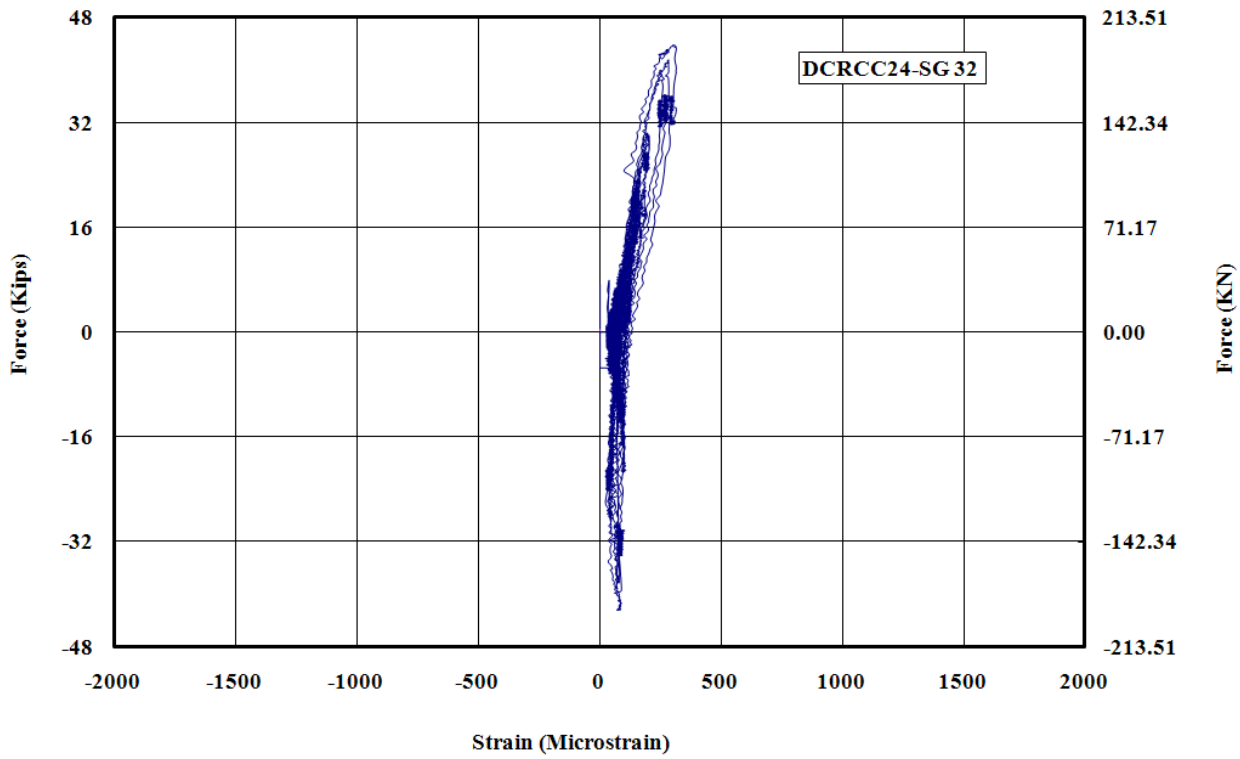

Figure C - 29: Measured Strain in Gauge No.32 for DCRCC24

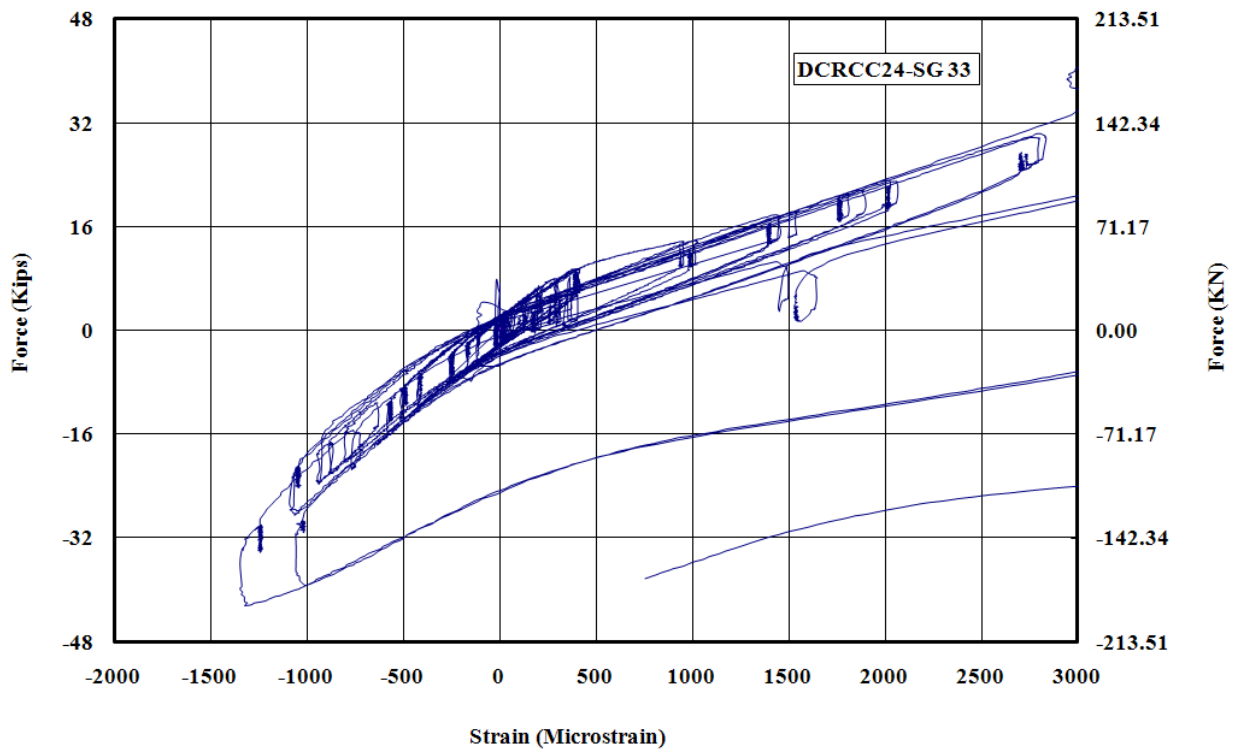

Figure C - 30: Measured Strain in Gauge No.33 for DCRCC24

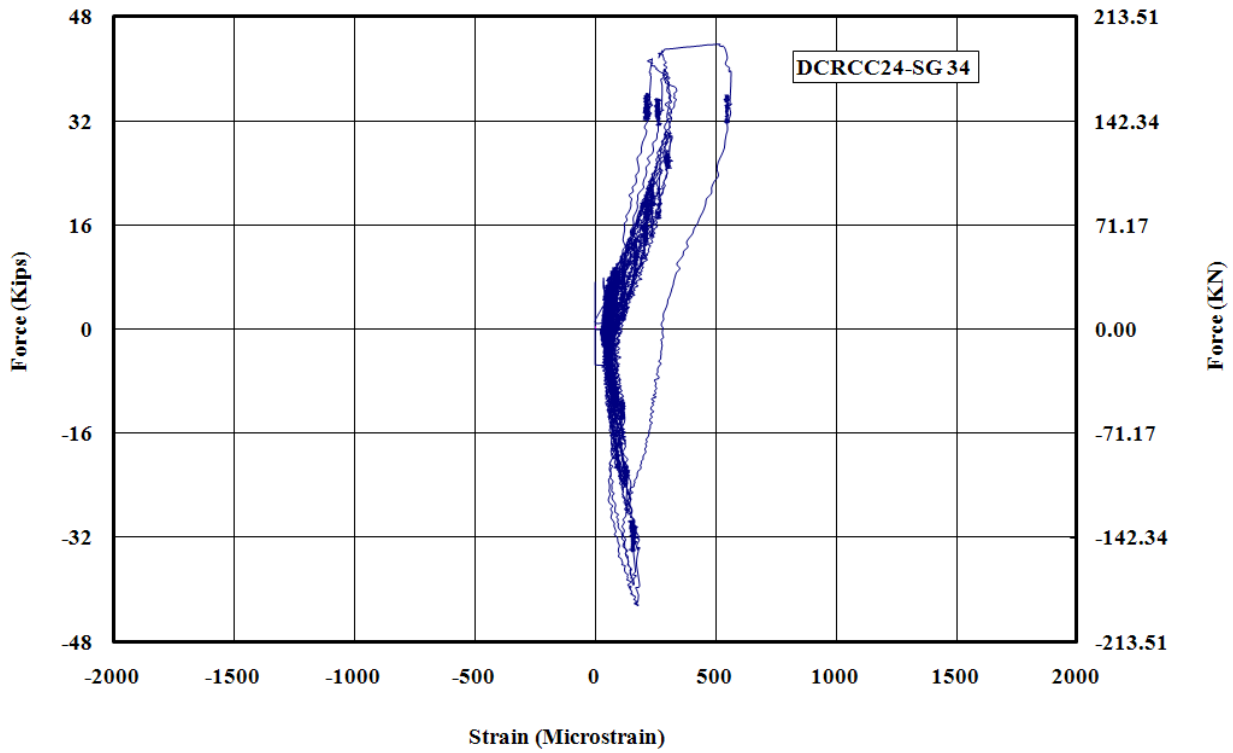

Figure C - 31: Measured Strain in Gauge No.34 for DCRCC24

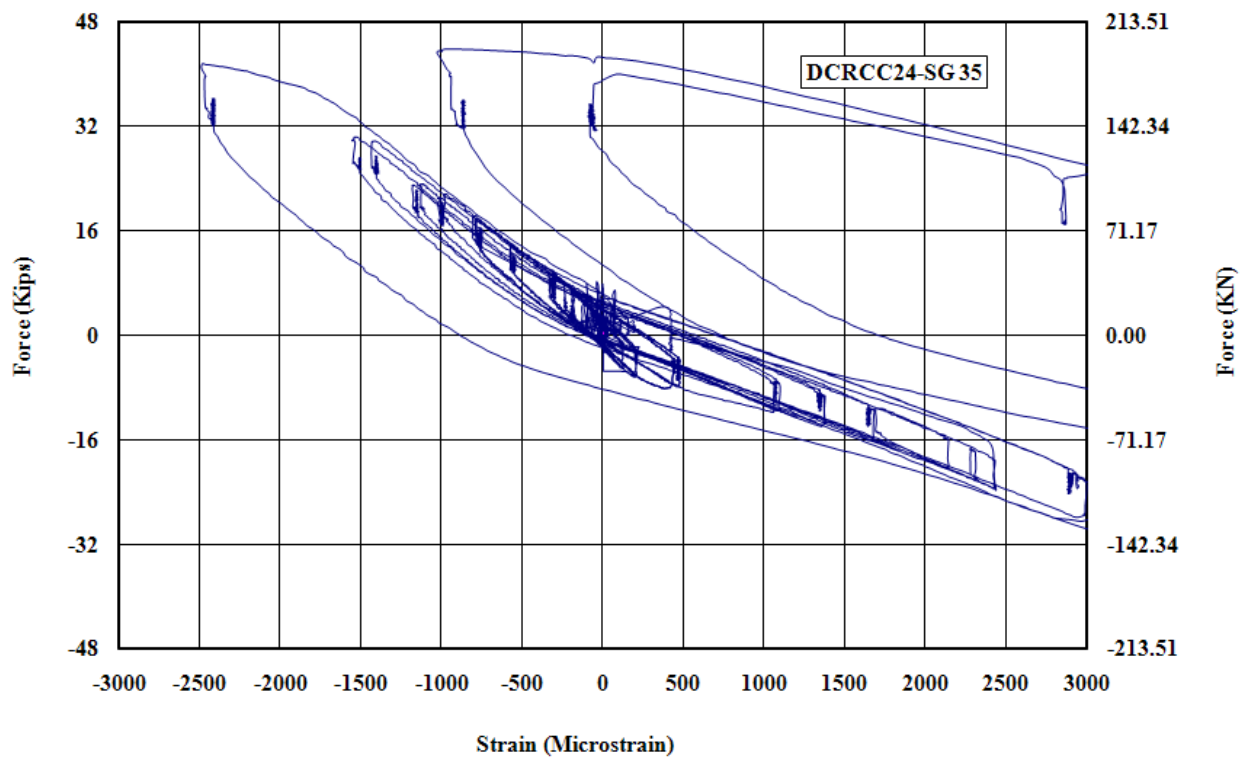

Figure C - 32: Measured Strain in Gauge No.35 for DCRCC24

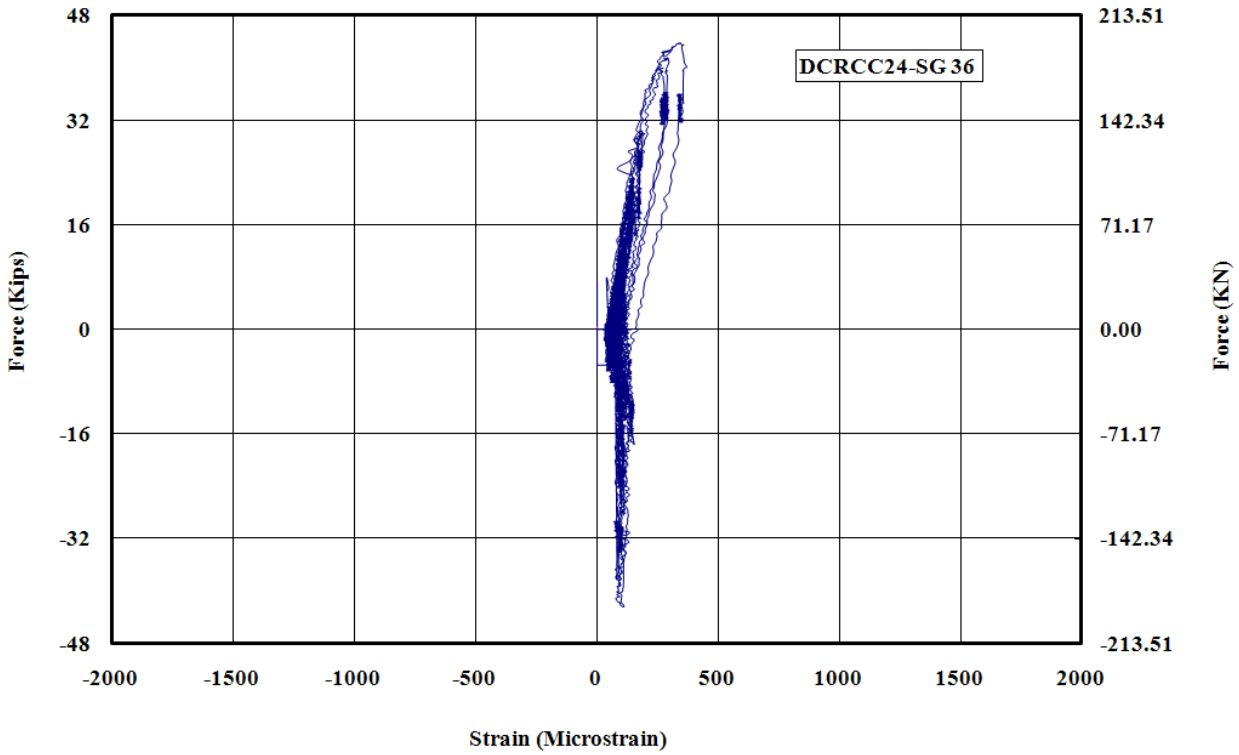

Figure C - 33: Measured Strain in Gauge No.36 for DCRCC24

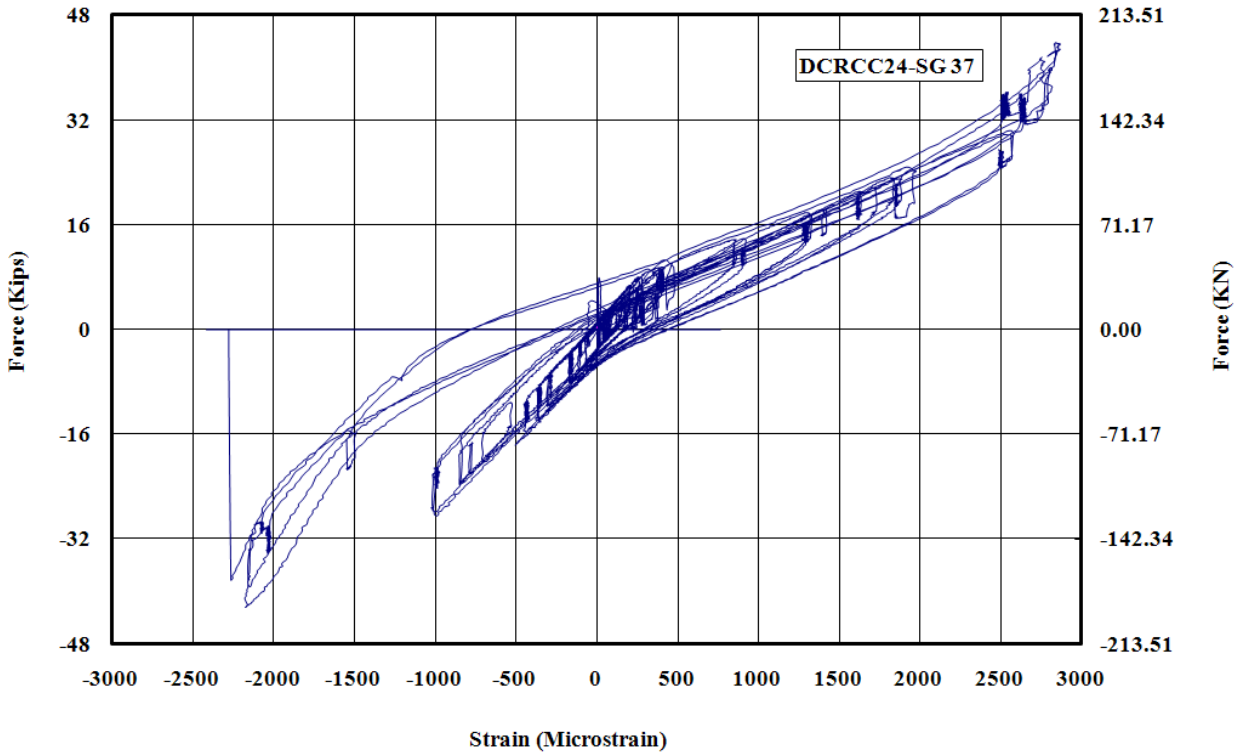

Figure C - 34: Measured Strain in Gauge No.37 for DCRCC24

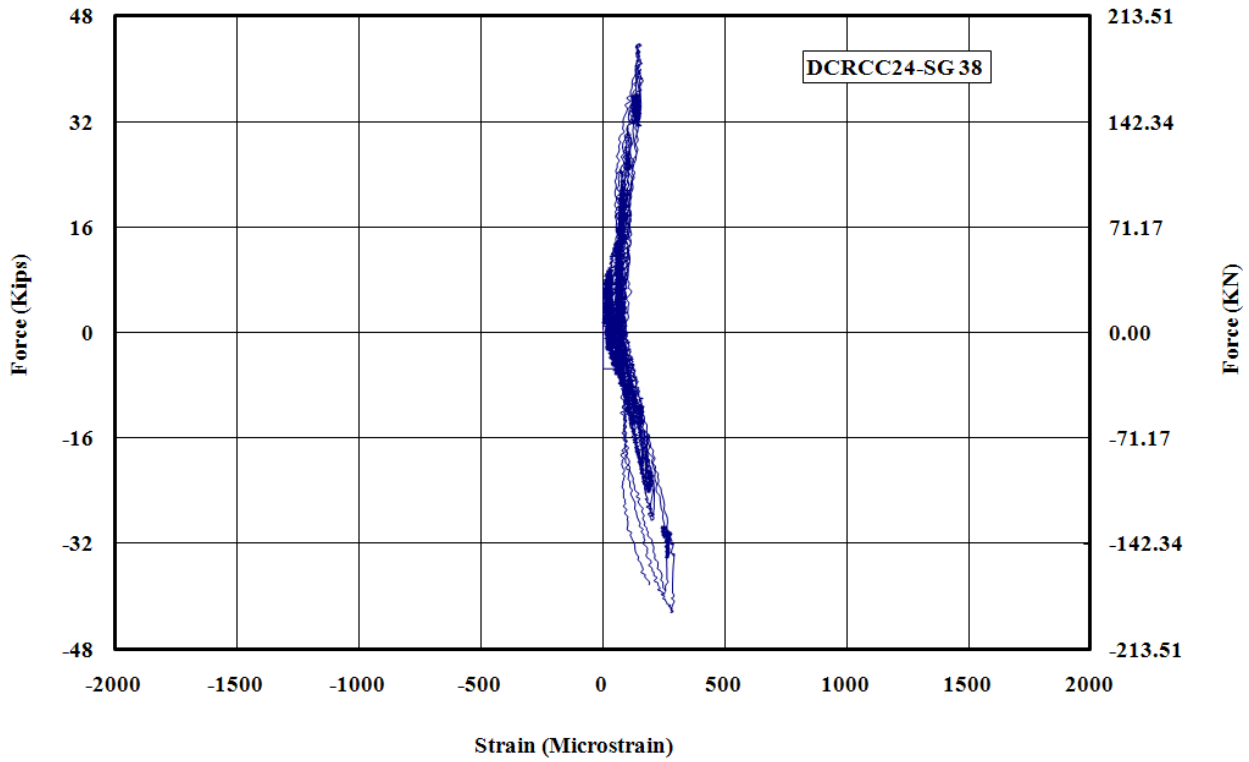

Figure C - 35: Measured Strain in Gauge No.38 for DCRCC24

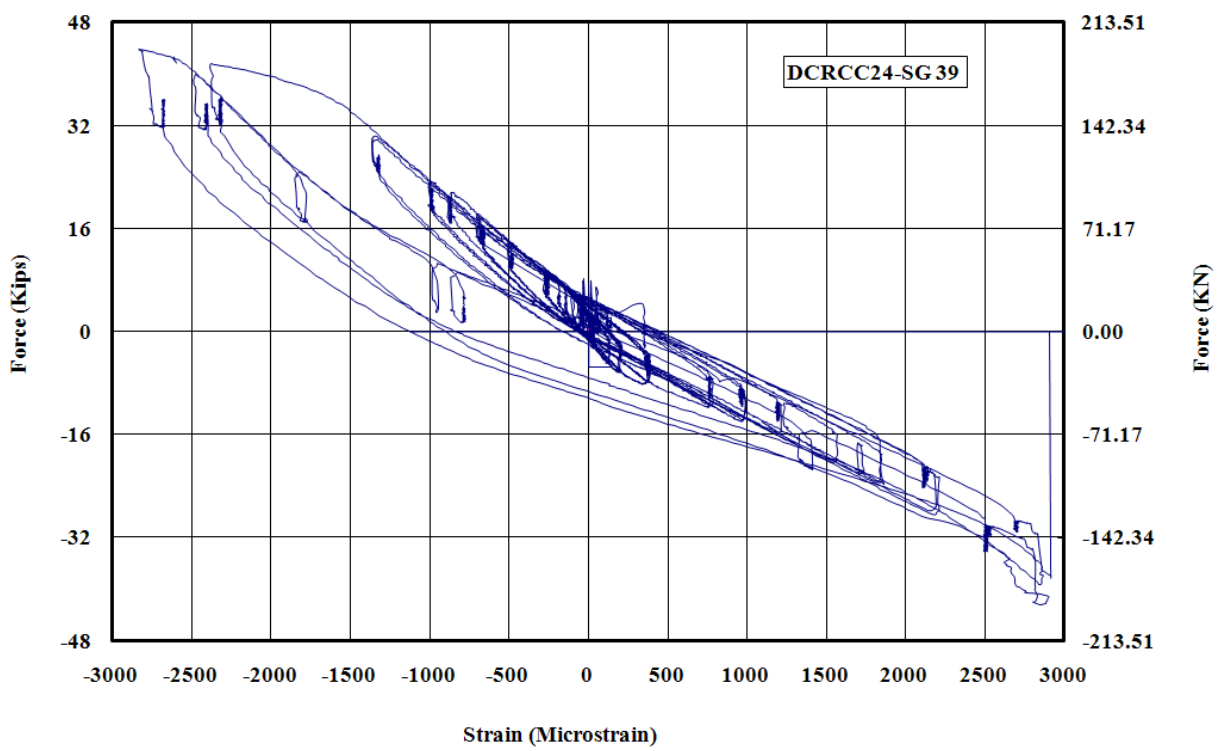

Figure C - 36: Measured Strain in Gauge No.39 for DCRCC24

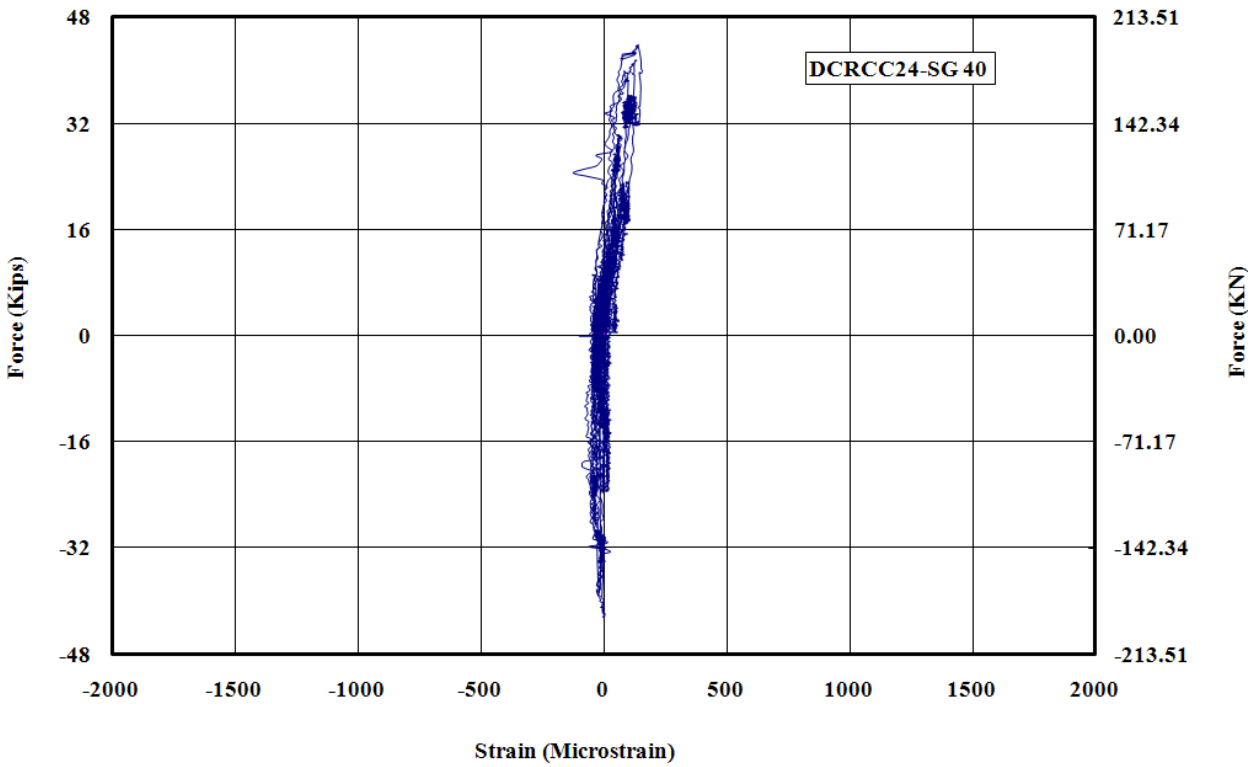

Figure C - 37: Measured Strain in Gauge No.40 for DCRCC24

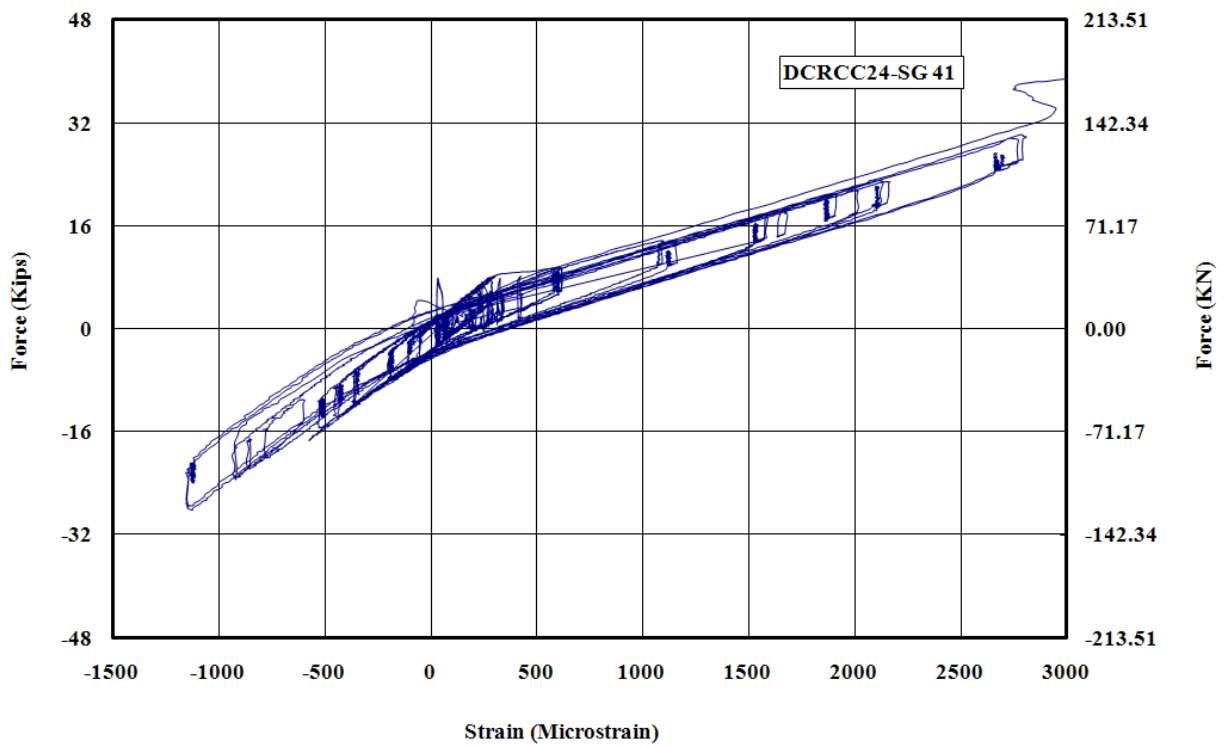

Figure C - 38: Measured Strain in Gauge No.41 for DCRCC24

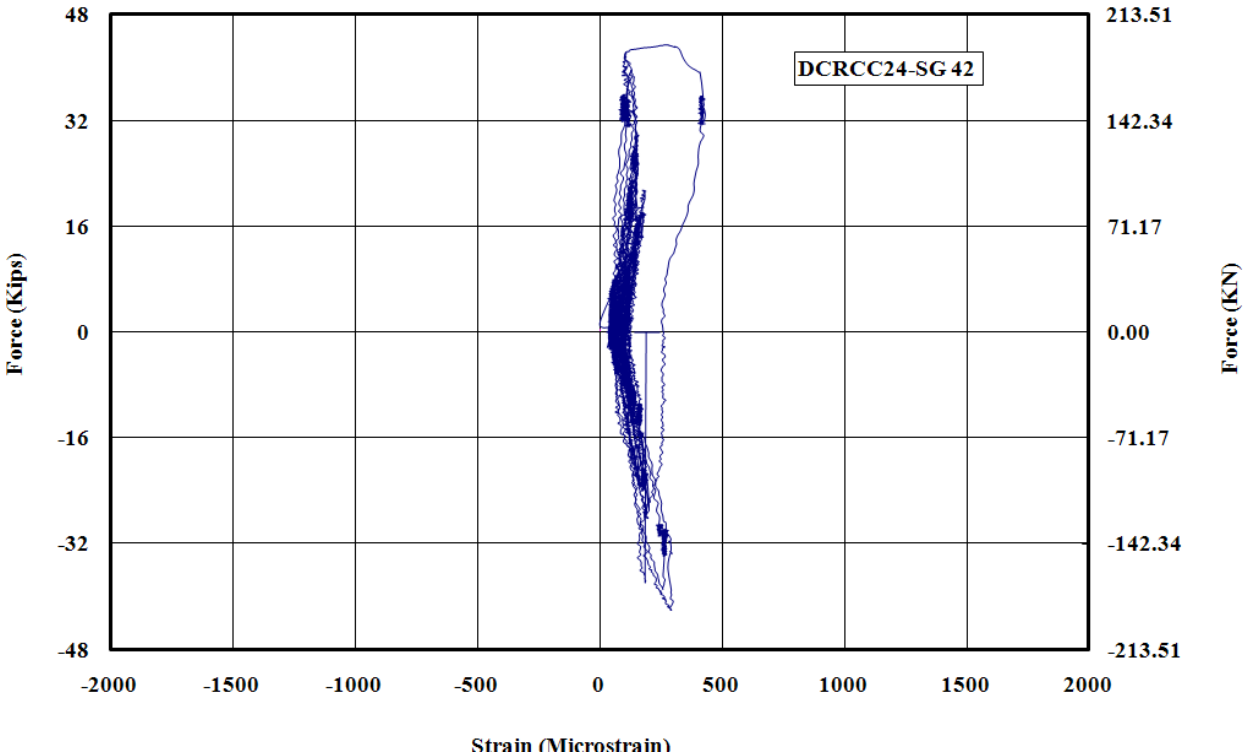

Figure C - 39: Measured Strain in Gauge No.42 for DCRCC24

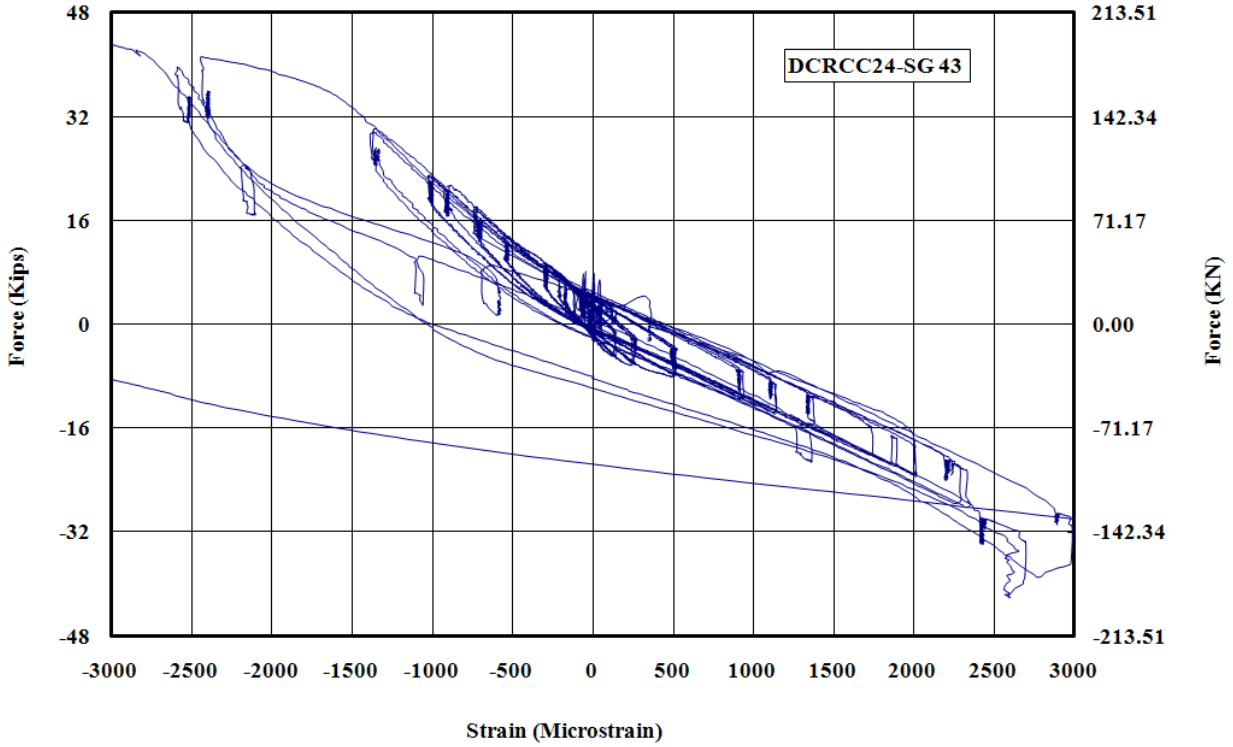

Figure C - 40: Measured Strain in Gauge No.43 for DCRCC24

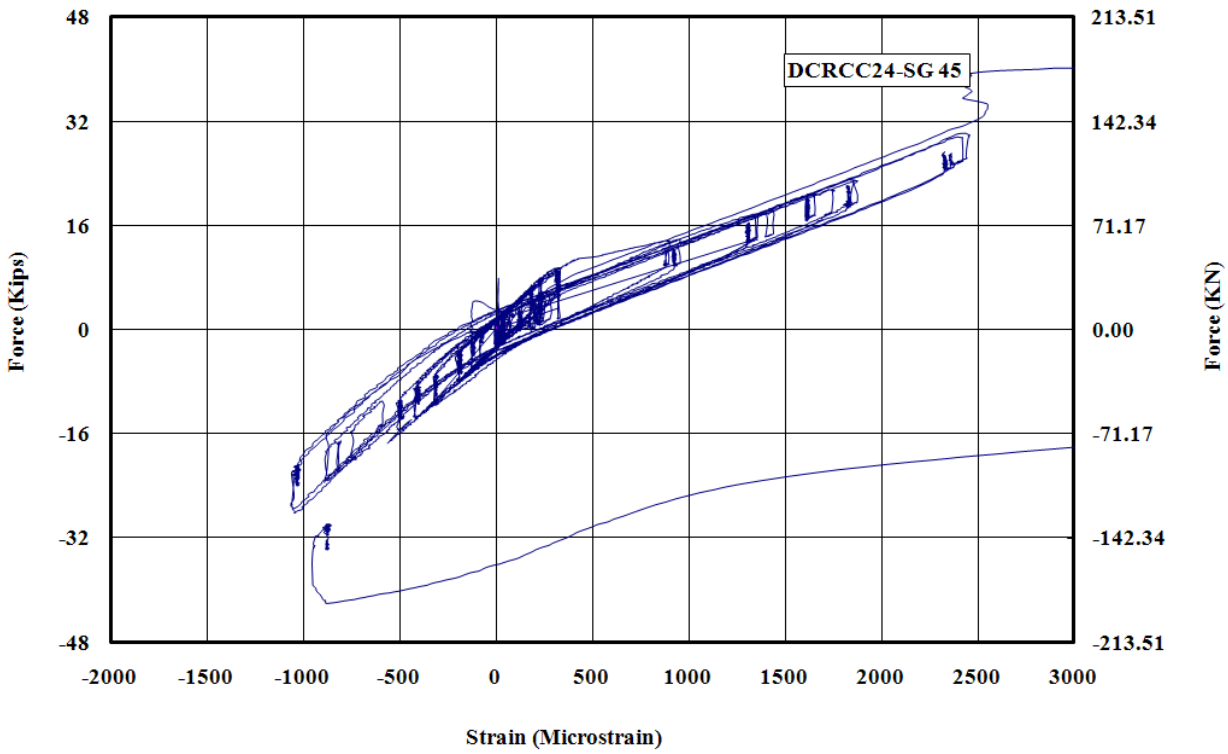

Figure C - 41: Measured Strain in Gauge No.45 for DCRCC24

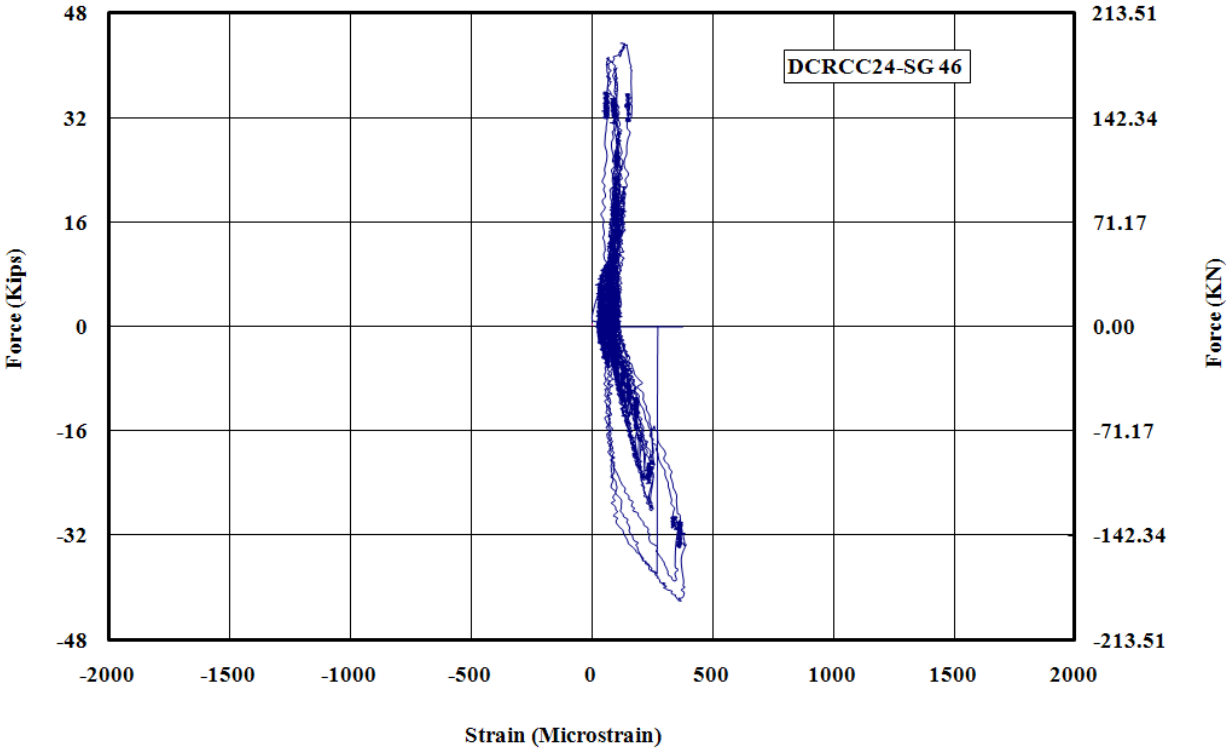

Figure C - 42: Measured Strain in Gauge No.46 for DCRCC24

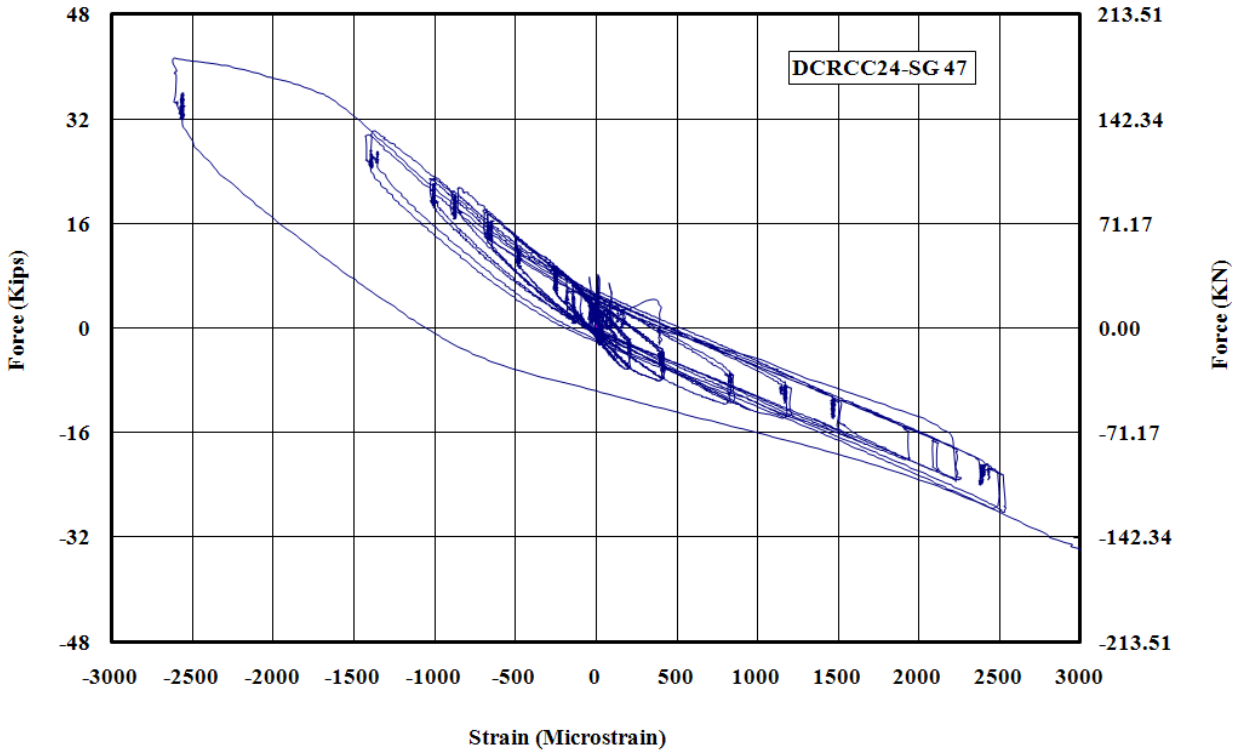

Figure C - 43: Measured Strain in Gauge No.47 for DCRCC24

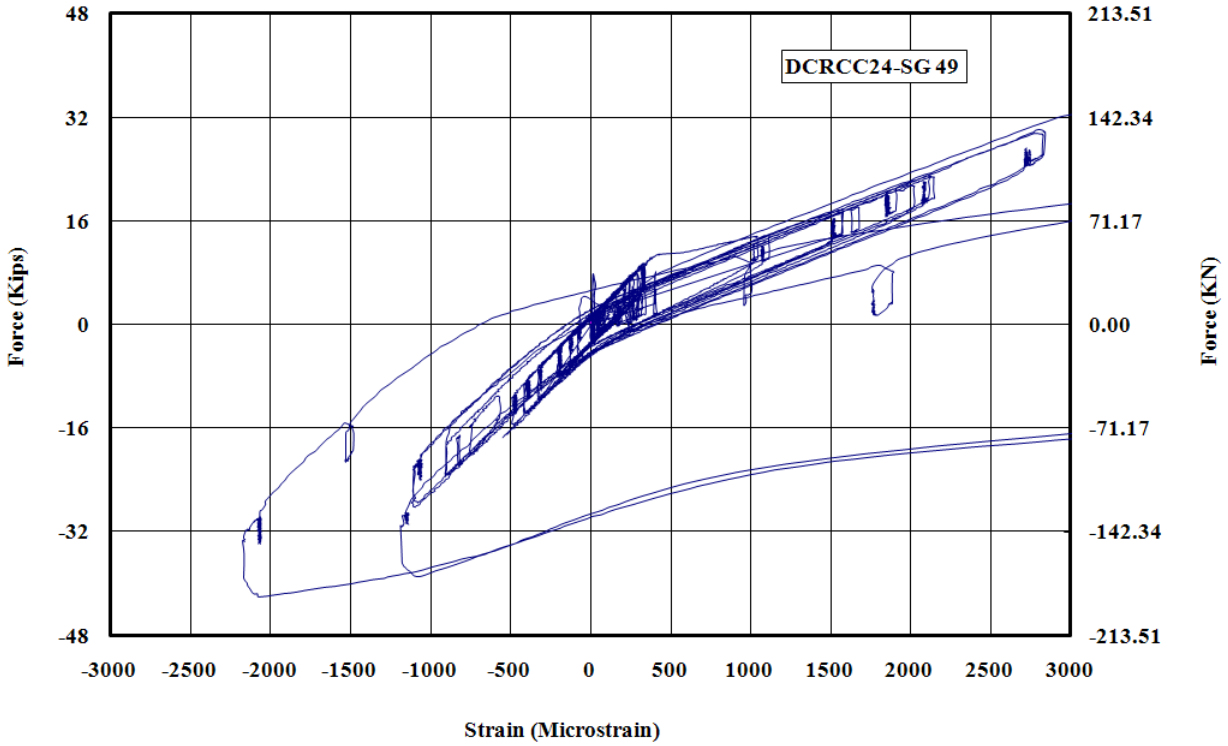

Figure C - 44: Measured Strain in Gauge No.49 for DCRCC24

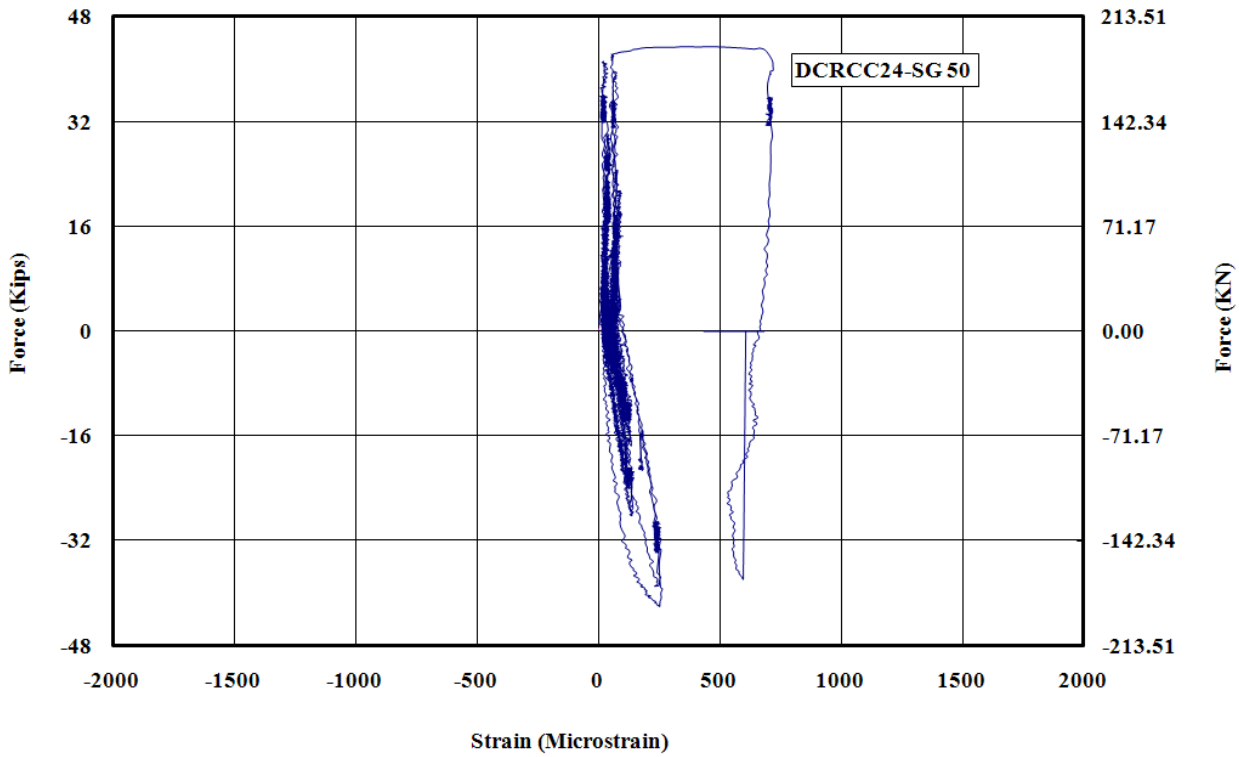

Figure C - 45: Measured Strain in Gauge No.50 for DCRCC24

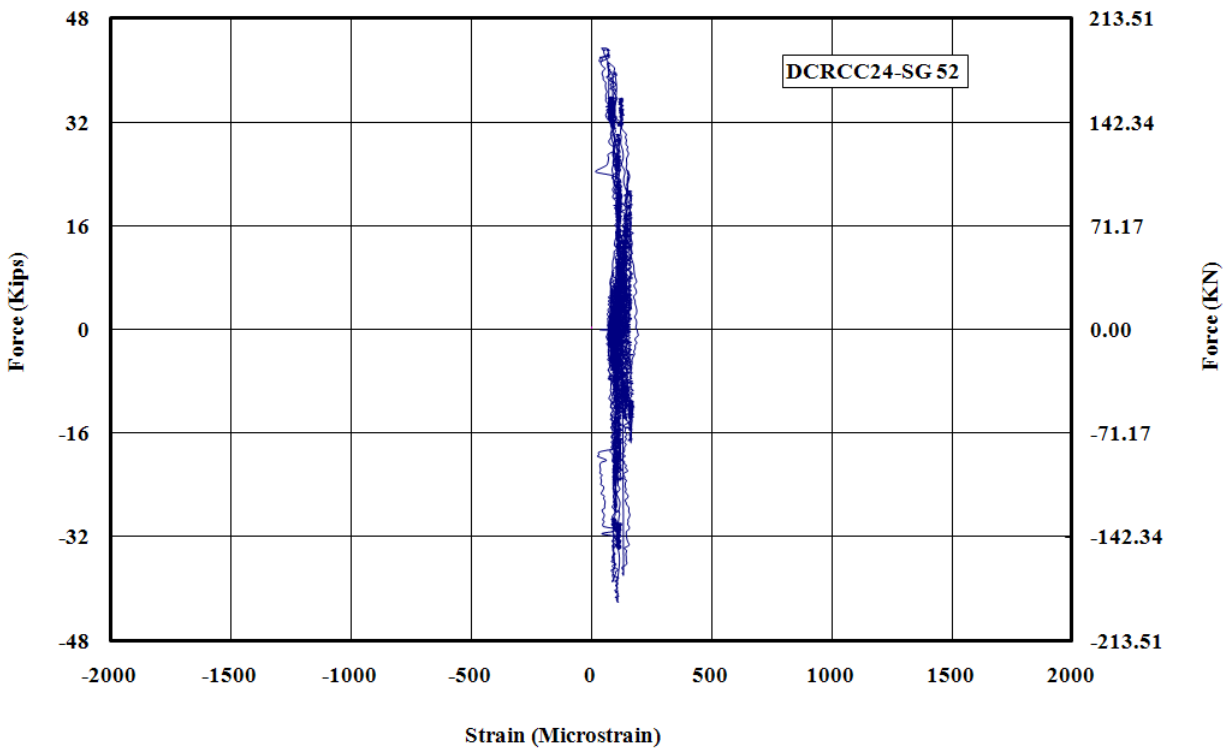

Figure C - 46: Measured Strain in Gauge No.52 for DCRCC24

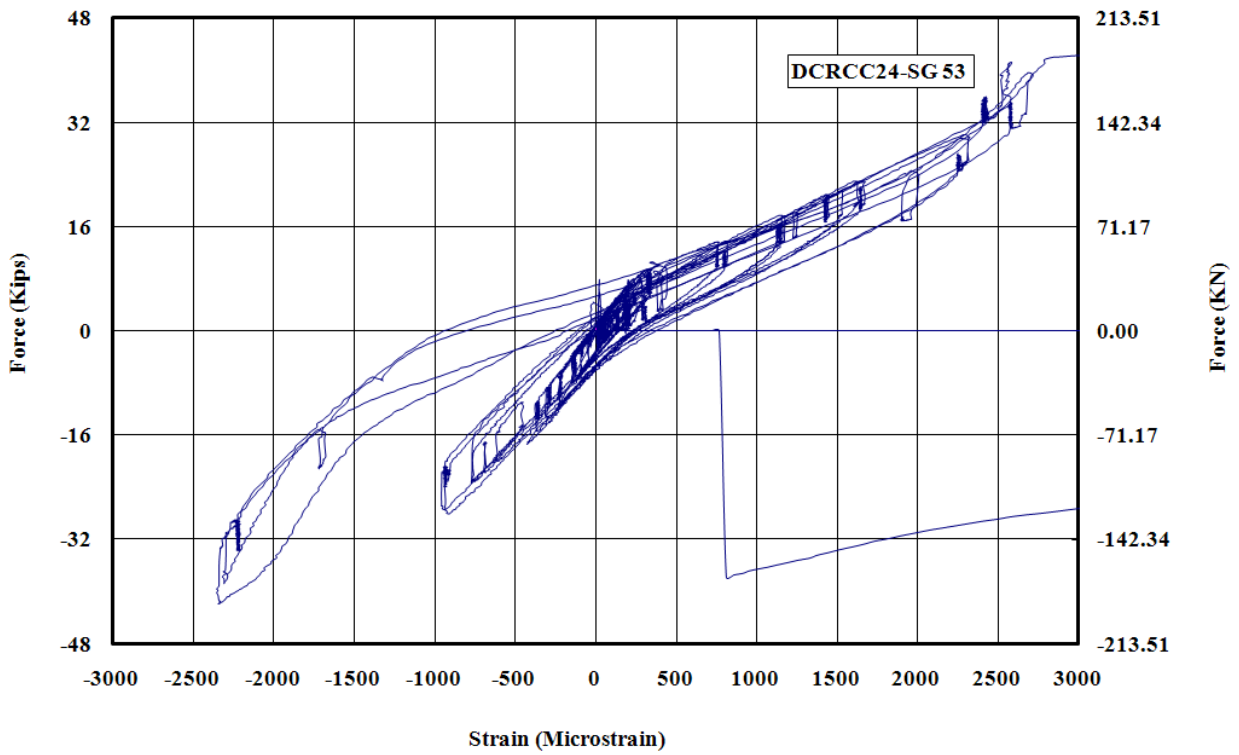

Figure C - 47: Measured Strain in Gauge No.53 for DCRCC24

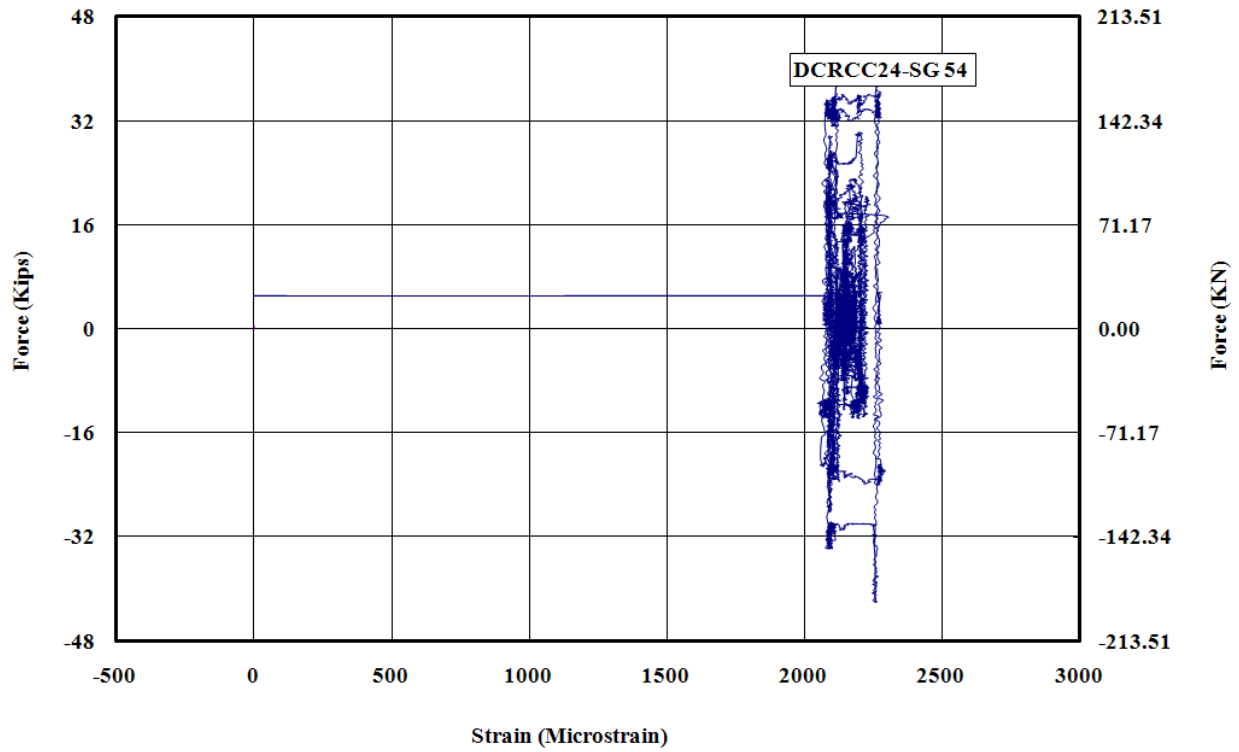

Figure C - 48: Measured Strain in Gauge No.54 for DCRCC24

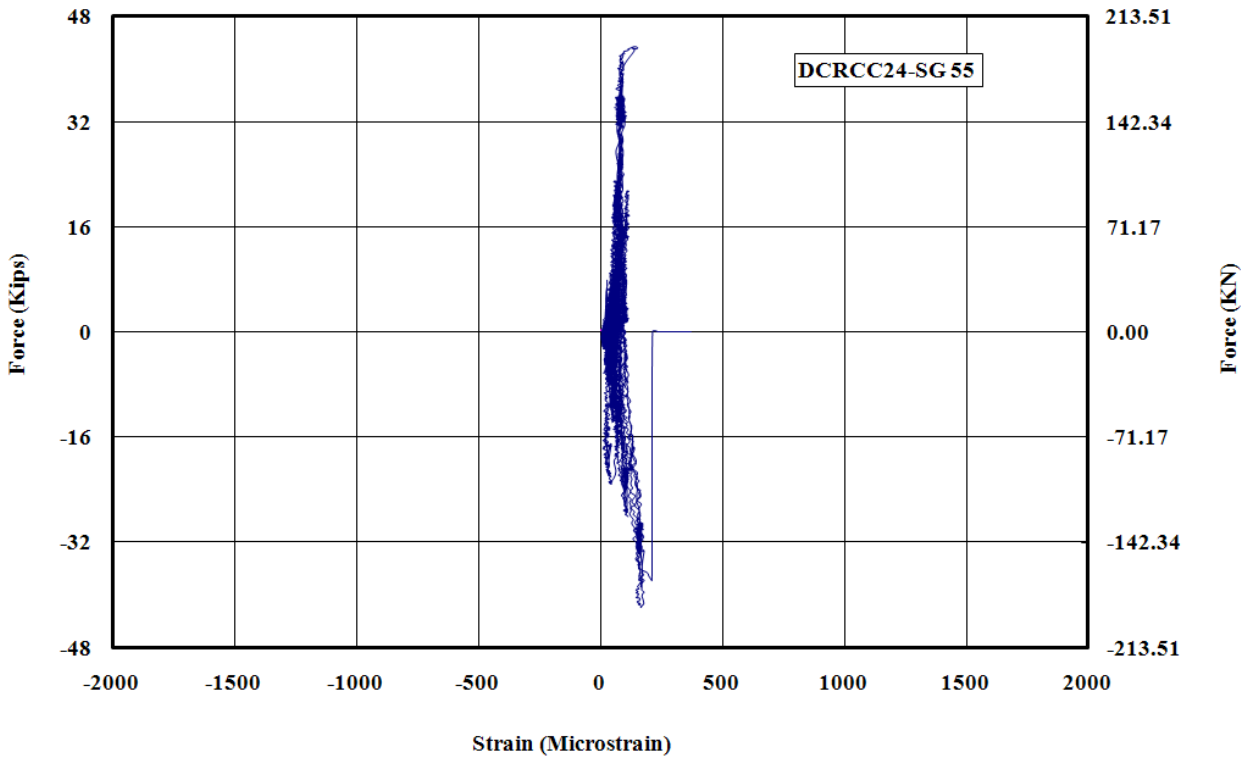

Figure C - 49: Measured Strain in Gauge No.55 for DCRCC24

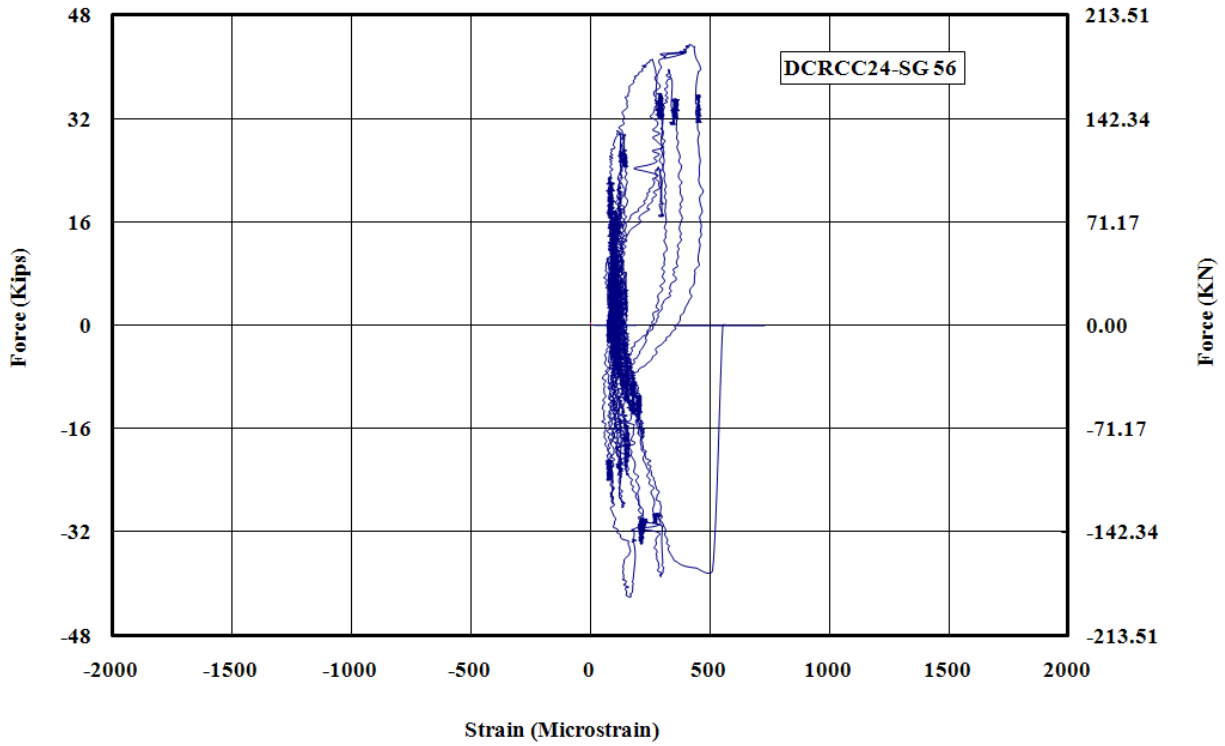

Figure C - 50: Measured Strain in Gauge No.56 for DCRCC24

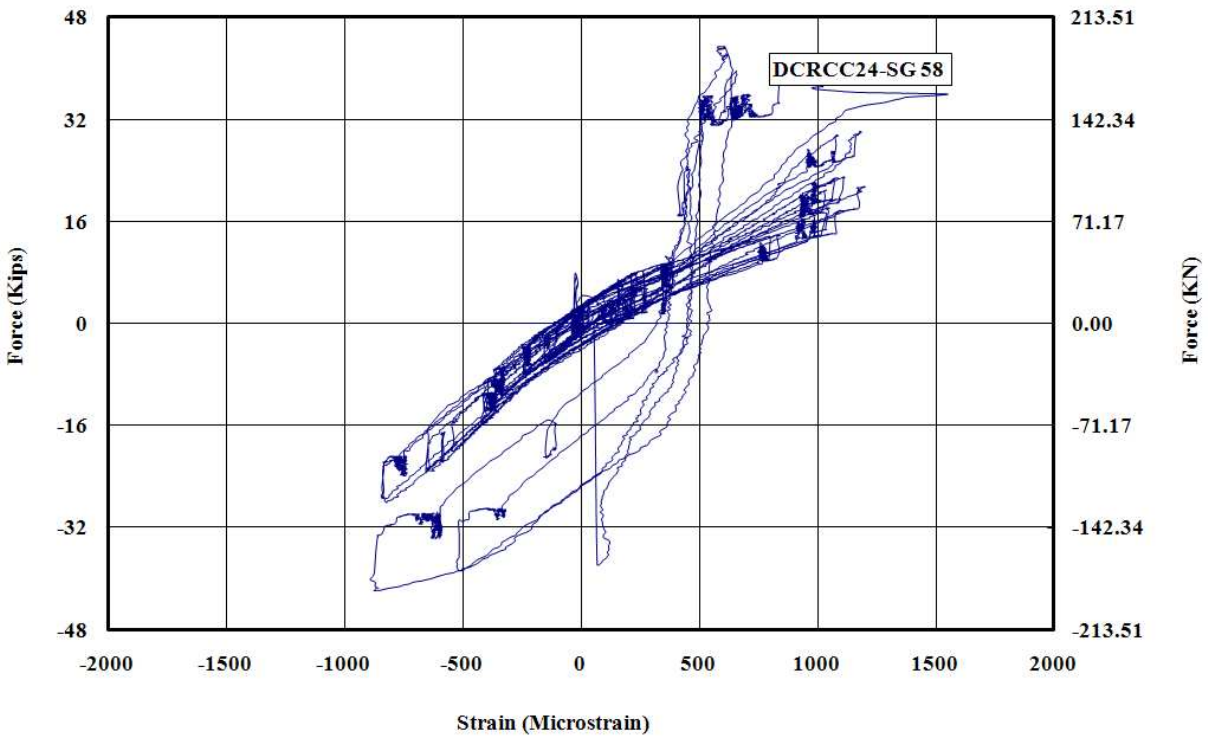

Figure C - 51: Measured Strain in Gauge No.58 for DCRCC24

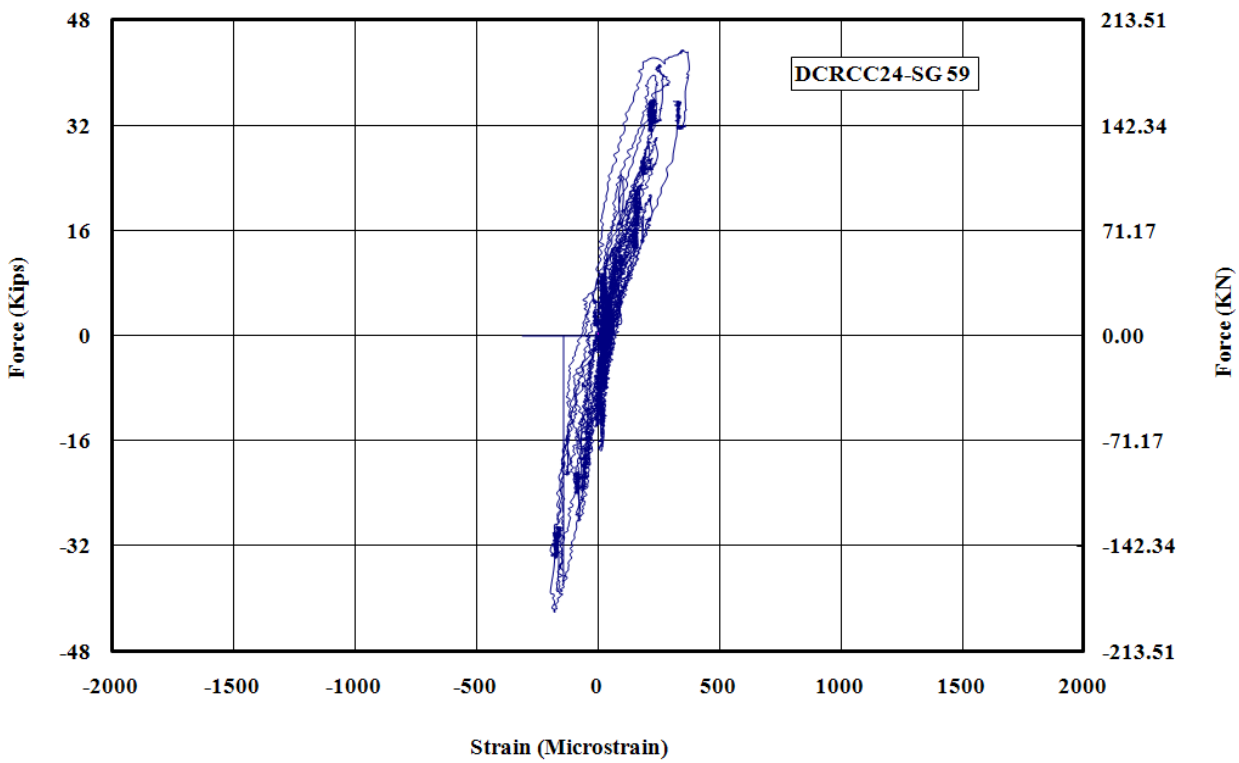

Figure C - 52: Measured Strain in Gauge No.59 for DCRCC24

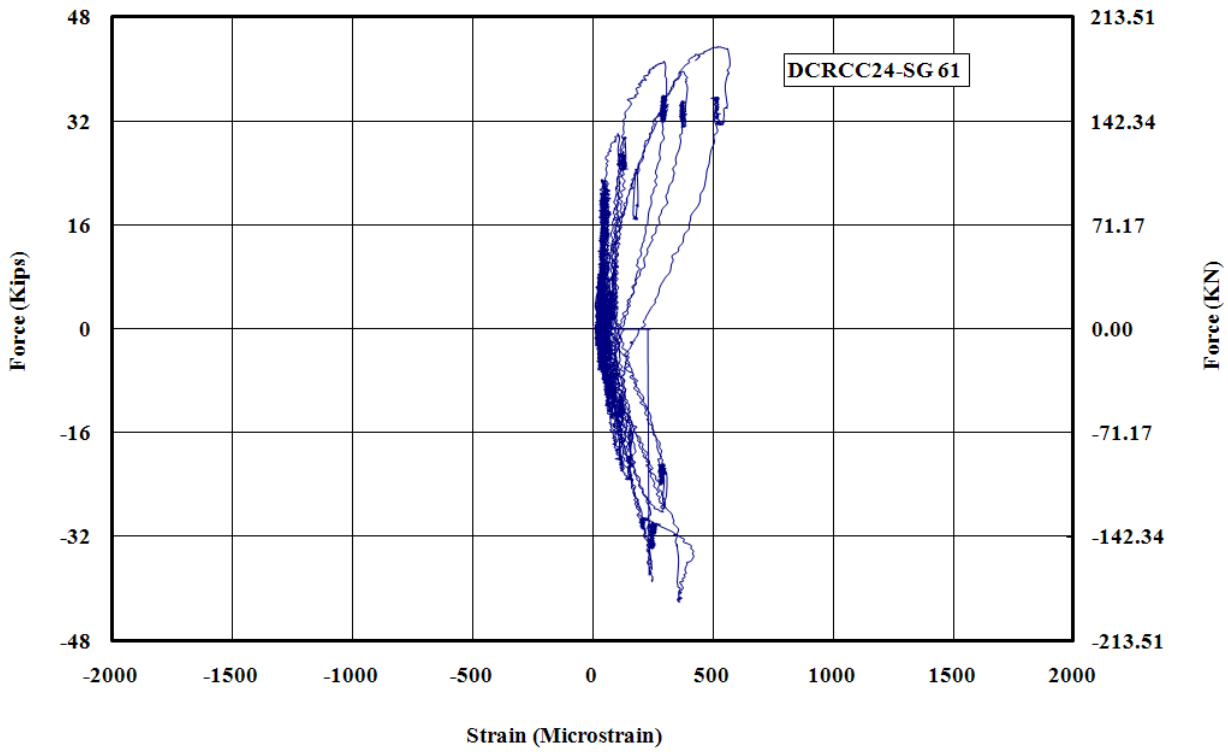

Figure C - 53: Measured Strain in Gauge No.61 for DCRCC24

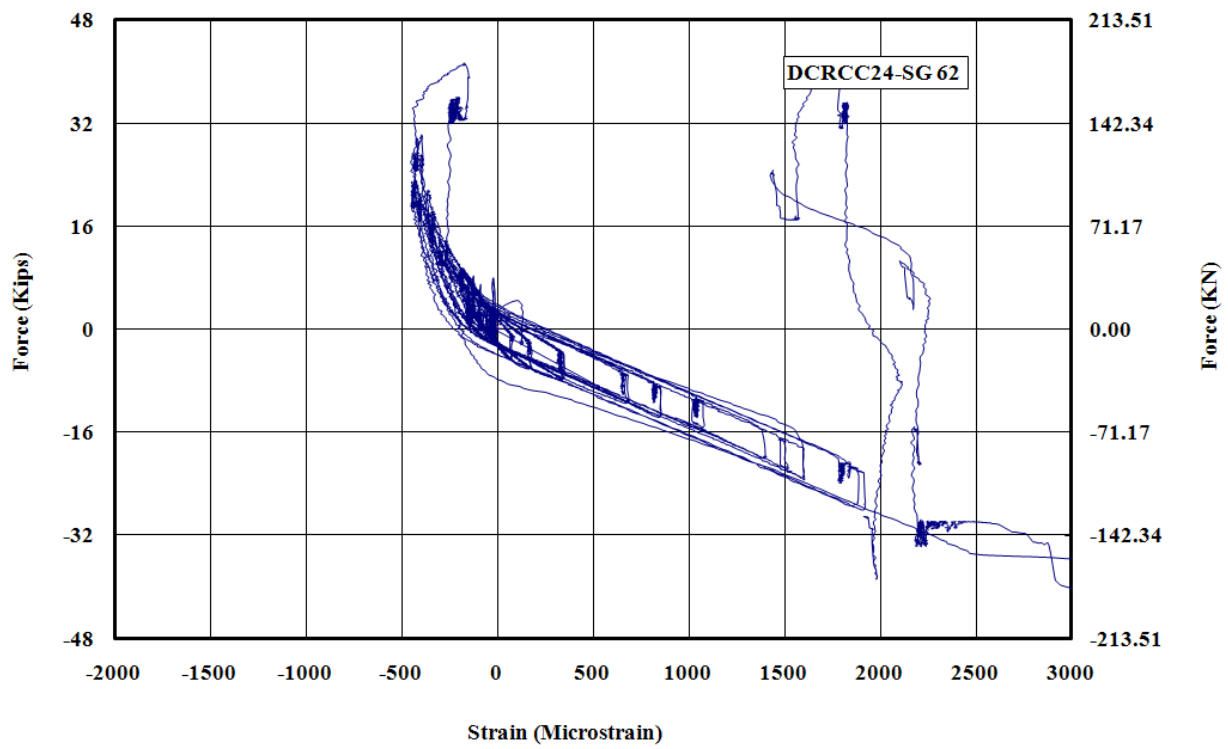

Figure C - 54: Measured Strain in Gauge No.62 for DCRCC24

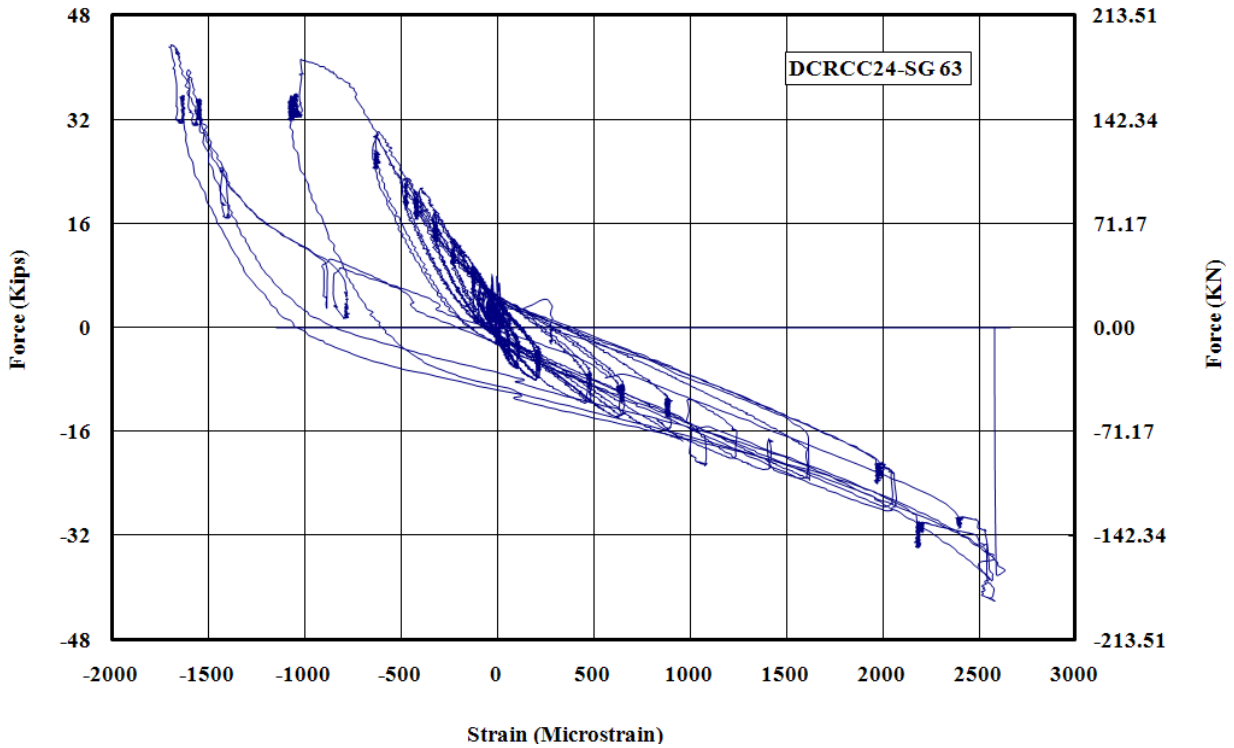

Figure C - 55: Measured Strain in Gauge No.63 for DCRCC24

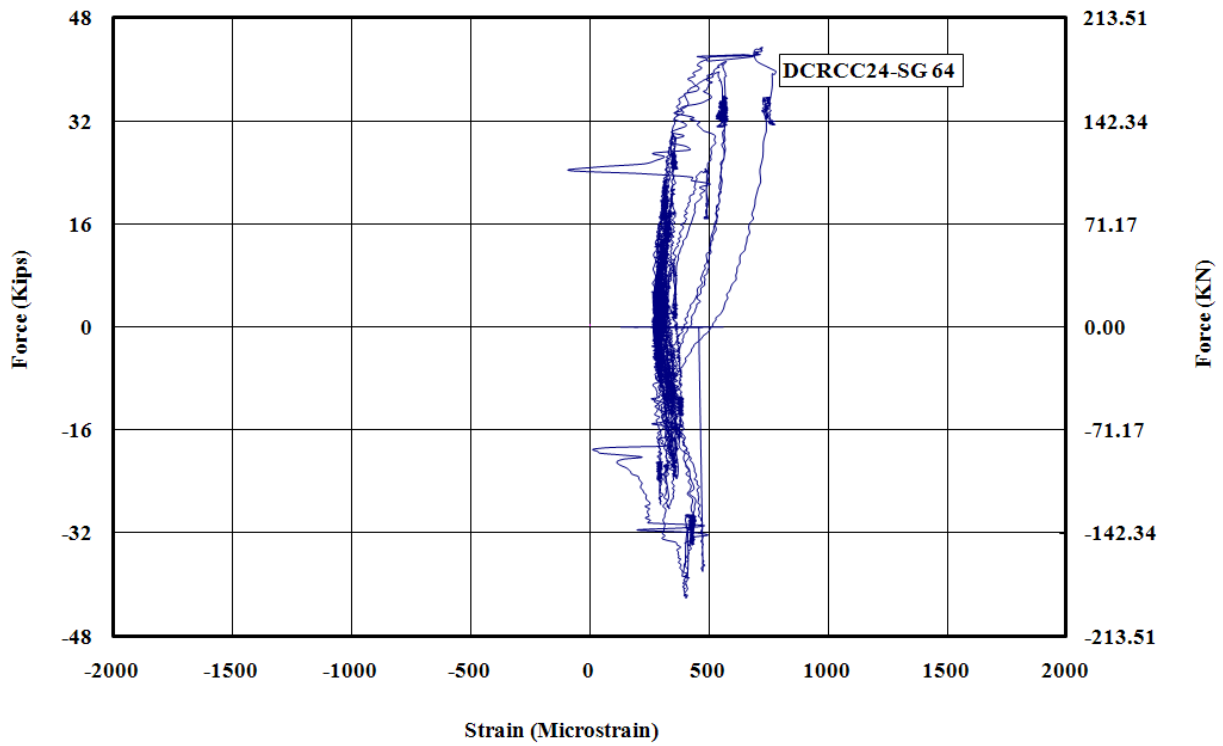

Figure C - 56: Measured Strain in Gauge No.64 for DCRCC24

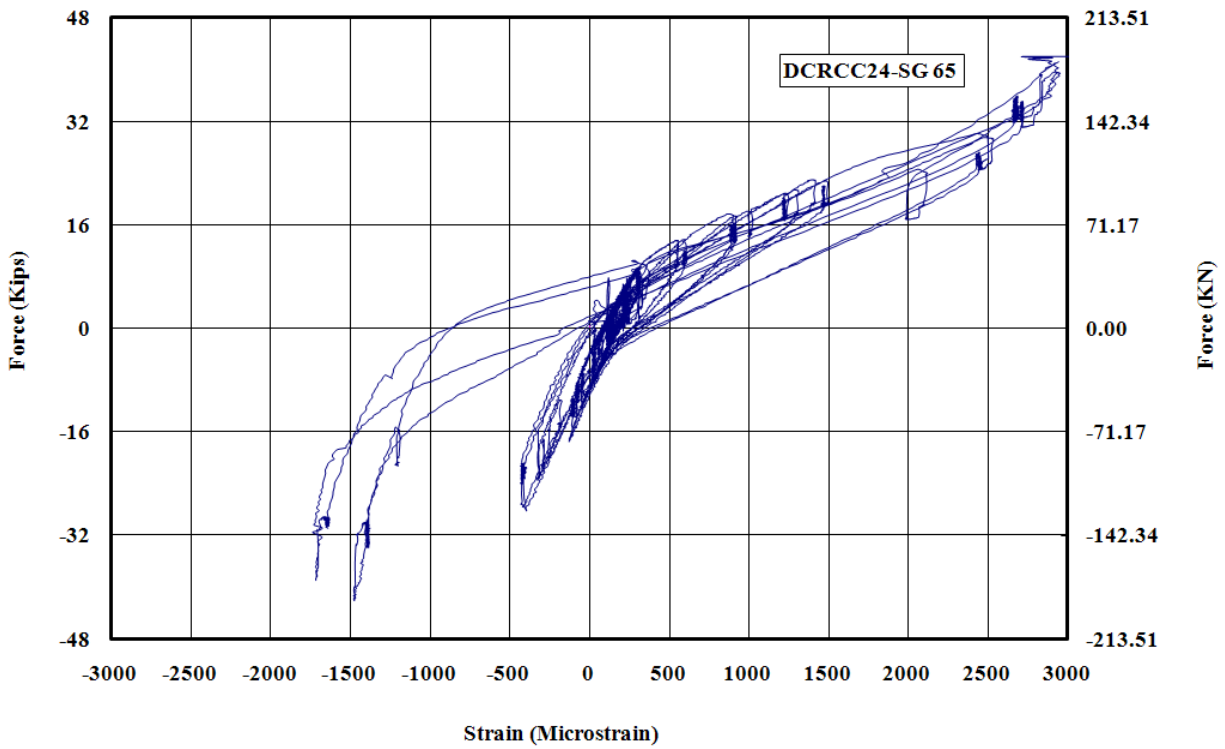

Figure C - 57: Measured Strain in Gauge No.65 for DCRCC24

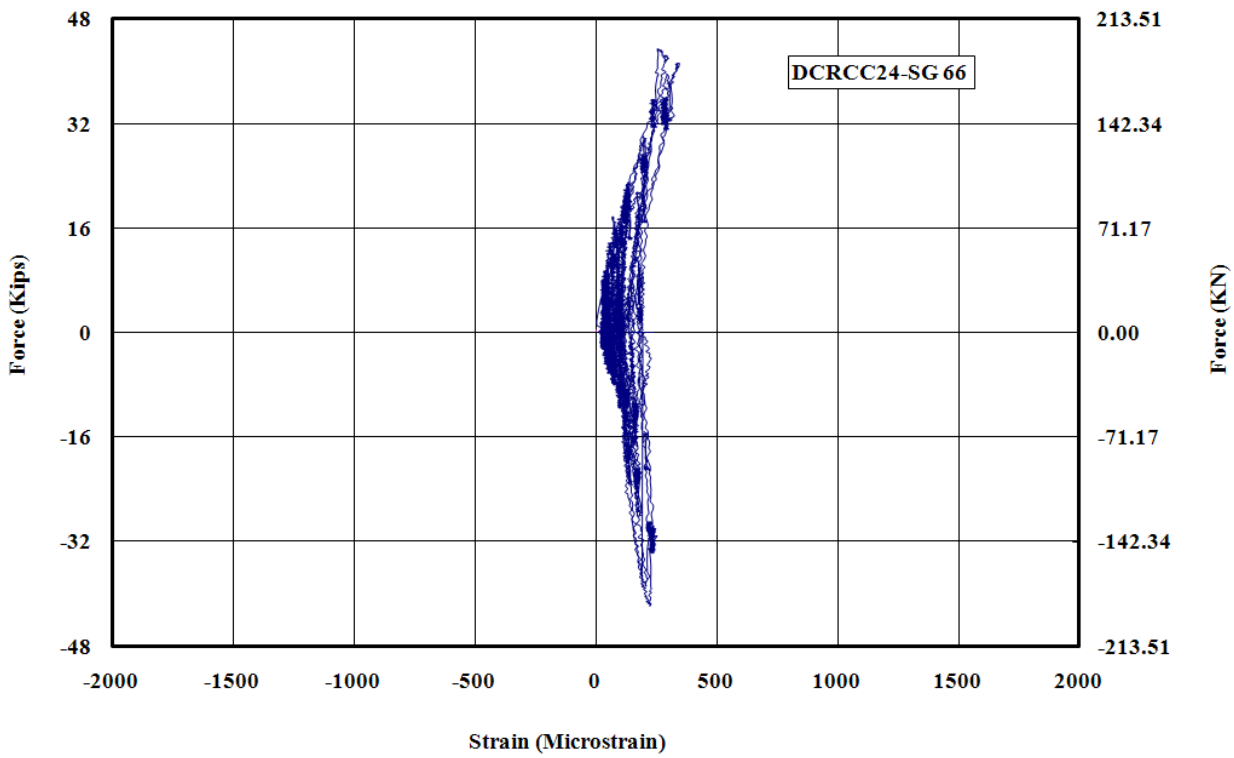

Figure C - 58: Measured Strain in Gauge No.66 for DCRCC24

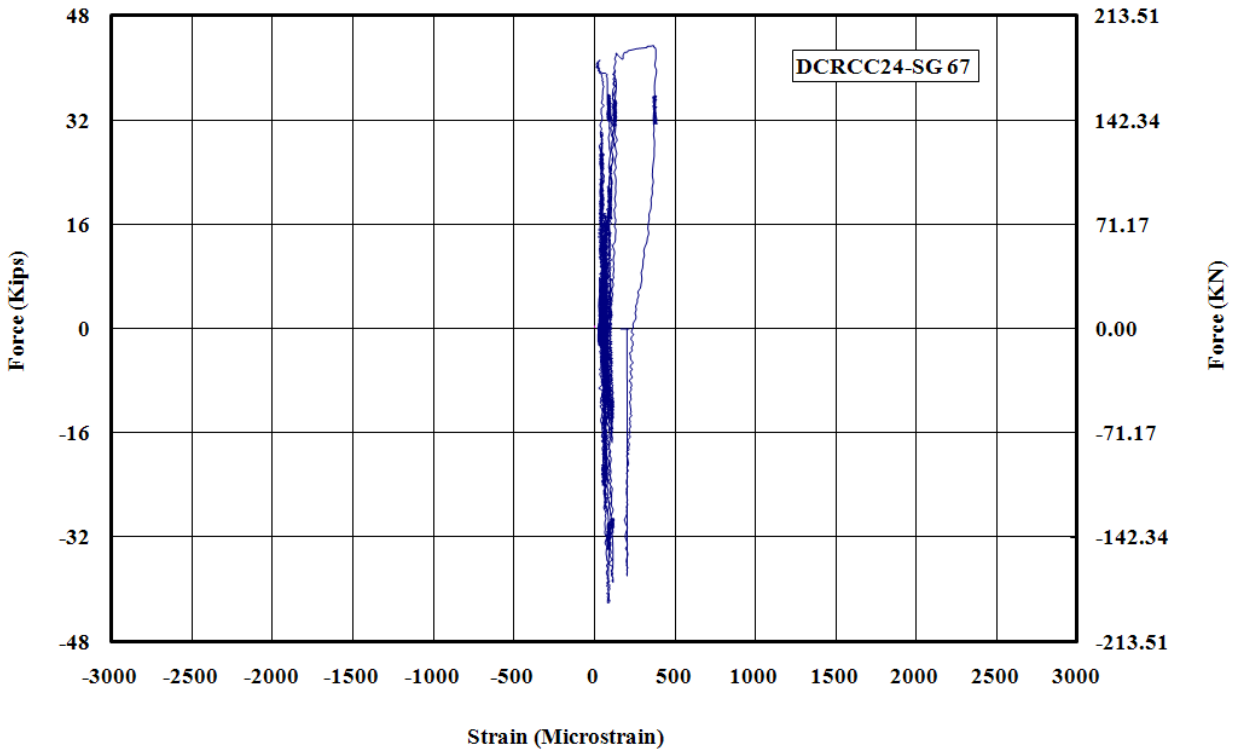

Figure C - 59: Measured Strain in Gauge No.67 for DCRCC24

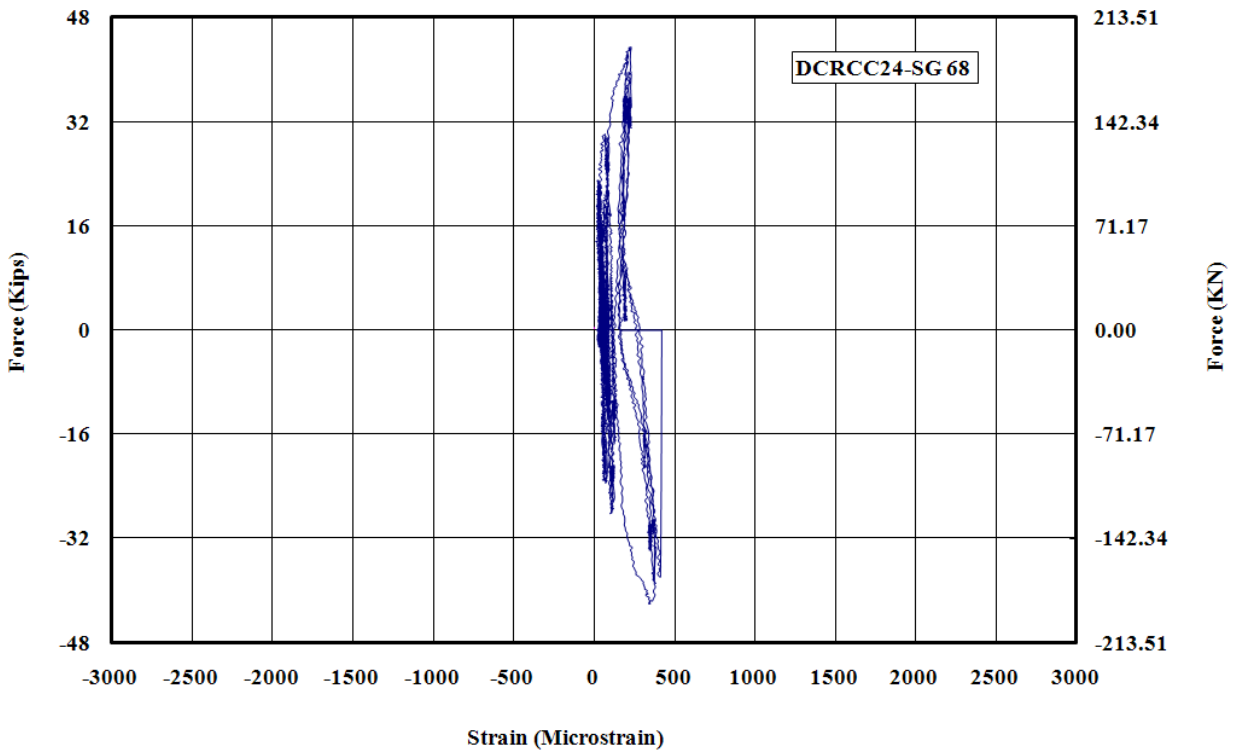

Figure C - 60: Measured Strain in Gauge No.68 for DCRCC24

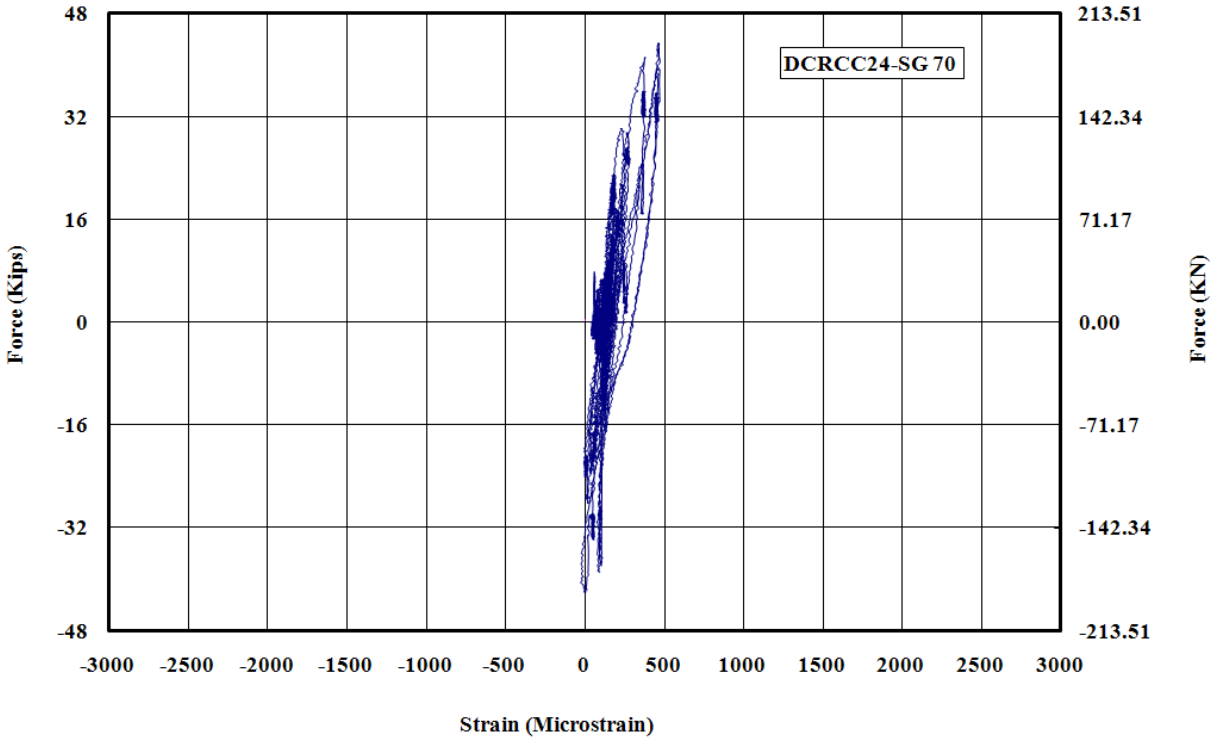

Figure C - 61: Measured Strain in Gauge No.70 for DCRCC24

Appendix D

Specimens FSRCC24

(Flat-Slab T-Joint with 24-in. diameter pile)

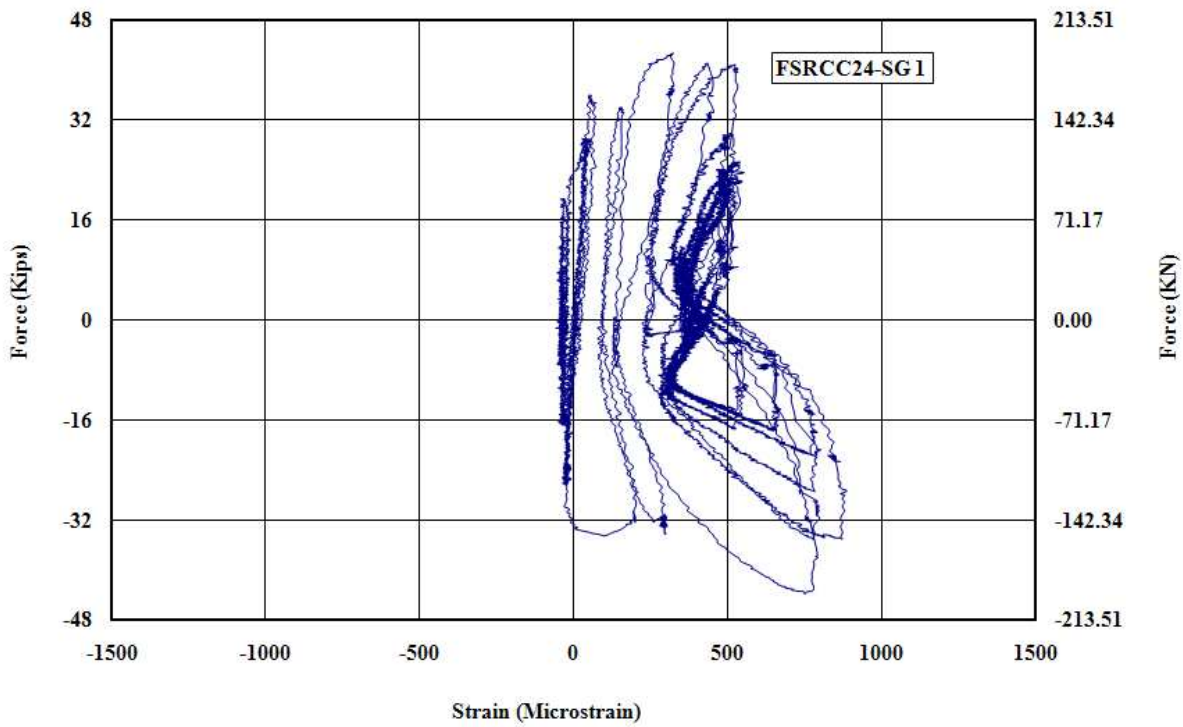

Figure D - 1: Measured Strain in Gauge No.1 for FSRCC24

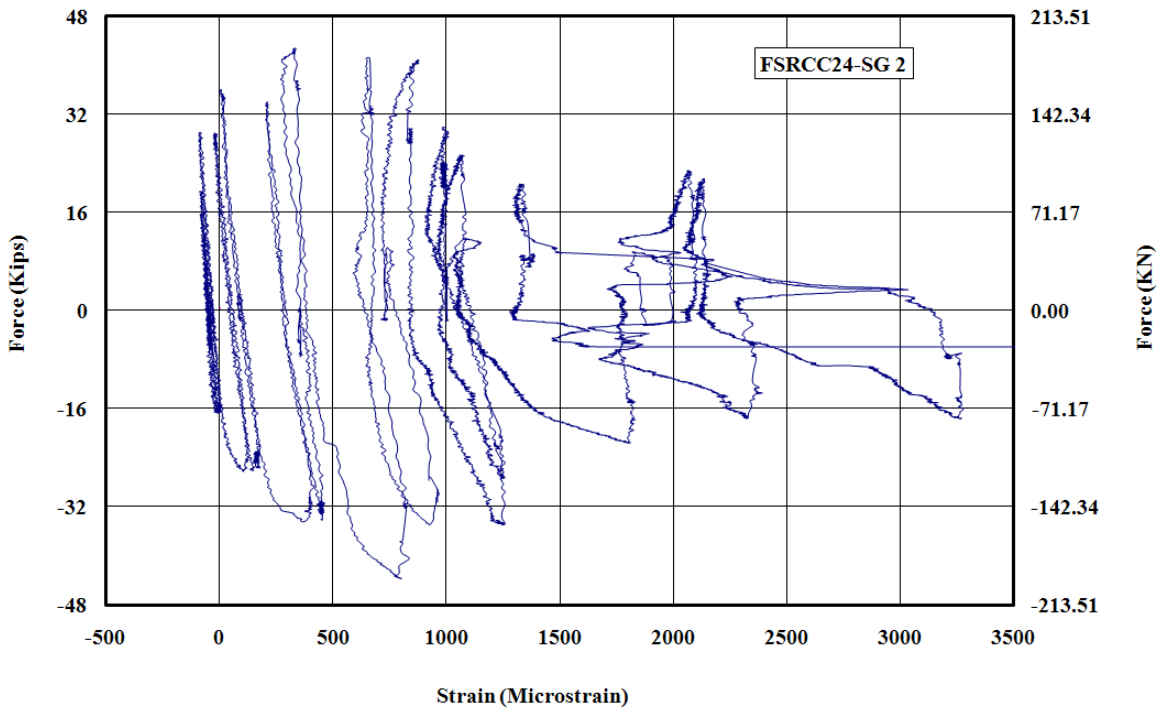

Figure D - 2: Measured Strain in Gauge No.2 for FSRCC24

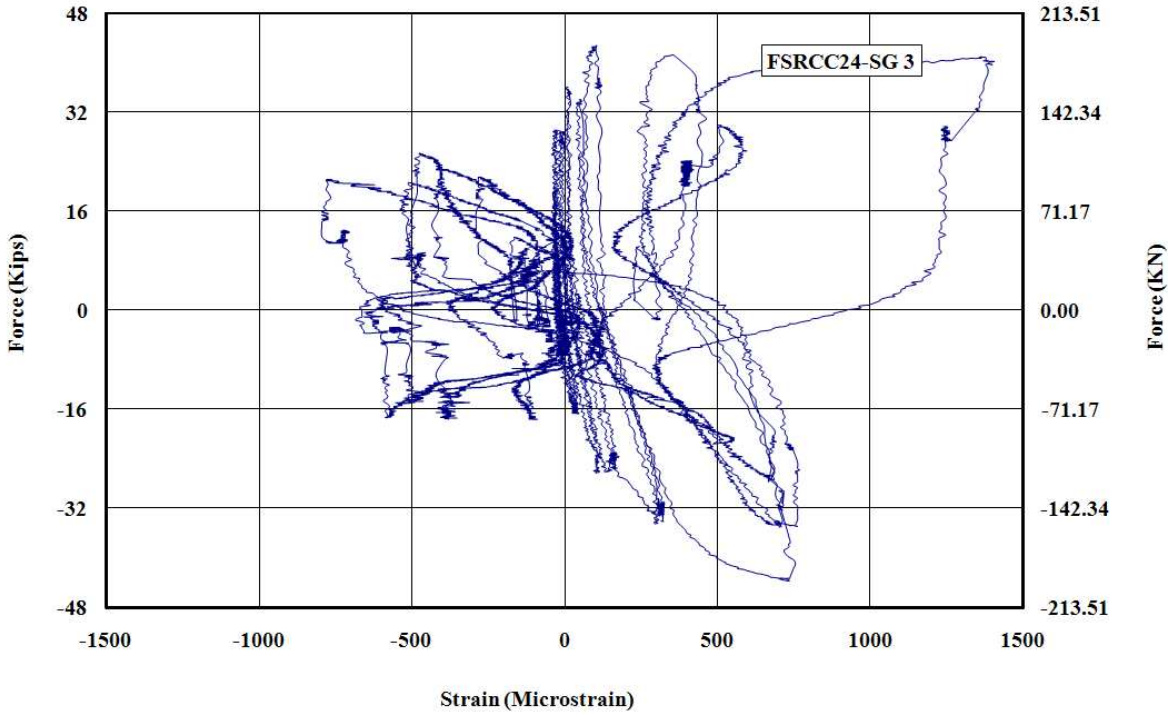

Figure D - 3: Measured Strain in Gauge No.3 for FSRCC24

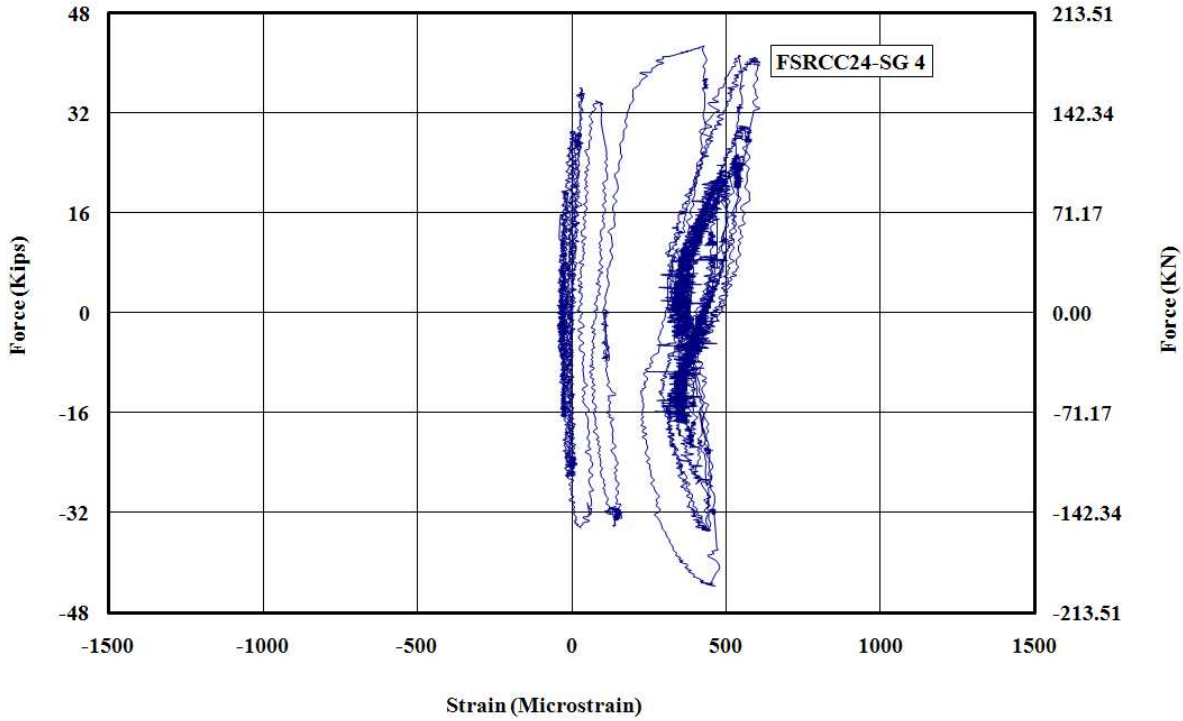

Figure D - 4: Measured Strain in Gauge No.4 for FSRCC24

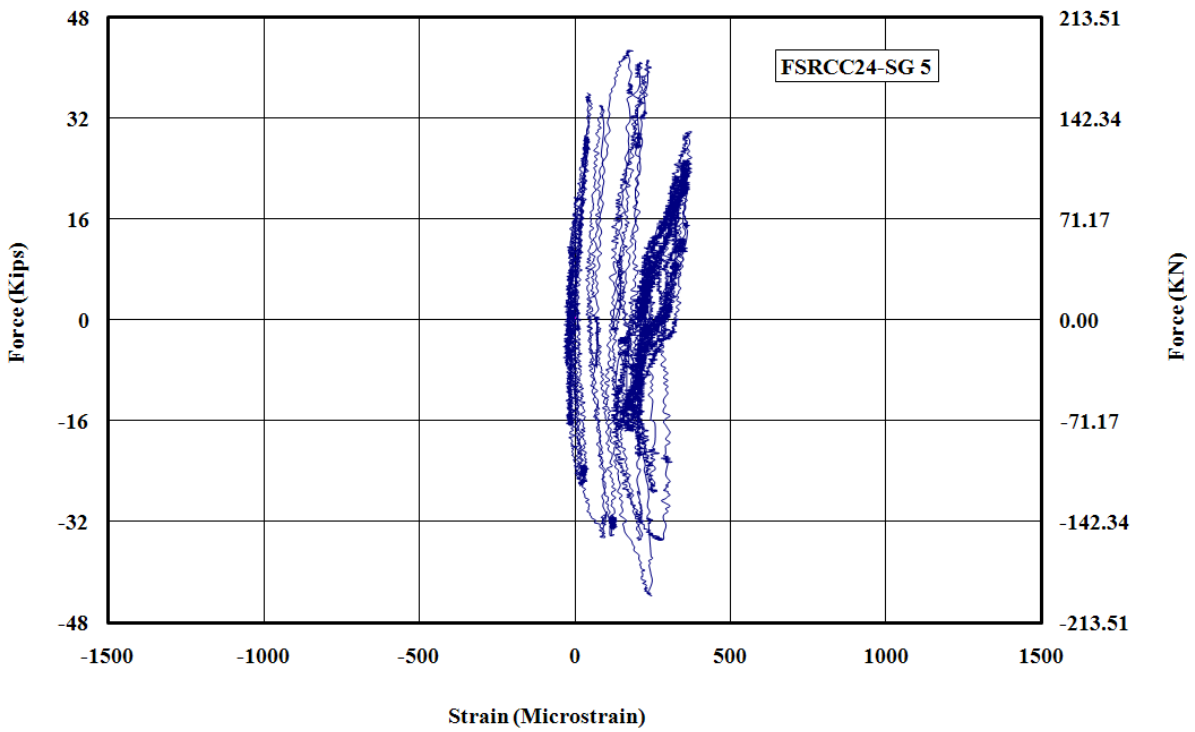

Figure D - 5: Measured Strain in Gauge No.5 for FSRCC24

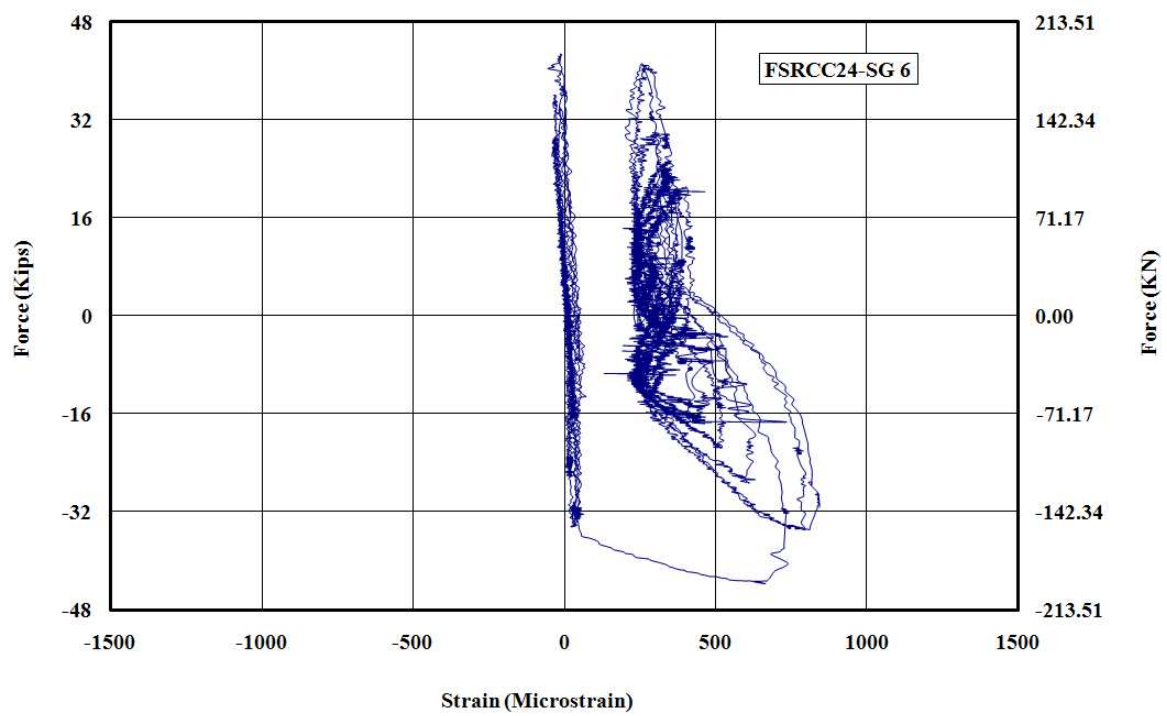

Figure D - 6: Measured Strain in Gauge No.6 for FSRCC24

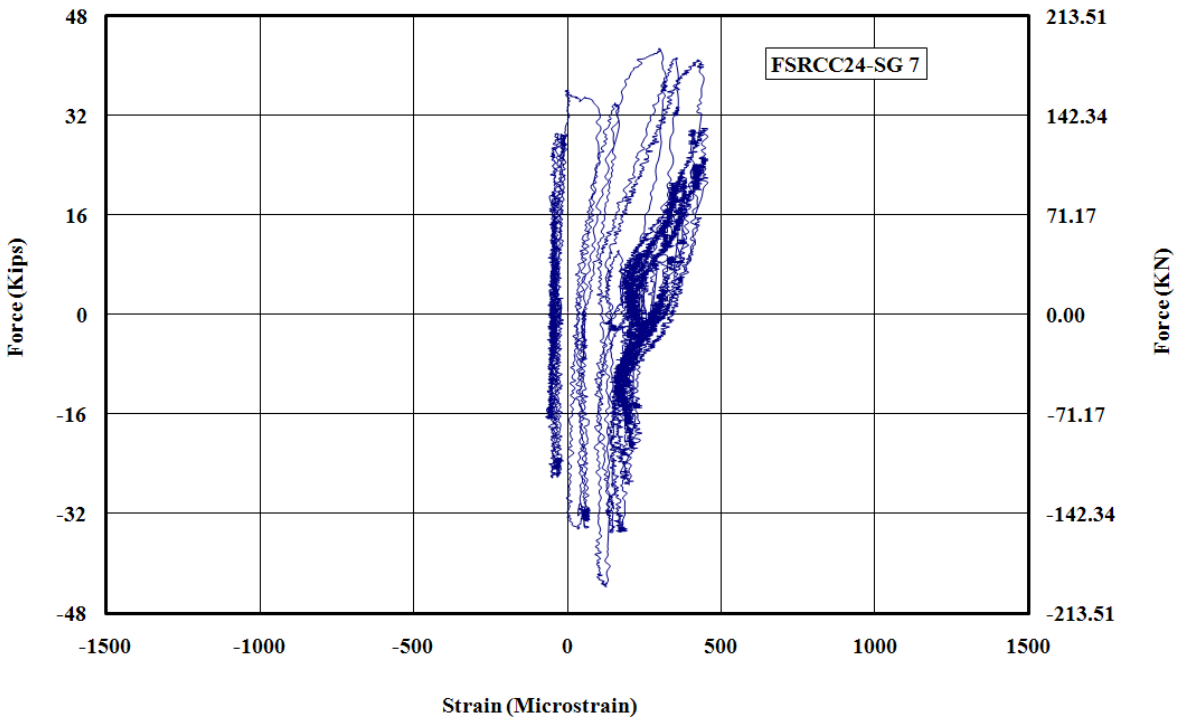

Figure D - 7: Measured Strain in Gauge No.7 for FSRCC24

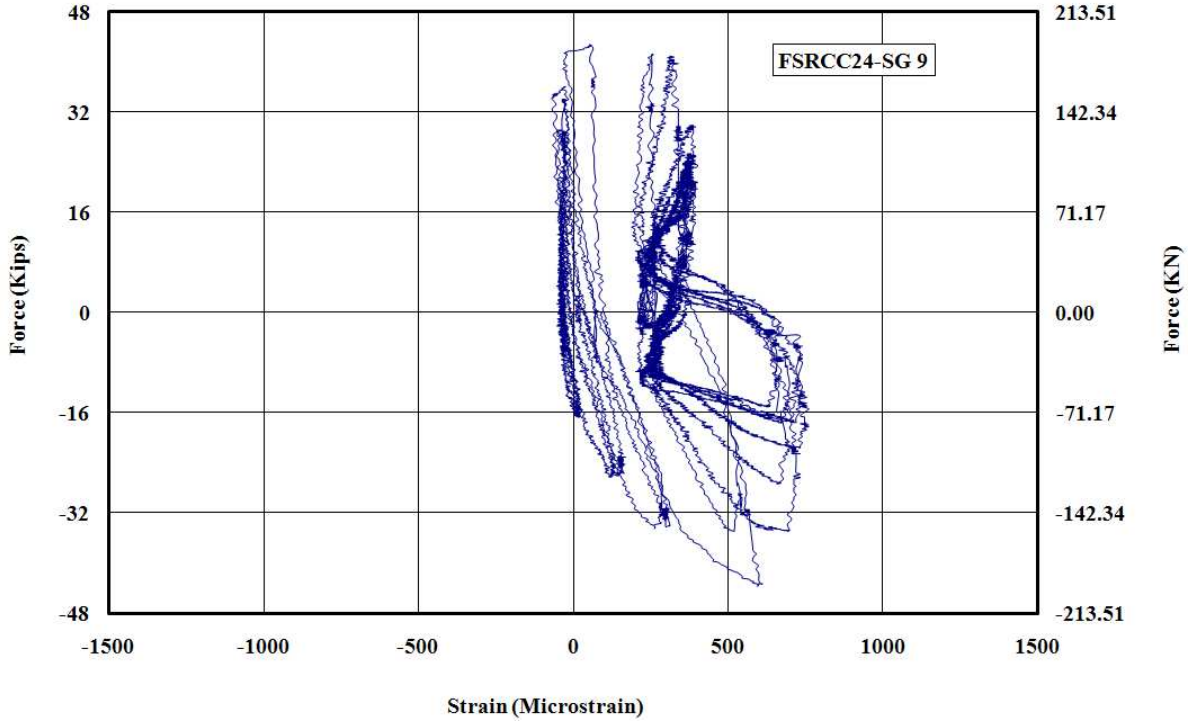

Figure D - 8: Measured Strain in Gauge No.9 for FSRCC24

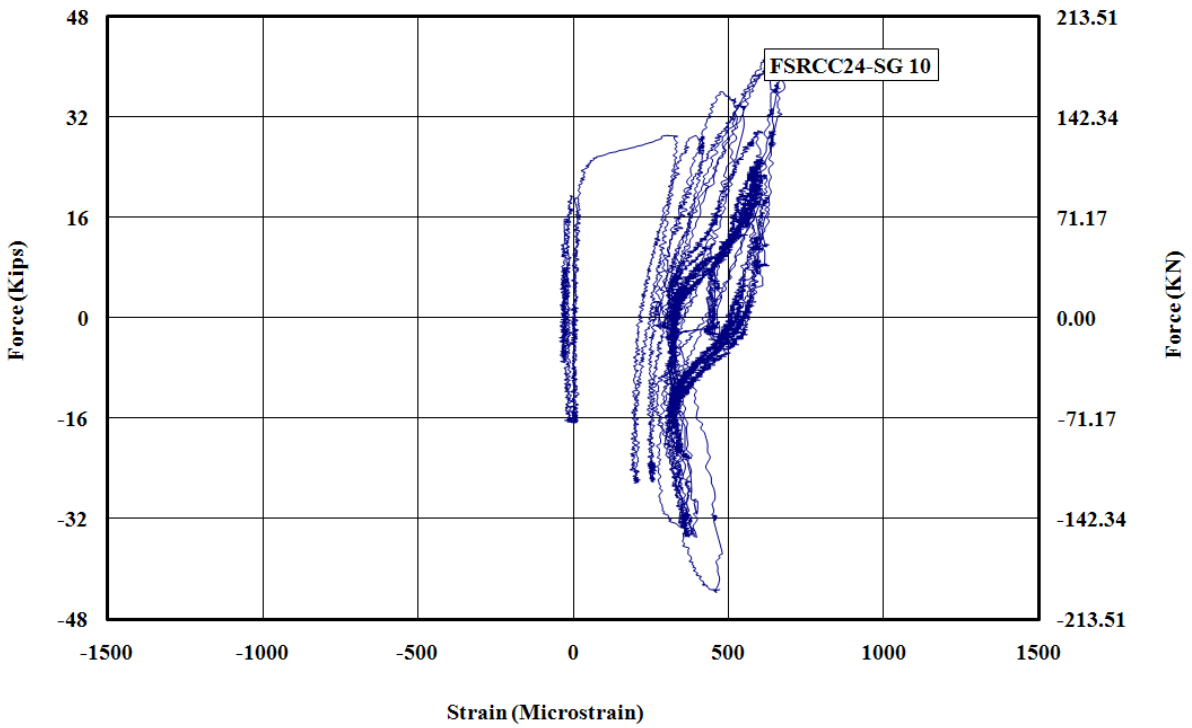

Figure D - 9: Measured Strain in Gauge No.10 for FSRCC24

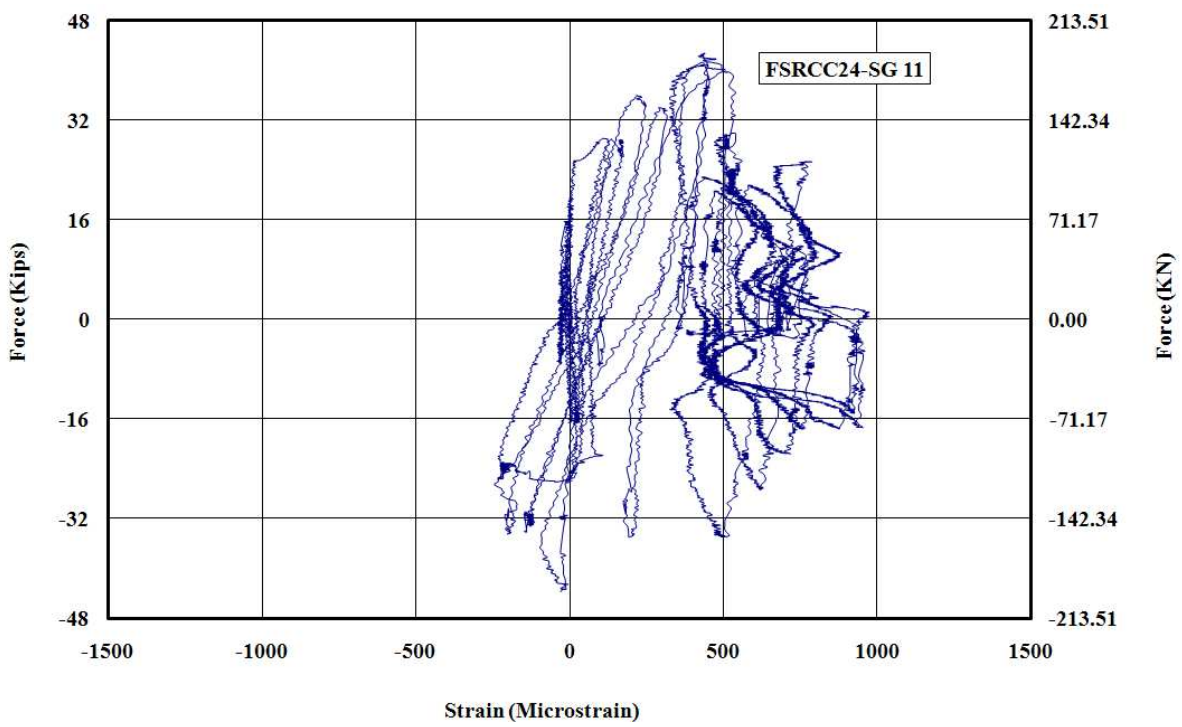

Figure D - 10: Measured Strain in Gauge No.11 for FSRCC24

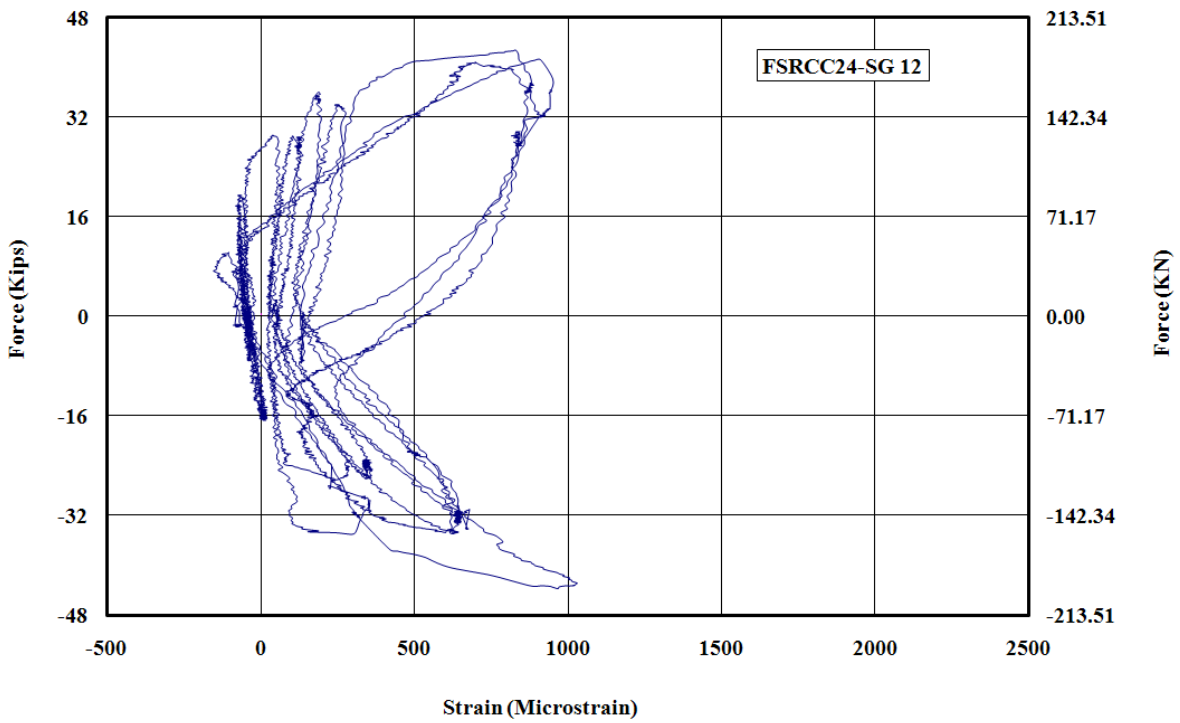

Figure D - 11: Measured Strain in Gauge No.12 for FSRCC24

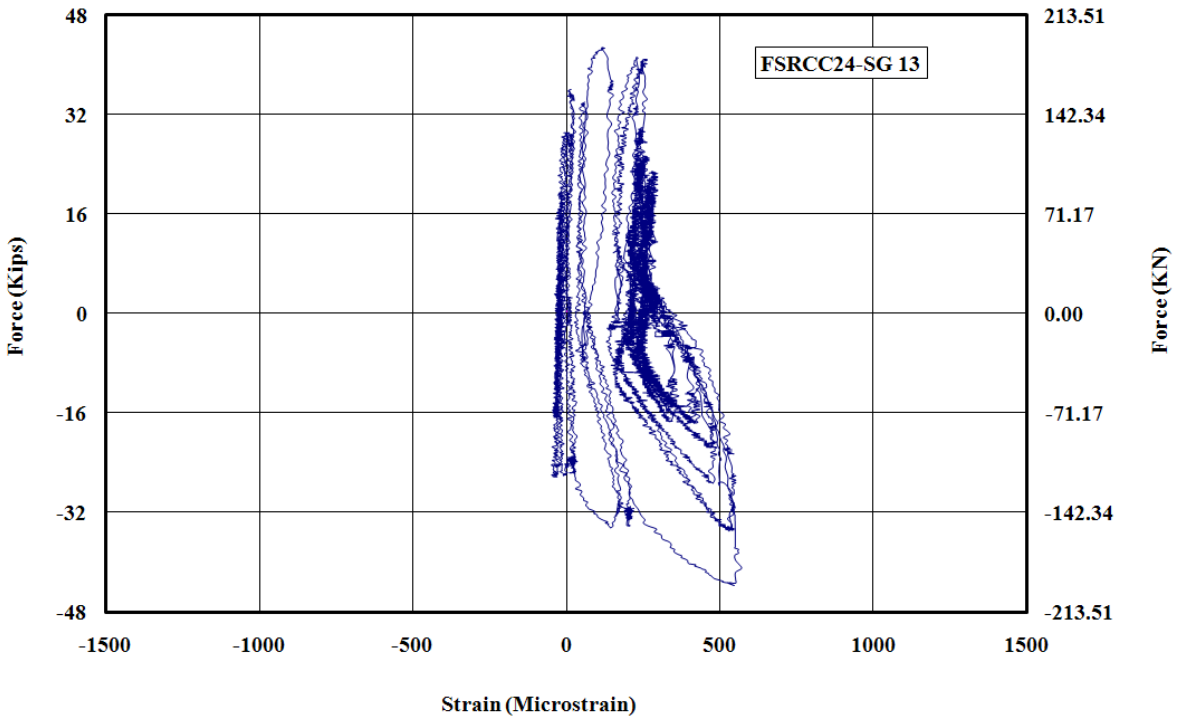

Figure D - 12: Measured Strain in Gauge No.13 for FSRCC24

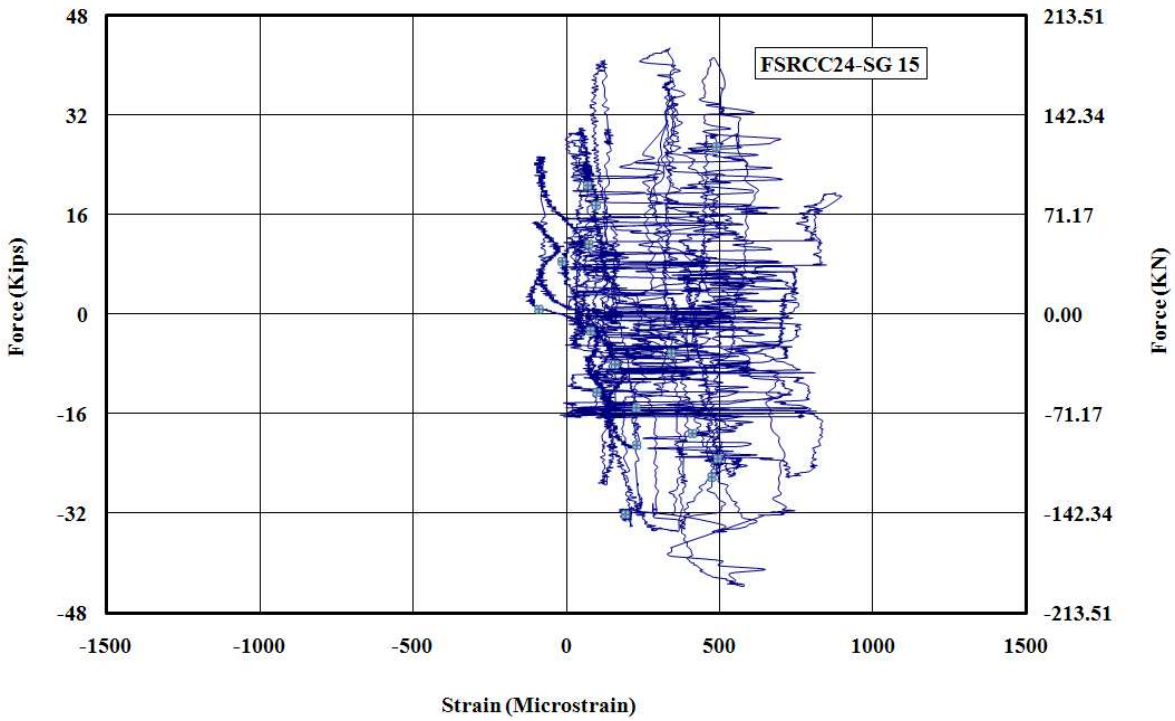

Figure D - 13: Measured Strain in Gauge No.15 for FSRCC24

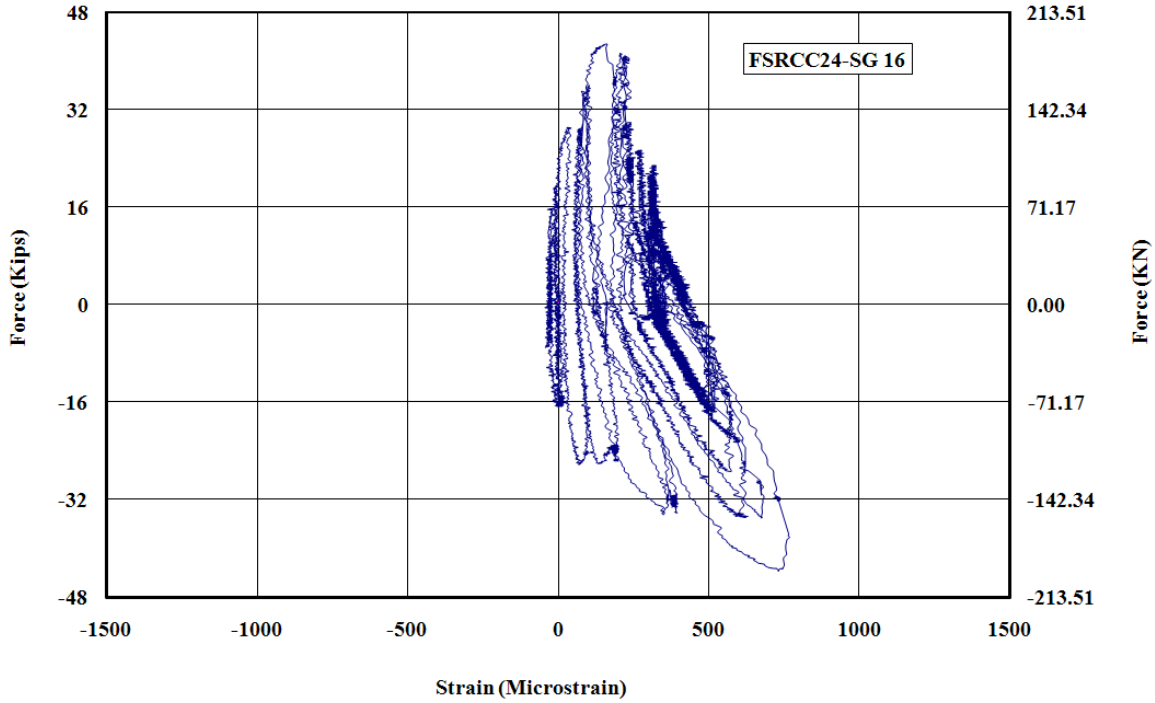

Figure D - 14: Measured Strain in Gauge No.16 for FSRCC24

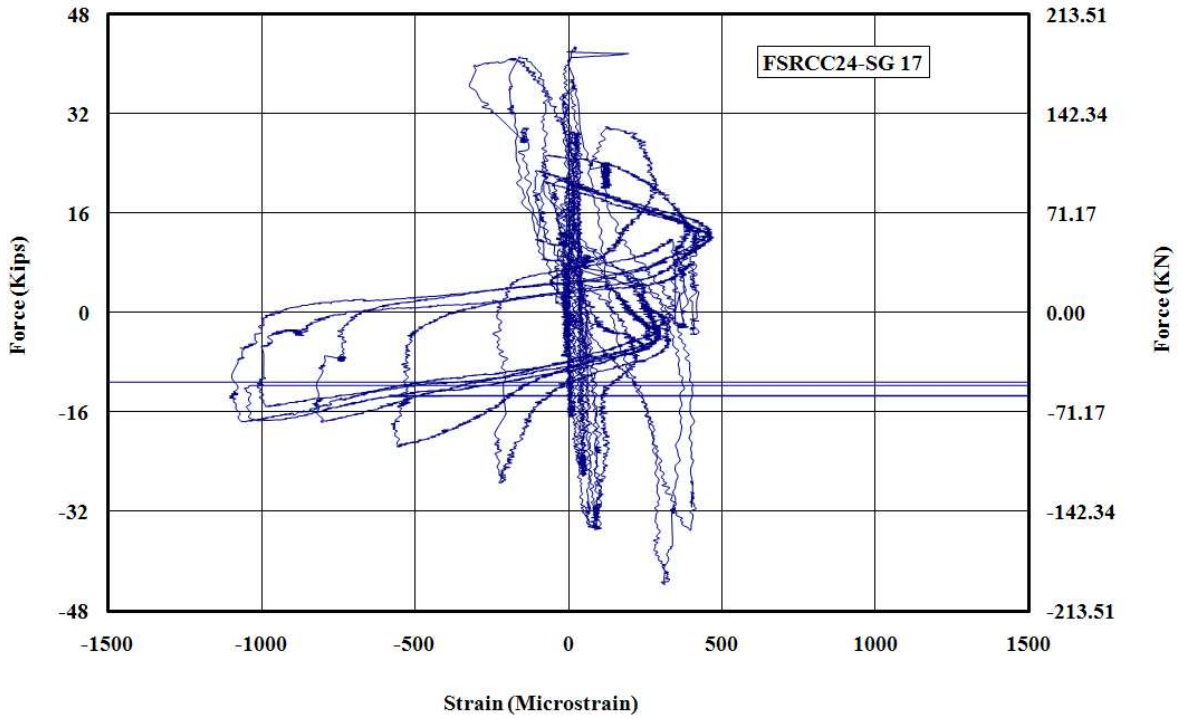

Figure D - 15: Measured Strain in Gauge No.17 for FSRCC24

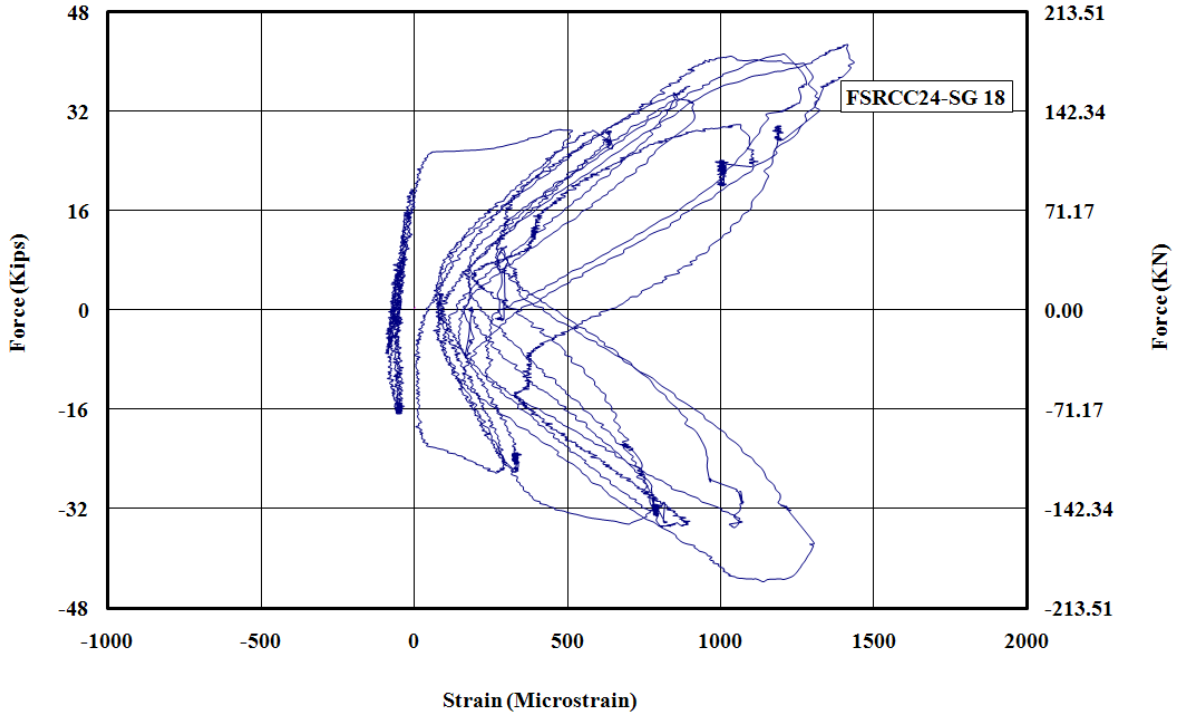

Figure D - 16: Measured Strain in Gauge No.18 for FSRCC24

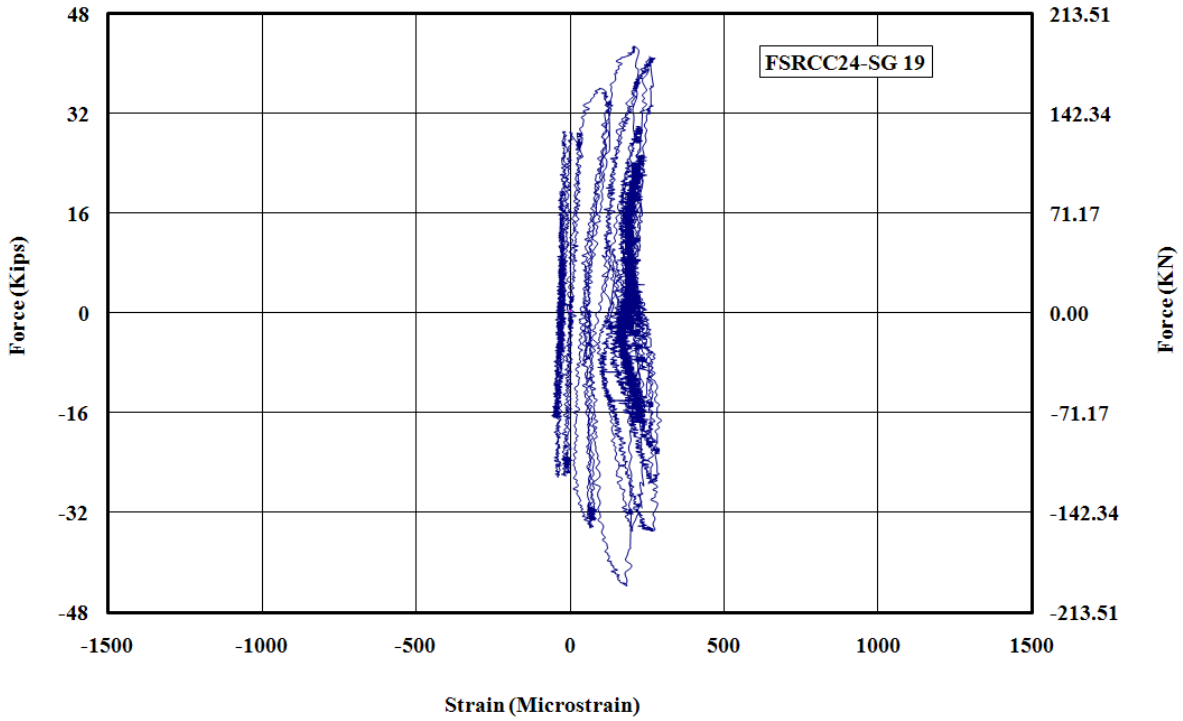

Figure D - 17: Measured Strain in Gauge No.19 for FSRCC24

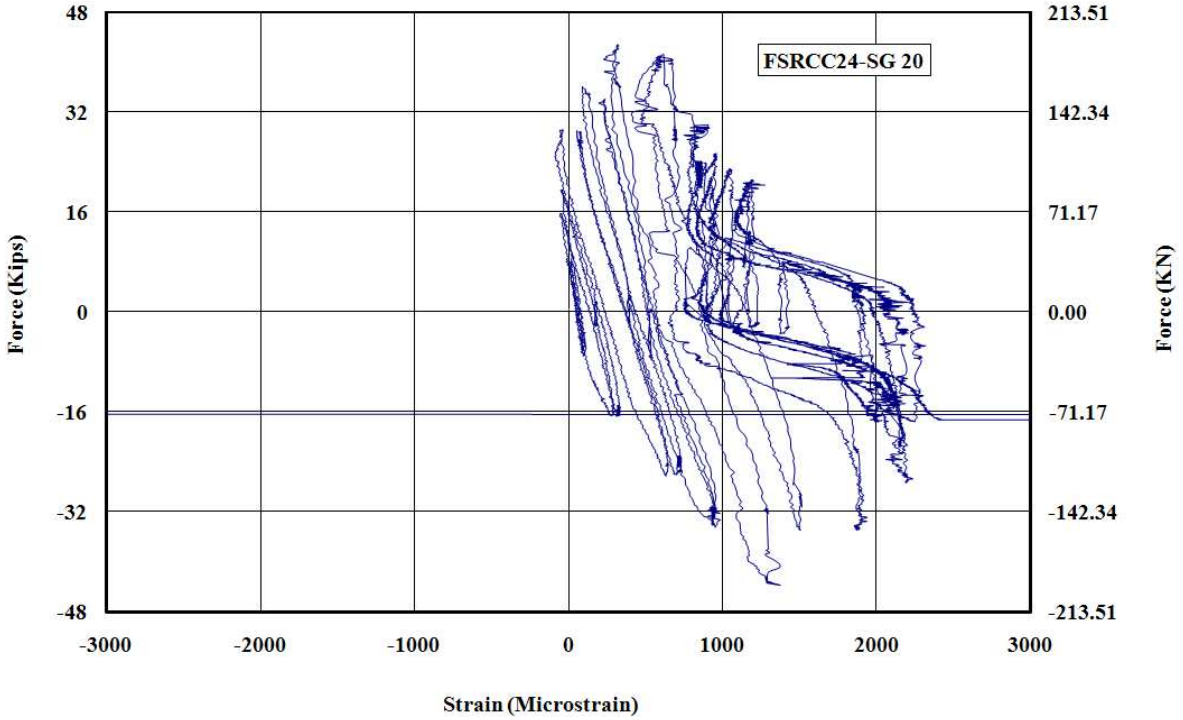

Figure D - 18: Measured Strain in Gauge No.20 for FSRCC24

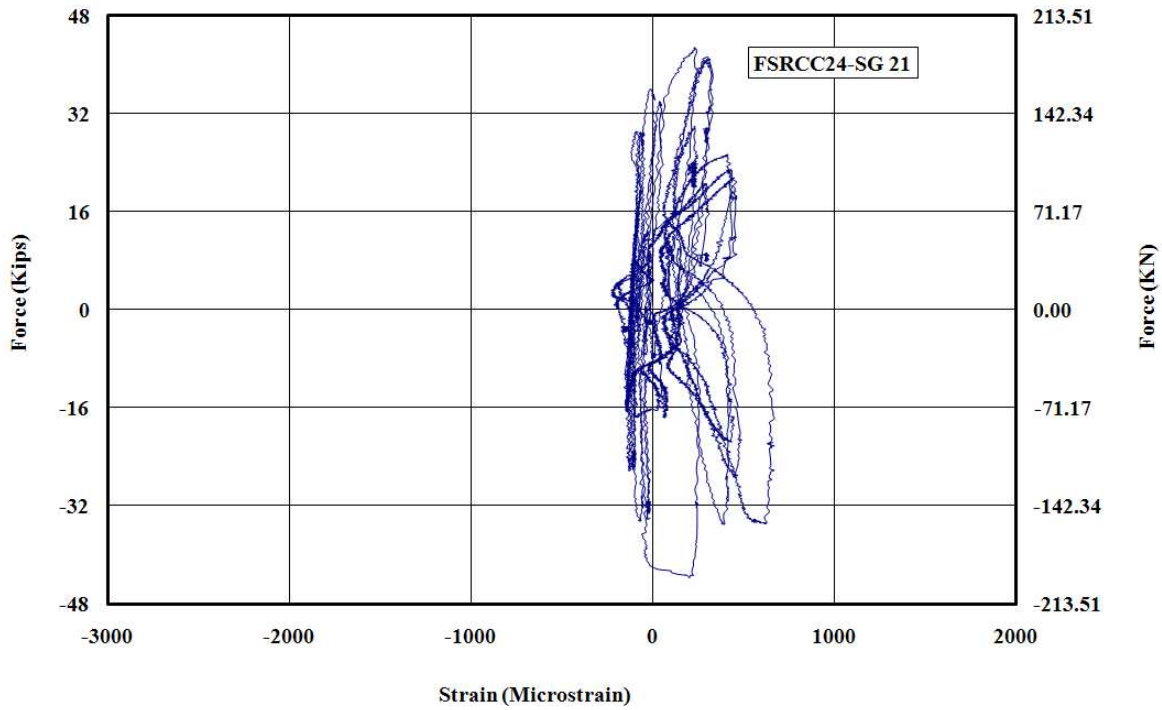

Figure D - 19: Measured Strain in Gauge No.21 for FSRCC24

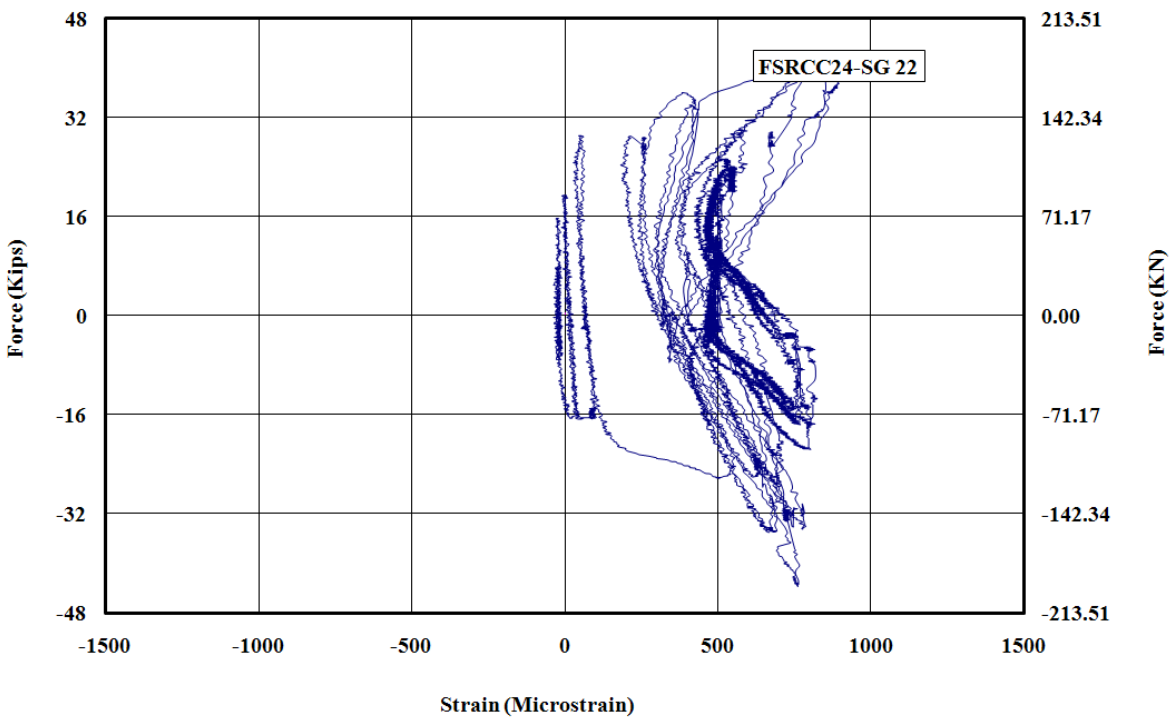

Figure D - 20: Measured Strain in Gauge No.22 for FSRCC24

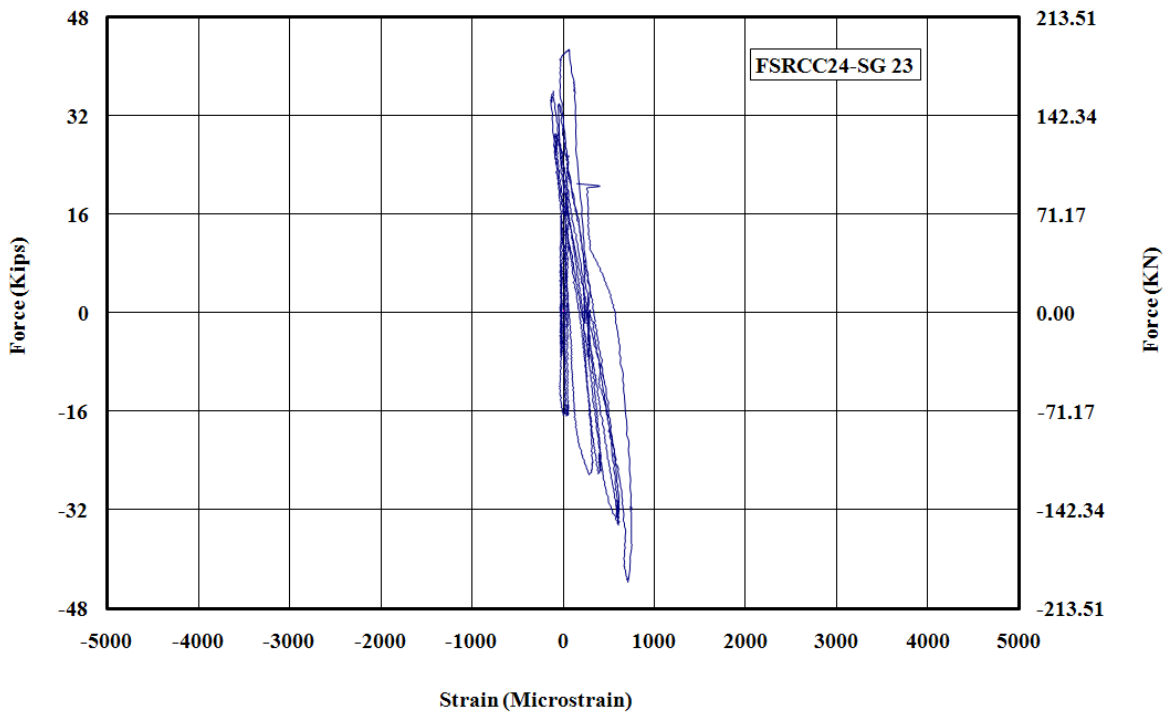

Figure D - 21: Measured Strain in Gauge No.23 for FSRCC24

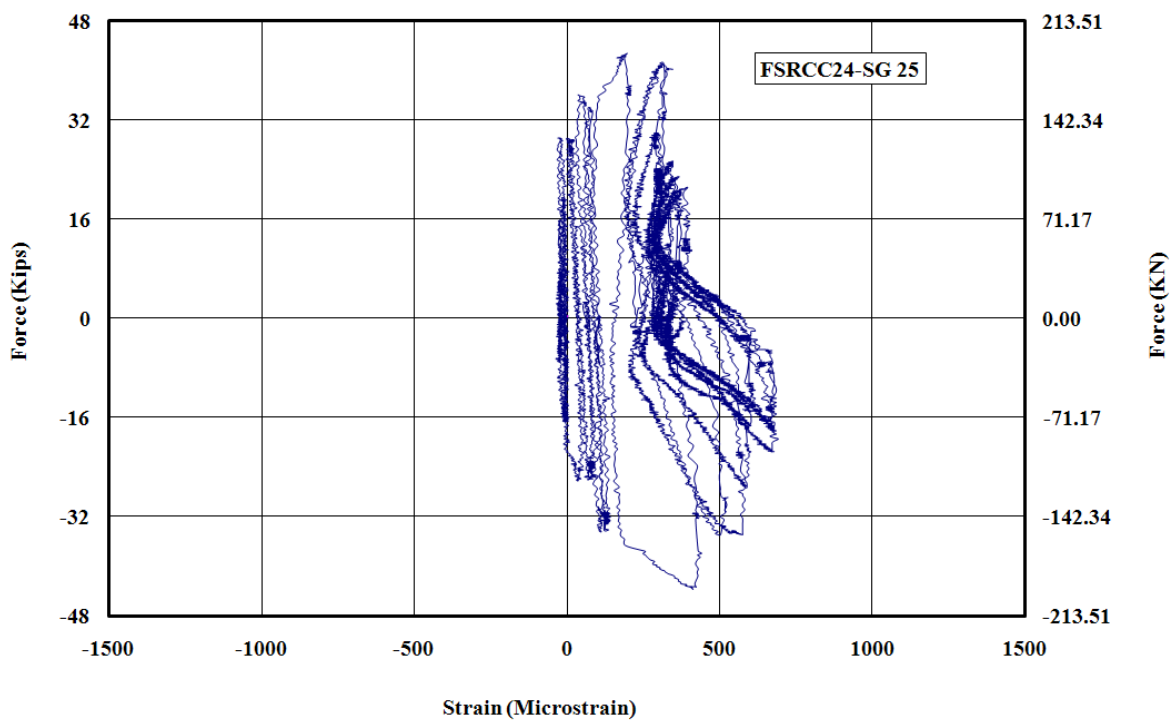

Figure D-21 Measured Strain in Gauge No.25 for FSRCC24

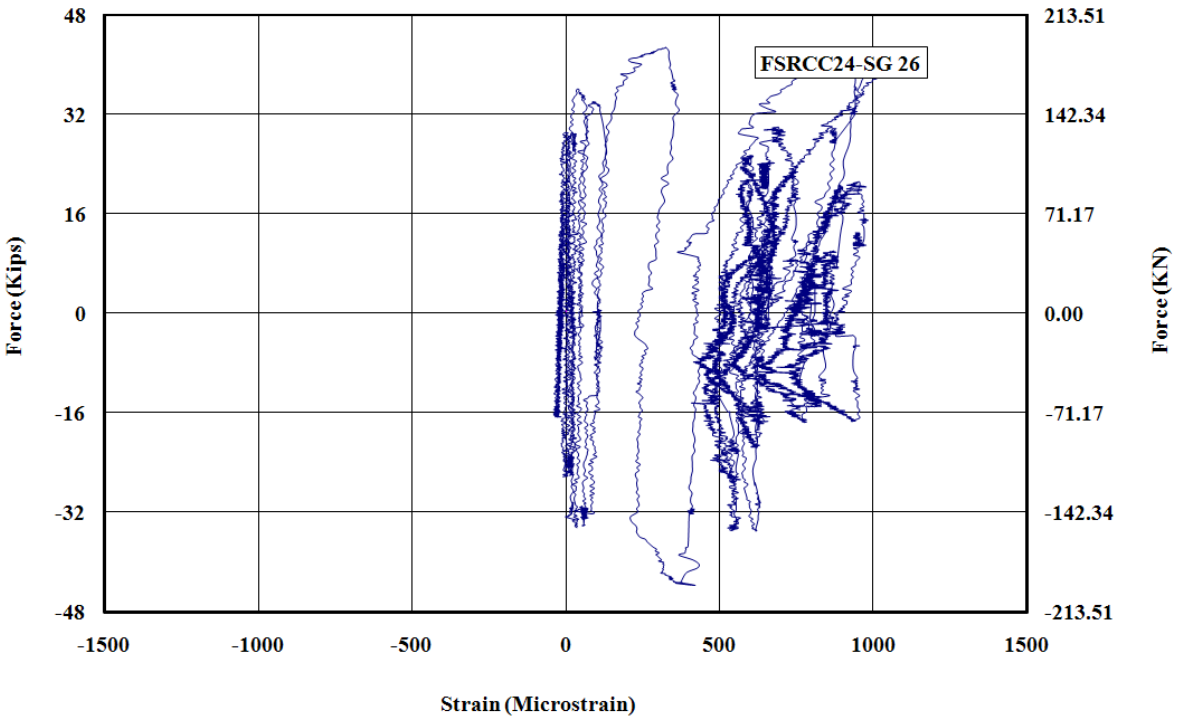

Figure D - 22: Measured Strain in Gauge No.26 for FSRCC24

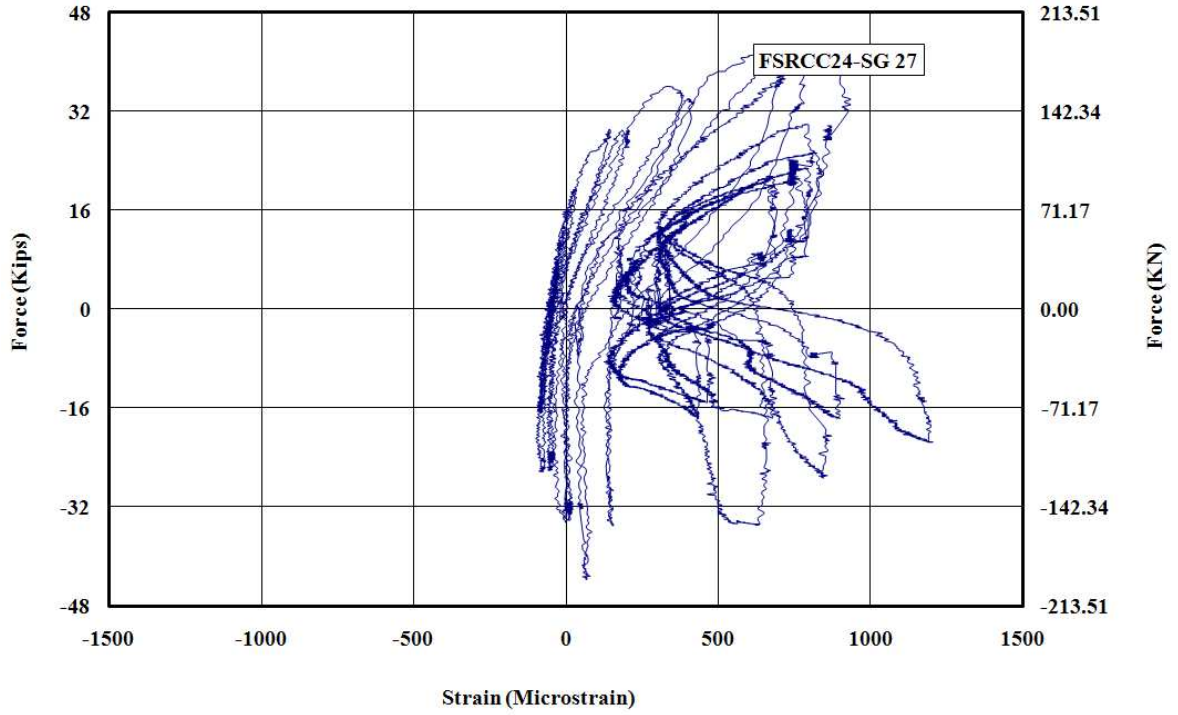

Figure D - 23: Measured Strain in Gauge No.27 for FSRCC24

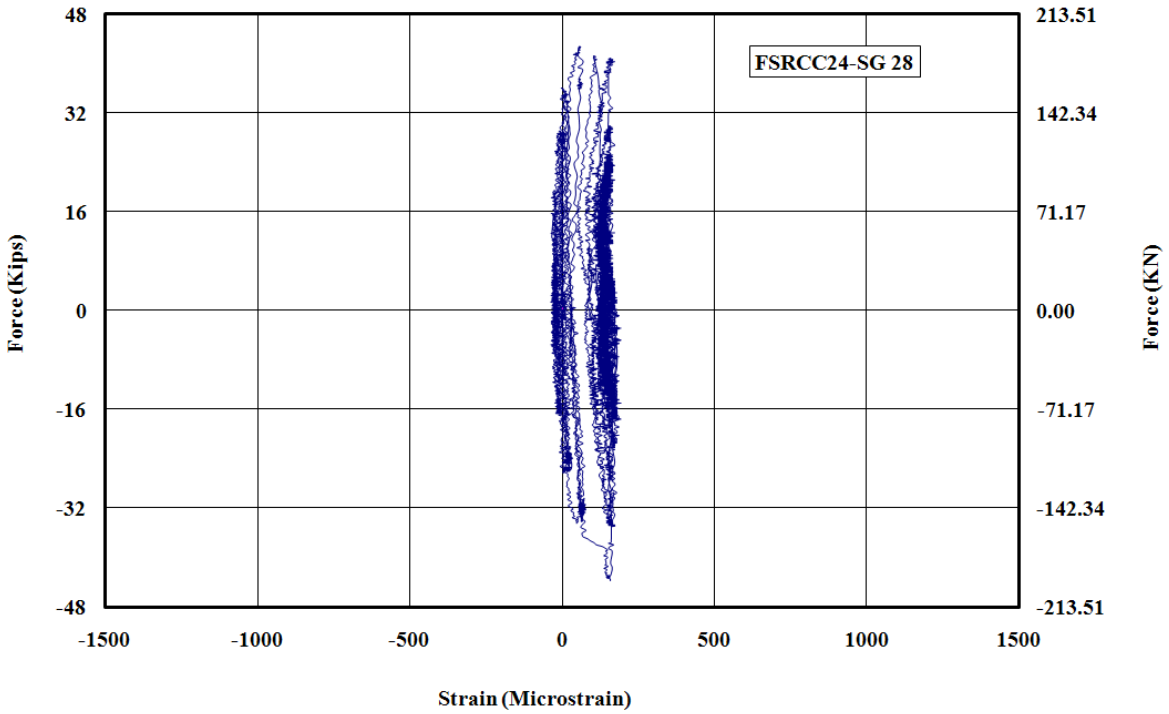

Figure D - 24: Measured Strain in Gauge No.28 for FSRCC24

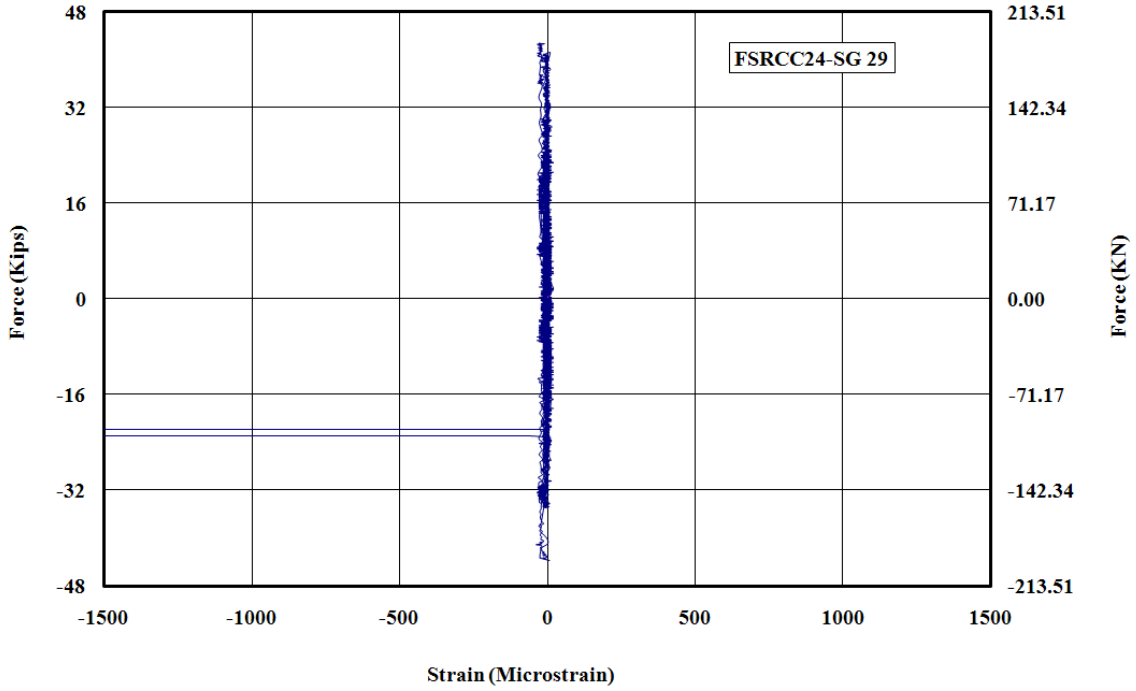

Figure D - 25: Measured Strain in Gauge No.29 for FSRCC24

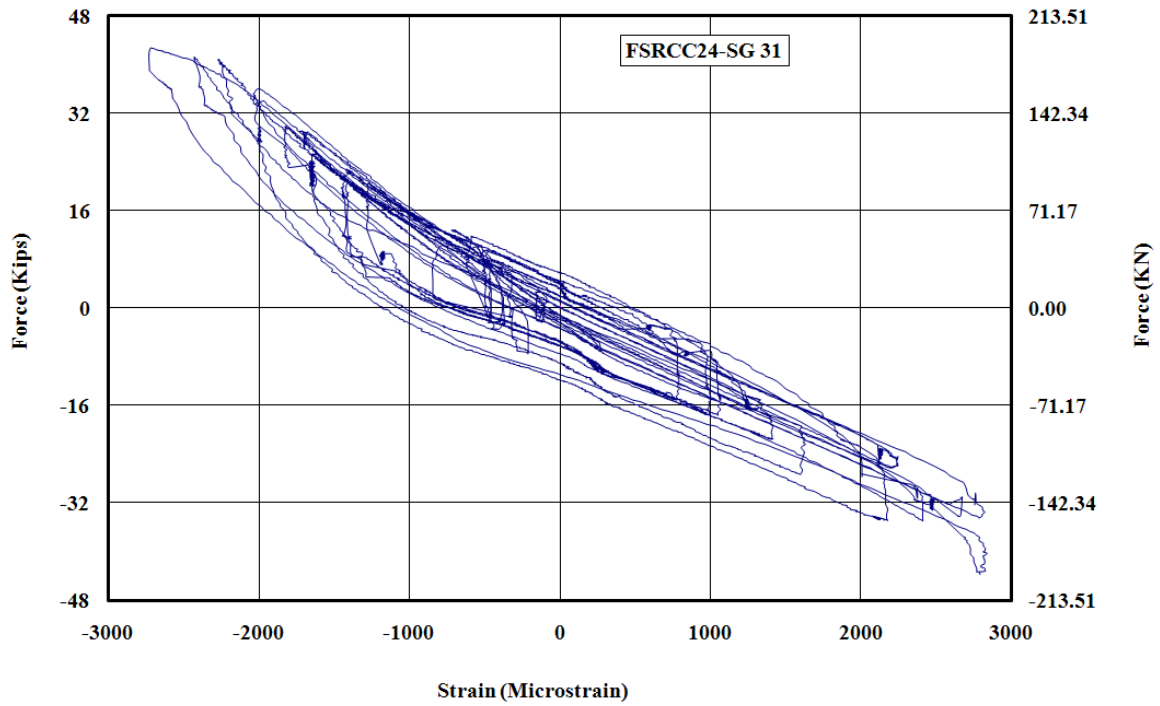

Figure D - 26: Measured Strain in Gauge No.31 for FSRCC24

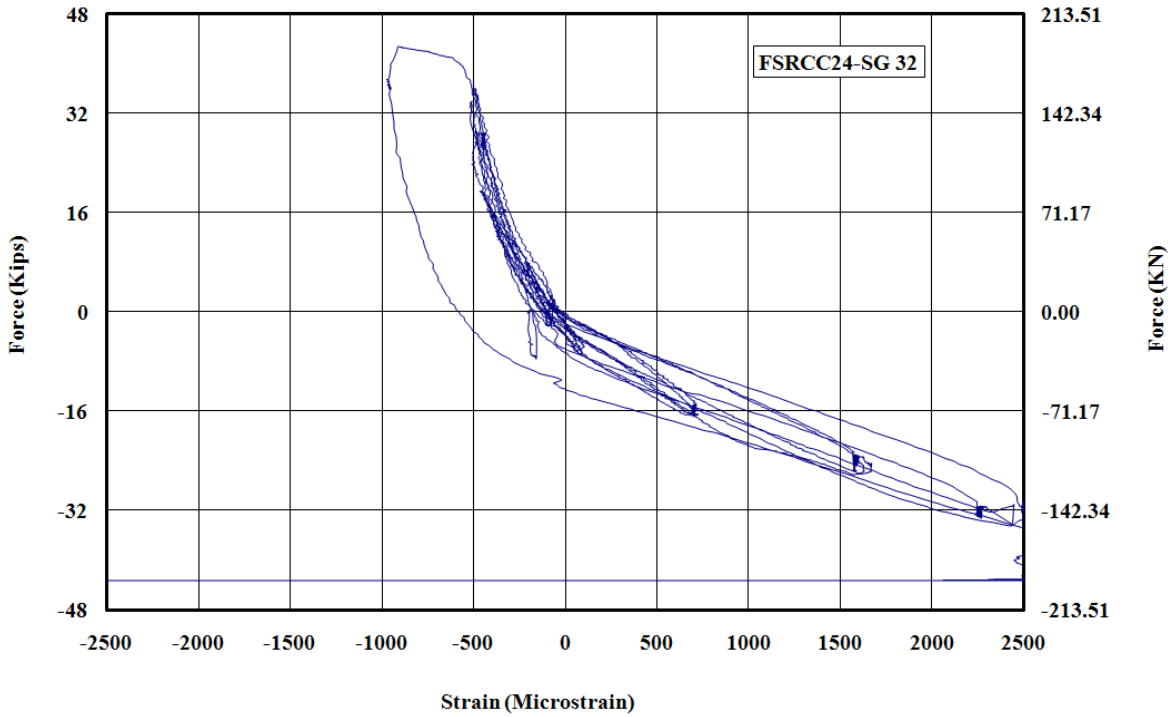

Figure D - 27: Measured Strain in Gauge No.32 for FSRCC24

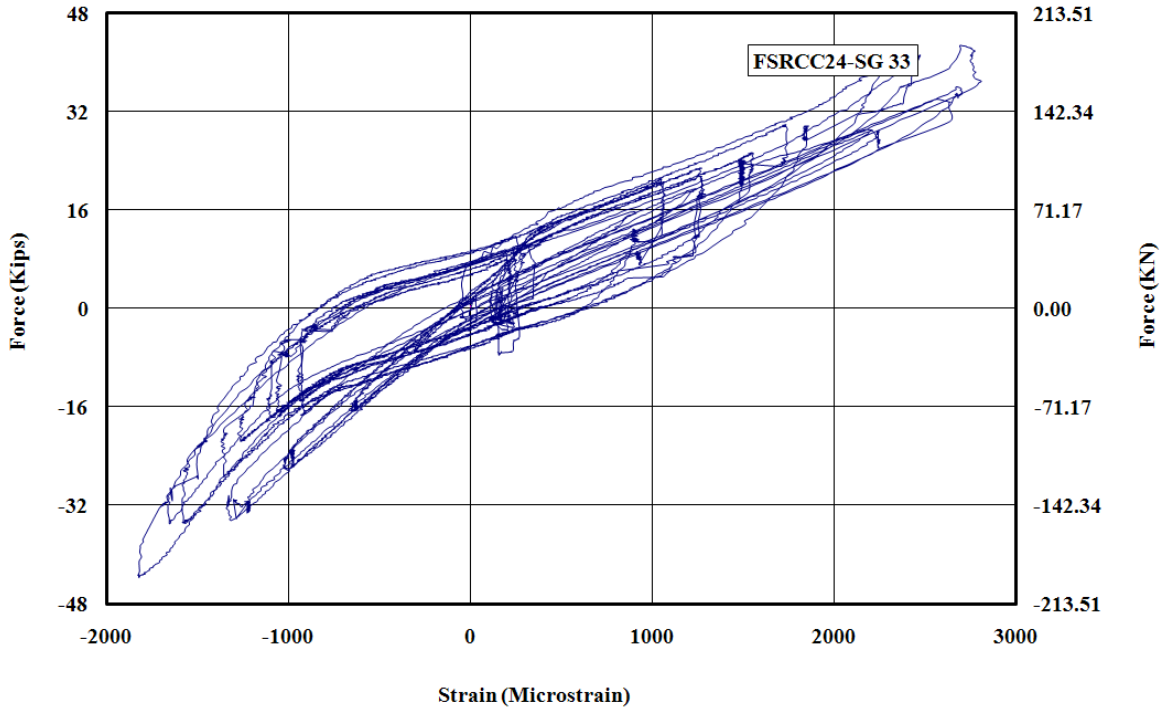

Figure D - 28: Measured Strain in Gauge No.33 for FSRCC24

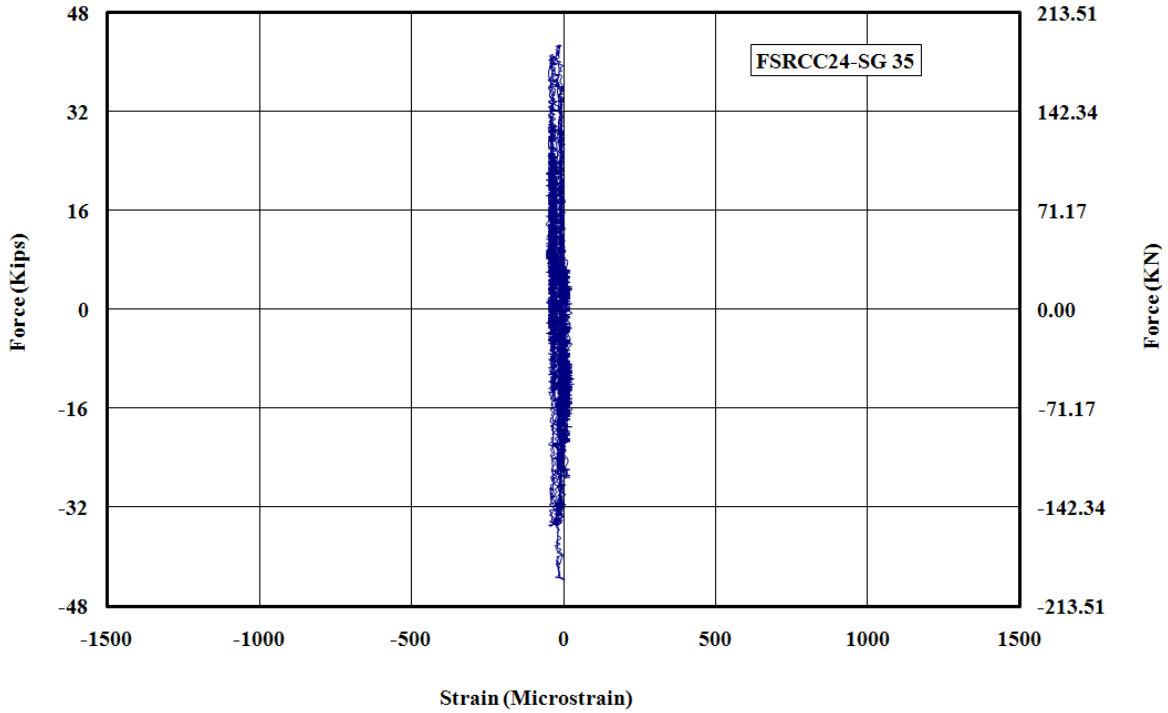

Figure D - 29: Measured Strain in Gauge No.35 for FSRCC24

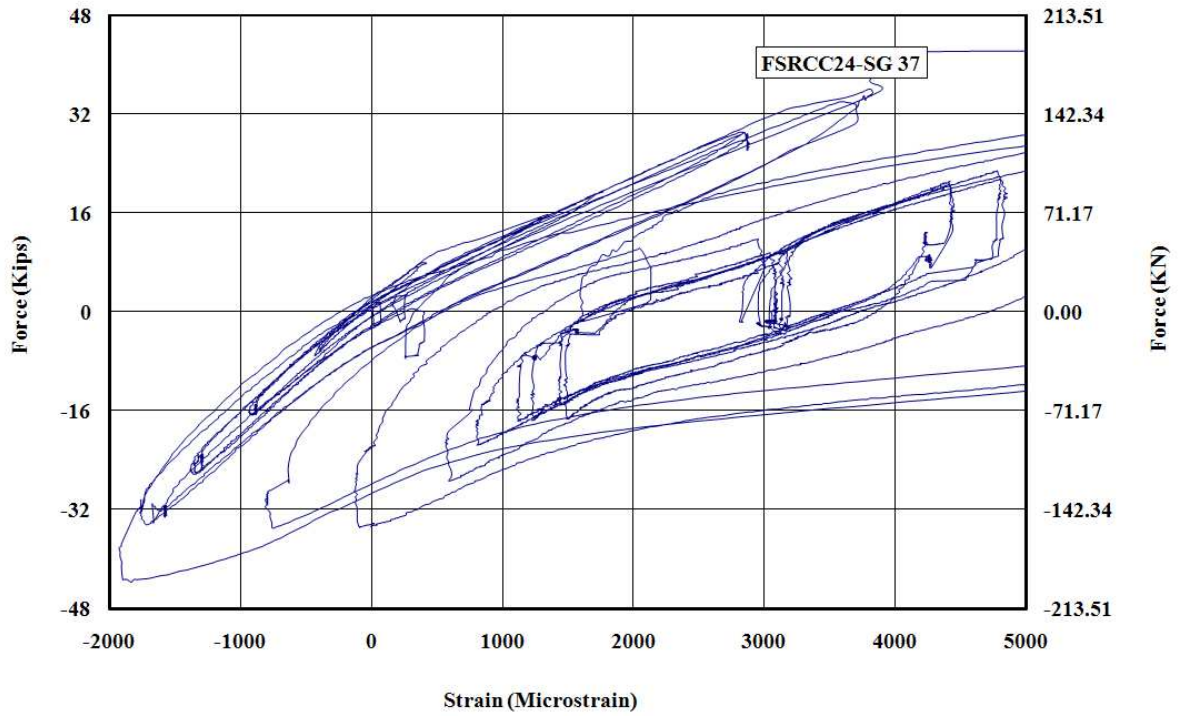

Figure D - 30: Measured Strain in Gauge No.37 for FSRCC24

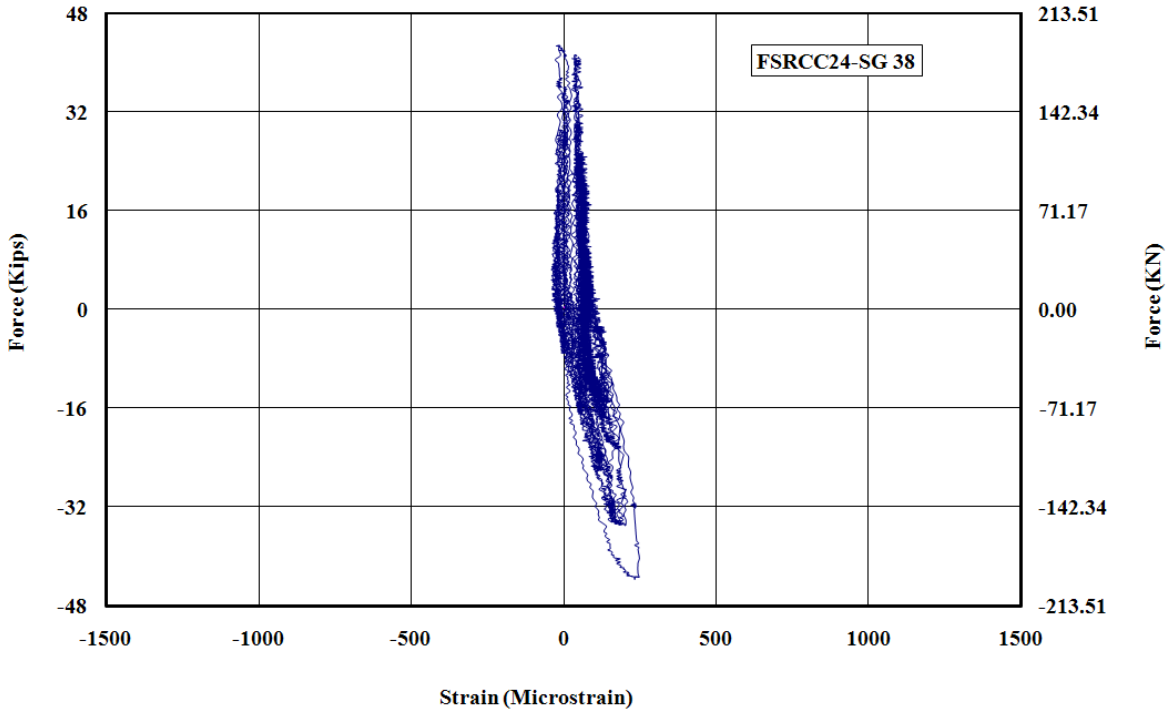

Figure D - 31: Measured Strain in Gauge No.38 for FSRCC24

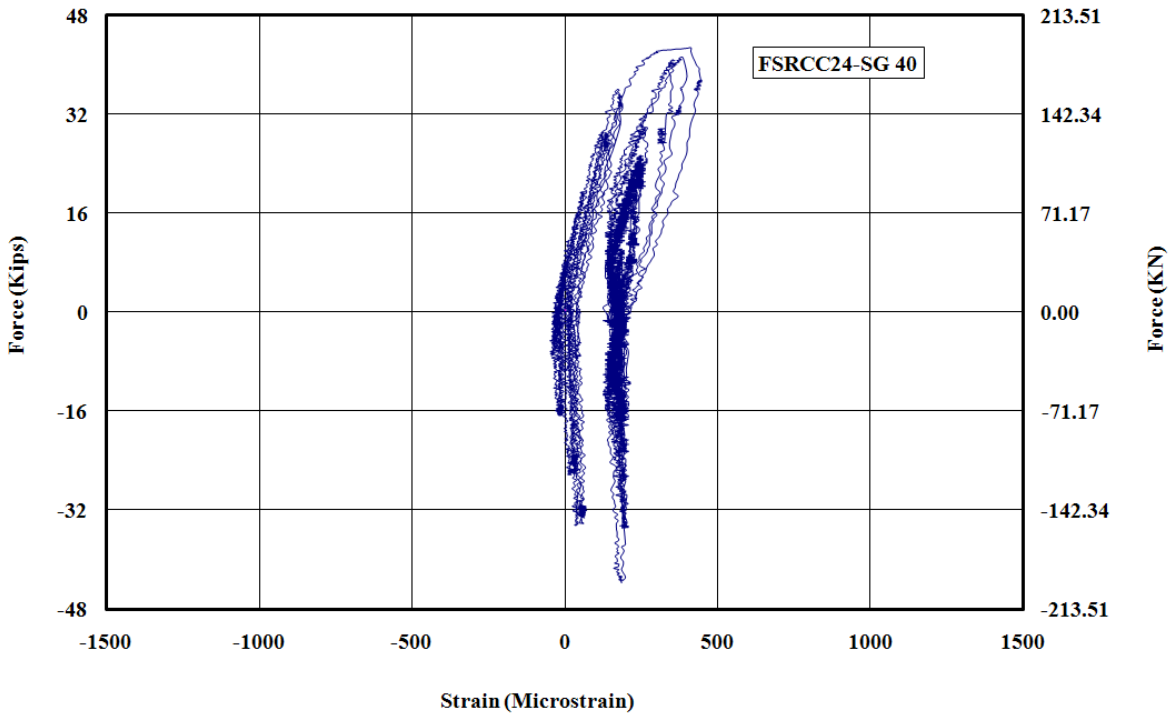

Figure D - 32: Measured Strain in Gauge No.40 for FSRCC24

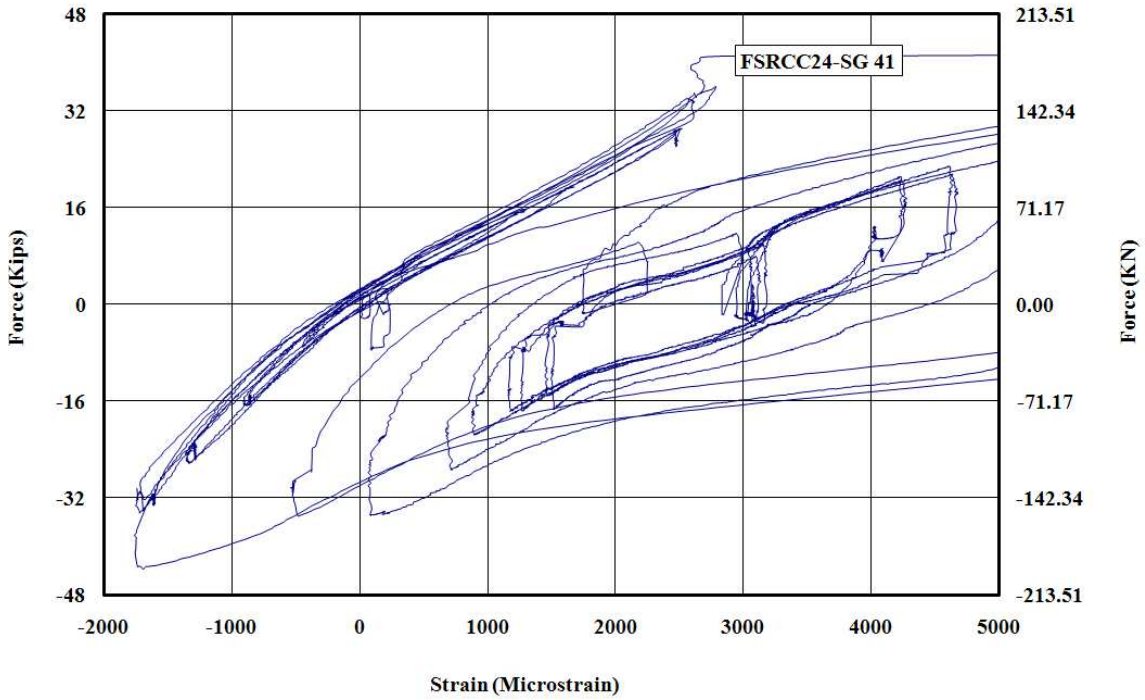

Figure D - 33: Measured Strain in Gauge No.41 for FSRCC24

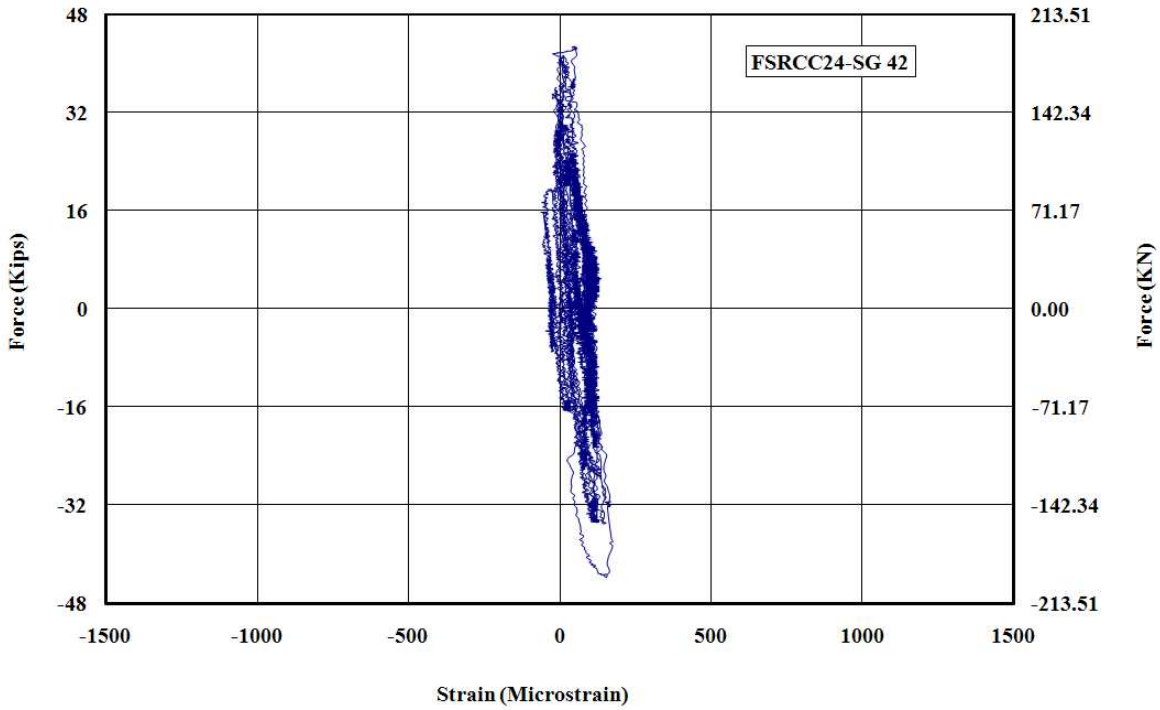

Figure D - 34: Measured Strain in Gauge No.42 for FSRCC24

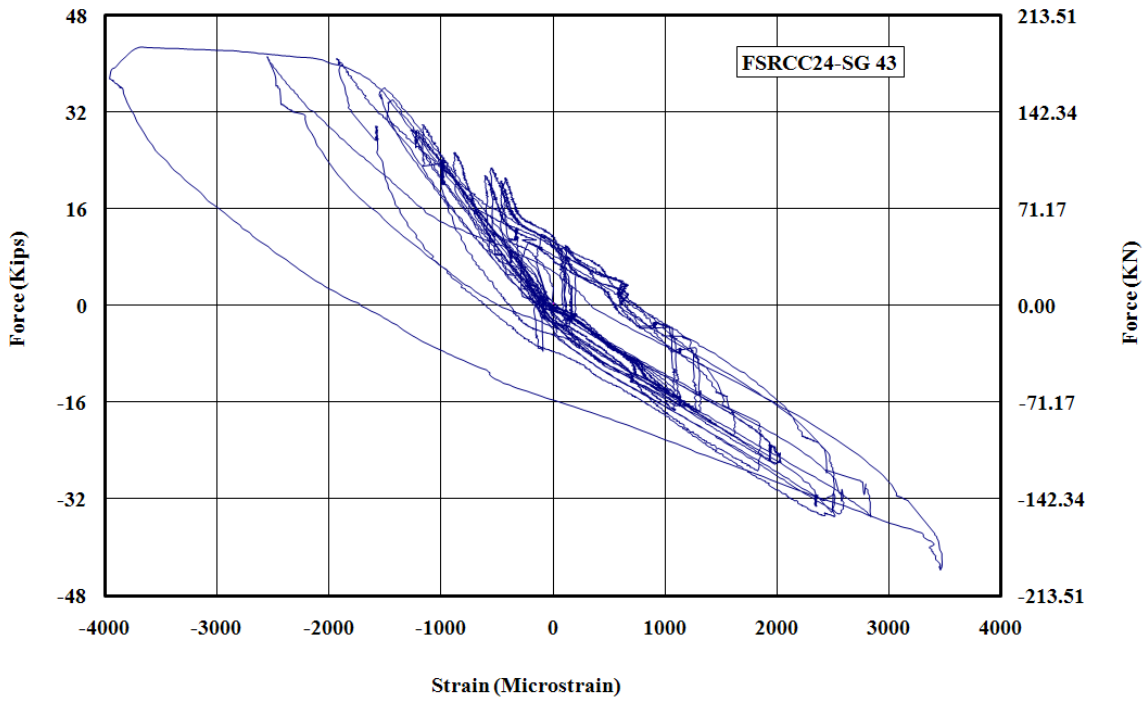

Figure D - 35: Measured Strain in Gauge No.43 for FSRCC24

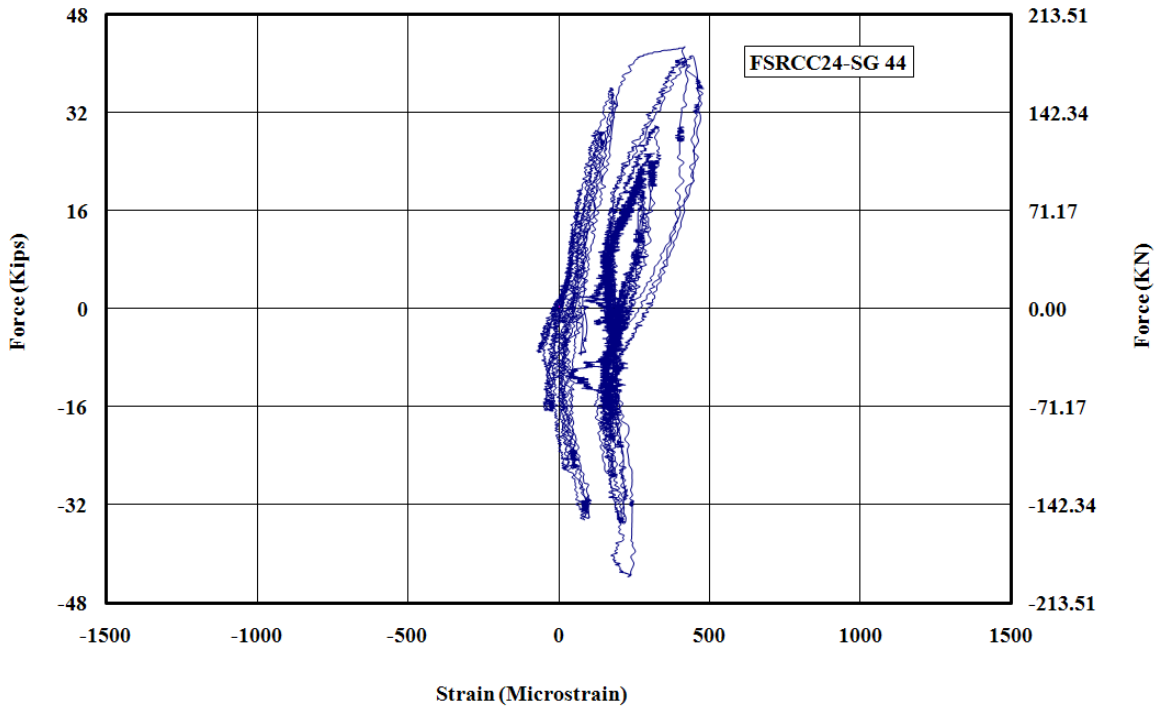

Figure D - 36: Measured Strain in Gauge No.44 for FSRCC24

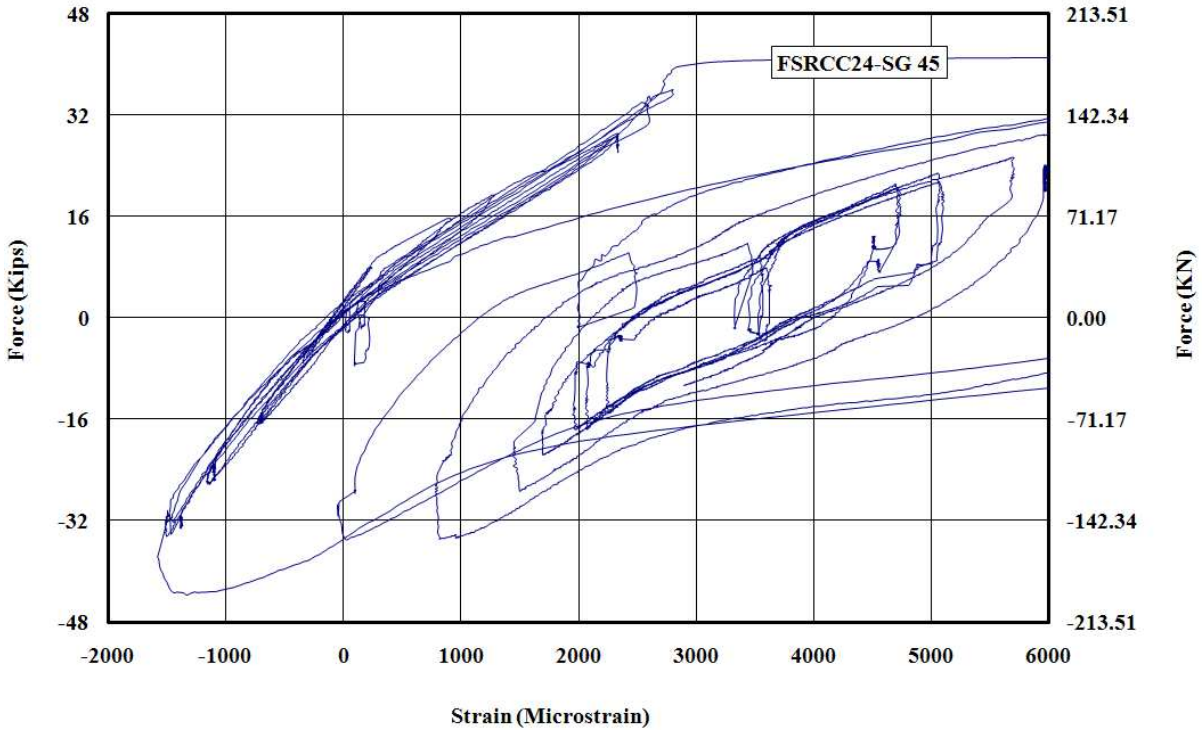

Figure D - 37: Measured Strain in Gauge No.45 for FSRCC24

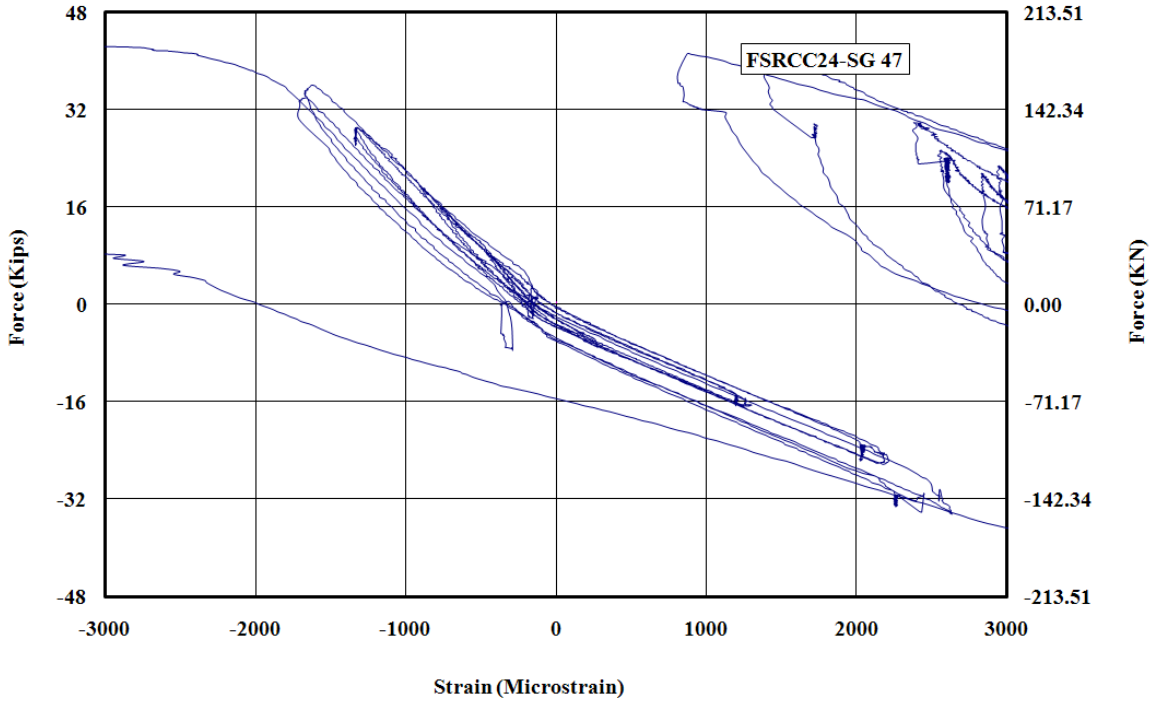

Figure D - 38: Measured Strain in Gauge No.47 for FSRCC24

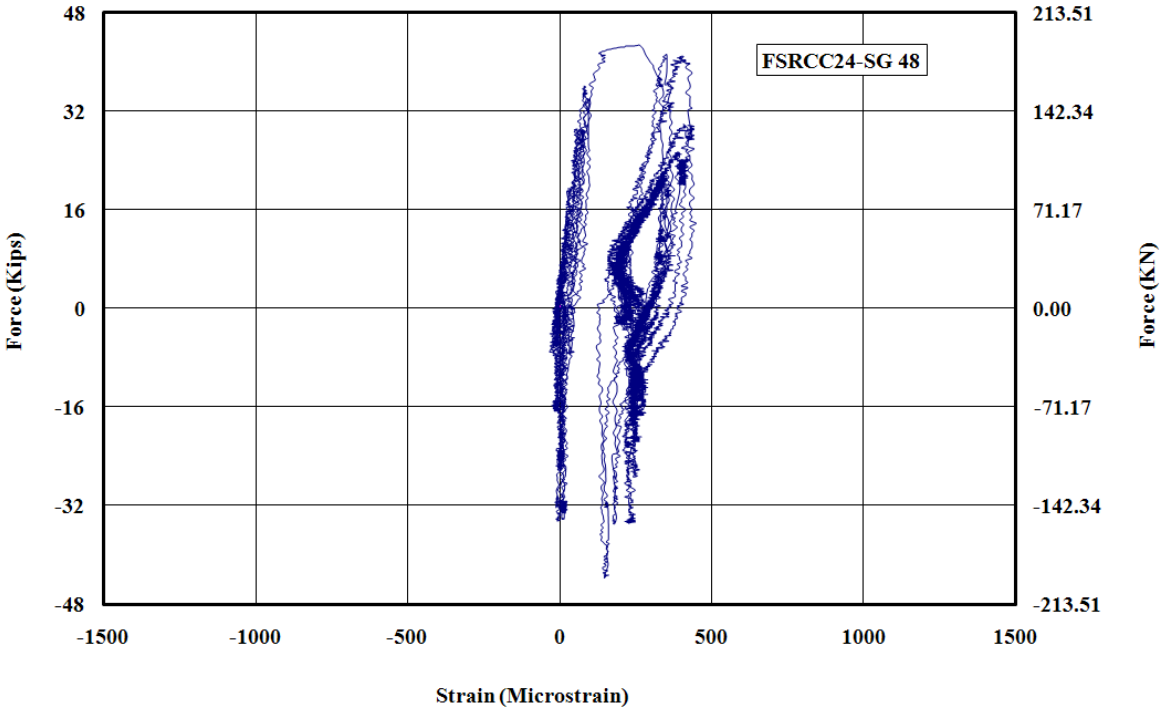

Figure D - 39: Measured Strain in Gauge No.48 for FSRCC24

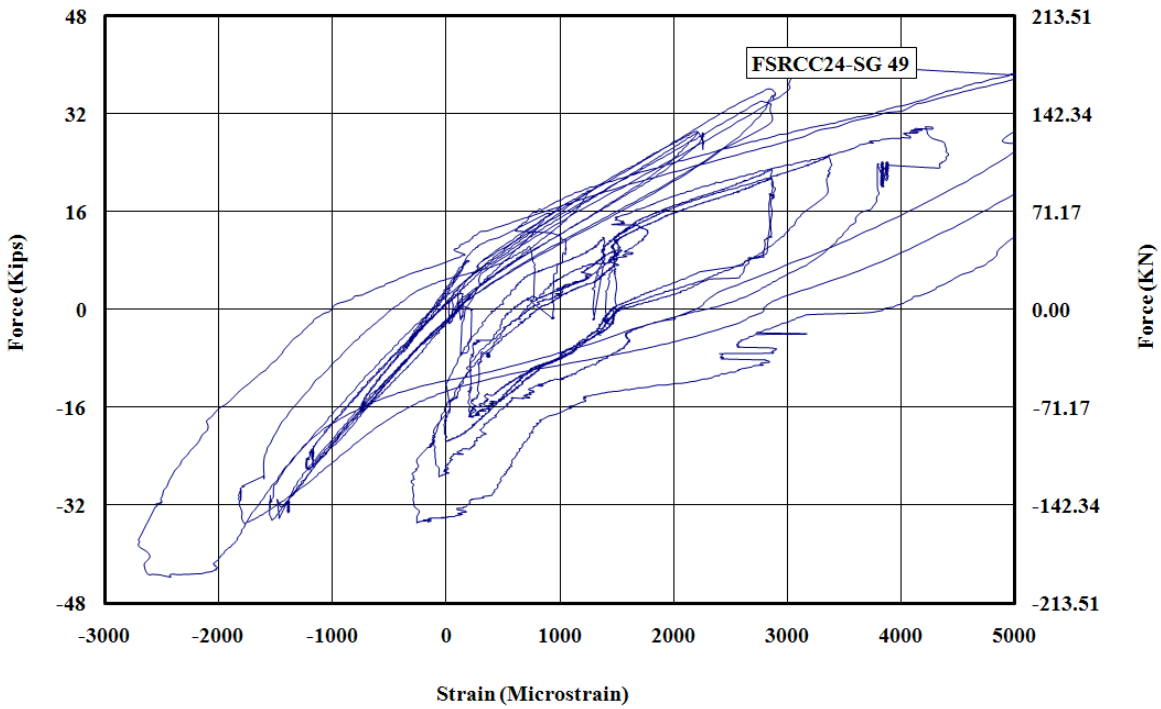

Figure D - 40: Measured Strain in Gauge No.49 for FSRCC24

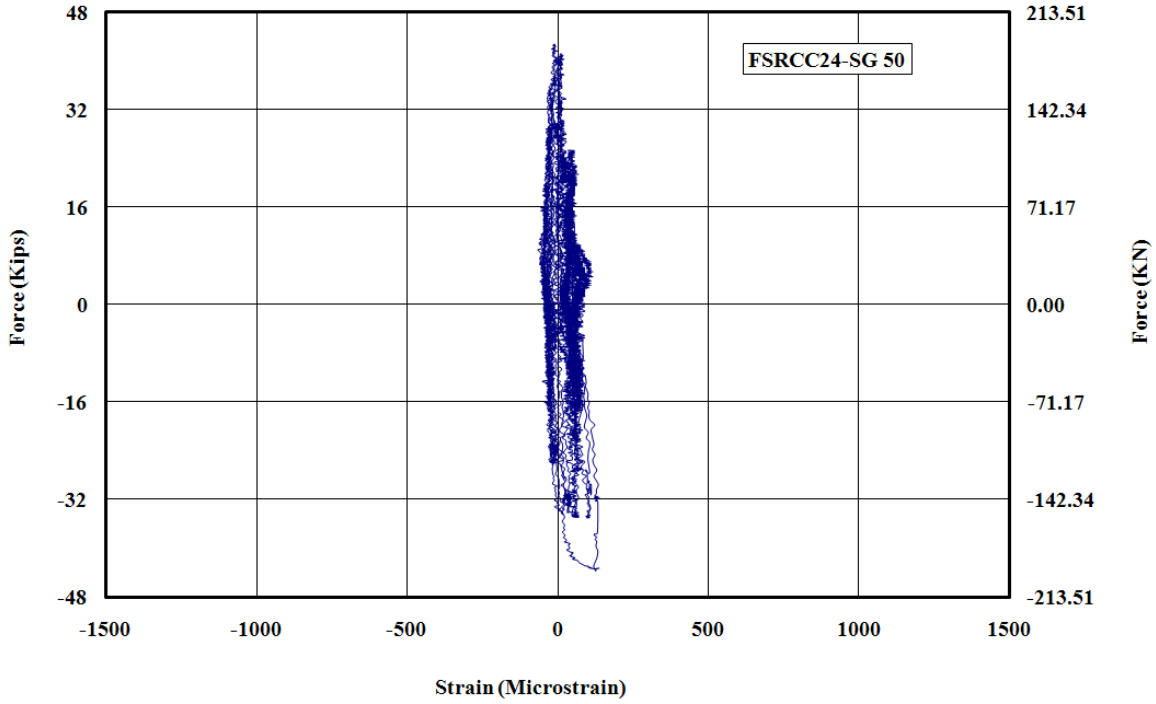

Figure D - 41: Measured Strain in Gauge No.50 for FSRCC24

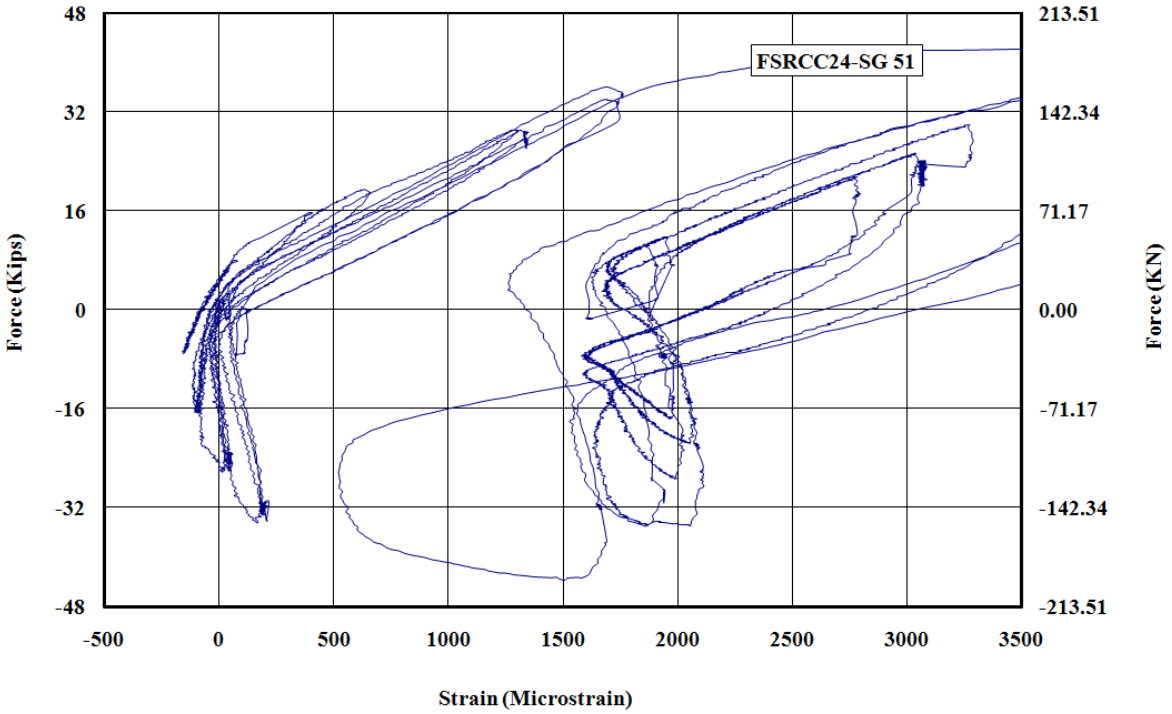

Figure D - 42: Measured Strain in Gauge No.51 for FSRCC24

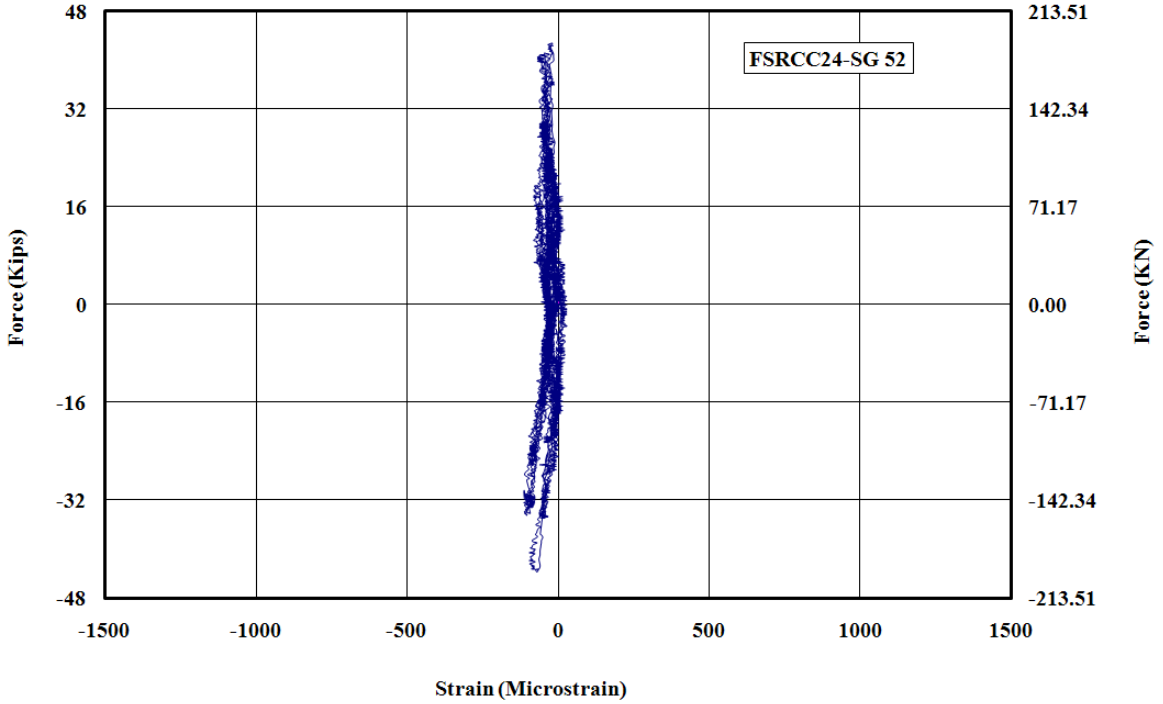

Figure D - 43: Measured Strain in Gauge No.52 for FSRCC24

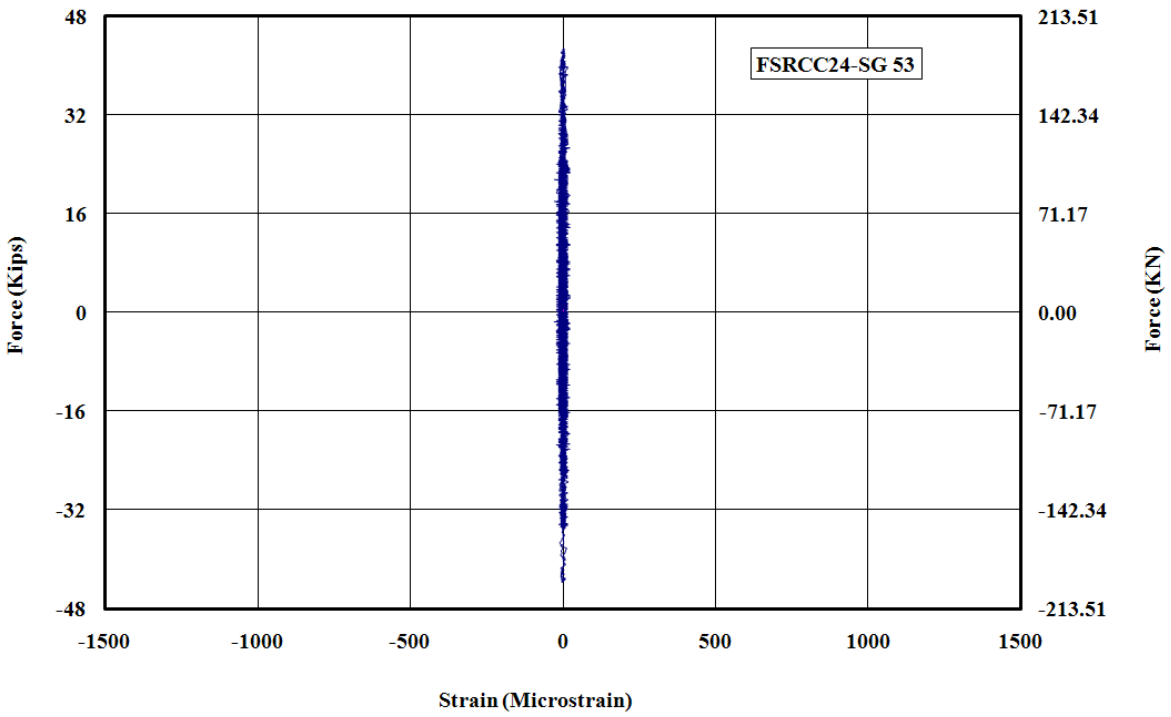

Figure D - 44: Measured Strain in Gauge No.53 for FSRCC24

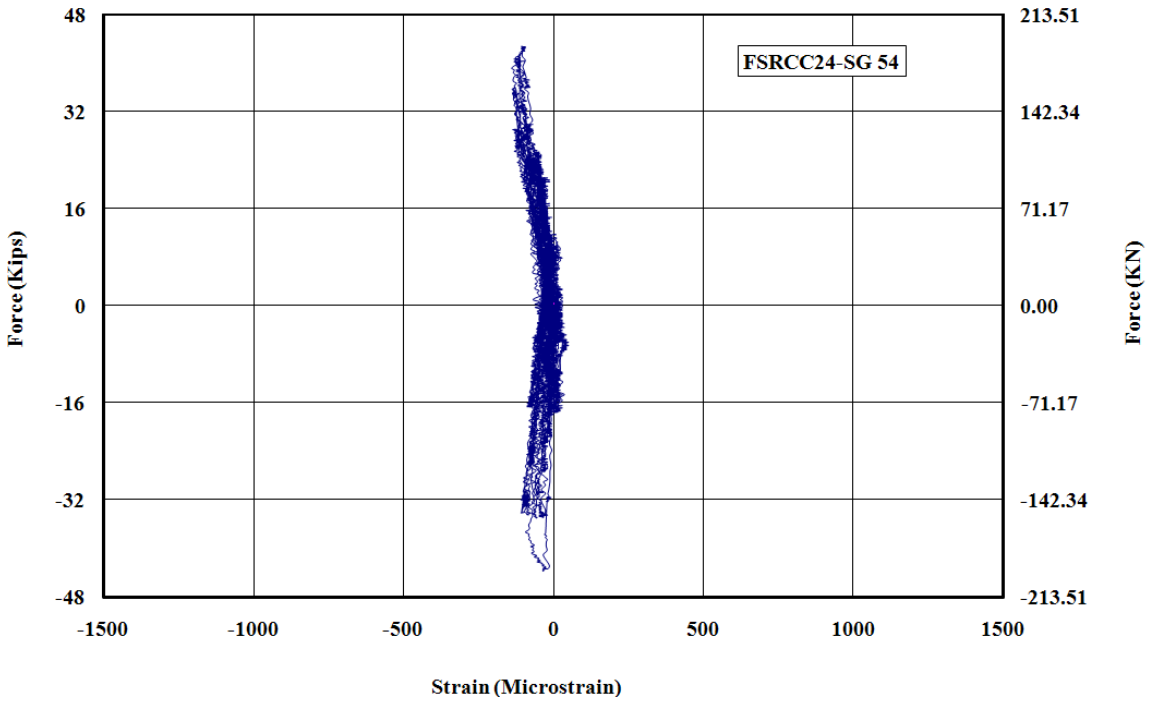

Figure D - 45: Measured Strain in Gauge No.54 for FSRCC24

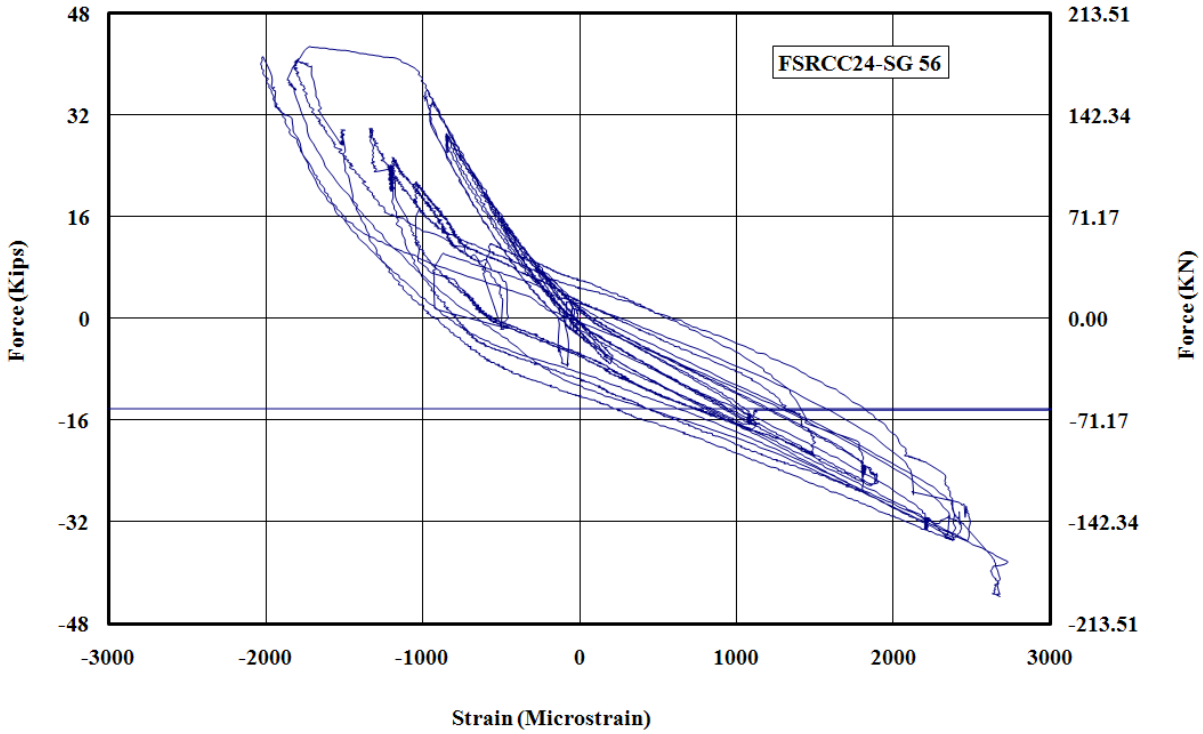

Figure D - 46: Measured Strain in Gauge No.56 for FSRCC24

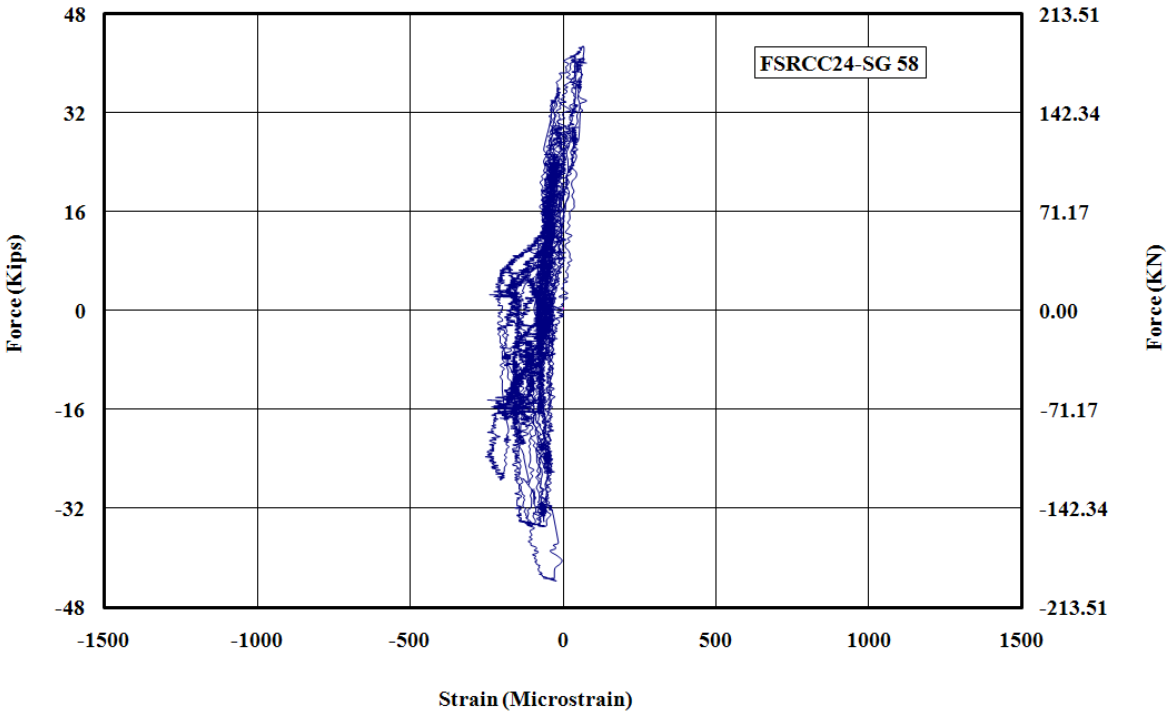

Figure D - 47: Measured Strain in Gauge No.58 for FSRCC24

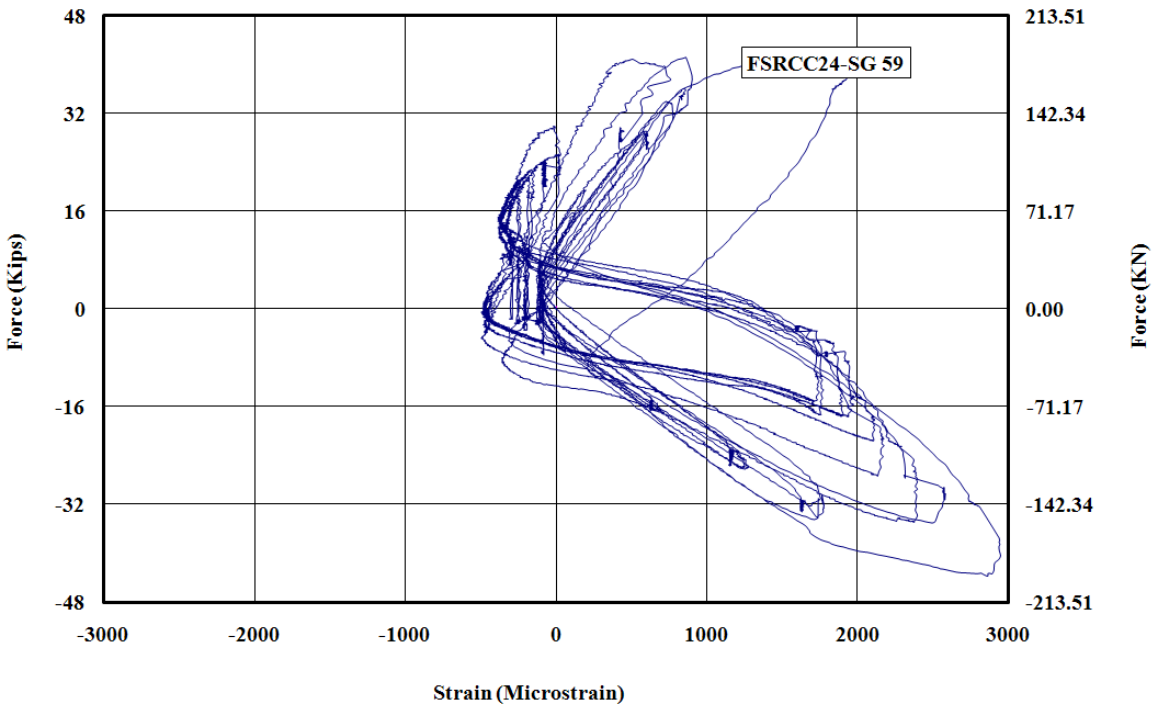

Figure D - 48: Measured Strain in Gauge No.59 for FSRCC24

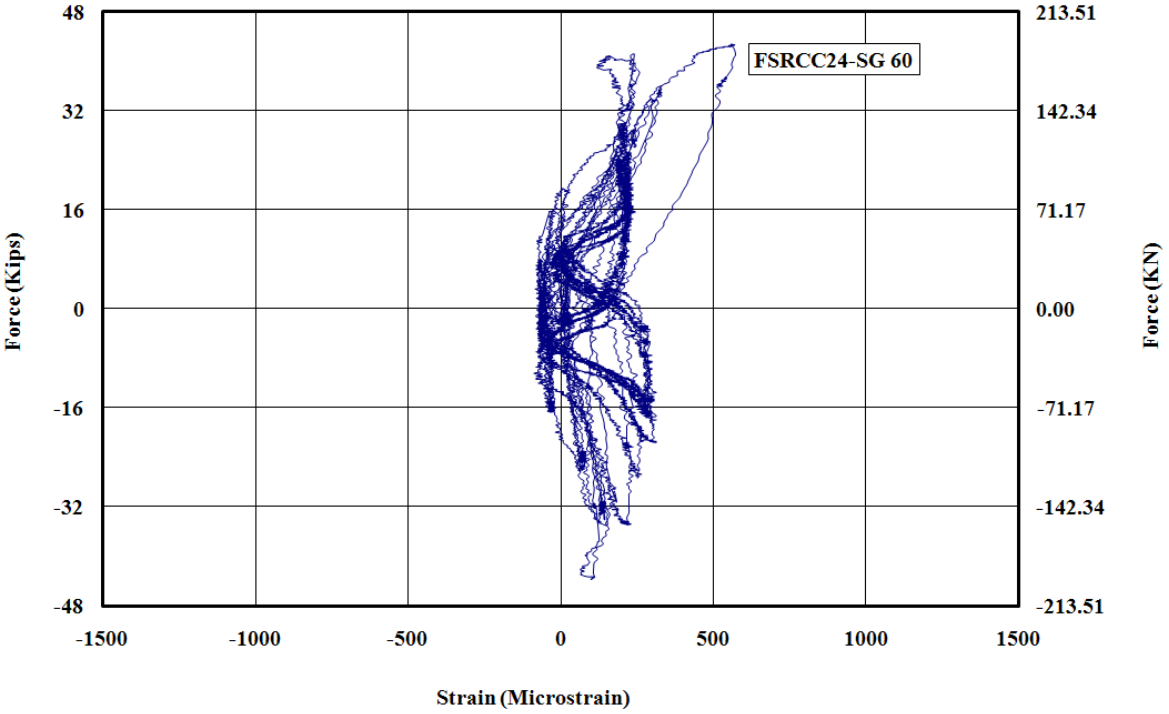

Figure D - 49: Measured Strain in Gauge No.60 for FSRCC24

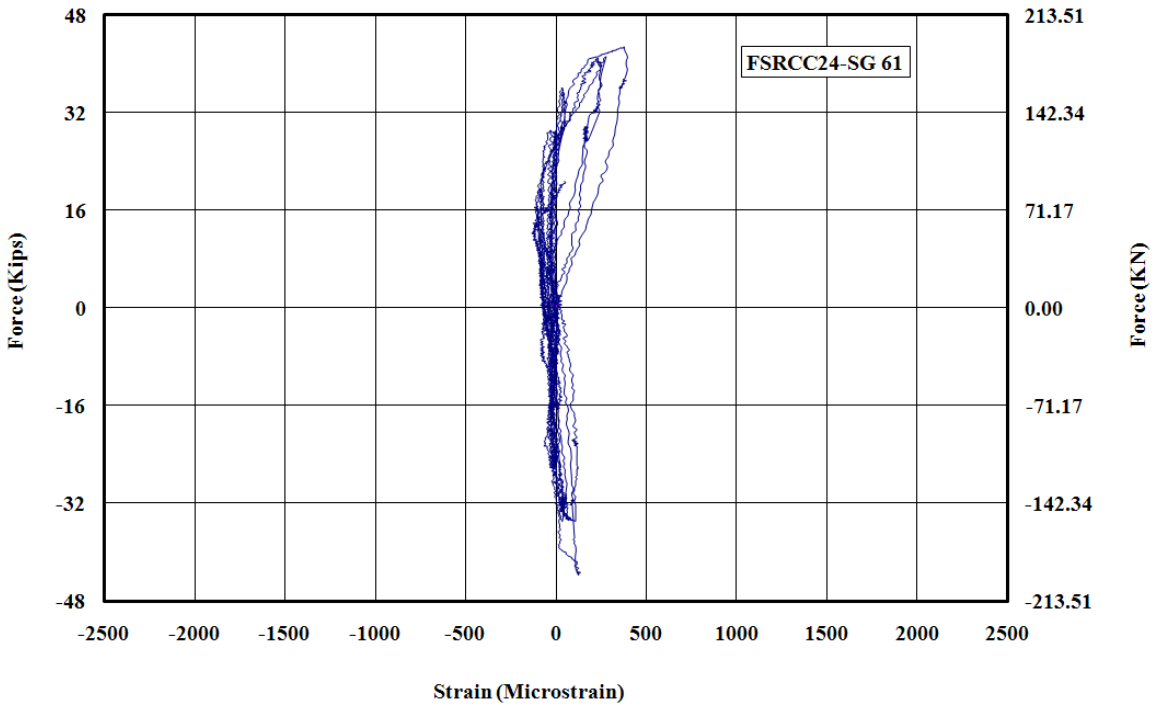

Figure D - 50: Measured Strain in Gauge No.61 for FSRCC24

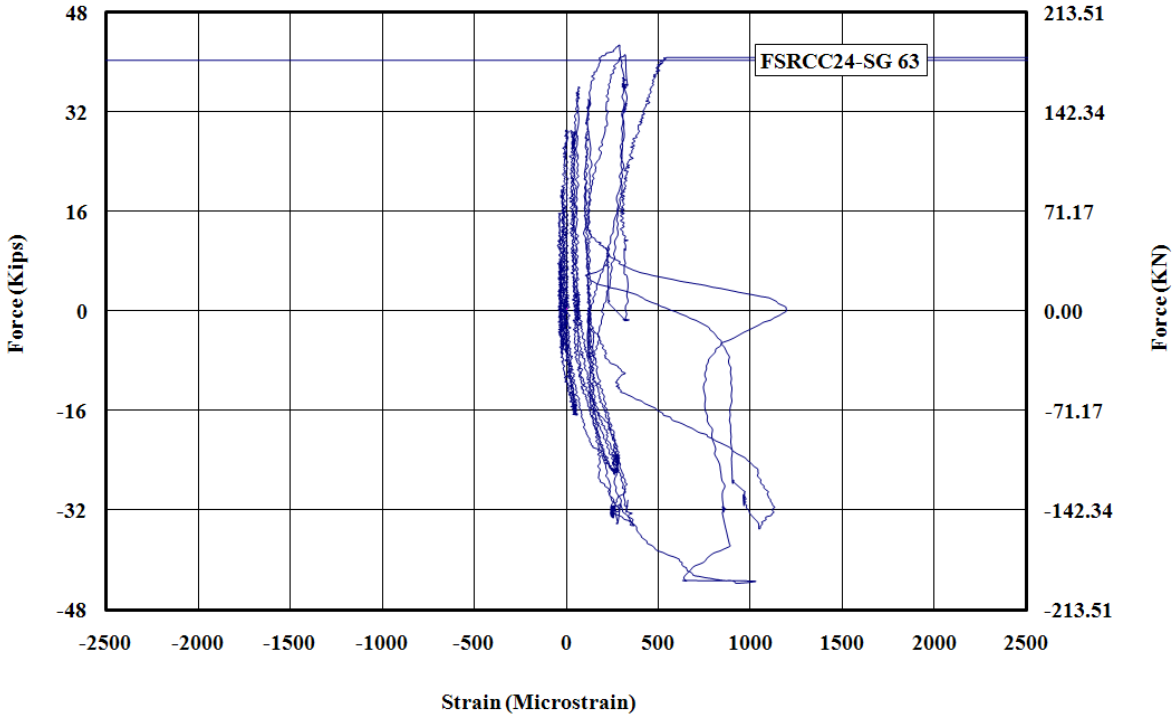

Figure D - 51: Measured Strain in Gauge No.63 for FSRCC24

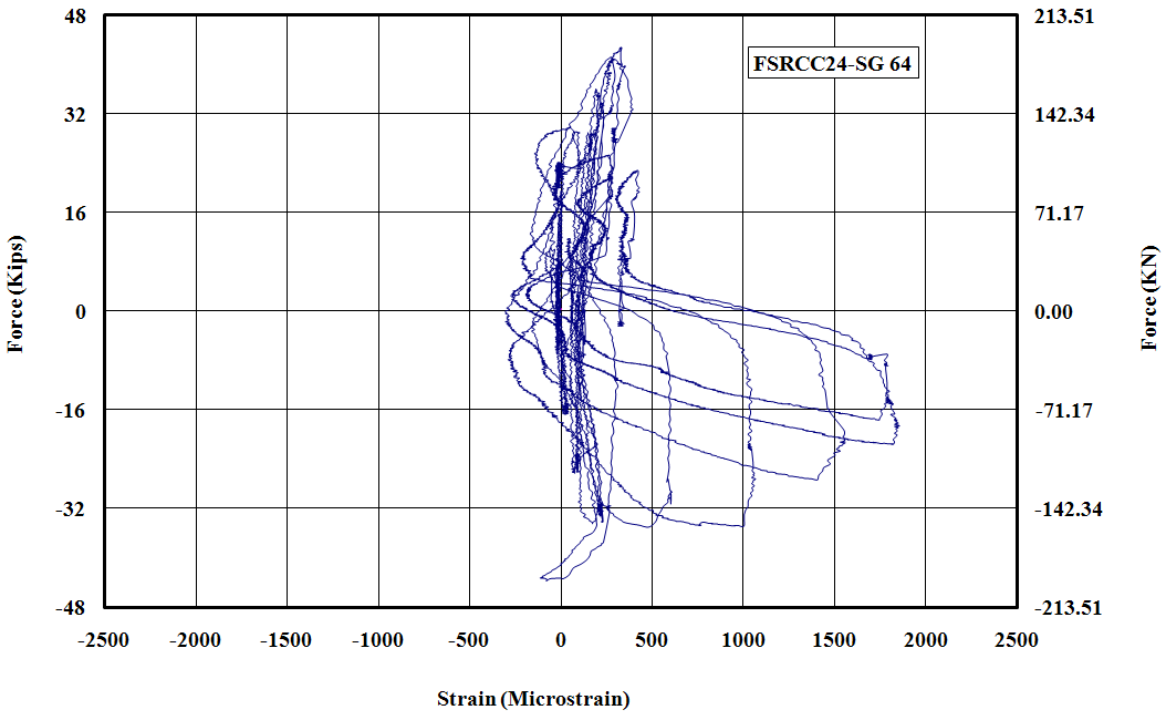

Figure D - 52: Measured Strain in Gauge No.64 for FSRCC24

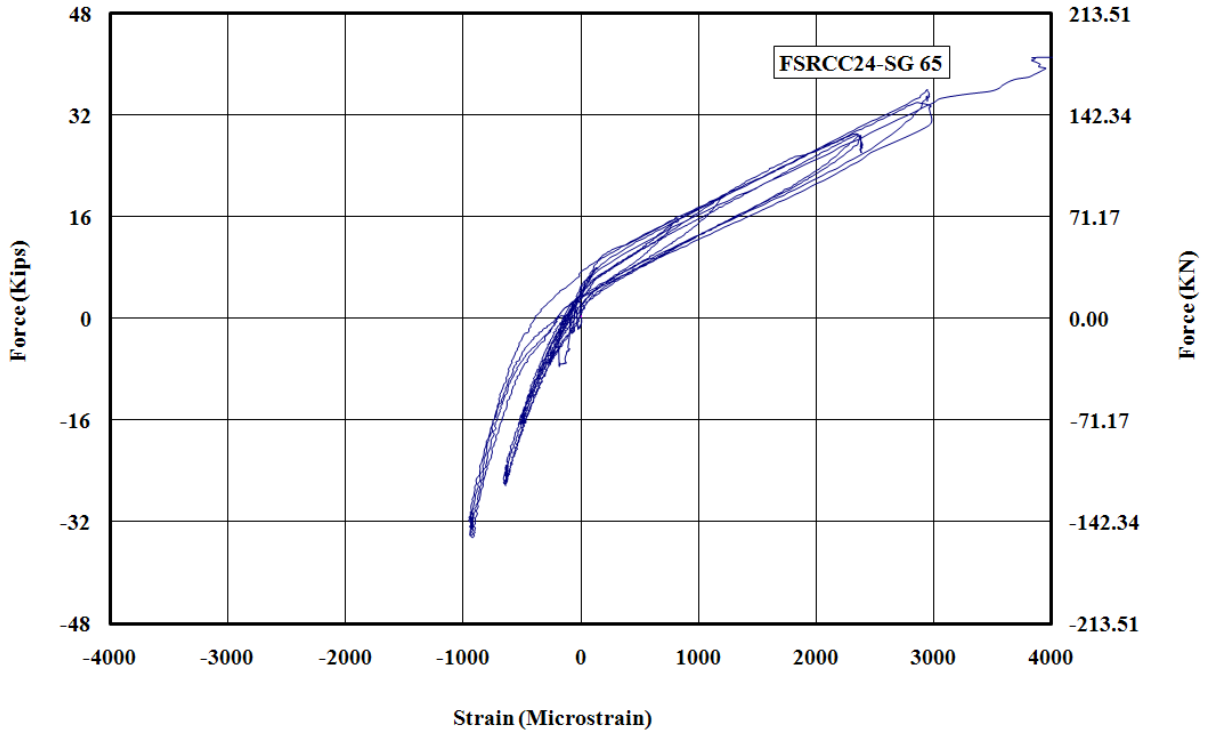

Figure D - 53: Measured Strain in Gauge No.65 for FSRCC24

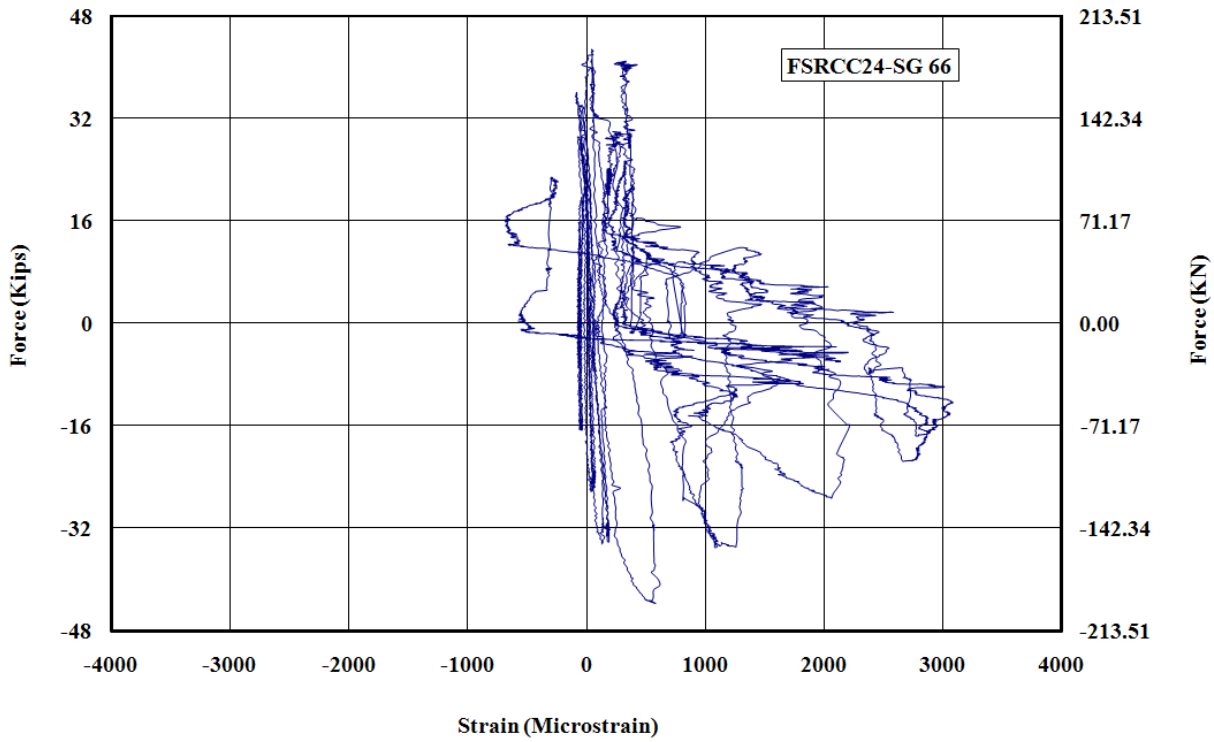

Figure D - 54: Measured Strain in Gauge No.66 for FSRCC24

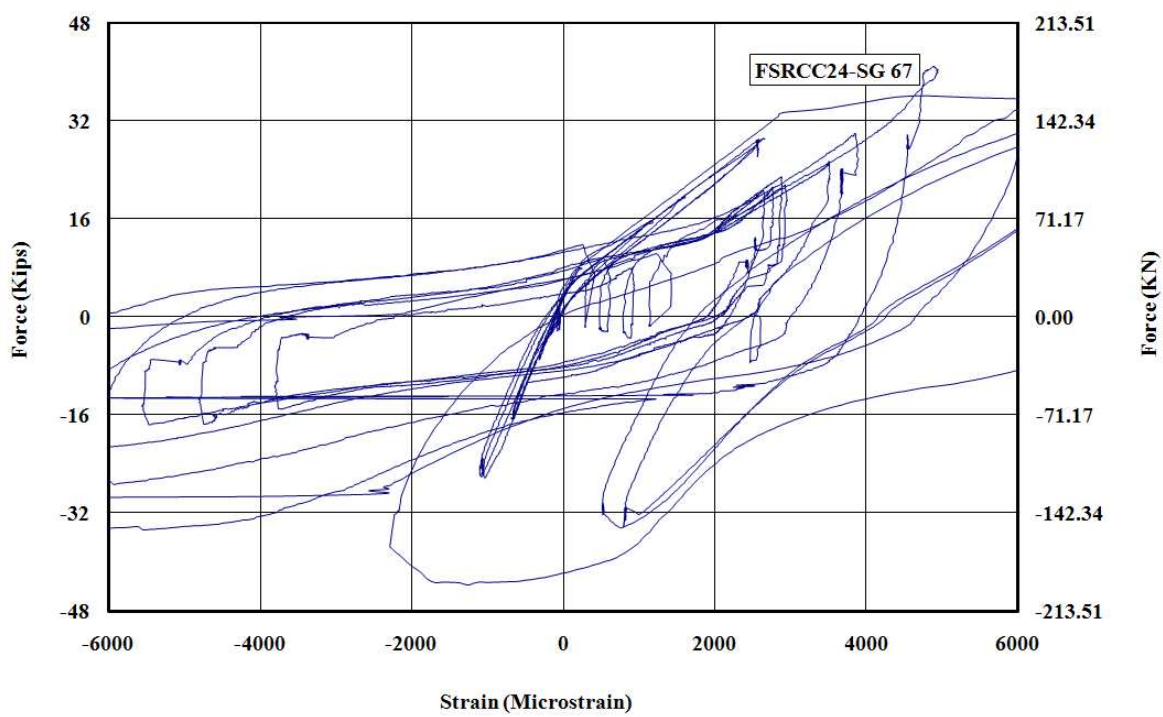

Figure D - 55: Measured Strain in Gauge No.67 for FSRCC24

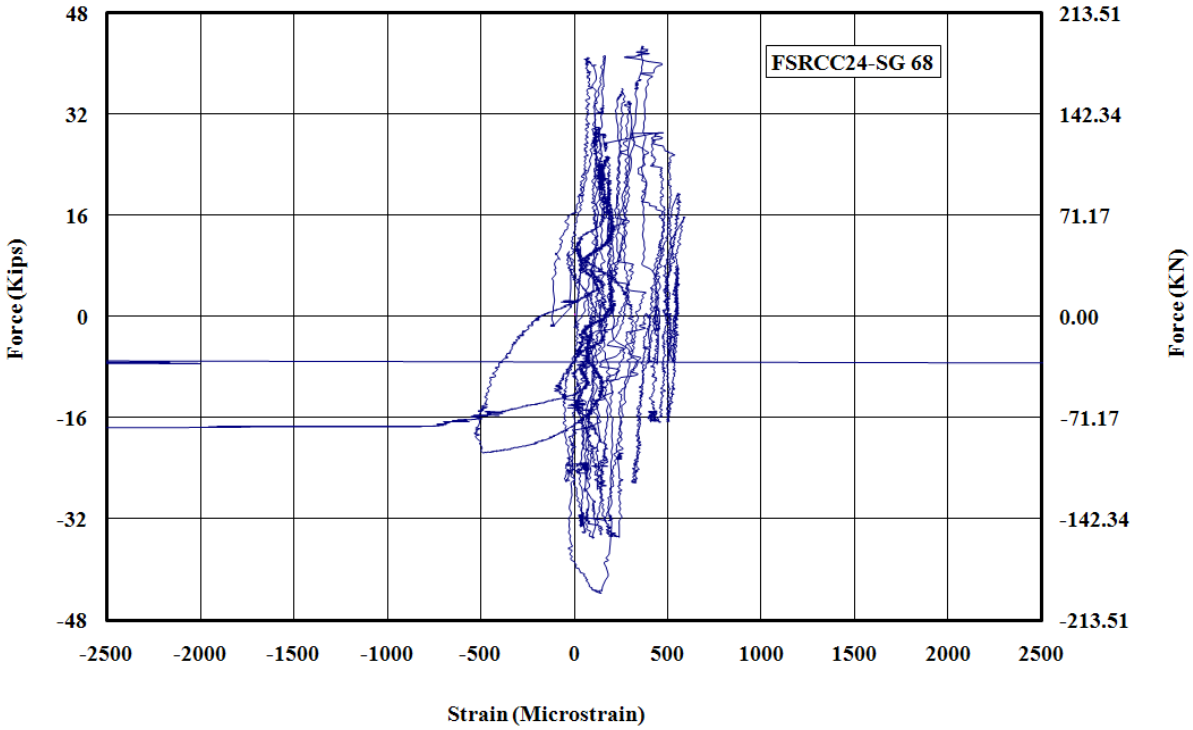

Figure D - 56: Measured Strain in Gauge No.68 for FSRCC24

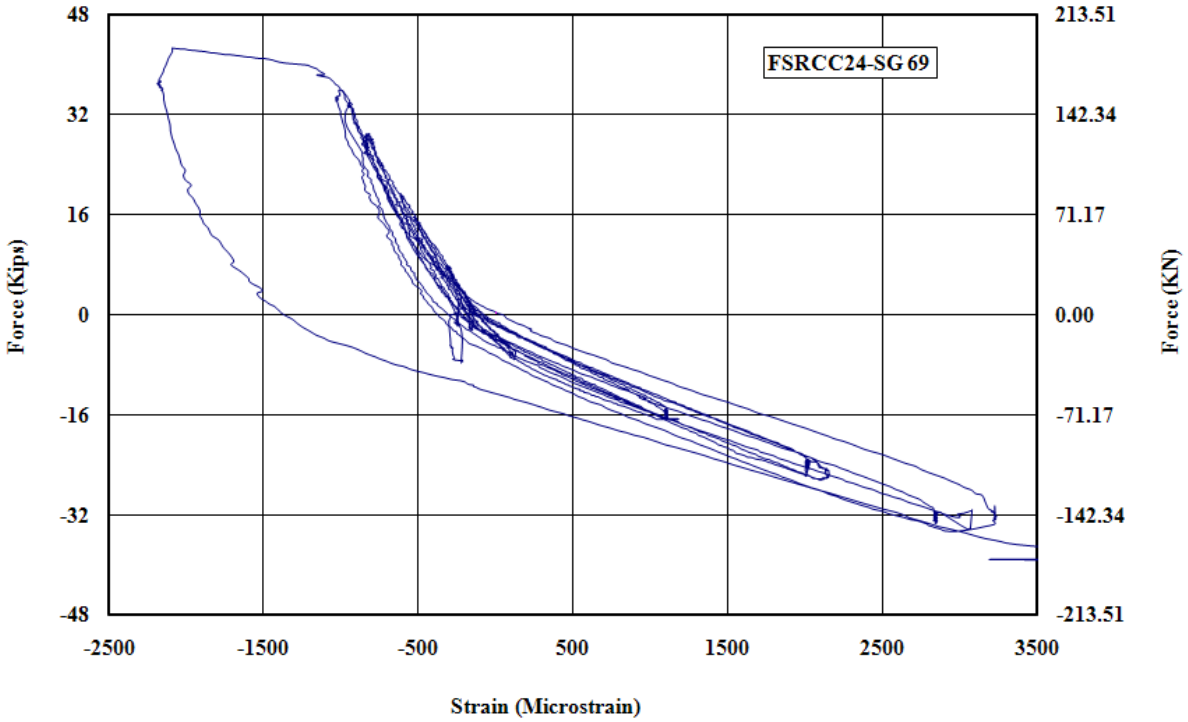

Figure D - 57: Measured Strain in Gauge No.69 for FSRCC24

Appendix E

Specimen DCKJ24

(Drop-Cap Knee-Joint with 24-in. diameter pile)

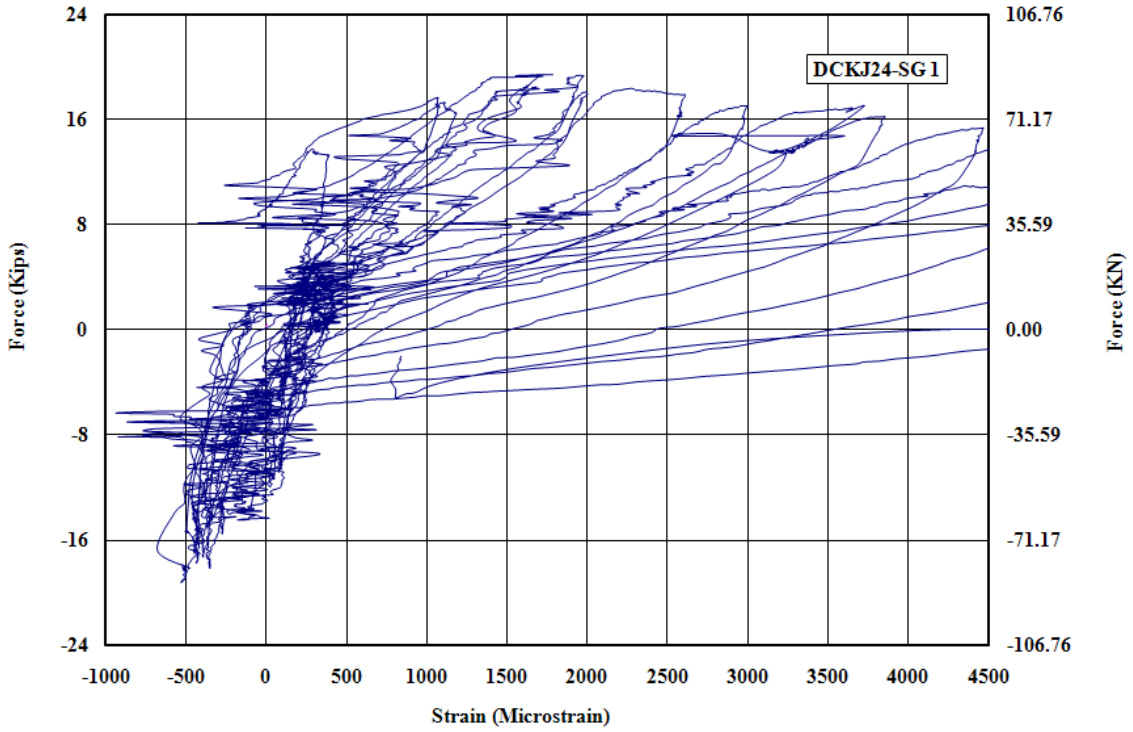

Figure E - 1: Measured Strain in Gauge No.1 for DCKJ24

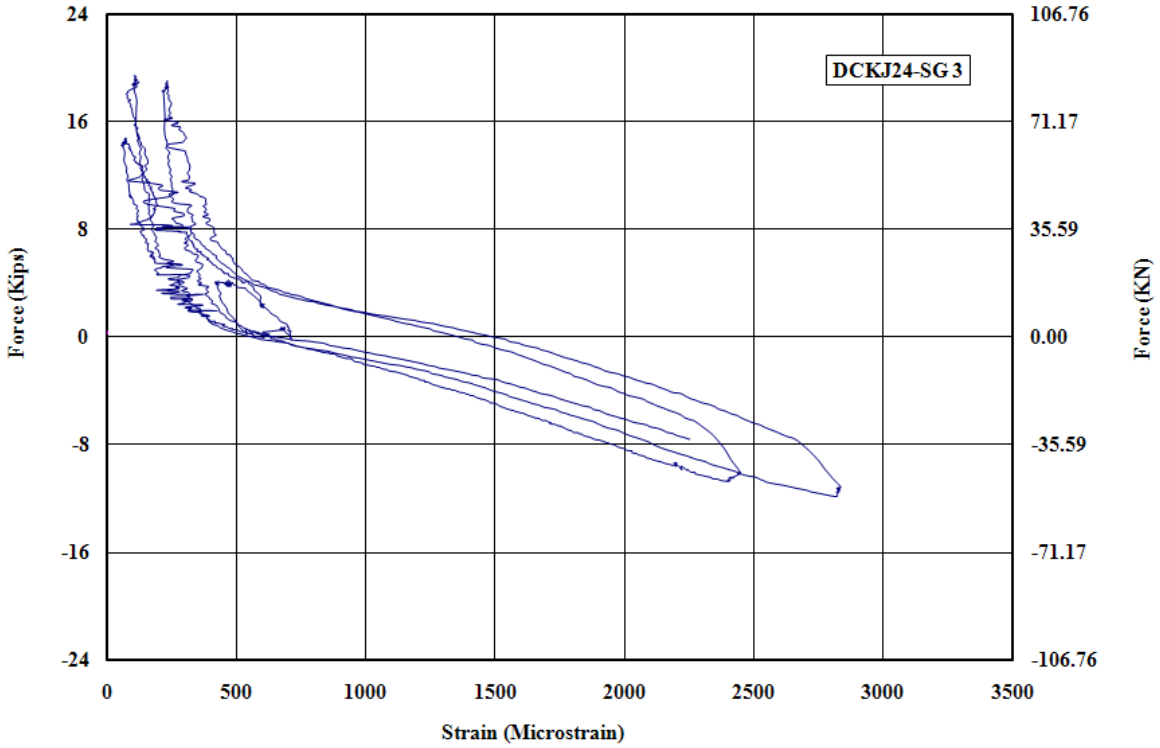

Figure E - 2: Measured Strain in Gauge No.3 for DCKJ24

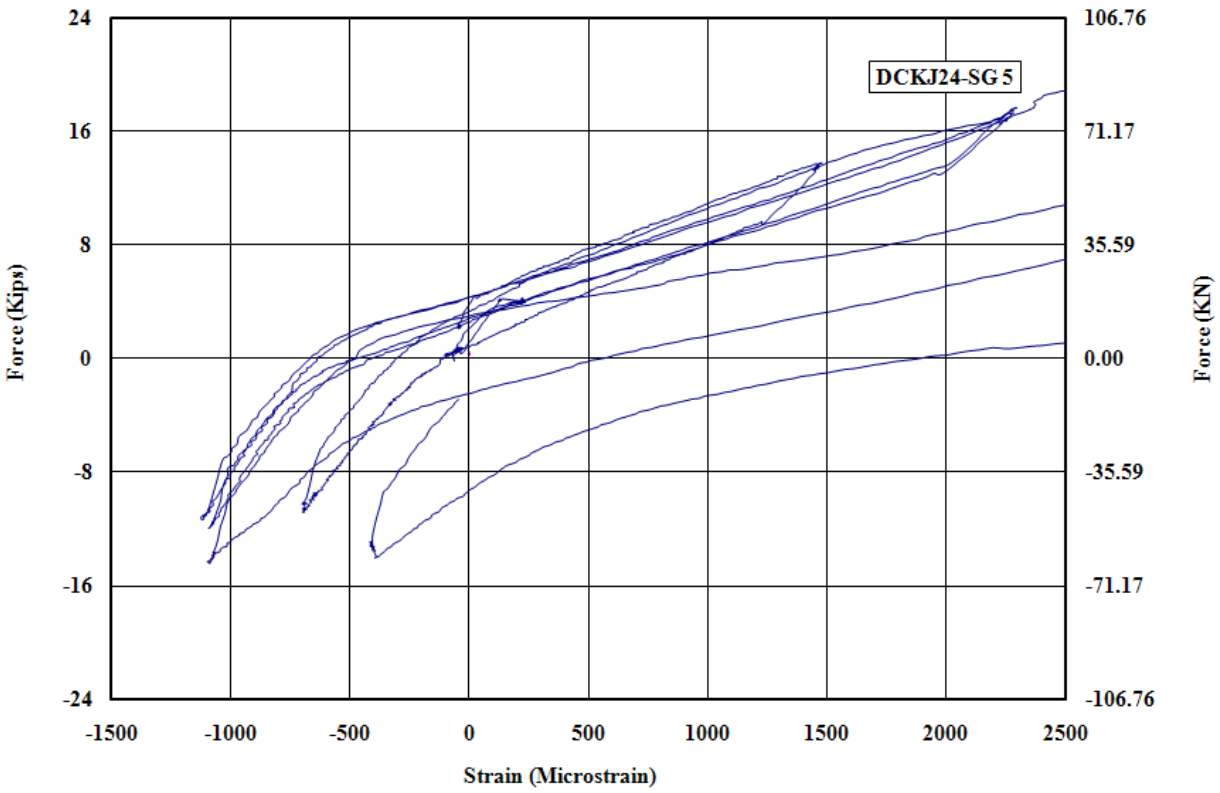

Figure E - 3: Measured Strain in Gauge No.5 for DCKJ24

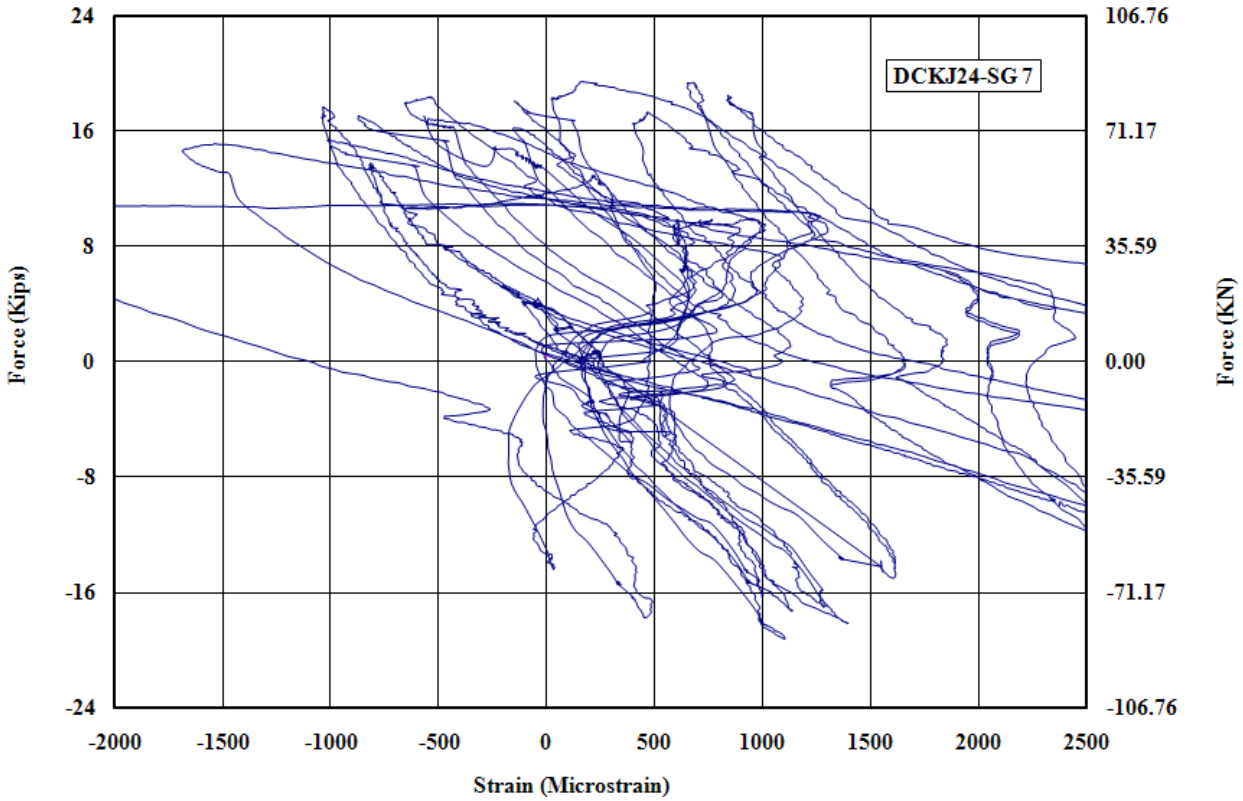

Figure E - 4: Measured Strain in Gauge No.7 for DCKJ24

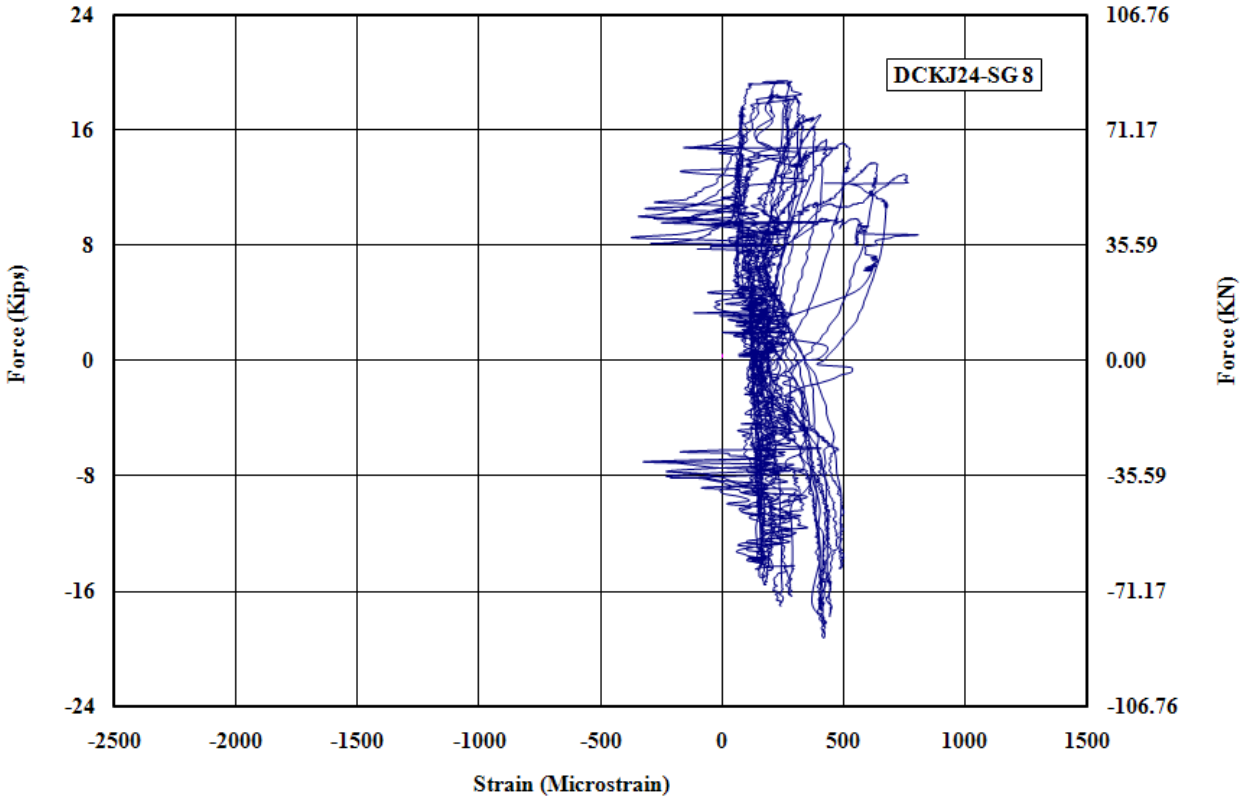

Figure E - 5: Measured Strain in Gauge No.8 for DCKJ24

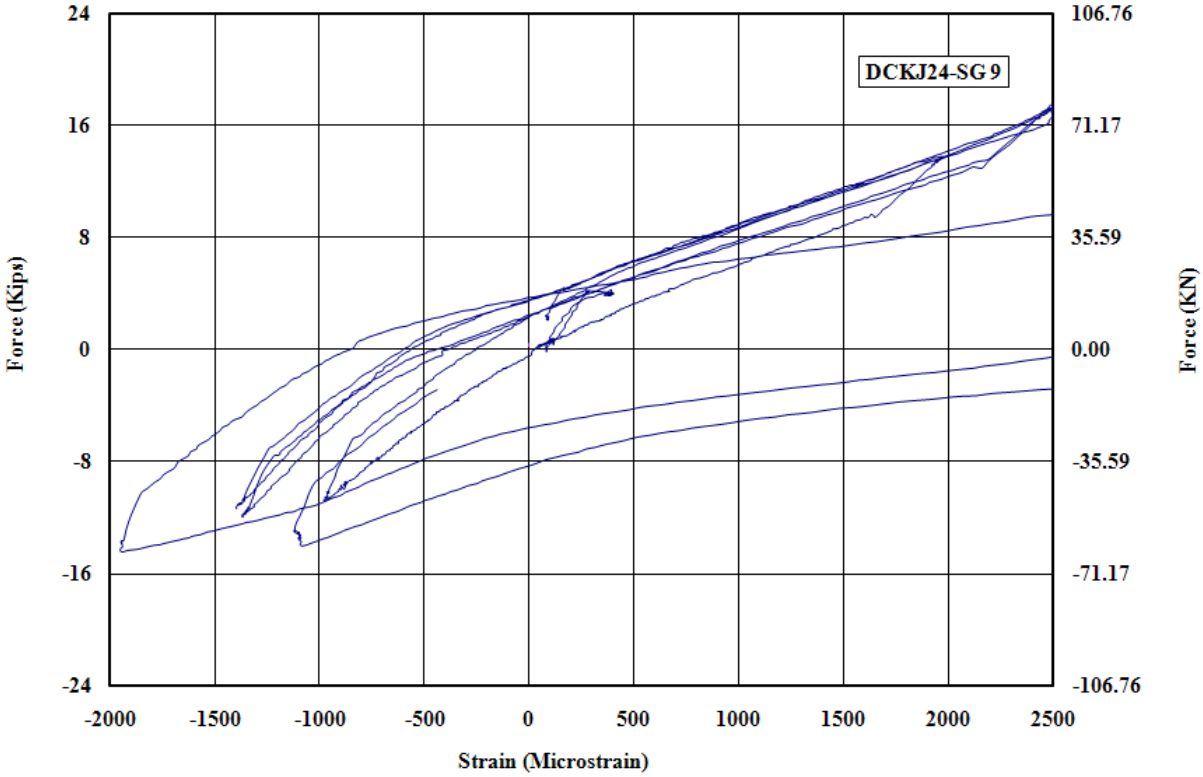

Figure E - 6: Measured Strain in Gauge No.9 for DCKJ24

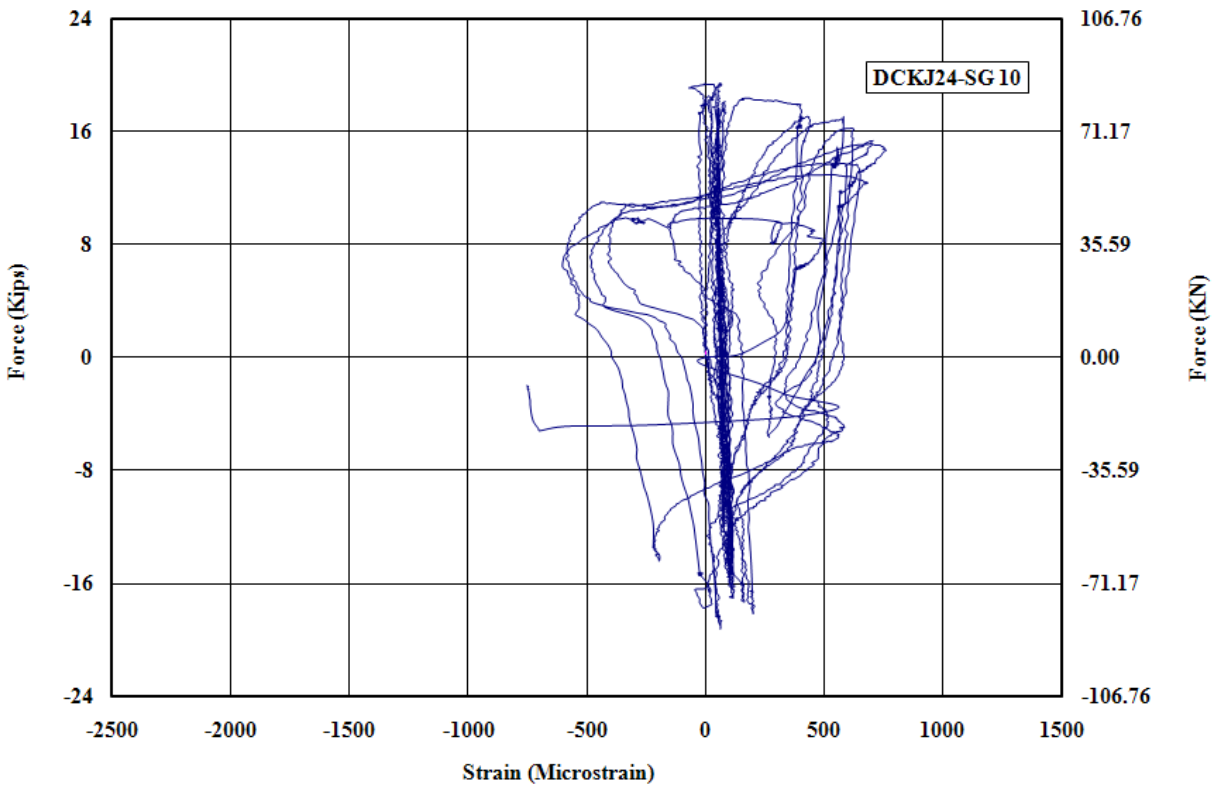

Figure E - 7: Measured Strain in Gauge No.10 for DCKJ24

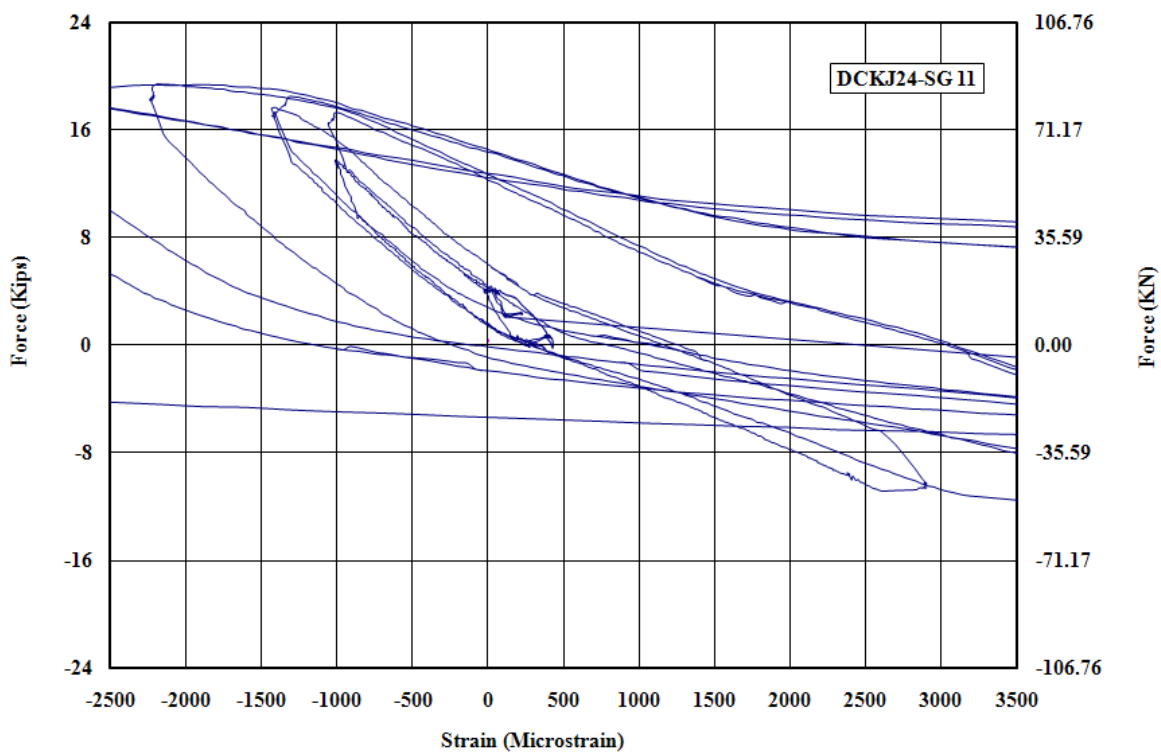

Figure E - 8: Measured Strain in Gauge No.11 for DCKJ24

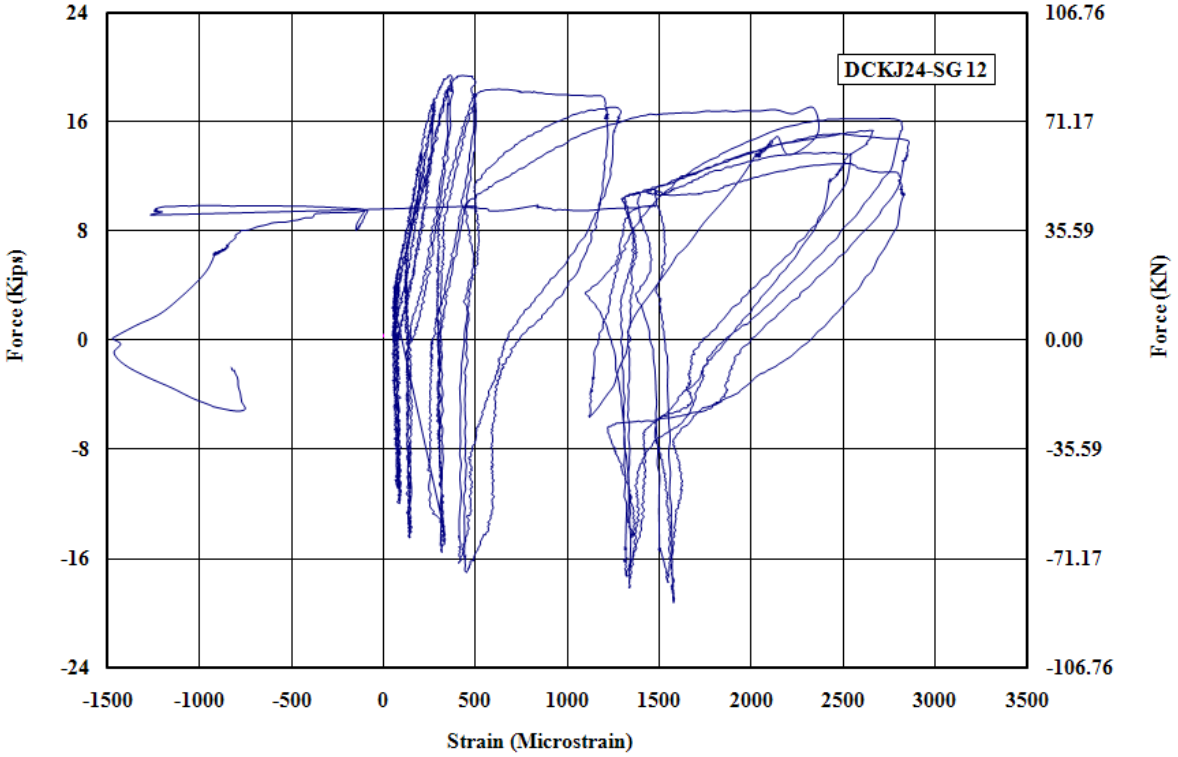

Figure E - 9: Measured Strain in Gauge No.12 for DCKJ24

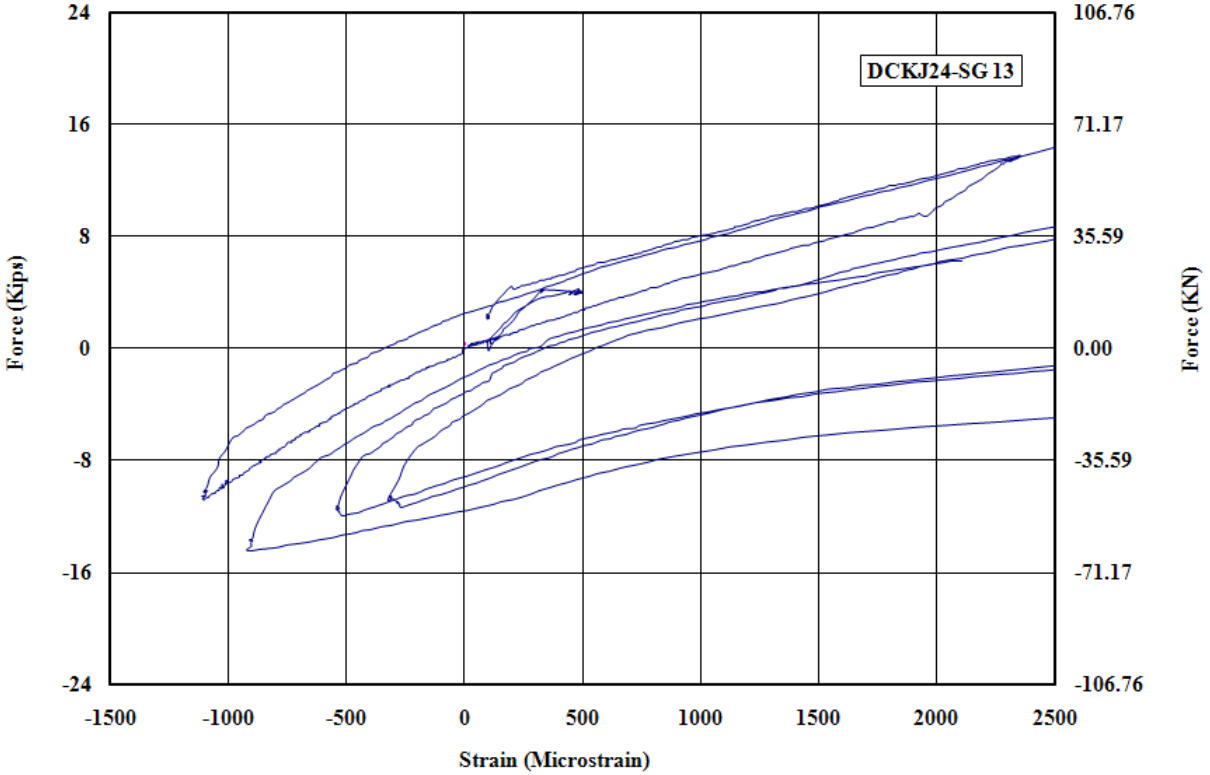

Figure E - 10: Measured Strain in Gauge No.13 for DCKJ24

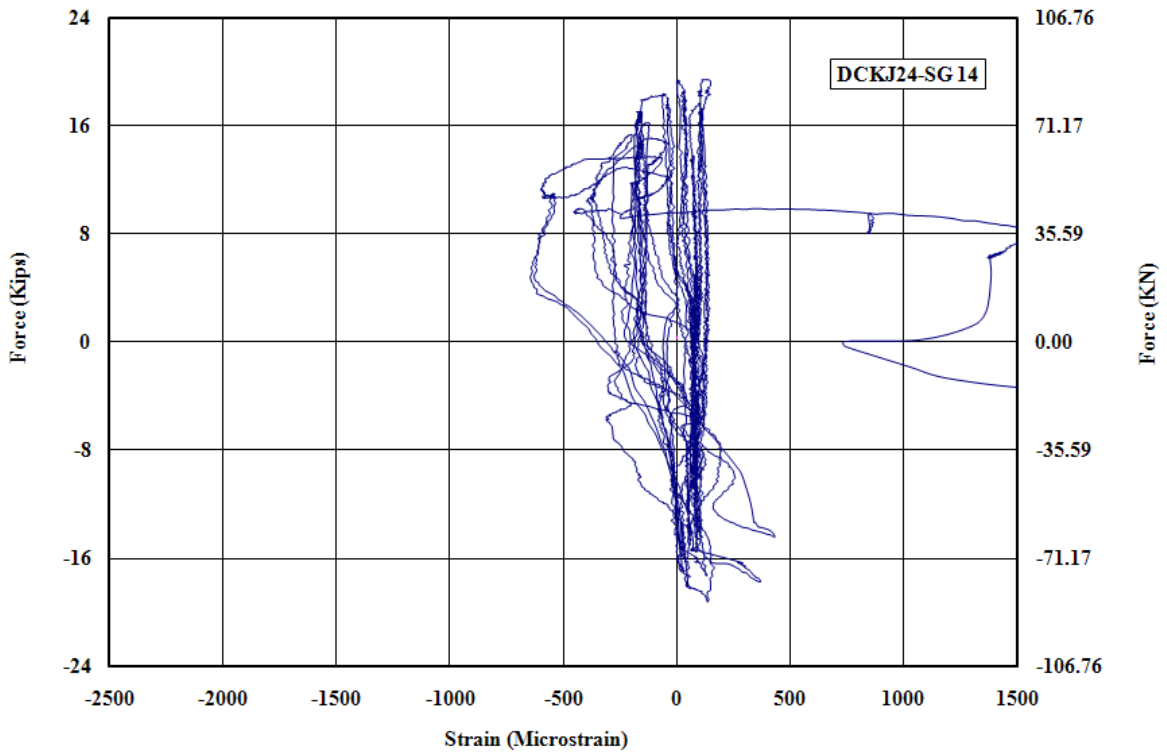

Figure E - 11: Measured Strain in Gauge No.14 for DCKJ24

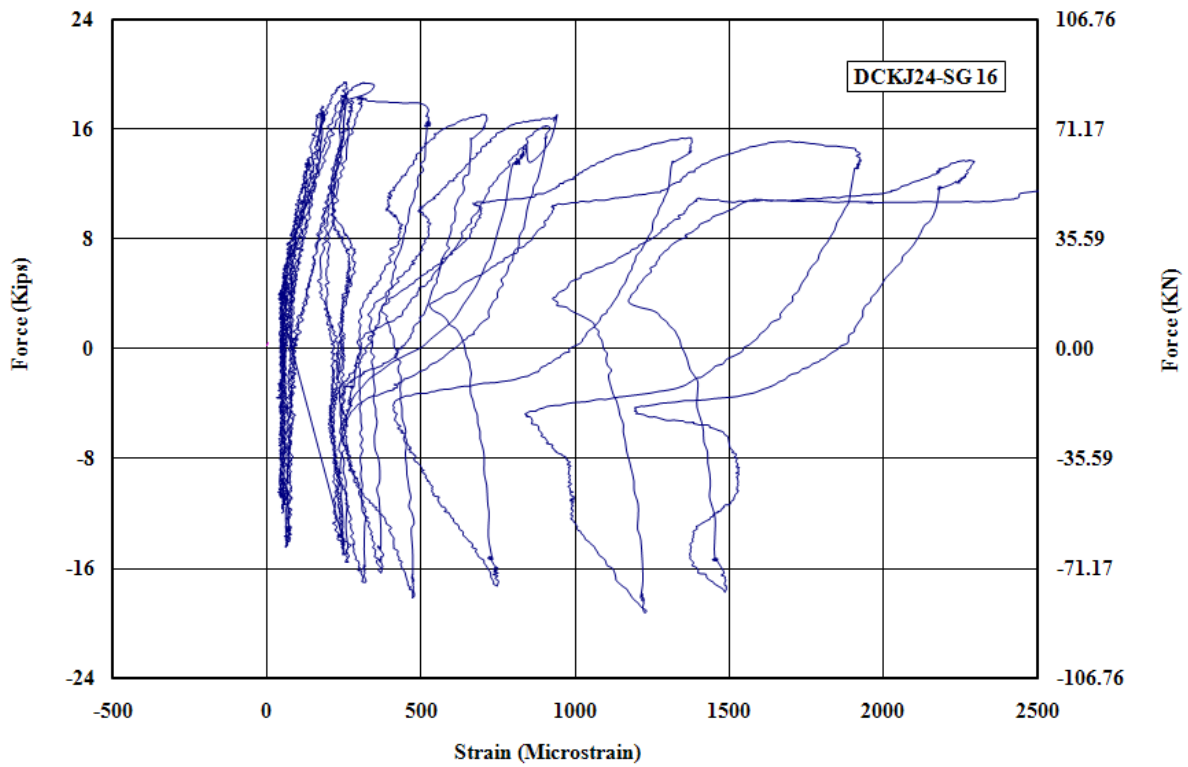

Figure E - 12: Measured Strain in Gauge No.16 for DCKJ24

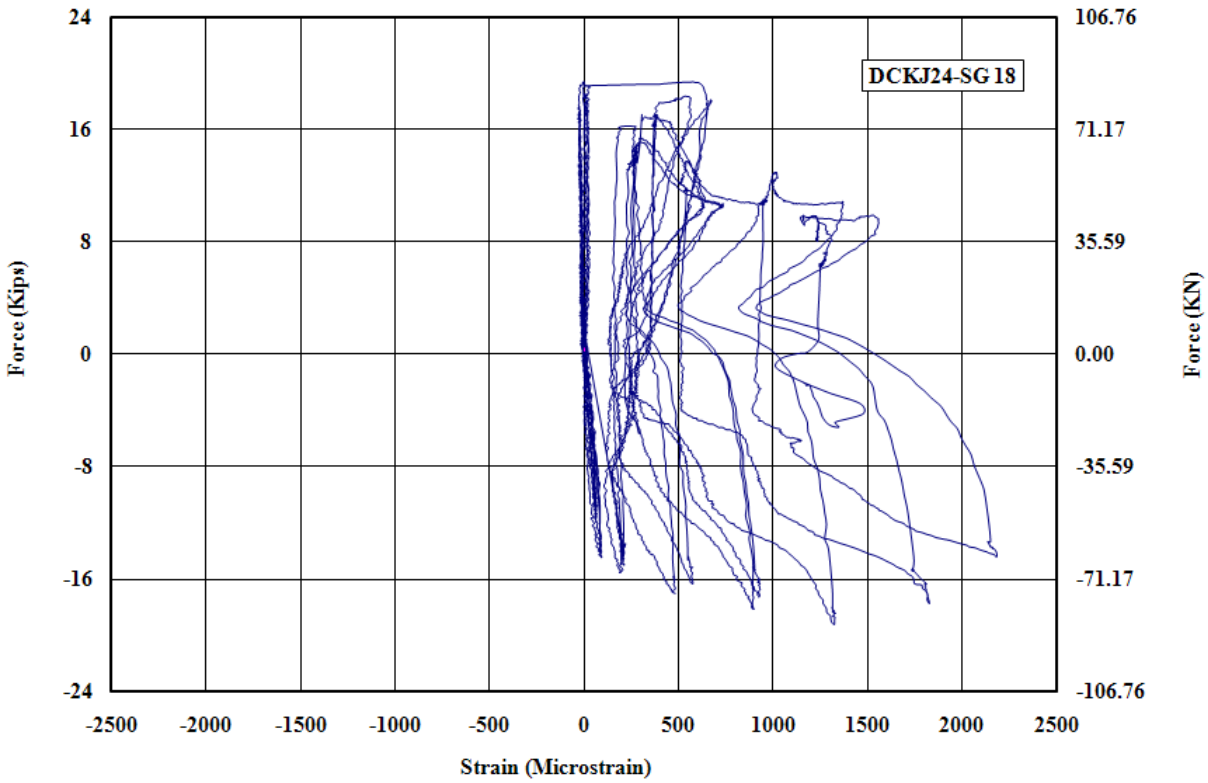

Figure E - 13: Measured Strain in Gauge No.18 for DCKJ24

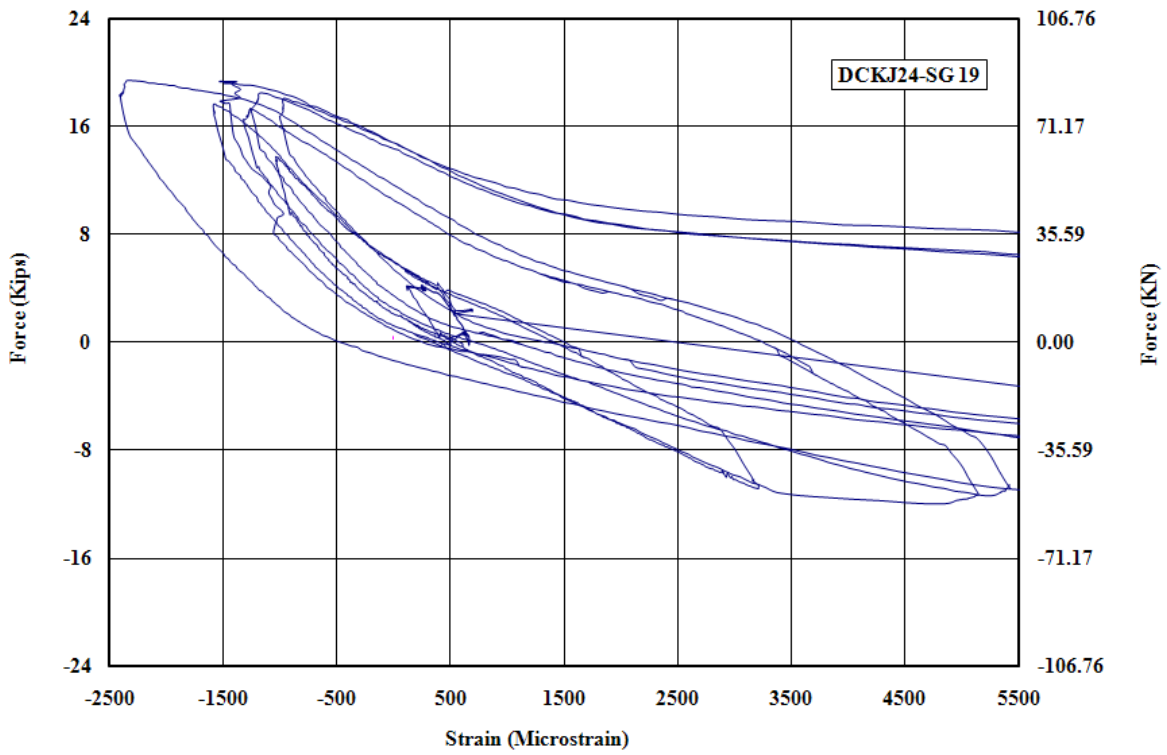

Figure E - 14: Measured Strain in Gauge No.19 for DCKJ24

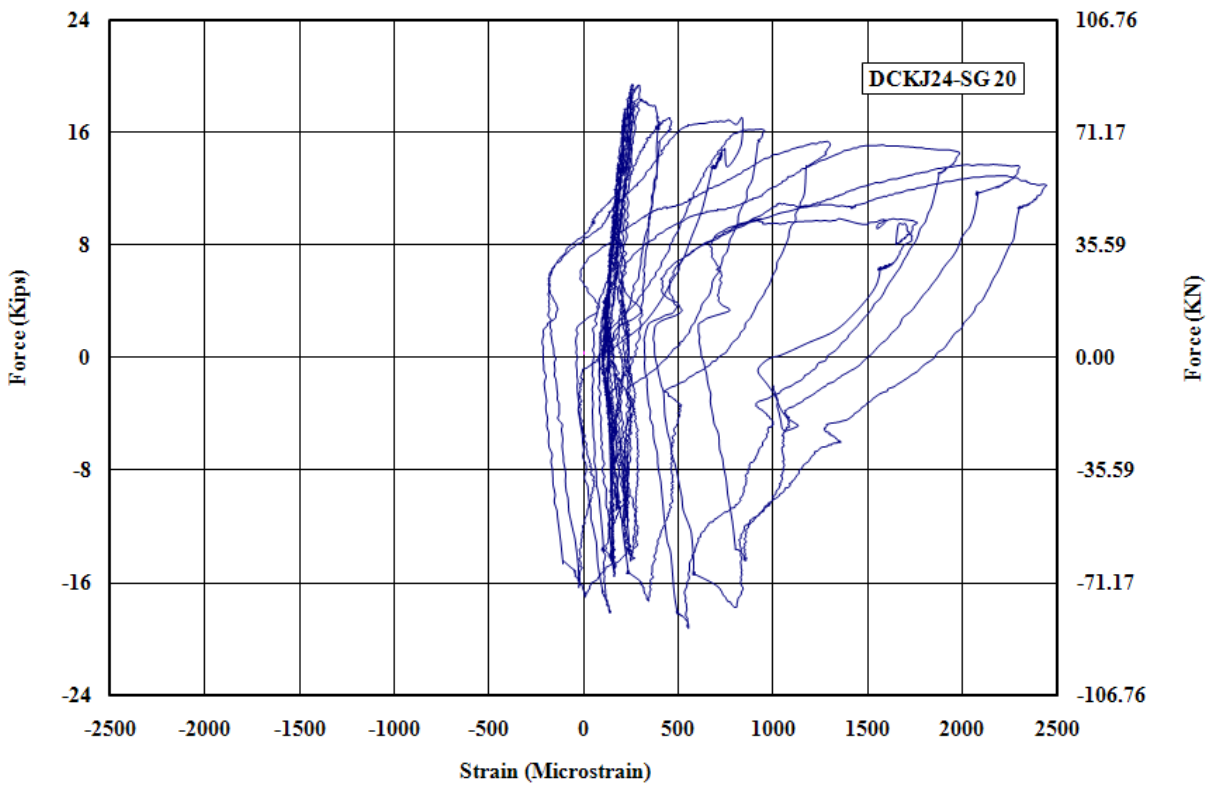

Figure E - 15: Measured Strain in Gauge No.20 for DCKJ24

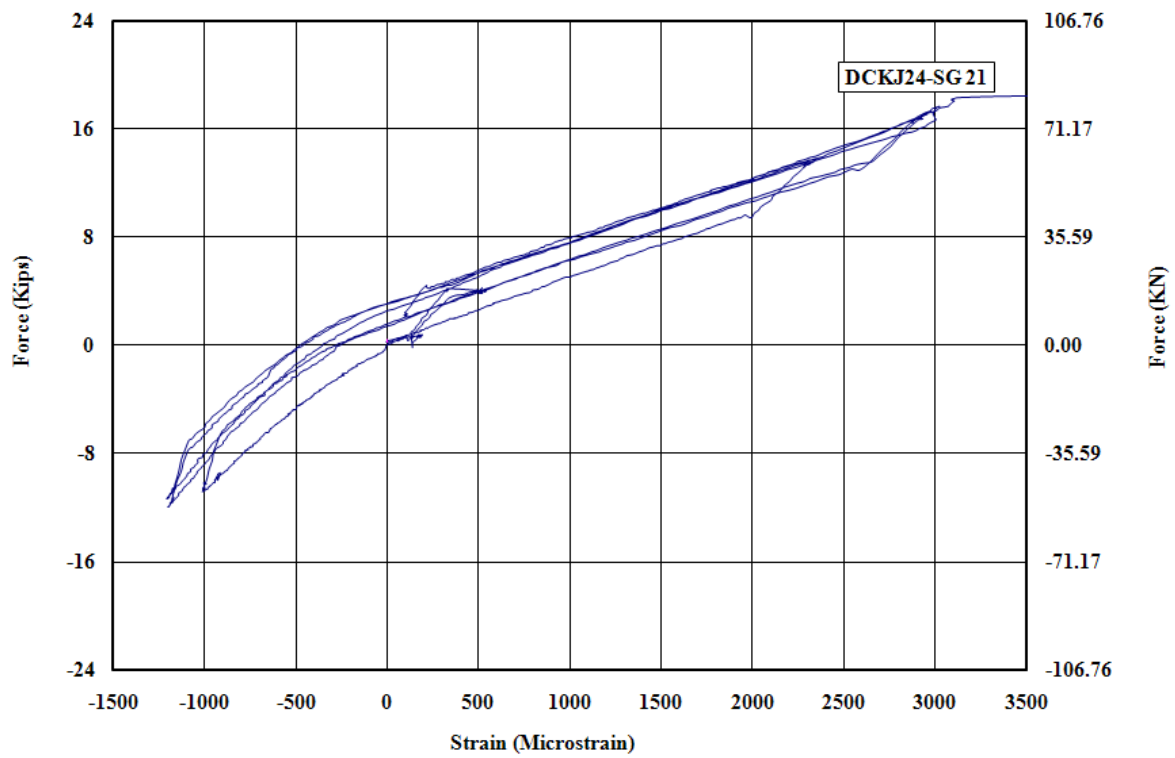

Figure E - 16: Measured Strain in Gauge No.21 for DCKJ24

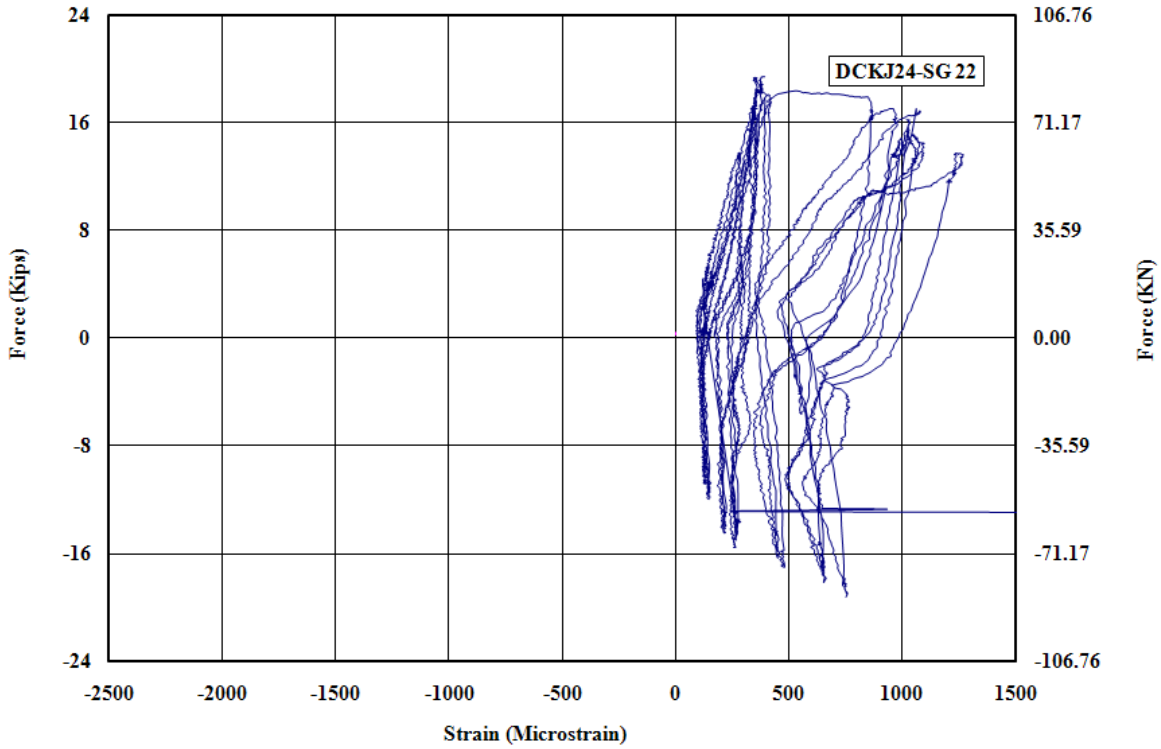

Figure E - 17: Measured Strain in Gauge No.22 for DCKJ24

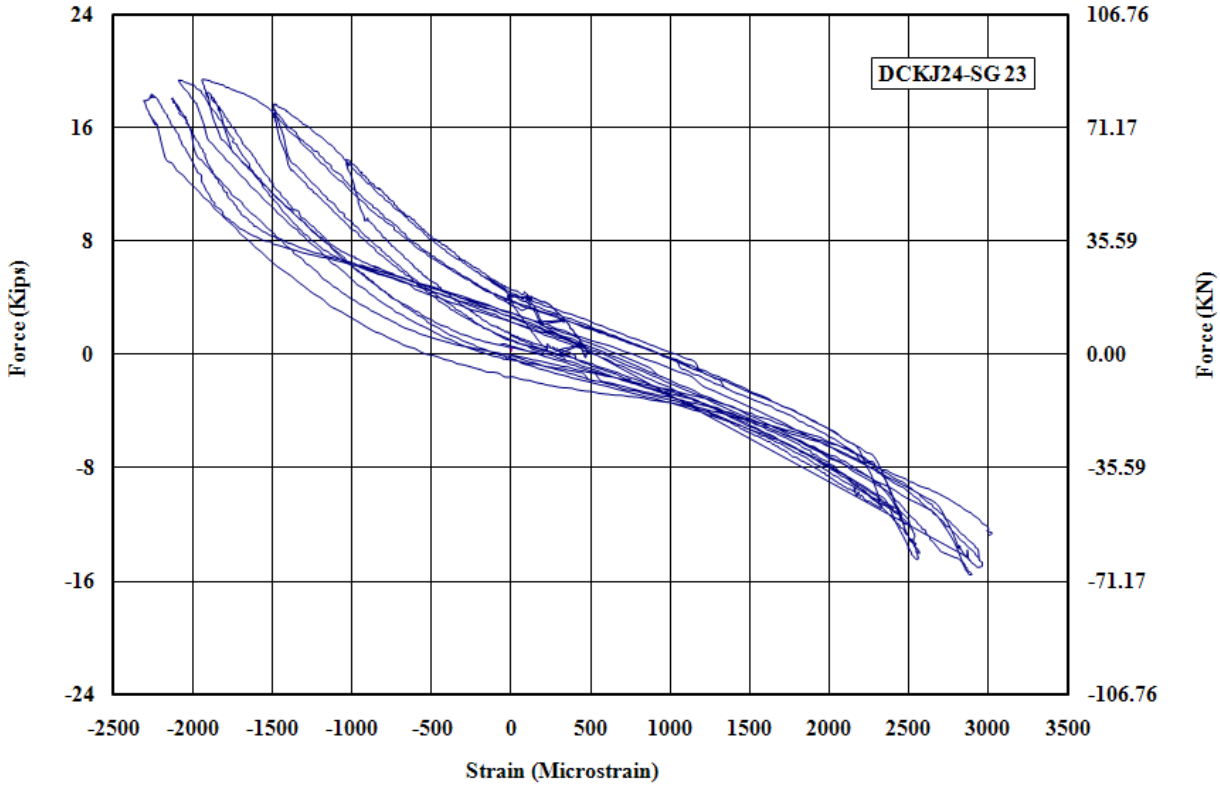

Figure E - 18: Measured Strain in Gauge No.23 for DCKJ24

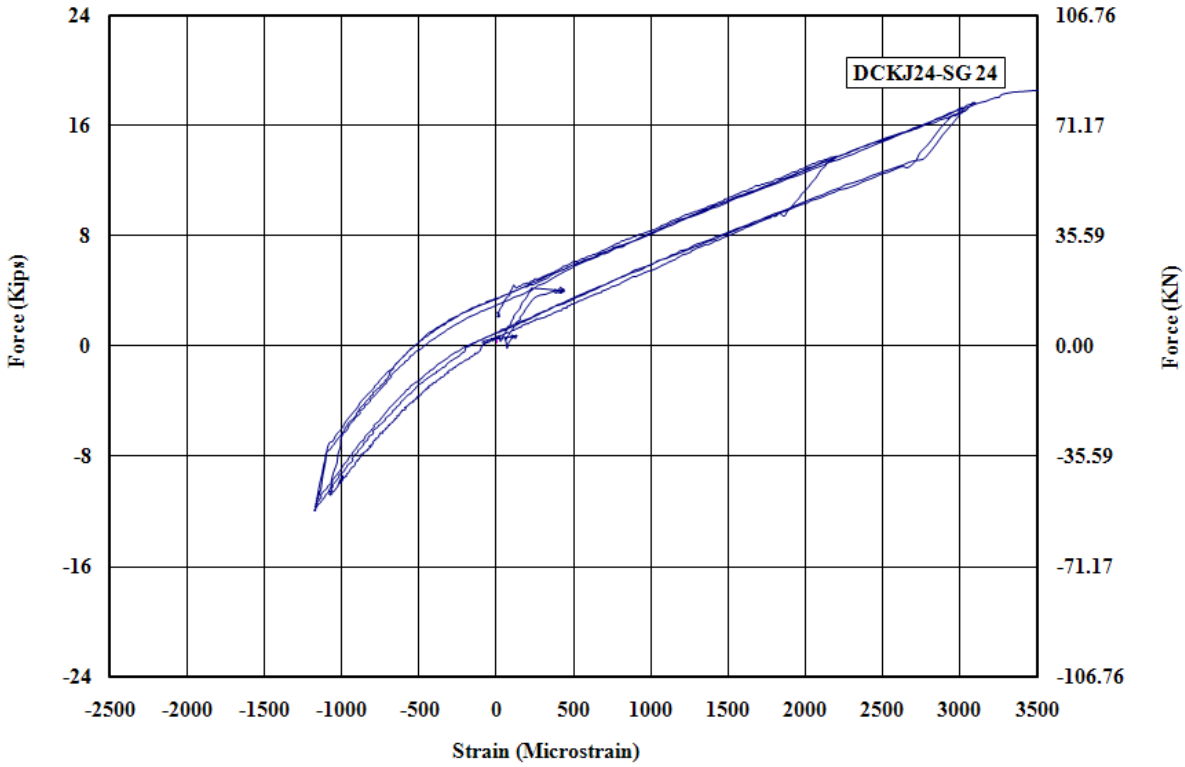

Figure E - 19: Measured Strain in Gauge No.24 for DCKJ24

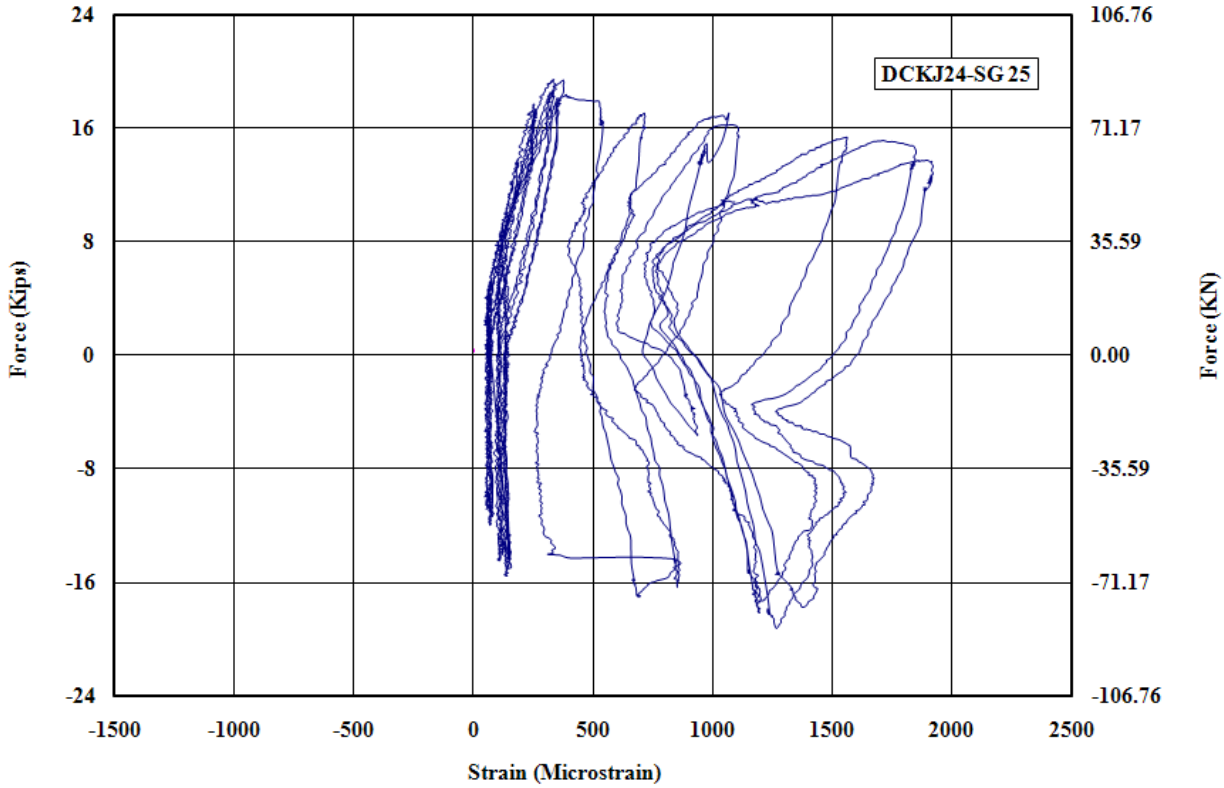

Figure E - 20: Measured Strain in Gauge No.25 for DCKJ24

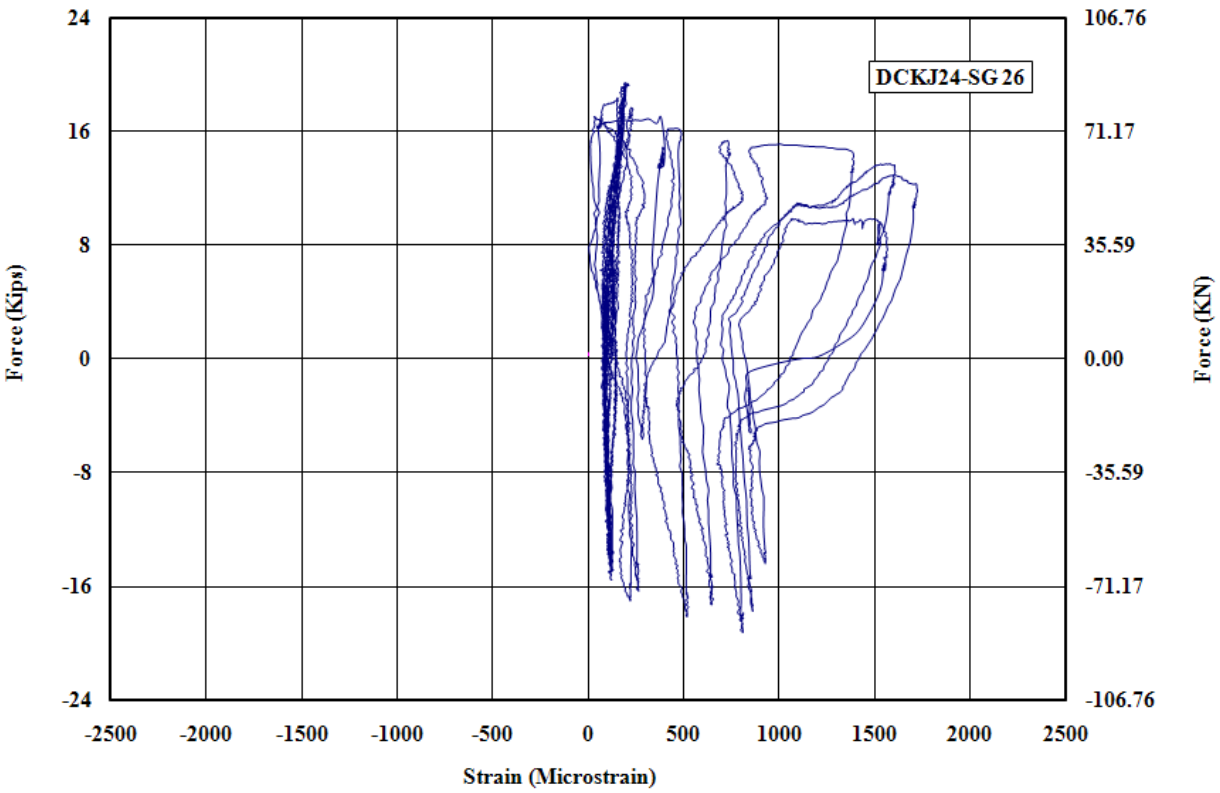

Figure E - 21: Measured Strain in Gauge No.26 for DCKJ24

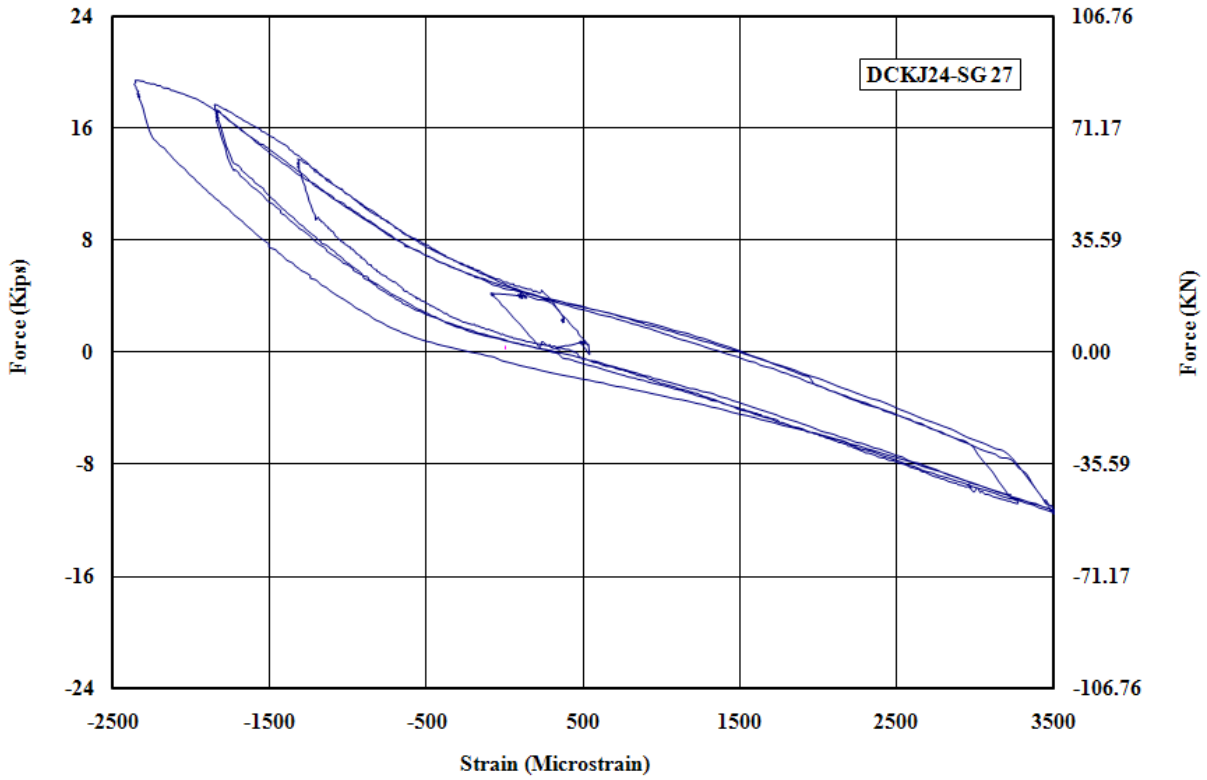

Figure E - 22: Measured Strain in Gauge No.27 for DCKJ24

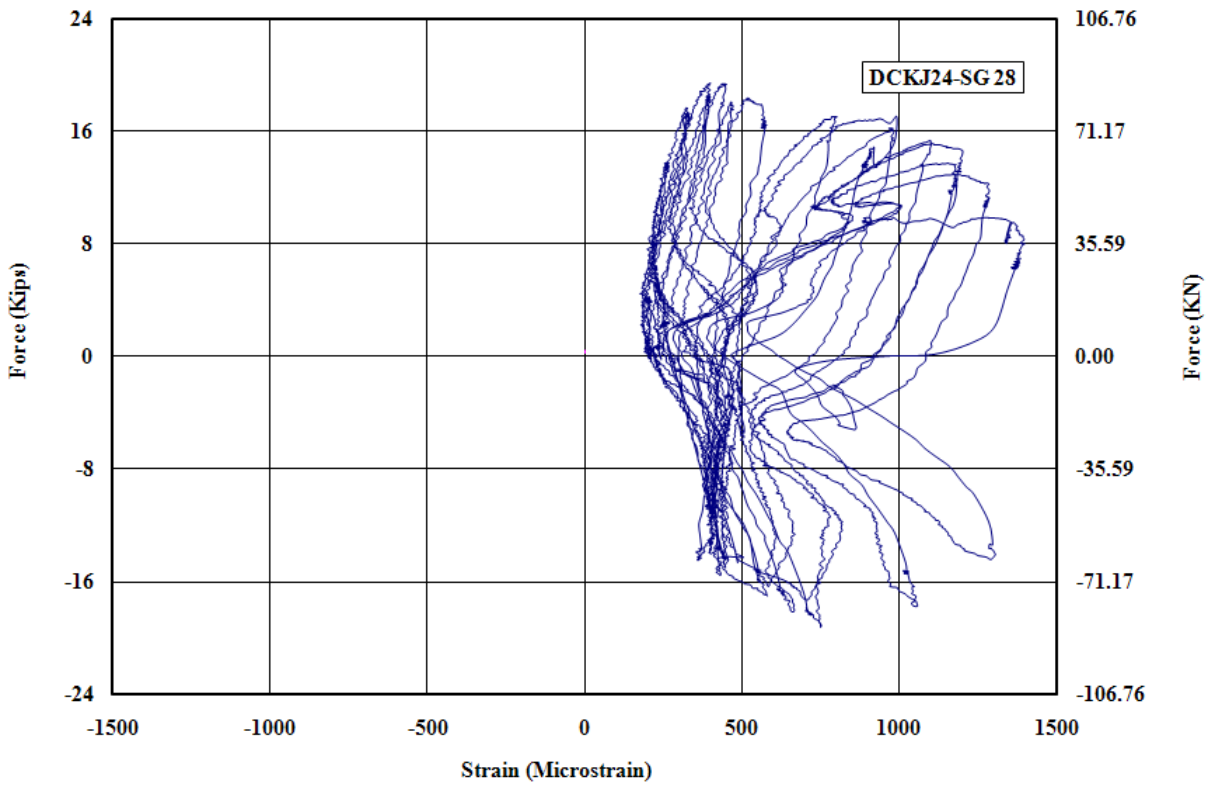

Figure E - 23: Measured Strain in Gauge No.28 for DCKJ24

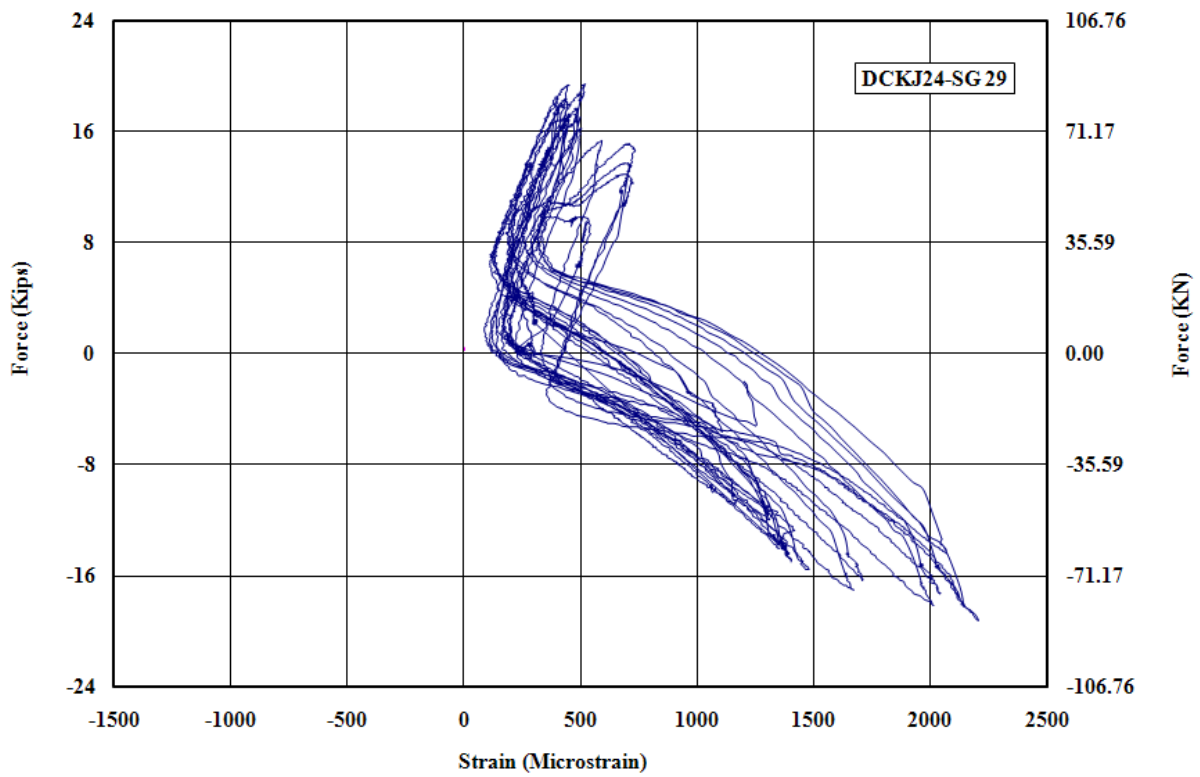

Figure E - 24: Measured Strain in Gauge No.29 for DCKJ24

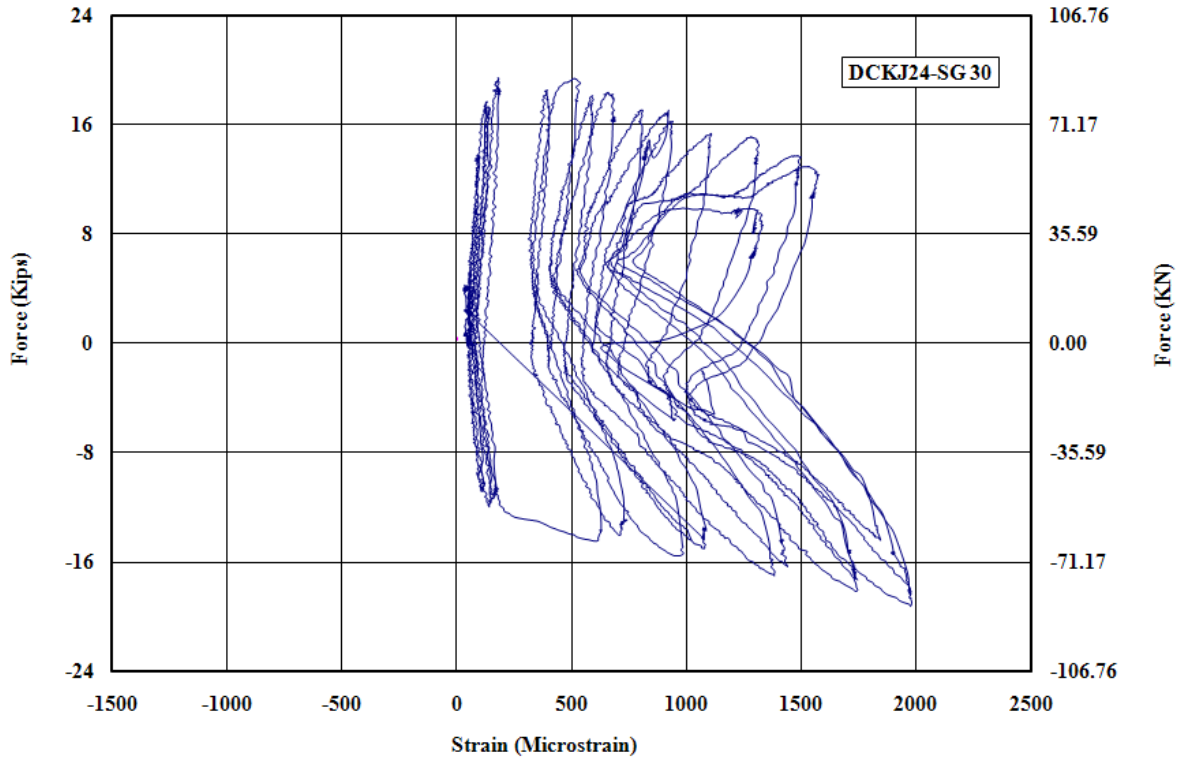

Figure E - 25: Measured Strain in Gauge No.30 for DCKJ24

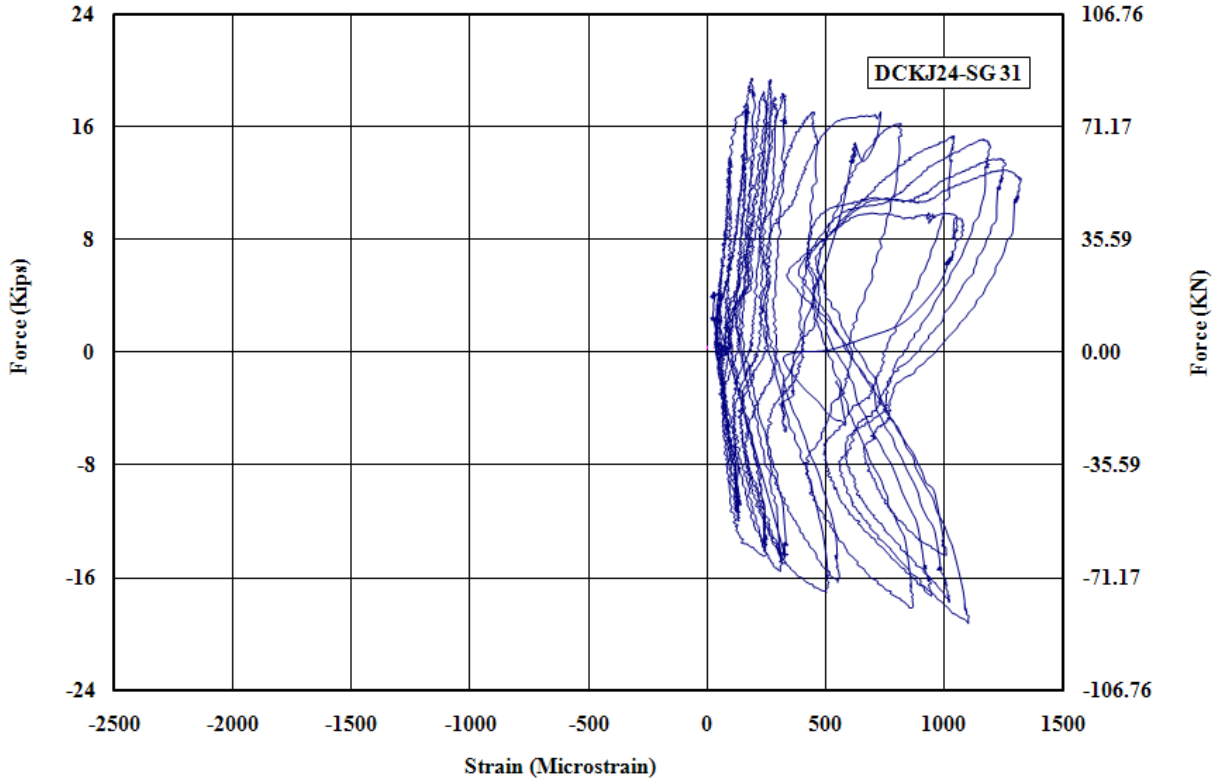

Figure E - 26: Measured Strain in Gauge No.31 for DCKJ24

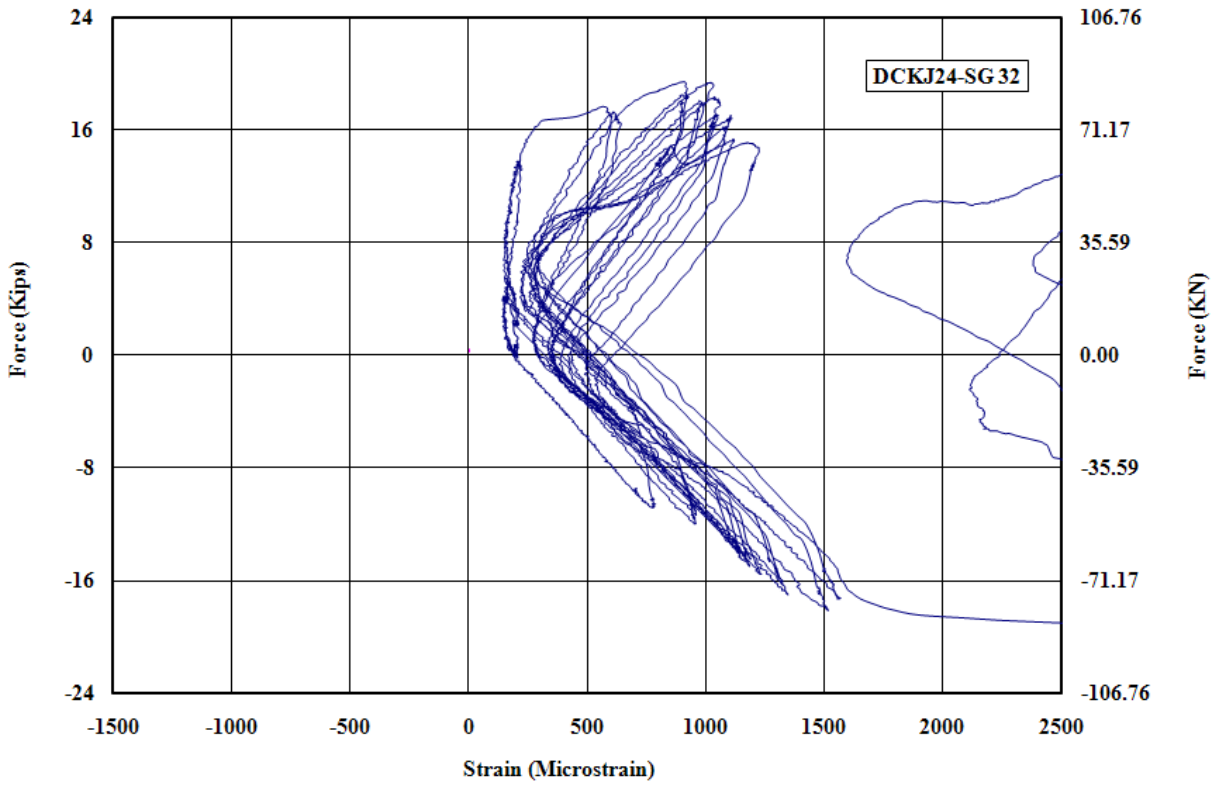

Figure E - 27: Measured Strain in Gauge No.32 for DCKJ24

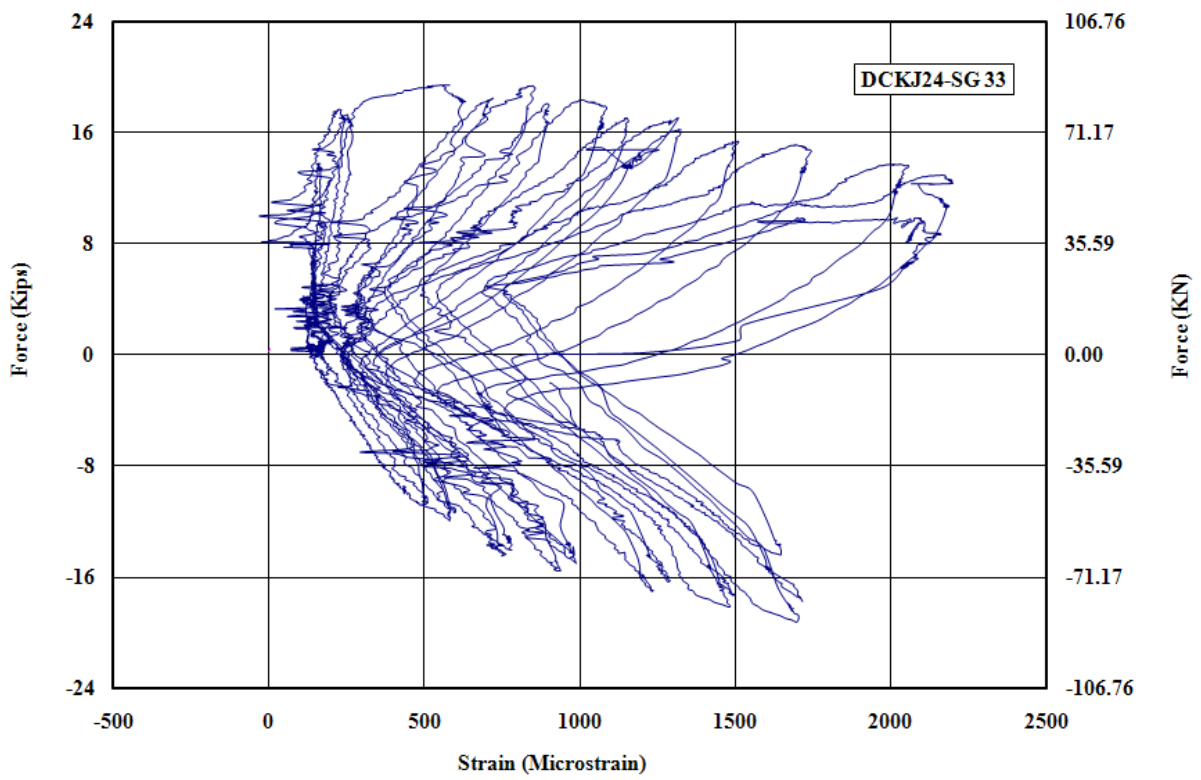

Figure E - 28: Measured Strain in Gauge No.33 for DCKJ24

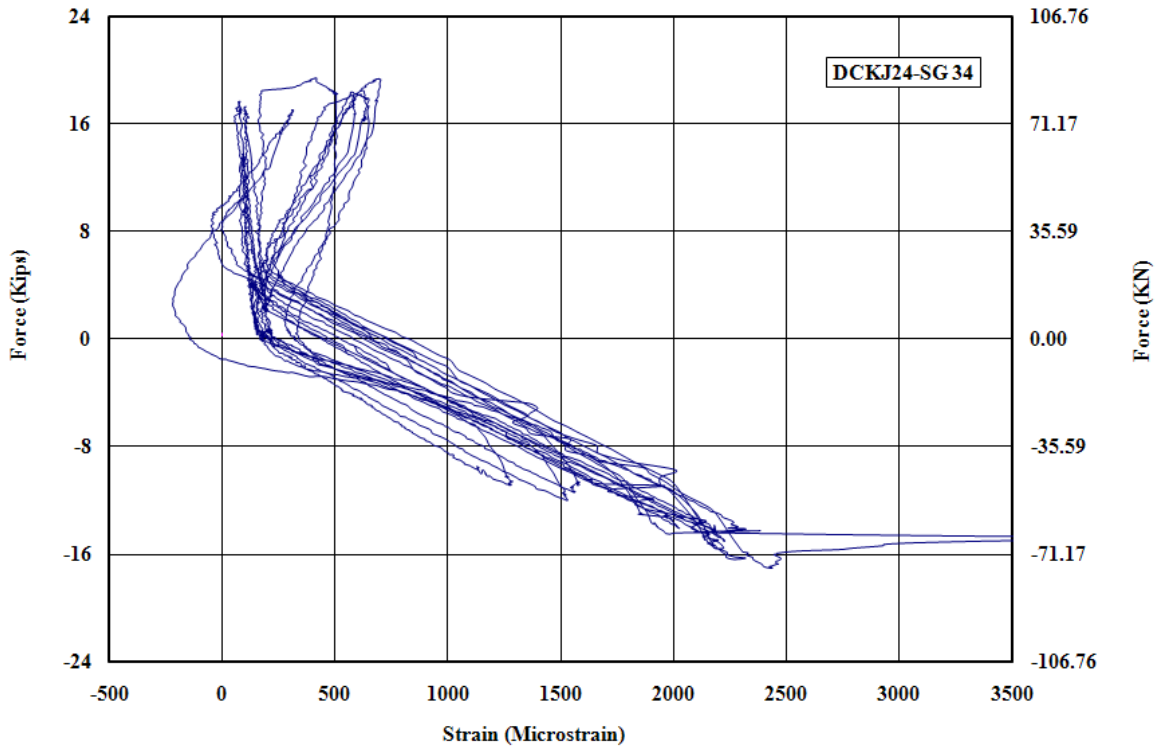

Figure E - 29: Measured Strain in Gauge No.34 for DCKJ24

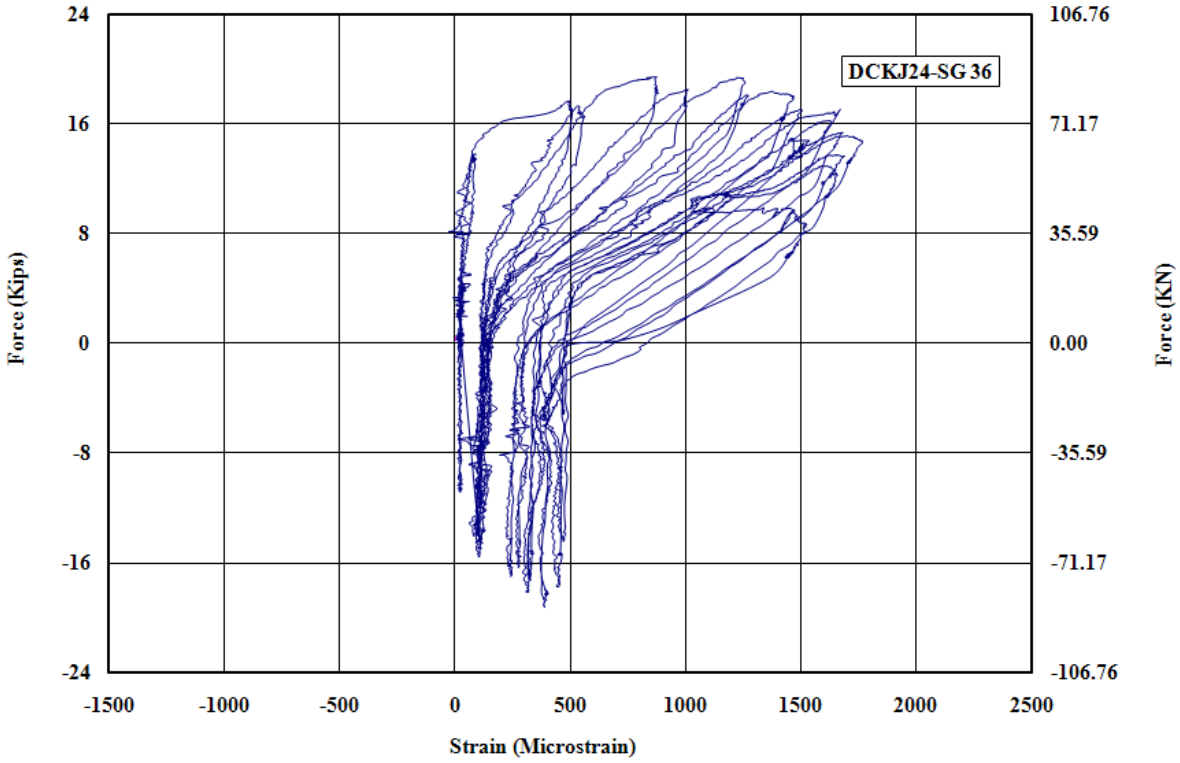

Figure E - 30: Measured Strain in Gauge No.36 for DCKJ24

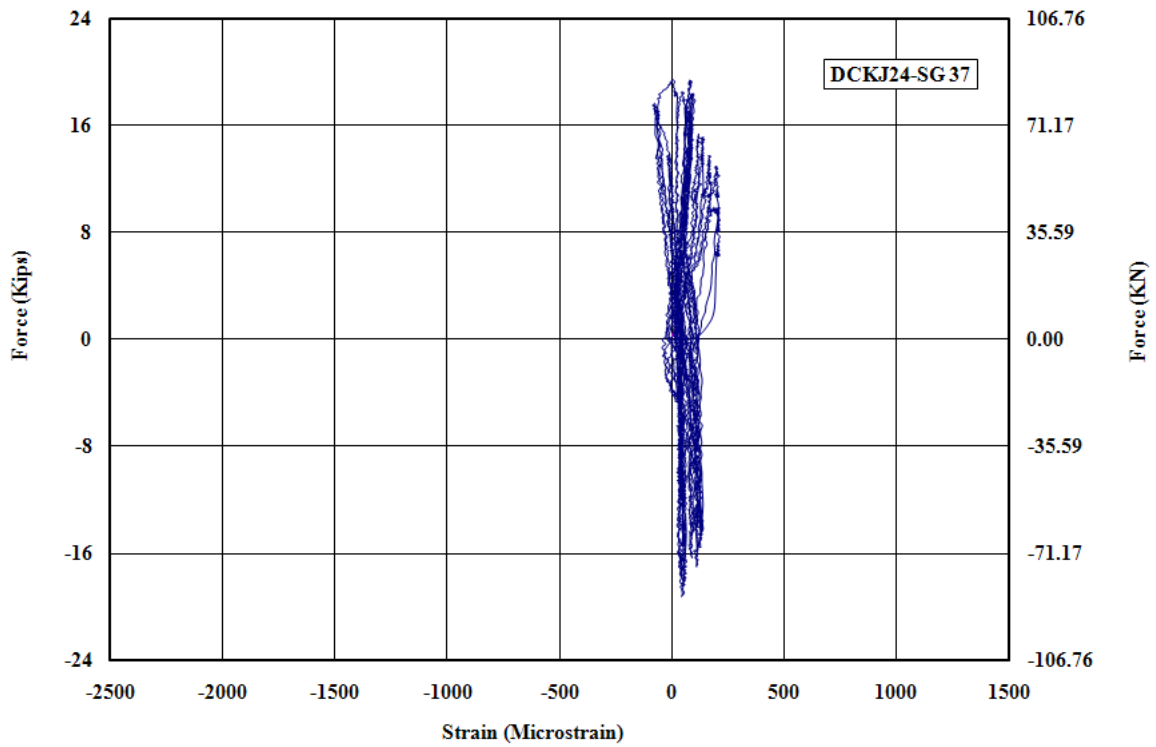

Figure E - 31: Measured Strain in Gauge No.37 for DCKJ24

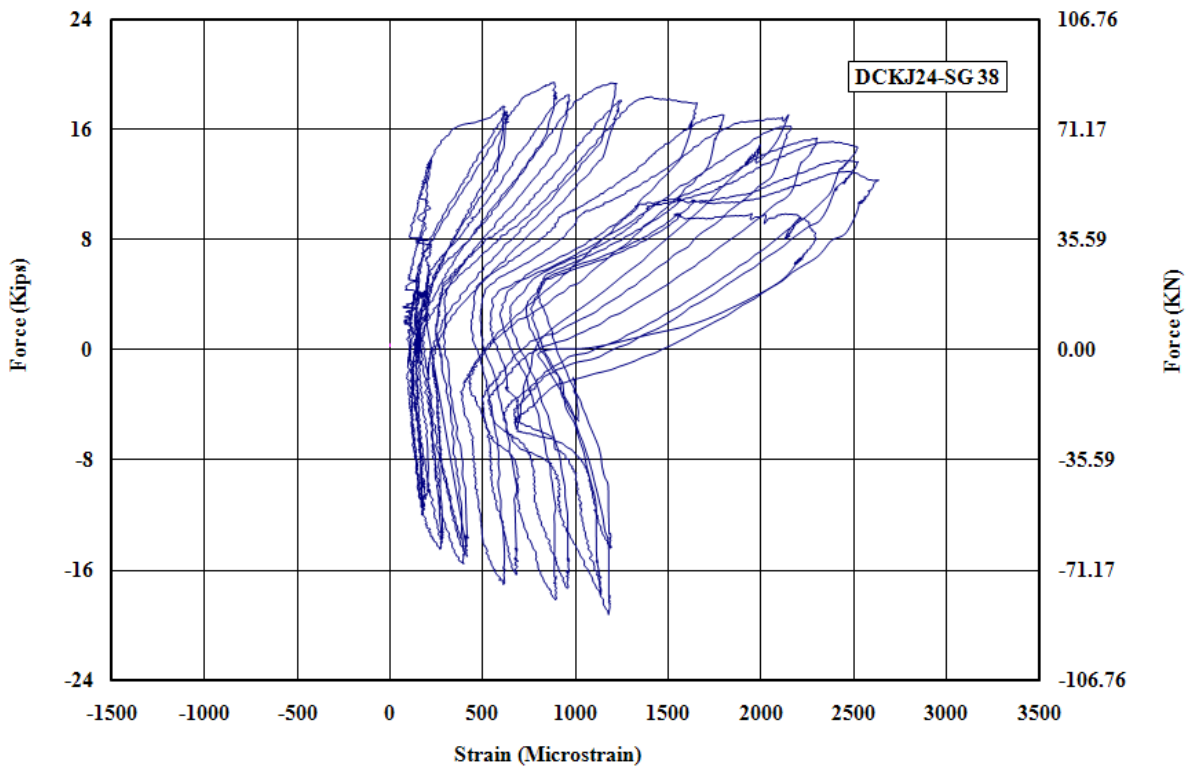

Figure E - 32: Measured Strain in Gauge No.38 for DCKJ24

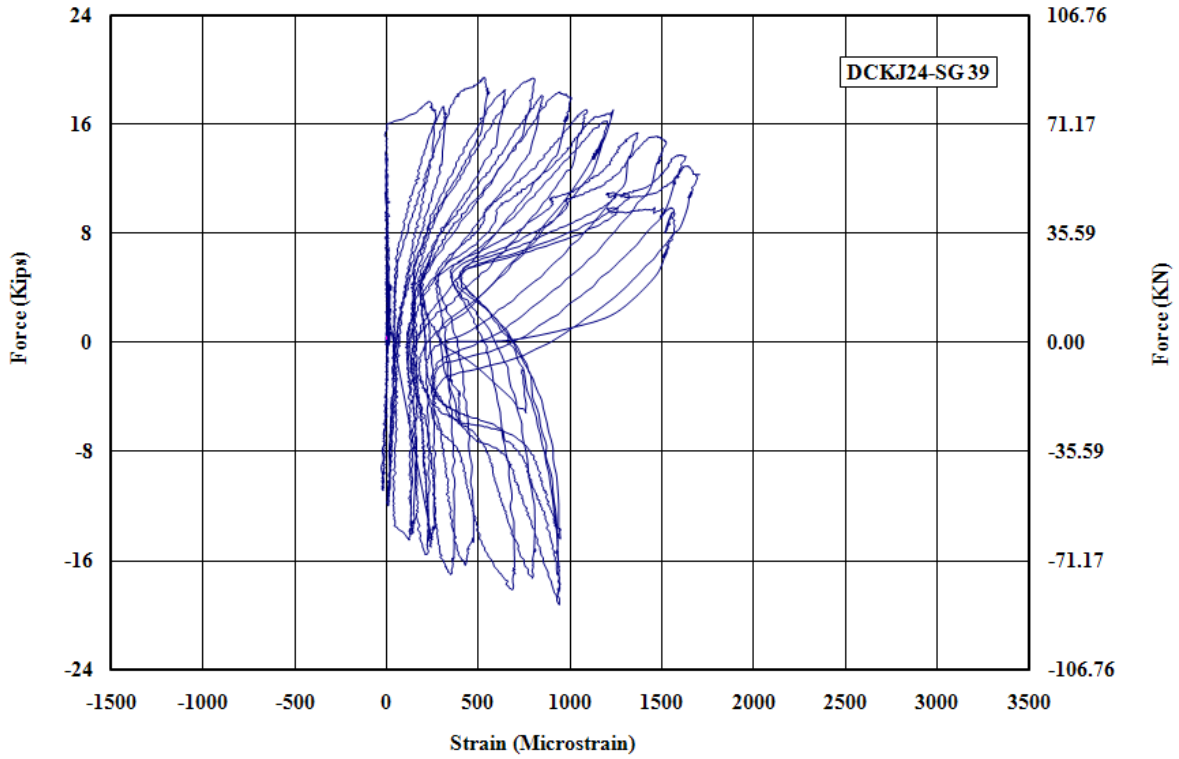

Figure E - 33: Measured Strain in Gauge No.39 for DCKJ24

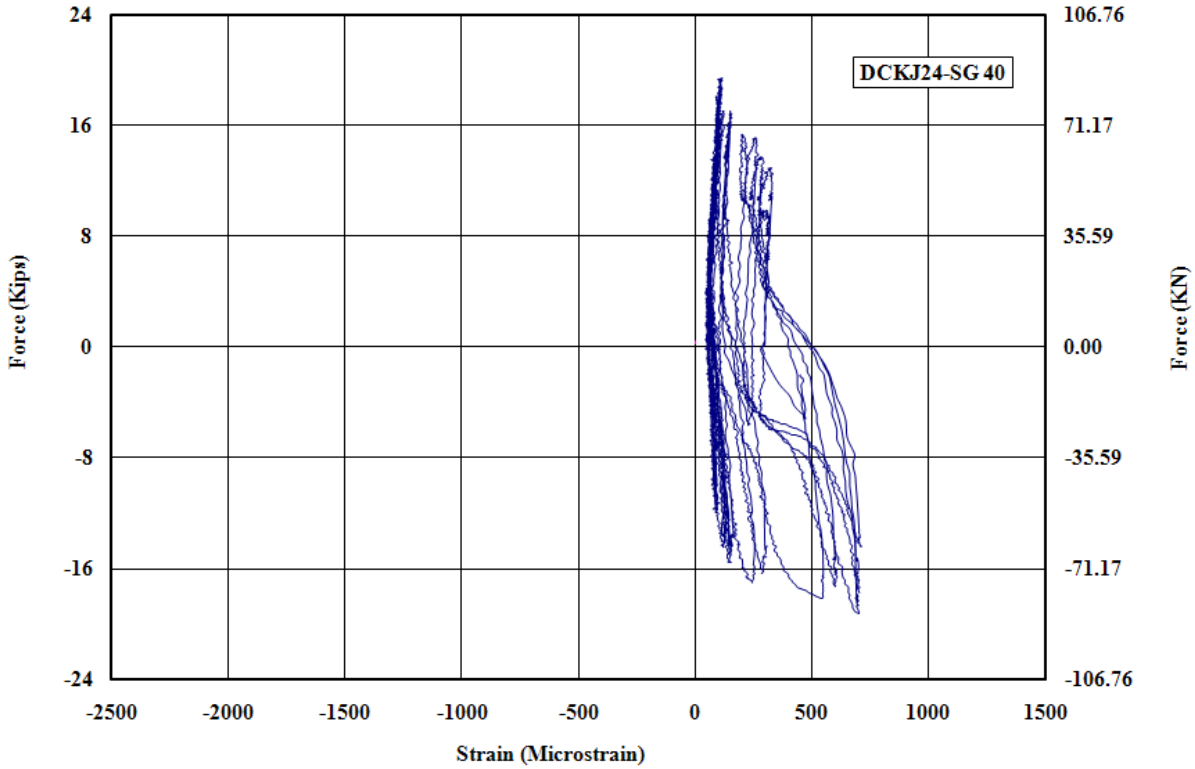

Figure E - 34: Measured Strain in Gauge No.40 for DCKJ24

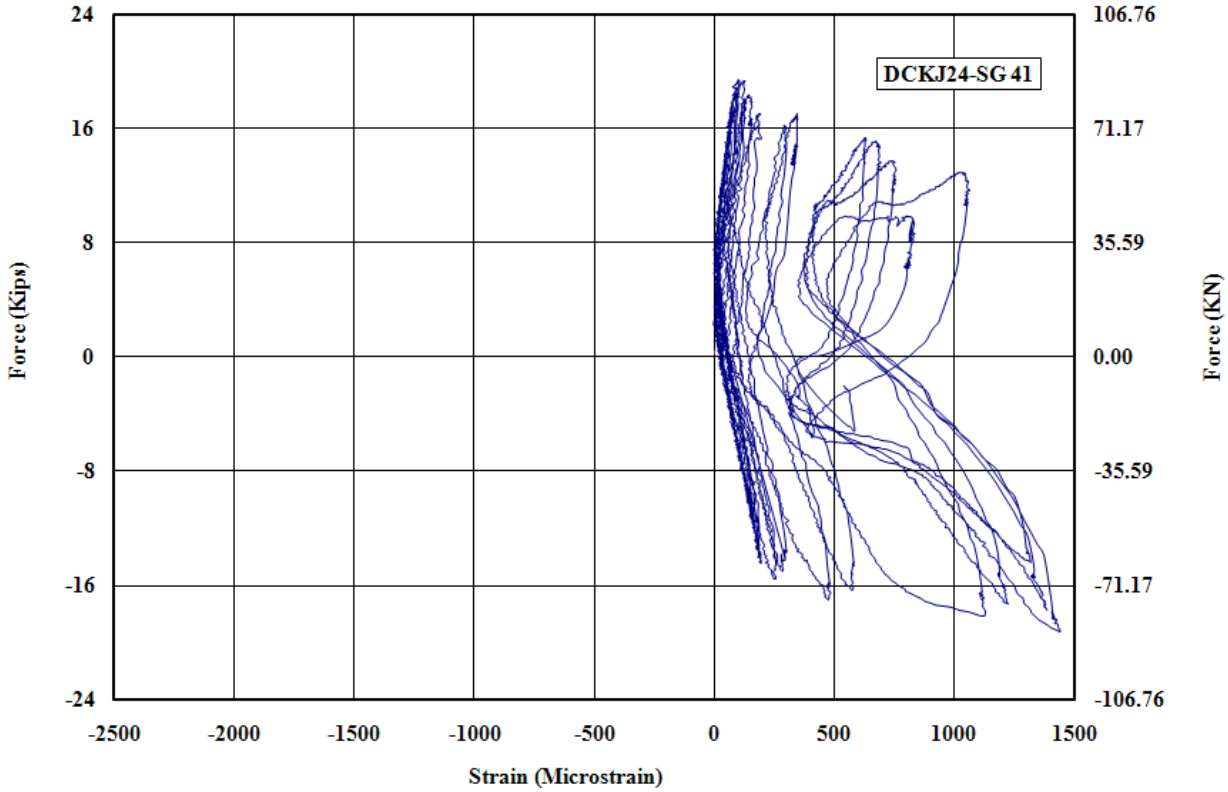

Figure E - 35: Measured Strain in Gauge No.41 for DCKJ24

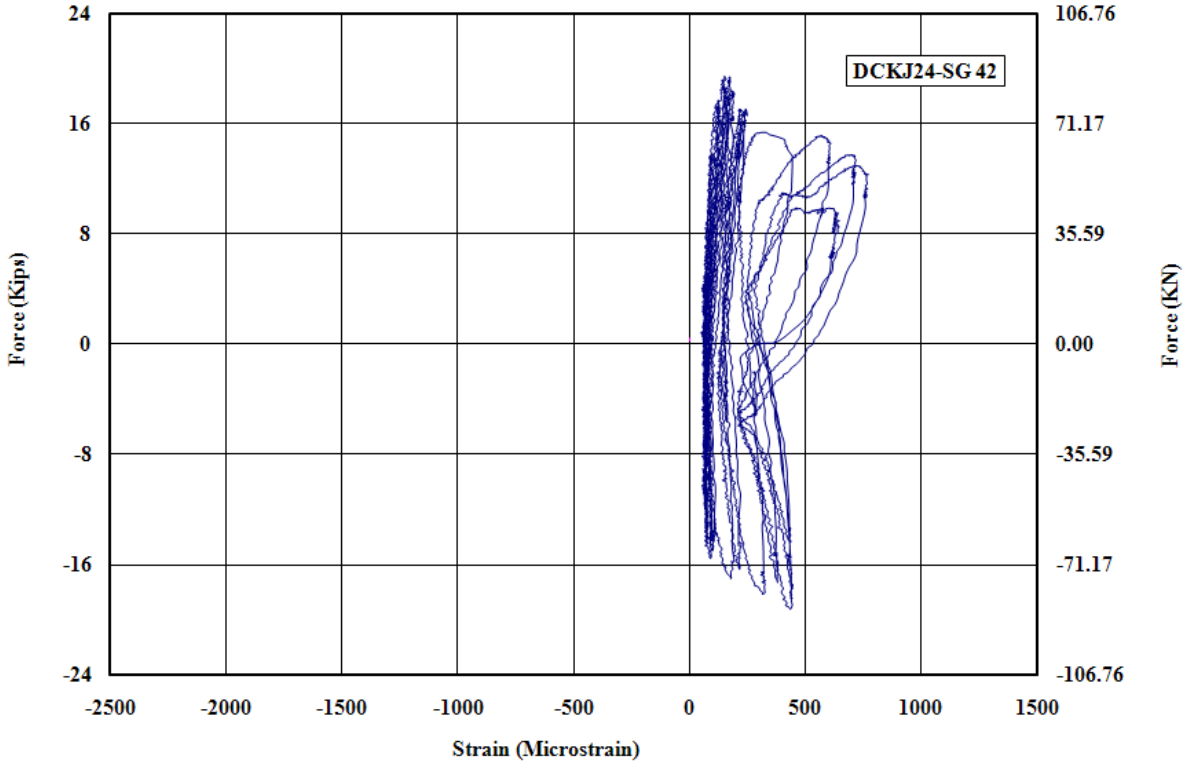

Figure E - 36: Measured Strain in Gauge No.42 for DCKJ24

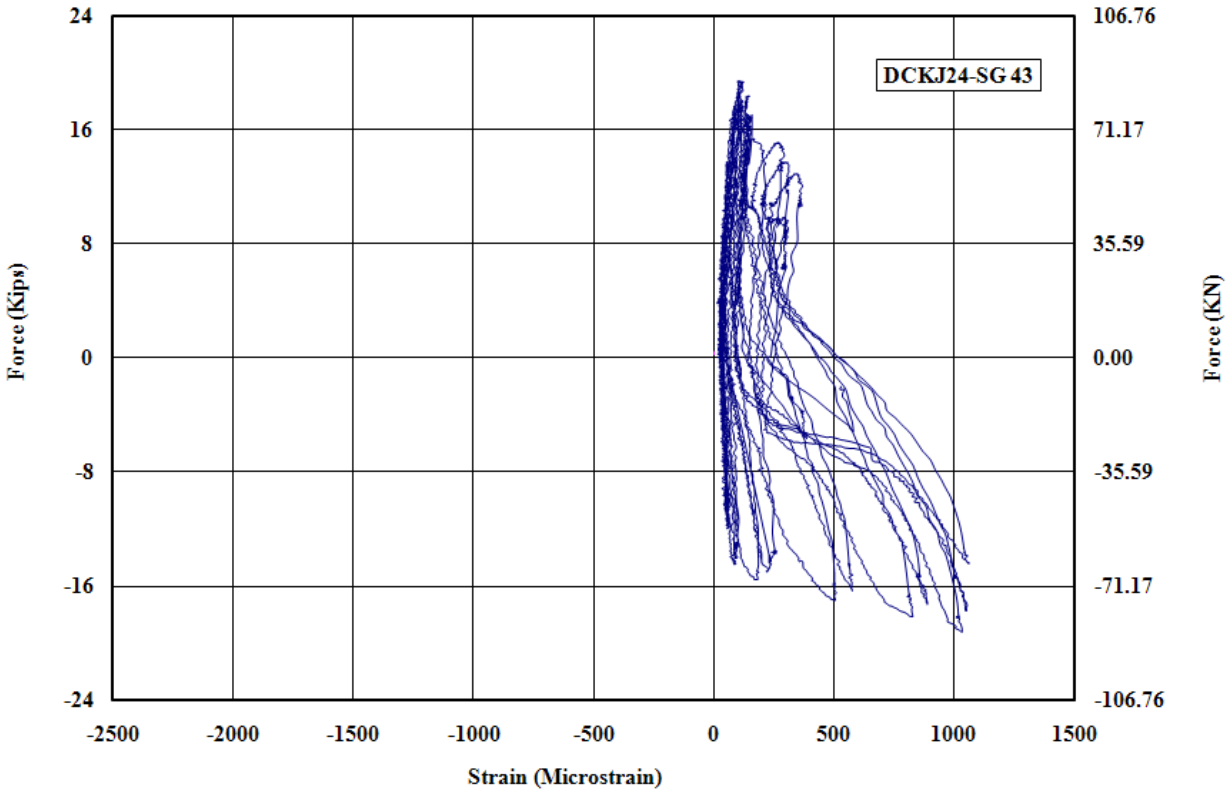

Figure E - 37: Measured Strain in Gauge No.43 for DCKJ24

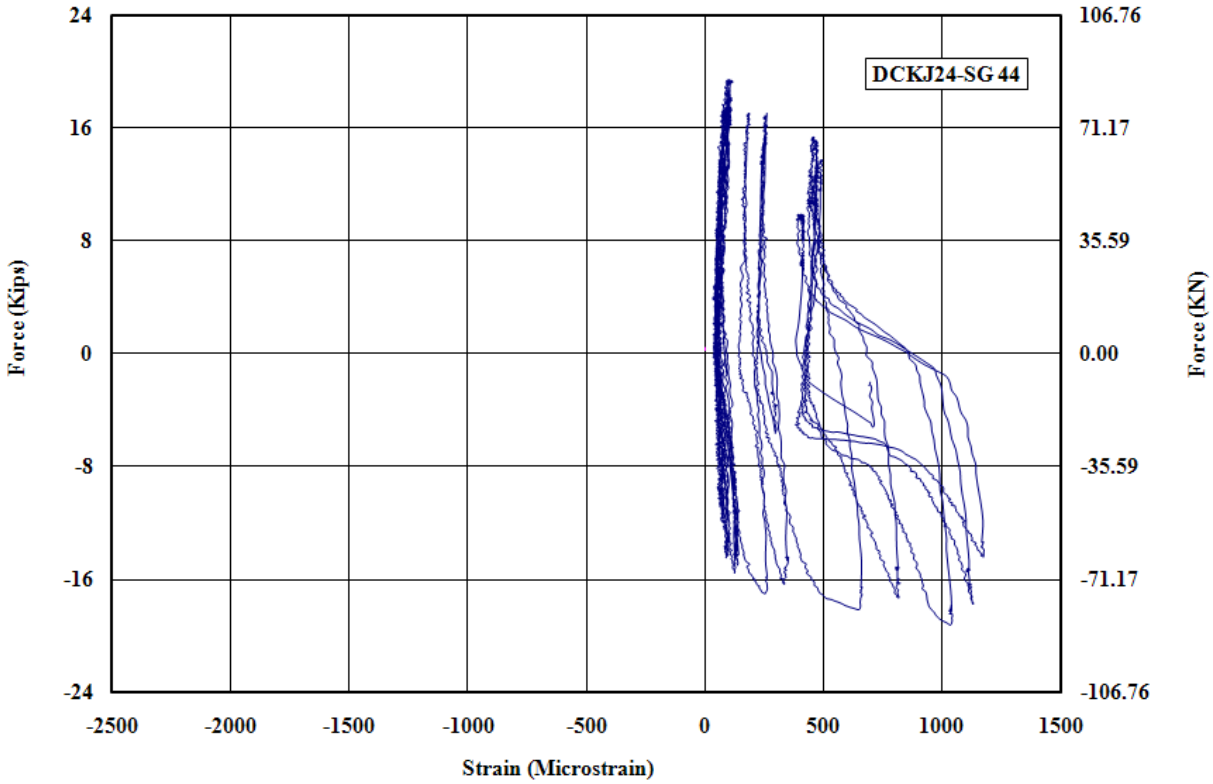

Figure E - 38: Measured Strain in Gauge No.44 for DCKJ24

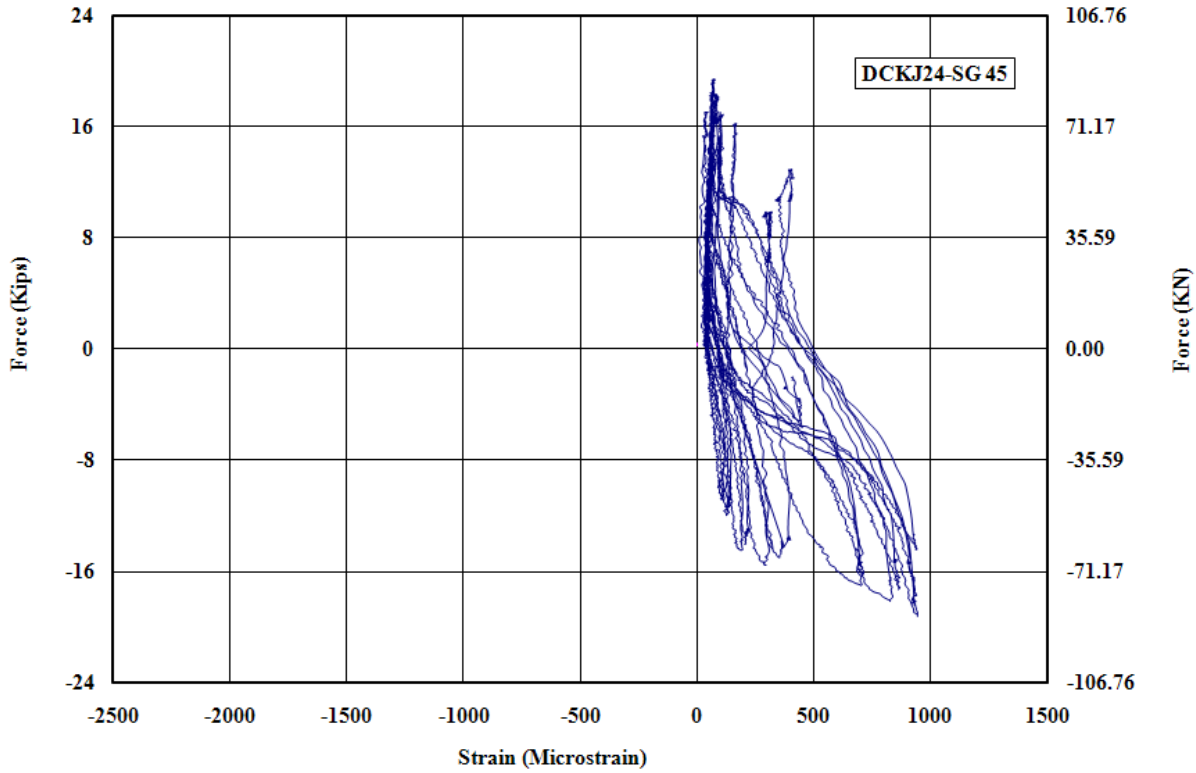

Figure E - 39: Measured Strain in Gauge No.45 for DCKJ24

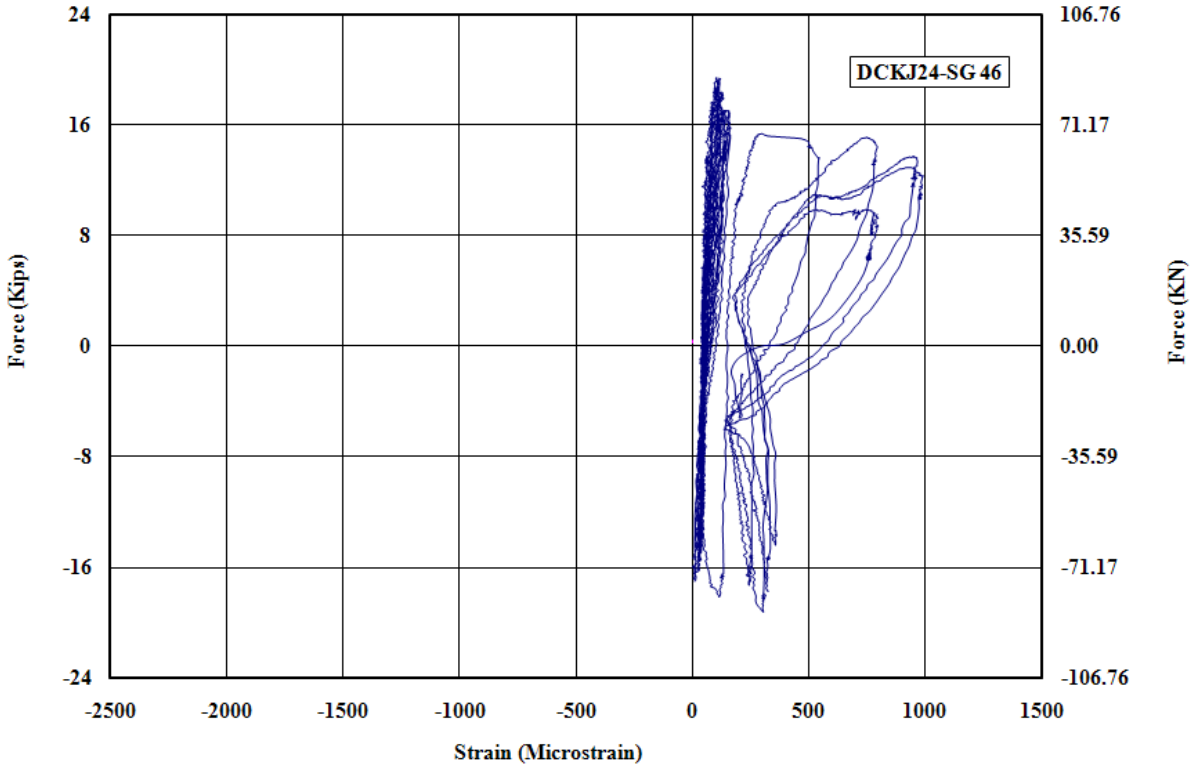

Figure E - 40: Measured Strain in Gauge No.46 for DCKJ24

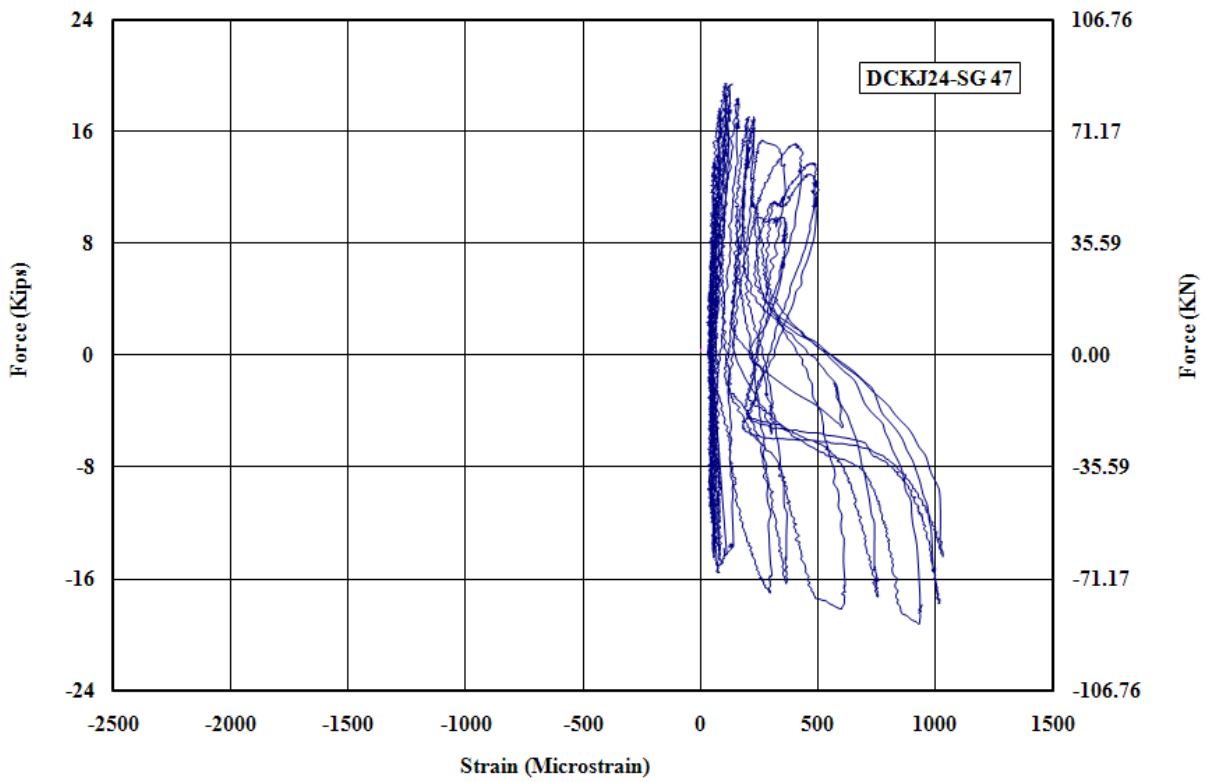

Figure E - 41: Measured Strain in Gauge No.47 for DCKJ24

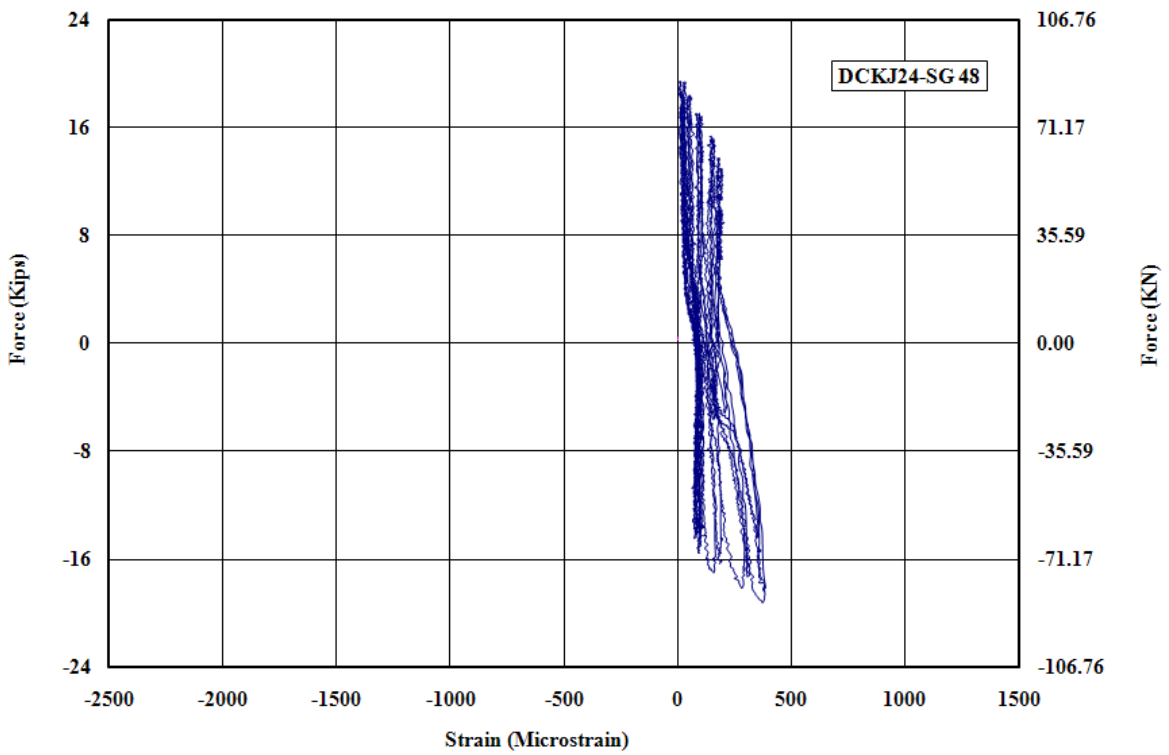

Figure E - 42: Measured Strain in Gauge No.48 for DCKJ24

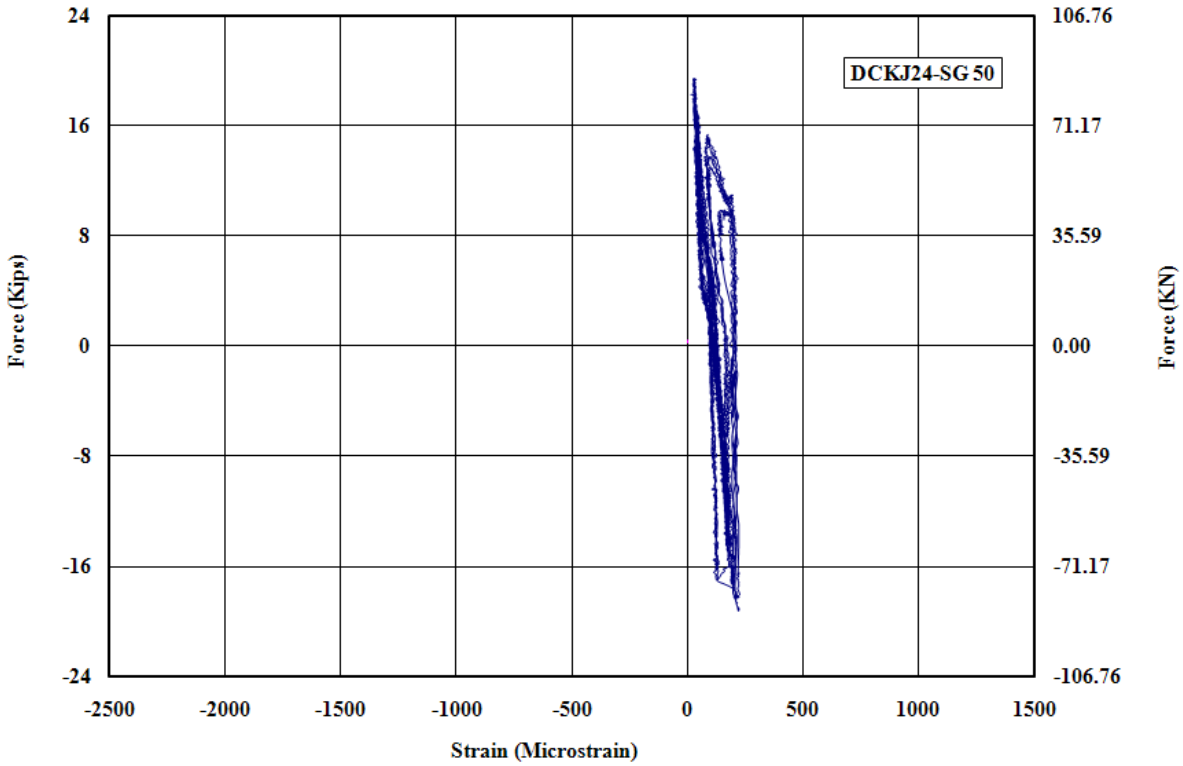

Figure E - 43: Measured Strain in Gauge No.50 for DCKJ24

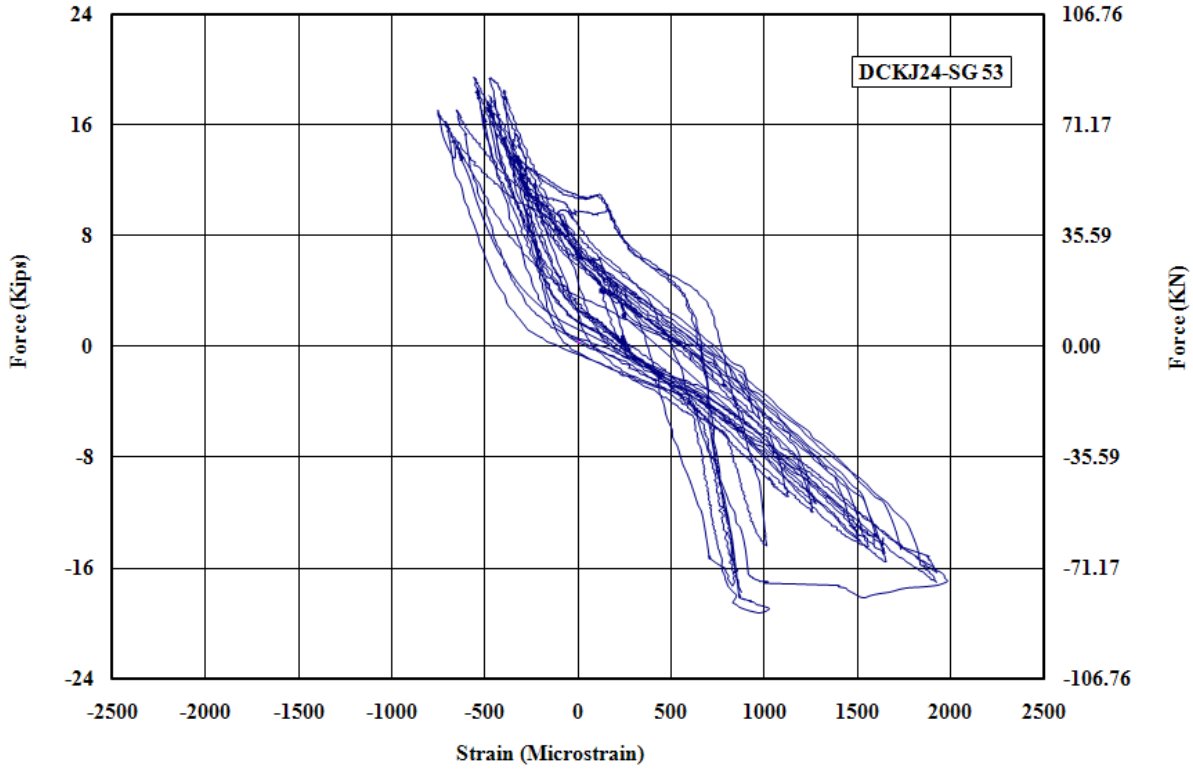

Figure E - 44: Measured Strain in Gauge No.53 for DCKJ24

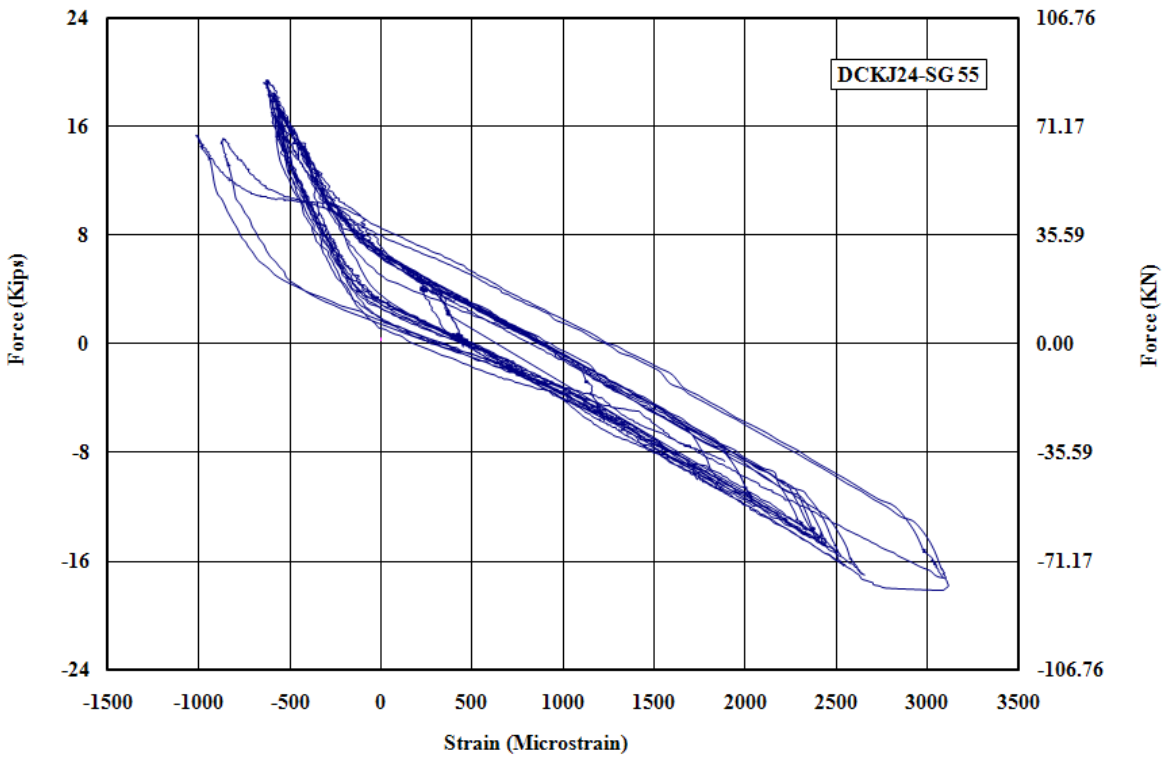

Figure E - 45: Measured Strain in Gauge No.55 for DCKJ24

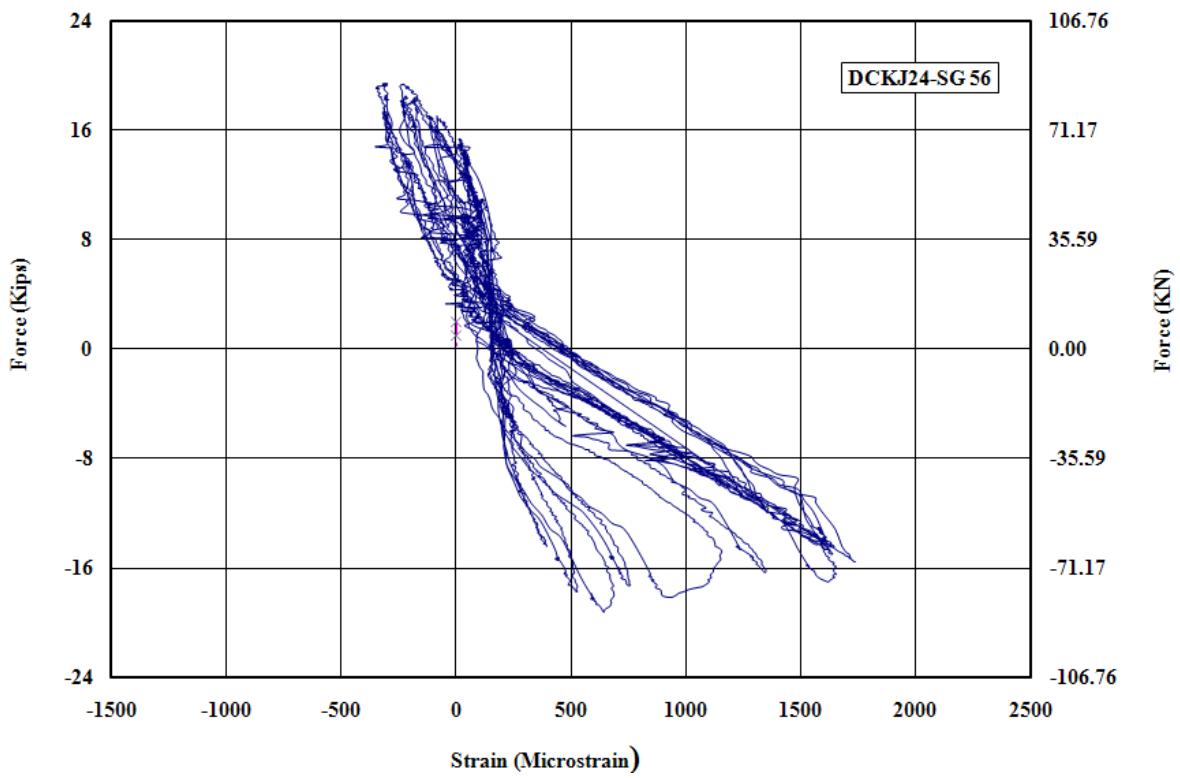

Figure E - 46: Measured Strain in Gauge No.56 for DCKJ24

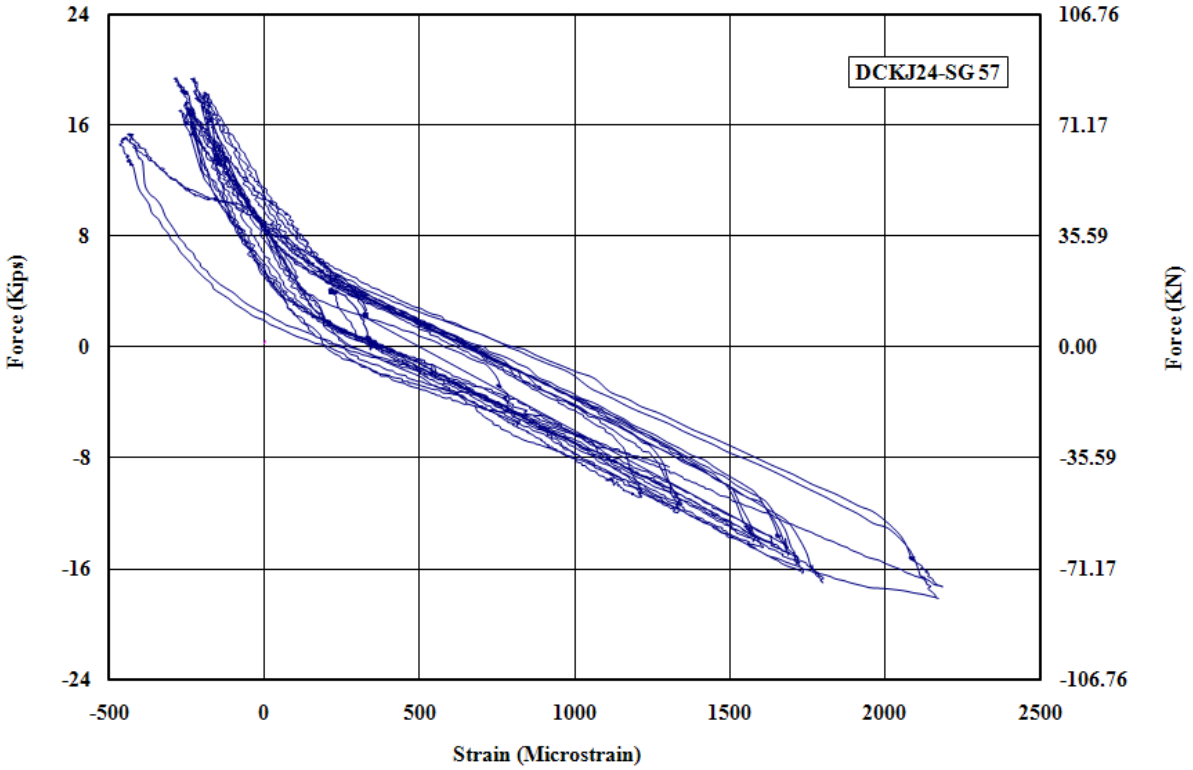

Figure E - 47: Measured Strain in Gauge No.57 for DCKJ24

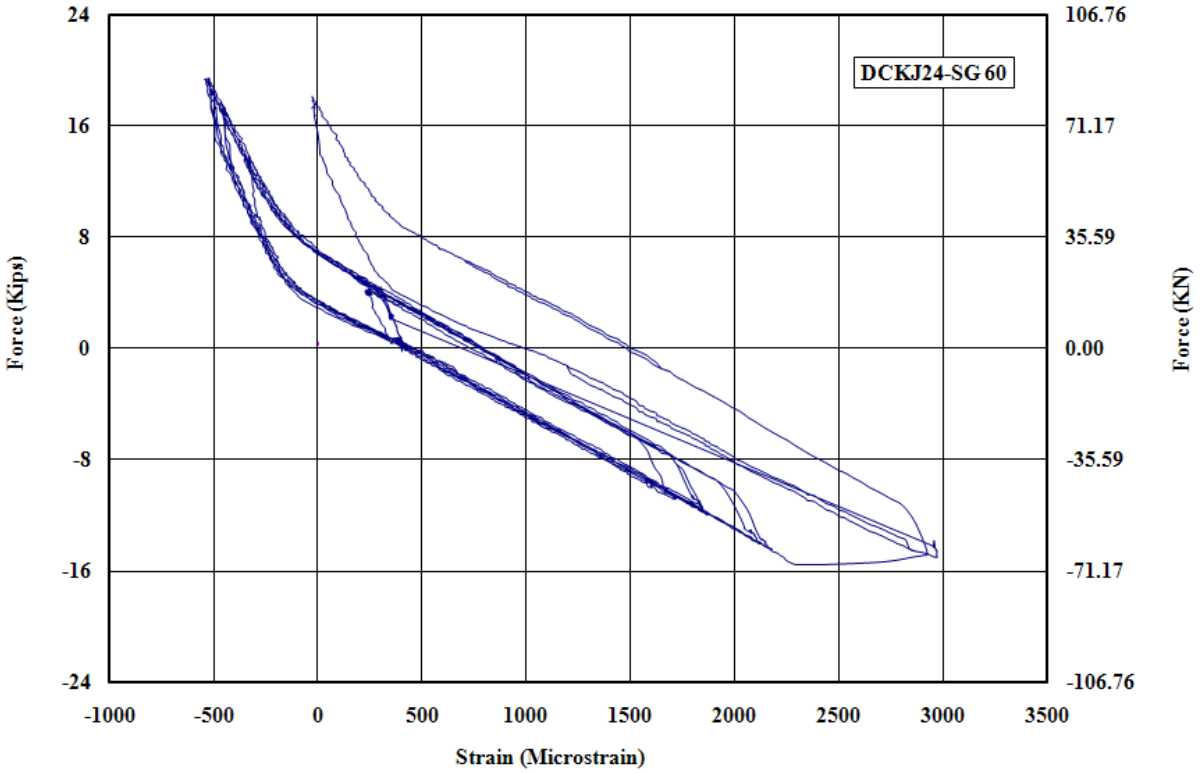

Figure E - 48: Measured Strain in Gauge No.60 for DCKJ24

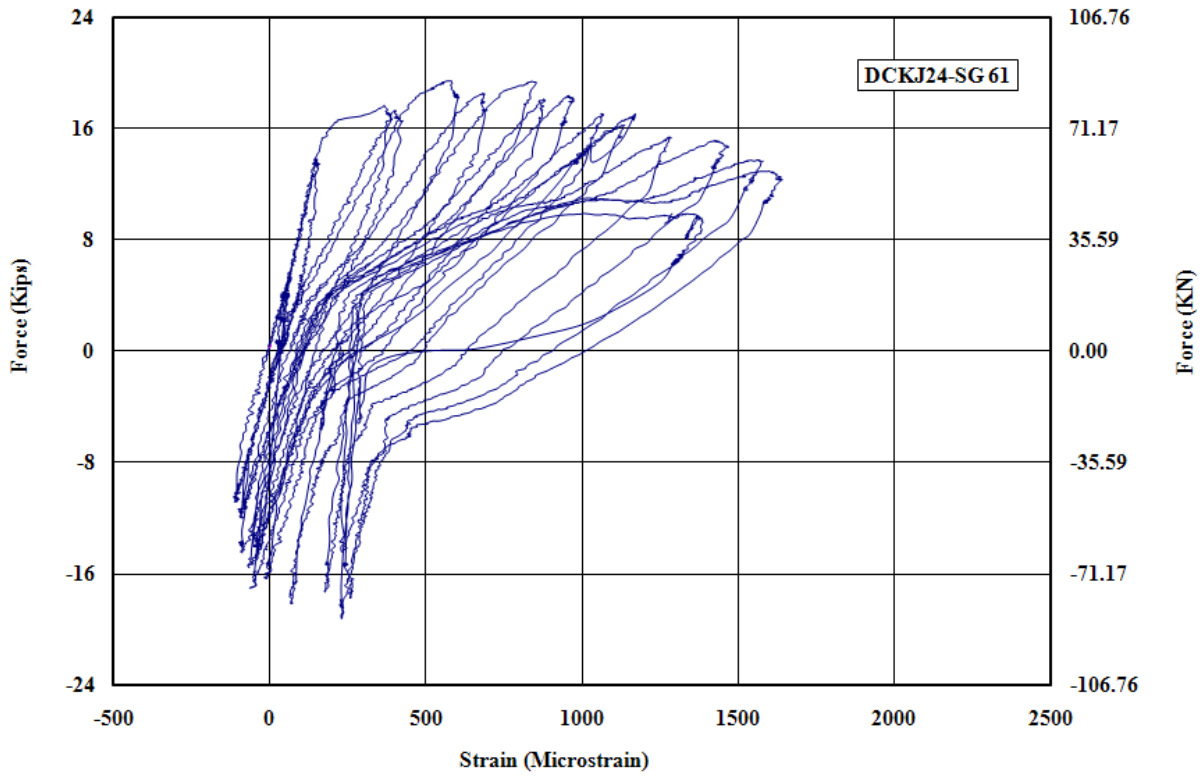

Figure E - 49: Measured Strain in Gauge No.61 for DCKJ24

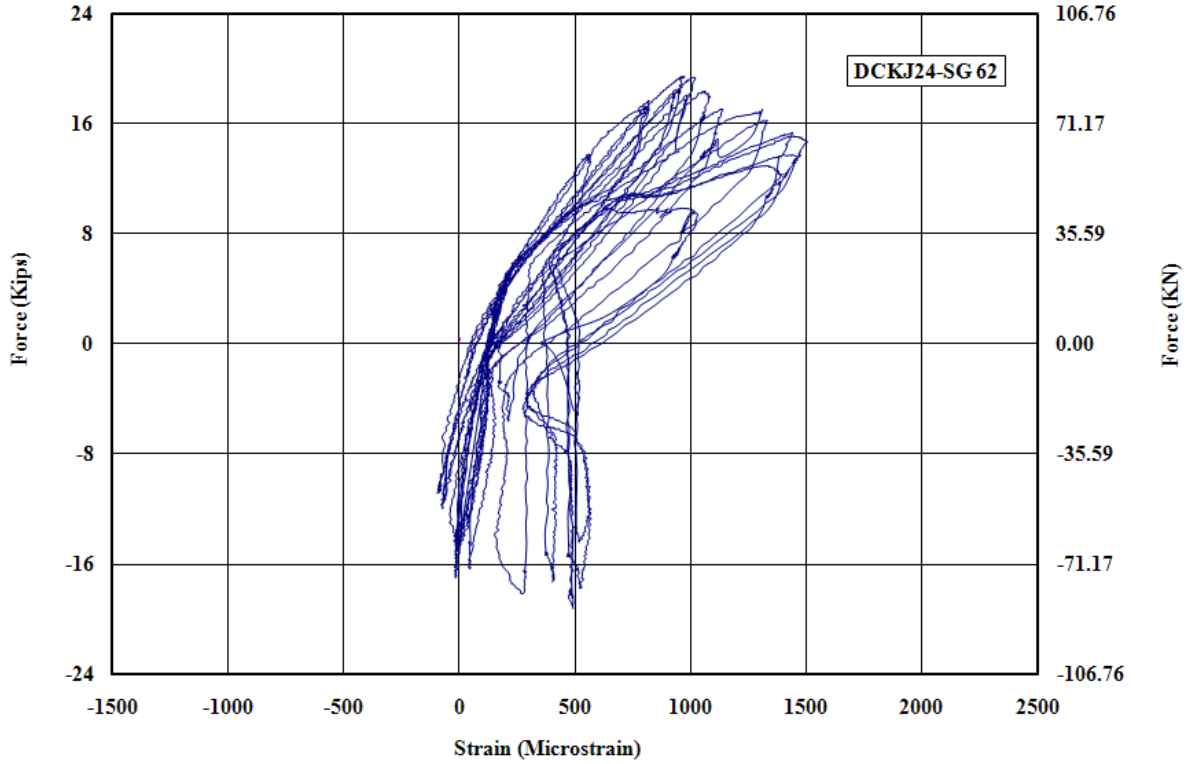

Figure E - 50: Measured Strain in Gauge No.62 for DCKJ24

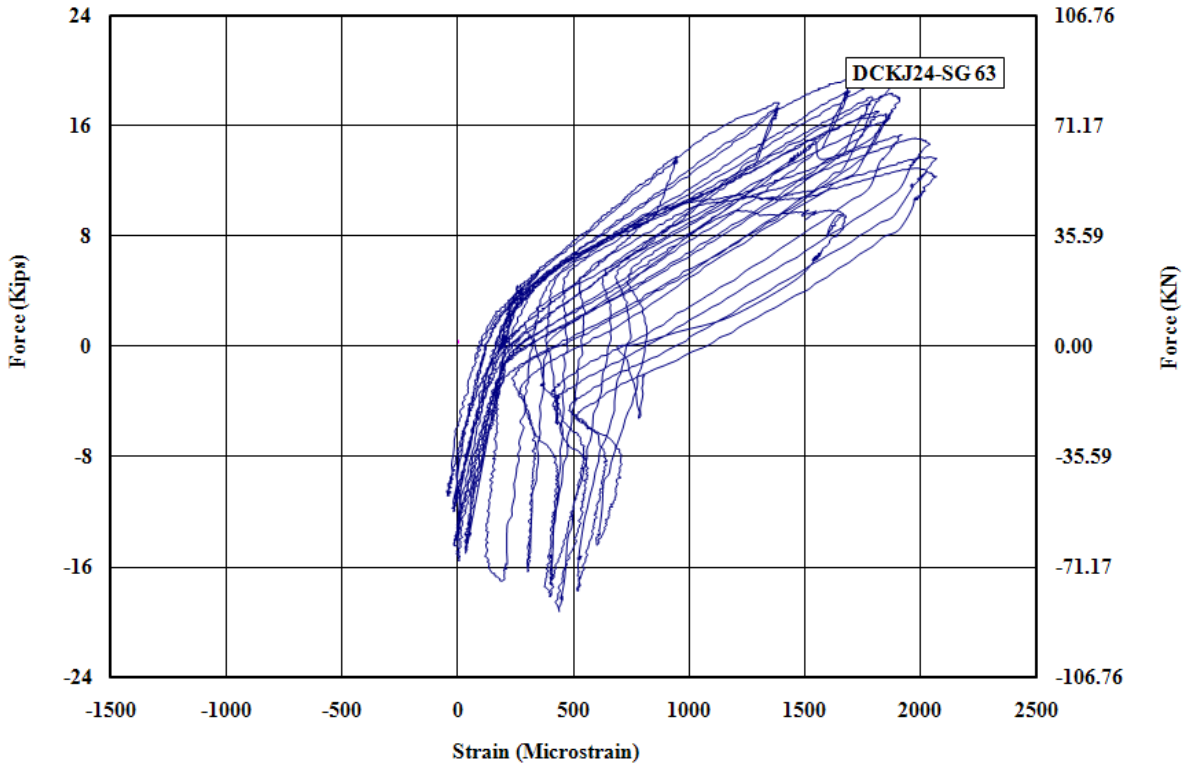

Figure E - 51: Measured Strain in Gauge No.63 for DCKJ24

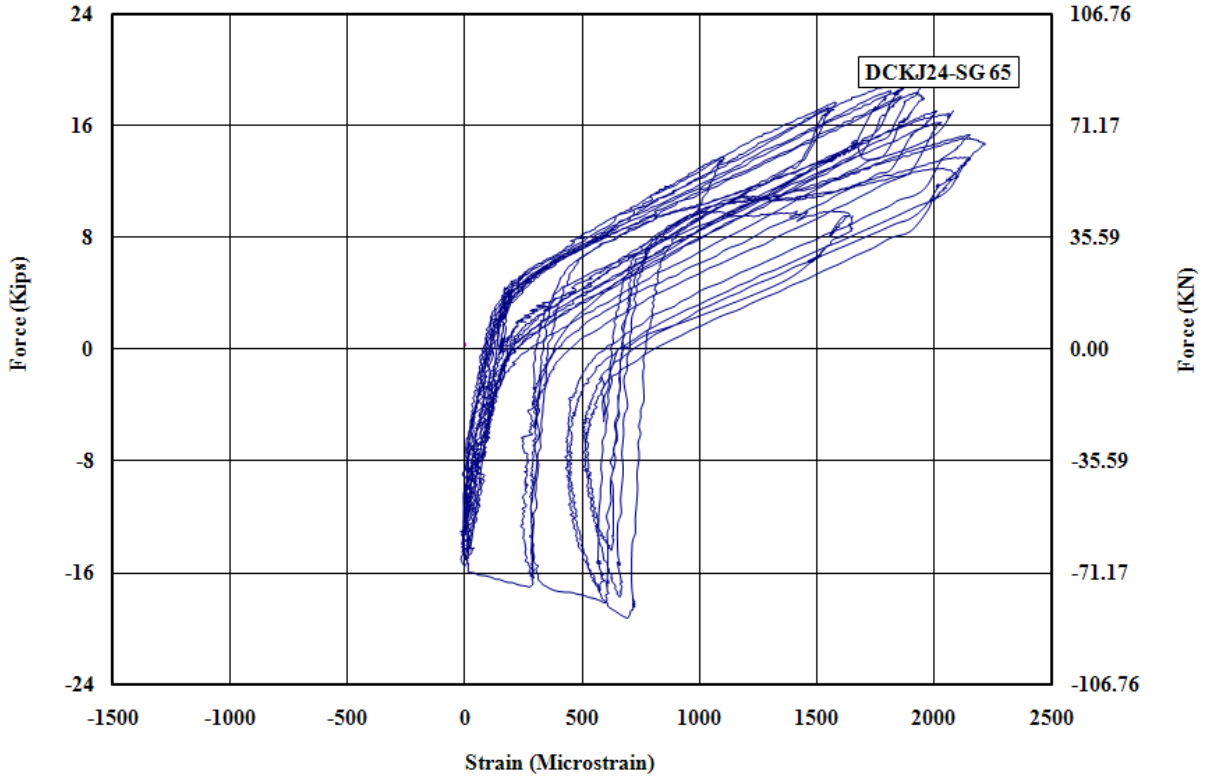

Figure E - 52: Measured Strain in Gauge No.65 for DCKJ24

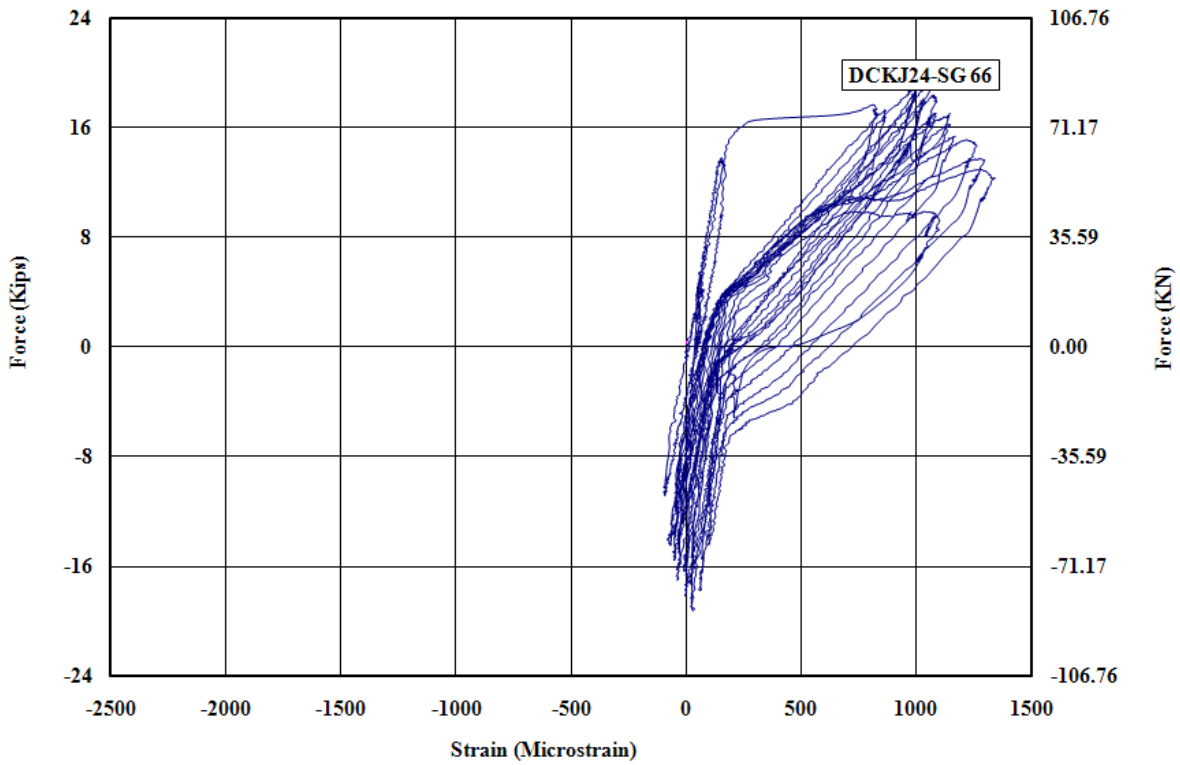

Figure E - 53: Measured Strain in Gauge No.66 for DCKJ24

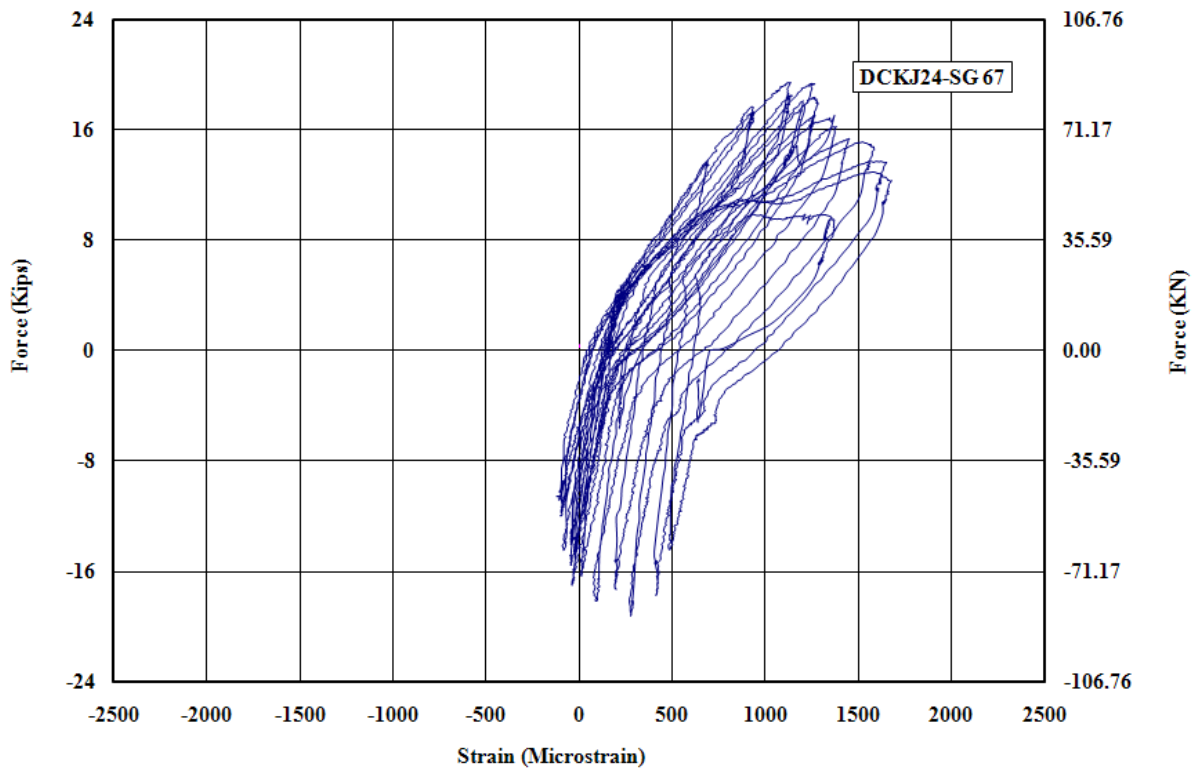

Figure E - 54: Measured Strain in Gauge No.67 for DCKJ24

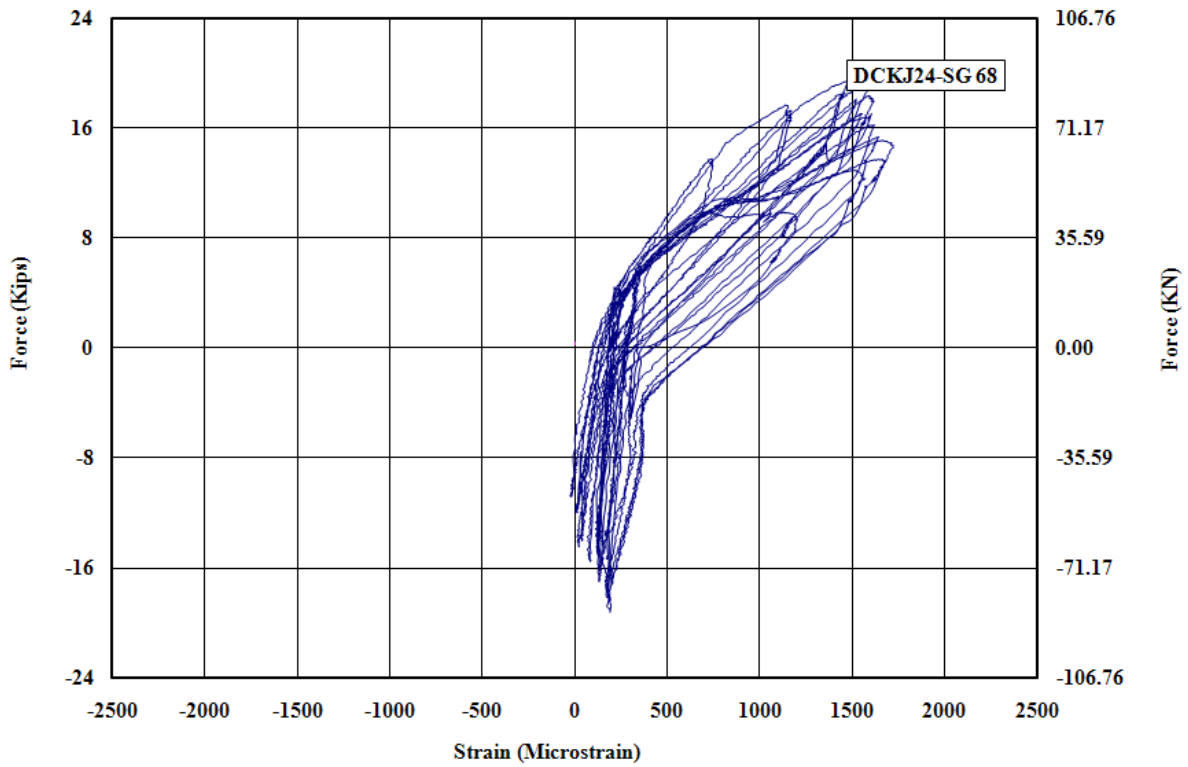

Figure E - 55: Measured Strain in Gauge No.68 for DCKJ24

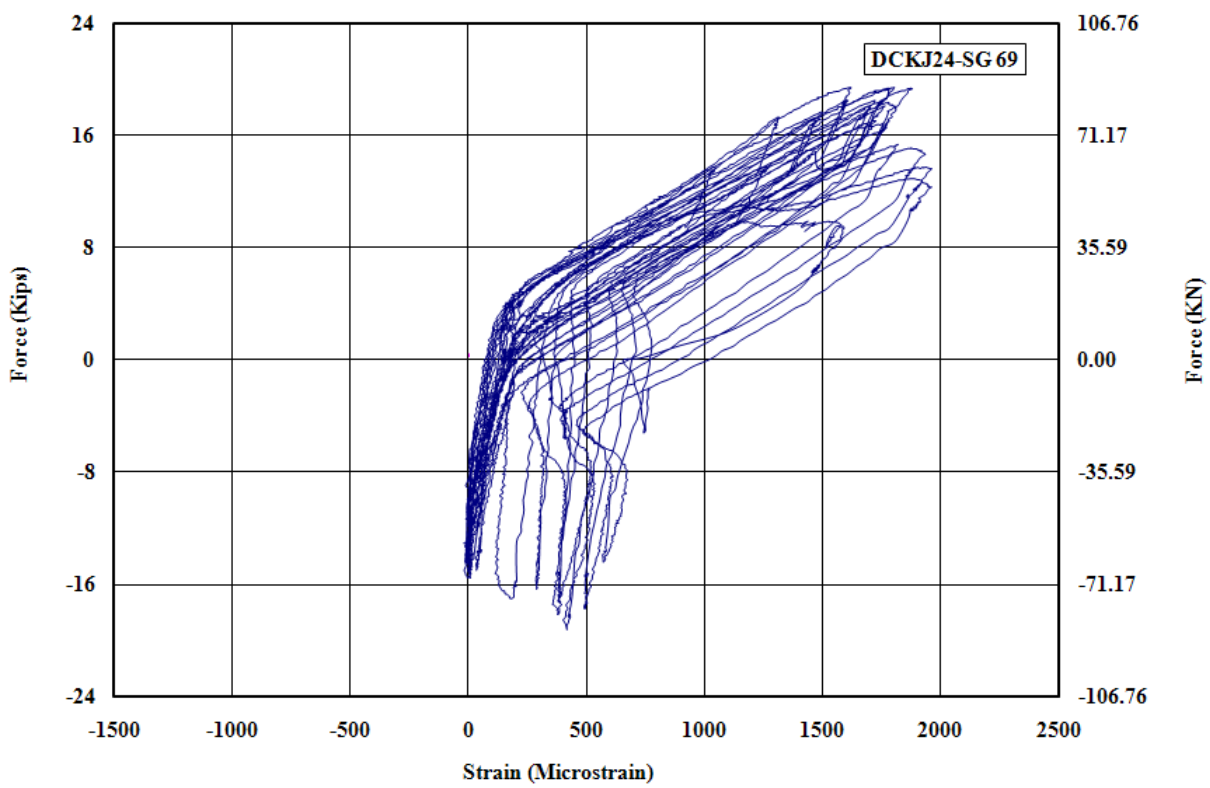

Figure E - 56: Measured Strain in Gauge No.69 for DCKJ24

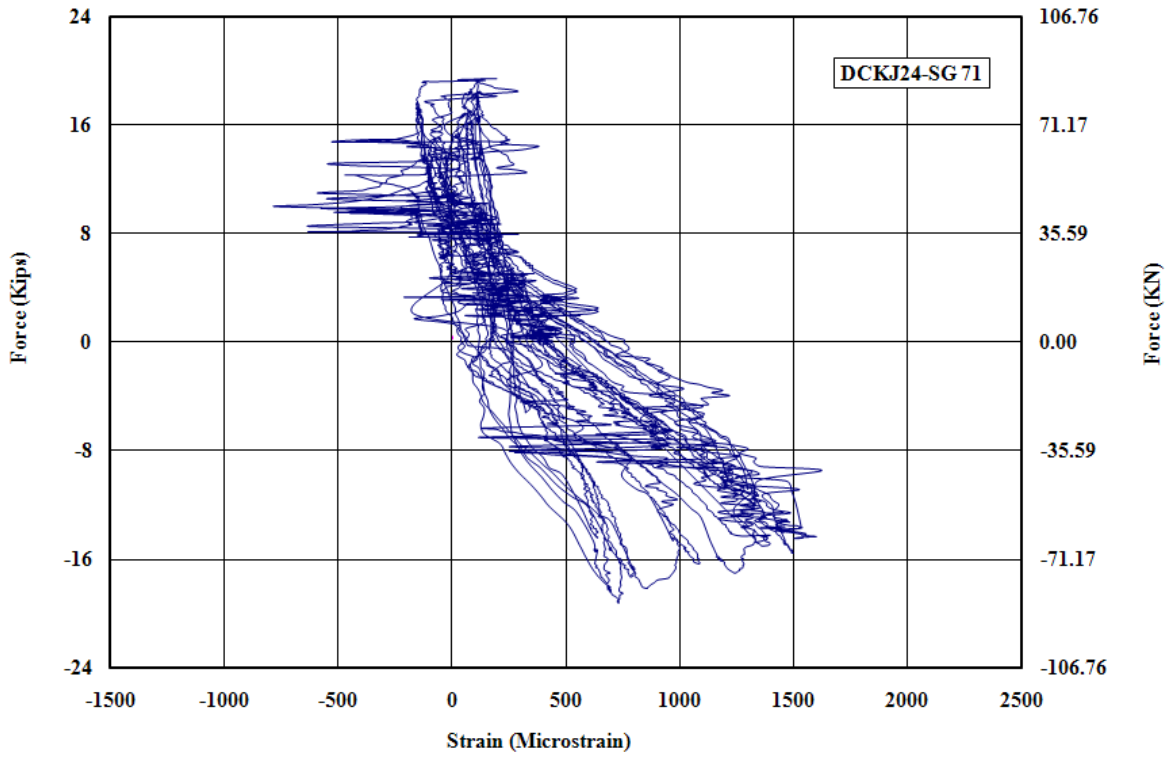

Figure E - 57: Measured Strain in Gauge No.71 for DCKJ24

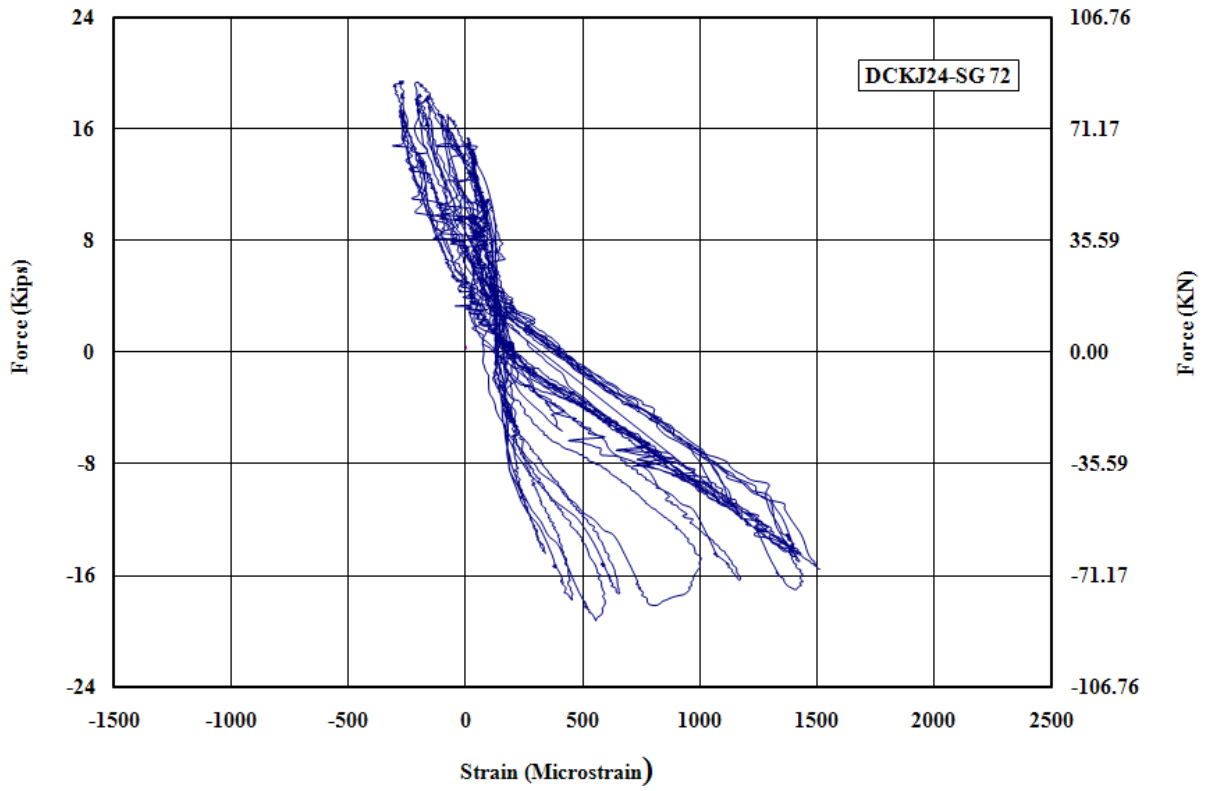

Figure E - 58: Measured Strain in Gauge No.72 for DCKJ24

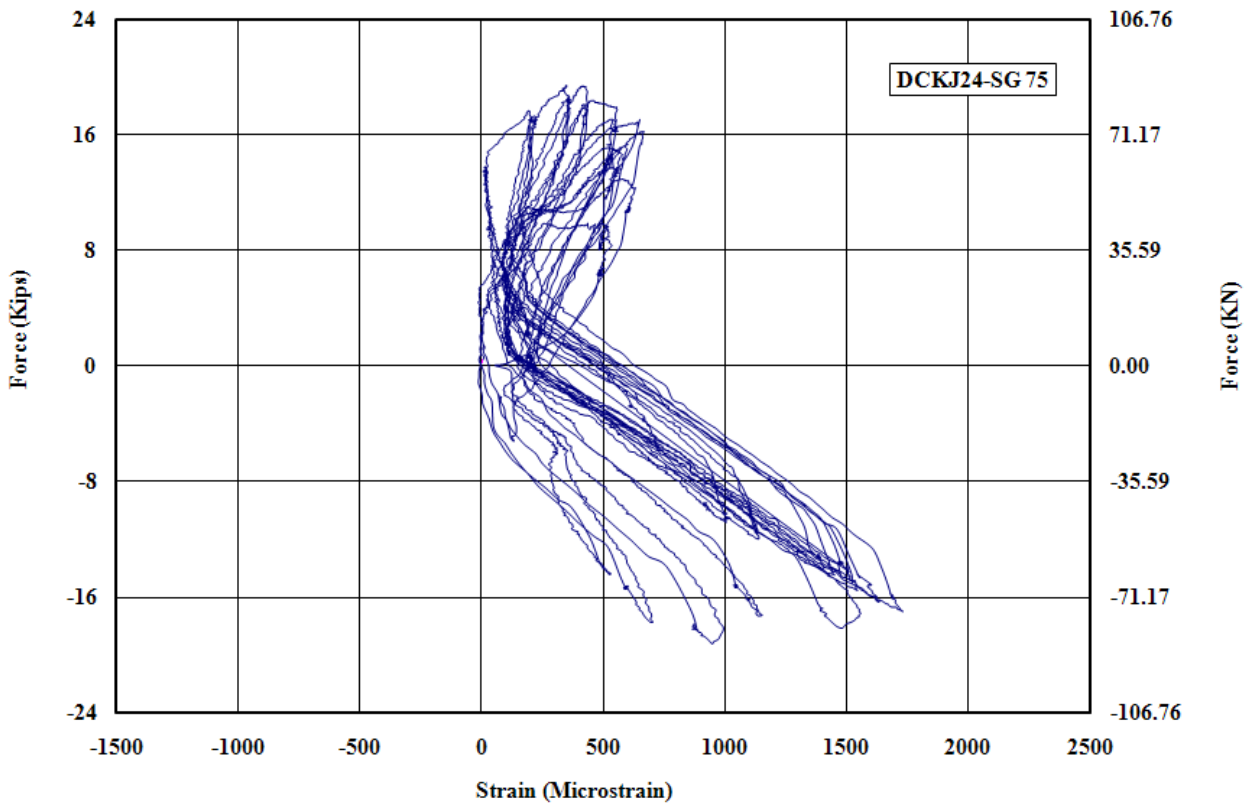

Figure E - 59: Measured Strain in Gauge No.75 for DCKJ24

Appendix F

Specimen FSKJ24

(Flat-Slab Knee-Joint with 24-in. diameter pile)

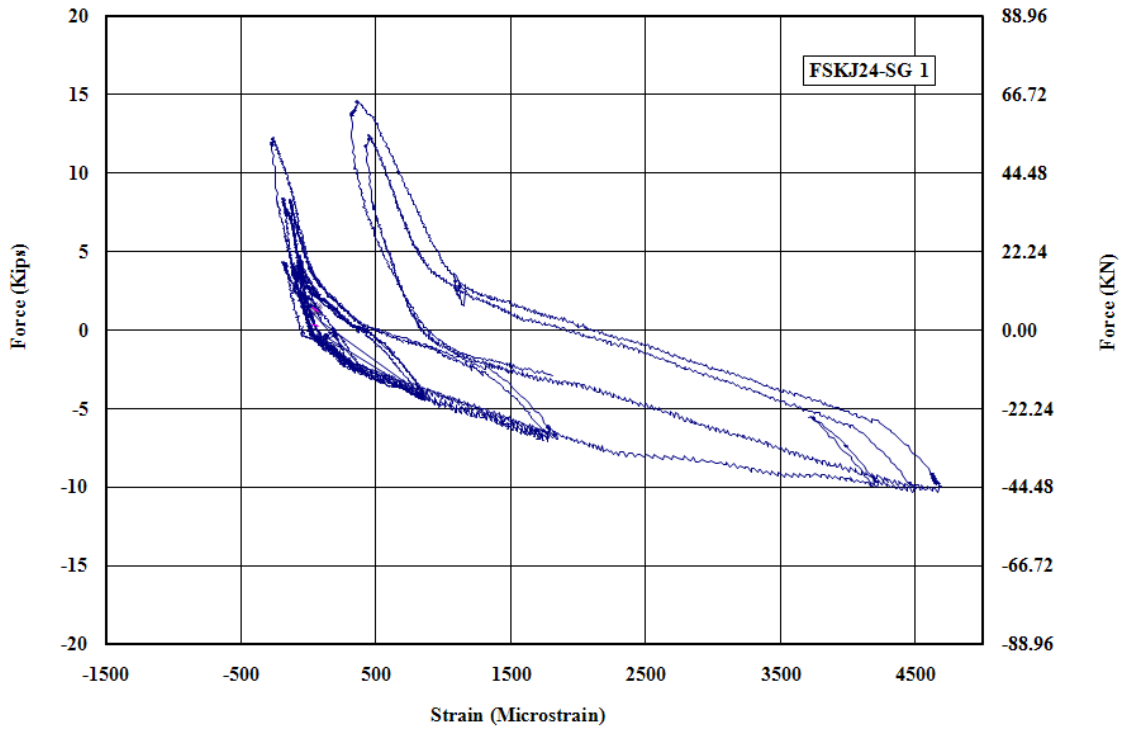

Figure F - 1: Measured Strain in Gauge No.1 for FSKJ24

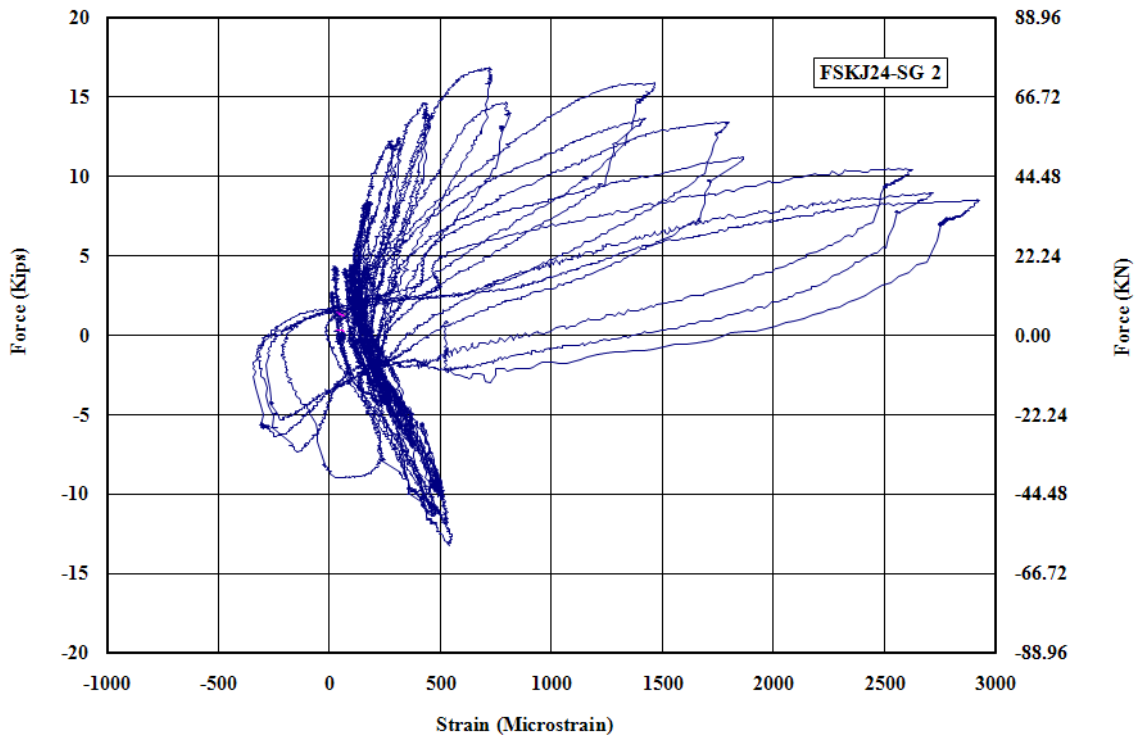

Figure F - 2: Measured Strain in Gauge No.2 for FSKJ24

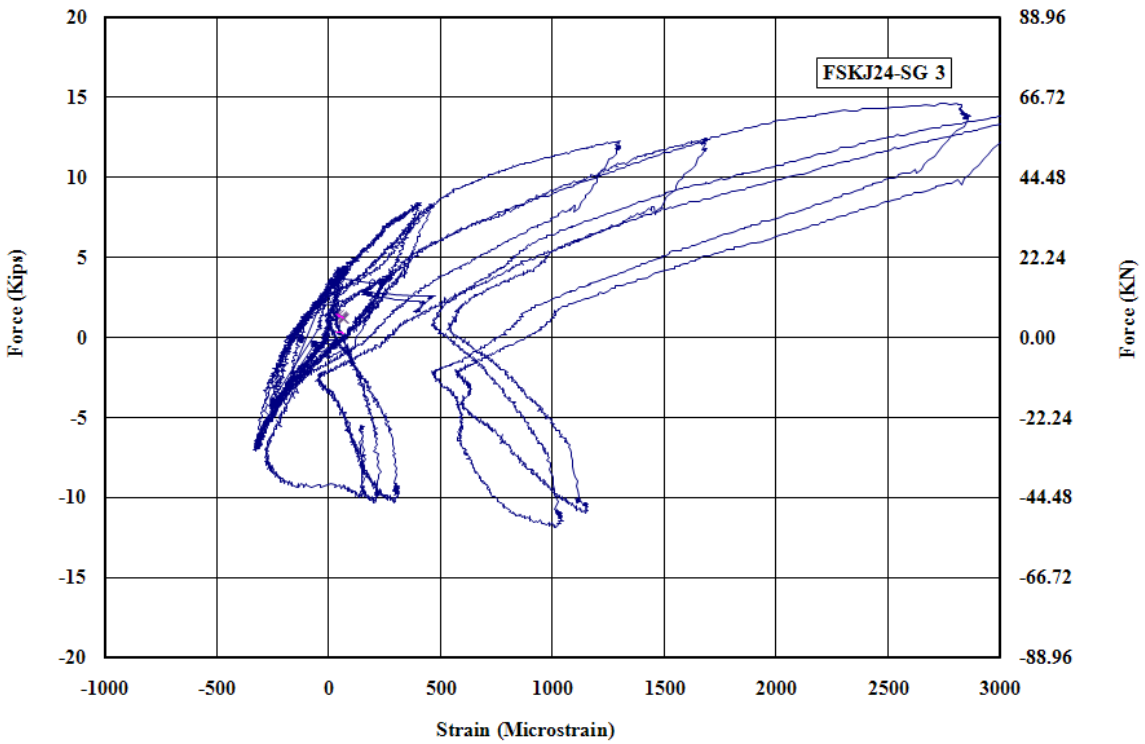

Figure F - 3: Measured Strain in Gauge No.3 for FSKJ24

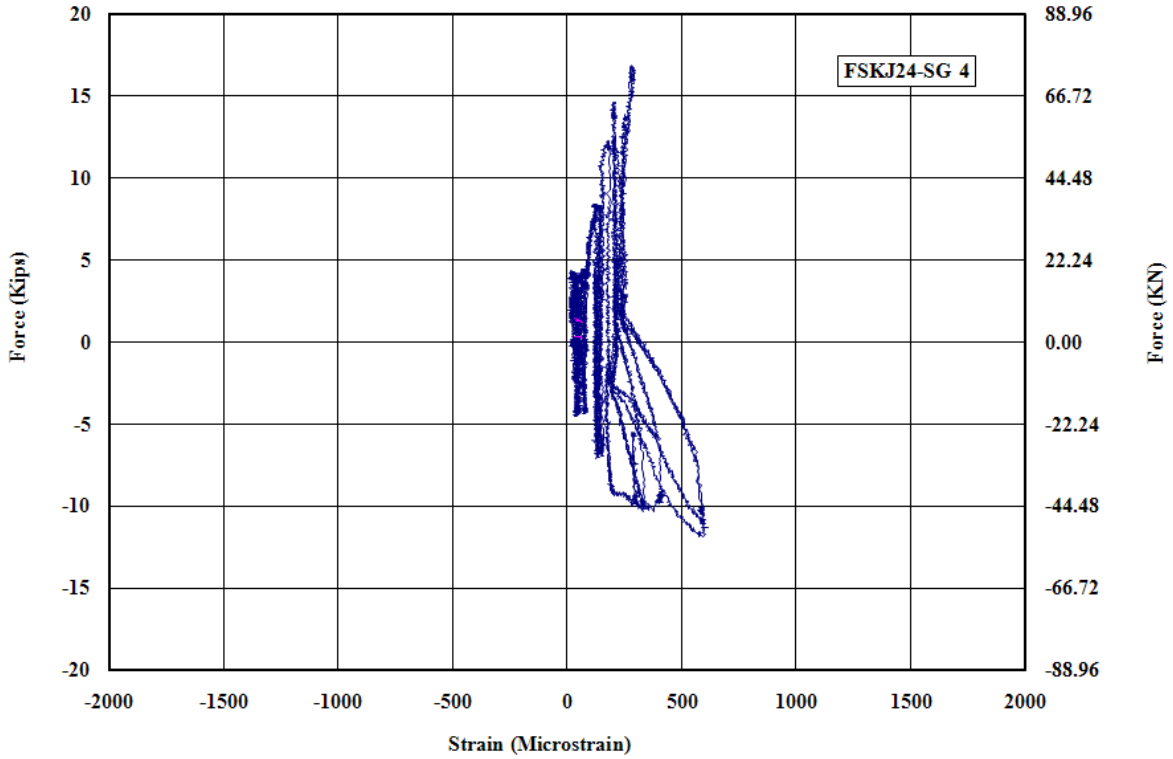

Figure F - 4: Measured Strain in Gauge No.4 for FSKJ24

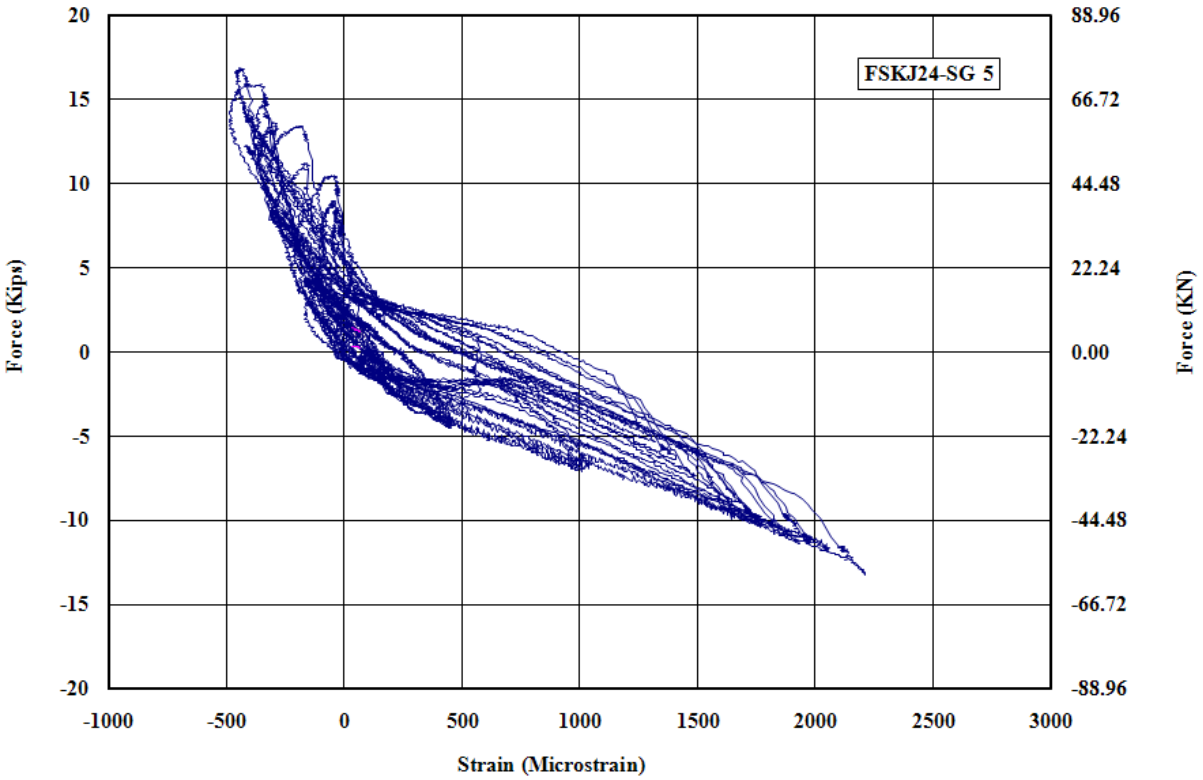

Figure F - 5: Measured Strain in Gauge No.5 for FSKJ24

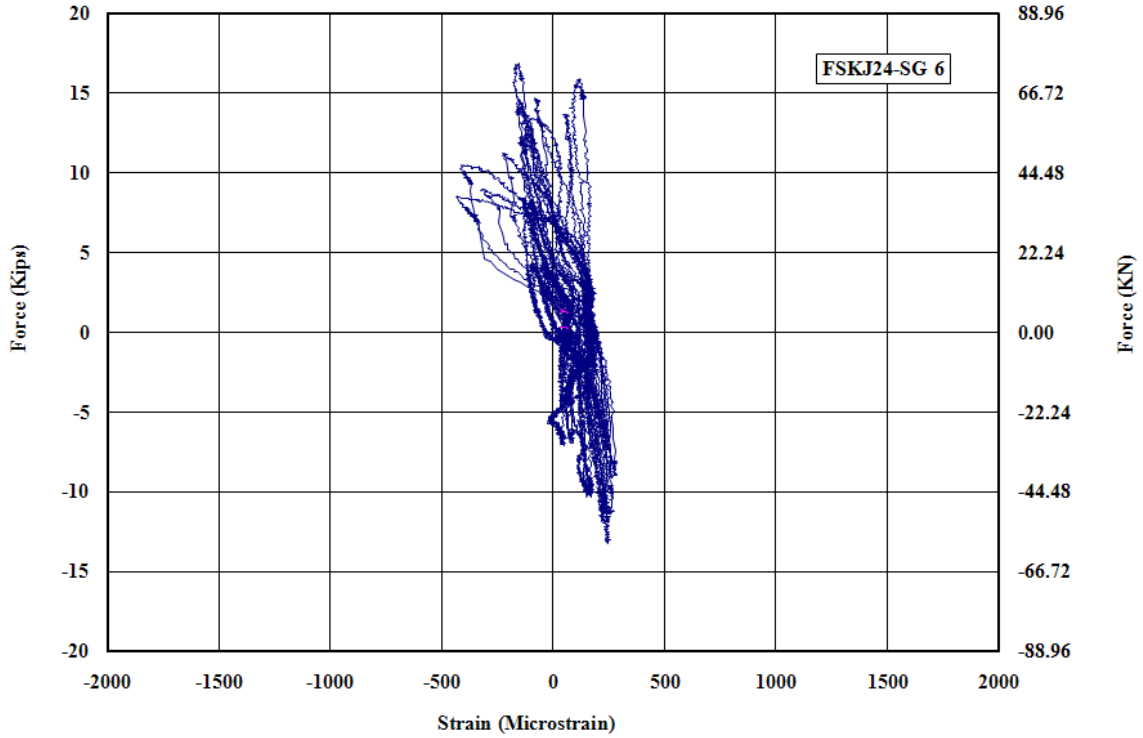

Figure F - 6: Measured Strain in Gauge No.6 for FSKJ24

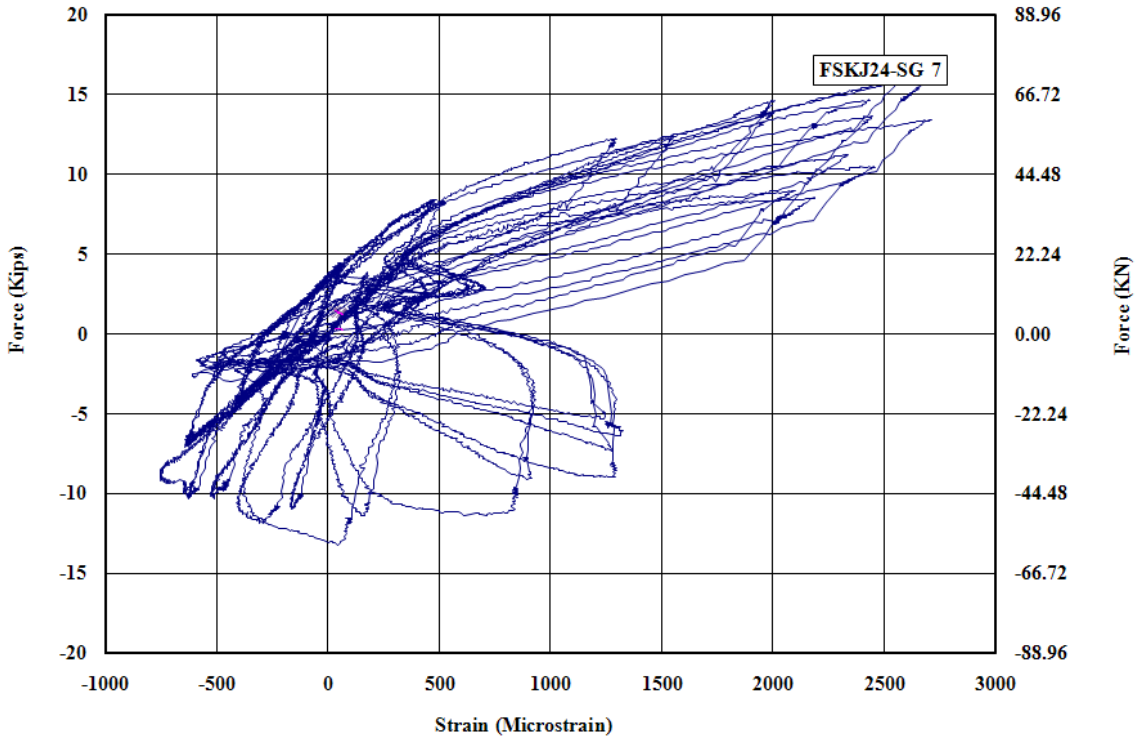

Figure F - 7: Measured Strain in Gauge No.7 for FSKJ24

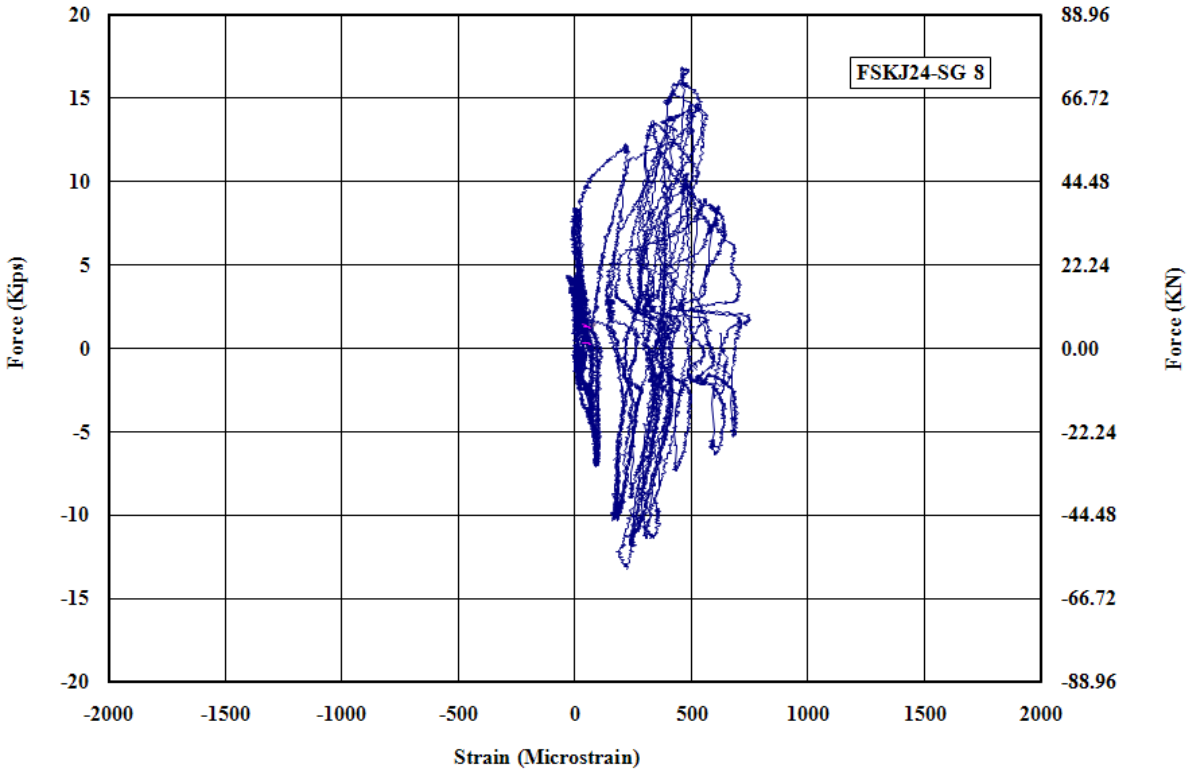

Figure F - 8: Measured Strain in Gauge No.8 for FSKJ24

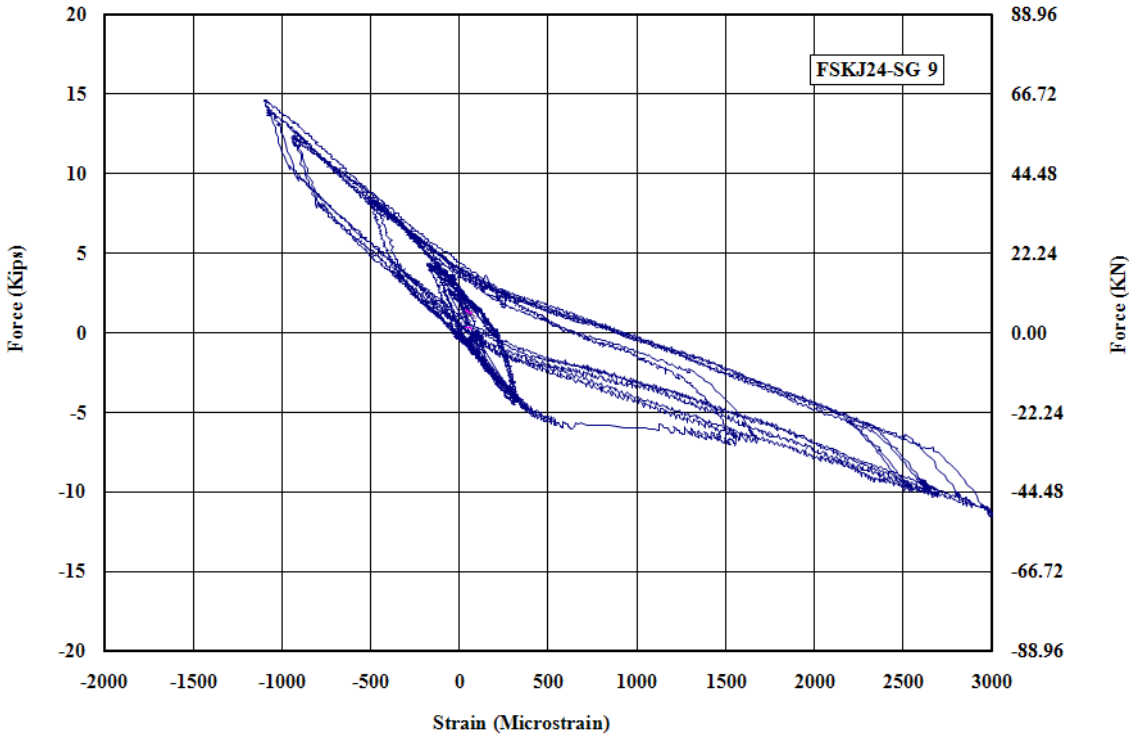

Figure F - 9: Measured Strain in Gauge No.9 for FSKJ24

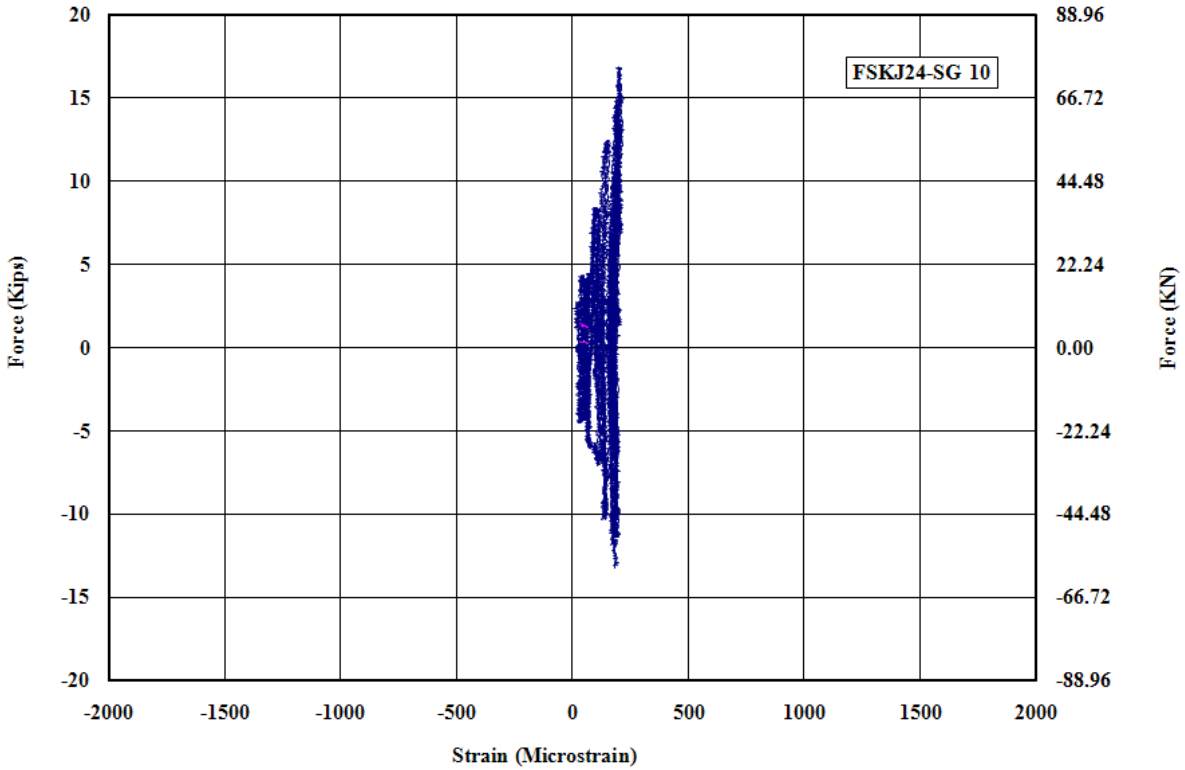

Figure F - 10: Measured Strain in Gauge No.10 for FSKJ24

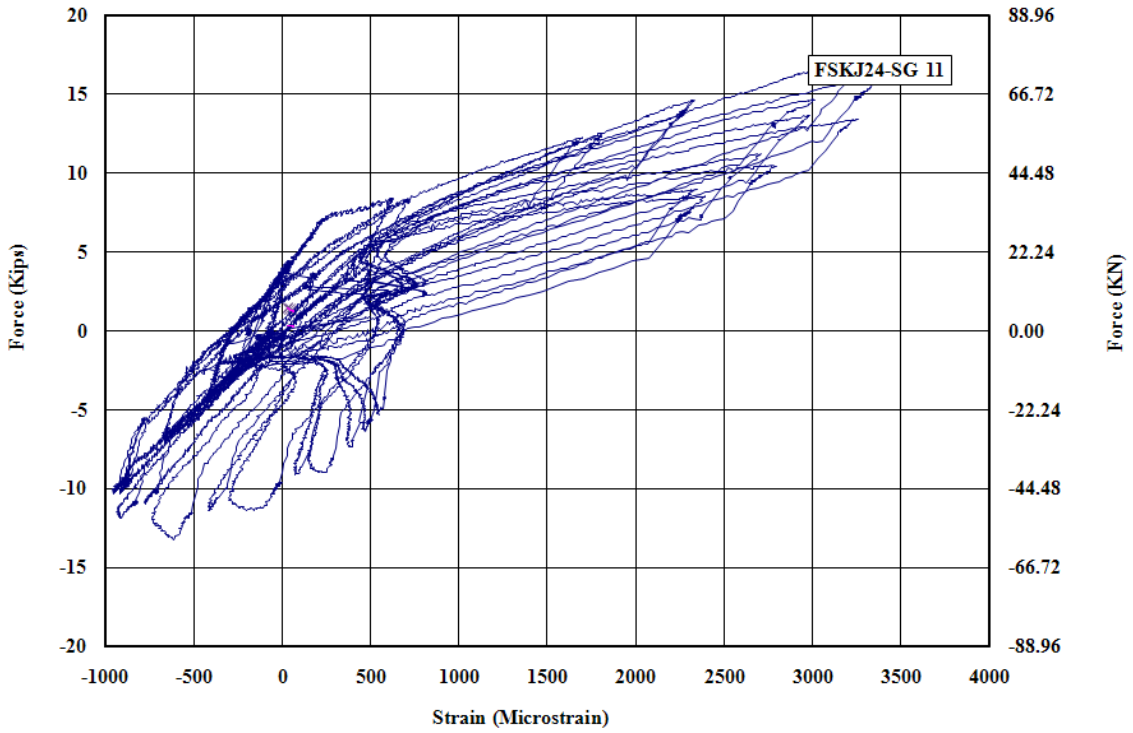

Figure F - 11: Measured Strain in Gauge No.11 for FSKJ24

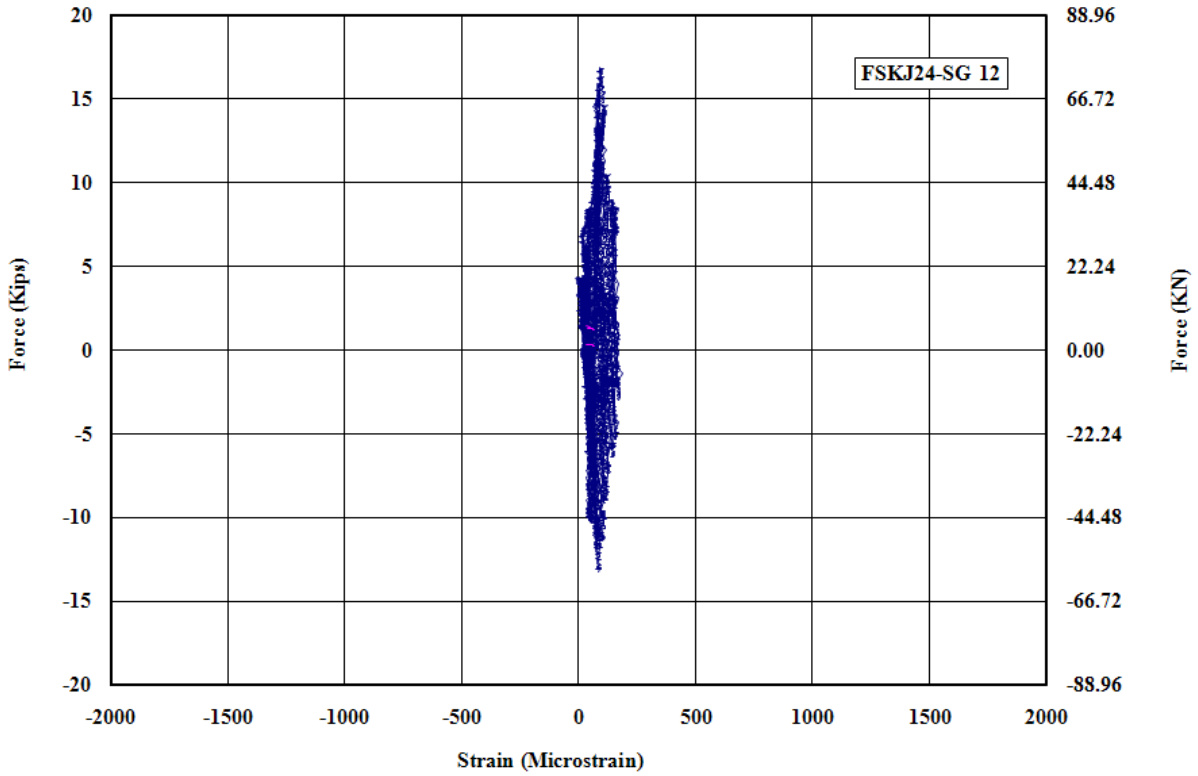

Figure F - 12: Measured Strain in Gauge No.12 for FSKJ24

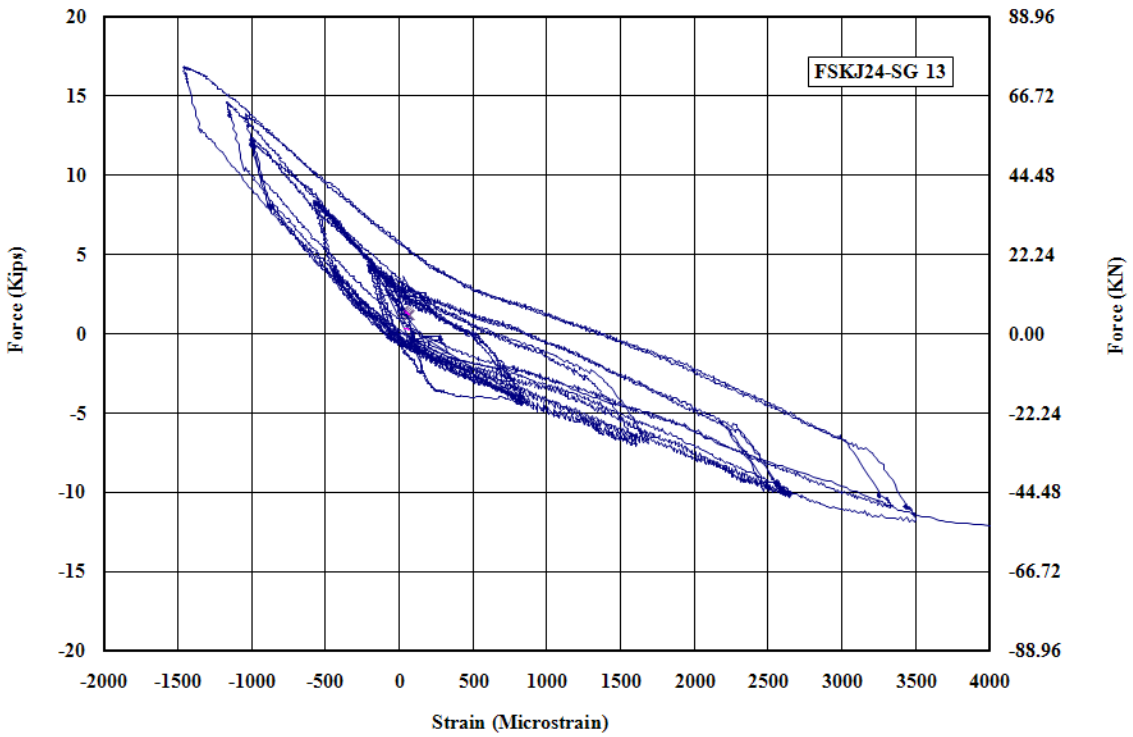

Figure F - 13: Measured Strain in Gauge No.13 for FSKJ24

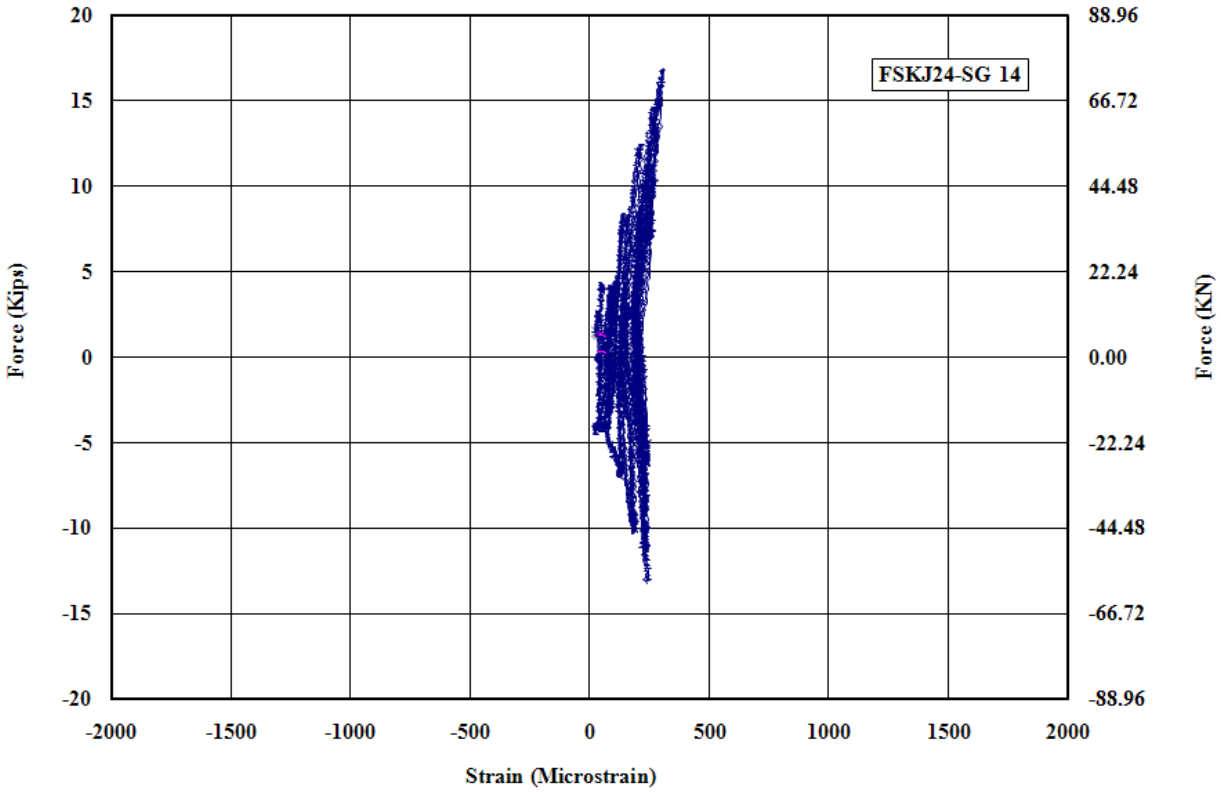

Figure F - 14: Measured Strain in Gauge No.14 for FSKJ24

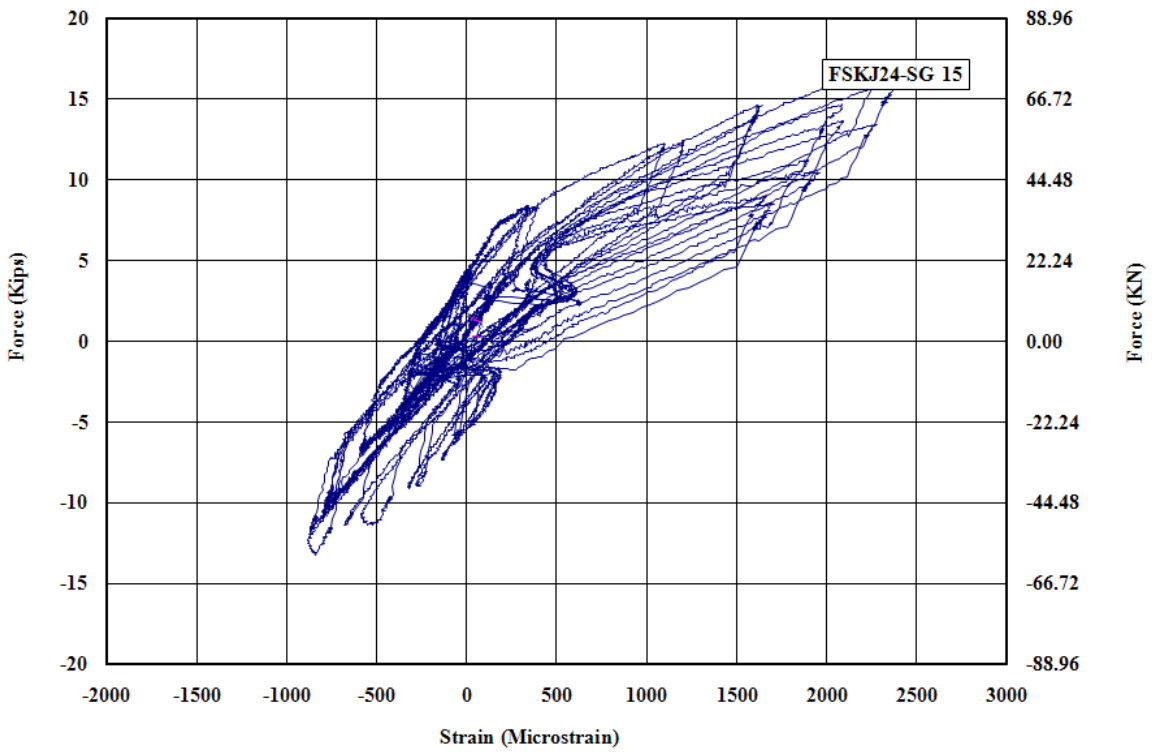

Figure F - 15: Measured Strain in Gauge No.15 for FSKJ24

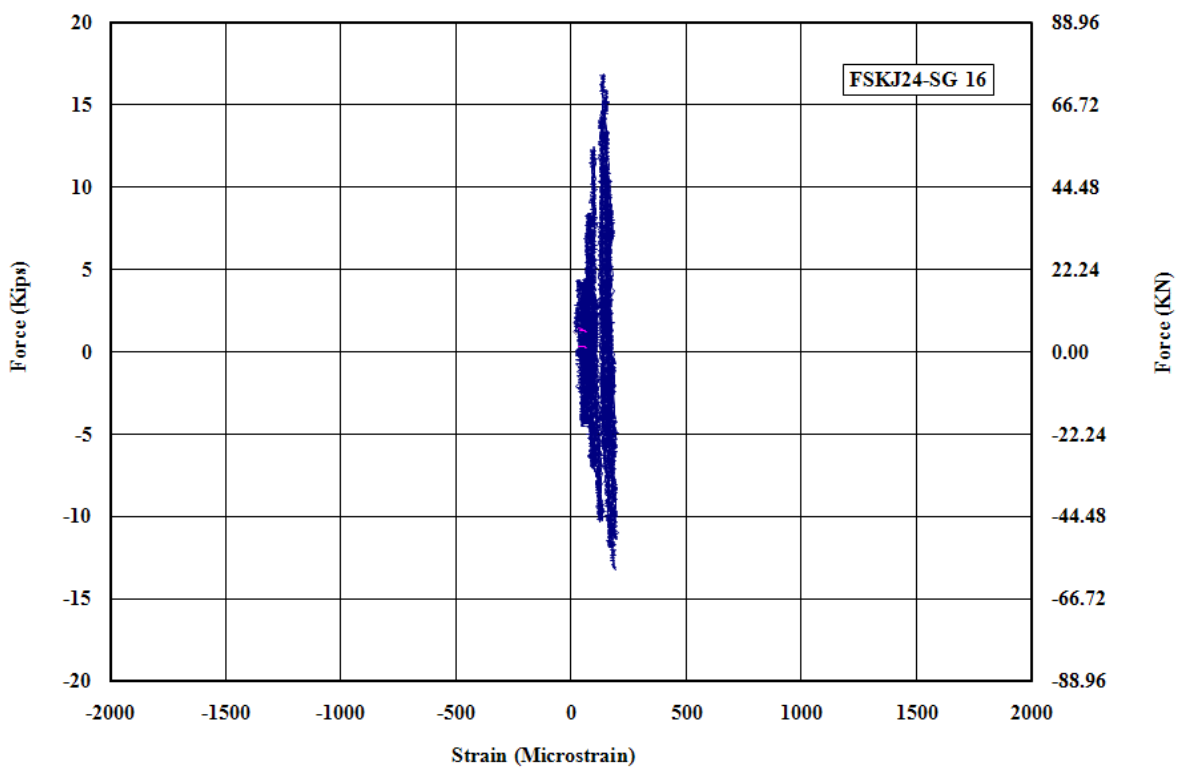

Figure F - 16: Measured Strain in Gauge No.16 for FSKJ24

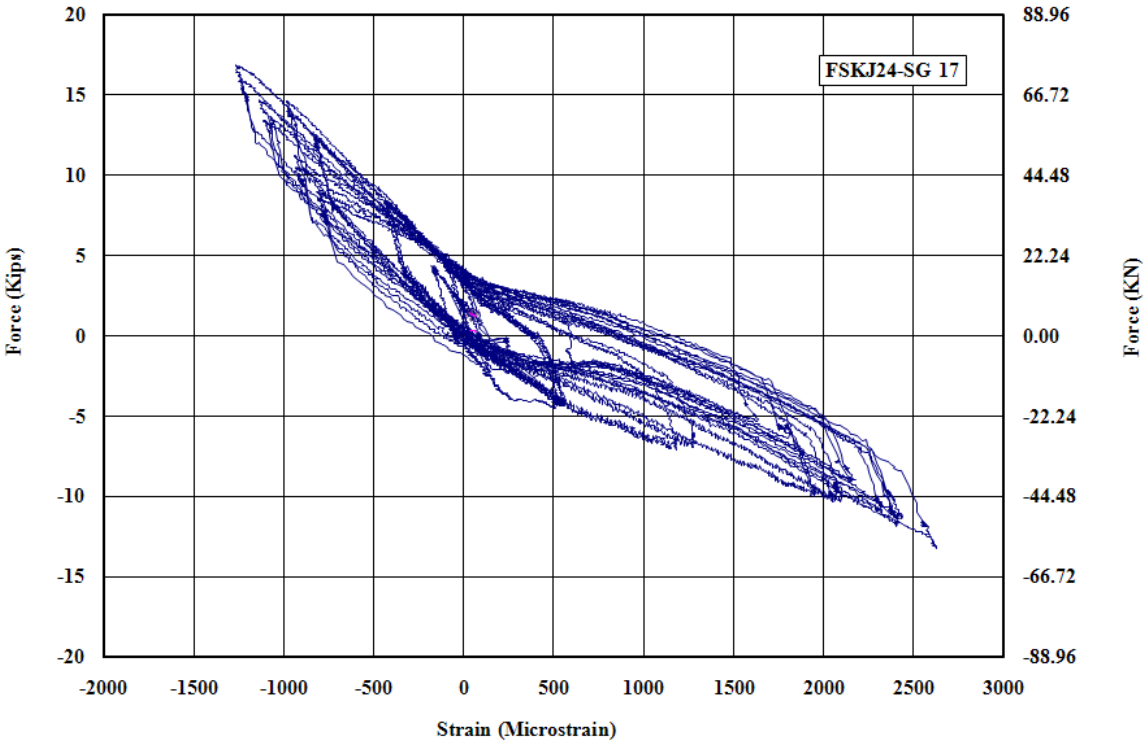

Figure F - 17: Measured Strain in Gauge No.17 for FSKJ24

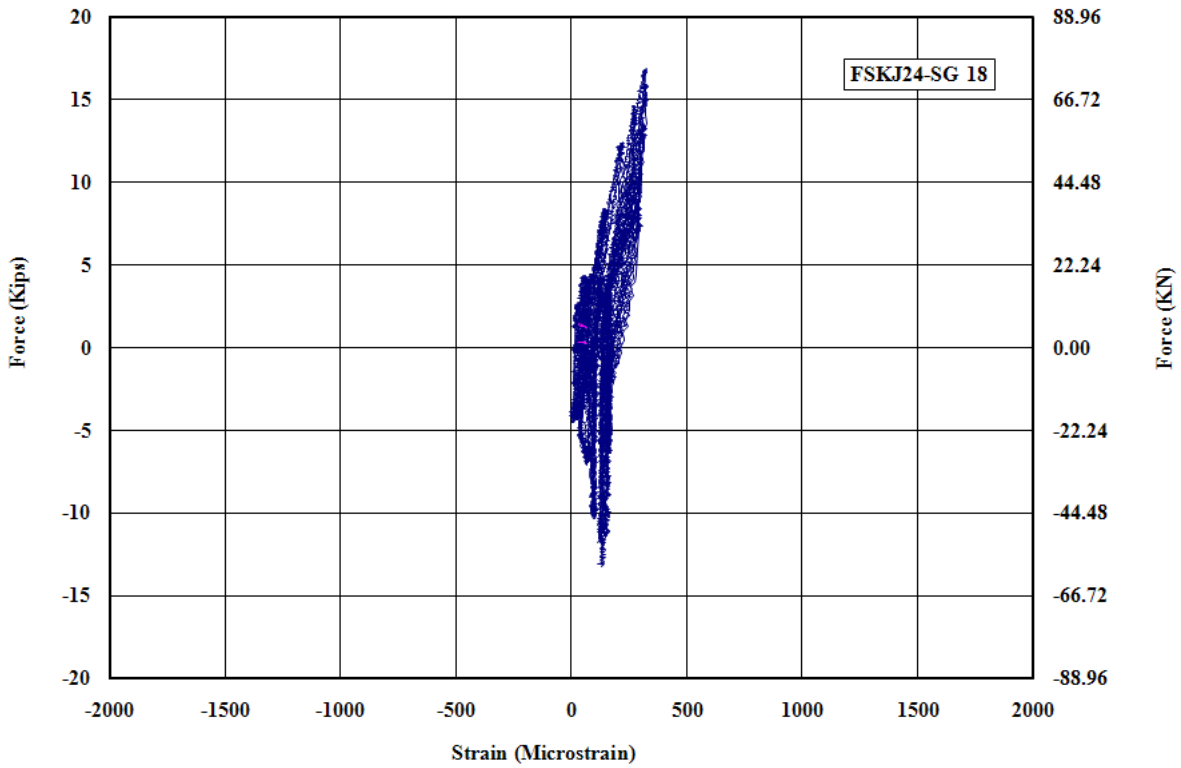

Figure F - 18: Measured Strain in Gauge No.18 for FSKJ24

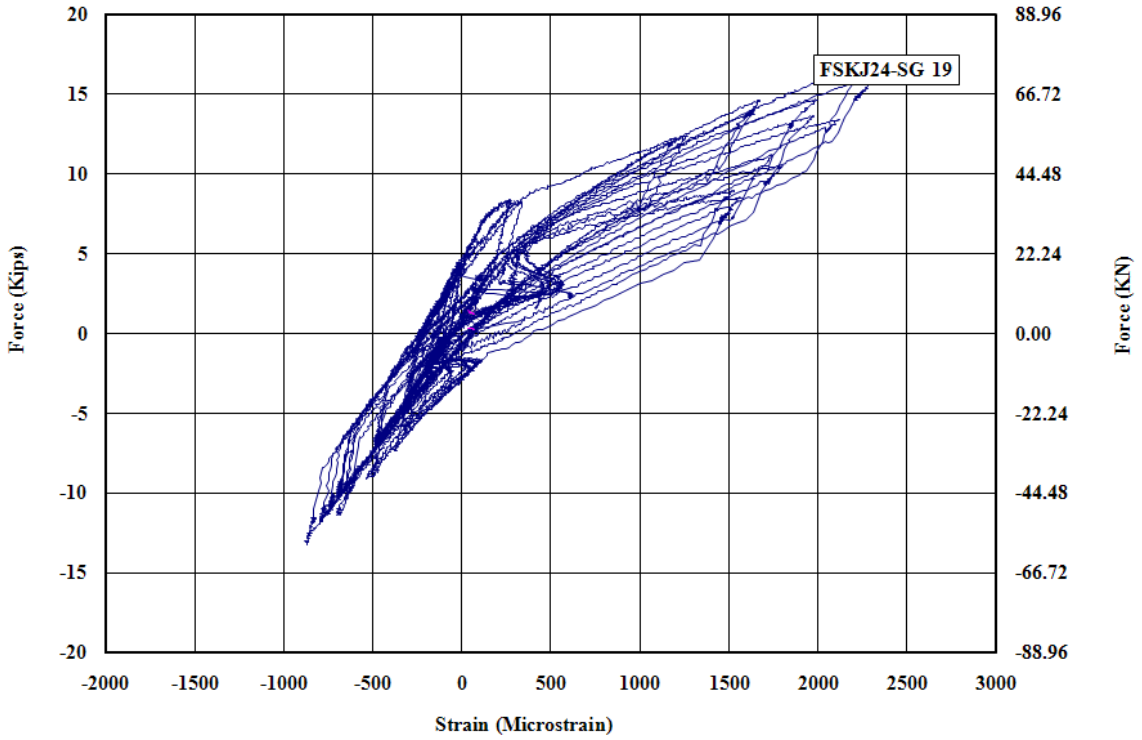

Figure F - 19: Measured Strain in Gauge No.19 for FSKJ24

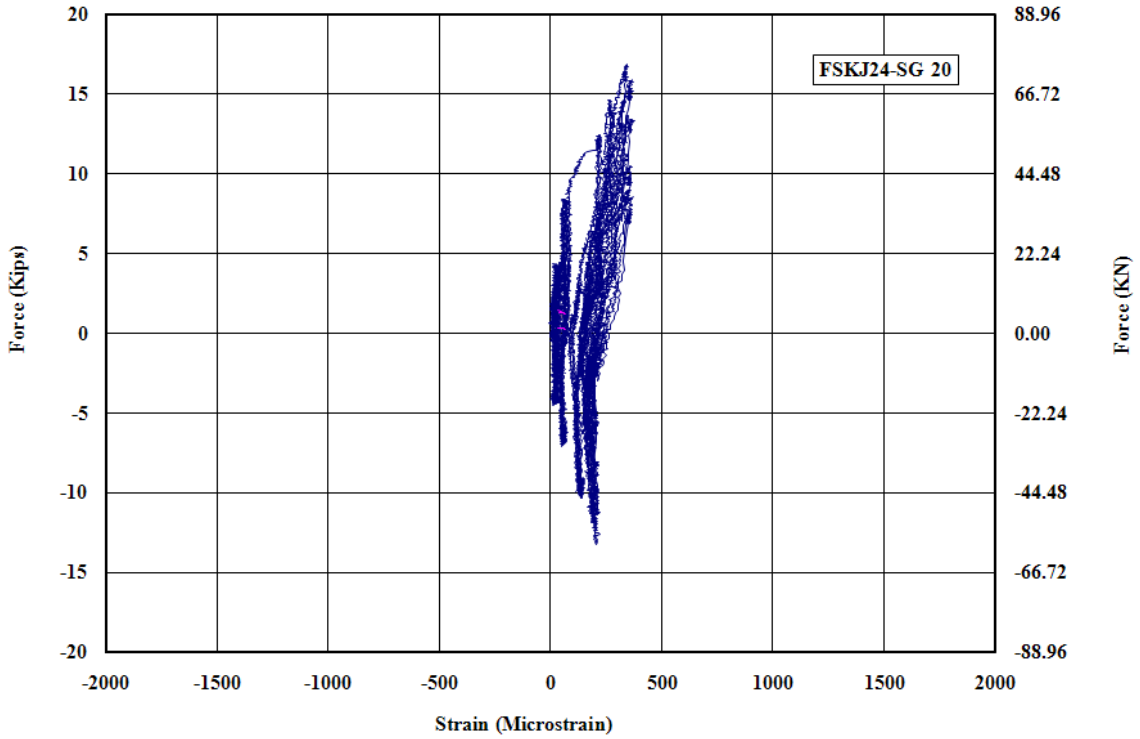

Figure F - 20: Measured Strain in Gauge No.20 for FSKJ24

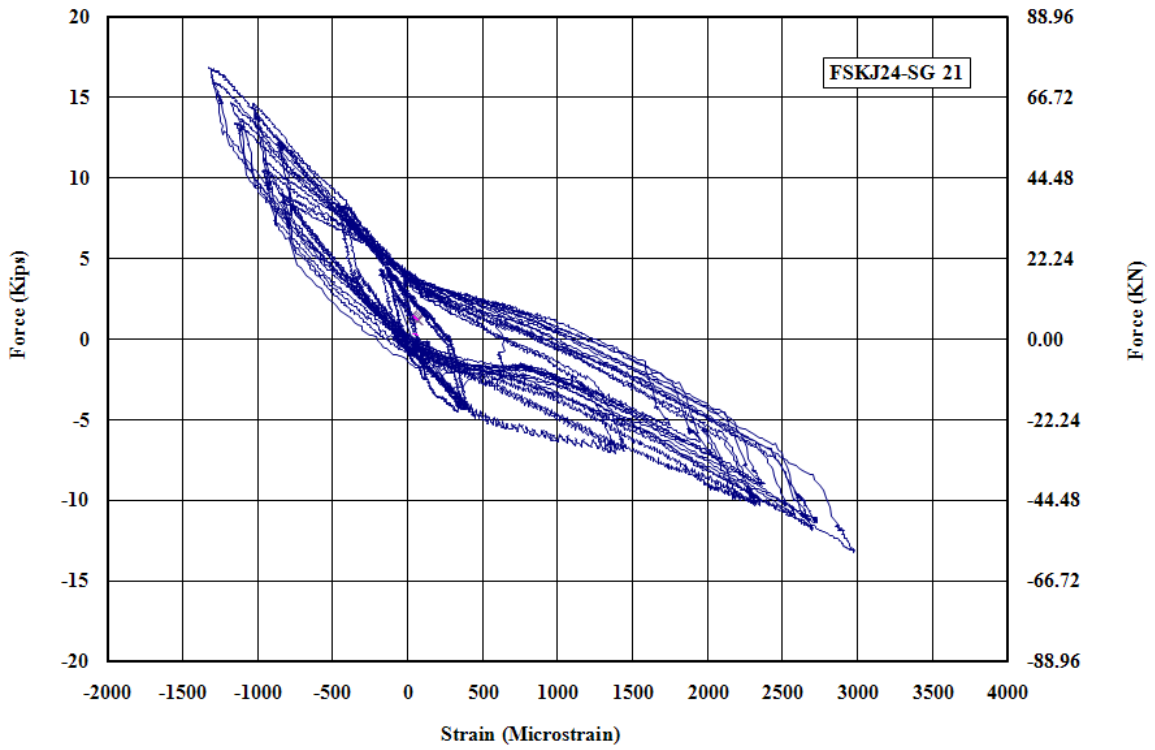

Figure F - 21: Measured Strain in Gauge No.21 for FSKJ24

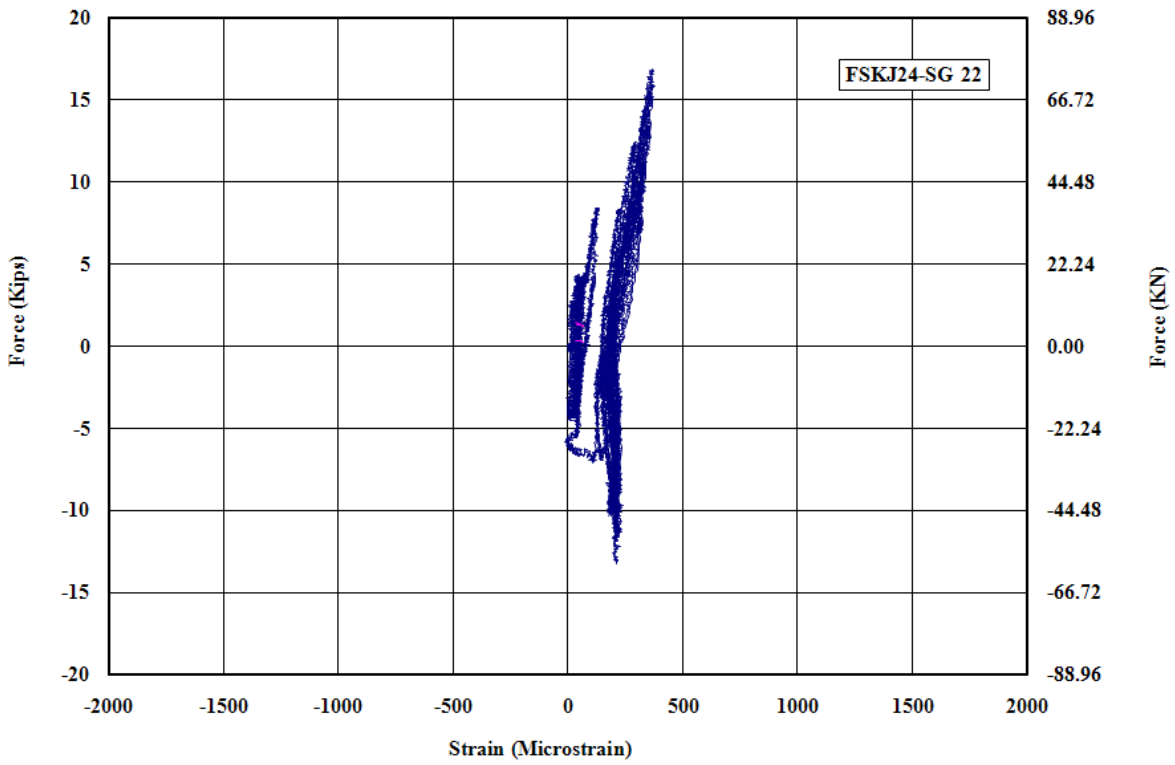

Figure F - 22: Measured Strain in Gauge No.22 for FSKJ24

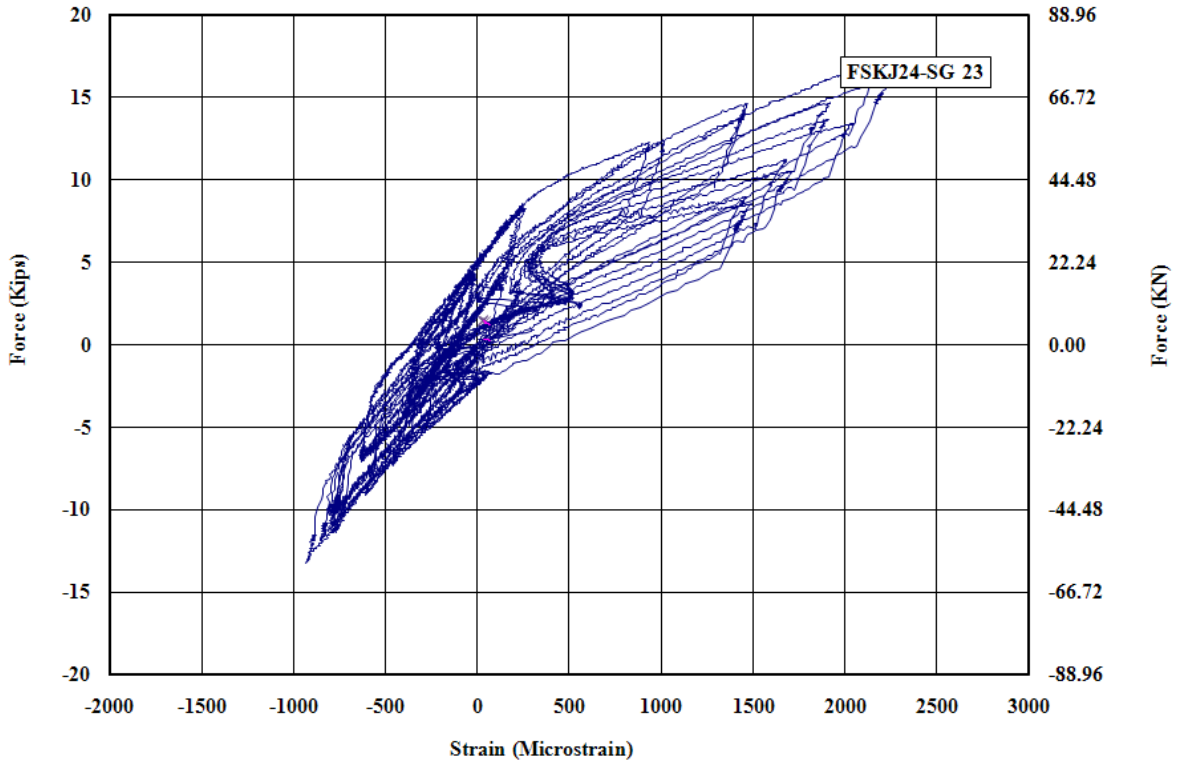

Figure F - 23: Measured Strain in Gauge No.23 for FSKJ24

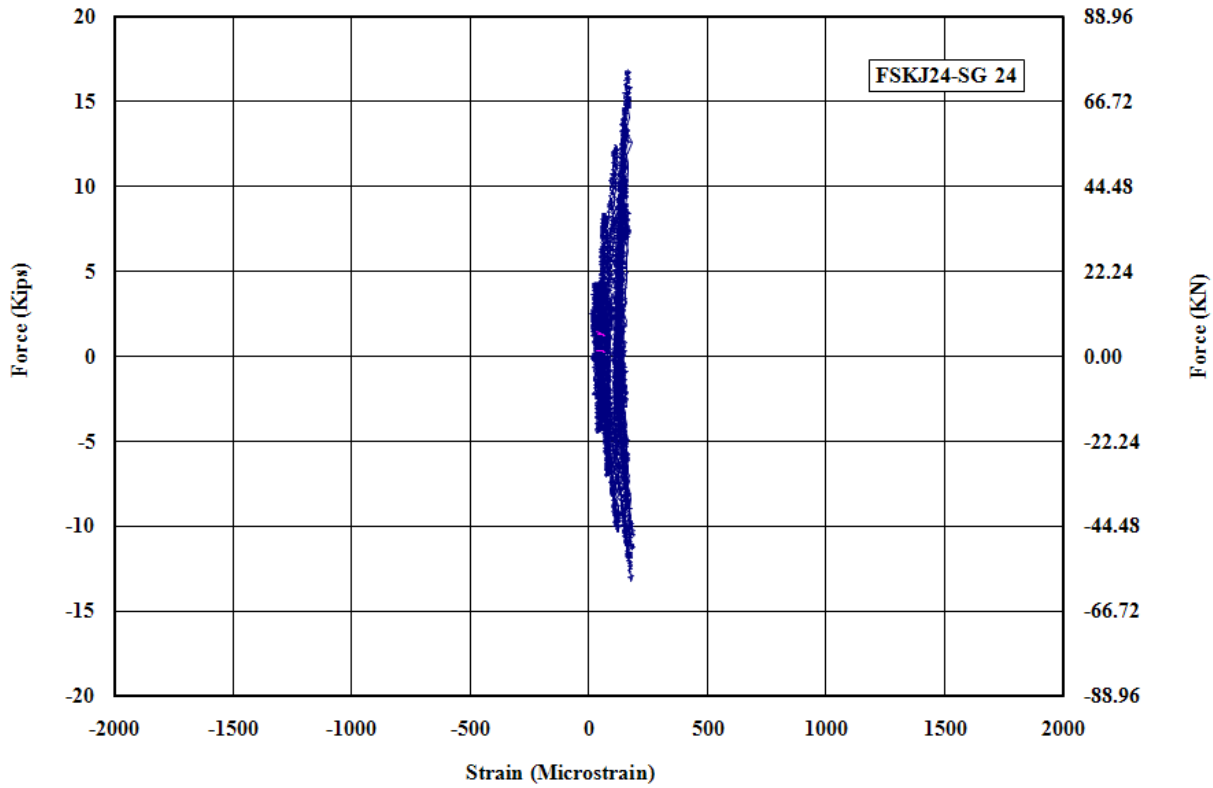

Figure F - 24: Measured Strain in Gauge No.24 for FSKJ24

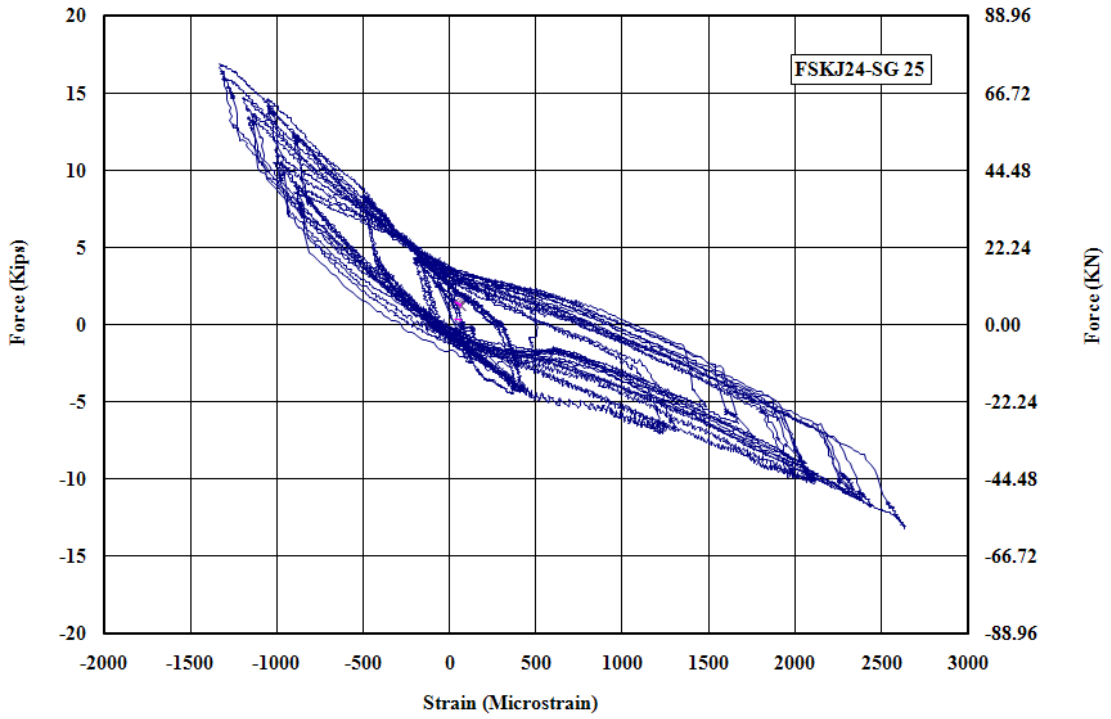

Figure F - 25: Measured Strain in Gauge No.25 for FSKJ24

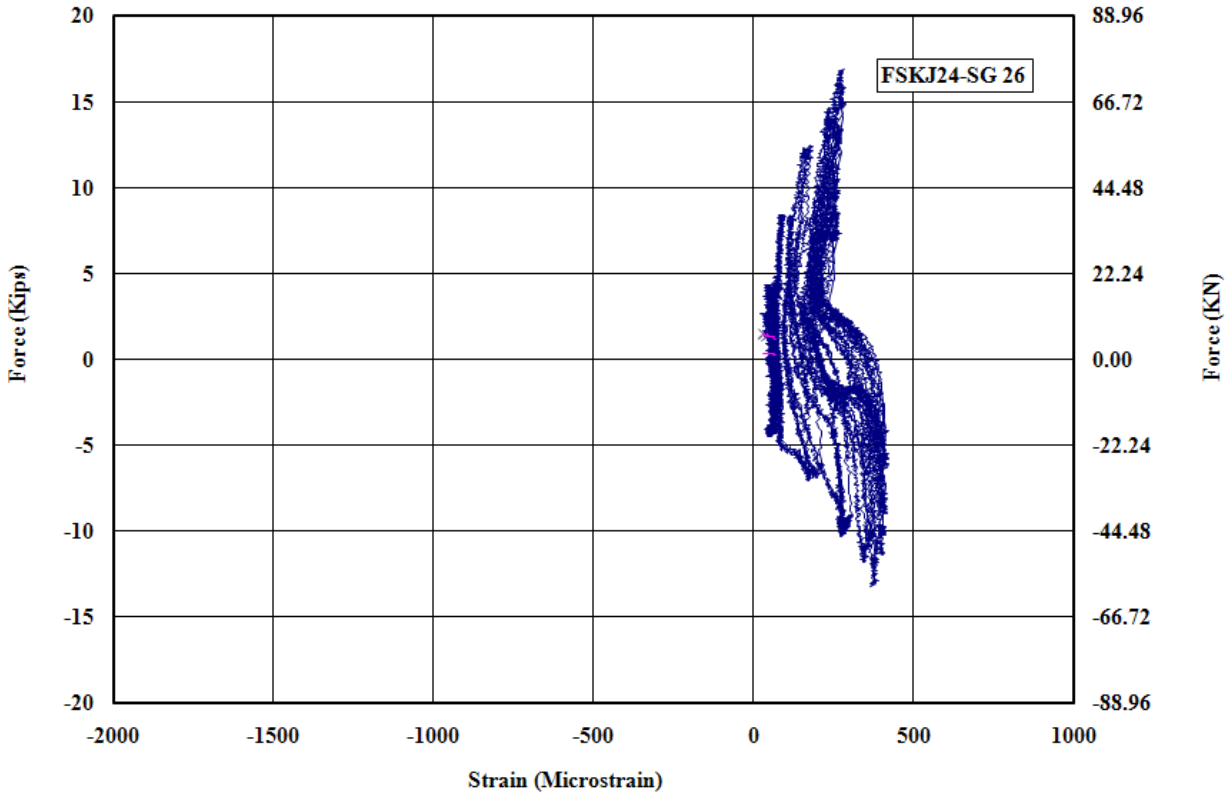

Figure F - 26: Measured Strain in Gauge No.26 for FSKJ24

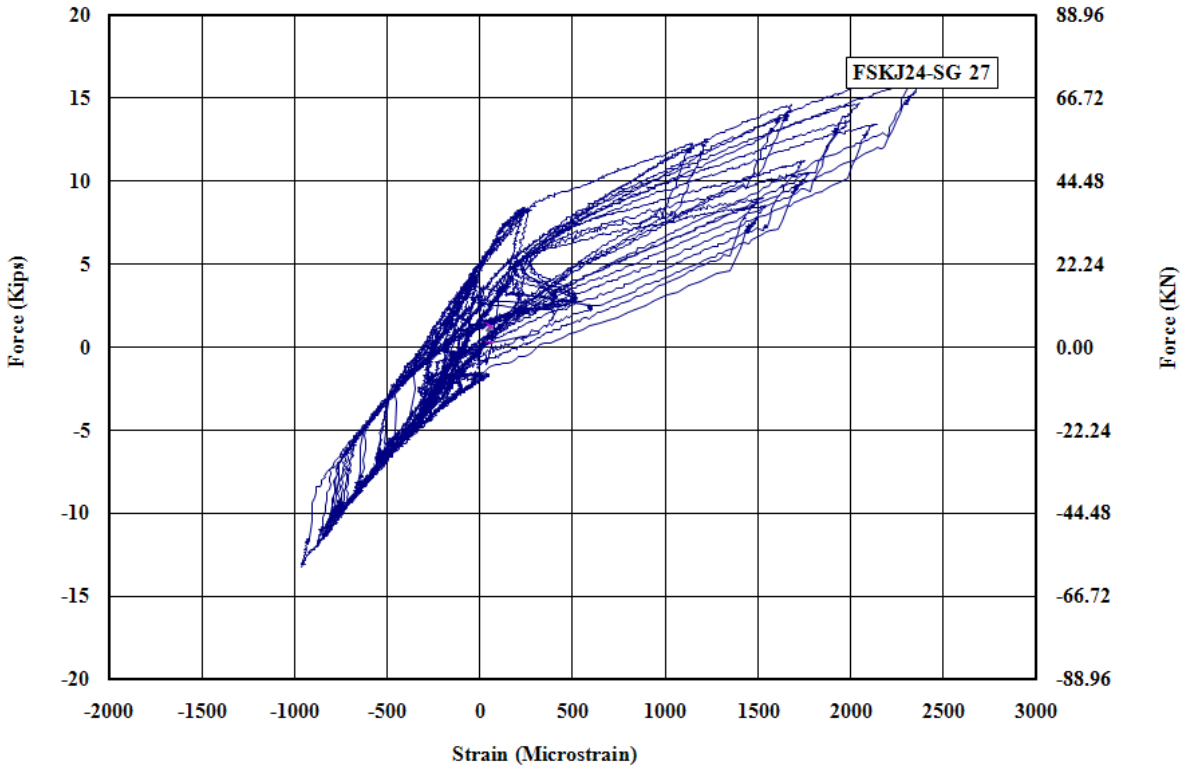

Figure F - 27: Measured Strain in Gauge No.27 for FSKJ24

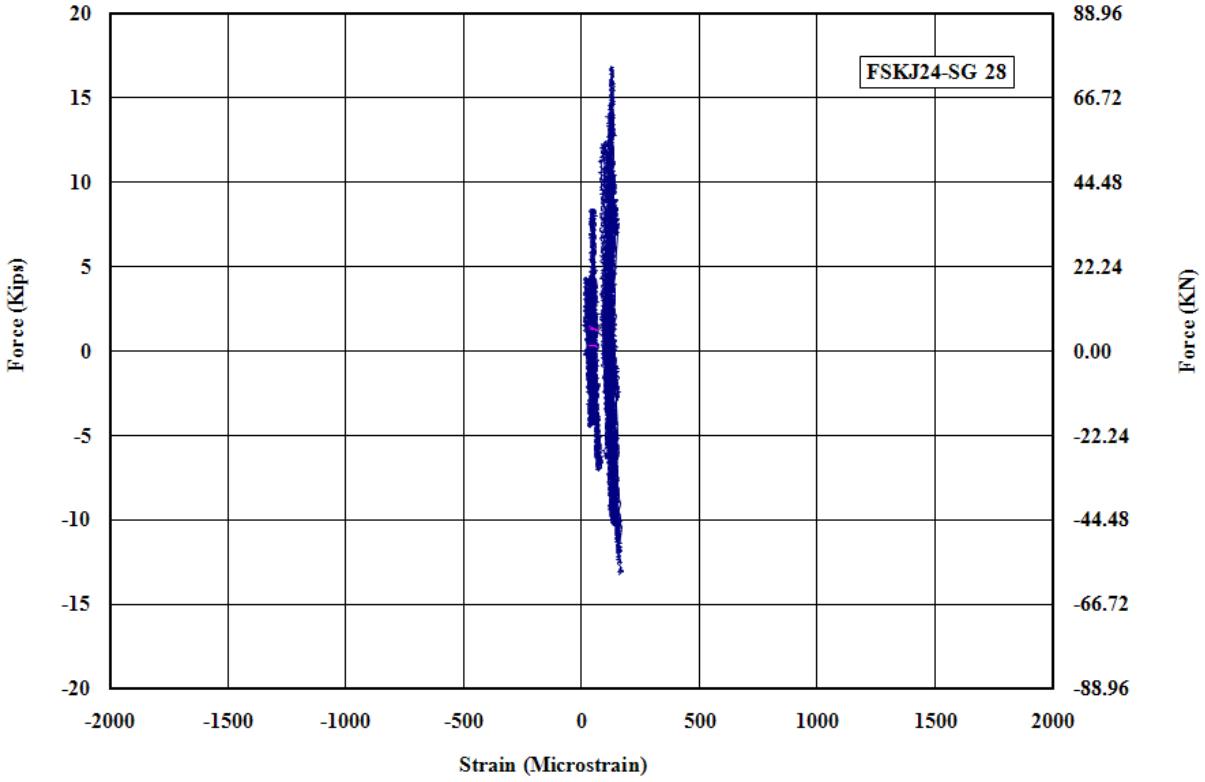

Figure F - 28: Measured Strain in Gauge No.28 for FSKJ24

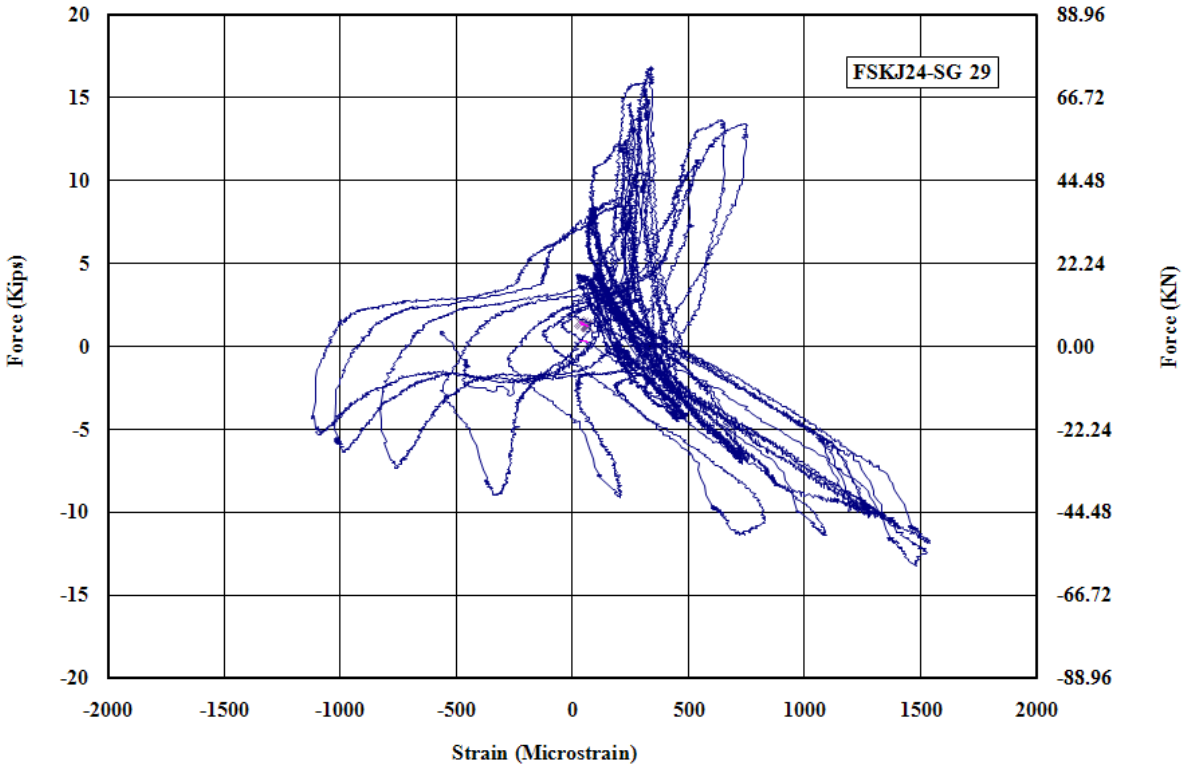

Figure F - 29: Measured Strain in Gauge No.29 for FSKJ24

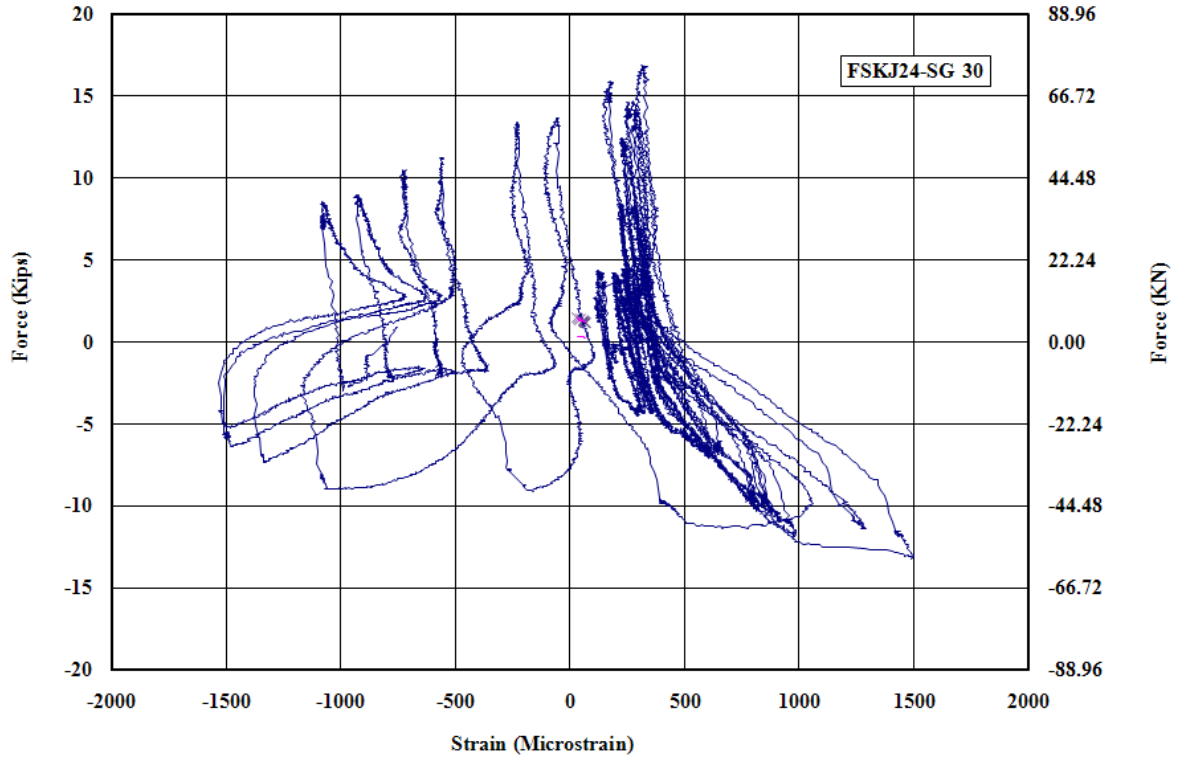

Figure F - 30: Measured Strain in Gauge No.30 for FSKJ24

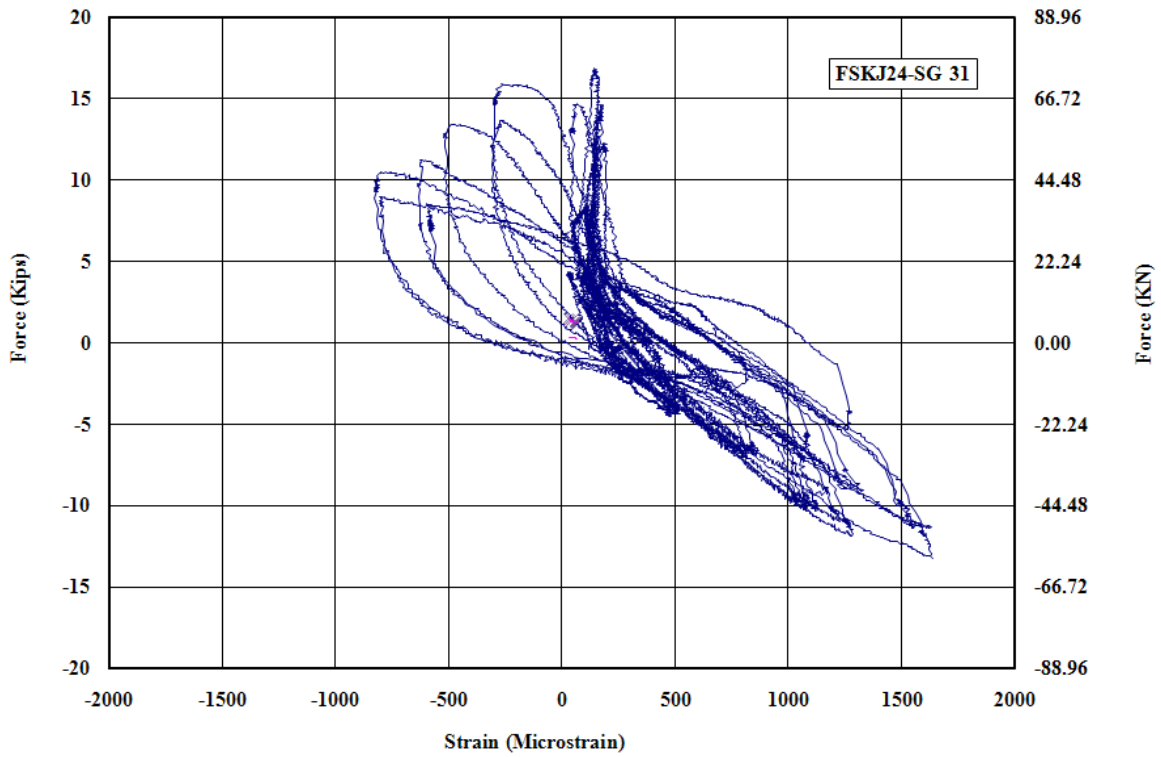

Figure F - 31: Measured Strain in Gauge No.31 for FSKJ24

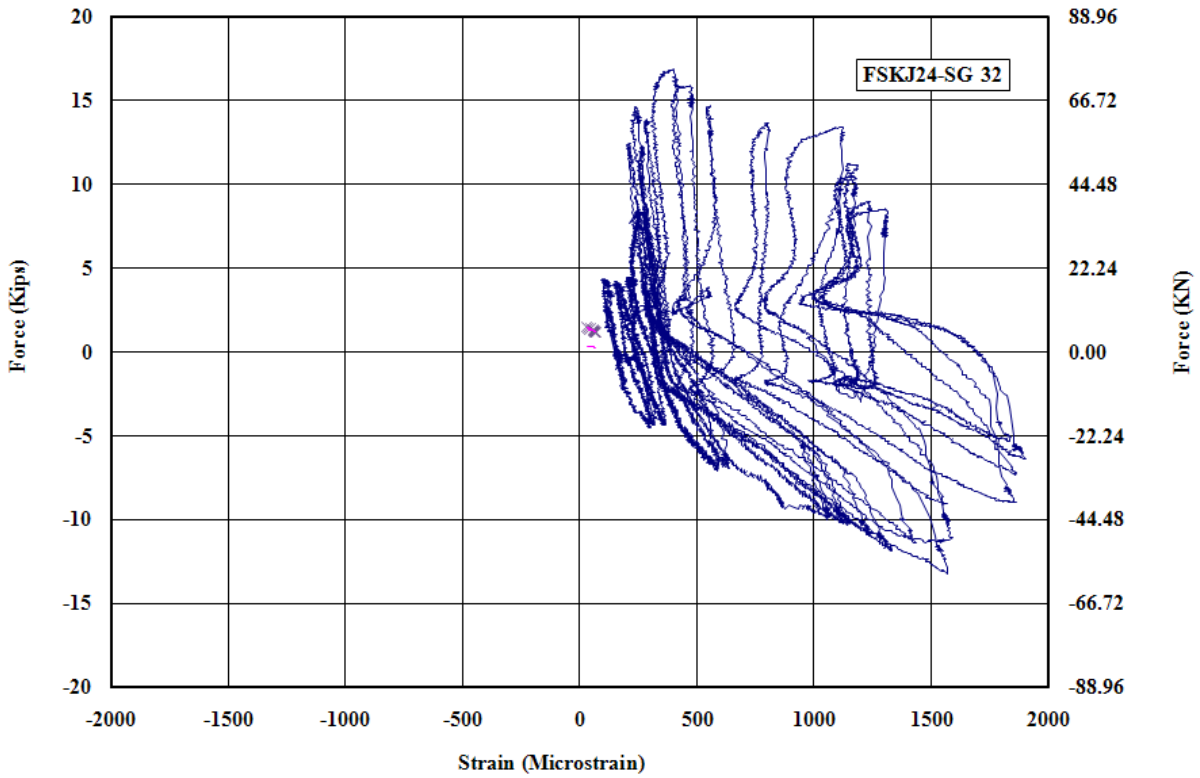

Figure F - 32: Measured Strain in Gauge No.32 for FSKJ24

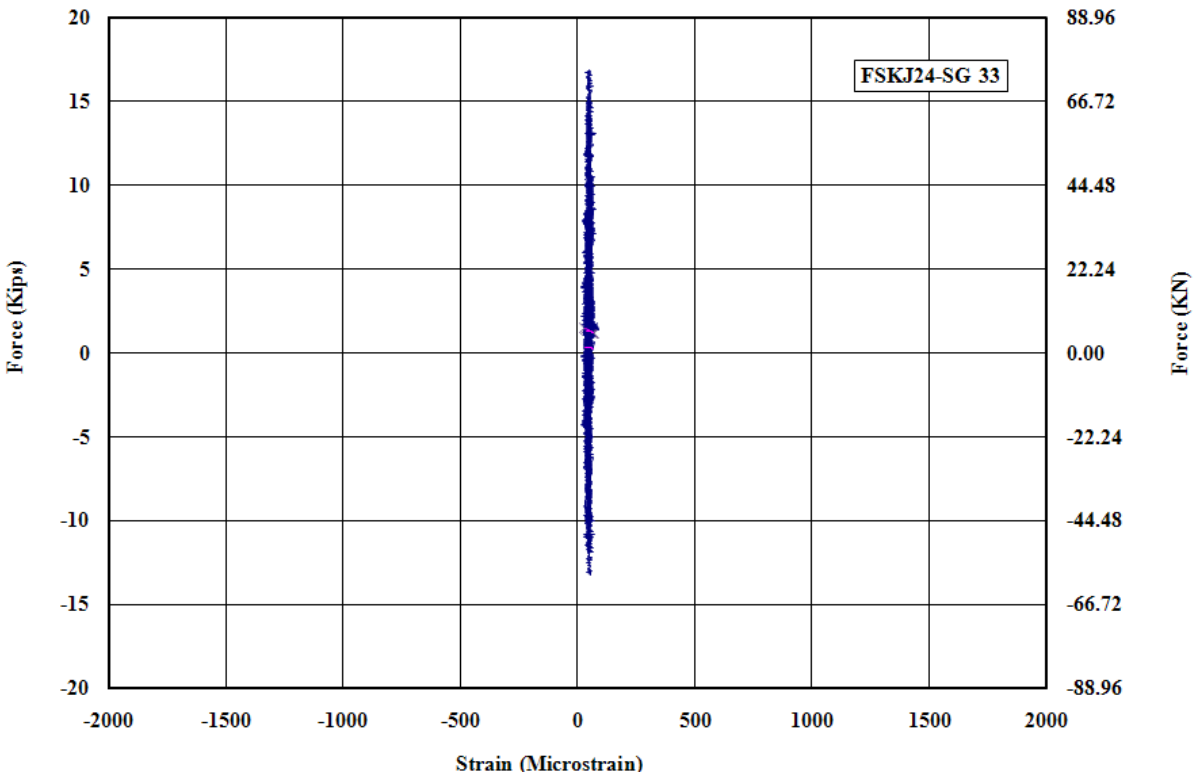

Figure F - 33: Measured Strain in Gauge No.33 for FSKJ24

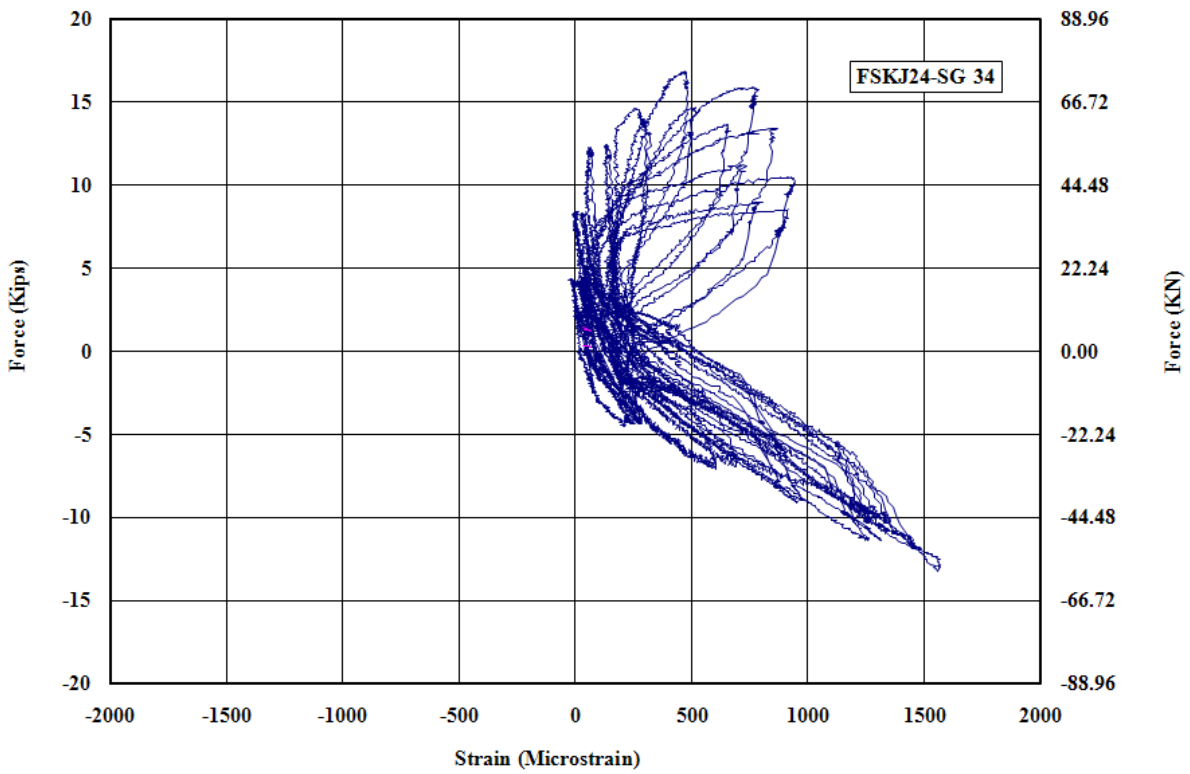

Figure F - 34: Measured Strain in Gauge No.34 for FSKJ24

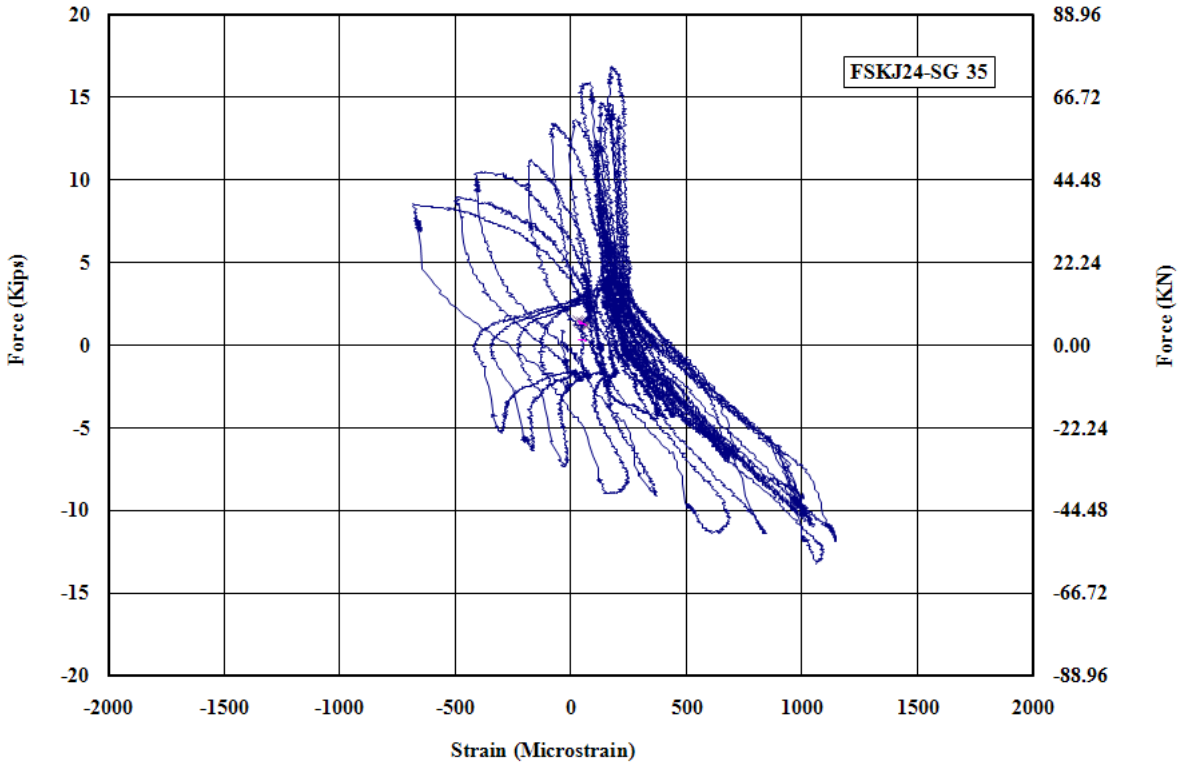

Figure F - 35: Measured Strain in Gauge No.35 for FSKJ24

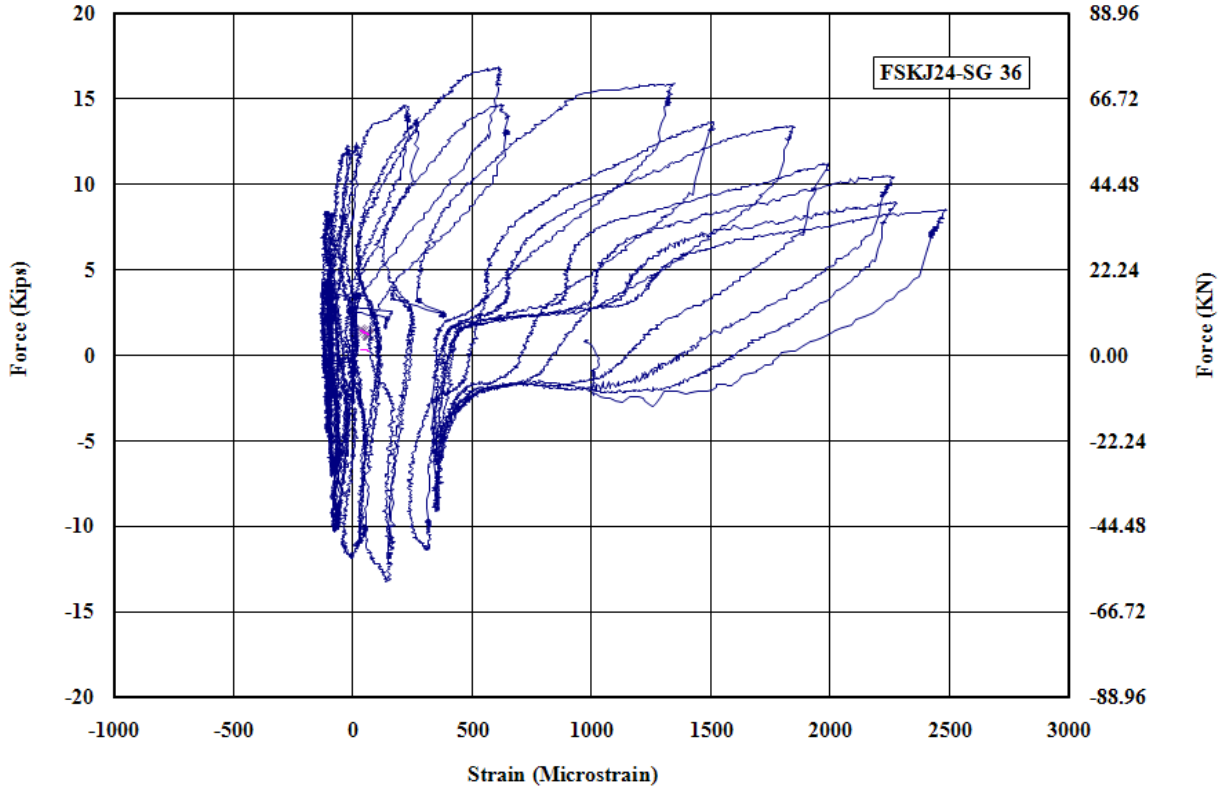

Figure F - 36: Measured Strain in Gauge No.36 for FSKJ24

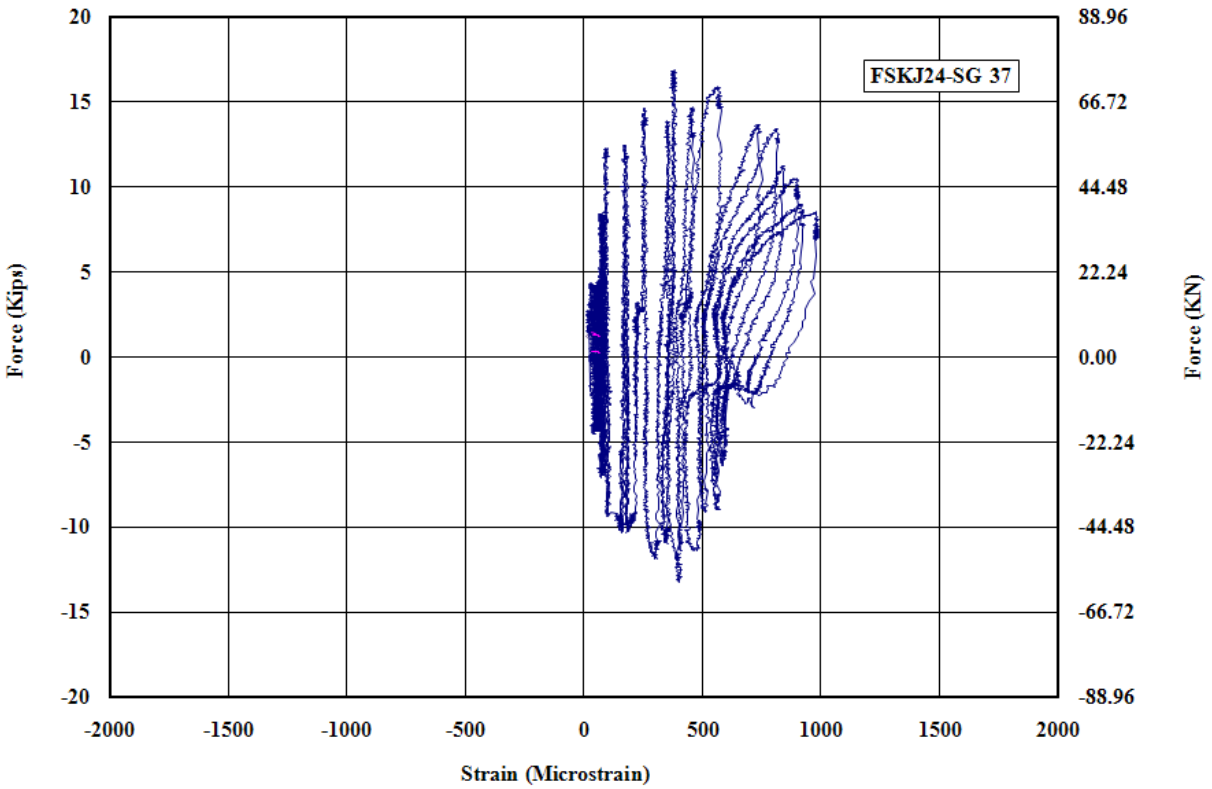

Figure F - 37: Measured Strain in Gauge No.37 for FSKJ24

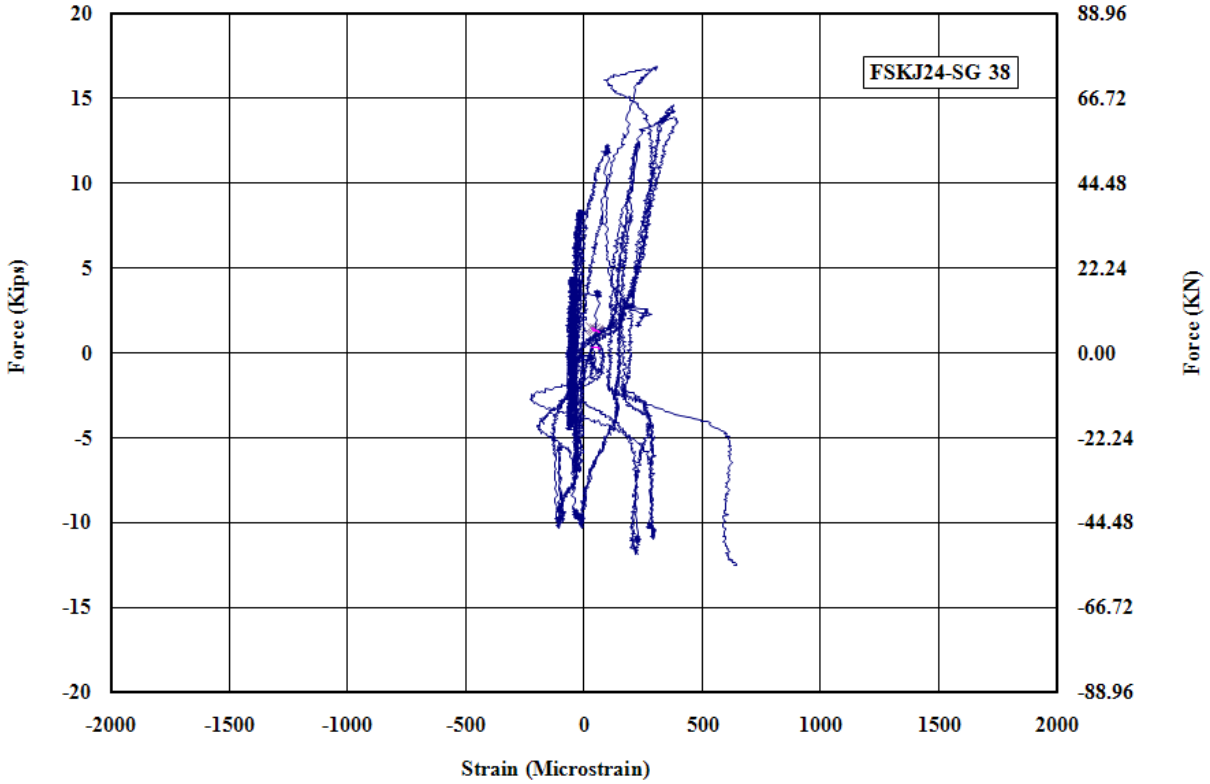

Figure F - 38: Measured Strain in Gauge No.38 for FSKJ24

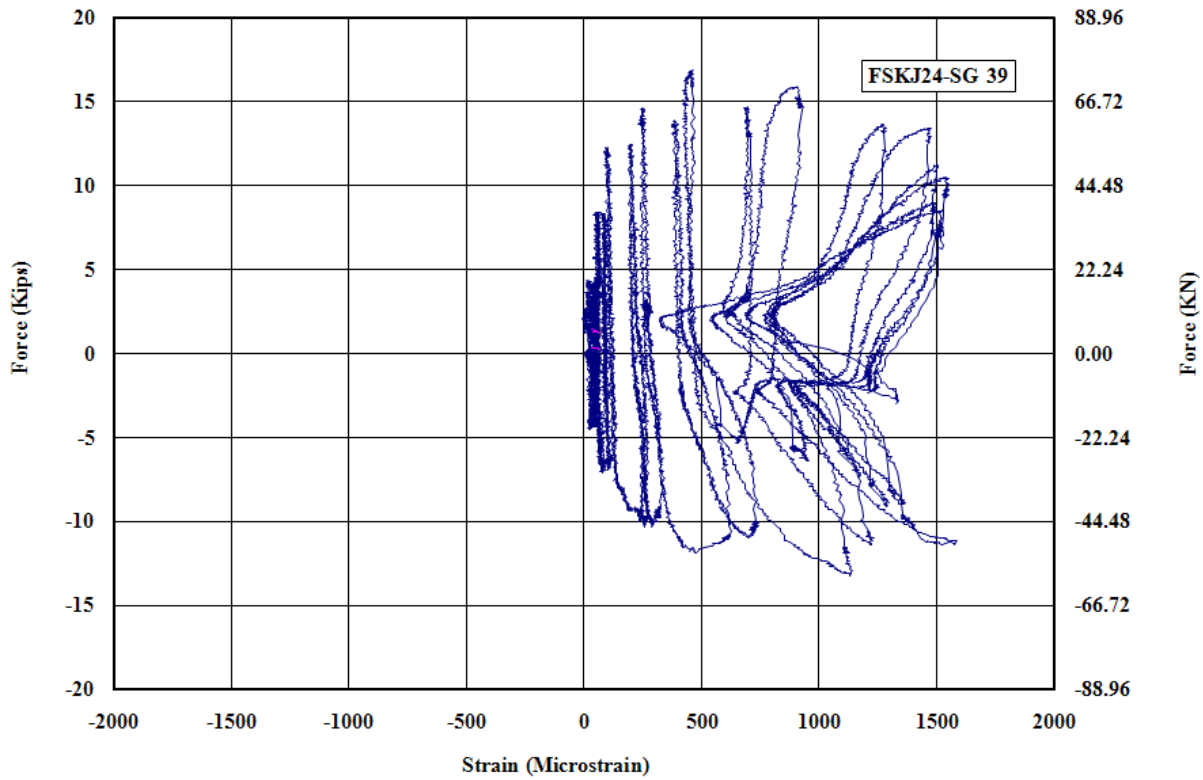

Figure F - 39: Measured Strain in Gauge No.39 for FSKJ24

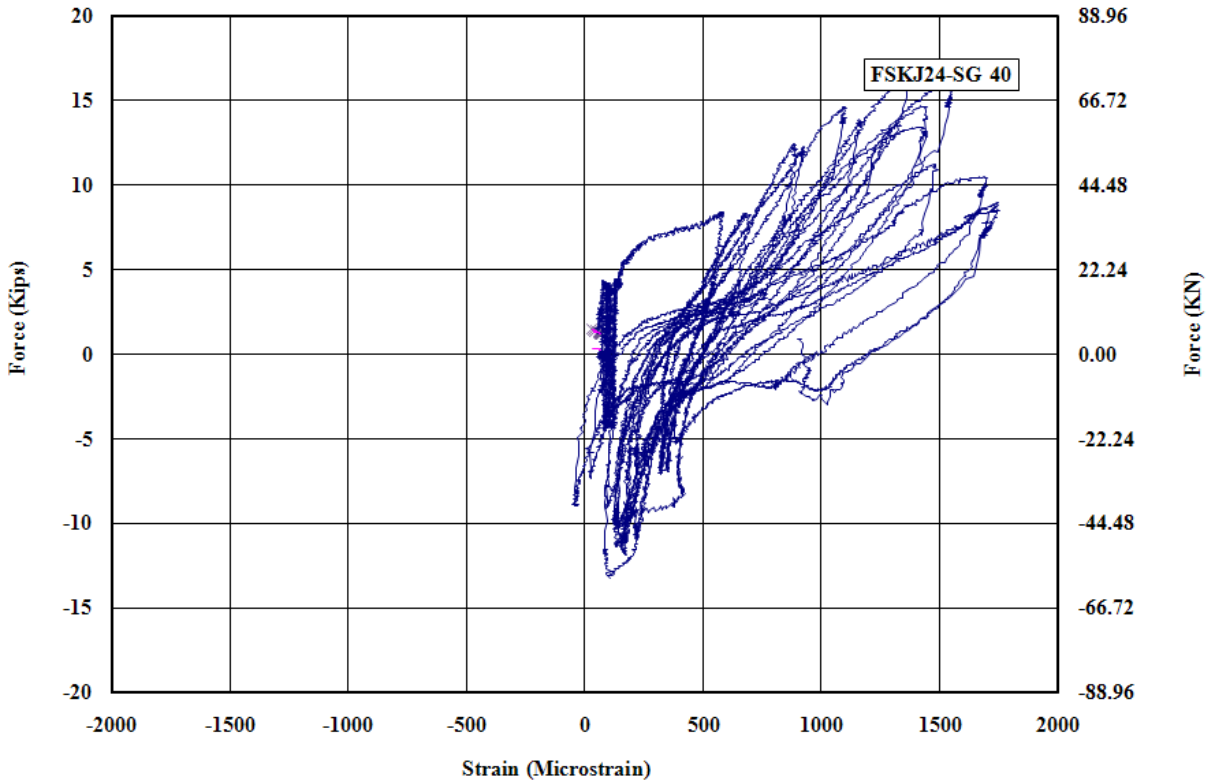

Figure F - 40: Measured Strain in Gauge No.40 for FSKJ24

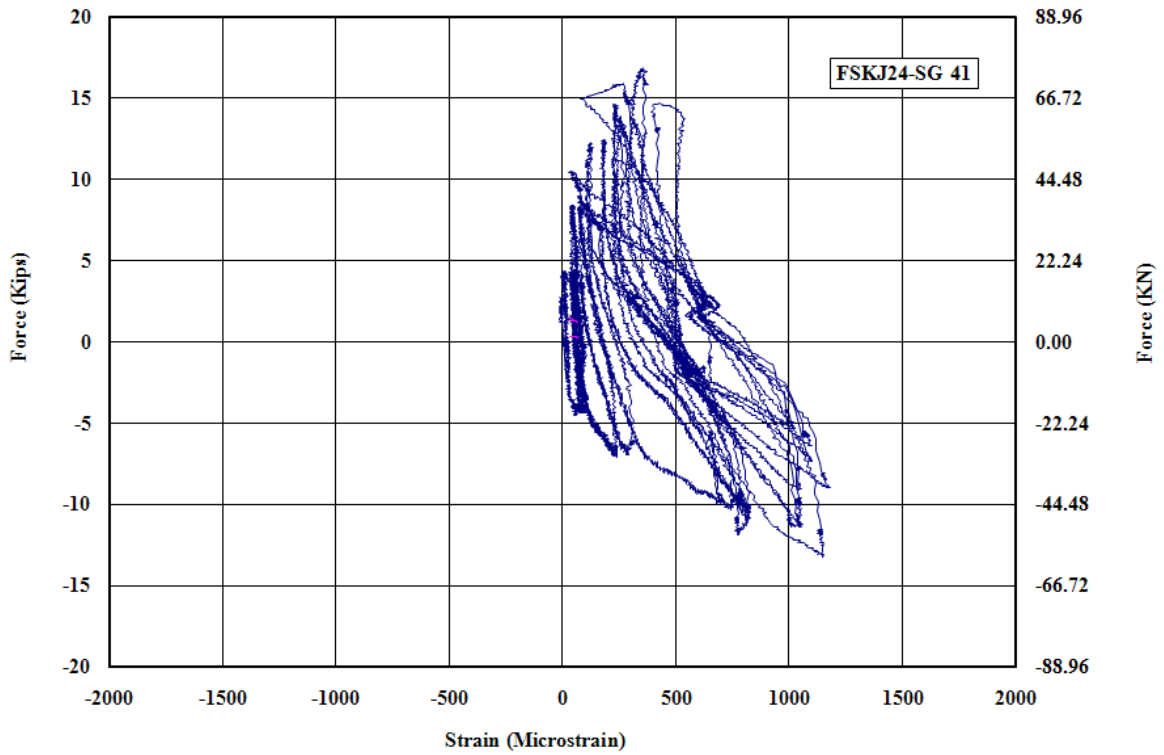

Figure F - 41: Measured Strain in Gauge No.41 for FSKJ24

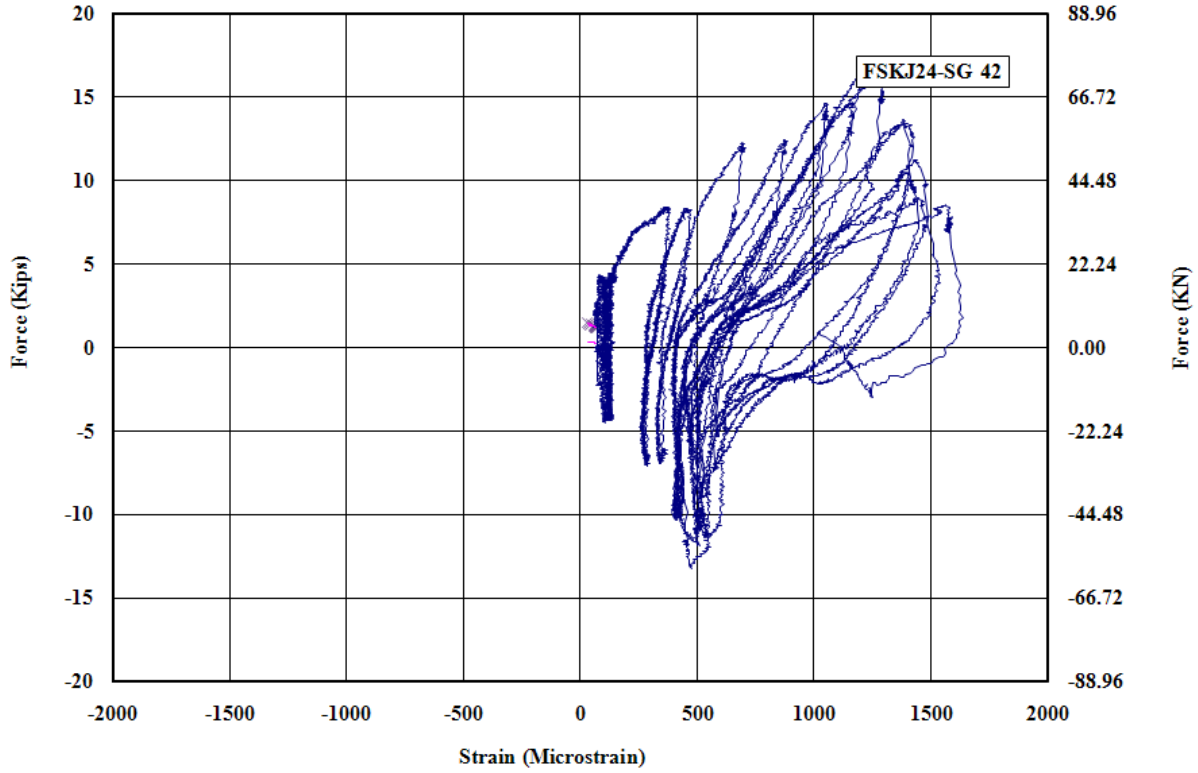

Figure F - 42: Measured Strain in Gauge No.42 for FSKJ24

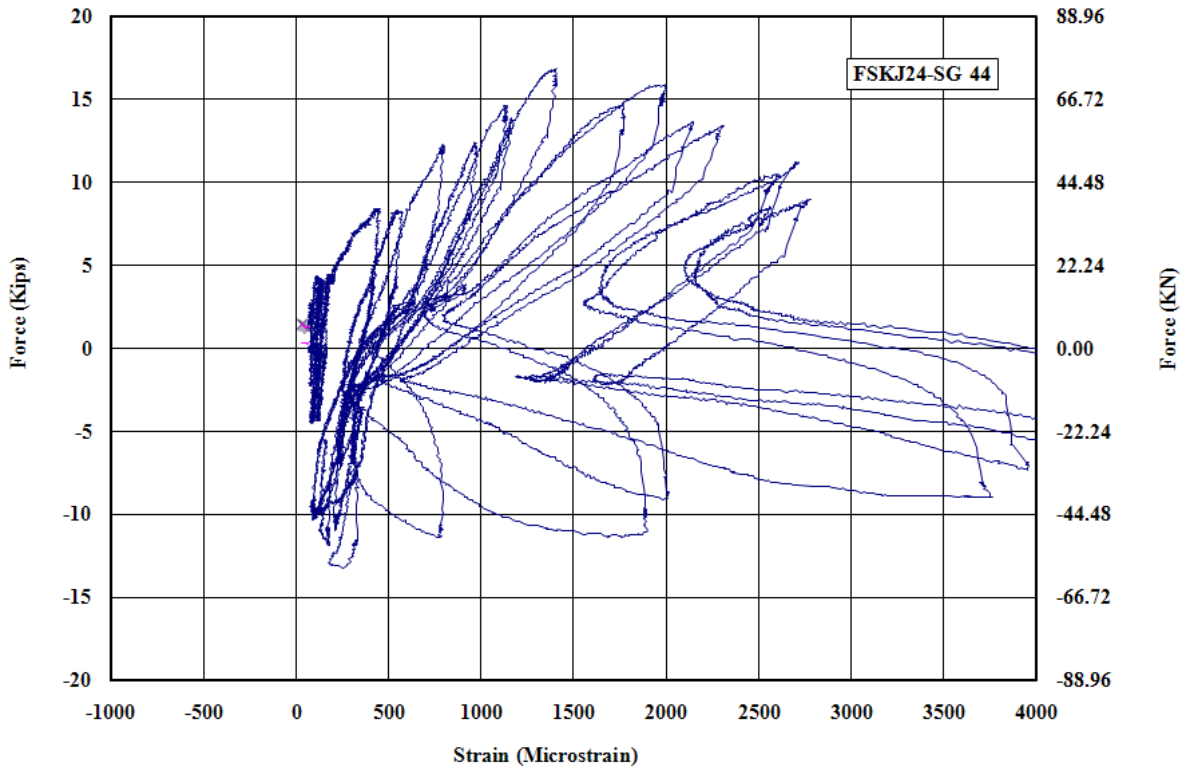

Figure F - 43: Measured Strain in Gauge No.44 for FSKJ24

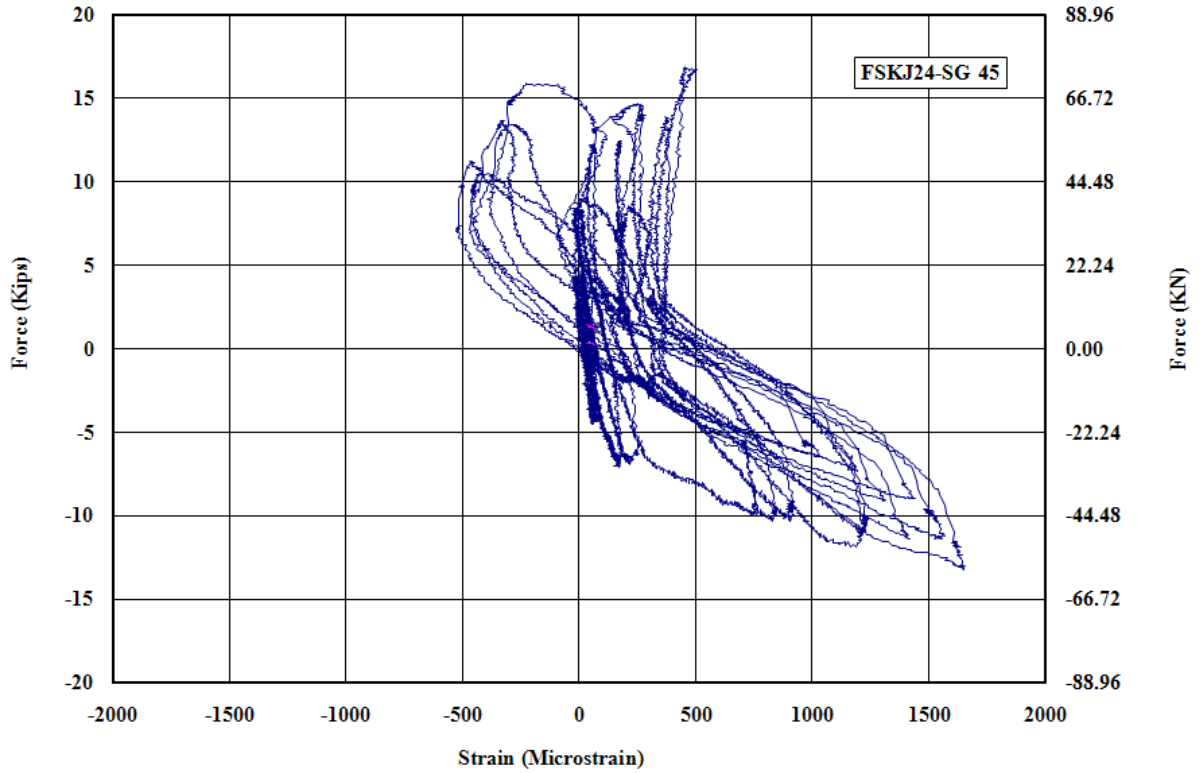

Figure F - 44: Measured Strain in Gauge No.45 for FSKJ24

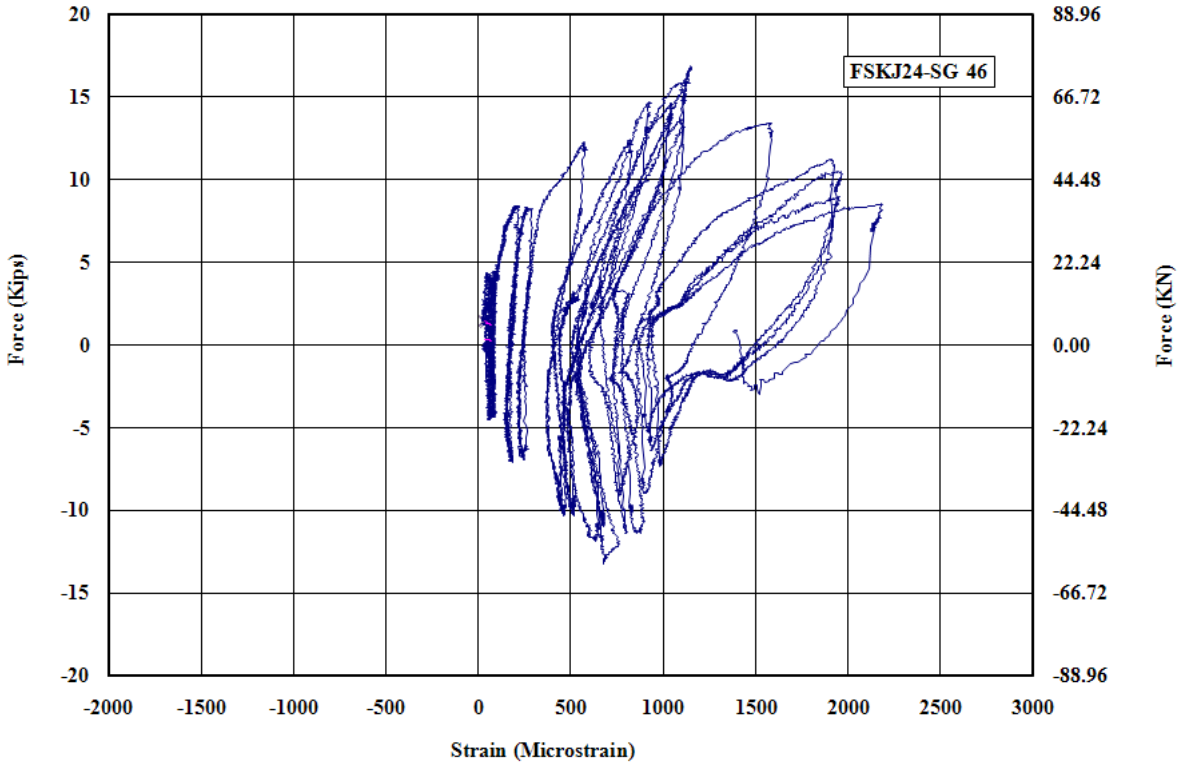

Figure F - 45: Measured Strain in Gauge No.46 for FSKJ24

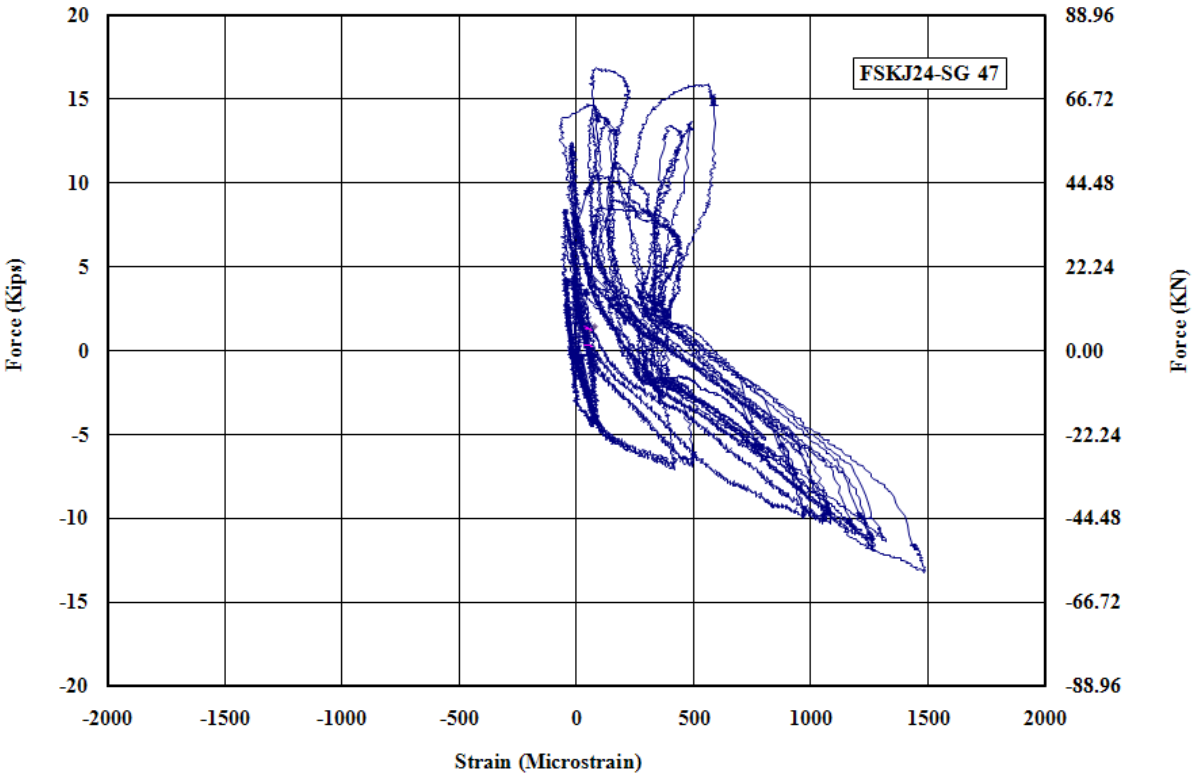

Figure F - 46: Measured Strain in Gauge No.47 for FSKJ24

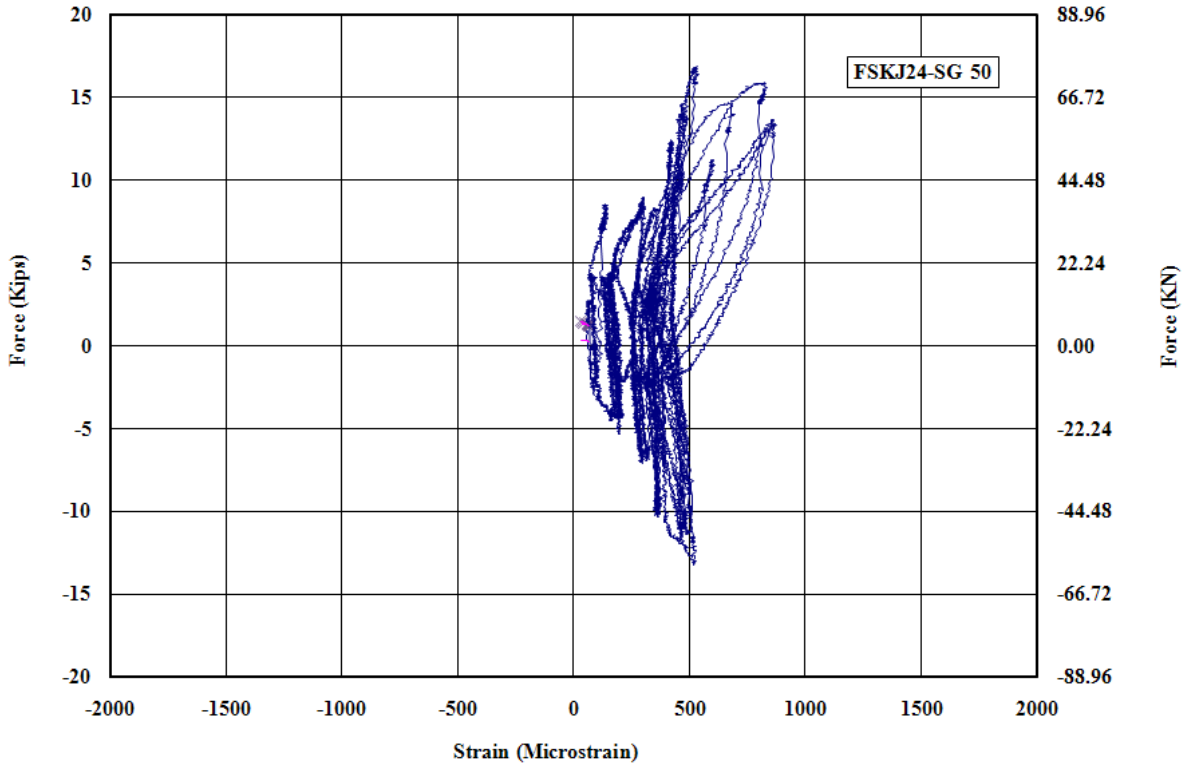

Figure F - 47: Measured Strain in Gauge No.50 for FSKJ24

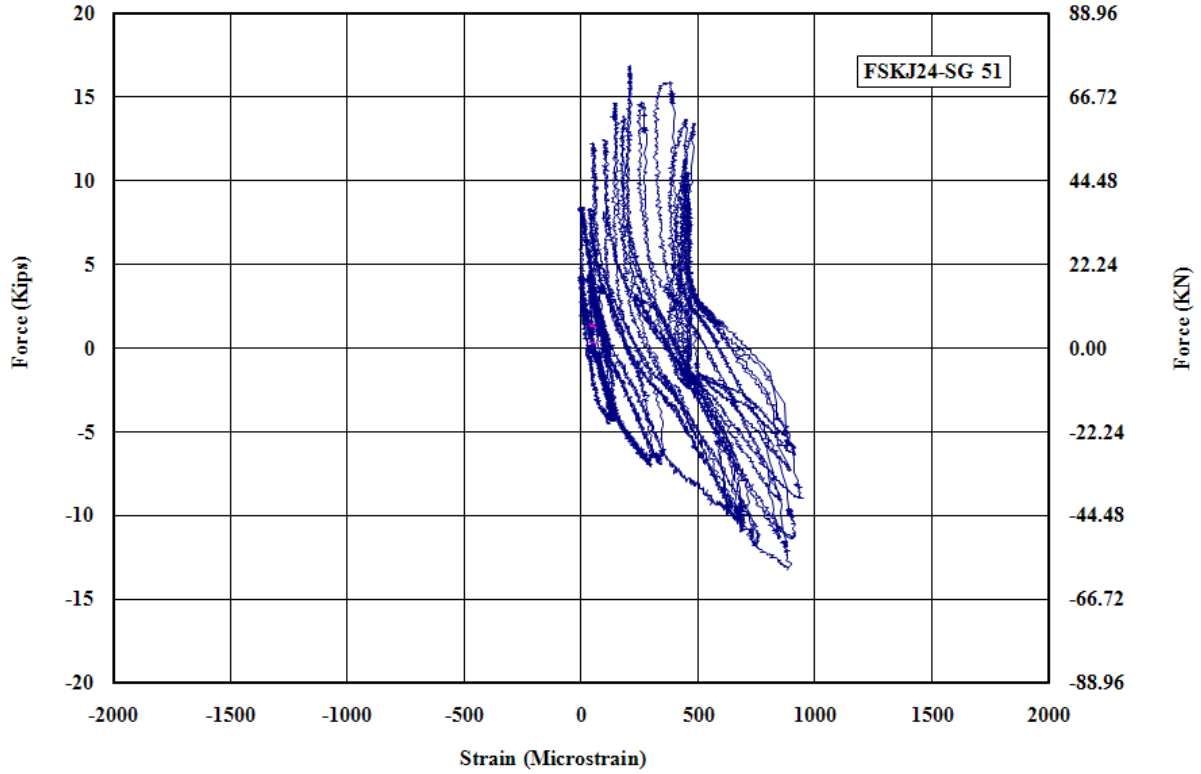

Figure F - 48: Measured Strain in Gauge No.51 for FSKJ24

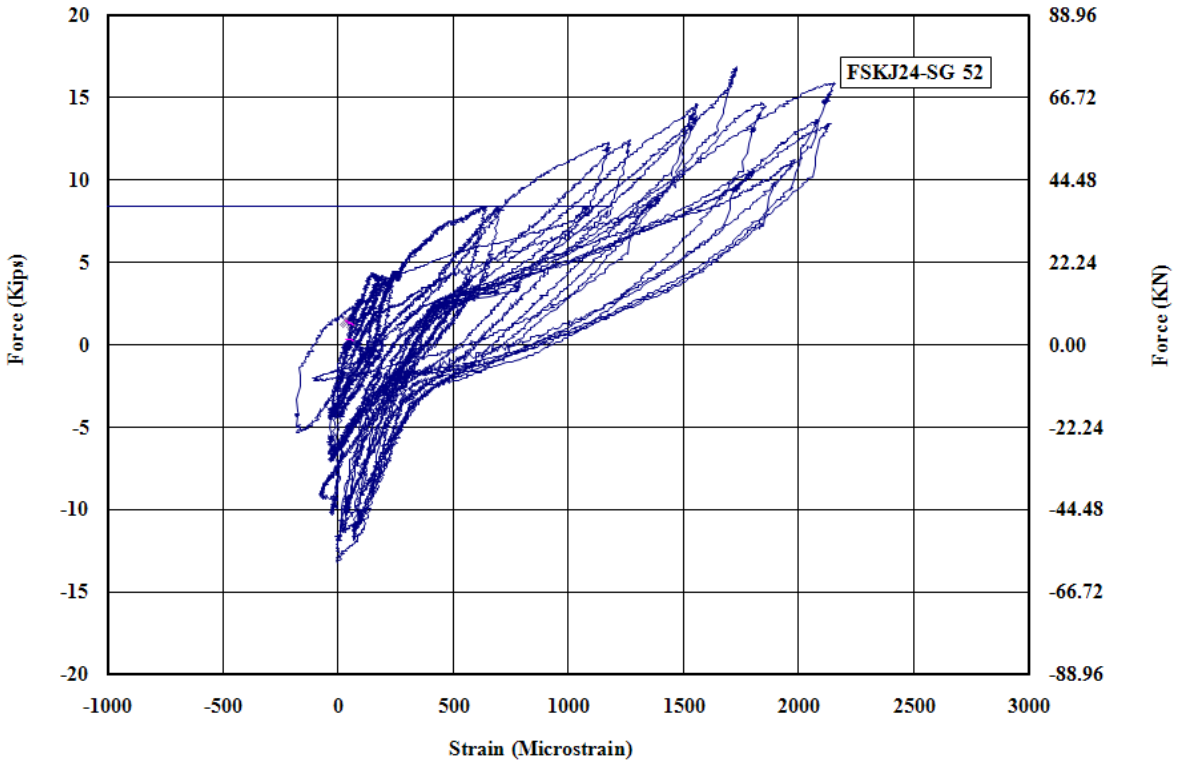

Figure F - 49: Measured Strain in Gauge No.52 for FSKJ24

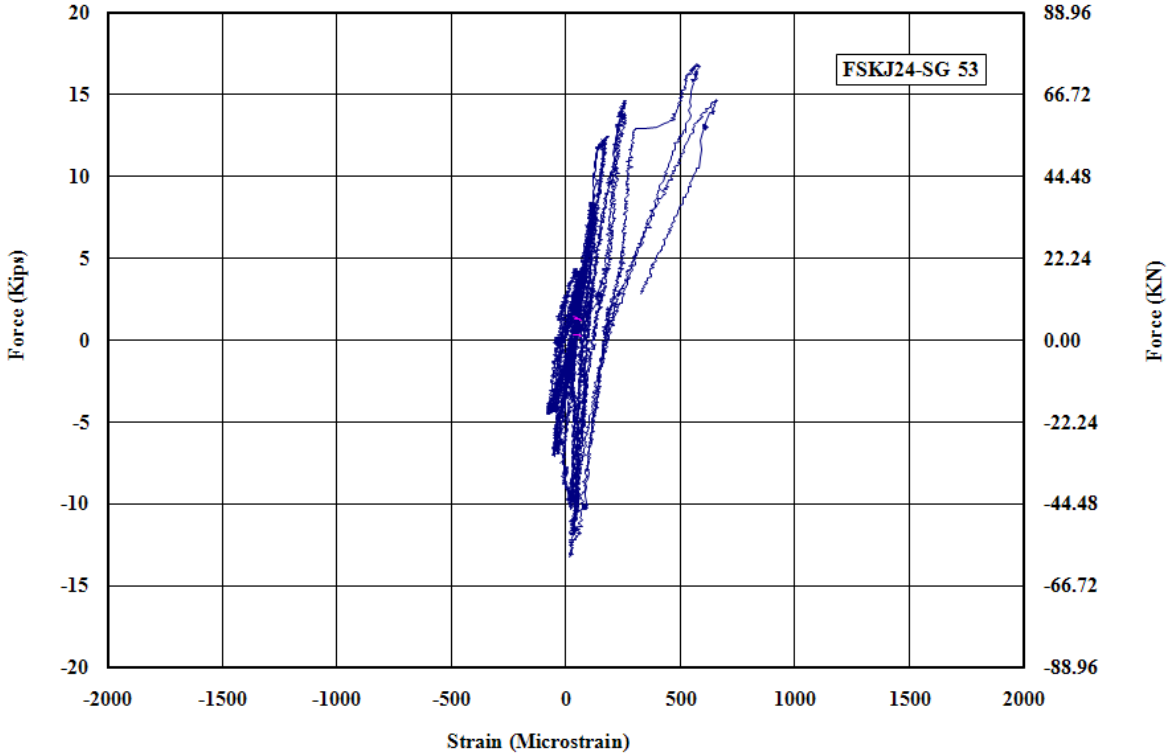

Figure F - 50: Measured Strain in Gauge No.53 for FSKJ24

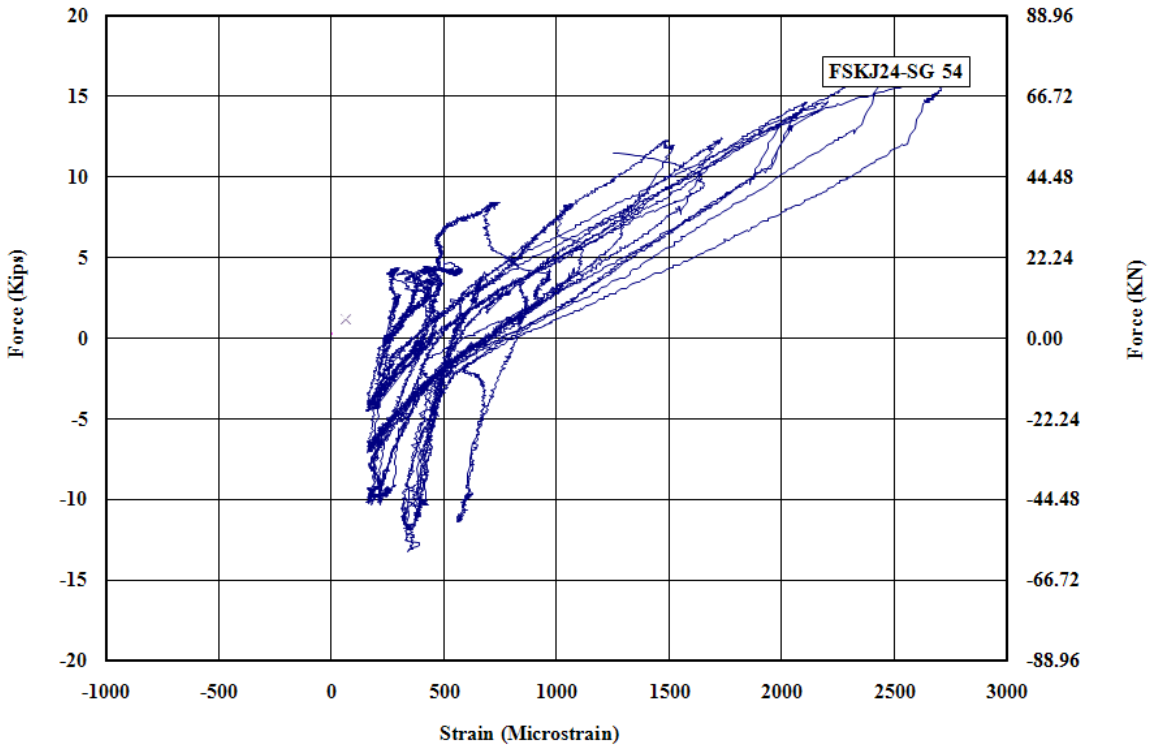

Figure F - 51: Measured Strain in Gauge No.54 for FSKJ24

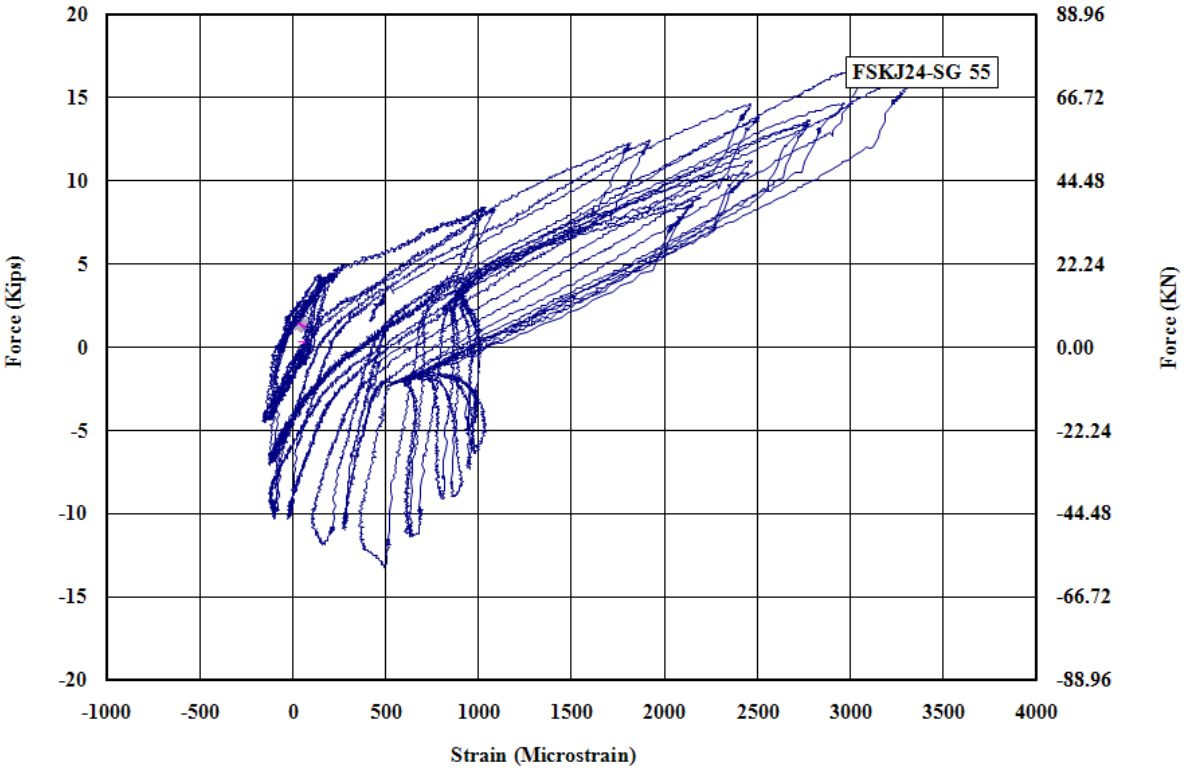

Figure F - 52: Measured Strain in Gauge No.55 for FSKJ24

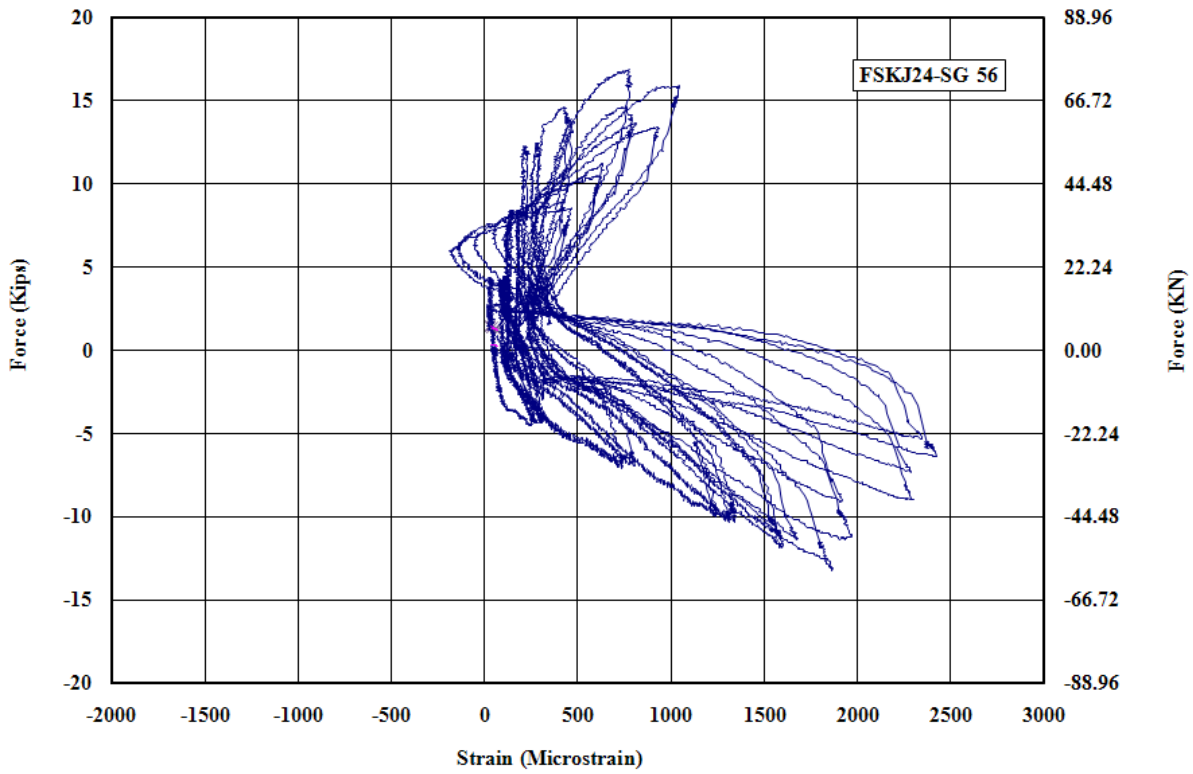

Figure F - 53: Measured Strain in Gauge No.56 for FSKJ24

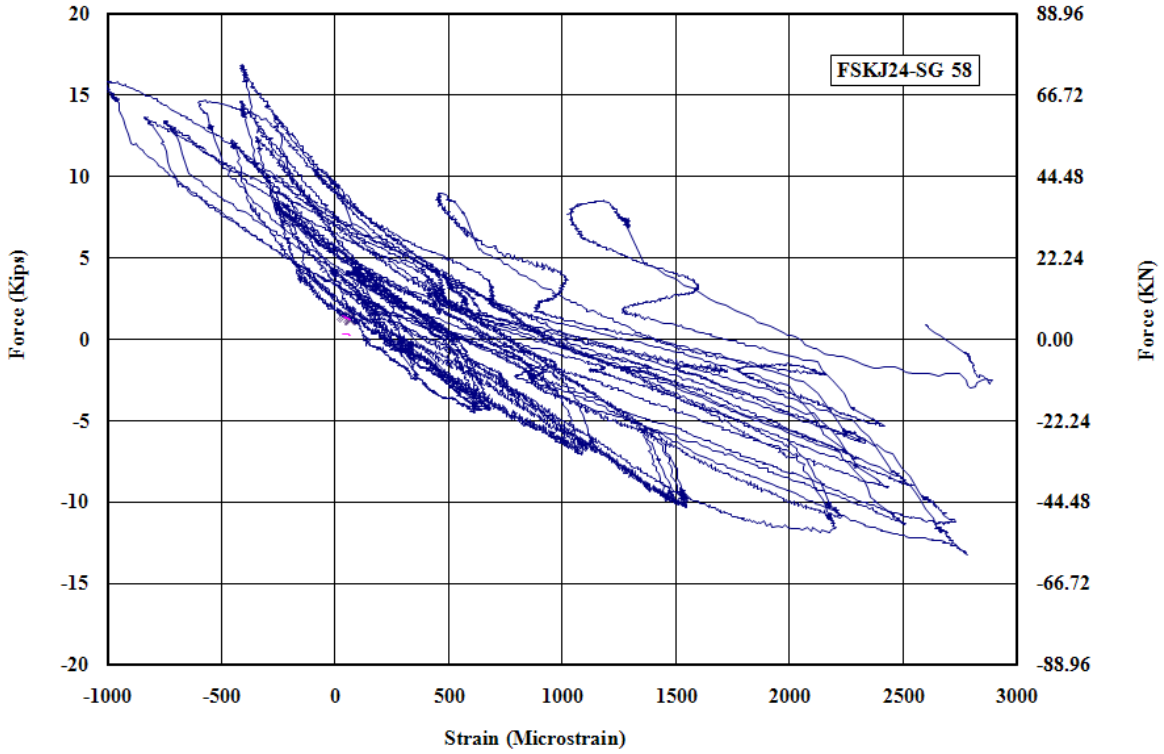

Figure F - 54: Measured Strain in Gauge No.58 for FSKJ24

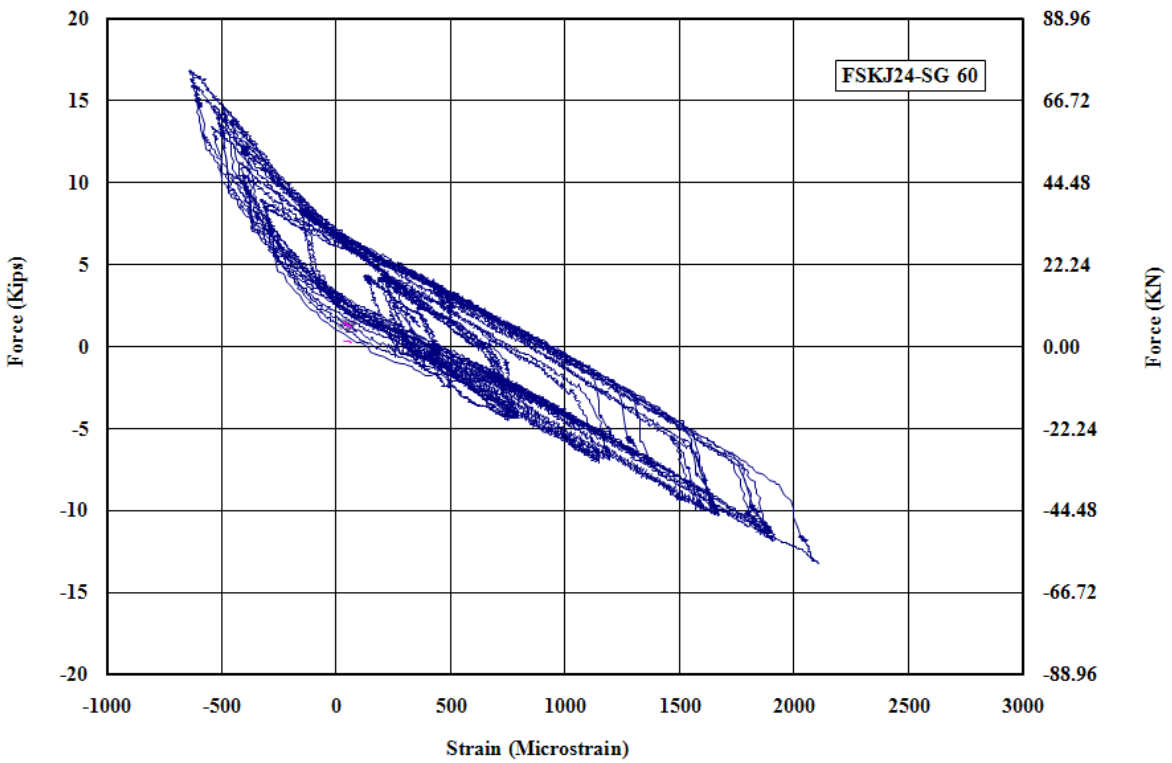

Figure F - 55: Measured Strain in Gauge No.60 for FSKJ24

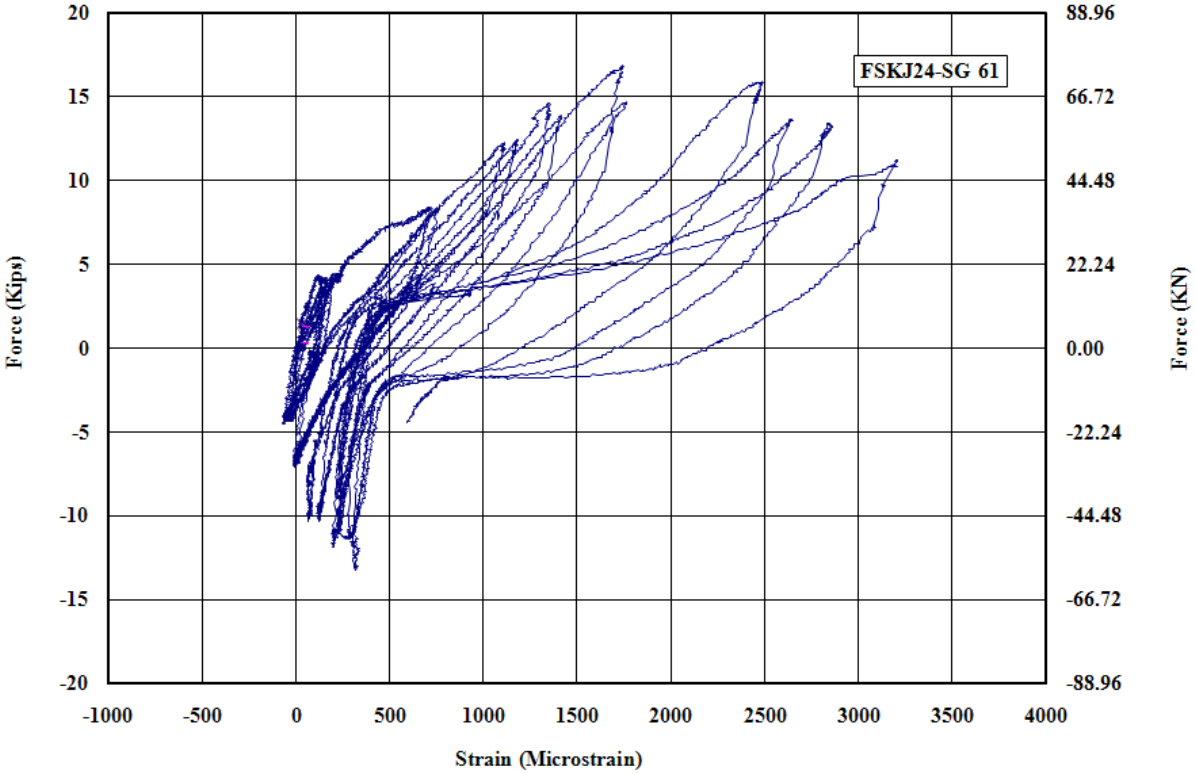

Figure F - 56: Measured Strain in Gauge No.61 for FSKJ24

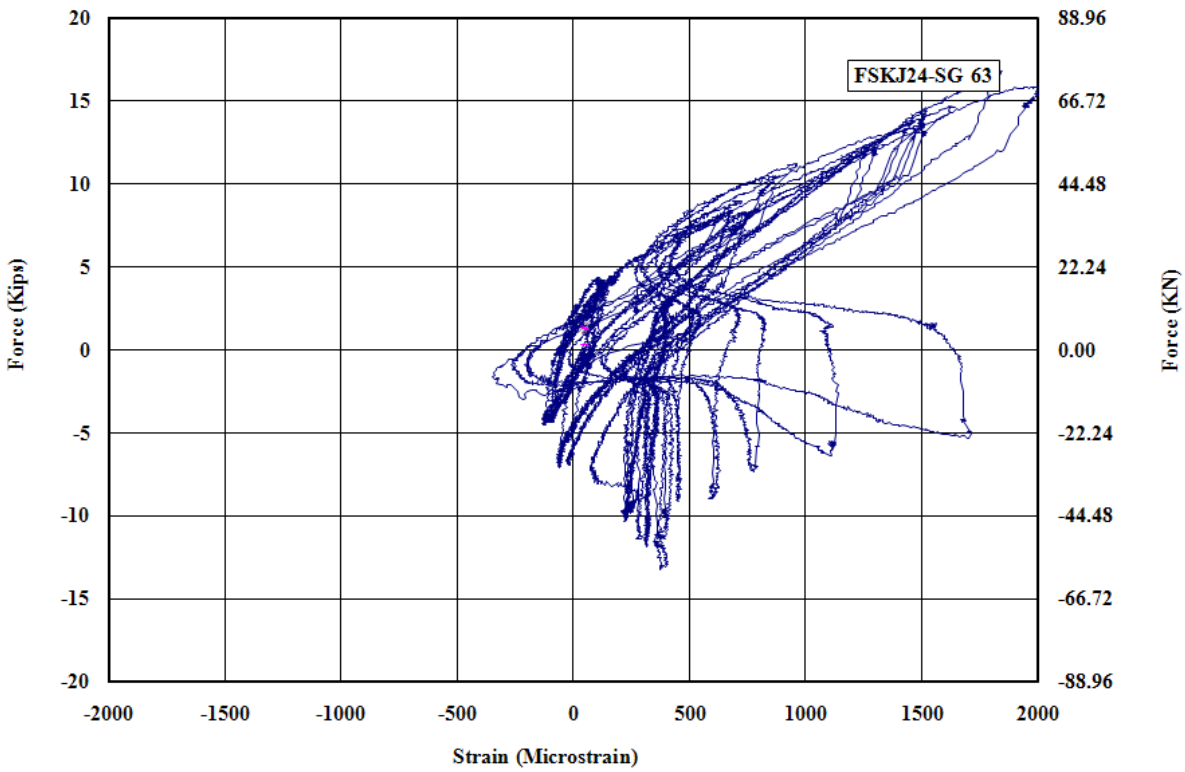

Figure F - 57: Measured Strain in Gauge No.63 for FSKJ24

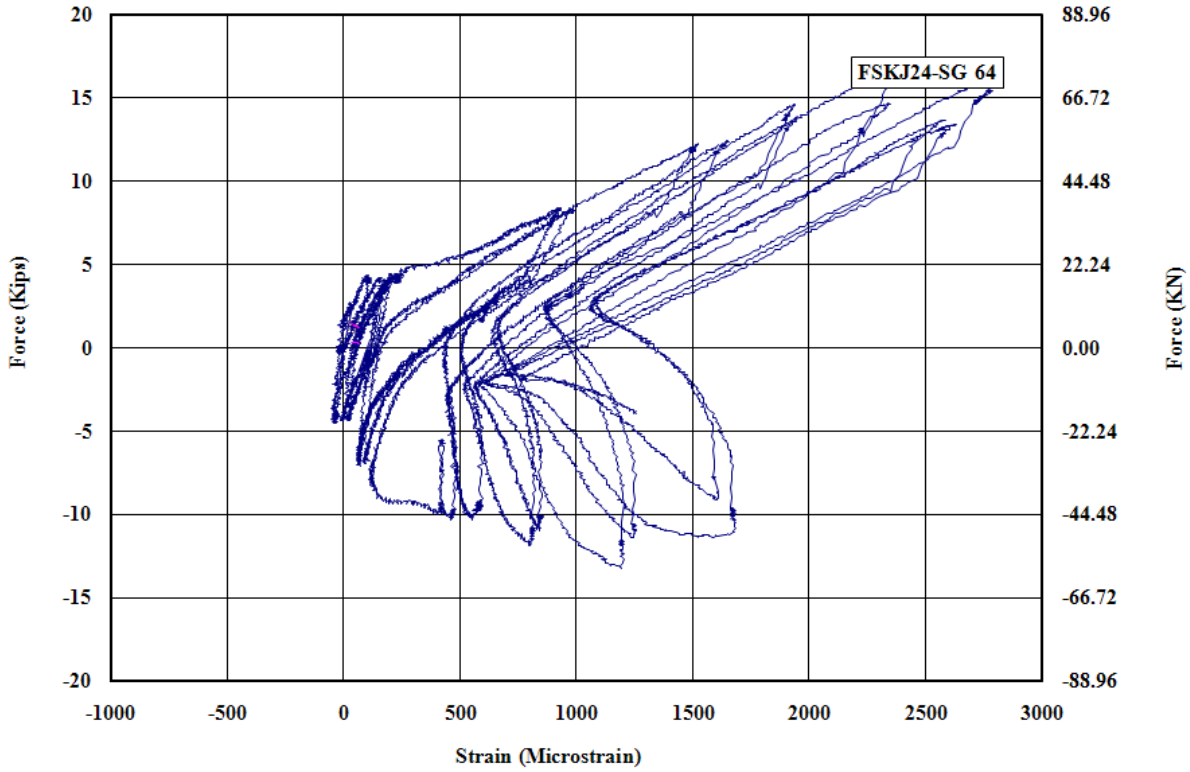

Figure F - 58: Measured Strain in Gauge No.64 for FSKJ24

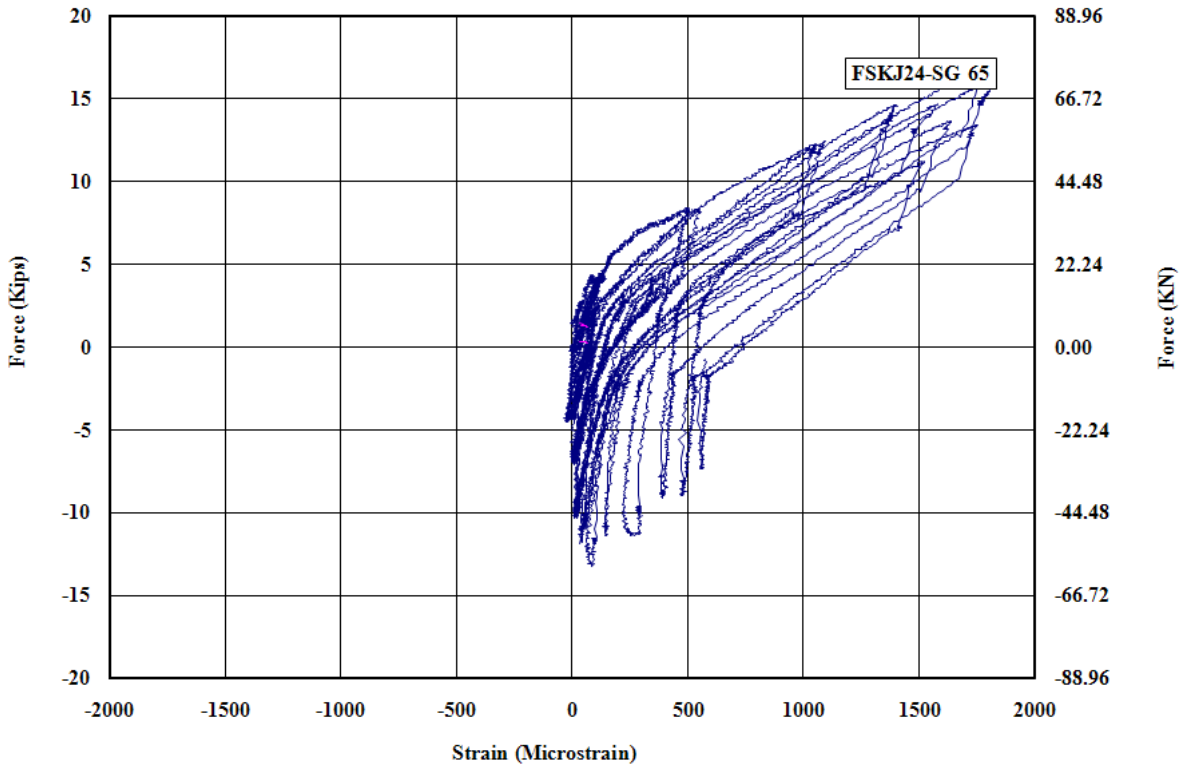

Figure F - 59: Measured Strain in Gauge No.65 for FSKJ24

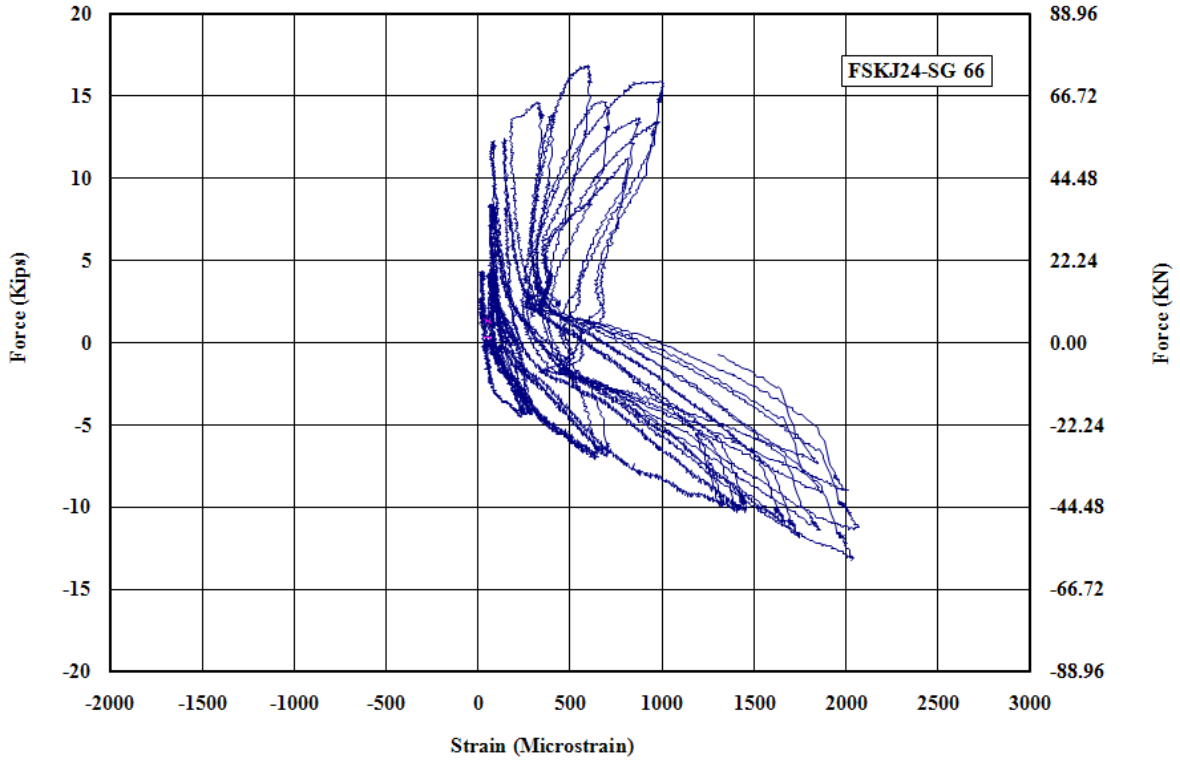

Figure F - 60: Measured Strain in Gauge No.66 for FSKJ24

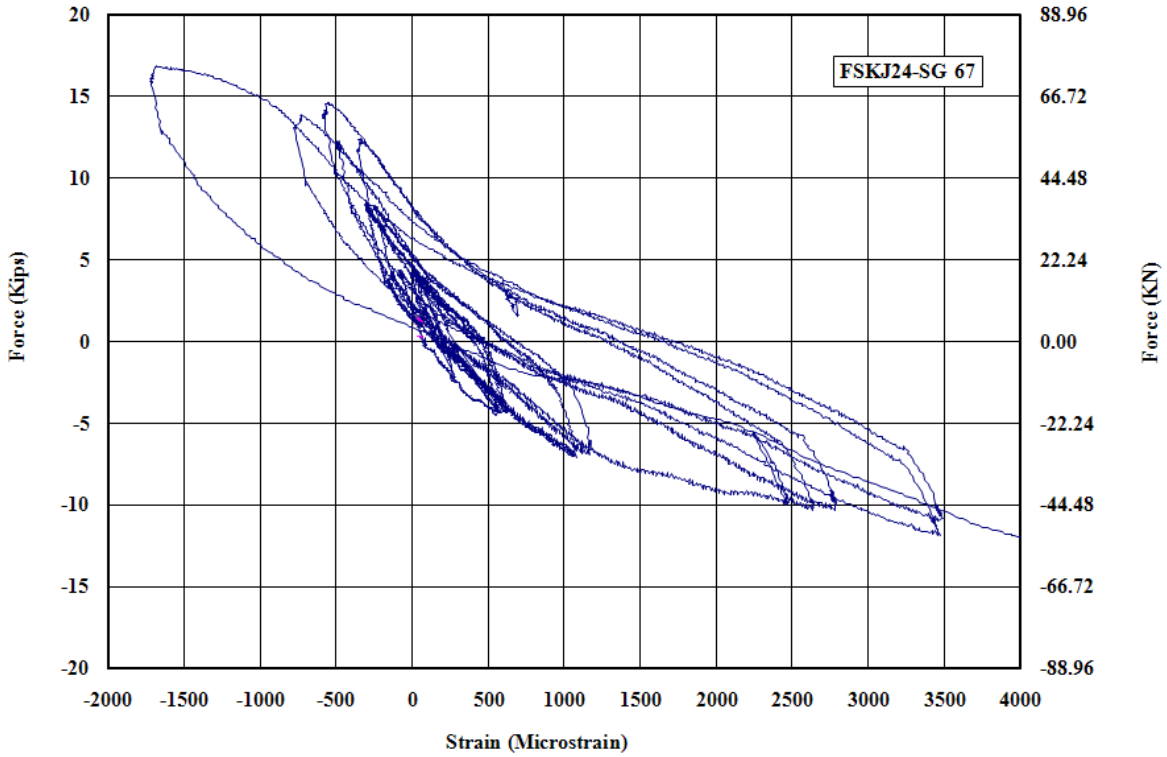

Figure F - 61: Measured Strain in Gauge No.67 for FSKJ24

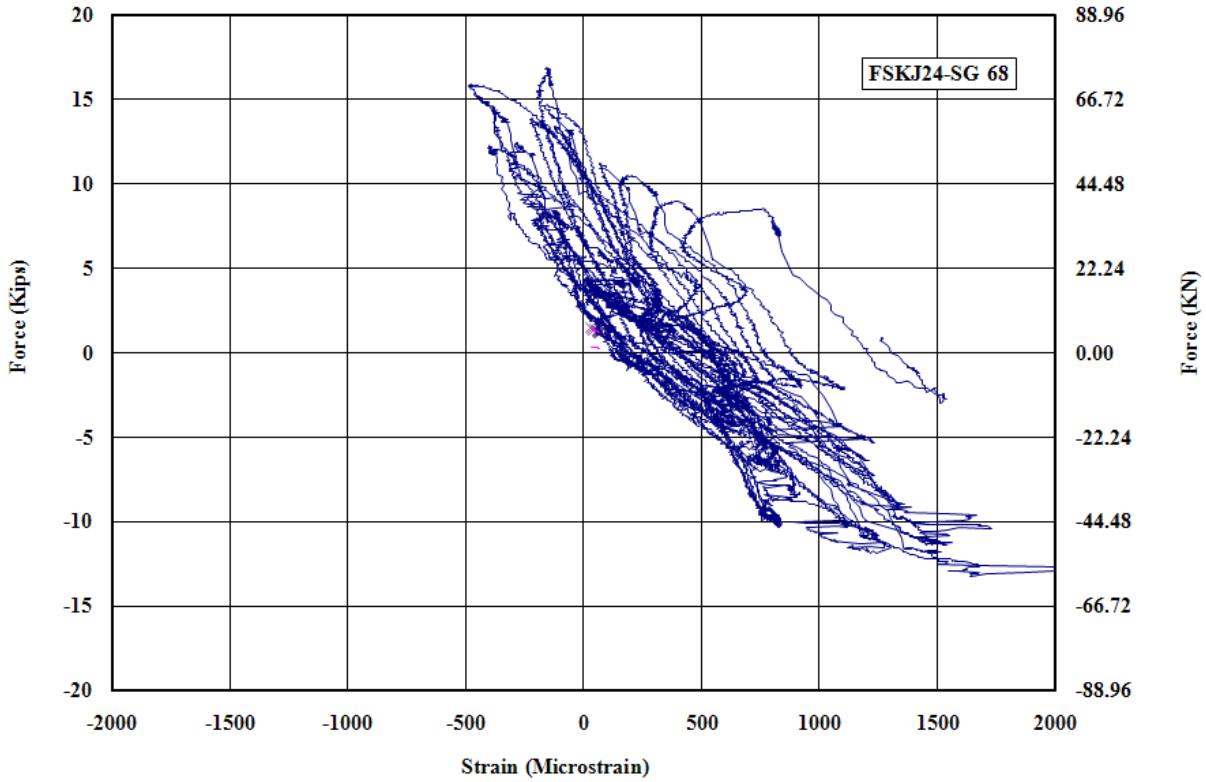

Figure F - 62: Measured Strain in Gauge No.68 for FSKJ24

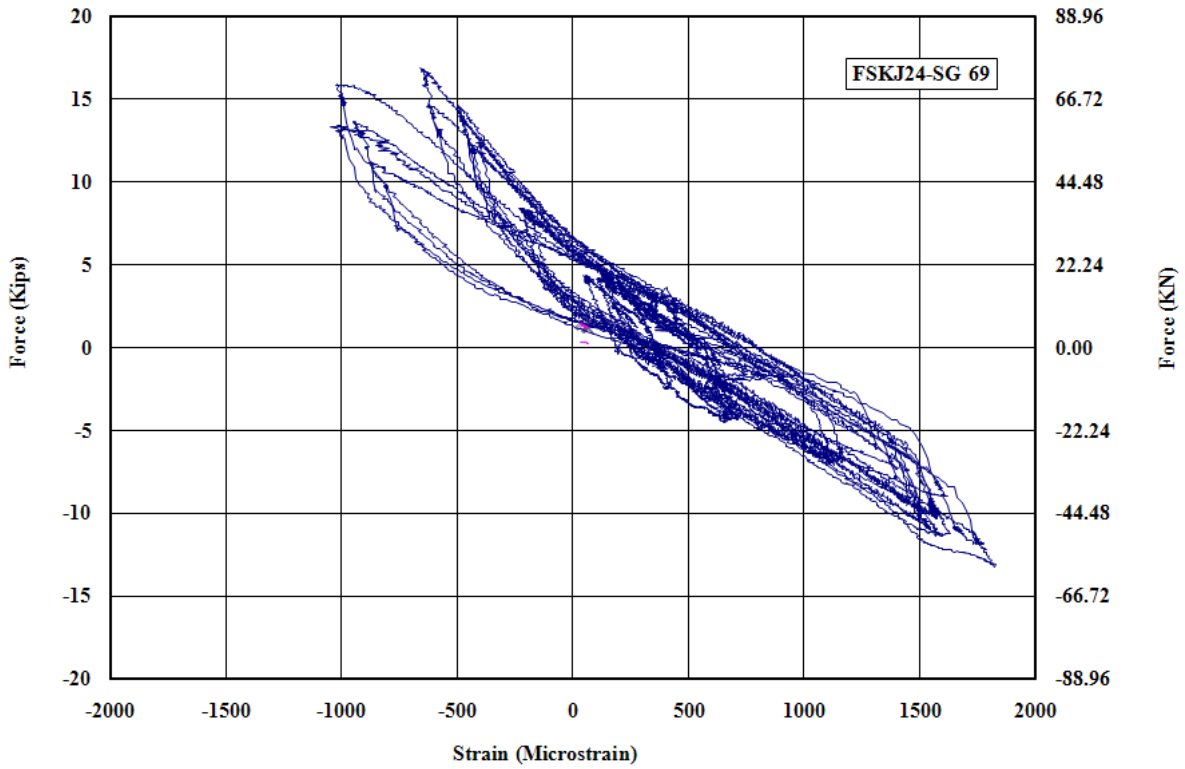

Figure F - 63: Measured Strain in Gauge No.69 for FSKJ24

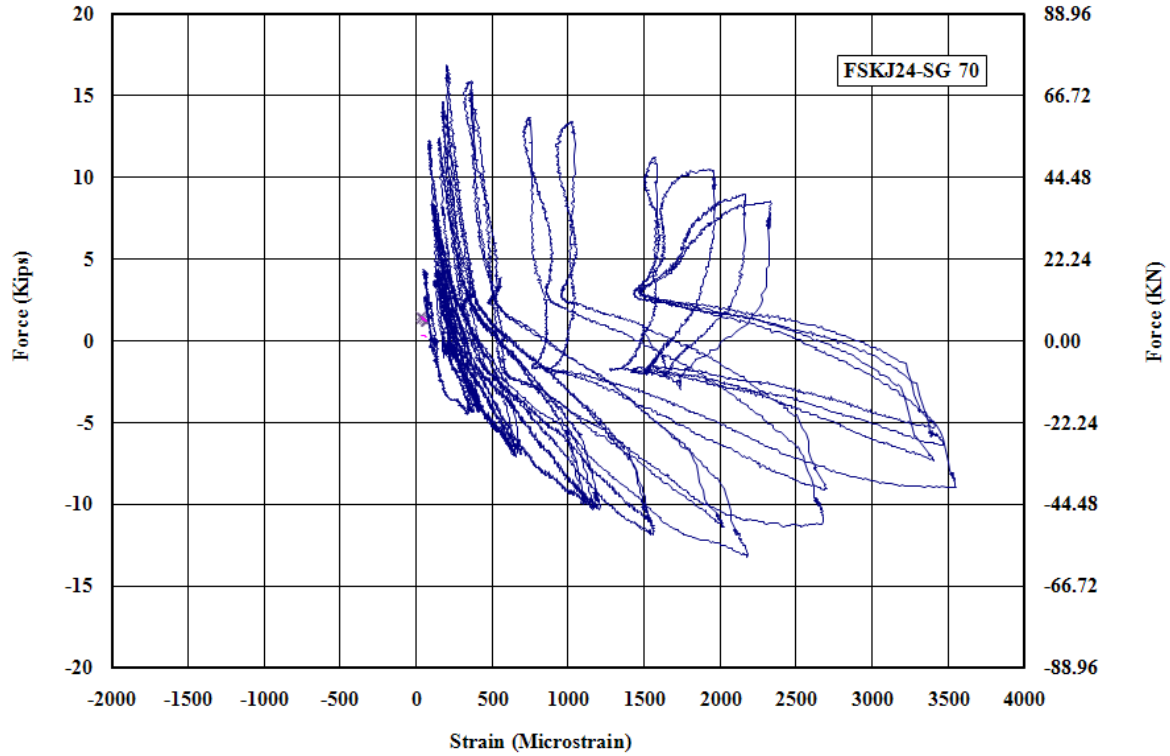

Figure F - 64: Measured Strain in Gauge No.70 for FSKJ24

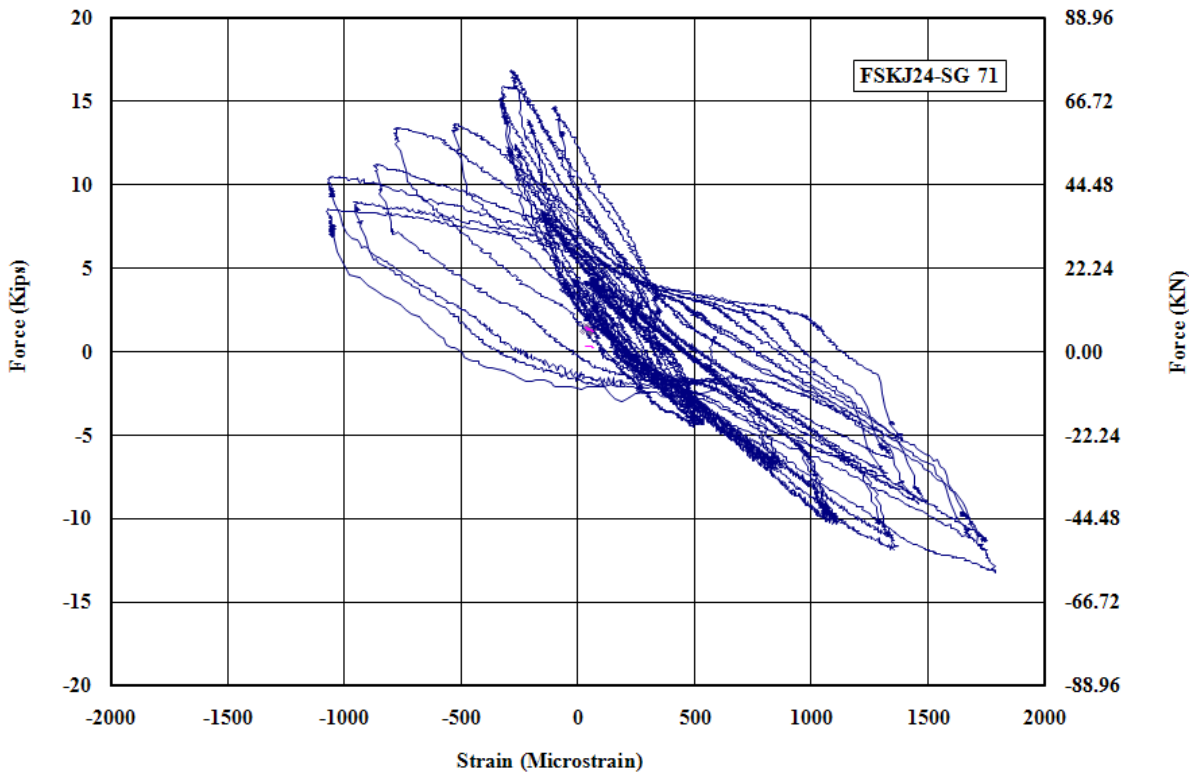

Figure F - 65: Measured Strain in Gauge No.71 for FSKJ24

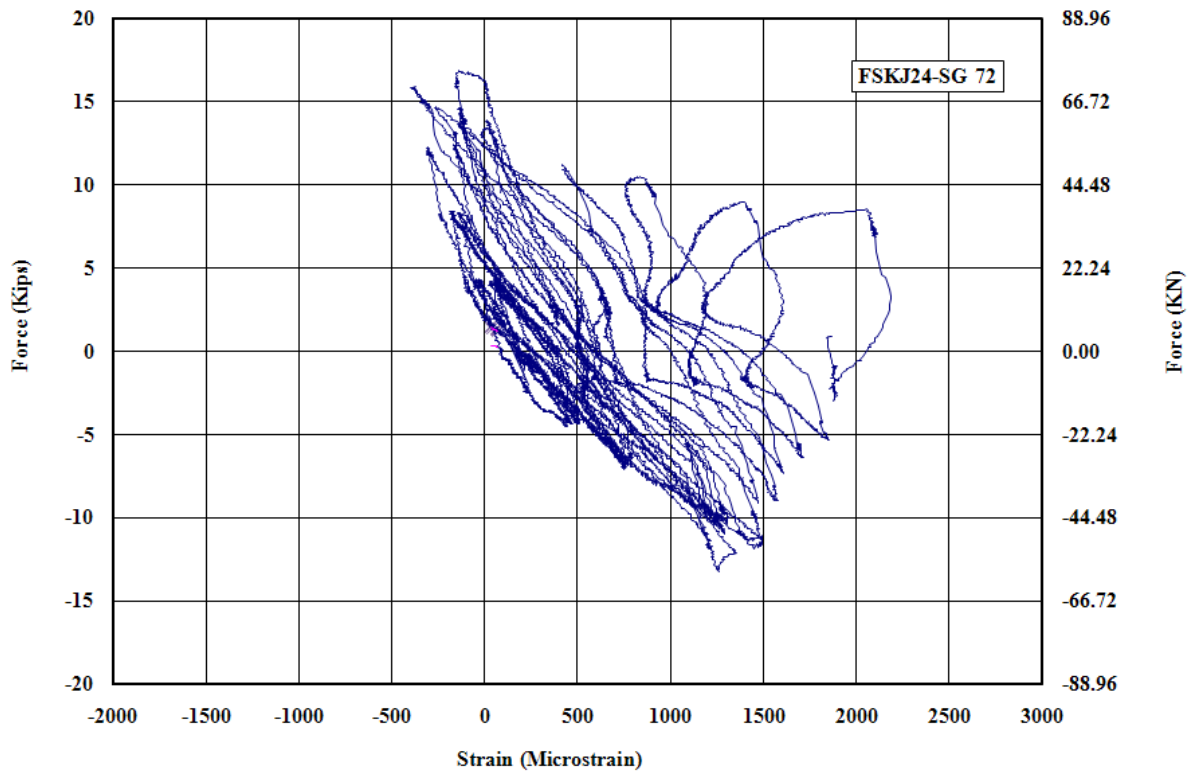

Figure F - 66: Measured Strain in Gauge No.72 for FSKJ24

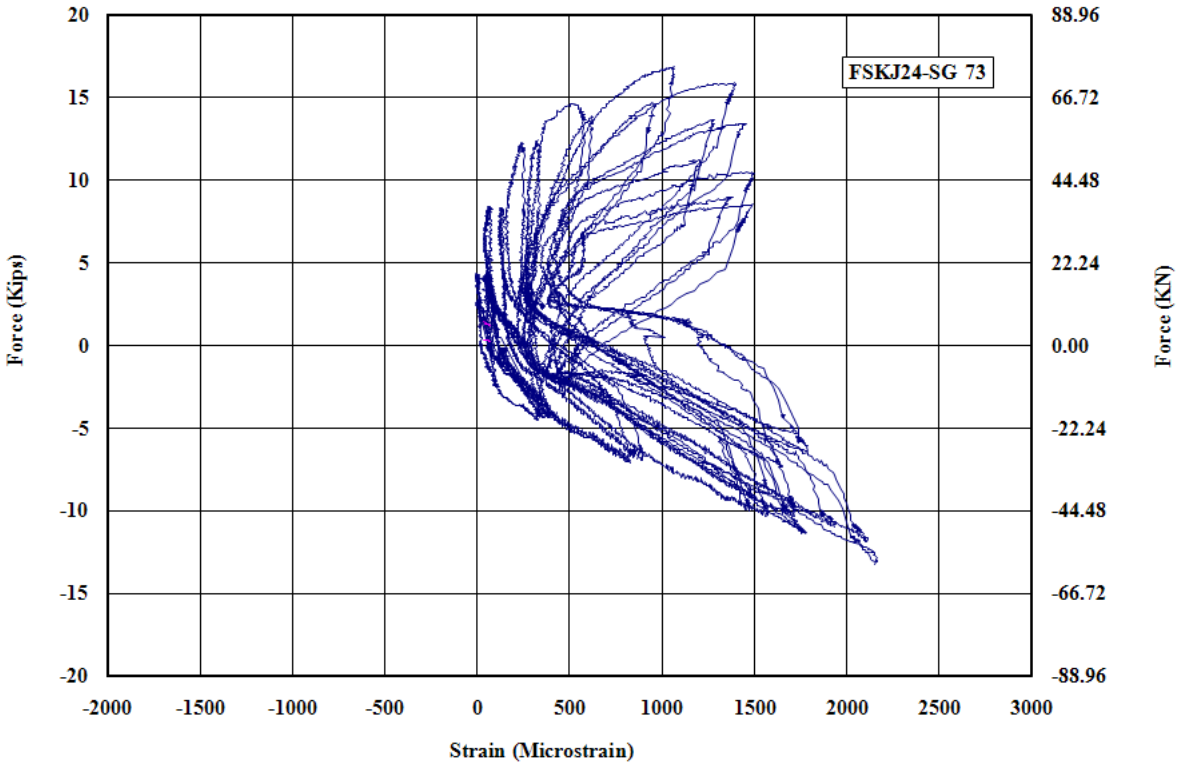

Figure F - 67: Measured Strain in Gauge No.73 for FSKJ24

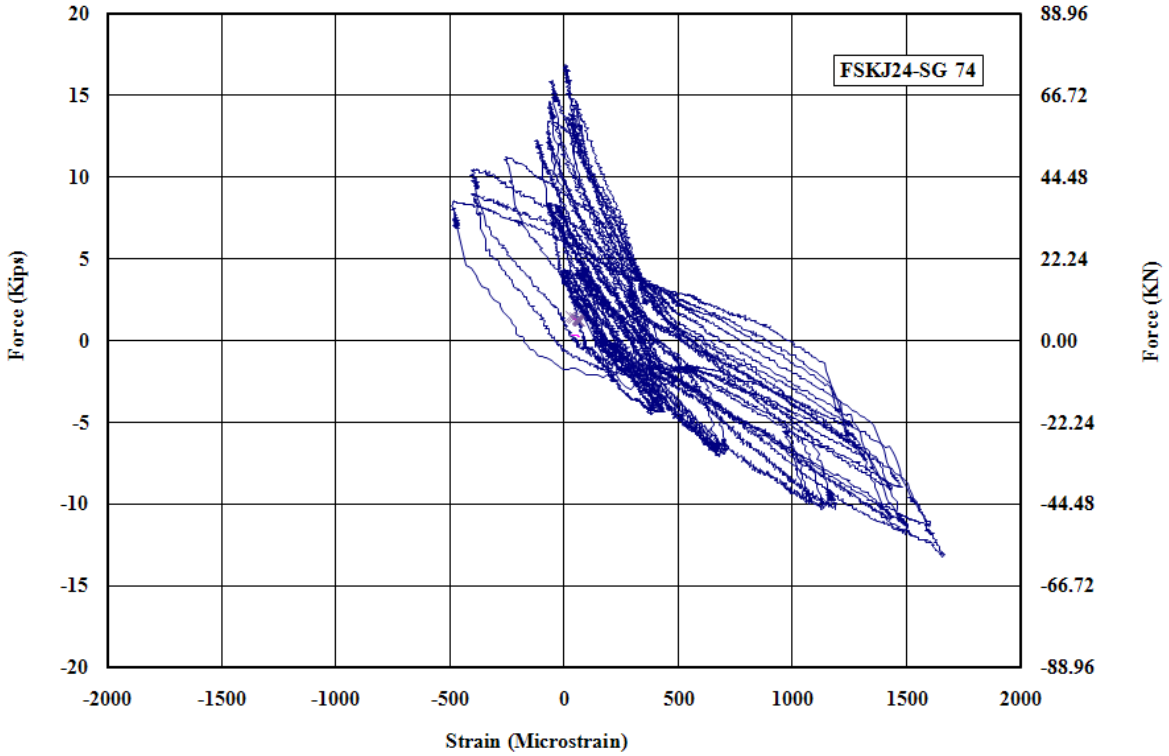

Figure F - 68: Measured Strain in Gauge No.74 for FSKJ24

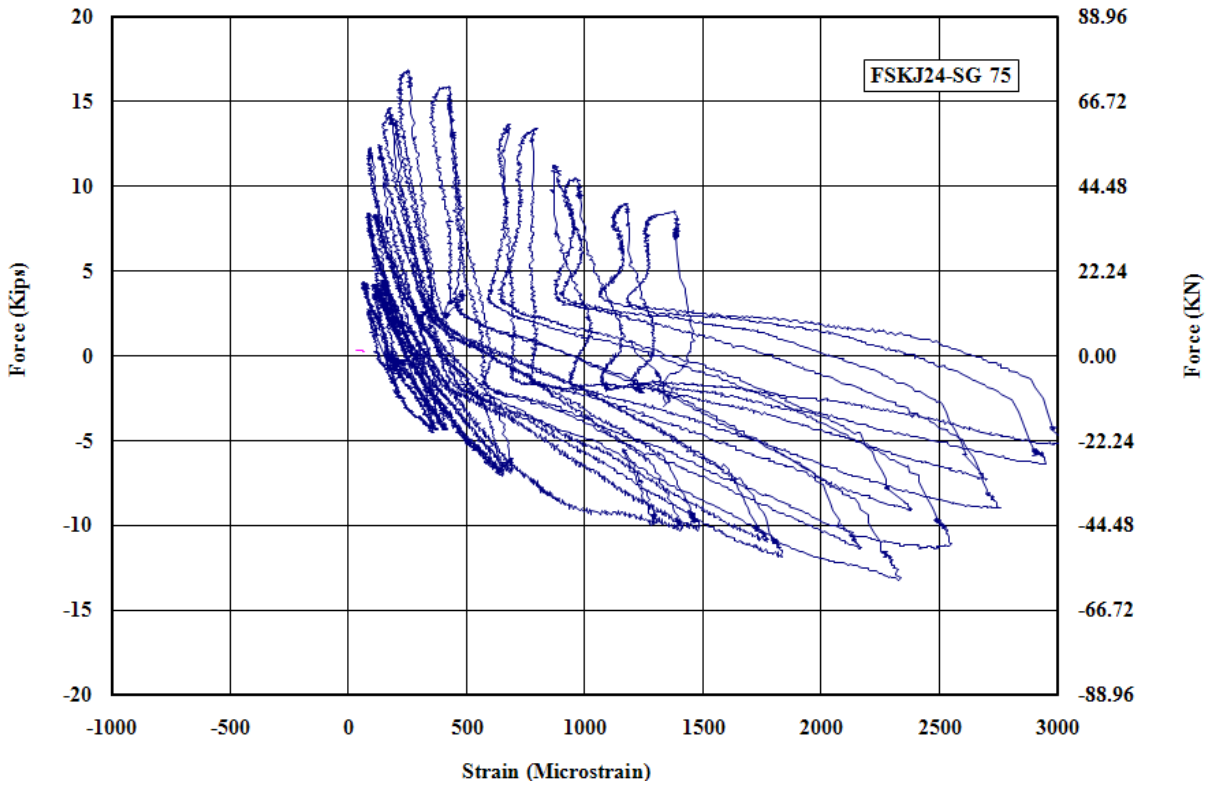

Figure F - 69: Measured Strain in Gauge No.75 for FSKJ24

Appendix G

Specimen FSRCC24-M

(Modified Flat-Slab T-Joint with 16-in. diameter pile)

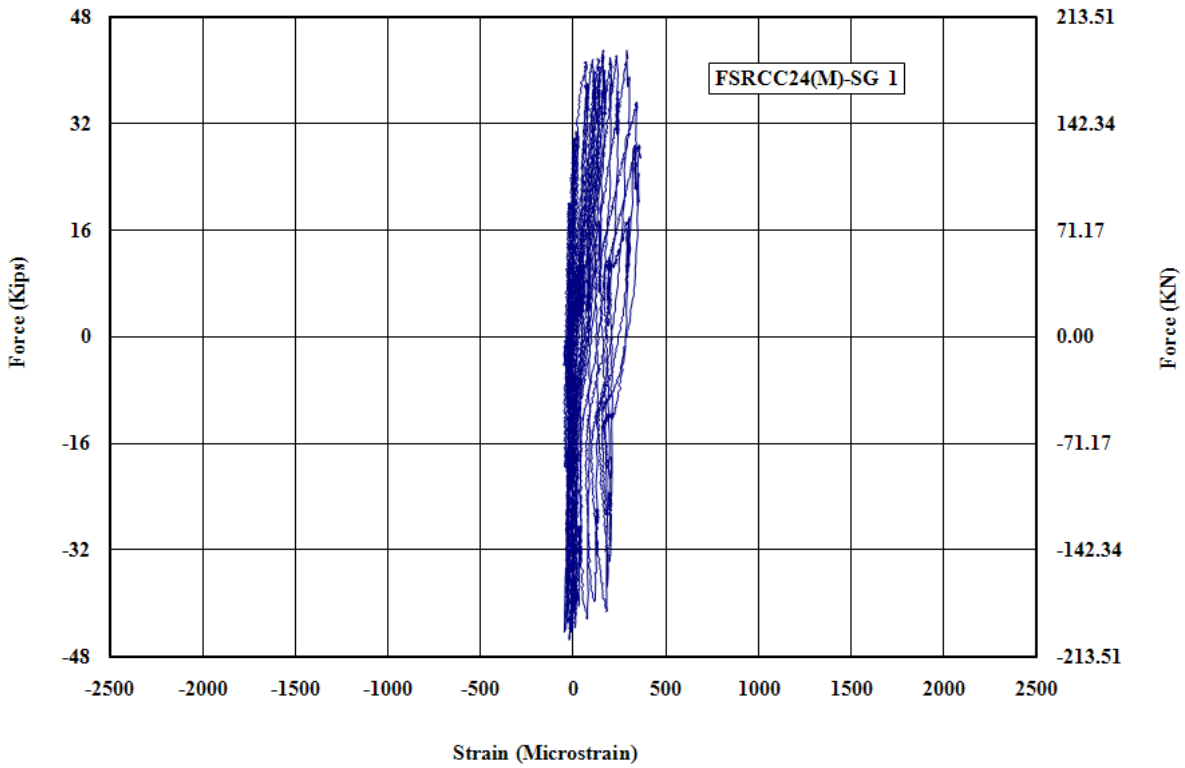

Figure G - 1: Measured Strain in Gauge No.1 for FSRCC24-M

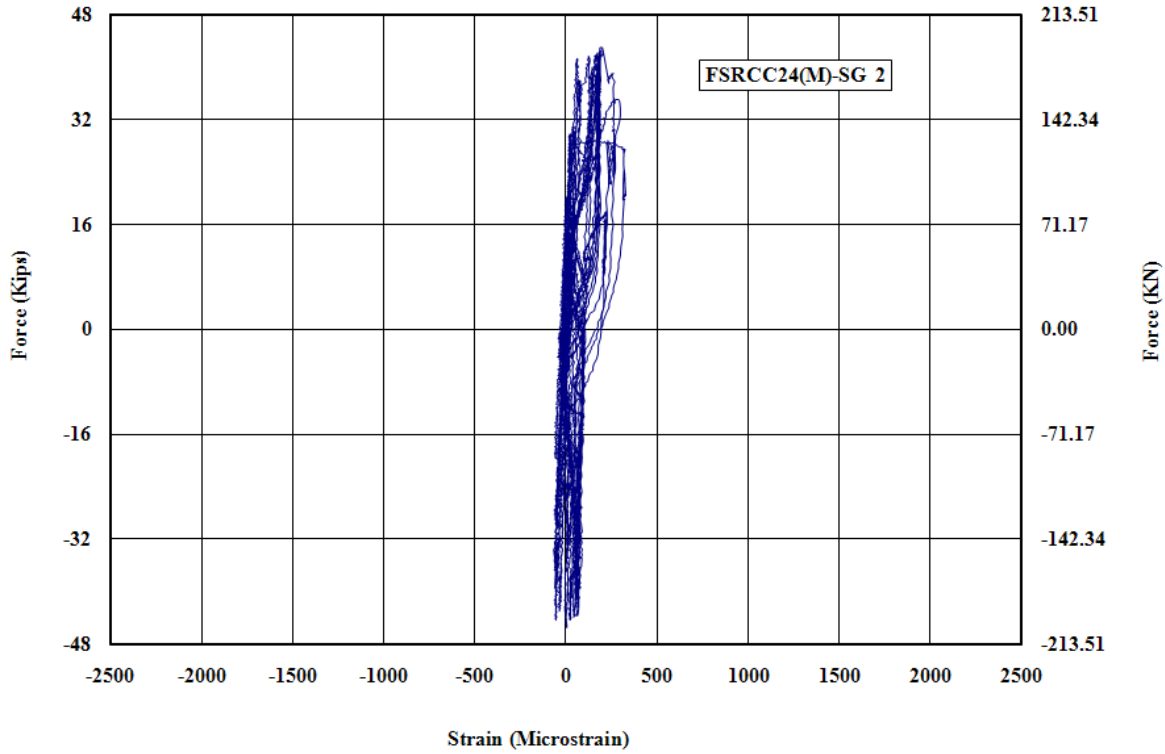

Figure G - 2: Measured Strain in Gauge No.2 for FSRCC24-M

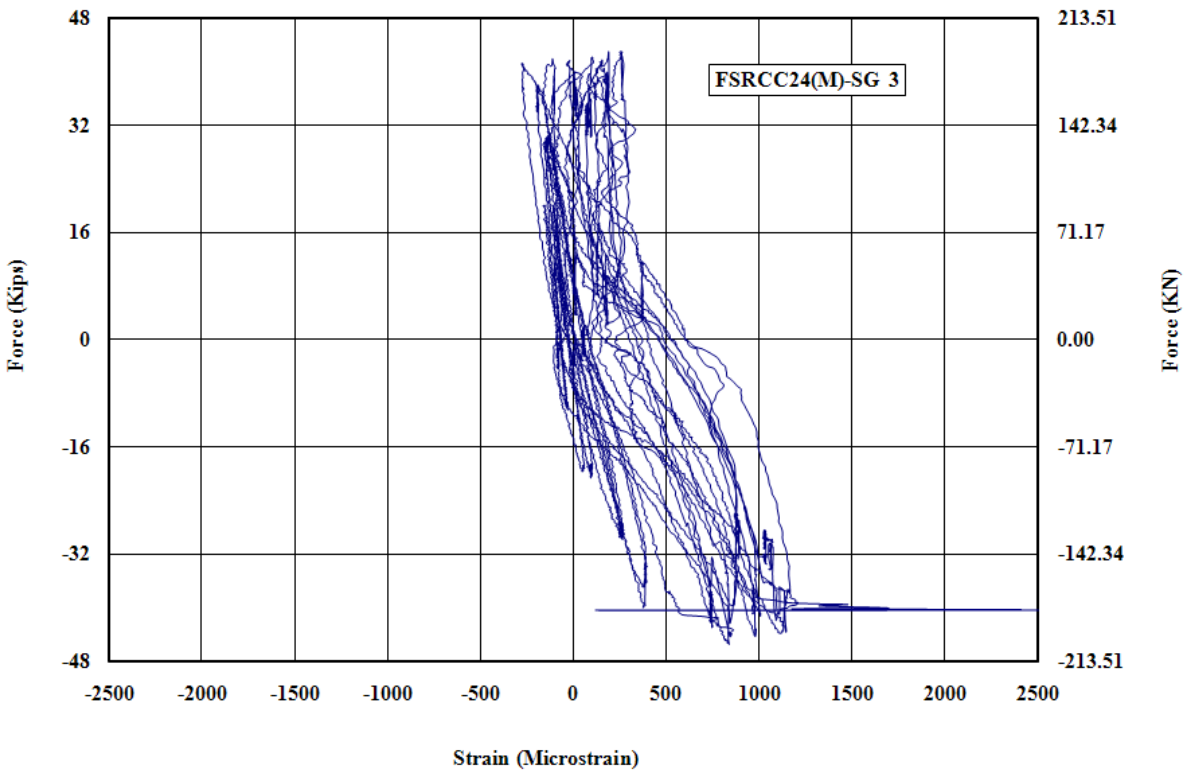

Figure G - 3: Measured Strain in Gauge No.3 for FSRCC24-M

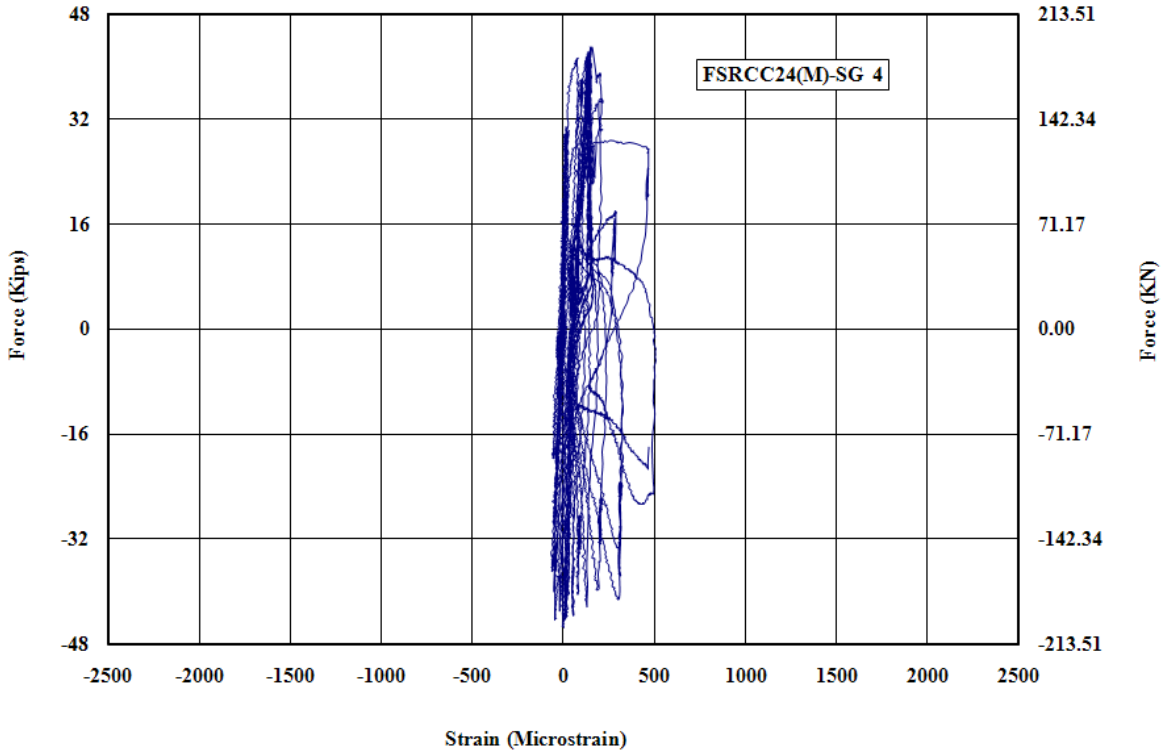

Figure G - 4: Measured Strain in Gauge No.4 for FSRCC24-M

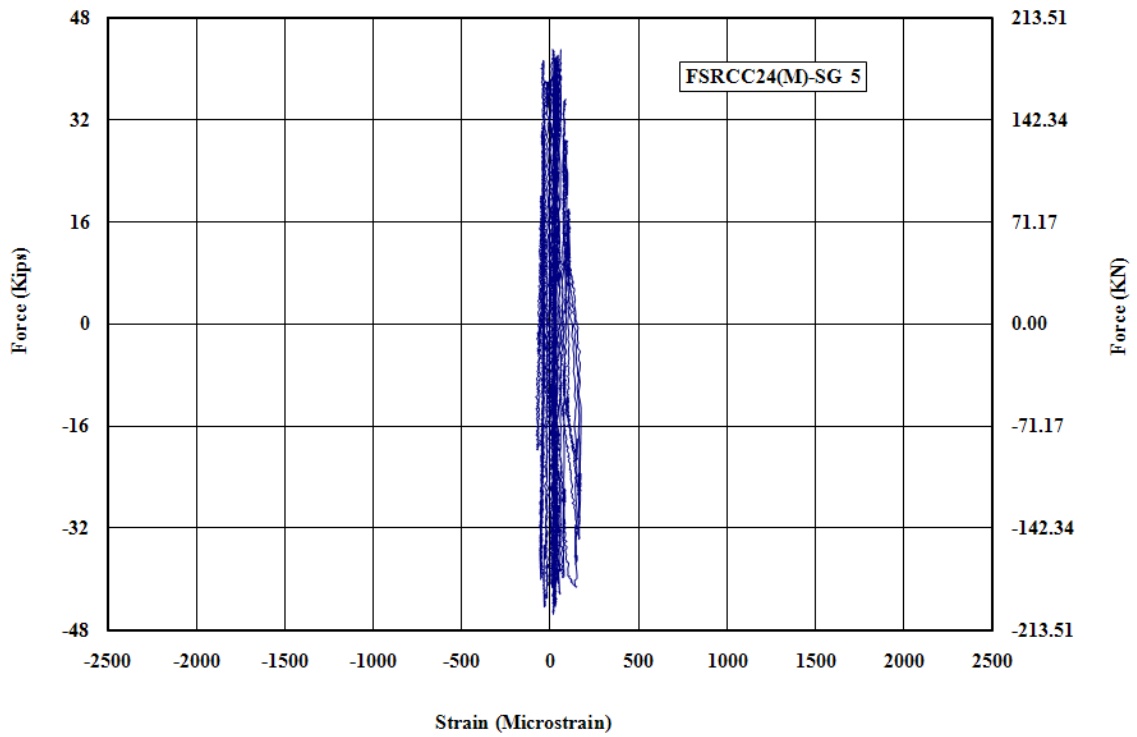

Figure G - 5: Measured Strain in Gauge No.5 for FSRCC24-M

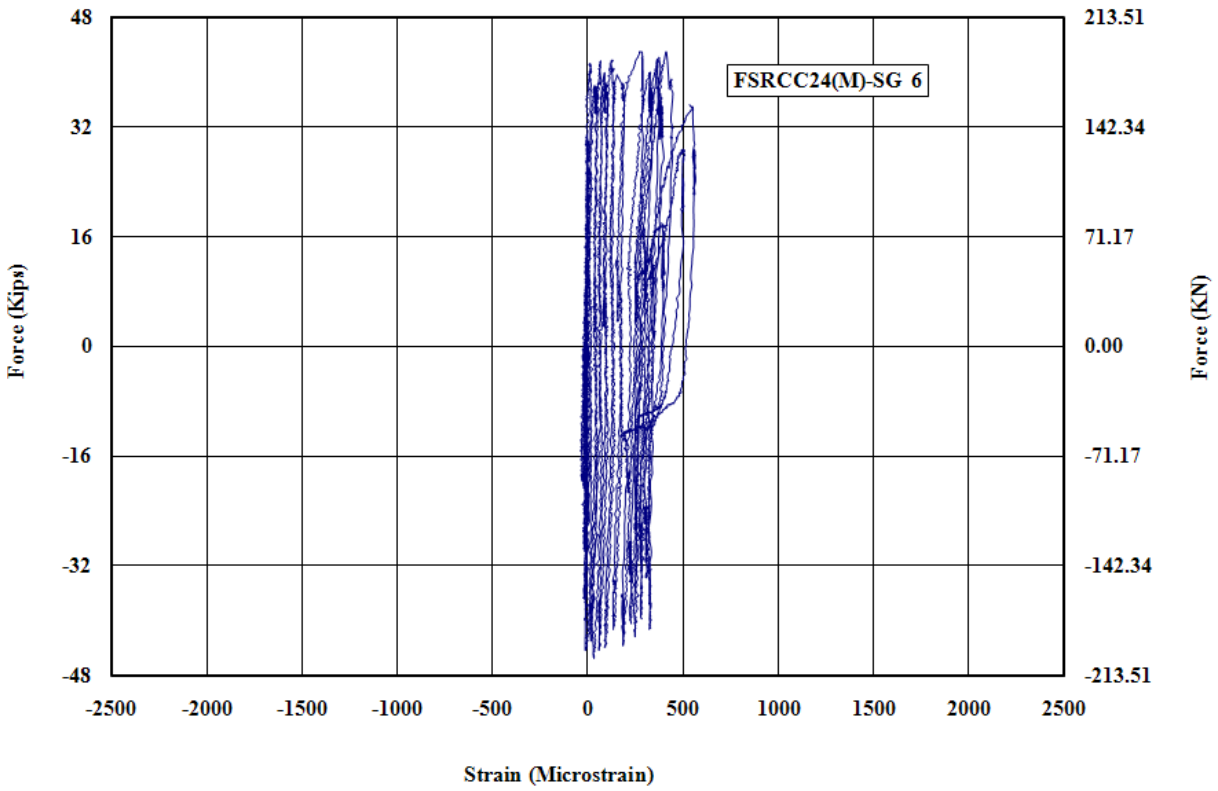

Figure G - 6: Measured Strain in Gauge No.6 for FSRCC24-M

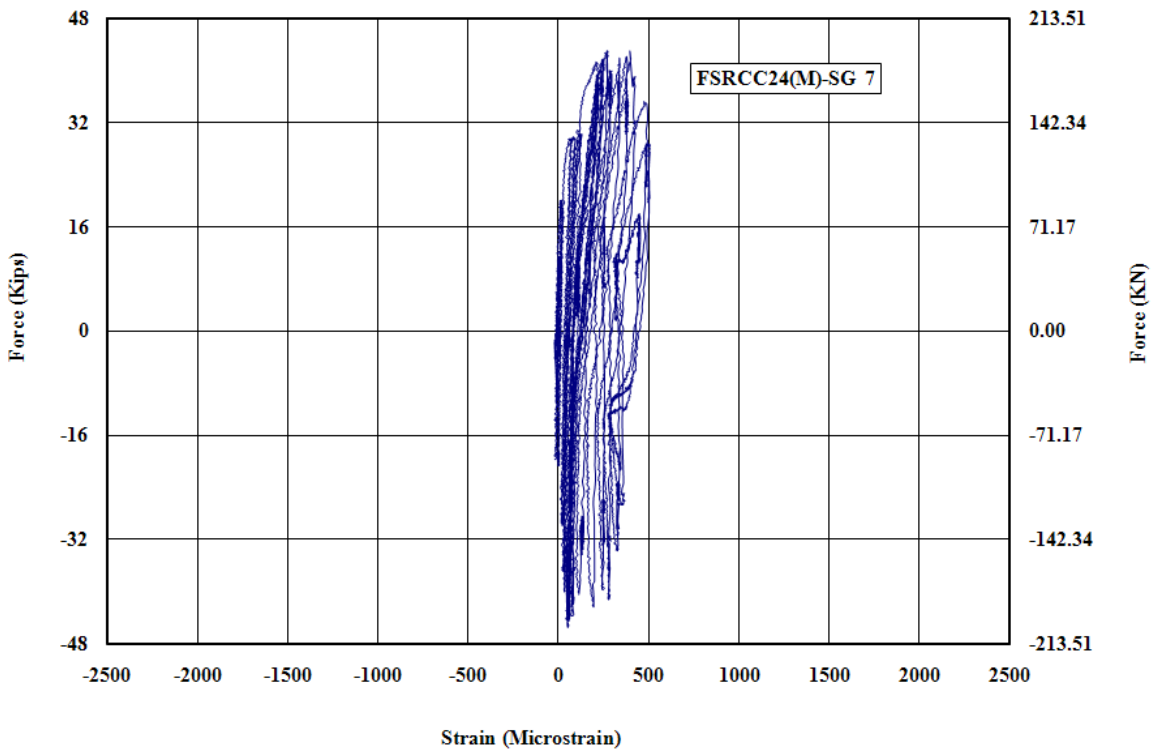

Figure G - 7: Measured Strain in Gauge No.7 for FSRCC24-M

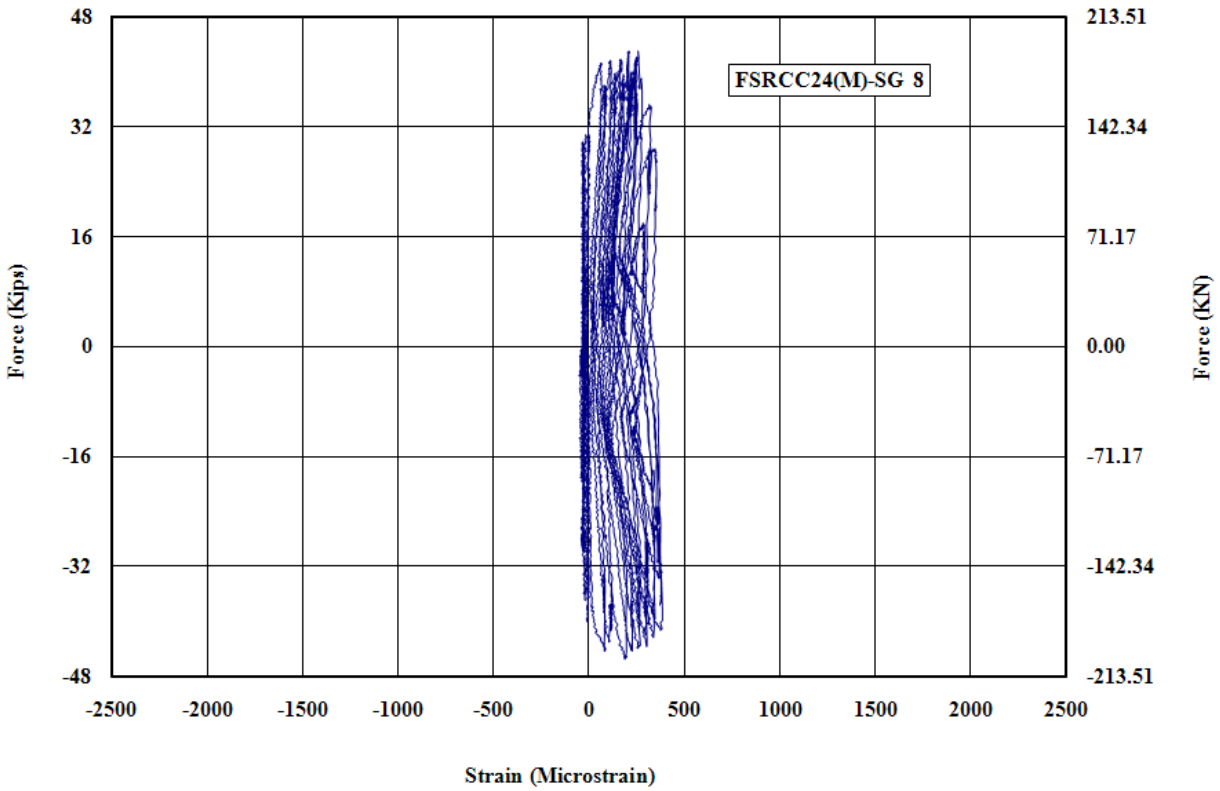

Figure G - 8: Measured Strain in Gauge No.8 for FSRCC24-M

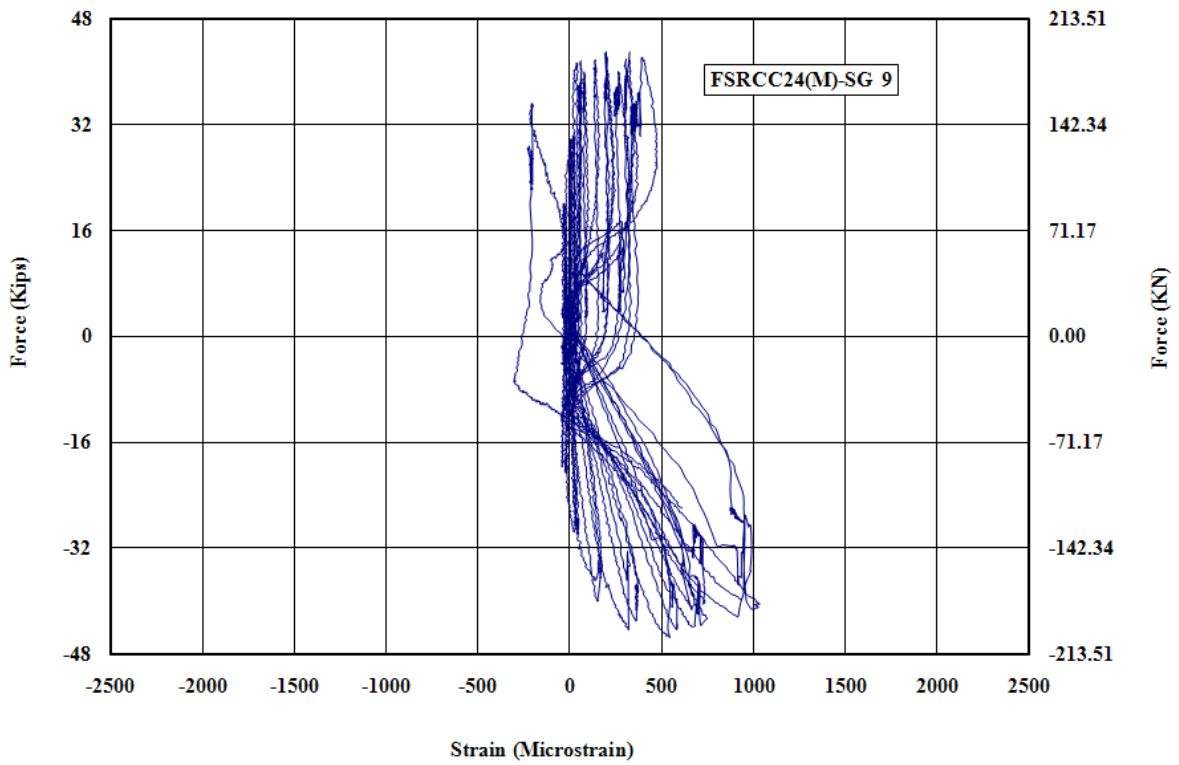

Figure G - 9: Measured Strain in Gauge No.9 for FSRCC24-M

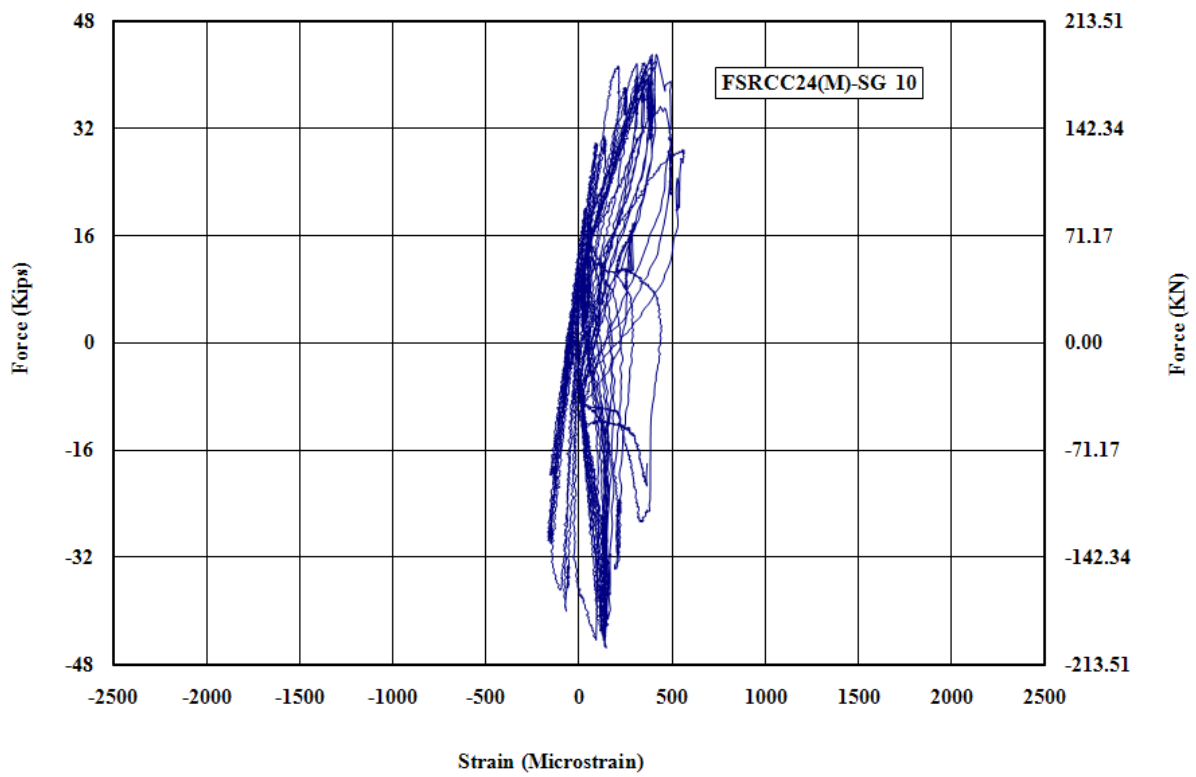

Figure G - 10: Measured Strain in Gauge No.10 for FSRCC24-M

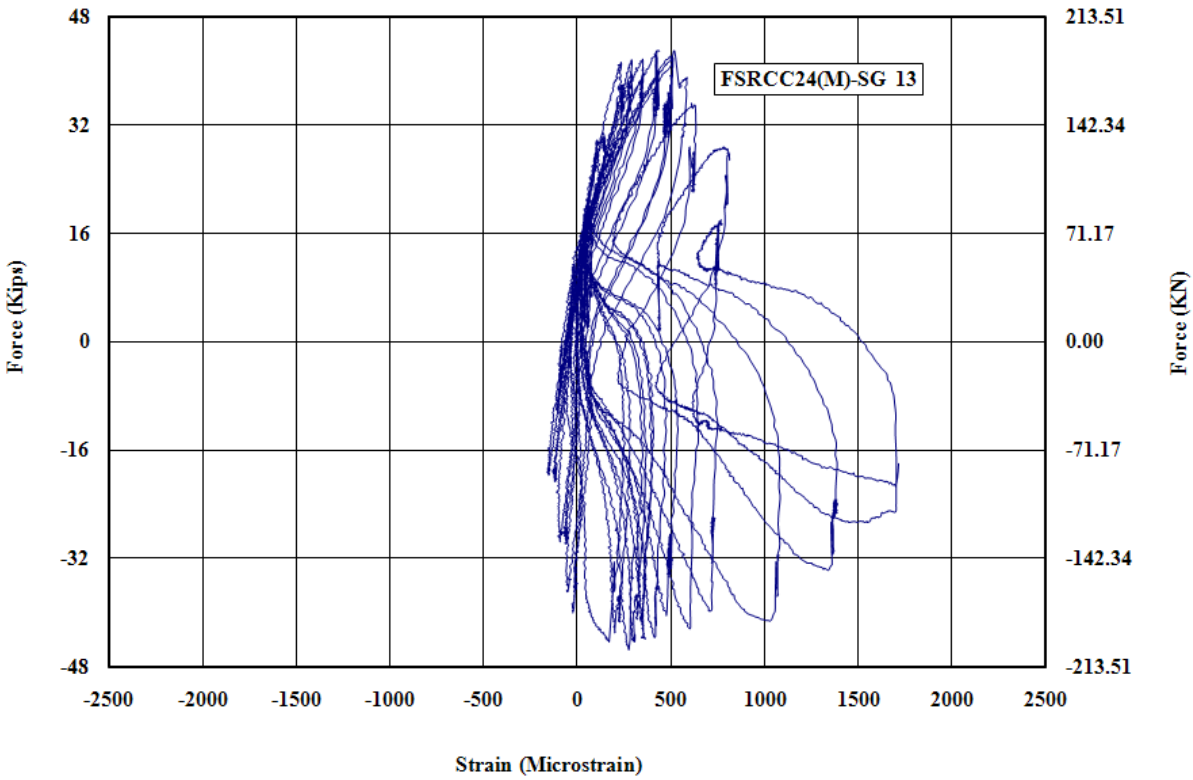

Figure G - 11: Measured Strain in Gauge No.13 for FSRCC24-M

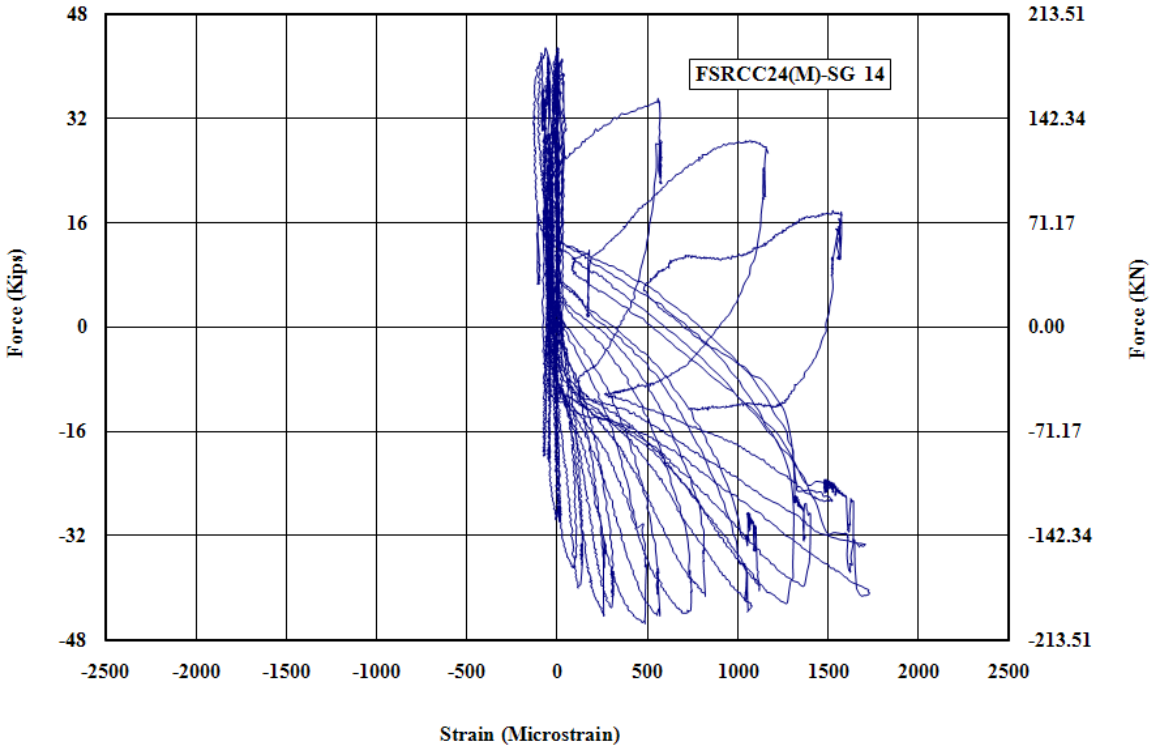

Figure G - 12: Measured Strain in Gauge No.14 for FSRCC24-M

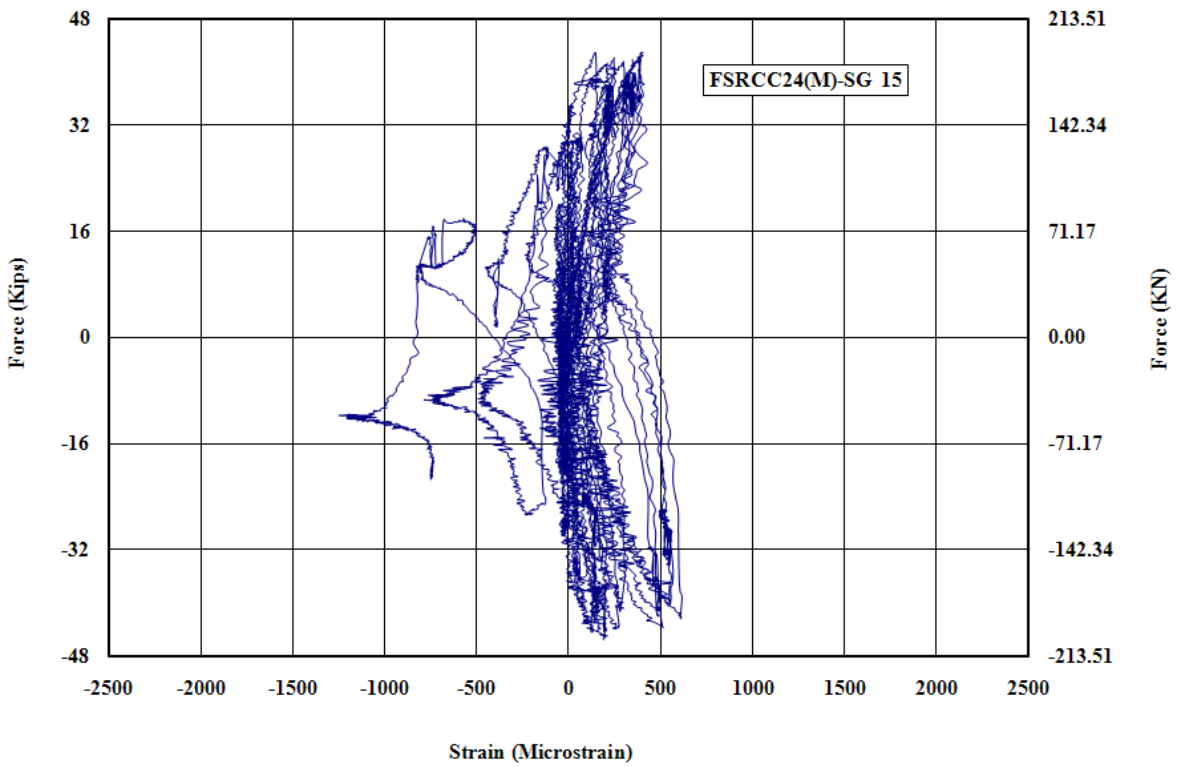

Figure G - 13: Measured Strain in Gauge No.15 for FSRCC24-M

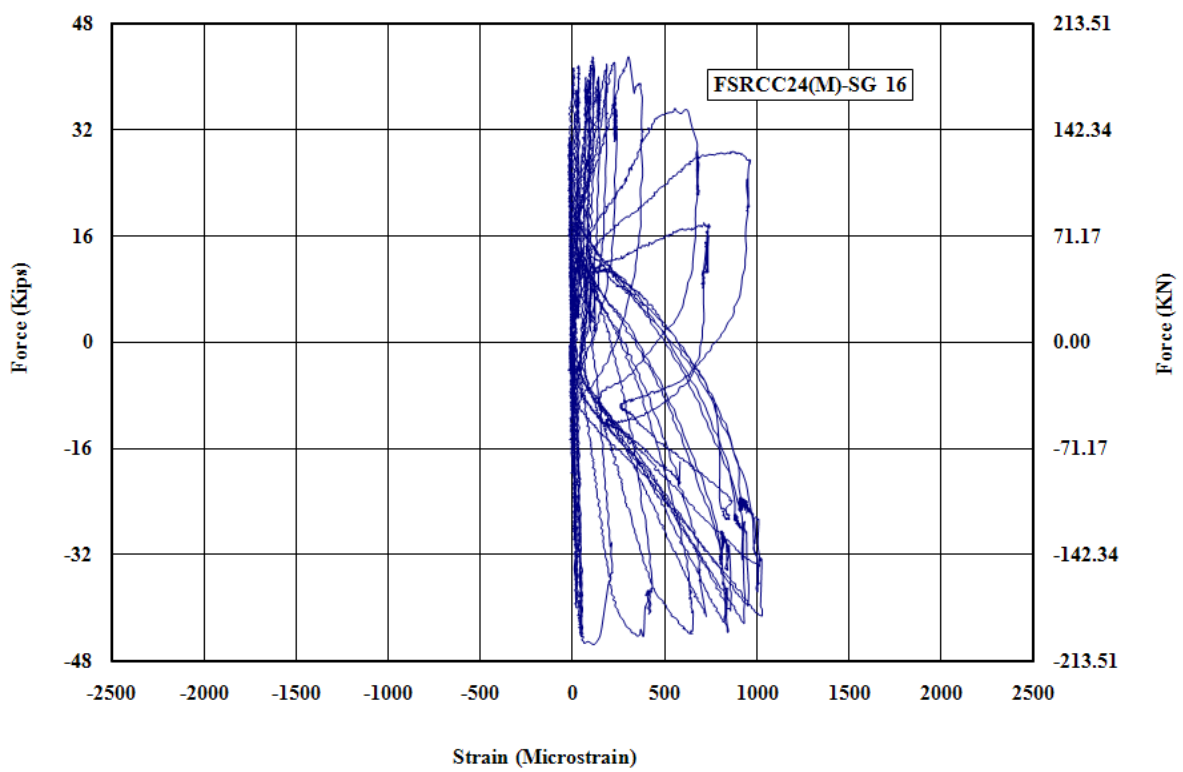

Figure G - 14: Measured Strain in Gauge No.16 for FSRCC24-M

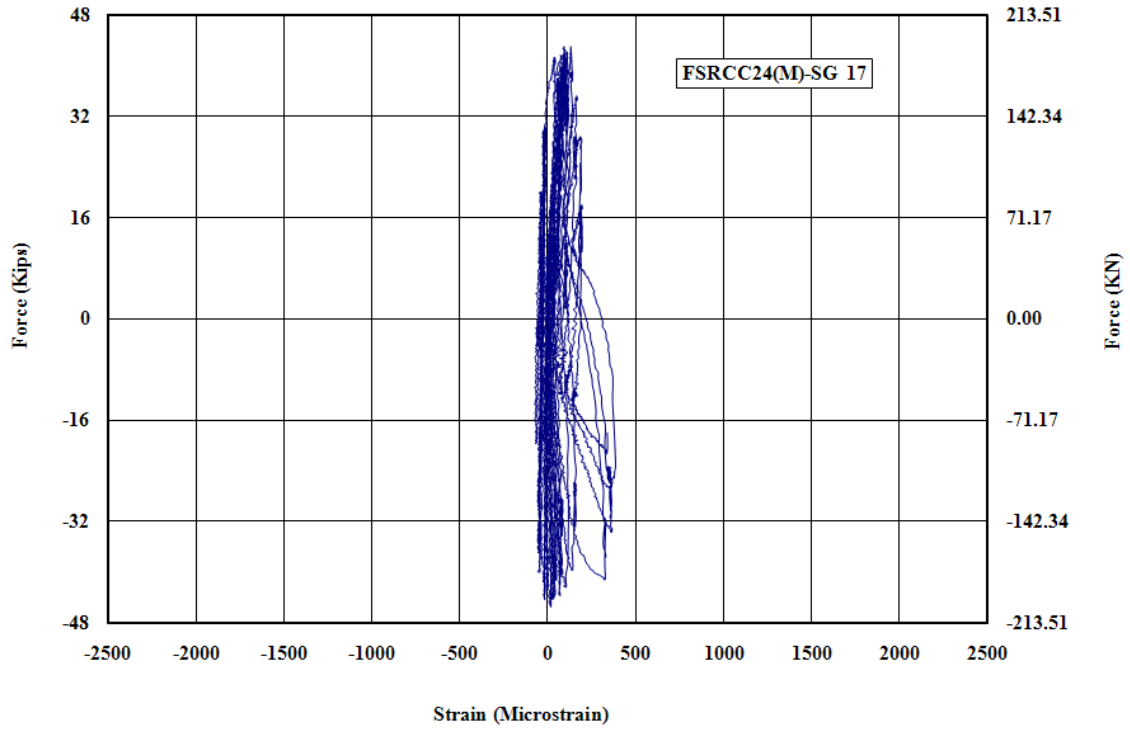

Figure G - 15: Measured Strain in Gauge No.17 for FSRCC24-M

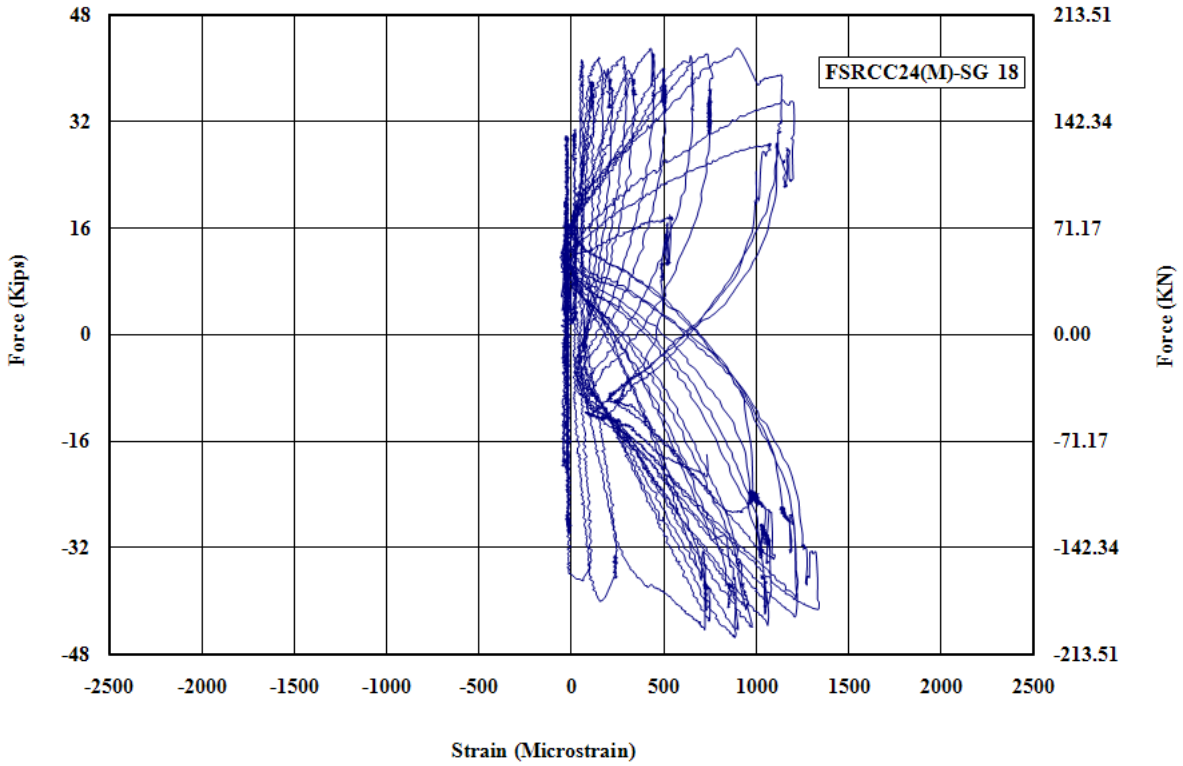

Figure G - 16: Measured Strain in Gauge No.18 for FSRCC24-M

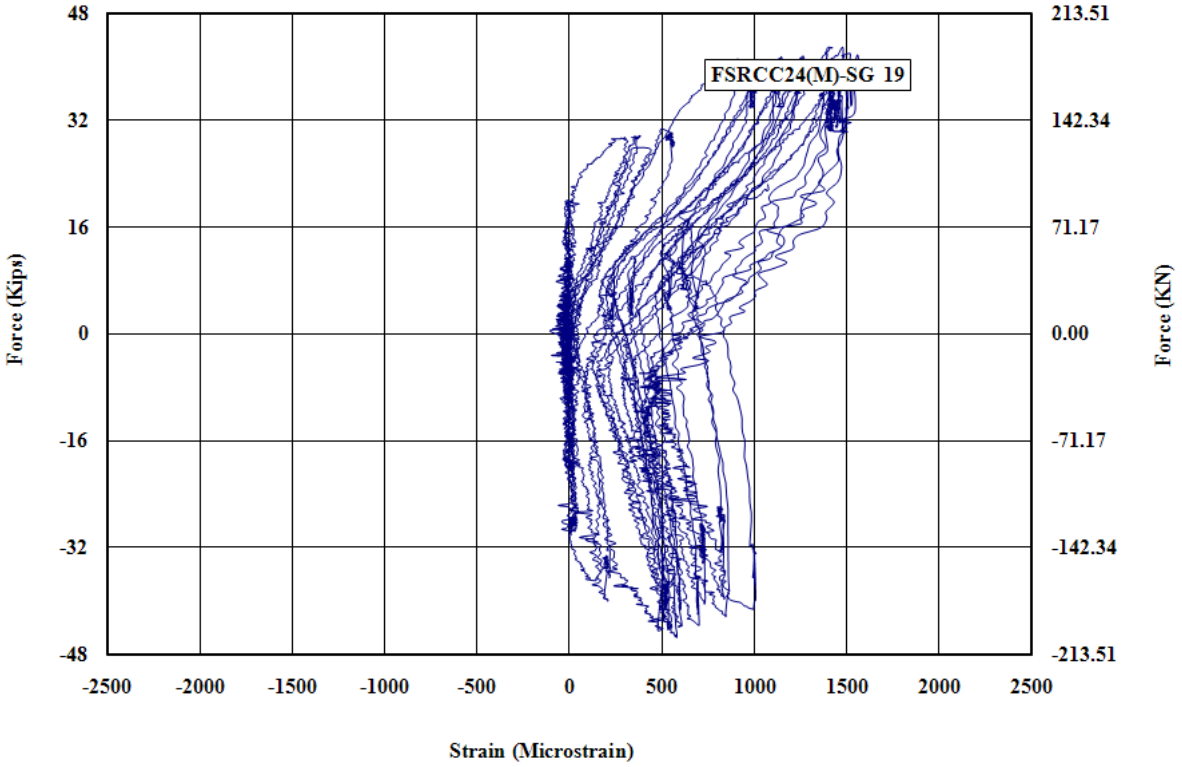

Figure G - 17: Measured Strain in Gauge No.19 for FSRCC24-M

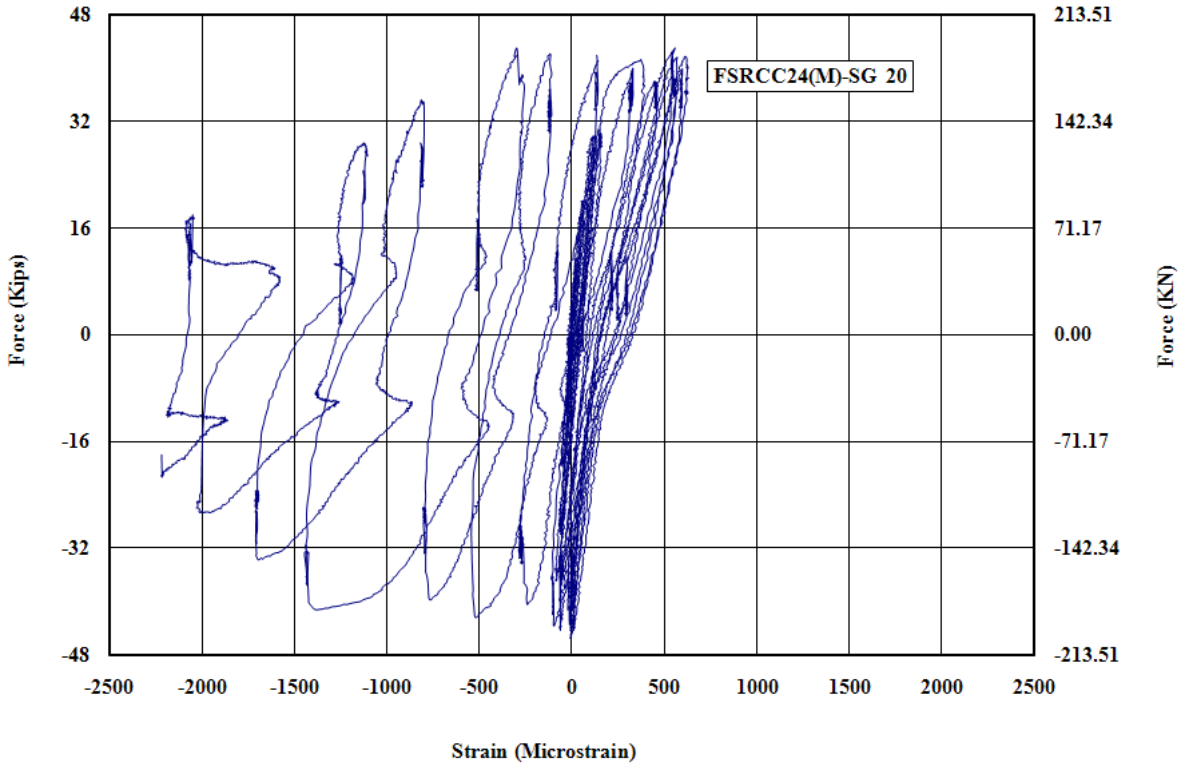

Figure G - 18: Measured Strain in Gauge No.20 for FSRCC24-M

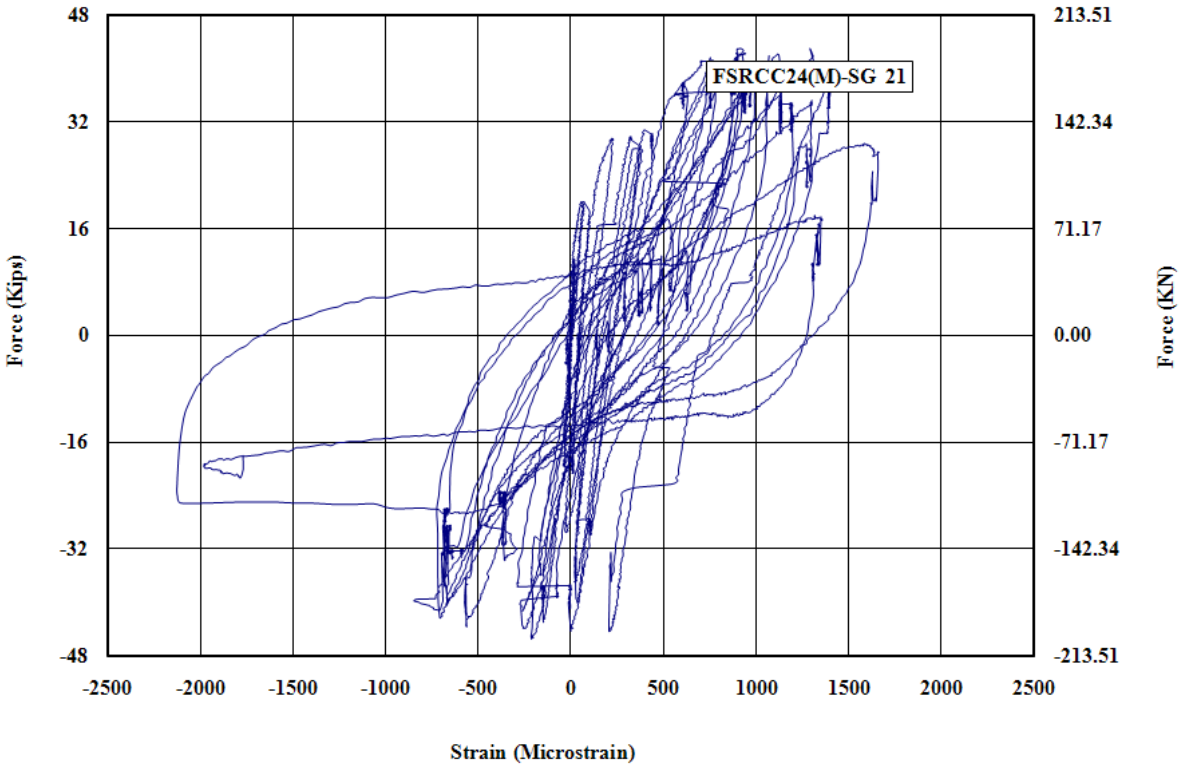

Figure G - 19: Measured Strain in Gauge No.21 for FSRCC24-M

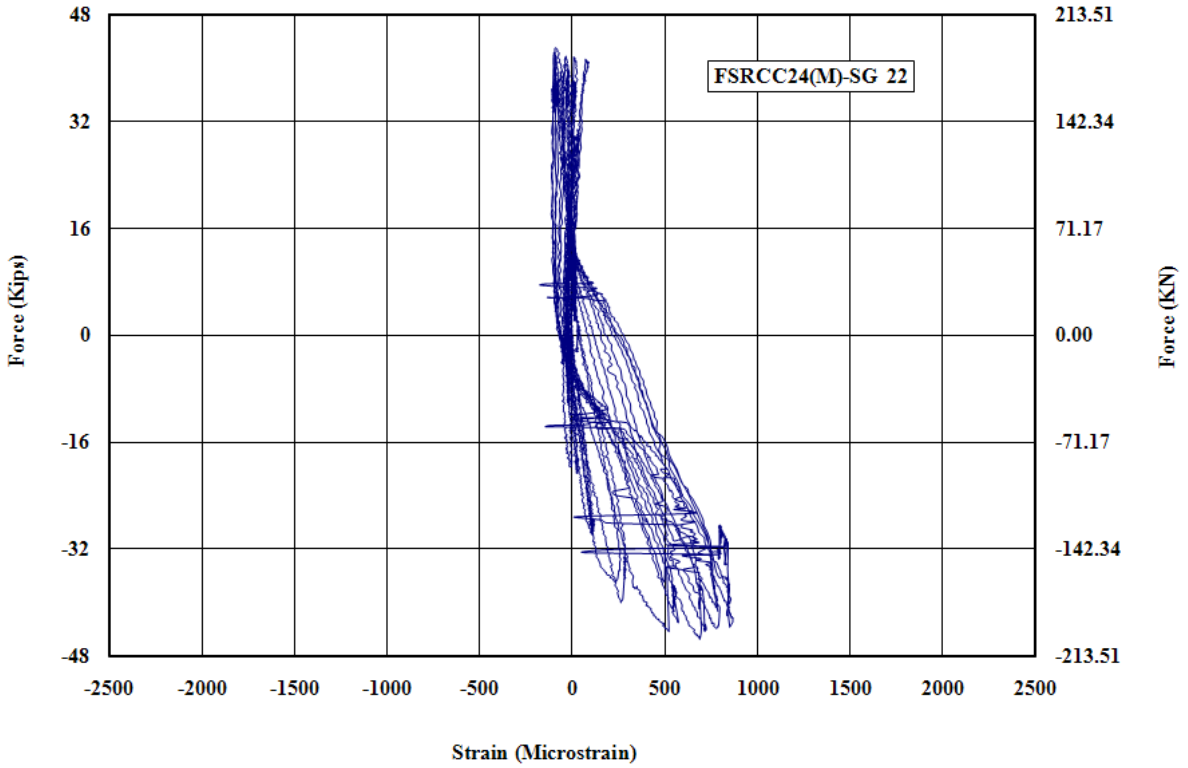

Figure G - 20: Measured Strain in Gauge No.22 for FSRCC24-M

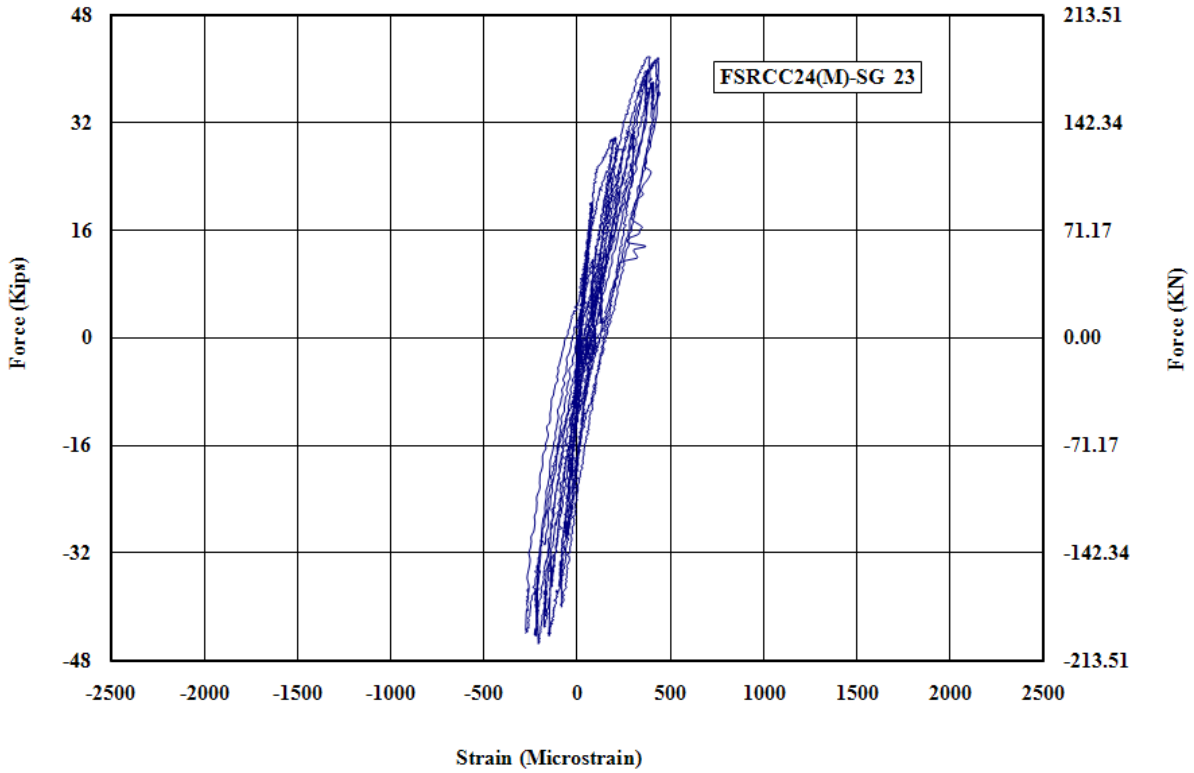

Figure G - 21: Measured Strain in Gauge No.23 for FSRCC24-M

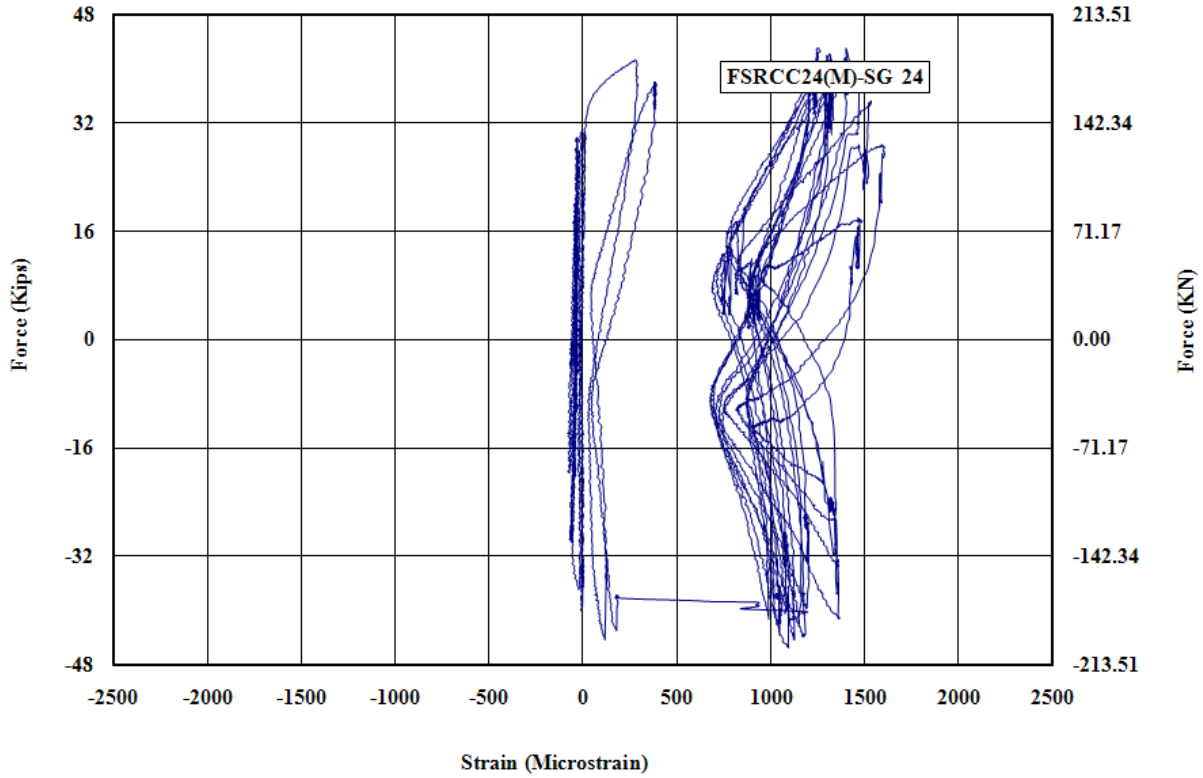

Figure G-20 Measured Strain in Gauge No.24 for FSRCC24-M

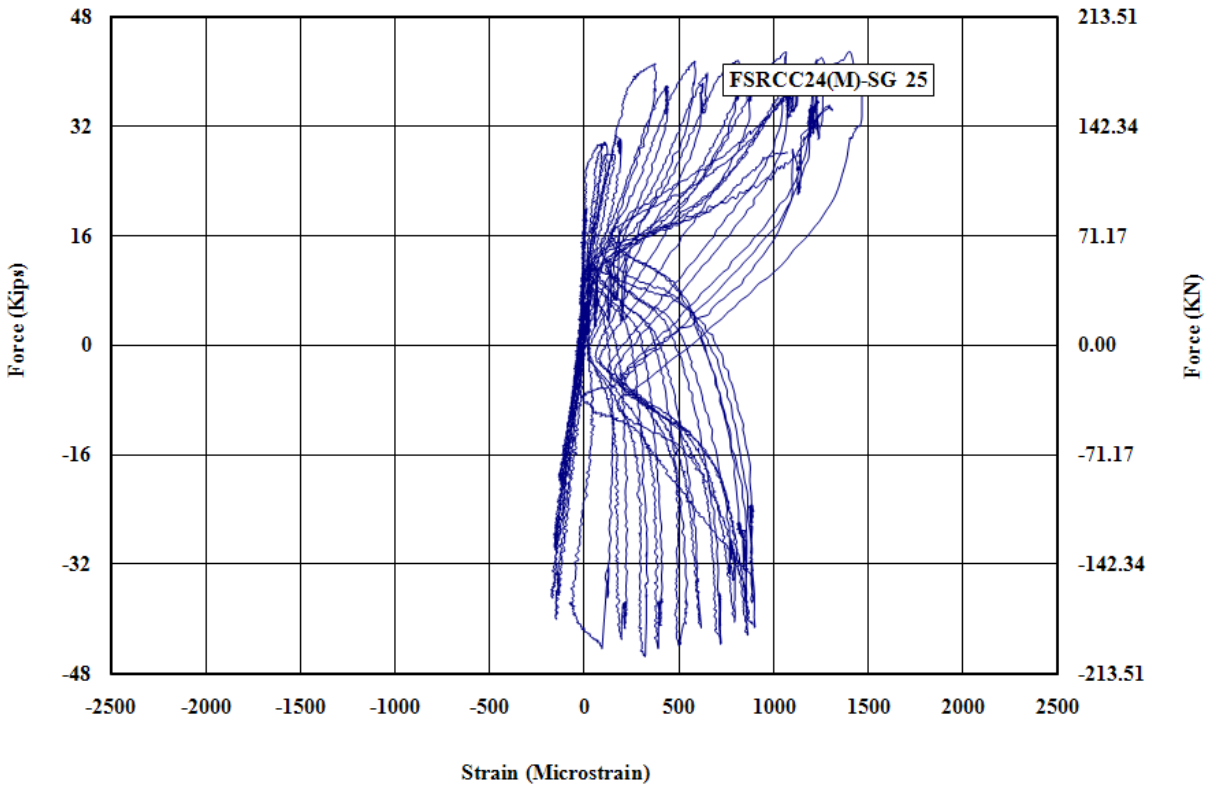

Figure G - 22: Measured Strain in Gauge No.25 for FSRCC24-M

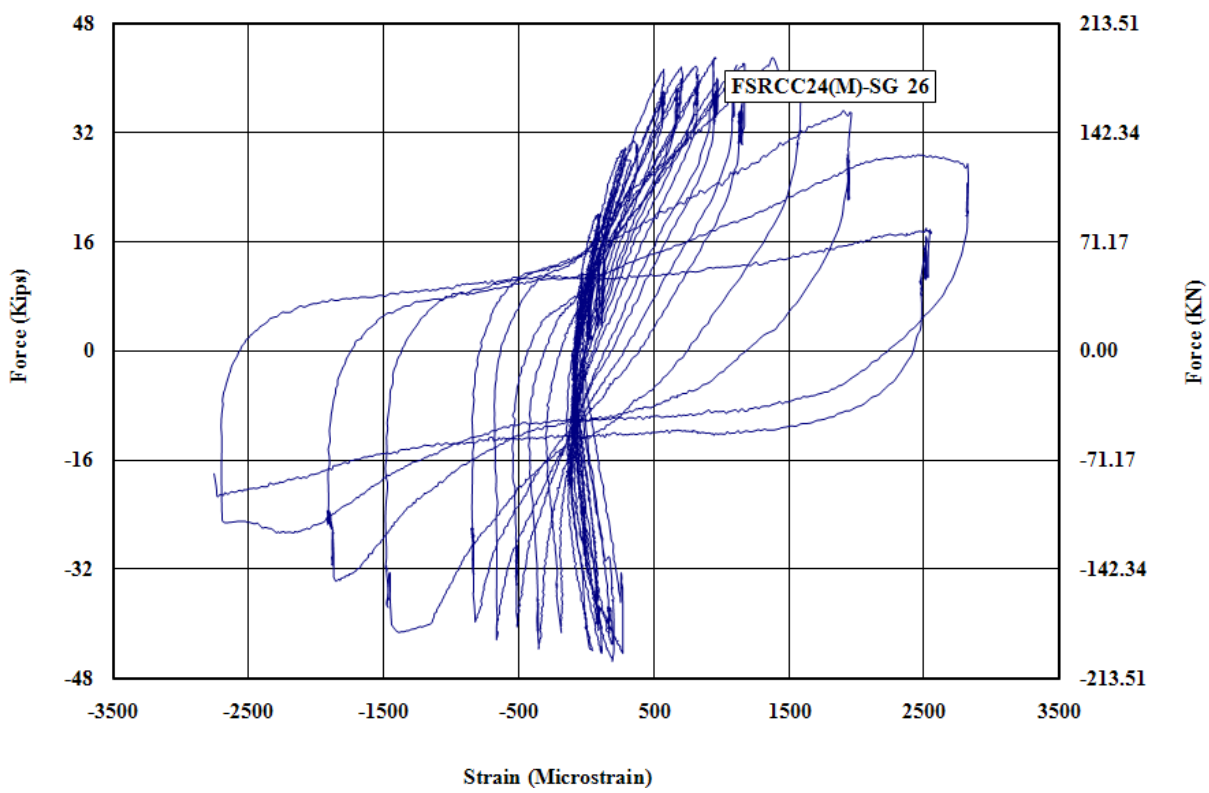

Figure G - 23: Measured Strain in Gauge No.26 for FSRCC24-M

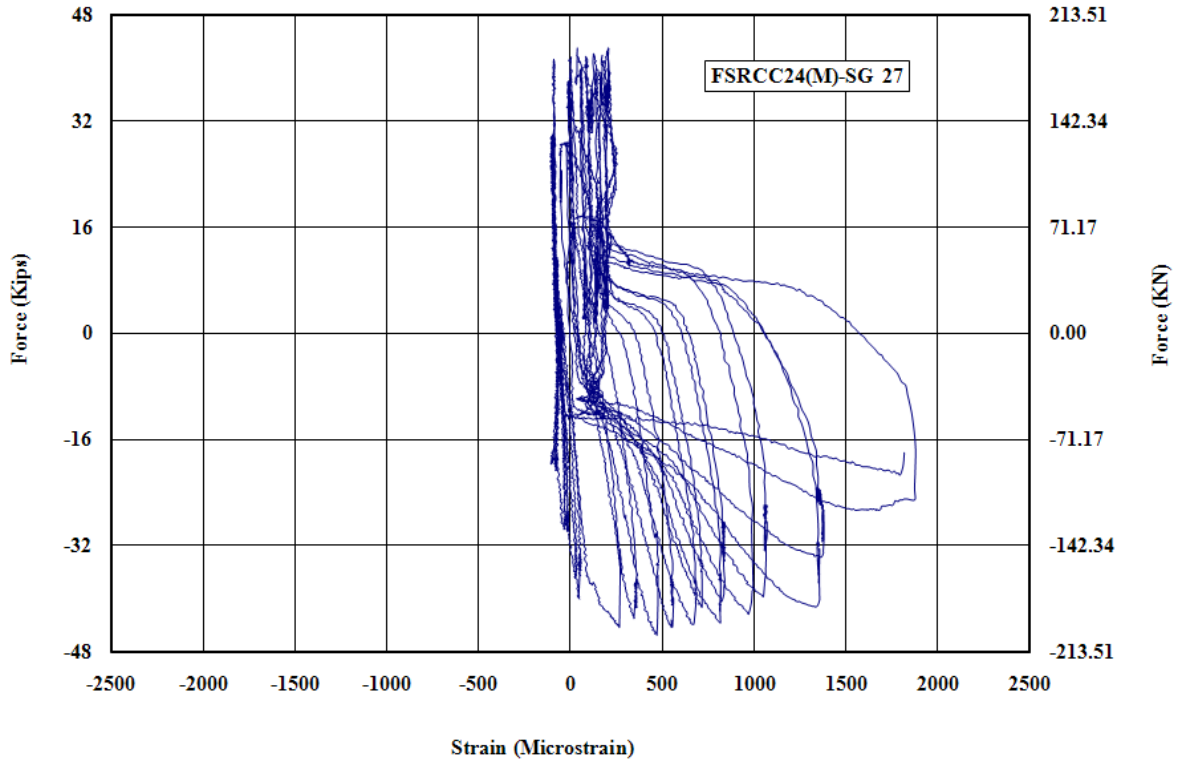

Figure G - 24: Measured Strain in Gauge No.27 for FSRCC24-M

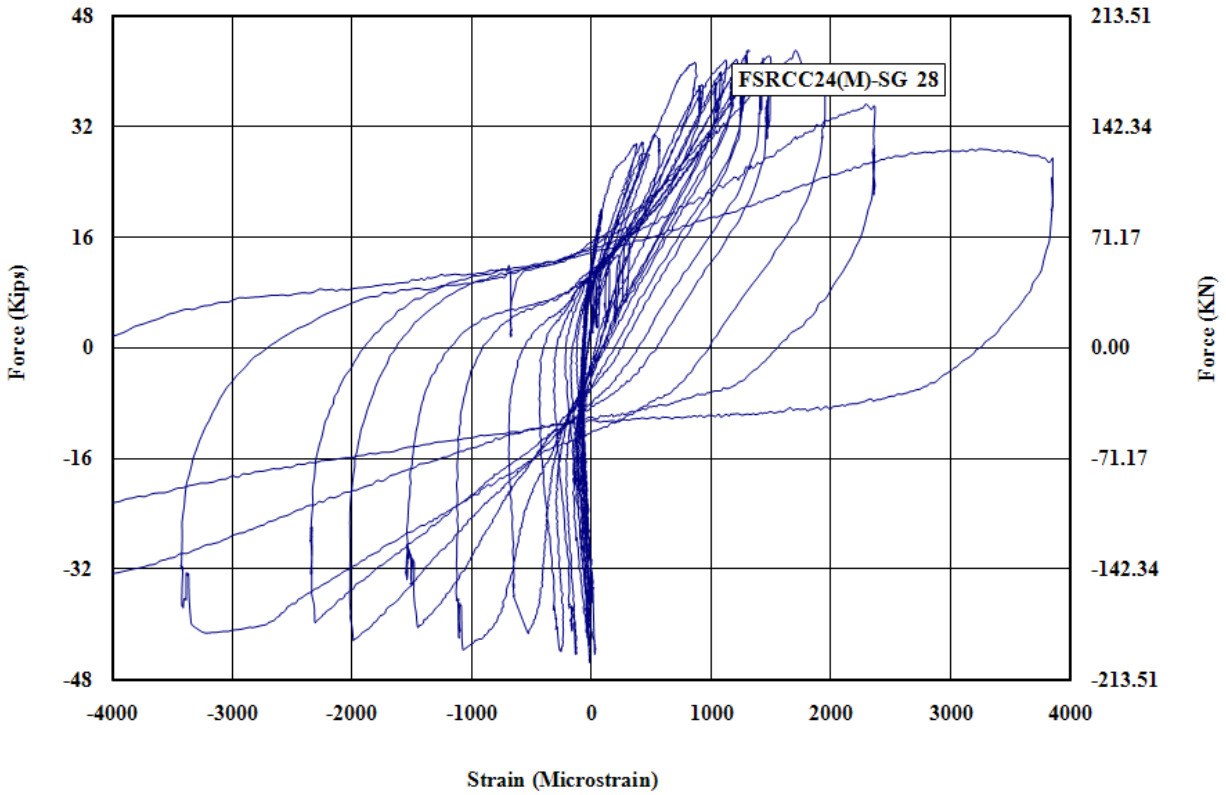

Figure G - 25: Measured Strain in Gauge No.28 for FSRCC24-M

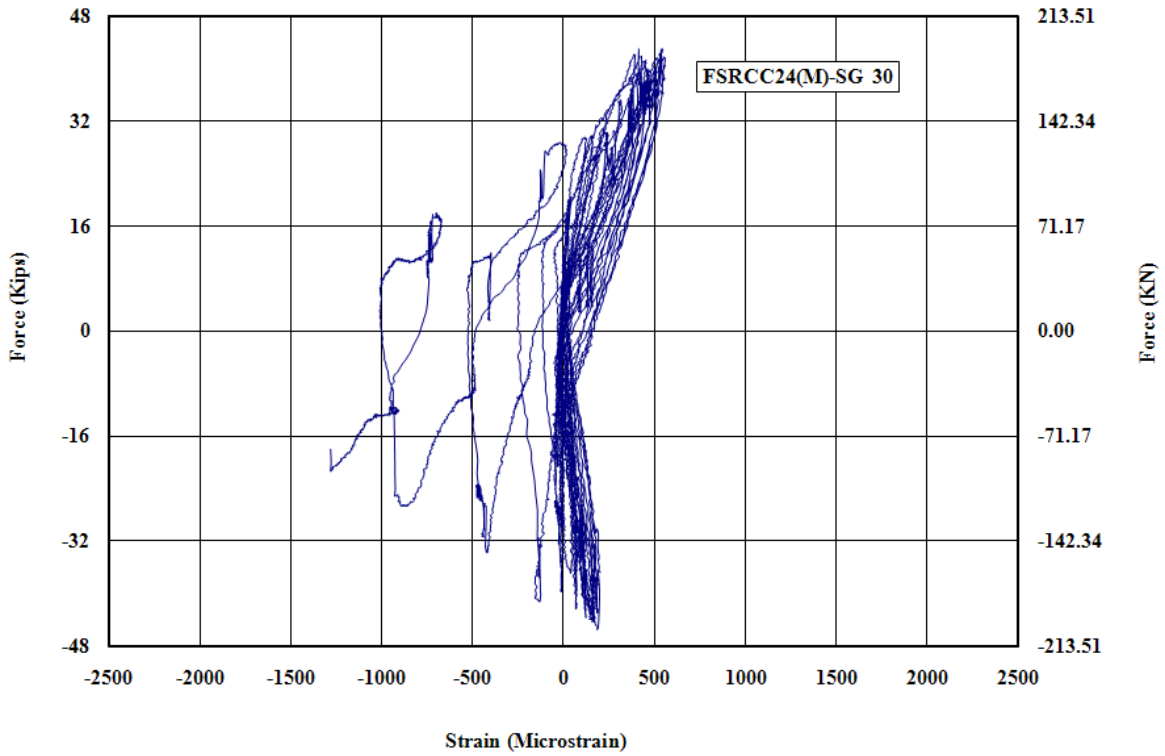

Figure G - 26: Measured Strain in Gauge No.30 for FSRCC24-M

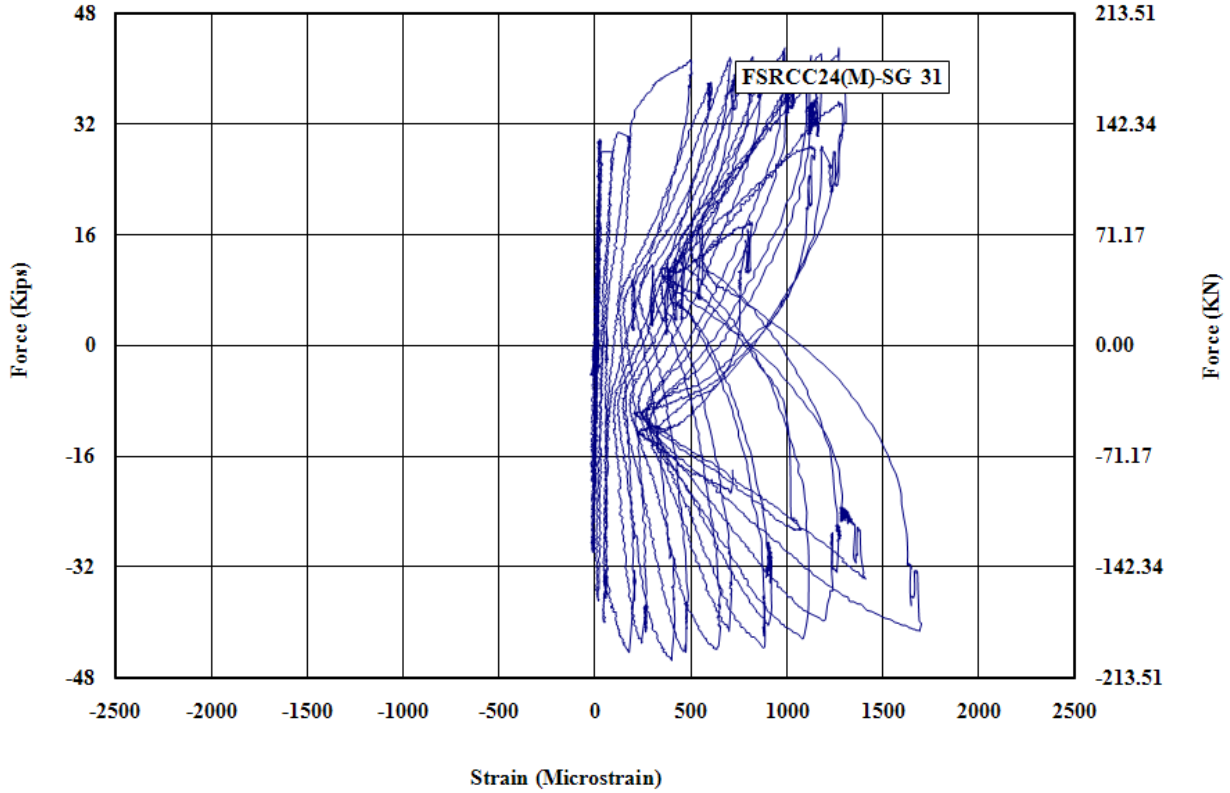

Figure G - 27: Measured Strain in Gauge No.31 for FSRCC24-M

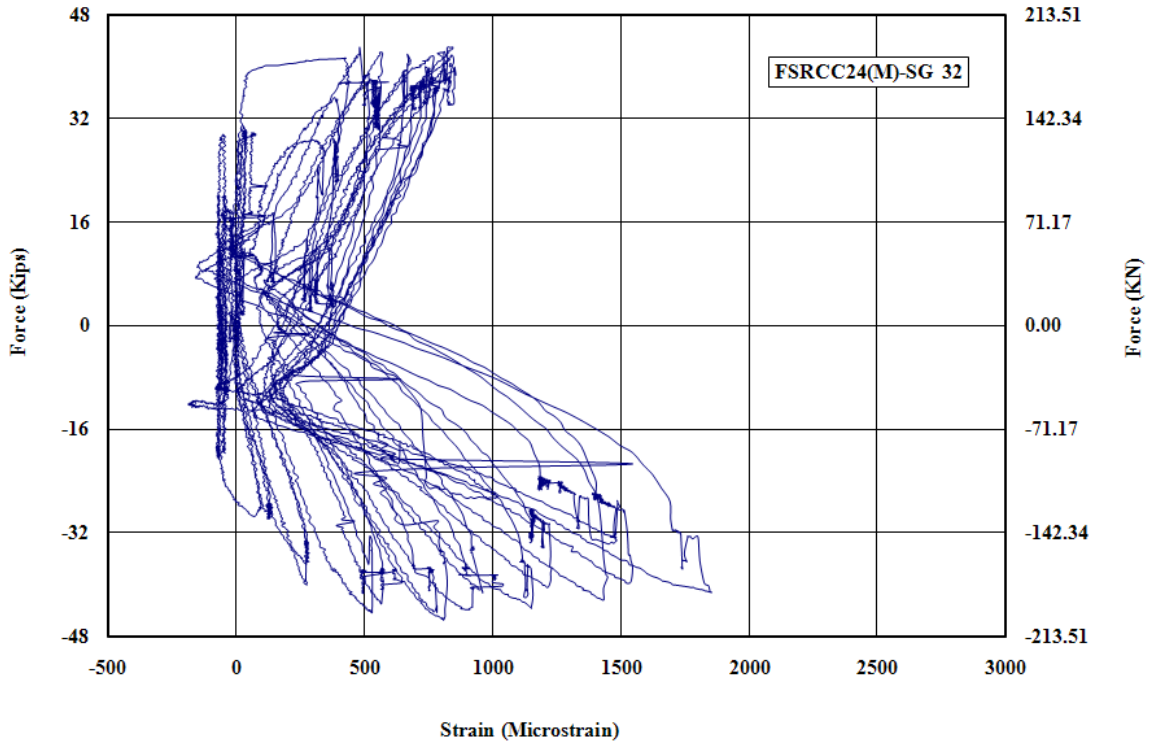

Figure G - 28: Measured Strain in Gauge No.32 for FSRCC24-M

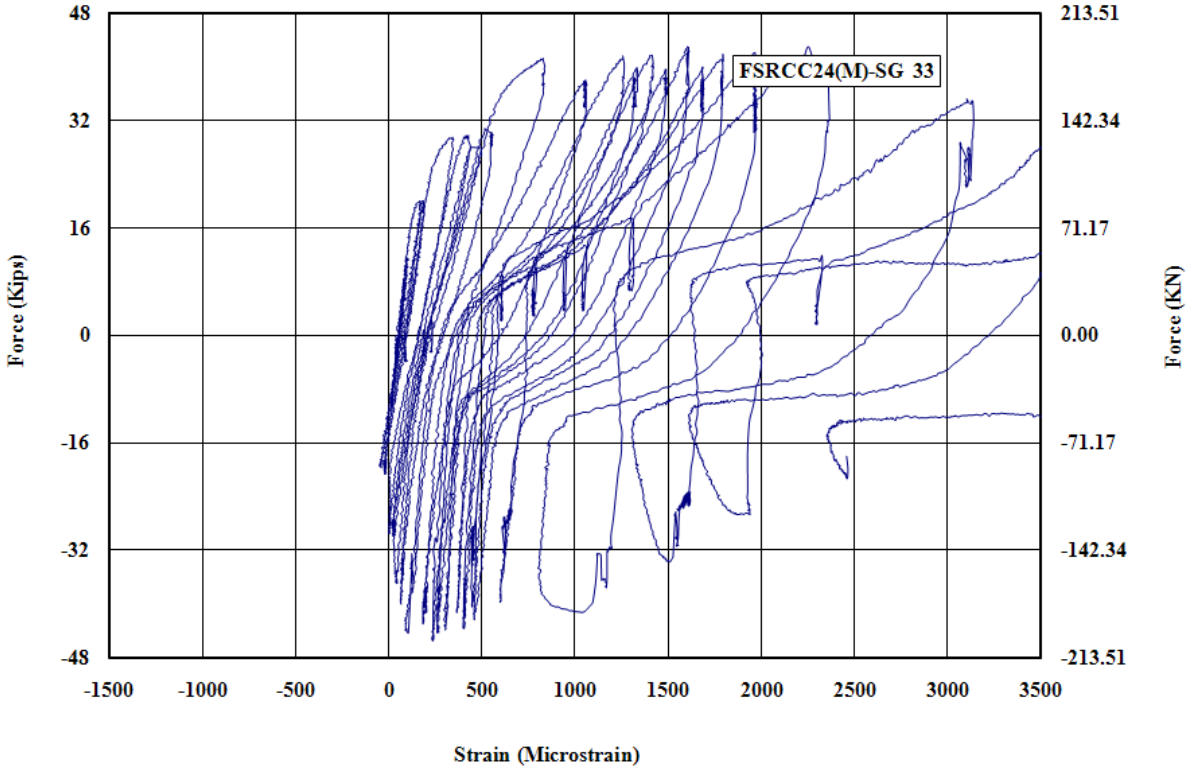

Figure G - 29: Measured Strain in Gauge No.33 for FSRCC24-M

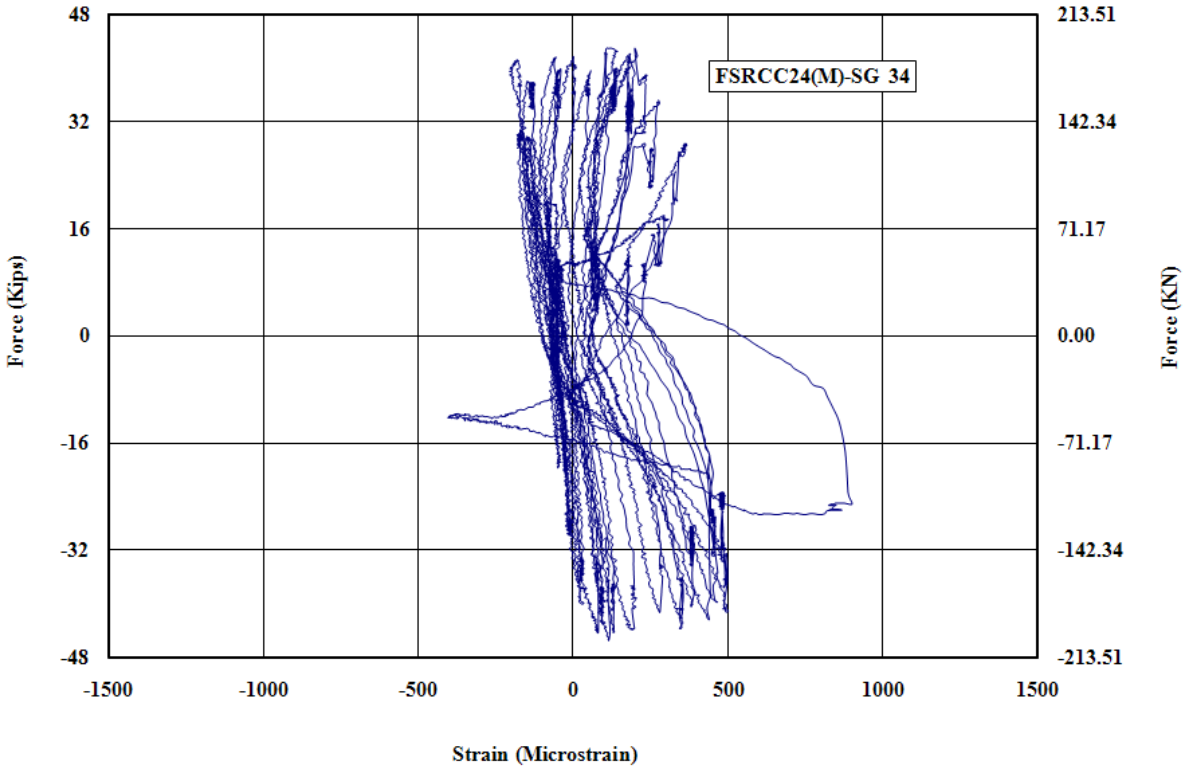

Figure G - 30: Measured Strain in Gauge No.34 for FSRCC24-M

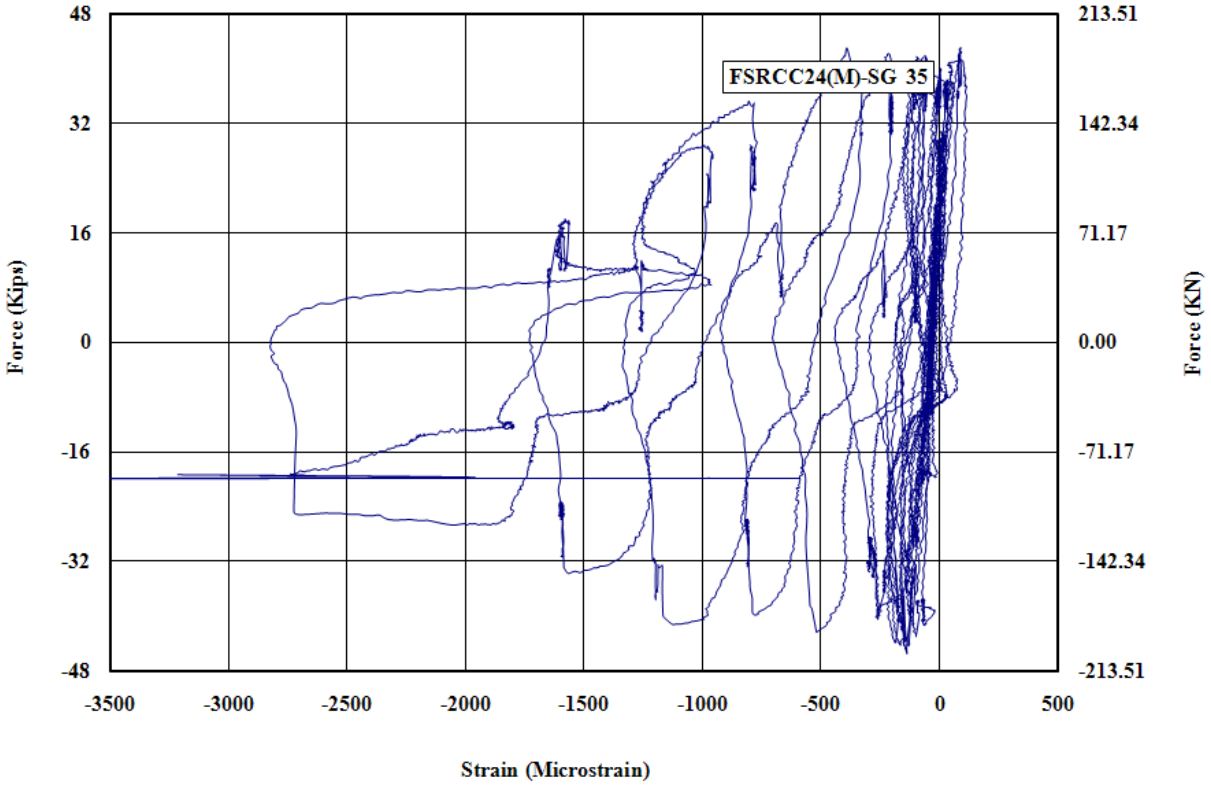

Figure G - 31: Measured Strain in Gauge No.35 for FSRCC24-M

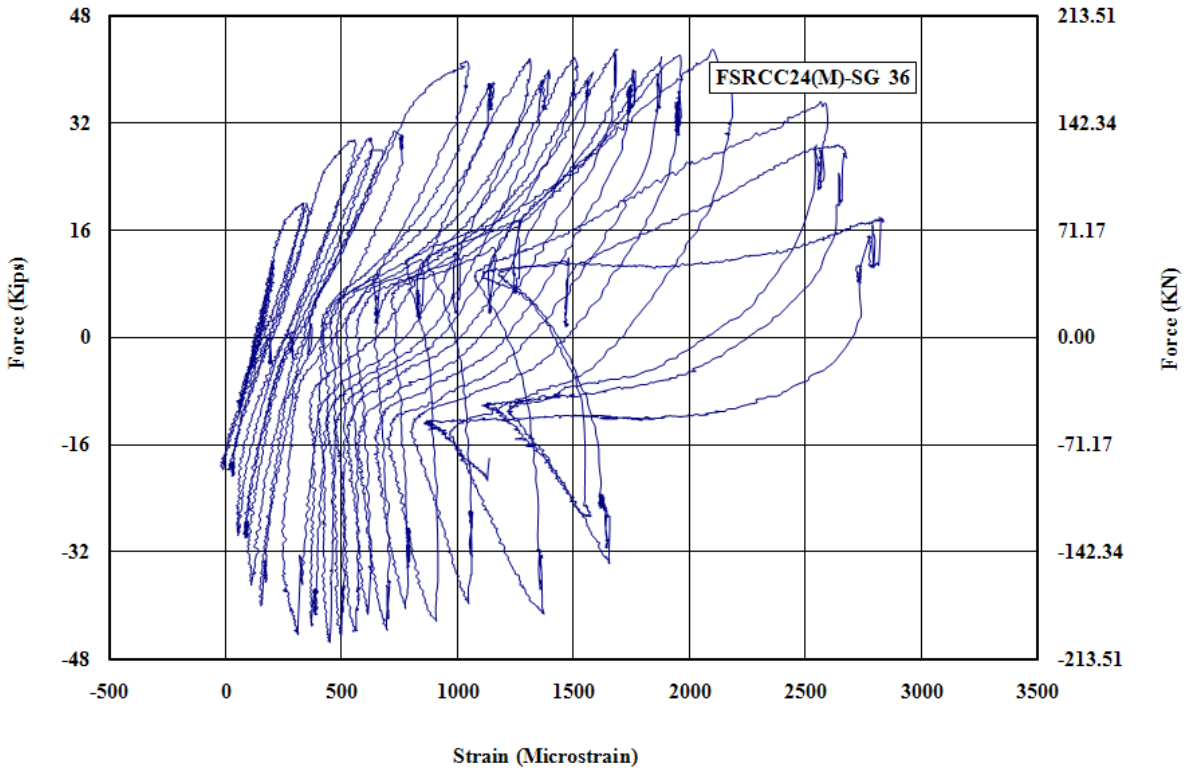

Figure G - 32: Measured Strain in Gauge No.36 for FSRCC24-M

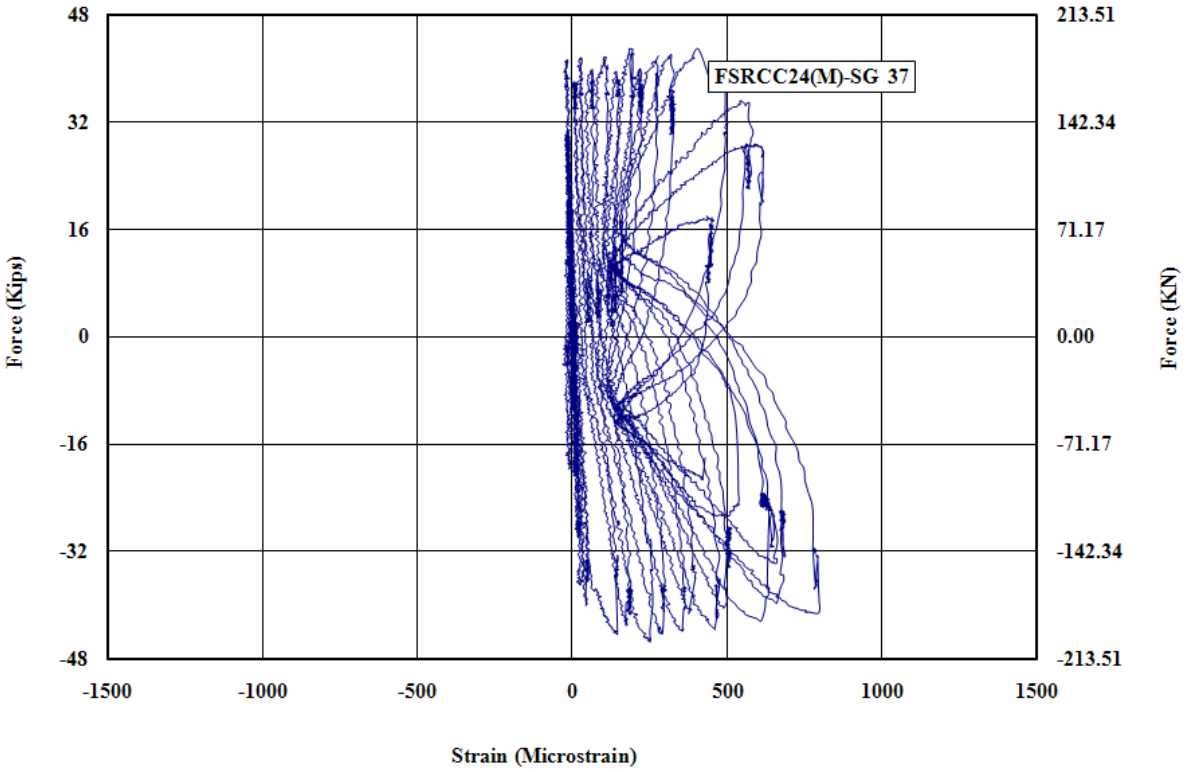

Figure G - 33: Measured Strain in Gauge No.37 for FSRCC24-M

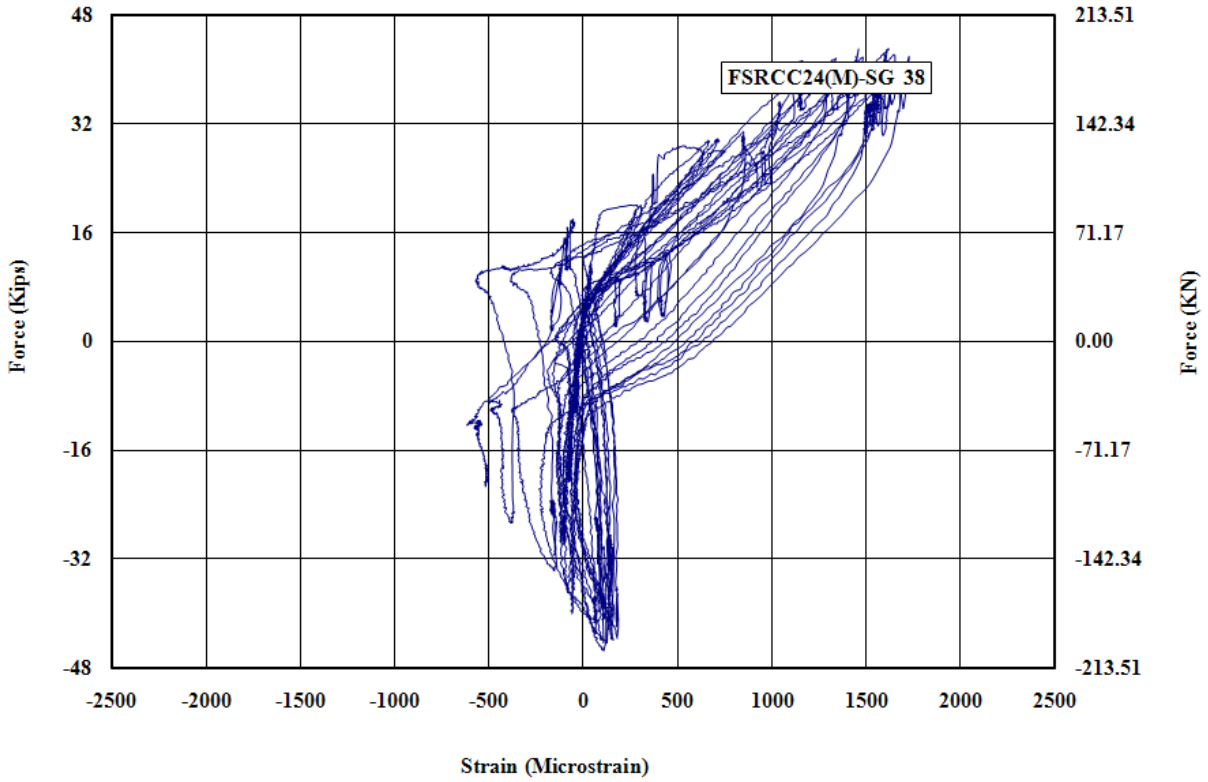

Figure G - 34: Measured Strain in Gauge No.38 for FSRCC24-M

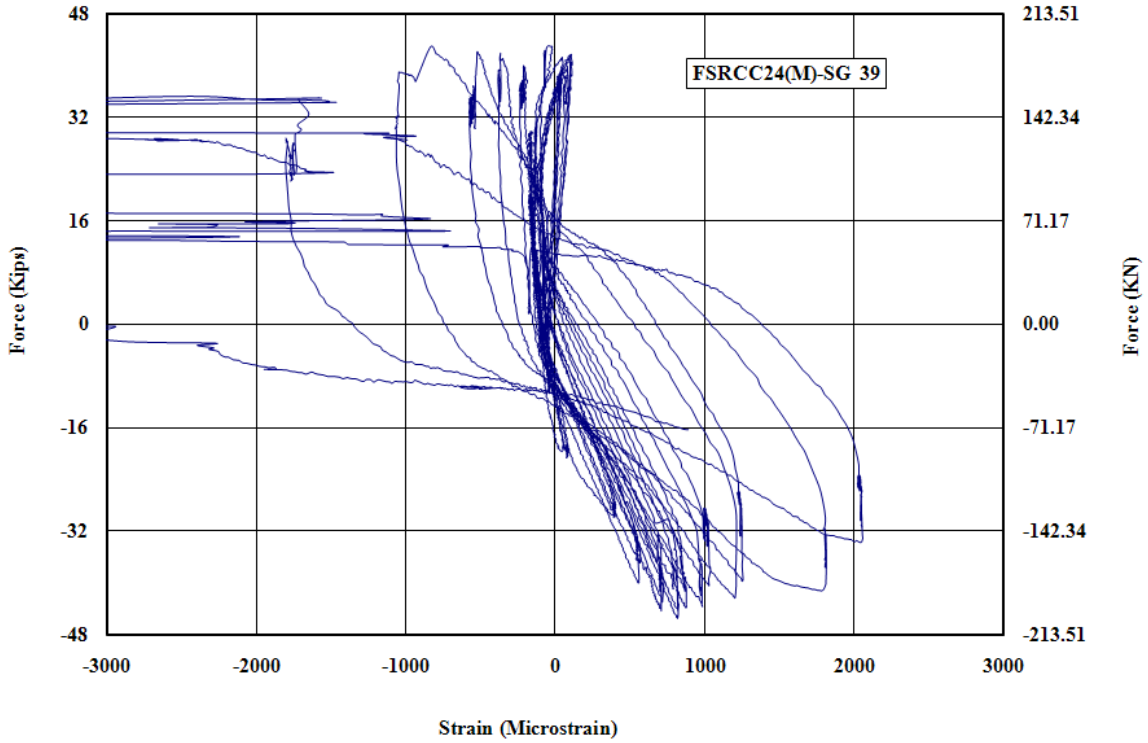

Figure G - 35: Measured Strain in Gauge No.39 for FSRCC24-M

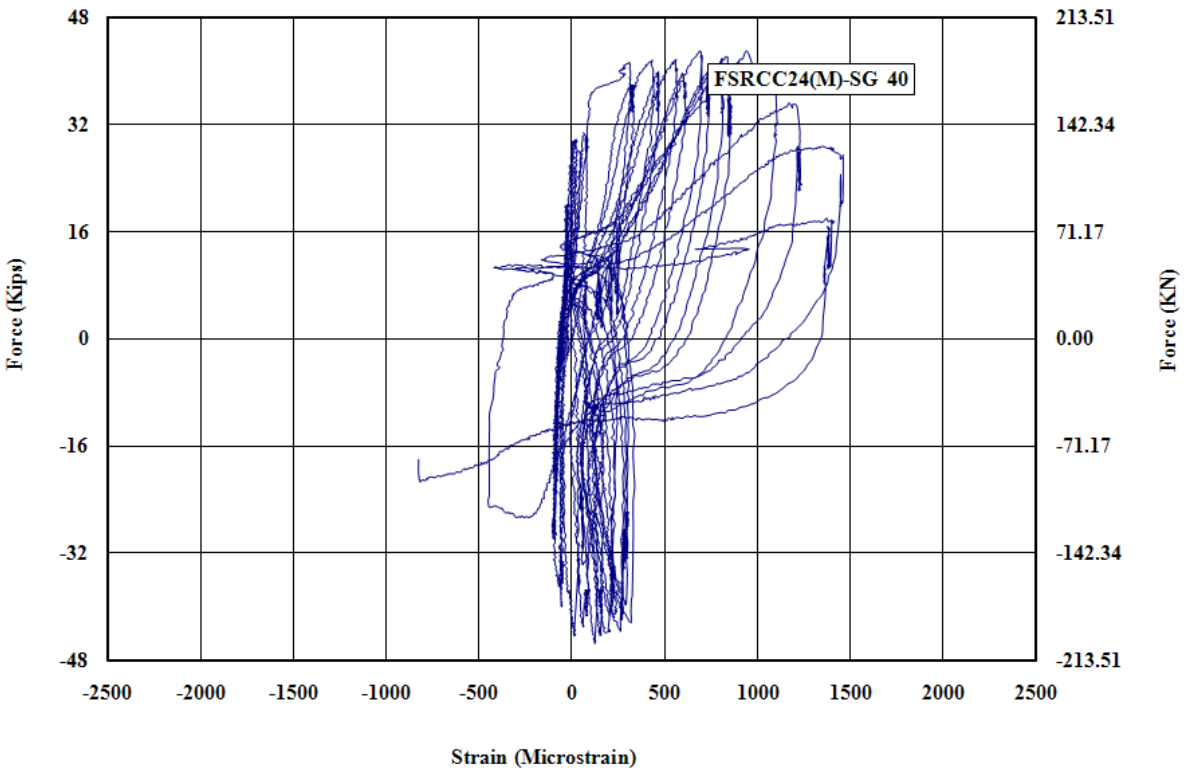

Figure G - 36: Measured Strain in Gauge No.40 for FSRCC24-M

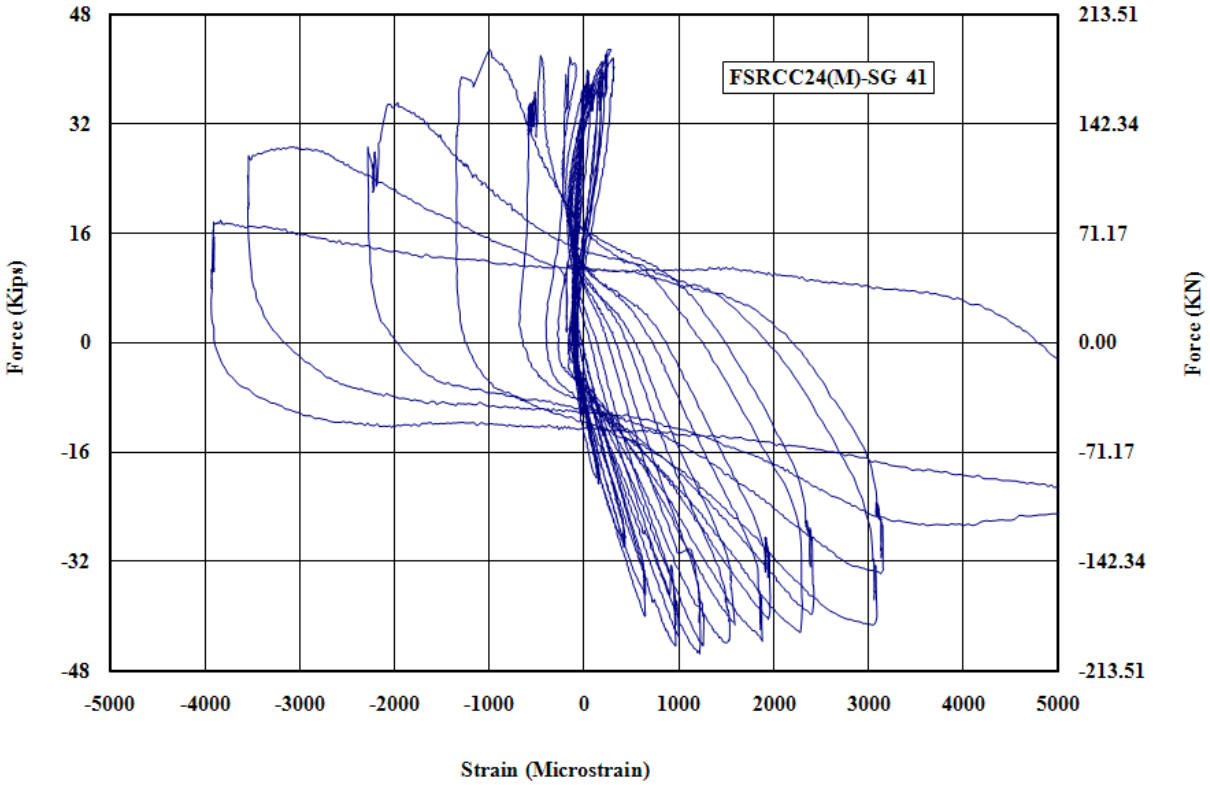

Figure G - 37: Measured Strain in Gauge No.41 for FSRCC24-M

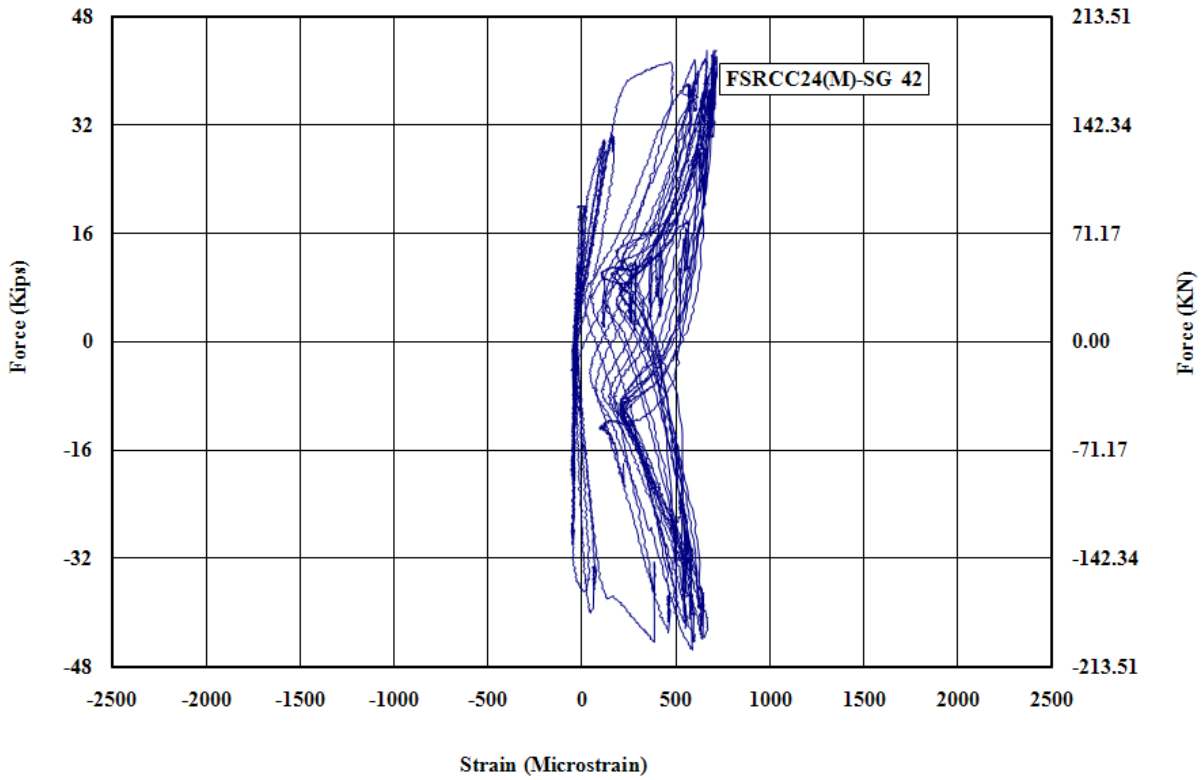

Figure G - 38: Measured Strain in Gauge No.42 for FSRCC24-M

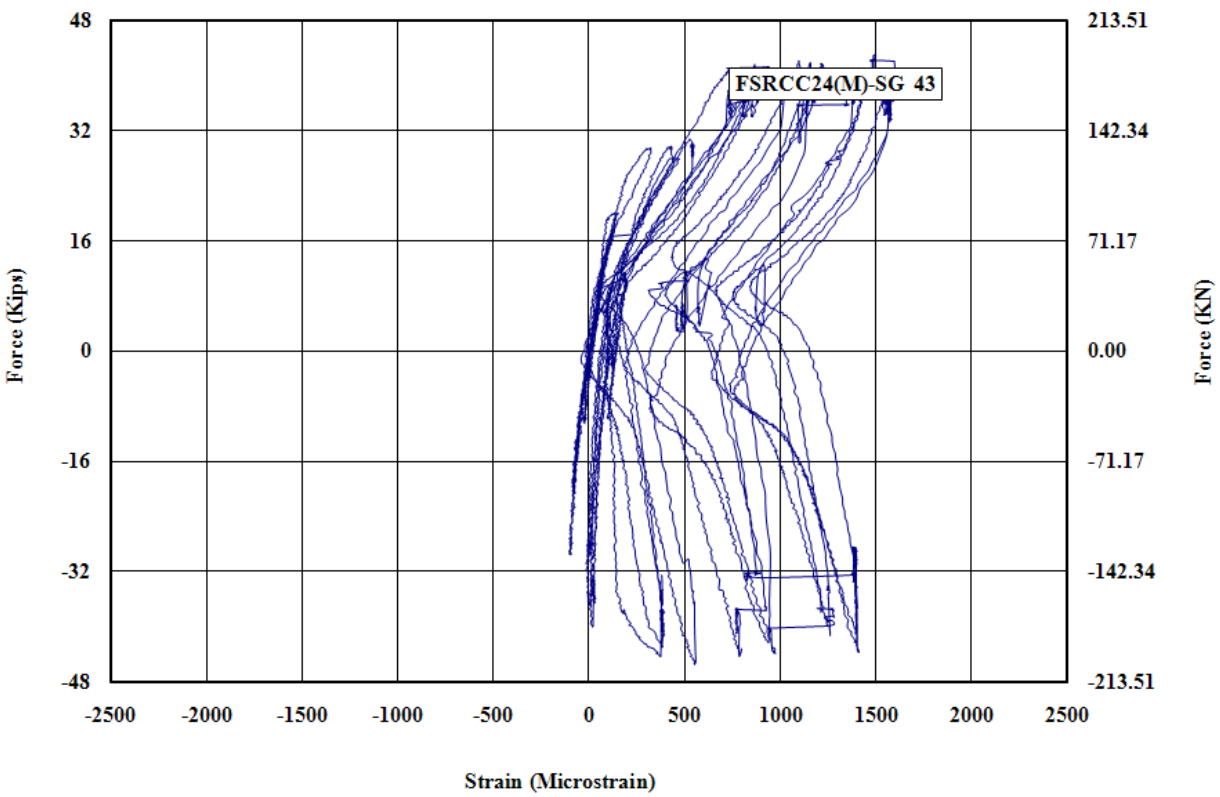

Figure G - 39: Measured Strain in Gauge No.43 for FSRCC24-M

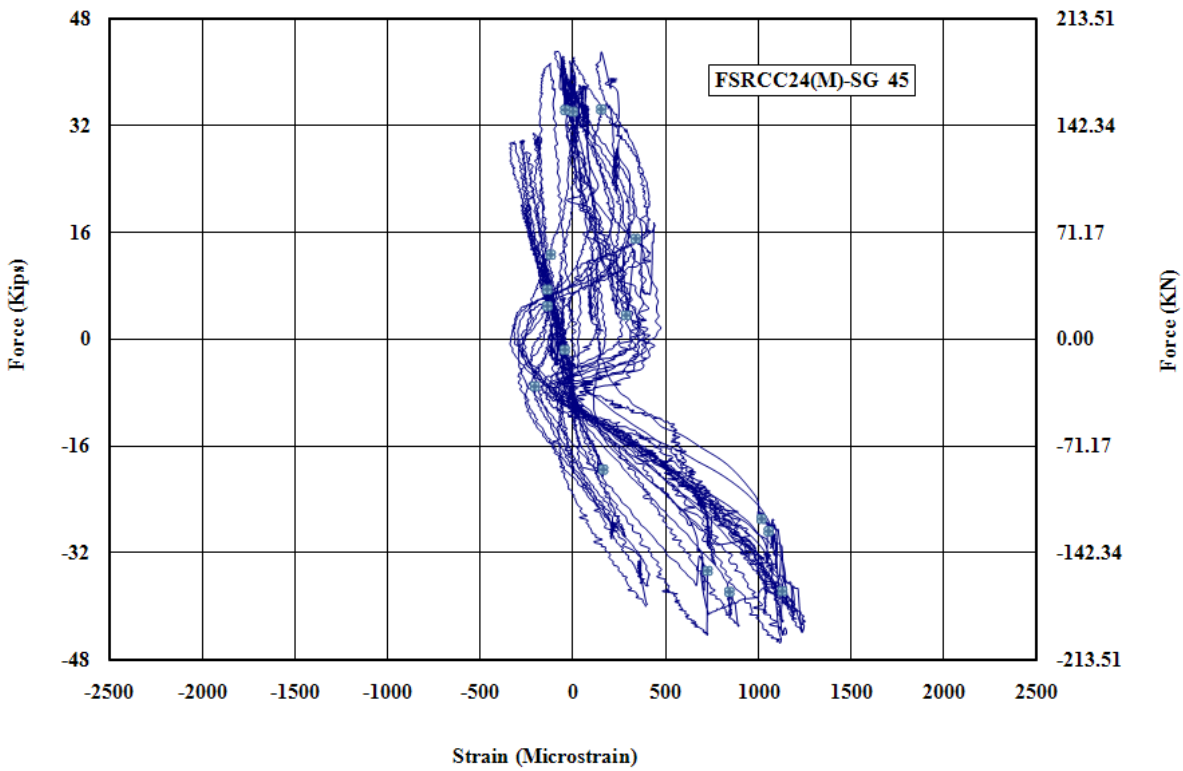

Figure G - 40: Measured Strain in Gauge No.45 for FSRCC24-M

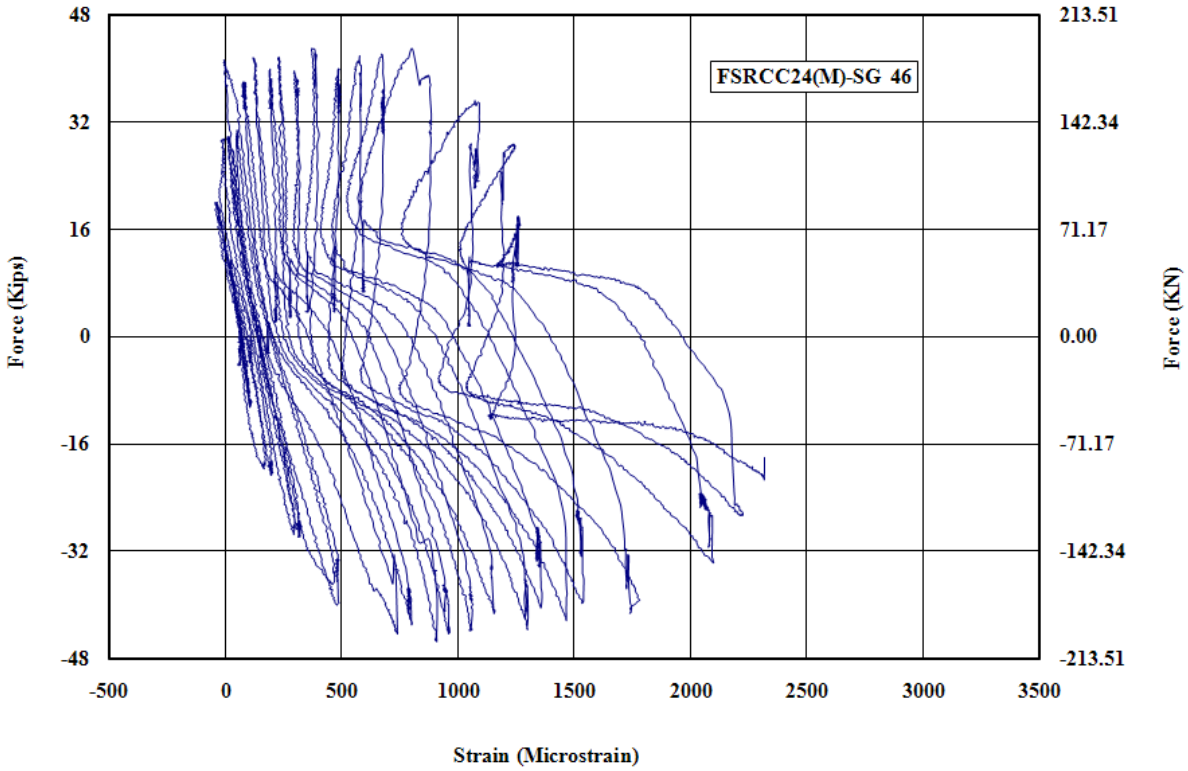

Figure G - 41: Measured Strain in Gauge No.46 for FSRCC24-M

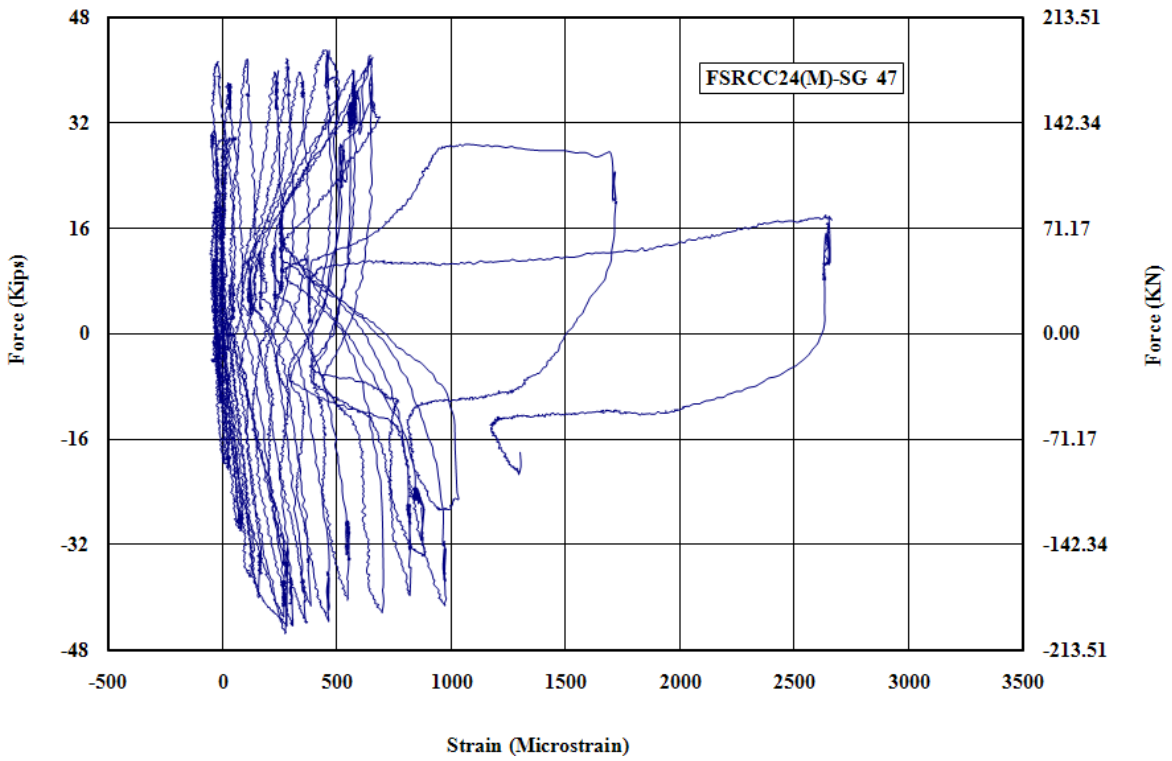

Figure G - 42: Measured Strain in Gauge No.47 for FSRCC24-M

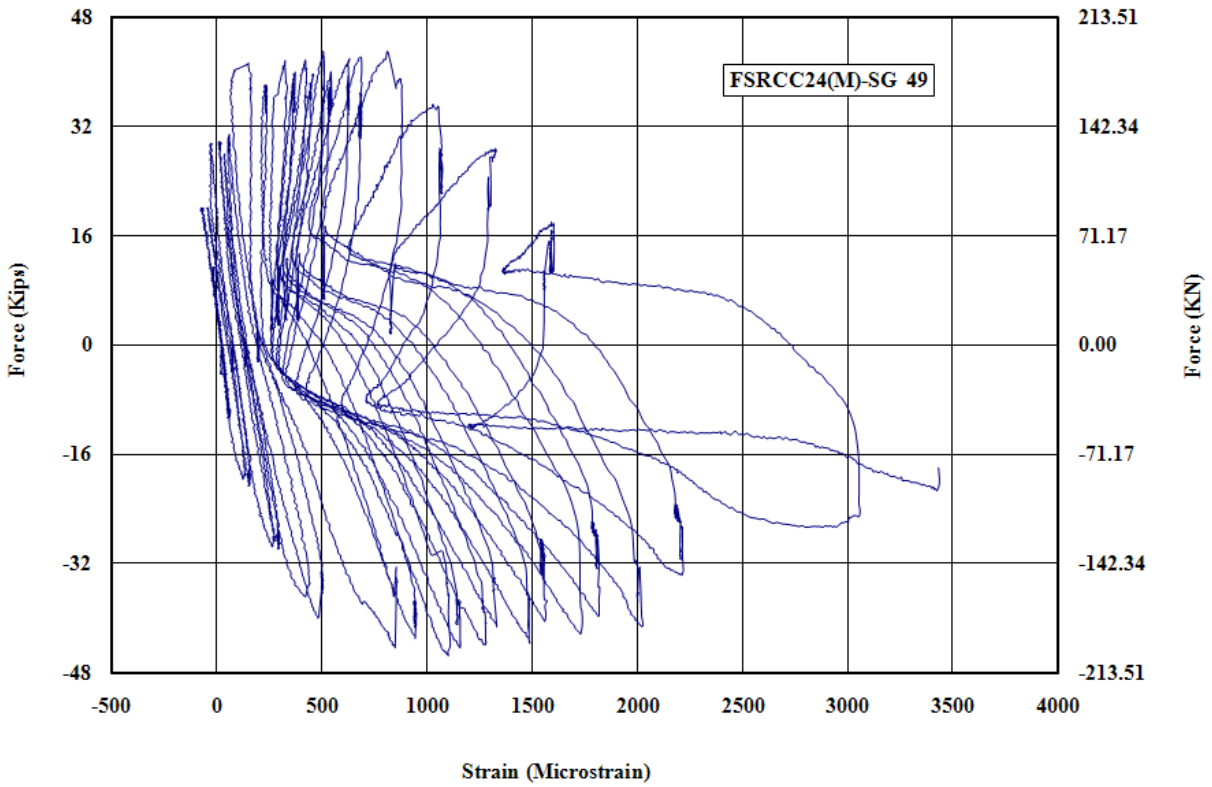

Figure G - 43: Measured Strain in Gauge No.49 for FSRCC24-M

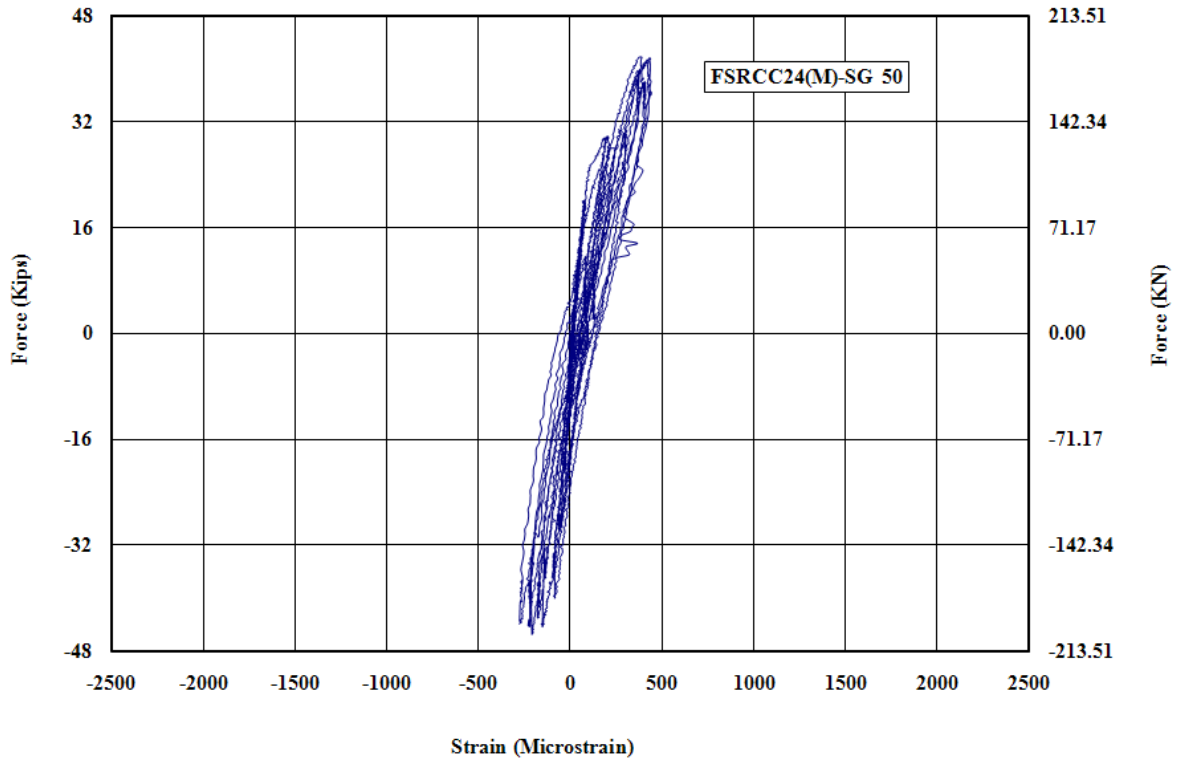

Figure G - 44: Measured Strain in Gauge No.50 for FSRCC24-M

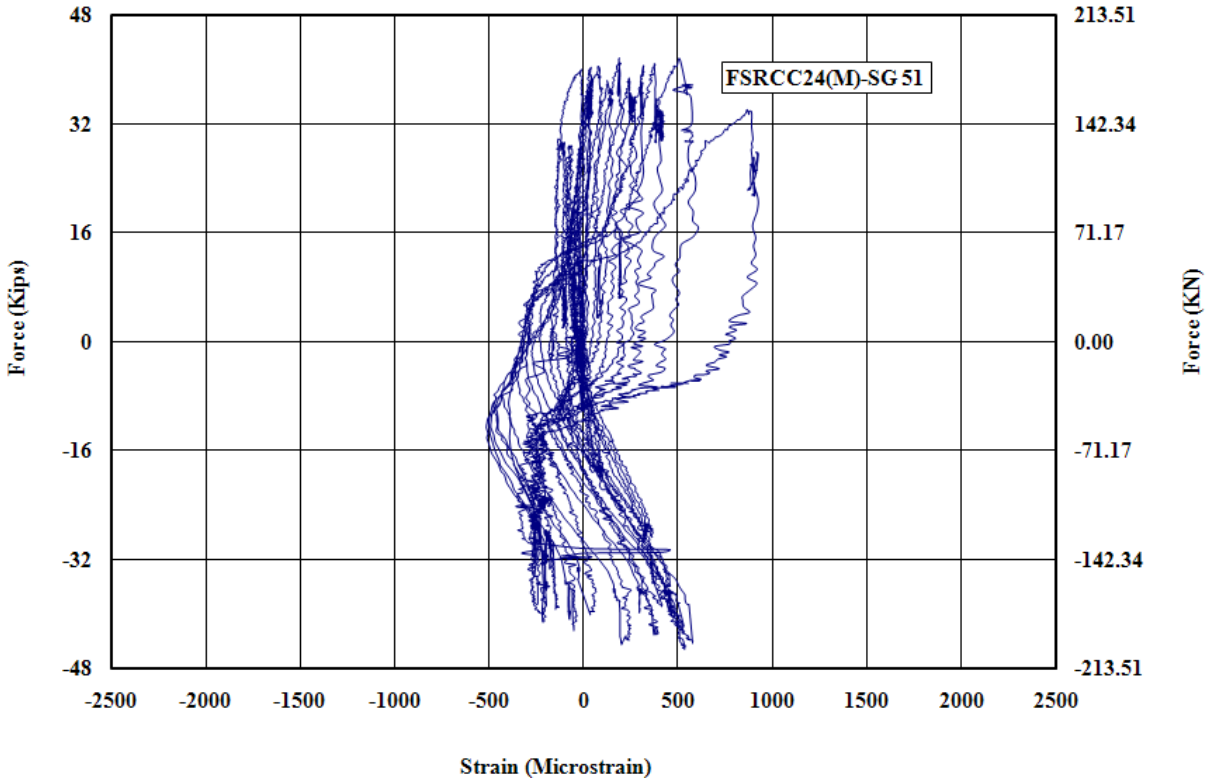

Figure G - 45: Measured Strain in Gauge No.51 for FSRCC24-M

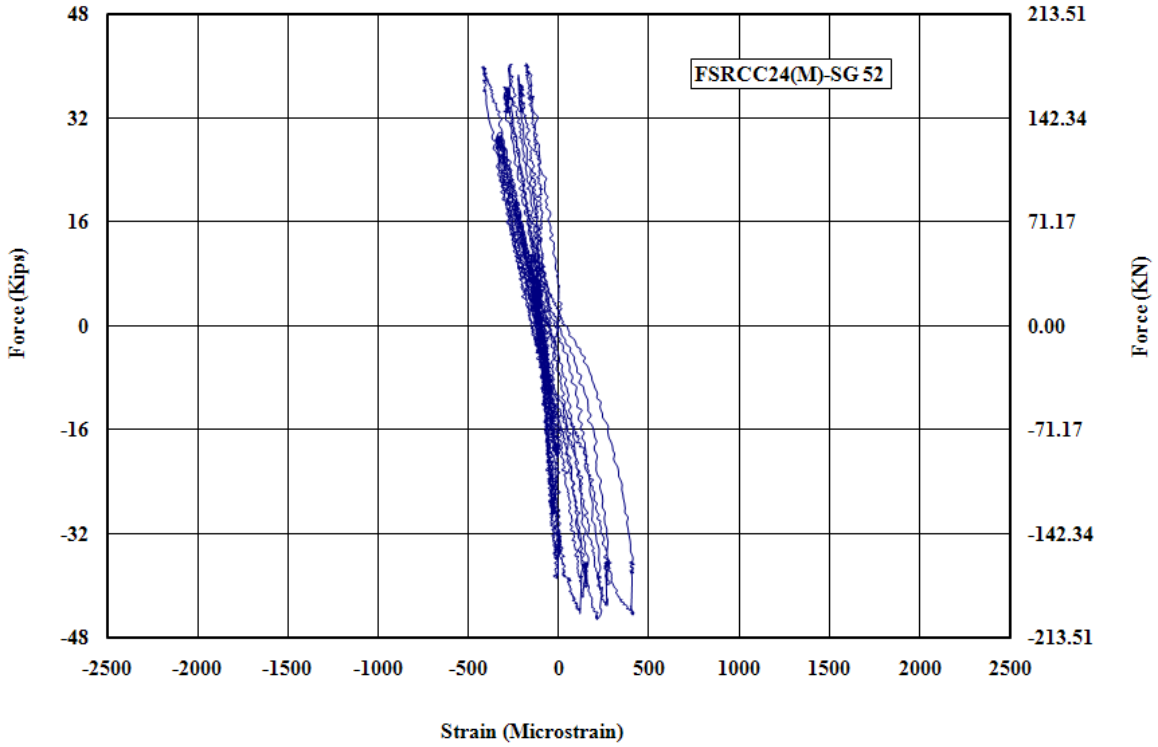

Figure G - 46: Measured Strain in Gauge No.52 for FSRCC24-M

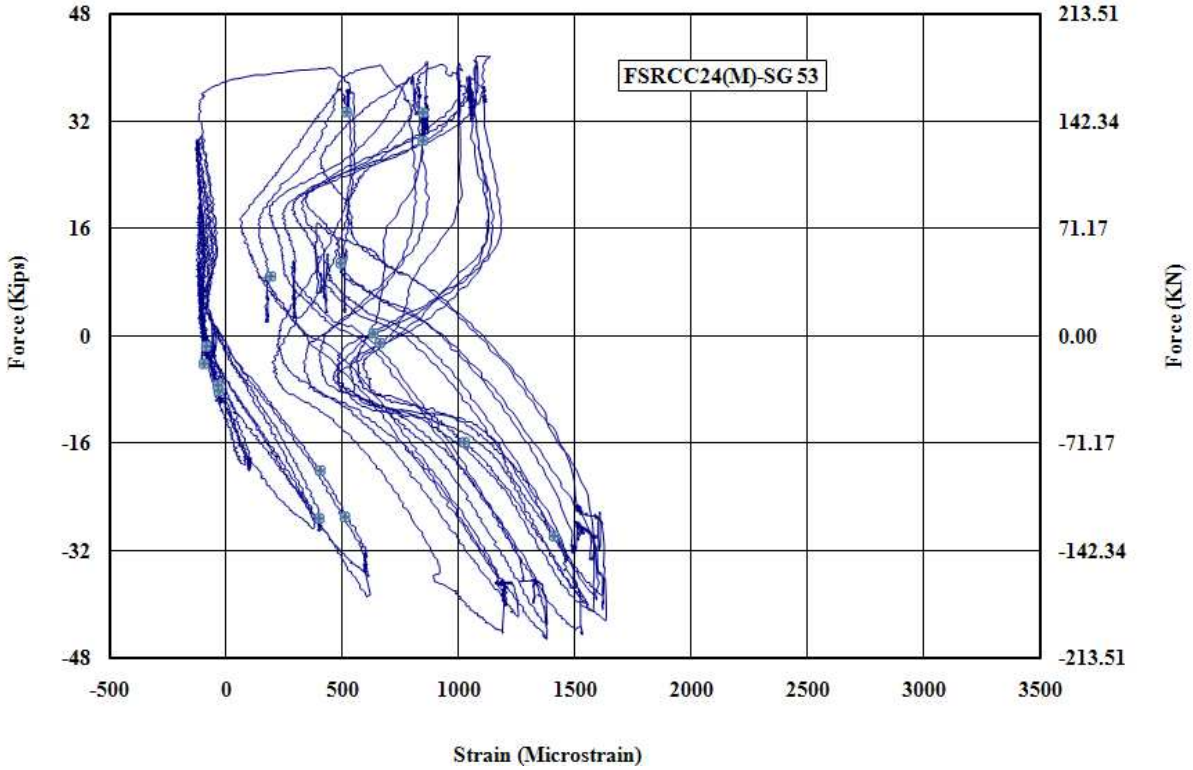

Figure G - 47: Measured Strain in Gauge No.53 for FSRCC24-M

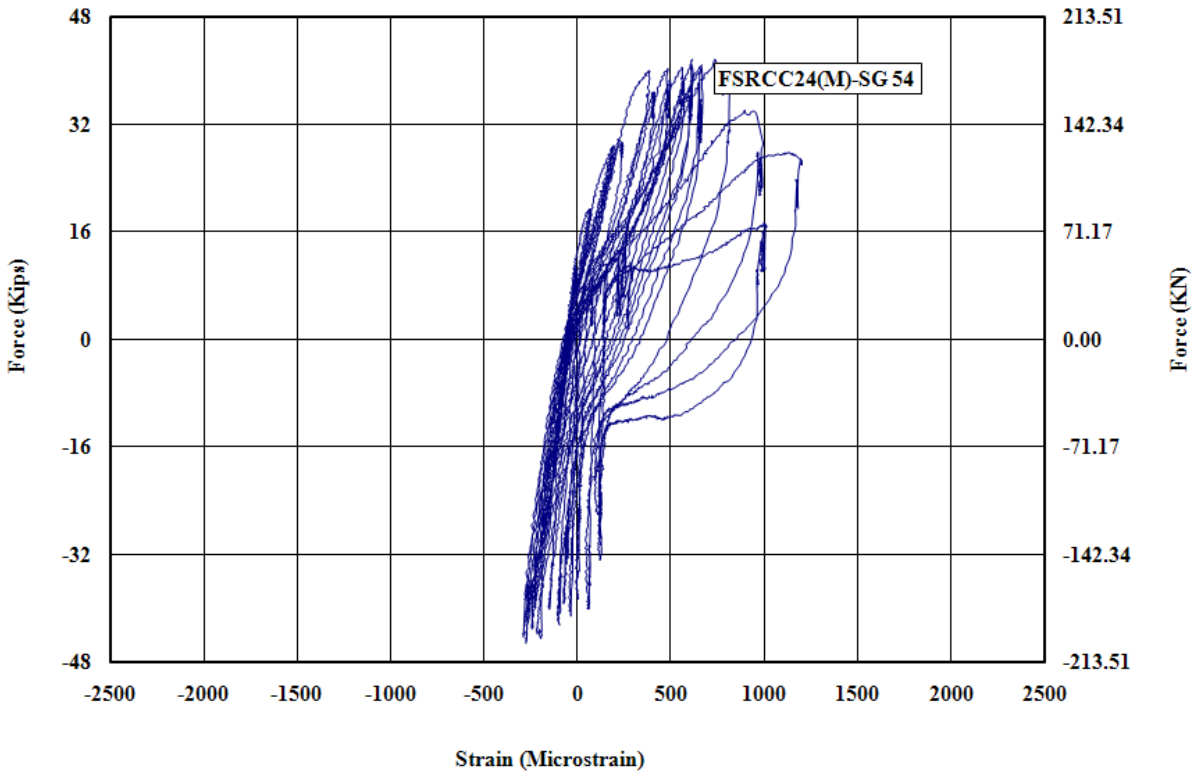

Figure G - 48: Measured Strain in Gauge No.54 for FSRCC24-M

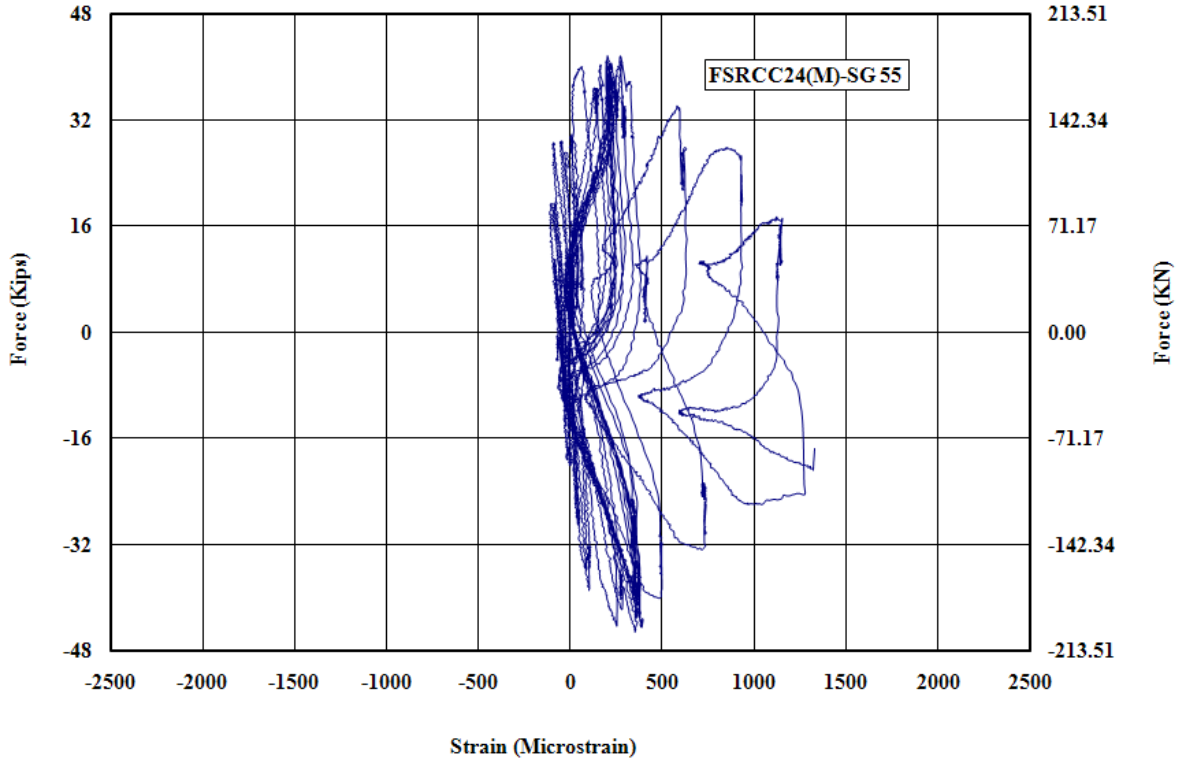

Figure G - 49: Measured Strain in Gauge No.55 for FSRCC24-M

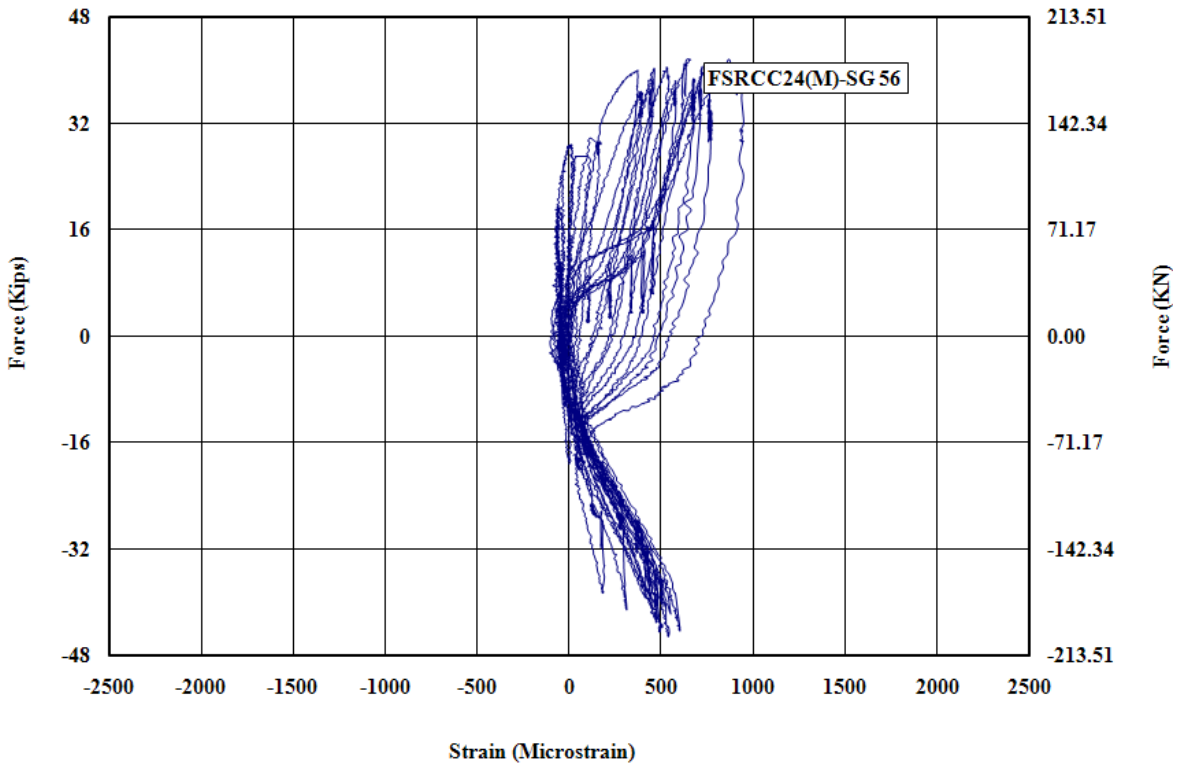

Figure G - 50: Measured Strain in Gauge No.56 for FSRCC24-M

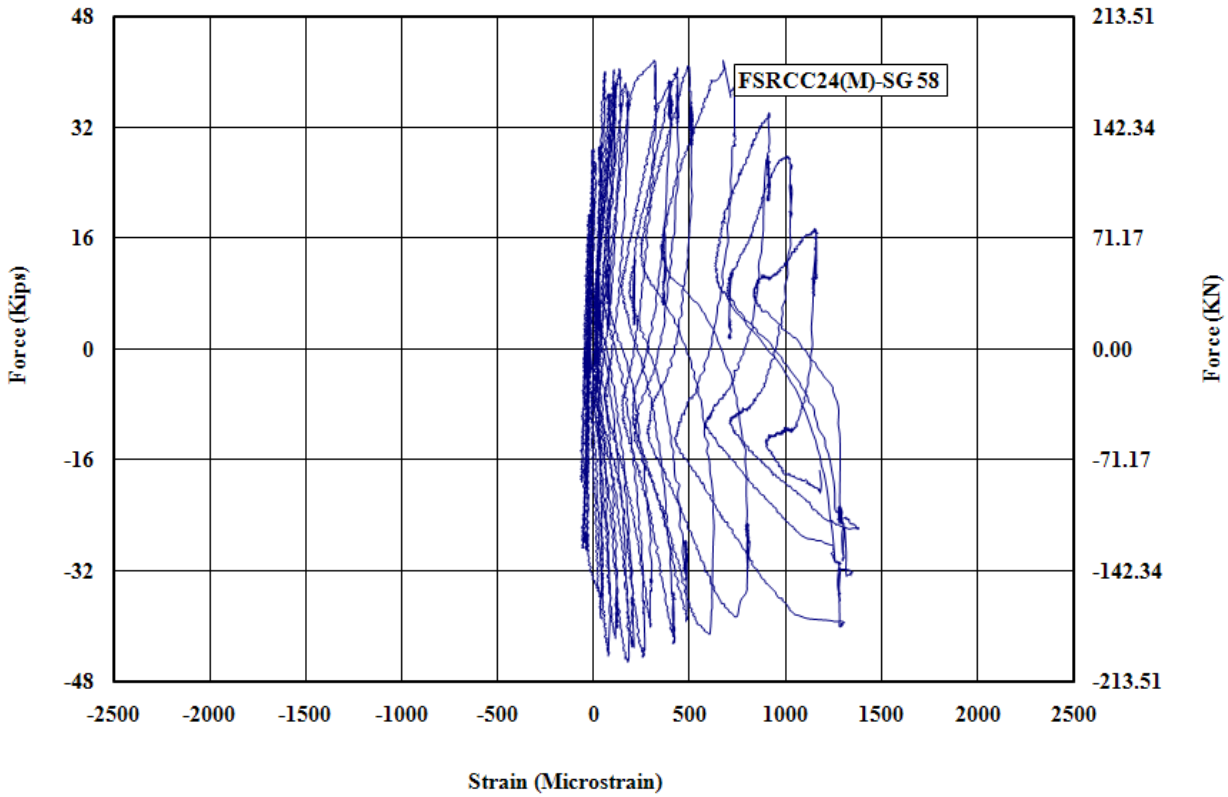

Figure G - 51: Measured Strain in Gauge No.58 for FSRCC24-M

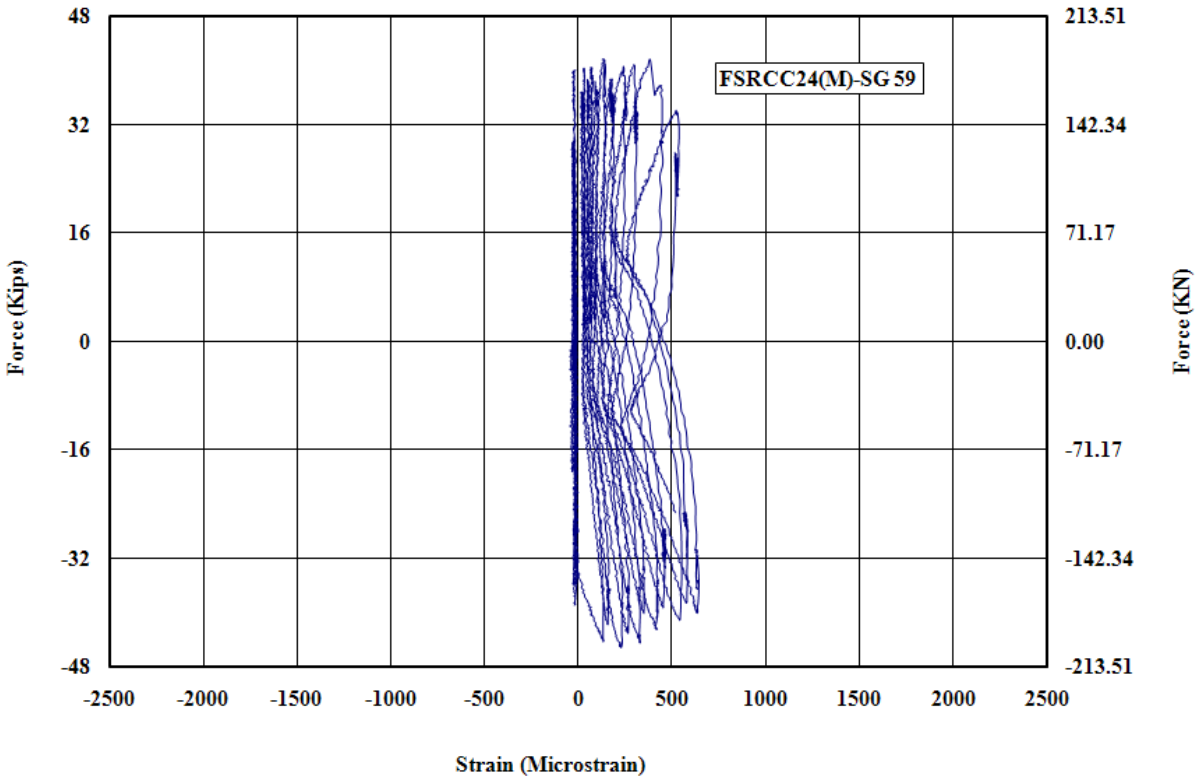

Figure G - 52: Measured Strain in Gauge No.59 for FSRCC24-M

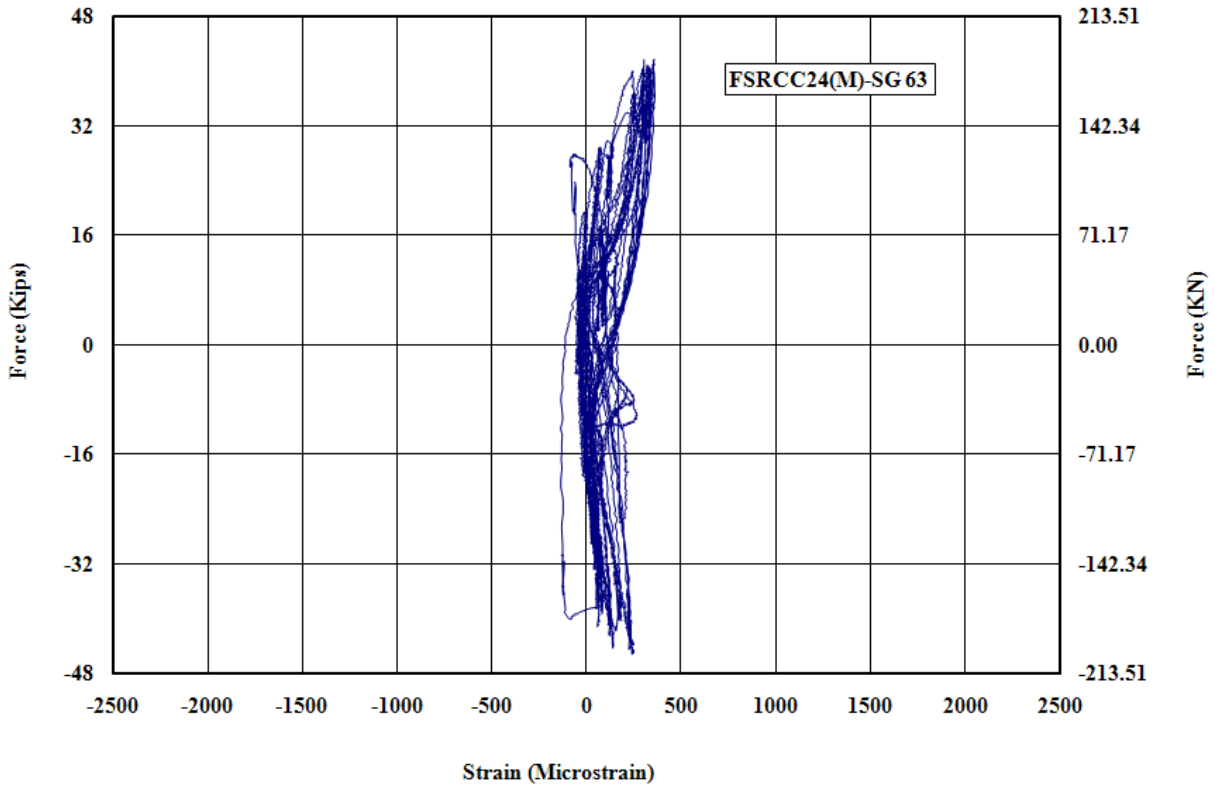

Figure G - 53: Measured Strain in Gauge No.63 for FSRCC24-M

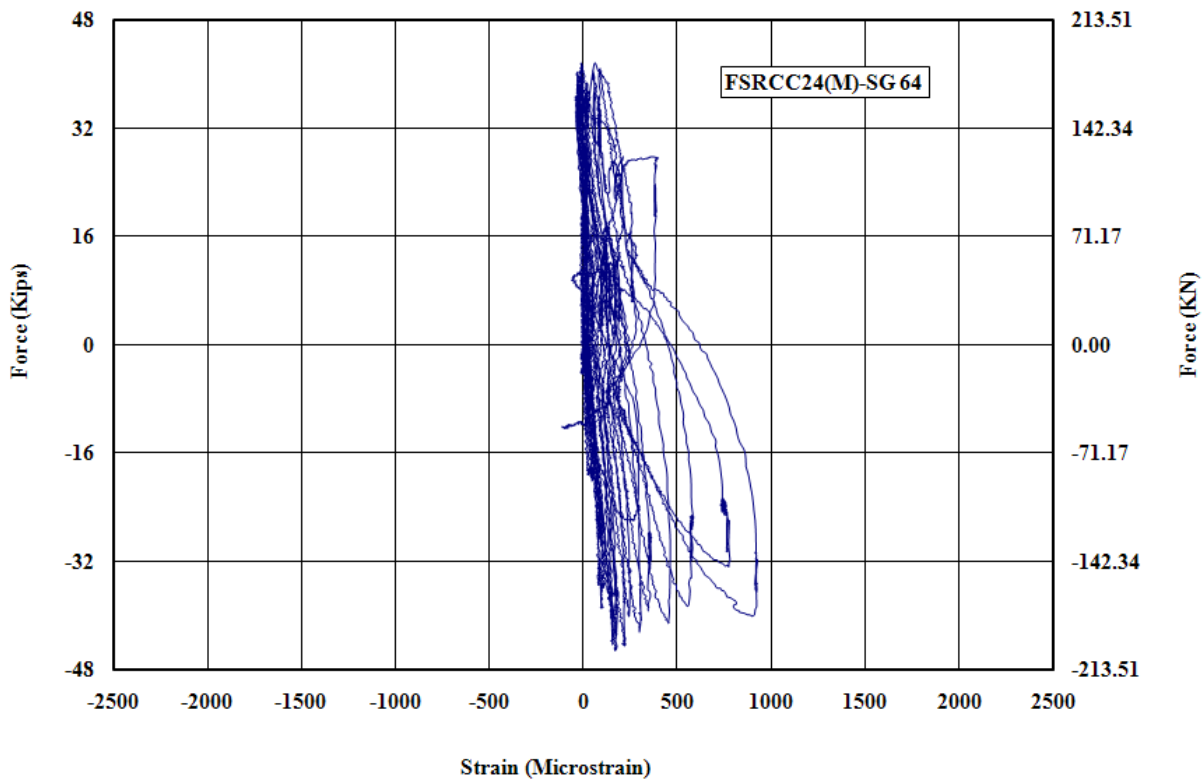

Figure G - 54: Measured Strain in Gauge No.64 for FSRCC24-M

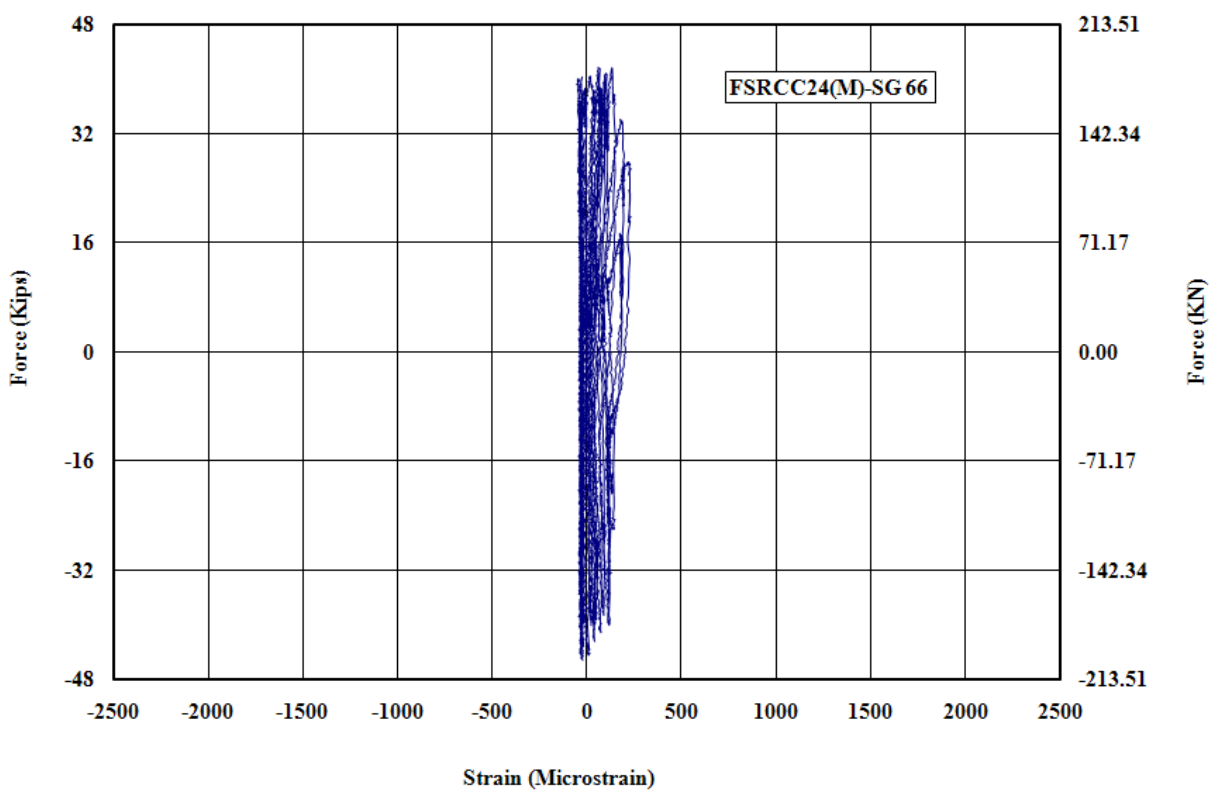

Figure G - 55: Measured Strain in Gauge No.66 for FSRCC24-M

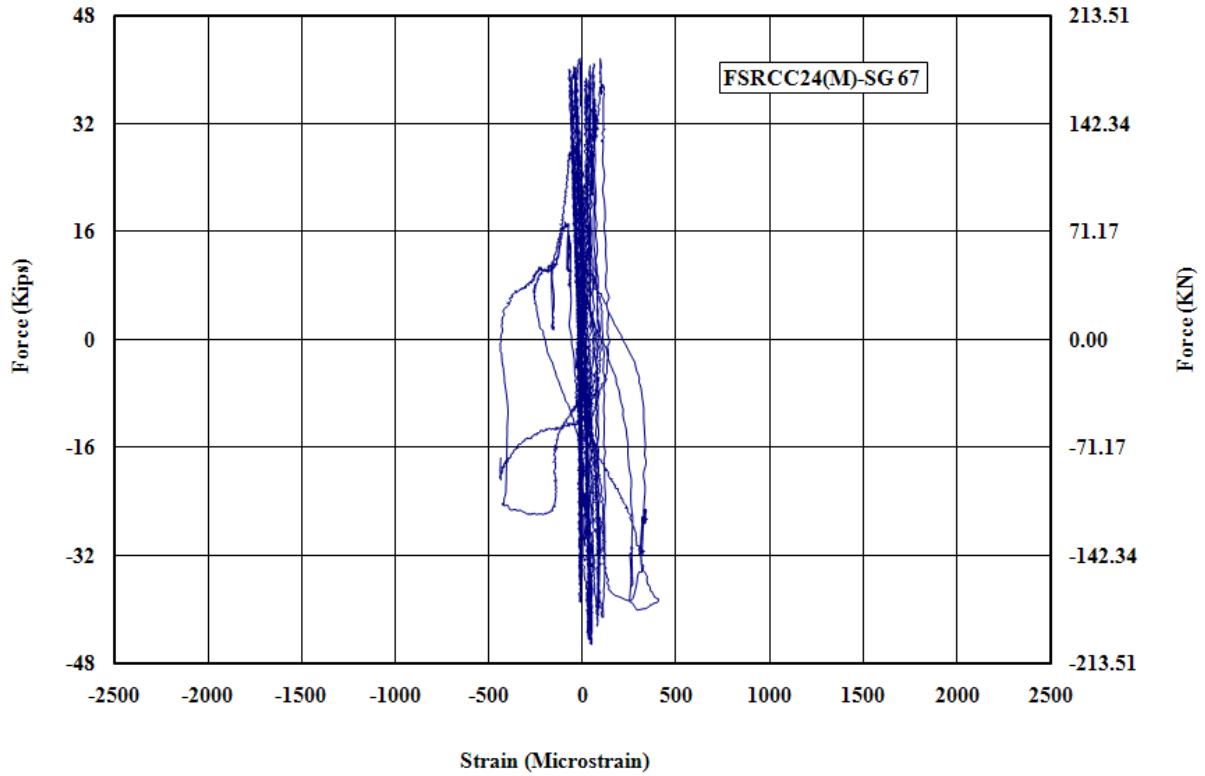

Figure G - 56: Measured Strain in Gauge No.67 for FSRCC24-M

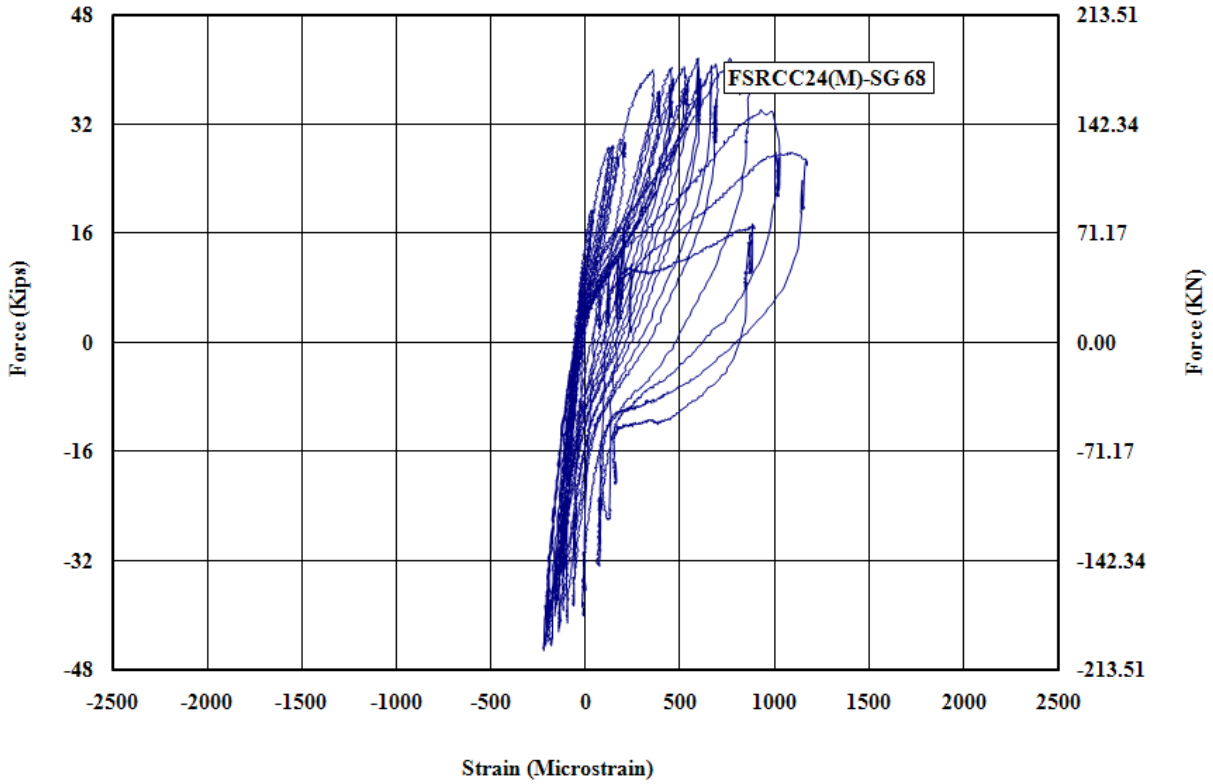

Figure G - 57: Measured Strain in Gauge No.68 for FSRCC24-M

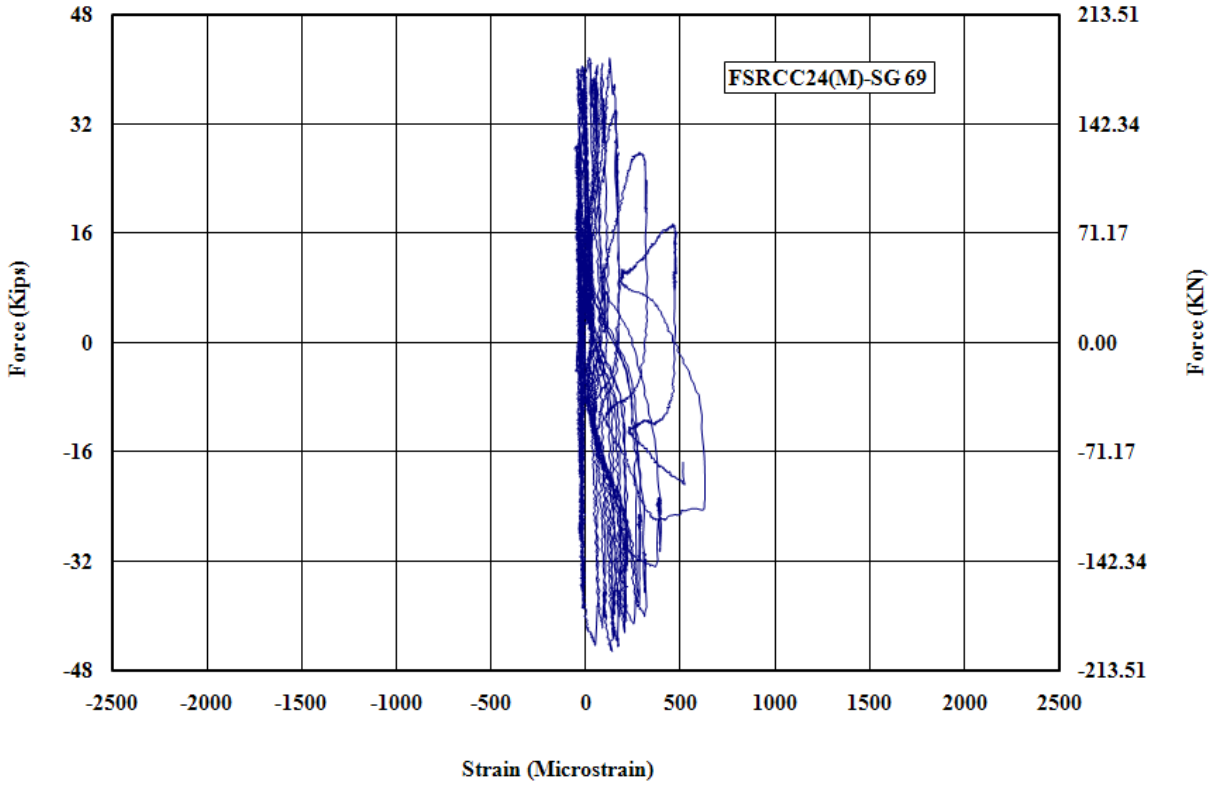

Figure G - 58: Measured Strain in Gauge No.69 for FSRCC24-M

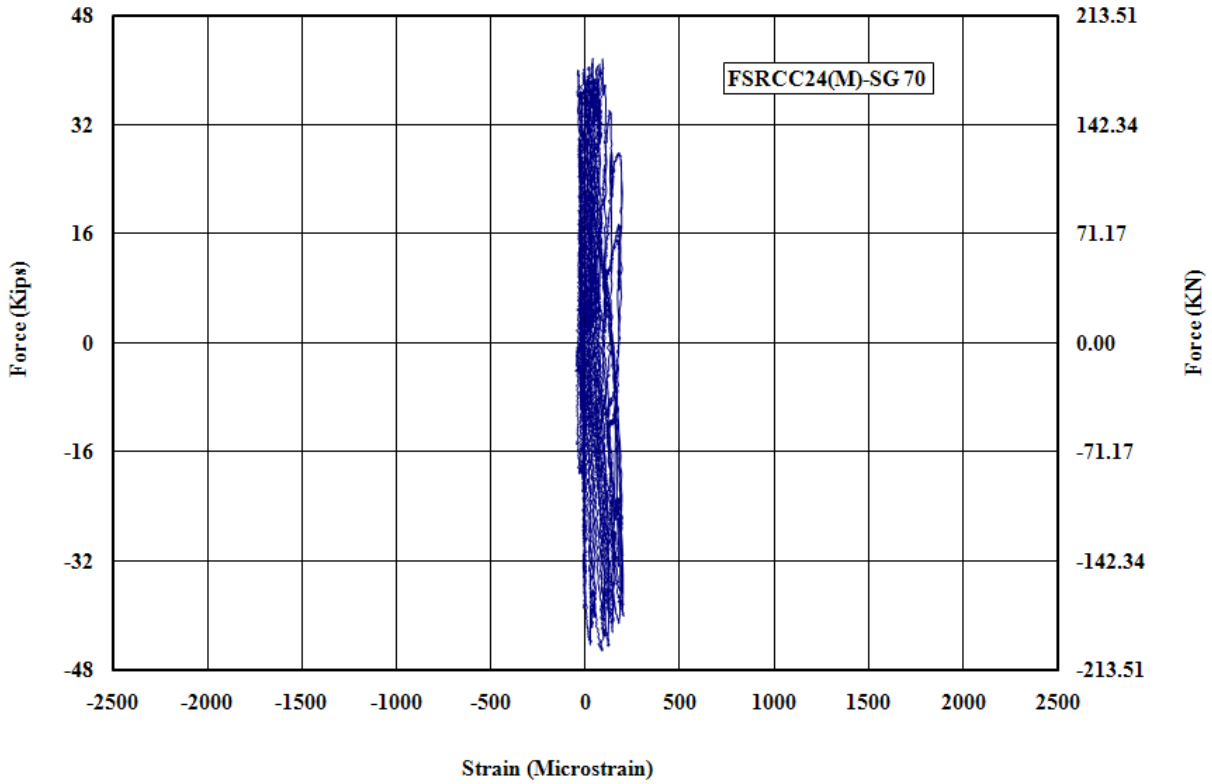

Figure G - 59: Measured Strain in Gauge No.70 for FSRCC24-M

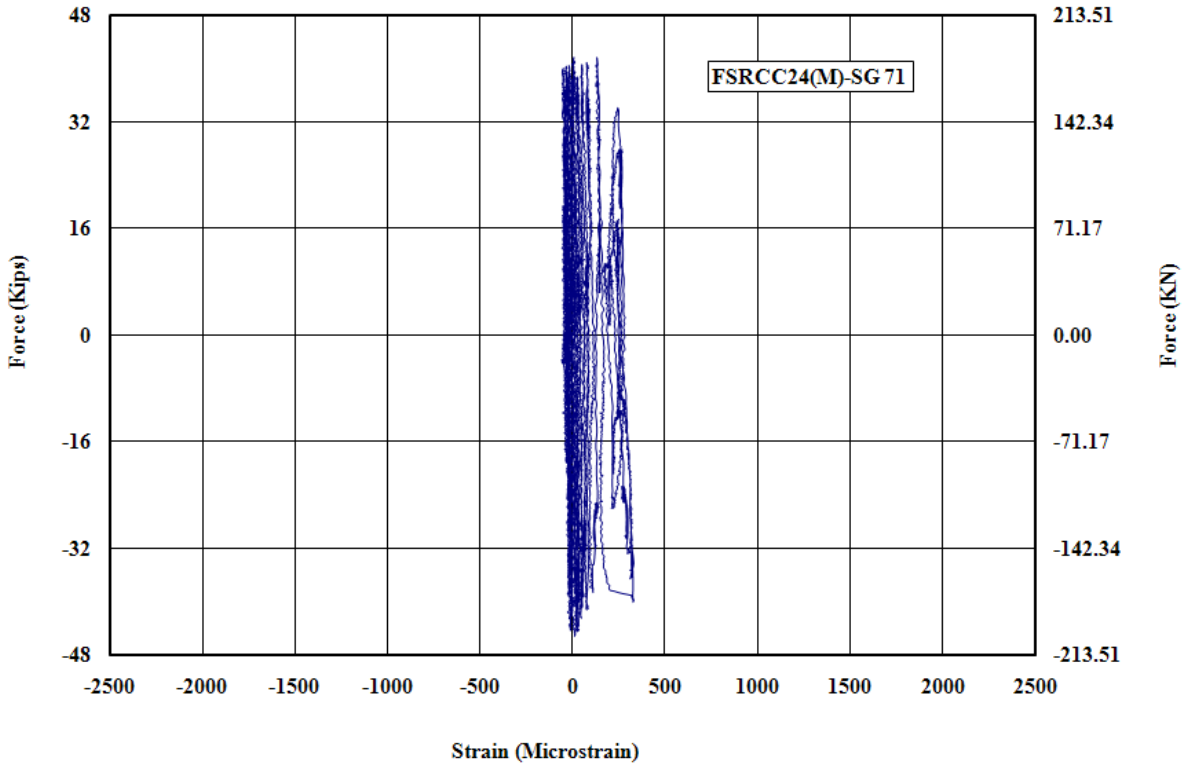

Figure G - 60: Measured Strain in Gauge No.71 for FSRCC24-M

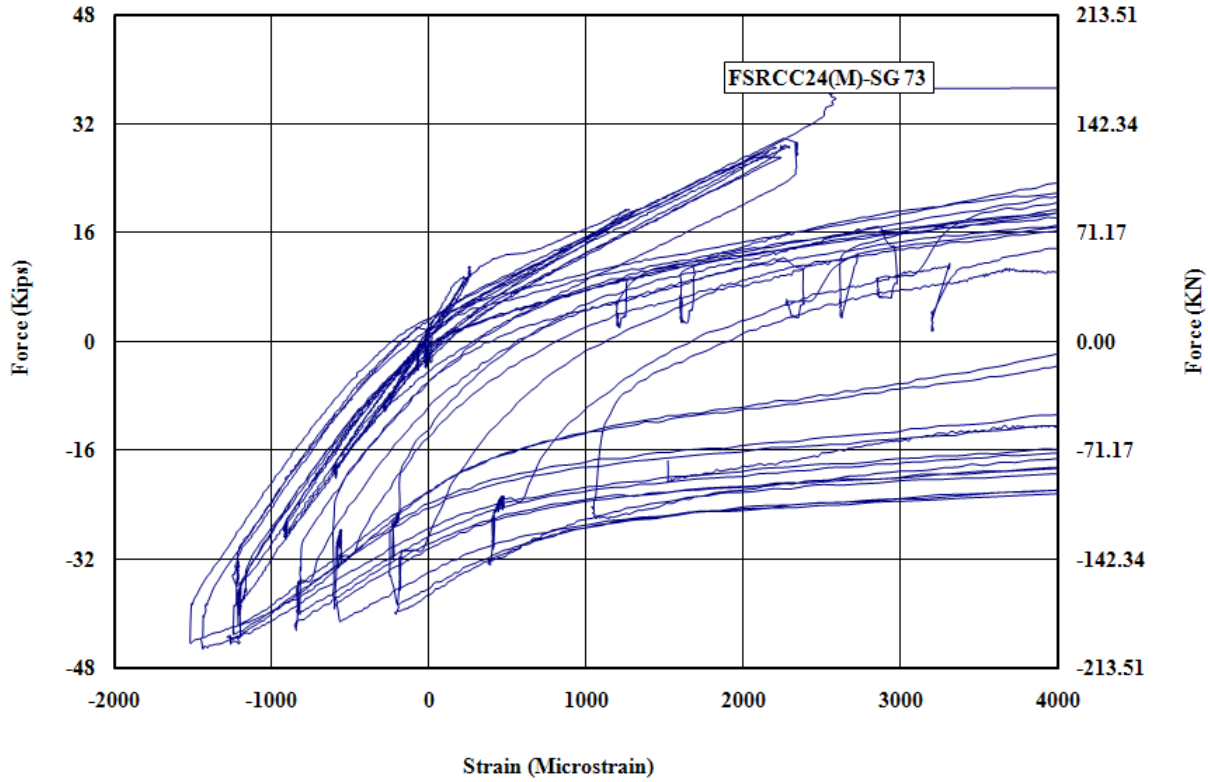

Figure G - 61: Measured Strain in Gauge No.73 for FSRCC24-M

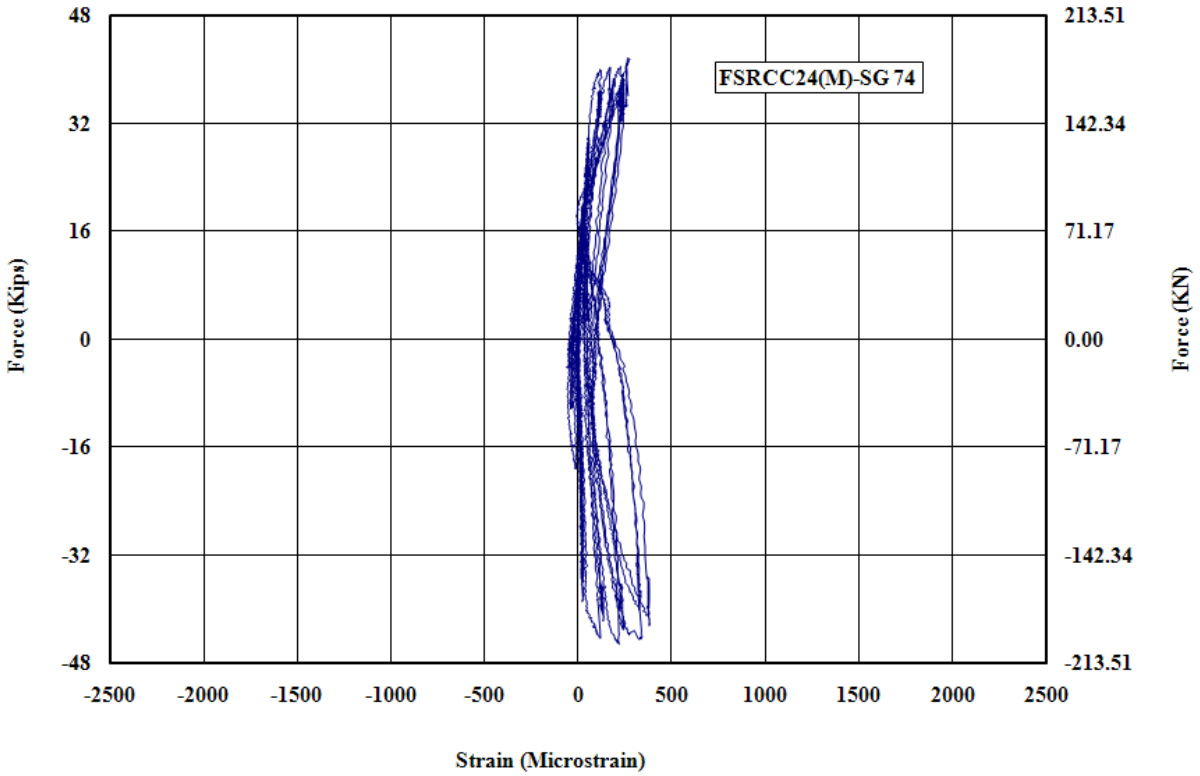

Figure G - 62: Measured Strain in Gauge No.74 for FSRCC24-M

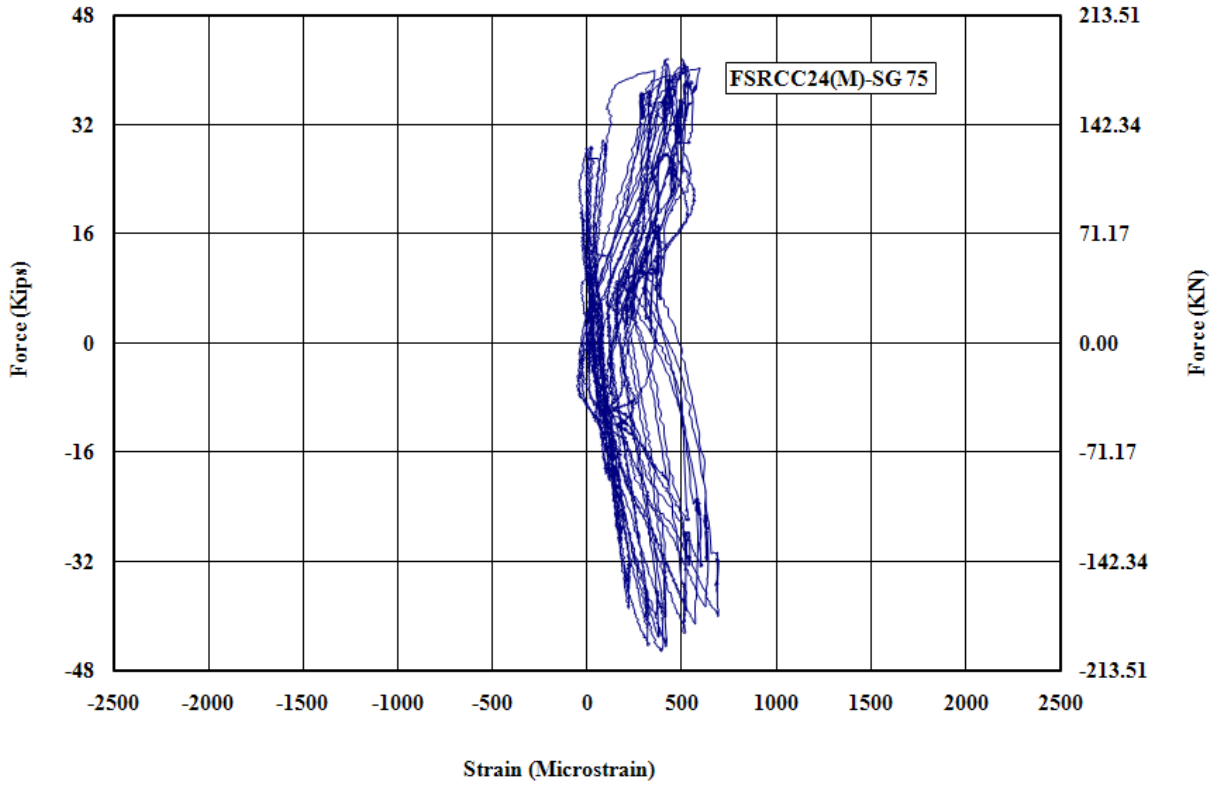

Figure G - 63: Measured Strain in Gauge No.75 for FSRCC24-M

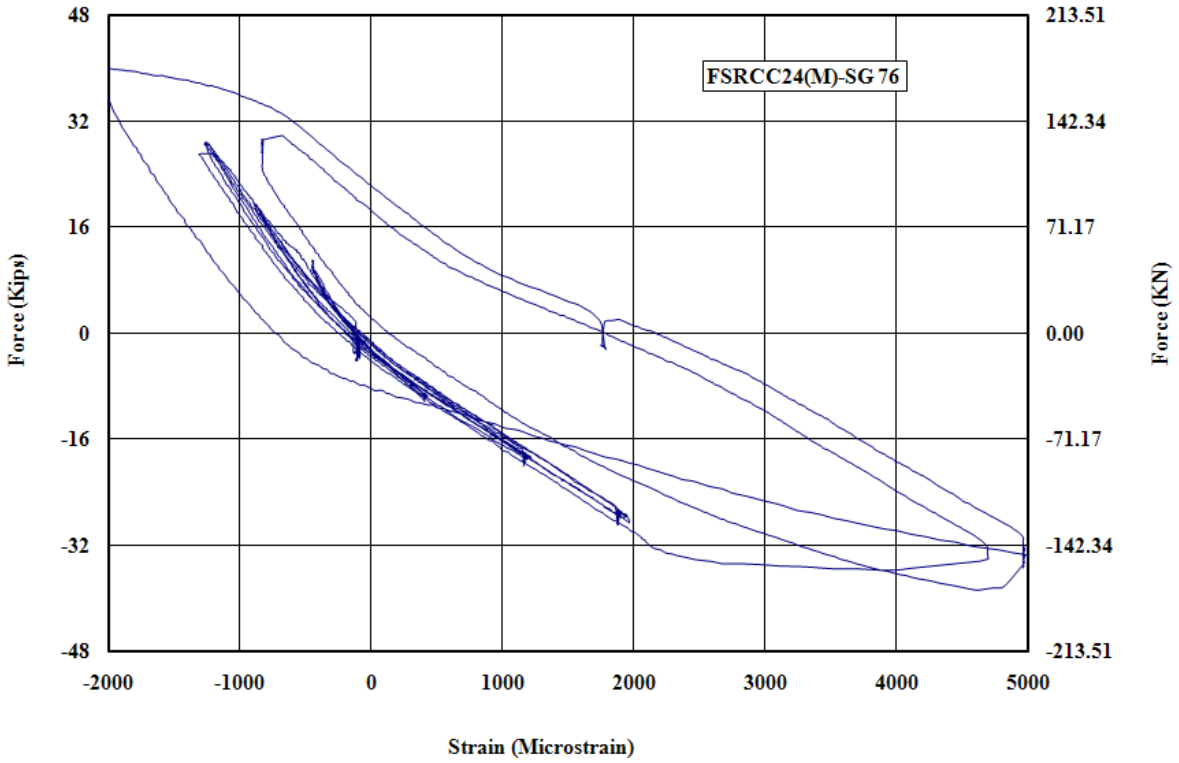

Figure G - 64: Measured Strain in Gauge No.76 for FSRCC24-M

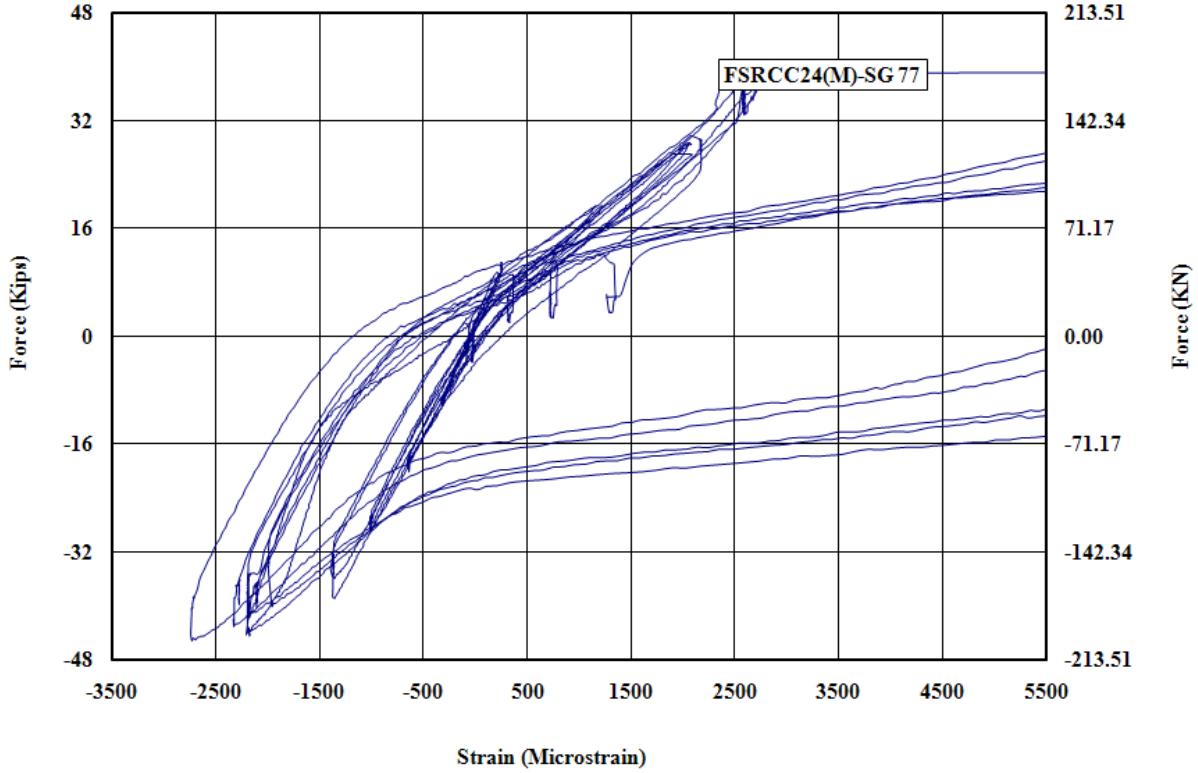

Figure G - 65: Measured Strain in Gauge No.77 for FSRCC24-M

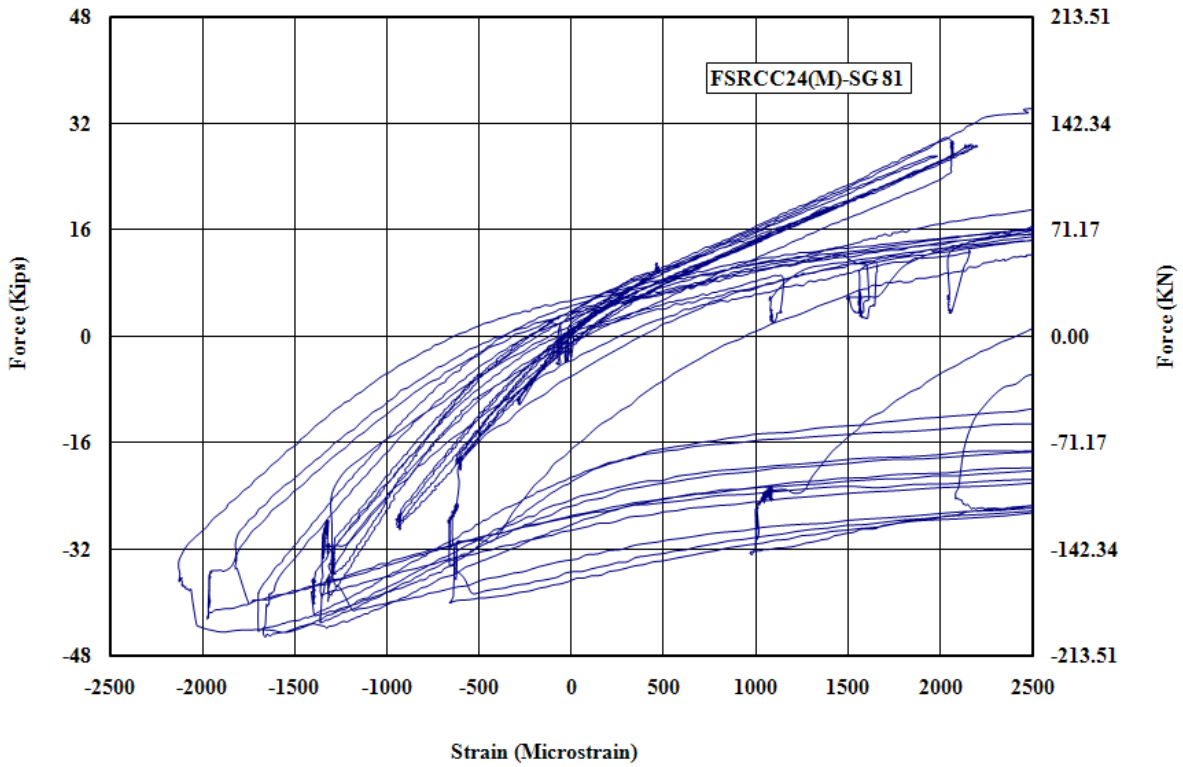

Figure G - 66: Measured Strain in Gauge No.81 for FSRCC24-M

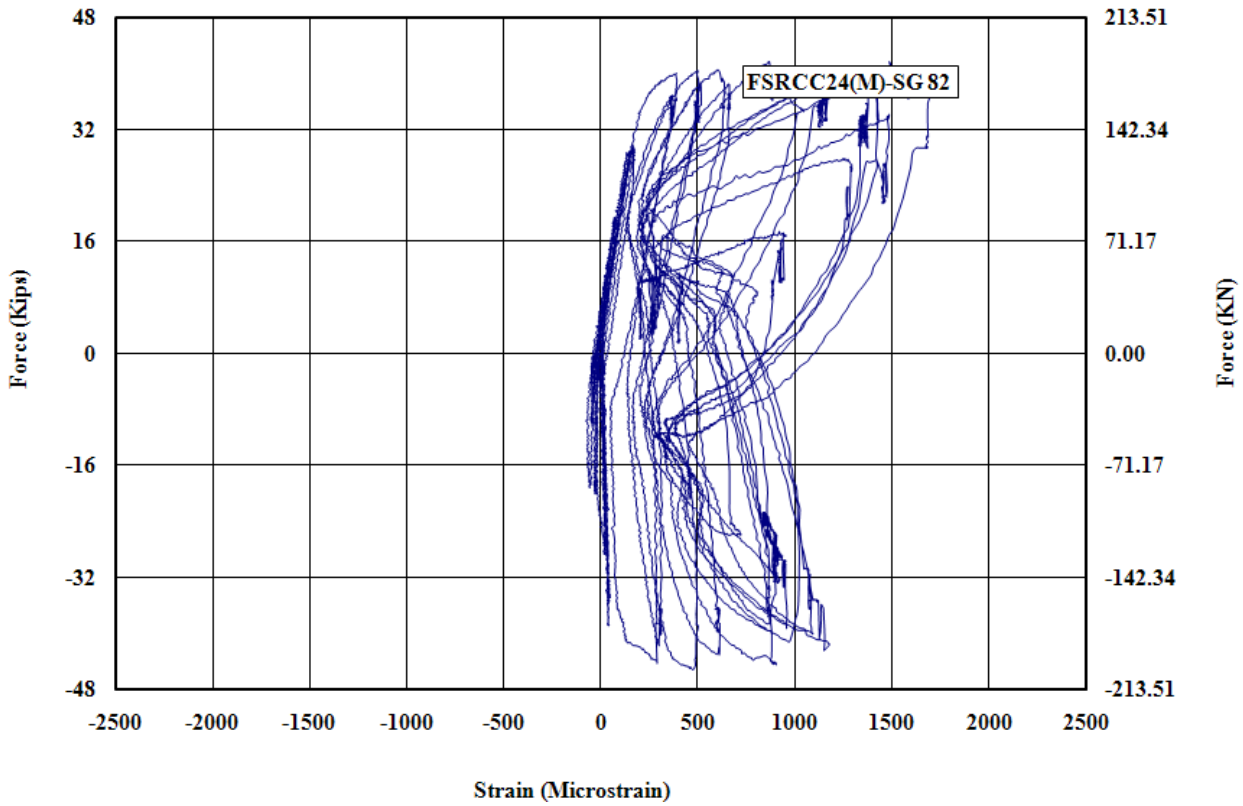

Figure G - 67: Measured Strain in Gauge No.82 for FSRCC24-M

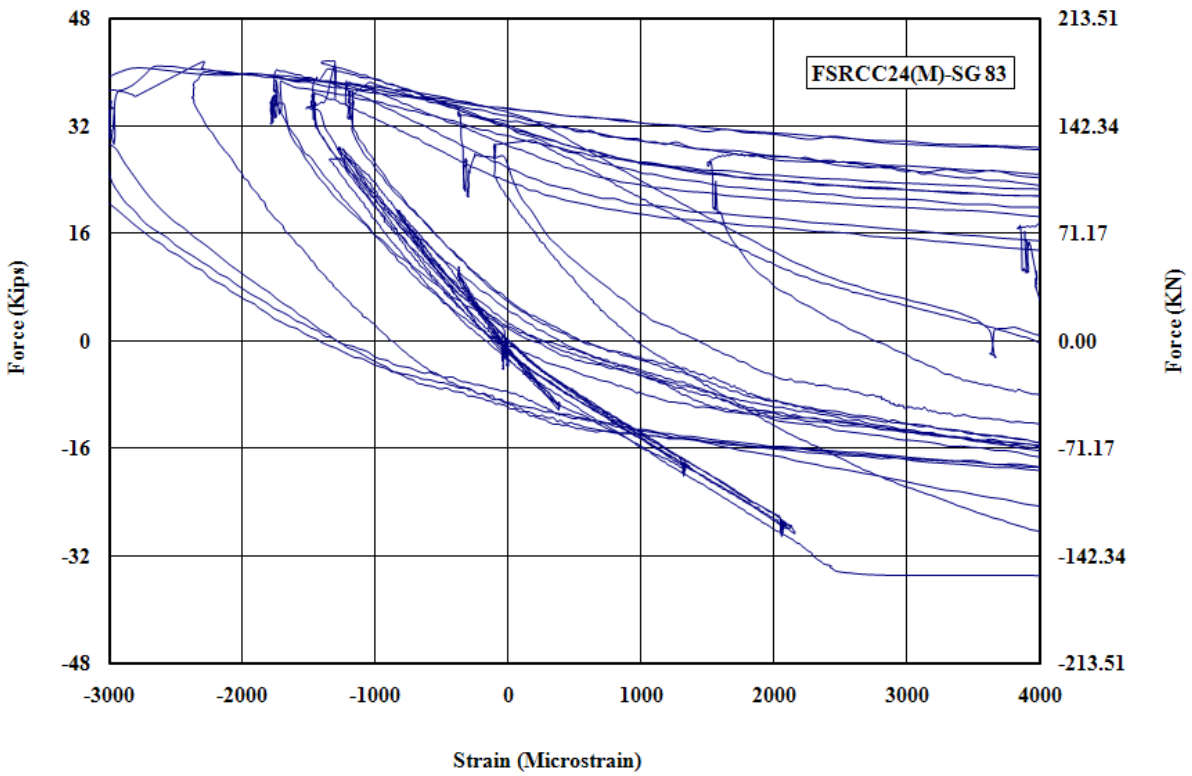

Figure G - 68: Measured Strain in Gauge No.83 for FSRCC24-M

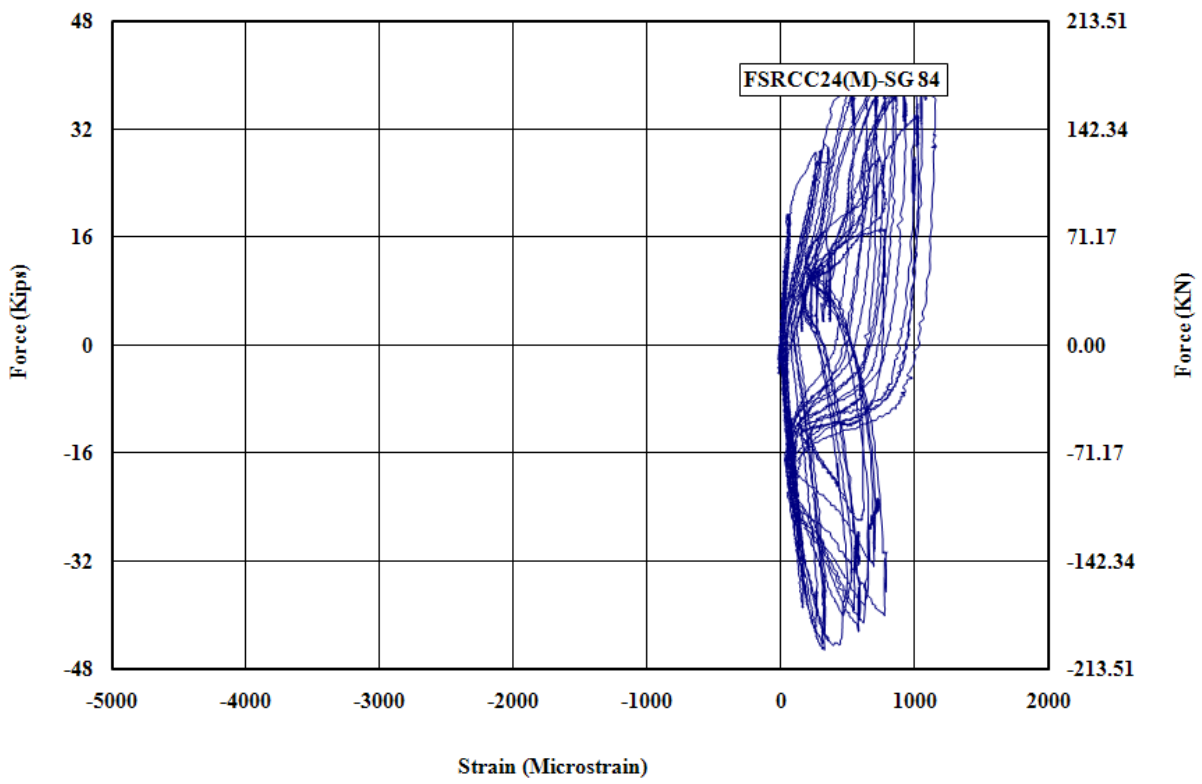

Figure G - 69: Measured Strain in Gauge No.84 for FSRCC24-M

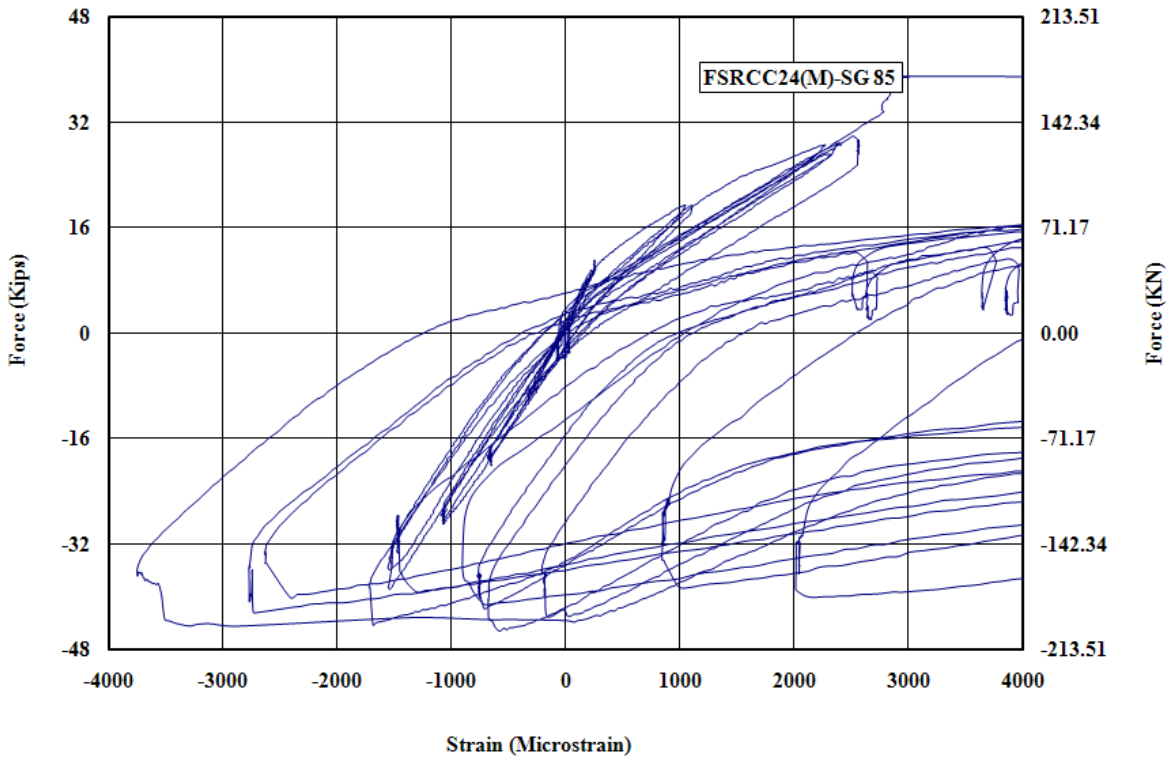

Figure G - 70: Measured Strain in Gauge No.85 for FSRCC24-M

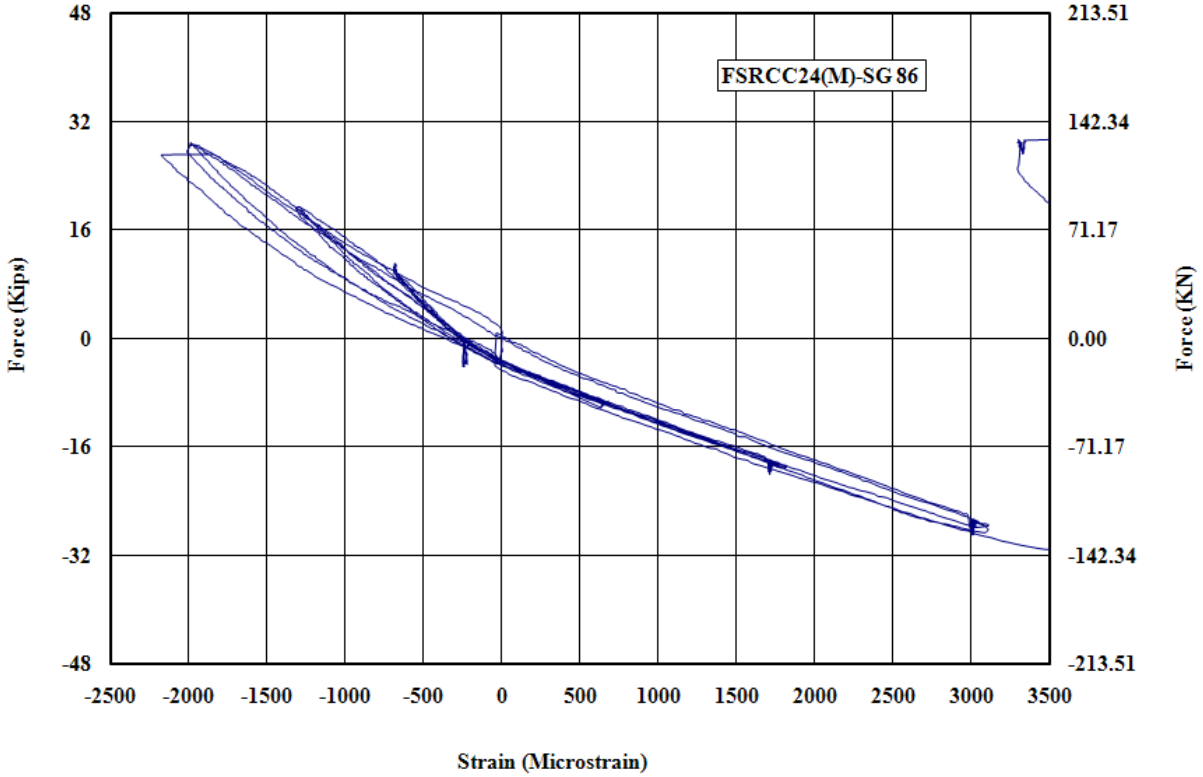

Figure G - 71: Measured Strain in Gauge No.86 for FSRCC24-M

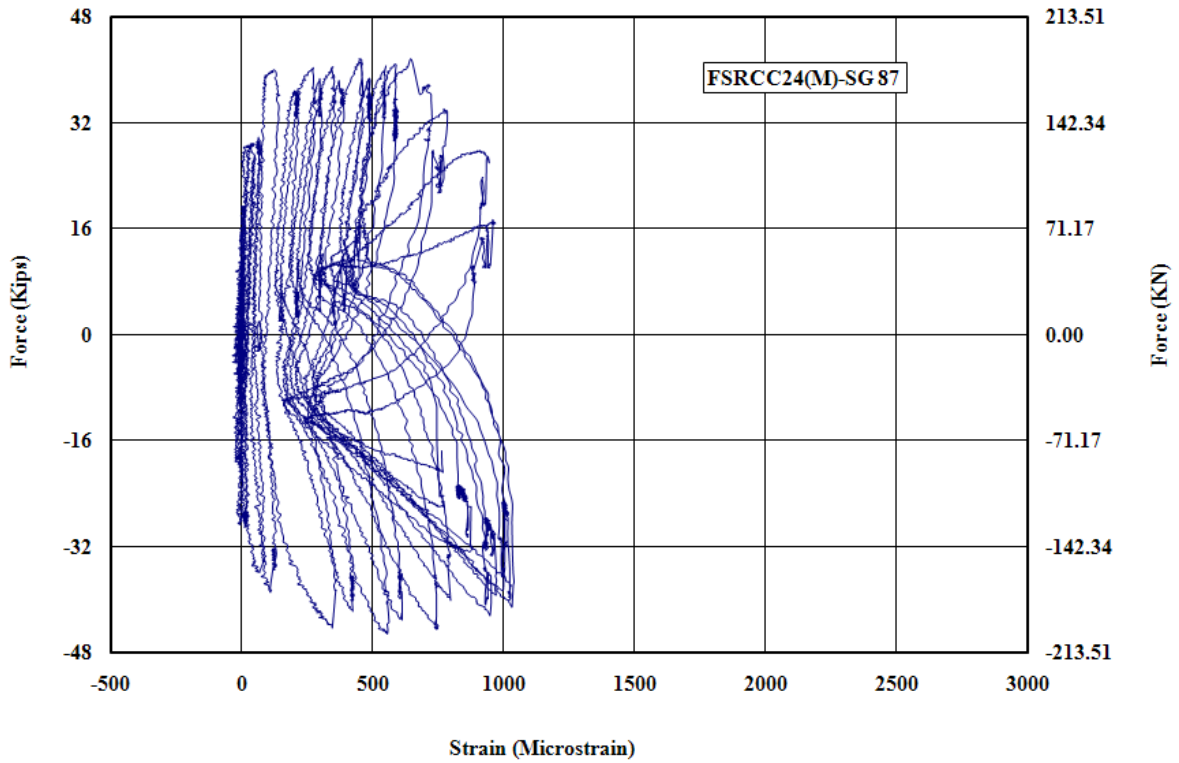

Figure G - 72: Measured Strain in Gauge No.87 for FSRCC24-M

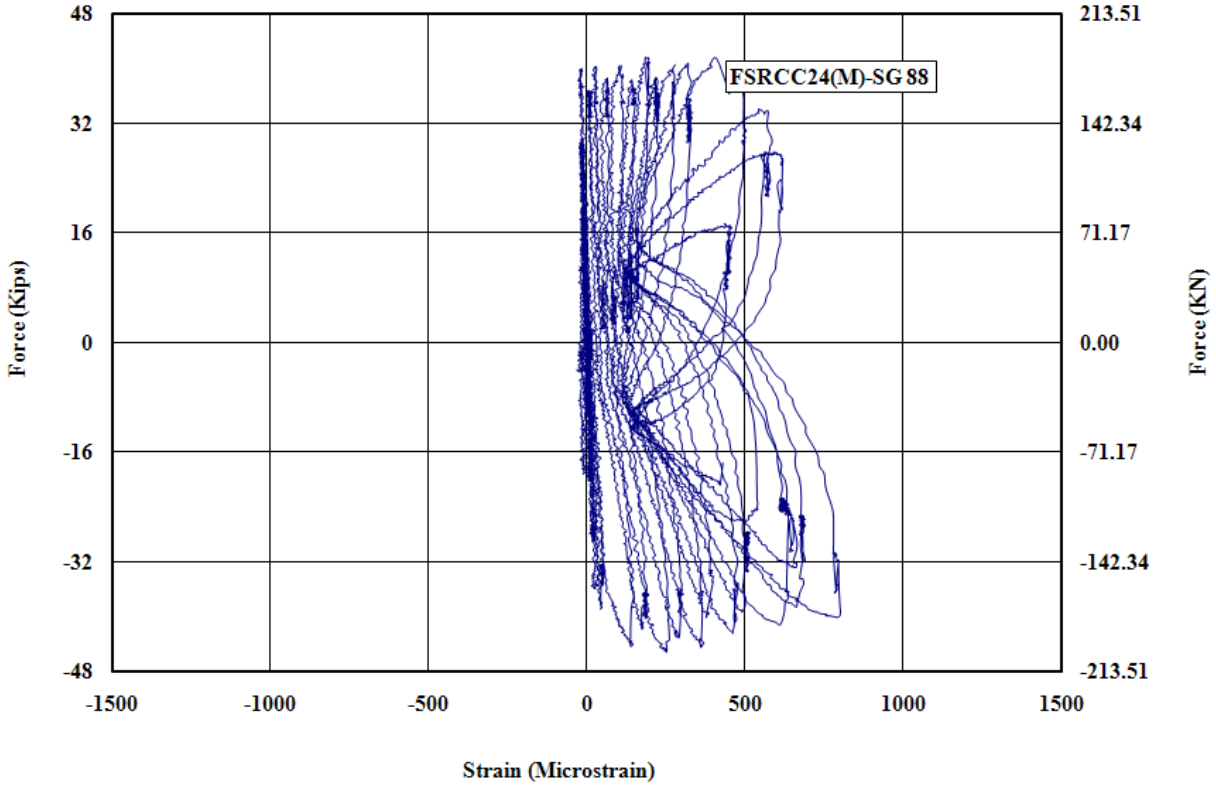

Figure G - 73: Measured Strain in Gauge No.88 for FSRCC24-M

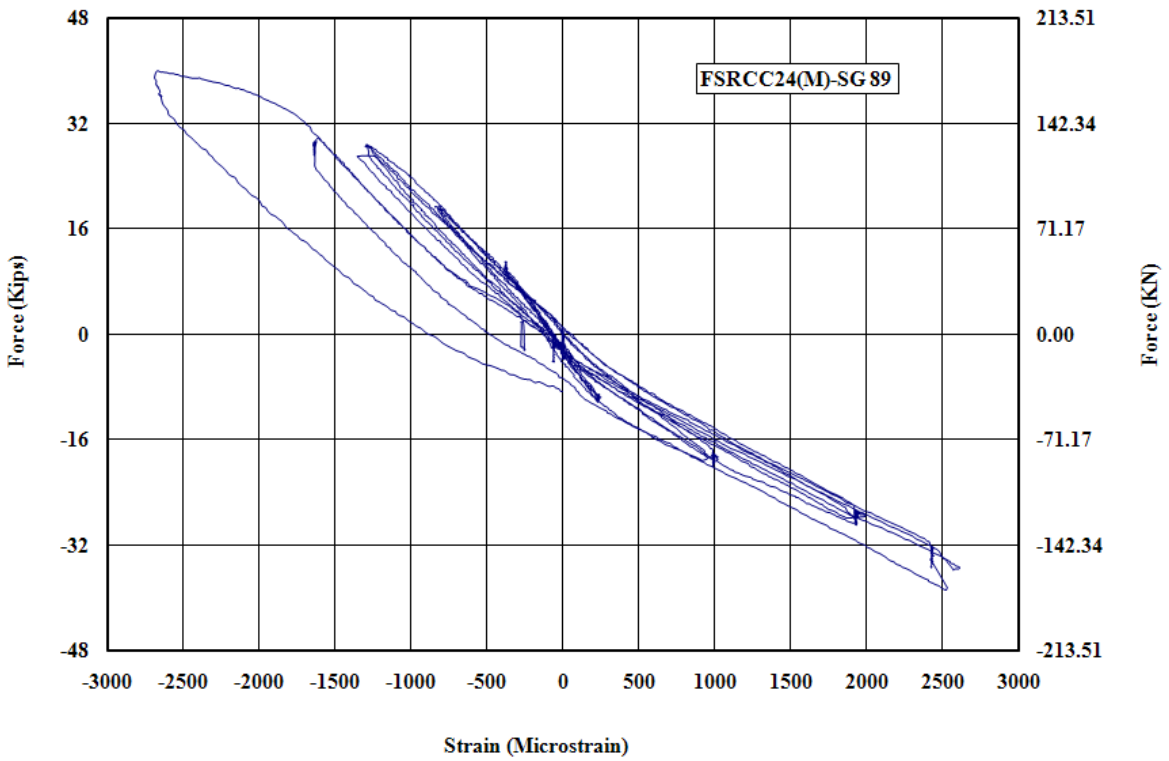

Figure G - 74: Measured Strain in Gauge No.89 for FSRCC24-M

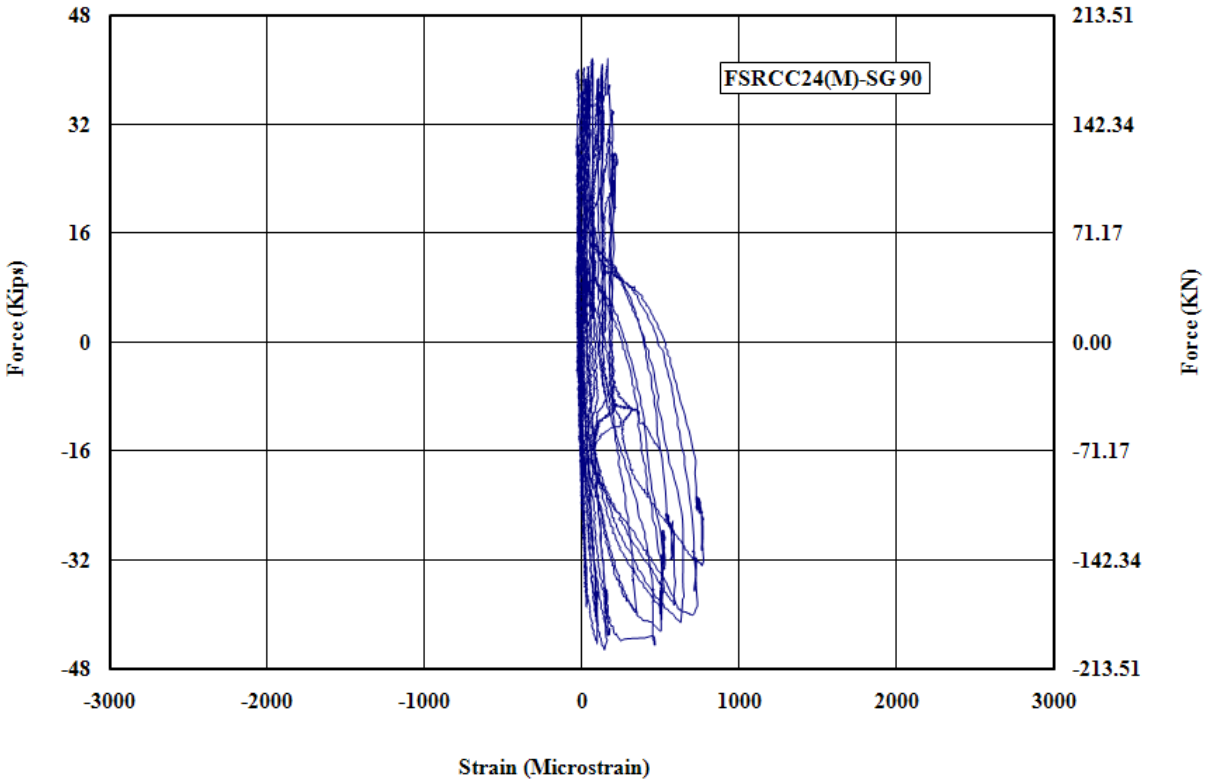

Figure G - 75: Measured Strain in Gauge No.90 for FSRCC24-M

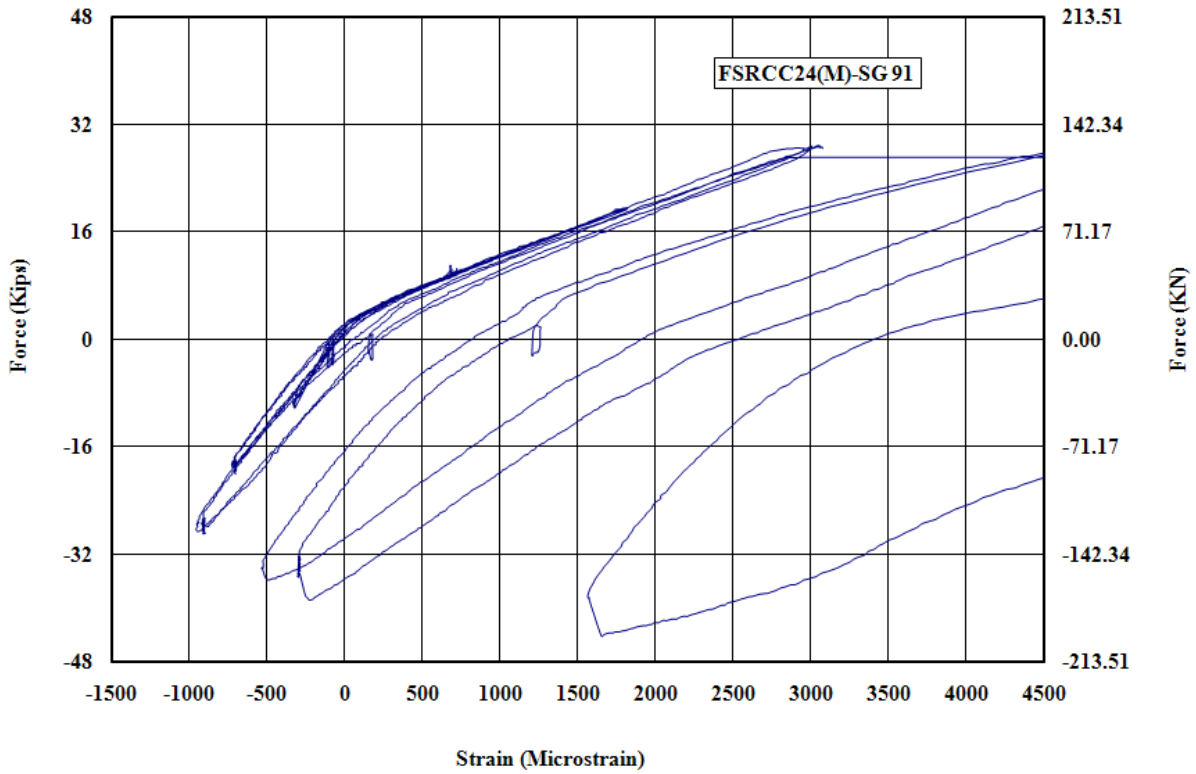

Figure G - 76: Measured Strain in Gauge No.91 for FSRCC24-M

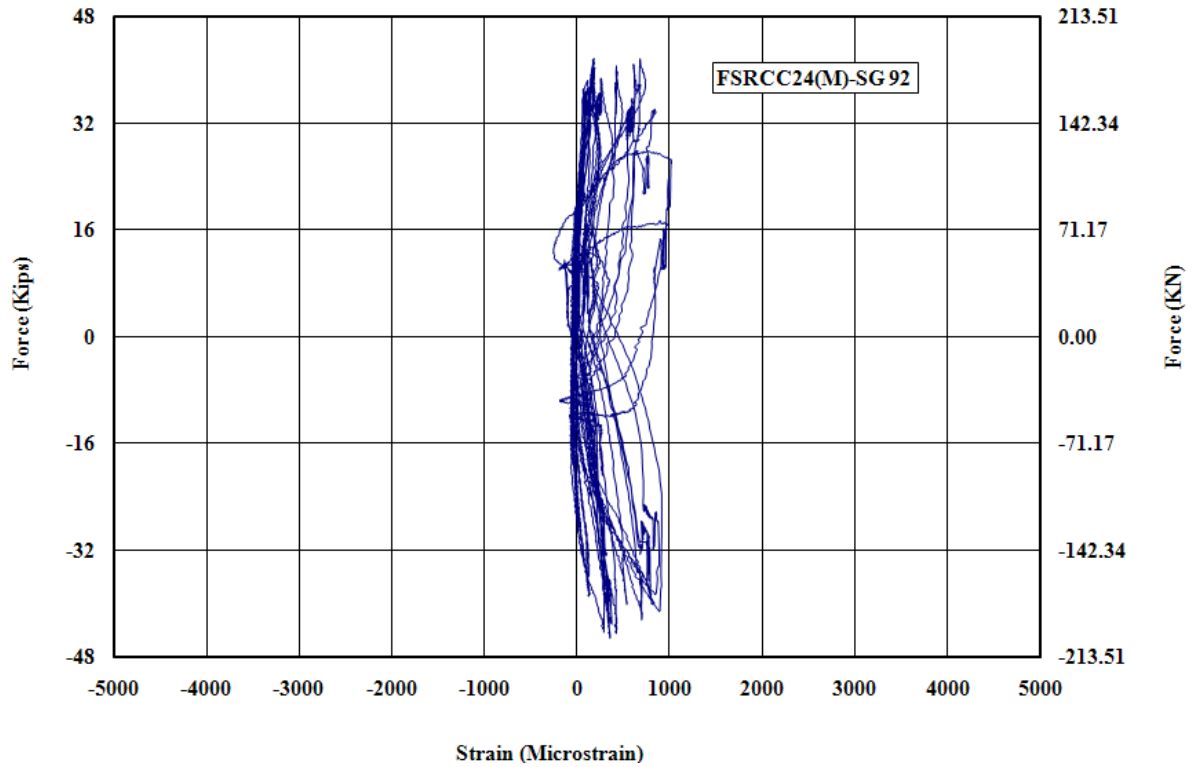

Figure G - 77: Measured Strain in Gauge No.92 for FSRCC24-M

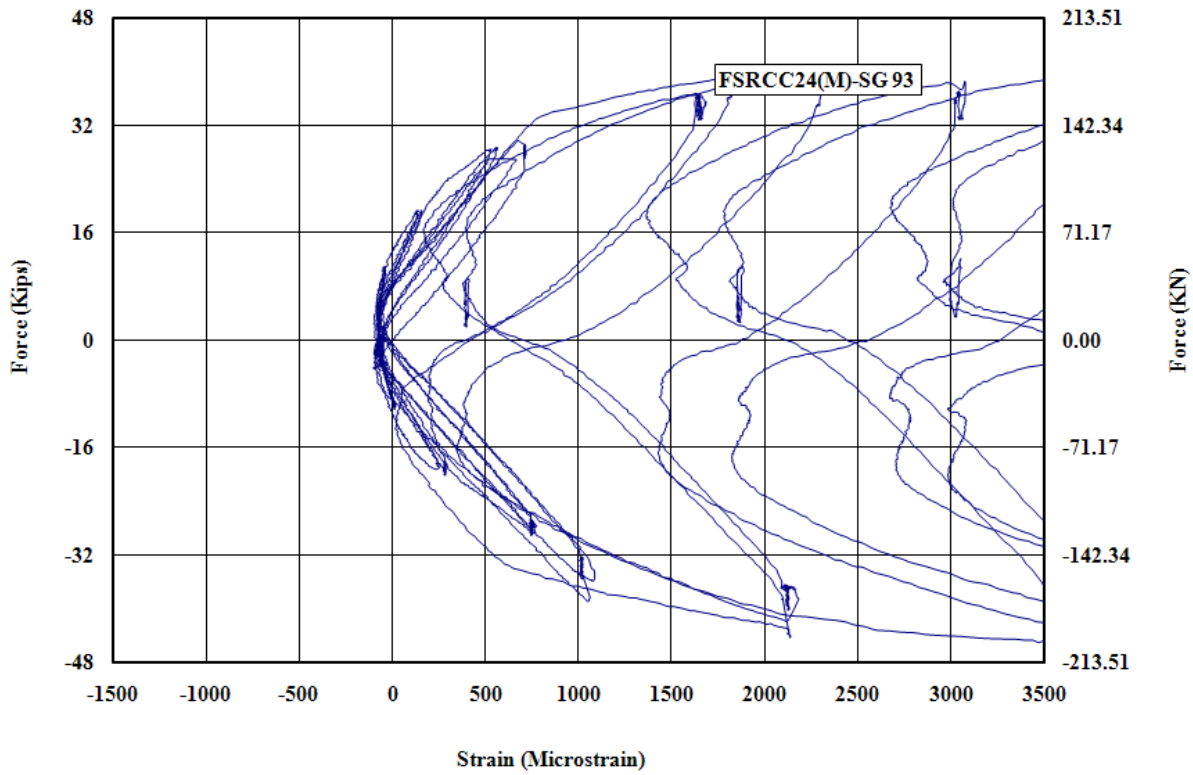

Figure G - 78: Measured Strain in Gauge No.93 for FSRCC24-M

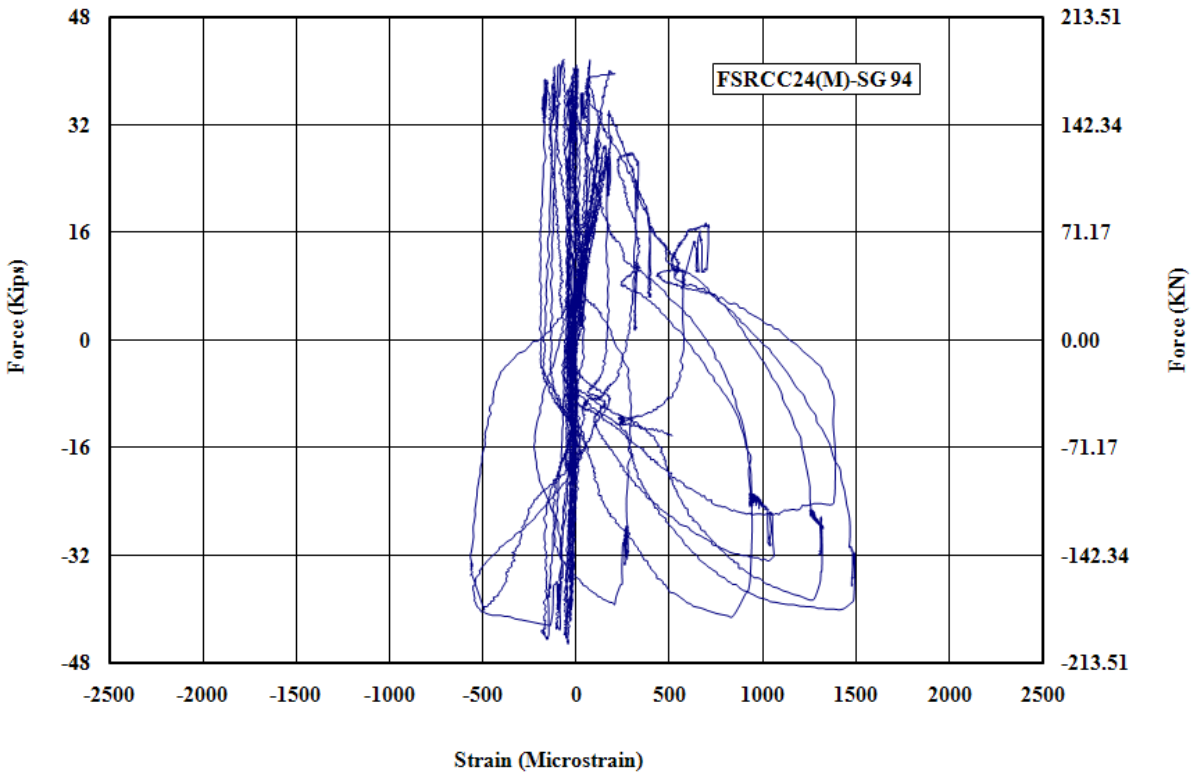

Figure G - 79: Measured Strain in Gauge No.94 for FSRCC24-M

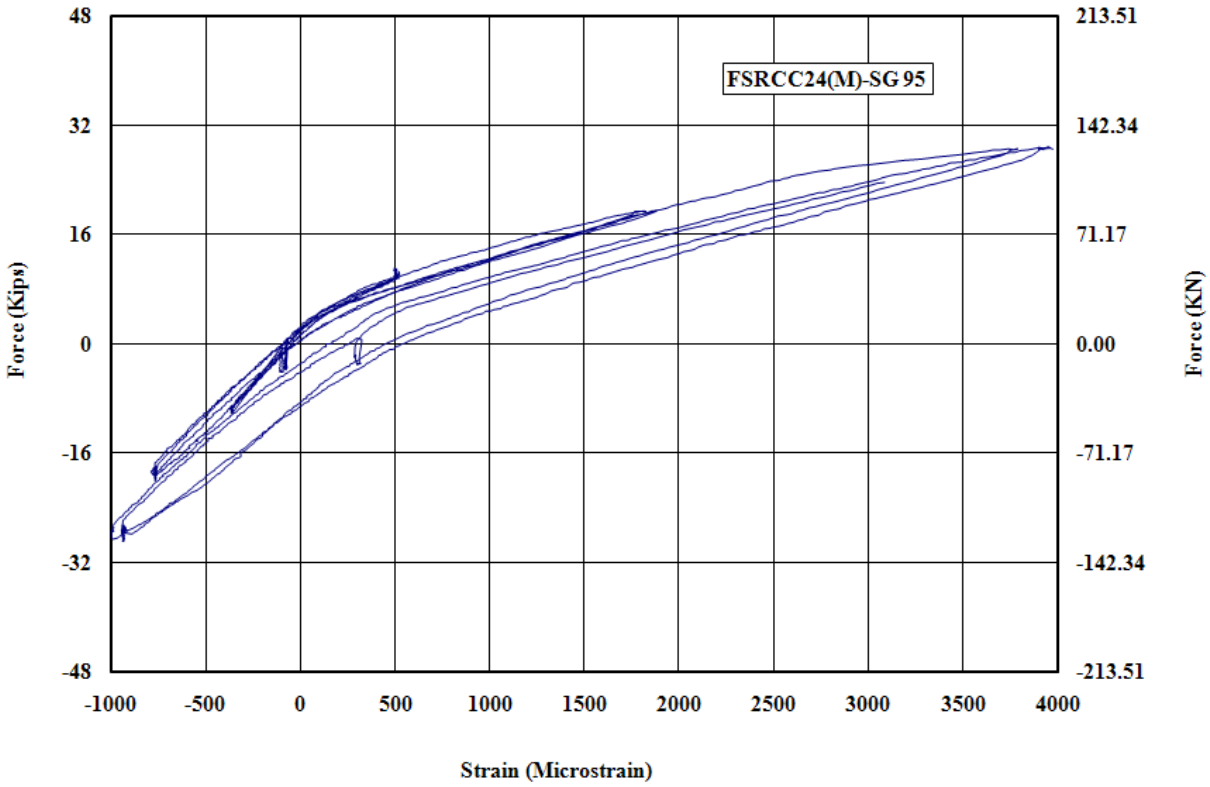

Figure G - 80: Measured Strain in Gauge No.95 for FSRCC24-M

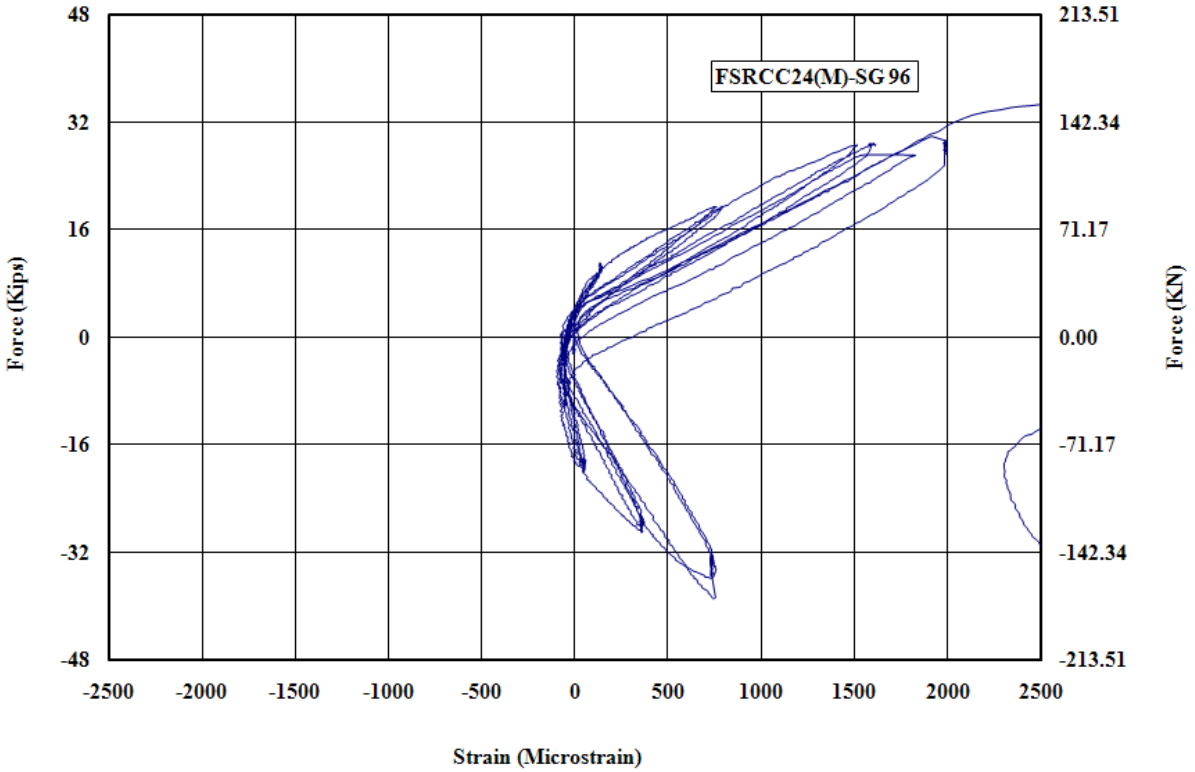

Figure G - 81: Measured Strain in Gauge No.96 for FSRCC24-M

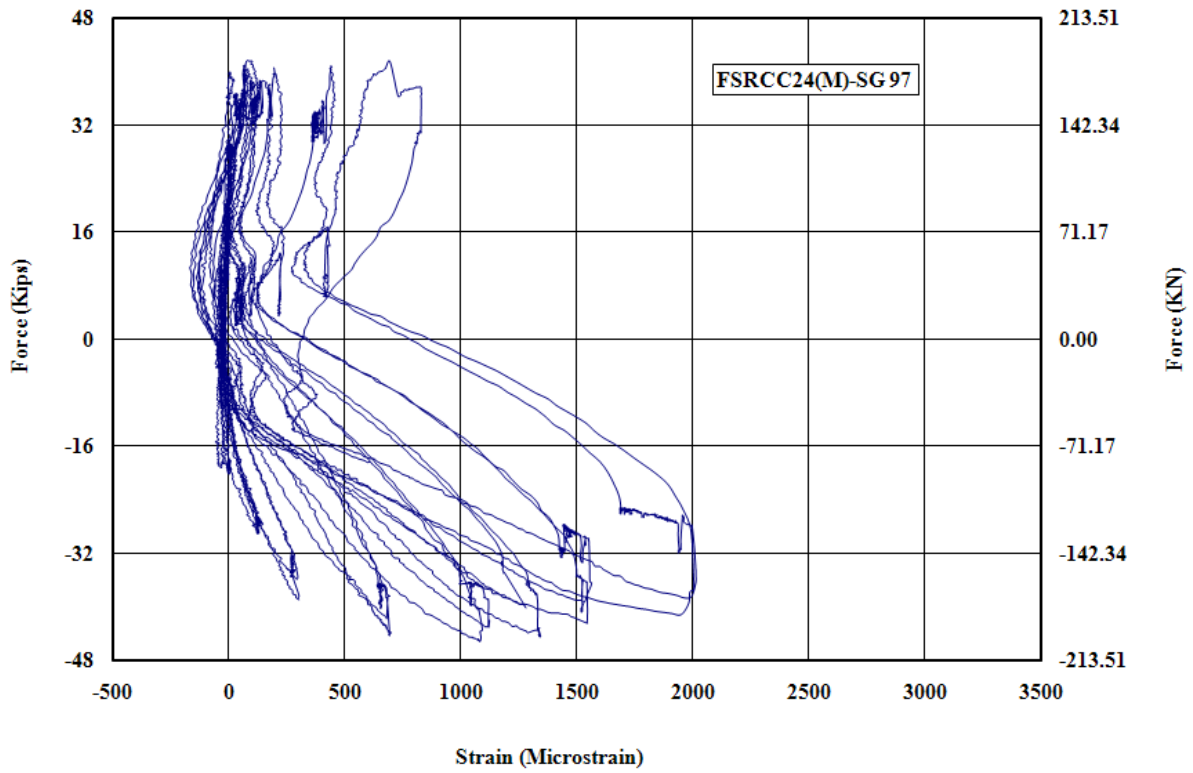

Figure G - 82: Measured Strain in Gauge No.97 for FSRCC24-M

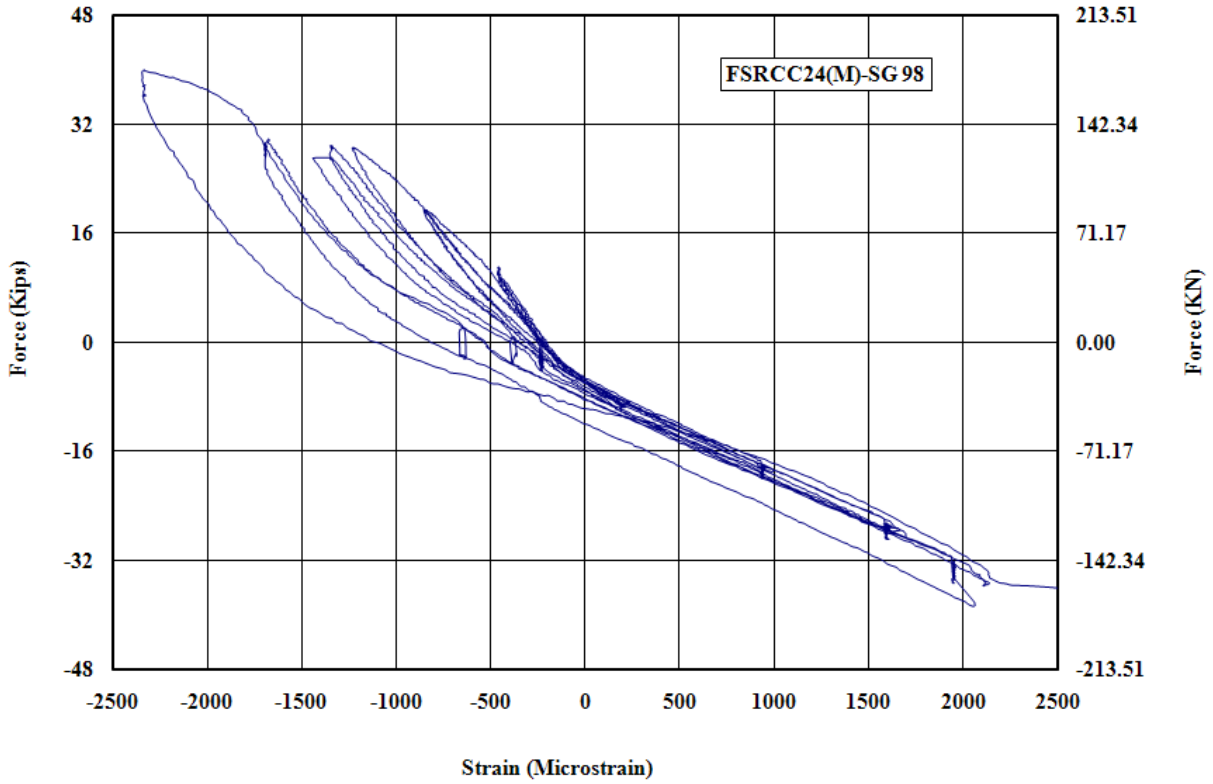

Figure G - 83: Measured Strain in Gauge No.98 for FSRCC24-M

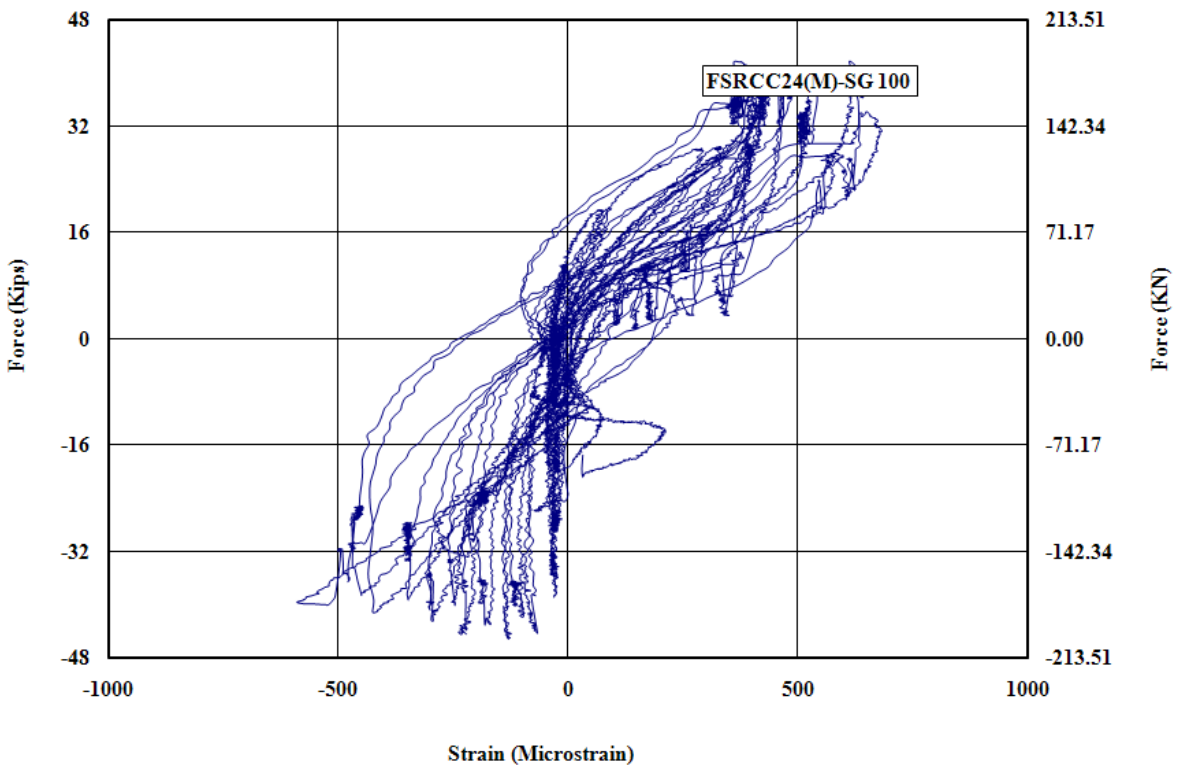

Figure G - 84: Measured Strain in Gauge No.100 for FSRCC24-M

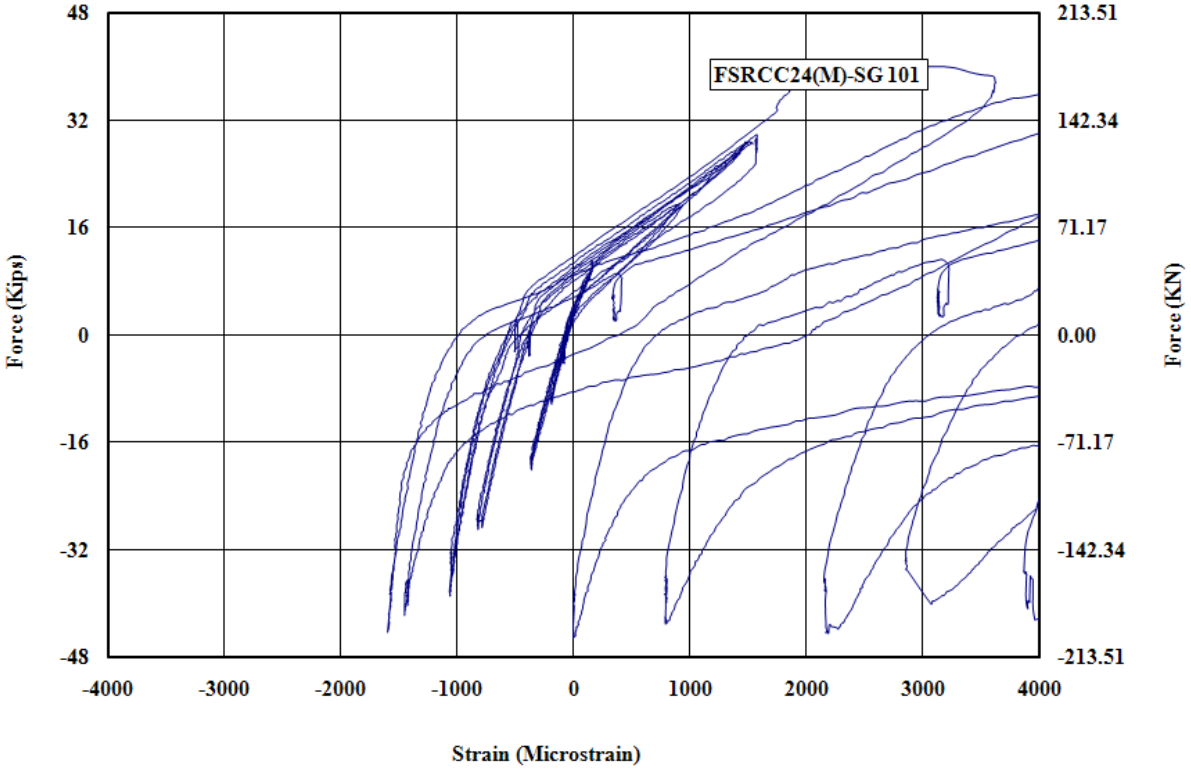

Figure G - 85: Measured Strain in Gauge No.101 for FSRCC24-M

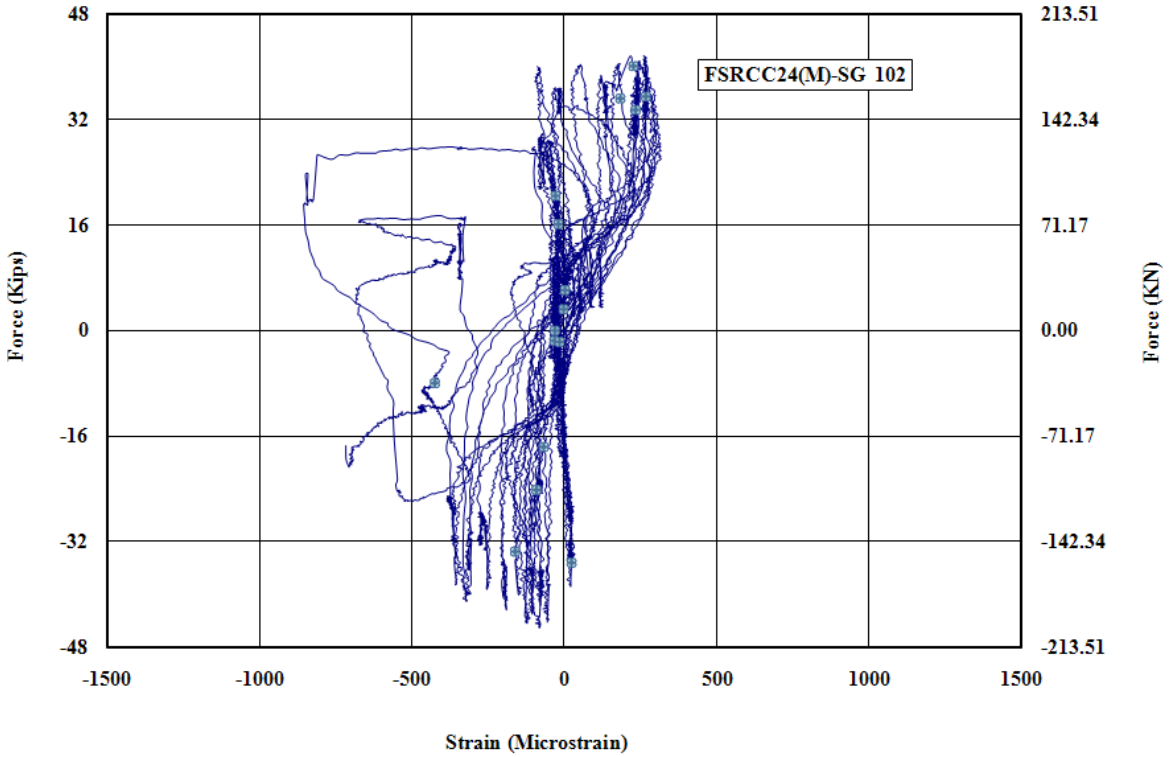

Figure G - 86: Measured Strain in Gauge No.102 for FSRCC24-M

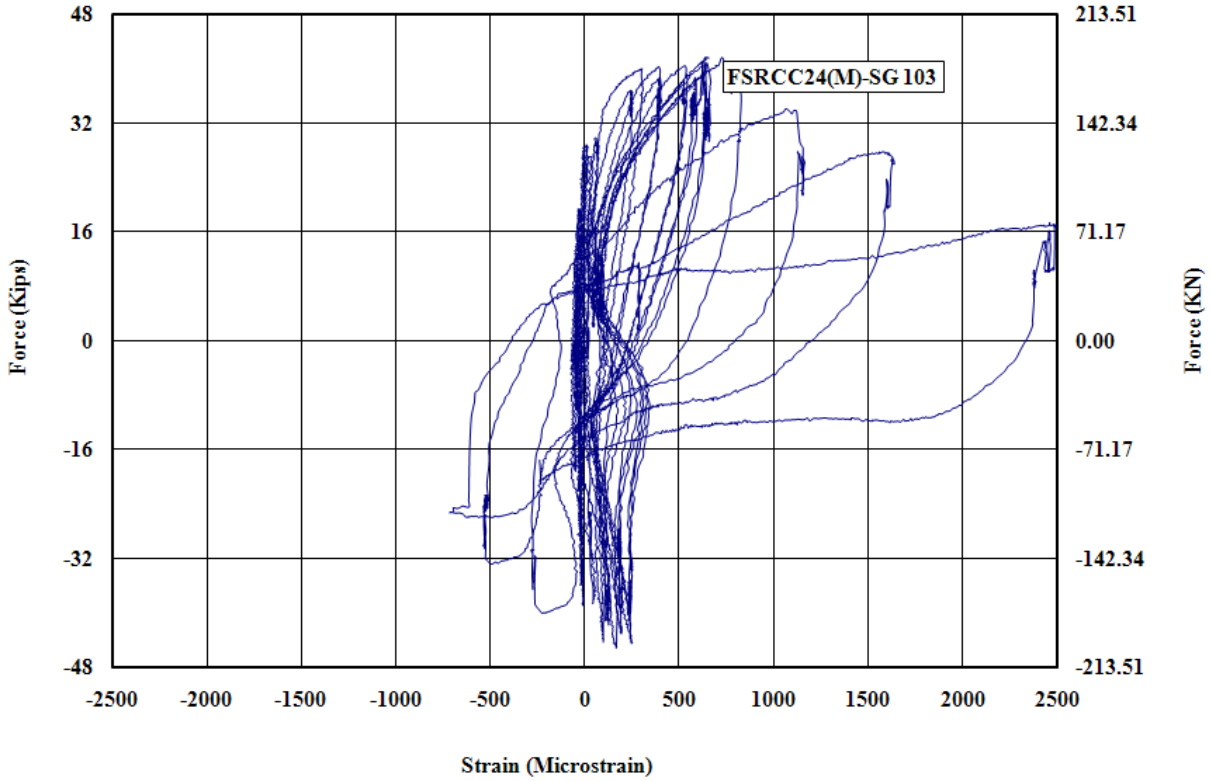

Figure G - 87: Measured Strain in Gauge No.103 for FSRCC24-M

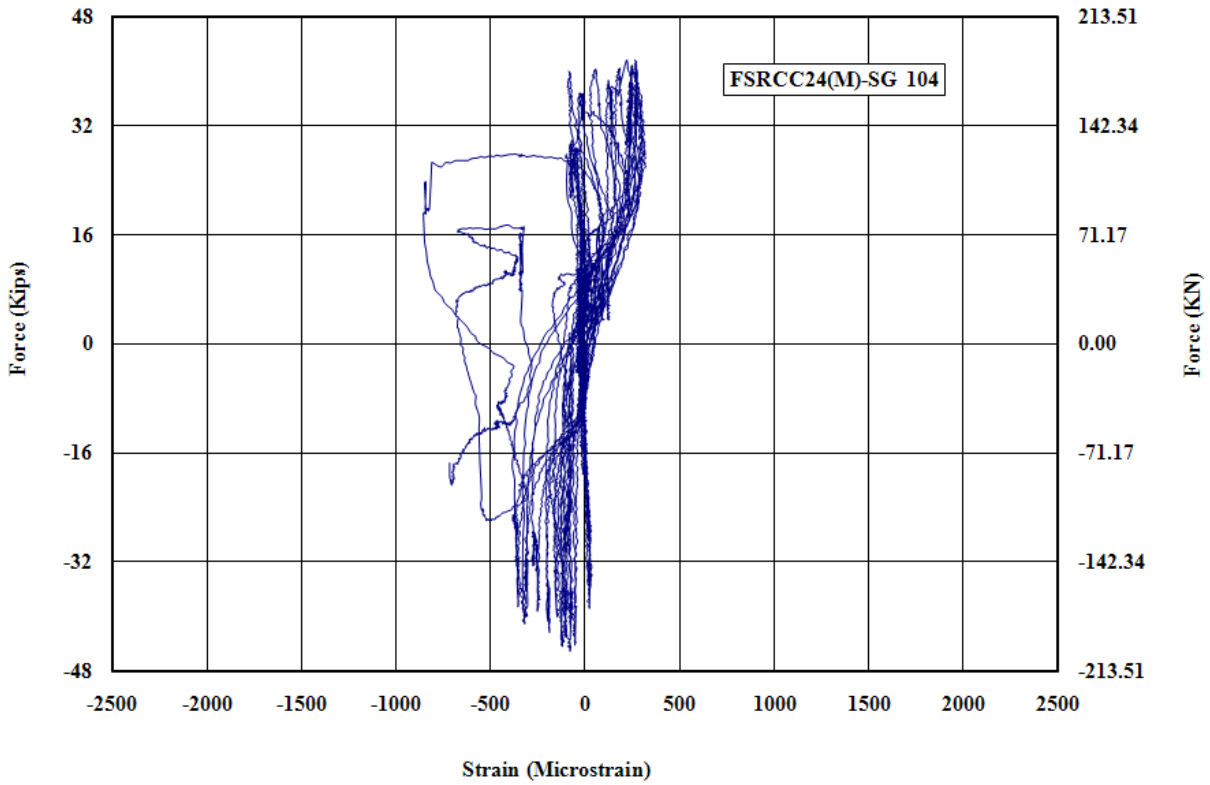

Figure G - 88: Measured Strain in Gauge No.104 for FSRCC24-M

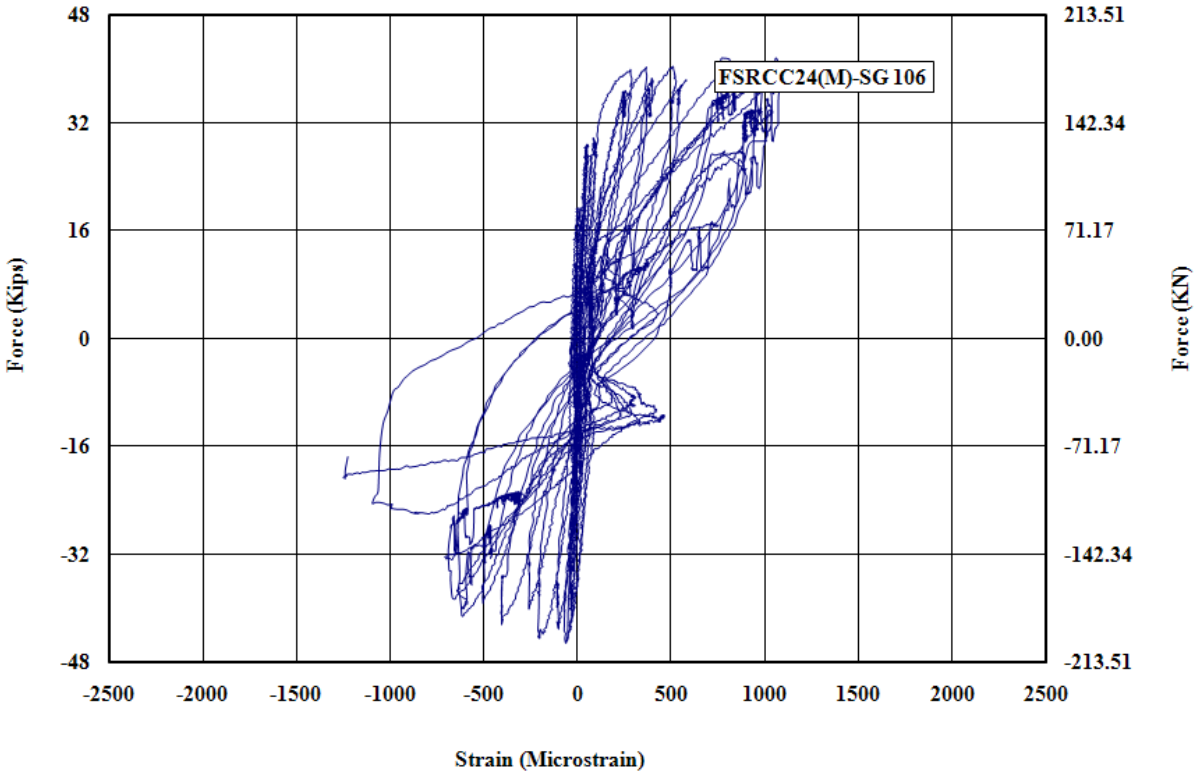

Figure G - 89: Measured Strain in Gauge No.106 for FSRCC24-M

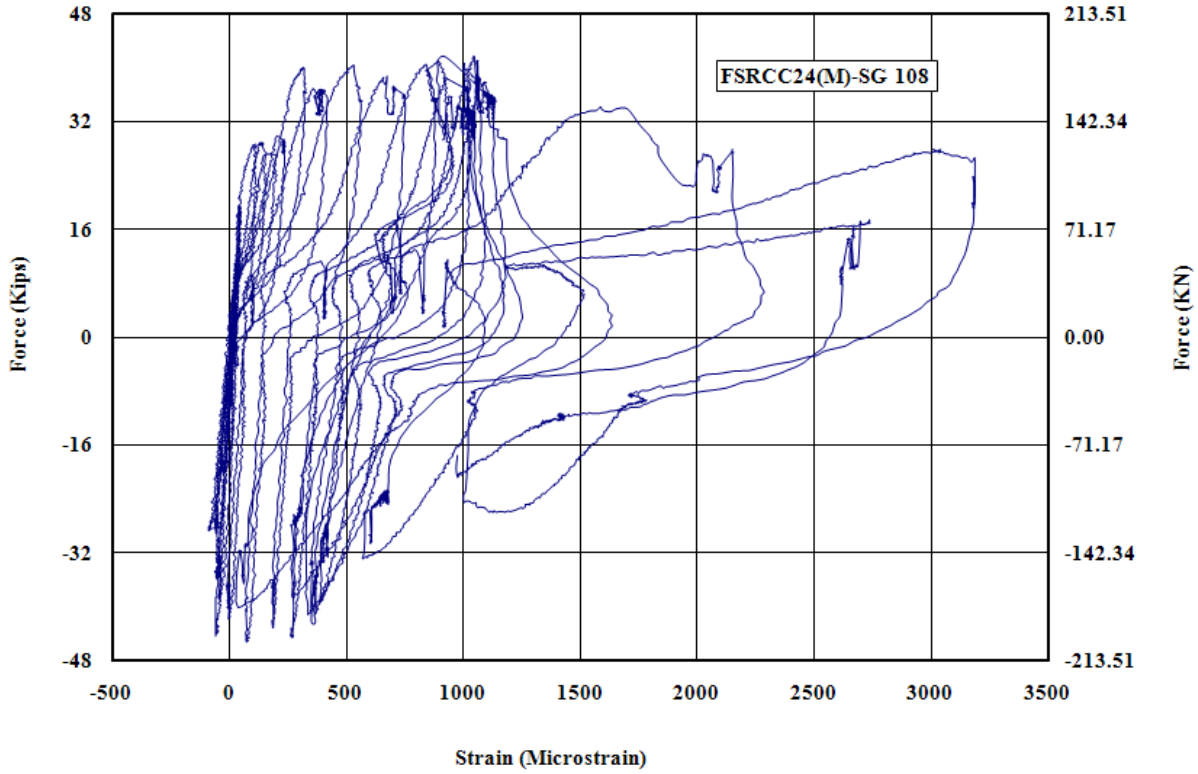

Figure G - 90: Measured Strain in Gauge No.108 for FSRCC24-M

Appendix H

Specimen FSKJ24-M

(Modified Flat-Slab Knee-Joint with 24-in. diameter pile)

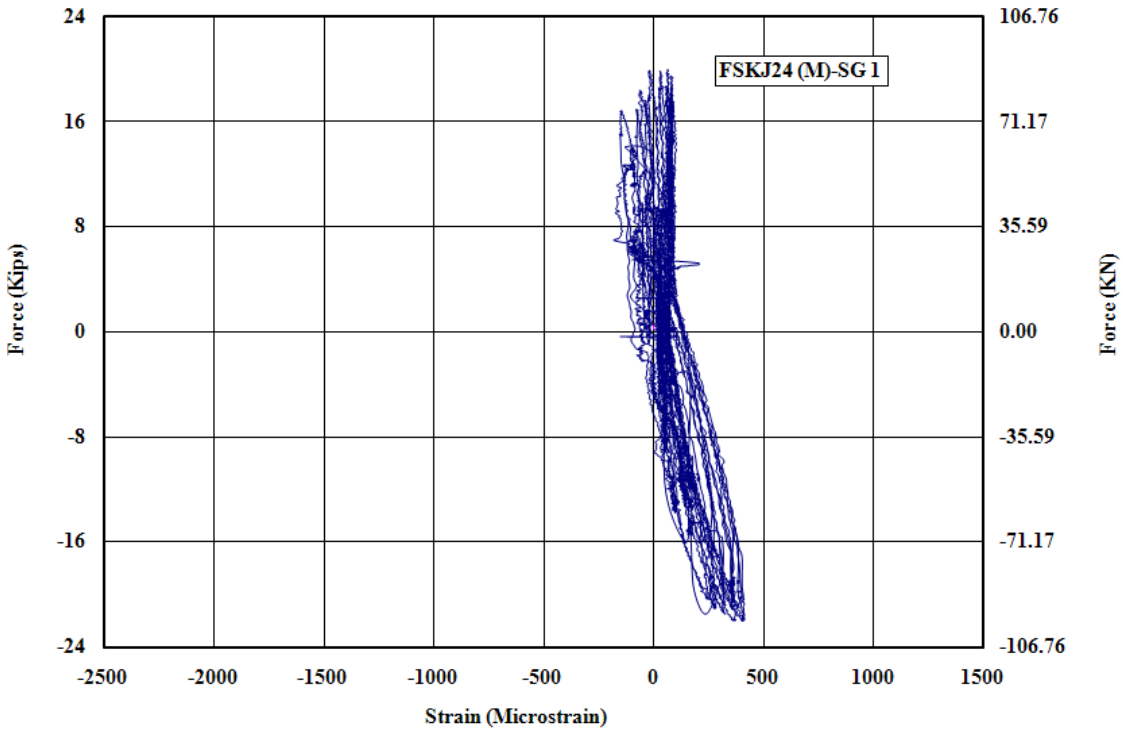

Figure H - 1: Measured Strain in Gauge No.1 for FSKJ24-M

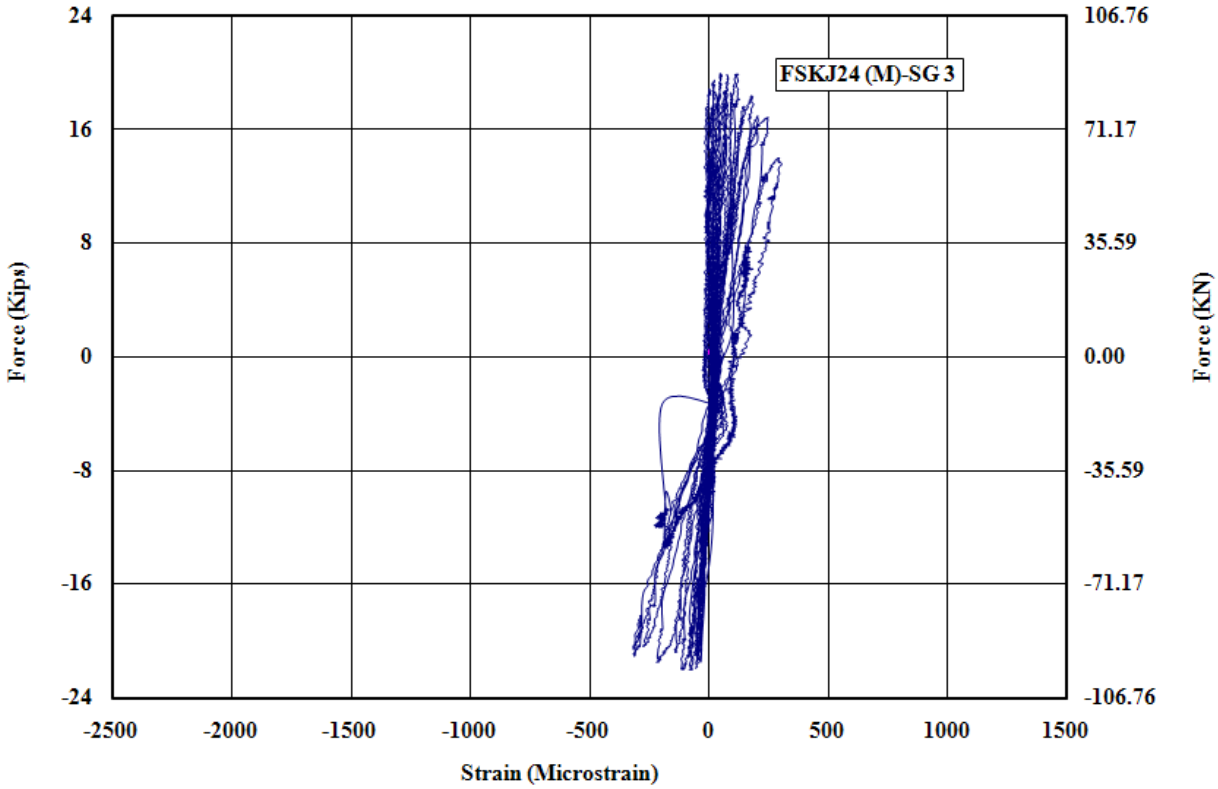

Figure H - 2: Measured Strain in Gauge No.3 for FSKJ24-M

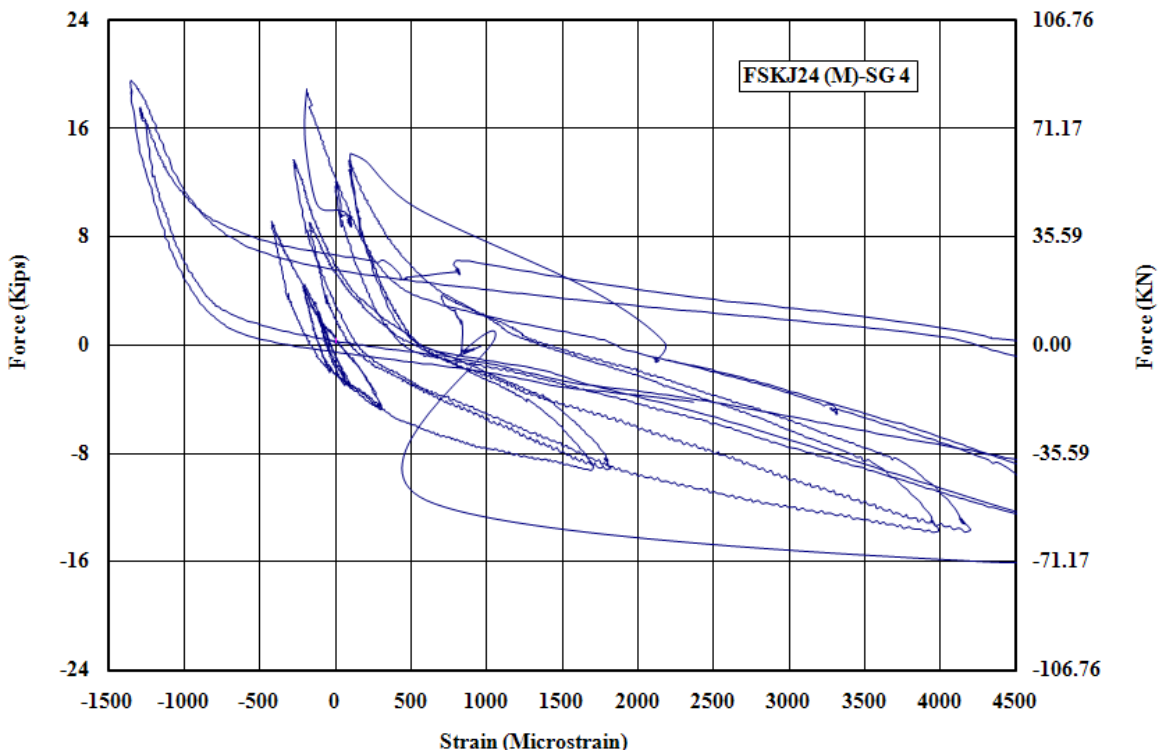

Figure H - 3: Measured Strain in Gauge No.4 for FSKJ24-M

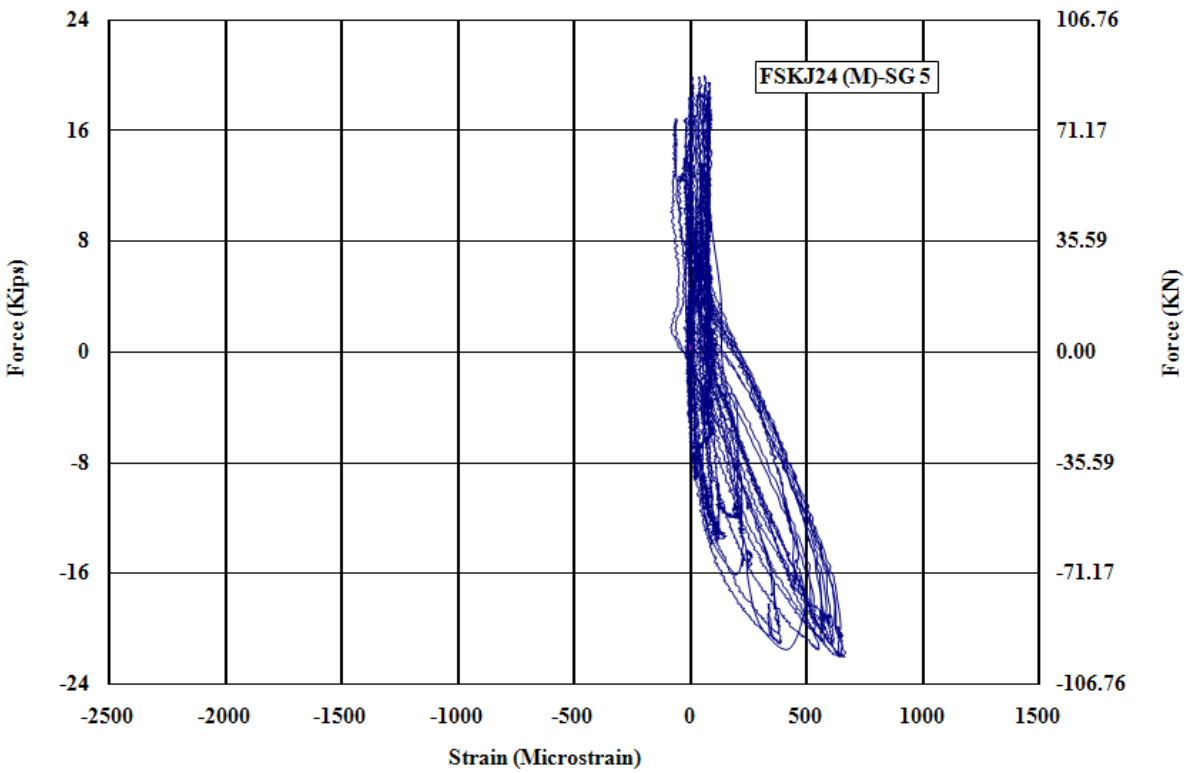

Figure H - 4: Measured Strain in Gauge No.5 for FSKJ24-M

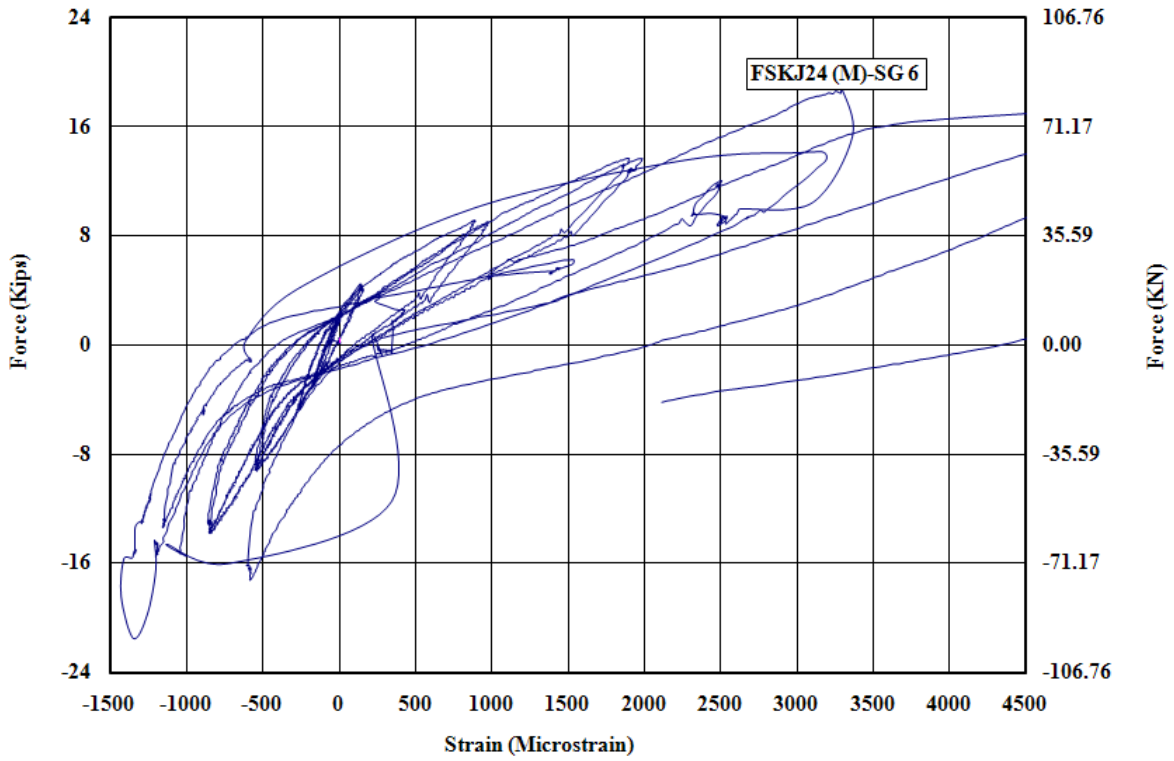

Figure H - 5: Measured Strain in Gauge No.6 for FSKJ24-M

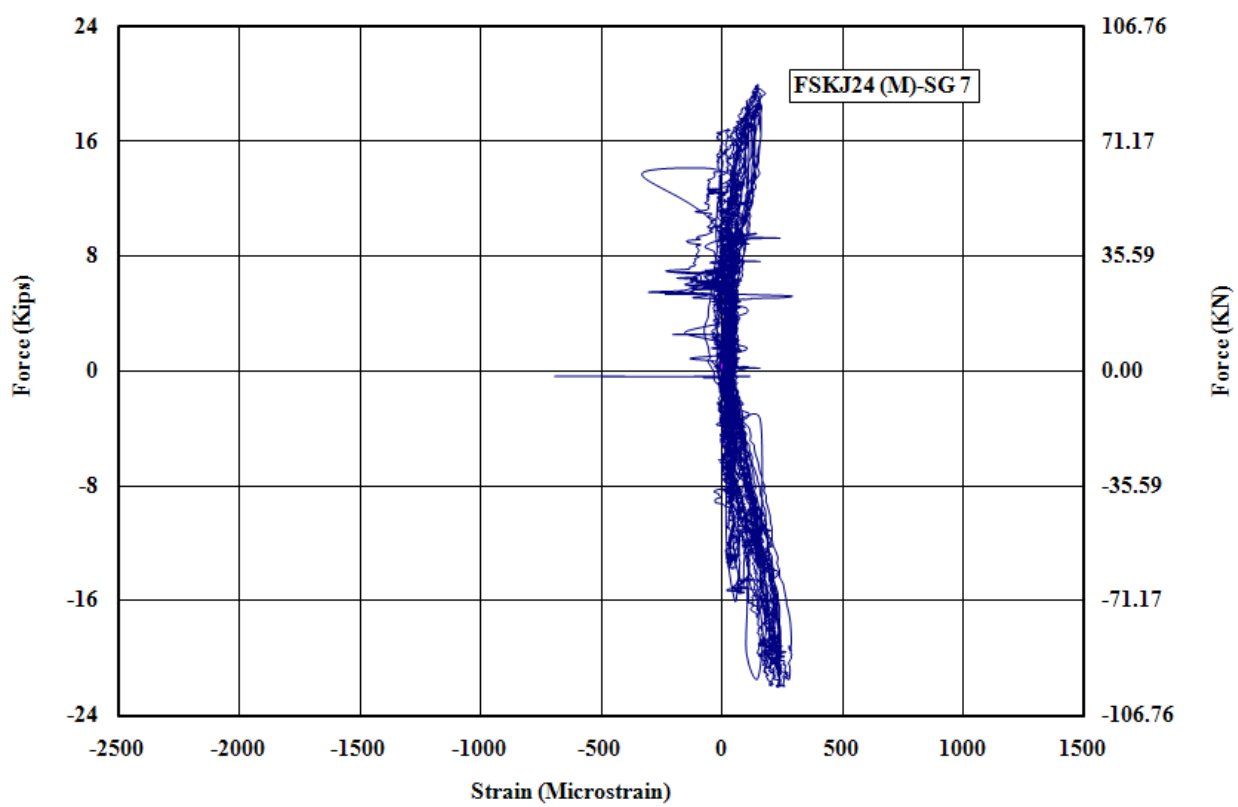

Figure H - 6: Measured Strain in Gauge No.7 for FSKJ24-M

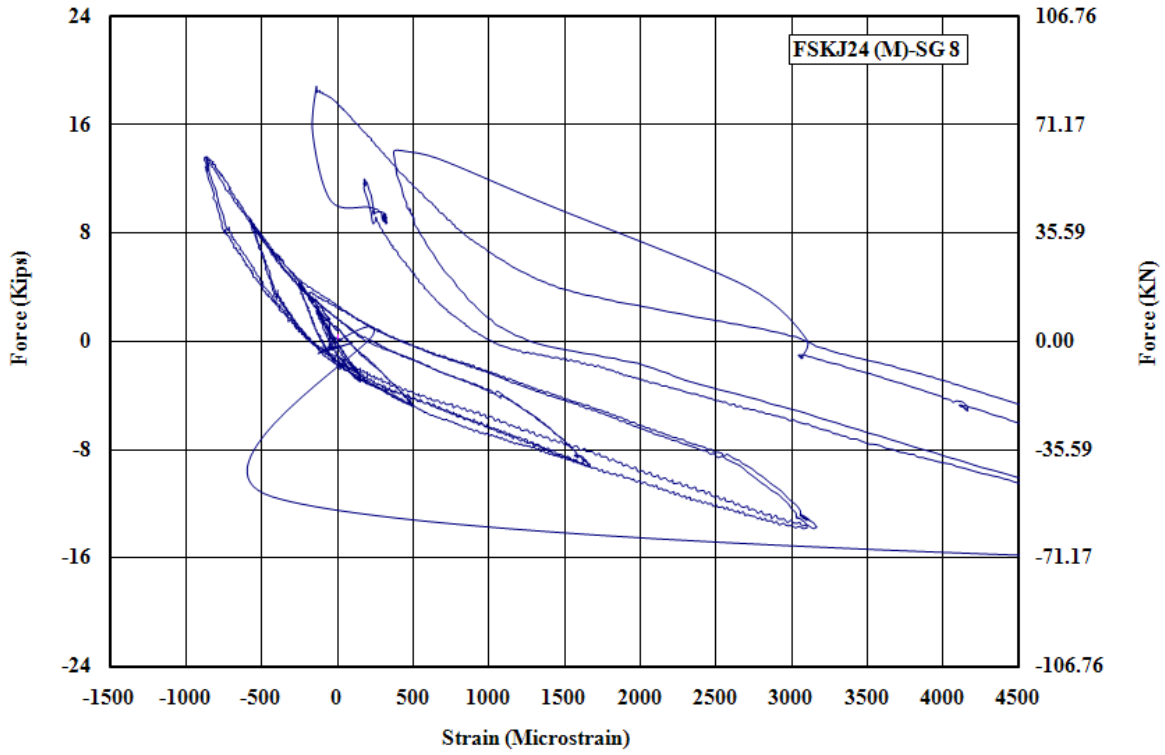

Figure H - 7: Measured Strain in Gauge No.8 for FSKJ24-M

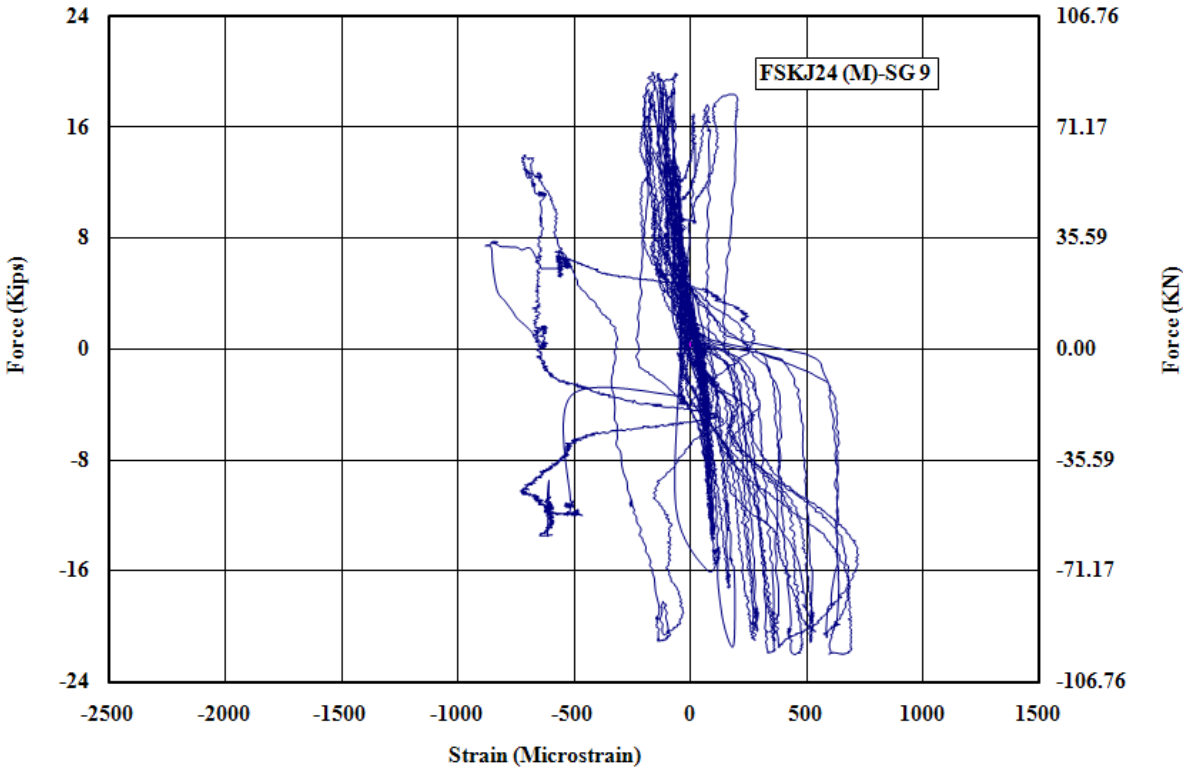

Figure H - 8: Measured Strain in Gauge No.9 for FSKJ24-M

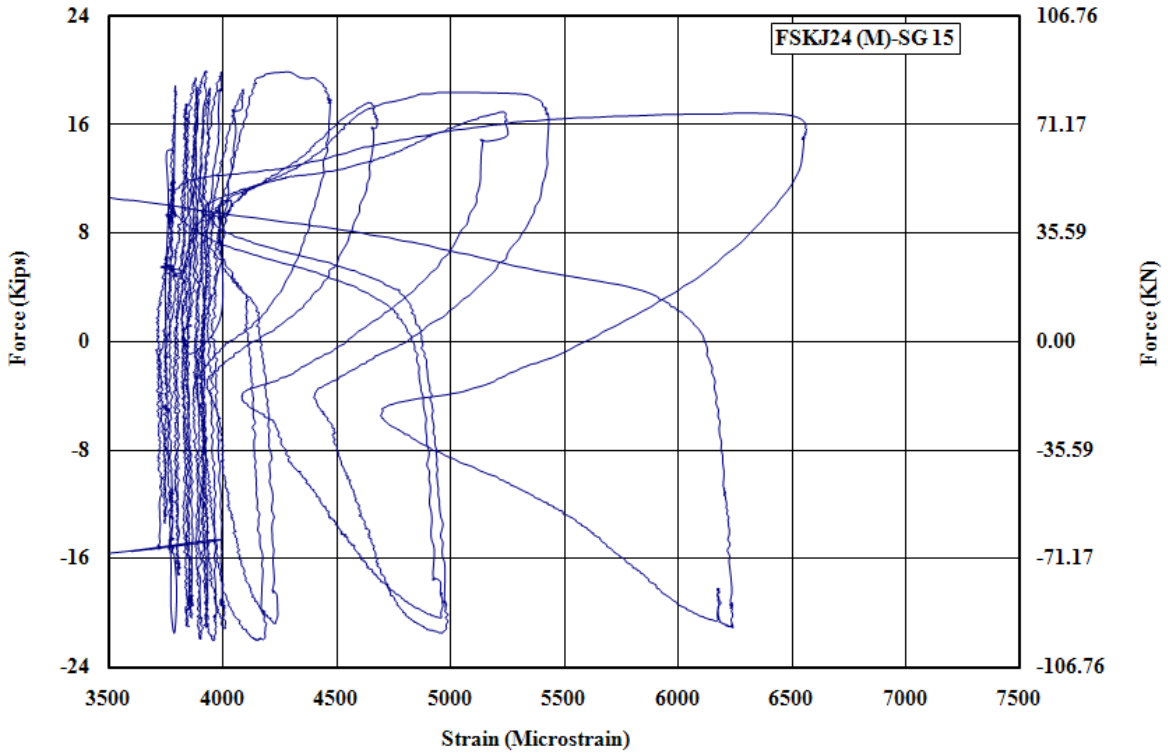

Figure H - 9: Measured Strain in Gauge No.15 for FSKJ24-M

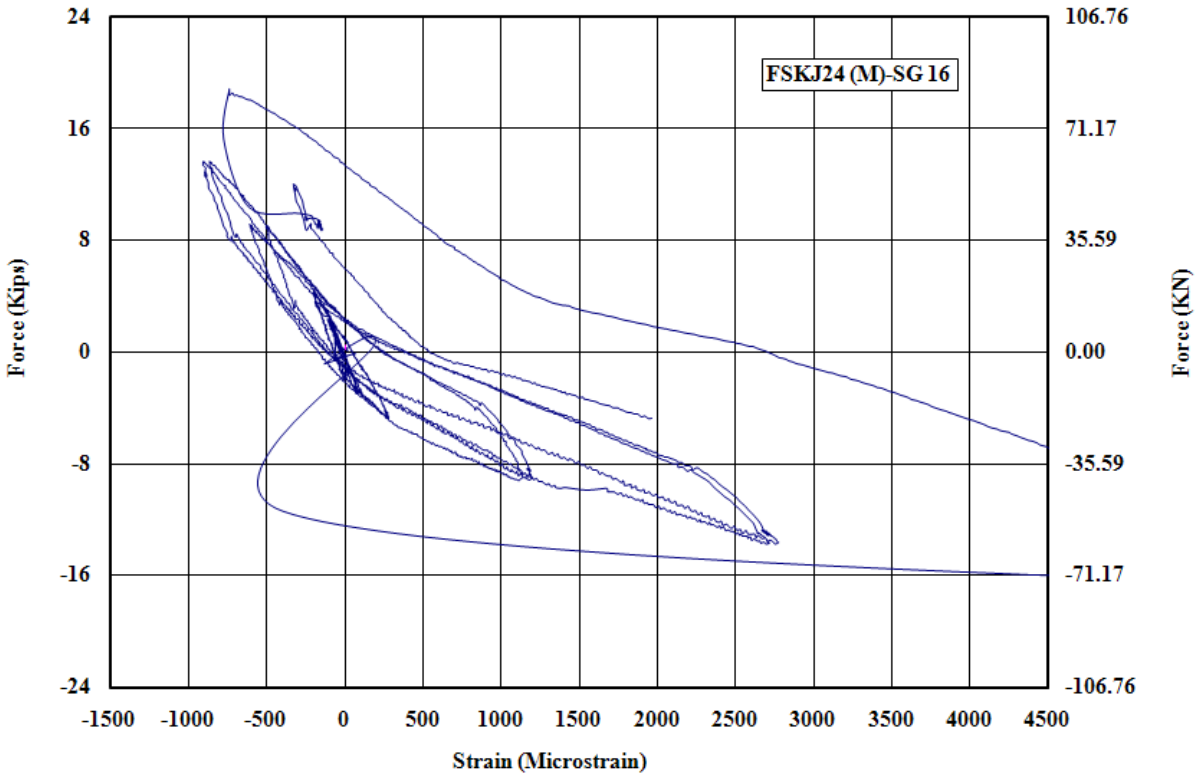

Figure H - 10: Measured Strain in Gauge No.16 for FSKJ24-M

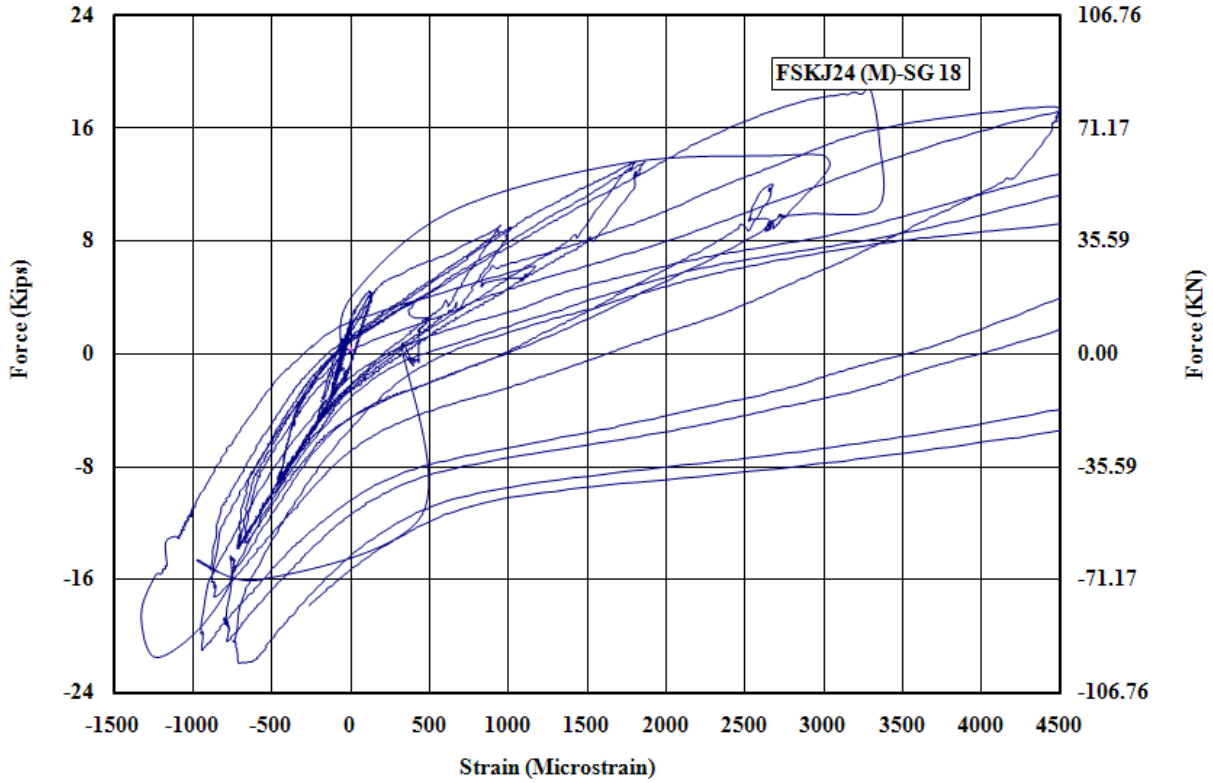

Figure H - 11: Measured Strain in Gauge No.18 for FSKJ24-M

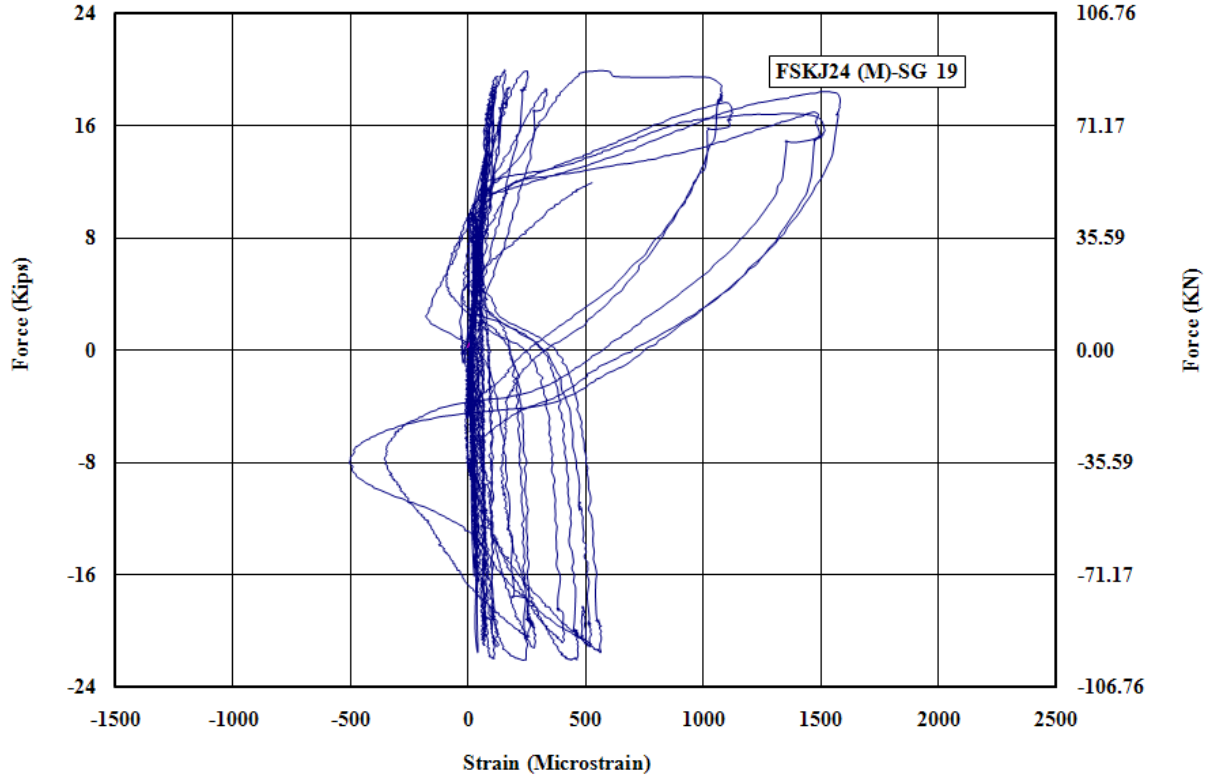

Figure H - 12: Measured Strain in Gauge No.19 for FSKJ24-M

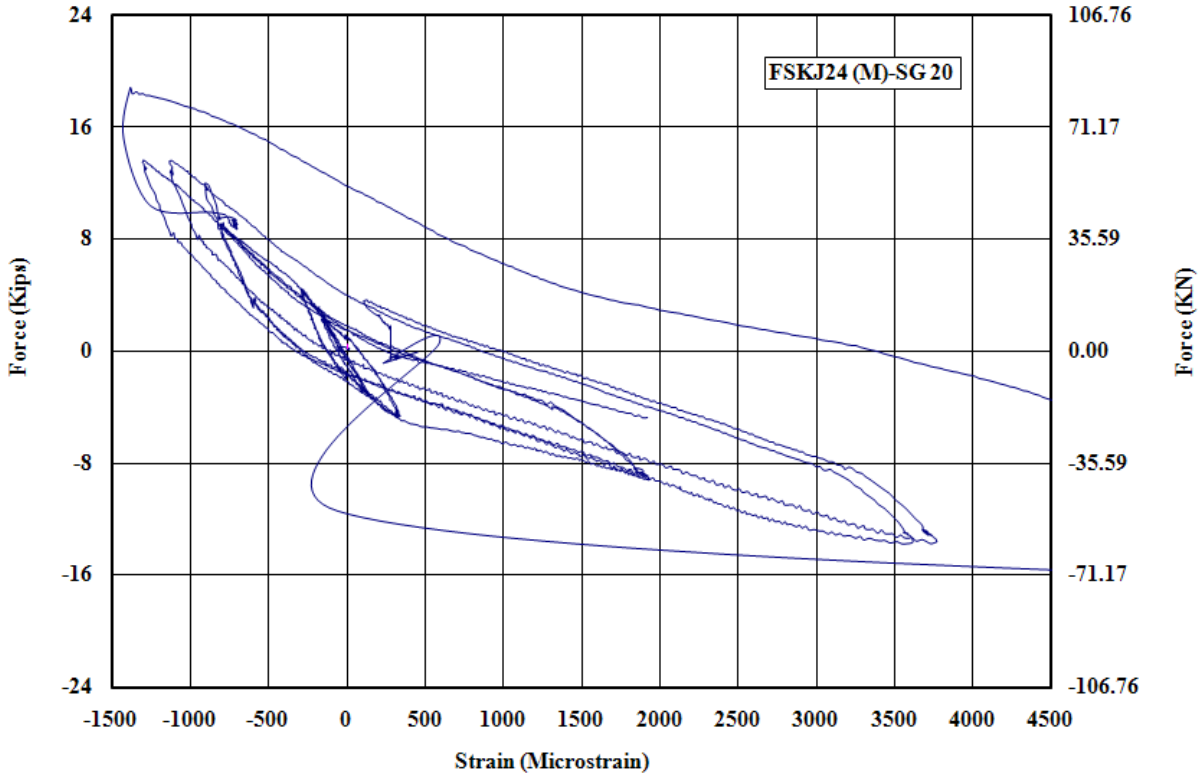

Figure H - 13: Measured Strain in Gauge No.20 for FSKJ24-M

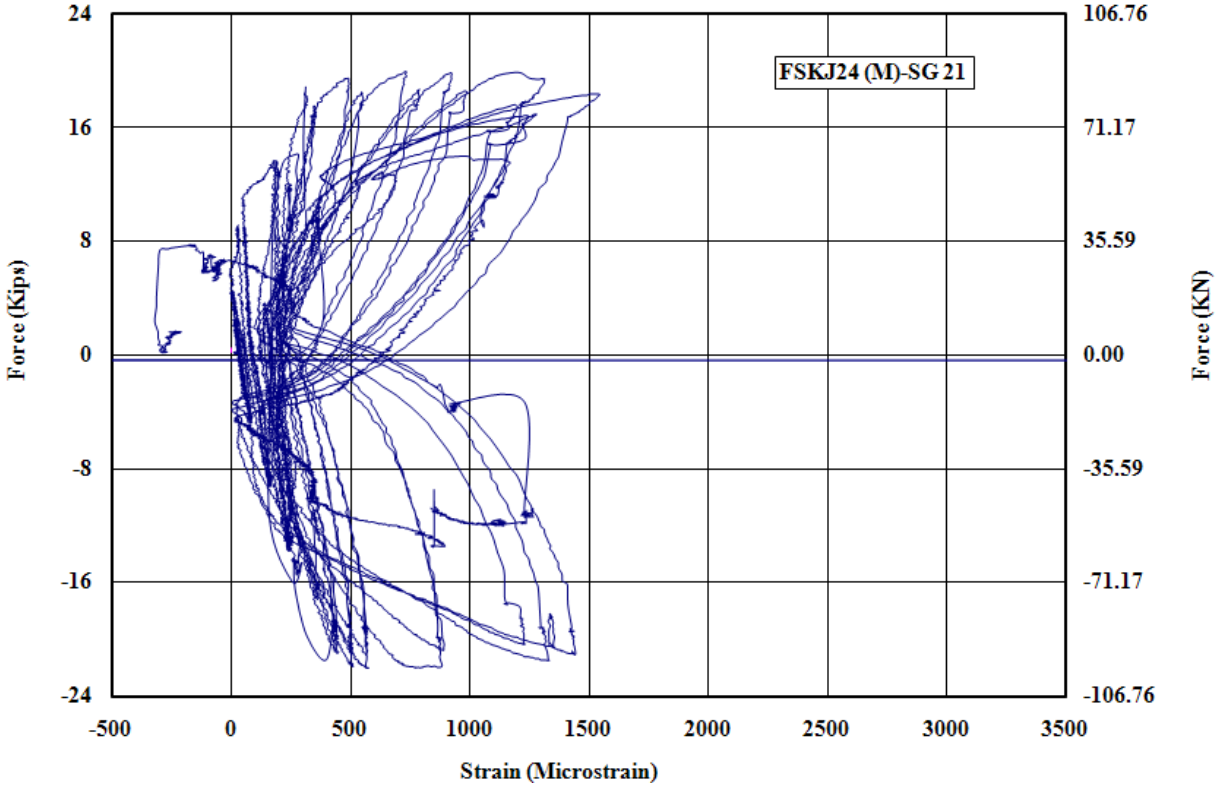

Figure H - 14: Measured Strain in Gauge No.21 for FSKJ24-M

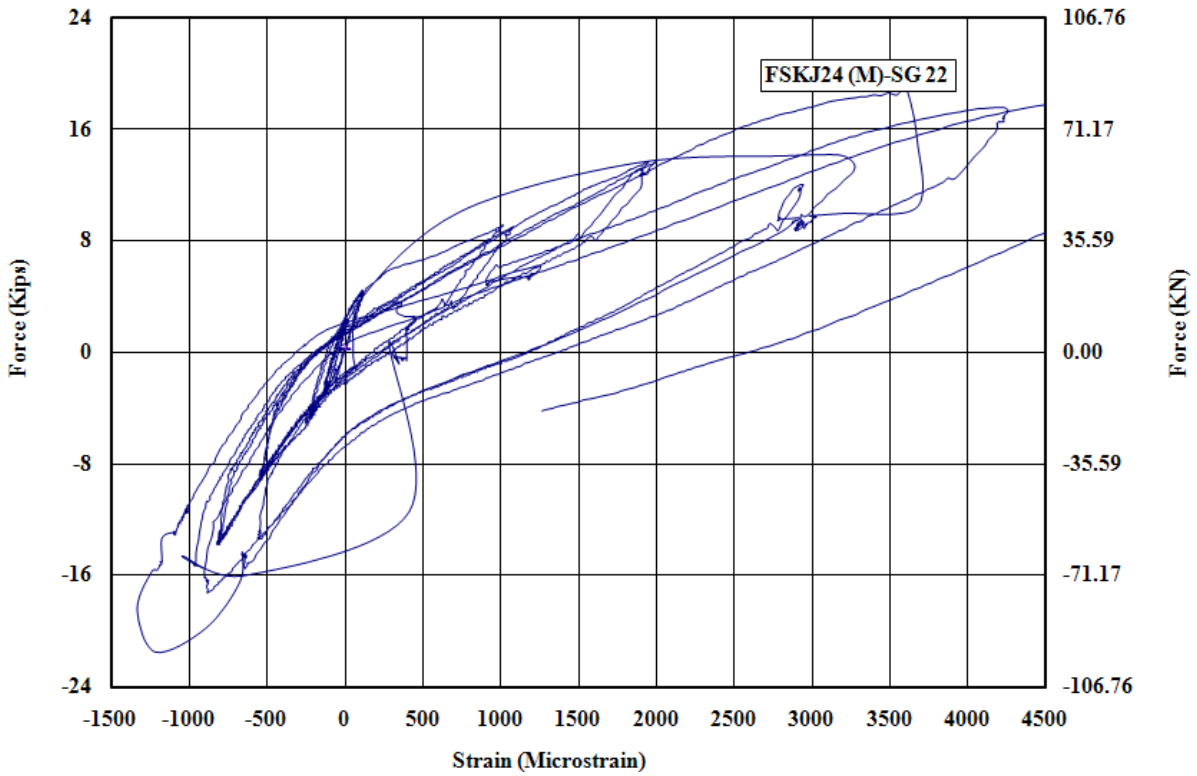

Figure H - 15: Measured Strain in Gauge No.22 for FSKJ24-M

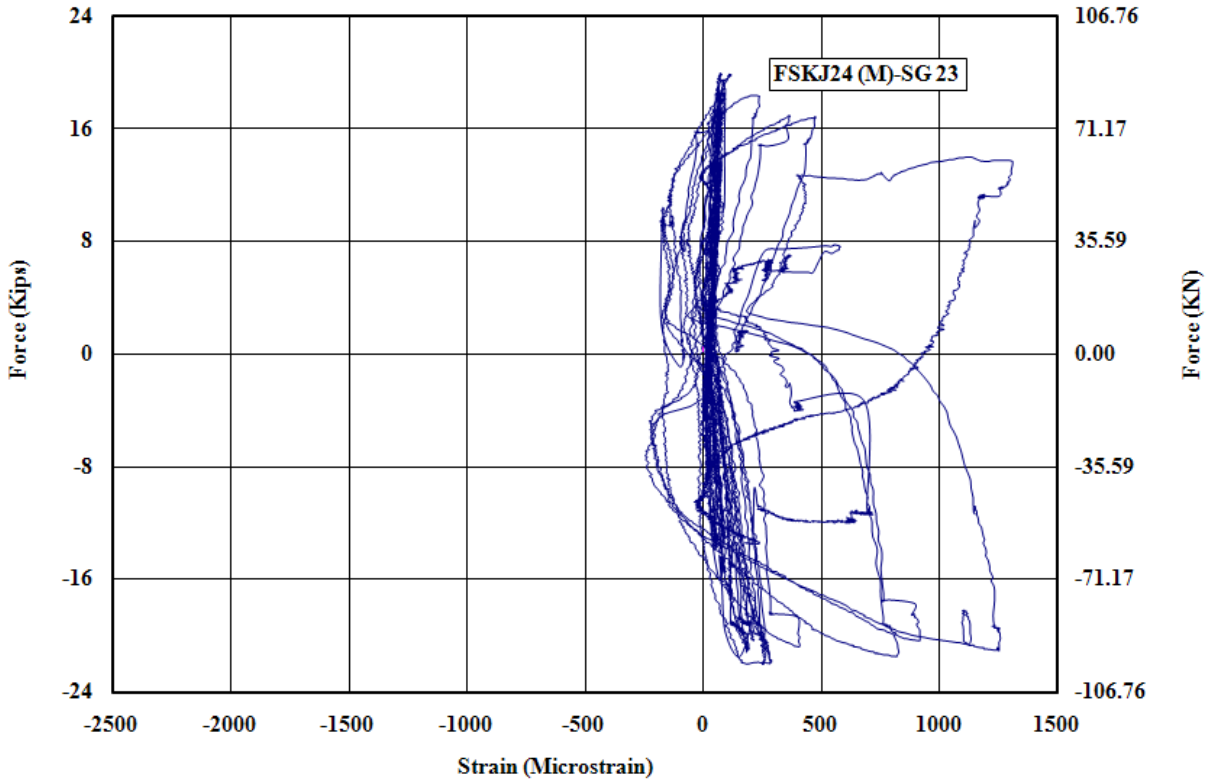

Figure H - 16: Measured Strain in Gauge No.23 for FSKJ24-M

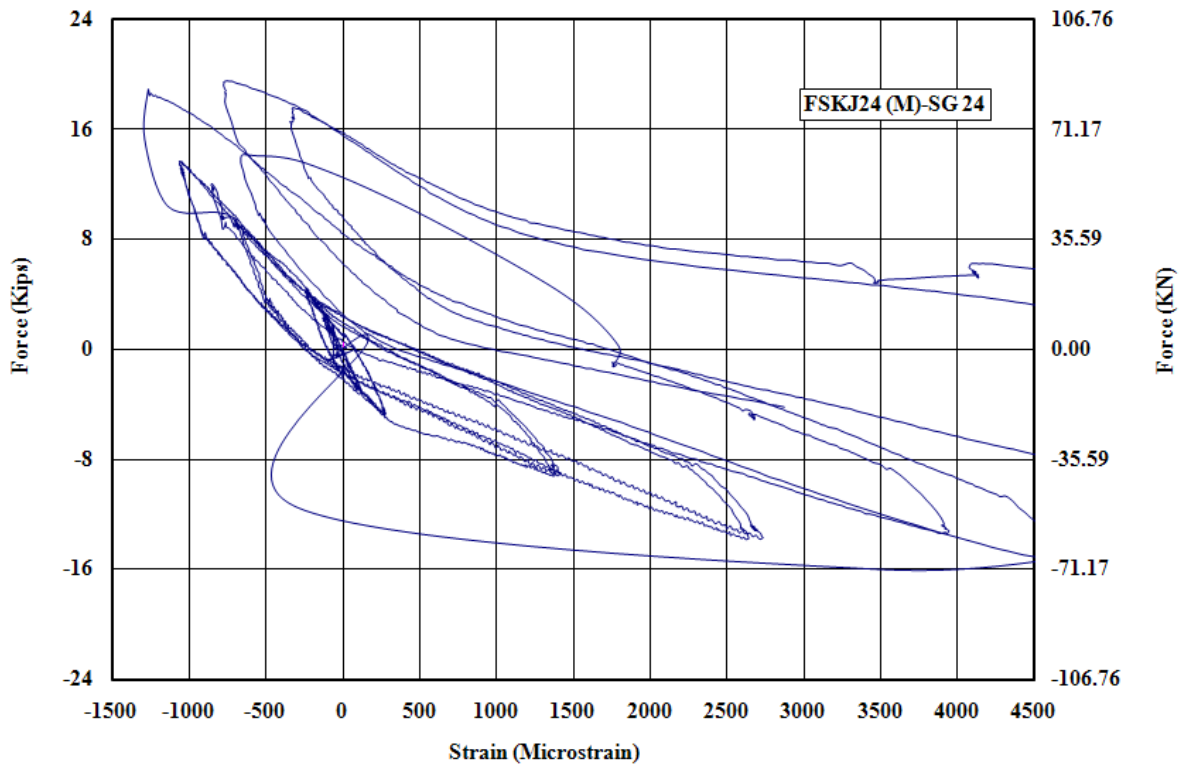

Figure H - 17: Measured Strain in Gauge No.24 for FSKJ24-M

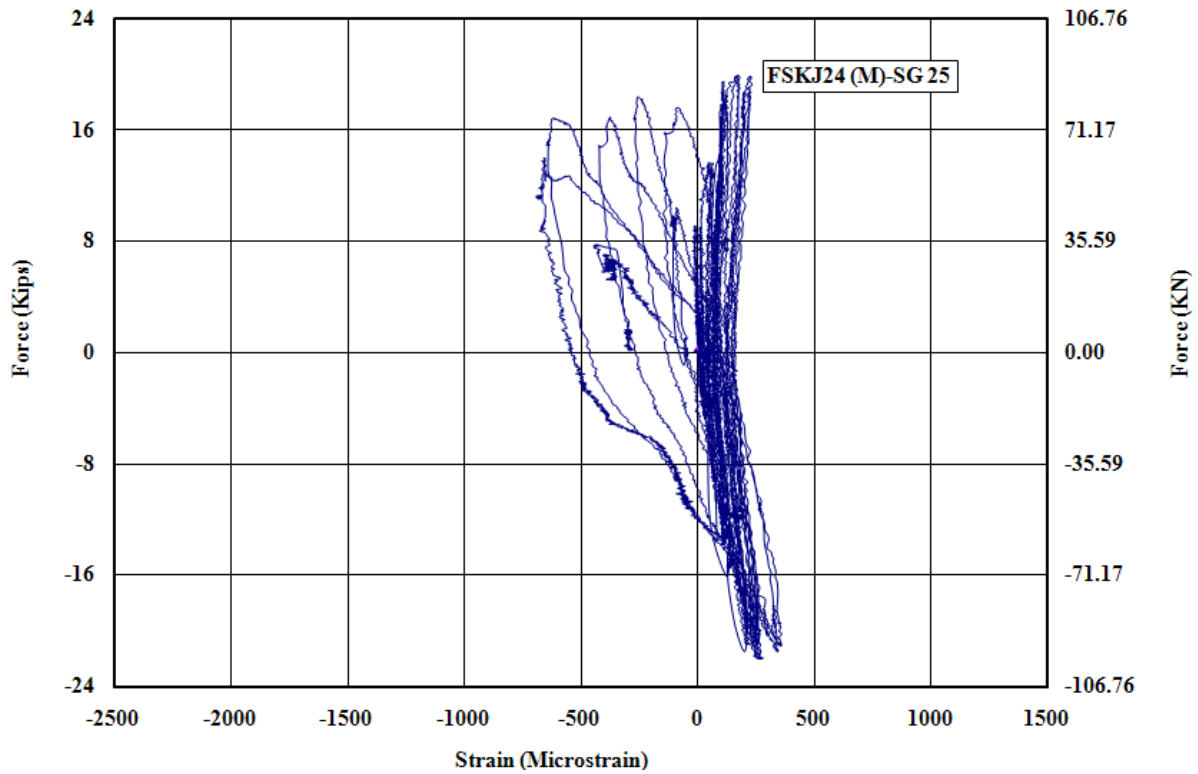

Figure H - 18: Measured Strain in Gauge No.25 for FSKJ24-M

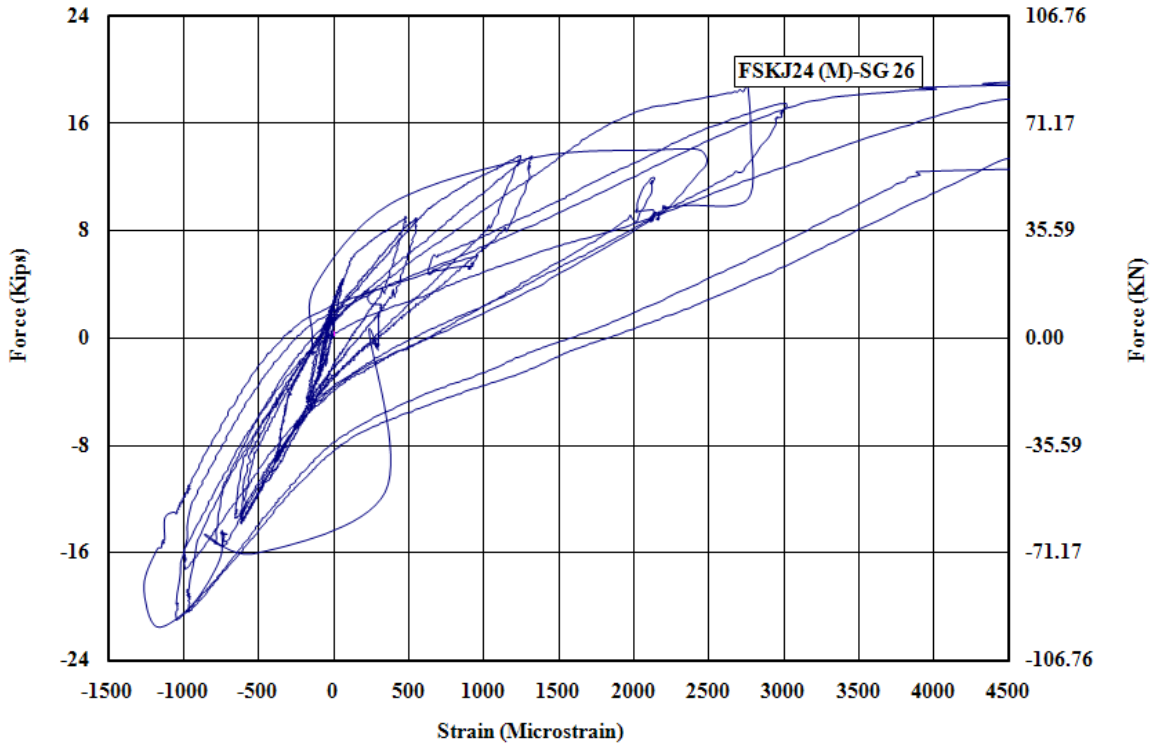

Figure H - 19: Measured Strain in Gauge No.26 for FSKJ24-M

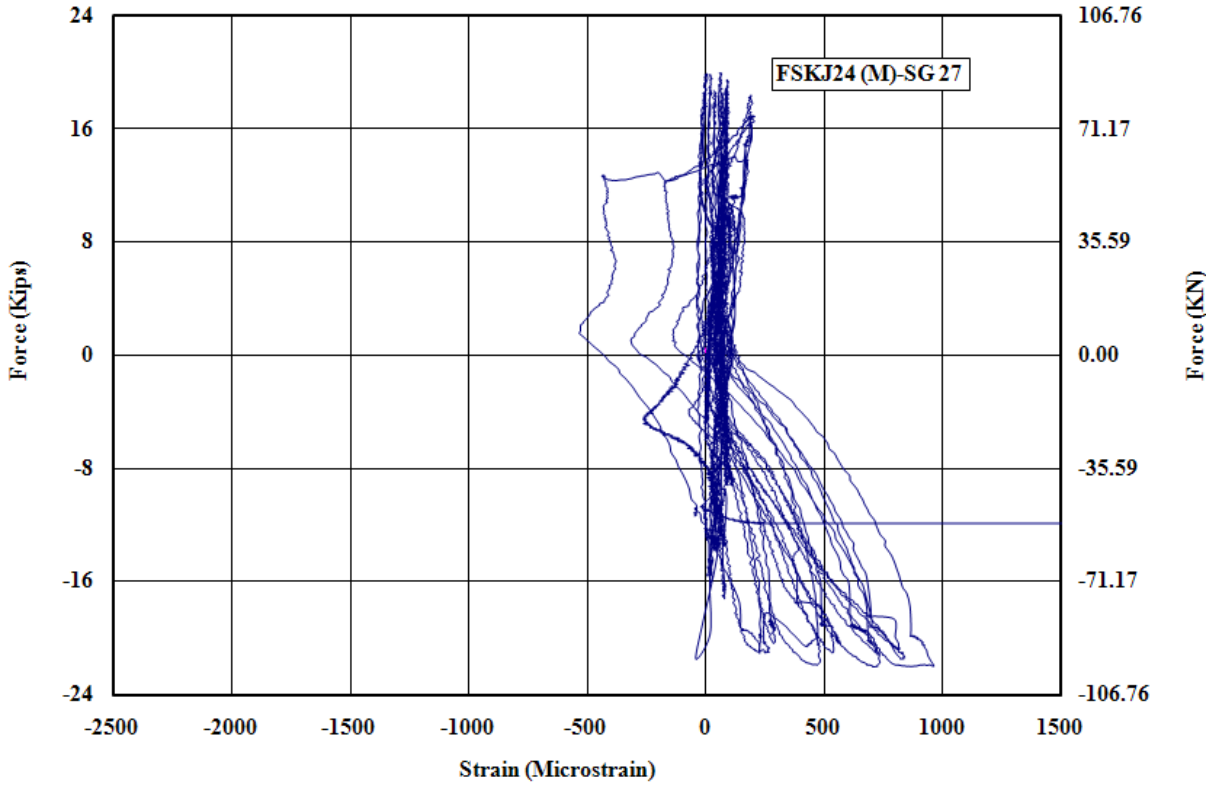

Figure H - 20: Measured Strain in Gauge No.27 for FSKJ24-M

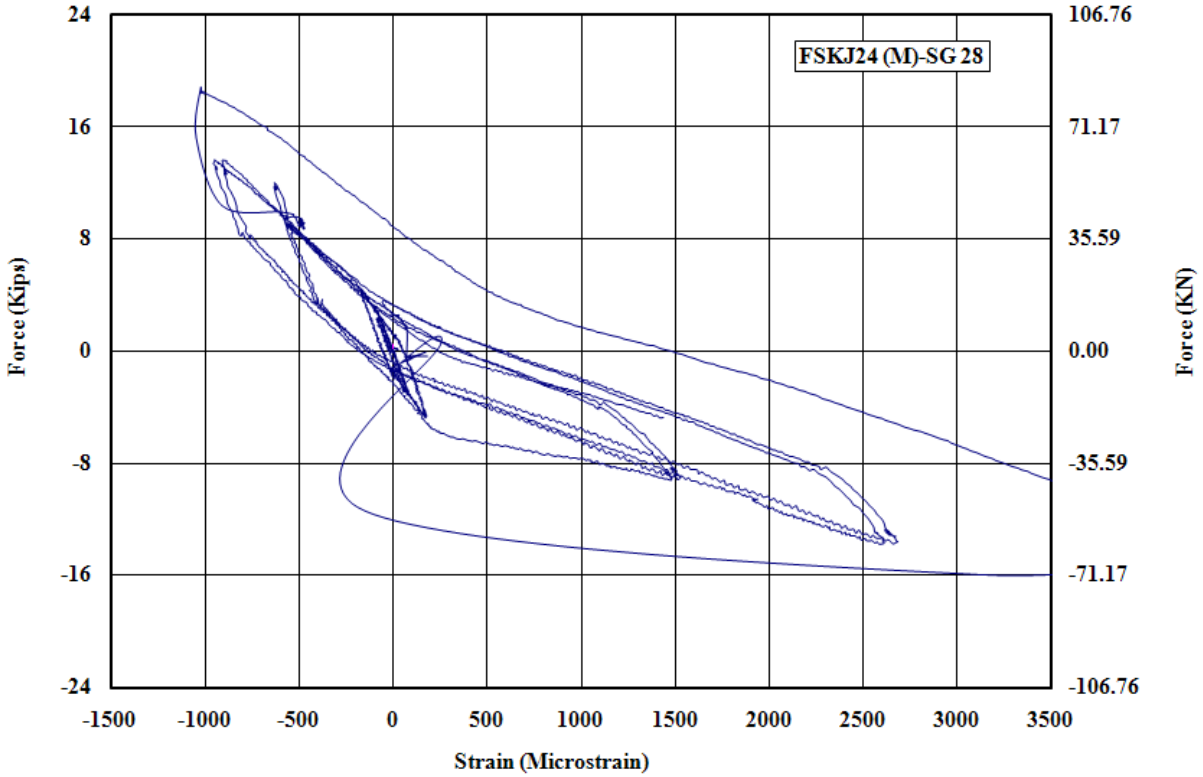

Figure H - 21: Measured Strain in Gauge No.28 for FSKJ24-M

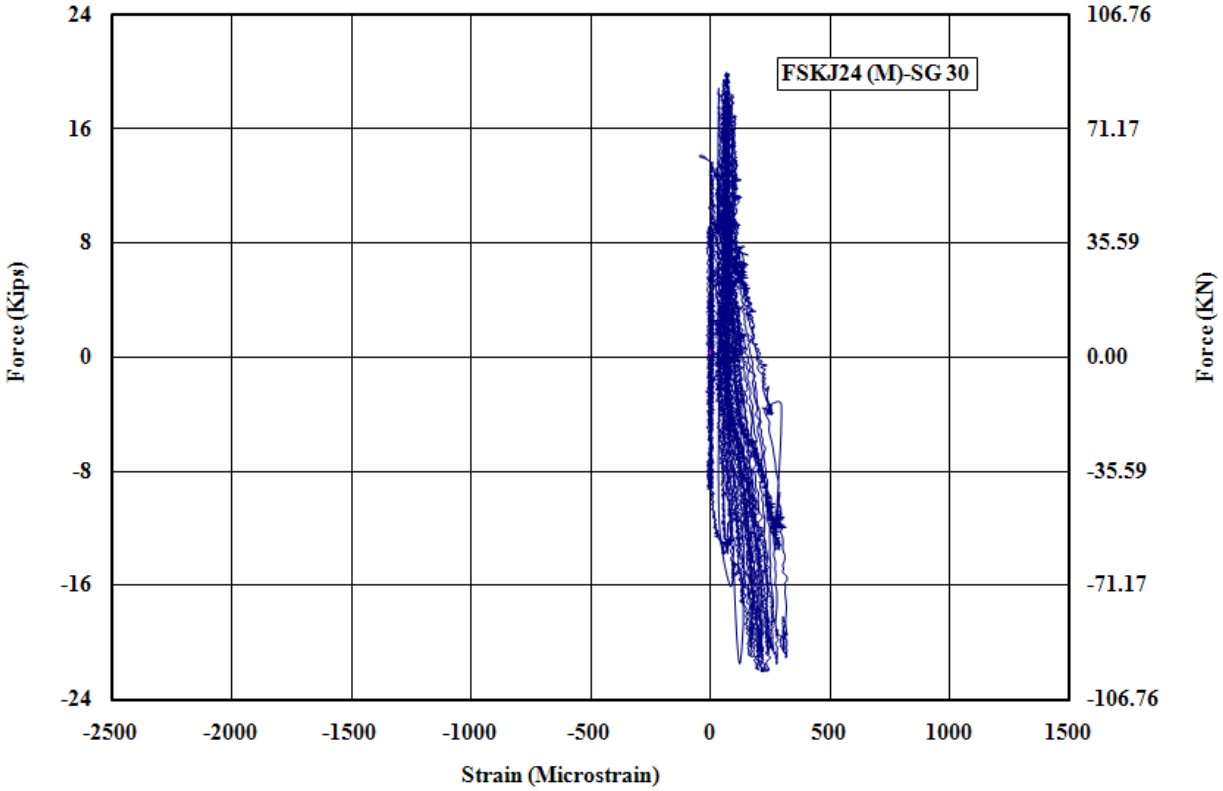

Figure H - 22: Measured Strain in Gauge No.30 for FSKJ24-M

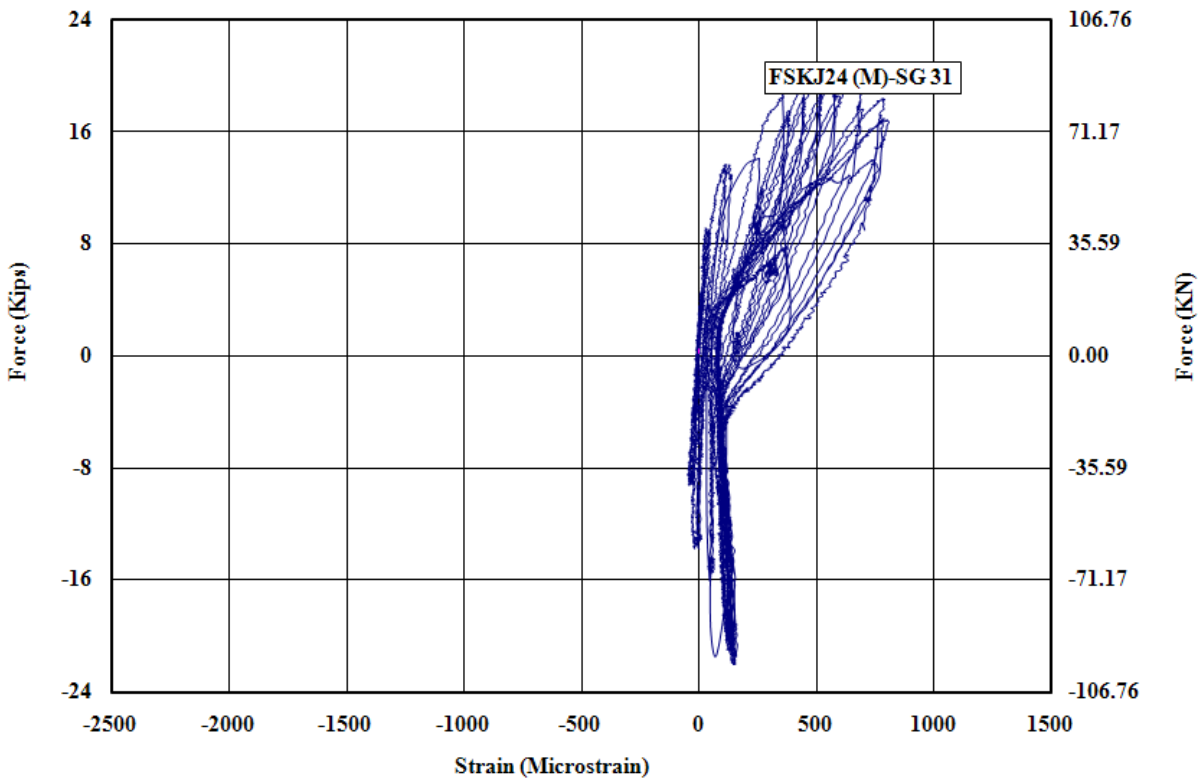

Figure H - 23: Measured Strain in Gauge No.31 for FSKJ24-M

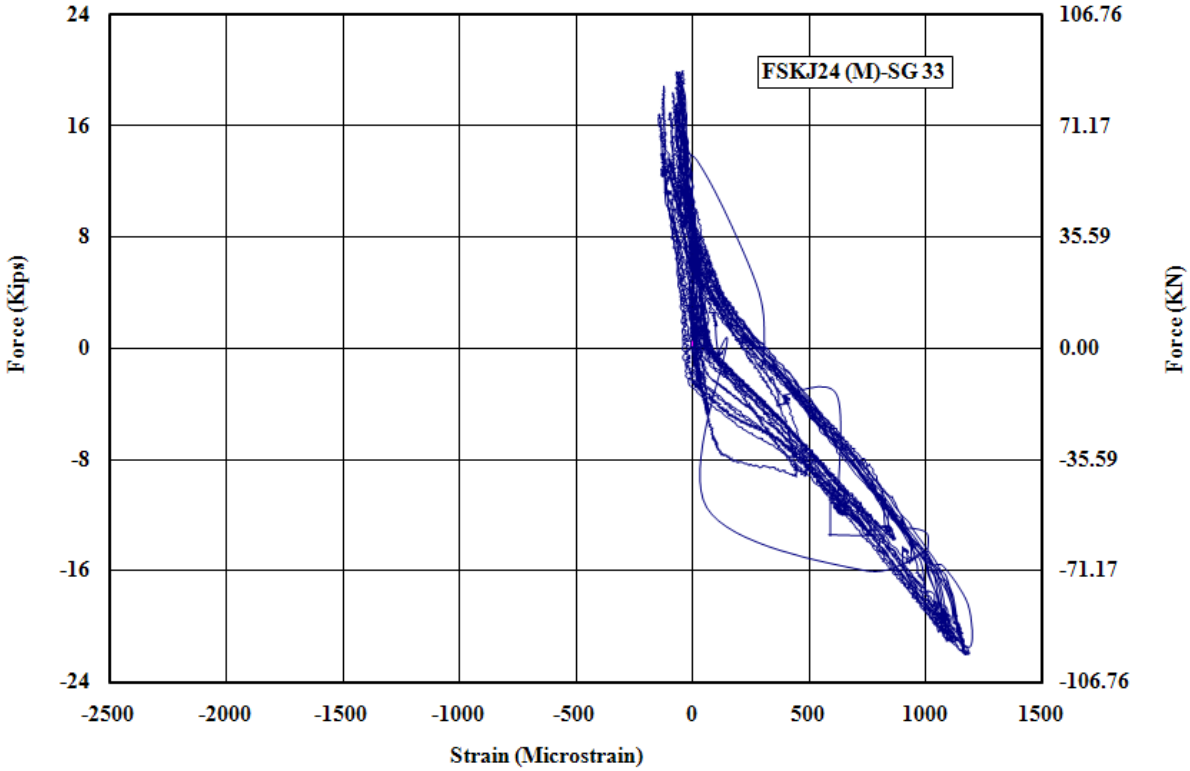

Figure H - 24: Measured Strain in Gauge No.33 for FSKJ24-M

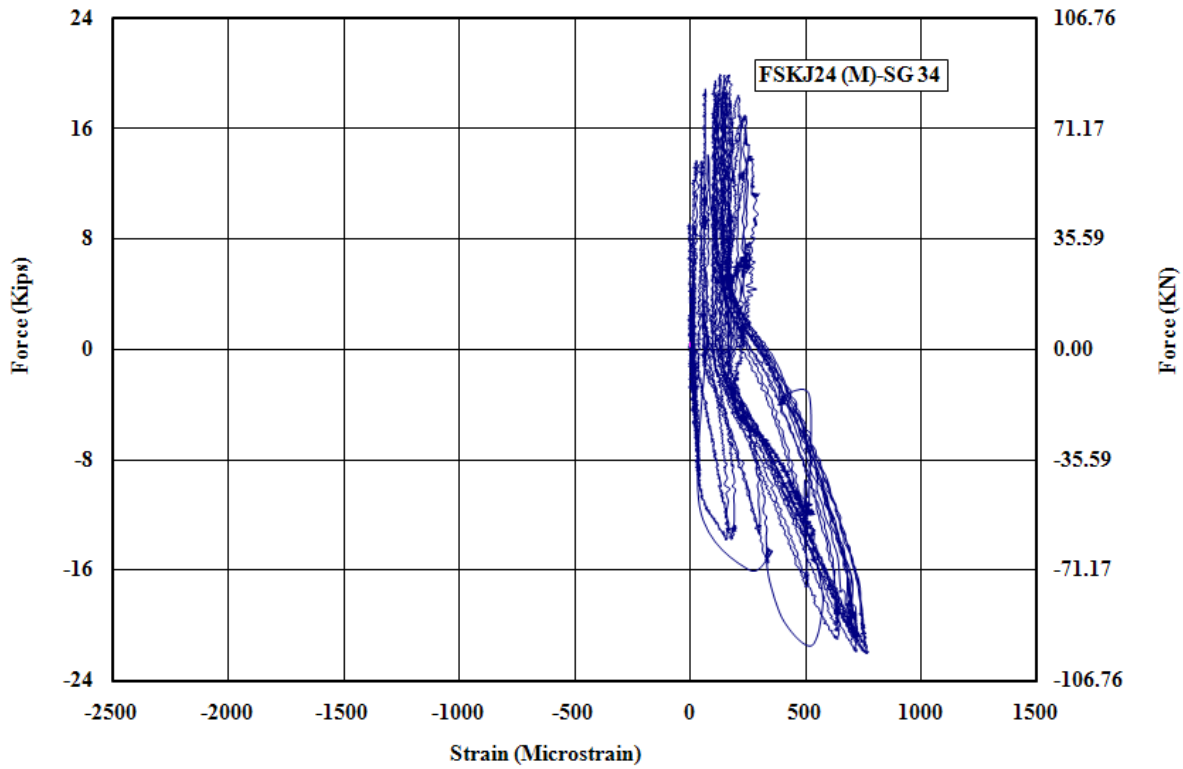

Figure H - 25: Measured Strain in Gauge No.34 for FSKJ24-M

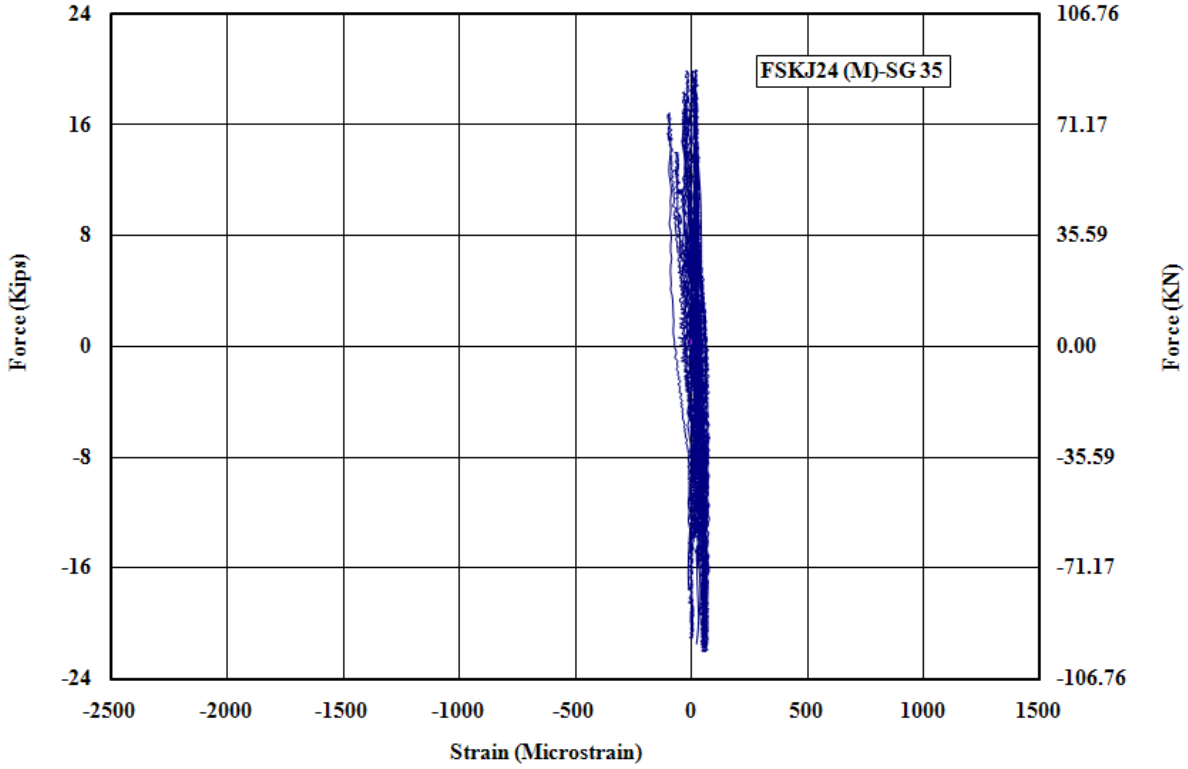

Figure H - 26: Measured Strain in Gauge No.35 for FSKJ24-M

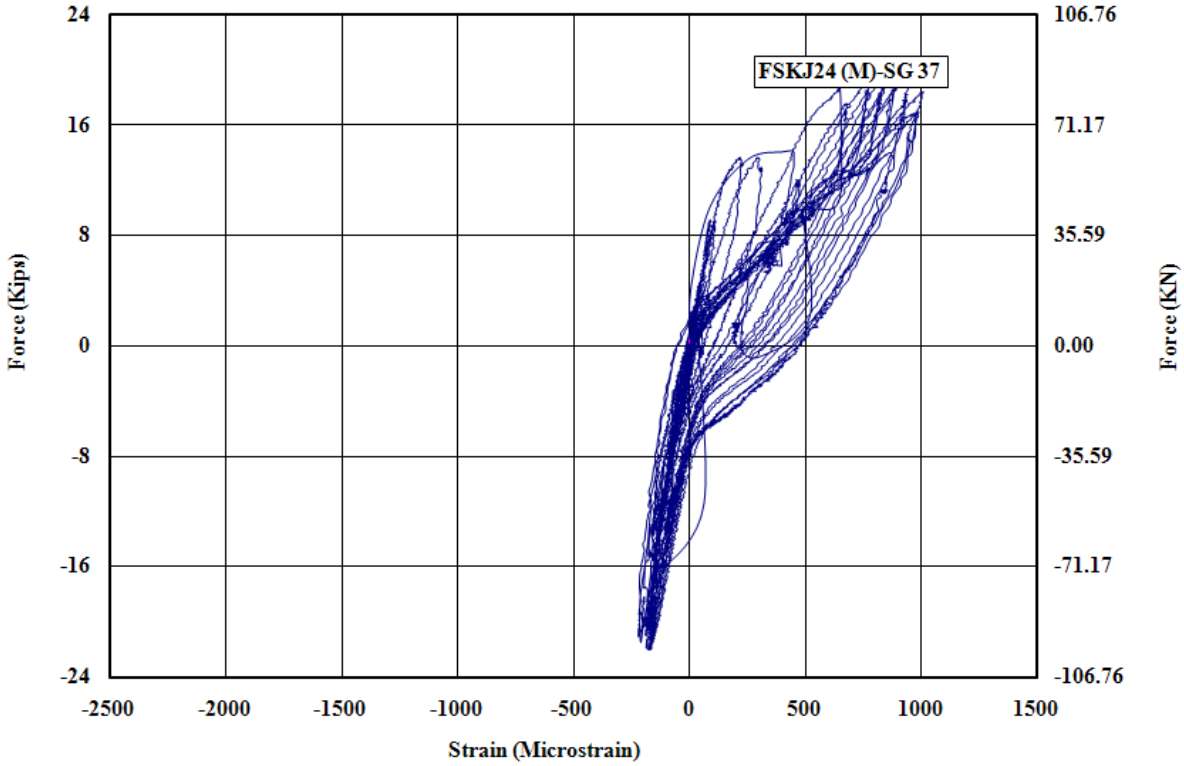

Figure H - 27: Measured Strain in Gauge No.37 for FSKJ24-M

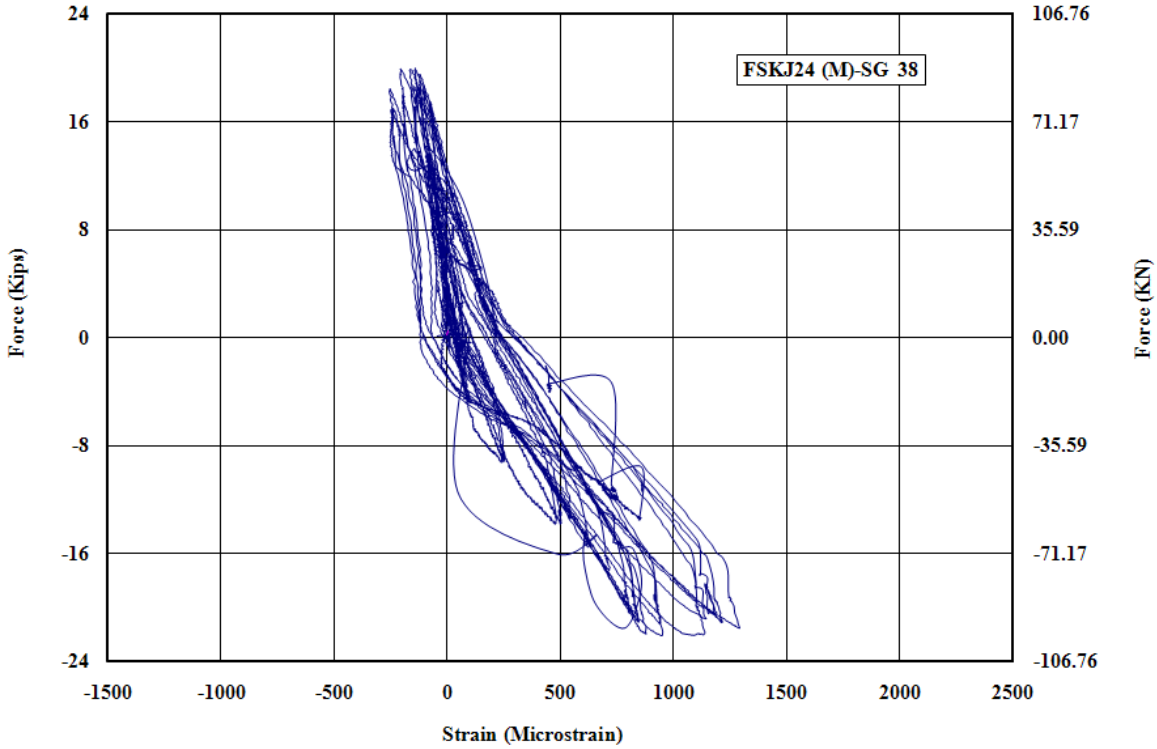

Figure H - 28: Measured Strain in Gauge No.38 for FSKJ24-M

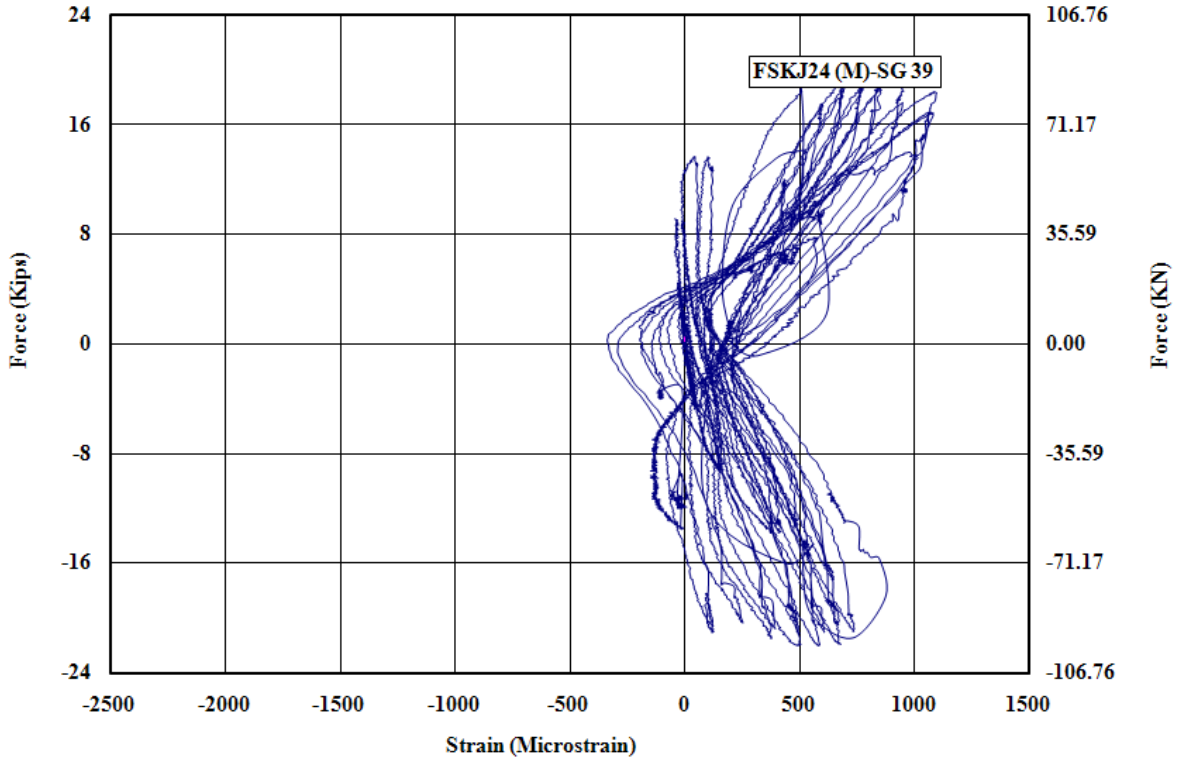

Figure H - 29: Measured Strain in Gauge No.39 for FSKJ24-M

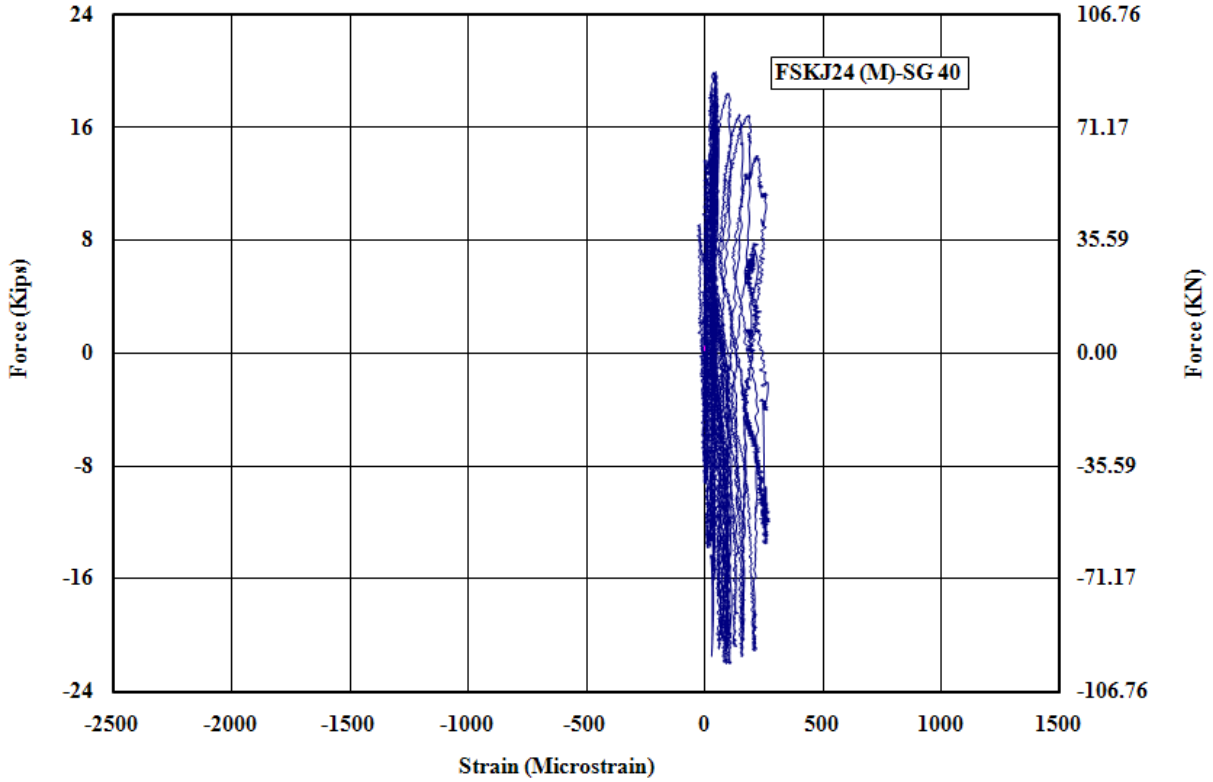

Figure H - 30: Measured Strain in Gauge No.40 for FSKJ24-M

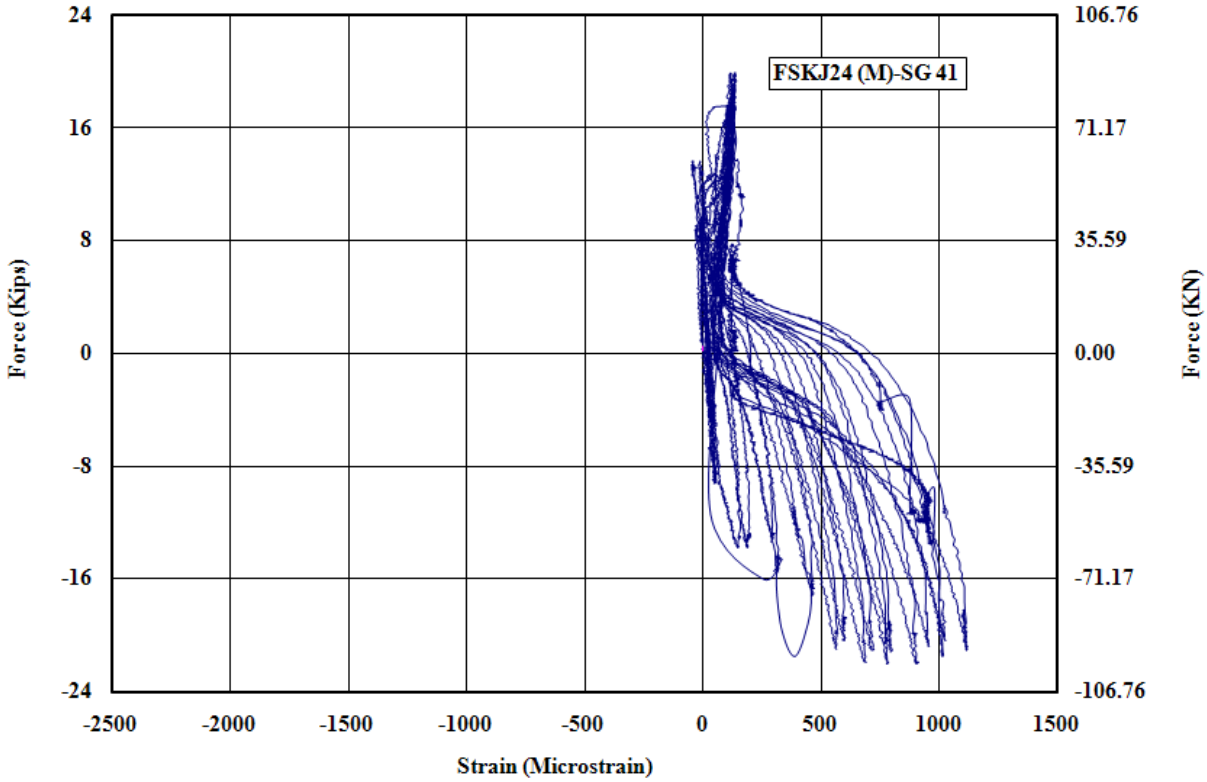

Figure H - 31: Measured Strain in Gauge No.41 for FSKJ24-M

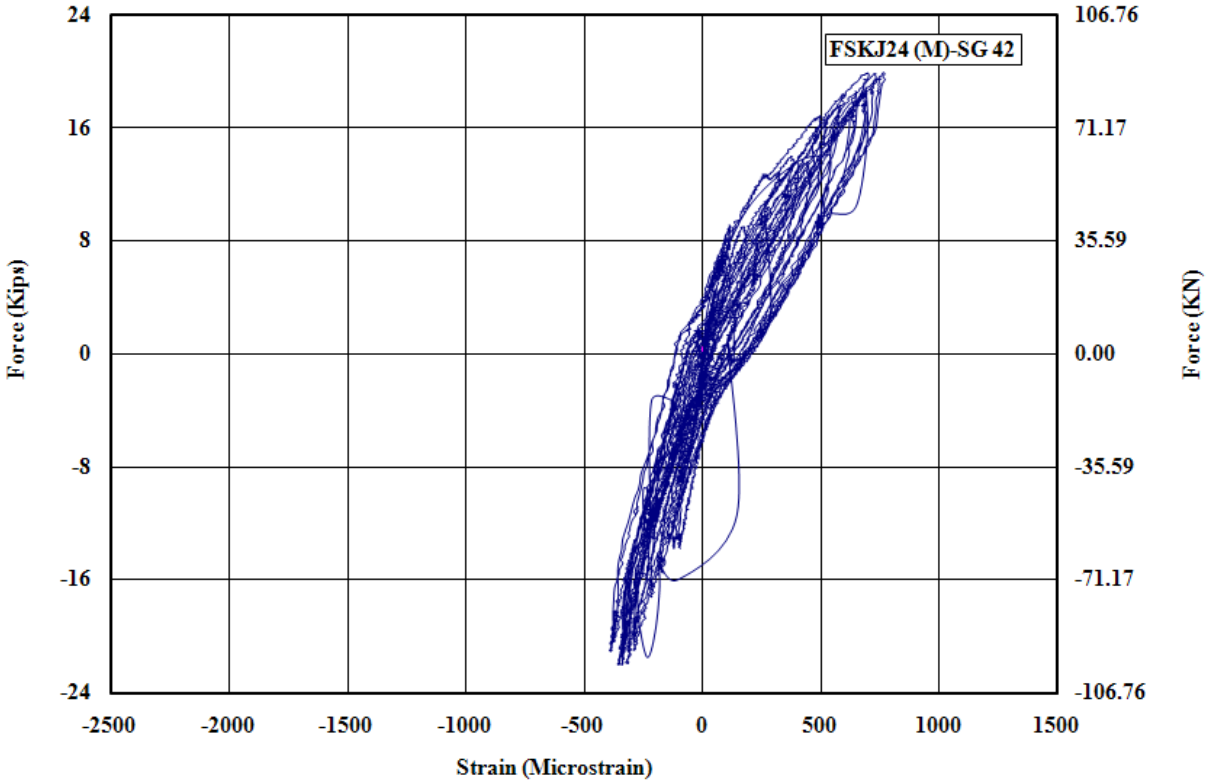

Figure H - 32: Measured Strain in Gauge No.42 for FSKJ24-M

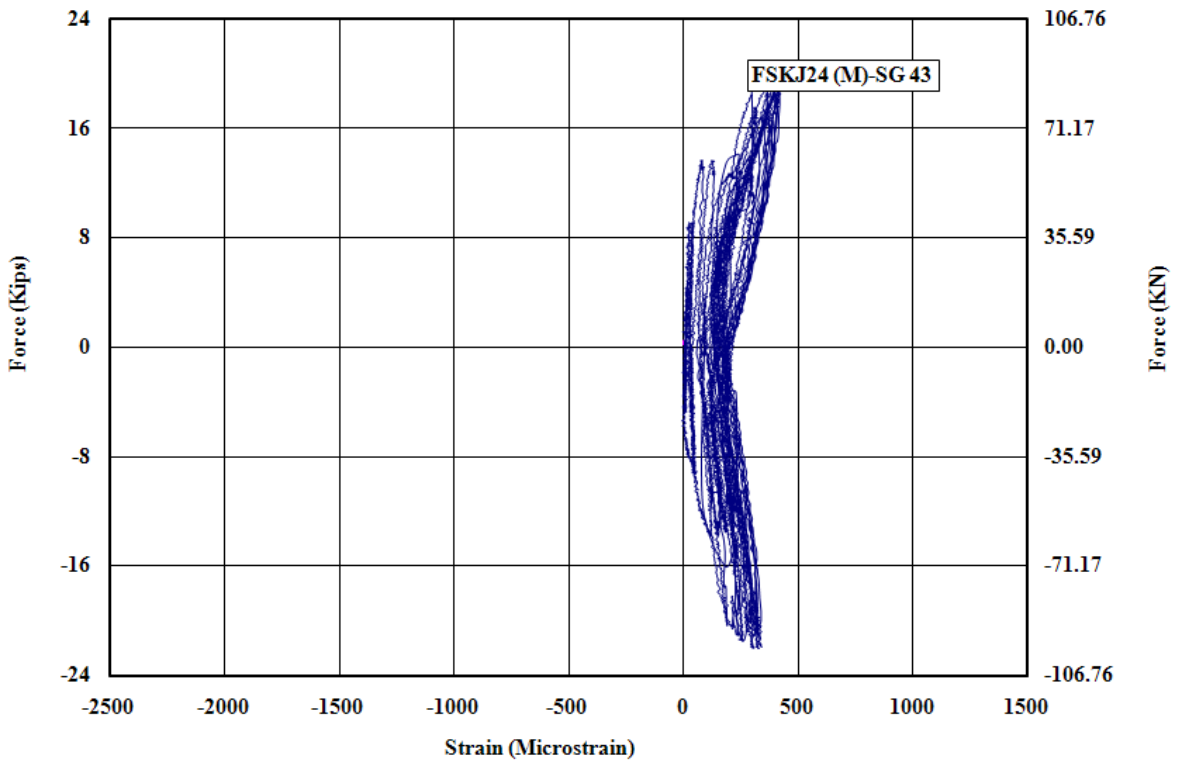

Figure H - 33: Measured Strain in Gauge No.43 for FSKJ24-M

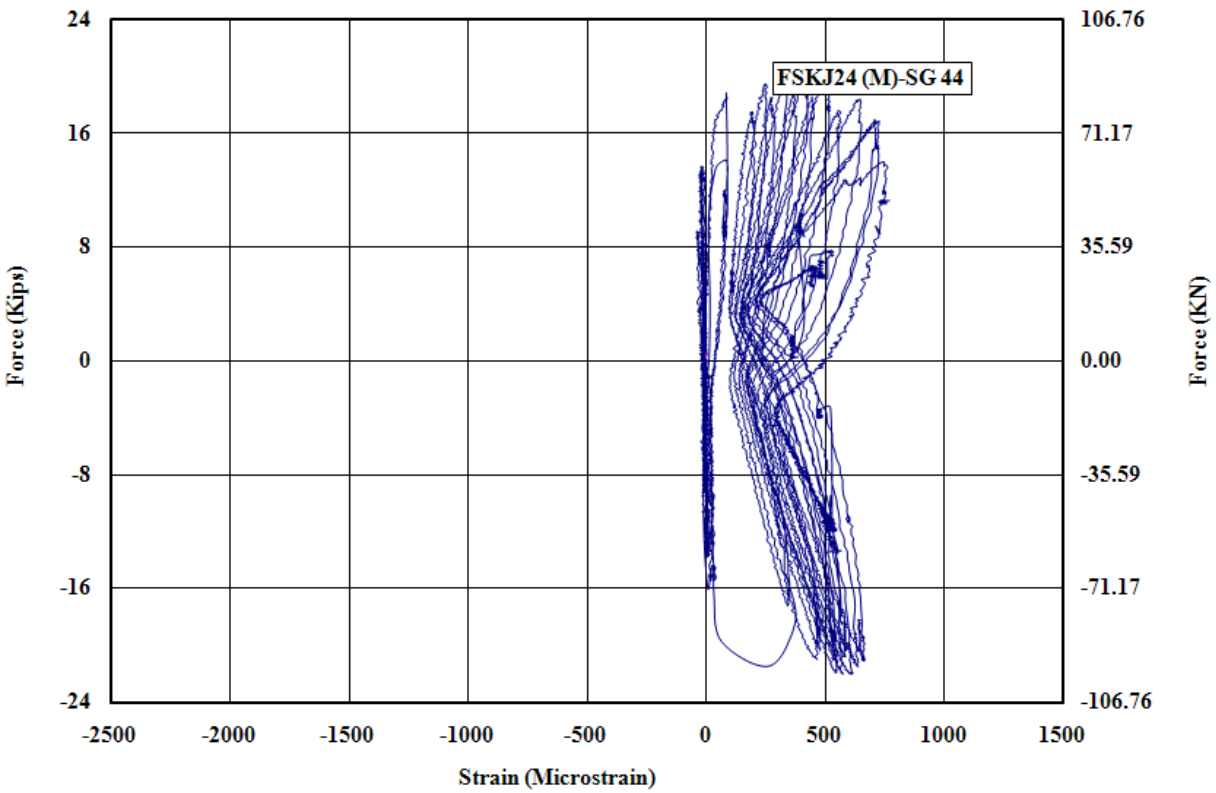

Figure H - 34: Measured Strain in Gauge No.44 for FSKJ24-M

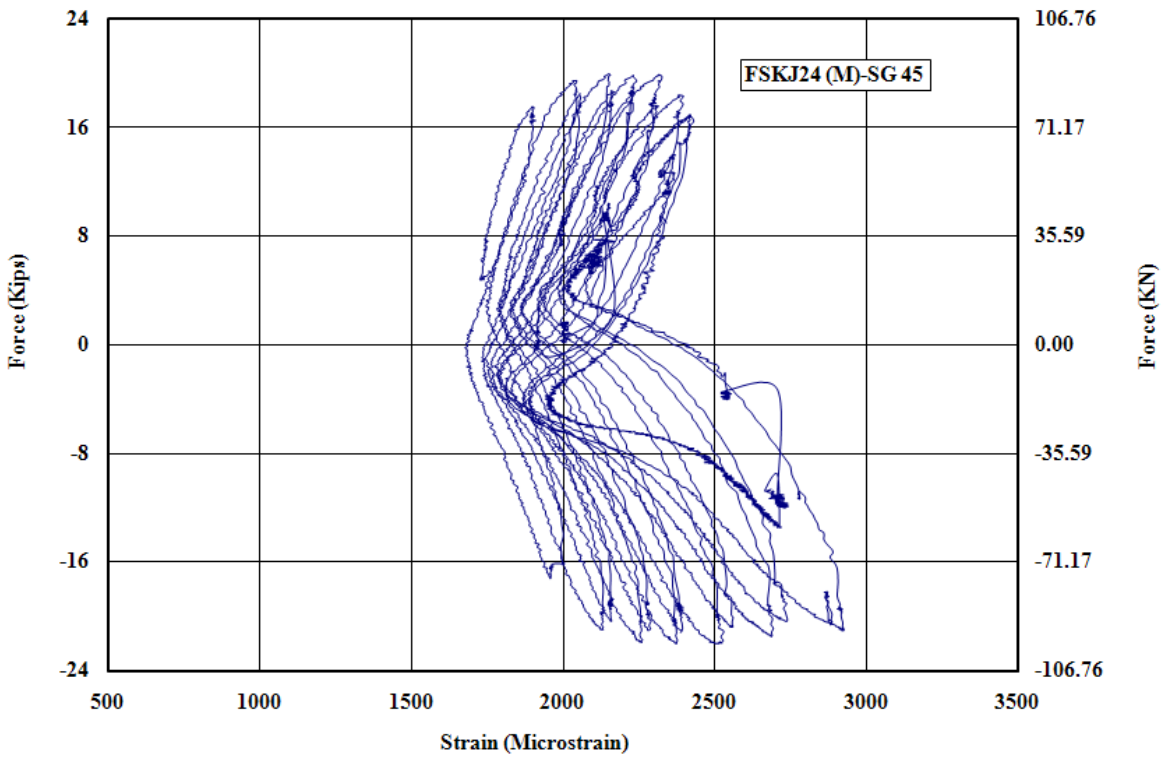

Figure H - 35: Measured Strain in Gauge No.45 for FSKJ24-M

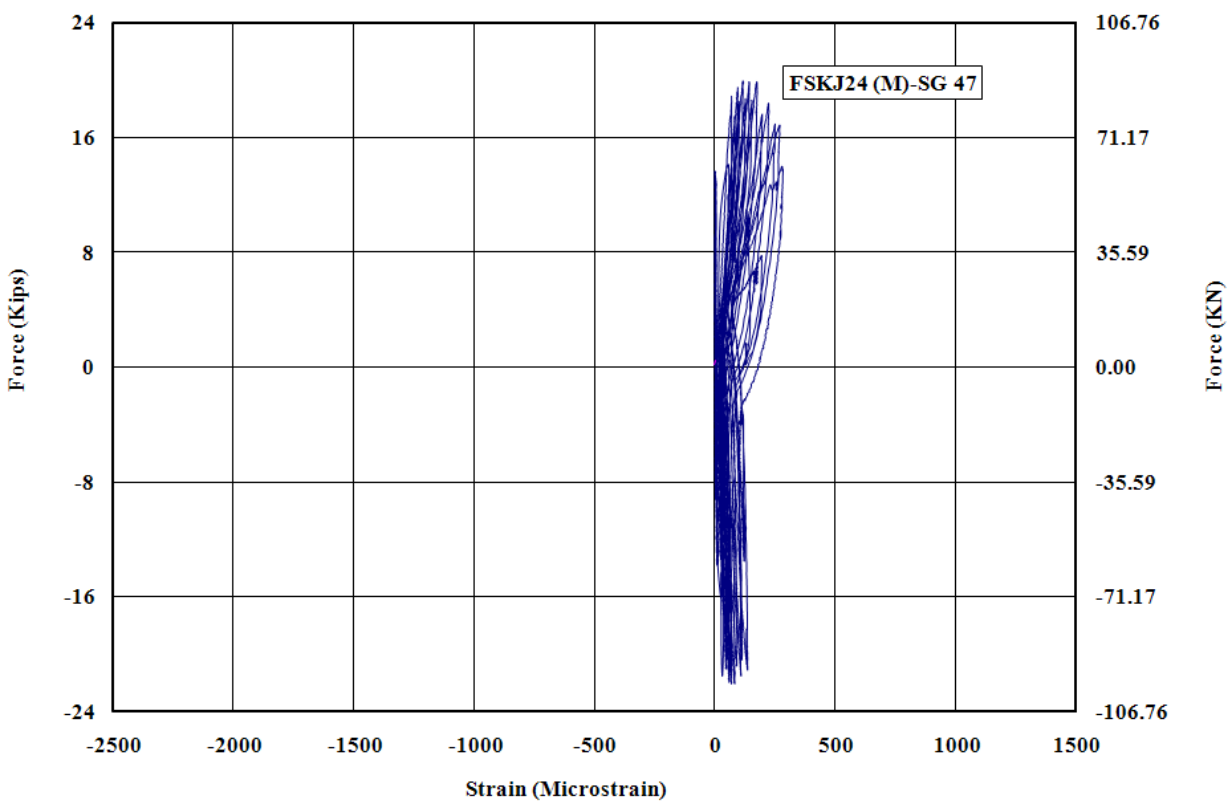

Figure H - 36: Measured Strain in Gauge No.47 for FSKJ24-M

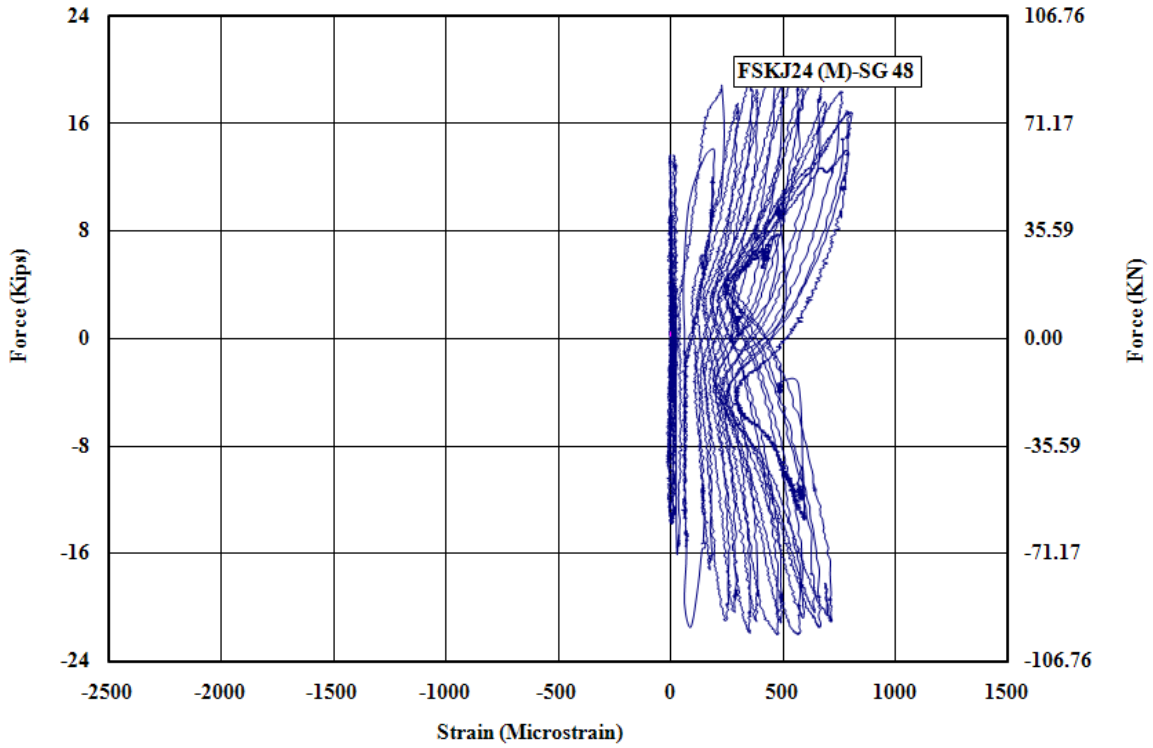

Figure H - 37: Measured Strain in Gauge No.48 for FSKJ24-M

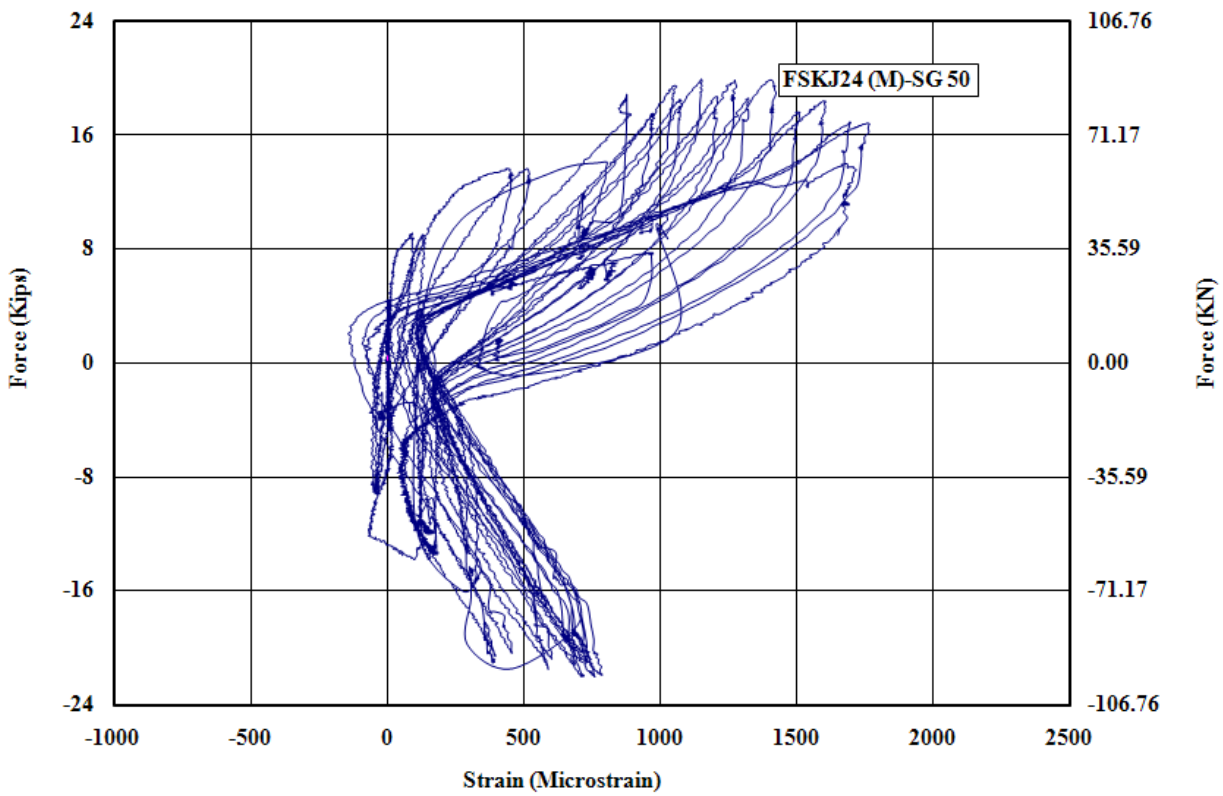

Figure H - 38: Measured Strain in Gauge No.50 for FSKJ24-M

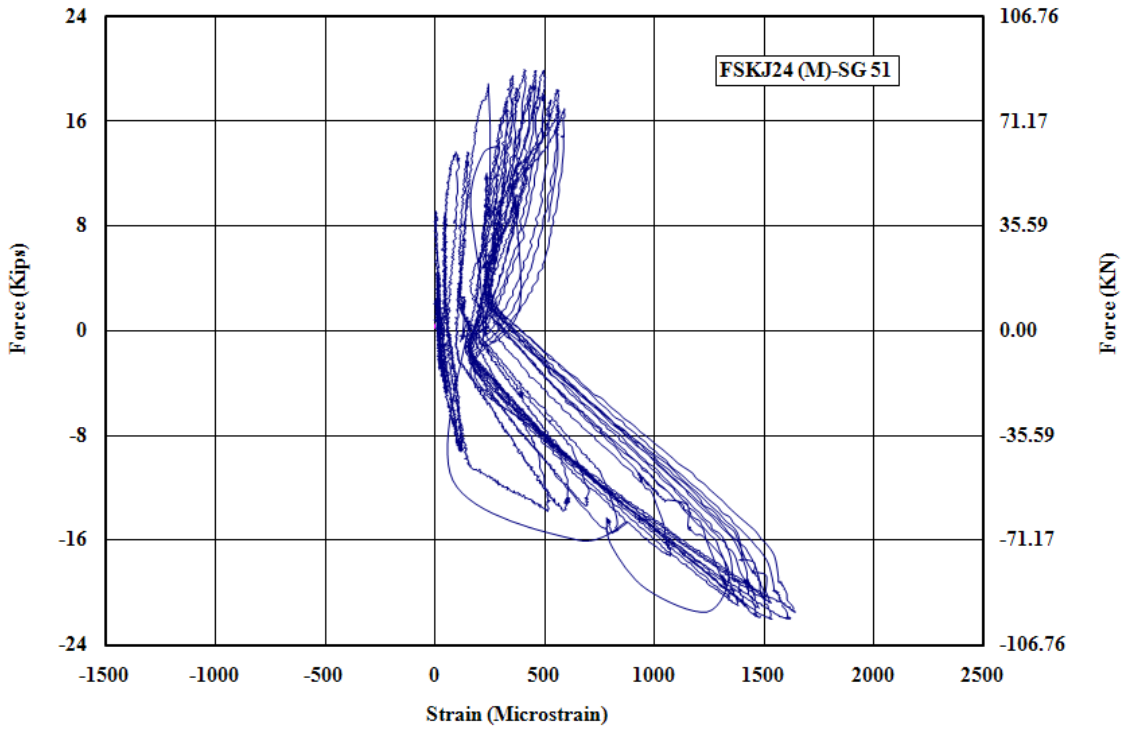

Figure H - 39: Measured Strain in Gauge No.51 for FSKJ24-M

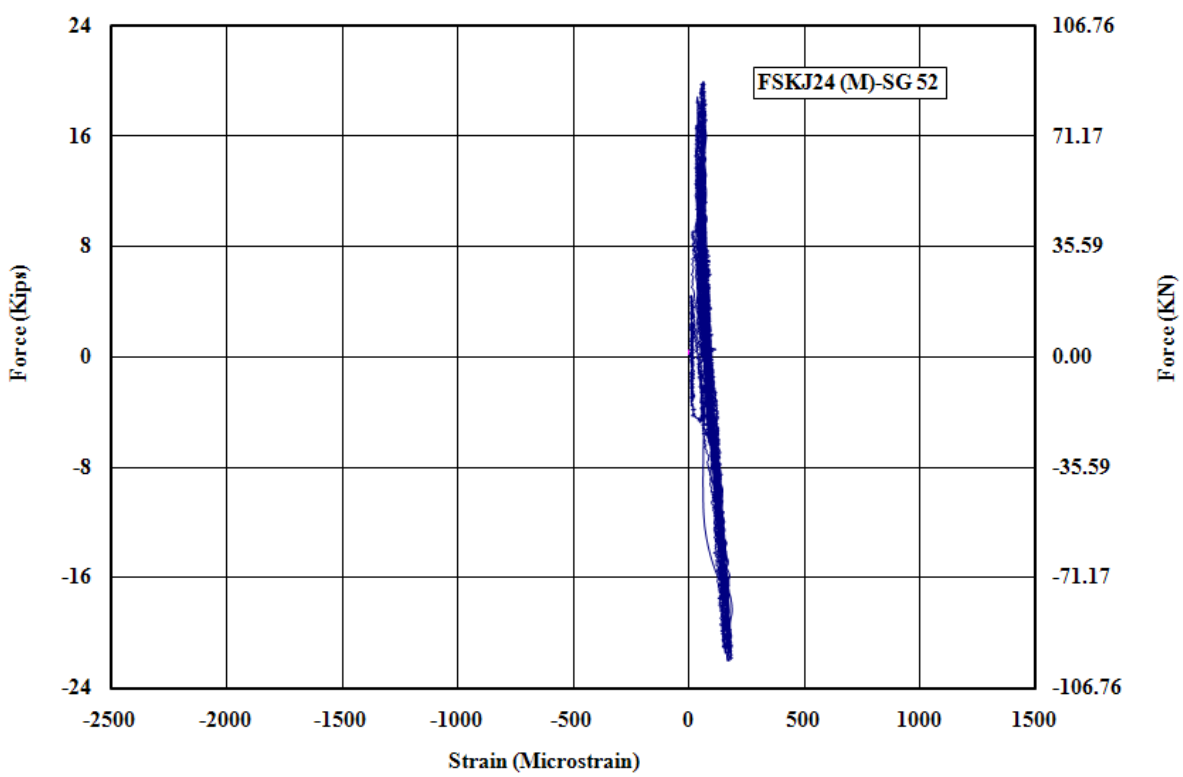

Figure H - 40: Measured Strain in Gauge No.52 for FSKJ24-M

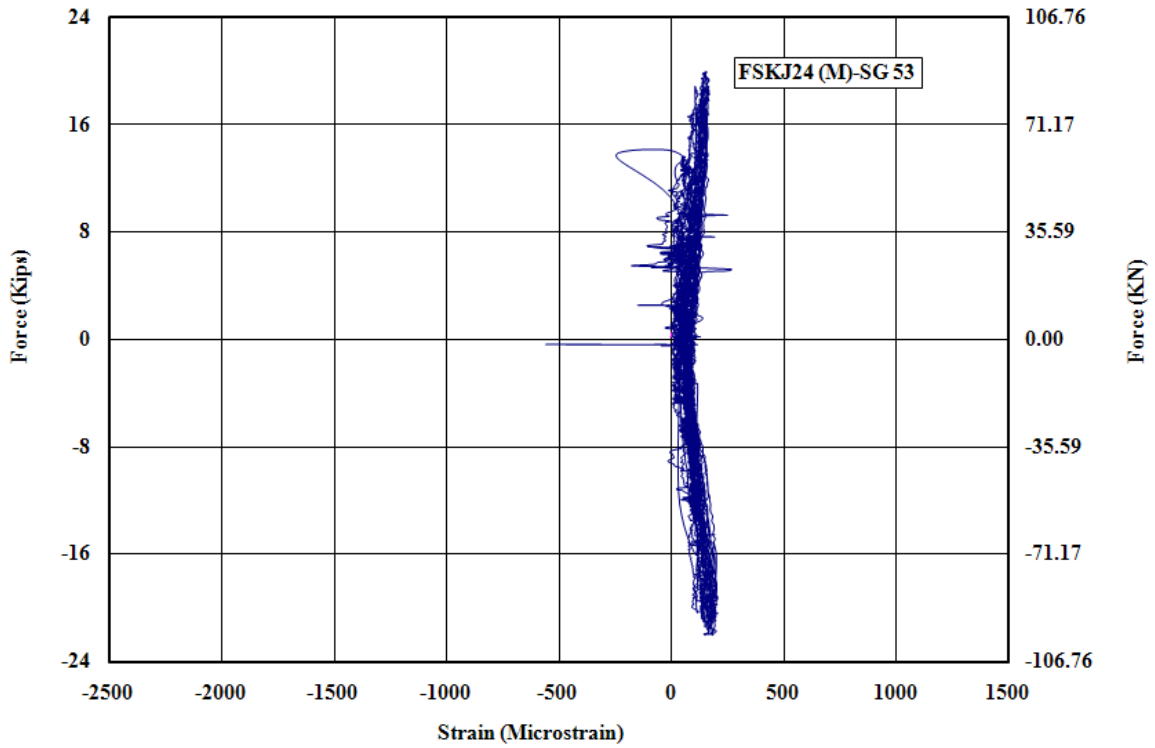

Figure H - 41: Measured Strain in Gauge No.53 for FSKJ24-M

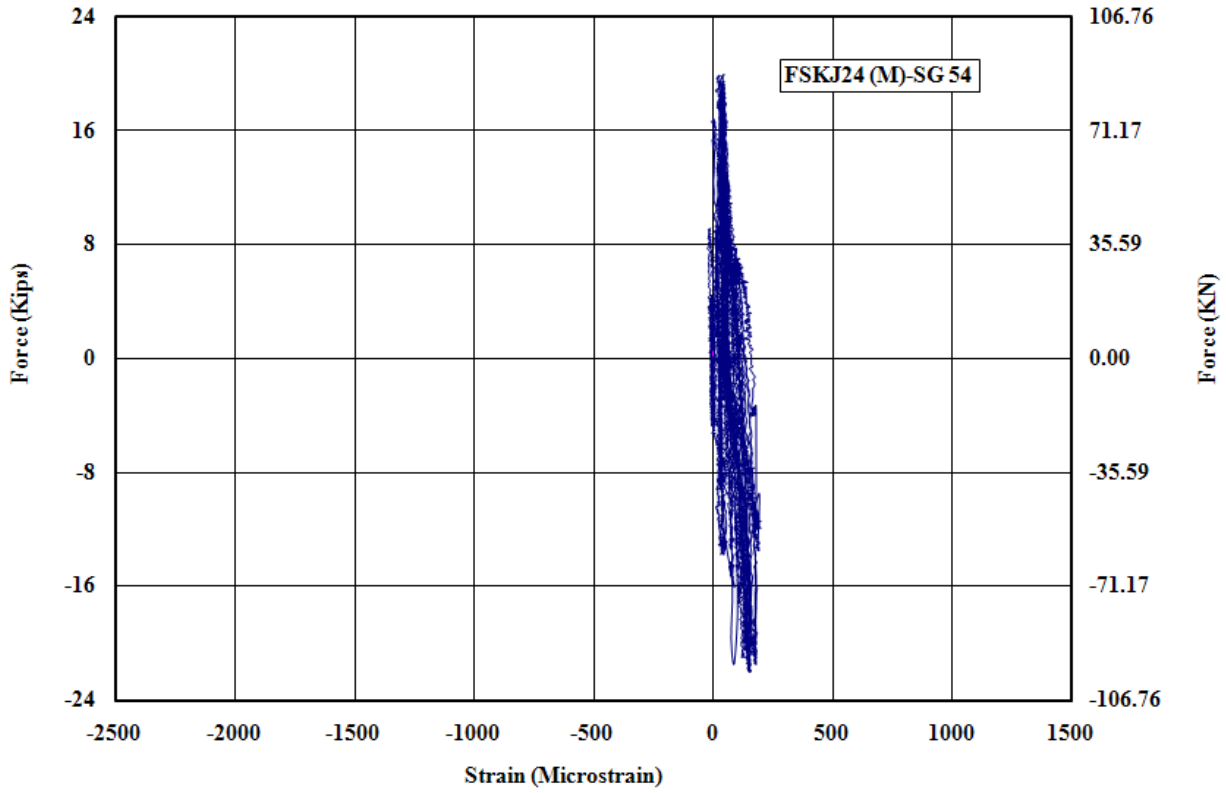

Figure H - 42: Measured Strain in Gauge No.54 for FSKJ24-M

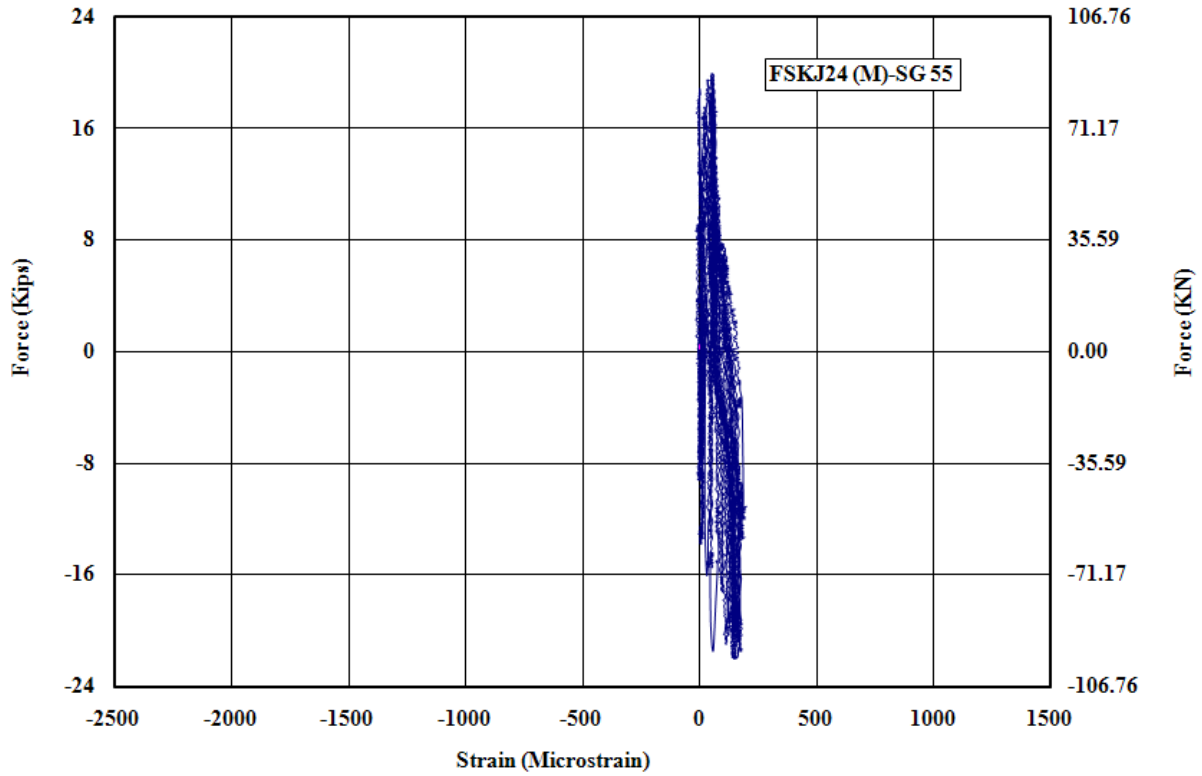

Figure H - 43: Measured Strain in Gauge No.55 for FSKJ24-M

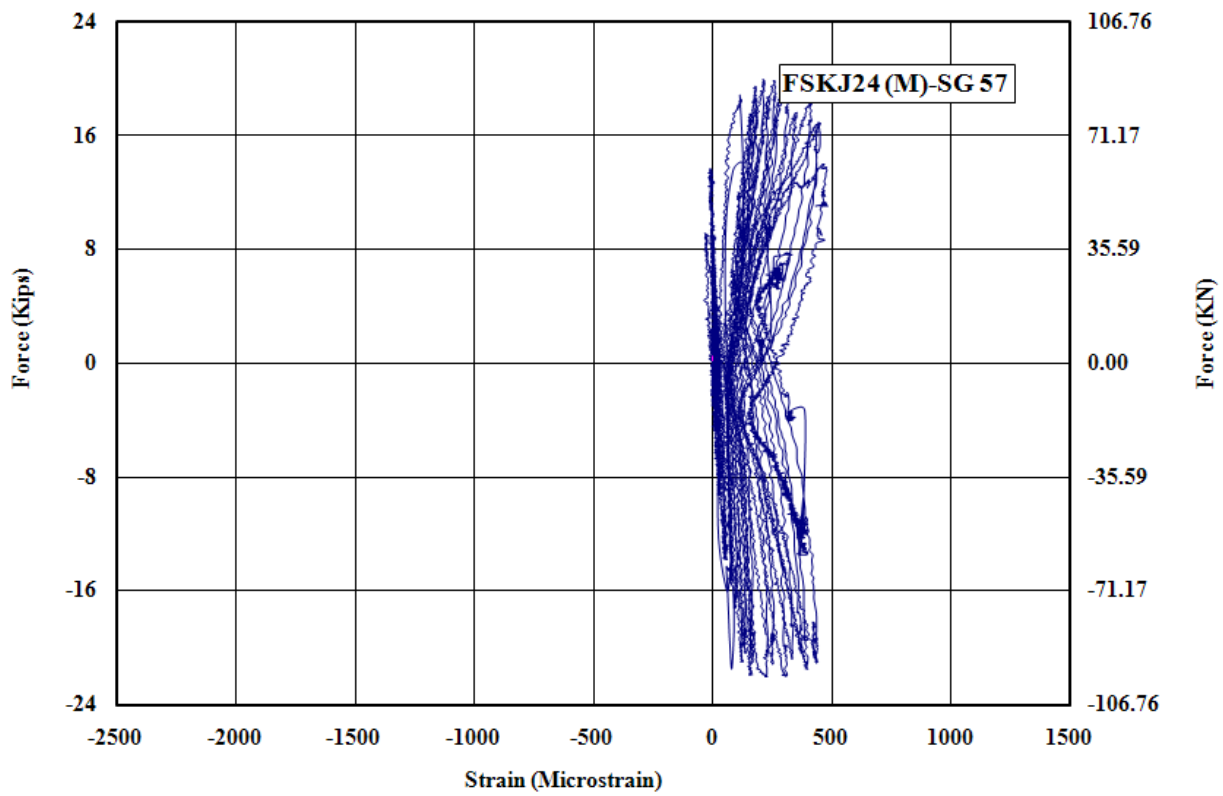

Figure H - 44: Measured Strain in Gauge No.57 for FSKJ24-M

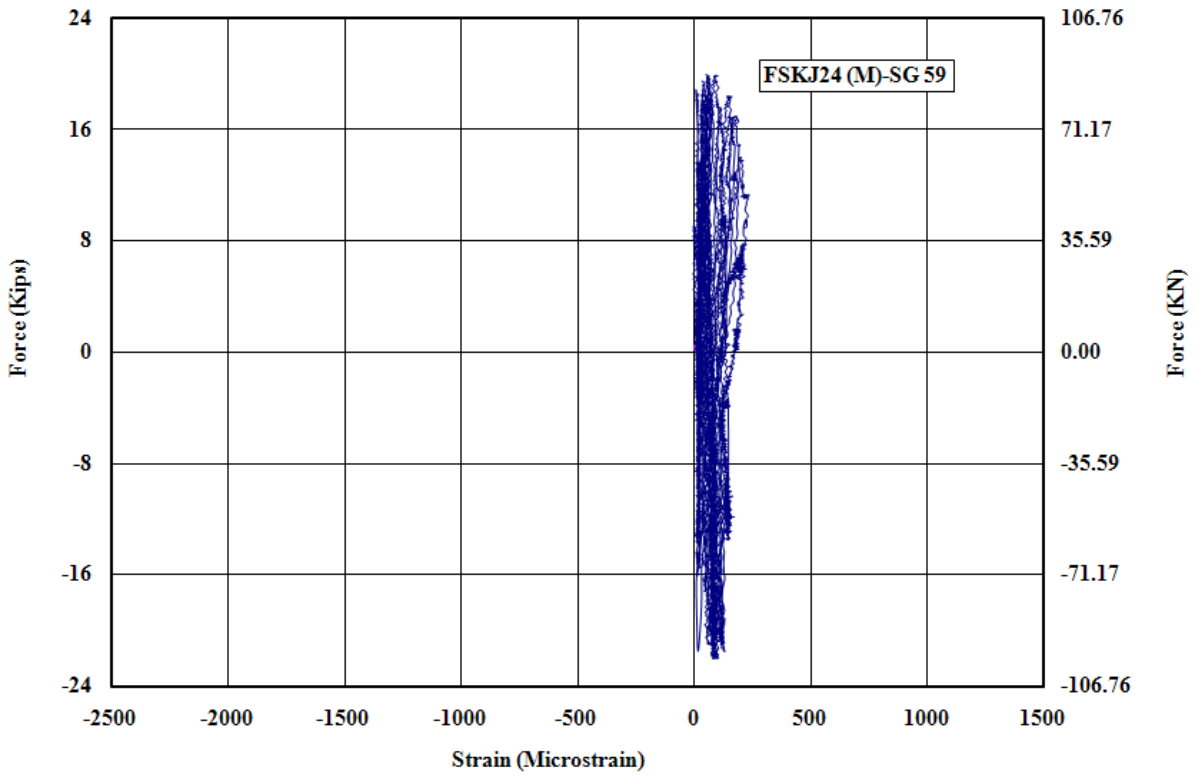

Figure H - 45: Measured Strain in Gauge No.59 for FSKJ24-M

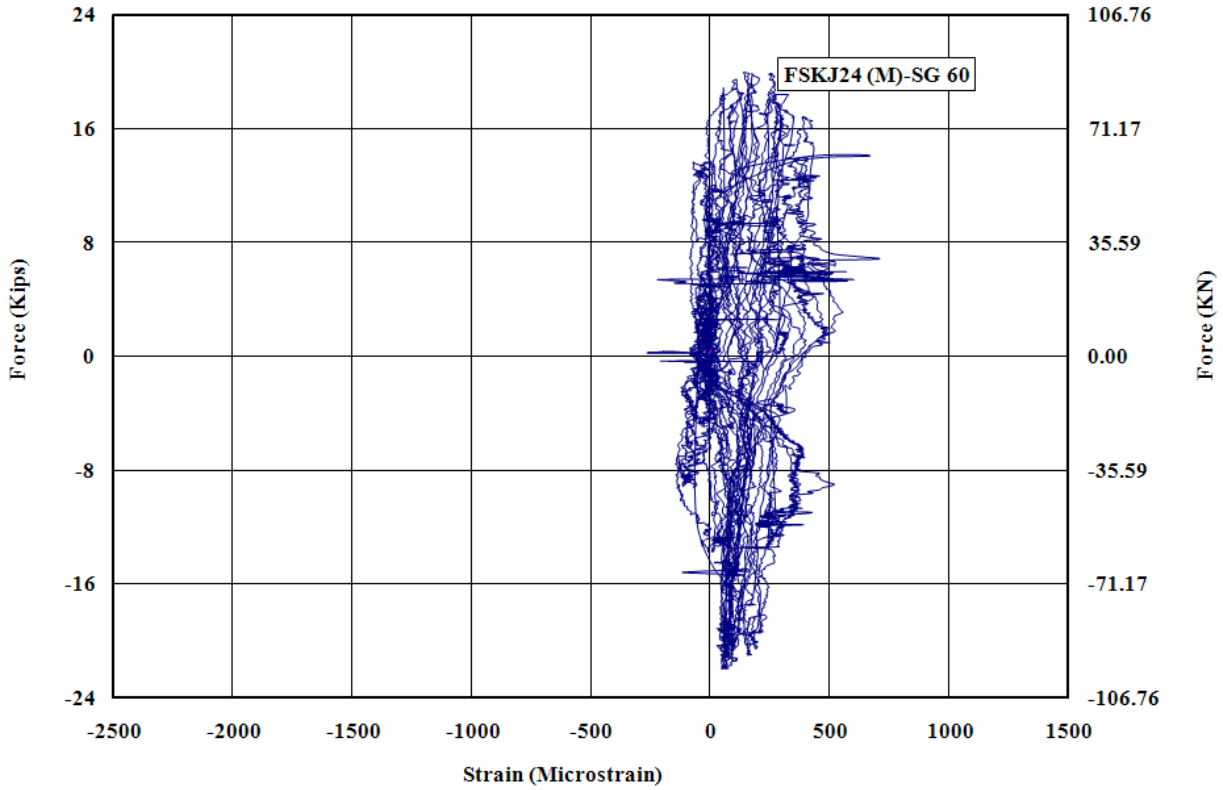

Figure H - 46: Measured Strain in Gauge No.60 for FSKJ24-M

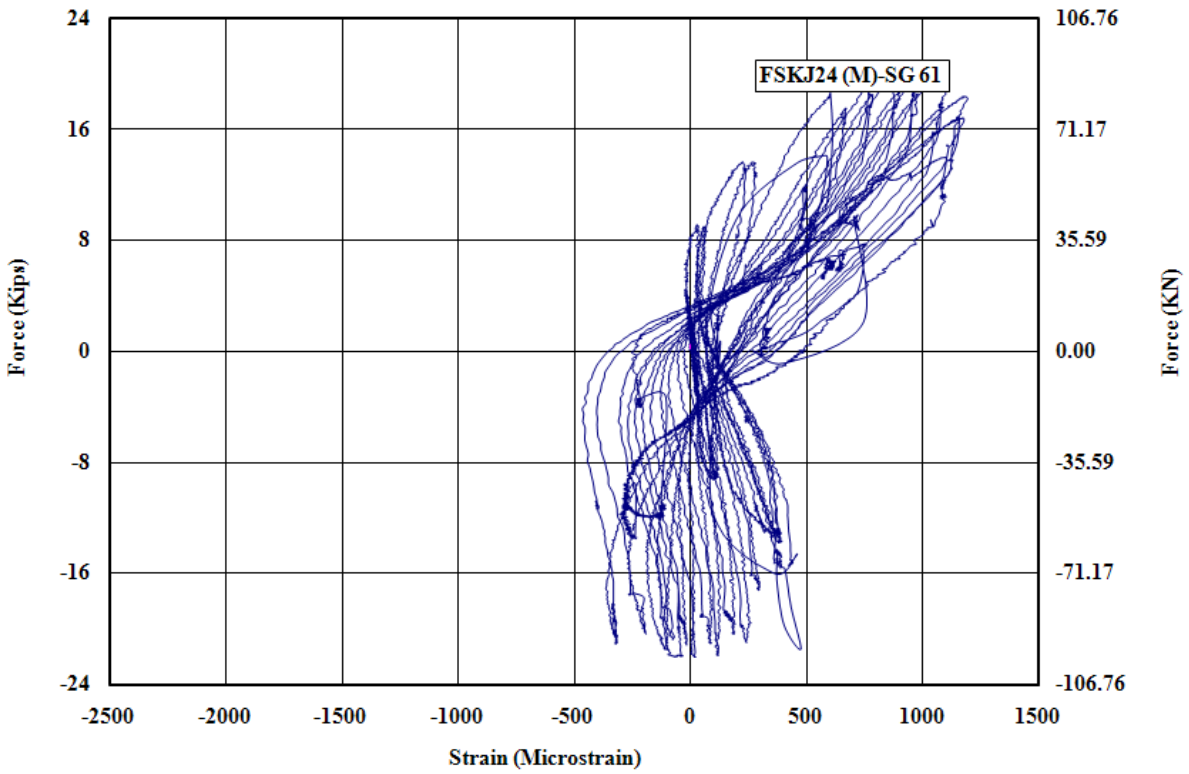

Figure H - 47: Measured Strain in Gauge No.61 for FSKJ24-M

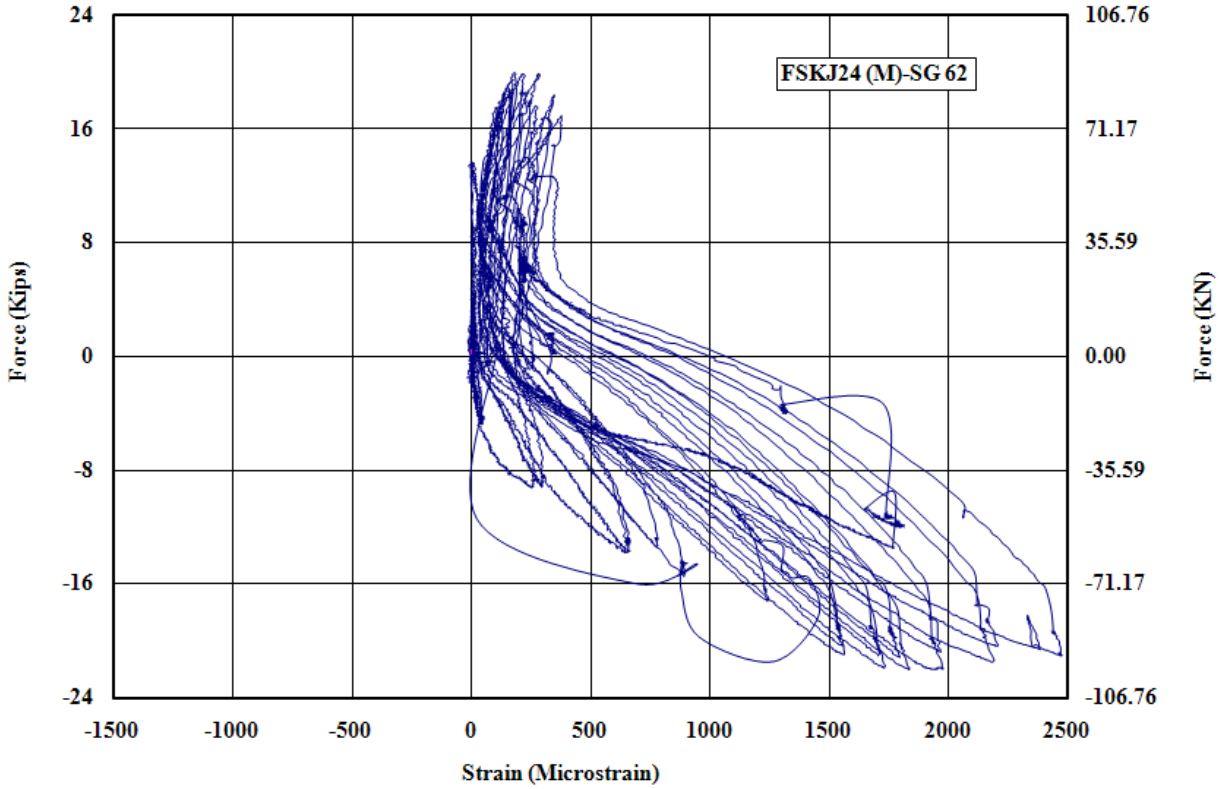

Figure H - 48: Measured Strain in Gauge No.62 for FSKJ24-M

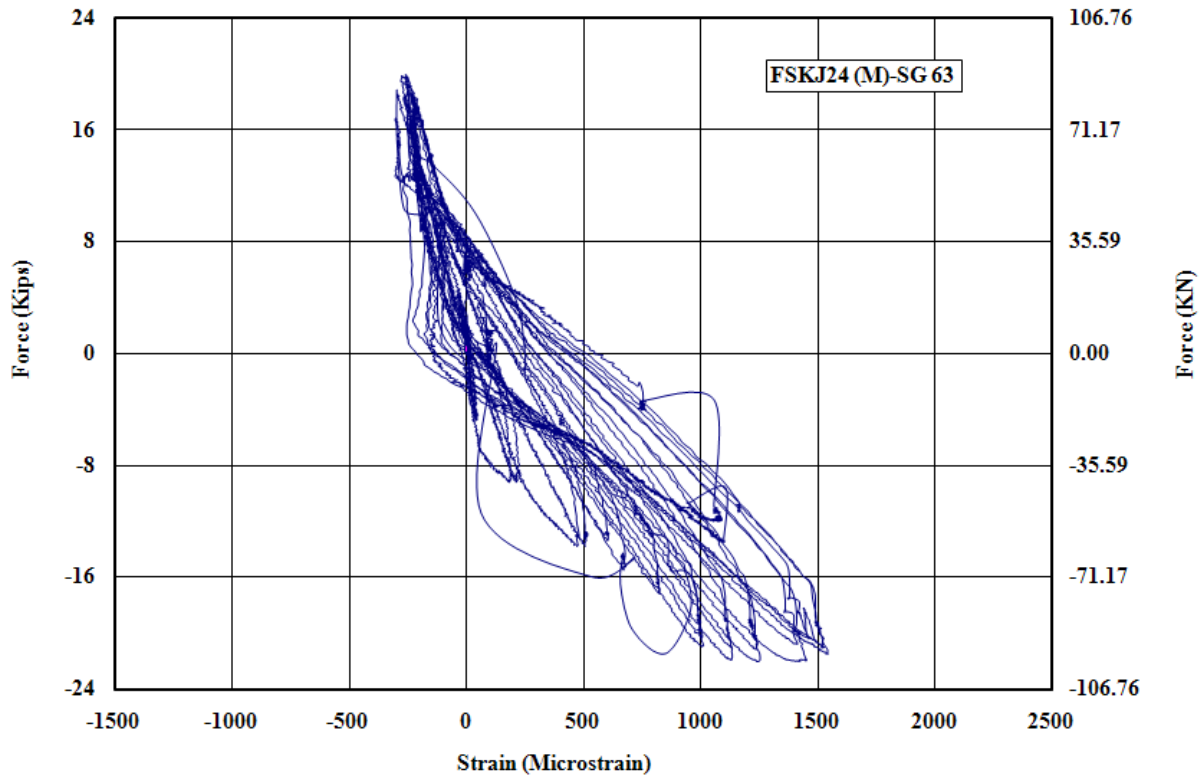

Figure H - 49: Measured Strain in Gauge No.63 for FSKJ24-M

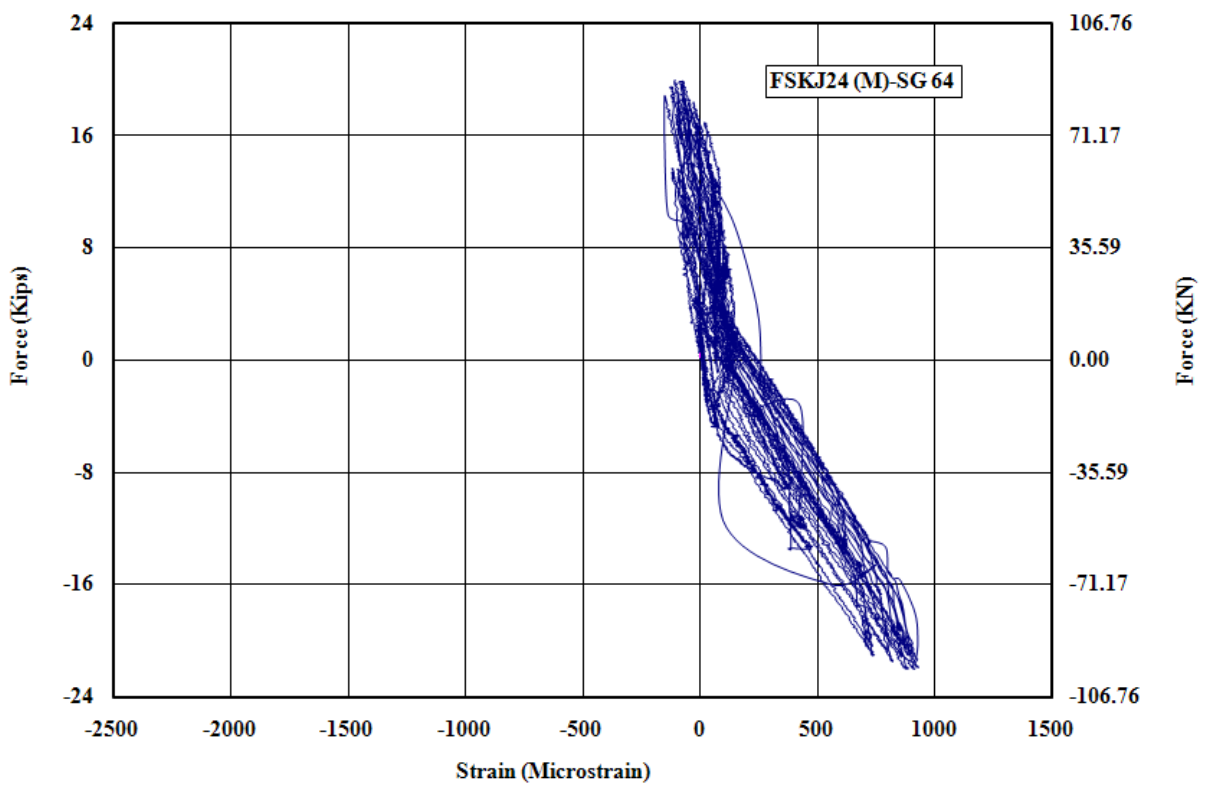

Figure H - 50: Measured Strain in Gauge No.64 for FSKJ24-M

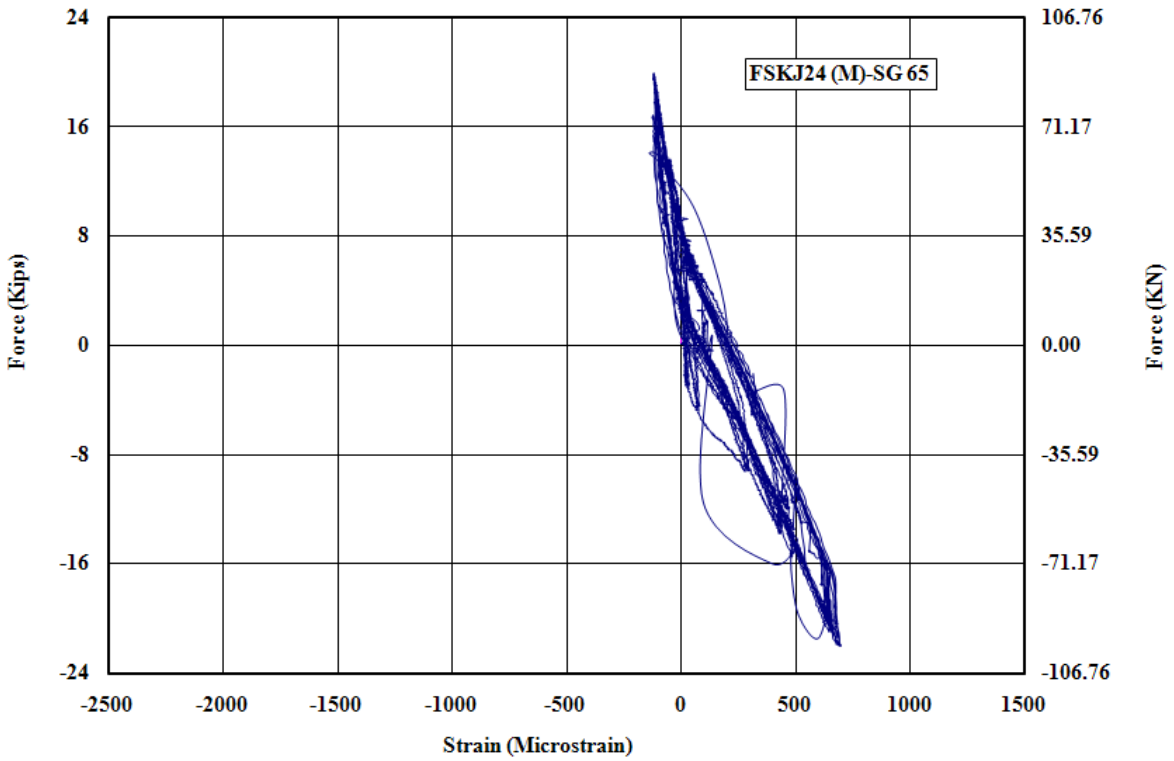

Figure H - 51: Measured Strain in Gauge No.65 for FSKJ24-M

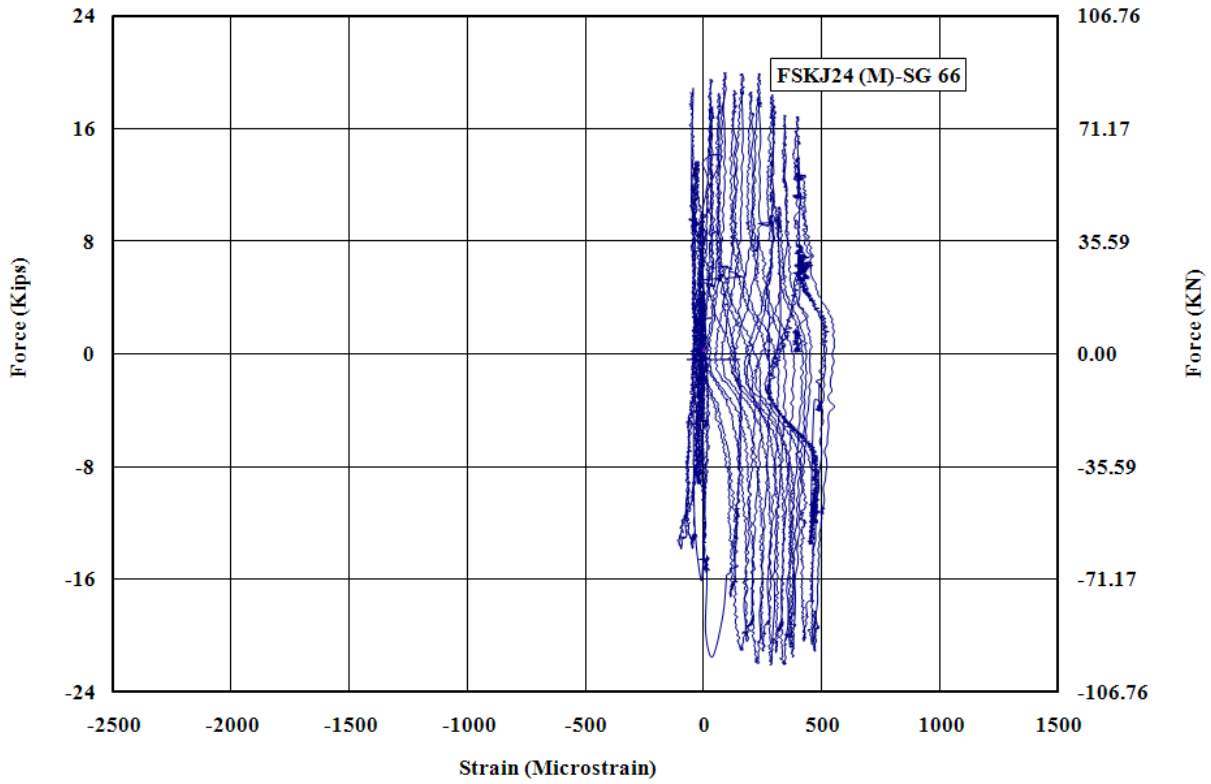

Figure H - 52: Measured Strain in Gauge No.66 for FSKJ24-M

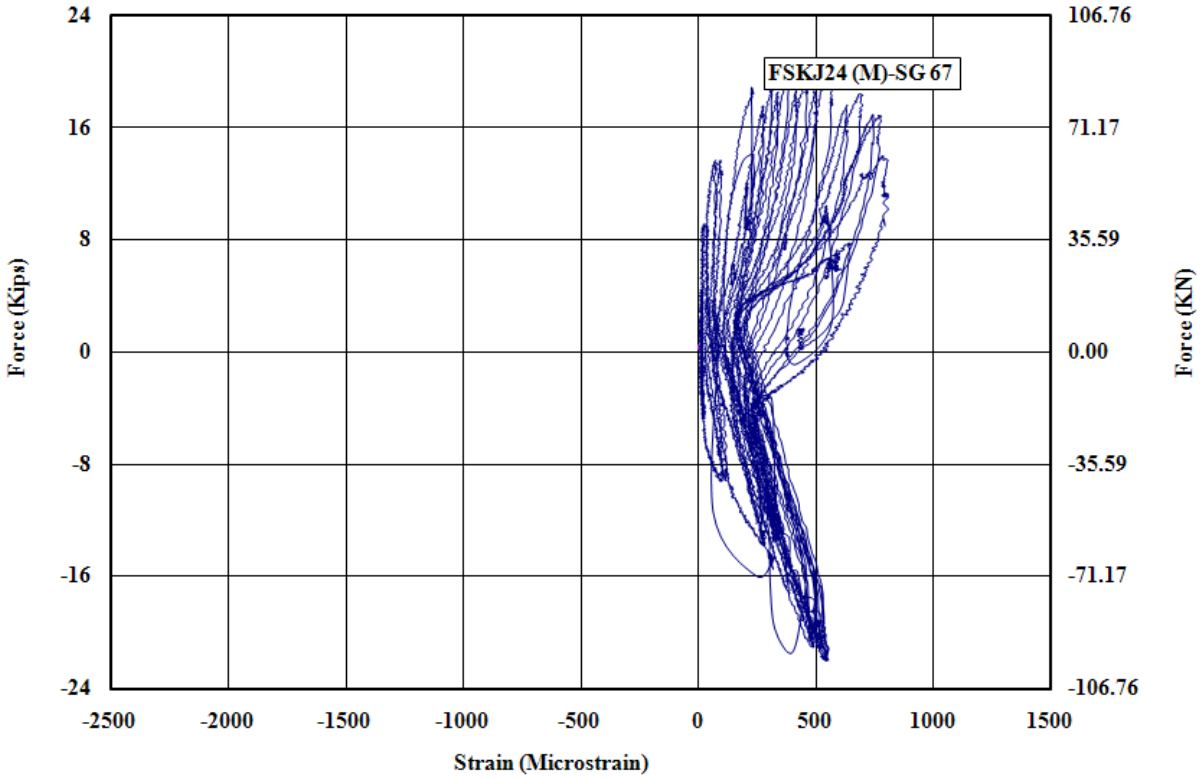

Figure H - 53: Measured Strain in Gauge No.67 for FSKJ24-M

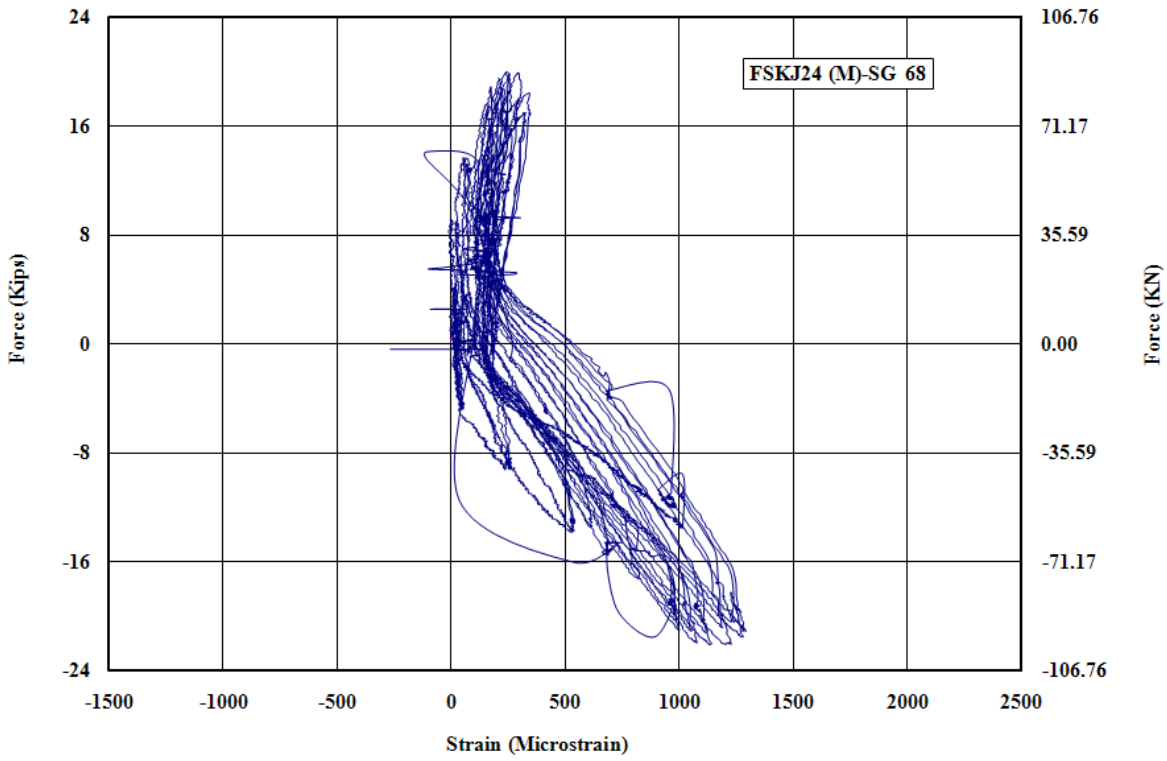

Figure H - 54: Measured Strain in Gauge No.68 for FSKJ24-M

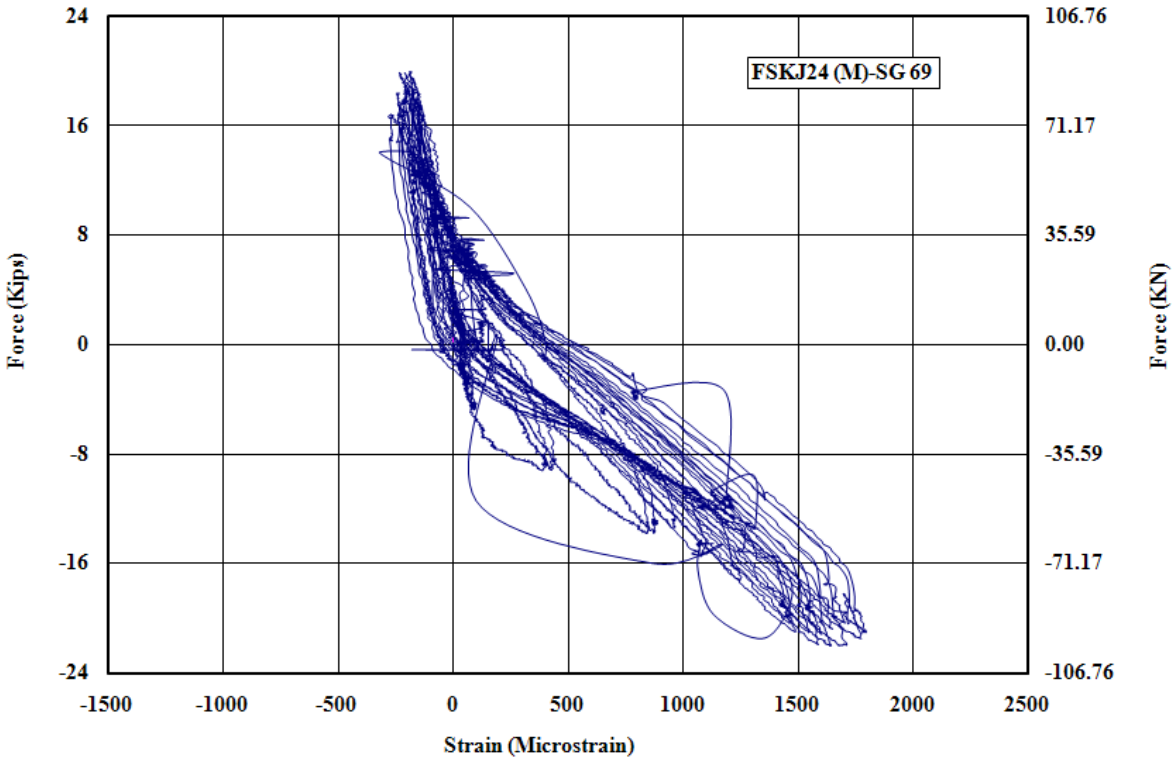

Figure H - 55: Measured Strain in Gauge No.69 for FSKJ24-M

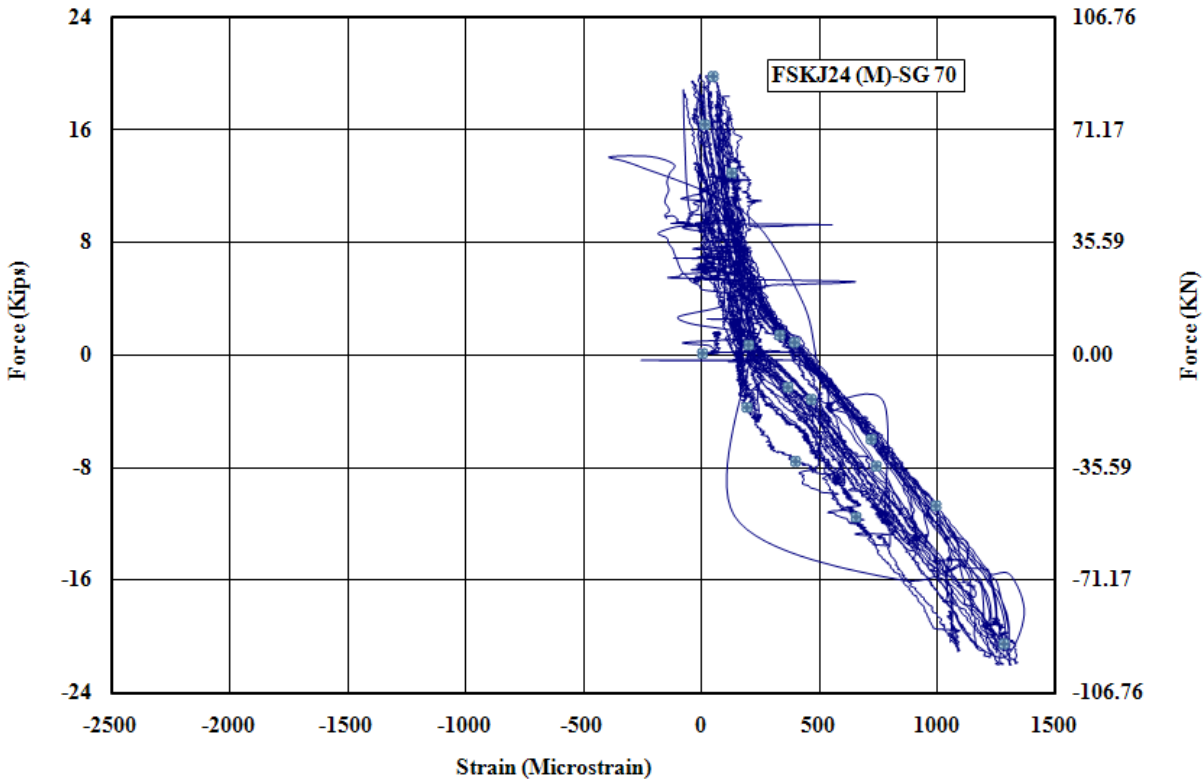

Figure H - 56: Measured Strain in Gauge No.70 for FSKJ24-M

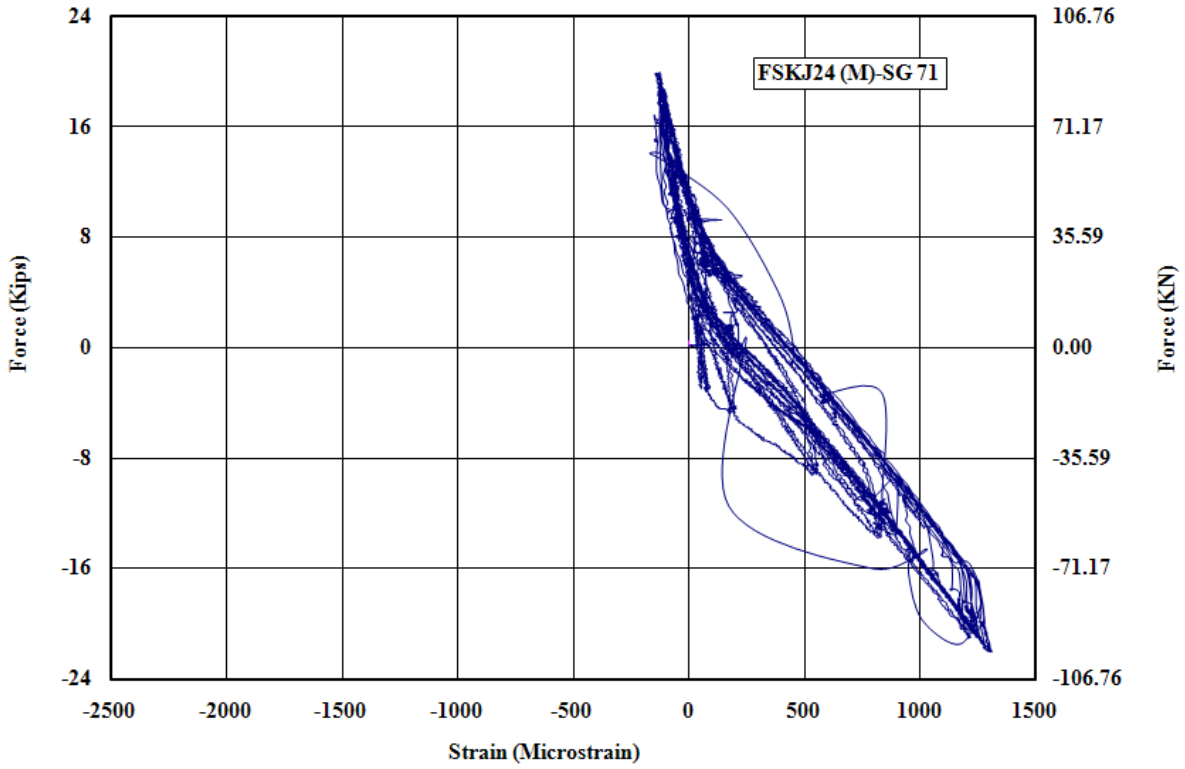

Figure H - 57: Measured Strain in Gauge No.71 for FSKJ24-M

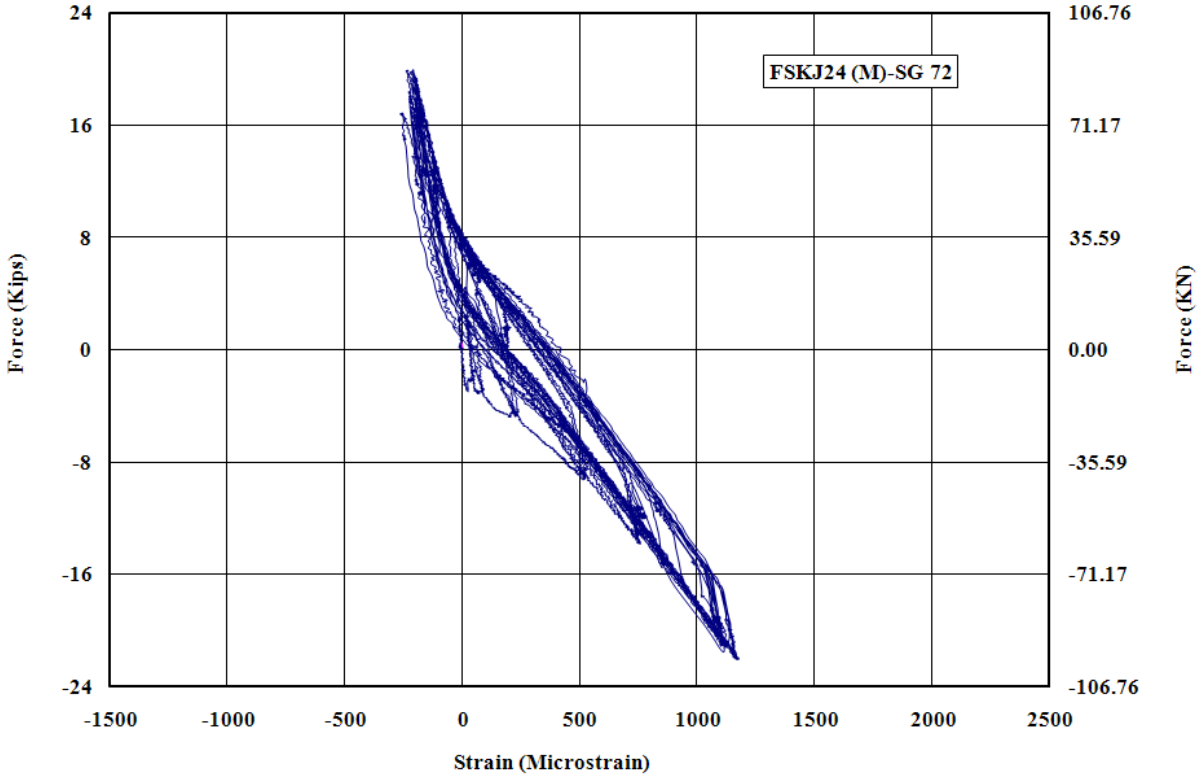

Figure H - 58: Measured Strain in Gauge No.72 for FSKJ24-M

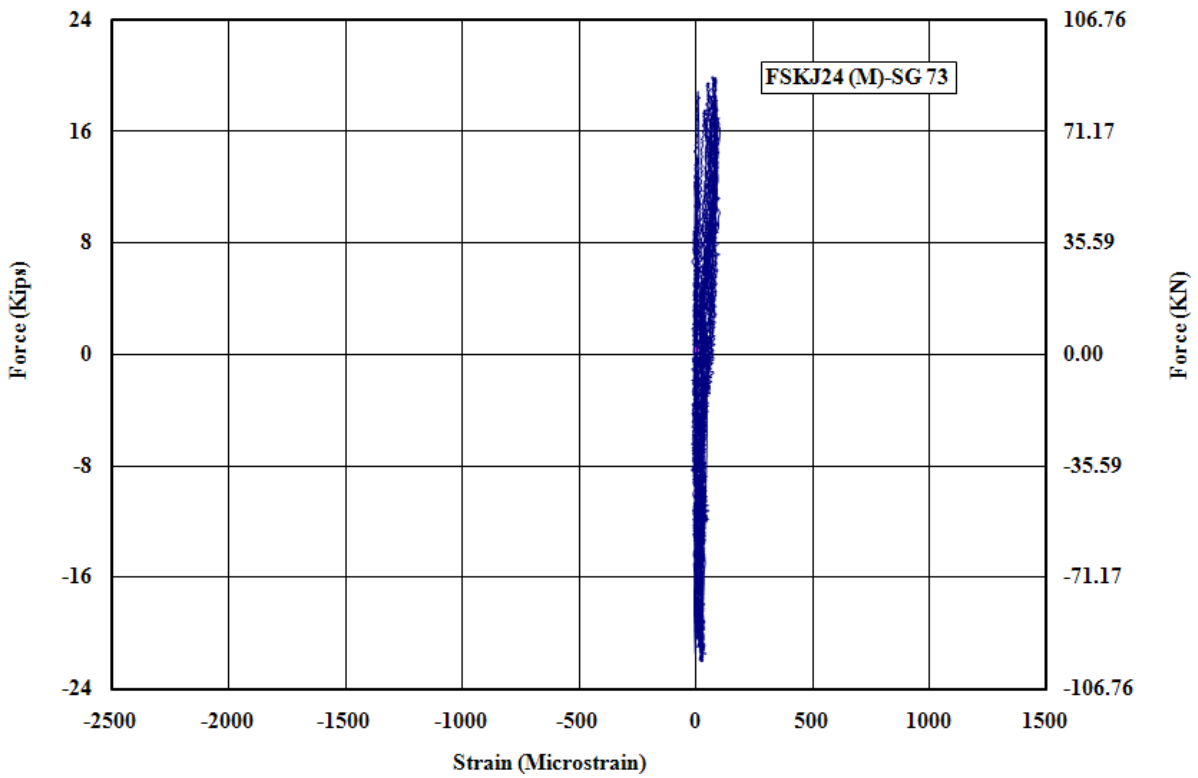

Figure H - 59: Measured Strain in Gauge No.73 for FSKJ24-M

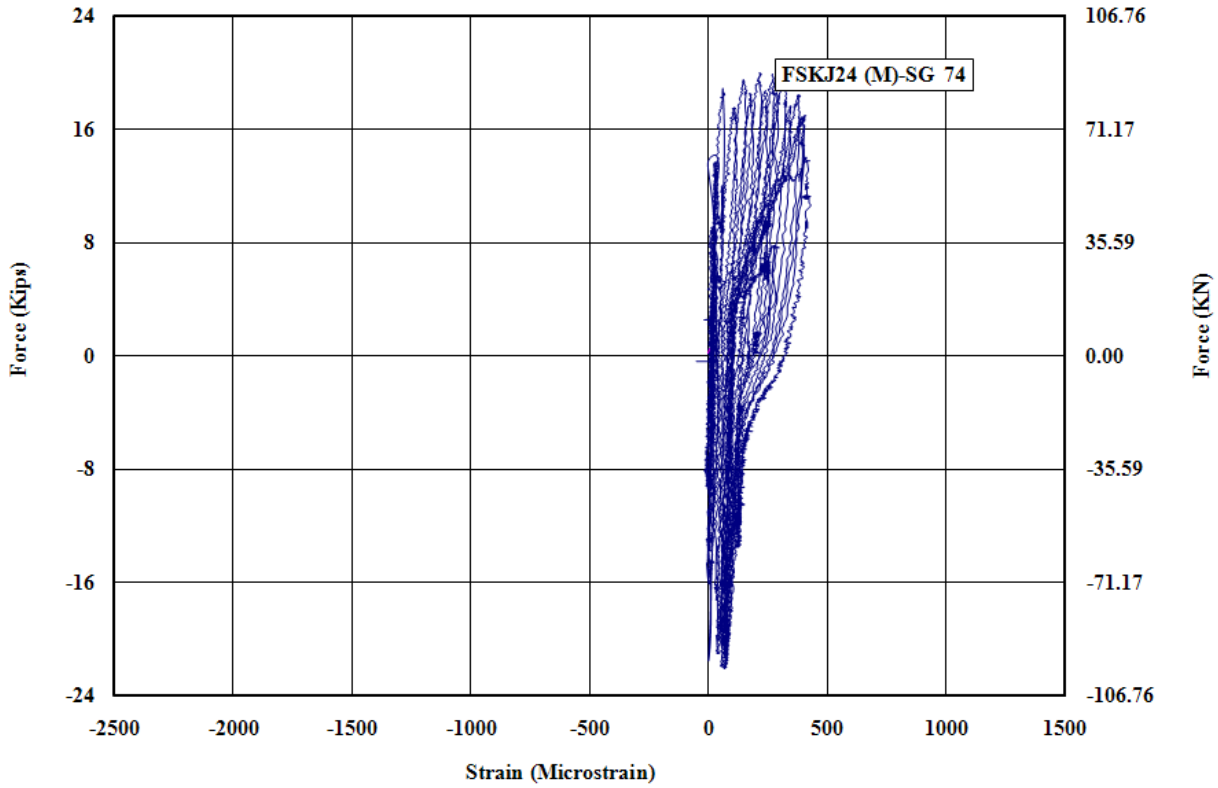

Figure H - 60: Measured Strain in Gauge No.74 for FSKJ24-M

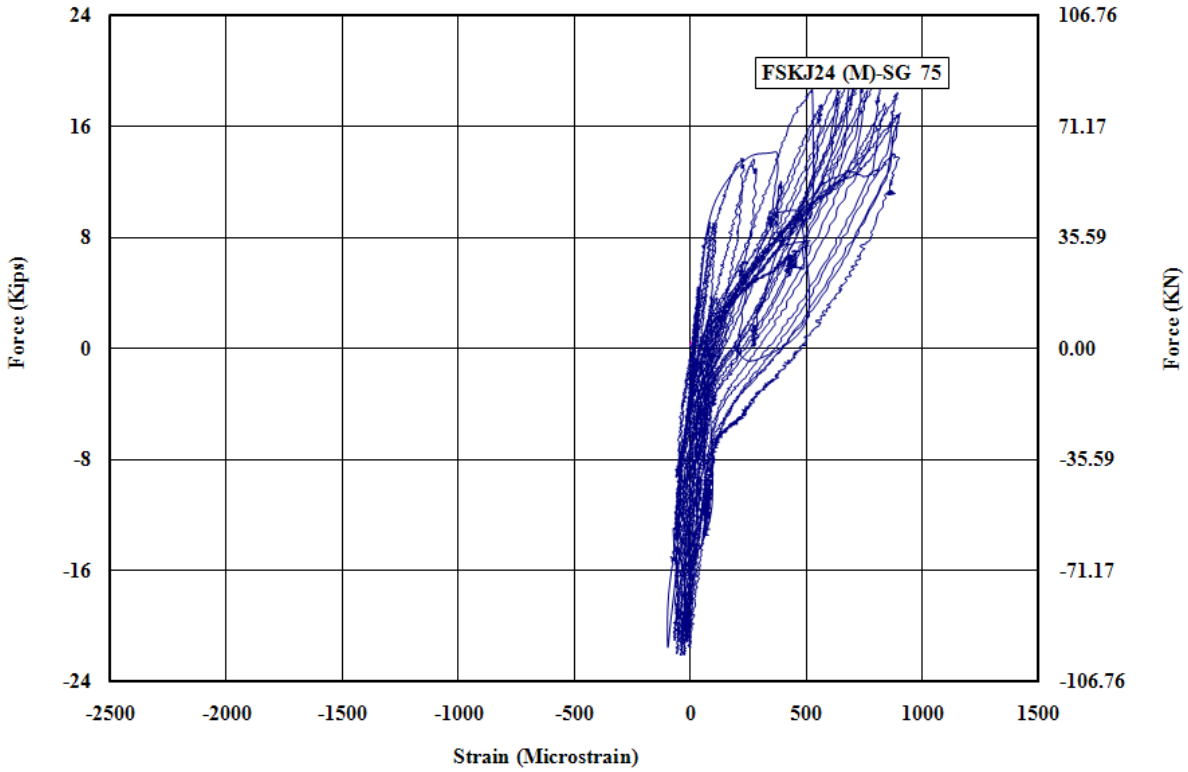

Figure H - 61: Measured Strain in Gauge No.75 for FSKJ24-M

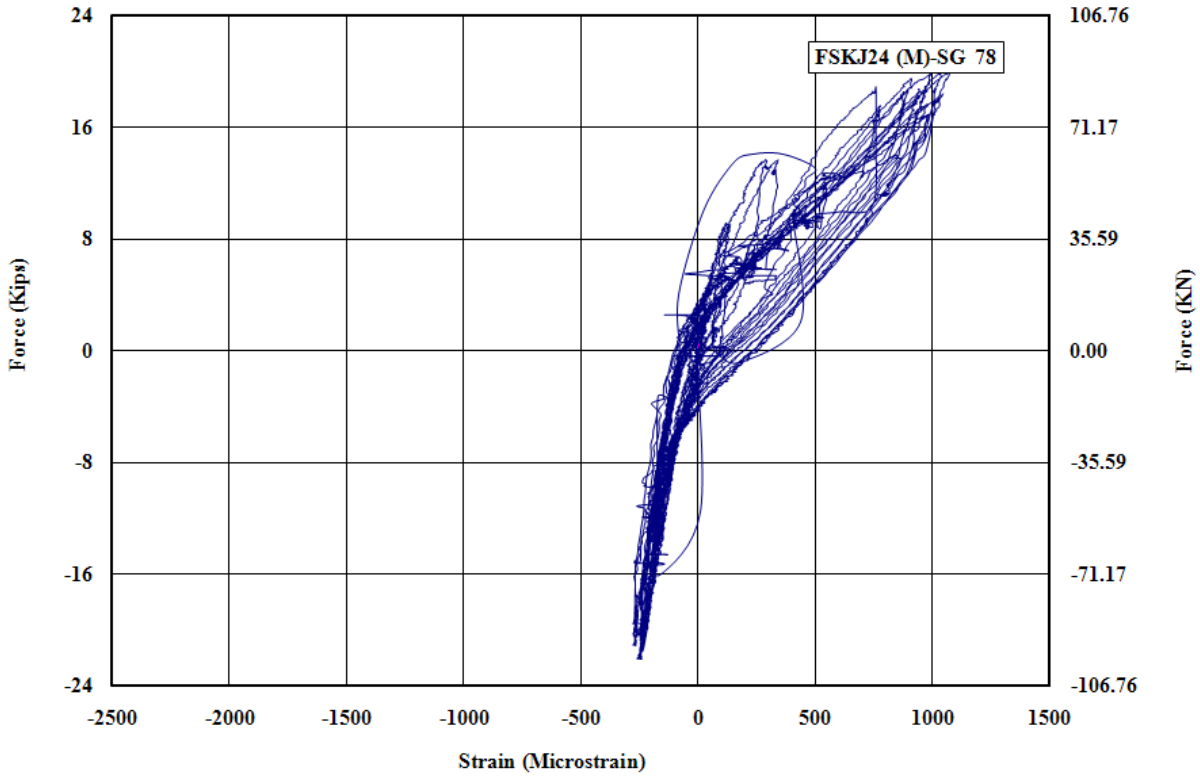

Figure H - 62: Measured Strain in Gauge No.78 for FSKJ24-M

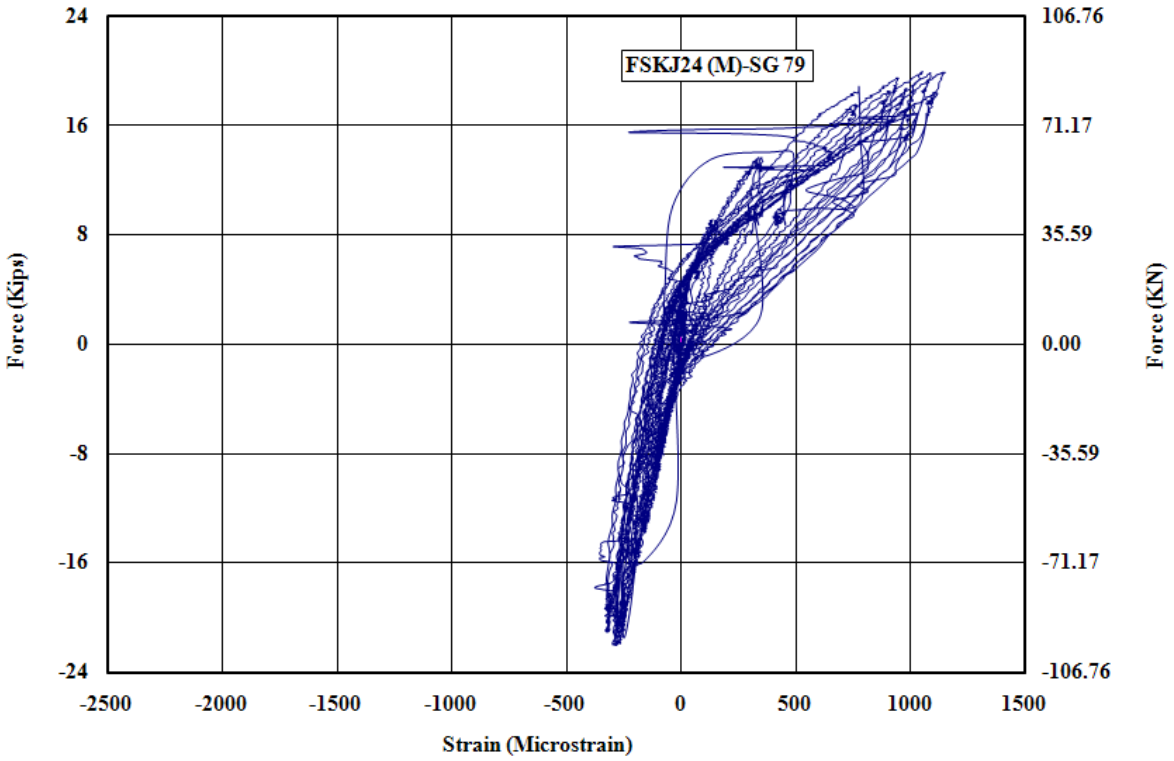

Figure H - 63: Measured Strain in Gauge No.79 for FSKJ24-M

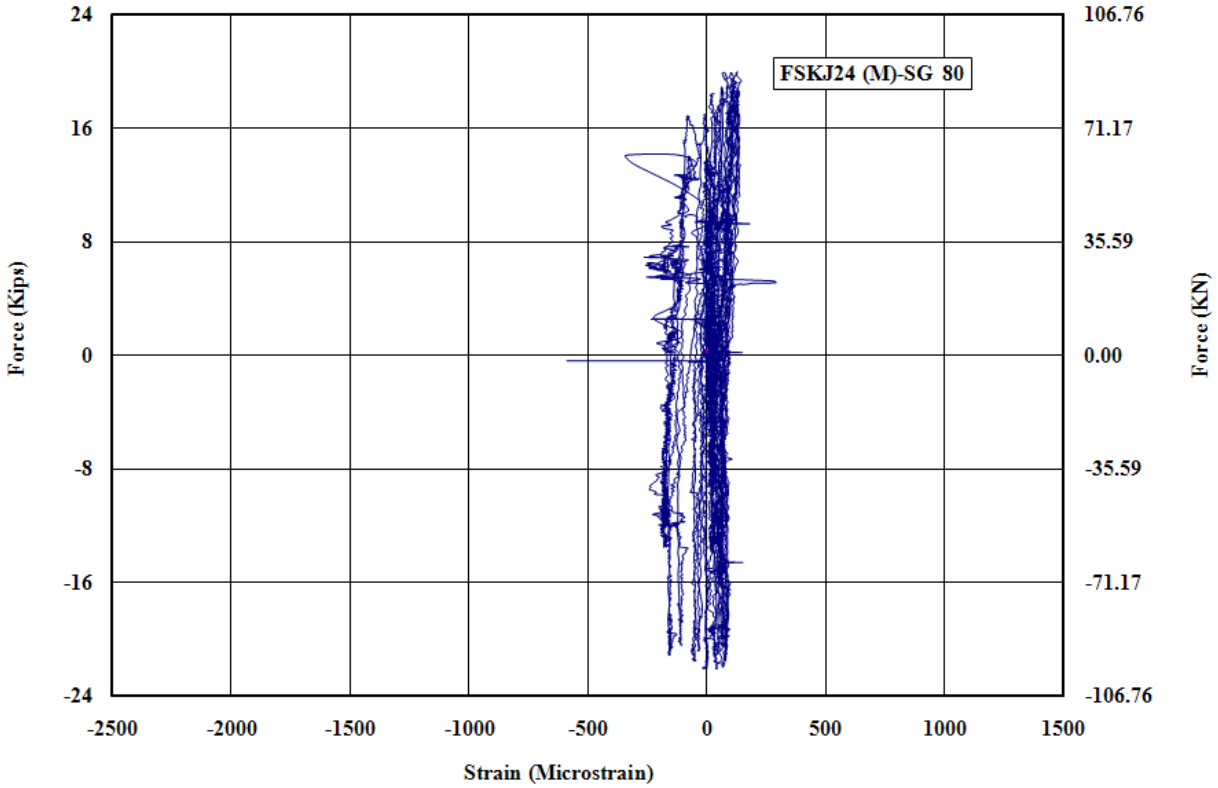

Figure H - 64: Measured Strain in Gauge No.80 for FSKJ24-M

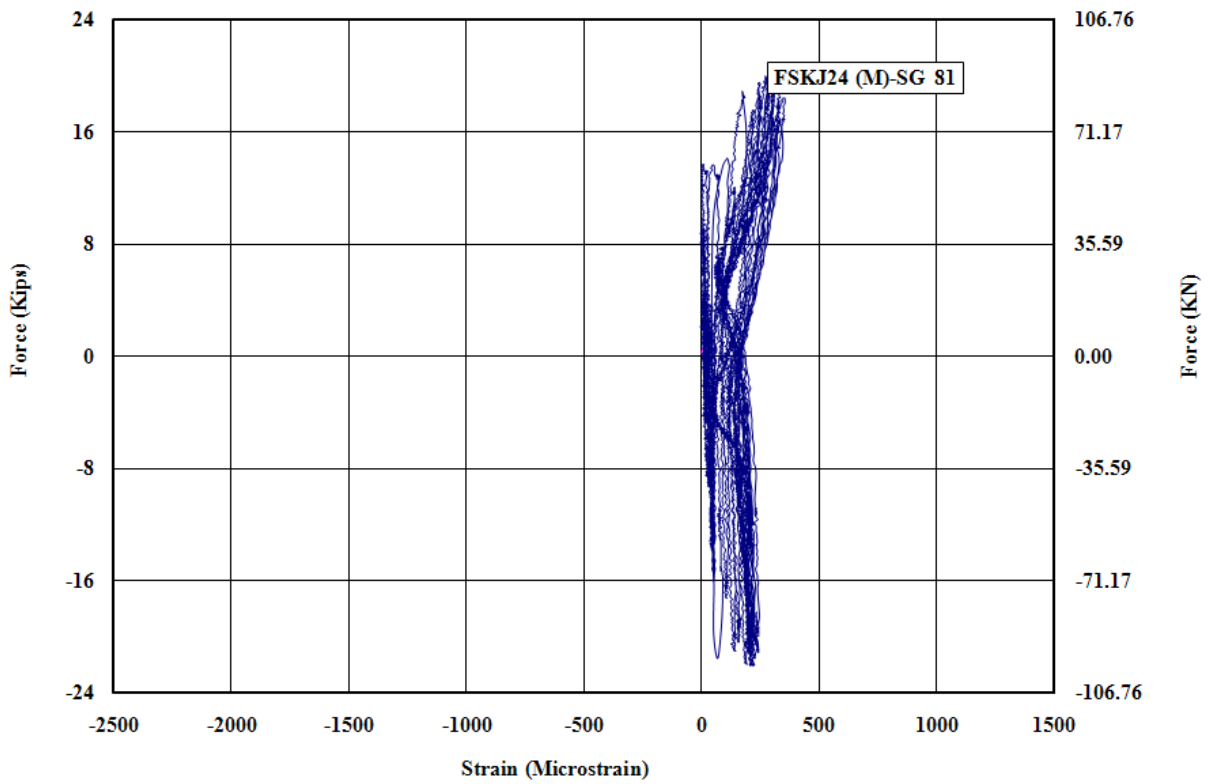

Figure H - 65: Measured Strain in Gauge No.81 for FSKJ24-M

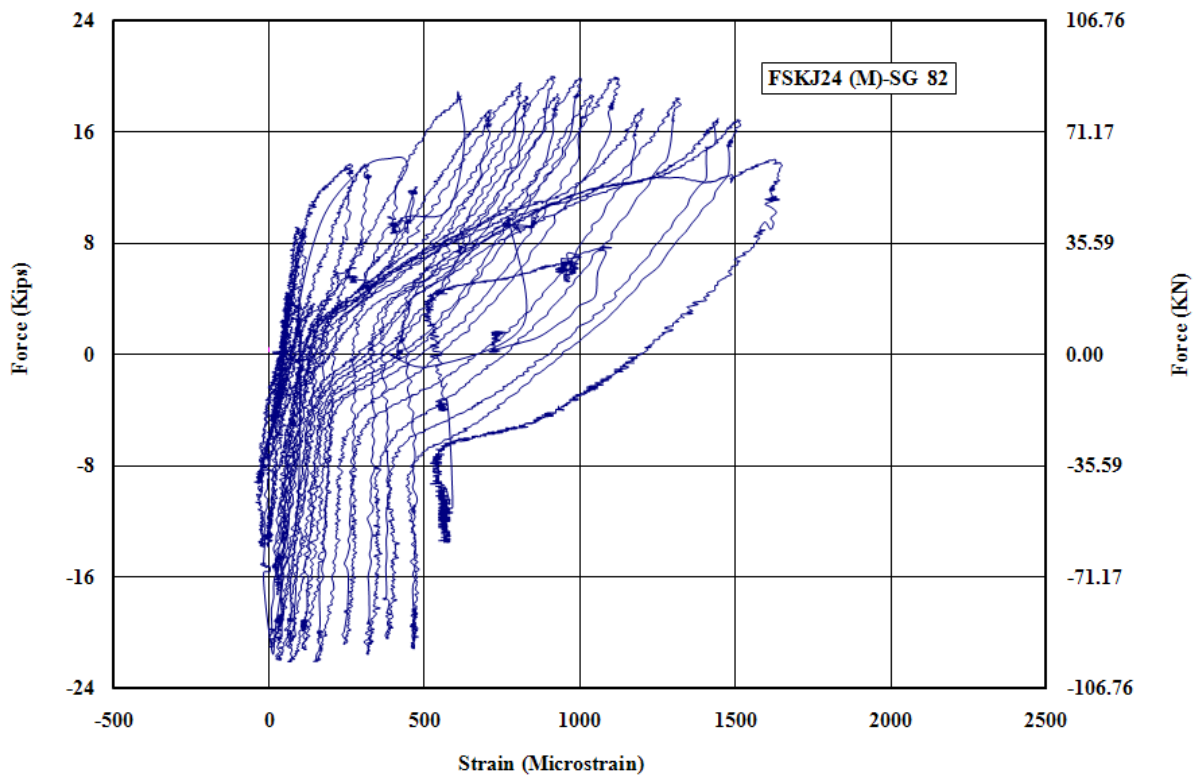

Figure H - 66: Measured Strain in Gauge No.82 for FSKJ24-M

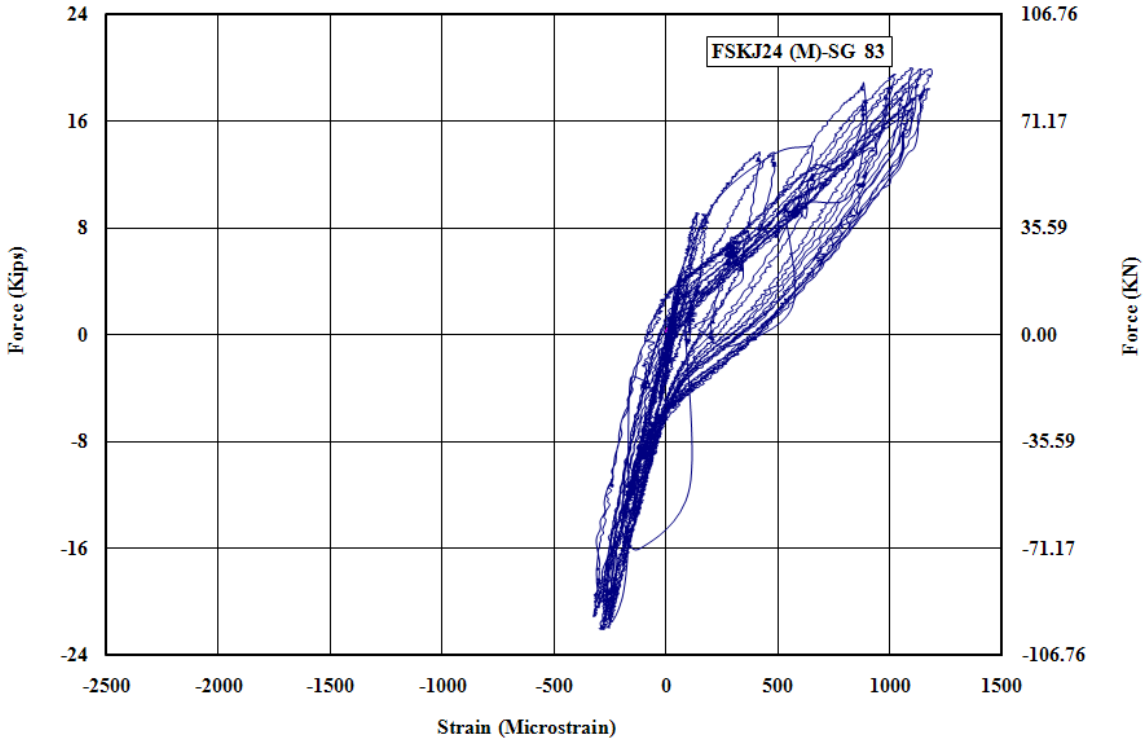

Figure H - 67: Measured Strain in Gauge No.83 for FSKJ24-M

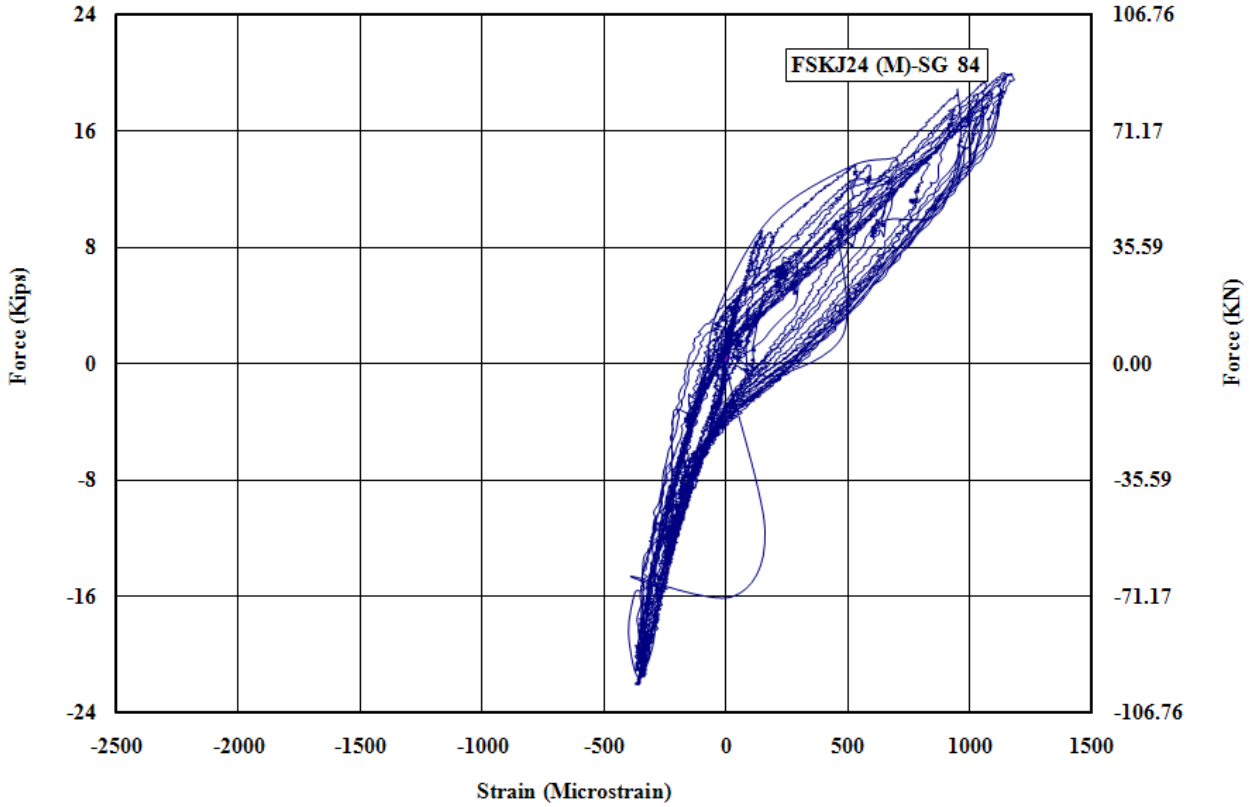

Figure H - 68: Measured Strain in Gauge No.84 for FSKJ24-M

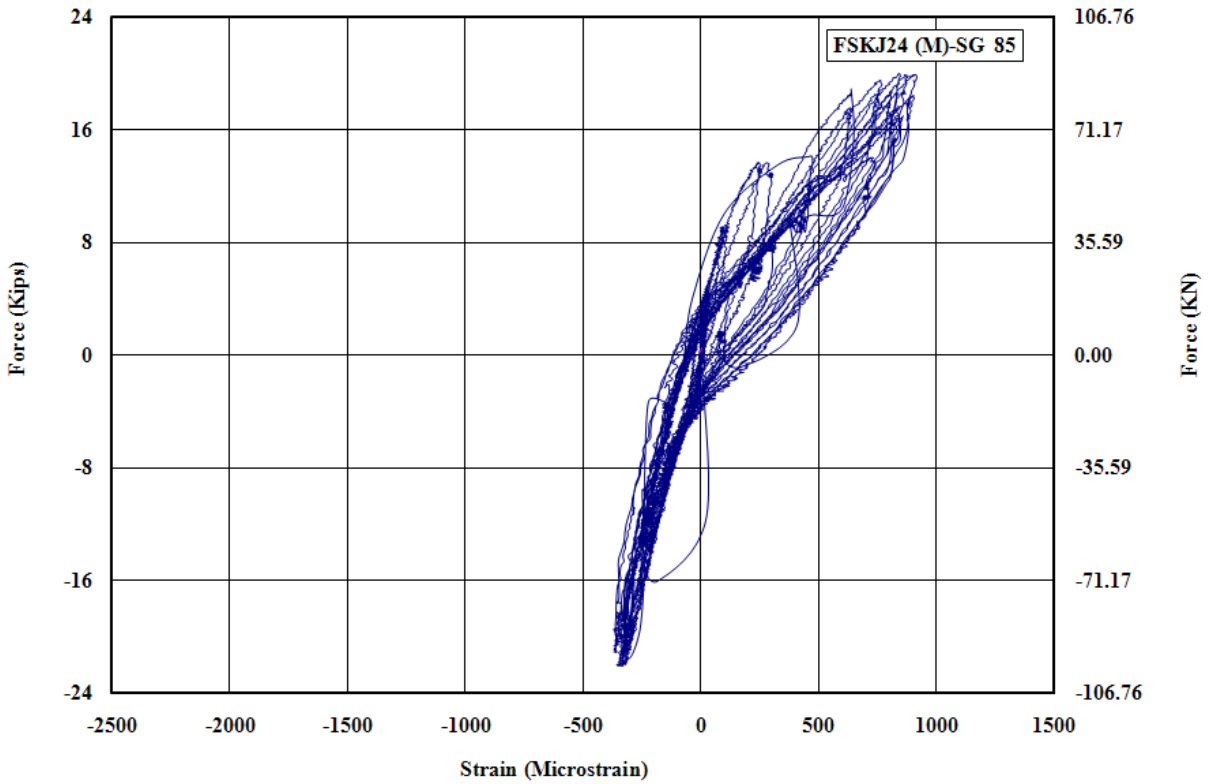

Figure H - 69: Measured Strain in Gauge No.85 for FSKJ24-M

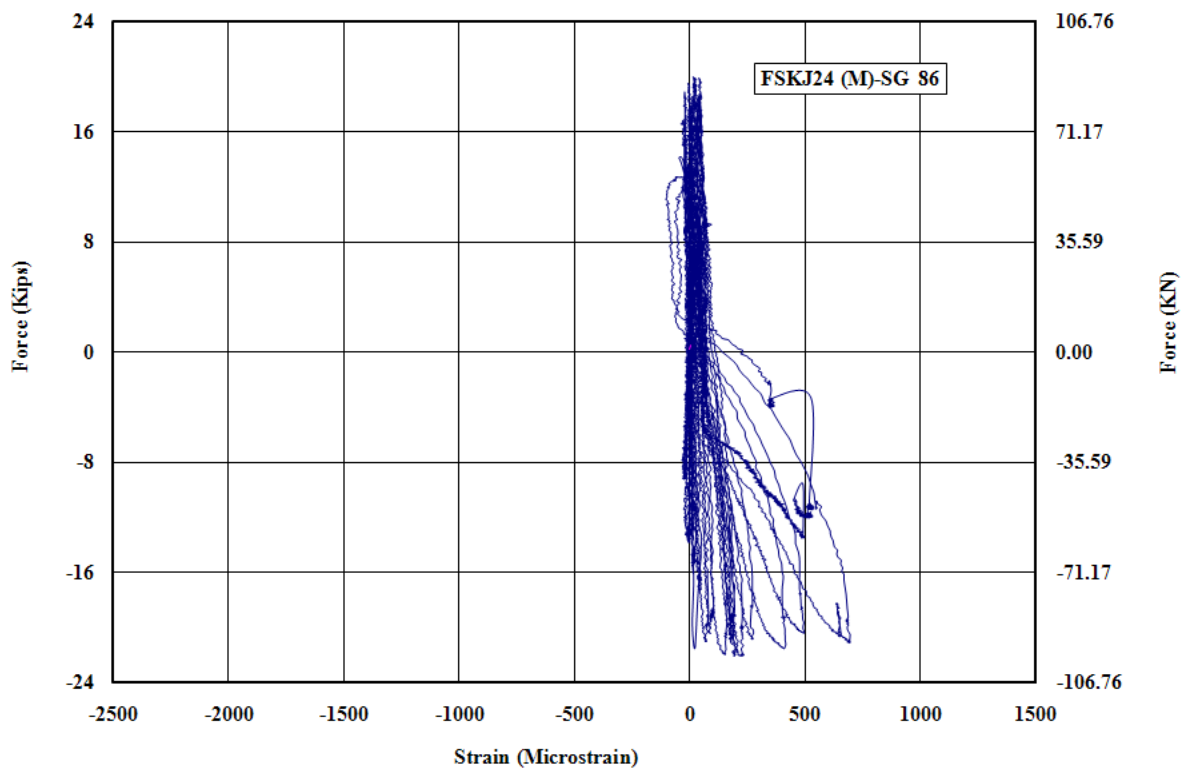

Figure H - 70: Measured Strain in Gauge No.86 for FSKJ24-M

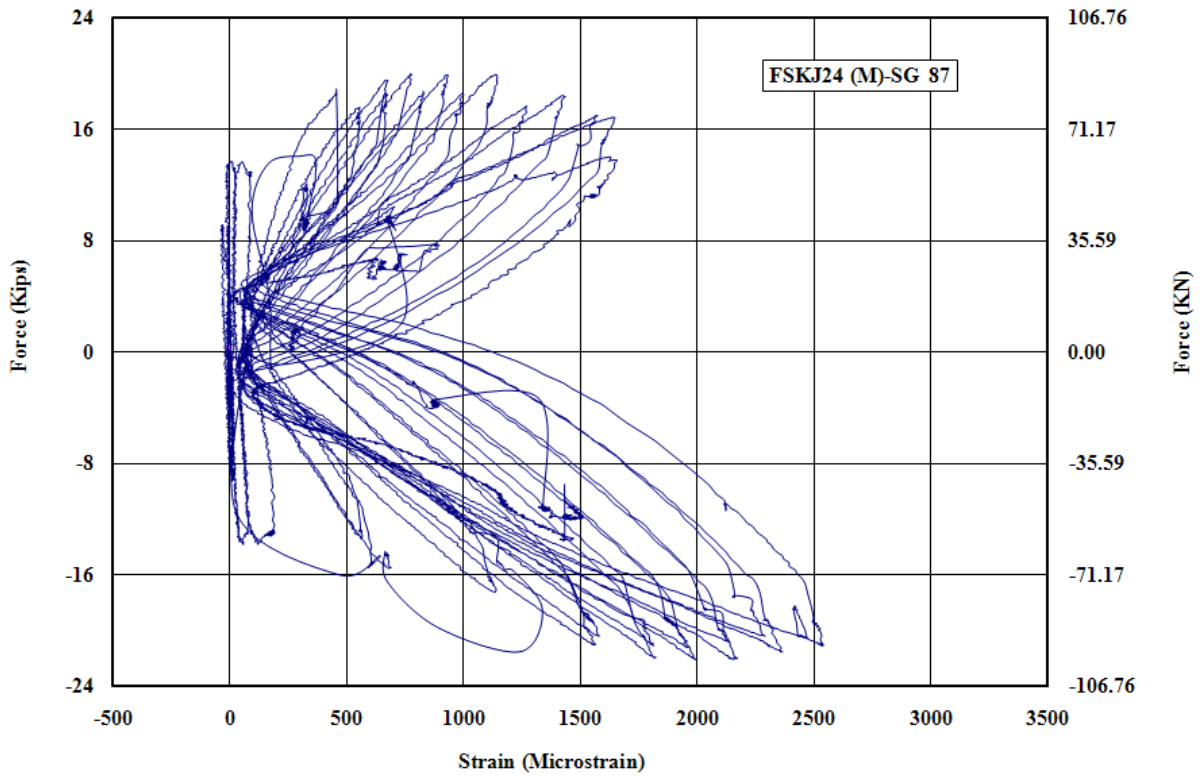

Figure H - 71: Measured Strain in Gauge No.87 for FSKJ24-M

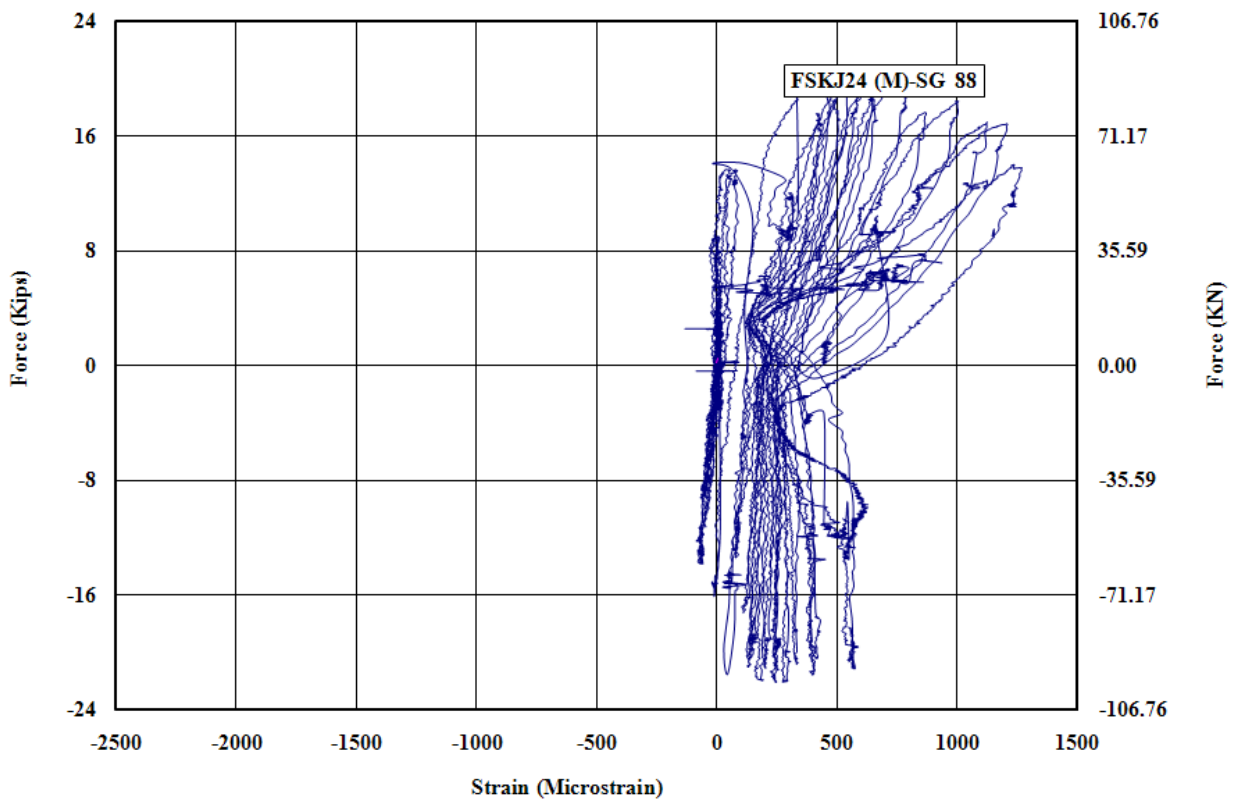

Figure H - 72: Measured Strain in Gauge No.88 for FSKJ24-M

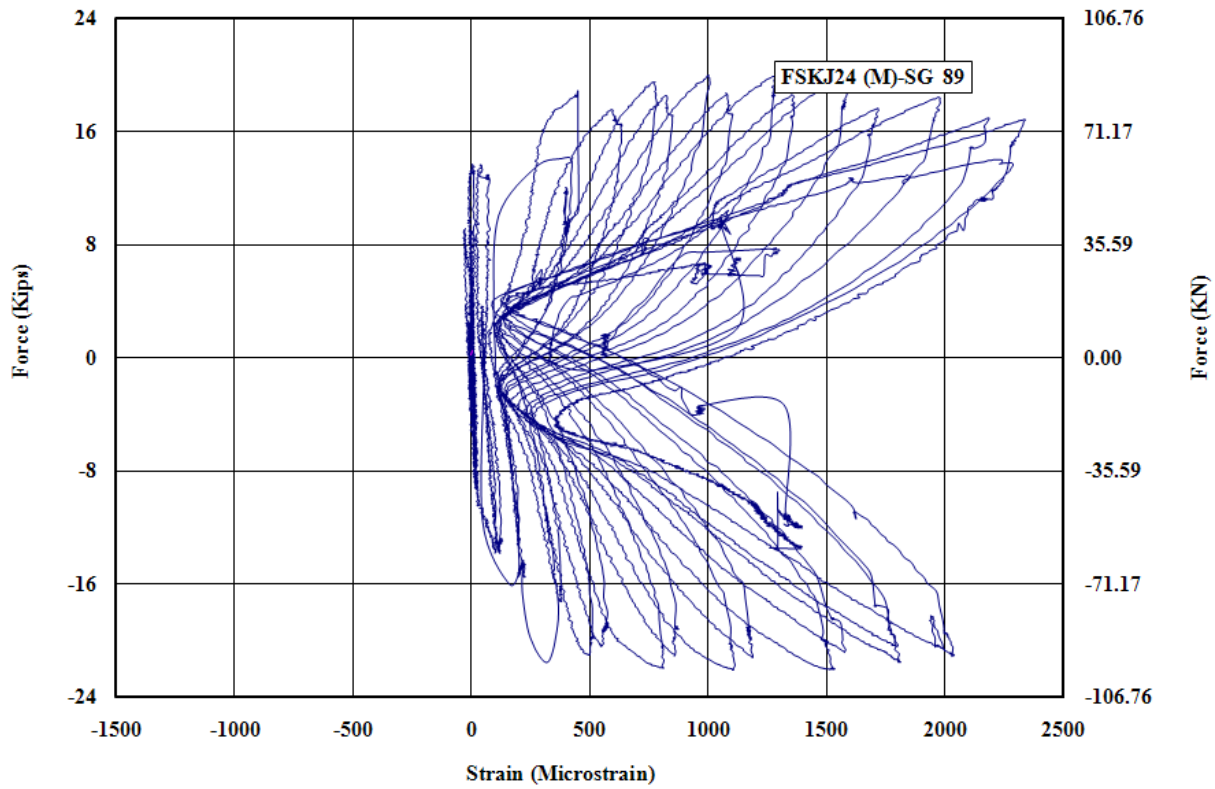

Figure H - 73: Measured Strain in Gauge No.89 for FSKJ24-M

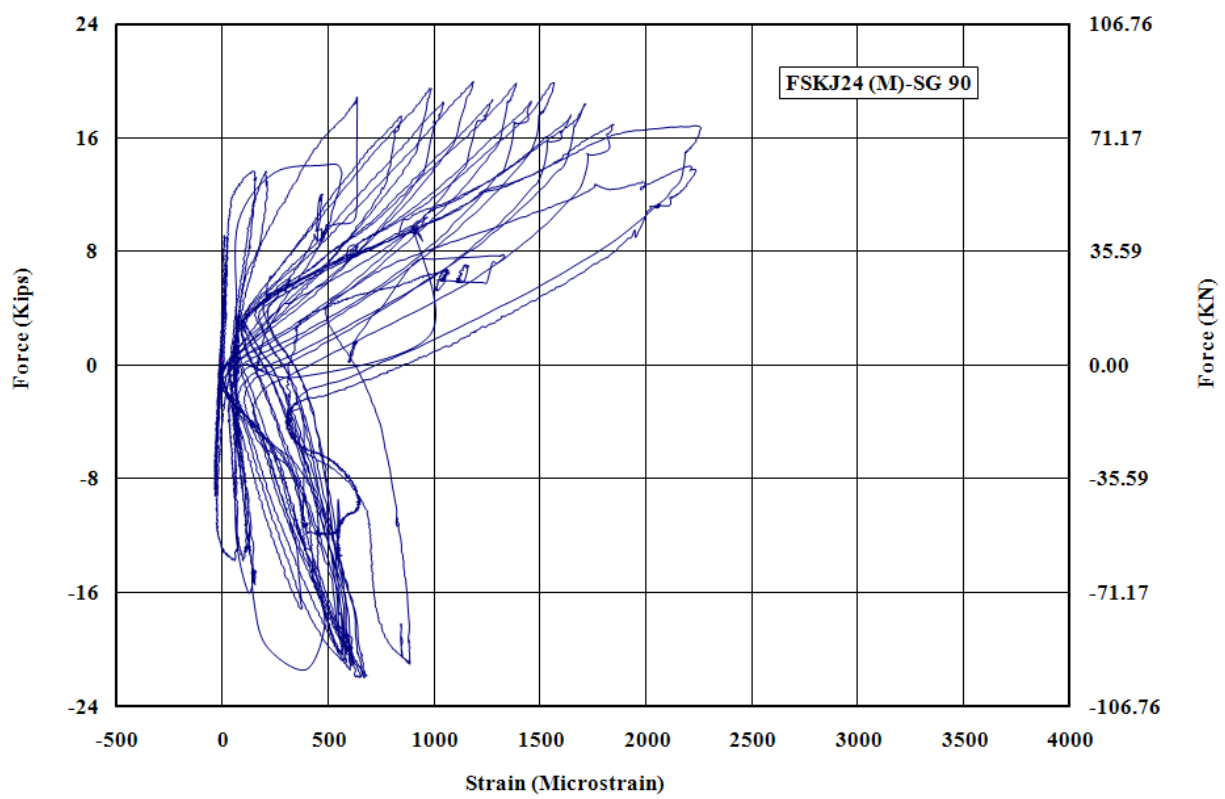

Figure H - 74: Measured Strain in Gauge No.90 for FSKJ24-M

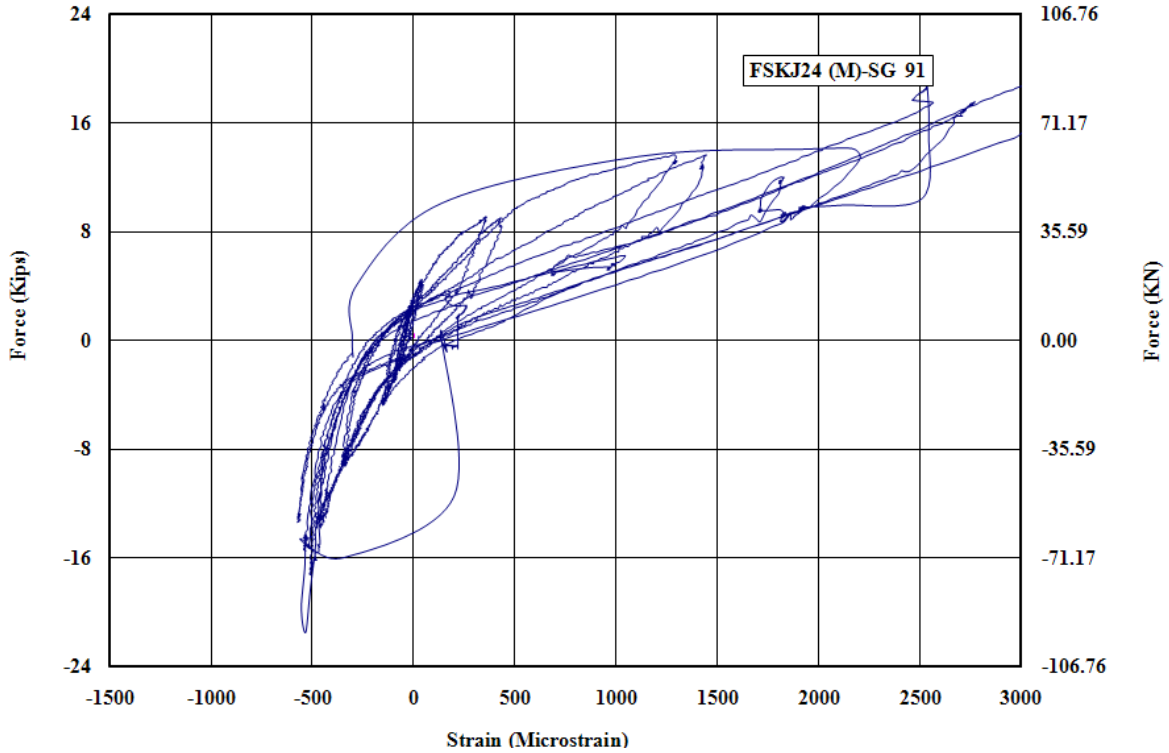

Figure H - 75: Measured Strain in Gauge No.91 for FSKJ24-M

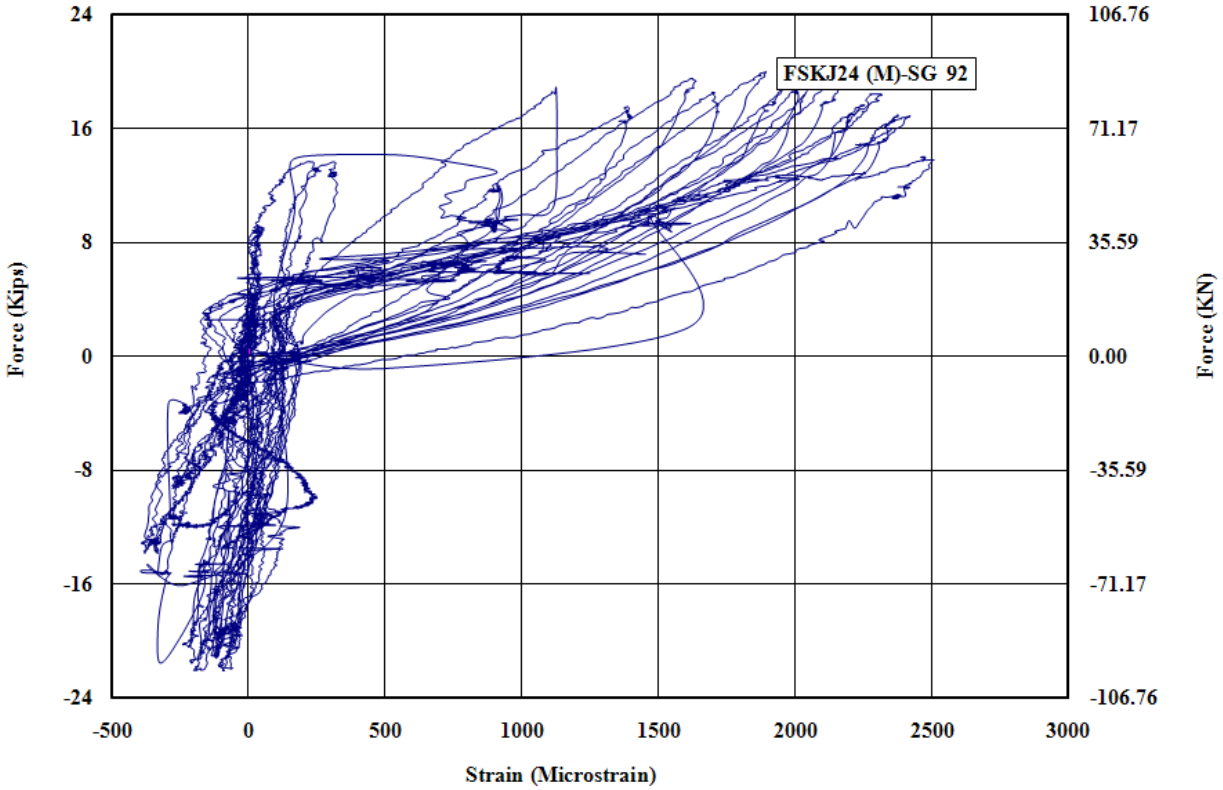

Figure H - 76: Measured Strain in Gauge No.92 for FSKJ24-M

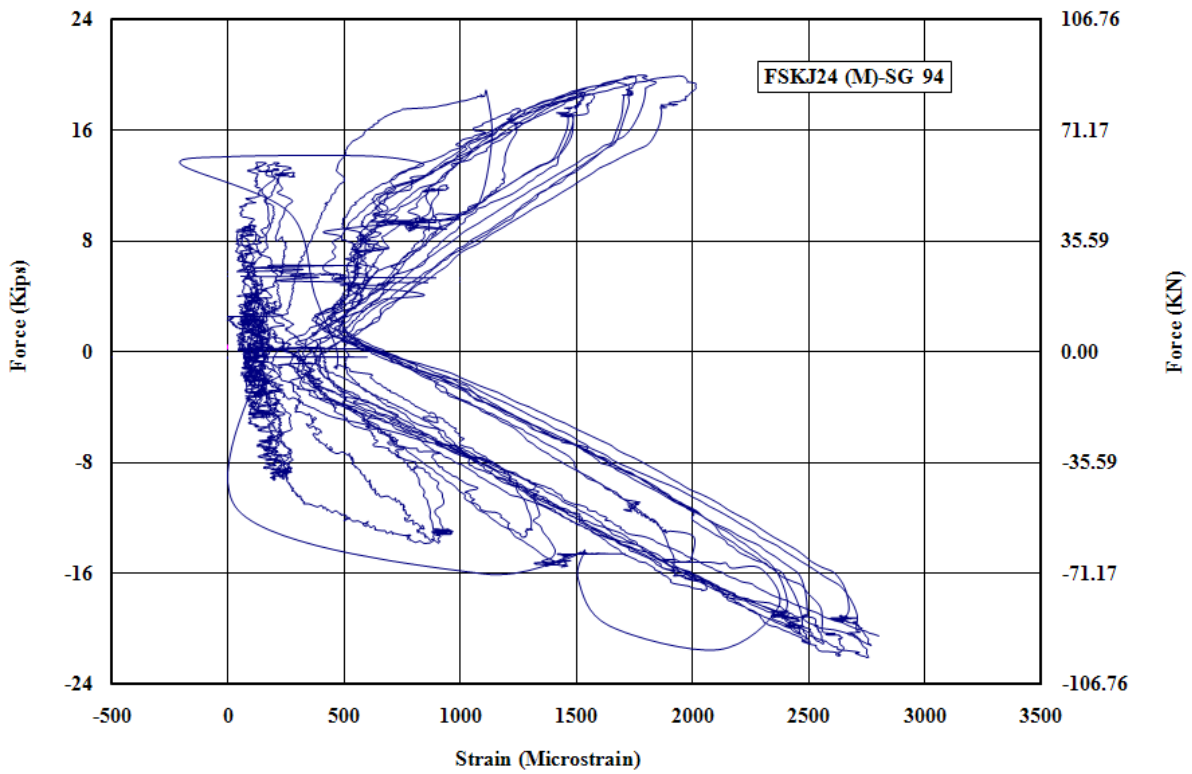

Figure H - 77: Measured Strain in Gauge No.94 for FSKJ24-M

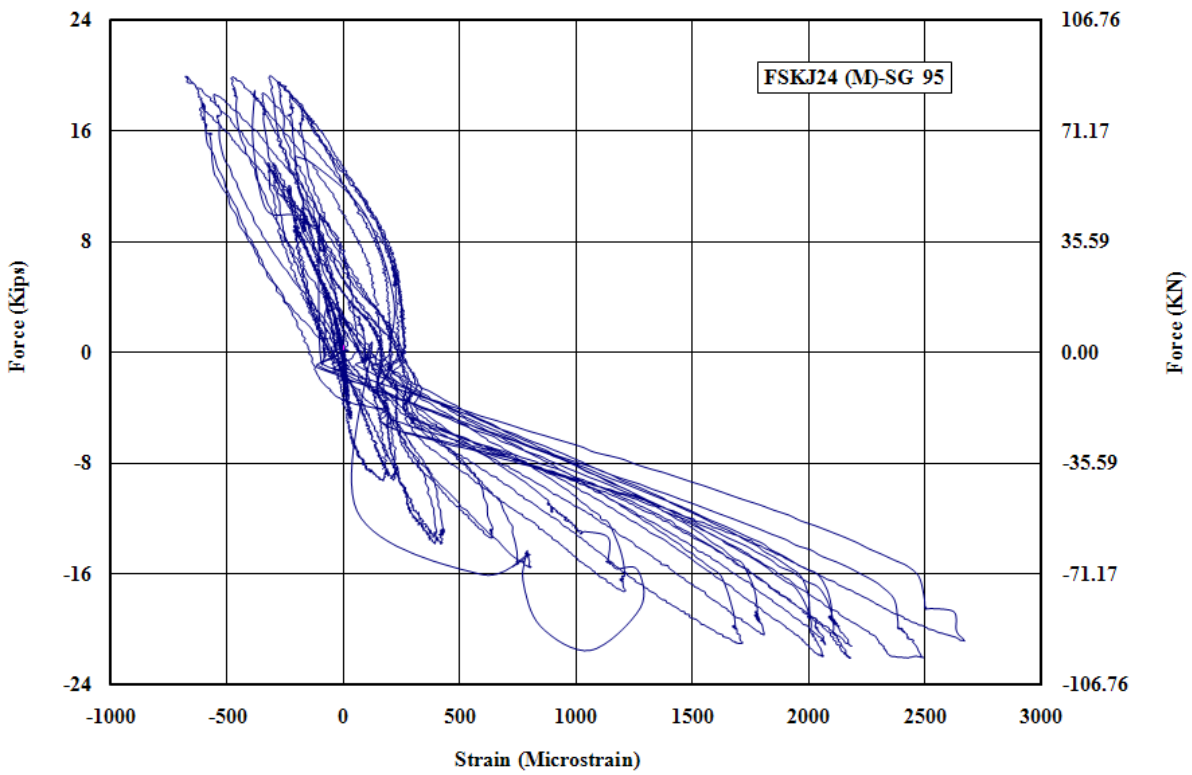

Figure H - 78: Measured Strain in Gauge No.95 for FSKJ24-M

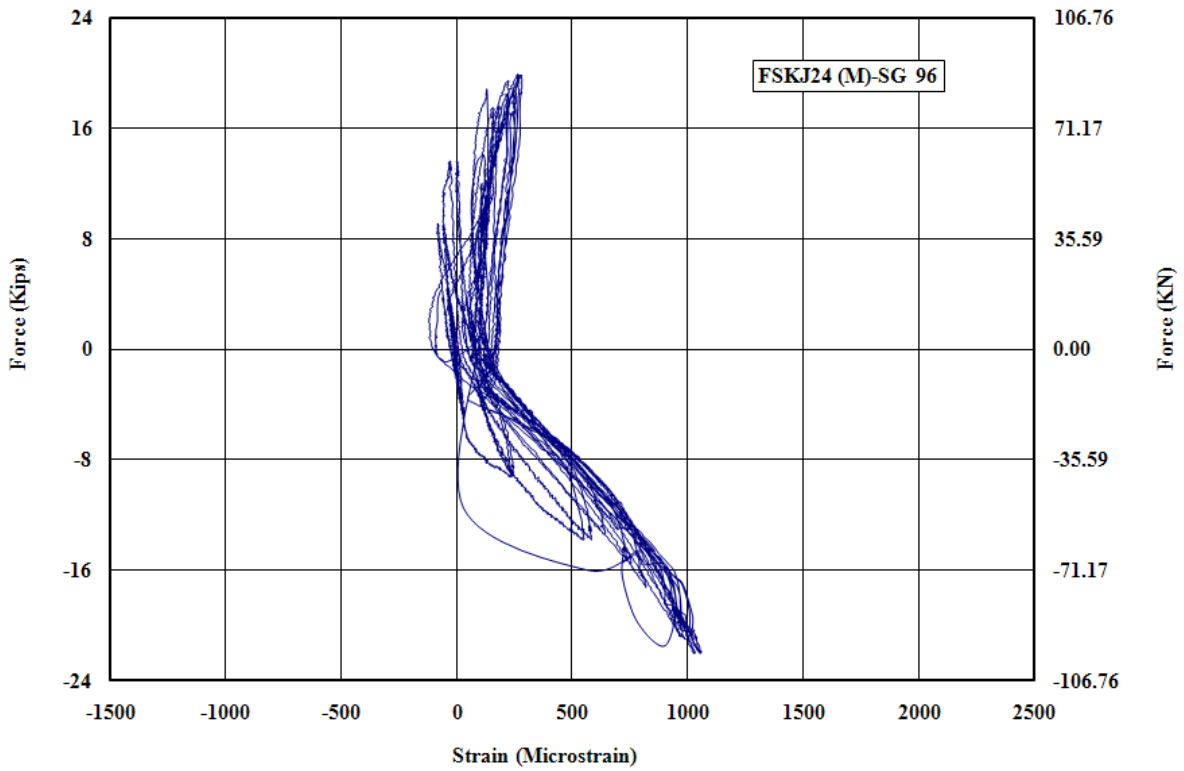

Figure H - 79: Measured Strain in Gauge No.96 for FSKJ24-M

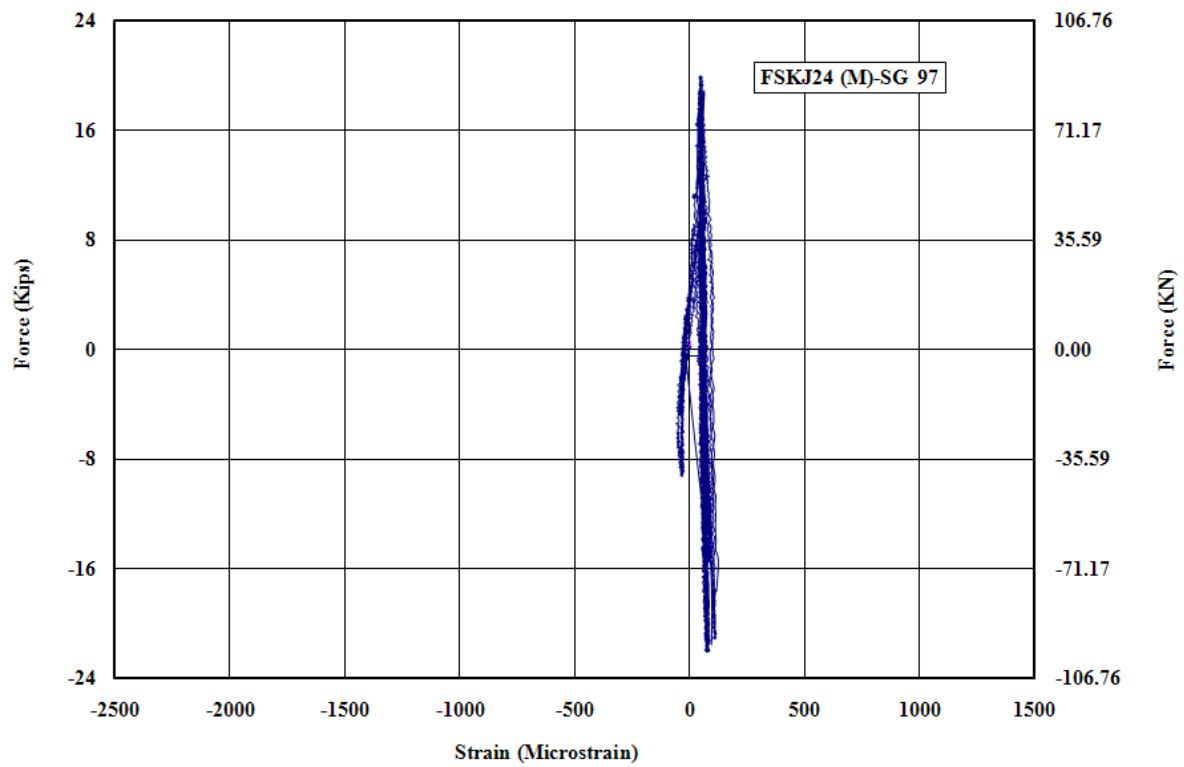

Figure H - 80: Measured Strain in Gauge No.97 for FSKJ24-M

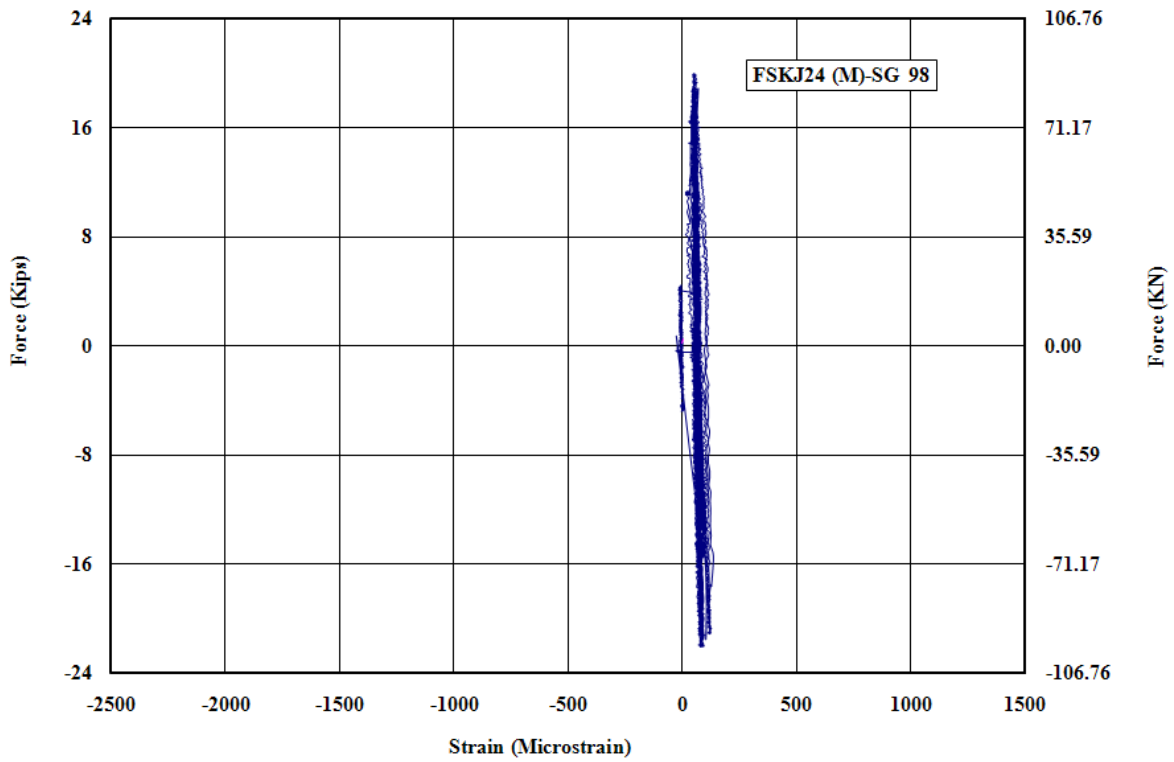

Figure H - 81: Measured Strain in Gauge No.98 for FSKJ24-M

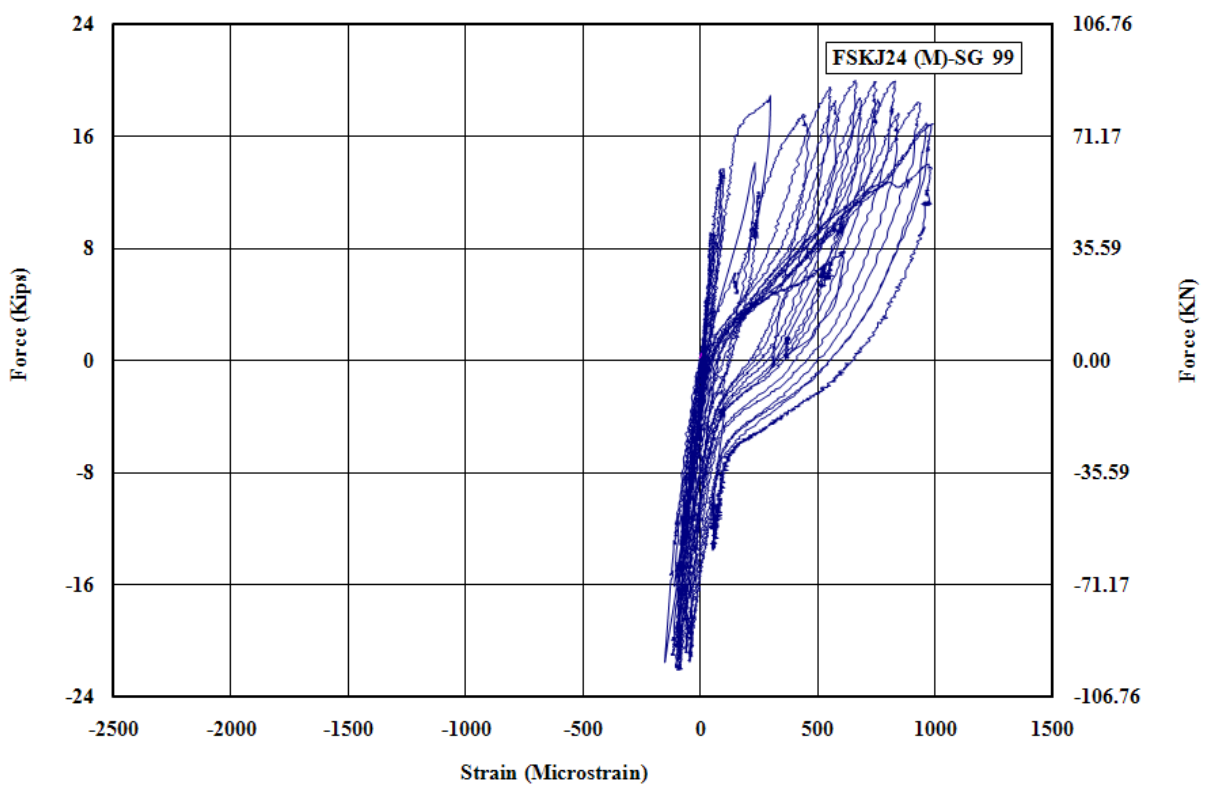

Figure H - 82: Measured Strain in Gauge No.99 for FSKJ24-M

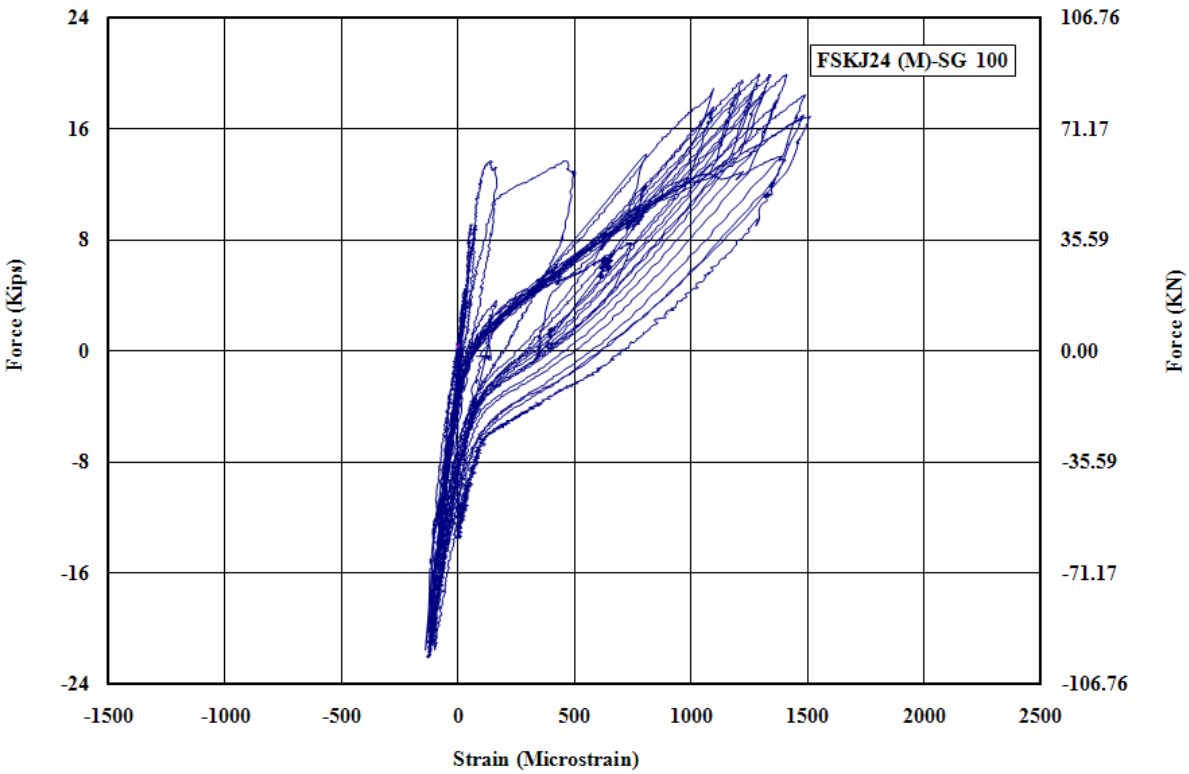

Figure H - 83: Measured Strain in Gauge No.100 for FSKJ24-M

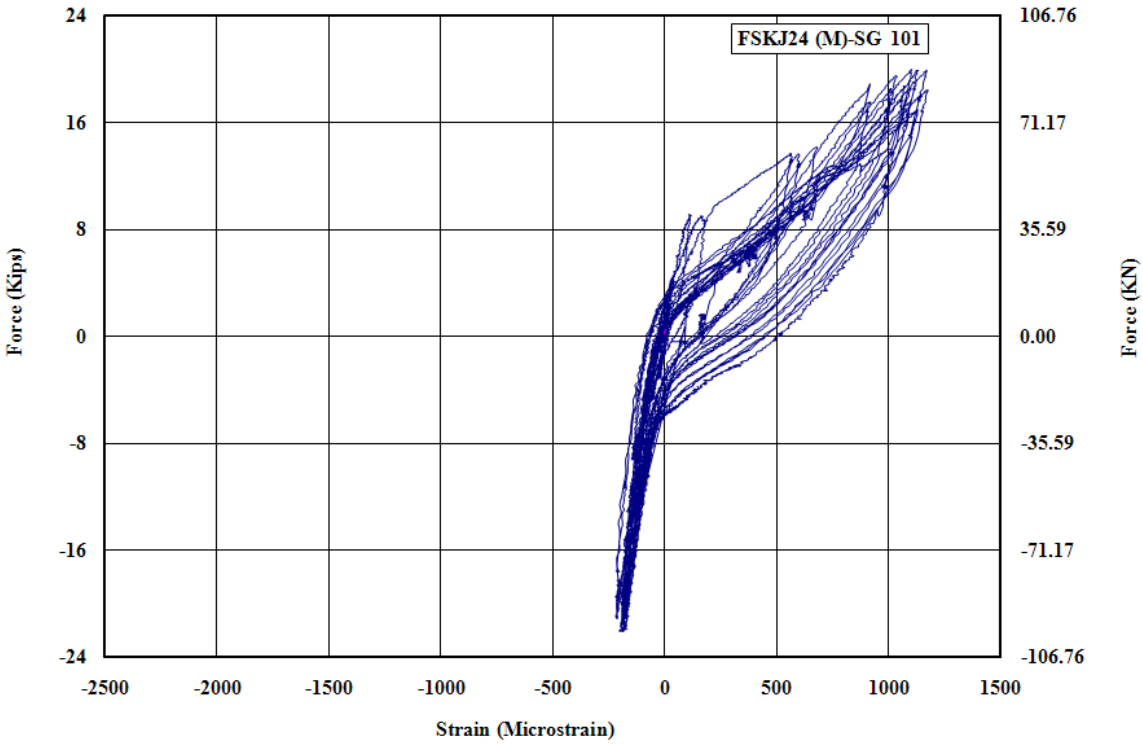

Figure H - 84: Measured Strain in Gauge No.101 for FSKJ24-M

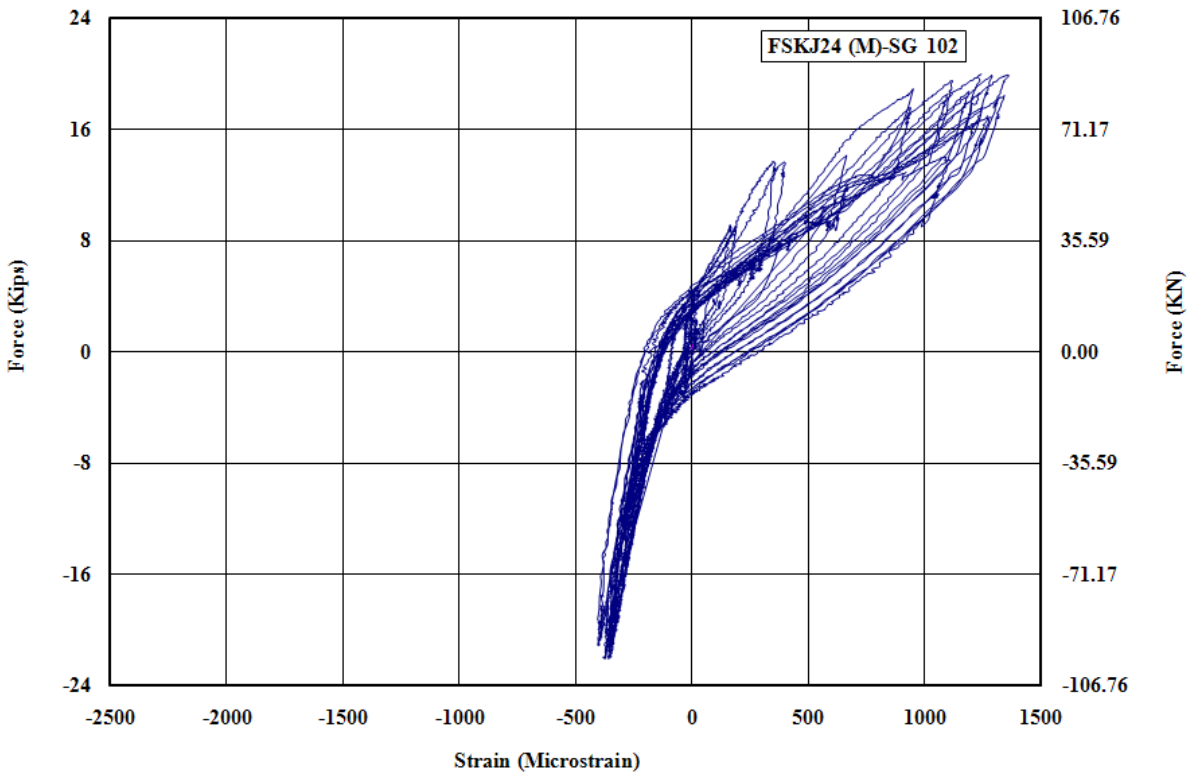

Figure H - 85: Measured Strain in Gauge No.1 02for FSKJ24-M

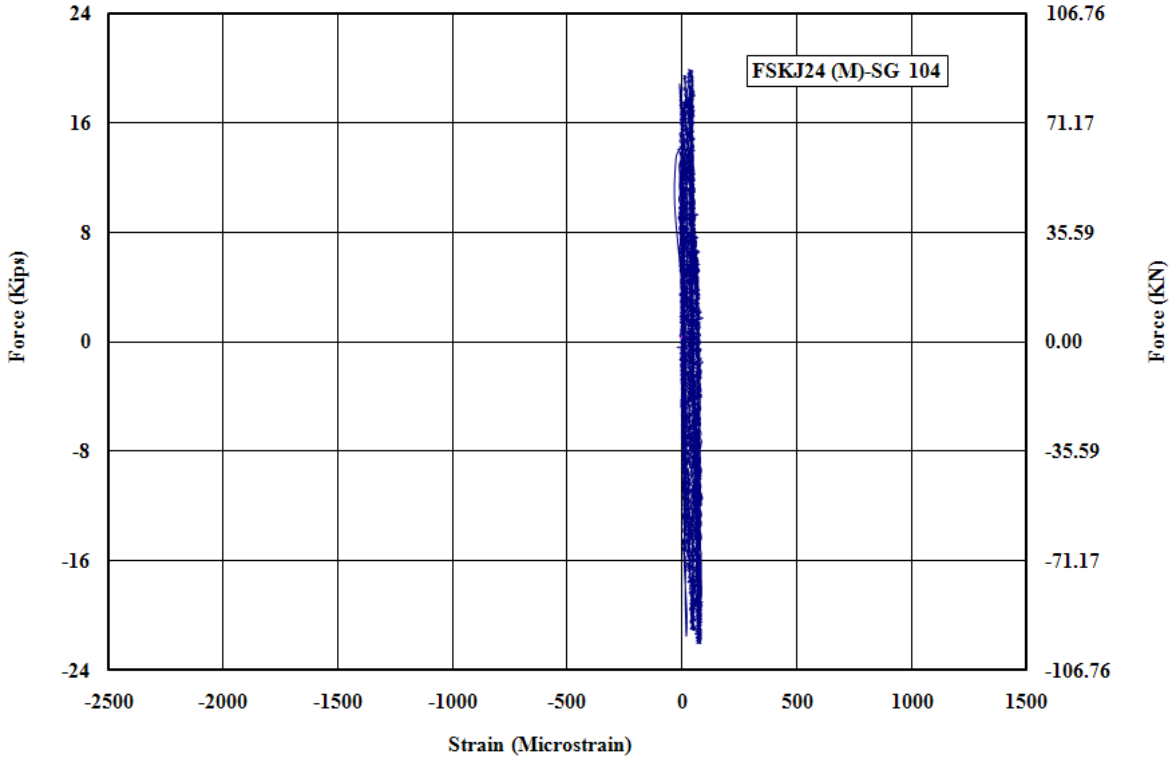

Figure H - 86: Measured Strain in Gauge No.104 for FSKJ24-M

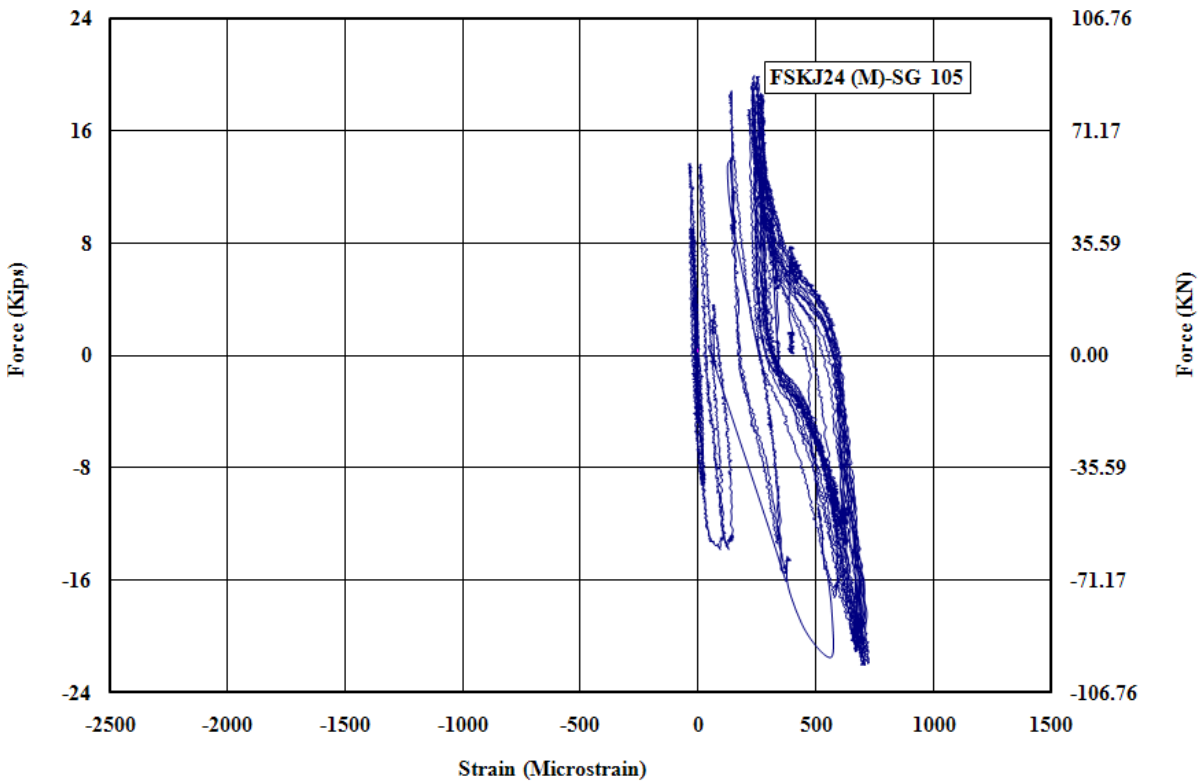

Figure H - 87: Measured Strain in Gauge No.105 for FSKJ24-M

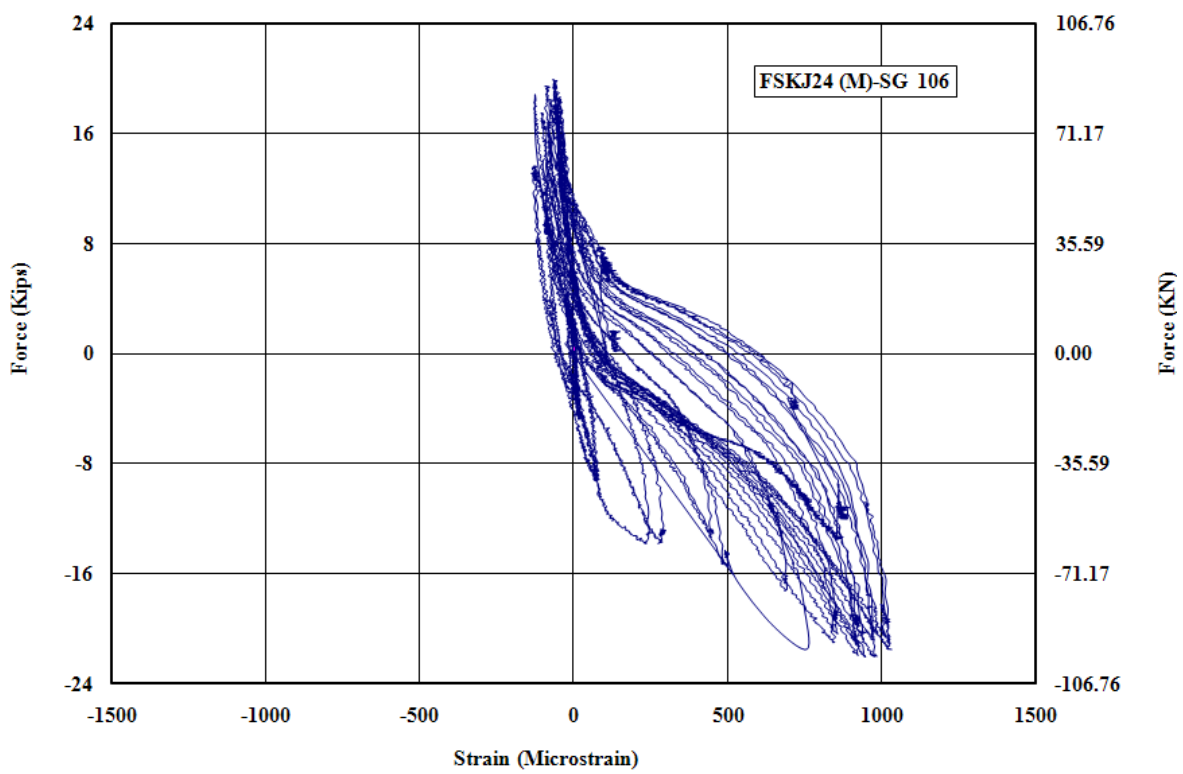

Figure H - 88: Measured Strain in Gauge No.106 for FSKJ24-M

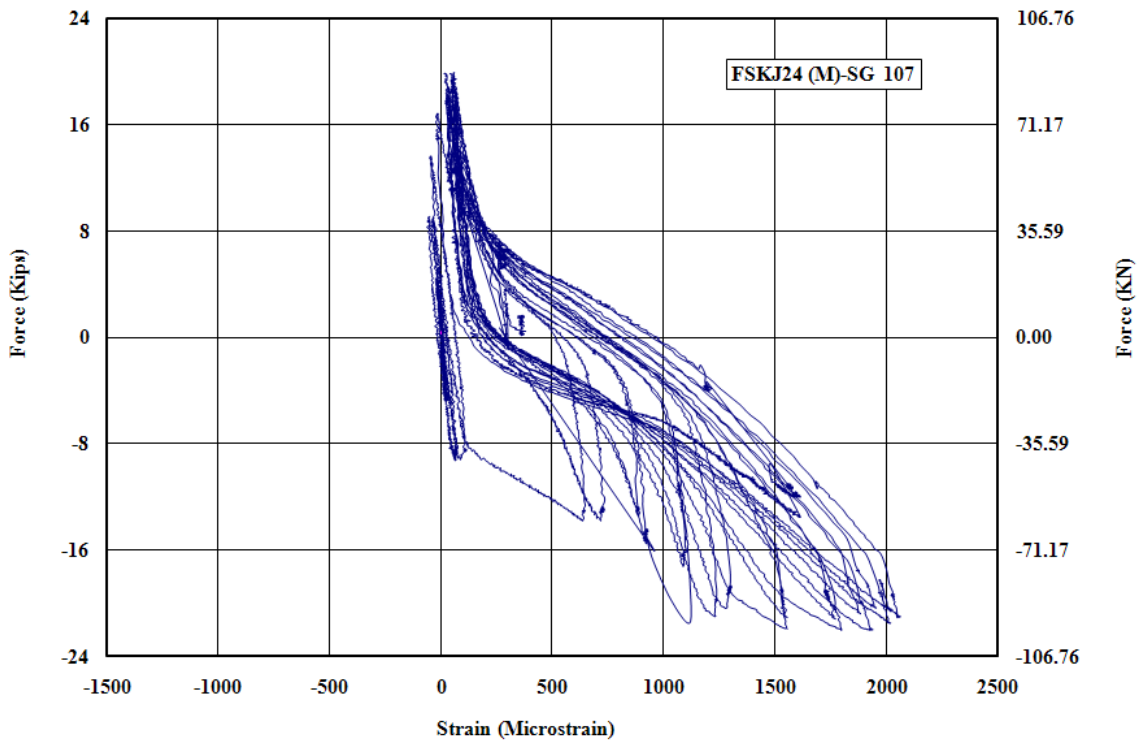

Figure H - 89: Measured Strain in Gauge No.107 for FSKJ24-M

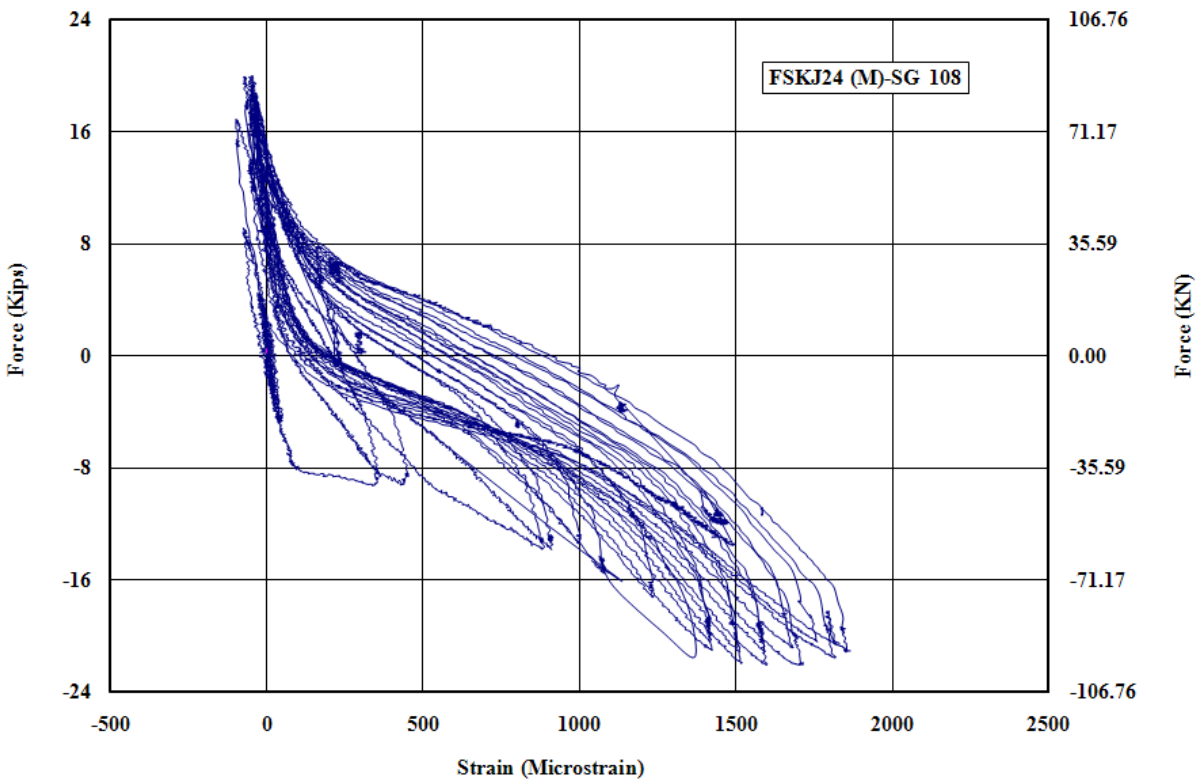

Figure H - 90: Measured Strain in Gauge No.108 for FSKJ24-M

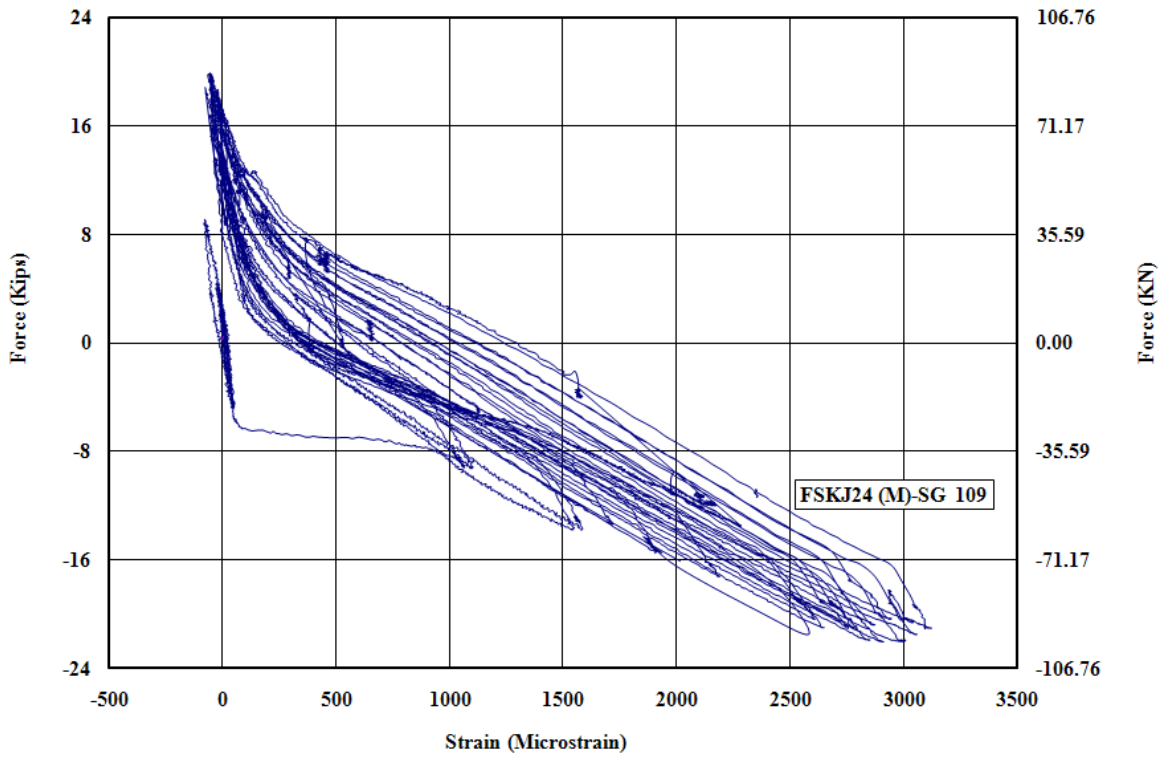

Figure H - 91: Measured Strain in Gauge No.109 for FSKJ24-M

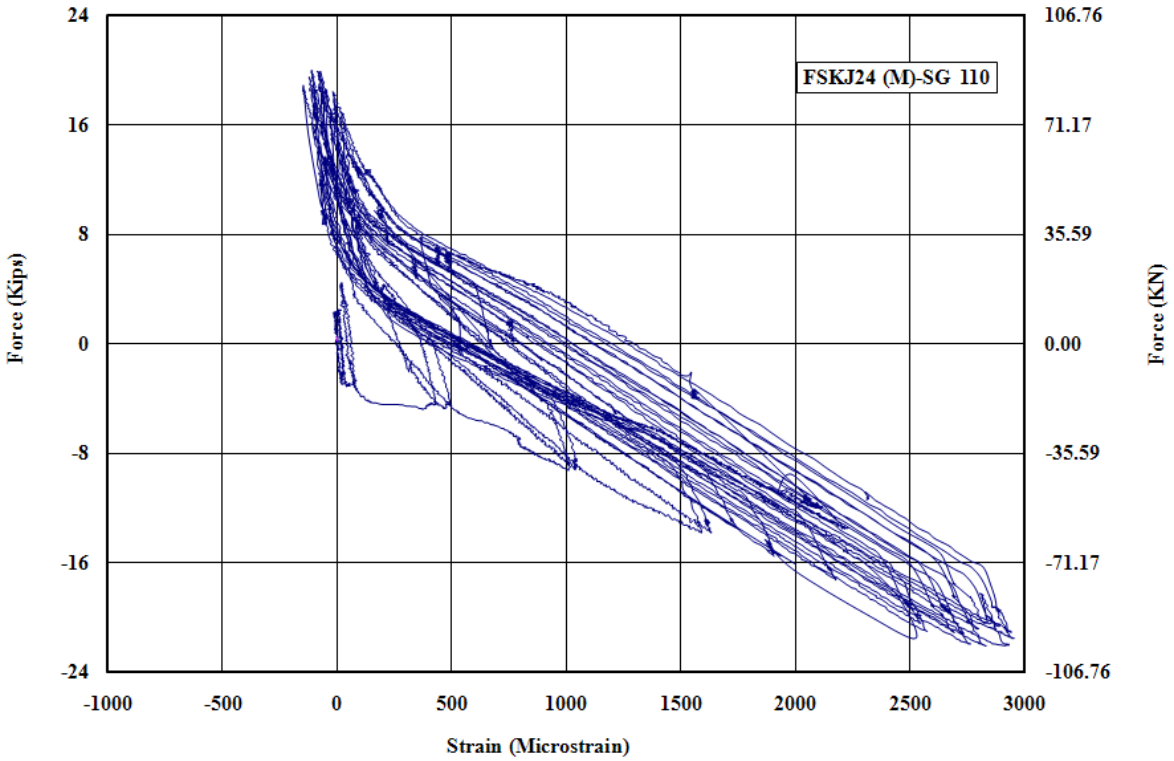

Figure H - 92: Measured Strain in Gauge No.110 for FSKJ24-M

LIST OF CCEER PUBLICATIONS

Report No.	Publication
CCEER-84-1	Saiidi, M., and R. Lawver, "User's Manual for LZAK-C64, A Computer Program to Implement the Q-Model on Commodore 64," Civil Engineering Department, Report No. CCEER-84-1, University of Nevada, Reno, January 1984.
CCEER-84-1 Reprint	Douglas, B., Norris, G., Saiidi, M., Dodd, L., Richardson, J. and Reid, W., "Simple Bridge Models for Earthquakes and Test Data," Civil Engineering Department, Report No. CCEER-84-1 Reprint, University of Nevada, Reno, January 1984.
CCEER-84-2	Douglas, B. and T. Iwasaki, "Proceedings of the First USA-Japan Bridge Engineering Workshop," held at the Public Works Research Institute, Tsukuba, Japan, Civil Engineering Department, Report No. CCEER-84-2, University of Nevada, Reno, April 1984.
CCEER-84-3	Saiidi, M., J. Hart, and B. Douglas, "Inelastic Static and Dynamic Analysis of Short R/C Bridges Subjected to Lateral Loads," Civil Engineering Department, Report No. CCEER-84-3, University of Nevada, Reno, July 1984.
CCEER-84-4	Douglas, B., "A Proposed Plan for a National Bridge Engineering Laboratory," Civil Engineering Department, Report No. CCEER-84-4, University of Nevada, Reno, December 1984.
CCEER-85-1	Norris, G. and P. Abdollaholiaee, "Laterally Loaded Pile Response: Studies with the Strain Wedge Model," Civil Engineering Department, Report No. CCEER-85-1, University of Nevada, Reno, April 1985.
CCEER-86-1	Ghusn, G. and M. Saiidi, "A Simple Hysteretic Element for Biaxial Bending of R/C in NEABS-86," Civil Engineering Department, Report No. CCEER-86-1, University of Nevada, Reno, July 1986.
CCEER-86-2	Saiidi, M., R. Lawver, and J. Hart, "User's Manual of ISADAB and SIBA, Computer Programs for Nonlinear Transverse Analysis of Highway Bridges Subjected to Static and Dynamic Lateral Loads," Civil Engineering Department, Report No. CCEER-86-2, University of Nevada, Reno, September 1986.
CCEER-87-1	Siddharthan, R., "Dynamic Effective Stress Response of Surface and Embedded Footings in Sand," Civil Engineering Department, Report No. CCEER-86-2, University of Nevada, Reno, June 1987.
CCEER-87-2	Norris, G. and R. Sack, "Lateral and Rotational Stiffness of Pile Groups for Seismic Analysis of Highway Bridges," Civil Engineering Department, Report No. CCEER-87-2, University of Nevada, Reno, June 1987.
CCEER-88-1	Orie, J. and M. Saiidi, "A Preliminary Study of One-Way Reinforced Concrete Pier Hinges Subjected to Shear and Flexure," Civil Engineering Department, Report No. CCEER-88-1, University of Nevada, Reno, January 1988.
CCEER-88-2	Orie, D., M. Saiidi, and B. Douglas, "A Micro-CAD System for Seismic Design of Regular Highway Bridges," Civil Engineering Department, Report No. CCEER-88-2, University of Nevada, Reno, June 1988.
CCEER-88-3	Orie, D. and M. Saiidi, "User's Manual for Micro-SARB, a Microcomputer Program for Seismic Analysis of Regular Highway Bridges," Civil Engineering Department, Report No. CCEER-88-3, University of Nevada, Reno, October 1988.

CCEER-89-1 Douglas, B., M. Saiidi, R. Hayes, and G. Holcomb, “A Comprehensive Study of the Loads and Pressures Exerted on Wall Forms by the Placement of Concrete,” Civil Engineering Department, Report No. CCEER-89-1, University of Nevada, Reno, February 1989.

CCEER-89-2 Richardson, J. and B. Douglas, “Dynamic Response Analysis of the Dominion Road Bridge Test Data,” Civil Engineering Department, Report No. CCEER-89-2, University of Nevada, Reno, March 1989.

CCEER-89-2 Vrontinos, S., M. Saiidi, and B. Douglas, “A Simple Model to Predict the Ultimate Response of R/C Beams with Concrete Overlays,” Civil Engineering Department, Report NO. CCEER-89-2, University of Nevada, Reno, June 1989.

CCEER-89-3 Ebrahimpour, A. and P. Jagadish, “Statistical Modeling of Bridge Traffic Loads - A Case Study,” Civil Engineering Department, Report No. CCEER-89-3, University of Nevada, Reno, December 1989.

CCEER-89-4 Shields, J. and M. Saiidi, “Direct Field Measurement of Prestress Losses in Box Girder Bridges,” Civil Engineering Department, Report No. CCEER-89-4, University of Nevada, Reno, December 1989.

CCEER-90-1 Saiidi, M., E. Maragakis, G. Ghusn, Y. Jiang, and D. Schwartz, “Survey and Evaluation of Nevada's Transportation Infrastructure, Task 7.2 - Highway Bridges, Final Report,” Civil Engineering Department, Report No. CCEER 90-1, University of Nevada, Reno, October 1990.

CCEER-90-2 Abdel-Ghaffar, S., E. Maragakis, and M. Saiidi, “Analysis of the Response of Reinforced Concrete Structures During the Whittier Earthquake 1987,” Civil Engineering Department, Report No. CCEER 90-2, University of Nevada, Reno, October 1990.

CCEER-91-1 Saiidi, M., E. Hwang, E. Maragakis, and B. Douglas, “Dynamic Testing and the Analysis of the Flamingo Road Interchange,” Civil Engineering Department, Report No. CCEER-91-1, University of Nevada, Reno, February 1991.

CCEER-91-2 Norris, G., R. Siddharthan, Z. Zafir, S. Abdel-Ghaffar, and P. Gowda, “Soil-Foundation-Structure Behavior at the Oakland Outer Harbor Wharf,” Civil Engineering Department, Report No. CCEER-91-2, University of Nevada, Reno, July 1991.

CCEER-91-3 Norris, G., “Seismic Lateral and Rotational Pile Foundation Stiffnesses at Cypress,” Civil Engineering Department, Report No. CCEER-91-3, University of Nevada, Reno, August 1991.

CCEER-91-4 O'Connor, D. and M. Saiidi, “A Study of Protective Overlays for Highway Bridge Decks in Nevada, with Emphasis on Polyester-Styrene Polymer Concrete,” Civil Engineering Department, Report No. CCEER-91-4, University of Nevada, Reno, October 1991.

CCEER-91-5 O'Connor, D.N. and M. Saiidi, “Laboratory Studies of Polyester-Styrene Polymer Concrete Engineering Properties,” Civil Engineering Department, Report No. CCEER-91-5, University of Nevada, Reno, November 1991.

CCEER-92-1 Straw, D.L. and M. Saiidi, “Scale Model Testing of One-Way Reinforced Concrete Pier Hinges Subject to Combined Axial Force, Shear and Flexure,” edited by D.N. O'Connor, Civil Engineering Department, Report No. CCEER-92-1, University of Nevada, Reno, March 1992.

CCEER-92-2 Wehbe, N., M. Saiidi, and F. Gordaninejad, “Basic Behavior of Composite Sections Made of Concrete Slabs and Graphite Epoxy Beams,” Civil Engineering Department, Report No. CCEER-92-2, University of Nevada, Reno, August 1992.

CCEER-92-3 Saiidi, M. and E. Hutchens, "A Study of Prestress Changes in A Post-Tensioned Bridge During the First 30 Months," Civil Engineering Department, Report No. CCEER-92-3, University of Nevada, Reno, April 1992.

CCEER-92-4 Saiidi, M., B. Douglas, S. Feng, E. Hwang, and E. Maragakis, "Effects of Axial Force on Frequency of Prestressed Concrete Bridges," Civil Engineering Department, Report No. CCEER-92-4, University of Nevada, Reno, August 1992.

CCEER-92-5 Siddharthan, R., and Z. Zafir, "Response of Layered Deposits to Traveling Surface Pressure Waves," Civil Engineering Department, Report No. CCEER-92-5, University of Nevada, Reno, September 1992.

CCEER-92-6 Norris, G., and Z. Zafir, "Liquefaction and Residual Strength of Loose Sands from Drained Triaxial Tests," Civil Engineering Department, Report No. CCEER-92-6, University of Nevada, Reno, September 1992.

CCEER-92-6-A Norris, G., Siddharthan, R., Zafir, Z. and Madhu, R. "Liquefaction and Residual Strength of Sands from Drained Triaxial Tests," Civil Engineering Department, Report No. CCEER-92-6-A, University of Nevada, Reno, September 1992.

CCEER-92-7 Douglas, B., "Some Thoughts Regarding the Improvement of the University of Nevada, Reno's National Academic Standing," Civil Engineering Department, Report No. CCEER-92-7, University of Nevada, Reno, September 1992.

CCEER-92-8 Saiidi, M., E. Maragakis, and S. Feng, "An Evaluation of the Current Caltrans Seismic Restrainer Design Method," Civil Engineering Department, Report No. CCEER-92-8, University of Nevada, Reno, October 1992.

CCEER-92-9 O'Connor, D., M. Saiidi, and E. Maragakis, "Effect of Hinge Restrainers on the Response of the Madrone Drive Undercrossing During the Loma Prieta Earthquake," Civil Engineering Department, Report No. CCEER-92-9, University of Nevada, Reno, February 1993.

CCEER-92-10 O'Connor, D., and M. Saiidi, "Laboratory Studies of Polyester Concrete: Compressive Strength at Elevated Temperatures and Following Temperature Cycling, Bond Strength to Portland Cement Concrete, and Modulus of Elasticity," Civil Engineering Department, Report No. CCEER-92-10, University of Nevada, Reno, February 1993.

CCEER-92-11 Wehbe, N., M. Saiidi, and D. O'Connor, "Economic Impact of Passage of Spent Fuel Traffic on Two Bridges in Northeast Nevada," Civil Engineering Department, Report No. CCEER-92-11, University of Nevada, Reno, December 1992.

CCEER-93-1 Jiang, Y., and M. Saiidi, "Behavior, Design, and Retrofit of Reinforced Concrete One-way Bridge Column Hinges," edited by D. O'Connor, Civil Engineering Department, Report No. CCEER-93-1, University of Nevada, Reno, March 1993.

CCEER-93-2 Abdel-Ghaffar, S., E. Maragakis, and M. Saiidi, "Evaluation of the Response of the Aptos Creek Bridge During the 1989 Loma Prieta Earthquake," Civil Engineering Department, Report No. CCEER-93-2, University of Nevada, Reno, June 1993.

CCEER-93-3 Sanders, D.H., B.M. Douglas, and T.L. Martin, "Seismic Retrofit Prioritization of Nevada Bridges," Civil Engineering Department, Report No. CCEER-93-3, University of Nevada, Reno, July 1993.

CCEER-93-4 Abdel-Ghaffar, S., E. Maragakis, and M. Saiidi, "Performance of Hinge Restrainers in the Huntington Avenue Overhead During the 1989 Loma Prieta Earthquake," Civil Engineering Department, Report No. CCEER-93-4, University of Nevada, Reno, June 1993 (in final preparation).

CCEER-93-5 Maragakis, E., M. Saiidi, S. Feng, and L. Flournoy, "Effects of Hinge Restrainers on the Response of the San Gregorio Bridge during the Loma Prieta Earthquake," (in final preparation) Civil Engineering Department, Report No. CCEER-93-5, University of Nevada, Reno.

CCEER-93-6 Saiidi, M., E. Maragakis, S. Abdel-Ghaffar, S. Feng, and D. O'Connor, "Response of Bridge Hinge Restrainers during Earthquakes -Field Performance, Analysis, and Design," Civil Engineering Department, Report No. CCEER-93-6, University of Nevada, Reno, May 1993.

CCEER-93-7 Wehbe, N., Saiidi, M., Maragakis, E., and Sanders, D., "Adequacy of Three Highway Structures in Southern Nevada for Spent Fuel Transportation," Civil Engineering Department, Report No. CCEER-93-7, University of Nevada, Reno, August 1993.

CCEER-93-8 Roybal, J., Sanders, D.H., and Maragakis, E., "Vulnerability Assessment of Masonry in the Reno-Carson City Urban Corridor," Civil Engineering Department, Report No. CCEER-93-8, University of Nevada, Reno, May 1993.

CCEER-93-9 Zafir, Z. and Siddharthan, R., "MOVLOAD: A Program to Determine the Behavior of Nonlinear Horizontally Layered Medium Under Moving Load," Civil Engineering Department, Report No. CCEER-93-9, University of Nevada, Reno, August 1993.

CCEER-93-10 O'Connor, D.N., Saiidi, M., and Maragakis, E.A., "A Study of Bridge Column Seismic Damage Susceptibility at the Interstate 80/U.S. 395 Interchange in Reno, Nevada," Civil Engineering Department, Report No. CCEER-93-10, University of Nevada, Reno, October 1993.

CCEER-94-1 Maragakis, E., B. Douglas, and E. Abdelwahed, "Preliminary Dynamic Analysis of a Railroad Bridge," Report CCEER-94-1, January 1994.

CCEER-94-2 Douglas, B.M., Maragakis, E.A., and Feng, S., "Stiffness Evaluation of Pile Foundation of Cazenovia Creek Overpass," Civil Engineering Department, Report No. CCEER-94-2, University of Nevada, Reno, March 1994.

CCEER-94-3 Douglas, B.M., Maragakis, E.A., and Feng, S., "Summary of Pretest Analysis of Cazenovia Creek Bridge," Civil Engineering Department, Report No. CCEER-94-3, University of Nevada, Reno, April 1994.

CCEER-94-4 Norris, G.M., Madhu, R., Valceschini, R., and Ashour, M., "Liquefaction and Residual Strength of Loose Sands from Drained Triaxial Tests," Report 2, Vol. 1&2, Civil Engineering Department, Report No. CCEER-94-4, University of Nevada, Reno, August 1994.

CCEER-94-5 Saiidi, M., Hutchens, E., and Gardella, D., "Prestress Losses in a Post-Tensioned R/C Box Girder Bridge in Southern Nevada," Civil Engineering Department, CCEER-94-5, University of Nevada, Reno, August 1994.

CCEER-95-1 Siddharthan, R., El-Gamal, M., and Maragakis, E.A., "Nonlinear Bridge Abutment , Verification, and Design Curves," Civil Engineering Department, CCEER-95-1, University of Nevada, Reno, January 1995.

CCEER-95-2 Ashour, M. and Norris, G., "Liquefaction and Undrained Response Evaluation of Sands from Drained Formulation," Civil Engineering Department, Report No. CCEER-95-2, University of Nevada, Reno, February 1995.

CCEER-95-3 Wehbe, N., Saiidi, M., Sanders, D. and Douglas, B., "Ductility of Rectangular Reinforced Concrete Bridge Columns with Moderate Confinement," Civil Engineering Department, Report No. CCEER-95-3, University of Nevada, Reno, July 1995.

CCEER-95-4 Martin, T.., Saiidi, M. and Sanders, D., "Seismic Retrofit of Column-Pier Cap Connections in Bridges in Northern Nevada," Civil Engineering Department, Report No. CCEER-95-4, University of Nevada, Reno, August 1995.

CCEER-95-5 Darwish, I., Saiidi, M. and Sanders, D., "Experimental Study of Seismic Susceptibility Column-Footing Connections in Bridges in Northern Nevada," Civil Engineering Department, Report No. CCEER-95-5, University of Nevada, Reno, September 1995.

CCEER-95-6 Griffin, G., Saiidi, M. and Maragakis, E., "Nonlinear Seismic Response of Isolated Bridges and Effects of Pier Ductility Demand," Civil Engineering Department, Report No. CCEER-95-6, University of Nevada, Reno, November 1995.

CCEER-95-7 Acharya, S.., Saiidi, M. and Sanders, D., "Seismic Retrofit of Bridge Footings and Column-Footing Connections," Civil Engineering Department, Report No. CCEER-95-7, University of Nevada, Reno, November 1995.

CCEER-95-8 Maragakis, E., Douglas, B., and Sandirasegaram, U., "Full-Scale Field Resonance Tests of a Railway Bridge," A Report to the Association of American Railroads, Civil Engineering Department, Report No. CCEER-95-8, University of Nevada, Reno, December 1995.

CCEER-95-9 Douglas, B., Maragakis, E. and Feng, S., "System Identification Studies on Cazenovia Creek Overpass," Report for the National Center for Earthquake Engineering Research, Civil Engineering Department, Report No. CCEER-95-9, University of Nevada, Reno, October 1995.

CCEER-96-1 El-Gamal, M.E. and Siddharthan, R.V., "Programs to Computer Translational Stiffness of Seat-Type Bridge Abutment," Civil Engineering Department, Report No. CCEER-96-1, University of Nevada, Reno, March 1996.

CCEER-96-2 Labia, Y., Saiidi, M. and Douglas, B., "Evaluation and Repair of Full-Scale Prestressed Concrete Box Girders," A Report to the National Science Foundation, Research Grant CMS-9201908, Civil Engineering Department, Report No. CCEER-96-2, University of Nevada, Reno, May 1996.

CCEER-96-3 Darwish, I., Saiidi, M. and Sanders, D., "Seismic Retrofit of R/C Oblong Tapered Bridge Columns with Inadequate Bar Anchorage in Columns and Footings," A Report to the Nevada Department of Transportation, Civil Engineering Department, Report No. CCEER-96-3, University of Nevada, Reno, May 1996.

CCEER-96-4 Ashour, M., Pilling, R., Norris, G. and Perez, H., "The Prediction of Lateral Load Behavior of Single Piles and Pile Groups Using the Strain Wedge Model," A Report to the California Department of Transportation, Civil Engineering Department, Report No. CCEER-96-4, University of Nevada, Reno, June 1996.

CCEER-97-1-A Rimal, P. and Itani, A. "Sensitivity Analysis of Fatigue Evaluations of Steel Bridges," Center for Earthquake Research, Department of Civil Engineering, University of Nevada, Reno, Nevada Report No. CCEER-97-1-A, September, 1997.

CCEER-97-1-B Maragakis, E., Douglas, B., and Sandirasegaram, U. "Full-Scale Field Resonance Tests of a Railway Bridge," A Report to the Association of American Railroads, Civil Engineering Department, University of Nevada, Reno, May, 1996.

CCEER-97-2 Wehbe, N., Saiidi, M., and D. Sanders, "Effect of Confinement and Flares on the Seismic Performance of Reinforced Concrete Bridge Columns," Civil Engineering Department, Report No. CCEER-97-2, University of Nevada, Reno, September 1997.

CCEER-97-3 Darwish, I., M. Saiidi, G. Norris, and E. Maragakis, "Determination of In-Situ Footing Stiffness Using Full-Scale Dynamic Field Testing," A Report to the Nevada Department of Transportation, Structural Design Division, Carson City, Nevada, Report No. CCEER-97-3, University of Nevada, Reno, October 1997.

CCEER-97-4-A Itani, A. "Cyclic Behavior of Richmond-San Rafael Tower Links," Center for Civil Engineering Earthquake Research, Department of Civil Engineering, University of Nevada, Reno, Nevada, Report No. CCEER-97-4, August 1997.

CCEER-97-4-B Wehbe, N., and M. Saiidi, "User's Manual for RCMC v. 1.2 : A Computer Program for Moment-Curvature Analysis of Confined and Unconfined Reinforced Concrete Sections," Center for Civil Engineering Earthquake Research, Department of Civil Engineering, University of Nevada, Reno, Nevada, Report No. CCEER-97-4, November, 1997.

CCEER-97-5 Isakovic, T., M. Saiidi, and A. Itani, "Influence of new Bridge Configurations on Seismic Performance," Department of Civil Engineering, University of Nevada, Reno, Report No. CCEER-97-5, September, 1997.

CCEER-98-1 Itani, A., Vesco, T. and Dietrich, A., "Cyclic Behavior of "as Built" Laced Members With End Gusset Plates on the San Francisco Bay Bridge," Center for Civil Engineering Earthquake Research, Department of Civil Engineering, University of Nevada, Reno, Nevada Report No. CCEER-98-1, March, 1998.

CCEER-98-2 G. Norris and M. Ashour, "Liquefaction and Undrained Response Evaluation of Sands from Drained Formulation," Center for Civil Engineering Earthquake Research, Department of Civil Engineering, University of Nevada, Reno, Nevada, Report No. CCEER-98-2, May, 1998.

CCEER-98-3 Qingbin, Chen, B. M. Douglas, E. Maragakis, and I. G. Buckle, "Extraction of Nonlinear Hysteretic Properties of Seismically Isolated Bridges from Quick-Release Field Tests," Center for Civil Engineering Earthquake Research, Department of Civil Engineering, University of Nevada, Reno, Nevada, Report No. CCEER-98-3, June, 1998.

CCEER-98-4 Maragakis, E., B. M. Douglas, and C. Qingbin, "Full-Scale Field Capacity Tests of a Railway Bridge," Center for Civil Engineering Earthquake Research, Department of Civil Engineering, University of Nevada, Reno, Nevada, Report No. CCEER-98-4, June, 1998.

CCEER-98-5 Itani, A., Douglas, B., and Woodgate, J., "Cyclic Behavior of Richmond-San Rafael Retrofitted Tower Leg," Center for Civil Engineering Earthquake Research, Department of Civil Engineering, University of Nevada, Reno. Report No. CCEER-98-5, June 1998

CCEER-98-6 Moore, R., Saiidi, M., and Itani, A., "Seismic Behavior of New Bridges with Skew and Curvature," Center for Civil Engineering Earthquake Research, Department of Civil Engineering, University of Nevada, Reno. Report No. CCEER-98-6, October, 1998.

CCEER-98-7 Itani, A and Dietrich, A, "Cyclic Behavior of Double Gusset Plate Connections," Center for Civil Engineering Earthquake Research, Department of Civil Engineering, University of Nevada, Reno, Nevada, Report No. CCEER-98-5, December, 1998.

CCEER-99-1 Caywood, C., M. Saiidi, and D. Sanders, "Seismic Retrofit of Flared Bridge Columns with Steel Jackets," Civil Engineering Department, University of Nevada, Reno, Report No. CCEER-99-1, February 1999.

CCEER-99-2 Mangoba, N., M. Mayberry, and M. Saiidi, "Prestress Loss in Four Box Girder Bridges in Northern Nevada," Civil Engineering Department, University of Nevada, Reno, Report No. CCEER-99-2, March 1999.

CCEER-99-3 Abo-Shadi, N., M. Saiidi, and D. Sanders, "Seismic Response of Bridge Pier Walls in the Weak Direction," Civil Engineering Department, University of Nevada, Reno, Report No. CCEER-99-3, April 1999.

CCEER-99-4 Buzick, A., and M. Saiidi, "Shear Strength and Shear Fatigue Behavior of Full-Scale Prestressed Concrete Box Girders," Civil Engineering Department, University of Nevada, Reno, Report No. CCEER-99-4, April 1999.

CCEER-99-5 Randall, M., M. Saiidi, E. Maragakis and T. Isakovic, "Restrainer Design Procedures For Multi-Span Simply-Supported Bridges," Civil Engineering Department, University of Nevada, Reno, Report No. CCEER-99-5, April 1999.

CCEER-99-6 Wehbe, N. and M. Saiidi, "User's Manual for RCMC v. 1.2, A Computer Program for Moment-Curvature Analysis of Confined and Unconfined Reinforced Concrete Sections," Civil Engineering Department, University of Nevada, Reno, Report No. CCEER-99-6, May 1999.

CCEER-99-7 Burda, J. and A. Itani, "Studies of Seismic Behavior of Steel Base Plates," Civil Engineering Department, University of Nevada, Reno, Report No. CCEER-99-7, May 1999.

CCEER-99-8 Ashour, M. and G. Norris, "Refinement of the Strain Wedge Model Program," Civil Engineering Department, University of Nevada, Reno, Report No. CCEER-99-8, March 1999.

CCEER-99-9 Dietrich, A., and A. Itani, "Cyclic Behavior of Laced and Perforated Steel Members on the San Francisco-Oakland Bay Bridge," Civil Engineering Department, University, Reno, Report No. CCEER-99-9, December 1999.

CCEER 99-10 Itani, A., A. Dietrich, "Cyclic Behavior of Built Up Steel Members and their Connections," Civil Engineering Department, University of Nevada, Reno, Report No. CCEER-99-10, December 1999.

CCEER 99-10-A Itani, A., E. Maragakis and P. He, "Fatigue Behavior of Riveted Open Deck Railroad Bridge Girders," Civil Engineering Department, University of Nevada, Reno, Report No. CCEER-99-10-A, August 1999.

CCEER 99-11 Itani, A., J. Woodgate, "Axial and Rotational Ductility of Built Up Structural Steel Members," Civil Engineering Department, University of Nevada, Reno, Report No. CCEER-99-11, December 1999.

CCEER-99-12 Sgambelluri, M., Sanders, D.H., and Saiidi, M.S., "Behavior of One-Way Reinforced Concrete Bridge Column Hinges in the Weak Direction," Department of Civil Engineering, University of Nevada, Reno, Report No. CCEER-99-12, December 1999.

CCEER-99-13 Laplace, P., Sanders, D.H., Douglas, B, and Saiidi, M, "Shake Table Testing of Flexure Dominated Reinforced Concrete Bridge Columns", Department of Civil Engineering, University of Nevada, Reno, Report No. CCEER-99-13, December 1999.

CCEER-99-14 Ahmad M. Itani, Jose A. Zepeda, and Elizabeth A. Ware "Cyclic Behavior of Steel Moment Frame Connections for the Moscone Center Expansion," Department of Civil Engineering, University of Nevada, Reno, Report No. CCEER-99-14, December 1999.

CCEER 00-1 Ashour, M., and Norris, G. "Undrained Lateral Pile and Pile Group Response in Saturated Sand," Civil Engineering Department, University of Nevada, Reno, Report No. CCEER-00-1, May 1999. January 2000.

CCEER 00-2 Saiidi, M. and Wehbe, N., "A Comparison of Confinement Requirements in Different Codes for Rectangular, Circular, and Double-Spiral RC Bridge Columns," Civil Engineering Department, University of Nevada, Reno, Report No. CCEER-00-2, January 2000.

CCEER 00-3 McElhaney, B., M. Saiidi, and D. Sanders, "Shake Table Testing of Flared Bridge Columns With Steel Jacket Retrofit," Civil Engineering Department, University of Nevada, Reno, Report No. CCEER-00-3, January 2000.

CCEER 00-4 Martinovic, F., M. Saiidi, D. Sanders, and F. Gordaninejad, "Dynamic Testing of Non-Prismatic Reinforced Concrete Bridge Columns Retrofitted with FRP Jackets," Civil Engineering Department, University of Nevada, Reno, Report No. CCEER-00-4, January 2000.

CCEER 00-5 Itani, A., and M. Saiidi, "Seismic Evaluation of Steel Joints for UCLA Center for Health Science Westwood Replacement Hospital," Civil Engineering Department, University of Nevada, Reno, Report No. CCEER-00-5, February 2000.

CCEER 00-6 Will, J. and D. Sanders, "High Performance Concrete Using Nevada Aggregates," Civil Engineering Department, University of Nevada, Reno, Report No. CCEER-00-6, May 2000.

CCEER 00-7 French, C., and M. Saiidi, "A Comparison of Static and Dynamic Performance of Models of Flared Bridge Columns," Civil Engineering Department, University of Nevada, Reno, Report No. CCEER-00-7, October 2000.

CCEER 00-8 Itani, A., H. Sedarat, "Seismic Analysis of the AISI LRFD Design Example of Steel Highway Bridges," Civil Engineering Department, University of Nevada, Reno, Report No. CCEER 00-08, November 2000.

CCEER 00-9 Moore, J., D. Sanders, and M. Saiidi, "Shake Table Testing of 1960's Two Column Bent with Hinges Bases," Civil Engineering Department, University of Nevada, Reno, Report No. CCEER 00-09, December 2000.

CCEER 00-10 Asthana, M., D. Sanders, and M. Saiidi, "One-Way Reinforced Concrete Bridge Column Hinges in the Weak Direction," Civil Engineering Department, University of Nevada, Reno, Report No. CCEER 00-10, April 2001.

CCEER 01-1 Ah Sha, H., D. Sanders, M. Saiidi, "Early Age Shrinkage and Cracking of Nevada Concrete Bridge Decks," Civil Engineering Department, University of Nevada, Reno, Report No. CCEER 01-01, May 2001.

CCEER 01-2 Ashour, M. and G. Norris, "Pile Group program for Full Material Modeling a Progressive Failure," Civil Engineering Department, University of Nevada, Reno, Report No. CCEER 01-02, July 2001.

CCEER 01-3 Itani, A., C. Lanaud, and P. Dusicka, "Non-Linear Finite Element Analysis of Built-Up Shear Links," Civil Engineering Department, University of Nevada, Reno, Report No. CCEER 01-03, July 2001.

CCEER 01-4 Saiidi, M., J. Mortensen, and F. Martinovic, "Analysis and Retrofit of Fixed Flared Columns with Glass Fiber-Reinforced Plastic Jacketing," Civil Engineering Department, University of Nevada, Reno, Report No. CCEER 01-4, August 2001

CCEER 01-5 Saiidi, M., A. Itani, I. Buckle, and Z. Cheng, "Performance of A Full-Scale Two-Story Wood Frame Structure Supported on Ever-Level Isolators," Civil Engineering Department, University of Nevada, Reno, Report No. CCEER 01-5, October 2001

CCEER 01-6 Laplace, P., D. Sanders, and M. Saiidi, "Experimental Study and Analysis of Retrofitted Flexure and Shear Dominated Circular Reinforced Concrete Bridge Columns Subjected to Shake Table Excitation," Civil Engineering Department, University of Nevada, Reno, Report No. CCEER 01-6, June 2001.

CCEER 01-7 Reppi, F., and D. Sanders, "Removal and Replacement of Cast-in-Place, Post-tensioned, Box Girder Bridge," Civil Engineering Department, University of Nevada, Reno, Report No. CCEER 01-7, December 2001.

CCEER 02-1 Pulido, C., M. Saiidi, D. Sanders, and A. Itani, "Seismic Performance and Retrofitting of Reinforced Concrete Bridge Bents," Civil Engineering Department, University of Nevada, Reno, Report No. CCEER 02-1, January 2002.

CCEER 02-2 Yang, Q., M. Saiidi, H. Wang, and A. Itani, "Influence of Ground Motion Incoherency on Earthquake Response of Multi-Support Structures," Civil Engineering Department, University of Nevada, Reno, Report No. CCEER 02-2, May 2002.

CCEER 02-3 M. Saiidi, B. Gopalakrishnan, E. Reinhardt, and R. Siddharthan, "A Preliminary Study of Shake Table Response of A Two-Column Bridge Bent on Flexible Footings," Civil Engineering Department, University of Nevada, Reno, Report No. CCEER 02-03, June 2002.

CCEER 02-4 Not Published

CCEER 02-5 Banghart, A., Sanders, D., Saiidi, M., "Evaluation of Concrete Mixes for Filling the Steel Arches in the Galena Creek Bridge," Civil Engineering Department, University of Nevada, Reno, Report No. CCEER 02-05, June 2002.

CCEER 02-6 Dusicka, P., Itani, A., Buckle, I. G., "Cyclic Behavior of Shear Links and Tower Shaft Assembly of San Francisco – Oakland Bay Bridge Tower," Civil Engineering Department, University of Nevada, Reno, Report No. CCEER 02-06, July 2002.

CCEER 02-7 Mortensen, J., and M. Saiidi, "A Performance-Based Design Method for Confinement in Circular Columns," Civil Engineering Department, University of Nevada, Reno, Report No. CCEER 02-07, November 2002.

CCEER 03-1 Wehbe, N., and M. Saiidi, "User's manual for SPMC v. 1.0 : A Computer Program for Moment-Curvature Analysis of Reinforced Concrete Sections with Interlocking Spirals," Center for Civil Engineering Earthquake Research, Department of Civil Engineering, University of Nevada, Reno, Nevada, Report No. CCEER-03-1, May, 2003.

CCEER 03-2 Wehbe, N., and M. Saiidi, "User's manual for RCMC v. 2.0 : A Computer Program for Moment-Curvature Analysis of Confined and Unconfined Reinforced Concrete Sections," Center for Civil Engineering Earthquake Research, Department of Civil Engineering, University of Nevada, Reno, Nevada, Report No. CCEER-03-2, June, 2003.

CCEER 03-3 Nada, H., D. Sanders, and M. Saiidi, "Seismic Performance of RC Bridge Frames with Architectural-Flared Columns," Civil Engineering Department, University of Nevada, Reno, Report No. CCEER 03-3, January 2003.

CCEER 03-4 Reinhardt, E., M. Saiidi, and R. Siddharthan, "Seismic Performance of a CFRP/ Concrete Bridge Bent on Flexible Footings," Civil Engineering Department, University of Nevada, Reno, Report No. CCEER 03-4, August 2003.

CCEER 03-5 Johnson, N., M. Saiidi, A. Itani, and S. Ladkany, "Seismic Retrofit of Octagonal Columns with Pedestal and One-Way Hinge at the Base," Center for Civil Engineering Earthquake Research, Department of Civil Engineering, University of Nevada, Reno, Nevada, and Report No. CCEER-03-5, August 2003.

CCEER 03-6 Mortensen, C., M. Saiidi, and S. Ladkany, "Creep and Shrinkage Losses in Highly Variable Climates," Center for Civil Engineering Earthquake Research, Department of Civil Engineering, University of Nevada, Reno, Report No. CCEER-03-6, September 2003.

CCEER 03- 7 Ayoub, C., M. Saiidi, and A. Itani, "A Study of Shape-Memory-Alloy-Reinforced Beams and Cubes," Center for Civil Engineering Earthquake Research, Department of Civil Engineering, University of Nevada, Reno, Nevada, Report No. CCEER-03-7, October 2003.

CCEER 03-8 Chandane, S., D. Sanders, and M. Saiidi, "Static and Dynamic Performance of RC Bridge Bents with Architectural-Flared Columns," Center for Civil Engineering Earthquake Research, Department of Civil Engineering, University of Nevada, Reno, Nevada, Report No. CCEER-03-8, November 2003.

CCEER 04-1 Olaegbe, C., and Saiidi, M., "Effect of Loading History on Shake Table Performance of A Two-Column Bent with Infill Wall," Center for Civil Engineering Earthquake Research, Department of Civil Engineering, University of Nevada, Reno, Nevada, Report No. CCEER-04-1, January 2004.

CCEER 04-2 Johnson, R., Maragakis, E., Saiidi, M., and DesRoches, R., "Experimental Evaluation of Seismic Performance of SMA Bridge Restrainers," Center for Civil Engineering Earthquake Research, Department of Civil Engineering, University of Nevada, Reno, Nevada, Report No. CCEER-04-2, February 2004.

CCEER 04-3 Moustafa, K., Sanders, D., and Saiidi, M., "Impact of Aspect Ratio on Two-Column Bent Seismic Performance," Center for Civil Engineering Earthquake Research, Department of Civil Engineering, University of Nevada, Reno, Nevada, Report No. CCEER-04-3, February 2004.

CCEER 04-4 Maragakis, E., Saiidi, M., Sanchez-Camargo, F., and Elfass, S., "Seismic Performance of Bridge Restrainers At In-Span Hinges," Center for Civil Engineering Earthquake Research, Department of Civil Engineering, University of Nevada, Reno, Nevada, Report No. CCEER-04-4, March 2004.

CCEER 04-5 Ashour, M., Norris, G. and Elfass, S., "Analysis of Laterally Loaded Long or Intermediate Drilled Shafts of Small or Large Diameter in Layered Soil," Center for Civil Engineering Earthquake Research, Department of Civil Engineering, University of Nevada, Reno, Nevada, Report No. CCEER-04-5, June 2004.

CCEER 04-6 Correal, J., Saiidi, M. and Sanders, D., "Seismic Performance of RC Bridge Columns Reinforced with Two Interlocking Spirals," Center for Civil Engineering Earthquake Research, Department of Civil Engineering, University of Nevada, Reno, Nevada, Report No. CCEER-04-6, August 2004.

CCEER 04-7 Dusicka, P., Itani, A. and Buckle, I., "Cyclic Response and Low Cycle Fatigue Characteristics of Plate Steels," Center for Civil Engineering Earthquake Research, Department of Civil Engineering, University of Nevada, Reno, Nevada, Report No. CCEER-04-7, November 2004.

CCEER 04-8 Dusicka, P., Itani, A. and Buckle, I., "Built-up Shear Links as Energy Dissipaters for Seismic Protection of Bridges," Center for Civil Engineering Earthquake Research, Department of Civil Engineering, University of Nevada, Reno, Nevada, Report No. CCEER-04-8, November 2004.

CCEER 04-9 Sureshkumar, K., Saiidi, S., Itani, A. and Ladkany, S., "Seismic Retrofit of Two-Column Bents with Diamond Shape Columns," Center for Civil Engineering Earthquake Research, Department of Civil Engineering, University of Nevada, Reno, Nevada, Report No. CCEER-04-9, November 2004.

CCEER 05-1 Wang, H. and Saiidi, S., "A Study of RC Columns with Shape Memory Alloy and Engineered Cementitious Composites," Center for Civil Engineering Earthquake Research, Department of Civil Engineering, University of Nevada, Reno, Nevada, Report No. CCEER-05-1, January 2005.

CCEER 05-2 Johnson, R., Saiidi, S. and Maragakis, E., "A Study of Fiber Reinforced Plastics for Seismic Bridge Restrainers," Center for Civil Engineering Earthquake Research, Department of Civil Engineering, University of Nevada, Reno, Nevada, Report No. CCEER-05-2, January 2005.

CCEER 05-3 Carden, L.P., Itani, A.M., Buckle, I.G, "Seismic Load Path in Steel Girder Bridge Superstructures," Center for Civil Engineering Earthquake Research, Department of Civil Engineering, University of Nevada, Reno, Nevada, Report No. CCEER-05-3, January 2005.

CCEER 05-4 Carden, L.P., Itani, A.M., Buckle, I.G, "Seismic Performance of Steel Girder Bridge Superstructures with Ductile End Cross Frames and Seismic Isolation," Center for Civil Engineering Earthquake Research, Department of Civil Engineering, University of Nevada, Reno, Nevada, Report No. CCEER-05-4, January 2005.

CCEER 05-5 Goodwin, E., Maragakis, M., Itani, A. and Luo, S., "Experimental Evaluation of the Seismic Performance of Hospital Piping Subassemblies," Center for Civil Engineering Earthquake Research, Department of Civil Engineering, University of Nevada, Reno, Nevada, Report No. CCEER-05-5, February 2005.

CCEER 05-6 Zadeh M. S., Saiidi, S, Itani, A. and Ladkany, S., "Seismic Vulnerability Evaluation and Retrofit Design of Las Vegas Downtown Viaduct," Center for Civil Engineering Earthquake Research, Department of Civil Engineering, University of Nevada, Reno, Nevada, Report No. CCEER-05-6, February 2005.

CCEER 05-7 Phan, V., Saiidi, S. and Anderson, J., "Near Fault (Near Field) Ground Motion Effects on Reinforced Concrete Bridge Columns," Center for Civil Engineering Earthquake Research, Department of Civil Engineering, University of Nevada, Reno, Nevada, Report No. CCEER-05-7, August 2005.

CCEER 05-8 Carden, L., Itani, A. and Laplace, P., "Performance of Steel Props at the UNR Fire Science Academy subjected to Repeated Fire," Center for Civil Engineering Earthquake Research, Department of Civil Engineering, University of Nevada, Reno, Nevada, Report No. CCEER-05-8, August 2005.

CCEER 05-9 Yamashita, R. and Sanders, D., "Shake Table Testing and an Analytical Study of Unbonded Prestressed Hollow Concrete Column Constructed with Precast Segments," Center for Civil Engineering Earthquake Research, Department of Civil Engineering, University of Nevada, Reno, Nevada, Report No. CCEER-05-9, August 2005.

CCEER 05-10 Not Published

CCEER 05-11 Carden, L., Itani., A., and Peckan, G., "Recommendations for the Design of Beams and Posts in Bridge Falsework," Center for Civil Engineering Earthquake Research, Department of Civil Engineering, University of Nevada, Reno, Nevada, Report No. CCEER-05-11, October 2005.

CCEER 06-01 Cheng, Z., Saiidi, M., and Sanders, D., "Development of a Seismic Design Method for Reinforced Concrete Two-Way Bridge Column Hinges," Center for Civil Engineering Earthquake Research, Department of Civil Engineering, University of Nevada, Reno, Nevada, Report No. CCEER-06-01, February 2006.

CCEER 06-02 Johnson, N., Saiidi, M., and Sanders, D., "Large-Scale Experimental and Analytical Studies of a Two-Span Reinforced Concrete Bridge System," Center for Civil Engineering Earthquake Research, Department of Civil Engineering, University of Nevada, Reno, Nevada, Report No. CCEER-06-02, March 2006.

CCEER 06-03 Saiidi, M., Ghasemi, H. and Tiras, A., "Seismic Design and Retrofit of Highway Bridges," Proceedings, Second US-Turkey Workshop, Center for Civil Engineering Earthquake Research, Department of Civil Engineering, University of Nevada, Reno, Nevada, Report No. CCEER-06-03, May 2006.

CCEER 07-01 O'Brien, M., Saiidi, M. and Sadrossadat-Zadeh, M., "A Study of Concrete Bridge Columns Using Innovative Materials Subjected to Cyclic Loading," Center for Civil Engineering Earthquake Research, Department of Civil Engineering, University of Nevada, Reno, Nevada, Report No. CCEER-07-01, January 2007.

CCEER 07-02 Sadrossadat-Zadeh, M. and Saiidi, M., "Effect of Strain rate on Stress-Strain Properties and Yield Propagation in Steel Reinforcing Bars," Center for Civil Engineering Earthquake Research, Department of Civil Engineering, University of Nevada, Reno, Nevada, Report No. CCEER-07-02, January 2007.

CCEER 07-03 Sadrossadat-Zadeh, M. and Saiidi, M., "Analytical Study of NEESR-SG 4-Span Bridge Model Using OpenSees," Center for Civil Engineering Earthquake Research, Department of Civil Engineering, University of Nevada, Reno, Nevada, Report No. CCEER-07-03, January 2007.

CCEER 07-04 Nelson, R., Saiidi, M. and Zadeh, S., "Experimental Evaluation of Performance of Conventional Bridge Systems," Center for Civil Engineering Earthquake Research, Department of Civil Engineering, University of Nevada, Reno, Nevada, Report No. CCEER-07-04, October 2007.

CCEER 07-05 Bahen, N. and Sanders, D., "Strut-and-Tie Modeling for Disturbed Regions in Structural Concrete Members with Emphasis on Deep Beams," Center for Civil Engineering Earthquake Research, Department of Civil Engineering, University of Nevada, Reno, Nevada, Report No. CCEER-07-05, December 2007.

CCEER 07-06 Choi, H., Saiidi, M. and Somerville, P., "Effects of Near-Fault Ground Motion and Fault-Rupture on the Seismic Response of Reinforced Concrete Bridges," Center for Civil Engineering Earthquake Research, Department of Civil Engineering, University of Nevada, Reno, Nevada, Report No. CCEER-07-06, December 2007.

CCEER 07-07 Ashour M. and Norris, G., "Report and User Manual on Strain Wedge Model Computer Program for Files and Large Diameter Shafts with LRFD Procedure," Center for Civil Engineering Earthquake Research, Department of Civil Engineering, University of Nevada, Reno, Nevada, Report No. CCEER-07-07, October 2007.

CCEER 08-01 Doyle, K. and Saiidi, M., "Seismic Response of Telescopic Pipe Pin Connections," Center for Civil Engineering Earthquake Research, Department of Civil Engineering, University of Nevada, Reno, Nevada, Report No. CCEER-08-01, February 2008.

CCEER 08-02 Taylor, M. and Sanders, D., "Seismic Time History Analysis and Instrumentation of the Galena Creek Bridge," Center for Civil Engineering Earthquake Research, Department of Civil Engineering, University of Nevada, Reno, Nevada, Report No. CCEER-08-02, April 2008.

CCEER 08-03 Abdel-Mohti, A. and Pekcan, G., "Seismic Response Assessment and Recommendations for the Design of Skewed Post-Tensioned Concrete Box-Girder Highway Bridges," Center for Civil Engineering Earthquake Research, Department of Civil and Environmental Engineering, University of Nevada, Reno, Nevada, Report No. CCEER-08-03, September 2008.

CCEER 08-04 Saiidi, M., Ghasemi, H. and Hook, J., "Long Term Bridge Performance Monitoring, Assessment & Management," Proceedings, FHWA/NSF Workshop on Future Directions," Center for Civil Engineering Earthquake Research, Department of Civil and Environmental Engineering, University of Nevada, Reno, Nevada, Report No. CCEER 08-04, September 2008.

CCEER 09-01 Brown, A., and Saiidi, M., "Investigation of Near-Fault Ground Motion Effects on Substandard Bridge Columns and Bents," Center for Civil Engineering Earthquake Research, Department of Civil and Environmental Engineering, University of Nevada, Reno, Nevada, Report No. CCEER-09-01, July 2009.

CCEER 09-02 Linke, C., Pekcan, G., and Itani, A., "Detailing of Seismically Resilient Special Truss Moment Frames," Center for Civil Engineering Earthquake Research, Department of Civil and Environmental Engineering, University of Nevada, Reno, Nevada, Report No. CCEER-09-02, August 2009.

CCEER 09-03 Hillis, D., and Saiidi, M., "Design, Construction, and Nonlinear Dynamic Analysis of Three Bridge Bents Used in a Bridge System Test," Center for Civil Engineering Earthquake Research, Department of Civil and Environmental Engineering, University of Nevada, Reno, Nevada, Report No. CCEER-09-03, August 2009.

CCEER 09-04 Bahrami, H., Itani, A., and Buckle, I., "Guidelines for the Seismic Design of Ductile End Cross Frames in Steel Girder Bridge Superstructures," Center for Civil Engineering Earthquake Research, Department of Civil and Environmental Engineering, University of Nevada, Reno, Nevada, Report No. CCEER-09-04, September 2009.

CCEER 10-01 Zaghi, A. E., and Saiidi, M., "Seismic Design of Pipe-Pin Connections in Concrete Bridges," Center for Civil Engineering Earthquake Research, Department of Civil and Environmental Engineering, University of Nevada, Reno, Nevada, Report No. CCEER-10-01, January 2010.

CCEER 10-02 Pooranampillai, S., Elfass, S., and Norris, G., "Laboratory Study to Assess Load Capacity Increase of Drilled Shafts through Post Grouting," Center for Civil Engineering Earthquake Research, Department of Civil and Environmental Engineering, University of Nevada, Reno, Nevada, Report No. CCEER-10-02, January 2010.

CCEER 10-03 Itani, A., Grubb, M., and Monzon, E, "Proposed Seismic Provisions and Commentary for Steel Plate Girder Superstructures," Center for Civil Engineering Earthquake Research, Department of Civil and Environmental Engineering, University of Nevada, Reno, Nevada, Report No. CCEER-10-03, June 2010.

CCEER 10-04 Cruz-Noguez, C., Saiidi, M., "Experimental and Analytical Seismic Studies of a Four-Span Bridge System with Innovative Materials," Center for Civil Engineering Earthquake Research, Department of Civil and Environmental Engineering, University of Nevada, Reno, Nevada, Report No. CCEER-10-04, September 2010.

CCEER 10-05 Vosooghi, A., Saiidi, M., "Post-Earthquake Evaluation and Emergency Repair of Damaged RC Bridge Columns Using CFRP Materials," Center for Civil Engineering Earthquake Research, Department of Civil and Environmental Engineering, University of Nevada, Reno, Nevada, Report No. CCEER-10-05, September 2010.

CCEER 10-06 Ayoub, M., Sanders, D., "Behavior of Pile Extension Connections to Slab Bridges Under Cyclic Loading Effect," Center for Civil Engineering Earthquake Research, Department of Civil and Environmental Engineering, University of Nevada, Reno, Nevada, Report No. CCEER-10-06, October 2010.